FIELD AND LABORATORY STUDIES OF MINE BACKFILL DESIGN CRITERIA

Luciano Piciacchia

B.Eng. (Mining)

M.Eng. (Mining)

Department of Mining and Metallurgical Engineering

McGill University

Montreal, Quebec

A Thesis Submitted to the Faculty of

Graduate Studies and Research in

Partial Fulfillment of the Requirements

of a Doctoral Degree in Mining Engineering

ACKNOWLEDGEMENTS

The author would like to extend his sincerest thanks to Dr. M.J. Scoble, McGill for his support, motivation and direction throughout the course of this project.

I would further like to acknowledge the Centre de Recherche Minerale de Quebec for their moral and financial support of these studies. Thanks are also extended to the numerous mines and their staff who cooperated with this work. The staff of the Noranda group of companies, especially Mssrs. J. Nantel and G. Sauriol deserve special mention in this respect, due to their involvement with this project from the outset.

Lastly I would like to express my thanks to the following members of the McGill rock engineering research group for their assistance and support: Dr. F.P. Hassani, Dr. H. Mitri, J. Hadjigeorgiou, L. Beauchamp, P. Chau, K. Shikatani, G. Wong, M. Vendramini, M. Vachon and M. Carter. Thanks are also due Mr. G. Toundjian for his translation assistance.

ABSTRACT

This work develops a backfill design procedure aimed to facilitate the optimization of an available mine material in order to meet target objectives in a particular mining role. This required the compilation and analysis of data on fill usage, established design procedures, physical and geomechanical properties, testing techniques and procedures, as well as behavioural modelling methods.

A backfill classification system is proposed based upon size distribution. A series of design equations are presented which relate to this system. These equations represent the means by which backfill geomechanical behaviour can be related to physical properties. This is considered to be fundamental to an effective backfill design procedure. Derivation of the equations has been based upon analysis of data from a program of laboratory and in situ testing conducted in ten operating Canadian mines by the author, together with other published work.

The in situ testing required the development of a pressuremeter testing procedure novel to underground mining. The theoretical basis for the employment of pressuremeter data has been examined and behavioral equations have been developed to describe the deformation and stress history during a backfill material test. In addition two new equations have been developed for the analysis of pressuremeter data. The in situ data collected has been correlated with laboratory derived geomechanical data for the same backfill materials.

The geomechanical properties associated with the proposed backfill classifications have also been related to their influence on backfill behaviour in three mine backfill roles: free standing stability during pillar recovery in bulk mining methods; dynamic interaction with stope walls in rockburst prone ground; and ability to reduce stresses in highly stressed rock masses. This work has been based on new and established modelling methods and aims to provide insight into the effectiveness of the backfill classes in these roles of growing practical significance.

ABSTRAIT

Ce Travail Developpe une procedure de dessin de remblai, ayant pour but de faciliter à une grande echelle d'un materiau de mine acceptable dans le but de rencontrer des objectifs en vue dans un rôle particulier de minage. Ceci requiert la compilation et analyse de donnees d'usage de remplissage, des dessins de procedures établies, des proprietes physiques et geomécaniques, testant des techniqués et procedures, aussi bien des methodes de modelage.

Un systeme de classification de remplissage de remblai est propose base sur une distribution de grandeur. Une serie d'équations de modeles sont presentees relatives a ce systeme. Ces équations representent les moyens par les quels le comportement geomecanique de remblai peut être relate a des proprietes physiques. Cesi est considere comme fondamental à un remplissage de remblai d'une procedure modelee, l'eloignement de ces equations a ete basee sur des donnees publiees aussi bien avec les resultats d'un programme de laboratoire et de test sur le champs de dix mines canadiennes operationnelles.

Le test sur le lien exiga le développment d'un pressiometre pourteter la procedure nouvelle à un minage de sous-sol. La base théorique pour l'usage de pressiometre couvrant les donnees a ete examinee et des equations d'equations de sensibilite developpees de decrire le deformation et l'histoire de contrainte dans contenant de test. En plus deux nouvelles equations on ete developees pour l'analyse des donnees du pressiometre. Les donnees sur le site

collectionnees on ete corroborées avec des donneés de laboratoire de proprietes de force geomécaniques pour les mêmes matériaux de comblement de remblai.

Les proprietes de force geomecanique associées avec le parachevement de classes de remblai ont ete aussi reliées a leur influence sur le comportement du remblai dans trois façons de minage: la stabilite d'une tenue libre pendant le recouvrement du pilier couvrant en gros de methodes minieres; une interation dynamiques avec des murs de chantier d'abattage dans un coup de charge rocheuse dans la rocaille; et habileté de reduire les contraintes des pilier.

TABLE OF CONTENTS
VOLUME 1

TABLE OF CONTENTS
VOLUME 1

TABLE OF CONTENTS
VOLUME 1

TABLE OF CONTENTS
VOLUME 1

TABLE OF CONTENTS
VOLUME 1

PAGE #

CHAPTER 6

TABLE OF CONTENTS
VOLUME 1

TABLE OF CONTENTS
VOLUME 1

TABLE OF CONTENTS
VOLUME 1

TABLE OF CONTENTS
VOLUME 1

TABLE OF CONTENTS
VOLUME 2

TABLE OF CONTENTS
VOLUME 2

LIST OF FIGURES

LIST OF FIGURES

CHAPTER 6

LIST OF FIGURES

LIST OF FIGURES

LIST OF FIGURES

LIST OF FIGURES

LIST OF FIGURES

CHAPTER 10

LIST OF FIGURES

LIST OF FIGURES

LIST OF TABLES

LIST OF TABLES

LIST OF TABLES

LIST OF TABLES

1.0 INTRODUCTION

The first reported uses of backfills for stablization of structures date back to 1864 (1) where hydraulic filling was used to protect the foundations of a church in the coal regions of Pennsylvania. The use of backfill became standard practice world - wide after World War II. The introduction of the use of Portland cement in the mid - sixties to stabilize backfill was the next most significant step towards current backfill technology.

It became apparent in the early 1980's that the use of backfill in Canada would grow significantly, mainly due to the occurence of rockbursting, trend towards bulk mining methods and increased mining depths. In parallel with the forseen increased usage it was apparent that there existed no design criteria for the prediction of the geomechanical behaviour of these materials. In addition, there was some confusion as to which behavioural properties were of greatest significance to the role of backfill in the various mining environments.

The geomechanical data available at the outset of this project predominantly related to the uniaxial compressive strength of Portland cement-stabilized fills. There was a sparsity of data on the mechanical behaviour of these materials, particularly for uncemented fine grained backfills and rockfill materials. In addition, the interdependance between the physical and geomechanical properties of such backfill materials was not clearly understood.

The existing data was not only limited to the uniaxial compressive strength of cemented fine grained backfills but also comprised laboratory test data only. A sparsity of in situ geomechanical characteristics of mine backfills existed. In addition it was not clear which in situ techniques were appropriate to determine such properties.

Recognition of this situation led to the submission of a proposal which aimed to help alleviate these severe constraints to mine design in 1983, to Centre de Recherche Minerale, Quebec. The research was launched at McGill University with the cooperation of the Noranda Research Center. The proposal focused on the development of backfill design criteria based on work including: the determination of backfill usage and properties from a mine survey and research review, laboratory and field testing; and to a lesser degree the evaluation of the effectiveness of backfills in various mine environments.

A backfill survey was initiated, by the author, in the summer of 1985 to verify the current and anticipated usage of backfill in Quebec mines. A similar survey was carried out cooperatively the following summer for the Ontario mining industry by the Ontario Ministry of Labour. The results of both surveys are reported in Chapter 4. In summary, it was found that 78% of Quebec mines presently use or plan to use backfill in their operations, with a similar trend observed in Ontario. The high degree of current and future backfill usage indicates the growing importance of this material in today's mining operations and further justified

the extent of the ensuing studies.

The primary objective of this thesis is to develop design criteria based on backfill function and material physical characteristics. A series of design equations have been developed, Chapter 9, which are intended to be universal in application. They aim to allow simulation of modifications of mine backfill systems in terms of their effect on physical backfill properties. The effect of these modifications can further be extended to the geomechanical properties by the developed equations . A further benefit of such an approach is the ability to predict backfill reponse with a limited availability of laboratory or field trials data. In this way backfill can be designed from basic principles rather than by trial and error.

Basic to the development of design criteria was the necessity to establish the geomechanical properties of backfills presently in use and test their effectiveness for different backfill support functions. This was considered as an important contribution since mines are increasingly employing backfill for support. Mines, however are only now beginning to consider geomechanical backfill requirements and thus the applicability and selection methods for behavioural modelling techniques have tended not to have been thoroughly verified by field data.

In order to meet the objectives outline above a backfill database was developed. Through the course of this research

project it has been found that backfills can be classified in four operational groups; fine grained or rock backfills, either of which can be cemented or uncemented. It was considered to be within the scope of this thesis to determine the operational geotechnical properties of each of these materials with the exception of cemented rockfills. This resulted from a lack of published data, and available testing locations for cemented rockfill material. The design equations developed are based on physical backfill characteristics and are an extension of a laboratory investigation, which focused on the relevent material properties defined. These design equations are further intended to be combined with field pressuremeter data to enable more accurate prediction of field properties by laboratory data.

The basic structure of this thesis thus goes from the general to the specific and is illustrated in Figure 1, commencing with a general review of present backfill classification and a review of important physical properties for design purposes. This is followed by the presentation of backfill design criteria aimed at backfill optimization. The laboratory and field testing procedures adopted are then outlined, followed by the presentation of the test data in the subsequent three chapters. The data relates to field and laboratory geomechanical properties as well as physical characteristics. The effectiveness of the properties derived is then tested against the functions related to three important mine settings in Chapter 10.

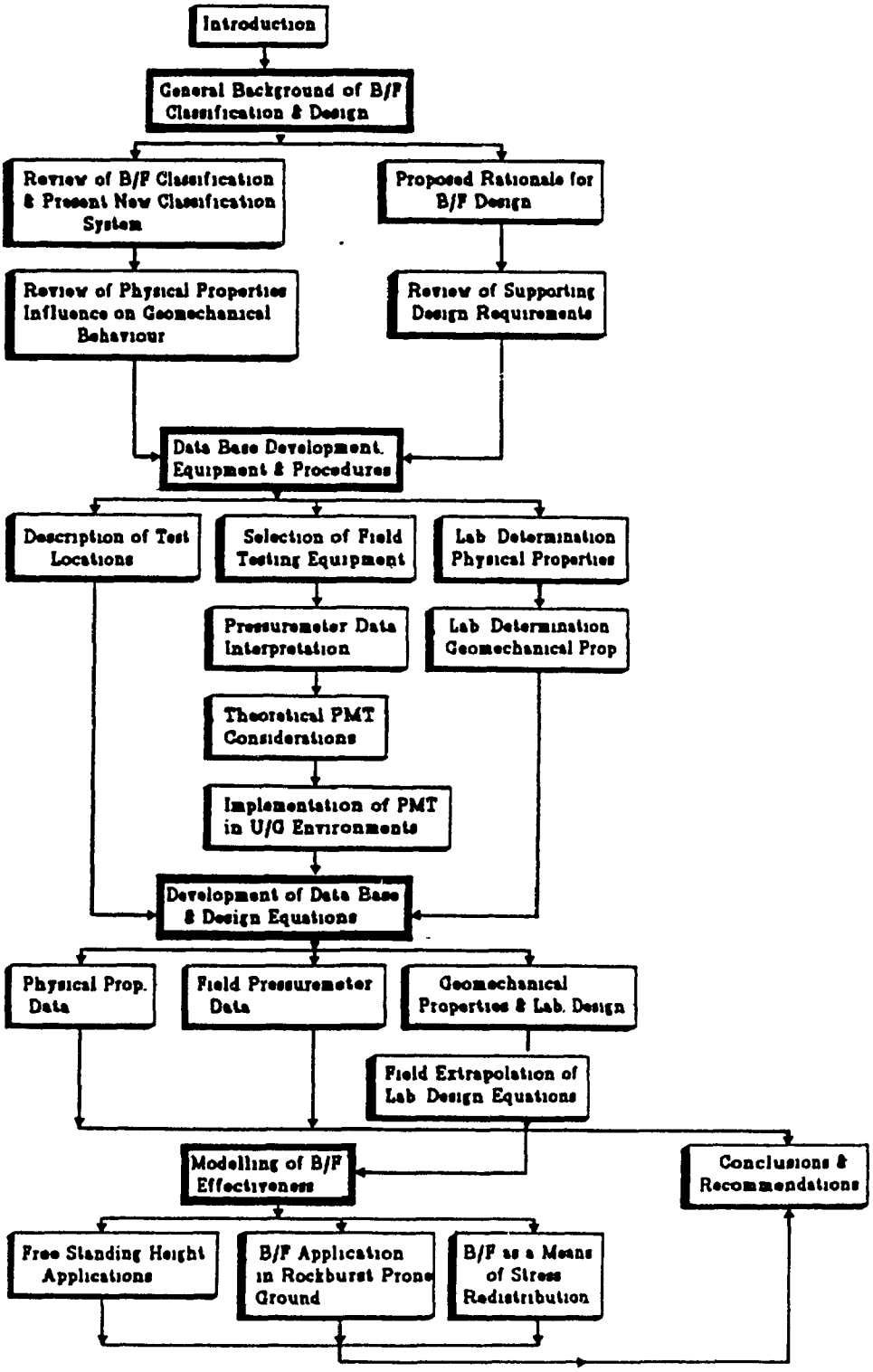

Figure 1.1 Thesis Rationale

A review of backfill usage and classification has been presented in Chapter 2, and a grading classification system has been developed. The benefit of this system of classification is its ability to uniformly and distinctly classify any backfill material, a process which to date has involved subjectivity without standardized criteria.

Having defined and categorized the available backfill material, a set of operational target properties must be met via some backfill design method. The present methods of backfill design have been characterized as methods of traditional usage based on past experience and/or trial and error. It was thus required to develop a backfill design system aiming to optimize design and account for the perceived role of the backfill and the interaction between physical and geomechanical properties. A backfill design system which fulfills the above criteria has been developed and outlined, Chapter 3. The design criteria presented focuses first on the determination of required backfill properties dependant on function. This further required that a number of modelling methods be evaluated or developed.

Once the target properties have been determined the available material is to be designed to meet these requirements via a series of interrelated design equations. The development of these equations required the formation of a database founded on published data, laboratory studies and field pressuremeter correlations. The various field testing equipment available for aquiring field data has been described in Chapter 5 and the rationale for finally

selecting the pressuremeter has been outlined. The use of the Pencel pressuremeter required the development of an innovative instrument insertion equipment and techniques appropriate to the underground environment. Arising from the field pressuremeter testing was the realization that the present equations describing the stress and strain distributions generated by the expansion of the probe within an infinite elastic undrained soil are not applicable to such mono-cellular probes. New equations have thus been developed which account for the elliptical deformation geometry of mono-cellular probes, Appendix 4 and Chapter 5.

The in situ backfill work has been substantiated by a laboratory testing program described in Chapter 6 and includes the tests required for the determination of both physical and geomechanical backfill properties. A series of tilt box tests were carried out for uncemented rockfill materials. These tilt box tests were first proposed by Barton (5), although such work had not been previously related to mine backfills. A procedure for the tilt box test was developed and described in Chapter 6.

After thus reviewing the various testing and a analysis techniques the thesis then reports on the test data . The physical characteristics of the tested mine backfills, Chapter 7, exhibited a wide range of grain mineralogy, grading and shape characteristics. The materials tested have been classified according to the textural classification system proposed in Chapter 2. It was found that the materials tested encompassed six of the nine available classifications.

Chapter 7, thus provides the required physical characterisitcs of mine backfills. Chapter 8 reports the in situ geomechanical properties of the tested mine backfills. The sensitivity and precision of the pressuremeter probe was also assessed. Data repeatability was found to be in the order of ±12% which was considered to be satisfactory. A number of empirical correlations have been used to extend the usefullness of the Pencel pressuremeter and two new relations have been developed.

Creation of a backfill properties database was undertaken via an extensive series of laboratory tests and published data survey. The published data has been described in Chapter 6 and used to develop backfill design equations for uniaxial compressive strength and axial stiffness of cemented fine-grained materials based on water : cement ratio. Similarly, design equations for shear stiffness, angle of internal friction and cohesion have been developed based on physical properties of uncemented fine grained materials. These equations stem from a laboratory direct shear testing program. The angle of internal friction of uncemented rockfills has also been related to porosity in the form of typical angle of internal friction - normal stress curves for varying porosities in Chapter 9. The laboratory data for uncemented fine-grained backfills has been extrapolated to field conditions by using the pressuremeter data described in Chapter 8. Strong correlation was found to exist between laboratory and field derived angles of internal friction. The laboratory derived cohesion has been indicated to be a good index for predicting the limit pressure in

the field. Similary, strong correlations have been achieved between laboratory shear stiffness and field measured deformation modulus.

The objective of developing backfill design equations for uncemented fine-grained, cemented fine-grained and uncemented rockfills had thus been addressed. An evaluation of the ability of these materials to act as support units under different field conditions was then under taken as the basis of the final section of the thesis. Chapter 10, thus investigates the support capabilities of the established classes of backfill materials.

2.0 BACKFILL TYPES AND USES

Over the years, the use of backfill has become widespread in underground mines. It has been integrated into numerous mining methods including cut and fill, blasthole stoping, room and pillar.

Hydraulic backfills comprise classified mill tailings, pit sands and combinations of the two. Alternately, rockfills consist of coarsely graded aggregate and varying degrees of fines. In addition, there are several speciality backfills, such as frozen backfill, of less widespread usage. This chapter aims to develop a backfill classification system for the wide range of backfill types in use, in order to enable consistent classification of backfill materials. The physical properties associated with each backfill class exert control over the in situ mechanical properties of the backfill. Section 2.2, thus, aims to clarify some of the interrelationships between specific physical properties and mechanical behaviour.

2.1 Backfill Classifications

Backfills can be classified into two broad categories, cemented or uncemented. Regardless of the presence of cementing agents a backfill can be further classified in terms of its grading characteristics. Hydraulic fills are composed of fine grained materials. In the case of rockfills, however, the material's final grading can vary substantially according to the source of material and the method of placement. Thus each combination of material

source and placement method can yield a different backfill type. A unified and consistent backfill classification system has yet to be established. It is thus the objective of the remainder of this section to review the existing soil classification systems and propose a new system covering the entire range of mine backfill materials from fine grained hydraulic fills to coarse rockfills with little fines.

Table 2.1 is a compilation of the existing six soil grading systems (2) and includes the proposed backfill classification scheme. It was noted that the existing classification systems were aimed to precisely define given ranges of material grading. For instance the MIT system defines precisely the grading characteristics of materials in the range of .1 to 1 mm. This type of system is adaptable to fine grained materials such as hydraulic backfills but would not be appropriate for coarse grained rockfills, as it poorly defines particle gradings above 2.0 mm. This is also true for the USDA and ISSS systems. On the other hand the remaining three systems attempt to focus on the coarser grained materials and would be appropriate for characterizing concrete aggregates. Each of the remaining systems, AASHTO, ASTM and USCS, fail to adequately represent the fine grained hydraulic backfills, however, with grain sizes in the range of 2 mm to <.001 mm, and further fail to characterize the coarse grained rockfill with particle sizes much greater than 76.2 mm. Thus the proposed classification system provides the benefits of the MIT system as well as improved definition of coarse material grades by adding a "boulder" classification, whilst better defining "gravel" sized material.

PARTICLE SIZE (mm)								
AGENCY	BOULDERS	GRAVEL	VERY COARSE SAND	COARSE SAND	MEDIUM SAND	FINE SAND	VERY FINE SAND	SILT CLAY
AASHTO		76.2 to 2.0		2.0 to .42		.42 to .075	.075 to .002	<.002
ASTM		76.2 to 2.0		2.0 to .42		.42 to .074	.074 to .005	<.005
USCS	COBBLES > 76.2 COARSE: 76.2 to 19.05 FINE: 19.05 to 4.76			4.76 to 2.0	2.0 to .42	.42 to .074	<.074	
USDA		>2.0	2.0 to 1.0	1.0 to .5	.5 to .25	.25 to .1	.1 to .05	.05 to .002	<.002
MIT		>2.0		2.0 to .6	.6 to .2	.2 to .06	.06 to .002	<.002
ISSS		>2.0		2.0 to .2		.2 to .02	.02 to .002	<.002
MCGILL	>114.3 COBBLES: 114.3 to 44.67 COARSE: 44.67 to 14.13 FINE: 14.13 to 4.76			4.76 to 2.0	2.0 to .42	.42 to .05	<.05	

AASHTO - Amer. Ass. of State Highway and Trans. Off. Desig.:M146-70
ASTM - American Society for Testing and Materials - Desig.: D422-63
USCS - U.S. Army Corps of Engineers
USDA - U.S. Dept. of Agriculture
MIT - Massachusetts Institute of Technology
ISSS - International Society of Soil Science
MCGILL - Proposed Backfill Classification System.

TABLE 2.1 Backfill and Soil Grading Classification Systems

Having defined ranges of particle sizes by terms such as "fine sand", the combinations and proportioning of particle size classifications for a given material can be used to texturally classify the material as a whole. Figure 2.1 represents a proposed textural classification chart for mine backfills. For the purposes of this classification chart material which is finer than fine sand or coarser than gravel is classified as "fine sand" and "gravel" respectively. Furthermore the coarse and medium sand materials are grouped in a single classification category of "coarse sand". Having said this a material containing 40% gravel, 30% coarse sand and 30% fine sand would be classified as a well graded rockfill. Thus the combination of Table 2.1 and Figure 2.1 should ensure that backfills will be classified in a uniform manner henceforth and will further ensure that a significant, presice meaning will be attached to each backfill classification. This is in contrast to the loose definition and interpretations of the term rockfill, for instance, where a wide range of material gradings are all termed rockfill. Furthermore, this classification removes the present subjective nature of backfill classification.

2.1.1 Fine Grained Backfills

The term "Hydraulic Backfill" is often used synonymously with the term "Sandfill", however this practice is misleading. The terms originate from the hydraulic transportation of backfill, at 60 to 70 % pulp density, to the underground workings. However, within the terms of reference of this thesis sandfill refers to a wide range material gradings which are independant of method of

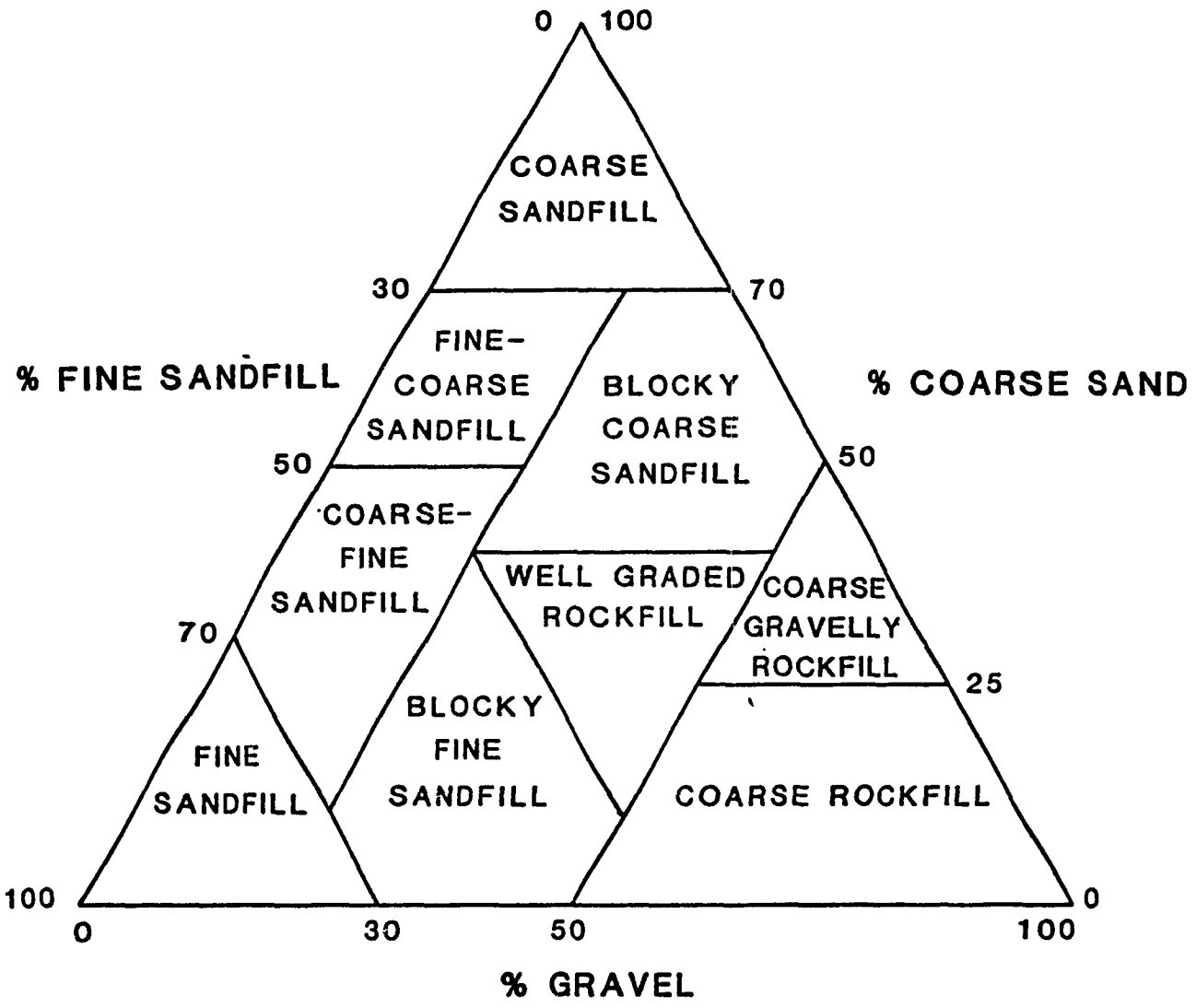

FIGURE 2.1 Proposed Textural Classification System For Mine Backfills

transportation. It has further been found that materials which are transported hydraulically tend to have a textural classification of "fine sandfill", with the occasional material classifying as "coarse - fine sandfill".

The materials used for hydraulic backfills typically include classified mill tailing and / or surficial sands. The use of surficial sands is employed if the tailings material is chemically inappropriate for use as backfill or if the quantity or quality of mill tailings are inadequate.

Hydraulic backfill is used in either cemented or uncemented form and accounts for over 65% of all backfill types used in both Quebec and Ontario. Typically, weakly cemented (< 6% portland cement) or uncemented hydraulic fills are used for bulk filling while hydraulic fills cemented at > 6% cement are used for stope floors to prevent loss of ore after lasting through floor penetration. Furthermore, some speciality fills such as high density backfills, described latter, could also be classified as hydraulic backfills.

2.1.2 Rockfills

The term rockfill is used universally to describe development waste, pit gravels, or combinations pit gravels,sands, tailings and development waste. Thus, the term rockfill is used to classify a wide range of material gradings and as such does not give specific definition for the individual gradings which may occur. It

was a further objective of the textural classification chart described in Figure 2.1 to subdivide the term rockfill further into three classifications, namely "well graded rockfills", "coarse gravelly rockfills" and "coarse rockfill". In addition, the "blocky coarse" and "blocky fine" sandfills are filling materials on the boundary between "rockfills" and "hydraulic fills". The textural classification for rockfill materials should be applied principally to in situ backfills as the transportation method from the production site to the materials' final placement can change the grading characteristics substantially (3).

Besides the textural classification of a rockfill material, its final in situ structure is governed by the method of placement, which will define the degree of segregation, as well as the method of cementation, if in fact the material is cemented. Several methods of placement are often used and include discharging material from one or several points, with the material dropping from 5 to 10 metres in cut and fill or Avoca mining. Alternately, it is dropped from 60 and 90 metres in delayed backfilling scenarios for blasthole stoping. A cementing slurry may be added in combination with hydraulic tailings, surficial sands or in a water / cement slurry. Furthermore, it may be transported from surface or mixed underground and can travel within the same fill raise as the rockfill aggregate or in a separate slurry raise. It can be seen that each combination can yield a different fill matrix. For instance if a tailings / cement slurry is used in conjunction with a rockfill aggregate and is transported within the same fill raises, then the final rockfill matrix will tend to be well mixed. The voids, created by the rock

aggregate, will be filled or partially fillied with a tailings / cement slurry, depending on the ratio of rock aggregate to cementing slurry. In addition if the same rock aggregate : cementing slurry were used as in the previous example with the slurry being transported separately and added to the inplace rockfill aggregate by percolating the slurry into the matrix then a substantially different in place backfill would result. This backfilling system would be limited by the depth to which the slurry could percolate. Thus the final fill matrix would be characterized by cemented and uncemented layers with filled or partially filled voids. In either of the above cases if a water / cement slurry is used in place of a tailings / cement combination then the voids will not be filled and the rock aggregate will be cemented at the rock to rock contacts only.

In summary, this section has demonstrated the wide range of material gradings which are classified as rockfills, along with the the complex and wide range of final fill matrices which can be achieved according to method of placement and addition of cementing slurry. The complexities of particle size range and lack of prior interest in geomechanical properties account for the fact that limited data is available on the strength and stiffness characteristics of such materials. The most extensive studies have been associated with the construction of rockfill dams, (4), (5), (6), (7), (8).

2.1.3 High Density Backfills

High Density Backfills are essentially hydraulic backfills with some transportation or placement variation which renders the final fill matrix into a denser state. Backfills can be densified in several ways (9), principally by the Head, Vibratory, Cement and Double Placed Methods.

The concept of the Head method is to introduce backfill from the bottom of the stope rather than the top. This allows the filling material to be placed under a constant pressure head, thus providing increased compaction of the fine grained material.

The Vibratory method consists of conventional fill placement followed by vibration through the use of concrete vibrators, see section 3.3.7. The objective is to reduce the void ratio in the vibration stage thus increasing the backfill stiffness and strength.

The Cement method has received much attention in the Canadian mining industry. Water contents which are normally used to transport hydraulic fills are normally in excess of that required to hydrate the small quantities of cement which may be present in mine backfills. Densification by the Cement method is by reduction of water within the fill matrix. Two approaches have been used to this end. The first is to transport the backfill at high pulp density, in the order of 70 to 80%. This presents the advantage of handling smaller quantities of water. However, flow plugs and equipment wear may become a problem. A further disadvantage is the additional cost

of plastisizers, nesessary in order to aid flow and reduce friction losses. The second method makes use of tailspinners (10) to dewater the backfill tailings prior to final placement. This system eliminates the problems associated with high density transport, however larger volumes of water must be handled. Furthermore the output rates for the tailspinners, in the range of 10 to 15 tonnes per hour may be insufficent to meet backfill requirements and scheduling (11). The Cement method as a whole is also characterized by an increase of fines in the fill matrix and lower percolation rates. A primary concern with high density backfills is thus the high retained moisture contents, in the order of 20%, and the potential of pore pressure buildup and subsequent liquefaction potential.

Lastly, the concept of "Double Placed Backfills" is a two step operation and involves a final fill matrix which can be texturally characterized as a "well graded rockfill". The coarse material is first placed and then a cementing slurry is introduced in such a way that the voids created by the coarse aggregate are completely filled by the slurry material. This may require the use of pressurized slurries and is thus the most expensive of high density, high modulus fills described. However, it has been shown that the use of this fill type can reduce maximum pillar stresses by as much as 27% (127).

2.1.4 Self Cementing Backfills

Self cementing backfills in terms of grading can be either fine grained or rockfill type. This classification is based on the materials' ability to cement itself. Two common types are used in Canadian mining practice; pyrrhotite and sulfate - rich backfills. In each of these an oxidation reaction occurs after placement, cementing the fill into a solid mass. The use, benefits and problems associated with self cementing fills has been reported by Patton (12), Lukaszewski (13), Swain (14) and Bayah (15). Self cementing fills offer the benefit of reduced cement costs for stabilization, however their usage can create heating and oxygen depletion problem which need to be recognized.

2.1.5 Evaporite Backfills

Evaporite backfills are used in salt and potash mines throughout Canada. Les Mine Seleine, a salt mine in Quebec, uses 1100 tonnes/ day of mill waste as underground backfill. A similar situation exists with Potash Corporation of Saskatchewan where salt waste is used as backfill material. The principle behind these backfill types is that upon placement, in a moist state, the salt first precipitates out of solution and then crystalizes into a competent mass (16). The advantage of this backfill type is that it is self cementing, however, it is important that additional water not be added upon solidification as this would cause the backfill to dissolve with disastrous consequences.

2.1.6 Frozen Backfills

The term frozen backfills applies to backfills which use ice as a cementing agent or as the actual backfill material. Two backfill structures are normally used. The first makes use of a bulkfilling material such as pelletized tailings or crushed shale which is then cemented by the addition of water. In the second instance, water is injected into the underground voids and is then frozen (17), (18). Typically, the ice is sprayed into the underground openings by use of snow making machines. This type of backfilling adds no dilution to mineable ore and is applicable to mining operations in both permafrost and sub-arctic regions.

2.2 Physical Property Influence On Geomechanical Behaviour

The interaction between physical and mechanical backfill properties is not clearly understood to the extent of providing a clear basis for backfill design. However, it is the case that the physical parameters govern the geomechanical and operational properties of mine backfills. The physical backfill properties which are of greatest importance to geomechanical behaviour comprise degree of cementation, grain size distribution, void ratio, particle shape, moisture content, particle density and segregation.

The optimization of physical parameters for geotechnical purposes can adversely affect the operational characteristics of backfill. For instance, a reduction in void ratio to achieve

increased stiffness may cause an unacceptable reduction in the rate of percolation. It is thus the intent of this section to define each of the physical parameters of interest and expand upon their influence on the operational and mechanical properties.

2.2.1 Void Ratio

Void ratio is defined as the ratio of the volume of voids to volume of solids. It thus describes the volume available for compression of the backfill material or alternately for the migration of water. It is thus a key design parameter and the influence of other parameters to void ratio will have a direct bearing on both geomechanical properties and percolation rate. The influence of grain size distribution and particle shape on void ratio will be examined later. An increase in void ratio will have a positive effect on percolation rate but will have adverse repercussions on strength and stiffness characteristics. Void ratios for hydraulic backfills have been noted in the range of .25 to .35 while rockfills exhibit void ratios in the range of .5 to .7. For the purposes of this thesis, it was found convenient to calcluate void ratio from the material dry density and the specific gravity of solids. The void ratio is related to these two properties by the following equation:

$$e = \frac{G_s \gamma_w - 1}{\gamma_d} \qquad \text{..... 2.1}$$

where: e = void ratio

G_s = specific gravity of solids

γ_w = unit weight of water

γ_d = dry unit weight of backfill

Furthermore, the term porosity is often used in place of void ratio. Porosity is related to void ratio by the equation:

$$n = \frac{e}{1+e} \qquad \text{..... 2.2}$$

where: n = porosity

Porosity represents the proportion of voids in a given volume of material.

2.2.2 Grain Size Distribution

The grain size distribution is used to represent the particle size composition of a granular material. Typically the size distribution is represented graphically, however, this form of representation is limited for design procedures. In order to quantify the distribution characteristics a number of indices have been used which attempt to summarize the graphical representation. The most widely used index is the coefficent of uniformity, C_u, which is defined in equation 2.3. The second is the coefficent of curvature, C_c, defined by equation 2.4. It has been noted that a well graded material is represented by a coefficient of uniformity of between 4 and 6, and a coefficient of curvature of between 1 and 3, (19).

$$C_u = \frac{U_{60}}{U_{10}} \qquad .....2.3$$

$$C_c = \frac{[U_{30}]^2}{[U_{60}]\ [U_{10}]} \qquad .....2.4$$

where: U_{10} = 10% passing size

U_{30} = 30% passing size

U_{60} = 60% passing size

The effect of grading on the geomechanical properties of backfill depends on its influence on void ratio. It is generally expected that a well graded material will yield a lower void ratio than a poorly graded one under the same conditions of consolidation and compaction. Furthermore, Talbot (20), proposed an optimum grading curve for granular materials, equation 2.5, which ensures that maximum compaction and minimum void ratio can be achieved.

$$P(u) = 100\ (U\ /\ U_m)^{.5} \qquad ..... 2.5$$

where: $P(u)$ = % finer than size U

U_m = maximum particle size

I can be showm, from equation 2.5, that the coefficent of uniformity and coefficent of curvature for the optimum grading curve are 2.45 and 1.22 respectively.

2.2.3 Particle Shape

Particle shape, along with material grading, has an effect on the achievable void ratio in a granular material. The particle shape can be represented by the coeffiecent of sphericity, the aspect ratio or the particle shape factor. The sphericity coefficent, S_s, is defined as,

S_s = intermediate grain size / maximum grain size

while the aspect ratio, A_r, is defined as,

A_r = maximum grain size / minimum grain size

and can be estimated by the reciprocal of the coefficient of sphericity. Lastly, the particle shape factor, S_f, is defined by the more comprehensive equation,

$$S_f = \frac{[\text{Perimeter}]^2}{\text{Area} \times 4}$$

Yong (22) contends that the angle of internal friction, φ, for a granular material is made up of two components; the basic friction angle, φ_b, and the interlocking friction angle, φ_i. Furthermore, the interaction, under normal stress, at the particle to, particle interface dictate that particles with aspect ratios close to 1 (spherical) would offer less resistance to shearing forces, as they offer less favorable interlocking potential.

2.2.4 Moisture Content

The effects of moisture on the geomechanical properties of backfill are twofold. Firstly, the effects of moisture and pore pressure in a structured backfill lattice have been demonstrated by Seed (23) to be potentially the cause of liquefaction. Secondly it has been suggested by Talbot (20) that a critical moisture content exists for granular material, whereby an increase or decrease in moisture content would cause a corresponding increase in void ratio and thus a decrease in stiffness and strength. This moisture content is denoted as the "Optimum Moisture Content" and generally increases with the overall fineness of the material in question. An index of this moisture content can be determined in the laboratory by the Proctor Test.

The two trends noted above; that of decreased strength with increased moisture and the suggestion of an Optimum Moisture Content, at first seem contradictory. However, upon further examination it is evident that the two observations are made at different stages of the construction and assemblage of the structural fill lattice. In the first instance, Seed (23) is concerned with an existing structure and therefore the introduction or presence of water will disrupt and thus weaken the structure through the build-up of pore pressures. On the other hand, Talbot (20) is interested in the formation of a granular structure, that is, the optimal packing of a material with a given material grading. Thus, it would be desirable to have an optimum moisture content during the inital stages of backfill placement to ensure optimum

packing, followed by a reduction in moisture content once the fill structure has been set.

Weaver (24) has noted that for pulp densities between 60 and 72%, representing moisture contents between 40 and 28% respectively, a notable increase in uniaxial compressive strength was evident. The data further illustrates a trend in strength which has not reached its peak at 72% pulp density. This would imply that the optimum moisture content has not been reached at an operational pulp density of 72%. The experience of increased strength high density backfills is consistent with this conclusion.

2.2.5 Macroscopic Fill Structure

The discussion in this section has dealt with the influence of individual backfill physical characteristics. The interrelation of the individual characteristics has been expanded upon and the sum effect on the geomechanical properties has been presented. Barrett (25) has attempted to qualitatively describe the various fills structures which can result from a combination of grading, moisture, particle shape, and method of placement which have a direct bearing on the degree on compaction and in rockfills, grading. Furthermore, Gonano (26) attempted to clarify Barretts' assertions and proposed a "visual classification" chart, presented here as Figure 2.2. The chart classifies backfill structures into nine categories. The major lines of distinction are for cemented and uncemented materials, and the ratio of coarse to fine aggregate.

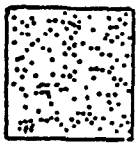

No. 1. Cemented sandfill - may be layered but no rocks present.

No. 2. Rock 'floaters' in a cemented sandfill matrix - no rock to rock contact.

No. 3. Rockfill with rock to rock contact with inter rock voids fully occupied with cemented sandfill - no air voids.

No. 4. Rockfill with rock to rock contact with inter rock voids partially occupied with cemented sandfill.

No. 5. Rockfill - uncemented. No fines.

No. 2a. Rock 'floaters' in uncemented matrix - no rock to rock contact.

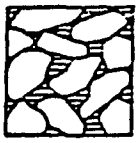

No. 3a. Rockfill with rock to rock contact with inter rock voids filled with uncemented material.

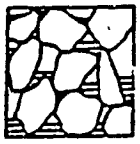

No. 4a. Rockfill with rock to rock contact with inter rock voids partially filled with uncemented material.

No. 6. Fine grained uncemented material e.g. rockfill fines.

FIGURE 2.2 Material Structural Classification System (After Gonano [26])

Figure 2.2, considers the differences in void ratio, density, the nature of particle contacts, and the particle grading curves for these structures. It is clear that both their strength and deformational properties would be expected to vary considerably.

2.2.6 Backfill Segregation

Segregation can be defined as the occurrence of a number of macroscopic structures within a rockfill mass. Segregation occurs as a result of differential settlement and the formation of segregation cones below the point of discharge. Barrett (25) reported that banding in cemented fine grained hydraulic backfill is most predominant at the stope edges, with some of the bands containing little or no cement. This study further concluded that at angles of segregation of 30^{o} or less the net strength of the backfill was not effected, and angles greater than 30^{o} decreased the backfill strength and stiffness. Gonano, further suggests that due to the large discrepancies in material structure, and thus geomechanical properties, of the different segregation layers each should be numerically modelled as a seperate material type. One ready conclusion from this assertion arises if a free standing height is required. The factor of safety calculations, under conditions of segregation should be based on the least favourable combination of material structure, strength and orientation.

2.2.7 Effects Of Polymeric Flocculants

The use of flocculants in backfill has grown recently as a result of the desire to control the migration and distribution of fines within a backfill matrix. The use of cement has increased the quantities of fines and thus amplified the problem. Use of flocculants offers the advantages of increased percolation rates, rates of sedimentation, retention of fines and contribution to an overall more homogeneous backfill structure. The use of flocculants also presents two major disadvantages, firstly increased costs and secondly the possible increase in porosity and moisture content with consequent decreased strength. However, the increased retention of fines would imply a greater retention of cement and thus would increase strength. Research has not as yet fully resolved these issues.

Braes (27), found that a 35 gram/tonne addition of flocculant to the mine backfill effectively reduced the slimes in the fill mass and completely removed slimes from the surface of the backfill. He further found that no increased strength was noted. In a similar study, the author in conjunction with Scoble and Robert (28) found that a 13.6 gram/tonne addition of flocculant confirmed the findings of Braes, however it was also found that the backfill stiffness was increased by 33%.

2.2.8 Effects Of Cementing Agent Addition

The primary purpose of cementing agent addition is to increase fill strength and stiffness. A number of cementing agents are typically used in backfill practice. These include Portland cement, fly ash, smelter slag, as well as sulphide fill mixes referred to in 2.1.4. The most common bonding agent is normal Portland cement. Thomas (29) illustrated that the cost of Portland cement in rich bulk mixes (8%) could constitute up to 50% of the mining costs. Thus the growing interest in Portland cement substitutes can be easily understood.

Portland cement contributes to fill strength by the formation and drying of a hydrate paste, producing lime as a byproduct. The hydrate coats individual particles and thus provides a means of interparticle cementation. Alymer (30) concluded that the full benefits of Portland cement could not be realized if it were used solely as a cementing agent since the lime which is formed is not utilized in the cementing process. However, it should be noted that the lime will sacrificially protect the cement bonds should acidic waters be present.

It was further indicated by Aylmer (30) and demonstrated by Thomas (29) that the use of pozzolans and fly ash would optimize the bonding properties of cement by utilizing the lime produced from the cement hydration reaction. This mechanism is certainly applicable to smelter slags and F-type fly ash which are pozzolanic and thus require lime for increased cementation (31). However, it has been

found that C-type fly ash is naturally cementitious and thus does not require lime to enhance fill strength (32). Lastly, the cementing characteristics for sulphate and pyrrhotite rich fills based on an oxidation reaction provides yet another means of increasing fill strength (12), (13).

2.3 Summary

It has been illustrated in this chapter that a wide range of backfill types are presently in use. These can be classified in two broad groups: cemented and uncemented. Furthermore, the textural composition of the backfill material can also used to classify backfills, the two groups normally cited are hydraulic backfills and rockfills. However, it has also been shown that the textural variations in mine backfills justify more than two simplistic groups. As such a textural classification system has been proposed to characterize all backfill types texturally.

The effects of various physical backfill parameters on geomechanical properties has been reviewed. It was concluded that, apart from cementation, void ratio is the most important physical property which contributes to backfill strength. Parameters such as moisture content, grain size distribution and particle shape effect fill strength primarily through their effect on void ratio. It can further be concluded that if at an early stage of backfill design the physical parameters are optimized to yield the stiffest and strongest backfill possible then the required cement addition to

attain the target geomechanical properties can be reduced.

The use of cementing agents to increase backfill strength, at increased cost, is becoming more popular, particularly the use of Portland cement substitutes. The mechanism of particle coating and hydration in the cementation process gives rise to the conclusion that cement addition should be based on the surface area of the particles to be covered rather than on the percentage weight methods currently used. This is later discussed in relation to the scatter of data observed in prior research by others, see section 6.2.1. This may be illustrated by the example of two materials with precisely the same grading but specific gravities of solids differing by 50%. This implies that for a given weight of material the denser material will have a correspondingly 50% lower volume. Furthermore, as the material gradings are identical the lower volume implies a lower surface area, and thus for a given weight addition of cementing agent, the denser particles will be coated more effectively.

3.0 DESIGN CONCEPTS AND PROCEDURES

Fresh impetus to backfill research has resulted recently from a renewed interest in the use of high quality, high modulus backfill for ground support in highly stressed ground and for pillar recovery in bulk mining methods. The investigations described herein have considered the usage of compaction, grading and reinforcement as well as cement binding agent to enhance the strength and stiffness of traditional backfill aggregates. A long history of research exists into various aspects of the addition of cement to aggregates for underground mine backfill usage. Industry faces the need to assess the cost benefits of cement addition to improve the mechanical behaviour of backfill, in light of its ground stability problems and efforts for higher productivity stoping.

Optimizing a backfill aggregate offers the potential for reducing cement requirements to meet target strength and stiffness properties with accompanying cost savings. This requires consideration of consequent effects on aggregate drainage characteristics. The use of Portland cement substitutes such as ground slag or fly ash and other additives such as flocculants increases even more the complex of factors involved in backfill design. This research has aimed to provide a rational approach to backfill design taking into consideration the wide range of interdependant design parameters.

The ground support characteristics of backfill materials, as related to compressive strength and stiffness, is becoming viewed as increasingly important particularly with the heightening interest in rockburst control. The mechanical behaviour of cemented backfill is governed by the materials' physical characterisitcs, confining stress and curing time. The environmental factors are defined by the in situ conditions and mine planning strategies. Mechanical behaviour is also governed by particle grading, pulp density and cementing agent content as well as placement method which contributes to segregation, section 2.2. Each of these are controllable design parameters the effects of which are described in section 3.1 of this chapter.

This chapter further aims to clarify the interactive processes between environmental and design factors. For this purpose a design procedure is proposed, with particular reference to cement content. The philosophy of this design procedure is to optimize the available source aggregate, whilst at the same time defining strength and stiffness requirements. This then enables calculation of cement content based upon a knowledge of its interaction with the aggregate and its control over mechanical behaviour. The design procedure in the form of a flowchart is cross-referenced within the text and at relevant points in Figure 3.2, to associated design equations (in square brackets) and publications (in parenthesis).

3.1 Philosophy of Backfill Design

An effective design process must initially define the target backfill properties. These may comprise a combination of the following: uniaxial compressive strength (σ_c), modulus of deformation (E), apparent cohesion (c) and angle of internal friction (φ), bearing capacity (S_b), grading factor (G_F), pulp density (P_d), and permeability (K). The particular properties and their priority will be governed by the function of the backfill and the characteristics of its particular mining environment.

The backfill design sequence involves consideration of permeability, pulp density and then the target mechanical properties. Through optimizing aggregate grading, whilst maintaining adequate permeability, materials handling can be considered in order to define the pulp density objectives. Interest in high pulp density backfills is growing and is due to improvements that result in strength, stiffness and drainage. Finally the pulp density and grading decisions enable the cementing agent requirements to be resolved so as to meet target strength and stiffness to contend with the mining environment. Past research has considered many parameters affecting the influence of cement on aggregate properties, singly or in combination. The need still exists however for a more integrated approach based on a rationale design concept. Figure 3.1, (139), has been developed by the author and indicates in summary this design concept, together with examples of cementing agent addition research to demonstrate the wide breadth of interactive factors which affect backfill behaviour.

FIGURE 3.1 Backfill Design Principles

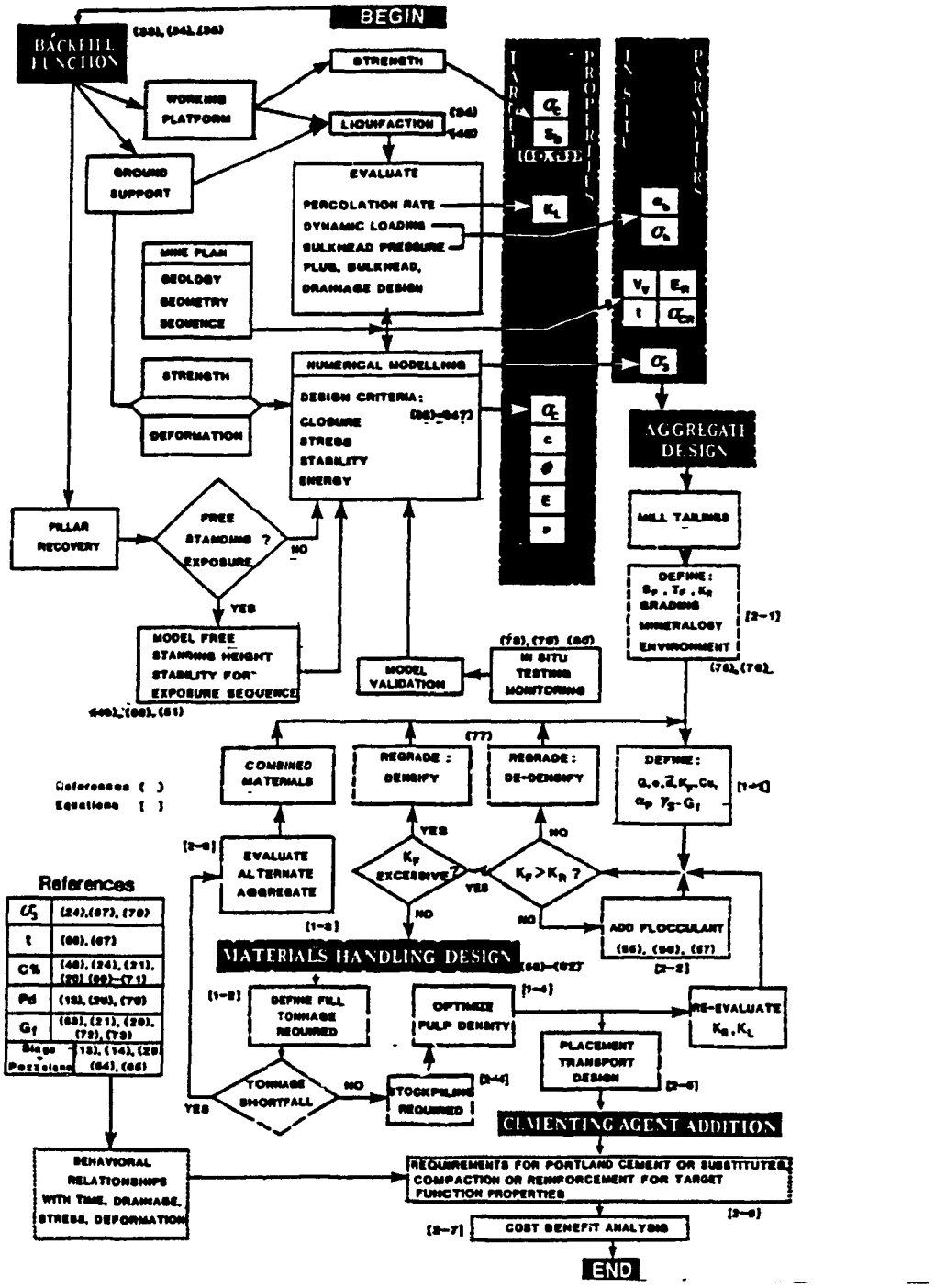

FIGURE 3.2 Backfill Design Flow Diagram

3.1.1 Backfill Design Procedure

Figure 3.2 shows a more detailed design flowchart which attempts to optimize aggregate grading in order to minimise cement addition whilst giving due consideration to both materials handling and drainage objectives. In order to achieve this a number of design equations can be employed to evaluate certain parameters of interest when designing the physical properties of the material. Where the same goal may be achieved by more than one alternative, then the final decisions may be based on economic considerations. Thus a number of associated costs must be accounted for in approaching the final design for a given alternative. Groups of design equations are given in Appendix 1 and cost equations in Appendix 2. These equations are cross-referenced by square brackets on the flow chart (e.g. [1-2] relates to the second set of design equations in Appendix 1).

In order to assist the reader acquire additional information about various stages of design, previous published work has been cross-referenced to the pertinent design stages in the flowchart, denoted by curved brackets (e.g. (33)).

3.1.2 Target Mechanical Properties

The target mechanical properties which will be used in subsequent design of the backfill depend on its intended function, Figure 3.3. The major backfilling functions are ground support, ore recovery and working platform. The determination of the primary

function of backfill is important in identifying the aspects of support which must be investigated. These are illustrated for each backfill function in the design flowchart, Figure 3.2, and fall into three categories; liquefaction, strength properties and deformational properties. Design procedure for the alleviation of liquefaction is identical for fills serving ground support or working floor functions. This should account for dynamic loading, time delay between filling and the application of the dynamic loads, permeability and the initial water content. A required miniumum permeability to inhibit liquefaction, K_L, can then be calculated for the in situ backfill.

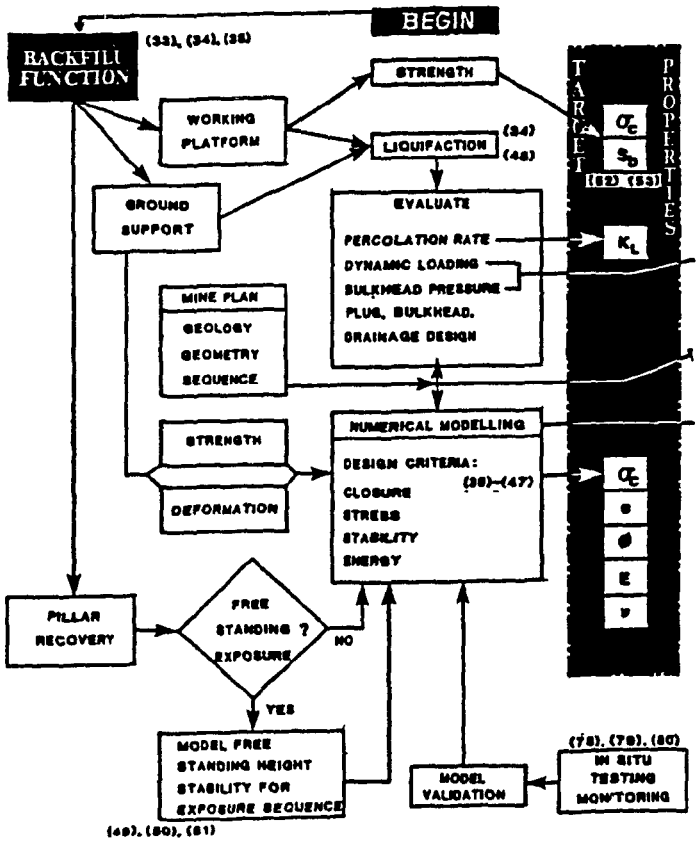

Figure 3.3 Backfill Function Flow Diagram

The strength and deformational properties for both ground support and ore recovery differ only in the approach used to determine these required properties. Considering ground support as the primary function, an evaluation based upon modelling to establish acceptable stope wall closure and pillar stress can be made for the rock mass in question. A second stage of modelling requires that account then be taken of backfill mechanical behaviour. Various backfill behavioural models have been proposed and range from simple linear-elastic (36,37) to non-linear elastic and elasto-plastic models (67,127). Appropriate modelling enables the backfill properties to be varied so that the preset limits of stope wall closure and pillar stresses are not exceeded. Meeting such design criteria leads to a set of operational properties, that the backfill must satisfy. The properties are for the subsequent design of the available aggregate grading. In the case of ore recovery, where the fill is not required to be free standing, i.e. crown or sill pillar recovery in cut and fill mining, the modelling process addresses the support contribution of backfill in influencing the stress concentration carried by the pillar. Initially the level of stress carried by the pillar at the cessation of normal stoping requires to be modelled. This then enables a reiteration of modelling with variation of backfill mechanical properties to design for acceptable pillar stress levels in both stoping and pillar recovery stages.

Several criteria for assessing the efficiency of backfill support have been proposed which account for the mechanical properties of both backfill and host rock. The first of these

relate the ratio of backfill stiffness (E_f) to rock mass stiffness (E_r), (E_f/E_r) to degree of closure as well as pillar and backfill stresses (36,37,42). Salamon (44,45,46), used an energy balance approach to determine the efficiency of backfill in inhibiting total closure in flat lying South African gold deposits thus combating rockbursting. Hedley (43) has subsequently applied the concept of energy balance to cut and fill mining, and described the backfill efficiency in terms of the ratio of the energy stored by the backfill to the energy which must be redistributed when a unit of ore is displaced during mining.

These methods and the modelling described so far in this chapter approach backfill as a passive support in a stressed environment. Backfill, however, may not necessarily be viewed as operating within a highly stressed or confined environment. This may be the case during pillar recovery in blasthole stopes, where backfill columns must remain free standing during the extraction of adjacent ore. Modelling methods for this type of backfill usage are simpler and well established (49,50,51). These tend to employ a plane failure analysis of the fill column with associated factor of safety derivation. A more detailed evaluation at these numerical method will be discuss later in this chapter, section 3.2.

The required design properties for backfill depend on its intended use and environment. If backfill is designed as a stressed medium then the deformational properties are required in order to determine the development of load in the given environment whilst

the strength properties are required to determine the material failure potential at various stages of loading. If, however, a free standing height is the main design function then the strength properties alone suffice.

The strength properties of backfill are usually expressed in terms of bearing capacity for the design of working cut and fill stope floors. It is suggested that the California Bearing Ratio (CBR) be used in the field. The details of this test are given in ASTM standard D1883-73, (190). The CBR test was developed by the U.S. Army to determine the suitability of soil surfaces for highway foundations (52,53).

3.1.3 Aggregate Design

Conventionally aggregates used in backfill design include mine waste rock, pit sands, smelter slags and commonly mill tailings. Backfill aggregate design for mill tailings, Figure 3.4, must be capable of coping with the current trend in milling towards finer grinds for ore liberation. This may result in tailings being unsuitable for backfill usage unless further grading modifications are made. Furthermore, the chemical composition of tailings materials may cause detrimental environmental impact, arising principally from either high sulphur content or radioactivity, thus requiring special design procedures (75,76). These special cases are discussed in section 3.3.

Once environmental considerations have been addressed then the available aggregate may be optimized in terms of permeability,

transportation and placement. Subsequentally the addition of cementing agents, in order to attain the target properties can be made at minimal cost.

The strength and deformational properties of backfill increase with increased cementation and decreased void ratio. If void ratios are decreased to optimize cement addition then problems of reduced percolation may result. It is thus important that material grading be optimized so that the use of cement is reduced whilst maintaining acceptable permeability. At this point a target in situ pulp density (Pd) must be assumed in order to determine a required fill permeability, K_r. This permeability can be compared to the permeability required to inhibit liquefaction, K_L, employing the greater of the two in the subsequent design as the target permeability, K_r. If the fill permeability K_f, is too far below K_r then the aggregate can be regraded or the addition of flocculants may be considered to meet the K_r requirements. Alternatively the tailings may exhibit an excessively high K_f value. In this case cement addition could not be subsequently optimized and thus the material would have to be regraded to densify, (i.e. approach the Talbot optimum particle size distribution (20)). Once the balance between acceptable permeability and maximum densification has been achieved then the materials handling aspect of design may be considered. It should also be noted that if regrading is undertaken, either to densify or de-densify the tailings, then the aggregate subsequently considered in materials handling design may be significantly different from the original available aggregate.

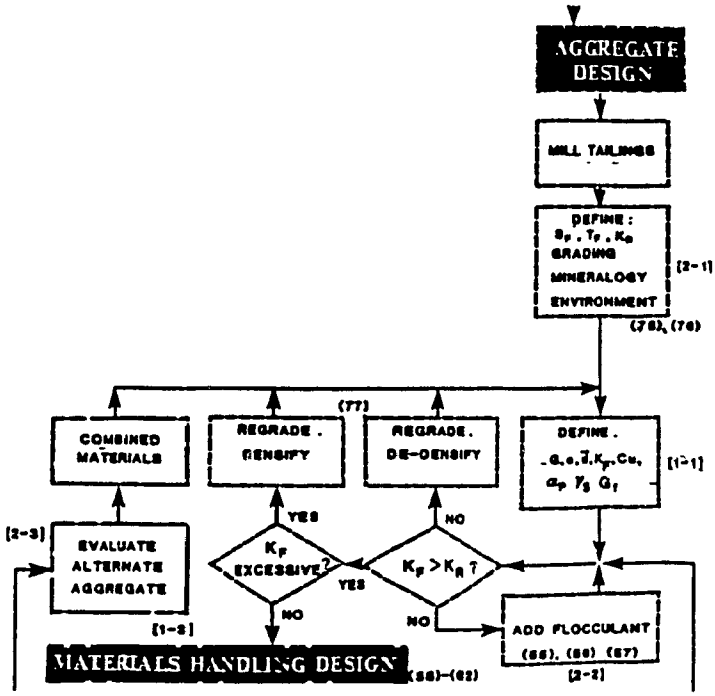

Figure 3.4 Aggregate Design Flow Diagram

3.1.4 Materials Handling Design

Design operational pulp densities for transportation and placement, Figure 3.5, can be considered once the original aggregate has met the requirements of environmental impact, optimum grading and permeability. Up to this stage an assumed pulp density in a desired range has been used to determine K_L and K_r. A graded aggregate has been designed to meet these requirements. Materials handling design must now be based on the aggregate properties determined to date.

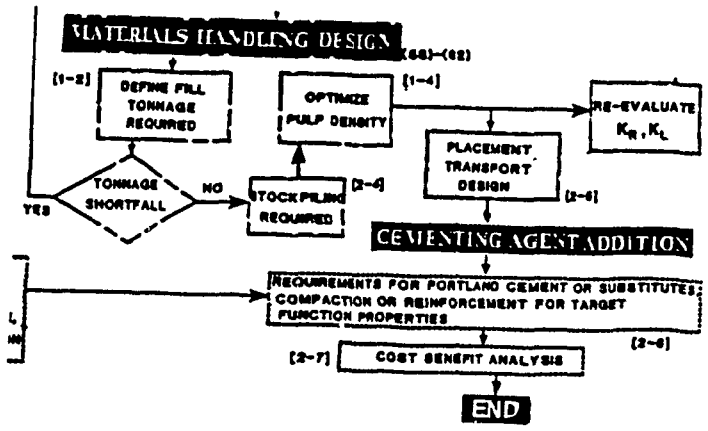

Figure 3.5 Materials Handling Design Flow Diagram

Materials handling can be designed at normal or high pulp densities. It must first be ensured, however, that the available aggregate is sufficient to fill the underground voids. If inadequate quantities are available then supplementary material will have to be sought. The new material and the original mill tails should be evaluated to meet the permeability and optimum grading requirements. Once the material available is sufficient to meet the required volumes, permeability and grading requirements then pulp density design can be considered using the concepts of normal or high density levels. The initial pulp density assumption and the calculated K_L and K_r values are now re-evaluated. Iteration through the permeability - grading - pulp density design then proceeds until changes in the resultant parameters lie within acceptable limits. The material which exits from this stage is thus optimized in terms

of materials handling, permeability and grading, thus ensuring that maximum stiffness and strength may subsequently be achieved with minimum cement addition and suitable drainage characteristics. The aggregate properties at this point can now be a basis for the determination of the required cement addition to meet the target properties under the predicted in situ ground conditions.

3.1.5 Cementing Agent Design

Reference has previously been made to the possibility of employing alternatives to cement, principally for reasons of economy. Portland cement still remains the most effective means of improving aggregate strength and stiffness. Calculating quantities of cement addition are based upon a full understanding of its interaction with the aggregate, whilst accounting for the influence of time on the behavioural characteristics of both the backfill and the enclosing rock mass.

Addition of Portland cement has in the past and presently remains the most accepted means of stiffening backfill. The high cost of Portland cement has prompted many users to seek less expensive substitutes which include smelter slags, pozzolans, fly ash and sulphides. Regardless of the cementing agent used, overall backfill costs can be reduced if the proportion of cementing agent is decreased. This, however, should not be done at the expense of backfill stiffness. The preceeding sections thus deal with a method of aggregate grading which yeilds the densest possible aggregate. In so doing we are assured that present backfill

stiffness is achieved with minimum cement agent addition. Futhermore, such a structured approach to design facilitates weighing of various alternatives which might include regrading, with its increased cost of grading and decreased cementing agent costs, versus the no regrading alternative with lower grading costs but higher cementing agent addition costs.

Although it may seem that the present levels of backfill stiffness used in industry, the regrading option is not the most attractive alternative, one need only consider the current trend towards stiffer backfills. This trend has been spurred by deeper mining environments which has increased the occurence of rockbursting in many mining camps. In light of this trend towards stiffer backfills, the cost of simply adding larger proportions of cementing agent to achieve stiffer fills have tended to become prohibitive and the regrading alternative has increased in appeal.

3.1.6 Discussion

Despite much past research there still remain many problems associated with existing backfill design techniques. These are becoming increasingly apparent with the trend of increased backfill usage in all forms of underground mining, the growing pressure to reduce costs and increased productivity, and the desire to adopt more scientific design procedures.

Uncertainty remains over the precise mechanism by which backfill interacts with surrounding rock masses and hence its ground support role, especially in rockburst-prone ground. The continued development of numerical modelling to account for the three - dimensional nature of most stoping geometries, the non-linear behaviour of backfills and the influence of arching will be required. In addition such work must be validated by increased monitoring of stress and deformation within backfills and rock masses. Little is also understood of the in situ mechanical properties of placed backfills, particularly rockfills. Existing insitu geotechnical engineering technology should be applied to backfills, such as pressuremeters, piezocones, and penetrometer testing, see Chapter 5. These also offer the advantage of providing the means to monitor quality control and segregation on a routine basis during backfill placement.

A clearer understanding of the support mechanisms of backfill should lead to a clearer definition of the means by which required stiffness and strength can be achieved most efficiently and economically. The effectiveness of backfill in alleviating rockbursting is beginning to be validated but the underlying mechanisms have yet to be clearly defined. Advances in the capability both to model regrading techniques and to densify and transport backfills are justified by prospects of reducing cementing agent requirements and costs. Similar motives support further research into substitute materials for Portland cement. Promising materials are fly ash and ground smelter slag. Alternative means of strengthening backfill in the vicinity of pillar recovery

operations, such as freezing, reinforcement and delayed consolidation should also be evaluated fully to optimize pillar support for optimum recovery and dilution control, as well as advance the industry - wide trend towards bulk mining methods.

3.2 Environmental And Supplementary Design Considerations

It is the objective of this section to provide design equations for backfill grading, drainage and transportation. This section further investigates the design procedures, for safety and environmental considerations such as oxygen depletion and bulkhead design.

3.2.1 Backfill Oxidation And Oxygen Depletion

The use of sulphide and sulphate rich backfills results in self-cementing materials. However the cementing action, provided by oxidation, presents the potential problem of oxygen depletion.

The exothermic oxidation of pyrite and pyrrhotite rich backfills requires oxygen in a dissolved form, usually in water, for the reaction to occur, (14). In a mining environment, the hydraulic transport of backfill provides the required water, while the ventilation system provides the oxygen, thus mine backfills may be under ideal conditions for oxidation to occur. Although oxidation may be is desirable for increased backfill strength it also creates heating and oxygen depletion concerns.

Patton (11), described the problems encountered at the Horne Mine, where granulated slag material was used. The exothermic nature of the oxidation reaction of the backfill was such that increased ventilation was required immediately after the filling cycle in order to remove excess heat and replenish depleted oxygen in working stopes.

Bayah et al (14) have described a similar problems in temporarily idle stopes at the Thompson Mine, Manitoba, noting the potential dangers upon re-entering stopes. It was further noted that oxygen concentrations as low as 7% were observed, while the minimum level required to sustain life is 15%. A detailed study of factors influencing oxygen depletion was carried out and it was noted that several mechanisms contribute to the phenomenon. Three mechanisms are prevalent:

1. The chemical reaction of oxygen at the pyrrhotite surface interface.
2. The diffusion of oxygen through the voids in the fill matrix.
3. The dissolution of oxygen from the air to oxygen depleted water.

Thus it can be summarized that the depletion of oxygen occurs at two interfaces, the gas /liquid interface and the liquid / solid interface. Bayah (14) presented a means of determining the rate of oxygen depletion at the gas / liquid, (air / water), interface. It was concluded that this was the depletion process of interest when concerned with safety. The rate of depletion was summarized mathematically:

$$\frac{dCr}{dt} = K_1 \frac{A}{V} (C_w - Cr) \quad ..... \quad 3.1$$

where: K_1 = 13.5 mm / min at 20^oc

A = interfacial area (cm^2)

V = volume of solution

C_w = saturated dissolved oxygen concentration

Cr = dissolved oxygen concentration

t = time

This equation provides a means of calculating the rate of oxygen depletion at the gas / liquid interface. Using this equation it was demonstrated that oxygen removal in sealed manways can occur at a rapid rate, even at low flow rates.

3.2.2 Air Contamination By Radioactive Mine Backfills

The introduction of radioactive backfills as ground support increases the health hazard of the underground mining operation. There thus exists a need to consider the possible environmental implications of using such materials as mine backfill. The solution will depend on the extent of the problem. As such, the first step is to determine the extent or rate of contamination and then choose the most cost effective solution.

Uranium backfills contain radioactive radon which was not extracted from the ore. Radon is a radioactive, chemically inert,

noble gas, and is the product of the disintegration of radium. It has a half-life of 3.8 days. The radon gas diffuses in air and water and is able to migrate within porous media according to gas laws.

The measurement of the rate at which this gases emanates from insitu backfill materials was presented by Franklin (75), and the equipment used is described by Franklin (105) and McVey (106). The study was undertaken at Rio Algom's Quirke Mine in Elliot Lake, Ontario. The tests involved the flushing of 5000 CFM of air in each of two stope (649 W & 650 E stopes) and the monitoring by four radon monitors of the concentration of radon gas at each of the four stations. The four monitors were located one in each stope, one at the intake and the last at the exhaust end of the access drive. It was found that when the fan was first turned on a steady state was achieved in the first four hours. It was also notable that the return air monitor indicated that the radon concentration showed little change, once steady state was achieved, whether the stopes were ventilated or not. This indicated that, in this particular case study, radon will convect out of a stope at the same rate as it emanates from the backfill. It was further found that the emanation rate of the Rio Algom backfill was .55 pCi / cm^2 sec^{-1}. This indicated that the emanation rate of backfill was 1000 times greater than exposed ore. This rate further indicates that the total contamination depends not only on time but on the exposed surface area of backfill. As such a filled stope with an exposed area equal to the crossectional area of the access will contaminate the air less than a half - filled stope under the same conditions.

Having defined the extent of the contamination problem several possible solutions are available and are discussed here. The first has already been indicated, i.e. the practice of completely filling stopes so as to reduce the exposed surface area of the backfill. This, in practical terms, implies that contamination can be reduced if the stopes are filled as quickly as possible. Another possible method is to remove the radium from the ore (107) or alternatively use uncontaminated surficial sands in place of mine tailings. Another possible solution is to increase localized ventilation in order to exhaust the work area more quickly. Lastly, the use of chemically stabilized radioactive mine backfills offer great potential (108,109,110). The premise of chemical stabilization is to form an impermeable layer at the fill - air interface. This layer will inhibit the diffusion of radon gas to the atmosphere. The actual process consists of physically spraying a 5 cm. thick layer of chemical grout onto the fill surface. The main requirement of the grout is that it have a coefficient of permeablility of 10^{-10} cm / sec. One such grout, Cyanamid's AM-9, has been reviewed by De Korompay (76). It was found that this material was acceptable in terms of it's permeability. Furthermore its cost in terms of a 5 cm. thick application was $7.47 (1977 dollars) per square metre.

In conclusion this section has reviewed the problems associated with the use of radioactive backfills. It further examines a means of measuring and remedying the problem of radon gas contamination.

3.2.3 Liquefaction Potential Of Backfill

The term liquefaction is used to define the mechanism by which a soil mass transforms into a liquid with flow potential. This phenomenon is well known in cohesionless granular materials. There are numerous reported cases of liquefaction, the most widely reported case in mining is presented by Sandy et al. (48). This case study concerned the no. 3 dump at the Mufulira mine in Zambia. A liquefaction failure in no. 3 dump on September 25th, 1970 resulted in the death of 89 miners. The dump material consisted of mill tailings. There are however few instances of liquefation failures occurring in classified mill tailings used as backfill. In order for liquefation to occur certain conditions must be met. These include:

1. The material must be fully saturated
2. The material must be subjected to dynamic loading
3. The fill should be cohesionless (uncemented)

Furthermore, the energy required to produce liquefaction depends on the inter-relationship between the characteristics of the material mass including , particle grading, grain shape and void ratio as well as the amplitude and frequency of the dynamic loading. In general liquefaction potential increases for materials at low confinements, for materials with high void ratios and materials with rounded grain shapes. Materials are also more susceptible to liquefaction when the pore water pressure is increased. The presence of fines in mine backfills will reduce the rate at which pore water pressures can dissipate and thus may create a liquefaction potential.

Several viewpoints on the principle reasons for the occurrence of liquefaction failures in cohesionless soils exist. These have been summarized by Whitman (117) and are listed below:

1. Seed et al (23), emphasized the buildup of excess pore pressure during cyclic straining as the main reason.

2. Casagrande (191) and Castro (192) have focused on the conditions under which sands deform continously under small shear stresses.

3. Schofield (193), has pointed out that a combination of low effective stresses and changing pore pressure gradients can create liquefaction conditions.

Void ratios in backill materials are normally very low and particle angularity is high for mill tailings, thus contributing to interlocking. Confining pressures are significantly higher than those of surface conditions and quoted permeabilities of 100 mm/hr are sufficent to allow pore pressures to dissipate rapidly. These typical backfill properties provide an explanation for the scarcity of published case studies of liquefaction failures for classified mill tailing in underground environments. However, it should be noted that high density backfills tend to contain a high degree of fines, and commonly contain as much as 20% moisture. These backfill may be suseptible to liquefaction failure if uncemented.

Liquefaction potential can effectively be reduced through the addition of cement, good drainage and desliming the mill tailings by classification.

In summary, liquefaction is a mode of failure occuring in cohesionless soils when such soils are saturated and subjected to cyclical or dynamic loading. Although few instances of liquefaction have been report for underground mine backfills, the potential for failure exists particularly soon after filling. As such a number of safeguards have been proposed and the design of bulkheads, is discussed in section 3.2.8.

3.2.4 Hydrocyclone Design For Backfill Grading

The purpose of cycloning is to render the percolation rate of tailings material acceptable for underground placement. This is done through separation of the original tailings material into two products, a coarse fraction and slimes. The performance and characterization of a cyclone circuit is measured by the distribution of its products, which can readily be predicted by existing cyclone models. Such models ensure that the backfill grading properties optimization, as described in section 3.1.3, can easily be integrated into the backfill design system. Two models, (77) and (126), in combination provide a means of estimating the final grain size distribution in the classified tailings portion of a hydrocylone circuit. It is useful initially to consider the operation of hydrocyclones. A slurry is introduced into the top of the cyclone and enters tangentially. Classification is achieved by

the centrifugal and drag forces which occur as a result of slurry velocity and cyclone geometry. The combination of these forces allow the larger particles to migrate to the walls of the cyclone and down through the apex of the cyclone (underflow) while the fines tend toward the center of the cyclone and move upwards and out through the vortex finder (overflow). Intermediate particle sizes will be suspended at proportionate distances from the core and thus account for a possible source of shortcircuiting of material within the cyclone. The shortcircuited portion will have to be considered in the final predicted grading curve. The design equations presented by Stratton-Crawley (77) are complex and need not be reproduced here, rather the reader is referred to the referecene. The complexity of these equations has lead Stratton-Crawley to computerize their characterization model. The model consists of seven basic equations which define the following characteristics:

1. Cyclone Capacity
2. Volume Split of Water Between the Underflow and Overflow
3. Cut Size
4. Probability of Particles of a Given Size Reporting to the Underflow
5. Seperation Modulus
6. Cyclone Seperation Efficency
7. Correction Factor for Classification of -45 um Particles

These modelling equations are all functions of cyclone dimensions including, height, diameter, diameter of vortex and apex.

They are also functions of of slurry and particle density and feed rate.

The Flow Ratio R_f is then used by Plitt (126) to predict the grain size distribution of the underflow product. This is expressed in one simple equation below:

$$R(u) = R_f + (1 - R_f)\ E(u) \quad .... \quad 3.2$$

where: u = particle size

R(u) = fraction of grain size, u, recovered in the underflow

$E(u) = 1 - \exp\ [-.693\ (u\ /\ U_{50})]$

Thus given the original grain size distribution and the cyclone operating parameters the retained portion in the underflow of each size fraction can be calculated and thus the final grainsize distribution determined.

3.2.5 Hydraulic Transportation

The design of transportation systems for hydraulic backfill slurries is based on calculations of friction losses in the transportation pipes. Once these friction losses are quantified the pump characteristics can be defined. It is the aim of this section to establish the relevant design parameters and equations for the hydraulic transport of backfill slurries. The first consideration for the hydraulic transport of backfill is the calculation of the

required backfill quantities at the stope site. Having determined the required quantities, pipe diameter selection will have a direct bearing on the total friction loss and thus is of crucial importance. The selection of pipe diameter depends on pipe orientation, flow velocities and flow quantity rates. Korompay (61) noted that if pipe diameters and flow velocities are properly matched then pipe wear and hence life is prolonged. The following equation was proposed for pipe or borehole diameter selection.

$$d = \frac{.409\ Q}{V\ u} \qquad \text{..... 3.3}$$

where d = optimum pipe diameter (in.)

Q = discharge rate (USGPM)

The values of velocity, V, and the constant, u, depend on pipe orientation and flow conditions. In the first instance we consider horizontal pipe sections. The value of u for these pipe sections is 1, and the optimum flow velocity is expressed by the following formulae:

$V = V_{crit} + 1$ if $V_{crit} < 4$ fps

$V = 1.25\ V_{crit}$ if $V_{crit} > 4$ fps

When fill is transported in vertical drops the value of V is equal to the selected flow line velocities, while the value of u remains equal to 1. These values are suggested by Korompay for vertical pipe sections having a uniform diameter. It was further

suggested that installation costs could be reduced if variable diameter pipe is used. In this instance the values of both V and u must be redefined as follows,

V = terminal fall velocity of slurry, fps

$u = A_s / A$

where: A_s = cross sectional area of pipe occupied by slurry (sq. in.)

A = cross sectional area of pipe (sq. in.)

The implication of this type of pipe selection is that smaller diameter pipes could be used at depth, thus reducing both capital and maintenance costs. The next stage of the transportation system design is the calculation of friction head losses for the selected pipe configuration.

When designing a filling system the most important consideration is friction loss which has a large effect on energy consumption. Friction loss is a function of pipe roughness, material grading and angularity, pulp density, slurry velocity and pipe diameter. A series of tests were initiated by Wayment (118) and Bardill (119) for slurry velocities between 2.8 and 19 ft/s for increments of .5 ft/s between the two values. Pulp densities were also varied between 5 and 70% in intervals of 3%. These tests were repeated for 2, 3 and 4 in. diameter pipes. The findings were expressed both in equation form and graphically. The following equation was developed:

$$\text{Head Loss} = A + B\,(\text{density}) + C\,(\text{velocity}) + D\,(\text{density})^2 + E\,(\text{velocity})^2 + F\,(\text{density})\,(\text{velocity}) \quad \ldots\ldots 3.4$$

where the coefficents A, B, C, D, E, and F vary with pipe diameter and are given in Table 3.1, and equation 3.4 yeilds head losses in psi./ 100 feet of pipe.

Pipe Size	A	B	C	D	E	F
2	47.08	-1.64	-2.49	.0149	.3003	.0403
3	25.48	-.744	-1.90	.0064	.1755	.0251
4	22.67	-.555	-2.58	.0038	.1829	.0366

Table 3.1 Regression Constants For Varying Pipe Diameters

3.2.6 Drainage Design

The mining industry regards drainage as a major design criteria for mine backfills. However, the terminology used is often inconsistant and incorrect with the applied units. The most commonly used term is permeability, this term applies to the physical properties of the medium only, (grading, porosity). Whereas, the terms of reference considered in mining refer to the migration of a fluid through a porous media. In this context, account must be taken of the interaction between the porous media and the fluid, the resulting index is refered to as hydraulic conductivity.

An example of the difference between permeability and hydraulic conductivity is thus provided here. For instance the Fair-Hatch (206) equation considers material packing, grading and shape characteristics only and is thus considered a permeability equation in the form presented by Todd (206), whereas the Kozeny-Carmen (207) equation also considers the fluid properties (viscosity

and specific gravity) and thus is a true hydraulic conductivity equation. A dimensional analysis of the two equations reveals that the resulting units are also different.

The inconsistancy thus arises from the units attached to various "permeability" equations. For instance a true permeability equation would have units in cm2, whereas the mining industry often uses the units cm/s. In fact a relationship between permeability and hydraulic conductivity exists, were one can be converted to the other by a factor which accounts for the fluid specific gravity and viscosity. The Fair-Hatch equation for instance has been reported as a hydraulic conductivity equation by Freeze and Cherry (208) by incorporating a term accounting for fluid viscosity and specific gravity. The assumption of the fluid being water at 20 C is often made in backfill technology without the appropriate change in terminology, from permeability to hydraulic conductivity. This error in terminology is evident with the Hazen equation (3.5), for example, which is refered to as a permeability equation by the mining industry. The constant "C" in equation 3.5 is taken to be between 90 and 120 by the mining industry, conversly in the Kozeny-Carmen equation the same "C" constant is taken to be in the order of 5, with seperate account being taken of viscosity and specific gravity of the fluid. The "C" constant used in equation 3.5 has thus incorporated viscosity and specific gravity, however the terminology has not been changed.

The units of equations 3.5 to 3.11 have similarly been expressed in cm/s thus impling that these equations are in fact hydraulic conductivity equations. However, within the context of

this thesis the term permeability has been used in place of hydraulic conductivity to be consistant with mining terminology.

Hydraulic backfill, after having been transported, generally in a 60 - 70% slurry, is placed in the stope. The excess water must be removed from the stope in order to ensure that the backfill solidifies. In addition there is often much concern about the turnaround time between filling and the resumption of mining. In this light the material permeability becomes a major design parameter for backfill drainage. The parameters controlling permeability include:

1. Backfill Grading
2. Stope Dimensions
3. Pulp Density
4. Desired Turnaround Time
5. Void Ratio
6. Mineralogy
7. Drainage System Design
8. Temperature
9. Use of Portland Cement
10. Use of Flocculants

The migration of water through the stope backfill occurs in two stages. In the first stage the water migrates through the backfill material. In this stage two mechanisms of interest are noted, these include the permeability of the backfill and in cemented backfills the hydration of Portland cement provides another means of expelling water. Once the backfill is graded such that the permeability is acceptable then the excess water must be expelled from the stope via the drainage system.

Examining firstly the permeability design, several empirical equation are available . The first is based on Hazen (113):

$$k = C\ (U_{10})^2 \qquad \text{..... 3.5}$$

where k = coefficient of permeablility (cm/s)
C = a constant (normally between 90 and 120)
U10 = 10% passing size

Although this equation is commonly used, the limitations of its' applicability to a range of material gradings, defined by the U_{10}, is not well documented. Another such equation was presented by Terzaghi (114) in the form:

$$k = 1.4\ e^2\ k_{.85} \qquad \text{..... 3.6}$$

where $k_{.85}$ = coefficent of permeability at a void ratio of .85
e = void ratio

Equation 3.5 relates permeability solely to U_{10}, whereas equation 3.6 relates permeability to void ratio alone. Shahabi et al (115) realized the limitations to such simplifications and thus proposed an equation which relates the permeability to the coefficient of uniformity (Cu), effective size (U_{10}) and void ratio (e).

$$k = 1.2\ Cu^{.74}\ (U_{10})^{.89}\ (\ e^3\ /\ 1+e\ ) \qquad \text{.....3.7}$$

This equation has been developed for materials having U_{10} values between .15 and .59 mm and Cu values between 1.2 and 8.07. Furthermore the term (e^3 / 1+e) must remain in the range between .05 and .22. The use of this equation outside these ranges is cautioned.

Yet another series of equations have been proposed by Bates (116). In his extensive review of material drainage characteristics Bates developed four different equations for the prediction of material permeability. In addition his work extended into the prediction of percolation rate and seepage velocity. However only the permeability equations are considered here. The applicability

of Bates' equations is subject to the conditions in Table 3.2.

The first of these equations was based simply on the U_{50} of the material and is represented by the equation:

$$k = 6100\ (U50)3.7 \qquad \text{..... 3.8}$$

PARAMETER	MINIMUM	MAXIMUM
VOID RATIO	.520	1.08
U10 (mm)	.003	.105
U50 (mm)	.060	.24
Cu	2.00	22.00

Table 3.2 Applicability of Bates' Equations

This equation was subsequently refined to include the coefficient of uniformity, equation 3.9, and refined again to include the void ratio, equation 3.10.

$$k = 1800\ (U50)2\ Cu-1.7 \qquad \text{..... 3.9}$$
$$k = 7300\ (U50)2.3\ Cu-1.3\ e4.1 \qquad \text{..... 3.10}$$

Bates was not satisfied with the performace of equations 3.8 to 3.10 and proposed a final more complicated and cumbersome equation:

$$k = 11.021 + \ln[(e)(U10)] - .085\ \ln(e)\ \ln(U50) + .194\ (e)(Cu) - 56.486\ U10\ U50 \qquad \text{..... 3.11}$$

The particle size in each of the Bates equations is in millimeters and the resultant permeability in in./hr.

In summary, seven different approaches have been illustrated for determining the coefficent of permeability of a material. It should further be noted that the author has not had the time or opportunity to determine the field validity of the above equations. However the applicability of the presented equations for different ranges of particle size, uniformity coefficient and void ratio has also been reviewed. It was found that the applicability of the Shahabi permeability equation, equation 3.7, is fcr coarser

materials than the four Bates equations. Furthermore, the Shahabi equation has been developed for a narrower and lower range of uniformity coefficients. Lastly none of the permeability equations presented have been developed for potential use with the coarse rockfill materials, see Chapter 7. It thus remains evident that future research should aim to develop permeability equations of application to rockfill.

Once it has been ensured that water can freely migrate within the backfill material, then the next consideration is the removal of water from the stope. This part of the design is site specific and depends on the stope dimensions and spacing of drainage towers.

3.2.7 Backfill Compaction

The most common method of backfill compaction is vibratory compaction. This is the practice of vibrating a backfill slurry to allow for optimium compaction of the in place material. Some of the main considerations for use of this system have been described by Nicholson et al. (111,112). These include the effectiveness of vibratory compaction for a particular material, methods of installation, required equipment compaction and possible mining cycle delays when including the compaction process as part of the mining cycle . The equipment described (111),(112) consists of a probe type concrete vibrator and the floating plate vibrator. It was found that the floating plate vibrator is less effective in compacting backfill than the probe type vibrators due to poorer energy coupling between the equipment and the material. On the

other hand probe type vibrators tend to settle to excessive depths. Each of the vibrator types operate at between 100 and 170 cps and apply a dynamic force of between 18 and 30 kN. Figure 3.6 illustrates dry density contours for compacted backfill using 50 and 75 mm probe type vibrators and the floating plate vibrator. This figure also illustrates that the probe type vibrator has a larger volume of influence than does the floating plate vibrator.

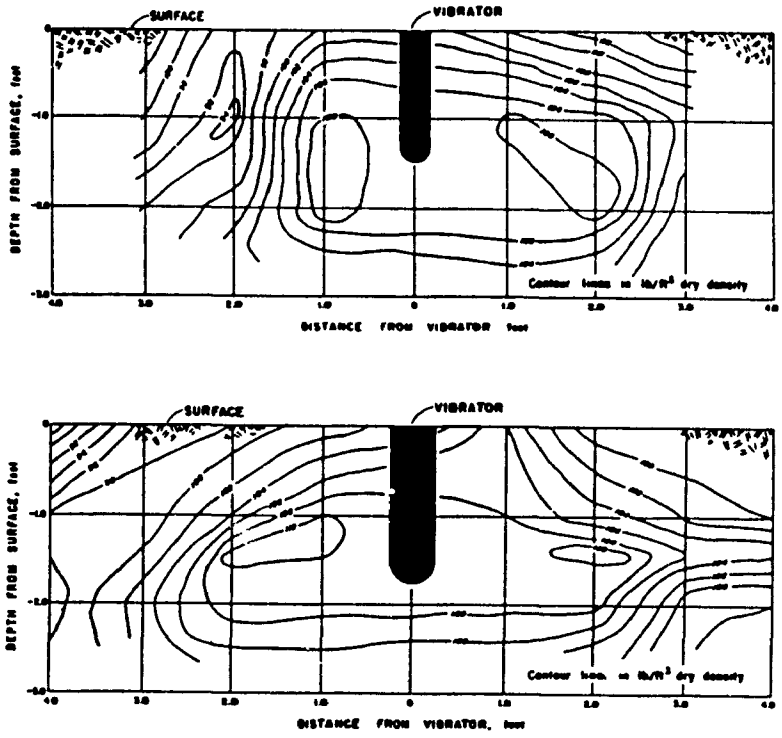

FIGURE 3.6 Effect of Vibartory Compaction on Backfill Dry Density (After Nicholson [112])

The effectiveness of the above vibrators is also dependent on the size of the probe, material grading and water content. It was found that the area influence of .9, 1.22 and 1.52 metres in diameter was achieved with 50, 100 and 150 mm probe type vibrators.

It was found that the lowest void ratios were achieved for well graded materials, while the effect of compaction equipment was greatest for uniformly graded materials. This is a result of a higher initial void ratio and thus a greater obtainable percentage reduction in void ratio. Lastly, the moisture content also has an effect on the compaction effectiveness. Increases in slurry pulp densities tends to show an increase the final density. An increase in slurry density further reduces the amount of effort required to compact the material.

3.2.8 Bulkhead Design

Bulkhead failures may occur as a result of inadequate drainage provisions behind the bulkhead or by leakage around the perimeter of the structure. Minor nuisance due to leakages are common but do not present major problems. However two major bulkhead failures have occured in Canada in the last 34 years.

The first occured in 1953 at the Kerr - Addison mine (120), where a bulkhead failure immobilized the cage and swept a miner into an open stope. The backfill material consisted of uncemented, classified mill tailings and pit sand with a percolation rate of 100 mm/hr. The failed timber bulkhead was constructed to an 20.3 cm. thickness and braced with two 15.24 cm. square whalers placed horizontally across the opening. The stope at failure contained 30,267 cubic yards of backfill.

Another failure occured at Hudson Bay Mining and Smelting's Centennial Mine, in 1979, Nantel (121). The failed timber bulkhead

was of lightweight construction and was observed to be poorly draining before the failure. The failure resulted in the death of one miner. The inplace backfill consisted of uncemented, classified mill tailings and Tyrell Lake sands, and again exhibited a percolation rate of 100 mm/hr.

These two case studies illustrate the need to standardize bulkhead design in order to prevent the reoccurance of such failures. The design procedure and equations are complex and need not be reiterated here. However the design principles will be reviewed and the design equations and standards for each bulkhead type referenced.

The use of cemented and uncemented fills, gives rise to different bulkhead requirements. In the case of cemented backfills, normal filling practice facilitates the solidification of cemented backfill plugs and thus subsequent filling will load both the backfill plug and the bulkhead. Typically, fills pressures range from 0 to 62 kPa for stopes filled to heights ranging between 18.3 and 61 m. Uncemented fills on the other hand present a much higher potential for hazard. The two case studies above illustrate the potential hazards. The most critical factor affecting the total pressure on the bulkhead is the water content in the stope. As such the percolation rate is the primary parameter of importance as it ensures reduced water buildup in the stope. Normally a 100 mm/hr. percolation rate is considered acceptable. However a draining column of backfill is sujected to both compaction and changing degree of saturation. The percolation rate is very sensitive to both these parameters. In fact, a 20% decrease in void ratio or a

10% decrease in degree of saturation would result in a 50% drop in the the percolation rate. As such uncemented fills can require bulkheads designed to a maximium of twice the hydrostatic head to a zero pressure. Nominally, for well drained backfills with bulkheads set back from the brow of the stope, the backfill pressure is in the order of 1.45 kPa.

Kivisto (120), summarized the types of bulkheads and categorized them as timber bulkheads, reinforced concrete and concrete/backfill plugs.

Timber bulkheads can be designed to resist pressures in the order of 4.35 kPa and are thus suitable for use with cemented hydraulic and well drained uncemented backfills. The use of timber bulkheads with well draining uncemented backfill should be considered only after careful investigation of the backfills permeability characteristics. Details on timber bulkhead design and anchoring are described in detail by Nantel (122).

Reinforced concrete bulkheads offer the advantage of being able to withstand greater loads and the design is facilitated (123,124) for standard size openings by design tables and relevant equations for non - standard openings. They present a disadvantage, however, in their cost, both in time and money. Concrete bulkheads further require drainage facilities as they are not permeable. The combination of cost and time constraints makes these bulkhead types suitable only for uncemented backfills.

The use of backfill/concrete plugs is gaining in popularity as a substitute for concrete bulkheads. The South Africans have used

and documented the design procedures (125). The basic approach is to construct a light timber bulkhead away from the brow of the stope. A highly cemented hydraulic fill is introduced and allowed to solidify, at which point the bulk-filling takes place. The resultant bulkhead is reported to be able to withstand pressures in excess of 145 kPa.

3.3 Summary

Section 3.1 of this chapter has dealt with a backfill design rationale in a qualitative fashion. The objective of section 3.2 was to link the design concepts illustrated in section 3.1 to design procedures and equations.

Sections 3.1.3 and 3.1.4 dealt with Aggregate Design and Materials Handling respectively. Parallel sections which deal with design equations for Hydraulic Transportation and Drainage are given in sections 3.2.6 and 3.2.7 respectively. Similarly, section 3.2.5 aims at providing a means of designing a backfill grading system which fulfills the requirements set out in section 3.1.3. The question of cementing agent addition, referred to in section 3.1.5, is the main thrust of this thesis and design equations for cemented hydraulic fills have been developed in section 9.1.1.

This chapter has thus covered a wide range of backfill design requirements, with the exception of geomechanical properties design. It is the intent of the remainder of this thesis to present, develop and correlate appropriate geomechanical behavioural equations, developed from laboratory and in situ studies, for application within the design rationale presented herein.

4.0 FIELD STUDIES

Prior to embarking on field and laboratory studies an appreciation was gained of the relative importance of backfill usage to the Canadian mining industry as well as the various backfill categories in use were established.

It was noted in chapter 1 that the data on backfill usage and properties at the outset of this project was sparse. Varying degrees of information on physical and geomechanical properties were available for each backfill type. Reference was made to published data where available. Such data, however, generally lacked in consistency and quantity. The need for a more complete series of testing was thus apparent.

It is the intent of this chapter to illustrate the importance of backfill in the context of mining in the provinces of Quebec and Ontario. Furthermore, this chapter delineates the program of laboratory and field study undertaken along with a geological and operational description of the mine locations involved in the study. Figure 4.1 illustrates the locations of these operations, and further illustrates the associated problems with the aquisition of field data. Field data aquisition involved mines ranging from the Abitibi region in Quebec, located 600 km. from Montreal, to the Red Lake District on the Ontario - Manitoba border, 2500 km from Montreal.

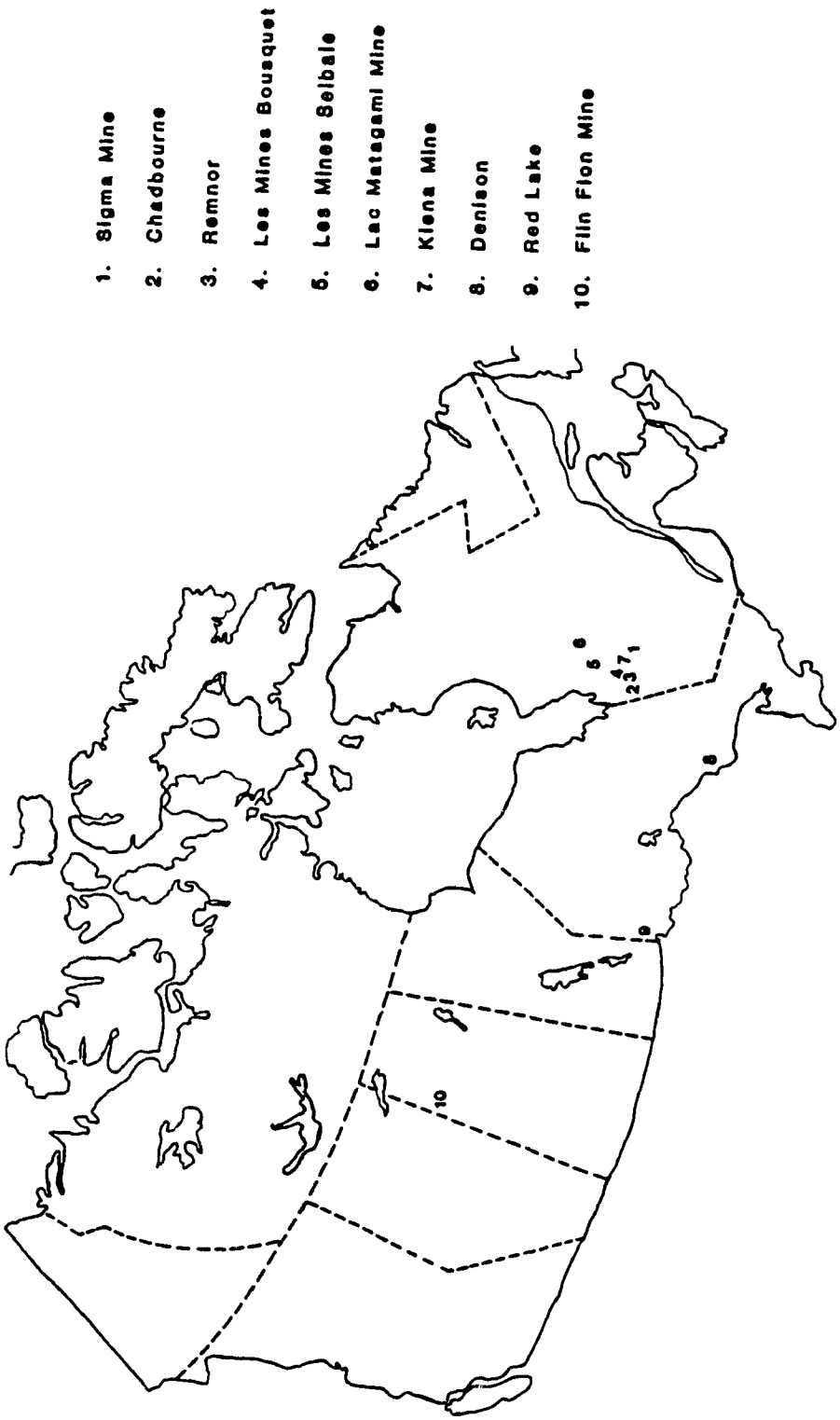

FIGURE 4.1 Geographical Location Of Field Sites

4.1 A Survey Of Backfill Usage

A survey of Quebec mines was initiated in the summer of 1985 with the assistance of the Centre de Recherche Minerale de Quebec. The survey comprised 19 questionaires which centered attention on the mining regions of Abitibi - Temiscamingue. A 90% response was achieved and the data showed that 60% of Quebec mines use some form of backfill and that an additional 18% planned to use backfill. This increasing trend is equally evident among South African gold mines, (201), where present backfill usage is limited to 1% of operating stopes at 7 mines. The projected usage for 1991 is for 25% of operating stopes at 25 mining operations. This illustrates the scope of backfill usage and its importance to Quebec, Canadian and world mining. A sample of the questionare is provided in Appendix 3.

Following the Quebec survey, a similar survey was issued in Ontario by the Ontario Ministry of Labour. These recent surveys of backfilling practices in Quebec mines (28,141) and its counterpart survey in Ontario (140) indicated that uncemented hydraulic fill is by far the most widely used backfill type in Quebec, accounting for almost half by weight of all backfill used (Table 4.1). In Ontario cemented hydraulic is by far the most popular. These surveys further illustrated that 34% of the backfill used in Quebec is of the rockfill type compared to 26% in Ontario.

The degree of cementation, for mines using cemented backfills in Ontario, is summarized in Table 4.2. The table illustrates that 57.5% of the cemented backfills contain less than

6% cement. These cement additions are typical in bulk filling practice. The second group consists of cement additions ranging from 6-12% and accounts for 38.5% of cemented backfill usage. Such additions of cement are most typical of cemented floor usage.

Although, 78% of Quebec mines reportedly use backfill only 11% of these mines reported comprehensive data on the backfill geomechanical behaviour. The reported data ranged from simple uniaxial compressive strength to triaxial compressive strengths at distinct curing periods and cement additions. Strikingly, however there were no reports of measured deformational properties for these same material. Furthermore, all the available data provided by the mine operators taking part in this survey pretains only to the laboratory environment.

FILL TYPE	PERCENT OF ALL BACKFILLS (by weight)	
	Quebec	Ontario
Cemented Hydraulic	20.0	57.5
Uncemented Hydraulic	46.0	16.5
Cemented rockfill	13.0	13.5
Uncemented rockfill	21.0	12.5
TOTAL	100.0	100.0

TABLE 4.1 - Distribution Of Backfills Used in Quebec and Ontario Mines, According to 1986 Survey (After Beauchamp [141])

CEMENT CONTENT (% by weight)	PERCENT OF ALL BACKFILLS (by weight)
0 - 2	2.5
2 - 4	32.0
4 - 6	22.0
6 - 8	16.0
8 - 10	16.0
10 - 12	6.5
12 - 14	0.0
14 - 16	2.5
16 - 18	2.5
TOTAL	100.0

TABLE 4.2 - Cement Addition in Mine Backfills, According To 1986 Survey, (After Campbell [140])

Lastly, the addition of 14-18% cement to backfills is limited to special uses such as the recovery of highly stressed pillars, and accounts for 5% of cemented fills in use.

4.2 Investigated Mine Sites

This study, undertaken over the last three years, has investigated backfills at ten different mine sites seven of which are located in Quebec with seven mines taking part in the study. Other materials tested include two from Ontario mines and one mine in Manitoba. This section provides background data on the individual mines involved.

4.2.1 Sigma Mines

Sigma Mines is located in Bourlamaque Township, Abitibi County in Northwestern Quebec; approximately one mile east of the town of Val d'Or. Sigma Mines has been producing gold for the last fifty years and covers an area of 1,469 acres (142).

Sigma Mines is situated within the Archean Malartic Group of steeply dipping, easterly striking, ultramafic flows, basalts, tuffs, agglomerates and andesites. In the mine area, the Malartic Group can be subdivided into North Flows, North Tuffs, C - Type diorites porphyry and G -Type diorite dykes. The mine is centered on the C - Type diorite with the vein systems lying outside this zone being unproductive.

The mine produces 1275 metric tonnes of gold bearing ore per day and employs four mining methods. These include Cut and Fill (38%), Shrinkage (20%), Room and Pillar (25%) and Long Hole (17%).

The cut and fill stopes are used in the quartz - tourmaline veins which dip at 70 degrees and have thicknesses between 2.44 and 3.66 metres. Longhole stoping is employed where such veins exceed 3.66 metres in thickness. Shrinkage stoping is also used where the viens are narrower than 2.44 metres in width. Shrinkage is also employed in the feldspar porphyry dykes zones. The average dip of these stopes is 80 degrees and the average width is 6.1 metres. Lastly the room and pillar mining method is used for flat lying veins. The average height of these stopes is 1.68 metres and the dip is 20 degrees.

Sigma uses 309 metric tonnes of backfill per day 90% of which is uncemented, it is further transported at a 65% pulp density. The use of backfill is limited to the cut and fill stopes and the cemented backfill is used for cemented floors only. These floors are 15.2 cm. in thickness and contain 7% cement.

In early November of 1985 pressuremeter tests were conducted by the author at the 1400 level breakthrough of a cut and fill stope at Sigma mines. The tests were performed to a depth of 8 metres in uncemented backfill material containing an average of 10% moisture.

Furthermore, laboratory shear box tests were conducted on 101.6 mm square samples of Sigma fill, to develop a failure envelope for the material. Other supporting data was also gathered via Proctor tests, sieve and hydrometer analysis along with pycnometer tests for determination of the specific gravity of soilds. Also a mineralogical assessment was made from analsyis on the scanning electron microscope.

4.2.2 Campbell Red Lake Mines

The Campbell Red Lake Mine (CRLM) is situated in the Red Lake District of northwestern Ontario. It is located in Balmertown and has been in production since 1948,(92).

There are two main vein structures at CRLM, with andesite being the main host rock. The ore structures consist of replacement veins, which range in width from .61 to 9.14 metres together with

quartz carbonate fracture filled structures with thicknesses between .15 and .9 metres. CRLM is a major gold producer. Its' daily output consists of 970 metric tonnes of gold bearing ore. The production comes from between the 300 and 900 metre horizons, from three sources; shrinkage (20%), overhand cut and fill (70%) and development (10%). Campbell attempts to recover 80% of the in situ ore, by these extraction methods. All stope development is in ore thus providing one source of muck. Both the shrinkage and cut and fill stopes have a south - west strike and dip at 65 degrees.

CRLM employs 460 metric tonnes of backfill daily. Both cemented and uncemented, fine grained sandfills are used in all cut and fill stopes. The bulk mix for the cemented backfill employs 5% Portland cement. Furthermore, cemented floors with a 10% cement addition are used to reduce dilution in scraper stopes.

A series of four field pressuremeter tests were conducted in early July of 1986 at two locations at CRLM. The first of these was a 5.5 metres test conducted in 1661 stope. The backfill in this stope was well drained and uncemented. The second series of pressuremeter tests were conducted in 1804-1 east-west stope and consisted of three test holes the first 2.5 metres in depth, the remaining two were conducted to a depth of 3.25 metres. 1804 stope has been filled with a 5% cemented bulk mix with 10% cemented floors. In each of these tests two distinct layers were encountered, including 14 day cured material in the first two tests and 160 day cured material in the second two tests conducted at depth.

4.2.3 Denison Mines

The Denison mine is situated in Elliot Lake, Ontario which 200 km. west of Sudbury, Ontario, was opened in 1954, (143). The orebody of the Denision mine consists of five stratigraphically separate quartz - pebble conglomerate reefs in the Proterozoic Matinenda quartzite formation. The mining property is located on the north limb of the Quirke syncline. The syncline overlies an Archaean basement complex and is itself overlain by a Mississagi Quartzite as well as Bruce Limestone and Conglomerates.

Denison mine is a uranium producer with daily output averaging 14,000 tonnes. The orebody dips approximately 20 degrees to the south and has a strike length of 4500 metres. It further consists of two main economic reefs which are 3 metres thick. These are seperated by a 2.5 metre low grade interbedded quartzite. The mining method presently consists of a room and pillar method which accounts for 100% of production.

Backfilling practise at Denison mine started in 27 panel, in 1982, in an attempt to control severe rockbursting of the barrier pillar between Denison mine and Rio Algom's Quirke mine. Presently, backfilling is carried out at rate reaching up to 3000 tonnes per day using, both cemented and uncemented backfills. The cemented backfills contain 3.3% portland cement and some experimentation is presently underway with pozzolans and fly ash. The backfill is pumped underground at a pulp density of 68%.

A series of pressuremeter tests were conducted in late June, 1986 at the Denison mine, centered around two stoping areas 37046 and 37036 stopes. The first of these, 37046 stope, included a series of tests conducted at the uppercut, or top of the stope, consisting of tests conducted to a 3 metres depth. A second series of tests were conducted on the same stope, however, the test location for this second series was on the stope bulkhead at its' base. Tests at this location were conducted to a depth of five metres. The backfill in 37046 stope was cemented at a 3.3% cement mix. The second stope involved in this study was 37036 stope. This stope was accessible in the down dip direction via the mining of 37037 pillar. It was observed that the exposed backfill showed distinct layers of segregation and a study was undertaken to determine the mechanical properties of the individual layers. Pressuremeter tests were conducted in each of three segregation layers. These tests were conducted at depths of 2 to 3 metres along the strike of the orebody.

Furthermore, laboratory shear box tests were conducted on 101.6 mm square samples of Denison backfill for both classified and unclassified mill tailing with no cement addition, to develop a failure envelope for the material. Other supporting data was also gathered via Proctor tests, sieve and hydrometer analysis and pycnometer tests for determination of the specific gravity of solids. A mineralogical assessment was made from analsysis by scanning electron microscope.

4.2.4 Kiena Gold Mines

Kiena Gold Mines operates a gold mine in the Abitibi region of north - western Quebec. The mine is situated in Dubuisson, approximately 10 kilometres west of the town of Val d'Or (144).

The Kiena orebody is a wide pyritic, albite - chlorite breccia zone and is relatively flat dipping. The ore itself is a competent rock mass enclosed within weak altered peridotite wall rocks. This gold and silver producer mines using two mining methods, cut and fill (60%) and long hole stoping (40%). A total of 1250 metric tonnes of ore are mined daily.

Backfill is transported to the underground workings via 7.6 and 10.2 cm. diameter plastic piping. All stopes are backfilled, the cut and fill stopes are filled with 3.3% cemented backfill and 12.5% cemented floors. Delayed backfill is used in the longhole stopes and is cemented at 5%. The backfill plant supplies 1000 metric tonnes of backfill underground daily.

In mid - November 1985 a series of pressuremeter tests were conducted at Kiena. This test series took place in cut and fill stope 23-25 in 5% cemented sandfill to a depth of six metres. A second series of tests were conducted, at the request of mine management, during the latter part of June, 1986. Their objective was to assess the effect of flocculant addition on the deformational properties of backfill. To this aim two test sites were selected. Each site contained 5% cemented backfill with 13.6 grams/tonne

flocculant. In the first of these locations tests were conducted to a depth of 8 metres while tests at the second site were executed to a depth of 4 metres.

Furthermore, laboratory shearbox tests were conducted on 50.8 mm square samples of Kiena 5% cemented backfill with no flocculant addition, to develop a failure envelope for the material. A uniaxial testing program was initiated for 101.6 mm diameter cylinders. The intent was to determine the effect of drainage characteristics on compressive strength. Other supporting data was also gathered via Proctor tests, sieve and hydrometer analysis along with pycnometer tests for determination of the specific gravity of solids. A mineralogical assessment of the backfill material was made by scanning electron microscope.

4.2.5 Les Mines Selbaie

Les Mines Selbaie is located in north western Quebec, 82 km west of Joutel and has been in production since 1974 (145). The orebody consists of one principal lens having a thickness ranging from 3 to 30 metres and a strike length of 550 metres. The dip of the orebody ranges from 40 to 55 degrees.

The mine produces 1,650 tonnes of ore consisting of copper, gold, silver, lead and zinc minerals. Two mining methods are employed: large diameter blasthole stoping (90%) and Avoca cut and fill (10%).

Delayed backfilling in the open stope areas is employed and a 5% cemented mixture is added to the mill tailings feed and

development waste rock to form the final backfill mass. The tailings and rock material is mixed in a 1:2 ratio. The same mix is used in the Avoca method, however, the backfill becomes an integral part of the mining cycle. In total the mine uses 700 to 900 tonnes/day of classified mill tailings and 1400 to 1800 tonnes/day of waste rock.

Tests on Selbaie backfill comprised laboratory tilt box tests to determine rockfill strength characteristics. The uniaxial rock compressive strength was estimated by the point load test. Joint shearbox tests were also conducted on sawcut rock samples to determine the base friction angle. Other supporting data was gathered via sieve analysis and pycnometer tests to determine the specific gravity of solids. A mineralogical assessment of the backfill material was made by scanning electron microscope.

4.2.6 Lac Matagami Mine

Lac Matagami mine is located in north - western Quebec, 5 km south of the towm of Lac Matagami. The orebody consists of a massive zinc sulphide ore zone, dipping at 80^{o}, with a nominal thickness of 100 m. This ore zone is bound by andesite and rhyolite country rocks on the hangingwall and footwall respectively. The footwall contact consists of talc and talc - chorlite schists. The major intrusive structures include rhyolite porphry and diabase dykes along with crosscutting gabbro and peridotite intrusions. The mine is a producer of zinc and copper concentrate. It produces 3000 tonnes of ore daily entirely by Vertical Crater Retreat (VCR)

stoping using 50 and 115 mm diameter blastholes.

The backfilling material consists of classified mill tailings. These were previously hydraulically transported through 100mm diameter diamond drill holes. Presently however the underground workings have broken through the floor of the old open pit and this access is being used to drawdown backfill to the underground workings where it is rehandled by LHD equipment. A total of 160 metric tonnes per day of backfill are used at Lac Matagami mine which contain 10 - 12 % moisture insitu.

In October 1985 pressuremeter tests were conducted at a fill access site on the floor of the old open pit at Lac Matagami mine. The tests were performed to a depth of 8 metres in uncemented backfill material, containing an average of 10% moisture.

Laboratory shear box tests were conducted on 101.6 mm square samples of Lac Matagami backfill, to determine the failure envelope for the material. Other supporting data was also gathered via Proctor tests, sieve and hydrometer analysis along with pycnometer tests for determination of the specific gravity of solids. A mineralogical assessment of the backfill material was made by scanning electron microscope.

4.2.7 Hudson Bay Mining & Smelting - Flin Flon Mine

The Flin Flon Mine is located in the city of Flin Flon on the Manitoba - Saskatchewan border, approximately 90 km. north of the southern extension of the Canadian Shield. The mine has been in production for over fifty years and production presently consists of

pillar and remnant recovery (146). The orebody consisted of six sulphide lenses extending to 1150 metres below surface with a strike length of 610m. These dip at between 60 and 70 degrees, with thicknesses up to 150m. The host rock is quartz porphyry, with the immediate hangingwall and footwalls consisting of andesite tuff and green chlorite and talc schists.

The Flin Flon mine is a producer of copper, zinc and some associated precious metals. It produces 1,500 metric tonnes of ore daily and employs one principal mining method; longhole stoping. Backfilling is an integral part of this method as mined out blocks must be filled prior to mining any adjacent blocks.

Flin Flon Mine uses 700 metric tonnes of coarsely ground uncemented smelter slag daily. The backfill is transported and placed via a conveyor system. The mine operators are presently interested in delayed cementing and grouting techniques so that pillars directly adjacent to previously filled stopes can effectively be mined, with minimum dilution from the backfill.

Tests on Flin Flon mine material were limited to laboratory tilt box tests. This test provided a means of determining rockfill strength characteristics. The slag uniaxial compressive strength was estimated by the point load test. Joint shearbox tests were also conducted on sawcut slag samples to determine the base friction angle. Other supporting data was also gathered via sieve analysis and pycnometer tests for determination of the specific gravity of solids. A mineralogical assessment of the backfill material was made by scanning electron microscope.

4.2.8 Chadbourne Mine

The Chadbourne mine is located in the town of Noranda in the Rouyn Township. The mine initally started production in 1923, (51,147). It is located in the Abitibi Greenstone Belt which trends northeast for 800 km and is 240 km wide. The Abitibi Greenstone Belt is central to the Archean Superior structural province of the Canadian Precambrian Shield. The Chadbourne orebody is contained within the Chadbourne Breccia, which has an area of 300m by 120 metres and plunges at 80 degrees. The Breccia host rocks are andesite and Lake Tremoy rhyolites. The Chadbourne mine is gold producer and mines 1000 metric tonnes per day via two mining methods, longhole stoping (30%) and VCR (70%).

The backfilling system consists of surface haulage of coarsely ground smelter slag from the Horne smelter to the surface access on the floor of the old open pit. The material is subsequently drawndown through a series of interconnected mined out stopes. It is further rehandled and placed in required stopes by Load Haul Dump (LHD) equipment. In total 200,000 tonnes of uncemented slag rockfill are used yearly.

In October 1985 pressuremeter tests were conducted at Chadbourne Mine. Three test sites were chosen: the first was at the fill access point on the old open pit floor. These tests were performed to a depth of 8 metres. A second and third series of tests were conducted in 4C and 4A North-West stopes, these were both conducted to a depth of 7m.

Laboratory tests on Chadbourne material included tilt box tests. This test provides a means of determining rockfill strength characteristics. The slag uniaxial compressive strength was estimated by the point load test. Joint shearbox tests were also conducted on sawcut slag samples to determine the base friction angle. Other supporting data was gathered via sieve analysis and pycnometer tests for determination of the specific gravity of solids. A mineralogical assessment of the backfill material was made by scanning electron microscope.

4.2.9 Remnor Mine

The Remnor mine is located in the town of Noranda in the Rouyn Township. The mine initially started production in 1925 under the name of the Horne mine. It subsequently fell on hard economic times and had to be closed. Recently the ore has been reevaluated and the mine has been reopened as Remnor mine. Within the last year the mine workings have linked up with those of Chadbourne mine and the two mines are now being run as one operation under the Remnor banner. The mine is located in the Abitibi Greenstone Belt which trends northeast for 800 km and is 240 km wide. The Abitibi Greenstone Belt is central to the Archean Superior structural province of the Canadian Precambrian Shield. The Remnor orebody is contained within the Chadbourne Breccia which has an area of 300m by 120 metres and plunges at 80 degrees. The host rock of the Chadbourne Breccia are andesite and Lake Tremoy rhyolites.

The Remnor mine is a gold producer and mines 500 metric tonnes per day via two mining methods, longhole stoping (70%) and shrinkage (30%).

The mine does not presently use backfill, however backfill has been used in the past. This consisted of granulated smelter slag and at times molten slag was also poured. No cementing agent was added to the granulated slag material however the high sulphide content in the material caused oxidation of the backfill and subsequent self - cementation.

In October 1985 pressuremeter tests were conducted at the Remnor mine in self - cemented granulated smelter slag. The access point for this series of tests was a vertical fill exposure on the 700 level. Tests were subsequently conducted to a depth of 7m.

Supporting data was gathered on grading characteristics and density of the material via sieve and pycnometer analysis. A mineralogical assessment of the backfill material was made by scanning electron microscope.

4.2.10 La Mine Bousquet

La Mine Bousquet is located north of the town of Cadillac near Preissac, Quebec and has been in operation since 1979 (148,149).

The ore zones lie in the Abitibi greenstone belt and are of stratabound volcanogenic origin, occuring within the the upper regions of the Blake River Group sediments. The Group is underlain

and overlain by the Kewagama and Cadillac Group sediments respectively. The orebody is steeply dipping and is known to extend 610m along strike and to a a depth of over 600m. The orebody is further contained in a halo of felsic tuffs and sericitic schists.

The mine produces 1500 metric tonnes of gold bearing ore per day and employs two mining methods: modified sublevel caving (80%) and the Avoca method (20%), which is used in areas where the orebody narrows to 3m or less.

Backfilling at La Mine Bousquet forms an integral part of the Avoca mining method. The backfill type used is uncemented rockfill originating from development waste. The backfill is transported underground by LHD equipment and placed directly into the stoping area. In total 760 metric tonnes of rockfill are used daily at La Mine Bousquet.

Tests on La Mine Bousquet material were limited to laboratory tilt box tests. This test provides a means of determining rockfill strength characteristics. The rock uniaxial compressive strength was estimated by the point load test. Joint shearbox tests were also conducted on sawcut rock samples to determine the base friction angle.

Supporting data was gathered on grading characteristics and density of the material via sieve and pycnometer analysis. A mineralogical assessment of the backfill material was made by scanning electron microscope.

4.3 Summary

Backfill is used or is intended to be used by 78% of Quebec mines. Thus backfill occupies an important role in Quebec mining operations. Although uncemented backfills are the most commonly used in Quebec mining, little is known of the geomechanical properties of such backfills.

An essential goal for this research was to establish a database for each backfill type: cemented hydraulic, uncemented hydraulic and uncemented rockfill. It was found that sufficient laboratory data was available for cemented hydraulic backfills, so that a re-analysis of the combined database could be used to define the required behavioural equations. The extension of this data to field conditions required subsequent field verification. Databases for both uncemented hydraulic and rock fills were formed as part of this work through laboratory and field tests. The extent of such testing along with a description of the mining operations involved has been given in this Chapter. The most important series of tests was the field pressuremeter tests which were carried out at seven of the ten mines involved in this study. Chapter 5 describes in detail the pressuremeter test and the data interpratation procedure. Chapter 6 then describes the laboratory tests including uniaxial compressive tests, shearbox and tilt box tests.

5.0 MINE BACKFILL IN SITU TESTING TECHNIQUES

The purpose of any in situ testing program is to determine the relevant physical and geomechanical parameters of the inplace material. For instance a civil engineer may be interested in the drainage characteristics of a given soil beneath a structure. On the other hand a mining engineer may be require the relevent rock strength characterisitcs in a given mining area of the mine. It can be appreciated that the testing techniques which apply to the two cases will be substantially diverse as both the material types and required properties are different. This range of in situ materials and property requirements has given rise to the development of a considerable number of different in situ testing techniques and instrumentation. The selection of the appropriate instrumentation is based on geological conditions under investigation, project requirements and the intended analysis and design methods to be subsequently used.

The main attraction of in situ testing is its ability to test a large volume of material, which otherwise could not be sampled in a cost effective manner. It further affords the ability to test the desired material under less disturbance than in a laboratory environment. There are however two limitations which must be considered; the inability to independently control drainage conditions and the stress environment within the material which may vary with time.

It is the objective of this chapter to briefly review the

range of in situ testing techniques and analysis methods which pertain to the aquisition of the physical and mechanical properties of soils. Furthermore, the rationale for the selection of the pressuremeter as the appropriate tool for testing in situ backfill conditions is presented. The data interpretation procedure for the selected instrument is explored in detail, for each of the material properties required. Lastly, some theoretical aspects of the Pencel pressuremeter are addressed and the necessary developments required for its usage in an underground environment are presented.

5.1 In Situ Testing Equipment And Selection

A wide range of in situ testing equipment has been developed over the years, from the simple, rugged and economical vane shear test to the highly sophisticated and expensive seismic crosshole method. Whatever the method, in situ tests can be subdivided into logging or profiling methods and those methods for the determination of a specific property. Robertson (150) has classified and assessed the applicability of 31 different testing techniques for the determination of specific material properties and ground conditions. Table 5.1 shows his classification which provides a means of equipment selection.

Table 5.1 however has several limitations, the table is based on the experience of one particular researcher with particular expertise in soil investigations. This is evident in the preceived "high applicability" of the prebored pressuremeter test in hard

Test method	Geotechnical information													Ground conditions						
	Soil type	Profile	Piezometric pressure (u)	Angle of friction (ϕ)	Undrained shear strength (S_u)	Density (D_r)	Compressibility (m_v, C_c)	Rate of consolidation (C_v, C_h)	Permeability (k)	Modulus: shear and Young's (G, E)	*In situ* stress (K_0)	Stress history (OCR)	Stress–strain curve	Hard rock	Soft rock—till, etc	Gravel	Sand	Silt	Clay	Peat—organics
Dynamic cone (DCPT)	C	B	—	C	C	B	—	—	—	C	—	—	C	—	C	B	A	B	B	B
Static cone:																				
Mechanical	B	A	—	B	C	B	C	—	—	C	C	C	—	—	C	—	A	A	A	A
Electronic friction (CPT)	B	A	—	B	C	B	C	—	—	B	C	C	—	—	C	—	A	A	A	A
Electronic piezo	B	A	A	B	B	B	C	A	B	B	C	B	B	—	C	—	A	A	A	A
Electronic piezo/friction (CPTU)	A	A	A	B	B	B	C	A	B	B	C	B	B	—	C	—	A	A	A	A
Electronic seismic/piezo/friction (SCPTU)	A	A	A	B	B	B	C	A	B	A	B	B	B	—	C	—	A	A	A	A
Acoustic probe	B	B	—	C	C	C	C	—	—	C	—	C	—	—	C	—	A	A	A	A
Flat plate dilatometer (DMT)	B	A	C	B	B	C	B	—	—	B	B	B	B	—	C	—	A	A	A	A
Field vane shear (VST)	C	C	—	—	A	—	—	—	—	—	C	B	—	—	—	—	—	B	A	B
Standard penetration test (SPT)	A	B	—	B	C	B	—	—	—	B	—	C	—	—	C	B	A	B	C	C
Resistivity probe	B	B	—	B	C	A	C	—	—	C	—	—	—	—	C	—	A	A	A	A
Electronic conductivity probe	A	B	—	C	C	A	B	—	—	B	C	C	C	—	—	—	A	A	A	B
Total stress cell	—	—	—	—	—	—	—	—	—	—	B	B	—	—	—	—	—	C	A	A
K_0 stepped blade	—	—	—	—	—	—	—	—	—	—	B	B	—	—	—	—	B	A	A	B
Screw plate	C	C	—	C	B	B	B	C	C	A	C	B	B	—	—	—	A	A	A	A
Borehole permeability	C	—	A	—	—	—	—	B	A	—	—	—	—	A	A	A	A	A	A	B
Hydraulic fracture	—	—	A	—	—	—	—	C	C	—	B	B	—	B	B	C	C	B	A	C
Borehole shear	C	C	—	B	C	—	—	—	—	C	—	C	—	B	B	C	B	B	C	C
Prebored pressuremeter (PMT)	B	B	—	C	B	C	C	C	—	A	C	C	C	A	A	B	B	B	A	B
Push-in pressuremeter (PPMT)	A	B	B	C	B	C	C	A	B	A	C	C	C	—	—	--	B	A	A	B
Full-displacement pressuremeter (FDPMT)	C	B	B	C	B	C	C	A	B	A	C	C	C	—	—	—	A	A	A	A
Self-boring pressuremeter (SBPMT)	B	B	A	A	B	B	B	A	B	A	A	A	A	—	C	—	B	A	A	A
Self-boring devices																				
K_0 meter	B	B	—	—	—	—	—	—	—	—	A	A	—	—	—	—	B	A	A	A
Lateral penetrometer	B	B	—	B	B	B	—	—	—	B	C	C	C	—	—	—	B	A	A	A
Shear vane	B	B	—	—	A	—	—	—	—	—	C	B	—	—	—	—	B	A	A	A
Plate test	B	B	—	C	B	B	B	C	C	A	B	A	C	—	—	—	B	A	A	B
Seismic cross/downhole/surface	C	C	—	—	—	—	—	—	—	A	—	—	—	A	A	A	A	A	A	A
Nuclear probes	—	—	—	B	—	A	—	—	—	—	C	—	C	—	—	--	A	A	B	A
Plate load tests	C	C	—	C	B	B	B	C	C	A	C	B	B	B	A	B	B	A	A	A

NOTE A = high applicability, B = moderate applicability, C = limited applicability, — = not applicable

TABLE 5.1 In Situ Test Methods And Their Appilcability (After Robertson [150])

rock. The pressuremeters' pressure capacity is an order of magnitude lower than the pressures required to effectively measure hard rock stiffnesses, thus the instrument and procedure have "limited applicability" in a hard rock environment. The rock dilatometer would be a more appropriate choice under such circumstances. Furthermore, the table does not classify the applicability of "combination tests" such as the electronic piezocone pressuremeter, with the benefits of both the piezocone and pressuremeter setups. Even with its limitations this table is a valuable asset to be used in equipment selection. Worth (151) has reviewed a range of in situ testing techniques from the point of view of data analysis and interperation.

It is the intent of this section to investigate the applicability of specific test methods, that is the penetrometer and pressuremeter type tests.

5.1.1 Standard Penetration Test (SPT)

The standard penetration test (SPT) is denoted as the workhorse of the practising civil engineer by Tavenas (152), who substantiates this claim by the statistic that 90% of all subsurface investigations for civil engineering projects is done with the SPT method. The instrument was developed in the early 1900's and has been applied mainly in foundation design, compaction control and liquefaction assessment. The testing procedure is based on the

measurement of the number of required blows (standard hammer weight and drop height) per unit length of penetration. The instruments' main attributes are its simplicity and ruggedness. The procedure is simple and thus permits frequent tests. Soil samples can usually be obtained and the instrument is applicable in most soils and many useful correlations having already been developed. Details of the testing procedure are given in CSA A119.1-1960 and ASTM D1586-67. However it has been shown that operator characteristics can effect test results significantly (153). In fact Kovacs (154) has shown that the energy delivered to the top of the rods averages 55% of the theoretical maximum and ranges between 30 and 80%. This problem has been somewhat alleviated by the developement of the automatic release hammer.

The usefulness of the SPT test is somewhat limited, with its most useful application being its use in material profiling and soil typing. Although the test parameters have be used in various correlations to determine the relative density, friction angle, undrained shear strength, and modulus, it has been shown in each case that the test remains too crude to be used in the determination of individual material properties. However it should be noted that if adequate controls on the test procedure are maintained, site specific data correlations can be developed.

5.1.2 Dynamic Cone Penetration Test (DCPT)

The dynamic cone penetration test is a continuous test in which an impacting weight drives rods and cone into the material

being tested. The test data is highly qualitative and is subject to the same limitations as the SPT method. It further lacks adequate standardization in both the procedure and equipment specifications. Some recent data from the Becker density test (BDT) has indicated that this particular variation of the test is very useful for liquefaction assessment in gravelly sands (155).

5.1.3 Static Cone Penetrometer Test (CPT)

The static cone penetrometer test was originally developed in Europe where it was extensively used prior to gaining some recent popularity in North America, (194). The CPT has the advantage of a simple test procedure, continuous recording system, reproducabiltiy of results and amenability of data to rational analysis. This test method is significantly superior to the dynamic methods previously described as the apllied load is more easily controllable and becomes operator independant.

The CPT method has been used traditionally for soil classification. The methods used is based on the ratio between the sleeve friction, f_s, and the cone bearing, q_c. Charts have already been developed which relate this ratio to a range of soil types. However, there presently exists little standardization in cone design, thus the cone bearing load can vary significantly. This presents a limitation in the use of this test in determining the undrained shear strength of the material. The CPT has been found to be useful for the design of shallow foundations, deep foundations

compaction control and liquefaction assessment, particularly in loose soils. This test is of special interest for the assessment of liquefaction potential in backfilled underground stopes.

5.1.4 Flat Plate Dilatometer Test (DMT)

The flat plate dilatometer test has developed in Italy, by S. Marchetti and is sometimes refered to as the Marchetti dilatometer. The instrument is a variation of th K_o stepped blade. The DMT has been the subject of much literature in recent years due to the claim that the instrument is highly applicable for the determination of in situ stresses. The dilatometer records the total stress measurements (P_o and P_1). These are then used in a series of three equations used to determine th material index, I_d, horizontal stress index, K_d and the dilatometer modulus, E_d.

Present evaluation of this test indicates that it provides excellent almost continuous identification of soil type. It has further been attempted to use this instrument in determining the angle of internal friction, however it has been found (156) that the correlations are at best highly empirical and the correlations are very poor. The most promising correlations have been presented by Marchetti (7) in tests conducted in uncemented insensitive clayey soils. The results indicate good correlations between K_o and K_d. This instrument, thus may provide a means of measuring K_o in backfills. Claims have also been made of this instruments' (157) applicability for determining deformation parameters. The applicability of this instrument for the determination of stiffness

parameters is doubtful. The instrument, for instance, is 14 mm in thickness and thus remolds the ground upon insertion. This is coupled with the test procedure which is based on the displacement of a small membrane a distance of 1 mm. Thus it seems reasonable to conclude from this that the entire test is being conducted in the remolded material. Furthermore the limited extent of the membrane area, 28 cm^2, entails that the testing of such a small volume of material makes extrapolate the results to the material mass somewhat difficult.

5.1.5 The Pressuremeter Test

Table 5.1 indicates that the pressuremeter is the most highly rated of specific test instruments available. The pressuremeter is basically an expandable probe which is placed in the material and expanded under controlled conditions. This testing method offers good potential for determining the deformational and strength characteristics of soil and backfill materials. The available tests can be classified according to three criteria (158); physical probe characteristics, method of inflation and insertion conditions.

The physical classification results from pressuremeter probes being available in a variety of diameters. The selection of probe diameter is dependant on the material grading and method of insertion. The instrument can also be of the tricellular variety, where two guard cells ensure that the applied deformation can be

estimated as a cylindrical cavity. Such probes have proven to be somewhat difficult to use in the field as the differential pressure between the guard cells and the test cell must be monitored at all times. Thus the monocellular probe has been developed to alleviate this problem. The advent of this probe required a new data evaluation as the deformation geometry was no longer representable by an expanded cylindrical cavity, rather the deformation is best approximated by an expanded ellipsoidal cavity. This fact has a significant effect on the equations describing the generated material stresses and strains during the pressuremeter test. This will be described in greater detail in section 5.3.

Pressuremeters can further be sub-classified by the method of probe inflation. That is, whether the probe is a strain or pressure control instrument. Although this should have no ef ct on the quality of data and analysis, it has been found in practice that the strain control instruments have experienced less operational problems than the pressure controlled instruments. The main problem encountered in stiff backfill materials using the pressure control instruments is the high incidence of probe bursting. This occurs as the stiff material does not readily accommadate the additional testing pressure. The pressure is thus borne by the pressuremeter sleeve which subsequent risk of probe failure.

Pressuremeters are also classified on the basis of insertion procedure. Three basic procedures are presently used and include the Prebored Pressuremeter Test (PMT), the Self-Boring Pressuremeter Test (SBPMT) and the Full Displacement Pressuremeter Test (FDPMT).

It can easily be seen that the amount of material distrubance can vary significantly from one instrument to the other. Furthermore, material disturbance becomes operator dependant for the PMT and SBPMT, which thus can be a source of variable results. The FDPMT creates the highest degree of material distrubance, however the disturbance becomes repeatable and is operator independant.

The applicablilty of the pressuremeter thus depends on the type of instrument used. The most common instrument is the PMT probe based on the Menard system, with a tricellular probe. The data for this probe is presented as volumetric strain at one minute after the pressure increment has been applied, versus the applied pressure. The PMT has been used to determine the modulus of deformation, E_m, and the limit pressure, P_l, directly from the primary data. Empirical correlations have also been derived to estimate the undrained shear strength and angle of internal friction. The Value of P_o is sometimes used as a crude estimate of the pre-existing lateral stress in the material. This is due to the disturbance which is created during the pre-boring stage.

Efforts to minimize this disturbance have given rise to the SBPMT. The instrument is essentially a thick-walled probe with a hollow core through which material is displaced to accomodate the probe. The problem of borehole wall compaction and disturbance are thus reduced substantially with this instrument. One should be advised that the SBPMT is a high cost method and the amount of borehole disturbance is dependant on operator characteristics. The probe can be used to determine the materials' strength and deformational characteristics with the same accuracy as the PMT.

The ideally less disturbed borehole conditions makes the SBPMT the most appropriate of the pressuremeter type tests for the determination of in situ stresses. The SBPMT insertion procedure has not as yet been standardized and the range of procedures in use are generally very slow and thus costly. In an effort to reduce the standardization problem Fahey (159) has evaluated the disturbance effects of five different SBPMT systems. Fahey took the approach of causing a disturbance by varying certain parameters, such as bit size, and recording the corresponding effect on the angle of internal friction and the dilatancy angle. The results indicated that the use of incorrect cutter settings increased the angle of internal friction by 4^{o} from 35^{o} to 39^{o}.

In an effort to reduce the costs which are normally associated with insertion for the SBPMT and to a lessor degree the PMT, the FDPMT was developed. Disturbance during probe installation is large but always repeatable. The costs involved with probe insertion and operator training are subtantially reduced. This probe type is generally of smaller diameter than the PMT or SBPMT in an effort to reduce probe wall friction during insertion. The data obtainable for material strength and stiffness are the same as for the PMT and SBPMT, and includes the angle of internal friction, shear modulus and undrained shear strength. Correlations with in situ stress are at best rough estimates due to insertion disturbance. The Shear Modulus for the FDPMT are calculated at 45% lateral displacement (160), this is compared to 15% lateral displacement for the PMT method. The full details of data interpretation are given in section 5.2.

5.1.6 Requirements For Mine Backfill Testing

The use and selection of an in situ test procedure for underground backfill testing is based primarily on the properties to be determined and desired accuracy. An additional constraint being the ability of the instrumentation to function efficiently in the hostile underground environment.

The primary purpose of conducting in situ tests as part of this project was to the determine reliable material properties for incorporating backfill into numerical models. Two sets of backfill properties are required, the first are the deformational properties which are used to represent the backfills' stress - strain characterisitcs in the linear range of material response, these consist of the shear modulus, G_p and the Menard deformation modulus, E_m. Next the backfills' failure characteristics need to be incorporated and thus the angle of internal friction and undrained shear strength need to be assessed. Furthermore, the in situ lateral stress would be an asset in the verification of the numerical model.

The review of available testing equipment has indicated that the cone penetration group of tests and the pressuremeter tests are applicable for physical and mechanical properties of sands and sand - like materials. Each of these test types have verified correlations already established, however the experiences with the pressuremeter are derived from "direct" measurements while the cone penetration type tests make use of empirical correlations and may

be applicable only in certain soil types. Thus, the pressuremeter offers greater potential for testing in a new material such as mine backfills. This conclusion is also reflected in Table 5.1. The Penetrometer type tests are rated at a "moderate" to "limited applicability" for the determination of the angle of internal friction, undrained shear strength and modulus of deformation. On the other hand the pressuremeter is rated as "highly applicable" for the assessment of these parameters. It is thus clear that the pressuremeter is the most appropriate instrumentation for determining the mechanical properties of mine backfills. This instrument also gives an estimate of in situ lateral stress.

Having decided upon the pressuremeter, a number of particular instruments are available and include the PMT, SBPMT and the FDPMT which have been described in the previous section. The main consideration in choosing from the available instrumentation was the applicabilty of the equipment and testing procedure to the range of underground mining environments normally encountered. These include the space limitations encountered in cut and fill mining, and the accessibility problems encountered in room and pillar, and blasthole stopes. The problems of testing underground are further extended to mobility of men and equipment, and the availability and accessibility of suitable drilling equipment for drilling undisturbed holes to be used for pressuremeter tests. The inaccessability of appropriate drilling equipment is a major problem if the PMT, or SBPMT systems are used. As such the full displacement pressuremeter test fills the practicle requirement of

doing a large number of tests in a varity of underground environments. The equipment for FDPMT insertion was not available at the begining of the this project and had to be developed. The developments are described in detail in section 5.4.

The pressuremeter chosen was the Pencel pressuremeter. The Pencel (162) is a 32 mm diameter, strain controlled, monocellular, full displacement probe instrument. The operating range is between 0 and 90 cc volume displacement at a maximum working pressure of 2500 kPa. The testing procedure consists of 18 equal steps of volume, V, in increments of 5 cc. The pressure, P, is noted at 30 seconds intervals at the end of each step. It has also been illustrated (163) that for monocellular probes with length to diameter ratios of greater than 6.5 the data obtained is similar to the data from a tricellular probe. This has been theoretically demonstrated in section 5.3.

5.2 Pressuremeter Data Interpretation

In this section the precise equations and processes required for the derivation of strength and stiffness characterisitcs of mine backfills from pressuremeter data is presented. The properties of interest include the angle of internal friction, the undrained shear strength and the moduli of shear and deformation. Furthermore the equations for the derivation of in situ stress are also presented.

Although a number of individual references are quoted, Wroth (151) and Baguelin (161) have exhaustively covered the interpretation of pressuremeter data. Typical pressuremeter data is presented in Figure 5.1. This data has been corrected for dilation in the pressurized lines and the inertia of the pressuremeter sleeve. The data in this form is now ready for subsequent processing into mechanical parameters.

5.2.1 Shear And Deformation Moduli

The shear modulus is the first parameter to be extracted from Figure 5.1. The derivation of the shear modulus G_m, is based on the Lame equation for the expansion of a cavity in an infinitely elastic medium (164) and is interpreted from the linear portion of the pressuremeter P-V curve. It can conveniently be represented in mathematical form as:

$$G_m = V_m \frac{\Delta P}{\Delta V} \qquad \text{..... 5.1}$$

The deformation modulus, E_m, is subsequently related to the shear modulus by the following:

$$E_m = 2(1+\nu)G_m \qquad \text{..... 5.2}$$

where: G_m = Shear Modulus

E_m = Deformation Modulus

V_m = Volume at Mid-Height of Linear Portion of Figure 5.1.

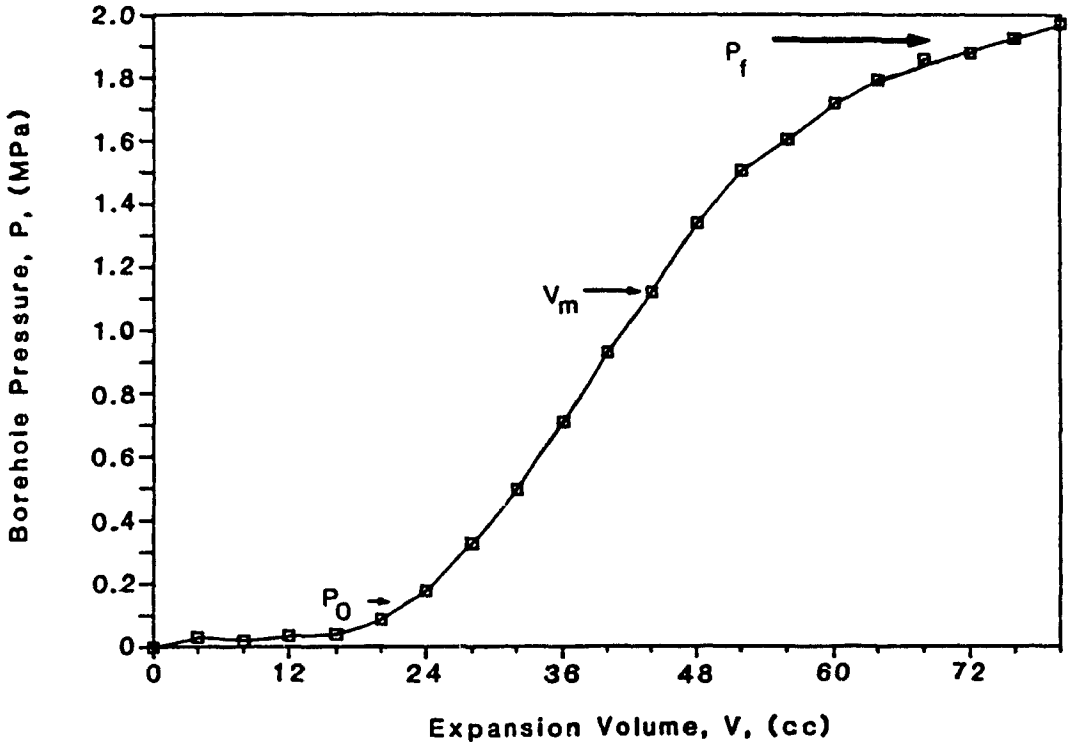

FIGURE 5.1 Typical Pressuremeter Data

P = Incremental Change in Pressure

V = Incremental Change in Volume

υ = Poisson's Ratio (assumed =.33)

5.2.2 In Situ Lateral Stress

The in situ lateral stress is estimated by the "take off" pressure (161), P_o, as illustrated in Figure 5.1. The use of the FDPMT yields a borehole with compacted walls, and a redistributed stress field. Thus, the data achieved can only serve as a crude estimate of lateral stress. Furthermore, the FDPMT data in many instances does not exhibit a take off pressure as the instrument remains in close contact with the borehole walls.

The lateral scress has also been related to the angle of internal friction. The coefficient of earth pressure at rest K_o, represents the ratio of lateral to vertical stress due to self weight and can be estimated by the equation:

$$K_o = 1 - \sin(\varphi) \qquad \text{..... 5.3}$$

where K_o = the ratio between the lateral stress to the vertical stress

Furthermore, the vertical stress can be obtained from backfill density and depth. Each of these data analysis methods will be evaluated as part of this thesis and are presented in Chapter 8.

5.2.3 Limit Pressure And Undrained Shear Strength

The limit pressure is defined as the pressure at double the initial volume of the pressuremeter. The operating volume of the Pencel is a maximum of 90 cc, with the initial volume of the pressuremeter being 230 cc. Thus it can easily be imagined that a method of extrapolating the experimental data to the theoretical definition of limit pressure is required. To this end four methods of data extrapolation have been reviewed by Piciacchia (158), and briefly listed here. The commonly used extrapolation methods include:

1. The Manual or Visual Method
2. Log - Log Method
3. Relative Volume
4. Inverse Volume Method

In methods 2,3 and 4 the objective is to linearize the volume displacement curve and then extrapolate the curve to twice the inital volume of the probe, thus obtaining the limit pressure. Conversely, the manual method is simply an observational method. It is see that the curve presented in Figure 5.1 tends to flatten out within the operating range of the test instrument, thus a visual asymptote is used to estimate the Limit pressure. It has been found that regardless of the method used the estimated limit pressure remains consistent.

The inverse volume method is used to estimate the limit pressure for purposes of this thesis. The method involves the development of a linear relation between the cell pressure, P and the inverse of the volume, 1/V. The relation is then extrapolated to 230 cc of injected volume, thus yielding the theoretical value for limit pressure.

Several approaches exist to obtain the undrained shear strength from the pressuremeter. The major theories are based on elastic - plastic assumptions. Three theoretical solutions have been reviewed (161). Setting Poissons' ratio to .5 (undrained loading) the three equations reviewed by Baguelin all reduce to:

$$P_{lc} = S_u \frac{[\ 1 + \ln (\ E\ )]}{3S_u} \qquad \ldots\ldots\ 5.4$$

where: P_{lc} = Limit Pressure (corrected for insitu stress)

$P_{lc} = P_l - P_o$

P_l = Limit Pressure

P_o = Take - Off Pressure

S_u = Undrained Shear Strength

E = Modulus of Deformation

Alternately, Amar (165) and Le Centre d'Etudes Menard (166) have proposed two empirical equations which have been reviewed by Felio (167),

$$S_u = \frac{P_{lc}}{10} + 25 \text{ kPa} \qquad \ldots\ldots 5.5$$

$$S_u = \frac{P_{lc}}{5.5} \qquad \ldots\ldots 5.6$$

It should be noted that each of these equations require the pre-existing horizontal stress which is estimated from the take off pressure, P_o. As such the evaluation of S_u is prone to the same source of error as the estimate of in situ lateral stress. For purposes of this study equations 5.5 and 5.6 will be evaluated in Chapter 8.

5.2.4 The Angle Of Internal Friction

The angle of internal friction has been found (168) to be related to the limit pressure by the relation:

$$P_{lc} = b\, 2^{[(\varphi - 24)/4]} \qquad \ldots\ldots 5.7$$

where: b = a constant which is material dependant

and = 1.8 for homogeneous, wet soil

= 3.5 for heterogeneous, dry soil

= 2.5 on average

We note that this particular formulation requires the in

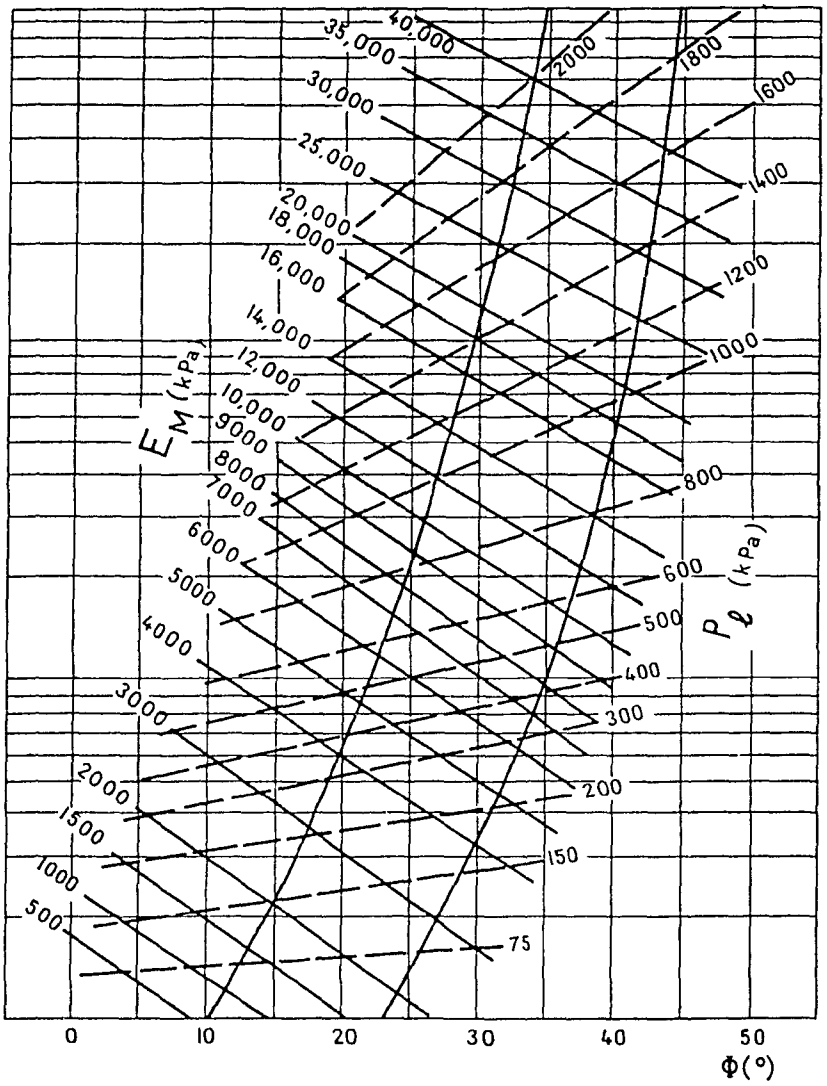

FIGURE 5.2 Empirical Correlation For Determining Angle Of Internal Friction - (After Calhoon [169])

situ lateral stress to be known. As such the equation is prone to the same limitations as the evaluation of the undrained shear strength.

Calhoon (169), has proposed an empirical method of deducing the angle of internal friction. The angle is graphically evaluated from the limit pressure, P_l and the Modulus of Deformation, E_m. The graph has been reproduced in Figure 5.2.

Furthermore, given equation 5.7 and Figure 5.2 an alternate means of estimating the lateral stress is evident. The limit pressure and the deformation modulus can be used to estimate the angle of internal friction using Figure 5.2. Subsequently, the angle of internal friction can be used in conjunction with equation 5.7 to yield the in situ lateral stress.

5.3 Theoretical Pressuremeter Considerations

The purpose of these theoretical studies is to assess the stress and strain distributions which occurs in the volume of influence of the pressuremeter during the testing procedure. The original pressuremeters where designed with three pressure cells; two gaurd cells and a testing cell. The purpose of the gaurd cells is to ensure that the deformation geometry of the test cell remains uniform throughout its length. The existing theoretical pressuremeter work (170,171,172,173,174) has been based on the expansion of a "cylindrical" cavity in an infinite elastic medium being tested under plane strain, undrained conditions.

The generated stress gradient has been expressed mathematically by Gibson (170) and reviewed by Palmer (171). The equation is based on the assumption that a uniform deformation occurs throughout the length of the pressuremeter testing cell. As such the equations employ a two dimensional simplification which is appropriate for tricellular probes. With this limitation in mind Fyffe (172) re-introduced the Gibson equations as:

$$(\sigma_r - \sigma_\theta) = \frac{2\ dp}{d\ (\ln \Delta V/V)} \qquad \ldots\ldots\ 5.8$$

This equation implies that the generated stress gradient can easily be obtained from the slope of the data plot relating change in $\ln(\Delta V/V)$ to change in pressure.

In a similar vein Fyffe (172) and Baguelin (173) have presented equations relating the generated radial and circumferential strains to injected volume, for tests conducted under conditions which are identical to those for equation 5.8.

$$e_r = 1 - (1 - \Delta V/V)^{1/2} \qquad \ldots\ldots\ 5.9$$

$$e_\theta = 1 - (1 - \Delta V/V)^{-1/2} \qquad \ldots\ldots\ 5.10$$

Houlsby (174), has related the generated radial pressure with the material to the test cell internal pressure and the materials' angle of internal friction. The following equation was presented.

$$\sigma_{ri} = \psi / [a/r_i]^{N-1} \quad \text{..... 5.11}$$

where: ψ = internal cell pressure

a = cell diameter

r_i = point of interest in material

N = constant dependant on the angle of internal friction

$$N = \frac{1 - \sin(\varphi)}{1 + \sin(\varphi)} \quad \text{..... 5.12}$$

However, equations 5.8 to 5.12 are only valid under the assumption that the deformation geometry is uniform along the entire length of the pressuremeter probe. Figure 5.3 illustrates the expanded geometry, in air, of a monocellular probe. It can thus be seen that the deformation geomerty is anything but uniform. In fact it was found that an ellipsoidal geometry best described the probe deformation. Using this deformation concept new equations have been developed as part of this thesis for use with the monocellular type probes, the details of which are contained in Appendix 4. The following sections present the relevant equations and the methodology for their derivation.

5.3.1 Displacement Geometry And Strain Evaluation

Figure 5.4 illustrates the anticipated deformation geometry. It was noted that the deformation at any point on the pressuremeter surface can be expressed in terms of the maximum displacement at y=0, the mid-height of the pressuremeter. Thus the pressuremeter

FIGURE 5.3 Expanded Monocellular Pressuremeter In Air

displacement at the mid-height has been expressed in terms of pressuremeter dimensions and injected volume in the following equation:

$$\delta = (r_o^2 + 3/2\ \frac{\Delta V}{\pi L})^{\frac{1}{2}} - r_o \qquad \text{..... 5.13}$$

Furthermore the displacement at any point on the pressuremeter surface can be expressed as a function of injected volume and distance from the mid-height.

$$\delta\ (\Delta V,Z) = = \frac{1}{L}\left[3/2\ \frac{\Delta V}{\pi L}\ (L^2 - 4Z^2) + r_o^2 L^2\right]^{\frac{1}{2}} - r_o \qquad \text{..... 5.14}$$

This equation can thus be used to illustrate the deformation geometry at various injected volumes. Figure 5.5 illustrates the deformation geometry for 25, 45 and 90 cc. of injected volume. This diagram further illustrates that the deformation model correctly predicts a zero displacement at the pressuremeter abutments. Equation 5.14 can be rewritten in terms of the instrument l/d ratio. This has been rewritten as equation 5.15.

$$\delta(\Delta V, Z) = \frac{1}{n r_o}\left[\frac{3}{4}\frac{\Delta V}{n r_o}\left(n^2 r_o^2 - z^2\right)\right] + n^2 r_o^4\Big]^{\frac{1}{2}} - r_o \qquad \text{..... 5.15}$$

Equation 5.15, has subsequently been used to produce Figure 5.6. This figure plots displacement differance between the probes mid-height and a point half-way to the abutment. These displacement differences are plotted for injected volumes of 45, 90 and 120 cc. If the 90 cc injected volume curves are used then the conclusion is

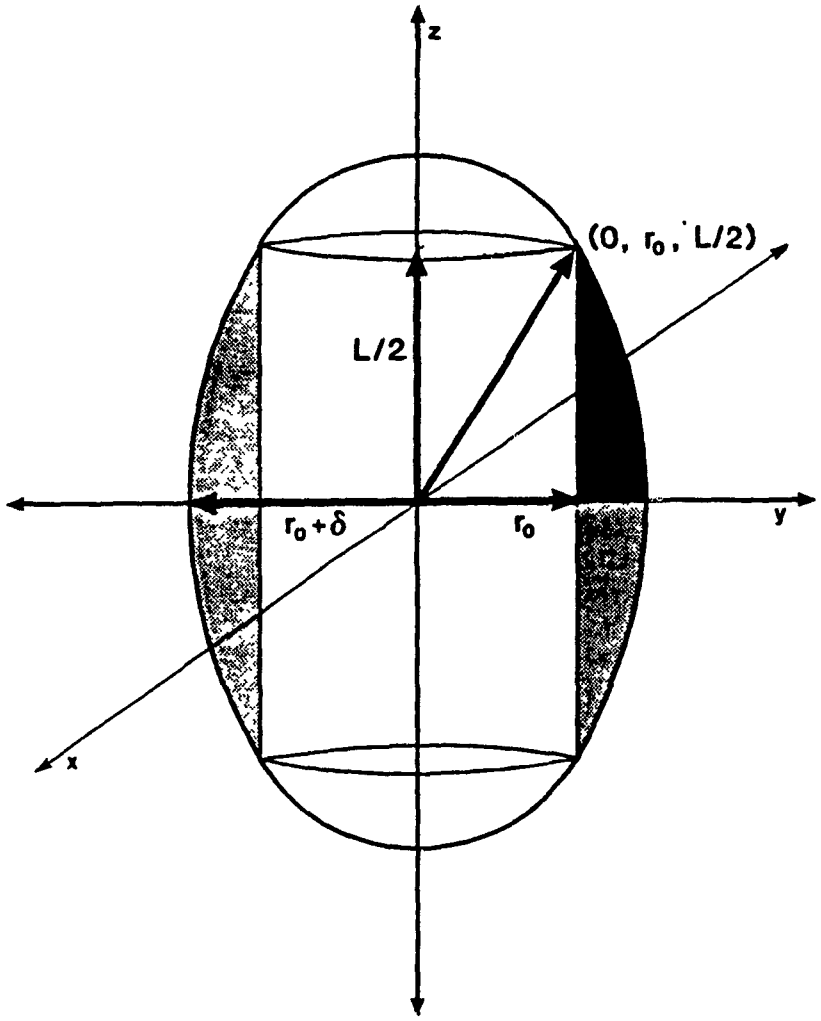

FIGURE 5.4 Idealized Monocellular Probe Deformation

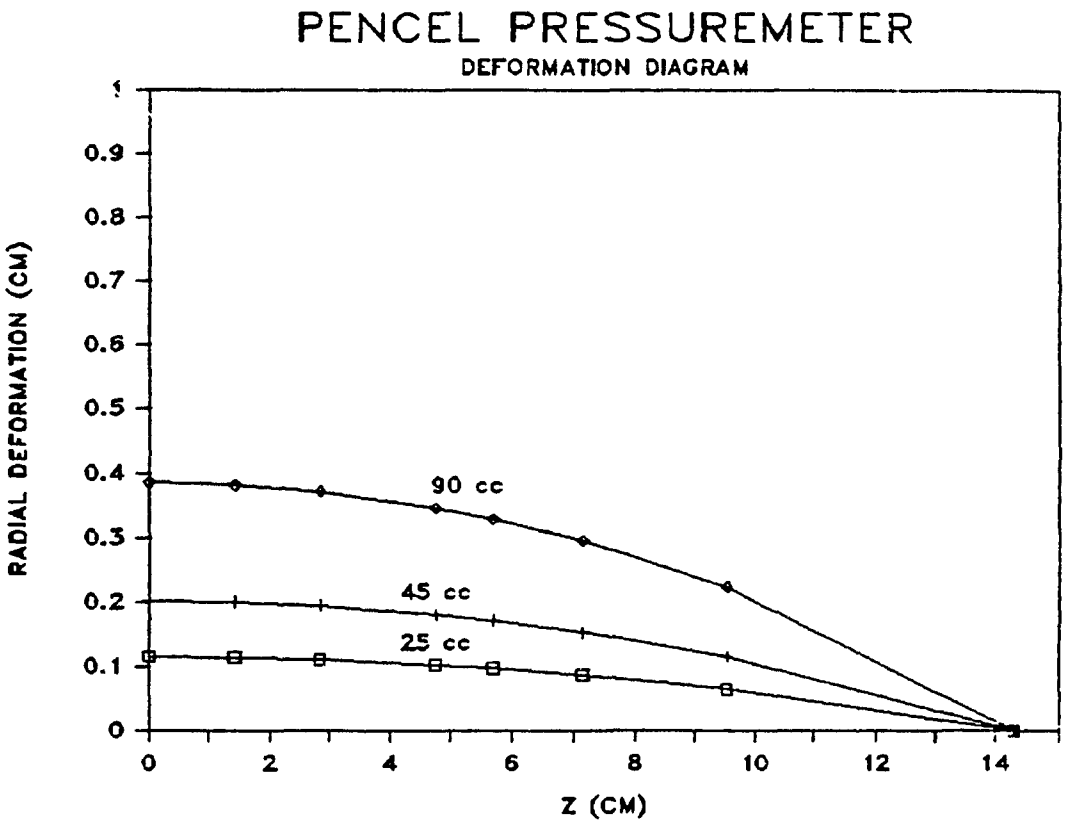

FIGURE 5.5 Deformation Prediction Diagram

that the displacement difference between these two points becomes negligible (.025 cm.) for an l/d ratio of 6.5. This conclusion is consistant with that of Capelle (163). In fact, an new ASTM standard is presently being set for the full displacement pressuremeter and the recommended l/d ratio is 6.5.

The circumferential and radial strains are developed from the basic equations:

$$e_\theta = \frac{y}{r-y} \qquad \text{..... 5.16}$$

$$e_r = \frac{1}{1+e_\theta} - 1 \qquad \text{..... 5.17}$$

Equation 5.16 is used in conjunction with equation 5.14 to develop the circumferential strain equation 5.18. This equation is subsequently used in association with equation 5.17 to develop the radial strain equation 5.19.

$$e_\theta(\Delta V,Z) = [1 - \delta(\Delta V,Z)(\frac{2+\delta(\Delta V,Z)}{r^2})]^{-\frac{1}{2}} - 1 \qquad \text{..... 5.18}$$

$$e_r(\Delta V,Z) = [1 - \delta(\Delta V,Z)(\frac{2+\delta(\Delta V,Z)}{r^2})]^{\frac{1}{2}} - 1 \qquad \text{..... 5.19}$$

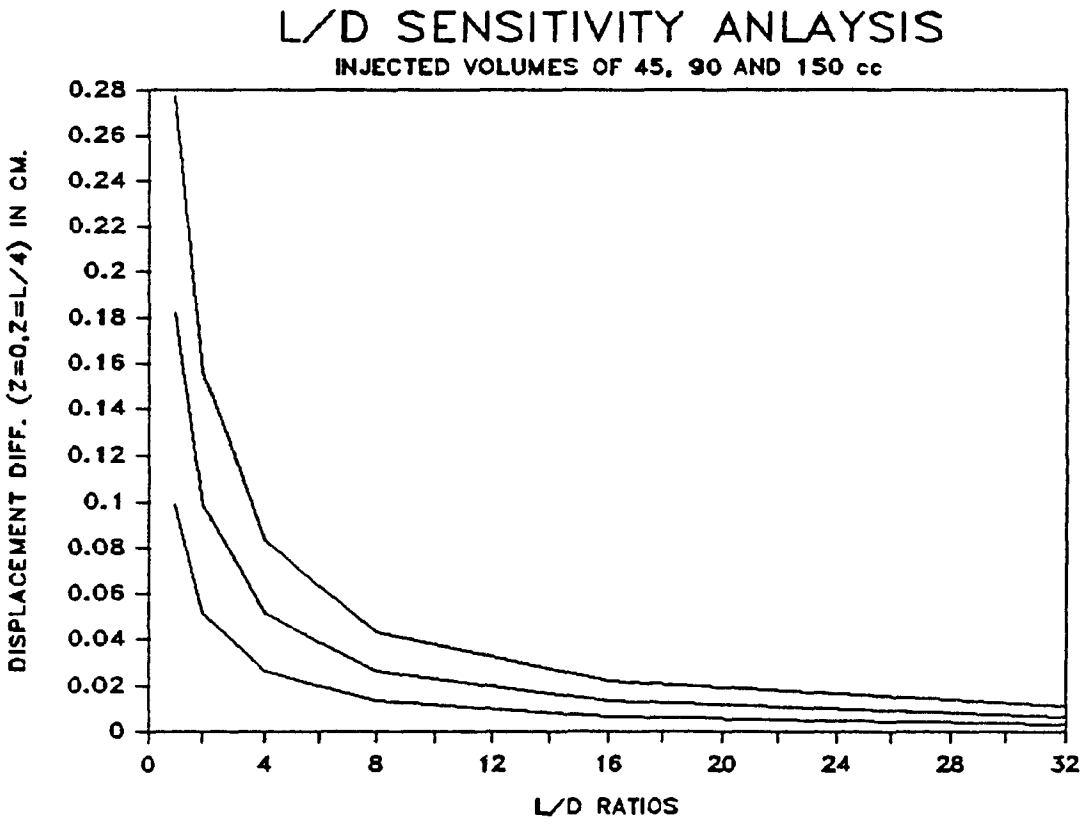

FIGURE 5.6 Length To Diameter Sensitivity Analysis

5.3.2 Stress Gradient And Generated Radial Stresses

The stress gradient equation developed from the radial equilibrium equations for the stresses is written:

$$\frac{rd\sigma_r}{dr} = \sigma_\theta - \sigma_r = -\phi(e_\theta) \qquad \text{..... 5.20}$$

It has been shown, in Appendix 4, that this equation after due substitutions and intergration becomes:

$$\phi(\delta) = \delta(1+\delta)(2+\delta)\psi'(\delta) \qquad \text{..... 5.21}$$

where: δ is defined by equation 5.14

Palmer (171) found that this equation could further be simplified and represented in such a manner that the stress gradient is given by twice the slope of the plot of ln (Δ V/V) vs. pressure. This has been accomplished by setting a function f(x) to,

$$f(x) = \delta(\delta+1)(\delta+2) \qquad \text{..... 5.22}$$

and seeking a second function g(x) such that,

$$f(x) = \frac{1}{g'(x)} \rightarrow g'(x) = \frac{1}{f(x)} \qquad \text{..... 5.23}$$

hence,

$$g(x) = \int \frac{1}{f(x)} \qquad \text{..... 5.24}$$

and equation 5.24 can be rewritten as:

$$g(x) = \frac{2}{D} \int \frac{x}{x^3 + Ex^2 + Fx + G}\, dx \qquad \text{..... 5.25}$$

where:

$A = 1.5 \,/\, \pi\, L$

$B = -6 \,/\, \pi\, L^3$

$C = (r_o)^2\, L^2$

$D = A + B\, Z^2$

$E = 3\, (1 - r_o)$

$F = [3\, (r_o)^2 - 6\, r_o + 2]$

$G = -\, [\, (r_o)^3 - 3\, (r_o)^2 + 2\, r_o]$

$X = (D \Delta V + C)$

The integral in equation 5.25 after several manipulations and substitutions reduces to

$$g(x) = \frac{1}{D} ln\left(\frac{x - \frac{E}{3} - 1}{x - \frac{E}{3} + 1} \right) + \frac{E}{3D}\, ln\left\{ \frac{(x - \frac{E}{3} - 1)\,(x - \frac{E}{3} + 1)}{x - \frac{E}{3}} \right\} \Bigg| \qquad \text{..... 5.26}$$

and the stress gradient equation can be rewritten as

$$\phi(\Delta V, Z) = \frac{d\psi}{dg(\Delta V, Z)} \qquad \text{..... 5.27}$$

In looking at the radial stresses generated by the pressuremeter while the test is in progress Houlsby (174) found the following

equation based on the stress equilibrium equations held true:

$$\frac{\Psi_r}{\sigma_r} = \left[\frac{r_o}{r_1}\right]^{N-1} \qquad \text{..... 5.28}$$

where, ψ , is the internal cell pressure. This is an applicable method for tricellular probes where ψ is always in the radial direction. However, given that the deformation geometry is not uniform throughout the probe length ψ is not applied radially throughout the probe. Pressure vessel theory dictates that the internal pressure, ψ , is always perpendicular to the interior surface of the probe, thus the radial internal pressure can be defined as a function of applied pressure, injected volume and location on the probe surface. This has been represented mathematically as:

$$\Psi_r = \frac{\psi\left(r_o^2 + \frac{3}{2}\frac{\Delta V}{\pi L}\right)^{\frac{1}{2}}}{\frac{1}{L}\left[\left(r_o^2 + \frac{3\Delta V}{2\pi L}\right)L^2 - \frac{6\Delta V Z^2}{\pi L}\right]^{\frac{1}{2}}} \qquad \text{..... 5.29}$$

Lastly, the radial stress at any point in the material being tested is defined by the combination of equations 5.27 and 5.28. and yields:

$$\Psi_r\left[\frac{r_o}{r_1}\right]^{1-N} = \sigma_r \qquad \text{..... 5.30}$$

Equations 5.18 and 5.19 along with equation 5.30 can be used to convert pressuremeter volumetric displacement - stress data to radial or circumferential stress - strain curves at any point in the test media.

It can be shown using equations 5.29 and 5.30 that if the Pencel pressuremeter is inflated to its' rated pressure of 2500 kpa the stress generated at the instruments mid-height, in a material with angle of internal friction of 32^{o}, would reduced to 5% or 125 kpa 2.5 radii from the instruments center. This is an important conclusion as it provides a means of determining minimum spacing requirements between pressuremeter test holes. For instance if the disturbance created by 125 kpa stress is acceptable then two test holes spaced 5 pressuremeter diameters (17.7 cm) apart could be considered as undisturbed in relation to the influence of adjacent holes.

5.4 Practical Considerations

The Pencel Pressuremeter has been developed extensively by civil engineers as a method for acquiring foundation design parameters for footings, piles, pavements and laterally loaded pylons. Each of these applications allows probe insertion by feed pressure provided by large surface drilling equipment which are not readily available in underground mines, where available space is often restrictive. Thus an alternate insertion system was developed for these studies, which comprises a heavy duty frame, 10 tonne hydraulic ram with a 1.1 m stroke and an air powered hydraulics control unit, Figure 5.7. A simple, rugged instrument for underground use the Pencel pressuremeter was selected.

The frame disassembles into components no larger than .8 x .8 m in size and so is capable of transport via confined spaces such as raises. The air powered hydraulic system was chosen due to the

ready availability of compressed air and the absence of electrical power in many underground mine locations. The maximum operating pressure of 35 MPa is achieved with .85 cu m/min. of compressed air at 415 kPa gauge pressure. This insertion system proved to be inexpensive and versitile in use, both on surface and in several different underground situations.

Four frame anchoring systems were also developed and tested. The first and simplest anchoring method for both surface and underground locations, where the roof was nonexistent or inaccessible, was to load two large plates on either side of the frame with waste rock or backfill, Figure 5.8. This requires the use of a LHD to handle the required volume of anchoring material. Alternately, when such vechiles were not available it was also possible to anchor the frame with double flighted, .15 m diameter, anchoring augers drilled to 1m depth with a hand - held, rotary drill, Figure 5.9. Next, where the roof was easily accessible, with 2.5 to 3 m of available height, the top of the frame was propped to the roof with timber cribbing, Figure 5.10. This system provided the quickest means of providing a rigid and stable frame assembly to counteract the stresses associated with forcing the pressuremeter probe and insertion rods up to 10 m into the various backfill types tested. Lastly, where the only access to the material to be tested is via a bulkhead, the frame is mounted horizontially and supported by 25 mm wire cables, Figure 5.11. This insertion method has proved effective to date in backfill of up to 65 Mpa in stiffness, beyond which pre-drilled holes have required.

FIGURE 5.7 Insertion Unit And Hydraulic Power Pack

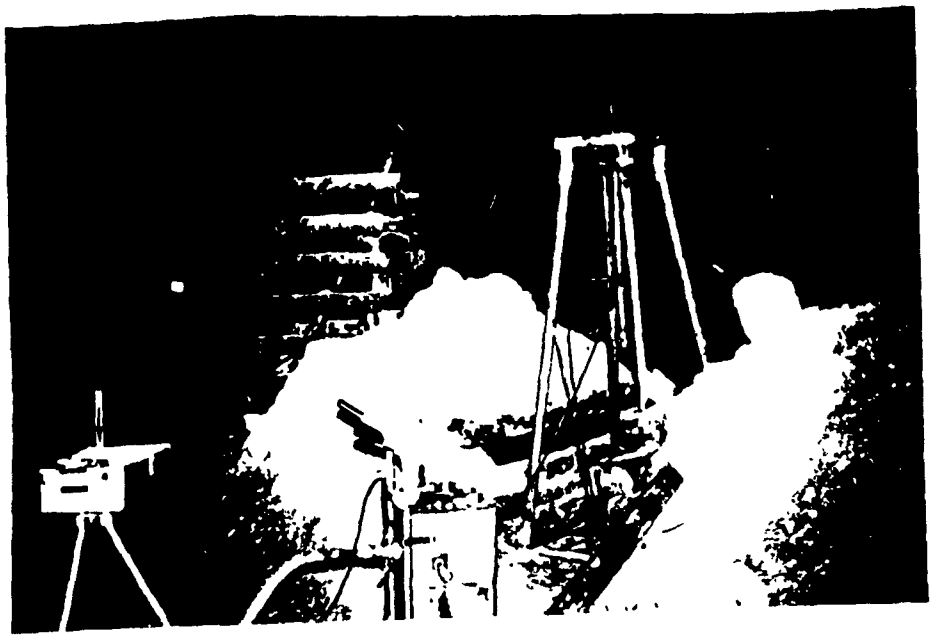

FIGURE 5.8 Anchoring System Using Muck Anchoring

5.5 Summary

This chapter has reviewed the role of in situ testing in engineering practice. A rationale for the selection of the appropriate testing equipment has been presented and possible equipment selections for the purposes of this project have been reviewed. The two basic categories of tests which would appear applicable for backfill testing are penetrometer type tests and the pressuremeter tests. Individual testing methods have been critically reviewed in section 5.1. The pressuremeter has emerged as the most appropriate instrument for backfill testing and the rationale for this selection has been presented.

The various options for the interpretation of pressuremeter data have been explored and the limitations outlined. Furthermore, a model has been developed which represents the generated strains and stress during a monocellular pressuremeter test. Lastly, an outline of the equipment and testing procedures developed as part of this project has been presented.

FIGURE 5.9 Anchoring System Using Auger Anchors

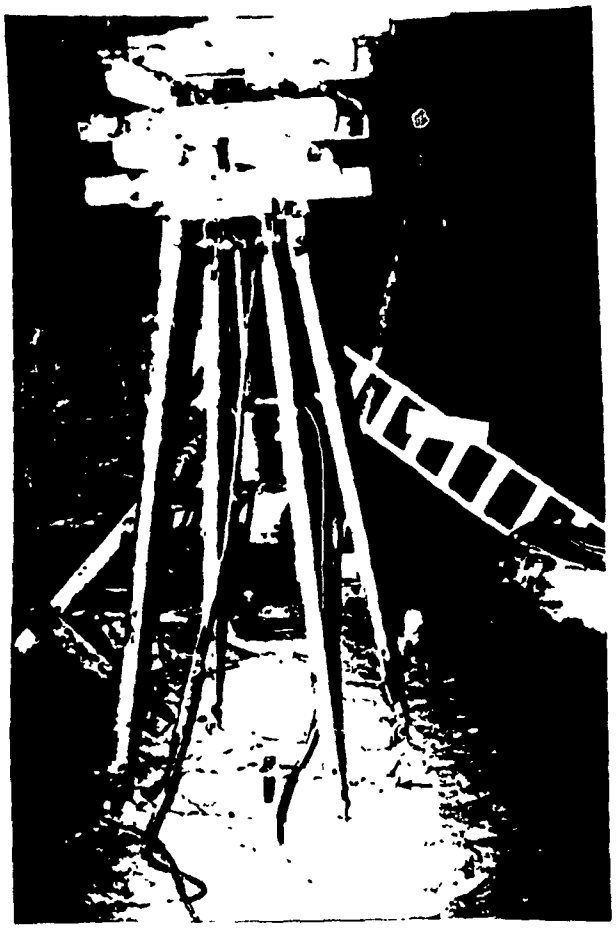

FIGURE 5.10 Anchoring System Using Wood Cribbing

FIGURE 5.11 Bulkhead Anchoring System Using Cables

6.0 MINE BACKFILL LABORATORY TESTING TECHNIQUES

The main objective of the laboratory testing program was to develop a backfill material properties data base from which a series of design equations could be developed and verified with field observations. To this end two categories of tests were performed. The objective of the first was to describe the physical properties of the available backfill materials. In the second instance the goal was to determine the geomechanical characteristics of these same backfill materials. The intent was then to match the physical and mechanical properties into a series of design equations.

With the objective having been defined, a battery of physical and geomechanical tests were conducted on the array of backfill materials accumulated from ten different mines in Quebec, Ontario and Manitoba. The physical properties tests included mineralogical analysis, determination of density, analysis of particle shape and grading, and the determination of optimum moisture content. The tests conducted for the determination of the geomechanical properties of backfills depended on the textural classification of the material to be tested. These materials included fine sandfills, coarse rockfills, and well graded rockfill material. It was evident that the applicability of tests conventionally conducted on fine grained materials to coarse ones was questionable. Therefore one set of tests, the tilt box test, was adopted for rockfill and another, the soil shear test, for uncemented sandfills. Design equations for cemented backfills have been developed from around 430 observations accumulated from published data.

The objective of this chapter is to describe the laboratory tests which were conducted for the determination of the physical and mechanical properties of mine backfills.

6.1 Backfill Physical Properties

Prior to undertaking any mechanical testing a number of physical properties require to be determined, both for the test specimens and the material particles.

The chemical characteristics of the backfill material were determined from the scanning electron microscope. Furthermore, representative material from each mine was used to determine material grading curves. The specific gravity of solids were determined with the null - pycnometer and the scanning electron microscope was further used to determine particle angularity.

The physical characteristics required for the test specimens stems from measurement moisture content. Having determined this property the dry density and void ratio can be determined from sample weight and specific gravity of solids respectively.

6.1.1 Determination Of Density

Two densities are required; the density of backfill particles and that of the samples tested. In the first instance we wish to determine the specific gravity of soilds. The specific gravity of soilds is defined as the ratio of a given volume of

material to the weight of an equivalent volume of water. The procedure for determining the specific gravity is outlined in (175), ASTM standard D854 - 58. The Quantachrome Corporation PY-5 Null Pycnometer (176) was used to determine the specific gravity of particles. The basic premise of the Pycnometer is to precisely measure the volume of a given weight of dried material. The Null Pycnometer used accurately measures the volume of particles to ±.33%, thus this is the accuracy to which specific gravity is measured.

The second procedure is used to determine the dry density and void ratio of the test specimens. Moist samples were measured and weighed prior to testing, thus a moist density could be calculated. The moisture content was determined (177) after the specimen was tested, hence the dry density could be determined. Lastly, the specific gravity of the solids and the dry density are used along with equation 2.1 to determine the void ratio of each sample tested.

6.1.2 Grading And Particle Shape Analysis

The method used to determine particle grading and shape depended on the textural classification of the material. For instance the fine sandfill required a procedure of sieve and hydrometer tests while the rockfills required screen and/or a manual dimensioning procedure.

The procedure used for grain size analysis of the fine grained material was consistent with ASTM D422 - 63 (178). The sieve analysis was conducted with a ten sieve stack with size ranges between 10 and 200 mesh. The material which passed the 200 mesh sieve was then used for the hydrometer analysis, with the 152-H type hydrometer.

This procedure was not applicable for the rockfill materials. A modified procedure was adopted whereby the rockfill was separated by a continuous, coarse screening. A screen stack of six screens, ranging in size between 20 mesh and 1.91 cm., was used. The oversized material was manually graded by measuring two particle dimensions and individual particle weight. A minimum of 200 particles were measured in this fashion for each rockfill material. The dimensioning portion of the grading data was also used to determine the coefficent of sphericity for the coarse fraction.

Representative samples of the fine grained material were scanned under the Joel 77 electron microscope at a magnification of 150 times. The Particle Recognition and Characterization (PRC) (179) data aquisition program was used to determine the particle angularity. Multiple frames were analysed so that between 400 and 700 particles were measured.

6.1.3 Determination Of Optimum Moisture Content

The testing procedure for determining optimum moisture content of granular materials is well documented and widely accepted. The test has often been termed the Proctor Test with two testing procedures being acceptable (180),(181). For the purposes of this thesis standard compaction was achieved with a 4.54 kg. hammer dropped from a 457mm height. This is the procedure outlined in ASTM D1557 - 78.

6.1.4 Mineralogical Investigations

The mineralogical investigation for each backfill material employed the use of the scanning electron microscope. This was used for the determination of elemental configurations of individual particles. The electron microscope enabled the isolation of individual particle on which a spectral analysis can be performed. The elemental data along with a visual assessment of particle structure provides a means of determining the minerology of the particle. Furthermore an overall spectral analysis can be conducted on the entire specimen, the height of the peaks recorded could theoretically be used to determine the elemental concentration in the sample.

The JOEL JSM - T300 (183) with the Tracor Northern (184) TN 5000 series Analyszer and asssociated software was used for this part of the work. The analyszer uses an x-ray diffraction method for particle analysis.

6.2 Determination Of Backfill Strength And Stiffness Characteristics

Prior to embarking on a laboratory testing program it was felt important to characterize the material to be tested. Upon further examination it was found that the materials fell into two broad categories: cemented and uncemented backfills. These two categories made logical sense as the parameters which enhance inherant strength and stiffness characteristics are different for each category. That is, for cemented backfills, the amount of cementing agent, curing period and moisture content are of greatest importance to stiffness and strength. Design equations for cemented backfills should thus be expressed in terms of these parameters. Upon considering uncemented backfills it was found that the important parameters are void ratio and degree of saturation. Therefore, in a similar manner as for cemented backfills, design equations for uncemented backfills should be expressed in terms of void ratio and degree of saturation. The available laboratory equipment enabled the testing of cemented and uncemented hydraulic fills and uncemented rockfills. The geomechanical properties of cemented rockfills were not determined as part of this study.

The design equations for cemented backfills have been developed from close to 430 observations accumulated from published data. Furthermore, 50 uniaxial compressive tests were conducted to verify the developed equations.

The testing program for uncemented backfill materials was undertaken by soil shear box testing. The testing covered material from five different mines and was conducted under conditions of

varying moisture contents and void ratios. In total 220 samples were tested in the soil shear box arrangement.

The question of determining the shear strength of uncemented rockfills with varying textural classifications brings with it a score of associated problems. This is due to the coarse grading of these materials. A testing procedure was proposed by Barton (5) which offers great potential in determining rockfill strength. A total of 100 box table tests were conducted, as part of this study, on mine rockfill materials from four different sources and with varying textures and degree of compaction.

The tilt box test requires supporting data in the form of surface base friction characteristics and uniaxial compressive strength of the rockfill particles. To this end the joint shear box test was used on saw cut rock samples for the determination of the base friction angle of the material, 4 such tests were conducted on each of four rockfill materials. In addition the uniaxial compressive strength of the material is also required. It was realized that the material was not suitable for coring and testing in uniaxial compression, thus some form of index test was required. The point load test was selected to fill this need and a total of 20 tests were conducted on each of the rockfill aggregates, (188,195).

6.2.1 Analysis Of Published Cemented Backfill Data

The literature contains abundant information on the variation of uniaxial compressive strength with the content of normal Portland cement, based on the testing of 152.4 mm diameter samples. The data accumulated in this study, represents test

results reported from 30 authors and more than 40 different mills representing mostly Canadian mines.

The number of observations of uniaxial compressive strength under varying cementing conditions have been tabulated in Table 6.1. These have further been separated in terms of observations at each curing time. The most abundant data was that for the 28 day cured samples. The tailings to cement ratios ranged from 40:1 to 5:1.

CURING TIME	NUMBER OF OBSERVATIONS OF U.C.S. vs. CEMENT CONTENT
7 DAYS	99
14 DAYS	76
28 DAYS	189
90 DAYS	66

TABLE 6.1 Availability And Demograhics of Published Cemented Backfill Uniaxial Compressive Strength Data

A statistical analysis package (SAS) was used to to correlate the reported uniaxial compressive strengths to the physical parameters which included cement content, curing time and moisture content. One possible source of error results from the degree of particle coating as a result of cement addition on a by weight basis. The problem can be rectified by converting cement additon to a per volume basis. However the specific gravity of solids is not reported in many instance which thus reduces the available data base.

6.2.2 Uniaxial Compressive Strength And Stiffness

Fifty uniaxial compressive tests were conducted on fine grained hydraulic backfills from Kiena Mines and Campbell Red Lake Mines.

The tests were conducted on 101.6 mm diameter cylinders of 20:1 cemented backfills and comply with ASTM D1633 - 33, (182). The Wykeham Farrance WF10072 100 kN press was used and the testing rate was .3 mm/min. Sample densities, void ratios and moisture content were measured for each sample. Furthermore, samples were allowed to cure for varying lengths of time under a range of curing conditions.

The cast samples from Campbell Red Lake had cured in an underground environment for a period of 28 days prior to being shipped to Montreal. The sample travelled a distance of 2500 km. and had been poorly packed, thus the Campbell Red Lake data from the ten samples tested should be viewed with caution.

NUMBER OF SAMPLES	MOIST CURING	DRY CURING	TOTAL CURING
10	14	52	66
10	35	0	35
10	35	7	42
10	63	4	67

TABLE 6.2 Curing Characteristics of Tested Uniaxial 20:1 Cemented Backfill Cylinders - Kiena Mine.

The cast cylinders from Kiena were encased within a backfill matrix in the transportation drum and were allowed to cure in this fashion for a period of 14 days. A total of forty samples were retrieved at that point and each was allowed to cure for different lengths of time under either moist or dry conditons. The precise conditions of curing are illustrated in Table 6.2.

6.2.3 Soil Shear Box Testing

Soil shearbox test were conducted on 220 - 101.6 mm square samples for uncemented backfills. Test were conducted with a standard soil shear box with load, lateral displacement and veritical dilation being measured. This enabled the measurement of shear strength, stiffness index Gp, and intermittent void ratio. These measurements were in keeping with ASTM D3080 - 72, (185) and Wray (186) and were conducted at 390, 780 and 1200 N nominal normal pressure.

The cemented samples were cured under the same conditions as the uniaxial samples illustrated in Table 6.2 and were tested at the same time as the uniaxial specimens. The testing rate for these samples was .5mm/min.

The uncemented samples were first brought to standard compaction as illustrated in 6.1.3. This was done for material at optimum moisture as well as above and below optimum moisture. Furthermore a series of tests were conducted for samples compacted at optimum moisture content and dried to 60% and 5% of optimum moisture. The overall strategy was to control the void ratio by

varying compaction moisture and subsequently controlling test sample moisture by drying samples for varying lengths of time, whilst observing the effects of changing these parameters on the failure envelope of the material. All tests were conducted at .5mm/min.

6.2.4 Tilt Box Tests

The testing of uncemented rockfills presents new challanges owing to the coarseness of these materials. Some testing data from civil engineering dam projects have been reported (4),(7), these, however, have been generated from triaxial tests on 1.05m diameter samples. This would not be a practicle means of testing for rockfills at mine sites as the required equipment is expensive and cumbersome. It was thus intented to determine the shear strength of uncemented rockfills in a fashion which is easily accessible to mine operators while maintaining high standards for data integrity. Barton (5) proposed one such test which is based on the determination of an equivalent roughness coefficent (R) and equivalent strength (S). The equivalent strength (S) is dependant the intact uniaxial strength of the fill aggregate and the U_{50} of the fill material, the precise relationship is illustrated in Figure 6.1.

Barton further proposed that the roughness coefficent could be determined by two methods. The first was through the estimation of particle angularity and porosity followed by the use of Figure 6.2 to determine R. The second method was to determine R by back - calculation and thus the usage of the tilt table test. It was

proposed that R could be back-calculated by the equation:

$$R = \frac{\alpha - \varphi_b}{\log\ (S/.\sigma_{no'})} \qquad \ldots\ldots\ 6.1$$

where: α = tilt angle at failure during test
φ_b = basic angle of internal friction
S = equivalent strength parameter
σ_n = normal stress of sample during testing

Equation 6.1 is then substituted into equation 6.2 where the angle of internal friction can be determined for a range of normal pressures.

$$\varphi = R \log\ (S\ /\ \sigma_n) + \varphi_b \qquad \ldots\ldots\ 6.2$$

where: σ_n = normal stress

Equation 6.2 thus implies that the total friction angle is comprised of two components, a basic friction angle and a stress, roughness, strength dependant component. In order to find the failure envelope these two components need to be defined. The base friction angle is determined by the joint shear test on saw - cut joints (6.2.5). The material strength is determined by the point load test (6.2.6). Thus the only parameter required at this stage is the roughness coefficent, equation 6.1. Having determined the base friction angle and the material strength then the tilt angle and the the normal load during the test need be determined. The normal load is easily calculated from the specific gravity of solids and the weight and volume of material above the failure plane. The tilt angle is determined by conducting the test.

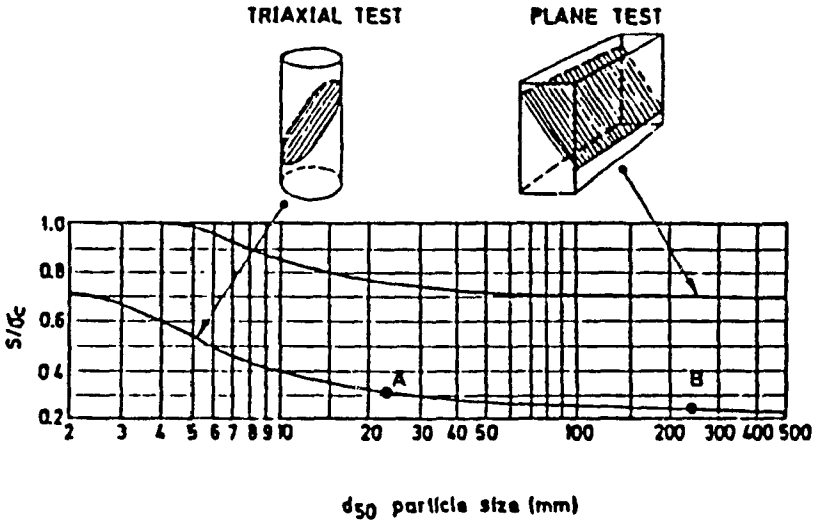

FIGURE 6.1 Method Of Estimating Equivalent Strength (After Barton [5])

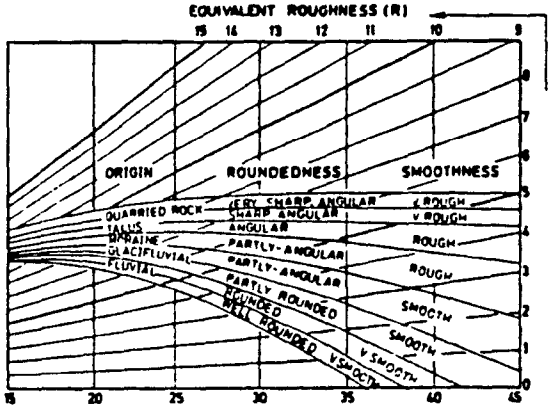

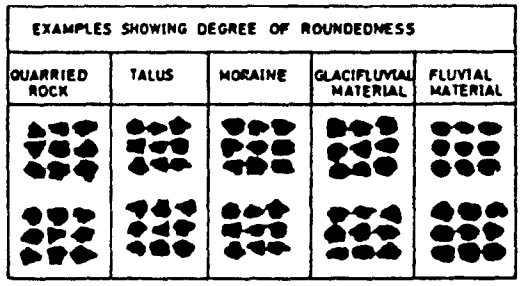

FIGURE 6.2 Method Of Estimating Equivalent Roughness (After Barton [5])

Barton proposed this method but did not propose guidelines for box construction and dimensioning. It is further implied that actual tests were never carried out to verify his hypothesis. Thus a set of guidelines were developed, the size of the required box was based on the size of the material which was to be tested. The rule of thumb used was to make the minimum dimension of the box 30 times the U_{50} of the material or 10 times the U_{max} whichever is greater. The testing apparatus and procedure used as part of this study was developed at McGill based on initial study of Bartons' (5) work. The testing apparatus is illustrated in Figure 6.3a. Figure 6.3a further illustrates a test at the onset of failure while Figure 6.3b illustrates the vibratory compaction system used. The containment area provides room for samples of up to .6 m^3 of material. Taking the box dimensions into consideration equation 6.1 can be rewritten to provide a roughness coefficent directly from the tilt height and the specific gravity of sample (equation 6.3).

$$R = \frac{SIN^{-1}(t/23.8) - \varphi_b}{LOG(S/.00034\gamma_s \times COS[SIN^{-1}(t/23.8)]} \qquad \ldots\ldots 6.3$$

where: t = tilt height
γ_s = specific gravity of sample

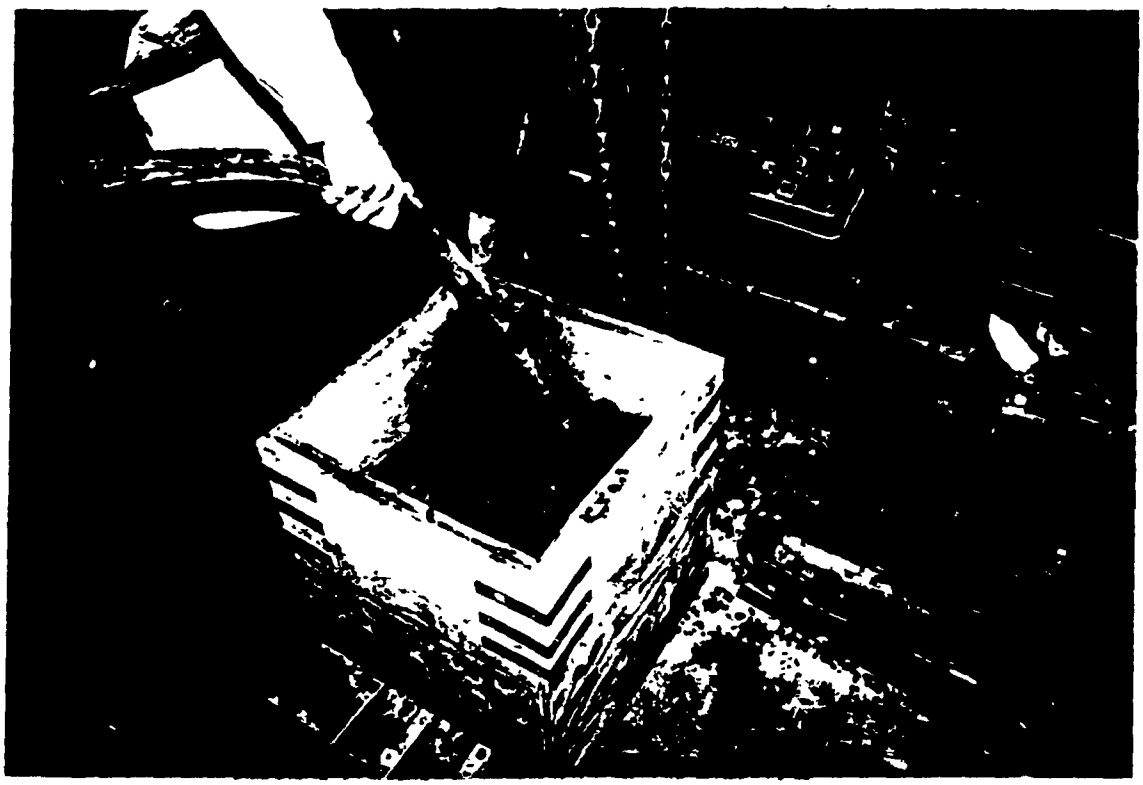

FIGURE 6.3 (A) Sample Preparation And Compaction For The Tilt Box Test

FIGURE 6.3 (B) Tilt Box Test At Point Of Failure

A total of 100 tests were conducted for nine differently graded material from four mine sites. Testing was conducted under compactions of 0, 15, 30 and 1 minute vibration times, and the tests were repeated five times under a particular set of conditions. The vibrator was a 25.4mm diameter probe - type instrument, vibrating at 10,000 vibrations per minute. The tests indicated excellent repeatability, with the tilt angle variations within a particular test group showing variation between .31^{o} and 1^{o}.

6.2.5 Joint Shear Box Tests

The joint shear box tests were conducted to determine the base friction angle of the rockfill materials tested in the Tilt Table. Test specimens were made by saw - cutting a large fill particle, the measured surface area of each sample is given in Table 6.3. Samples were tested to ISRM standard (187), under normal loads of 10, 15 and 20 kN. Readings were taken every .03 mm of axial displacement.

MINE LOCATION	SPECIMEN AREA (CM^2)
BOUSQUET	77.42
SELBAIE	125.81
CHADBOURNE	51.6
HBM&S	41.94

TABLE 6.3 Shear Surface Area For Joint Shear Box Tests

6.2.6 Point Load Testing

The uniaxial compressive strength of the rockfill material needs to be determined in order to calculate an equivalent strength for insertion into equation 6.3. The material available was not large enough for coring and thus an index test was required. The point load test was selected as it is a widely accepted and well documented test. The procedure and analysis followed is that for lump samples (188,195), and 20 tests were conducted for each material type. The average variation in predicted uniaxial compressive strength for a material type was $\pm$6.7 MPa.

6.3 Summary

This chapter has summarized the laboratory tests which were conducted as part of this work. The tests were conducted to determine the physical and geomechanical properties of mine backfills. The applicable standards have been quoted although not expanded upon in the interest of brevity. Any variations from these standards have been mentioned and the particular testing conditions have been outlined.

7.0 PHYSICAL CHARACTERISTICS OF MINE TESTED BACKFILLS

The objective of this chapter is to describe the physical characteristics of the mine backfills tested. The physical properties covered in this chapter fall into two categories; physical properties of the backfill material (sections 7.1, 7.2 and 7.3) and properties of the test specimens (section 7.4). The individual properties used to describe the backfills tested include the material grading and particle shape, dry density and void ratio and permeability. The backfill material mineralogical composition, specific gravity and optimum moisture content are also used to characterize the materials tested.

This chapter further evaluates the consistancy of the seven permeability prediction equations listed in Section 3.3.6. Having evaluated their consistancy the use of these equations is commented upon and recommendations for determination of material permeability are made.

The use of a 25.4 mm diameter, 10,000 vib. / min., industrial vibrator was required for the compaction of rockfill samples in the tilt box tests. It was recognized that the vibration times and procedures for sample preparation were carried out without the benefit of knowing the precise effect vibration time had on void ratio. Thus it is further intended to evaluate the effectiveness of vibration time on the change in void ratio. The resultant relation can be used for future tilt table sample preparation and also to illustrate the benefits of vibratory compaction.

7.1 Mineralogical Composition

The objective of the mineralogical investigation was to define the chemical composition and mineralogical phases. Both these objectives were met by the scanning electron microscope. In the first instance, Figure 7.1, the chemical composition of the entire field is evaluated, with the relative heights of the spectral peaks being used to determine the relative proportions reported in Table 7.1. The table indicates that the most common elements found in the mine backfills examined included silica, sulphur, calcium and iron.

MINE LOCATION	ELEMENTAL PROPORTIONING (%)											
	Na	Mg	Al	Si	S	Cl	K	Ca	Fe	Cu	Zn	Ti
SIGMA	2.7	4.8	18.1	34.7	5.9	9.1	4.0	15.5	5.3	-	-	-
LACMAT	-	1.3	5.1	14.6	32.9	3.8	2.5	3.2	36.7	-	-	-
HBM&S	-	-	6.2	45.1	4.1	4.1	3.1	4.1	31.8	1.	.5	-
BOUS.	-	-	12.3	57.3	2.1	3.8	4.1	13.0	4.1	-	-	3.4
KIENA	1.2	2.4	9.7	39.3	5.3	5.8	3.6	20.9	11.7	-	-	-
DEN.	-	-	6.6	66.2	6.6	6.6	5.3	4.0	2.7	2.0	-	-
SELB.	-	4.3	8.6	62.9	5.7	2.9	3.8	2.9	9.1	-	-	-
CHAD.	-	-	4.4	26.3	10.1	6.0	3.2	7.3	42.7	-	-	-
REMNOR	-	-	4.4	26.3	10.1	6.0	3.2	7.3	42.7	-	-	-

TABLE 7.1 Elemental Composition of Mine Backfills

Although this table presents the elemental composition of the various backfills, it does not identify the material mineralogy. Thus, a series of spot analyses were initiated in which elemental analysis on individual material phases were conducted, Figure 7.2. The interpretation of the spot analysis directly gives the mineralogy of the phase being examined and the repetition of

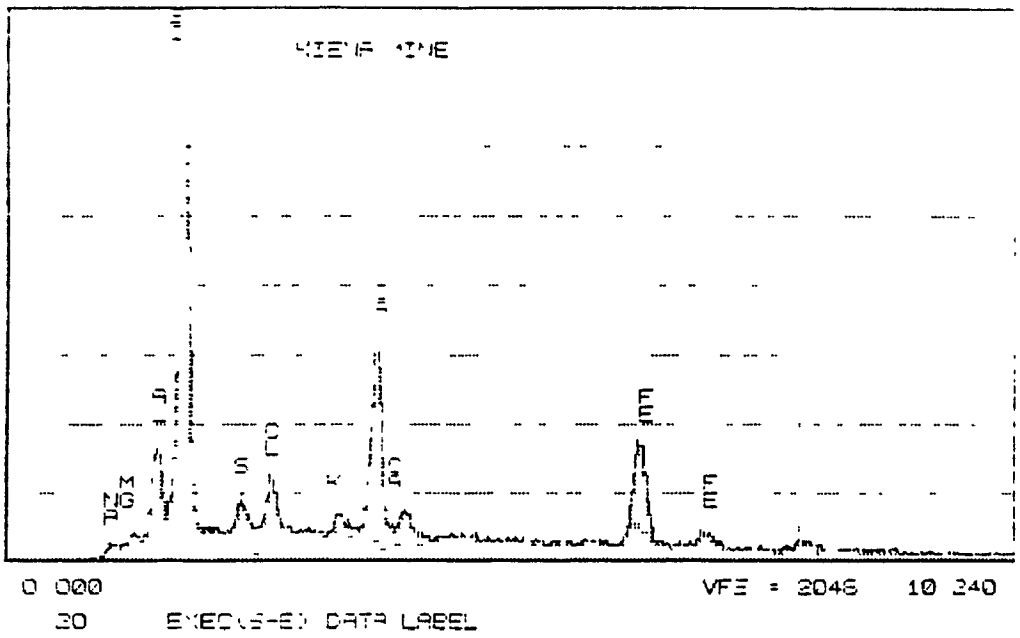

FIGURE 7.1 Global S.E.M. Spectrum Analysis - Kiena Mine

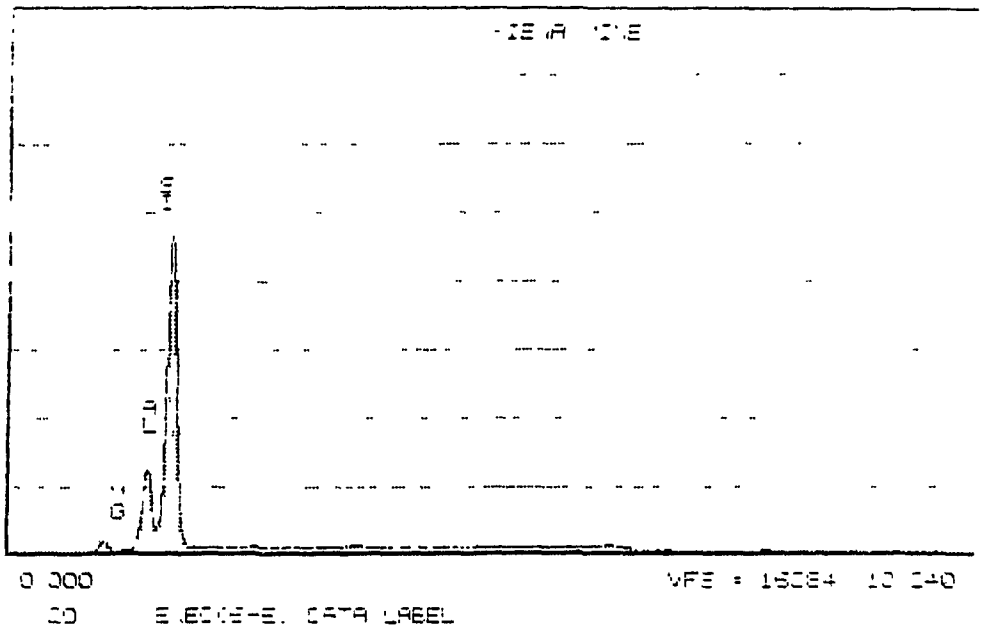

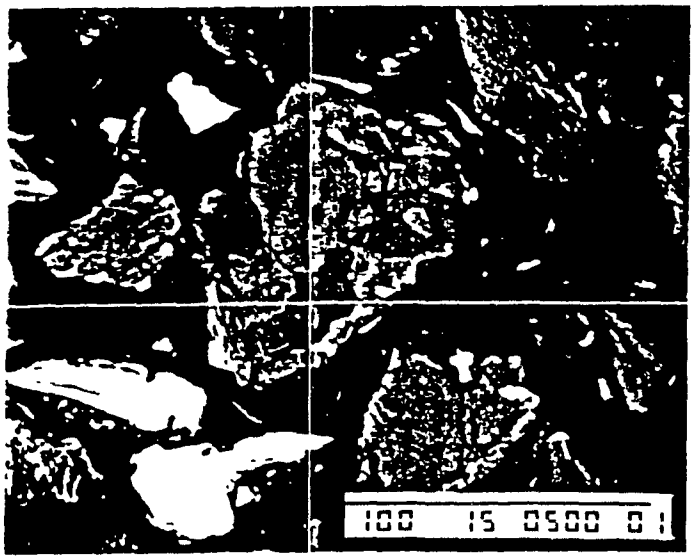

FIGURE 7.2 Spot S.E.M. Spectrum Analysis - Kiena Mine

this process for each phase present yielded the backfill mineralogy presented in Table 7.2. The global and spot spectrums along with the particle shape analysis for each of the backfills investigated is presented in Appendix 5.

MINE LOCATION	MINERALOGICAL COMPOSITION
LAC MATAGAMI	PYRITE, HAEMATITE, ALMANDINE
KIENA	PYRITE, DOLOMITE, KYANITE
SIGMA	PYRITE, DOLOMITE, PLAGIOCLASE
BOUSQUET	QUARTZ,PLAG.,AMPH.,ILMENITE
DENISON	PYRITE, QUARTZ
HBM&S	SLAG
CHADBOURNE	SLAG
SELBAIE	PYRITE,QUARTZ,PHYRRH.,GOETHITE
REMNOR	SLAG

TABLE 7.2 Mineralogical Composition of Mine Backfills

7.2 Specific Gravity Of Solids

The specific gravity of the materials tested ranged from 2.6 to 3.57. This range respresents the the wide assortment of mineralogical compositions encountered. The specific gravity for most of the tailing backfill is in the range 2.6 to 3.0 which is a relatively narrow band and is representative of a high silica content at the lower end of the scale and an even mixture of silica and sulphates at the higher end. Outside this band the materials with the higher specific gravities comprise the smelter slags used at Remnor, Chadbourne and HBM&S. The lone exception is the Lac Matagami material due to its' high content of sulphides and sulpates. Table 7.3 illustrates the specific gravities of eight of the mine backfills and have been derived from the pycnometer tests

as described in 6.2.1. The specific gravity of solids is subsequently used to convert the sample dry densities to void ratio.

MINE LOCATION	SPECIFIC GRAVITY
SIGMA	2.60
CHADBOURNE	3.41
REMNOR	3.41
LAC MATAGAMI	3.57
KIENA	2.82
DENISON	2.70
BOUSQUET	2.76
SELBAIE	3.00
HBM&S	3.48

TABLE 7.3 Specific Gravity of Mine Backfill Materials

7.3 Material Grading And Classification

The aim of this section is to describe the granulametric composition and particle structure of the range of mine backfills tested. This is done by describing the material grading and angularity. The material grading is then used in conjunction with the grading classification system (developed as part of this thesis) presented in section 2.1 to categorize the textural structure of the backfill materials.

7.3.1 Material Grading

The backfill materials examined as part of this study exhibit a wide range of grading characteristics. This is illustrated by the range of U_{10} values encountered. The values can be as low as 15.14 microns and as large as 42.17 mm. Similarly the

coefficient of uniformity ranges from 1.18 to 83.43. Large uniformity coefficients such as that exhibited by the Mine Selbaie material are typical of rockfill materials embedded in fine grained matrices. The matrix material yields a low U_{10} value while the coarse rockfill portion gives a large U_{60}, the combination of these two factors gives a large uniformity coefficient.

The individual material grading curves are presented in Appendix 6. Figure 7.3a and 7.3b illustrate the grading curves for the entire range of materials tested, from the fine grained tailings at Kiena to the coarse development waste at La Mine Bousquet.

	DIMENSIONS IN MICRONS				GRADING COEFF.	
MINE LOCATION	U_{10}	U_{30}	U_{50}	U_{60}	C_u	C_c
CHADBOURNE	11481.5	15848.9	17378.0	18071.7	1.57	1.21
LAC MATAGAMI	15.14	56.23	100.46	104.23	6.88	2.00
SIGMA	15.14	131.83	153.11	181.13	11.96	6.34
KIENA	10	38.02	70.8	89.13	8.91	1.62
REMNOR	749.3	1513.6	1972.4	2213.1	2.81	1.29
BOUSQUET	42169.7	53703.2	66834.4	74131.0	1.76	0.92
SELBAIE	158	1778.3	7943.3	13182.6	83.43	1.52
DENISON CLS.	177.83	331.13	478.6	630.96	3.55	1.29
DENISON UNC.	77.62	134.9	167.88	186.21	2.40	1.26
HBM&S (insitu)	2545.0	6309.6	10000.0	12023.0	4.72	1.30
HBM&S (regrade)	1230.3	2818.4	6456.5	25118.9	20.4	0.26
HBM&S -3/4,+1/2	13335.2	14454.4	15848.9	16218.1	1.22	0.97
HBM&S -1/2, +3m	7244.6	8128.3	9332.5	10000.0	1.38	0.91
HBM&S -3M, +4M	5000.4	5308.5	5623.4	5888.4	1.18	0.96
HBM&S +3/4						

TABLE 7.4 Backfill Grading and Particle Dimensioning

Although these curves provide a visual assessment of material grading and coarseness they are unwieldy in any analytical role. Therefore, the use of coefficents

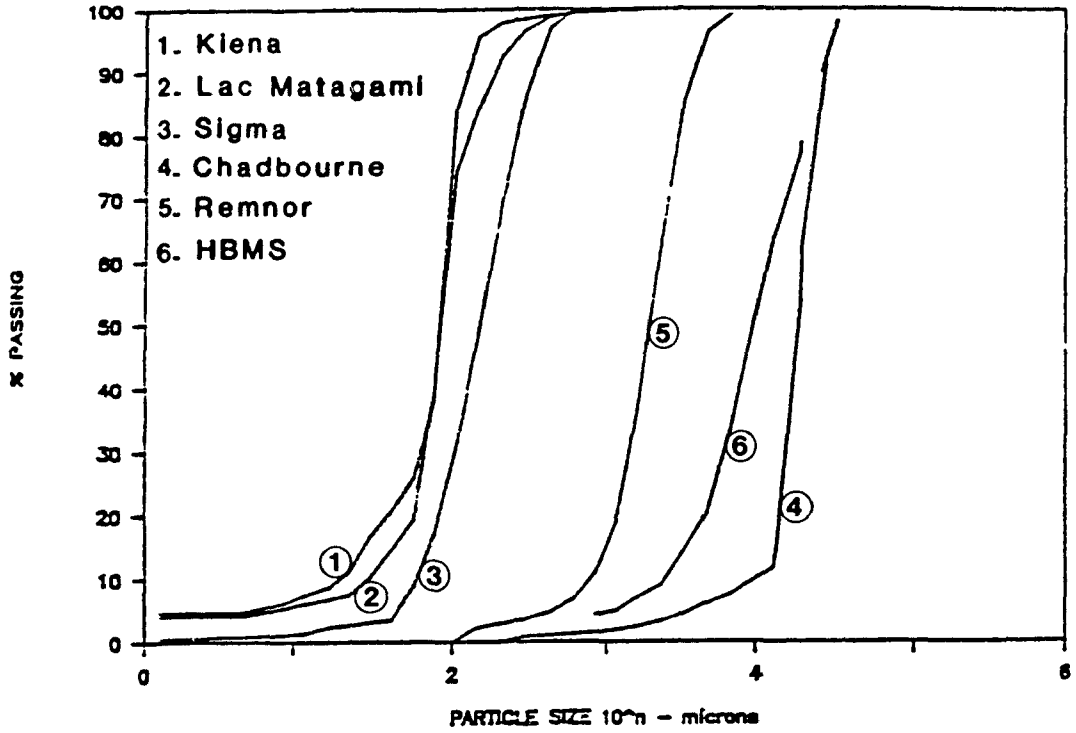

FIGURE 7.3 (A) Material Grading Curves

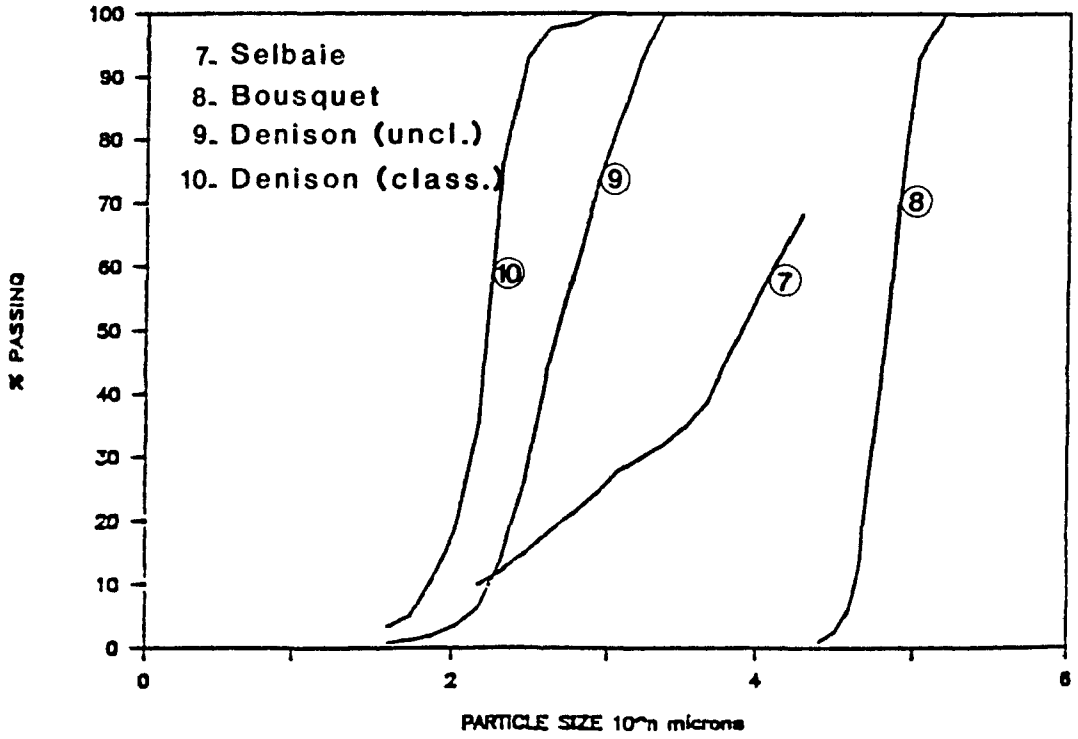

FIGURE 7.3 (B) Material Grading Curves

and representative grain sizes is often employed, as is the case in permeability models. Each of these are extracted directly from the curves and have been tabulated in Table 7.4. This table lists four representative grain sizes and two material coefficents; the coefficent of curvature C_c and the coefficent of uniformity, C_u.

The HBM&S material was used extensively for tilt box testing and the individual grain fractions were used to represent different material gradings. Figure 7.4 illustrates the different HBM&S material gradings employed for tilt box test and these gradings have been included in Table 7.4.

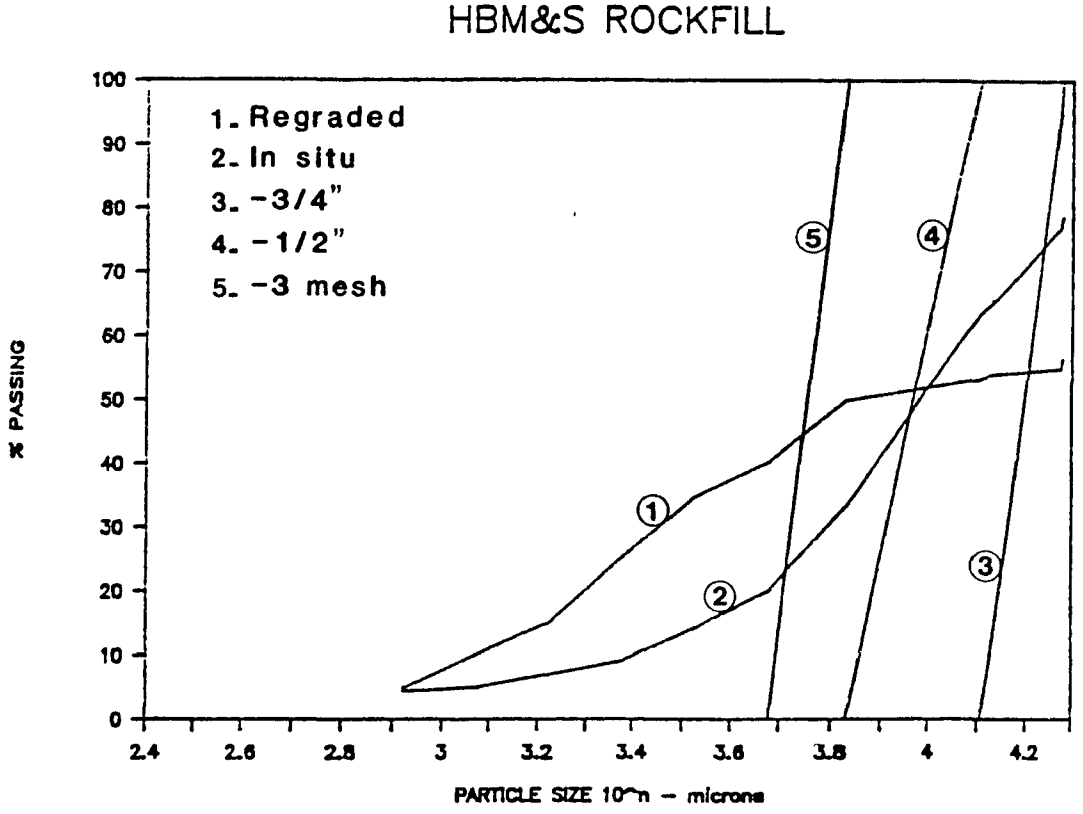

FIGURE 7.4 HBM&S MATERIAL GRADING CURVES FOR REGRADED SAMPLES

7.3.2 Particle Shape And Angularity

Nine backfill samples were examined under the scanning electron microscope and analyzed using its particle recognition and characterization software. This program has the ability to quantify particle dimensions and calulate the average crossectional area and perimeter dimensions of the particles. These are then used to calculate a particle shape factor. In addition the program automatically calculates an average aspect ratio for the particles encountered.

The data obtained is summarized in Table 7.5, which includes the number of particles measured, the aspect ratio, the coefficient of sphericity and the shape factor. It was found that the aspect ratio ranged from 2.6 to 11.3 and the coefficent of sphericity ranged from .09 to .39. Similarly the shape factor ranged from 1.3 to 2.94. These parameters are used later to verify their influence on the interlocking component of the angle of internal friction, φ_i .

MINE LOCATION	NUMBER OF PARTICLES	ASPECT RATIO	COEFFICENT OF SPHERICITY	SHAPE FACTOR
CHADBOURNE	338	7.77	.129	1.84
LAC MATAGAMI	689	2.60	.385	1.30
REMNOR	338	7.77	.129	1.84
SIGMA	390	5.85	.171	2.94
KIENA	404	3.93	.254	2.51
DENISON	323	9.37	.107	2.21
BOUSQUET	362	5.88	.170	1.40
SELBAIE	274	9.51	.105	2.16
HBM&S	353	11.30	.088	1.60

TABLE 7.5 Particle Shape and Angularity

7.3.3 Textural Classification

A textural classification system has been proposed in section 2.1 which encompasses the entire range of mine backfills encountered in practice. The classification system was applied to the backfill gradings described in Figure 7.3. The breakdown of the three major size fractions required to classify the backfills is reported in Table 7.6. The data in Table 7.6 is subsequently used to locate the individual material classification on Figure 7.5.

It is further noted that of the nine backfill classifications available on Figure 7.5, six are represented by the mine backfills of this study. This verifies the attempt made to test a wide range of material gradations as part of this study. It is noted that the three poles of the grading diagram are well represented and a number of intermediate gradations have also been considered.

MINE LOCATION	% FINE SANDS	% COARSE SANDS	% GRAVEL
CHADBOURNE	.5	14.5	85
LAC MATAGAMI	99	1	-
REMNOR	5	95	-
SIGMA	99	1	-
DENISON CLS.	31	69	-
DENISON UNC.	98	2	-
BOUSQUET	-	-	100
SELBAIE	17	61	22
HBM&S	5	65	30
HBM&S COMB.	3	45	52
KIENA	99	1	-

TABLE 7.6 Breakdown of Major Size Classes

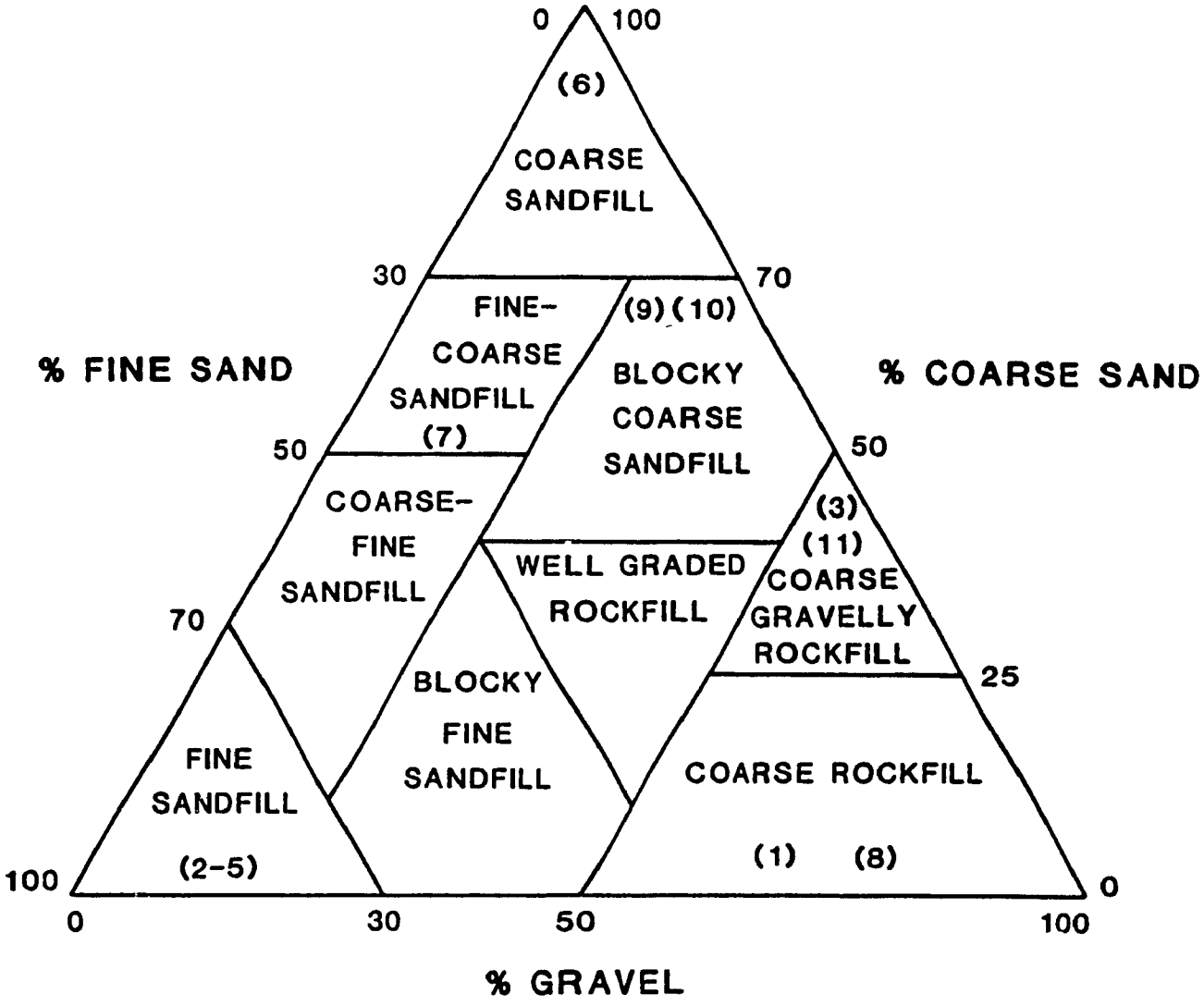

1- Chadbourne
2- Lac Matagami
3- Sigma
4- Kiena
5- Denison (unclassified)
6- Remnor
7- Denison (classified)
8- Bousquet
9- Selbaie
10- HBMS (in situ grading)
11- HBMS (regraded)

FIGURE 7.5 Textural Classification Of The Backfills Tested

7.4 Sample Properties

The physical properties described thus far apply to the individual grains of material used as backfill. However, once the material has been structured into a sample lattice, new properties are required to describe the sample and its structure. These properties include the sample dry density, void ratio and moisture content. Furthermore, void ratio is used in conjunction with the grading characteristics described in 7.3.1 to define the sample permeability.

It has long been realized that the moisture content of a soil sample during compaction has a direct effect on the sample void ratio. An optimum moisture content also exists at which a minimum void ratio is achieved. Section 7.4.1 thus reports on the optimum moisture content and resultant dry density and void ratio at standard compaction as described in 6.1.3.

7.4.1 Optimum Moisture Content

The optimum moisture content can only be determined for fine grained backfill materials, and thus could only be determined for five of the mine backfills examined. A typical proctor curve is illustrated for Denison classified backfill in Figure 7.6. The curve represents the plot of compaction moisture versus sample weight. The optimum moisture is defined as the moisture at which maximum sample weight is achieved. The Denison classified tailings, in the example, has an optimum moisture of 9.42%. Similar curves

have also been developed for the Lac Matagami, Sigma, Kiena and Denison unclassified materials and are presented in Appendix 7.

The compaction moisture can also be reduced after compaction to yield drier samples as represented by the curves in Figure 7.7. These curves represent samples with moisture contents ranging from 0% to 100% of the compaction moisture. The bottom curve, representing 0% of proctor moisture has been used to calculate the sample dry density. This format of proctor curve presentation has been adopted for each of the mines listed above and reported in Appendix 7.

The data extracted from these curves have been summarized in Table 7.7. The table indicates that the optimum moisture ranges from 9.42% to 15.6% for the materials listed. The calculated void ratio, however, indicated a more consitent trend with void ratios between .29 and .38, with an some values of .45 for the Kiena backfill.

MINE LOCATION	OPTIMUM MOISTURE	OPTIMUM DRY DENSITY	OPTIMUM VOID RATIO
LAC MATAGAMI	12.9	2.58	.38
KIENA	15.6	1.94	.45
SIGMA	15.0	1.91	.36
DENISON UNC.	13.9	2.00	.35
DENISON CLS.	9.4	2.10	.29

TABLE 7.7 Description of Optimum Physical Parameters

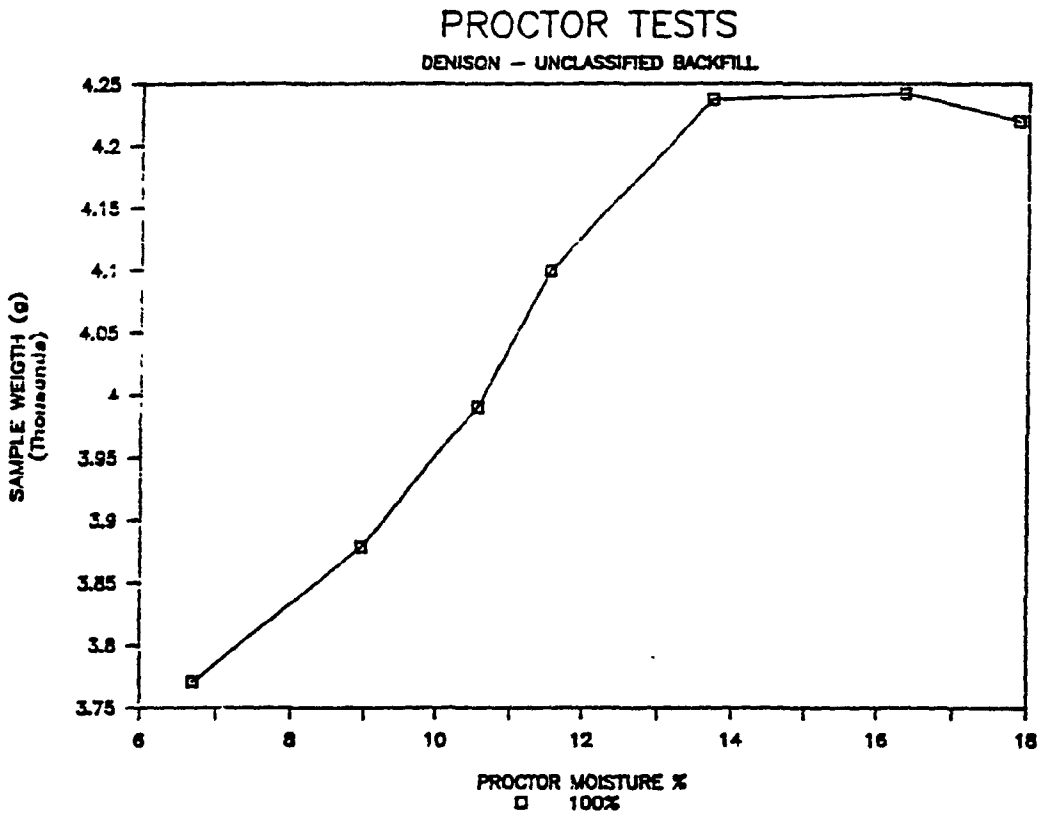

FIGURE 7.6 Typical Proctor Test Results - Denison Mine

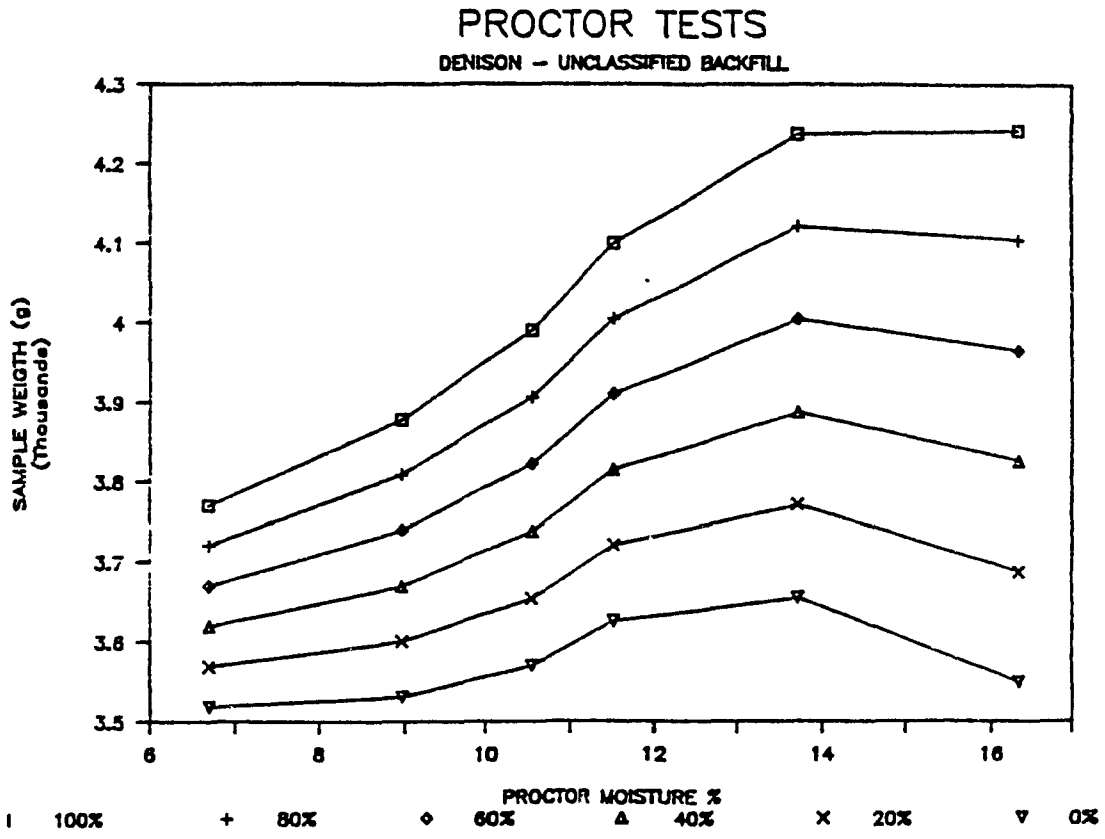

FIGURE 7.7 Modified Proctor Analysis - Denison

7.4.2 Density and Moisture Content

The tested backfill samples were prepared under a variety of conditions. The aim of sample preparation was to vary void ratio. This was achieved through vibration compaction for the tilt box tests and by varying the compaction moisture for the soil shearbox tests. A total of 64 sample groups were incorporated into this study and the sample conditions are reported in Appendix 8. The nominal sample conditions are reported in Table 7.8. The void ratios for the soil shearbox tests varied from .30 to .82 while the moisture content ranged from .063% to 18.24%. The ranges for the tilt tests were between .30 and 2.59 for the void ratio and the samples were tested in a dry state.

MINE LOCATION	AVERAGE DRY DENSITY	AVERAGE VOID RATIO	AVERAGE MOISTURE CONTENT
SIGMA	1.46	.78	8.00 %
LAC MATAGAMI	1.73	.61	5.31 %
DENISON CLS.	2.00	.35	4.36 %
DENISON UNC.	1.67	.62	8.54 %
CHADBOURNE	2.11	.62	-
SELBAIE	1.77	.69	-
BOUSQUET	1.27	1.17	-
UNVIBRATED HBM&S			
HBM&S #1	2.68	.57	-
HBM&S #2	1.78	.96	-
HBM&S -3m,+4m	1.63	1.13	-
HBM&S -1/2,+3m	1.32	1.64	-
HBM&S +1/2,-3/4	1.41	1.47	-
HBM&S +3/4	.97	2.59	-

Table 7.8 Average Physical Properties For Tested Materials

7.4.3 Sample Permeability

Seven permeability equations have been presented in section 3.3.6, four were presented by Bates and individual equations were set forth by Casagrande, Hazen and Shahabi. The Casagrande equation requires laboratory permeability data to be of any use and has thus not been considered further. Each of the six remaining permeability equations have been evaluated and their limits of applicability defined. The data presented in Table 7.9 indicates that none of the permeability equations give reasonable results for materials with U_{50} values of greater than 480 microns. The study of permeability characteristics of coarse grained materials should thus be the focus of future research.

It is further evident that two distinct formulations of permeability equations exist. The two groups consist of those equations which make use of material grading characterisitics only (equations 3.22, 3.25 and 3.26), and those which also make use of void ratio (equations 3.24, 3.27 and 3.28).

The first group of equations shows little consistency in predicting permeability for any of the materials. The variation in predicted permeability using the Hazen and two of the Bates (3.25 and 3.26) equations range from close agreement in one instance to a 21 fold difference in another material.

A similar inconsistency is evident in the second group of equations. Three equations fall into this category and include the

TABLE 7.9 Analysis Of Available Permeability Equations

MINE	D10	D50	Cu	Vr (Min.)	Vr (Max.)	EQUATION 3.5 HAZEN'S (cm/sec)	EQUATION 3.7 SHAHABI'S (Min) (cm/sec)	EQUATION 3.7 SHAHABI'S (Max) (cm/sec)	EQUATION 3.10 BATES 81 (Min) (cm/sec)	EQUATION 3.10 BATES 81 (Max) (cm/sec)	EQUATION 3.9 BATES 82 (cm/sec)	EQUATION 3.8 BATES 83 (cm/sec)	EQUATION 3.11 BATES 84 (Min) (cm/sec)	EQUATION 3.11 BATES 84 (Max) (cm/sec)
BIBRA	15.14	153.11	11.96	0.71	0.82	0.000229	0.037360	0.054075	0.000671	0.001210	0.000438	0.004221	0.000345	0.000694
LAC RATAGAMI	15.14	100.46	6.88	0.44	0.66	0.000229	0.007033	0.020589	0.000073	0.000387	0.000483	0.000888	0.000028	0.000132
DENISON UNC	77.62	167.88	2.4	0.55	0.67	0.006025	0.025204	0.042288	0.002347	0.005272	0.008081	0.005935	0.002504	0.004849
KIENA	10	70.8	8.91	0.45	0.55	0.000100	0.006246	0.010668	0.000026	0.000059	0.000155	0.000243	0.000011	0.000025
DENISON CLS.	177.83	478.6	3.55	0.3	0.41	0.031624	0.013600	0.032006	0.001308	0.004709	0.033757	0.286300	0.000079	0.000216
HBMS+1/2,-3/4	13335.2	15848.9	1.22	1.11	1.47	177.83	9.03	17.5	3510.82	11106.71	727.50	120481.31	0.00	0.00
HBMS-1/2+3 MSH	7244.6	9332.5	1.38	1.27	1.64	52.48	7.99	14.80	1536.75	4583.96	63.97	16979.13	0.00	0.00
HBMS-3MSH+4MSH	5000.35	5623.41	1.18	0.7	1.13	25.00	1.15	3.85	51.09	363.94	30.31	2605.69	0.00	0.00
HBMS 81	2544.97	10000	4.72	0.3	0.57	6.48	0.18	1.02	0.98	13.64	9.08	21924.16	0.00	0.00
HBMS 82	1230.3	6456.54	20.4	0.57	0.96	1.51	1.56	5.98	0.74	6.30	0.31	4344.33	.00	.00
CHADBOURNE	11481.5	17378	1.57	0.62	0.62	131.82	2.16	2.16	287.07	287.07	178.15	169403.41	0.00	0.00
SELBAIE	158	7943.3	83.43	0.69	0.69	0.02	1.17	1.17	0.42	0.42	0.04	9352.47	.00	.00
BOUSQUET	42169.69	66834.4	1.76	1.17	1.17	1778.26	37.50	37.50	74088.32	74088.32	2169.86	24741333.31	0.00	0.00

Shahabi equation and two Bates equations (3.27 and 3.28). The differences encountered for this set of equations show discrepancies of two orders of magnitude.

In conclusion, the range of available permeability equations provides little consistency in predicting material permeability. It is thus not possible to recommend any of these equations as predictors of material drainage characteristics. The limitations of these equations extend beyond those stated in Chapter 3, as even within these limits, little consistency is observed. The only alternative to making use of predictor type equations is to perform laboratory and field permeability tests, (196). This solution would alleviate mine site problems of permeability assessment but provides little contribution to the general knowledge of material drainage characteristics.

7.4.4 Compaction Control

The use of vibrators for compaction of granular materials has been presented in section 3.3.7. The effects of vibratory compaction as it applies to the preparation of tilt box samples of the size previously described was not documented at the outset of this study. A total of 120 compacted samples were prepared for the tilt box test under controlled vibration times. The void ratio was calculated for each vibration condition prior to conducting the tilt test.

The prepared samples all started out with different initial void ratios and it was desired to correlate the effect of vibration time to change in initial void ratio. After examining the available data, equation 7.1 was developed, and yields a correlation coefficent of .90.

$$\% \Delta e = 2.296 + .555 \text{ [time (s)]} \quad \ldots\ldots \quad 7.1$$

Thus, for example, given a vibration time of 40 s, it would be expected that the uncompacted void ratio would be reduced by 24.5%.

7.5 Summary

This chapter has summarized the physical characteristics of the mine backfills which have been examined as part of this study. It further illustrates that the backfills involved encompass a wide spectrum of material gradings, mineralogy and structure. As a result the geomechanical testing, reported in chapters 8 and 9 is considered to be representative of the wide range of backfill material encountered in practice.

This chapter has also examined the available permeabiltiy prediction equations and has illustrated their inconsistency. The use of these equations appears to be dubious at best, and laboratory and field permeability tests have been recommended in their place.

Equation 7.1 has been developed to control compaction in the preparation of tilt box test samples. It relates vibration time to reduction in void ratio.

8.0 FIELD EVALUATION OF MINE BACKFILL PROPERTIES

This chapter reports on the results of 100 pressuremeter tests conducted at 17 different mine test sites, located on 7 mining properties. The chapter begins with an overview of pressuremeter correction, calibration and verification procedures. It further examines the geomechanical properties of mine backfills as interpreted from pressuremeter data. The applicability of various empirical relations used to expand the usefulness of the pressuremeter are also reviewed.

The pressuremeter data is then placed in the context of its limitations by describing the typical data variations observed. Furthermore a series of pressuremeter tests designed to assess the instrument's sensitivity are reviewed.

8.1 Pressuremeter Calibration And Verification

This section examines the procedure used to correct raw pressuremeter data. Two data corrections are required: pressure and volume corrections. Furthermore, a simplified pressure correction procedure for the Pencel instrument is proposed.

Data repeatability and instrument sensitivity have also been examined and the results of this investigation have been reported. The analysis for data repeatability was made from three adjacent test locations underground at Campbell Red Lake mine. This data also illustrated the Pencel pressuremeter's sensitivity for

detecting different material phases as subsequent tests traversed different, detectable material horizons.

8.1.1 Data Correction

Field or raw pressuremeter data must be corrected for instrument characteristics before any use can be made of the pressure - volume curves. It can be visualized that as the instrument is inflated the injected volume is applied in theory to deform the soil. In practice, however, internal instrument dilation occurs under the applied fluid pressure. The dilation occurs in the readout fittings and valves, fluid lines and due to elastic slippage at the pressuremeter membrane coupling ring. Thus, these sources of volume dilation must be measured and accounted for. In a similar manner the inertial pressure of the membrane must be accounted for.

It is thus required that two calibration tests be carried out, one for the pressure correction, the other for volume correction. Figure 8.1 illustrates both correction procedures. The Figure indicates that the pressure correction reduces the measured pressure and volume. As such the corrected data is shifted downwards and to the left of the raw data curve.

The test procedure for determining the pressuremeter calibration curves must be repeated with each new membrane used and was found to be a laborious task. It was further felt that any developments towards reducing calibration times would provide a significant benefit to the testing procedure.

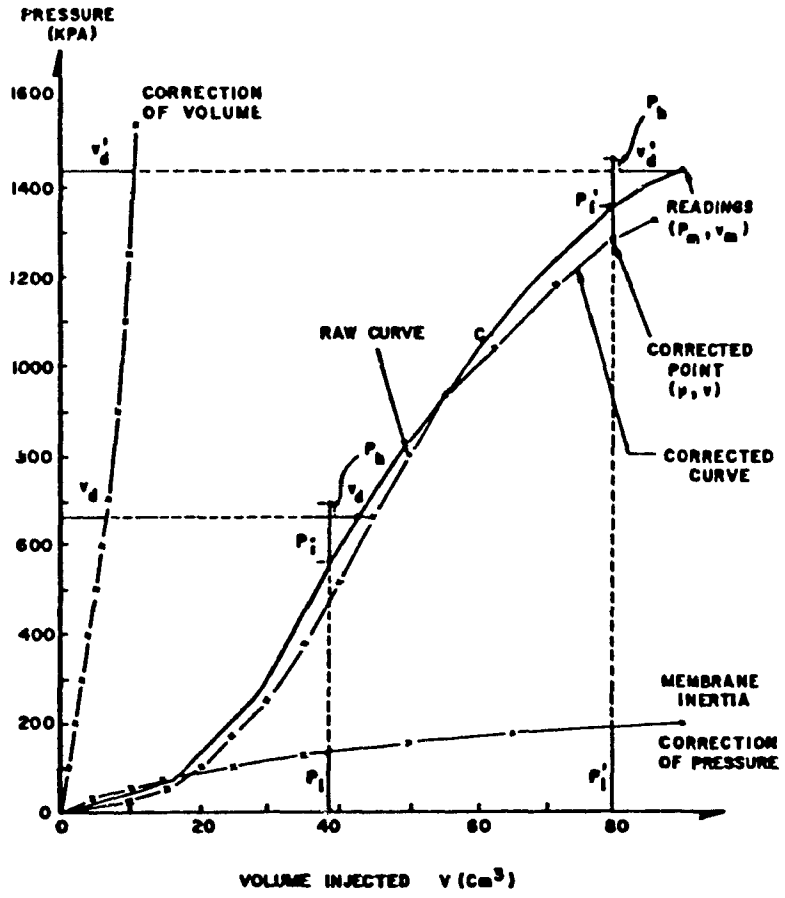

FIGURE 8.1 Raw Pressuremeter Data Correction

It was found that the volume correction curves for individual membranes showed significant variations. A simplified or reference volume calibration curve could thus not be developed. Furthermore, the volume calibrartion testing procedure must be repeated for each new membrane used. Conversly, little variation of the pressure correction curves was observed. An average curve, Figure 8.2, was used for pressure corrections and the pressure correction test was eliminated. The calibration curve presented in Figure 8.2 has been plotted with the calibration data of nine of the 25 membrane sleeves membranes used during the course of this study. This plot indicates that the maximum variation from the reference

correction curve was ± 25 kPa. The use of this reference curve may generate a source of error, however, this is not considered to be significant. For instance the ± 25 kPa variation translates into a ± 7% shift in the value of the limit pressure at Chadbourne mine, while the same variation represents only a ± 1% variation for the Campbell Red Lake material. It is thus proposed that the pressure calibration curve presented in Figure 8.2 be used in place of the pressure calibration test for the Pencel pressuremeter.

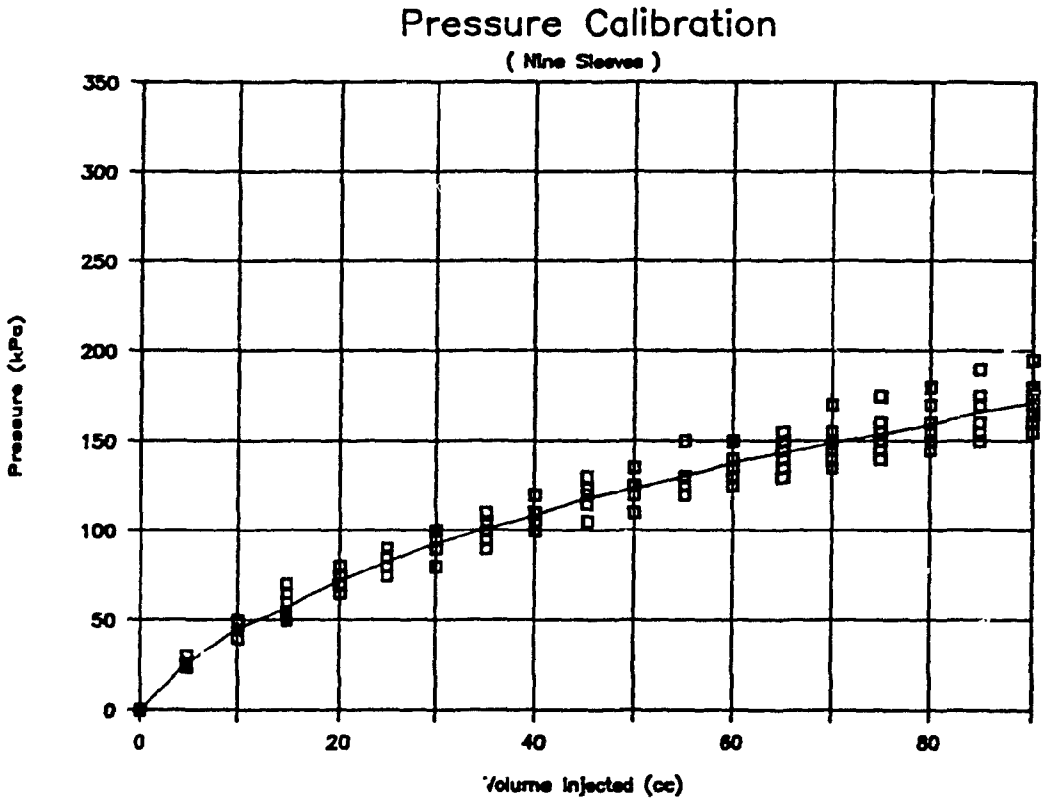

FIGURE 8.2 Proposed Pressure Correction Curve

8.1.2 Data Repeatability And Instrument Sensitivity

The question of instrument reliability is one that must be addressed before the data can be used with any confidence. The Pencel pressuremeter has been used for a number of years and its reliability remains unquestioned, however the instrument's sensitivity has not been quantified or even qualitatively assessed.

Two series of tests were included in the overall testing program. The aim of these tests was to address the question of data repeatability within a given material and instrument sensitivity characteristics.

The first series of three tests were conducted at the Campbell Red Lake mine, in 1804 stope. The aim of these tests was to verify the repeatability of pressuremeter data when tests were conducted within the same material. With this objective in mind a series of tests were conducted within a radius of .25 m to a depth of 3.25 m. It was found that two distinct materials were encountered: a 14 day cured backfill was encountered within the first 2.25 m and a 60 day cured material to a depth of 3.25. The data above and below the 2.25 m cutoff was grouped separately and the repeatability of each group is analysed. Figure 8.3 illustrates that the natural variation in pressuremeter data is in the order of $\pm$ 12% for both the 14 and 60 day cured data in three adjacent test holes. It is thus indicated that given a mean backfill stiffness it will not be possible to distinguish surrounding backfill zones with material properties varying less than $\pm$ 12% from the mean.

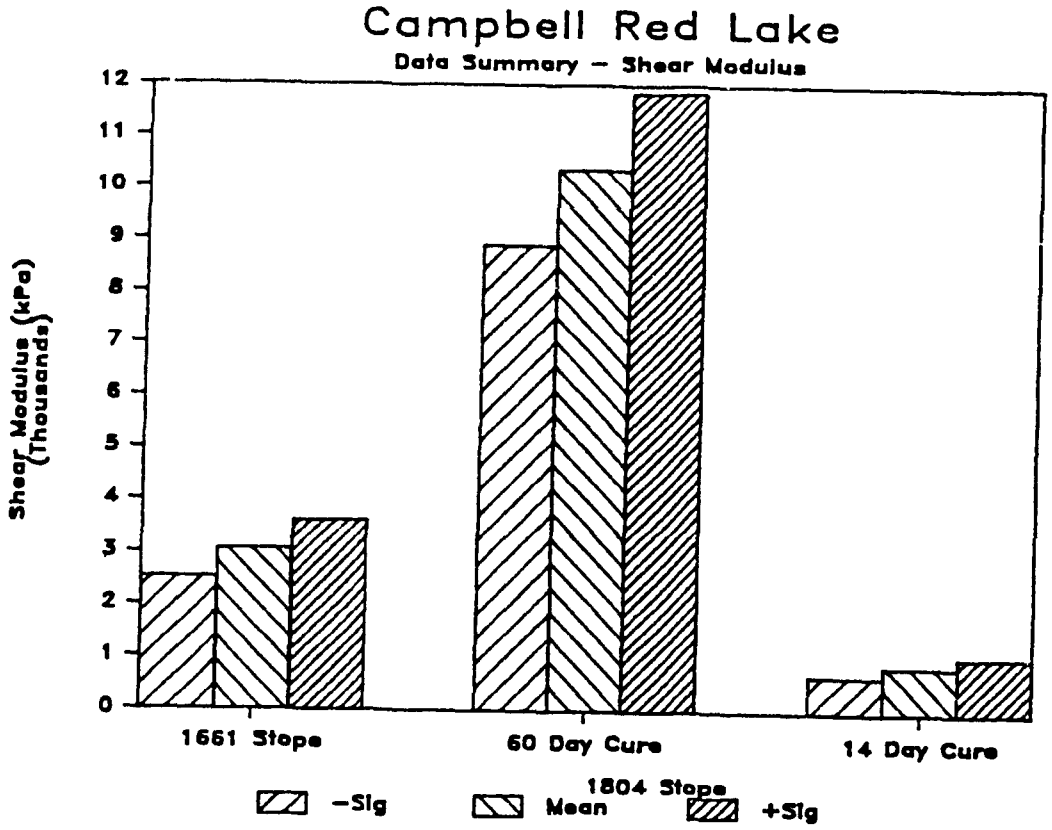

FIGURE 8.3 Data Repeatability, Demonstrated By Variation From The Mean

The data illustrates good repeatability within a uniform material. It further illustrates that it is possible to distinguish between backfills with wide ranging material properties such as the 14 and 60 day cured materials. The properties for the two materials indicate a 10 fold difference in terms of shear modulus. This indicates the Pencel's ability to distinquish between very discrete backfill properties.

This last example illustrated the coarse discretionary ability of the Pencel pressuremeter. However, a more refined series of tests were conducted in which the objective was to determine the ability of the pressuremeter to detect more subtle changes in

material properties. With this objective in mind a series of three tests were conducted in stopes 37036 and 37038 at Denison mines. The access to these areas was the pillar recovery phase between the two stope. As pillar recovery progressed the backfill in the two stopes was exposed. Figure 8.4 illustates the banding which had occured during the placement of the backfill. The tests conducted in each of these bands indicated that the difference in

FIGURE 8.4 Banding Characteristics Of Denison Mine Backfill

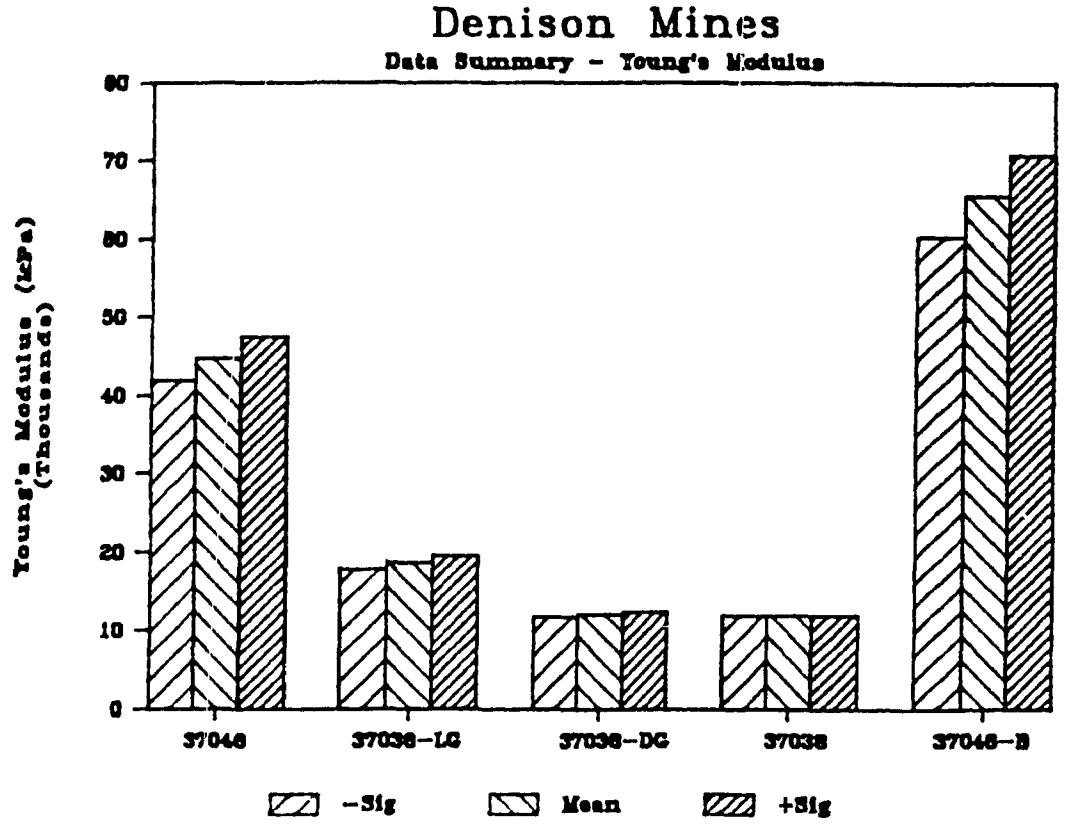

FIGURE 8.5 Pencel Pressuremeter Sensitivity

material properties measured 42%, Figure 8.5. This finding is consistant with that of the repeatability tests conducted at Red Lake, that is if the 42% difference in material properties were to represent data scatter it would imply that the natural scatter would be ± 21%, which is beyond the natural scatter which was measured in the controlled repeatabilty tests. It is thus concluded that scatter in material properties of less than ±12 % cannot be construed as actual variations in material properties. On the other hand the instrument's sensitivity is such that provided the insertion procedures are controlled in each test case a data scatter of ± 21 % or beyond represents a true variation in material

properties. Unfortunately, no comment can be made of changes in material properties of between ± 12 and ± 21% as suitable tests could not be performed to determine the pressuremeters' sensitivity within this range.

Table 8.1 has been assembled to show the natural data variation encountered. It illustrates that the first two materials, Denison and Kiena backfills, showed scatter in the data of less than the natural scatter eluded to earlier. This implies that the material in these instances can be considered to be homogeneous. The next three materials from Lac Matagami, Sigma and Campbell Red Lake indicate data variations in close order to that of natural scatter, that is a ± 12% to ± 15% variation about the mean. This data can thus also be considered as a homogeneous backfill. The last two materials are special cases. The Remnor backfill is considered a special case as a pre-hole was required and was drilled crudely by pneumatic jackhammer, Figure 8.6. The Chadbourne backfill is also considered to be an exception as the material is much coarser than either of the materials used for the repeatability or sensitivity test series.

MINE LOCATION	% VARIATION IN DATA
DENISON	± 4.0
KIENA	± 7.0
LAC MATAGAMI	± 12.0
SIGMA	± 12.3
CAMPBELL RED LAKE	± 15.0
REMNOR	± 17.6
CHADBOURNE	± 20.0

TABLE 8.1 Observed Variations in Pressuremeter Data

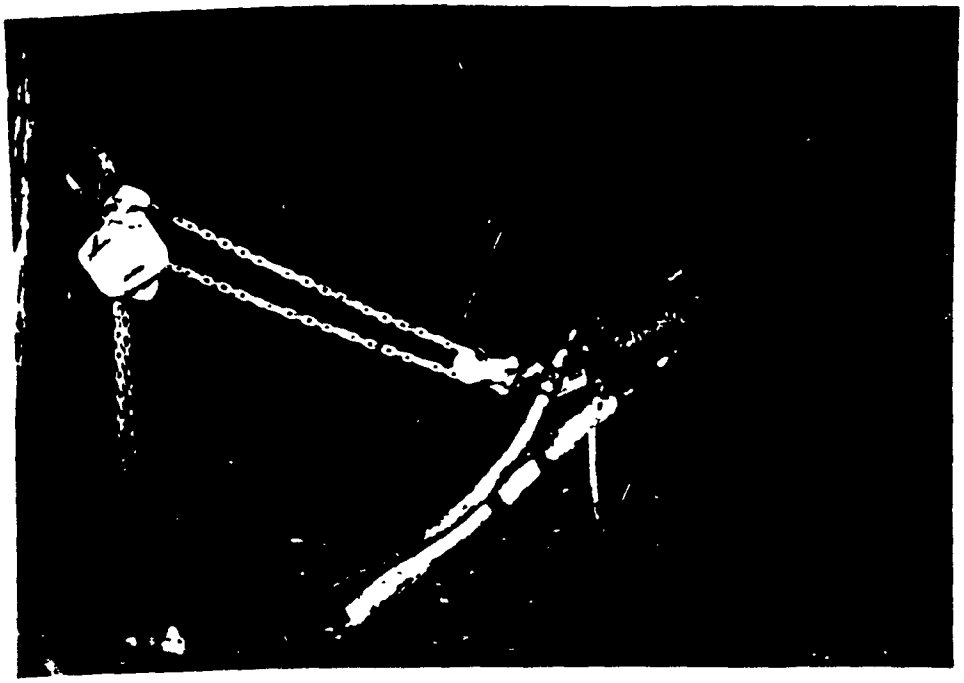

Figure 8.6 Drilling Of Pre-Hole By Jackleg At Remnor Mine

8.2 In Situ Geomechanical Properties

The geomechanical properties of mine backfills have been extracted from the corrected data curves, these curves have been provided in Appendix 9. Three basic parameters are extracted from these curves: the shear modulus, the limit pressure and with a lesser degree of confidence the pre-existing lateral stress. The shear modulus is easily converted to a modulus of deformation by equation 5.2. The limit pressure is another important parameter as it has been empirically correlated to the materials undrained shear strength and angle of internal friction. The angle of internal

friction is subsequently used to estimate the stress distribution within the material due to its own weight. Lastly, the P_o value is used as an estimate of the total lateral stress. The total lateral stress is the sum of the stresses due to the material's own weight and the stresses absorbed by the redistribution of stresses in the adjacent rock structure.

8.2.1 Material Stiffness

The stiffness properties of mine backfills are characterized by the shear modulus, G_m and the deformation modulus, E_m. Table 8.2 and Figure 8.7 represents the stiffness characteristics of the mine backfills tested in this study. Measured deformation moduli range from 1.06 to 65.17 MPa.

The E_m / P_1 ratio has been historically used to develop soil profiles and have been useful for backfill characterization. Three groups of backfill materials have been observed and include coarse grained loose gravels at Chadbourne with E_m / P_1 ratios in the order of 4 tc 8. The second group includes the largest number of backfills tests; the uncemented fine grained tailings at Lac Matagami, Sigma and Denison, the E_m / P_1 ratio for these materials is in the range of 10 to 15. Lastly, the cemented tailing used at Red Lake, Denison and Kiena and the Remnor cemented smelter slag indicated E_m / P_1 ratios between 15 and 24 and is typically in excess of 20. This ratio has thus proven itself very useful in assessing the classification of cemented mine backfills whether

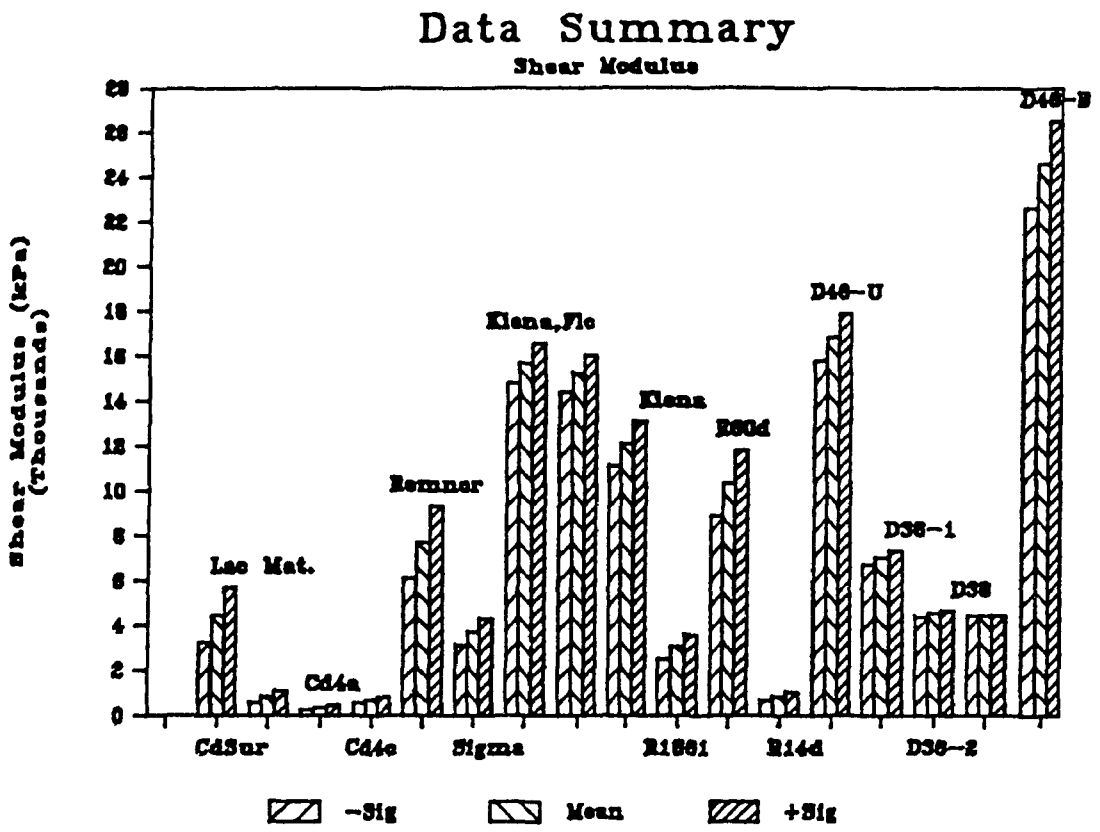

FIGURE 8.7 (A) Data Summary Of Measured Shear Moduli

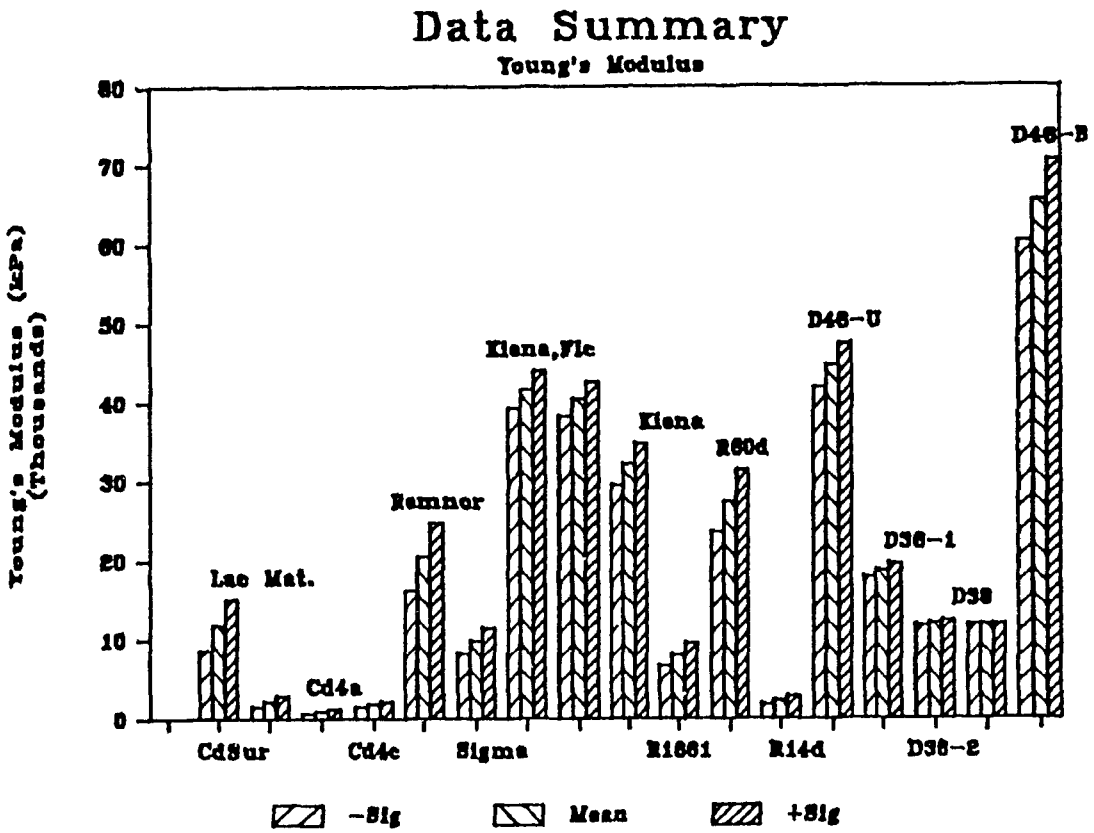

FIGURE 8.7 (B) Data Summary Of Measured Young's Moduli

loose gravel or cemented backfills.

Upon further examination of Table 8.2 and Figure 8.7 it is evident that the shear modulus and deformation modulus show significant variations with cementing characteristics, curing periods and addition of flocculants. The addition of cementing agents, for instance, increases the stiffness characteristics from the 2.4 to 12 MPa in range for uncemented backfills to 20 to 40 Mpa in range for typical 20:1 cemented backfills,together with exceptional examples of stiffness greater than 65 MPa.

The tests conducted at Campbell Red Lake mine indicated the effects of curing in cemented fine grained backfills. Two stopes were examined, 1661 and 1804 stopes. The tests conducted in 1804 traversed two horizons of similarly cemented backfills (20:1) at different stages of curing, (14 and 60 days). The backfill in the second stope had been cured to for 30 days. Figure 8.8 illustrates the deformation modulus data for these three backfills. It indicates that a 5.6 MPa increase in deformation modulus occurs as the backfill cures from 14 to 30 days. Similarly, a 25.5 MPa increase is observed as the material cures from 30 to 60 days. This is in contrast to the trends observed with concrete , where 80% of the material stiffness is achieved in the first 28 days. The explanation for this discerpancy is the high moisture content which mine backfills originally contain. The high original moisture retards the hydration process and thus the achieved stiffness.

MINE LOCATION	P_1 (MPa)	G_m (MPa)	E_m (MPa)	E_m/P_1
LAC MATAGAMI	1.00	4.50	11.97	11.97
CHADBOURNE				
SURFACE	.41	.86	2.29	5.59
4a STOPE	.27	.40	1.06	3.93
4c STOPE	.24	.74	1.96	8.17
REMNOR	.86	7.74	20.60	23.95
CAMPBELL RED LAKE				
1661 STOPE	.75	3.00	8.00	10.67
1804 STOPE 14D	.21	.90	2.40	11.43
1804 STOPE 60D	2.50	10.50	27.93	11.17
SIGMA	.66	3.75	9.97	15.11
DENISON MINES				
37046 U/C	1.97	16.50	43.89	22.28
37046 BULKHEAD	-	24.5	65.17	-
37036 LIGTH GREY	.91	7.0	18.50	20.33
37036 DARK GREY	1.19	4.10	10.91	9.16
37038	1.10	4.14	11.00	10.00
KIENA				
FLOCCULANTED	2.11	12.12	32.25	15.28
NON-FLOCCULATED #1	2.07	15.50	41.23	19.92
NON-FLOCCULATED #2	1.85	15.40	41.00	22.16

TABLE 8.2 Geomechanical Characteristics of Mine Backfills

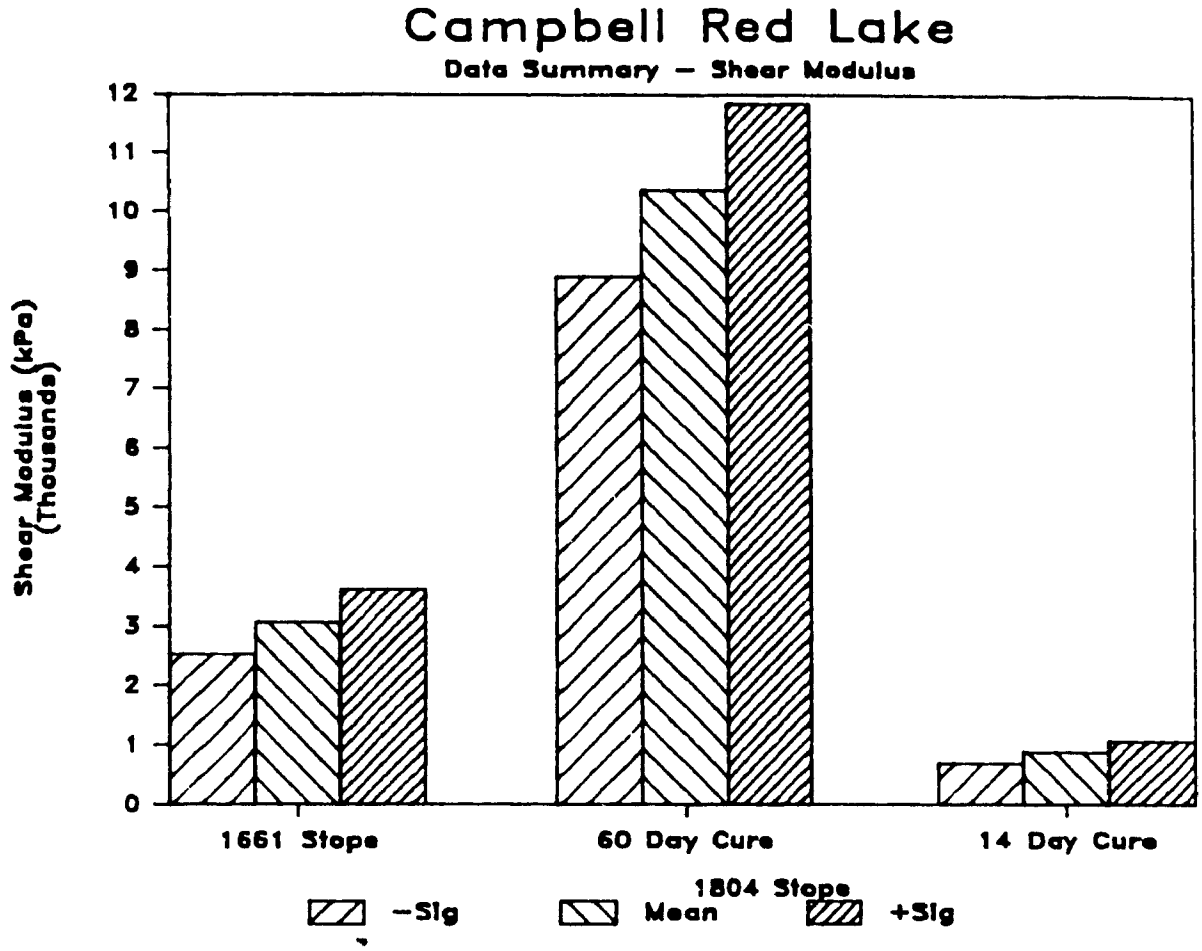

FIGURE 8.8 In Situ Curing Characteristics of Mine Backfills

After an inital vist to Kiena Mines in the fall of 1985 a return vist was requested by the mine management in June of 1986. The objective of the second test program was to assess the effect of flocculants on the stiffness characteristics of the cemented mill tailings. Figure 8.9 gives a comparative analysis of the measured shear and deformation moduli for flocculated and unflocculated backfill materials. The figure illustrates that the use of flocculants increases the shear and deformation moduli by 27.5% for similarly cemented and cured backfill materials.

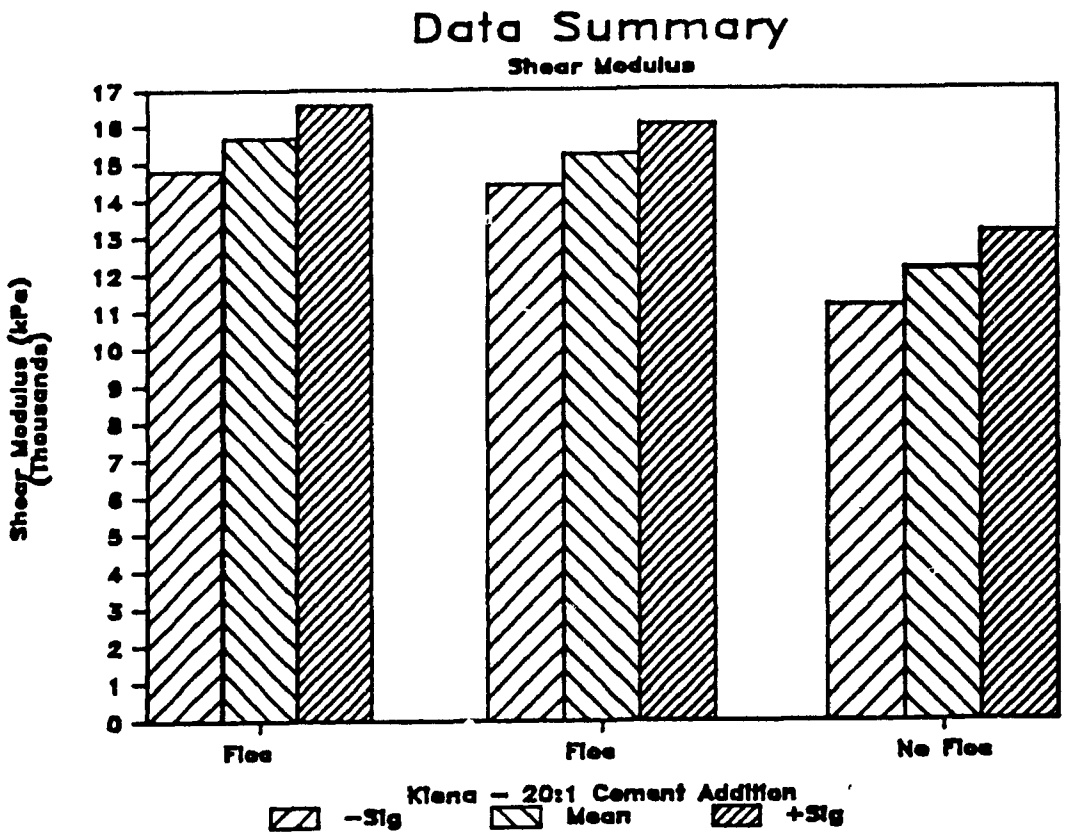

FIGURE 8.9 (A) Effect Of Flocculants On Shear Modulus

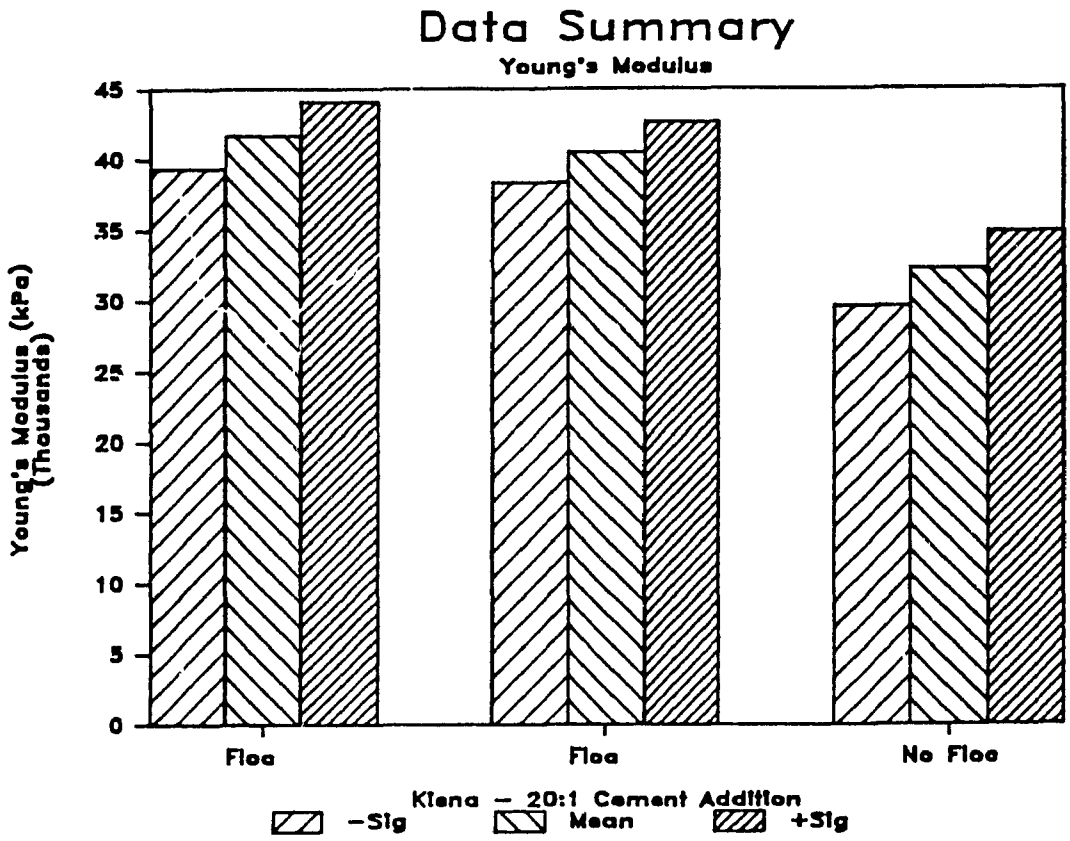

FIGURE 8.9 (B) Effects Of Flocculants On Young's Modulus

8.2.2 Limit Pressures Of Mine Backfills

The curves provided in Appendix 9 were also used to extract the limit pressure as described in Chapter 5. The limit pressure was subsequently used to estimate the undrained shear strength, S_u. Table 8.2 and Figure 8.10 illustrate the relevant limit pressure data. The data indicates that a 1 MPa cutoff can be applied, with the material lying below the cutoff representing uncemented materials and those with limit pressures above 1 Mpa constituting cemented materials.

The uncemented backfill materials further indicate two distinct groups; namely the coarse grained materials with limit

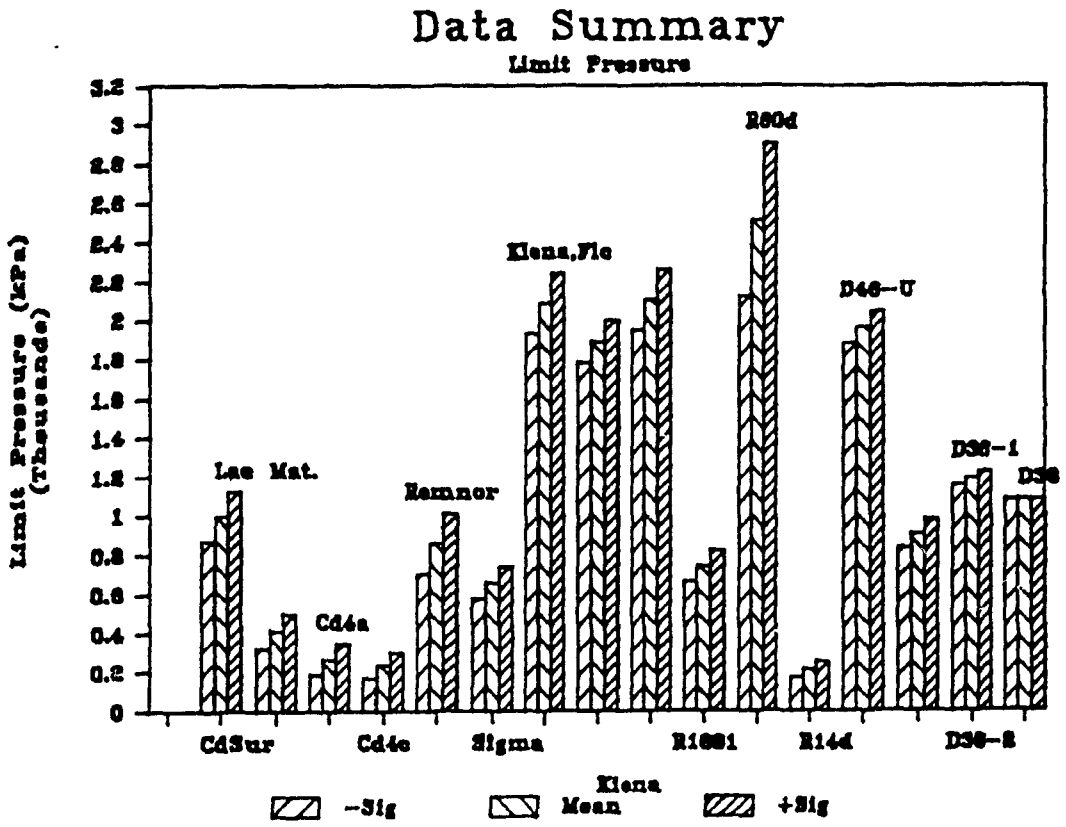

FIGURE 8.10 Summary of Measured In Situ Limit Pressure

pressures in the range of .2 to .4 and fine grained backfills with limit pressures between .66 and 1.00. The only exceptions to the rule are the 14 and 30 day cured 20:1 fine grained backfills at Campbell Red Lake Mines. These material were not fully drained, and as such they behaved more fluidly, being reflected in the limit pressure.

The effect of curing is illustrated in Figure 8.11. The limit pressure increases from .21 to .75 between days 14 and 30, representing a .54 MPa increase. Subsequently, the limit pressure increases by 1.75 MPa in the next 30 days, to 2.5 MPa. This represents the same delayed curing trend as that observed for the stiffness characteristics.

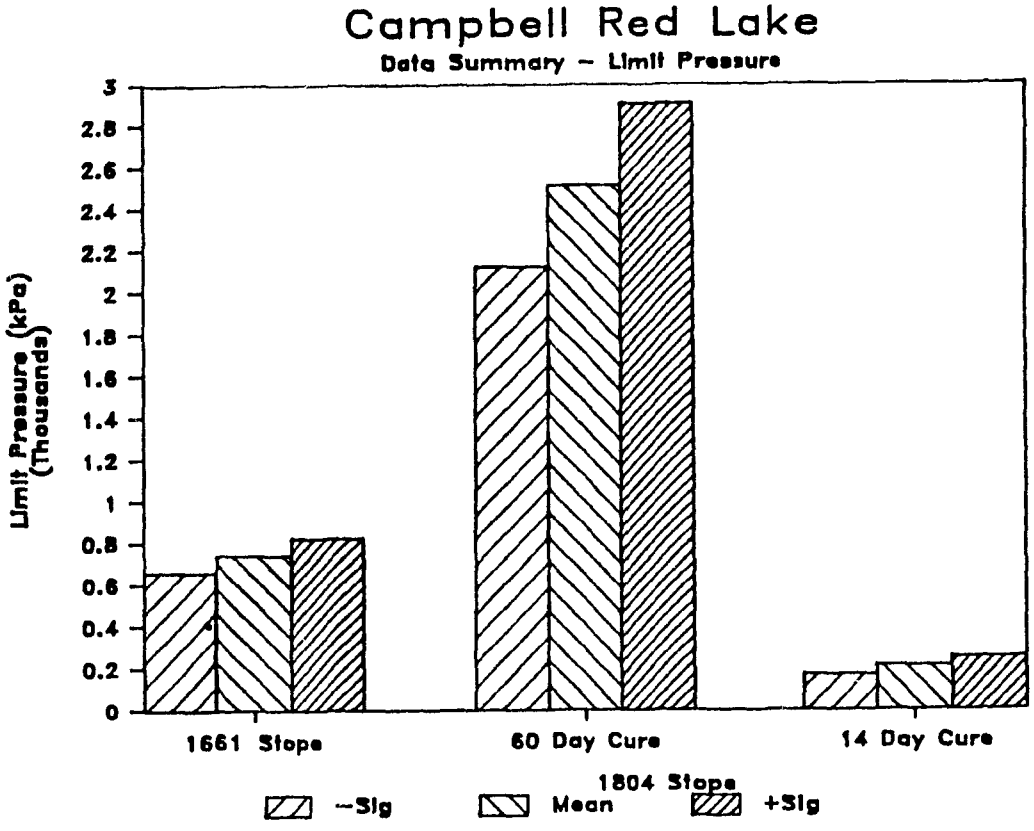

FIGURE 8.11 Effects of Curing on Limit Pressure - Campbell Red Lake

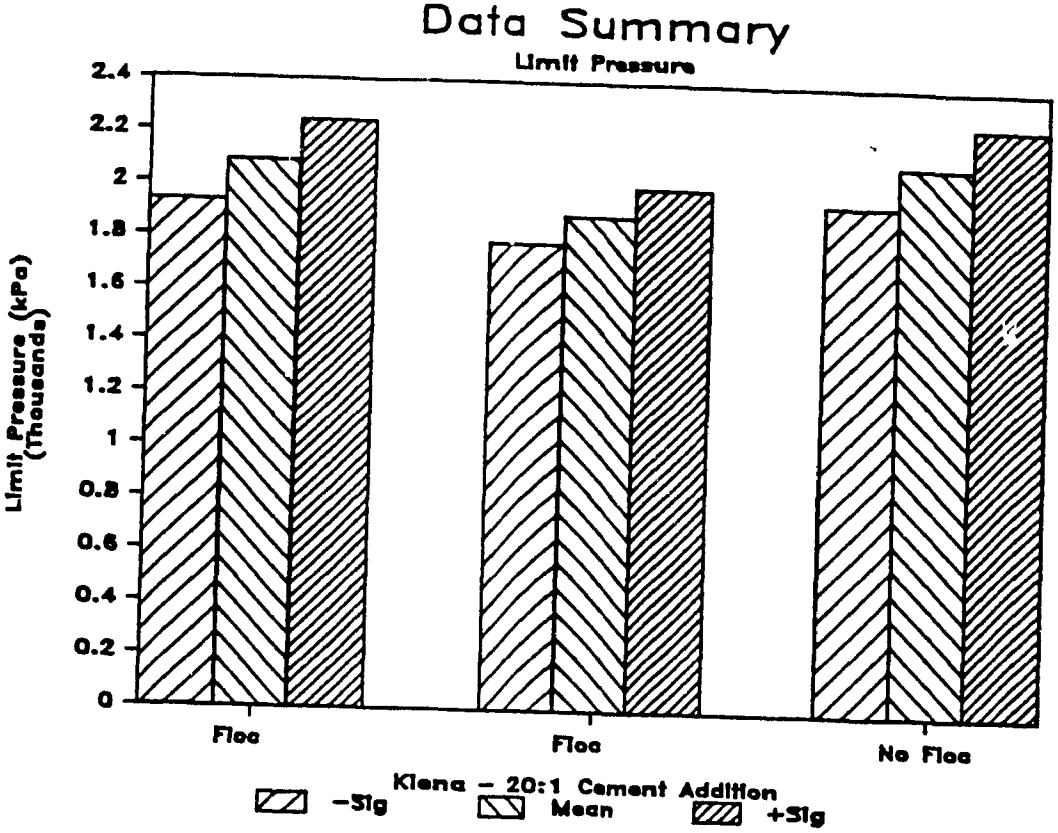

FIGURE 8.12 Effect of Flocculants On Backfill Limit Pressure

The use of flocculants on limit pressure has been summarized in Figure 8.12. This figure suggests that within the bounds of experimental variation the limit pressure has not changed with the addition of flocculants.

8.2.3 Undrained Shear Strength

The undrained shear strength is defined as one half the compressive strength of an undrained soil sample (19). It has further been empirically correlated to the limit pressure derived from the pressuremeter test. In this section two such correlations are examined, these have been presented as equations 5.5 and 5.6 in

Chapter 5. The predictions of these two equations are contrasted in Table 8.3. The table presents the undrained shear strength as estimated by the two empirical equations. Furthermore, it includes the percentage difference between the two predictions. The data further indicates that a large dispersion in predicted strengths, as much as 40%, is possible between the two equations. It was further found that the amount of error increased with increased shear strength, as illustrated in Figure 8.13. This figure shows that equation 5.5 gives more conservative estimates for shear strength values greater than 55.5 KPa, while equation 5.6 gives lower values at for shear strengths ranging between 0 and 55.5 KPa.

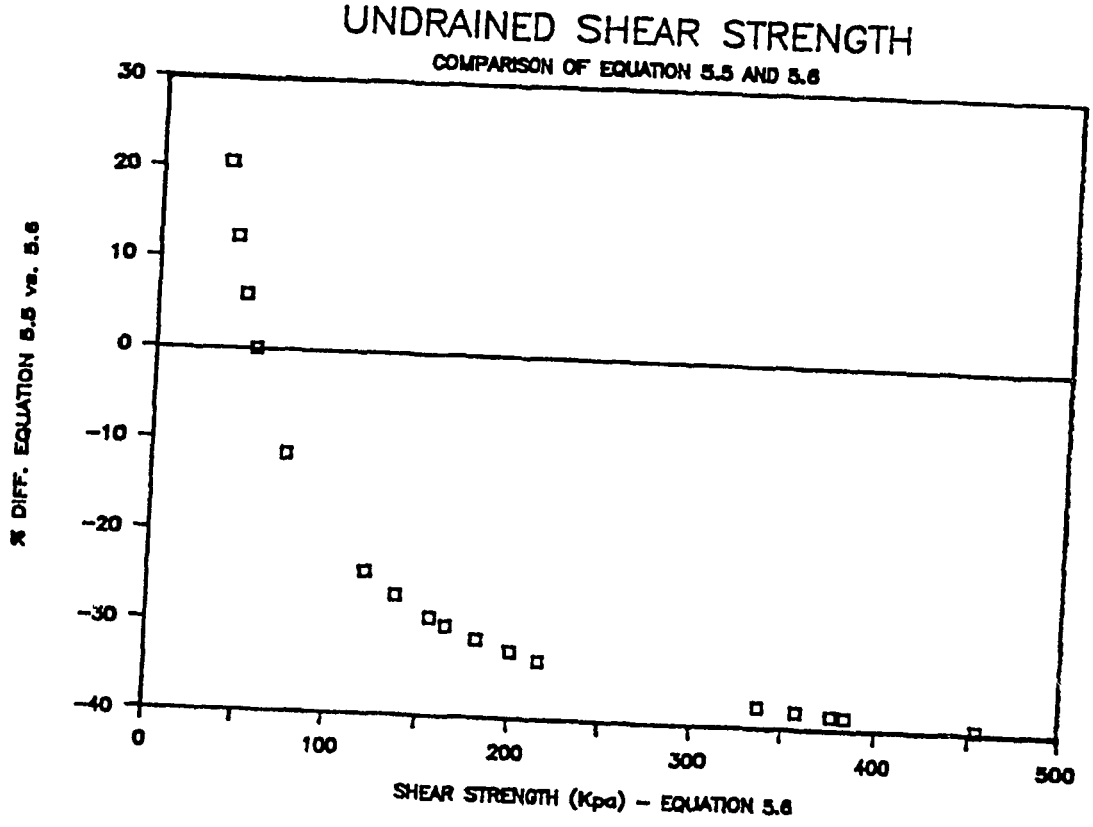

FIGURE 8.13 Comparison Of Undrained Shear Strength Predictions

The large observed scatter in predicted undrained shear strength is a cause of some concern as the use of either equation could incure a possible error of up to 40%. In an effort to reduce this error an alternate equation was developed based on equations 5.5 and 5.6. This equation, reduces the possible maximum error from 40% to 20% and is presented as equation 8.1.

$$S_u = .141\ P_1 + 12.5\ (kPa) \qquad ..... \ 8.1$$

MINE LOCATION	EQUATION 5.5	EQUATION 5.6	% DIFF.
LAC MATAGAMI	125.00	181.82	-31.25
CHADBOURNE			
SURFACE	66.00	74.55	-11.46
4a STOPE	52.00	49.09	5.93
4c STOPE	49.00	43.64	12.29
REMNOR	111.00	156.36	-29.01
RED LAKE			
1661 STOPE	100.00	136.36	-26.67
1804 STOPE 14D	46.00	38.18	20.48
1804 STOPE 60D	275.00	454.55	-39.50
SIGMA	91.00	120.00	-24.17
DENISON			
37046 U/C	222.00	358.18	-38.02
37046 BULKHEAD	-	-	-
37036 LIGTH GREY	116.00	165.45	-29.89
37036 DARK GREY	144.00	216.36	-33.45
37038	135.00	200.00	-32.50
KIENA			
FLOCCULATED	210.00	336.36	-37.57
NONFLOCCULATED #1	236.00	383.64	-38.48
NONFLOCCULATED #2	232.00	376.36	-38.36

TABLE 8.3 Estimated Undrained Shear Strength of Mine Backfills

8.2.4 Angle Of Internal Friction

The angle of internal friction has been empirically correlated to the limit pressure by Gambin in equation 5.7. Furthermore, Calhoon proposed a graphical means of determining the angle of internal friction from the modulus of deformation and the limit pressure, Figure 5.2. Each of these have been applied to the pressuremeter data presented in Table 8.2 and the results have been reported in Table 8.4.

Table 8.4 further illustrates that Calhoon's graphical method consistently underestimates the angle of internal friction when compared to Gambin's equation. In many instances Calhoon's equation predicts anomalously low angles of internal frictions in the order of 25^{o}. However, the largest limitation of Calhoon's method is the narrow range of applicability. Although the method proposed by Calhoon is, at first glance, applicable to stiffnesses in the range of .05 to 40 MPa and limit pressures between 75 and 2000 kPa there is an additional inherant problem. The problem being that combinations of high limit pressure and low deformation modulus or vise versa fall outside the bounds of the graphical method.

The Gambin equation, on the other hand, is applicable to the entire range of limit pressures encountered. Furthermore, it predicts angles of internal friction in the order of 30^{o} to 37^{o} as expected. It also correctly predicts the expected lower angle of internal friction for the loose granular Chadbourne backfill. These predicted angles of internal friction are also observed to fall within a narrow band of 3^{o}.

MINE LOCATION	ANGLE OF INTERNAL FRICTION EQUATION 5.7	CALHOON
LAC MATAGAMI	32.11	28.00
CHADBOURNE		
SURFACE	26.97	-
4a STOPE	24.55	-
4c STOPE	23.88	-
REMNOR	31.24	-
CAMPBELL RED LAKE		
1661 STOPE	30.45	25.00
1804 STOPE 14D	23.10	15.00
1804 STOPE 60D	37.40	-
SIGMA	29.71	28.00
DENISON		
37046 U/C	36.02	35.00
37046 BULKHEAD	-	-
37036 LIGHT GREY	31.57	-
37036 DARK GREY	33.11	24.00
37038	32.66	23.00
KIENA		
FLOCCULATED	36.42	-
NON FLOCCULATED	36.31	-
NON FLOCCULATED	35.66	34.00

TABLE 8.4 Estimated Angle of Internal Friction

It is thus concluded that the Gambin equation has a wider range of applicability and consistency. This is to be expected as the consistency of Gambin's predictions is dependant on the consistency and repeatability of the limit pressure measurement.

It is also interesting to note that, although the limit pressure increases with increased cementation and the addition of flocculants, the angle of internal friction is little affected. Conversely, the effect of curing as demonstrated by the Campbell Red Lake data has a pronounced effect on the angle of internal friction. Numerically, a 7^{o} increase is noted in each of the curing periods between 14 and 30 days and the subsequent curing to 60 days.

8.2.5 Lateral Stress Evaluation From Pressuremeter Data

The determination of in situ lateral stress must be preceded by a definition of which component of lateral stress is of interest. It has already been mentioned that the total lateral stress in mine backfills is comprised of two components; stresses due to self-weight and stresses which are absorbed or transmitted through the backfill mass by the redistribution of stresses around the mine opening. It is this second component that represents the backfill's ability to absorb pillar stresses.

Although the stress redistribution component cannot be measured directly by the pressuremeter, an indirect measurement can be made. This stems from the above definition of total lateral stress. The stresses generated by the backfill's self-weight is

directly related to the angle of internal friction and yields the K_o parameter. This parameter can be subsequently used in conjunction with the materials bulk density to estimate the lateral stresses due to self weight.

Total lateral stress has traditionally been measured by PMT and SBPMT type pressuremeter tests and can also be measured in some instances with the Pencel pressuremeter, a FDPMT push - in type pressuremeter . The data from Remnor, Lac Matagami and Kiena were amenable to measurement of total lateral stress since a P_o is distinguishable on their data curves. The combination of the K_o estimator and the measurement of total lateral stress enables the prediction of absorbed stresses.

Following this logical process of data analysis the first stage is to determine the K_o parameter. This parameter is readily determined from the angle of internal friction and equation 5.3. The results of this analysis are presented in Table 8.5. The K_o parameter has then plotted against limit pressure in Figure 8.14 and was found to decrease with increases in limit pressure. This implies that as the limit pressure increases the stresses due to self-weight tend to remain in the vertical direction. Conversely, as the limit pressure decreases then the lateral component takes on a role of greater prominance. This trend is observed consistently within the range of data presented in Table 8.2 and 8.5. A statistical analysis of this data yielded the empirically derived equation 8.2, with a regression coefficent of .998. The predicted and actual K_o are presented in Figure 8.14 and are plotted as functions of the limit pressure.

MINE LOCATION	Ko	DRY DENSITY
LAC MATAGAMI	.47	1.73
CHADBOURNE	.97	2.11
REMNOR	.48	2.11
CAMPBELL RED LAKE		
1661 STOPE	.49	1.80
1804 STOPE 14D	.61	1.80
1804 STOPE 60D	.39	1.80
SIGMA	.50	1.46
DENISON	.45	2.00
KIENA	.41	1.80

TABLE 8.5 Estimated K_o Values For Mine Backfills Based on The Angle of Internal Friction

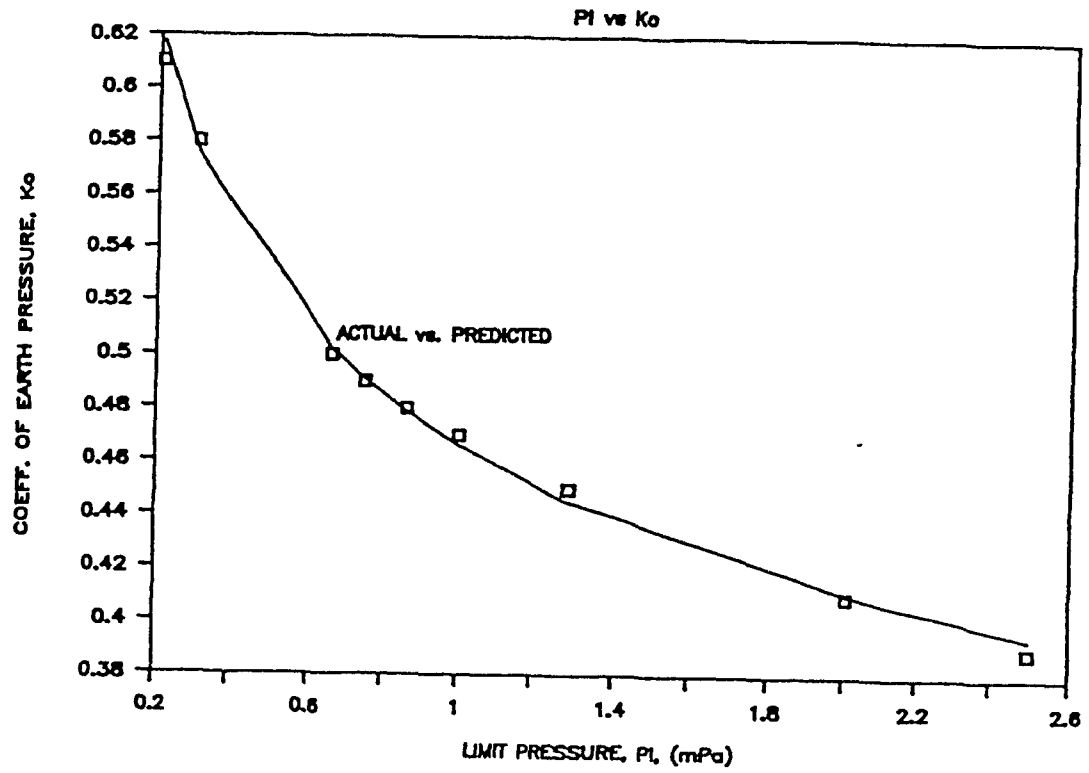

FIGURE 8.14 Estimated and Predicted K_o Values Based on Limit Pressure

$$K_o = .466 / (P_1)^{.18} \qquad \text{..... 8.2}$$

Once the K_o value has been determined by equation 8.2 then an estimate of bulk density is required to calulate the vertical component of in situ stress and finally the lateral stress. The values of dry density quoted in Table 8.5 have been derived from laboratory tests and have been reported in Chapter 7 and Appendix 8. The result of this phase of the analysis is an estimate of vertical and lateral stresses due to self weight. This is graphically represented for the Kiena Mine in Figure 8.15. Similar curves are presented in Appendix 10 for each of the mines listed in Table 8.5.

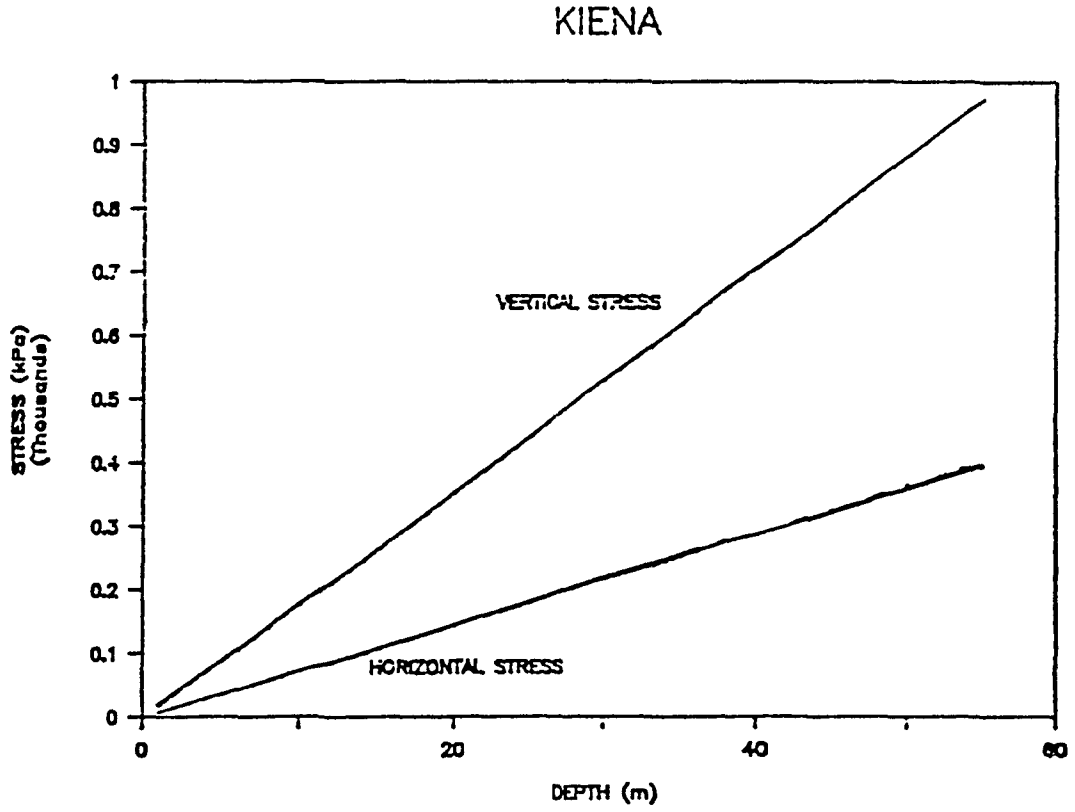

FIGURE 8.15 Vertical And Horizontal Stresses Due To Self - Weigth at Kiena

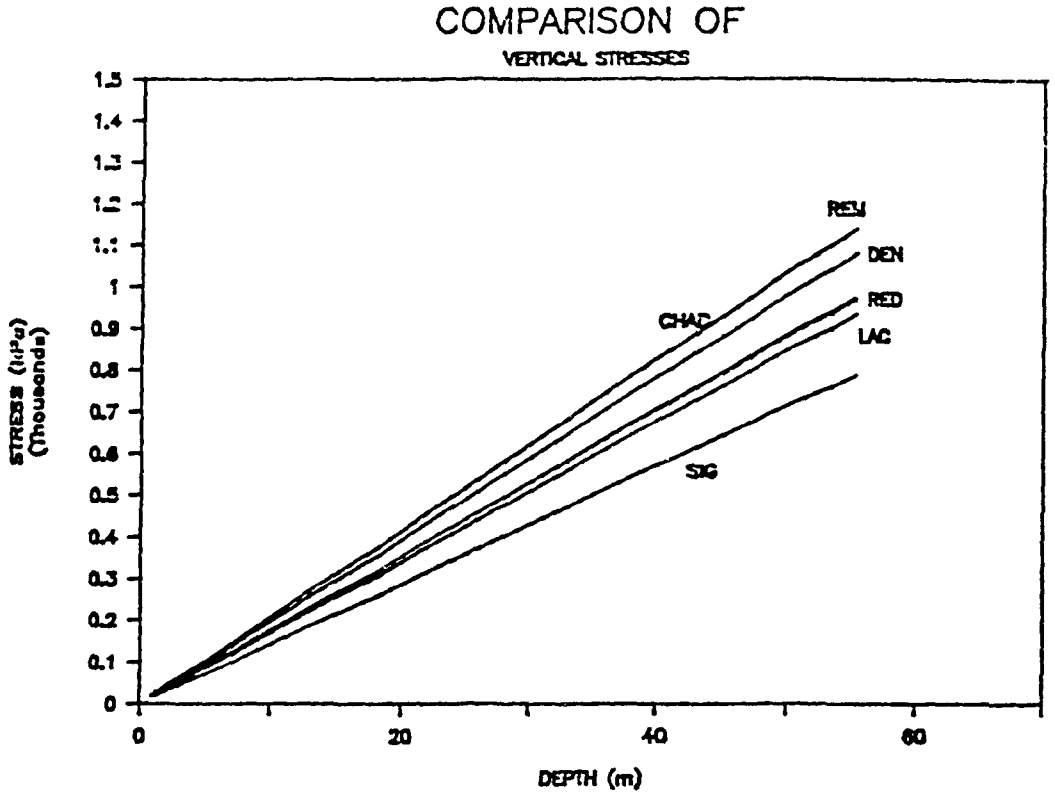

FIGURE 8.16 (A) Comparison Of Vertical Stresses

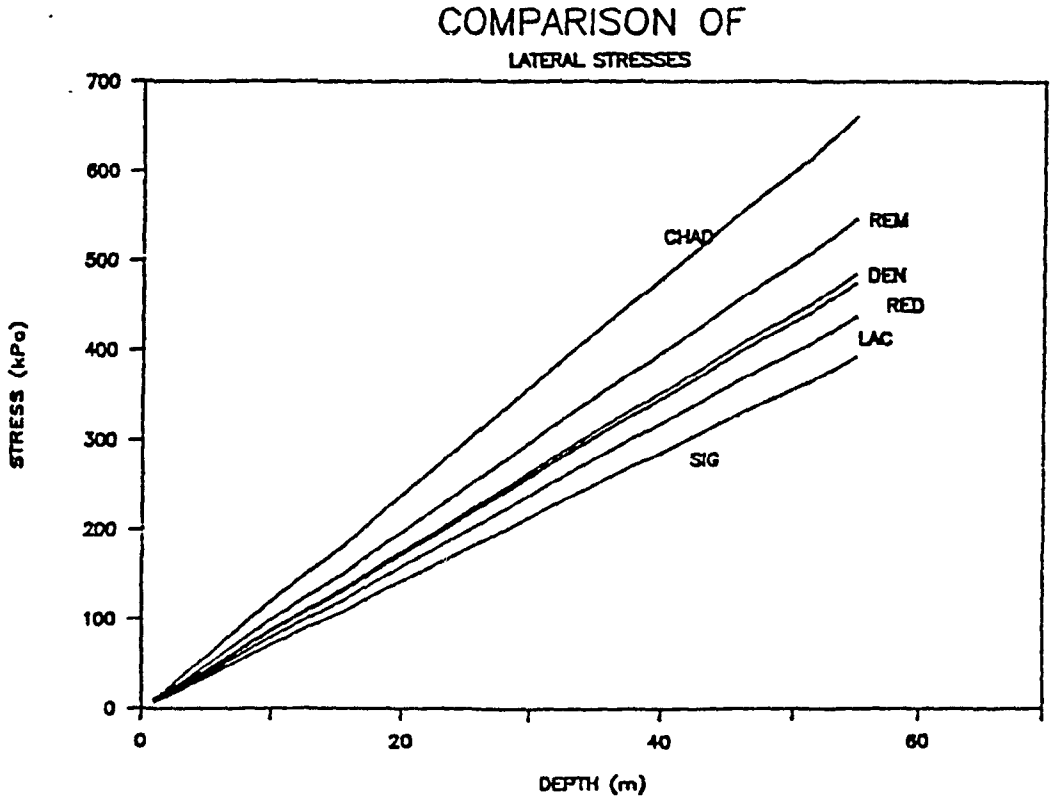

FIGURE 8.16 (B) Comparison Of Lateral Stresses

MINE LOCATION	STRESSES (kPa) VERTICAL	HORIZONTAL	PREDICTED EQUATION 8.3
LAC MATAGAMI	509.1	239.3	237.3
CHADBOURNE	621.0	360.3	357.3
REMNOR	621.0	298.1	297.3
CAMPBELL RED LAKE			
1661 STOPE	529.7	259.6	260.0
1804 STOPE 14D	529.7	323.1	326.9
1804 STOPE 60D	529.7	206.6	209.3
SIGMA	429.7	214.8	215.8
DENISON	588.6	264.9	262.0
KIENA	529.7	217.2	217.7

TABLE 8.6 Estimated Vertical and Horizontal Stress For Mine Backfills at a Depth of 30 m.

The vertical and horizontal stresses due to self weight have been plotted in a comparative fashion in Figure 8.16 (a) and 8.16 (b). The data has been plotted to a depth of 50m and shows a significant variation due to the range of K_o and material densities.

As an example Table 8.6 represents the data for the vertical and lateral stresses at a depth of 30m. The vertical stresses vary between 430 and 620 kPa and are solely dependant on material density, as illustrated by the Campbell Red Lake backfill. The horizontal stress on the other hand is dependant on the vertical stress and the K_o parameter and thus on equation 8.2. Combining

equation 8.2 with the definition of K_o yields equation 8.3.

$$\text{Horizontal Stress} = .466 \quad d / (P_l)^{.18} \quad \ldots\ldots \quad 8.3$$

Table 8.6 also presents the predicted horizontal stresses by equation 8.3 at a 30m depth and indicates good correlation. Equation 8.3 has the benefit of predicting horizontal stresses directly from the the limit pressure and material density.

The discussion to date has centered around the determination of the stresses generated by self weight. These stresses represent only one component of total stress, thus our attention now focuses on the determination of total stress and absorbed stress. The total stress is determined directly from the pressuremeter data when a P_o is distinguishable. Table 8.7 represents the total lateral pressure as measured with the Pencel pressuremeter. The P_o values were only obtainable for data from three of the seven mines surveyed, due to obtained curve forms. These values are comparable, though lower, to those measured by Corson (80) and Zahary (79) which ranged from 200 to 700 kpa.

	MINE LOCATION		
DEPTH (m)	KIENA	REMNOR	LAC MATAGAMI
1	90	-	-
2	135	-	50
3	185	175	75
4	200	195	95
5	250	210	150
6	300	220	205
7	-	250	-

TABLE 8.7 Measured Total Lateral Stresses (kPa)
By Pencel Pressuremeter

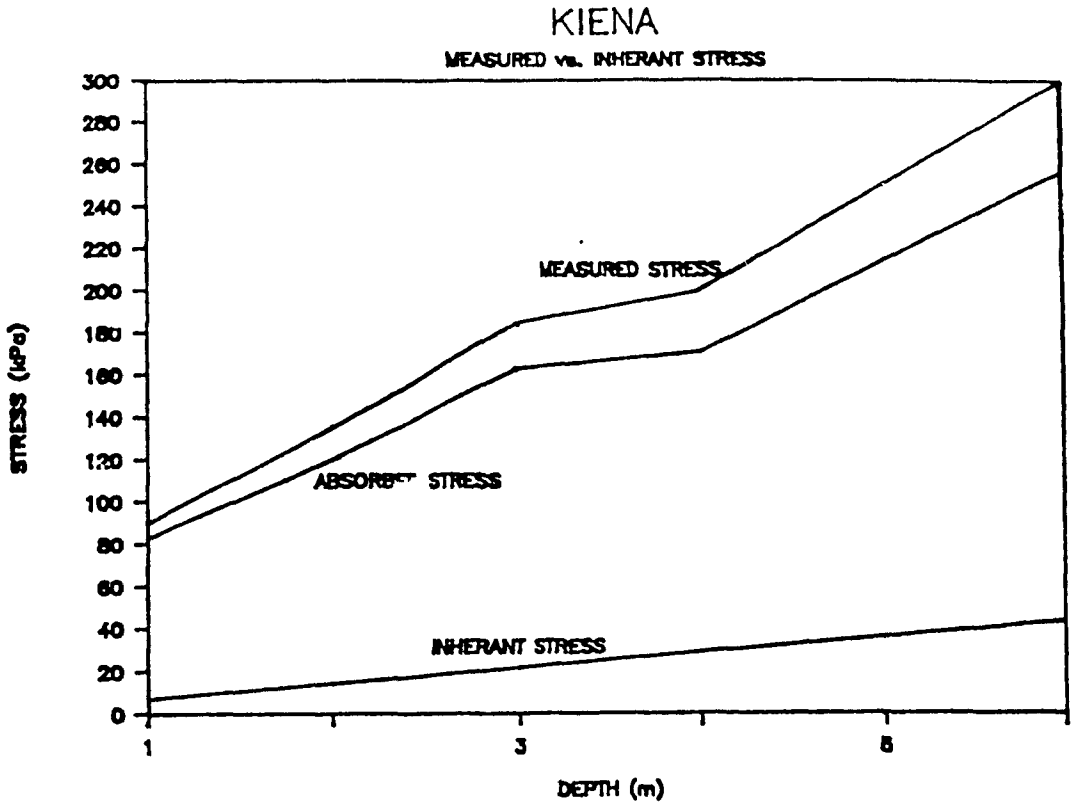

FIGURE 8.17 Lateral Stress Components at Kiena

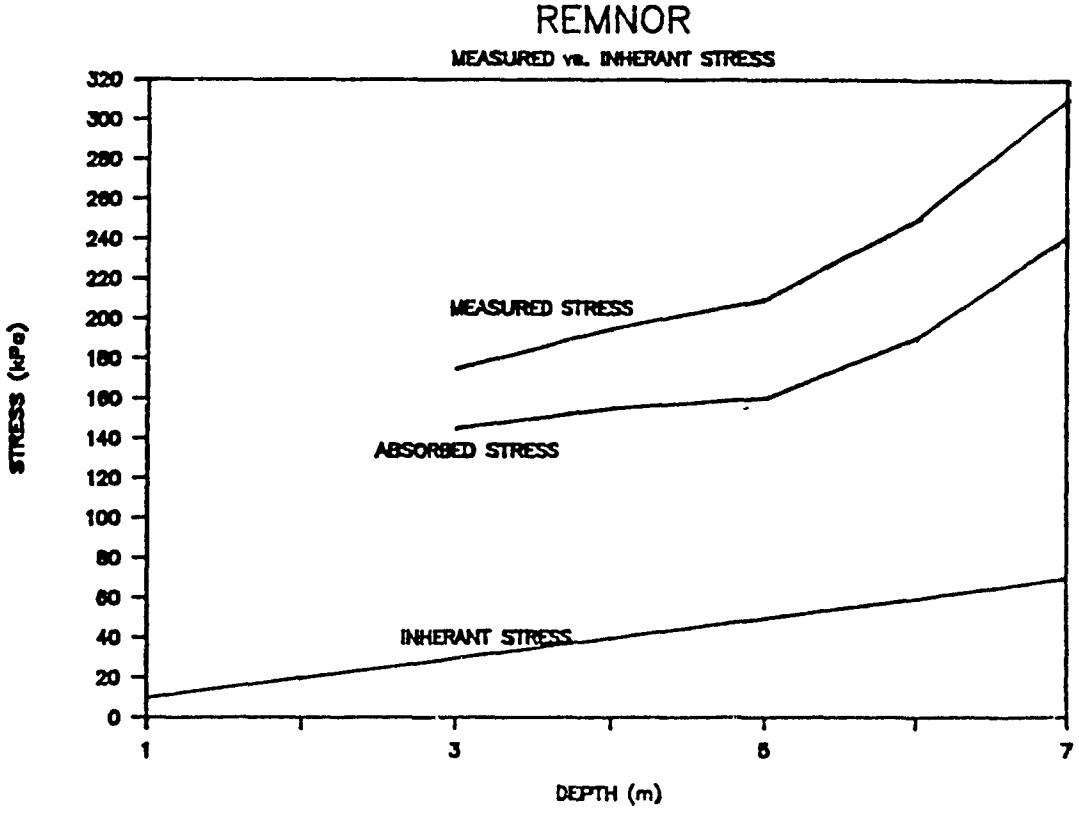

FIGURE 8.18 Lateral Stress Components at Remnor

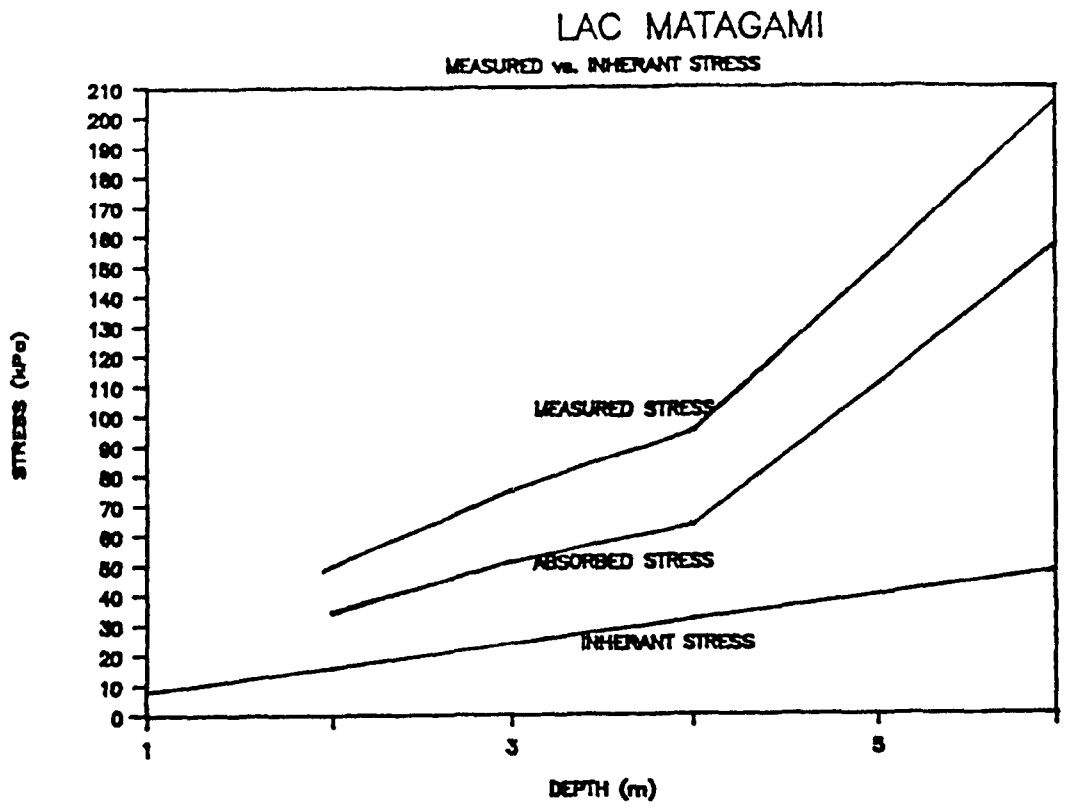

FIGURE 8.19 Lateral Stress Components at Lac Matagami

The lateral stress component due to self weight, or inherant stress, must be subtracted from the data presented in Table 8.7 to give the absorbed stress. Figures 8.17, 8.18 and 8.19 graphically represents the three components of horizontal for the three mine locations listed in Table 8.7.

The comparison of the absorbed lateral stresses, Figure 8.20, for the Lac Matagami (uncemented) and Kiena (cemented 20:1) materials indicates that the absorbed lateral stresses at Kiena are consitantly 60 to 250 % higher than in the uncemented backfill at

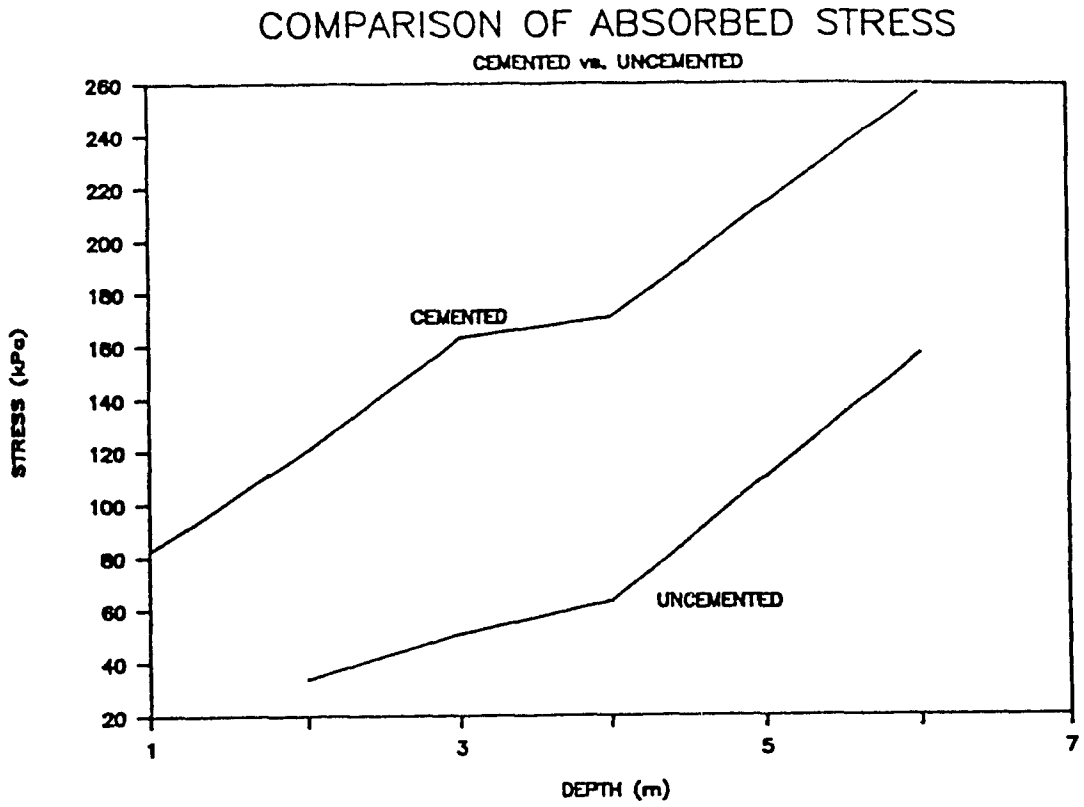

FIGURE 8.20 Comparison of Absorbed Stresses

Lac Matagami. This leads to the conclusion that the addition of cementing agents significantly increases the stresses absorbed by the backfill. This conclusion should be qualified as the backfill materials at Lac Matagami and Kiena exist in different stress environments.

8.3 Summary

This chapter has summarized the techniques for data correction and instrument calibration. A modified instrument calibration procedure has also been proposed. The pressuremeter data has been put in the context of the Pencel pressuremeter sensitivity.

The chapter subsequently presented the in situ geomechanical properties of mine backfills tested. It is possible to conclude from the available data that both the strength and stiffness characteristics increase with cementation and length of curing. The wide range of geomechanical properties observed for the uncemented backfills implies that the physical characteristics exert control over the material strength and stiffness. The stiffness properties also show a significant increase with the addition of flocculants while the strength parameters remain unchanged.

Several empirically derived geomechanical parameters, including the undrained shear strength, angle of internal friction and the coefficient of earth pressure at rest, K_o, have been presented. The available undrained shear strength equations show a 40 % variation in the predicted shear strengths, thus a new equation has been proposed which reduces the variability of predicted shear strengths to 20 %. New relations for the K_o parameter and the horizontal stress have been proposed. These are based on the limit pressure and material density. The K_o parameter along with the total lateral pressure have been used to estimate the stresses absorbed by the backfill.

The geomechanical properties described in this chapter are subsequently correlated to the laboratory derived properties in Chapter 9.

9.0 LABORATORY GEOMECHANICAL PROPERTIES AND IN SITU CORRELATIONS

The objective of this chapter is to present the backfill design and field correlation equations which have been developed as part of this study. This chapter begins by describing the results of an extensive laboratory testing program including results from 220 shear box, 100 tilt box and 50 uniaxial compression tests. This test data is combined with some 430 data points accumulated from published works to form the basis for backfill design for cemented fine-grained backfills. In a similar manner the laboratory data is used to develop backfill design equations for uncemented fine-grained backfills and uncemented rockfills. The chapter further describes the relations which have been developed to extrapolate laboratory data to the field environment. The combination of laboratory design equations and field correlations are aimed to enable the mine engineer to predict field response from laboratory tests for uncemented fine grained backfills.

It further noted here that a downloaded version of STATPAK (209) is used for all regression analysis performed in this thesis. The program predicts the regeression coefficents by the least squared method. The assumption is made that the measurement of the independant variable is made error free. In addition it is not known if "linearizing parameterization" is conducted automatically by the program formulation.

9.1 Laboratory Strength And Stiffness Parameters

This section describes the laboratory data for cemented and uncemented fine grained backfills and uncemented rockfill materials.

The method of analysis is described and the relevant design equations outlined. It is noted that design equations have been developed for three of the four backfill types; with cemented rockfill having been excluded due to lack of data. The relations developed for each of the backfill types analyzed indicated strong correlations between physical and mechanical parameters.

9.1.1 Cemented Fine-Grained Backfills

The literature contains abundant information on the strength characteristics of cementeted fine-grained backfills which have been used for this analysis and reported in Appendix 15. The data accumulated and reported on herein is based uniaxial laboratory tests on 15.25 cm. diameter by 30.5 cm. in length. The precise curing conditions includings moisture and temperature, sample preparation techniques, Portland cement type used and the details of the testing techniques were often not reported. The can thus account for some of the residual scatter remaining in the data after the final analysis. The analysis carried out in the literature normally consists of the correlation of compressive strength to Portland cement content and thus a significant variation with curing time still exists. In this light the first attempts at analysis of the accumulated data is on the basis of strength variations with cement content. A follow up analysis is also carried out with the objective of eliminating curing time variations and decreasing data scatter.

The number of observations of uniaxial compressive strength has been presented in Table 6.1. The accumulated data is based on

the work of over 30 authors on more than 40 different mill tailings fills, representing mostly Canadian mines. Although substantial data was available a careful screening was required to eliminate non - conforming procedures. For instance a abundance of data available from Thomas (16) (29) could not be used as the tests were conducted at .1 MPa confinement. It was with this same meticulous screening process that the final data base was established. Considerable data was available for 28 day curing while less than half as many values were found at 7, 14 and 90 days curing. The cement mixes represented by this data ranges from 2.5% to 20% with a decrease in the number of observations with increased cement addition.

The regression analysis for each of the curing periods showed strong positive correlations with cement addition. Figures 9.1 to 9.4 illustrate the data for each curing period and the prediction curves resulting from the regression analysis along with the 90% confidence interval. The regression constants and coefficients are summarized in Table 9.1.

Figures 9.1 to 9.4 further illustrate that although a strong positive correlation exists in each case, large variations can occur between predicted and observed values. This variation is further demonstrated by Table 9.2 which presents the 90% confidence interval for the regression constants a and b. This table further also provides the length of the confidence interval as a precentage of the established regression coefficent. An increase in this ratio corresponds to and increases in scatter. The inconsitancy between acceptable correlation coefficient and observed scatter results from

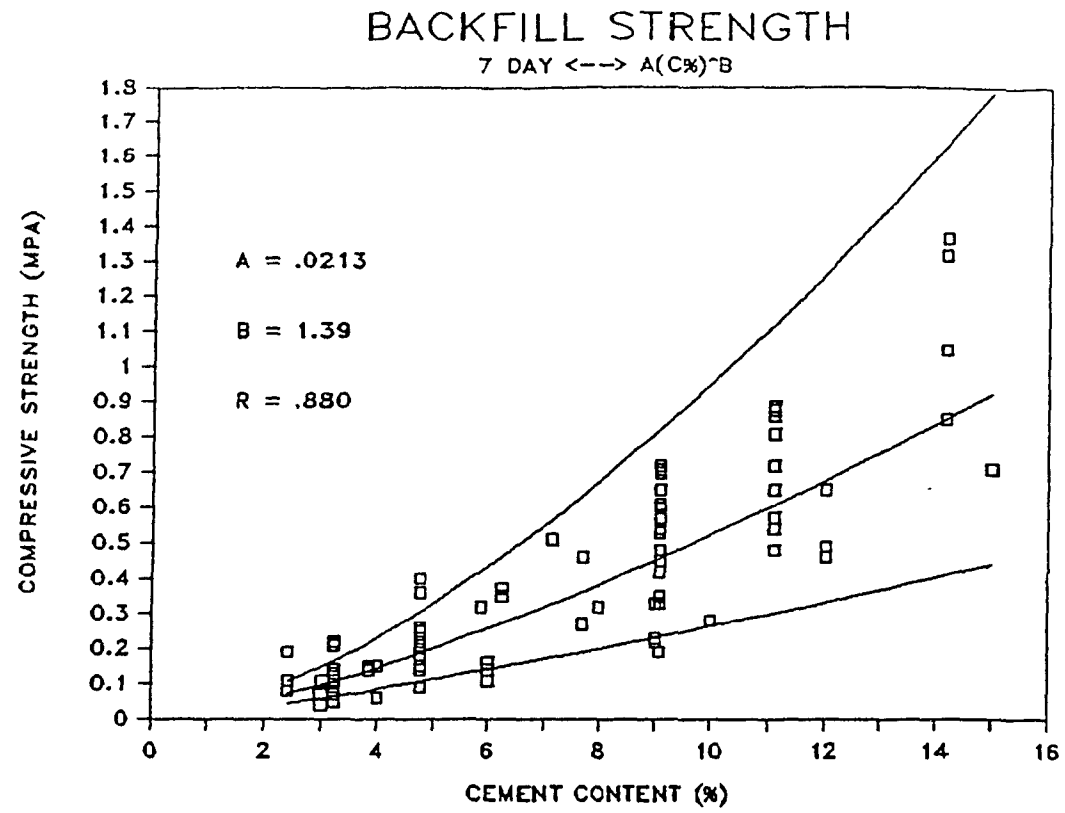

FIGURE 9.1 Uniaxial Compressive Strength vs. Cement Content 7 Day Curing Period

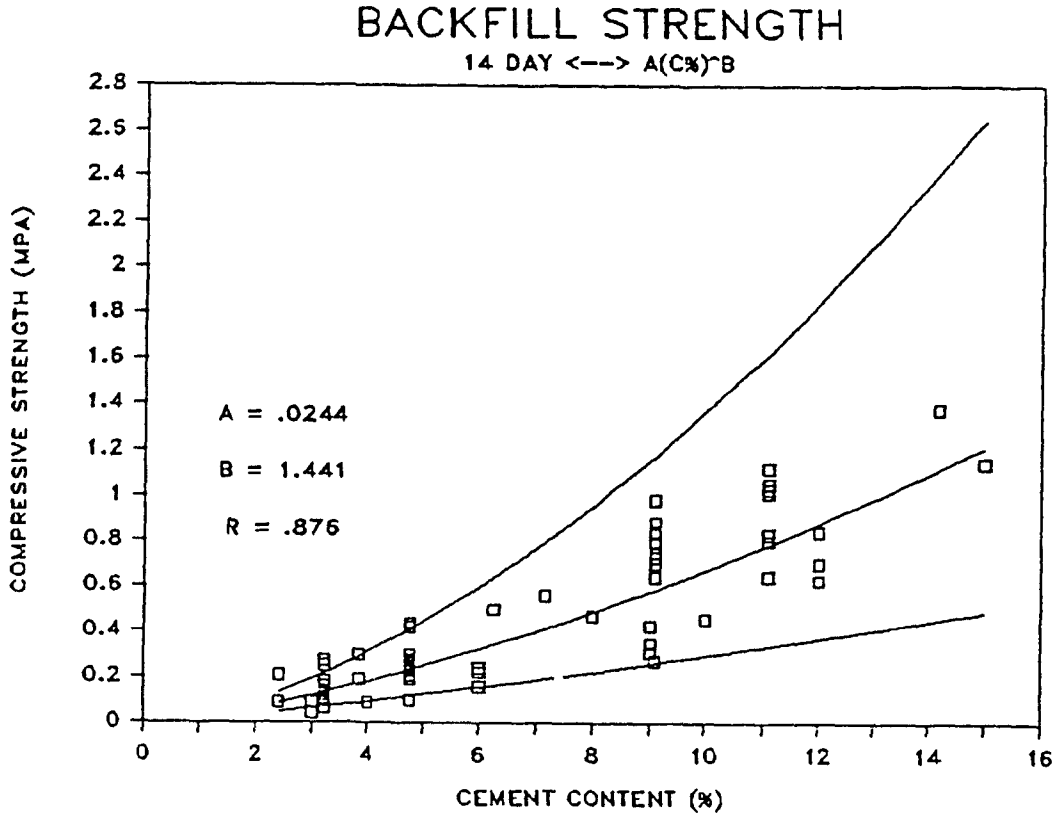

FIGURE 9.2 Uniaxial Compressive Strength vs. Cement Content 14 Day Curing Period

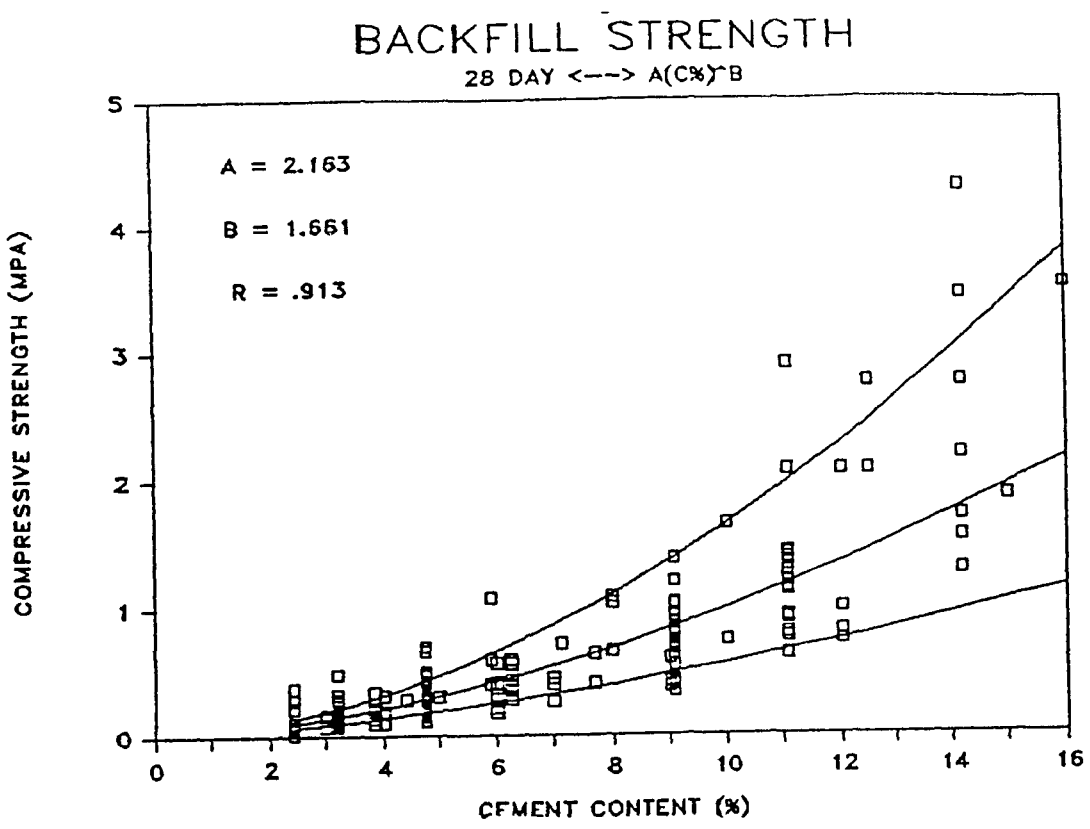

FIGURE 9.3 Uniaxial Compressive Strength vs. Cement Content
28 Day Curing Period

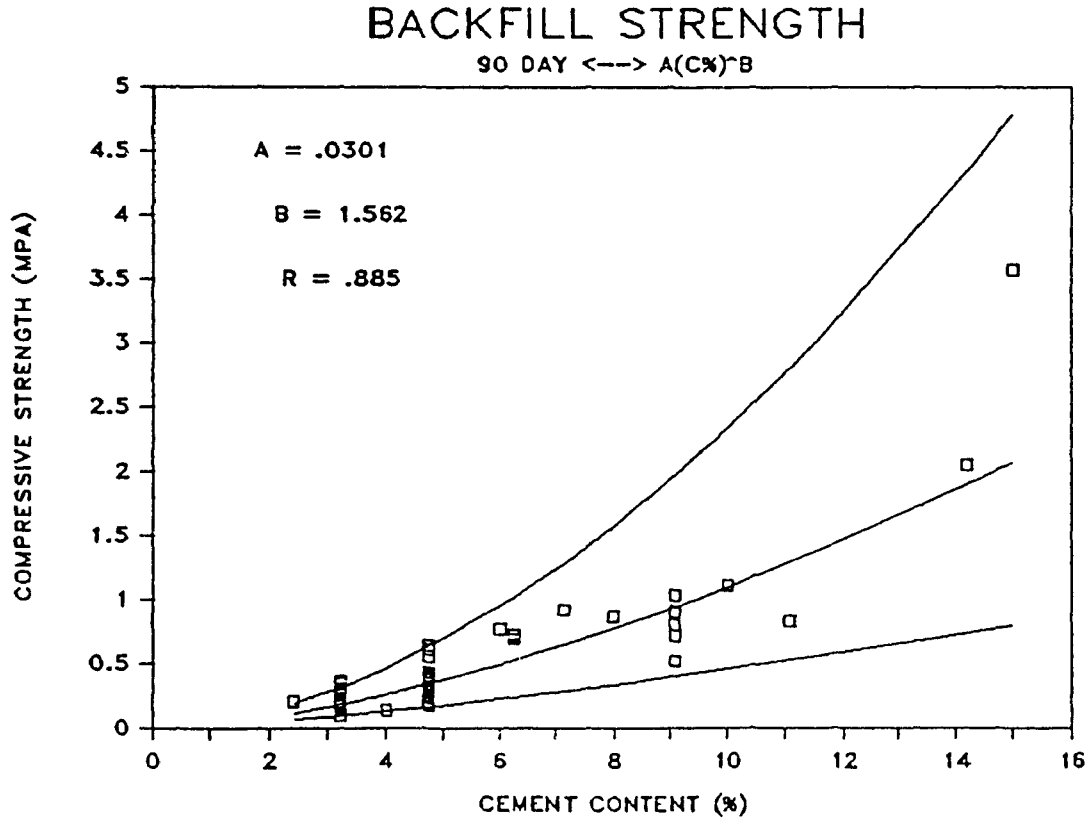

FIGURE 9.4 Uniaxial Compressive Strength vs. Cement Content
90 Day Curing Period

EQUATION FORM: UCS = A*(C%)^B

where:

S = UNIAXIAL COMPRESSIVE STRENGTH
C% = CEMENT CONTENT
A, B = EMPIRICAL CONSTANTS

CURING TIME	A	B	R
7 DAYS	0.0213	1.392	0.880
14 DAYS	0.0244	1.441	0.876
28 DAYS	0.0216	1.661	0.913
90 DAYS	0.0301	1.562	0.885

TABLE 9.1 Regression Equations For Uniaxial Compressive Strength vs. Cement Addition

the symmetric scatter of data above and below the prediction curve. The symmetric scatter results in counterbalanced positive and negative scatter which have cancelling effects and thus results in high regression coefficients. On the other hand visual inspection indicates that the trend is appropriate but the potential regression error still remains large. It should be emphasized, however, that the equations presented in Table 9.1 still provide a good basis for preliminary design, as the equations provide a means of obtaining an average value for backfill strength for a given cement content and curing period.

CURING TIME	90% CONFID. INTERVAL FOR "A"	INTERVAL AS % OF "Amean"	90% CONFID. INTERVAL FOR "B"	INTERVAL AS % OF "Bmean"
7 DAYS	.0153 - .0272	±28.0	1.239 - 1.545	±11.0
14 DAYS	.0163 - .0325	±33.1	1.257 - 1.625	±12.8
28 DAYS	.0165 - .0267	±23.6	1.532 - 1.789	±7.70
90 DAYS	.0202 - .0400	±32.9	1.356 - 1.767	±13.2

TABLE 9.2 Assessment of Data Scatter for Cement Addition Correlation to Uniaxial Compressive Strength

Figure 9.5, represents the empirical curves for each curing period on the same graph. It is noted that only a small increase in strength is obtained as the material cures from 28 to 90 days. This is consistent with experience in concrete technology where 80% of concrete strength has been found to be gained in the first 28 days of curing. It is also noted from Figure 9.5 and regression constant "B", in Table 9.1, that an increase in curvature is observed with increased curing. This implies that the effects of an incremental increase in cement content, particularly for cement contents above 10% (1:10, cement:tailing mixes by weight), are more pronounced at longer curing periods. This is a significant fact as the survey of Quebec and Ontario mines indicates that 59% of Quebec and 29% of Ontario mines presently use uncemented backfills, see Table 4.1.

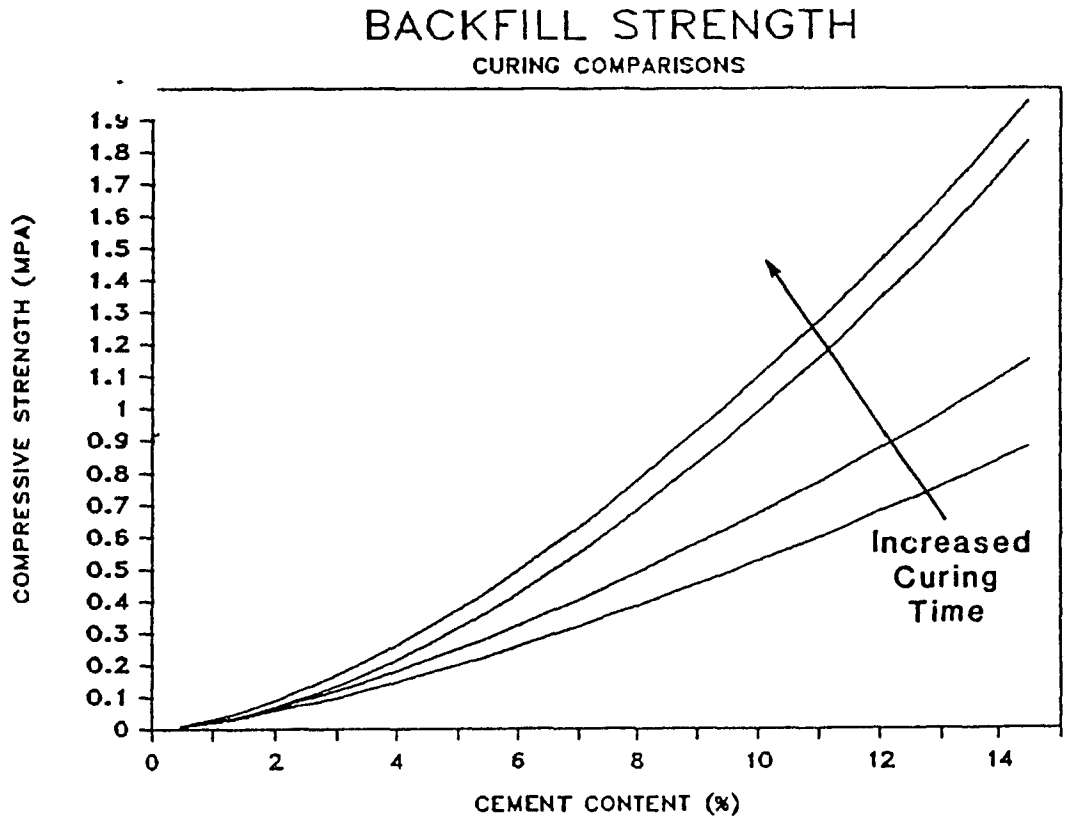

FIGURE 9.5 Empirical Equations Relating Uniaxial Compressive Strength To Cement Content

Furthermore, the data related to the Ontario mining industry indicates that 88.5% of the cemented backfill in use employs less than 10% cement, see Table 4.2. The implication of this is that the cement additions presently being used do not provide maximized marginal strength increases. That is, an increase of .6 MPa is observed for an increase of 2 percentage points in cement addition from 10 to 12%. Similar increases in backfill strength are observed for increases in cement additions from 6 to 10% thus indicating that cement additions above 10% are twice as effective as similar additions below 10%.

The series of equation presented in Table 9.1 provides valuable insight into the behaviour of cemented backfill and the influence of cement addition. However, the scatter of data as reported in Table 9.2 curve indicates that these curves are not suitable for refined design applications. The curves illustrated in Figure 9.5 apply to particular curing periods, furthermore the uneven spacing between the curves indicates a non-linear relation between curing time and backfill strength. The combination of distinct curing periods and their non-linear relation to strength makes the interpolation to intermediate values of curing difficult. The problem is further compounded by poor correlation (R=.531) when curing is incorporated into the equations described in Table 9.1. A different approach was thus required to refine these backfill design equations. The new approach must fulfil two criteria; reduce the amount of data scatter while maintaining acceptable regression coefficients and reduce the effect of curing time on the regression equations.

It was found that by incorporating the initial moisture content; the moisture present when the material is being introduced into the stope, the observed scatter from the design equations is subsequently reduced as account is taken of one further controlling parameter, the moisture content. The use of W/C ratios is consistant with those analysis conducted for concrete design, (202), (203) and the backfill analysis, based on limited backfill data, reported by Manca (65) . The moisture content is incorporated by means of a water to cement ratio (W / C). Figures 9.6 to 9.9 illustrate the regression prediction equations along with the raw data for 7, 14 ,28, and 90 days curing. These curves relate backfill strength to the W / C ratio. Each of the curves illustrates a much tighter packing of raw data around the prediction equation than did the simple cement addition analysis.

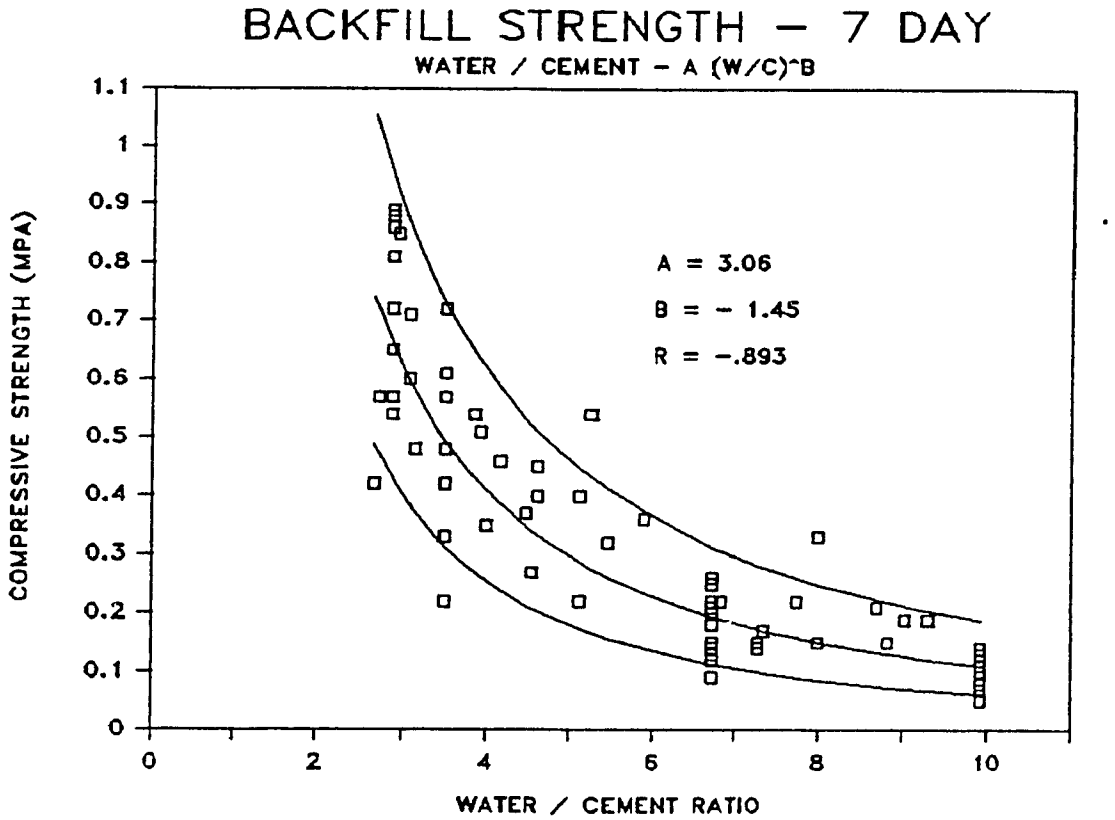

FIGURE 9.6 Uniaxial Compressive Strength vs. Water:Cement Ratio 7 Day Curing Period

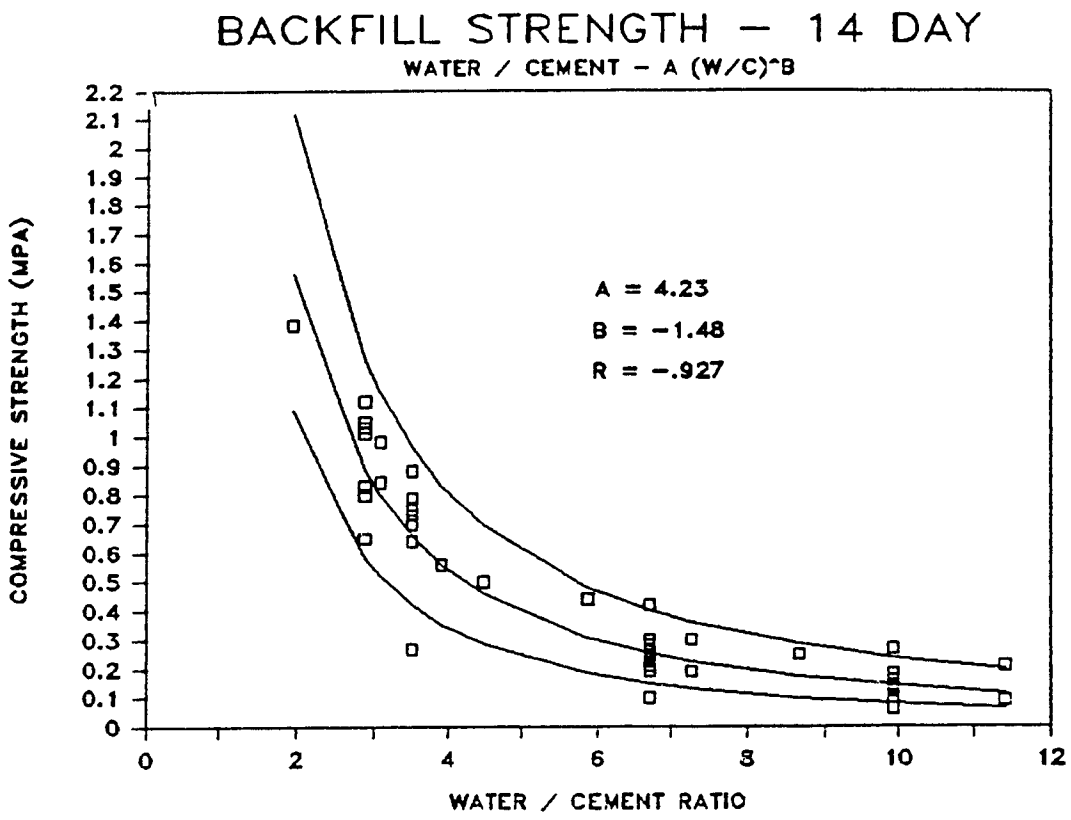

FIGURE 9.7 Uniaxial Compressive Strength vs. Water:Cement Ratio 14 Day Curing Period

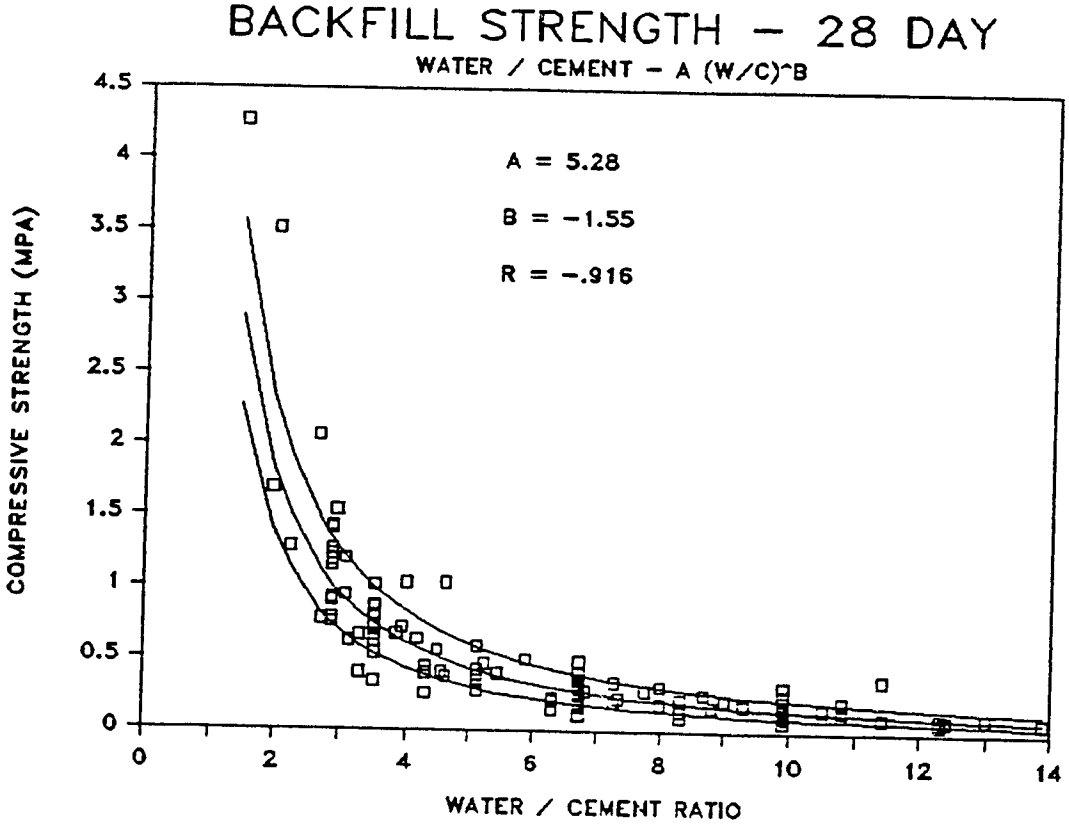

FIGURE 9.8 Uniaxial Compressive Strength vs. Water:Cement Ratio 28 Day Curing Period

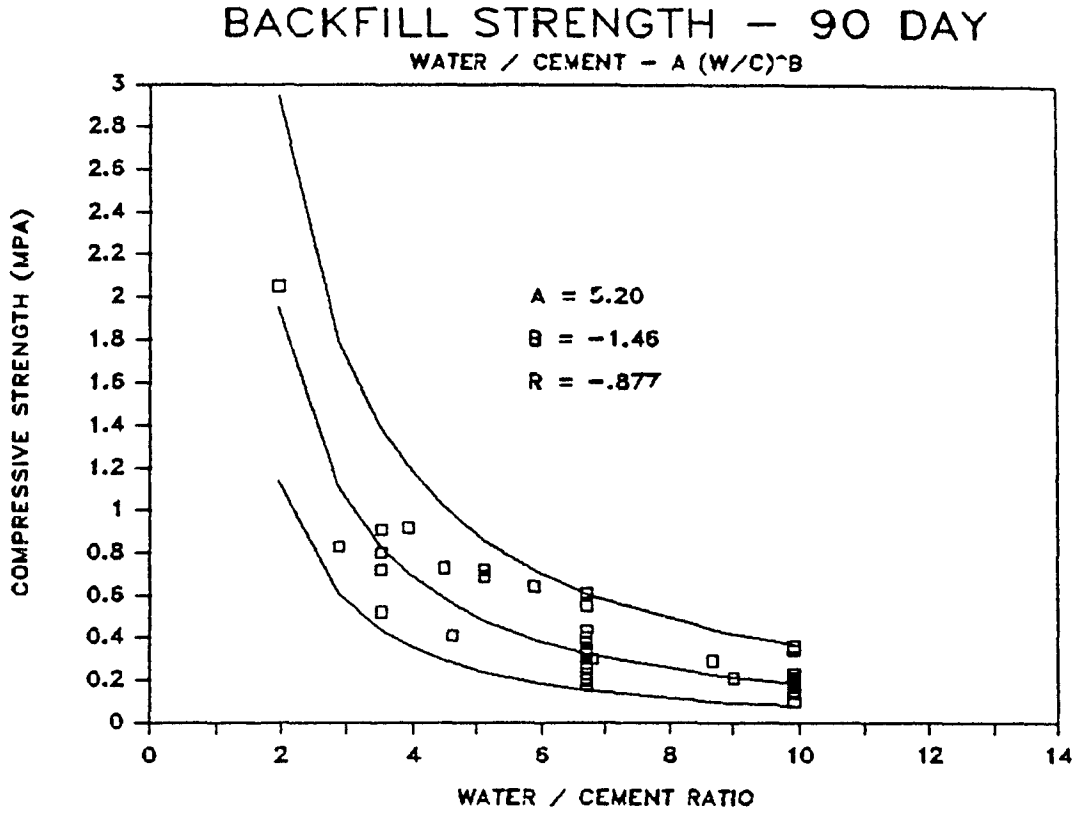

FIGURE 9.9 Uniaxial Compressive Strength vs. Water:Cement Ratio 90 Day Curing Period

EQUATION FORM: $S = A*(W/C)^B$

where:

S = UNIAXIAL COMPRESSIVE STRENGTH
W/C = WATER:CEMENT RATIO
A, B = EMPIRICAL CONSTANTS

CURING TIME	A	B	R
7 DAYS	3.055	-1.449	- 0.893
14 DAYS	4.232	-1.479	- 0.927
28 DAYS	5.280	-1.553	- 0.916
90 DAYS	5.200	-1.458	- 0.877

TABLE 9.3 Regression Equations For Uniaxial Compressive Strength vs. Water:Cement Ratio

CURING TIME	90% CONFID. INTERVAL FOR "A"	INTERVAL AS % OF "Amean"	90% CONFID. INTERVAL FOR "B"	INTERVAL AS % OF "Bmean"
7 DAYS	2.307 - 3.803	±24.5	-1.59 - -1.31	±9.50
14 DAYS	3.212 - 5.250	±24.1	-1.61 - -1.35	±8.80
28 DAYS	4.312 - 6.247	±18.3	-1.65 - -1.45	±6.50
90 DAYS	3.420 - 6.980	±24.3	-1.63 - -1.28	±12.0
TOTAL DATA	3.208 - 4.194	±13.3	-1.48 - -1.34	±5.10

TABLE 9.4 Assessment of Data Scatter for Water:Cement Ratio Correlation to Uniaxial Compressive Strength

Table 9.4 represents the 90% confidence interval for the "A" and "B" regression constants reported in Table 9.3. The reduced scatter is evident in the decreased length of the confidence interval for the A and B regression coefficients, Table 9.4. This table indicates a reduction in the scatter of the A and B regression coefficents when compared to similar parameters in Table 9.2. Compressive strength decreases with increased W / C ratio. This is to be expected as both increased cement addition and decreased moisture have a decreasing effect on the W / C ratio while maintaining a beneficial effect on backfill strength. The relevant equations are summarized in Table 9.3.

The regression constant "A" varies from 3.06 to 5.28 while the "B" coefficient shows a smaller variation between -1.45 and -1.55. The small variation in both the A and B constants suggests the entire backfill strength data base is amenable to analysis as a whole regardless of curing time. This is supported by Figure 9.10, which illustrates that a variation still exists between compressive strength and curing period, but has been substantially reduced from the previous analysis which considered cement content alone as the independant variable. Having said this, an analysis on the data for

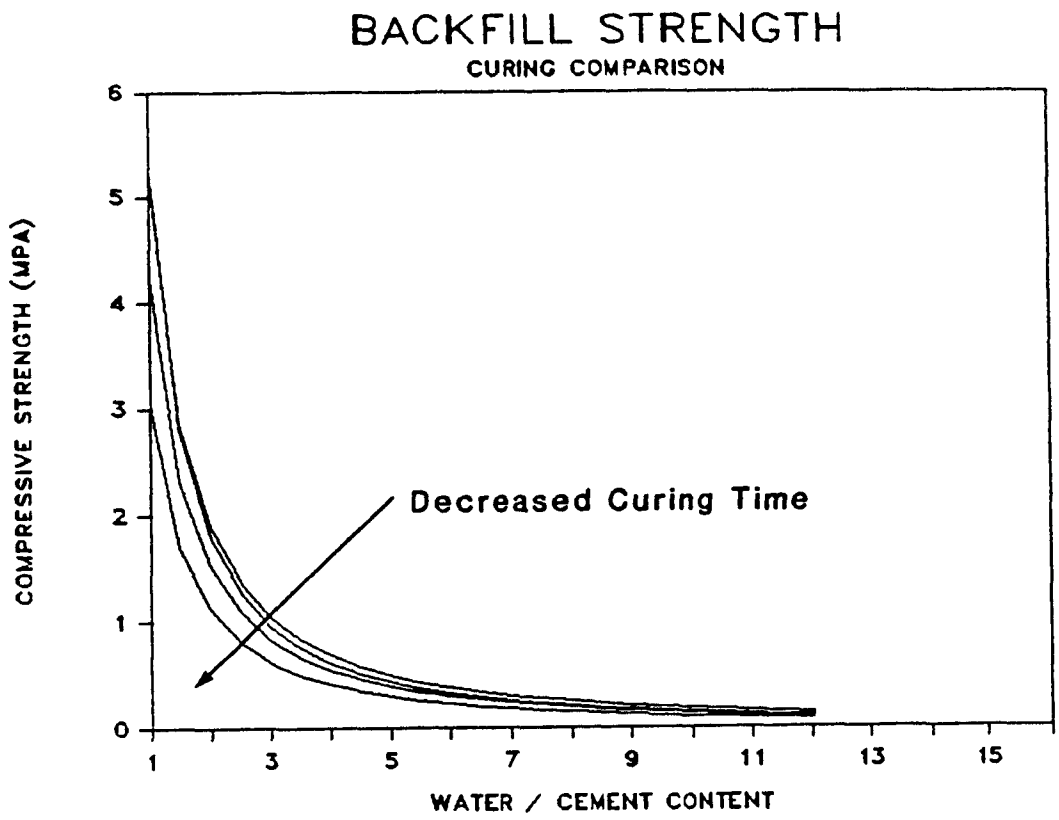

FIGURE 9.10 Empirical Equations Relating Uniaxial Compressive Strength To Water:Cement Ratio

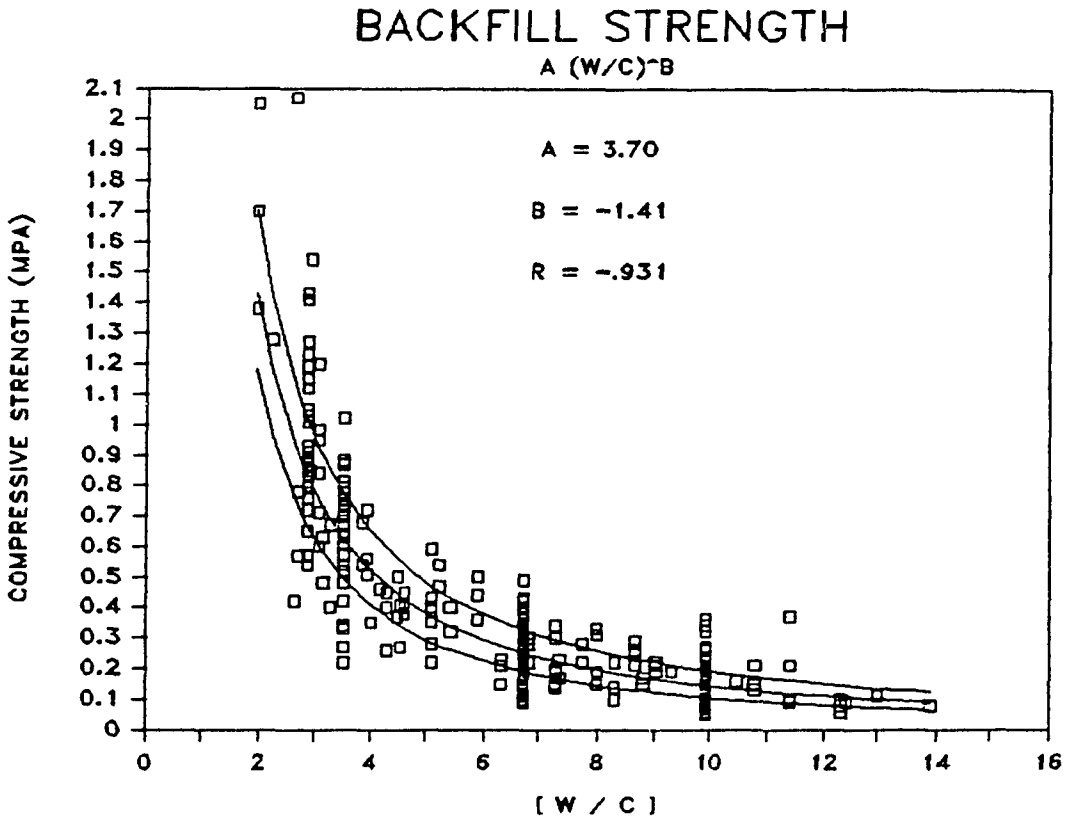

FIGURE 9.11 Averaged Empirical Equation Plotted Against Raw Data For All Curing Periods

all curing periods has been performed. The analysis produced the curve illustrated in Figure 9.11 and equation 9.1. Equation 9.1 also yields a regression coefficient of -.931, indicating a strong negative correlation. In addition the scatter is further reduced when compared with the curves relating the W/C ratio to compressive strength for individual periods, this is also illustrated in Table 9.4.

$$UCS = 3.70\ (W/C)^{-1.41} \qquad \text{..... 9.1}$$

It is further noted that if the averaged regression equation is compared to each of the curves described in Table 9.3 the estimation error due to curve averaging, which represents the elimination of curing time as a variable, can be measured. Figure 9.12 has been produced to represent the estimation error encountered by curve averaging. It is further noted that the estimation error is dependant on the curing curve being considered and the range of W/C which is of interest. Using the 28 day data as a yardstick, and if we consider a 10% cement mixed in a 60% pulp density (W/C=4) the estimation error associated with Equation 9.1 in relation to Table 9.2 is consistantly below 20% and is 8.22% for this example. Figure 9.12 further indicates that that for W/C ratios greater than 4 the estimation error is reduced below 8%. It should be noted here that error induced by the elimination of curing is smaller than that associated with the 90% confidence interval. thus this error need not be considered separately as it falls within the prescribed confidence limits. This is of interest as the bulk of data represented in Figure 9.11 is for W/C ratios above 4.

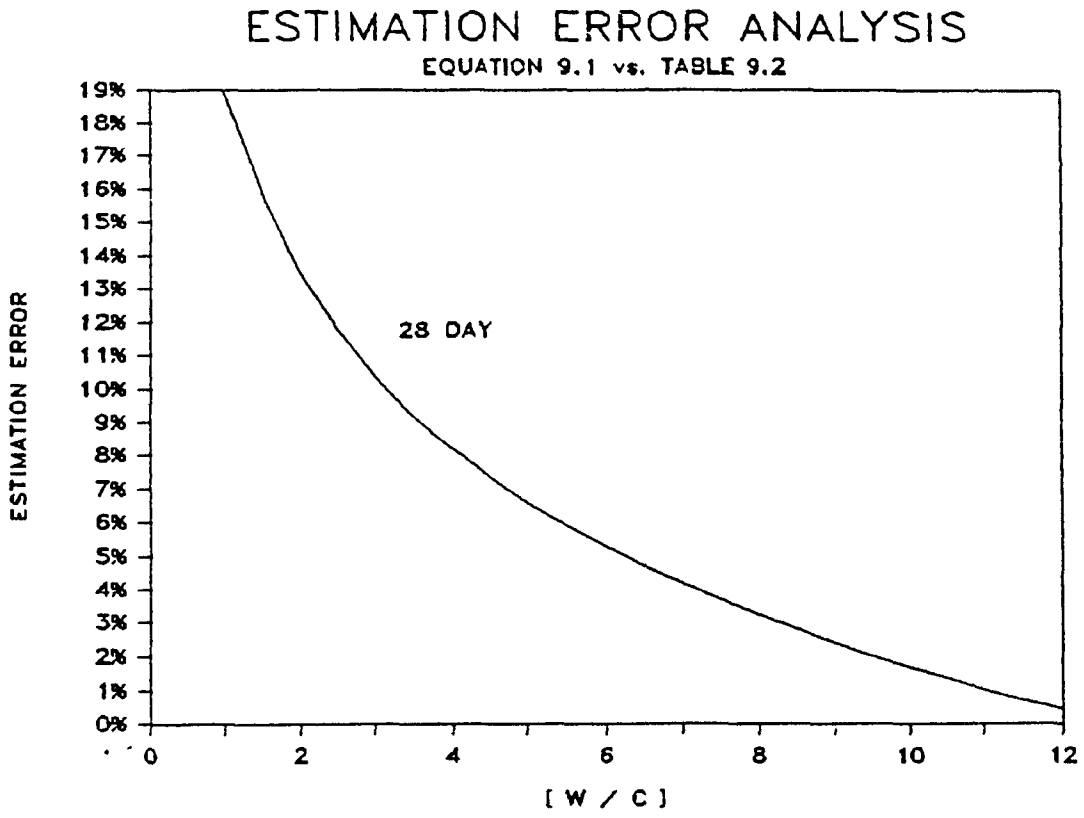

FIGURE 9.12 Estimation Error For Equation 9.1

The conclusion must thus be drawn that for the range of backfills involved in this study the effect of curing would seem to be negligible. This conclusion would seem to be inconsistant with the expected trends observed in concrete design technology, thus the conclusion warrants further investigation. We must first recognize that cemented fine grained backfills attain their strength by the addition and hydration of Portland cement. Furthermore, any part of a sample preparation or field implementation procedure which directly affects the distribution of Portland cement or the hydration process itself will have an effect on the the compressive strength of the backfill. It is with this in mind that the apparent

inconsistancy is investigated, with further examination of the effect of W/C ratio on compressive strength and by the investigation of excess water on the hydration process of Portland cement.

Teychenne (202) found that although most concrete is mixed at a W/C ratio of .5 some of the variations in concrete strength can be accounted for by variations in this ratio. He found that as the W/C ratio increased then the compressive strength correspondingly decreased, this trend is consistant with that reported in this chapter. Figure 9.13 illustrates this finding and shows consistent

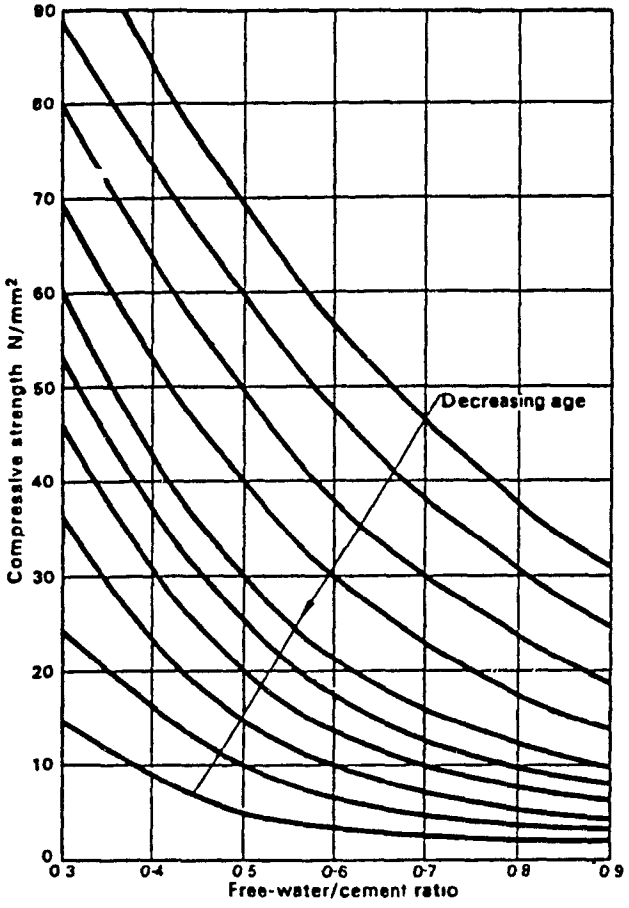

FIGURE 9.13 Effect of Curing and W/C Ratio on Compressive Strength, After Teychenne (202)

trends for all curing periods. Although the actual curing periods are not illustrated in Figure 9.13 a further trend is revealed. These curves indicatr a trend towards convergence as the W/C ratio increases. It is further noted that the W/C ratios illustrated in Figure 9.13 extend to a maximum of .9. In fact, the preliminary data presented by Manca (65) applies to W/C ratios between 1.25 and 1.75 which remains. These ratios remain too low to observe the reduced effect of curing. The data base for cemented fine grained backfills in this study, however, indicates a range of W/C ratios between 2 and 14. Thus the convergence indicated by Figure 9.13 in more pronounced and the curing curves will be more tightly packed at the W/C ratios normally encountered in cemented mine backfills. The tighter packing of the curing curves indicates that at higher W/C ratios such as those encountered in mining backfill practice the effects of curing would be much less pronounced than at low W/C ratios, thus supporting the authors hypothesis that the effects of curing are negligible.

Further reference to research on the hydration process of Portland cement, is relevant to the mine data analysis. Illston (203), on commenting on the limits of Portland cement hydration, suggested that at high W/C ratios there will exist capillary space not reached by the cement gel at the end of hydration, thus yielding a weaker, hardened cement paste, hcp. Furthermore, this inherent weakness becomes the predominant control of hcp strength at high W/C ratios. This in turn will weaken the concrete or backfill matrix. This also reinforces the conclusion that at high W/C ratios (>2) the predominant controls on backfill strength is the effect of excess water on the hydration process rather than the curing time.

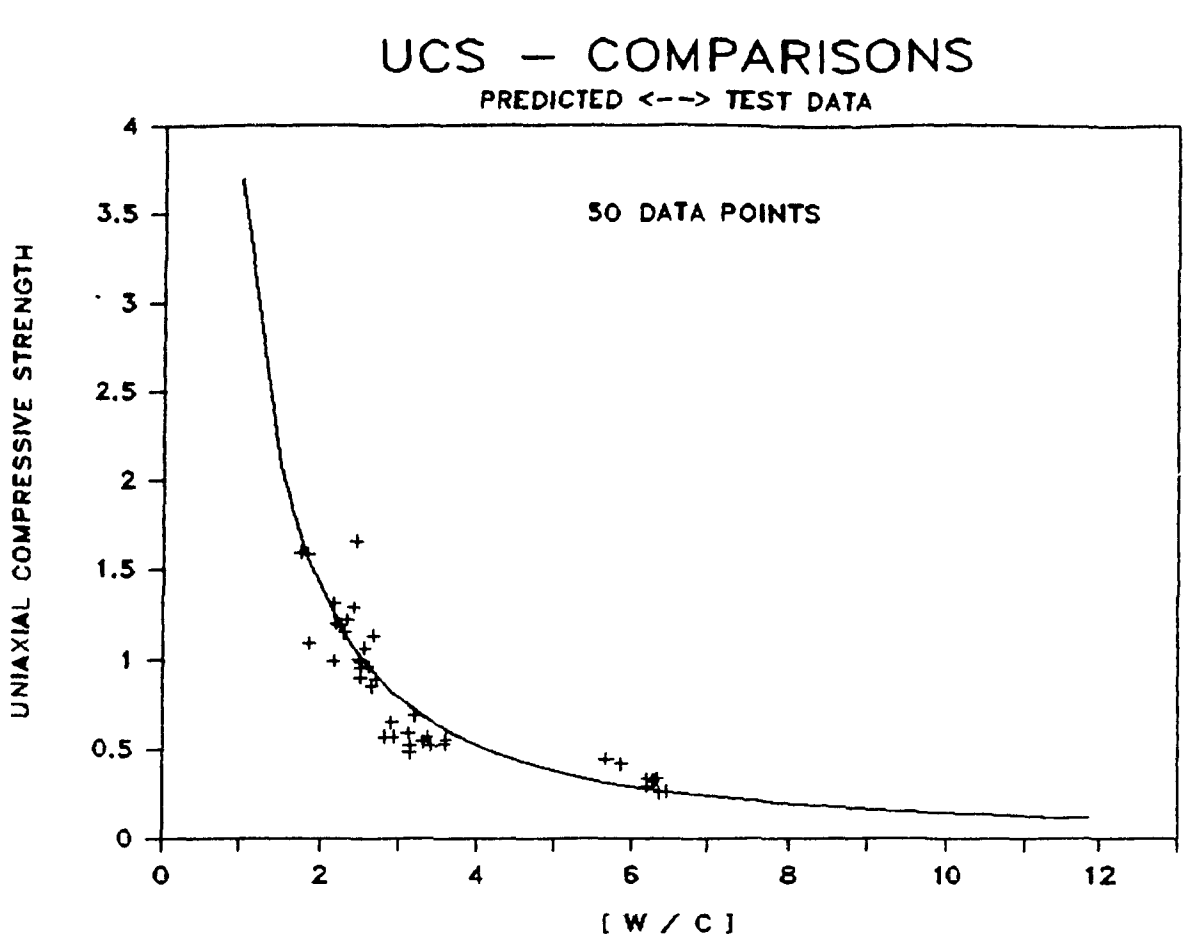

FIGURE 9.14 Comparison Of Uniaxial Compressive Strength Prediction To Laboratory Data

The only remaining limitation of equation 9.1 is related to the reduced scatter still remaining in the data. This is not viewed as significant when the variations in sample preparation and testing techniques exist for the procedures employed by the 30 authors from whom the original published data has been extracted. Although, the results of the regression analysis yielded satisfactory results and the observed trends and conclusions seem reasonable, it was further felt that a series of controlled verification tests were required. To this end a series of 50 uniaxial compression tests were conducted for a 5% Portland cement mix over a range of curing time and

moisture. The results of these tests were plotted against equation 9.1 and are represented in Figure 9.14. The laboratory data is presented in Appendix 11. The close correlation illustrated between laboratory test data and equation 9.1 further increases our confidence the final design equation.

It shoud be noted that although equation 9.1 has been made independant of curing, part of the residual scatter illustrated in Figure 9.11 is due to curing and is not representable in mathemathical form for this database. Equation 9.1 is presented thus as an acceptable means of prediction of backfill strength characteristics from physical parameters. The implications of this design criterion will now be considered.

There are several profound operational implications of equation 9.1 which should be explored in further detail. The objective of backfill design in light of equation 9.1 should be to decrease the W/C ratio. This can be achieved in two ways; by increasing the cement content or by decreasing the water content. Illston (203), suggests that a minimum W/C ratio of .4 be maintained to ensure that complete hydration of Portland cement occurs. The curve form further indicates that maximized marginal increases in compressive strength are achieved for W/C ratios below 3.5, see Figure 9.15.

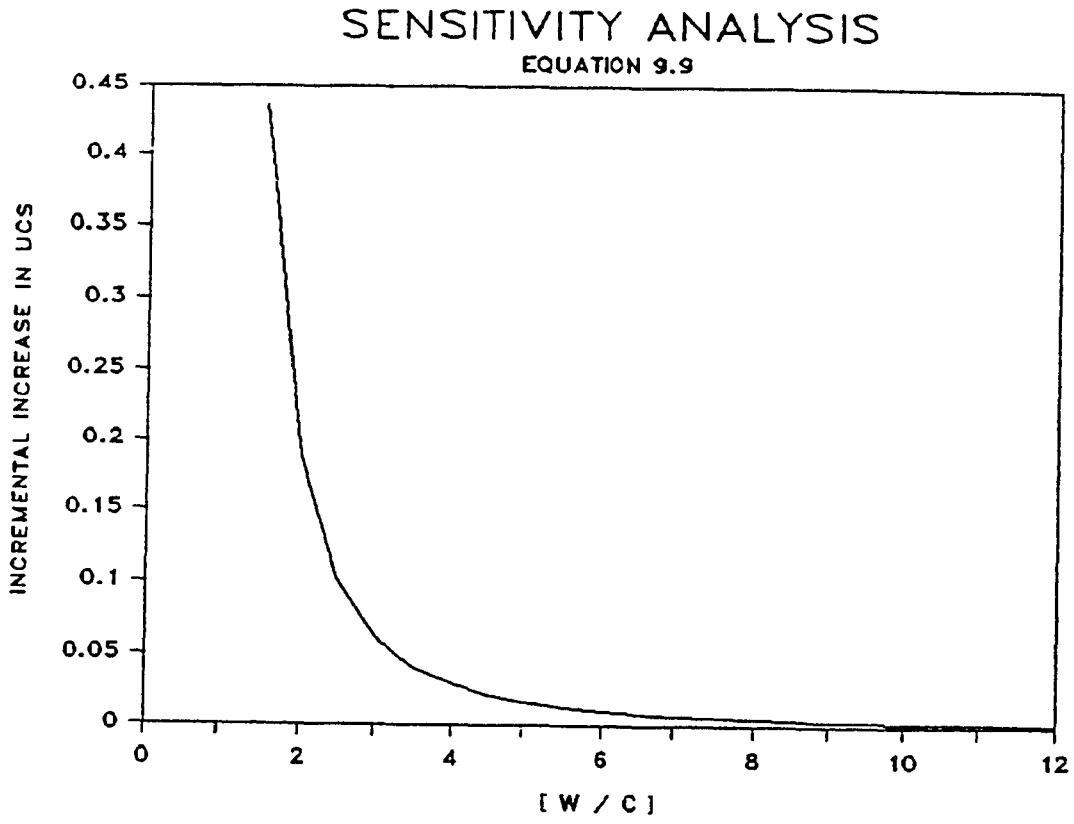

FIGURE 9.15 Sensitivity Analysis Of Equation 9.1

From an operational point of view this would imply that for typical mining pulp densities of 65% (moisture: 35%) cement additions above 10% provide maximized marginal increases in compressive strength. It should further be noted that such a backfill system could further be optimized by increasing the pulp density to 68.5 (moisture: 31.5%). In so doing the same backfill compressive strength can be achieved with 9% cement addition, resulting in a saving of 1% point in cement content. It is also evident from Figure 9.15 that W/C ratios above 6 are to be avoided.

The previous example illustrates a means of predicting backfill strength given a set of physical parameters. However, from a design point of view it is required that Equation 9.1 be reworked

so that the W/C ratio can be calculated from a desired uniaxial compressive strength. This has been done and represented in Equation 9.2

$$W/C = 2.53\ (UCS)^{-.709} \qquad \text{..... 9.2}$$

The use of this equation provides a means of determining the required W/C ratio to achieve a desired strength. One further step is still required to convert the W/C ratio to operational parameters such as cement content and pulp density. Such a conversion would enable the optimized design of backfill with respect to cement content and pulp density. Figure 9.16 has been plotted for W/C ratios between 1 and 6, the curves have been cut -off at cement contents of 20% and pulp densities of 40% as any values beyond this are considered impractical.

The use of Figure 9.16 for optimizing backfill design is best illustrated by an example. Given that a cemented backfill with a uniaxial compressive strength of .79 MPa is required. This requirement is inputted into Equation 9.2, also provided on Figure 9.16, to determine a necessary W/C ratio. The ratio for a uniaxial compressive strength of .79 MPa is 3.0. It is further noted that a W/C of 3.0 can be obtained anywhere on the line labeled "3" on Figure 9.16. Thus, both a combination of 20% cement at a 40% pulp density or a cement content of 8% at 76% pulp density would yield the same results. It would then be up to the design engineer to determine the optimum combination of pulp density and cement

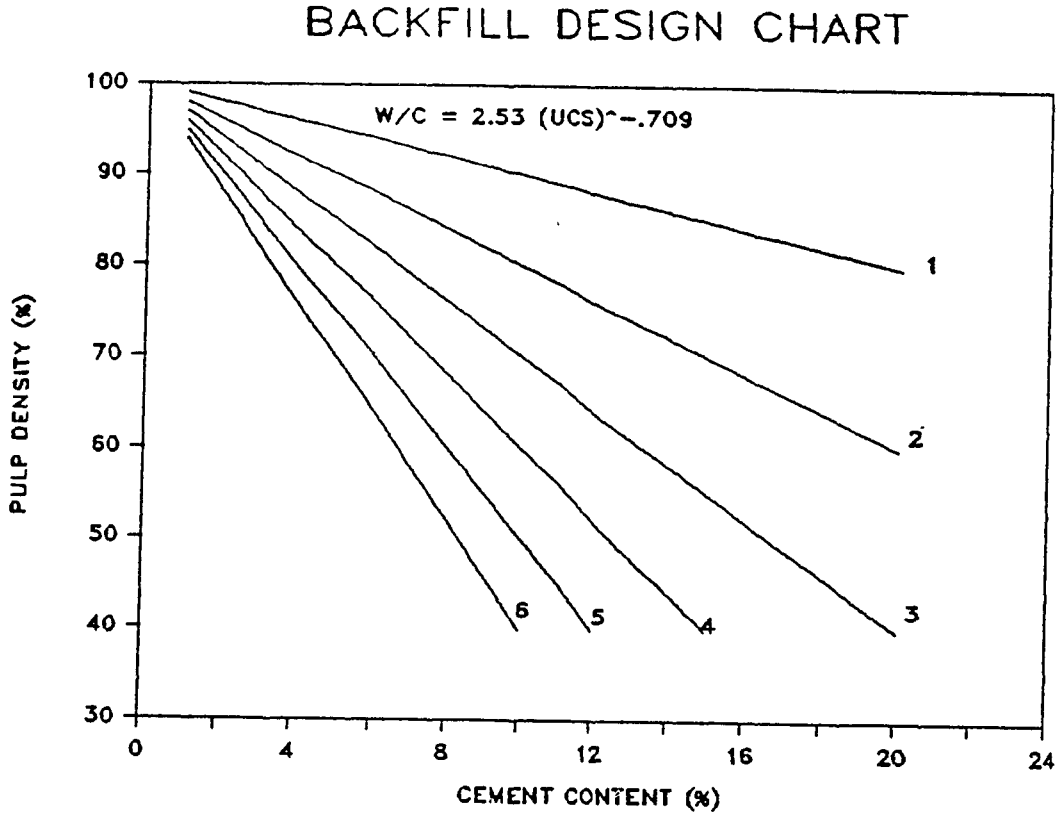

FIGURE 9.15 Backfill Design Chart

content. This decision should be based on a marginal cost benefit analysis between increasing the pulp density with the associated costs of plastizers in transportation lines or dewatering using tailspinners versus the option of increasing cement content.

The discussion to date has centered around the relation between uniaxial compressive strength and the W/C ratio. However, it is often required to use a backfill stiffness for modelling purposes. The literature, however, does not contain the abundance of stiffness data which was available for uniaxial compressive strength. Swan (189) has produced a relation between backfill stiffness and uniaxial compressive strength. This empirical relation has been presented here as Equation 9.3.

$$E = 210\ (UCS)^{1.44} \qquad \ldots\ldots\ 9.3$$

where: E and UCS are the stiffness and uniaxial compressive strength respectively, MPa.

Equation 9.3 has not been verified in the literature and the specific test conditions have not been outlined. The 50 uniaxial compression tests which were used to verify equation 9.1 were also instrumented so that the material stiffness could be measured. The measured stiffnesses and uniaxial compressive

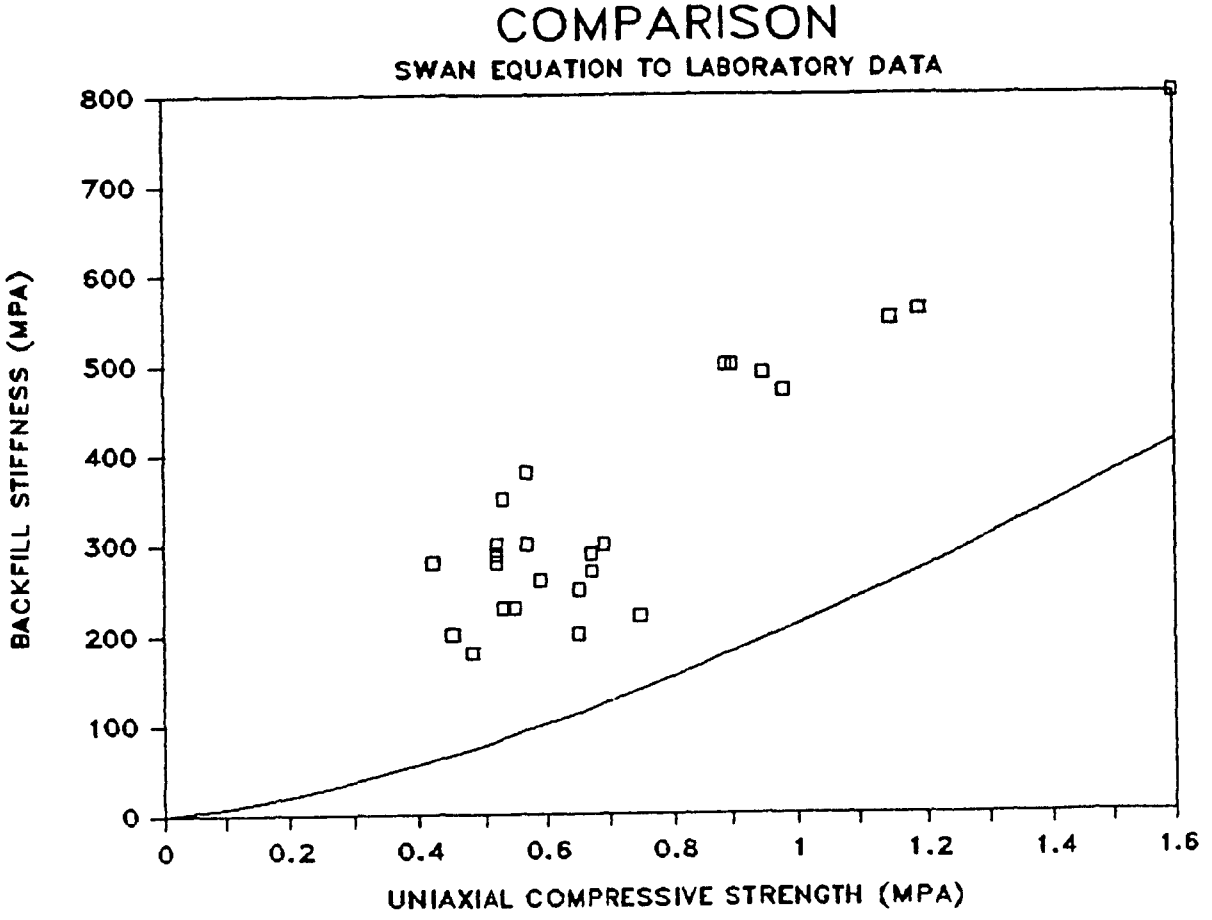

FIGURE 9.17 Verification Of Equation 9.3 Using Laboratory Data

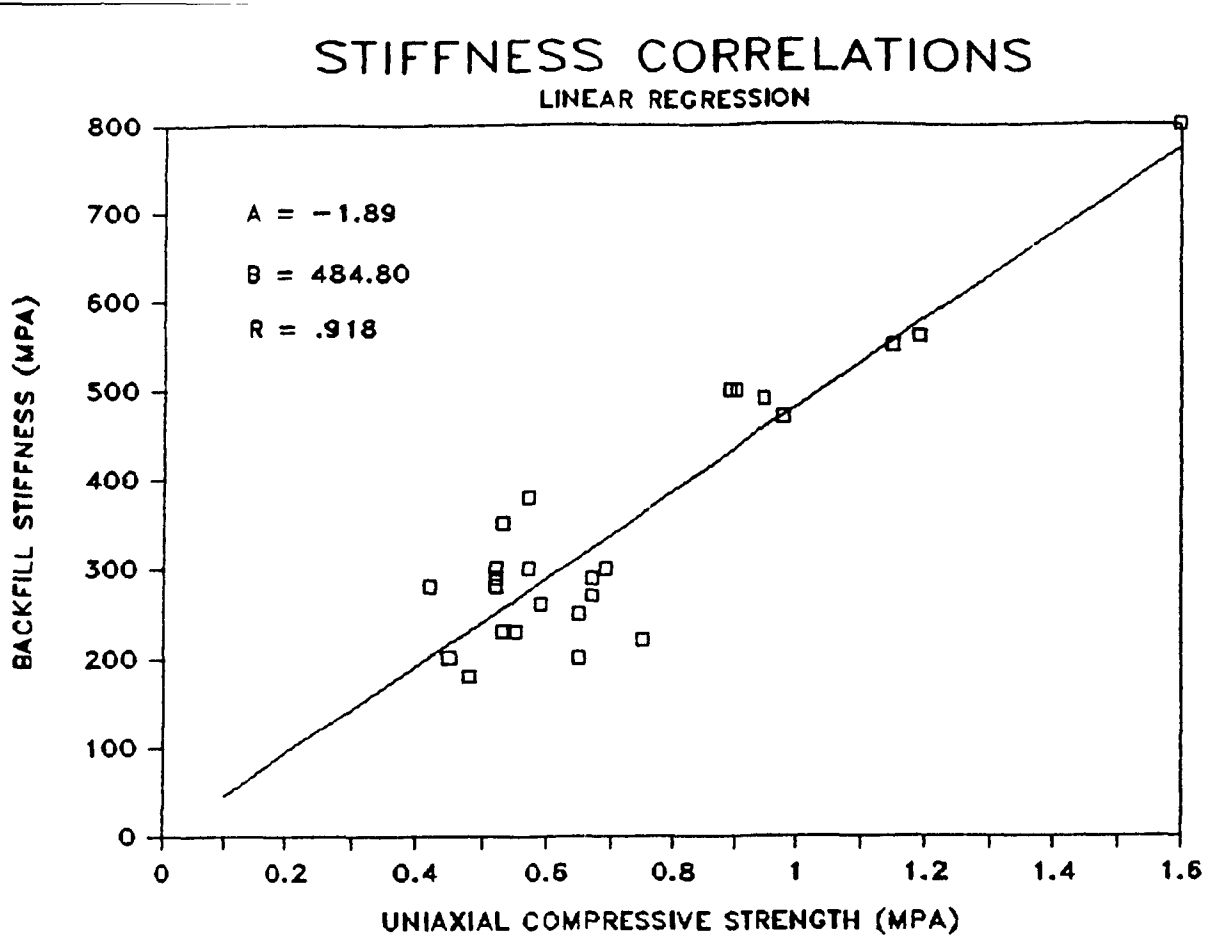

FIGURE 9.18 Analysis Of Laboratory Stiffness And Compressive Strength Correlations

strengths were plotted against Equation 9.3 to verify its applicability and reliability, as illustrated in Figure 9.17. This figure shows that the Swan model consistantly under - predicts the material stiffness as illustrated by the laboratory data.

The data obtained from the laboratory study has thus been analyzed in order to develop a new relation, Equation 9.4. This equation has subsequently been plotted against the raw data in Figure 9.18 and produced a correlation coefficient of .918.

$$E = 484.8\ [UCS] - 1.89 \qquad \ldots\ldots\ 9.4$$

Equation 9.4 can be combined with equation 9.1 to form the basis of stiffness design from the physical parameters; moisture and cement contents. This procedure has been summarized in equation 9.5. The form of this equation implies that an increase in void ratio also decreases the material stiffness.

$$E = 1793.8 \left[W / C \right]^{-1.41} - 1.89 \quad \ldots\ldots 9.5$$

A final transformation may now be undertaken so that equation 9.5 can be used in a design role, i.e. to determine the operational parameters which are required to achieve a given stiffness. This is a similar procedure to that used for the unconfined compressive strength. The relevant equation for backfill stiffness is given in Equation 9.6. This equation can be used to determine the required W/C ratio to achieve our goal. Figure 9.16 may subsequently be used to determine the appropriate combination of pulp density and cement content.

$$W/C = 202.7 \left[E + 1.89 \right]^{-.709} \quad \ldots\ldots 9.6$$

9.1.2 Uncemented Fine-Grained Backfills

Uncemented backfills comprise 59% of backfills used in Quebec and 29% of those employed in Ontario. Despite the significant usage of uncemented backfill, the geomechanical properties of these materials have been investigated by few workers and the literature contains little data on these materials. A laboratory testing program was thus initiated to provide the required geomechanical data.

The previous section has dealt with the geomechanical behaviour of cemented fine-grained backfills. It was found that although physical material parameters such as void ratio may have an effect on the geomechanical properties, the effect of such parameters are dwarfed by that of cement and moisture content. The strength and stiffness of cemented backfills increase with increased cement content and decreased moisture. The effect of moisture on geomechanical properties does not relate to mechanical influence, rather moisture effects backfill strength and stiffness through its' influence on the chemical reaction of Portland cement hydration. Excessive water during curing effectively weakens the rigid structure formed by the cement gel.

The geomechanical properties of uncemented backfills on the other hand are governed by the physical characteristics of the material alone. The parameters which are of greatest interest are the material grading, C_c and C_u, void ratio, V_r and moisture content. The effect of moisture content on uncemented granular

materials relates a mechanical process, thus the moisture content alone does not adequately describe the mechanical process. A more appropriate parameter would incorporate both the moisture content and the volume available to accomodate the moisture. The correct parameter is thus the degree of saturation, S_r. The strength and stiffness of uncemented backfill is also governed by the stressed condition of the potential failure plane, S_n.

The testing program to be undertaken, thus had to encompass the measurement of each of these required physical parameters along with the continuous measurement of the stress environment during the test. Related to the geomechanical properties of interest for uncemented backfills is the failure envelope, defined by the angle of internal friction and material cohesion. A further parameter, describing stiffness is also require. To this end a series of shear box tests were conducted for a range of material gradings and moisture contents, see section 6.2 for details.

Four parameters were measured during the shear box tests, i.e. the normal and shear stresses as well as the normal and shear displacements. The horizontial displacement was used to correct the shear stress for changing cross-sectional area during the test and to plot the shear displacement - shear stress diagram from which the peak shear stress and shear stiffness was determined. The horizontial displacement was also used to correct the normal stress for changing area and thus provide a means of tracking the change in normal stress throughout the test. The horizontal and normal

displacements were also used to monitor the void ratio throughout the test. Figure 9.19 provides the summarized data plot for one such test. It further indicates that having determined the peak shear stress, the void ratio and normal stress existing at peak shear can be determined. Similar data for each of the 220 tests is provided in Appendix 12.

The data was subsequently grouped according to intital void ratio, moisture content and material origin. This was then used to develop a material failure envelope, see Figure 9.20 and Appendix 13. Table 9.5 summarizes the angles of internal friction, cohesion and the uniaxial compressive strength for each of the material groups tested. It is noted that the uniaxial compressive strength is estimated graphically from the failure envelope diagram, by plotting the circle which passes through the origin and is tangent to both the shear strength axis and the failure envelope.

The data summarized in Table 9.5 is combined with the backfill physical properties reported in Tables 7.4, 7.8 and Appendix 8. This combination of data enabled the characterization of the geomechanical properties by physical parameters. Empirical design equation were then developed which relate the cohesion and the angle of internal friction to physical material properties.

It was found that material cohesion linearly ccrrelated with the degree of saturation. Figure 9.21 and Equation 9.7 describe the relation between degree of saturation and cohesion. The relation indicates that increased cohesion results from increased degree of saturation.

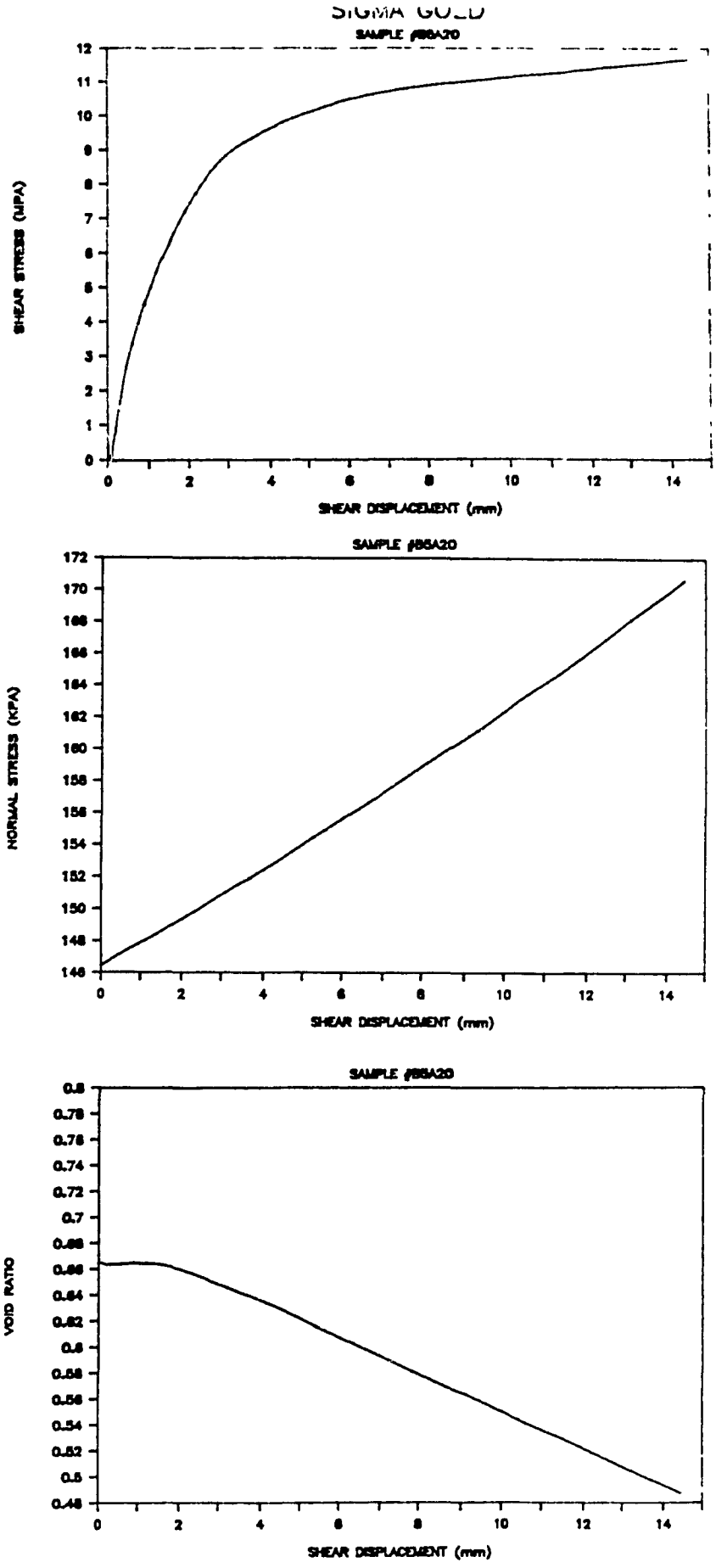

FIGURE 9.19 Summarized Data Plot Of Raw Data

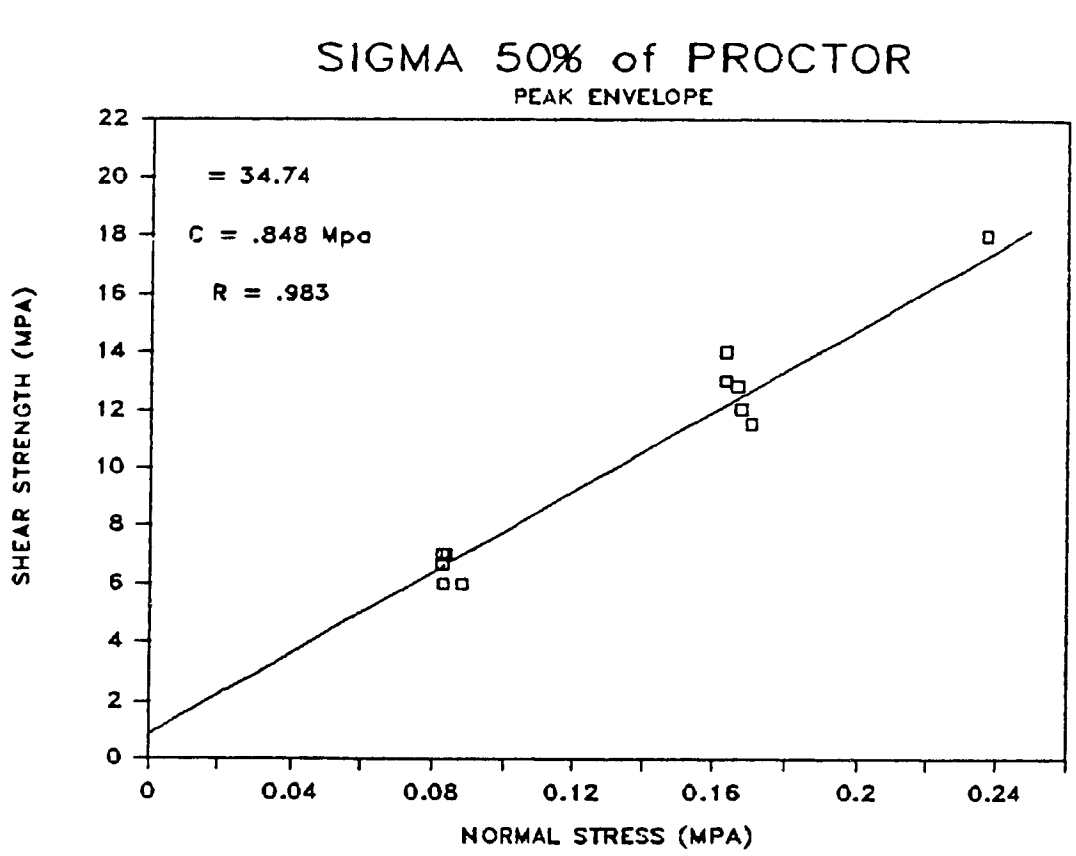

FIGURE 9.20 Material Failure Envelope

SAMPLE SERIES	ANGLE OF INTERNAL FRICTION	COHESION (MPa)	UCS (KPa)
DENA5	34.11	2.34	70
DENA50	36.21	2.33	70
DENA100	34.04	3.53	101
DENB20	36.36	1.59	38
DENB50	34.72	2.52	49
DENB100	37.50	2.69	50
LAC5	33.97	0.87	27
LAC50	37.19	0.0	0
LAC100	31.78	4.36	120
SIG5	34.75	0.21	10
SIG50	34.74	0.85	25
SIG100	33.92	4.08	121

TABLE 9.3 Summary Of Strength And Frictional Properties

$$C = .64 + 4.80\ [S_r]\ ;\quad (R = .907) \quad \ldots\ldots\ 9.7$$

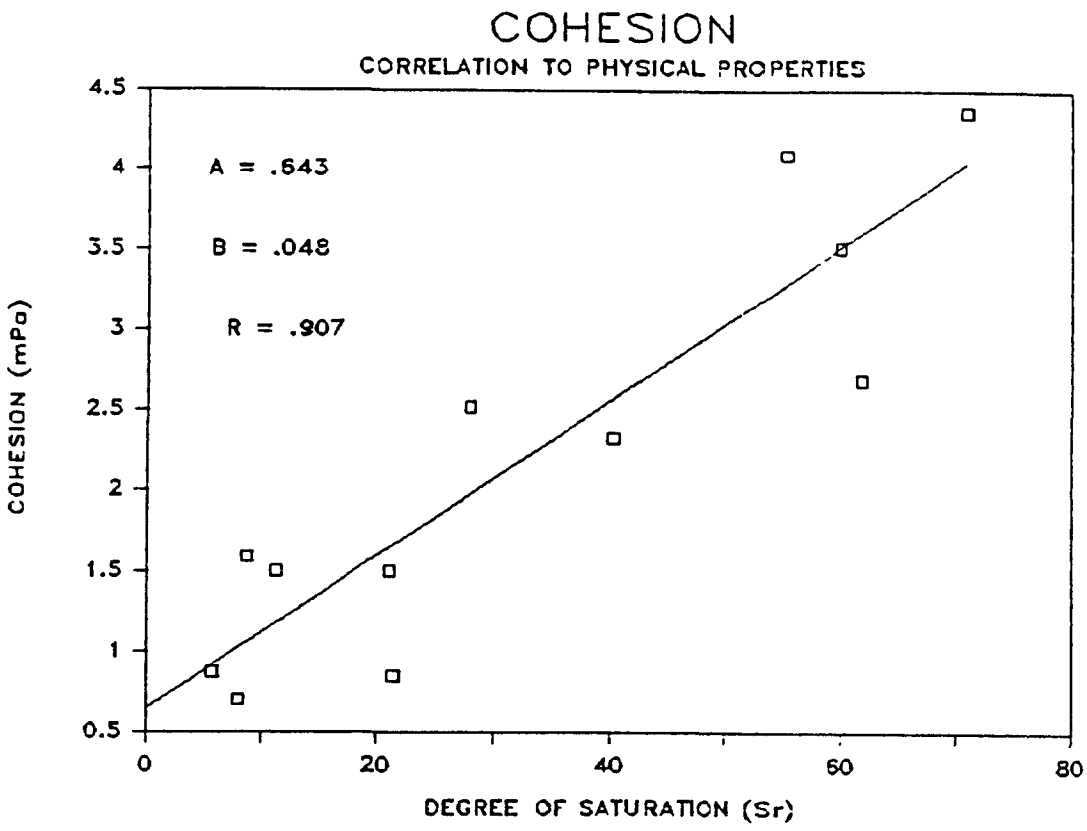

FIGURE 9.21 Cohesion Design Curve

It was further found that the angle of internal friction was not only dependant on the degree of saturation but also on the material grading chacteristics, C_c and C_u. The same trend with degree of saturation was observed with cohesion as for the angle of internal friction. In addition increases in either of the grading coefficients resulted in an adverse effect on the angle of internal friction. Figure 9.22 and and Equation 9.8 describe the relationship derived.

$$= 34.16 + .165\ [\ S_r/C_c/C_u\ ] \quad (R=.9) \quad \ldots\ldots\ 9.8$$

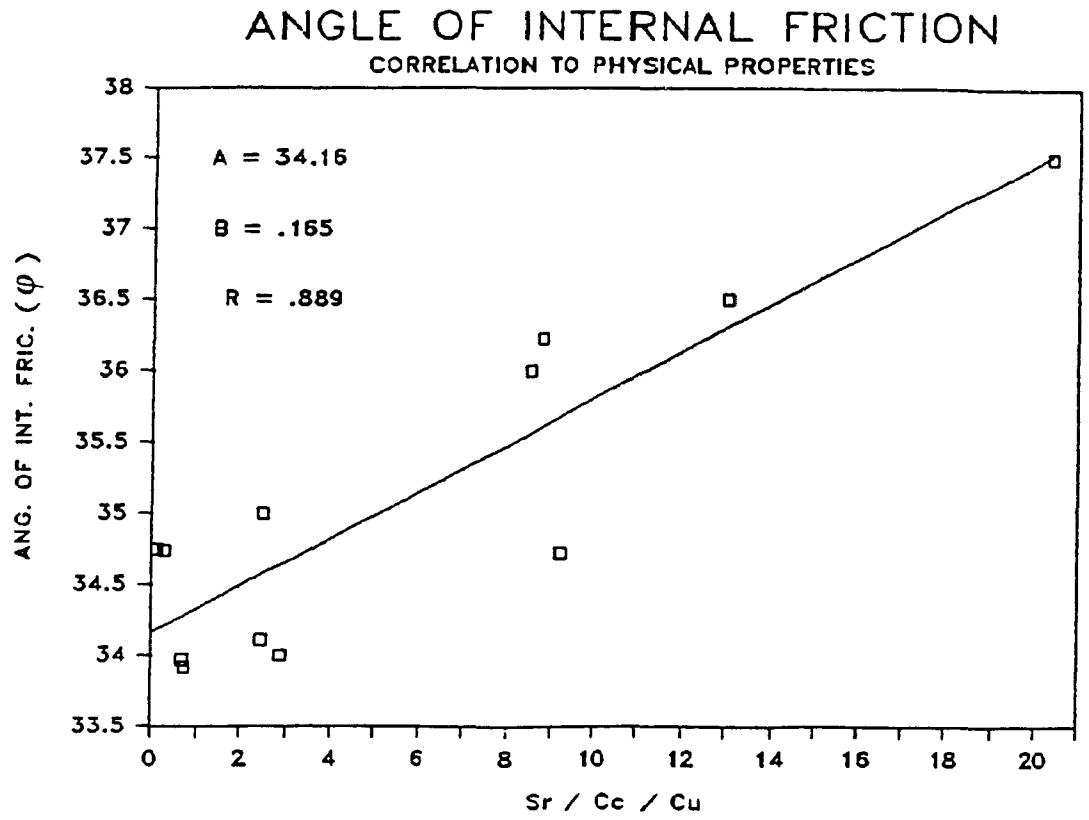

FIGURE 9.22 Design Curve For The Angle Of Internal Friction

Finally, a similar regression analysis was carried out for the determination of shear modulus values for the materials tested. The test data was again grouped by inital void ratio, moisture content and material origin. Each of these material groups were analyzed separately and it was found that the material stiffness was governed by the degree of saturation, void ratio, specific gravity of solids and the existing state of stress as defined by the normal load. Increasing the normal stress and the specific gravity of solids increased the shear modulus. Conversely, an increase in void ratio and degree of saturation resulted in a reduction of the shear modulus. Figure 9.23, illustrates one such analysis and the remainder are reported upon in Appendix 14. Table 9.6 summarizes the regression constants for each of the backfill groups tested.

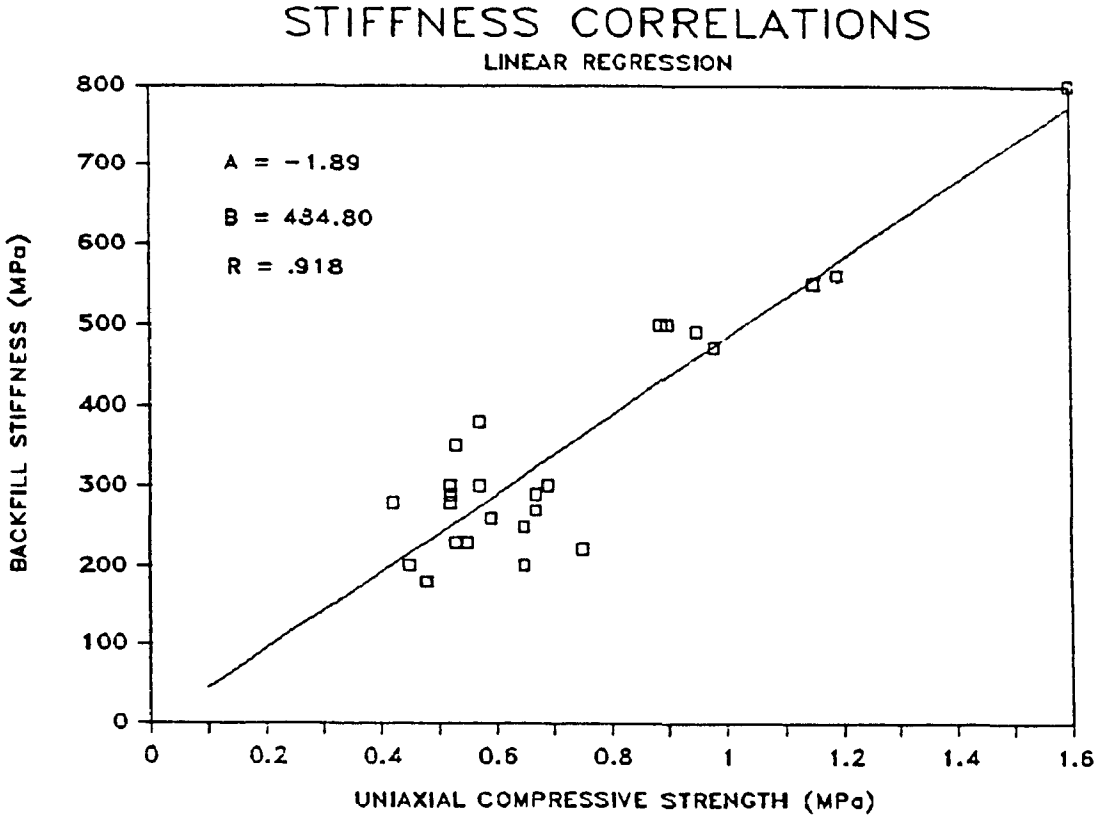

FIGURE 9.23 Sample Analysis Of Shear Modulus

SAMPLE SERIES	A	B	R
DENA5	212.5	651.7	.947
DENA50	115.7	695.6	.948
DENA100	138.6	548.5	.942
DENB20	126.8	958.1	.913
DENB50	94.3	1016.0	.941
DENB100	179.6	1012.4	.907
LAC5	118.2	1055.4	.925
LAC50	99.7	921.2	.914
LAC100	67.6	723.0	.977
SIG5	133.7	898.0	.919
SIG50	52.4	984.6	.962
SIG100	239.1	720.5	.960

TABLE 9.6 Regression Analysis Summary For Shear Modulus

Table 9.6 further illustrates that good correlations can be achieved with a linear curve form for specific test conditions. It is thus concluded that the determination of the shear modulus by the method described above is repeatable. It is further recommended that similar relations be developed on a site specific basis as wide variation in the "A" and "B" parameters are evident. However, a preliminary design equation has been developed using the combined database for all samples tested. A linear regression proved to be equally effective in analyzing the entire database. The results of this analysis are summarized in Equation 9.9 and illustrated in Figure 9.24.

$$G_p = 183.4 + 652.7 \times S_n \times [1/V_r - S_r/G_s] \quad \ldots\ldots 9.9$$

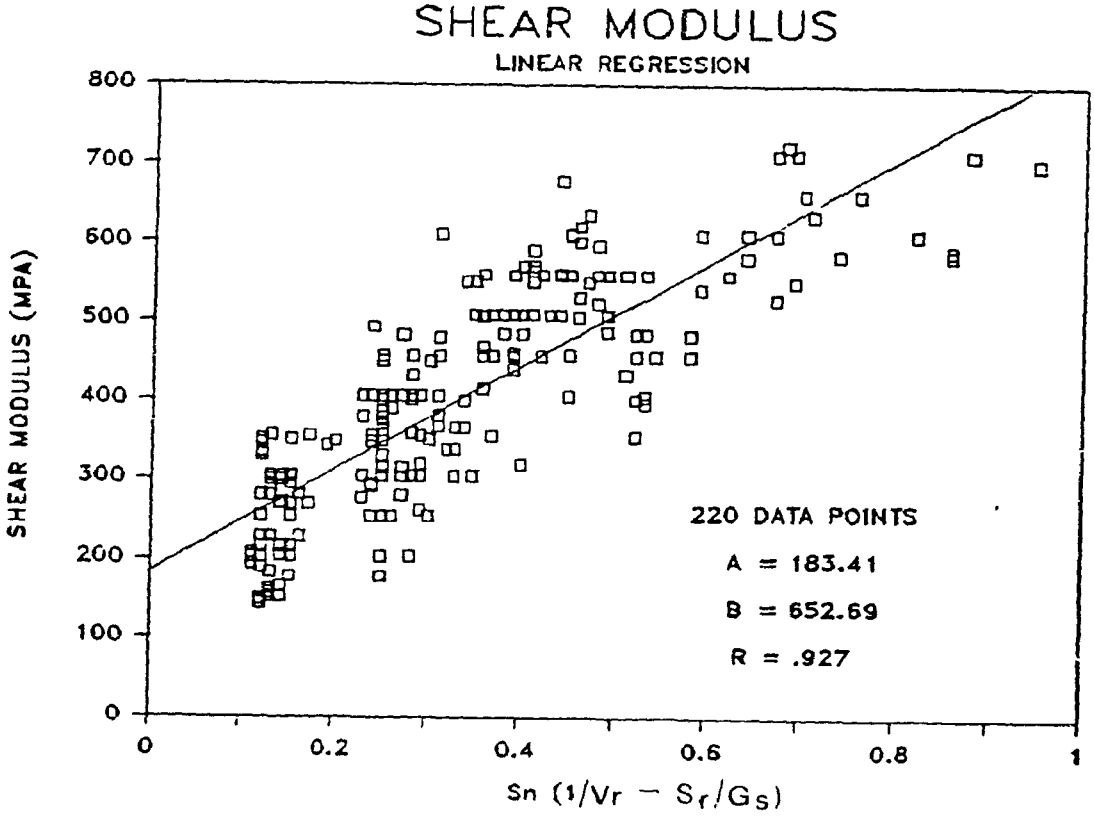

FIGURE 9.24 Shear Modulus Design Curve

9.1.3 Uncemented Rockfills

Uncemented rockfills comprise 21% and 12.5% of backfills used in Quebec and Ontario respectively. The main attraction of this material is its' low cost and availability. Geomechanically it is characterized by its' lack of cohesion and low stiffness. The only property which may be designed for is the angle of internal friction as uncemented rockfill, as a class, behaves like a granular material. This leads to the conclusion that this material is unsuitable for use where exposed fill faces are required since the maximum angle at which this material will stand freely is equal to the angle of internal friction.

The intent of this section is to provide a guideline for maximizing the angle of internal friction of uncemented rockfills. To this end 100 laboratory tilt box test were conducted. The samples were compacted to different porosities, and were tested dry. The porosities as calculated and reported in Table 9.7 are based on the assumption that the individual rockfill particles contain no voids inaccessable to the helium gas employed in the pycnometer test. This assumption may create slight inaccuracies in the calculated porosities. This material is characterized by a nonlinear failure envelope. The implication of a nonlinear envelope is that the angle of internal friction is dependant on the normal stress. The form of the curve indicates that the angle of internal friction decreases with normal stress. The angle of internal friction has been related to Barton's (5) equivalent strength parameter (S) and roughness coefficient (R), as well as normal stress and base friction angle. The relation has been summarized in Equation 6.2.

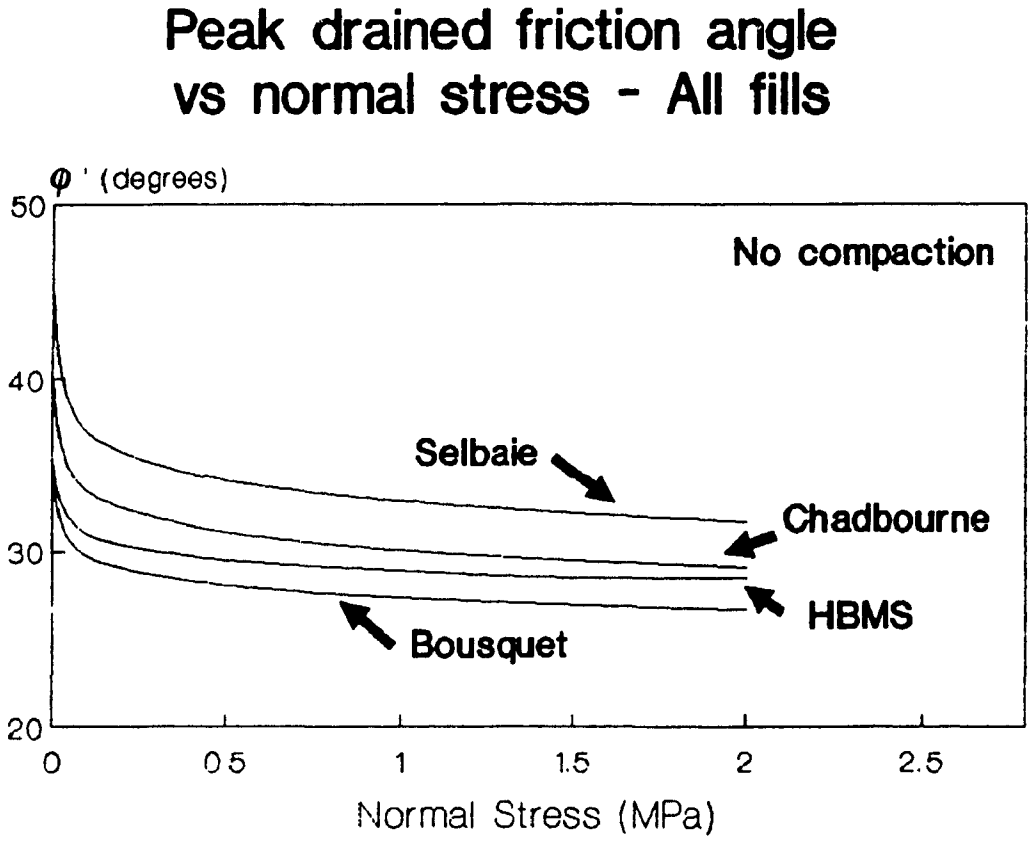

FIGURE 9.25 Angle Of Internal Friction As A Function Of Normal Stress For Materials Tested

Figure 9.26 illustrates the curves generated using Equation 6.2 and laboratory test data for the four rockfill marterials tested, at their natural gradation and no compaction. The natural porosities for these four materials range between 34 and 53%.

The curves generated in Figure 9.25 require three parameters to be know; coefficient of roughness, equivalent strength and the base friction angle. These parameters have been reported in Table 9.7 for each set of test conditions.

The base friction angle has been determined from the joint shear box test on sawcut rockfill material. This parameter is a basic material parameter and as such little can be done to increase the inherent value which the available material exhibits.

Increasing the equivalent strength parameter increase the total undrained friction angle. It is estimated from the uniaxial compressive strength, which has been determined from point load test, and the materials' U_{50}. The uniaxial compressive strength is again an inherent parameter, however the equivalent strength increases with a decrease in U_{50}, see Figure 6.1. The greatest benefits are achieved with U_{50}'s lower than 50 mm. This would imply that the angle of internal friction can be increased by crushing the rockfill material finer.

Increasing the roughness coefficient also increases the angle of internal friction. Figure 6.2 provides a means of estimating the roughness coefficient from the porosity and a visual

MINE SITE	n	R	S	0_b
HBM&S IN SITU GRADING				
NO COMPACTION	.51	2.1	71.1	25
15 SEC.	.48	4.5	71.1	25
30 SEC.	.44	5.1	71.1	25
60 SEC.	.41	5.1	71.1	25
HBM&S -1/2" +3 MESH				
NO COMPACTION	.43	1.2	69.5	25
15 SEC.	.41	2.3	69.5	25
30 SEC.	.37	2.8	69.5	25
60 SEC.	.34	3.2	69.5	25
HBM&S +1/2" -3/4"				
NO COMPACTION	.54	2.4	64.6	25
30 SEC.	.50	3.6	64.6	25
60 SEC.	.49	3.8	64.6	25
HBM&S +3/4"				
NO COMPACTION	.57	0.7	60.5	25
15 SEC.	.53	2.1	60.5	25
30 SEC.	.50	2.2	60.5	25
60 SEC.	.45	2.2	60.5	25
BOUSQUET MINE IN SITU GRADING	.53	2.3	98.0	22.8
CHADBOURNE IN SITU GRADING	.47	3.3	162.2	22.8
SELBAIE MINE IN SITU GRADING	.34	4.0	114.3	22.8

TABLE 9.7 Frictional Parameters For Uncemented Rockfills

assessment of particle angularity. A back calculation technique has been used, however, based on the tilt box test. Figure 9.26 illustrates the effect porosity has on the angle of internal friction. As the other parameters are kept constant on Figure 9.6 the conclusion can be made that a decrease in porosity increases the roughness coefficient. It was also found that the range of test conditions used in this test program complemented the existing rockfill dam data. Figure 9.27 illustrates the lower and upper ranges of mine rockfill friction angle characteristics as observed from the test program and the equivalent rockfill dam data as reported from Leps (4). This figure indicates that the upper range of the test data reported in Table 9.7 corresponds to the lower range of the available rockfill dam data. This is to be expected as

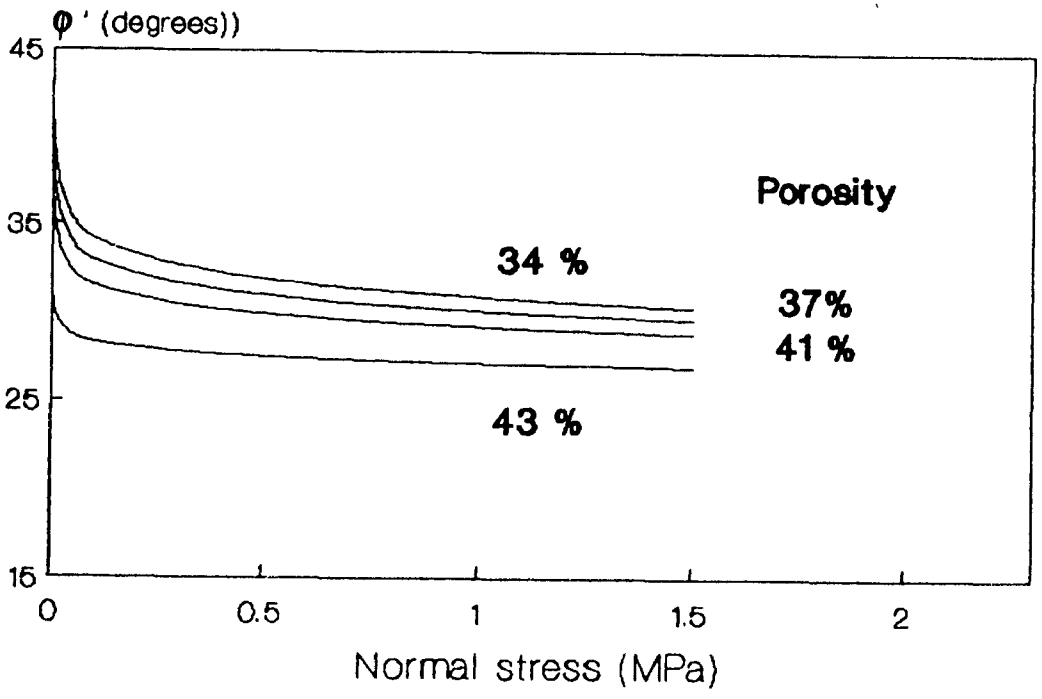

FIGURE 9.26 Effect Of Porosity On The Angle Of Internal Friction

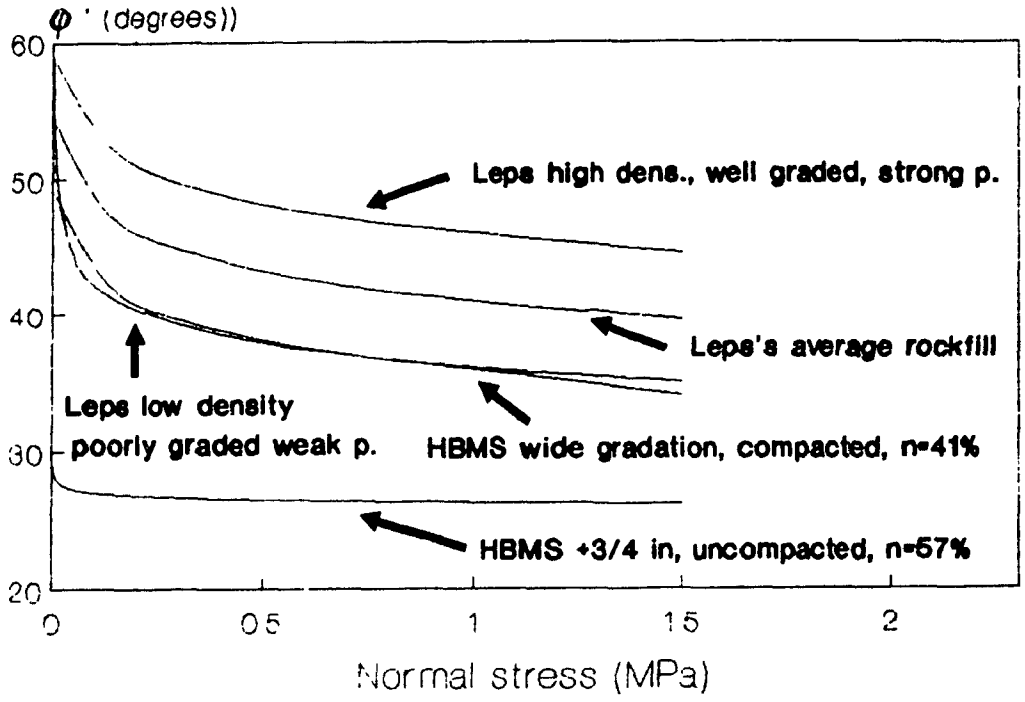

FIGURE 9.27 Comparison Of Mine Rockfill And Dam Rockfill Data

Barton (5) reports typical porosities between 18 and 31%. It is also noted that the upper range of porosities for the rockfill dam data corresponds with the lower range of porosities for the mine backfill.

In essence two basic methods of increasing the angle of internal friction for uncemented rockfills are possible. These relate back to equation 6.2, which implies an increase in the angle of internal friction is obtained by increasing the equivalent strength parameter or the equivalent roughness coefficent. In practical terms the equivalent strength parameter can be increased

by regrading or regrinding the backfill material. Additional increases in the angle of internal friction can be obtained with an increase in the equivalent roughness, this parameter too is a function of the material grading characteristics and the degree of compaction.

9.2 Correlation Of Laboratory And In Situ Data

This chapter to date has centered around the evaluation of laboratory data. It is evident however that if this data is to be useful it must be correlated to the field environment. The overall project has focused on this concept. This chapter section examens the relation between laboratory strength, stiffness and frictional properties and similar properties measured in the field with the pencel pressuremeter, reported in Chapter 8.

The correlation of field and laboratory data results from 220 laboratory tests and 100 field pressuremeter tests. After data reduction, however, fewer points are available for laboratory to field data extrapolation. Strong correlations, however, were achieved, with this limited data.

9.2.1 Stiffness Correlations

The deformation modulus is measured in the field by the Menard modulus, E_m, and are summarized in Table 8.2. A similar parameter, the laboratory shear modulus, G_p, has also been measured. The unconfined laboratory shear modulus proved to be a effective

index for predicting the field modulus. It should be noted that the laboratory data remains an order of magnitude higher that the measured fields response. Furthermore an exponential curve form proved to adequately represent the relation between these two parameters. The correlation coefficient for this curve form, R=.990, implies that Equation 9.10 gives a strong positive correlation.

$$E_m = 6.31 \text{ EXP } [.0092\ G_{po}\ ] \text{ ; } (R=.990) \quad \ldots\ldots 9.10$$

Equation 9.10 has been represented in Figure 9.28 along with the actual data for uncemented materials.

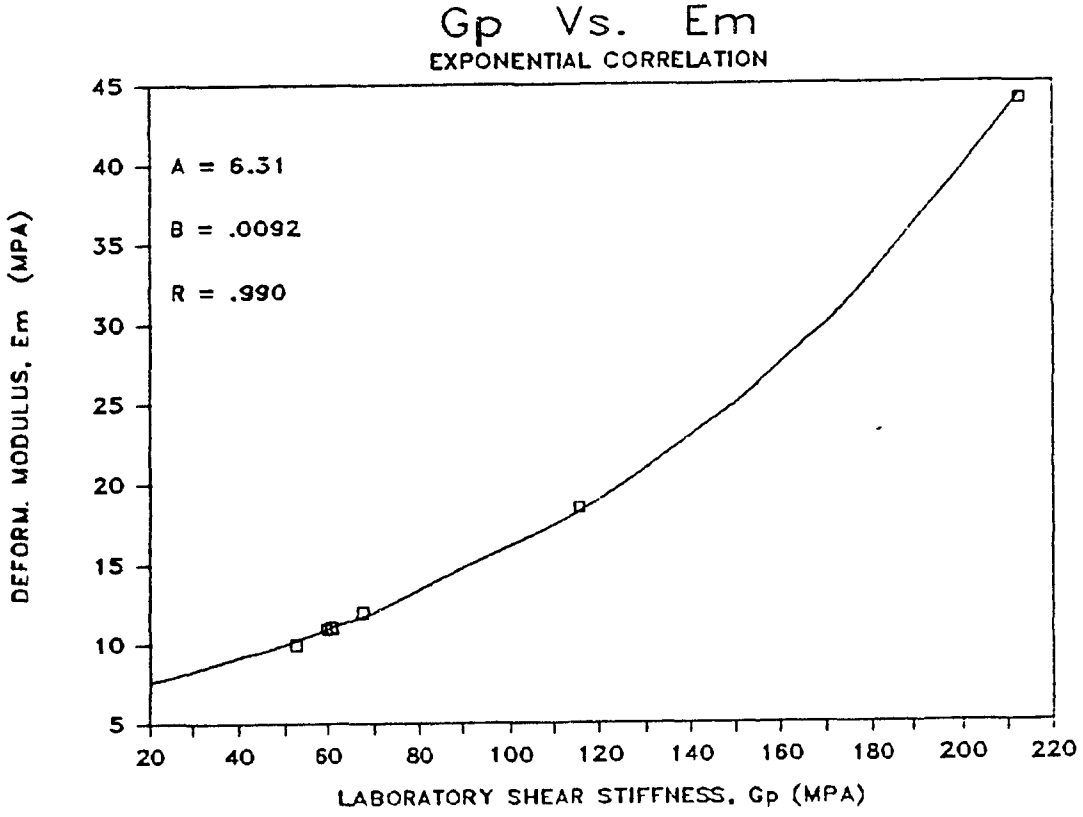

FIGURE 9.28 Correlation Of Laboratory Shear Stiffness And Field Deformation Modulus

9.2.2 Strength Parameter Correlations

Two strength parameters have been recorded in the laboratory; the uniaxial compressive strength and the material cohesion. The uniaxial compressive strength was determined directly for cemented backfill materials and was estimated graphically from the failure envelope for uncemented fine-grained backfills. These two means of determining the same property lead to discrepancies which make correlation to field conditions impossible. On the other hand the laboratory cohesion for uncemented materials proved to correlate well with the pressuremeter limit pressure, see Table 8.2.

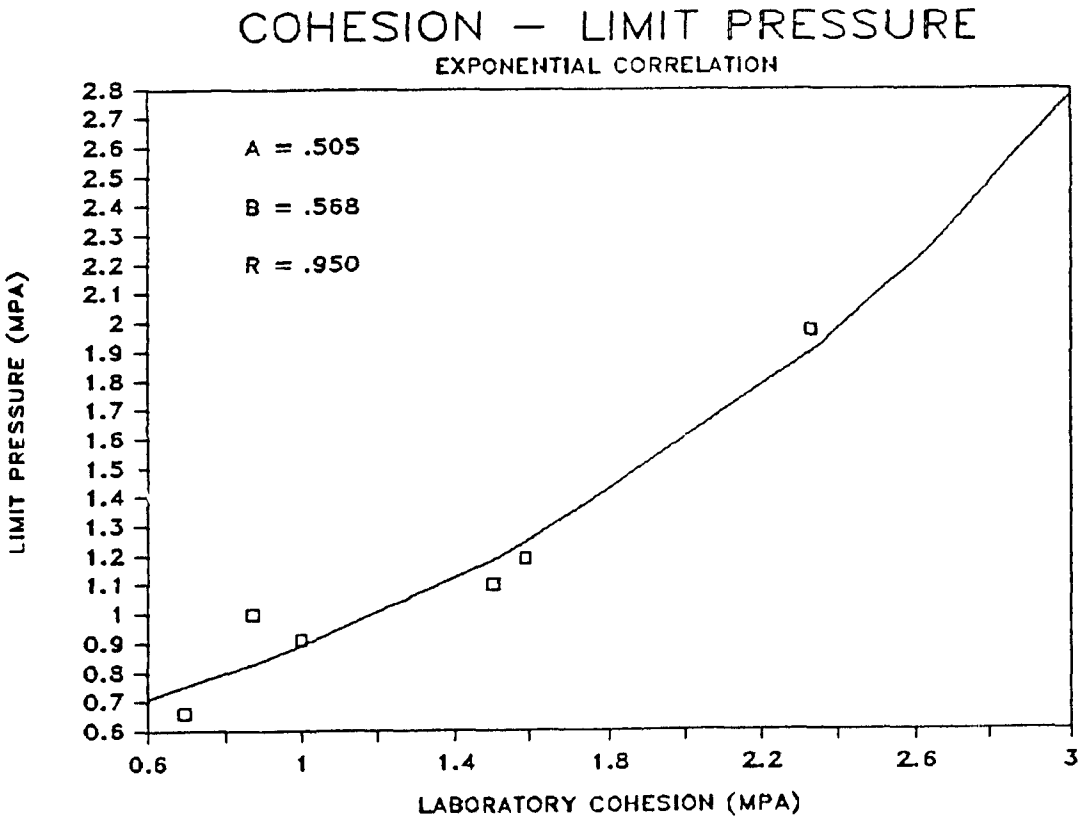

FIGURE 9.29 Correlation Of Laboratory Cohesion And Field Limit Pressure

An exponential curve form was also used to relate cohesion and limit pressure. Equation 9.11 gives the precise numerical representation, while Figure 9.29 diagramatically represents this relation.

$$P_l = .51 \text{ EXP } [.57 \text{ C }] \text{ ; } (R=.950) \quad \ldots\ldots 9.11$$

Equation 9.11 can be combined with Equation 9.7 ,the resulting equation, Equation 9.12, can be used to estimate the anticipated limit pressure directly from the degree of saturation.

$$P_l = .51 \text{ EXP } [.37 + 2.74 \, S_r] \quad \ldots\ldots 9.12$$

9.2.3 Frictional Characteristics Correlations

The frictional characteristics of uncemented mine backfills are defined by the angle of internal friction. This parameter has been determined by two test methods; shear box and tilt box test, for uncemented fine-grained and uncemented rockfills respectively. The analysis of the relavent laboratory data for each of these materials has been described in sections 9.1.2 and 9.1.3. The corresponding field data for uncemented rockfill is limited to the tests conducted at Chadbourne mine, thus laboratory to field correlations for uncemented rockfills was not possible.

The extrapolation of laboratory angle of internal friction, as determined in section 9.1.2, has been limited to uncemented fine grained materials. Figure 9.30 graphically illustrates the relation between laboratory and field angle of internal friction. This relation is mathemathically represented by Equation 9.13.

$$\varphi_{field} = 1.046[\ \varphi_{lab}\ ] - 3.59 \ ; \quad (R=.945) \quad ..... \quad 9.13$$

This strong correlation confirms the applicability of Equation 5.7 for the determination of the angle of internal friction from the pressuremeter limit pressure. It further allows corrections to be made to laboratory angle of internal friction to

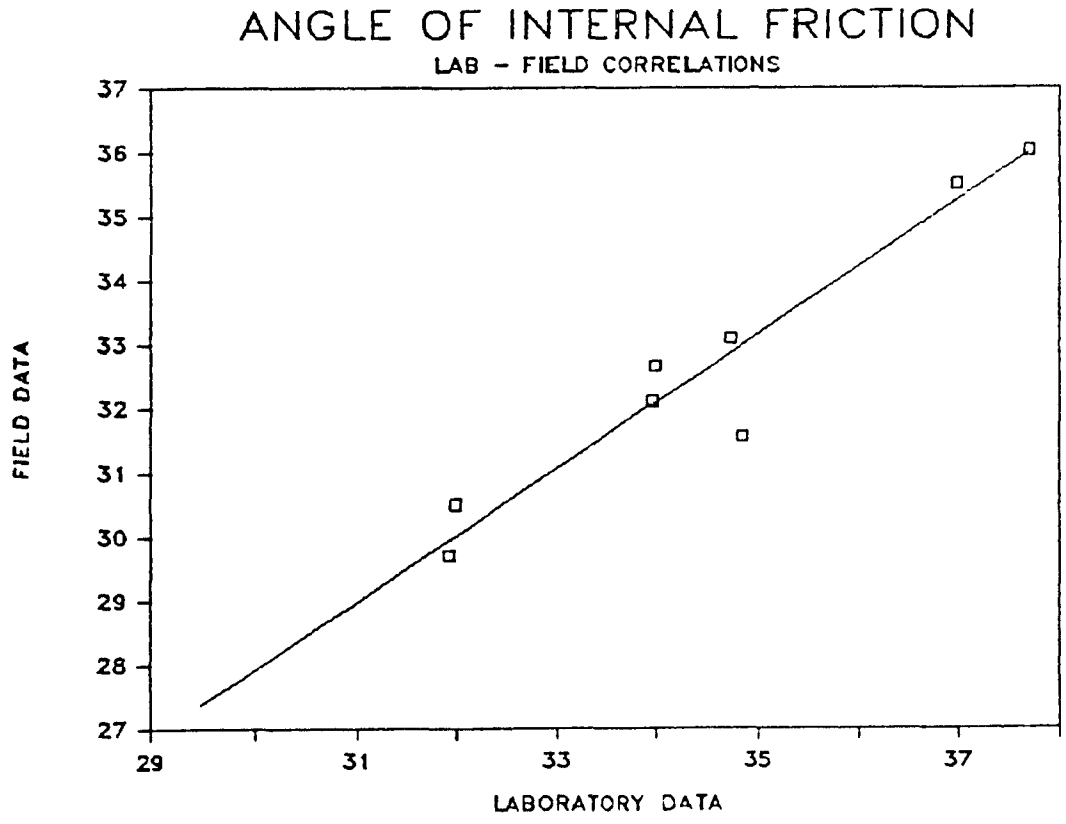

FIGURE 9.30 Correlation Of Laboratory And Field Angle Of Internal Friction

reflect field conditions. A further modification can be made to Equation 9.13 by combining it with Equation 9.8 to yield a field value of angle of internal friction directly from physical parameters, Equation 9.14.

$$\varphi_{field} = 32.15 + .173 \left[S_r / C_c / C_u \right] \quad ..... \quad 9.14$$

9.3 Summary

This chapter has presented design equations for three materials; cemented fine-grained backfill, uncemented fine-grained backfill and uncemented rockfill. The design properties vary with material type, for instance the uniaxial compressive strength, and stiffness are the major design properties for cemented fine-grained backfills. Design equations for these geomechanical properties have been developed for cemented backfill and presented in this chapter.

Similarly, design equations for uncemented fine-grained backfills are based on the material shear modulus, cohesion and angle of internal friction. These geomechanical properties have been equated to degree of saturation, void ratio, specific gravity of solids and state of stress.

The tilt box tests described in sections 6.2.4 and 9.1.3 have been used to correlate the degree of compaction as defined by the void ratio to angle of internal friction of the test material.

Particular attention has been focused on the relationship between laboratory and field observations for uncemented fine-grained backfills. Strong correlation has been observed between laboratory shear stiffness and field deformation modulus. Equally good correlation was observed between laboratory cohesion and pressuremeter limit pressure as well as for field and laboratory angle of internal friction.

The thesis thus far and this chapter in particular has focused on the geomechanical properties of existing backfill materials. Reference has not yet been made to the interaction between these materials and the stoping environment. As such conclusions cannot as yet be made of the effectiveness of backfill in a ground support role. Chapter 10, will thus investigate the effectiveness of backfill under the various enivronments which may be encountered.

10.0 BACKFILL EFFECTIVENESS AND STABILITY IN GROUND CONTROL

The focus of previous chapters has been on the determination of geomechanical mine backfill properties and their relationship to physical properties in order to develop appropriate design equations for each backfill type. The effectiveness of backfill types in fulfilling different ground control roles in various mining environments is important to establish. Only with such knowledge can a design engineer define the required target properties for a backfill type in a particular environment. The objective of this chapter is to investigate the requirements of backfill in three significant mining environments. These include; rockburst - prone ground, free standing stability and static stress redistribution applications. These environments and the models used to idealize them are described in detail later in this chapter.

Included in predictive design methods are any numerical or analytical models which attempt to simulate a mine environment. These models include limit equilibrium analysis, used in assessing free standing heights, dynamic energy balance approaches for assessment of backfill behaviour in rockburst-prone ground , displacement discontinuity or finite element models for assessing stresses around mine openings and in backfill structures. The appropriate choice of model is crucial to the successful prediction of backfill behaviour. Such choices should thus be based on the preconceived backfill function, mining dimensions, geometry and geology as well as model validity and costs.

Models can be used to evaluate the performance of a given

fill material. This may be measured in terms of a backfills' free standing height, ability of the fill to redistribute stresses or other criteria which the backfill designer considers appropriate for the preconceived function. Alternately these models can be used in an iterative fashion to determine the target mechanical properties required to meet a desired performace criterion as described in section 3.1.2.

BACKFILL TYPE	COHESION (kPa)	FRICTION ANGLE	COMPRESSIVE STRENGTH (MPa)	E (MPa)
UNCEMENTED				
FINE GRAINED FILL	0 - 45	31 - 38	0 - .15	2 - 15
MINE ROCKFILL	0	25 - 35	0	1 - 2
DAM ROCKFILL	0	35 - 55	0	3 - 5
CEMENTED				
FINE GRAINED FILL	48 - 62	35 - 38	.5 - 2	20 - 85
MINE ROCKFILL	150 -350	50 - 55	6 - 11	500-1000
VIBRATED F.GRAIN.	38 - 85	35 - 38	.4 - 2.8	16 - 117
DOUBLE PLACED R.F.	95 - 150	37 - 42	1 - 5.5	44 - 230

TABLE 10.1 Typical Backfill Properties
For A Range Of Backfill Types

Each section in this chapter first describes the mining environment and modelling method used and then determines the required backfill properties for particular design criteria. These properties are then compared to a table of typical backfill properties, Table 10.1, to determine backfill type suitabilitY for each application. This table is an attempt to broadly summarize the geomechanical properties of the backfill types and is based on both the thesis laboratory and in situ testing as well as published work. The chapter further investigates the effects of dimensional, environmental and saturation conditions on backfill effectiveness.

10.1 Free Standing Height Applications

During pillar recovery against backfill stopes the stability of the exposed backfill faces becomes of critical importance to maintain ground support and minimize dilution. Although backfill free standing stability can be analyzed using numerical methods (128), simpler closed form solutions exist,such as the two dimensional limit equilibrium method (49,50,51,136,137). The method stems from the factor of safety equation developed by equating driving and resistance forces along an assumed plane of failure, Figure 10.1. Failure is assumed to occur at:

$$\alpha = (45 + \varphi / 2) \qquad .....10.1$$

The problem of free standing heights is illustrated in Figure 10.1

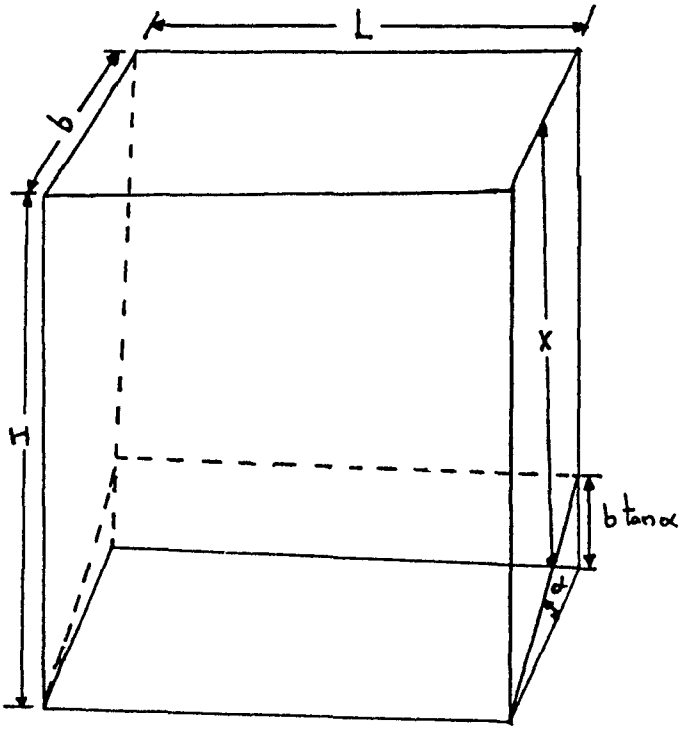

Figure 10.1 Mode Of Failure Diagram

The factor of safety equation for this failure mode thus can be written as:

$$F = \frac{CLB/\cos(\alpha) + W_n \cos(\alpha) \tan(\varphi)}{(LBX\gamma - 2CBX)\sin(\alpha)} \quad \ldots\ldots 10.2$$

where: F = factor of safety

C = cohesion

L = strike length of exposed fill

B = width of block

$\alpha = 45 + \varphi/2$

γ = unit weight of backfill

φ = angle of internal friction

and $W_n = BLX$

The above equation is applicable to all backfill types ranging from cohesive backfills, cemented hydraulic and rockfills, and cohesionless fills such as uncemented rockfill. However it should be noted that equation 10.2 can be simplified for cohesionless materials, and becomes:

$$F = \frac{\tan(\varphi)}{\tan(\alpha)} \quad \ldots\ldots 10.3$$

Equation 10.3 implies that for cohesionless materials such as uncemented rockfill a free standing vertical height is not possible. In summary, there is little difference between various limit equilibrium equations described thus far. However, experience in soil mechanics and analysis of failure modes in such

structures shows that failure in soils occurs in what is known as circular arch failure mode. Hoek and Bray (138) proposed a series of design charts for the stability of soil slopes and defined the two following terms:

$$X = C / \gamma H \tan(\varphi)$$

$$Y = \tan(\varphi) / F$$

where C = cohesion (kN/m^2)

φ = angle of internal friction

γ = backfill density (kG/m^3)

H = vertical height

F = factor of safety.

The relationship between the two quantites, X and Y is dependant on the slope angle and degree of saturation. A free standing height requirement is analogous to a vertical slope. A statistical analysis of the Hoek design charts was carried out by the author and the following equation developed:

$$F = \frac{\tan(\varphi)}{A} \left(\gamma H \tan(\varphi) / C \right)^B \qquad \ldots\ldots 10.4$$

where A and B are regression constants depending on saturation conditions. Furthermore equation 10.4 can be used to determine the free standing height of a particular material. This is done by setting $F = 1$ and rearranging equation 10.4, so that in S.I. units:

$$H = 203.9 \ (A/\tan(\varphi))^{1/B} \left(C/ \gamma \tan(\varphi) \right) \qquad \ldots\ldots 10.5$$

Both equations, 10.4 and 10.5 are applicable over a certain range of X values and saturation conditions, defined by the saturation number, n. The saturation number represents the fraction of total height which is saturated; i.e a saturation number of 8 implies that backfill is saturated to 1/8 its total height. These ranges and the regression constants are given in Table 10.2.

n	X - range	A	B	Coeff. Corr.
	.07 to .9	.376	-.628	.970
8	.08 to .8	.379	-.631	.999
4	.095 to .6	.415	-.616	.999
2	.13 to .5	.424	-.655	.999

Table 10.2 Regression Constants For Varying Saturation

Using equation 10.2, Nantel (51) found that for a backfill having a density of 2402 kg/m^3, an angle of internal friction of 42^o and a cohesion of 74.2 kPa. a free standing height of 40 m was attainable, assuming planar failure. Using these same input parameters equation 10.5 can be used to estimate the free standing height under circular failure conditions. It was found that equation 10.5 predicted a free standing height of 28 m. It is felt that as equation 10.5 best represents the failure mode of soil and soil - like materials such as backfills, it should be used in place of equation 10.2. Furthermore, both of these models have the inherant idealization of homogeneous material properties, thus segregation or banding, which would reduce the free standing height, cannot be modelled. This further supports the use of the more conservative predictions provided by equation 10.5.

The effectiveness of backfill in free standing height applications is dependant on the required height of exposed face and the backfill employed. Equation 10.5 was used to assess the backfill property requirements to meet a range of free standing height objectives. This equation has also been used to verify the sensitivity of free standing height to the angle of internal friction, material cohesion, material density and degree of saturation.

A base series of model parameters, representing vibrated cemented fine grained backfill properties, were used. These included a cohesion of 74.2 kPa, angle of internal friction of 35^{o} and material density of 2402 kg/m^3. Each of these parameters were then varied independantly so that their influence and sensitivity on free standing height could be assessed.

Table 10.1, indicates that the angle of internal friction ranges from 25 to 55 degrees for the materials presented. The angle of internal friction has thus been varied from 20 to 60 degrees to encompass the entire range. Figure 10.2 illustrates the variation of free standing height, as predicted by equation 10.5, with the angle of internal friction. It was found that for the range of internal friction angles given above the safe free standing height ranged from 16.5 to 41.5 metres. This represents a significant variation and the internal friction angle should thus be optimized. The relation shown in Figure 10.2 further indicates a quasi-linear relation between angle of internal friction and free standing fill height. The relationship further indicates that a 5m increase in free standing height is obtained for each increase of 8^{o} in the

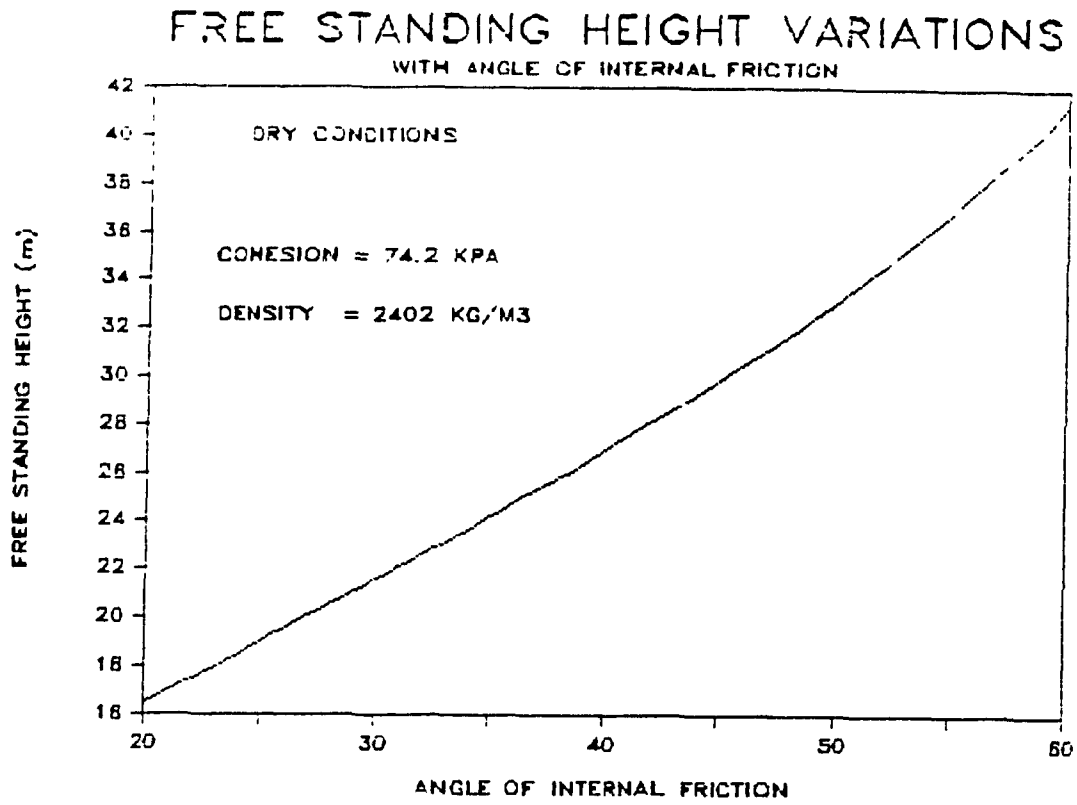

FIGURE 10.2 Free Standing Height Sensitivity To The Angle Of Internal Friction

angle of internal friction. This relation only indicates the sensitivity of the angle of internal friction on Equation 10.5.

Material cohesion ranges from 0 to 350 kPa in Table 10.1. The higher end of the scale represents cemented rockfill alone with the range for the remainder of the backfill types ranging from 0 to 150 kPa. Furthermore, Equation 10.3 indicates that for cohesionless materials a safe condition (F=1) can only be obtained for a face angle equal to the angle of internal friction. This implies that a vertical free standing height is not possible for cohesionless materials. This would thus exclude all uncemented rockfill, or uncemented dam rockfill materials for use in free standing height applications. Some uncemented fine grained materials, particularly

at low degrees of saturation, as implied by Equation 9.7, would not be suitable for free standing heights either. Given these restrictions on material cohesion, a sensitivity analysis was conducted with material cohesion ranging from 30 to 150 kPa. The linear relation between cohesion and attainable free standing height, Figure 10.3, indicates that a 2m increase in free standing height is achieved for incremental increases of 6 kPa in material cohesion. Again this relation only represents the sensitivity of Equation 10.5 to cohesion.

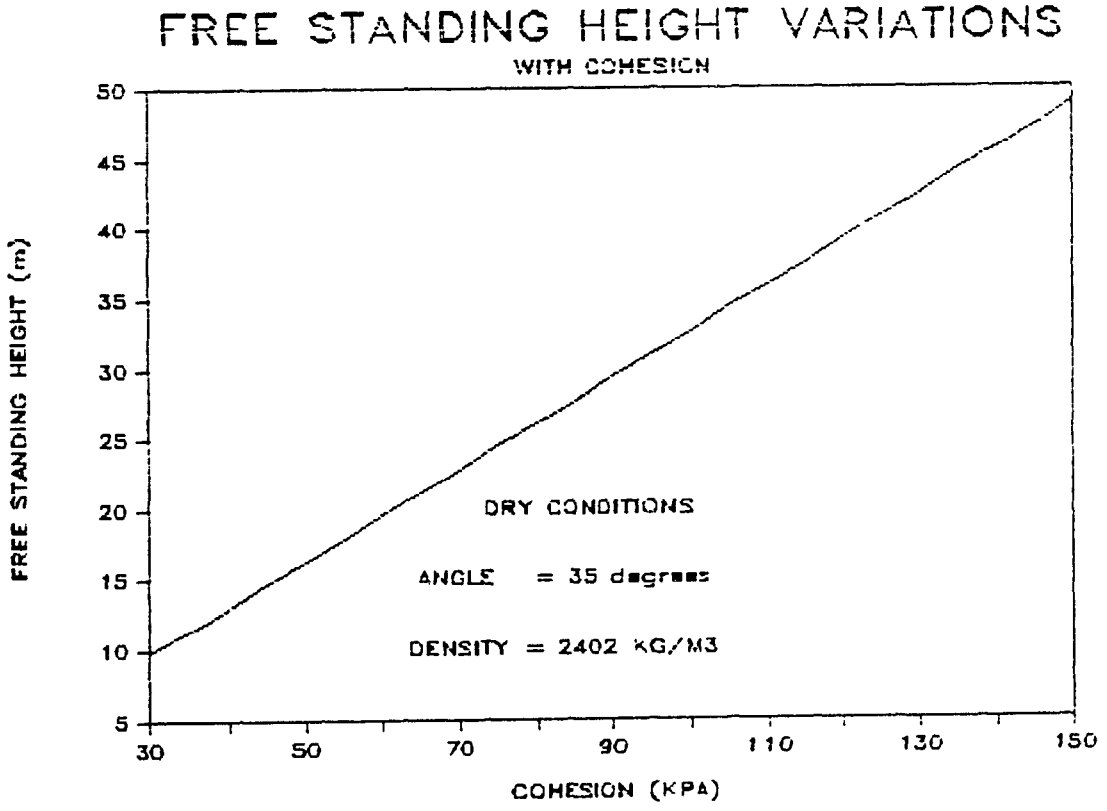

FIGURE 10.3 Free Standing Height Sensitivity To Material Cohesion

Material density in equation 10.5 influences the driving forces on the failure surface, and as such an increase in density will have a detrimental effect on free standing height. This conclusion is seemingly in contradiction to the objectives of material densification. However, it should be pointed out that as the material density increases both the cohesion and angle of internal friction increase. The material density was varied from 1200 to 2700 kg/m^3 as this range covers the entire spectrum of material densities expected. Figure 10.4 illustrates that a decrease in free standing height occurs with an increase in material density. The relation shown is notably nonlinear, however, it can be linearized for discrete ranges. Backfill densities typically range between 1800 and 2000 kg/m^3. If this range is considered a 10%

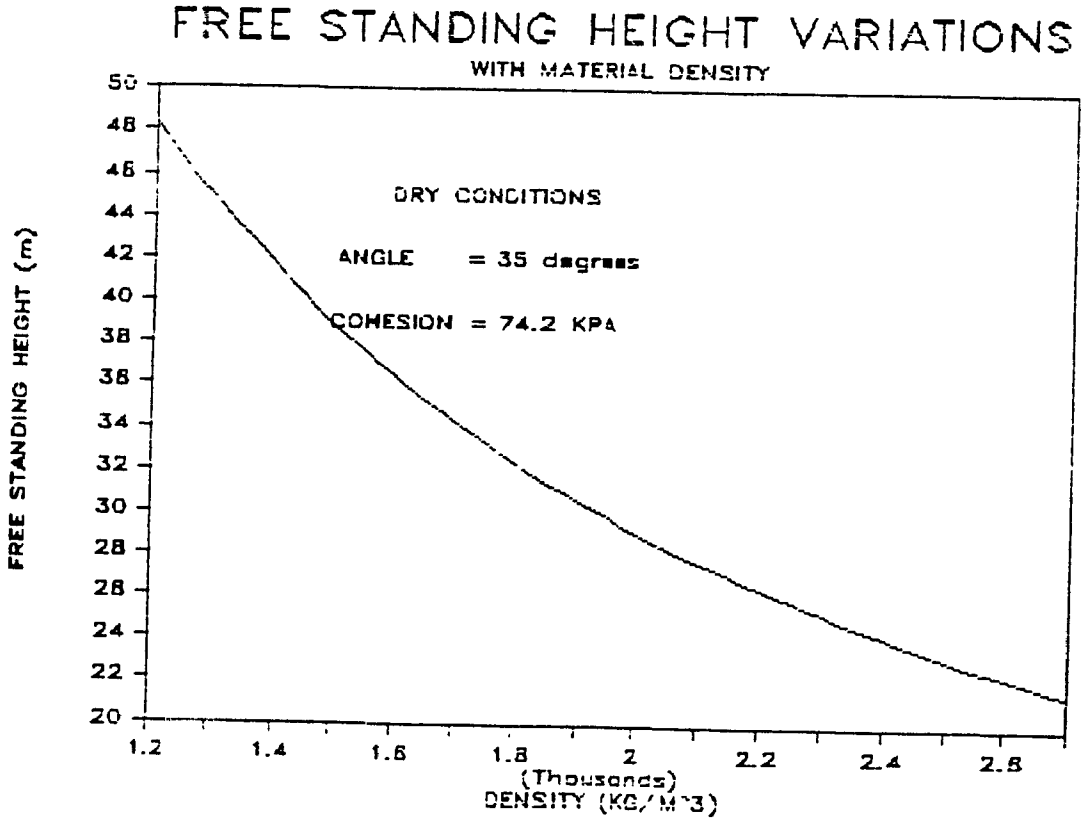

FIGURE 10.4 Free Standing Height Sensitivity To Material Density

decrease in free standing height is observed.

The sensitivity analysis conducted thus far sheds light on the effect of cohesion, angle of internal friction and material density on free standing height. It is not possible at this stage, however, to assess the effectiveness of the backfill types represented Table 10.1 in a free standing environment. To this end Table 10.3 has been created, which indicates the calculated free standing heights for the different backfill types considered in Table 10.1 using average backfill properties. In addition it has been demonstrated by equation 10.5 and Table 10.2 that the attainable free standing height is also dependant on the degree of saturation as described by the saturation constant, n.

Table 10.3 indicates that none of the uncemented backfill materials are suitable for free standing height applications, due to their lack of cohesion. Uncemented fine grained backfills

BACKFILL TYPE	COHES. (kPa)	FRIC ANG.	SATURATION NUMBER, n dry	2	4	8
UNCEMENTED				HEIGHT (m)		
UNCEMENTED HYDR.	22.5	34.5	9.7	7.8	8.4	9.5
UNCEMENTED ROCK.	0	30.0	0.0	0.0	0.0	0.0
UNCEMENTED DAM ROCK.	0	45.0	0.0	0.0	0.0	0.0
CEMENTED						
CEMENTED HYDR.	55.0	37.0	25.0	19.9	21.8	24.6
CEMENTED ROCK.	260.0	47.0	145.7	113.2	128.3	142.8
VIBRATED FILL	61.5	37.0	28.0	22.2	24.3	27.5
DOUBLEPLACED R.F.	132.5	38.5	62.2	49.3	54.3	61.1

TABLE 10.3 Attainable Free Standing Heights For Various Backfill Types

may, however, achieve free standing heights in the range of 10m under the best of material saturation conditions, few practical applications are foreseen. It was further found that cemented fine grained backfills could attain free standing heights of 25m on average. This compares with a 40 m free standing height predicted by Nantel (51) and Arioglu (49). In addition, vibration of these fills would increase the average free standing height by 3m. However if the double placed method of placement is used the fill height can be increased to 62m. Finally, the cemented rockfills is the only material suitable for free standing heights greater than 100m. This conclusion has been supported by field observations at Kidd Creek mine, (197,198), where cemented rockfill mixed at a W/C ratio of 1.2 and containing 5% Portland cement is capable to stand unsupported to heights of 100 m and withstand blast vibrations.

The conclusions drawn thus far have been based on dry fill structures. The saturation conditions however, have a significant effect on attainable free standing heights. This is evidenced by the heights calculated in Table 10.3. It was further found that if the intital free standing calculations were based on dry conditions then a simple correction factor could be used to determine the free standing height under a range of saturation conditions. This relation has been developed using the data in Table 10.3 and is graphically expressed in Figure 10.5. This figure relates the correction factor to the saturation number, n. The curve illustrates that for n=1 (fully saturated) the correction factor is 0.7, implying that a 30% reduction in free standing height results due to the saturation condition. On the other hand as "n"

approaches 10.8 then the correction factor approaches 1, indicating that for "n" values greater than 10.8 the saturation condition can be considered dry.

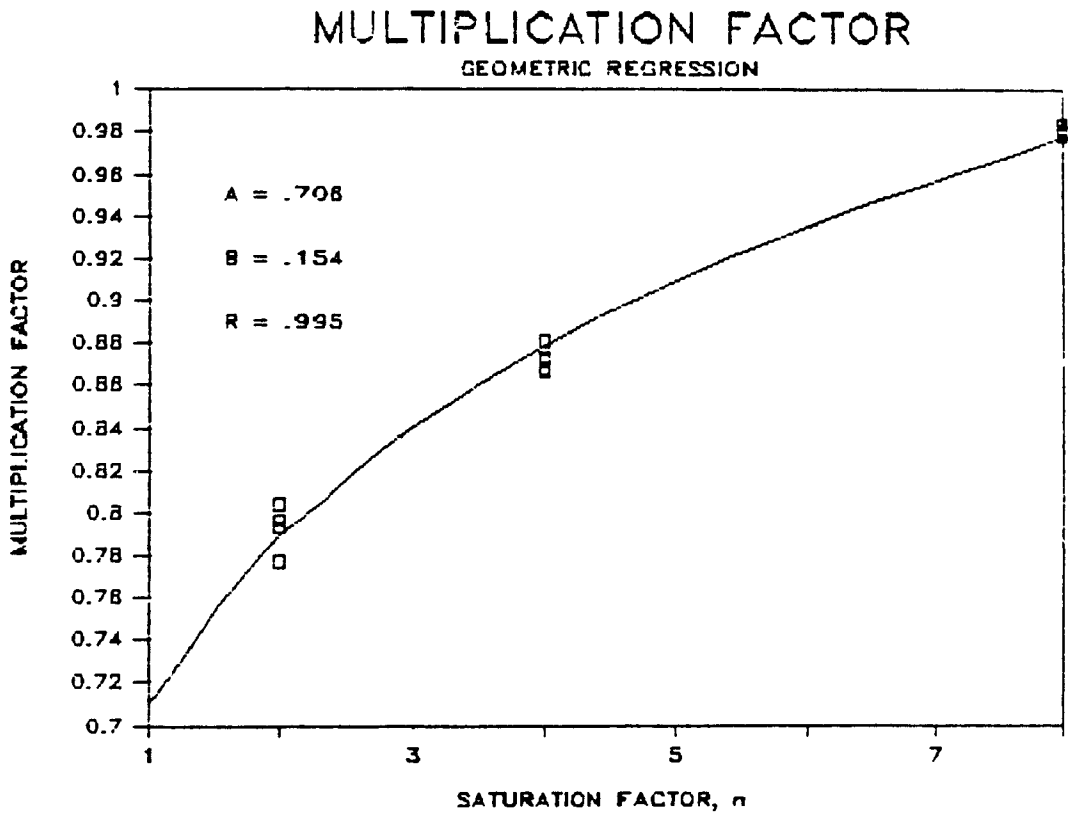

FIGURE 10.5 Saturation Correction Factors

10.2 Rockburst-Prone Ground Applications

Rockbursting has been a ground control hazard in both soft and hard rock mines in Canada for over 50 years (83). It has been responsible for severe losses in production and in several instances the closure of mines. Even more significant is its influence on the safety and morale of miners. Renewed recognition of the need to combat this phenomenon arose after a sequence of rockbursting activity in 1984 at several mines, principally in the province of Ontario. In the Sudbury area a sequence of rockbursts up to 2.6 Richter scale in magnitude culminated in the loss of four lives and the eventual closure of the Falconbridge No. 5 Shaft Mine (84). A few weeks later at the Creighton Mine in the same area a sequence of rockbursts including one of Richter scale 4.0 were experienced (85). The need to alleviate the rockbursting hazard is further compounded as Canadian mines recognize the future need to work with improved safety, productivity and recovery, often at increased depth.

Many Canadian mining camps, soft and hard rock, have experienced a history of rockbursting problems. In the Maritime provinces the coal mining operations have experienced some significant outbursting and bump activity at depths in excess of 500 m. The major associated tragedy occured at the Springhill Mine, Nova Scotia, where a sequence of bumps culminated on October 1958 in the destruction of one entire production district with the loss of 75 lives and the eventual closure of the mine (86). Currently some operating Potash mines in Saskatchewan are experiencing seismic

activity in carbonate sandstone and shale horizons, overlying the evaporite deposits (87).

The principal rockbursting activity has been associated with hard rock mining in the Canadian PreCambrian Shield. Rockbursting has been experienced in Newfoundland, New Brunswick and Quebec mines. Although Quebec has not yet experienced a major share of rockbursting, there have been instances of activity, such as that at the East Malartic Mine (88). The main rockburst - prone geological structure at this mine was a highly brittle porphyritic intrusion. Seismic velocity measurements indicated velocities in the range of 6.1 to 7.6 km/s. These very high velocities were indicative of highly stressed and competent rock. The measured country rock major minor and intermediate principal stresses were 83.1, 69.6 and 74 MPa respectively.

The more proliferous base metal and gold mines of Ontario however have suffered more frequently and severely. In 1940 a growing anxiety over rockbursting prompted Ontario's Mining Association to invite R.G.K. Morrison to apply his expertise, developed through exposure to rockbursting on the Kolar Gold Field in India, to the Ontario mining environment (83). The early forties saw initial experimentation with microseismic monitoring systems in mines of the Sudbury and Kirkland Lake areas. An inability to predict bursting appears to have led to their application lying dormant until the late seventies (89). In the intervening period rockbursting activity continued in Ontario mines,

e.g. 22 of 208 fatalities due to falls of ground arose from rockbursts in the period 1960 - 1979 (90). 1984, however, saw 4 fatalities arising from rockbursts in Ontario. Serious sequence of seismic activity have been experienced in fourteen mines in the last two years in Ontario. The principal affected mining districts have been Sudbury (83,84), Elliot Lake (91), Red Lake (92) and Kirkland Lake (93). Although only the rockbursting history of Canadian mines has been described, problem of rockbursting extends across international borders. A long history of rockbursting exists in South Africa particularly the Val Reefs and Western Deep Levels regions. The brittle rock sequences of the Coeur D'Alene region in Idaho have also exhibited much rockbusrting and has been the subject of much research.

Backfill as a support unit in rockburst-prone ground may be subjected to dyanamic as well as static loading. In this light the design of backfill will differ according to the type of loading being considered.

10.2.1 Dynamic Interaction

In the case of dynamic loading one must first concede the occurence of a seismic event. The backfill is designed so as to minimize the damage to the underground opening by reducing closure. On this basis the author has developed a series of design equations relating stope geometry and orientation, seismic velocity, and backfill material properties to stope wall closure. The peak ground velocity, V, is used as the major design parameter for determining

stiffness, E, in equation 3.1, which was developed as part of this study.

$$E = (2A\delta + (2600)\ V^2\ /\ d\ ) /\delta^2 \ \ldots\ldots\ 10.6$$

In this equation "A" is a parameter dependant on rock mass weight and stope inclination, δ is the acceptable closure of the opening as strain, d is the original size of the opening, V is the peak ground velocity and E is the stiffness of the support, in our case the support is backfill. With this equation a number of design curves have been developed.

The role of backfill can be considered both a strategic and tactical measure for rockburst alleviation. In the broadest sense backfill may be considered a strategic support system when the original design of backfill is based on a pre-set failure criteria which accounts for rockburst conditions. Such a failure criteria may concede a rockburst and attempt to reduce the extent of damage to the stope opening under dynamic loading. Similarly, the initial objective may be to alleviate rockbursts under a prolonged or gradually increasing static load. In both these cases the original design of the backfill to meet these failure criteria can be considered as strategic design.

Often, however, it is not possible to encompass every eventuality into an original design, or to consider possible local variations. It is therefore quite possible that the original failure criteria be exceeded at some point, in such a case remedial measures may have to be taken. Such as stiffening of the backfill

over a localized area where the original design was inadequate. Such a remedial design of backfill would be considered to be tactical.

Regardless of whether backfill design is based on a strategic or tactical philosophy the failure criteria and prevalant stress conditions form the basis for design. In this vein two scenarios are considered. The first looks at the behaviour of backfill once a rockburst has occured. In such a case the backfill is under a dynamic load, as a predetermined block of ground is accelerated into the opening at an anticipated ground velocity. Under such loading conditions, a failure criteria would be based on the amount of closure which would be deemed acceptable. The relevant equations for such a senario have been developed and are based on an energy balance approach (100).

The second scenario occurs when, at the outset, backfill design is being used to alleviate rockbursts. In such a case the energy balance of interest is that at stable and unstable equilibrium of the rock mass. The introduction of backfill into this energy balance and the subsequent design of backfill aims to turn an unstable or rockburst condition into one of stable equilibrium. This case clearly illustrates that failure of the backfill occurs when it is incapable of absorbing enough energy to transform an unstable equilibrium to a stable one. Another approach has been taken by some authors where the degree of closure has been related to the occurence of rockbursts. When such data is available the failure criteria for rockburst alleviation becomes the closure at which rockbursts occur.

The dynamic loading case is first considered. The basic premise of such a design is that a backfill column "d" metres in length and having a cross-sectional area of 1m is dynamically loaded by a column of rock having the same dimensions. The rock - backfill system is arranged in such a way that the rock mass lies in the hangingwall. The rock mass, on initiation of the rockburst, has an initial velocity of "V" m/s. The energy balance of such a system yields the required backfill stiffness to obtain a desired closure . Figure 10.6 illustrates this problem in two dimensions. The rock mass has at the beginning of impact a velocity, V, and the backfill column is stationary. During the short interval of impact the rock mass is rapidly decelerated and the backfill column is rapidly accelerated until a new velocity, V' is obtained: from conservation of momentum we thus have:

$$V' = M_r \, V \, / \, (M_r + M_s) \qquad \ldots\ldots \; 10.7$$

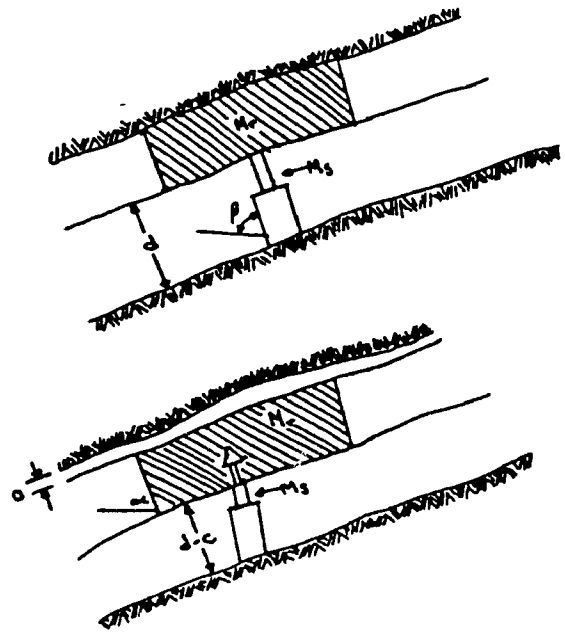

FIGURE 10.6 Two Dimensional Representation Of Dynamic Loading

Equating the work done by all forces the change in kinetic energy of the system is obtained for:

$$-.5\ (M_s + M_r)\ ([M_r]^2\ V^2)\ /(M_r + M_s)^2 =$$
$$-\int_0^C F\ (x)\ dx + M_r gcSin(\alpha) + M_s gcSin(\beta)\ .....\ 10.8$$

Since $M_s << M_r$,equation (10.8) can be simplified and rewritten as follows:

$$.5\ (M_r\ V^2) + M_r gcSin(\alpha) = \int_0^C F_s(x)\ dx\ .....\ 10.9$$

If we now consider the in place backfill to behave linearly then $F(x) = Ex$ and equation (10.9) can be simplified. The integral on the right hand side of equation (10.9) becomes:

$$\int_0^C Ex\ dx$$
$$= .5\ Ex\ /_0^C = .5\ EC^2$$

thus

$$.5\ EC^2 - M_r\ gSin(\alpha)C - (M_r\ V^2)\ /\ 2 = 0$$

and

$$C = (M_r gSin(\alpha) + \sqrt{(M_r gSin(\alpha))^2 + EM_r V^2})\ /\ E\ .....\ 10.10$$

Assuming a failure or yeild zone around the opening, d, the cross sectional dimension of the stope.

then

$$M_r = \rho \, d \times 1 \times 1 \qquad \text{..... 10.11}$$

Then if equation 10.11 is inserted into equation 10.10 and both sides of the equation is divided by the stope dimension "d" we obtain

$$\delta = C/d = (\rho g \mathrm{Sin}(\alpha) + \sqrt{(\rho g \mathrm{Sin}(\alpha)^2 + E \rho V^2 / d)} / E \qquad \text{..... 10.12}$$

At this stage equation 10.12 is in terms of closure strain rather than absolute closure. Furthermore if

$$A = \rho \, g \mathrm{Sin}(\alpha) \qquad \text{..... 10.13}$$

then

$$\delta = (A + (A^2 + E \rho V^2/d)^{.5}) / E$$

$$E (E \delta^2 - 2A\delta - V^2 \rho / d) = 0$$

The trivial solution E = 0.0 is not useful for practical purposes then

$$E = (2A\delta + \rho V^2 / d) / \delta^2 \qquad \text{..... 10.14}$$

returning to equation 10.14 $\alpha = 90 - \gamma$ where, γ = stope dip angle, and assuming $\rho = 2600$ kg / m^3 then:

$$A = 25500 \, \mathrm{Cos}(\gamma) \qquad \text{..... 10.15}$$

Equation 10.15 was subsequently used to develop Figure 10.7, for stope angles ranging from 0 to 90 degrees. Next if $Z = V^2/d$ in equation 10.14 then equation becomes a linear function of "A". Figure 10.8 provides a rapid means of determining Z, for stope dimensions between 1 and 20 metres and ground velocities between .1 and 6 m/s.

Equation 10.14 thus becomes:

$$E = (2A\delta + \rho Z)/\delta^2 \qquad \text{..... 10.16}$$

Constructing graphs, for specific values of A, with "Z" as the independant variable for closure strains δ, then the required stiffness corresponds to the Y - axis.

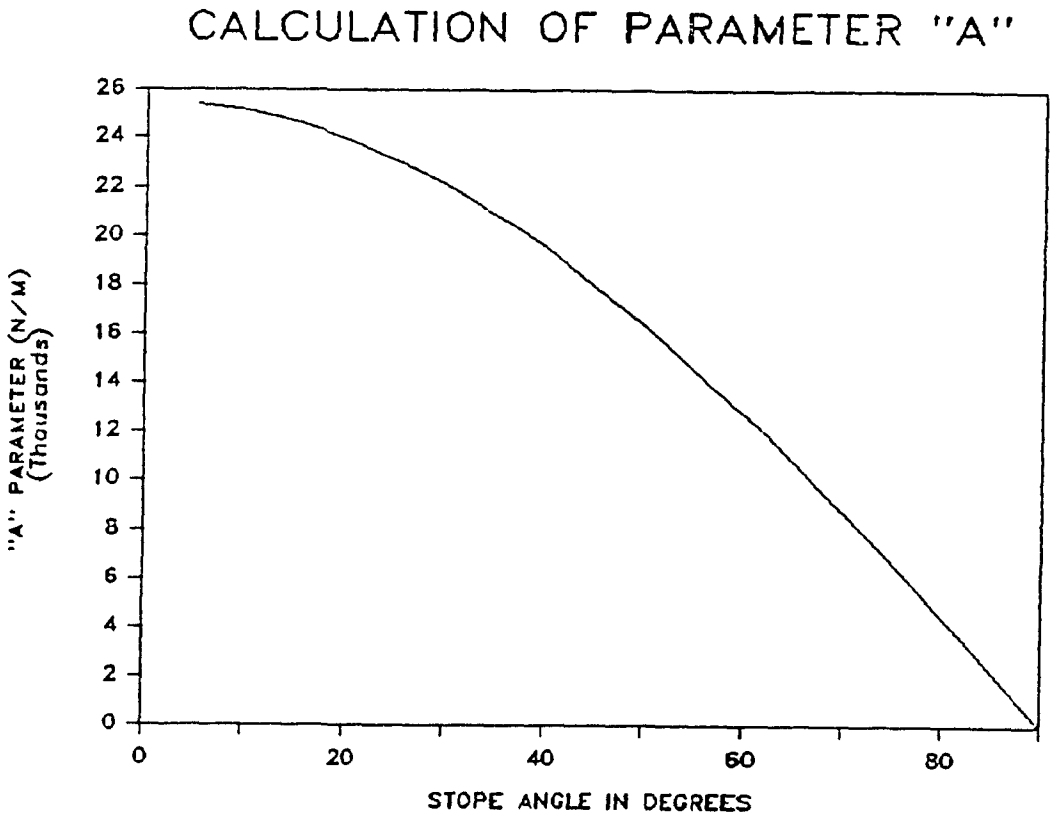

FIGURE 10.7 Determination Of Parameter "A"

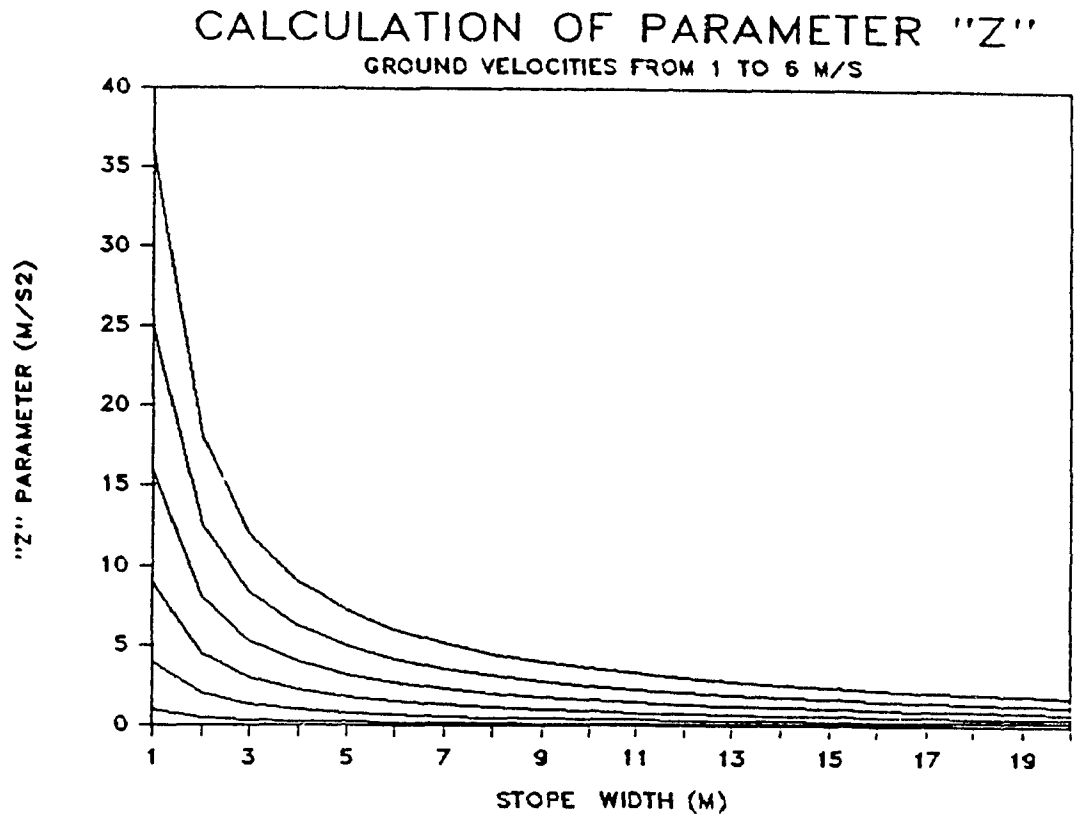

FIGURE 10.8 Determination Of Parameter "Z"

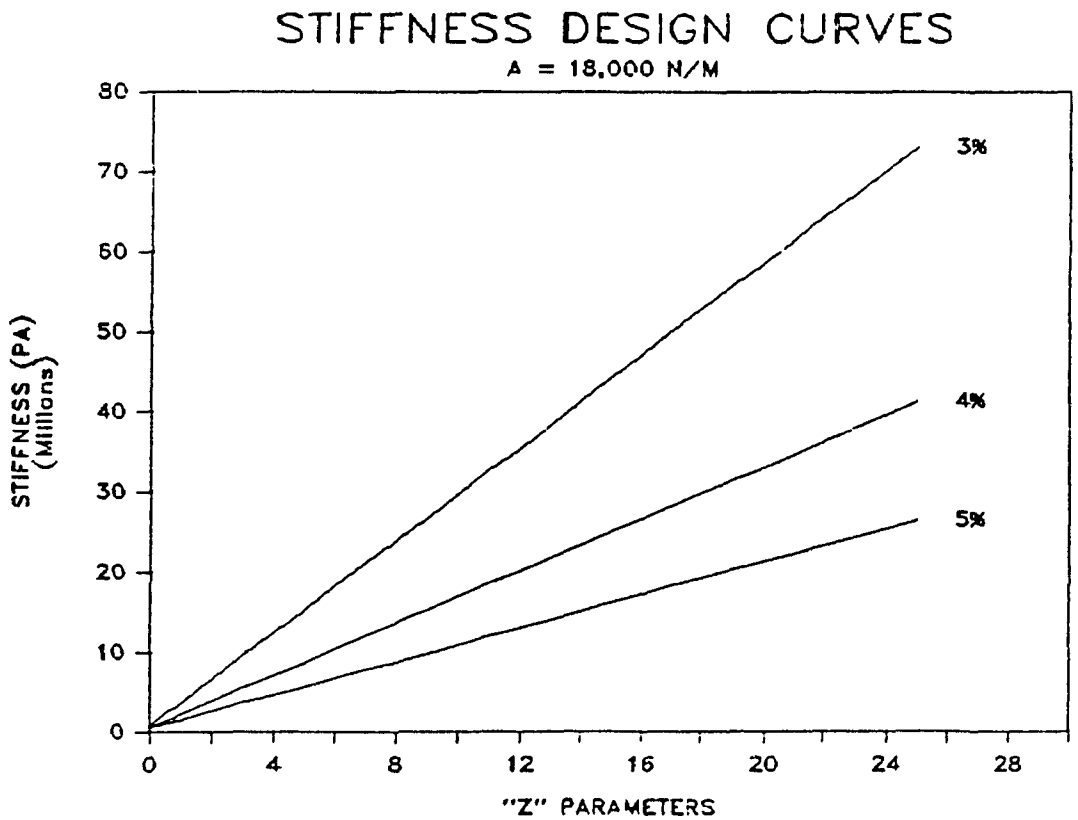

FIGURE 10.9 Backfill Stiffness Design Curves

The use of Figures 10.7, 10.8 and 10.9 in backfill design can best be illustrated through an example. Given that an orebody dips at 45^{o} in a rock mass of specific gravity of 2.6 and stope dimensions of 8m. If the design objective was for the backfill to withstand a peak ground velocity of 4 m/s then the required fill stiffness could be derived, for example, if 5% closure of the opening was considered to be the limit of acceptable deformation.

The first step would be to determine the "A" parameter from Figure 10.7 Given that $\rho = 2600$ kg / m and $\gamma = 45^{o}$ the "A" parameter becomes 18000. Similarly the Z parameter is obtained from Figure 10.8, given a design velocity of 4 m/s and an 8m stope width we find that Z = 2.04. The next step is to go to Figure 10.9, which is designed for an "A" value of 18000, and using the calculated "Z" value and the 5% acceptable closure given, then the "E" value related to these conditions can be derived. For this example a 2.8 MPa fill stiffness would be required to meet the preset failure criteria.

The prededing design process was based a peak ground velocity. It is, however, possible to design to a Richter magnitude of seismic event occuring at a specified distance from the opening. It has been proposed (101) that peak ground velocity can be correlated to local Richter magnitude, M_L, and distance from the source, R, by the equation 10.17. This equation implies that a 5 Richter Magnitude rockburst occuring 100 m from a stope would yield a 6 m/s ground velocity at the stope wall.

$$\text{Log } (R \times V) = 3.95 + .57\ M_L \quad \ldots\ldots\ 10.17$$

In summary, given that a rockburst of a given Richter magnitude will occur at an anticipated distance from an opening we are now in a position to design an adequate backfill to maintain stope closure within specified limits. Conversely, given the same information we are also equipped to predict stope wall closure knowing that a fill of specified stiffness is being used.

This thesis section has developed a series of backfill design curves for use under dynamic loading. It has also reviewed the implications of designing backfill to reduce seismic activity in mining. The two methods, although they are both derived from energy balances, are for the design of backfill under different conditions. The first is used to design backfill to reduce closure resulting from a seismic event. As such the energy balance is based on kinetic energy. The design criteria used in this case is closure, under a pre-defined seismic environment and stope dimensions.

The use of backfill in rockburst prone ground requires that a precise purpose be defined prior to design. Two purposes are outlined in this chapter and include backfills ability to absorb strain energy in its' role for rockburst prevention. In addition backfill may be used in a dynamic role to limit the amount of damage caused by a rockburst which has occurred. This role is termed "dynamic interaction" as a ground velocity is generated at the rockbursts' epicenter which will cause a net closure of the

stope walls. The total closure is dependant on the magnitude of the ground velocity at the stope boundaries, and the backfill stiffness.

Thus from a design point of view the required backfill stiffness depends primarily on the closure expectations or requirements and the anticipated ground velocity. The required stiffness is also dependant on the stope angle and width. As such each of the four design parameters have been used as part of a sensitivity analysis on the effect of these parameters on the required stiffness.

The parameters mentioned above fall into two categories including stope geometry, described by the stope width and the dip angle and the environmental expectations for both the backfill material in terms of required closure and the anticipated ground velocity. Again, a series of base parameters including a stope width of 4m, stope angle of 45^{o}, ground velocity of 4m/s and a design closure of 5%, have been employed.

Keeping all other parameters constant, the stope angle was varied from 20^{o} to 90^{o} to encompass a wide range of stope orientations. Equation 10.6 was then used to perform a sensitivity analysis with respect to stope inclination. Figure 10.10 illustrates the variation of required stiffness with stope inclination. It illustrates a 1 mPa variation, from 4.1 to 5.1 MPa over a 70^{o} range in stope angle. Thus the required stiffness appears to be relatively insensative to stope inclination. The required stiffness tends to decrease with an increase in stope

angle.

A similar investigation of the effect of stope width on required stiffness was conducted. The stope widths were varied between 2 and 13m. The effect of stope width is illustrated in Figure 10.11. This figure indicates increased sensitivity of required backfill stiffness with a decrease in stope width. It was further found that over the range of widths covered in this analysis, the required stiffness ranged from 2 to 7 MPa, thus illustrating a relative insensitivity of required stiffness to stope

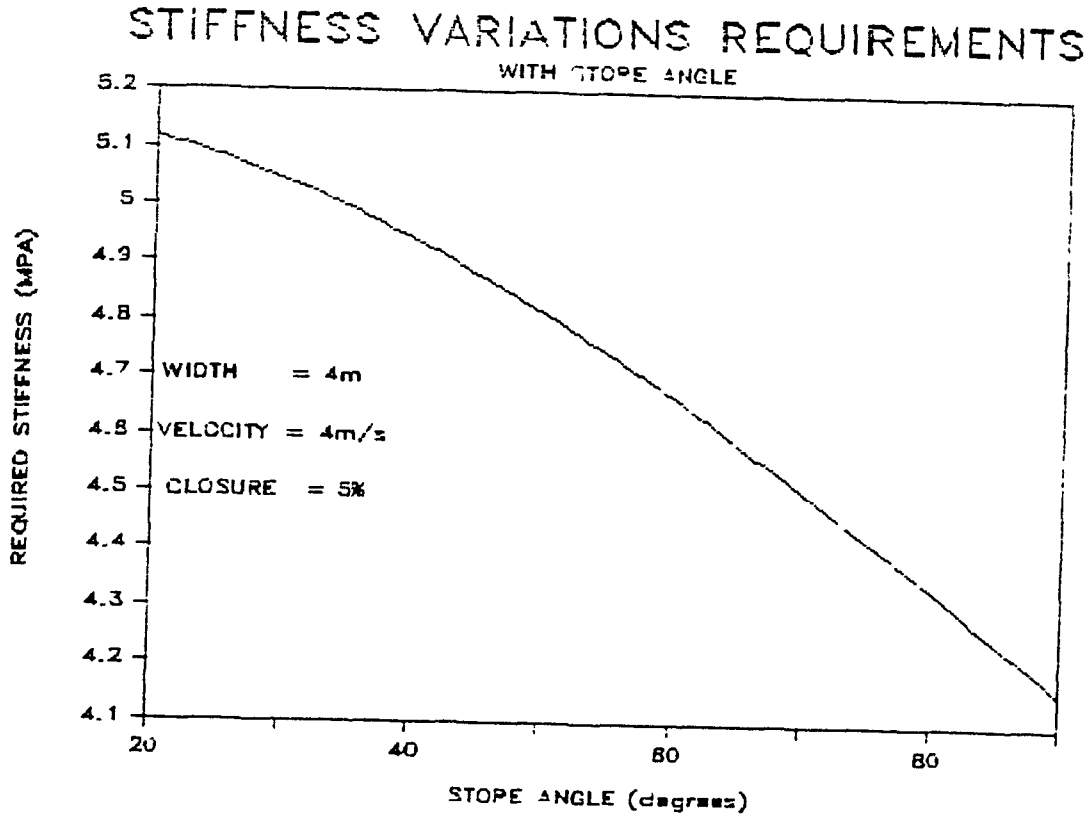

FIGURE 10.10 Stiffness Requirement Sensitivity To Stope Inclination

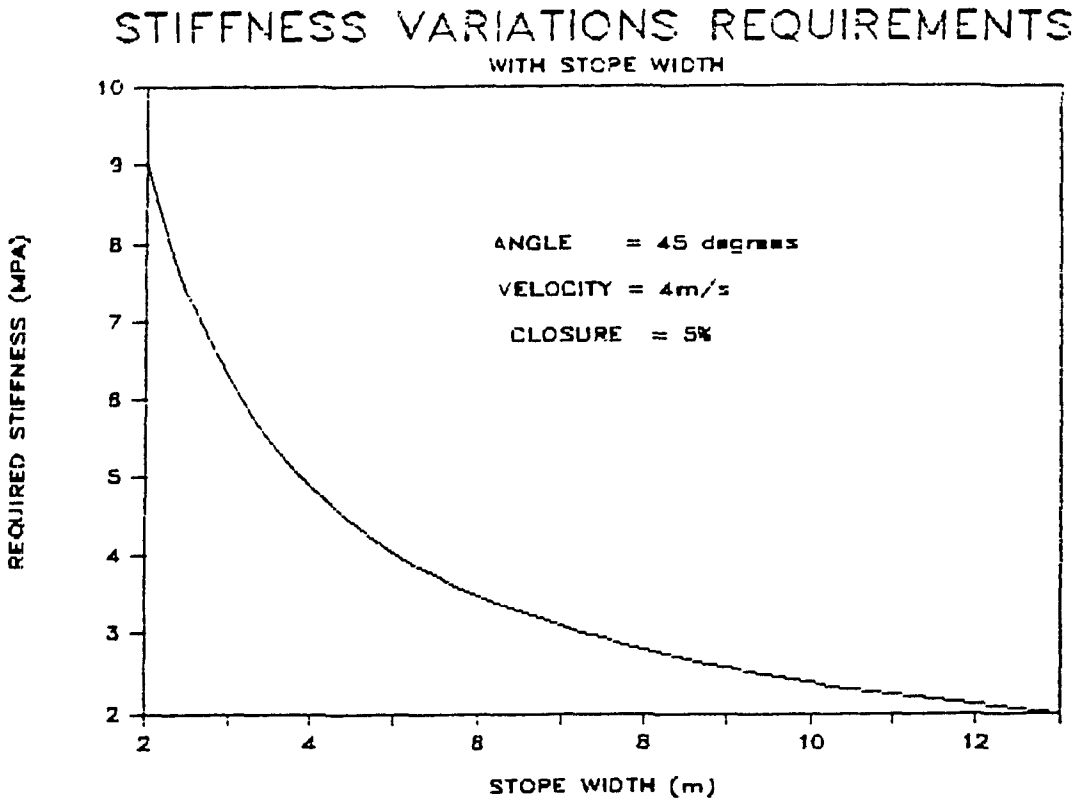

FIGURE 10.11 Stiffness Requirement Sensitivity To Stope Width

width. Furthermore, as the stope width approaches 13m, it is found that the required stiffness approaches 2 MPa for the stope inclination, seismic environment, and desired closure requirements listed in Figure 10.11. This is a significant fact when taken in the context of Table 10.1, as it would imply that under these conditions any of the listed materials would be suitable in a dynamic role.

Although both the stope inclination and width have an effect on the required stiffness the most significant effects result from the expected ground velocity and the closure which is considered acceptable. The effects of ground velocity for a range

between .5 to 11 m/s have been illustrated in Figure 10.12. The required stiffness ranged from 1 to 32 MPa over this range of ground velocities. This indicates increased sensitivity of required stiffness to anticipated ground velocity. Figure 10.12 further illustrates that if 5% closure is deemed acceptable in a 4m stope inclined at 45° then uncemented backfills may have some applicability for reducing damage which may be caused by dynamic loading. This is a significant conclusion as Pariseau (36) found that if stope wall closure in a cut and fill mining environment is limited to below 5% the damage to host rock remains insignificant. It is noted that uncemented rockfills may be applicable for ground velocities up to 2 m/s. A regrading and compaction of this material to properties similar to that of rockfill dam materials would increase the uncemented rockfills' applicability to ground

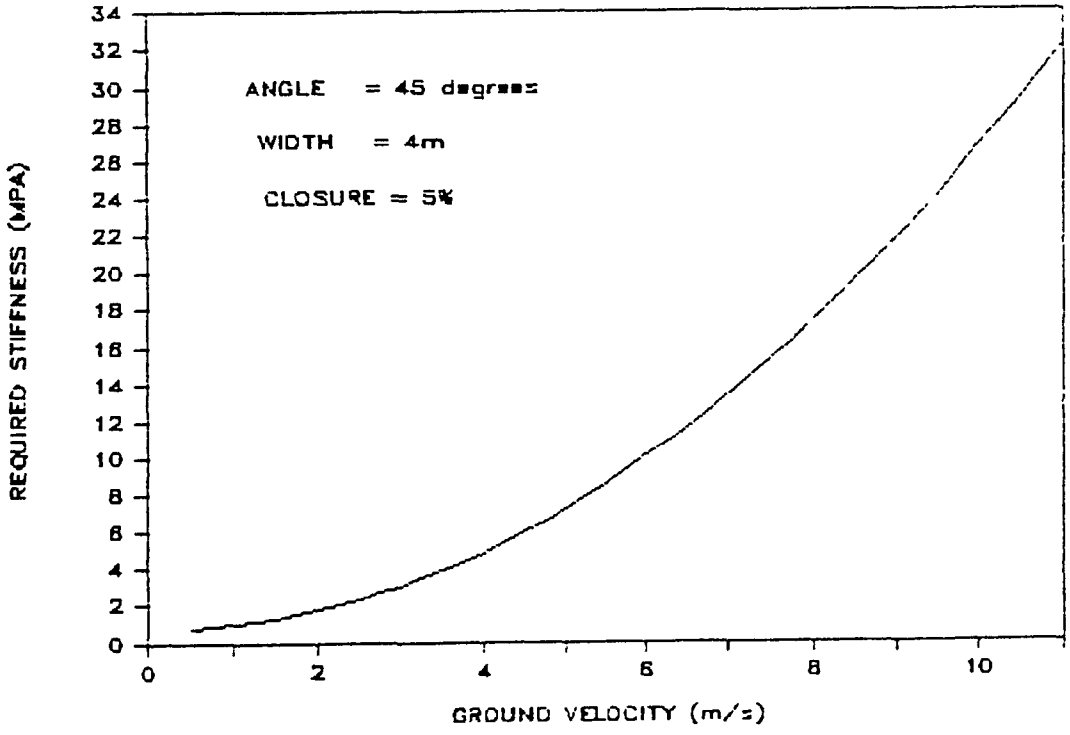

FIGURE 10.12 Stiffness Requirement Sensitivity To Ground Velocity

velocities up to 4.2 m/s. In addition uncemented fine grained backfills are applicable for ground velocities up to 7.5 m/s. It is further noted that any of the cemented backfills would perform satisfactorily for ground velocities up to 11 m/s.

The parameters discussed thus far reflect the in situ environment or anticipated conditions in the case of ground velocity. The acceptable closure, however, is a parameter which reflects a design requirement rather than an in situ condition. The required material stiffness was found to be most sensitive to the design closure, or acceptable closure. A wide range of acceptable closures have been illustrated in Figure 10.13. The design closures on Figure 10.13 range from .7 to 8% acceptable closure. The figure

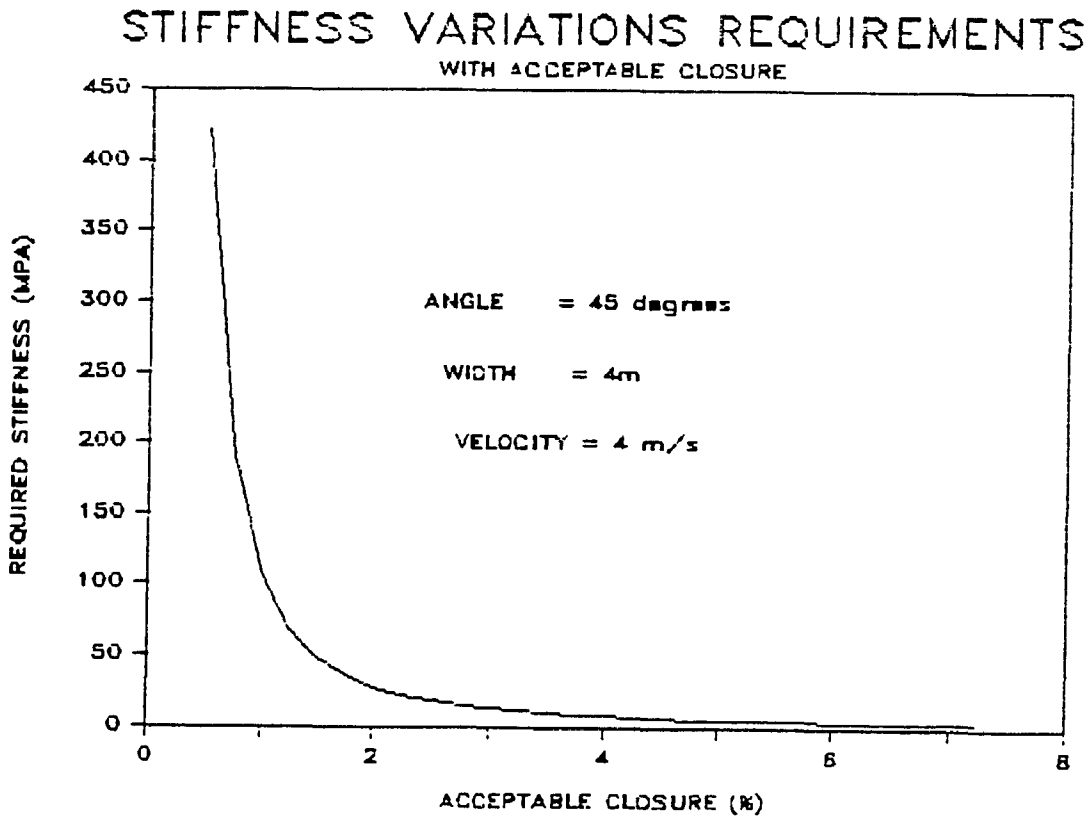

FIGURE 10.13 Stiffness Requirement Sensitivity To Acceptable Closure

further illustrates that a decrease in acceptable closure requires stiffer materials. In addition design closures below 1% are impractical and design closures of .75% approach the limit of present backfills available. It should further be noted that the limit of practical design closures increases with an increase in anticipated ground velocity. The 1% limit on design closure is applicable for the conditions set out on Figure 10.13. Cemented fine grained materials are applicable for design closures in excess of 1.1%. Vibrated fills on the otherhand can extend the design closure down to .9%. A further decrease in acceptable closure is indicated to be achieved if the double placed method of fill placement is used. Lastly, cemented rockfills would appear to be the only practical materials for use in design applications requiring less than .8% closure.

It has thus been concluded that although stope angle and widths have some influence on required backfill stifffness, the predominant effect is that of ground velocity and acceptable closure. The ability of the materials listed in Table 10.1 to reduce wall closure to acceptable limits has only been touched upon. It is the objective of the remainder of this section to more fully explore the applicability of the materials in Table 10.1 for closure control in rockburst prone ground. To this end two case studies have been examined; the first is a narrow stope 2m wide dipping at 20^{o} and the second is a 6m wide stope dipping at 75^{o}. These two cases represent two possible extremes geometry. In addition a ground velocity of 6m/s and design closure of 3% is used to access the effectiveness of the materials in Table 10.1. In the first

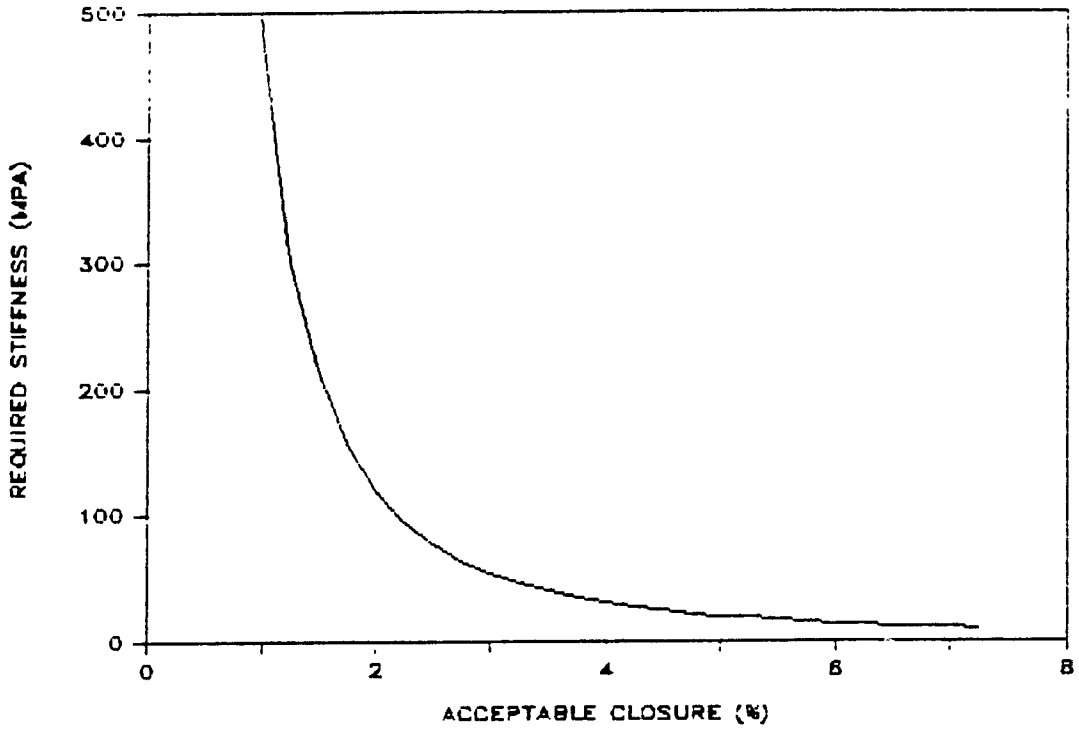

FIGURE 10.14 Stiffness Requirements For Shallow, Narrow Stope Arrangement - Ground Velocity = 6m/s

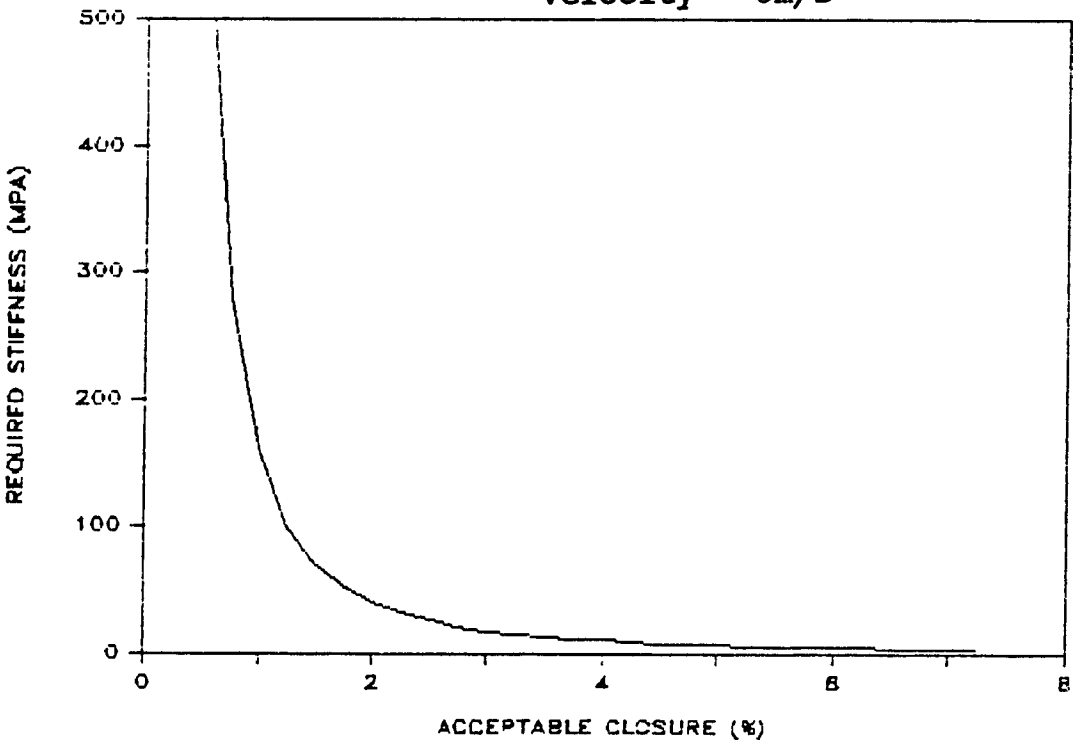

FIGURE 10.15 Stiffness Requirements For Steep, Wide Stope Arrangement - Ground Velocity = 6m/s

instance it is observed, see Figure 10.14, that for narrow, shallow dipping stopes in evironments of anticipated ground velocities of 6m/s the limiting design closure is 1.2%. This implies that extremely stiff fill materials are required for limiting closures below 1.2%. Under similar seismic conditions the limiting design

	STOPE ARRANGEMENT	
CLOSURE	WIDTH = 2m DIP = 20°	WIDTH = 6m DIP = 75°
	REQUIRED STIFFNESS (MPa)	
3%-4%	30 - 55	10 - 17
4%-5%	20 - 30	6.5 - 10
5%-7%	9.5 - 20	3 - 6.5

TABLE 10.4 Stiffness Requirements For Ranges Of Design Closures - Ground Velocity = 6 m/s

closure, from Figure 10.15, approaches .5% for the second mine geometry. This drastic decrease in unrestrainable closure is also reflected in stiffness requirements for the entire range of design closures. Table 10.4 summarizes the required stiffnesses for ranges of closure requirements for both case studies.

Figures 10.14, 10.15 and Table 10.4 indicate that for gently dipping narrow stopes then cemented backfills should be used exclusively for all design closures. The lone exception is the use

of uncemented fine grained backfills if design closures in the range of 7% become acceptable. Conversely, if a wide, steeply dipping stope orientation is considered then a wider range of materials becomes applicable. For instance if large closures in the order of 5%-7% are acceptable, then uncemented rockfills, graded and compacted to dam rock densities are indicated to be suitable choices. Furthermore, uncemented fine grained backfills could have applicability down to 3% closure. In addition to providing a means of backfill selection, the contrast illustrated between the two case studies indicates that although the required stiffness is relatively insensitive to both the stope angle and stope width a significant effect is observed when the two extremes are combined.

FIGURE 10.16 Stiffness Requirements For Ranges Of Anticipated Ground Velocities - Closure = 3% Narrow, Shallow Stope Arrangement

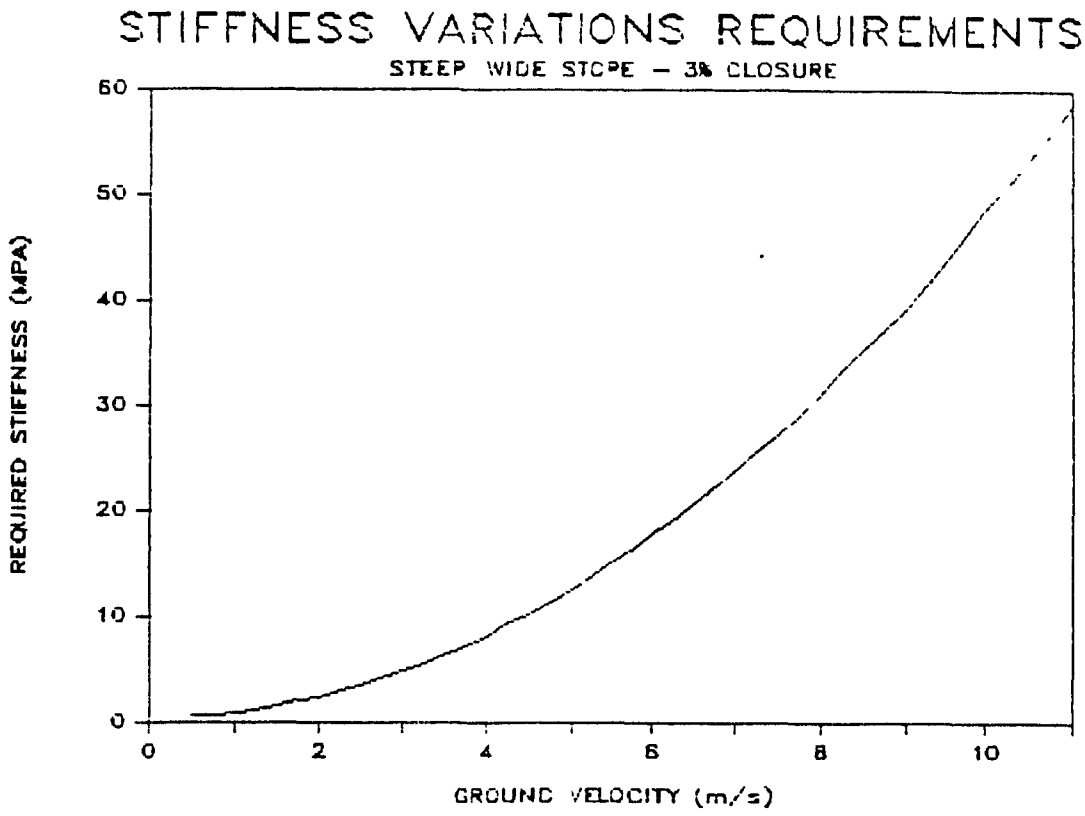

FIGURE 10.17 Stiffness Requirements For Ranges Of Anticipated Ground Velocities - Closure = 3% Wide, Steep Stope Arrangement

The design process outlined for the two case studies above starts from the basis that a seismic event of known magnitude occurs and that the applicability of the different backfills in Table 10.1 is verified. However. it may be required in some instances to limit closure where the seismic evironment is not known. The objective of design in this instance is to determine the maximum magnitude of seismic activity which can be supported by the materials in Table 10.1 and still limit closure within deemed acceptable norms. Figures 10.16 and 10.17 have have thus been developed. These figures represent the required stiffness for a particular design

closure (3%) and geometric stope arrangements. The required closure is illustrated as a function of anticipated ground velocity. In this way the maximum seismic ground velocity can be determined for any of the materials in Table 10.1 for a 3% closure requirement. The maximum stiffness scales on Figures 10.16 and 10.17 indicate a three-fold difference between narrow and wide stope arrangements. This again reflects the combined influence of stope dip and width. The data from Figures 10.16 and 10.17 has been summarized for distinct ranges of ground velocities, see Table 10.5.

	STOPE ARRANGEMENT	
GROUND VELOCITY (m/s)	WIDTH = 2m DIP = 20°	WIDTH = 6m DIP = 75°
	REQUIRED STIFFNESS (MPa)	
2 - 3	7 - 15	2.5 - 4.8
3 - 7	15 - 70	4.8 - 24
7 - 11	70 - 175	24 - 59

TABLE 10.5 Stiffness Requirements For Ranges Of Anticipated Ground Velocities Closure = 3%

Table 10.5 indicates that if a maximum 3% closure is required, which is in keeping with Pariseau's (36) minimum requirement for reduction wall rock failure in a narrow stope arrangement then uncemented fine grained backfills are suitable for ground velocities up to 3 m/s. The other uncemented materials are not suitable for ground velocities above 2 m/s. Cemented fine

grained backfills are applicable for ground velocities up to 7 m/s. The usefullness of cemented backfills can be extended to 11 m/s if special placement techniques (vibration, double placement) are used.

If the same design requirments are placed on a wide, steeply dipping stope then, the backfill material applicability can change. For instance, uncemented rockfills, both regular and compacted, have some degree of applicability for ground velocities up to 3 m/s. Uncemented fine grained backfills have some applicability for ground velocities between 3 and 7 m/s. Beyond this range, cemented backfills must be used to met the design requirements.

This section has thus reviewed the role of backfill in rockburst prone ground and its dynamic interaction with the surrounding rock mass. Some general comments as to the applicability of the materials in Table 10.1 have been made for particular mine geometries. Generally, as stope dimensions increase then weaker backfills appear to gain some applicability. Furthermore, a sensitivity analysis revealed that the required stiffness is primarily dependant on the design closure and anticipated ground velocity. In addition the required stiffness showed little sensitivity to the stope width and dip when considered independantly. However, the data produced from the two case studies indicates that when stope width and dip are taken in combinations which form extreme cases the total effect becomes significant. Lastly, all of the materials presented in Table 10.1 appear to have some applicability in rockburst prone ground.

10.2.2 Static Stress and Energy Reduction Applications

The trend towards increased mining depths and ore recovery has led to the need to design for high effective stresses in mining abutments. Blake (204) suggests that when the stresses in mine abutments is in excess of the rock strength and the stiffness of the abutment is greater than that of the static system of rock and support, then a rockburst situation exists. Thus as mining depths increase and the rock mass becomes more highly stressed then a rockburst-prone situation exists. The need exists to be able to predict such stress in advance of mining. The introduction of backfill as a structural component in such models has given rise to questions of backfill in situ support capabilities and actual in situ properties.

Methods used to assess rockburst potential include the use of numerical models to determine the stresses generated by the mine opening. These model types may also be used to incorporate backfill and evaluate its effectiveness at stress redistribution. An alternate model considers the energy release rate of the rock mass as a means of assessing rockburst potential.

A number of numerical models will be reviewed in this section and include a displacement discontinuity model (MINTAB), a two dimensional linear elastic finite element model (SAP2D), a two dimensional non-linear elastic finite element model (ADINA) and three dimensional non - linear elastic and non - linear elastoplastic and visco - plastic models (NONSAP, ASQUARE). It has

previously been noted that "calibrated" two dimensional linear and non-linear elastic models have performed well in backfill stoping environments (36),(37),(128). On the other hand, the use of the more complex model types presented here have not been supported by field calibration, rather they have been used to compare data with other complex models. The use of three dimensional models have not as yet been widely accepted due to computer memory requirements and runtime constraints.

A finite element model was used by Beer (47) to measure the effect of crown pillar removal on regional stability and the feasibility of mining under in place backfill. The concern was the stability of a backfill plug, see section 3.3.8, upon removal of a an underlying confining pillar. An elaborate, elasto-visco-plastic, two dimensional finite element program was used under plane strain conditions. Beer found that upon complete removal of the crown pillar, an extensive failure of the backfill material occured. This, however could not be verified in the field as the complete extraction of the pillar was not undertaken. He further pointed out that the backfill was modelled as an elastic, perfectly plastic material and that a yet more elaborate model, accounting for strain - hardening of the backfill, would have enhanced the results.

A more simplified technique was used by Pariseau (36),(37) for modelling stresses generated in sill pillar abutments between steeply dipping cut and fill stopes. Pariseau recognized that backfill is essentially non - linear and thus approximated its behaviour as being bi - linear in a two dimensional linear elastic

finite element model. He reported that the model was capable of predicting wall closures to within 10% and fill pressures to within 15% of observed field values. He further noted a significant decrease in sill pillar stress when backfill was used.

The case study described by Pariseau (36,37), illustrates that good correlations between predicted and measured in situ closures and stresses is possible. With the use of such models Pariseau concluded that pillar stresses could be reduced by 5 to 24% for ranges of backfills with stiffness between 6 and 60 MPa. The effects of backfill stiffness on maximum pillar stress is illustrated in Figure 10.18. This figure represents the variation in peak pillar stresses in a cut and fill mining situation for the range of backfill stiffness previously mentioned. Such stiffnesses represent backfills ranging from uncemented to cemented fine grained backfills. Under similar mining conditions Van Eeckhout (127) modelled backfill using ADINA, a non - linear elastic two dimensional finite element code. This work considered the use of various backfill types, ranging from conventional fine grained hydraulic backfill to double placed backfill. It was found that the maximum abutment stresses could be reduced by 7 to 27% over the no backfill scenario, depending on the backfill type used. The stress reduction observed by Van Eekhout is consistant with the findings of Pariseau (36,37). Using a different approach Hustrulid (39) considered Blakes' (204) assessment of conditions for rockburst potential and concluded from a closed form non-linear elastic solution for stress around a slender slot, that this rockburst

potential can be reduced in two ways. The first suggested method was to reduce the stiffness of the abutments so that the abutment stiffness is less than that of the loading system. Secondly the stiffness of the loading system was suggested to be increased, to this end he suggested that "high modulus" backfills be used.

The three case studies presented thus far are two dimensional and illustrate that backfill is an effective means of redistributing stresses.

Coulthard (128), on the other hand, attempted to model a fill pillar by three dimensional linear elastic finite element modelling. These results were compared with a two dimensional model of the same pillar. He observed that the two dimensional analysis showed that displacements on exposed faces of backfill pillars were greater when the analysis was performed with non - linear rather than linear elements. That is, an apparently larger stiffness is simulated with linear elements as compared with non-linear. He extrapolated this to his three dimensional linear elastic model and recommended that non - linear three dimensional calculations, using a fine mesh, be used before predicted behaviour can be relied upon.

The programming case studies described thus far have been for various finite element codes. Yu (42) illustrated the use of a displacement discontinuity model for backfill assessment. A trial analysis for the Copper Cliff South Mine, assessed the effect of varying backfill to rock stiffness ratios. These were varied from .01 to .1, and it was concluded that the larger ratios provided greater

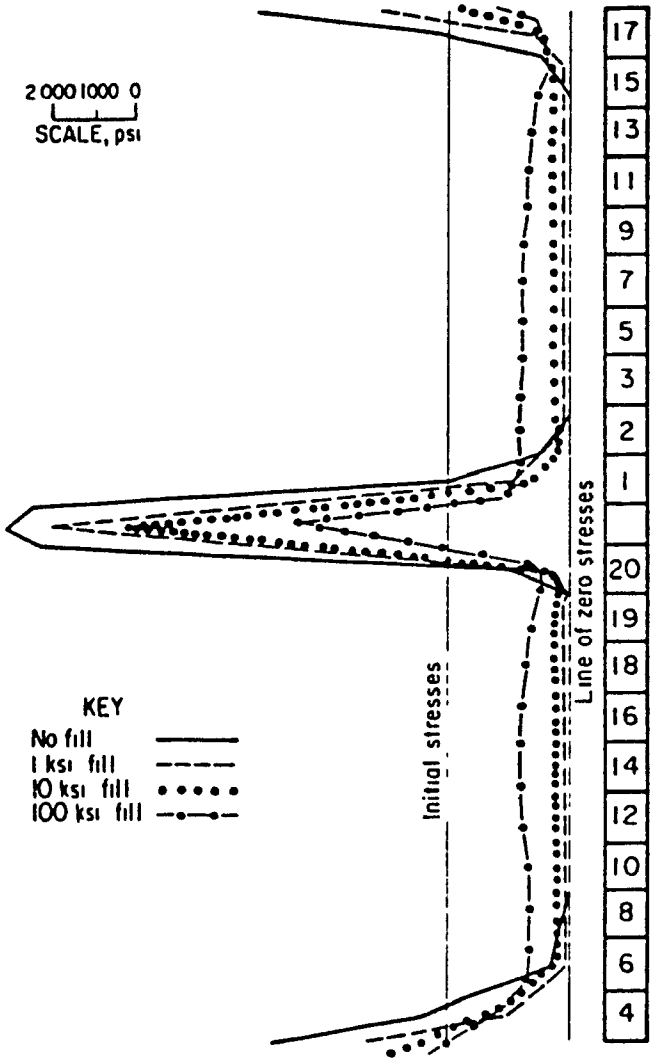

FIGURE 10.18 Effect of Backfill Stiffness on Peak Pillar Stress, After Pariseau (36)

resistance to stope wall closure and reductions in pillar stresses. It was found however that for the stiffest fill material investigated the resultant reduction in pillar stresses was in the range of 2%, this is in contrast to Van Eeckhout's (127) findings of a decrease of 7 to 27% in maximum pillar stresses. This difference is one illustration of how opinions as to the effectiveness of backfill in stress redistribution currently vary. Furthermore these discrepancies may have occured due to the use of different backfill properties in each case or as a result of the model formulation. It is not possible to accurately comment on the over-riding factor for the dicrepancy as Van Eeckhout does not present the backfill properties used in his model.

These programs, be they finite element or displacement discontinuity, are prone to a number of possible sources of numerical error. In the mining environment, the prevalent sources of error in finite element simulations stem from the idealization of mine structures. Two categories of such errors exist, idealization of mine opening geometry and idealization at mesh boundaries through the assumption of virgin principal stress at the boundaries. These are also sources of error for the displacement discontinuity model. Boundary stresses are applied to the structure, compatible with the virgin stress reported by Herget (94).

Other idealization errors result from simplification of material behaviour. It has already been previously discussed that idealization of backfill as linear elastic material does not represent the non-linear , plastic behaviour of mine backfill

observed in reality. It has been shown by Piciacchia (135), however, that for backfills confined at pressures of 2.75 MPa, the material response remains linear up to 3% strain and 1.6 MPa applied stress. This represents 40% of the failure strain and 50% of the confined failure stress. Other material idealization errors occur as a result of modelling the rock mass as a uniform structure, thus no account is taken of the possible effects of jointing and faulting. Furthermore, the zones directly surrounding the mine openings are often fractured and destressed. Account is often not taken of this fact.

In view of the number of possible idealization errors which can occur with these numerical codes and the ability of particular models to cope with these possible errors to varying degrees, the observed discrepancies as to backfills' effectiveness for redistribution of stresses around mine openings is not surprising. Perhaps the most logical means of overcoming these idealization errors is to calibrate the model by reference to field measurements. The model presented by Pariseau (36) (37) is one such model. In view of the remaining discrepancy between the conclusions drawn by Yu (42) and the other three case studies presented, the following comments are presented in partial explanation of the disparities:

- MINTAB uses a linear elastic formulation for representing material properties while the other case studies presented are all non -linear and thus represent the material characteristrics more accurately.

- The presented idealization errors may have effected each of the case studies to differing degrees.

- The range of material properties varied from case study to case study.

Having considered the possible explanations for the discrepancy between Yu (42) and the other three casestudies, particularly the first, and considering in conjunction with this the calibration procedure carried out by Pariseau (36) (37), the author concludes that linear elastic models are not suitable for modelling backfill materials. This conclusion is supported by Coulthard's (128) findings that linear - elastic models tend to be more conservative than non-linear models.

In the second instance, we are concerned with the redistribution of strain energy. Rock masses in their virgin state have a certain amount of strain energy stored within, due to their own weight and tectonic history. Furthermore, as a block of ore is removed from the original rock mass through mining then changes in the energy balance take place. Firstly, the strain energy previously stored in the ore removed must be dissipated. Secondly the system must achieve a state of energy equilibrium. It is on this basis that the effectiveness of backfill to reduce seismic activity is measured. Hedley (43) has expressed the energy balance which occurs as a result of mining. It is possible on the basis of this energy balance to evaluate the effectiveness of backfill in absorbing strain energy.

The assumption is made that as a block of ore is removed, the only two means for energy dissipation is as seismic energy or in compressing the backfill. Therefore if we ensure that more of the available energy released goes into compressing the backfill then

less energy will be available to be dissipated as seismic energy. The strain energy redistribution equations indicate that seismic activity can be reduced by destress blasting, a practice being examined at the Campbell Red Lake mine, as this would reduce rock mass stiffness, or by stiffenening the backfill. Furthermore a combination of the two techniques would be most effective. We also note that at lower rock mass stiffnesses the energy balance equations become more sensitive to backfill stiffness. Hence, another conclusion that can be drawn is that the benefits of stiffening backfill are more apparent in lower modulus rock masses or in a destressed rock mass. This conclusion is consistant with Blakes' (204) theory of rockburst conditions and with Hustrulid's (39) recommendation of reducing pillar stiffness or increasing the stiffness of the loading system.

Hart (205) used a non-linear energy balance approach to assess the effectiveness of backfill for reducing the total stored energy in the rock mass. Figure 10.19, illustrates the comparison between a stope which is fill with backfill (case C) and one which is not (case B). The figure illustrates that as a mining stage occurs the total stored energy increases to a peak value. Over time, between mining phases, a gradual ajustment and energy balance is observed, a new mining sequence brings the total energy above the old peak value. Hart concluded that backfill effectively lowered the energy release rate by 20% through its ability to absorbing energy which would otherwise be released if no backfill was present.

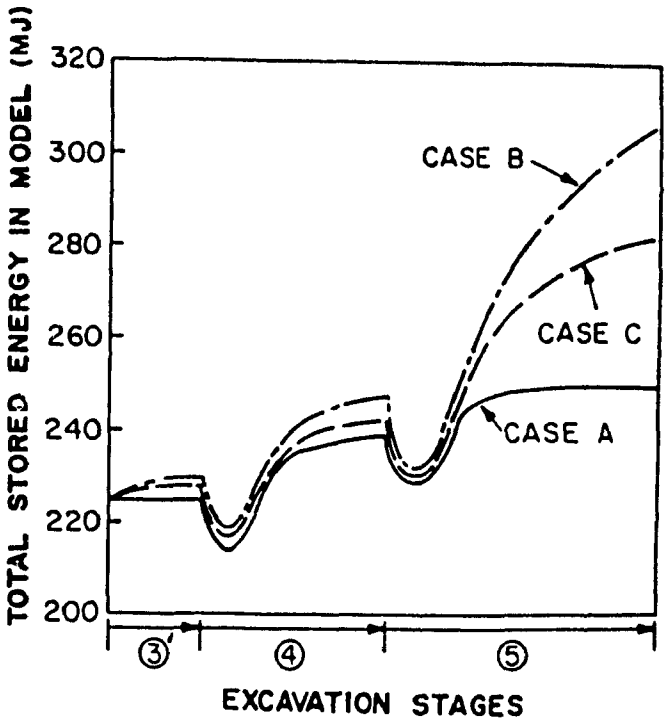

FIGURE 10.19 Stored Energy Buildup With and Without Bacfill, After Hart (205)

10.3 SUMMARY

The objective of this chapter was to determine the effectiveness of backfill in various roles in the mine environment. The applicability of backfill in its' role as a free standing pillar has been examined. Furthermore, the applicability of backfills in dynamic interaction with the surrounding rock mass in rockburst prone ground has been investigated. Lastly, the applicability of various fill materials for stress reduction in has been examined.

Backfills role in free standing applications is particularly sensitive to material cohesion, density and angle of internal friction. Uncemented rockfill have no free standing applicability due to their lack of cohesion. The remainder of the fill materials have limited applicability, defined by the maximum attainable height, see Table 10.2. Furthermore, as much as a 30% decrease in attainable height is observed when saturation corrections are made.

The role of backfill in rockburst prone ground has also been examined. It was found that as stope dimensions increase then weaker backfills gain some applicability. Furthermore, a sensitivity analysis revealed that the required stiffness is primarily dependant on the design closure and anticipated ground velocity. In addition the required stiffness showed little sensitvity to the stope width and dip when considered independantly however, two casestudies indicated a significant effect is possible when the effects of these parameters are considered in combination. The materials presented in Table 10.1 all have some applicability in rockburst prone ground.

The published works investigating the effectiveness of backfill for the redistribution of stresses and energy absorption, seems to come to some contradictory conclusions. However, the comprehensive modelling study and field calibration reported by Pariseau implies the applicability of cemented and uncemented fine grained backfills. This conclusion was further supported by a similar study conducted by Van Eeckhout (127) and a study by Hustrulid (39).

The effectiveness of backfill in rockburst-prone ground judged on the basis of energy absorbtion have been illustrated by Hedley (43) and Hart (205). Their findings concur with those of Pariseau (36), (37), Van Eeckhout (127) and Hustrulid (39). Their conclusion was that backfill can be an effective means of decreasing pillar stress and absorbed energy for rockburst applications. The literature, however, contains scant information on the precise relationship between backfill stiffness and effectiveness. This should be the aim of future research.

11.0 SUMMARY AND CONCLUSIONS

The backfill design procedure comprises material design, to account for the selection of backfill type and material properties, as well as transportation and placement design. There exists a need for an integrated approach to backfill design. A design rationale has been presented, the structure of which could be contemplated as an backfill design expert system, based primarily on geomechanical considerations.

The main objective of this thesis was to develop a backfill design criteria based on backfill function and material physical characteristics. This objective was met by the formation and analysis of a backfill geomechanical and physical properties database from which design equations were developed. The database required the development of an insitu and laboratory testing program of backfills from ten mines, together with reference to other workers. These equations are to be used within the framework of the design rationale to be applied to target mechanical properties, which are dependant on backfill function and mining environment. The effectiveness of backfill in different mining roles has thus also been investigated in order to relate backfill properties to function and demonstrate the concept of defining target material properties.

11.1 Pressuremeter Usage And Applicability

Mono - cellular and Tri - cellular pressuremeters have been used in geotechnical engineering for over 25 years, but have only been introduced to the underground mining sector in this decade. Their applicability and limitations in mining environments justified a full assessment.

The Pencel pressuremeter, a mono-cellular probe, was used as part of this study in a program of 100 pressuremeter tests, conducted at 17 different mine test sites in conjunction with 7 mine operators.

Two empirical equations for pressuremeter data interpretation have thus been proposed in this thesis. These include a simplified correlation between K_o and the limit pressure, P_1, equation 8.2. Secondly the existing available undrained shear strength equations give a wide dispersion of predicted strength for identical input data, as great as 40%. A new equation, 8.1, has been proposed which reduces the scatter to a maximum of 20%.

Several other conclusions can be drawn on the application of the pressuremeter and the interpretation of its data.

- The pressuremeter has proven itself, through the course of this study, to be a reliable and highly applicable tool for determining field geotechnical properties of backfills including:
    - angle of internal friction
    - shear and deformation moduli
    - K_o parameter
    - undrained shear strength

- The use of the Pencel pressuremeter indicates that natural data scatter to the extent of 12% is to be expected

- A series of tests were conducted in which two distinct material bands in a backfill mass were tested. The difference in material properties was detected and measured 21%. This implies that measured variations of $\pm$21% or greater represent actual variations in material properties.

- Variations of less than $\pm$12% cannot be construed as actual variations in material properties. Unfortunately, no comment can be made of data variations between 12 and 21%.

- It is recommended that laboratory pressuremeter testing should be conducted to more accurately quantify instrument sensitivity and data repeatability under controlled conditions.

- The P_o value from the pressuremeter curves has been used to determine the total lateral pressure. This total pressure along with the K_o parameter have been used to calculate total absorbed stress by the backfill material. However, it is not possible to verify the predicted total lateral stress due to lack of availability of field measurments.

- It is recommended that the applicability of the FDPMT for measurement of total lateral stress become the focus of a future study.

- The testing procedure itself has been improved by eliminating the pressure calibration of individual membranes, see Figure 8.2.

- Furthermore, prior to the work carried out in this thesis it was not possible to conduct FDPMT in confined environments such as those encountered in underground mining. A new system was thus developed which could contend with the space and transportability requirements for underground usage, section 5.4. The system described in section 5.4 proved to reliably fulfil these requirements.

- Several theoretical equations have been developed since the pressuremeters' inception. The aim of these equations has been to describe the stress and strain distributions which are generated around the pressuremeter probe upon inflation. It is noted, however, that the pressuremeter instruments for which existing equations have been developed are of the tri-cellular variety and are not applicable to other probe types.

- The deformation of mono-cellular probes is elliptical. As such, the existing equations do not adequately represent the stresses and strains which are generated around a mono-cellular probe. Several equations have thus been developed which assume the deformation geometry of mono-cellular to be elliptical. These equations indicate that if a length to diameter ratio of greater than 6.5 is maintained the difference in deformation over the length of the probe is negligible and the generated stress tends towards uniformity.

- When the Pencel is inflated such that the internal pressure reaches the quoted instrument capacity, 2500 kPa, the stress at 2.5 pressuremeter diameters from the probe has fallen off to 5% of the internal membrane pressure.

- In light of the stress regime about the inflated pressuremeter probe, it is thus recommended that if closely spaced tests are required, they should be spaced no closer than 17.7 cm, assuming an angle of internal friction of 32^{o}.

- It is recommended that the stress and deformation equations developed as part of this thesis be verified with laboratory tests. This would include comparing laboratory measured stresses and strains within a test media during a pressuremeter test to predicted values of theoretical equations.

- It was not possible within the scope of this thesis to assess the material damage generated by instrument insertion. This should be the scope of an extensive laboratory study with the aim of providing insertion damage correction equations for limit pressure and modulus of deformation.

11.2 In Situ Geomechanical Data

There has been and still exists a large deficiency of backfill field data. The data presented as part of this study represents the most ambitious Canadian undertaking for the determination of in situ mine backfill properties on record. It forms the foundation for a future database of in situ geotechnical backfill properties. It is recommended that this database be further expanded to include a wider variety of backfill types and conditions, relating to the proposed backfill classification scheme.

A summary of conclusions drawn form the present database is outlined:

- the addition of flocculants can significantly increase material stiffness without additional cement.

- A series of tests conducted in differently aged backfills indicates that the curing characteristics of in situ backfills may be retarded due to high initial moisture contents and their effect on the hydration process.

- It was found that the pressuremeter E_m / P_l ratio is a good indicator of backfill material type. The following ratios are typical for the materials tested

    - uncemented rockfill: 4 --> 8
    - uncemented fine grained backfill: 10 --> 15
    - cemented fine grained backfill: 15 --> 24

- This ratio may thus be suitable for use in quality control applications or for detecting segregation

- Backfill limit pressures have been measured as .3 to .4 MPa for uncemented rockfills, with a notable increase to .6 to 1.5 MPa for uncemented fine grained materials. The limit pressures for cemented fine grained materials ranged from .75 to 2.5 MPa. Similarly, the deformation modulus followed the same trend.

- Although, it has already been mentioned that the reliability of the Pencel for measuring total lateral stress has not been verified, the present data point to some interesting trends. It idicates that lightly cemented backfill (5% wt.), absorb as much as three times the stress than uncemented backfills. It is recommended that this observation be investigated further.

- The influence of environmental and geological factors on measured stress is also concluded to justify further work.

- Study of a possible correlation between measured stress and cement addition would appear to be of significant interest and should be the object of further in situ investigations.

11.3 Laboratory Data And Field Correlations

A laboratory testing program formed the basis for developing design equations for three backfill types. The work on uncemented fine grained backfills produced laboratory design equations relating physical and geomechanical properties. The laboratory equations have also been related to field conditions via appropriate correlations. Laboratory design equations for cemented backfills have been developed but field extrapolation, however, was not possible due to lack of in situ test data. Lastly, the data for uncemented rockfill serves purely as a guide to determining the angle of internal friction from porosity. Data for cemented

rockfills is particularly sparse and it was beyond the scope of this study to consider these materials. It is, however, recommended that each of these study areas be brought to a more final state of completion comparable to that of uncemented fine grained materials.

It is further concluded of the analysis conducted for uncemented fine grained backfills that:

- The analysis of the uncemented fine grained backfill can be extended to relate the base friction angle to particle angularity.

The data correlations and design equations for cemented fine grained backfills have been developed mainly from a data base of published work. The initial analysis consisted of direct correlation of strength to cement addition for distinct curing periods.

- It was noted that the scatter reported in Table 9.2 was in excess of desired limits although the correlation coefficients proved acceptable.

- A second analysis was performed using water to cement ratio, W/C, which yielded equally good correlations whilst the observed scatter was substantially reduced.

- Subsequently, if was found that when the data is presented in this format the effects of curing are minimized.

- Distinct curing curves tend to converge as W/C ratios increase. This accounts for the decreased influence ofcuring at common W/C ratios used in mining.

- It was found that an averaged curve, relating strength to W/C, could be used to represent the entire body of data with only a nominal error resulting due to the elimination of curing characteristics and the scatter is also further reduced.

- The averaged curve is represented as equation 9.1. adequately predicted the strength of laboratory test specimens cured for different curing periods and moisture contents.

- This equation was then used to develop a backfill design procedure aimed at optimizing the selection of cement addition and pulp density.

- Guidelines for the selection of W/C ratios arose from a sensitivity analysis. It was found that W/C ratios below 3.5 are required in order to maximize marginal from increases in cement addition or increases in pulp density. It was also indicated that W/C ratios greater than 6 should be avoided.

- It follows that at normal pulp densities (65%) optimized mariginal increases in strength can only be achieved at cement additions above 10%. A 10% cement addition is at the boundd of economic limits for bulk fills.

- Cement additions above 10% are not part of present practice and the conclusion thus follows that present cement addtions fail to provide optimized marginal strength increases.

- Recent research has trended towards increasing the pulp densities in the range of 78%, this would enable optimization of cement additions as low as 6%.

- Equation 9.4 was developed to relate the material stiffness to uniaxial compressive strength. Exisiting equations tend to underextimate the material stiffness. The equaiton was reworked so that the material stiffness could be predicted from the W/C ratio.

- It was found that the literature contained a marked absence of data on the compressive strength and stiffness charateristics of uncemented fine grained backfills. A study of these parameters was thus undertaken, and included extensive pressuremeter and laboratory shearbox testing. The parameters of interest in the laboratory study included the material cohesion, angle of internal friction and the shear stiffness. It was found that each of these parameter correlated best with different physical properties. Strong correlations were found between thefollowingphysicaland geomechanical properties:

    - cohesion with degree of saturation
    - angle of internal friction with degree of saturation, C_c , C_u
    - shear modulus with void ratio, degree of saturation, specific gravity of solids normal stress

- The laboratory data for individual mine siteswas studied with parallel in situ data, resulting in effective correlations. This is considered to be an important contribution as it enables field response to be predicted from laboratory testing. Three correlations studies have been made, including:

    - laboratory cohesion with limit pressure
    - unconfined laboratory with in situ stiffness
    - laboratory with in situ friction angles

- It is recommended that the observed relationships be reinforced with additional in situ and laboratory data.

The tilt box test (5) was applied to determine the angle of internal friction of uncemented rockfill. The testing program undertaken enabled characteristic angles of internal friction to be determined for materials having different porosities. The

repeatability and reproducibility of tilt box data suggests the applicability of this technique for determining the angle of internal friction of uncemented rockfills. The measured angle of internal friction at normal loads of 1 MPa for the Chadbourne mine material is in the order of 30^{o}, this is compared with 27^{o} as estimated from the pressuremeter data. It is recommended that a full parametric study be undertaken so that the angle of internal friction can be determined directly from physical parameters.

11.4 Backfill Effectiveness In Ground Control

In addition to developing design equations for three backfill types this thesis has investigated the effectiveness of backfill materials in different structural roles in the underground environment. These include:

- backfills' role in rockburst prone-ground
- free standing height applications
- backfills' ability to reduce static stresses

Free standing height applications are the first to be considered and a curvilinear model is developed and used to represented the backfill material.

- the curvilinear approach has found to be yield more conservative free standing heights than the linear models available

- the estimated free standing heights for cemented rockfills are consistant with observed field evaluations

- The curvilinear failure mode represented by Equation 10.5 illustrates that cohesionless backfill materials such as uncemented rockfills are not suitable for free standing height applications as a free standing height is not possible due to their lack of cohesion.

- This equation further showed a significant sensitivity to the angle of internal friction, the material cohesion and to a lesser degree the backfill density.

- Table 10.3 was developed, which illustrates the nominal expected heights which can be achieved for various backfill types. It indicates that:

    - uncemented fine grained backfills are stable to heights of 10m.

    - cemented fine grained materials would increase the attainable height 25m.

    - double placed rockfill or cemented rockfill materials would yeild free standing heights of 60 and 100m

- It was further found that these values are dependant on the degree of saturation of the backfill material and a saturation correction curve has been presented, Figure 10.5.

Backfill may also be required to perform in rockburst prone environments where it may be required to serve to counteract dynamic and/or static loading. In the first instance a dynamic model based on energy conservation has been developed in Chapter 10. The model has subsequently been used to predict backfill stiffness requirements for limiting closure to desired levels for given seismicity and geometry.

- A sensitivity analysis revealed that the required stiffness is insensitive to the stope inclination and width, when these parameters are considered separately. The combined effect, however, can become significant.

- The general trend revealed that as stope width and inclination increase then the required stiffness decreases.

- The required stiffness is most sensitive to the anticipated ground velocity and design closure limit.

- It was found to be impractical to design for closures below 1% for some values of ground velocity.

Two case studies were contrasted for different stope dimensions and inclinations. Two alternate design processes were investigated for each of these environments; design for an anticipated ground velocity (6m/s) and a range of design closures; or design for a desired closure (3%) and a range of seismic environments. The fixed velocity design process indicated that:

- In narrow, shallow dipping stopes for 6 m/s, ground velocity, then cemented backfills should be used exclusively.

- The use of uncemented backfills for stope wall closures of 7% is considered the lone exception.

- Within this environment a limiting design closure of 1.2% is noted, where extremely stiff fill materials are required beyond this limit.

- A similar analysis was conducted for a wide, steeply dipping stope in the same seismic environment as the narrow stope. It was apparent that the required stiffness was substantially reduced, and the use of uncemented rockfills became acceptable for closures between 5 and 7%. Uncemented backfills become acceptable for closures as low as 3%.

The second design process, a fixed closure method, indicated that:

- Uncemented fine grained backfills are applicable for ground velocities of 2 - 3 m/s.

- Cemented materials are recommended for ground velocities greater than 3 m/s.

- The analysis of wide, steeply dipping stopes illustrated that uncemented rockfills may be applicable for ground velocities as high as 3 m/s.

- Uncemented backfills are acceptable for ground velocities between 3 and 7 m/s. Beyond this range cemented backfill materials are exclusively required.

- The analysis conducted indicatedavarieddegree of backfill applicability in rockburst-prone environments depending primarily on geometric considerations, support expectations and seismic intensity.

The effectiveness of backfill for stress and energy redistribution has been reviewed from the literature. It was found that differing opinions on backfills' effectiveness in redistributing stress still exists. However, the evidence seems to indicate that backfill is an effective means of stress and energy redistribution. The following detailed conclusions can thus be made:

- Pariseau (36) (37) and Van Eeckhout (127) both concluded that cemented fine grained backkfills could effectively reduce the maximum pillar stress by 26%.

- The findings of Pariseau and Van Eeckhout have been further colaborated by Hustrulid (39).

- Although these analyse provided some valuable insight into the effectiveness of backfills for stress redistribution it is recommended that a more detailed analysis be conducted. The analysis should provide a more realistic representation of rock and backfill properties, particularly throught the use of non-linear models.

- A rational approach for model development and selection in studying backfill performance is still required. Generally, the use of an F.E.M. program should be preceded by a series of field evaluations of the major structural components which include:

    - stiffness characteristics of the backfill
    - stiffness chatacteristics of the rock mass
    - the properties of the joint elements
    - the stress environment should measured
    - the underground structure needs to be monitored and the monitoring results compared with the predicted values

This approach requires that each of these areas of model development, in situ monitoring and properties determination be undertaken in parallel. This overall approach has successfully been used at the Nasliden mine, Kolsrud (199), and Krauland (200).

The use of energy balance approaches for the assessment of backfill effectiveness has further corroborated the findings of Pariseau and Van Eeckhout. Hart (205) indicated that the use of backfill could reduce the energy release rates by 20%.

11.5 Summary

This thesis has developed a series of design equations for cemented and uncemented fine grained backfills. In addition it has provided some initial data for the evaluation of uncemented rockfills. The properties determined have subsequently been used to

evaluate the ground support and stability of these materials in a range of mining environments.

This chapter first summarizes the use and applicability of the pressuremeter for testing backfill materials. Reference has been made to the sensitivity, data scatter and practical aspects of pressuremeter usage. In addition the implications stemming from the developed stress and strain equations for the pressuremeter tests are outlined. The in situ properties data base has further enabled tha author to provide insight into the effect of in situ curing characteristics, the effects of flocculants and the applicability of the instrument for quality control applications. In addtion the data base has provied valuable insight into typical in situ properties for different backfill types.

The development and analysis of a backfill properties database formed the core of the work undertaken. The analysis of the data base yielded design equations for cemented fine grained backfills. These equations are based on the water to cement ratio and were developed from over 500 data records accumulated from the literature and from laboratory tests. Similarly, design equations have been developed for uncemented fine grained materials. The geomechanical properties were related to the physical characteristics. The data for uncemented fine grained materials was related to parallel in situ characteristics which resulted in a design capability to predict filed response from physical parameters. In the case of uncemented rockfill materials a series of preliminary design curves relating the angle of internal friction

to the normal stress have been presented and the practical quidelines for increasing the angle of internal friction have been presented. Lastly, the effectiveness of backfill for free standing applications and in rockburst-prone ground has been investigated using existing and developed models as well as published casestudies.

1. Lightfoot W.E., 1951. "Hydraulic Filling in Metal Mines". Special Report 12, State of California, Dept. of Natural Resources.

2. Spangler and Handy, 1973. "Soil Engineering". Third edition, Intext Educational Publishing, New York.

3. Mathews K.E. and F.E. Kaesehagen, 1973. "The Development and Design of a Cemented Rock Filling System at the Mount Isa Mine Australia". Proc. Jubil. Sympo. on Mine Filling, Aug. 1973, pp 13-23.

4. Leps T.M., 1970. "Review of Shearing Strength of Rockfill". Journ. of the Soil Mech. and Found. Div., Proc. of the A.S.C.E., pp. 1159 - 1170.

5. Barton N. and B. Kjaernsli, 1981. "Shear Strength of Rockfill". Journ. of the Geotech. Engineering Div., Proc. of the A.S.C.E., pp. 873 - 891.

6. Stephenson D., 1979. "Rockfill in Hydraulic Engineering". First Edition, Elsevier Scientific Publishing Company, Amsterdam.

7. Marachi D.N., Chan C.K. and Seed H.B., 1972. "Evaluation of Properties of Rockfill Materials". Journ. of the Soil Mech. and Found. Div., Proc. of the A.S.C.E., pp. 95 - 114.

8. Hribar J., Dougherty M., Ventura J. and P. Yavorsky, 1986. "Large Scale Direct Shear Tests on Surface Mine Spoils". Proc. Inter. Symp. on Geotech. Stability in Surface Mining, Calgary, Nov. 1986, pp. 295 - 303.

9. Anon, 1983. "Placement and Evaluation of High - Modulus Backfills". Prepared for USBM, Washington by Montana Coll. of Mineral Science and Technology on Contract J0295052, OP 151-84.

10. Wayment W.R., "Backfilling With Tailings - A New Approach". Internal Report, Joy Manufacturing Co.

11. Churcher D., 1986. "Evaluation of A High Density Backfill System at Dome Mines". Proc. McGill Backfill Short Course, Nov. 1986.

12. Patton F.E., 1952. "Backfilling at Noranda". Trans.Can. Inst. Min. Met., vol. LV, 1952, pp. 127 -133.

13. Lukaszewski G.M., 1973. "Sulphides in Underground Mine Filling Operations". Proc. Jubil. Sympo. on Mine Filling, Aug. 1973, pp. 87 - 96.

14. Swain H.D., 1973. "An Investigation into the Use of Pyrrhotite as a Cementing Agent For Backfill".Proc. Jubil. Sympo. on Mine Filling, Aug. 1973, pp. 77 - 85.

15. Bayah J., Meech J.A. and G. Stewart, 1984. "Oxygen Depletion of Static Air by Backfill Material at The Thompson Mine". Min. Sci. Tech., Jan., 1984, pp.93-106.

16. Thomas E.G., Nantel J.H. and K.R. Notley, 1979. "Fill Technology in Underground Metalliferous Mines". Dept. of Mining Engineering, Queens University, Kingston, Ontario.

17. Sprott D.L. and W.F. Bawden, 1986. "Ice as a Backfill Material in Underground Mines". Proc. McGill Backfill Short Course, Nov. 1986.

18. Fangel H., 1986. "Backfilling with Ice". Proc. Inter. Sympo. on Mining With Backfill, Lulea, June 1983, pp. 445 - 464.

19. Das B.M., 1983. "Advanced Soil Mechanics". McGraw - Hill Book Company, New York, New York.

20. Talbot A., 1921 "Strength and Proportioning of Concrete", Proc. ASTM, Vol. 21, pp 240.

21. Swan G., 1983. "Compressibility Characteristics of Cemented Backfill", Div. Rep. 83-60 (op) (J); Canmet, EMR Canada,

22. Yong R.N.and B.P Warkentin, 1975. "Soil Properties and Behaviour". Elsevier Scientific Publishing Co., New York.

23. Seed H.B., 1979. "Soil Liquefaction and Cyclic Mobility Evaluation for Level Ground During Earthquakes". J. ASCE (105) GT2, pp. 201 - 255.

24. Weaver W.S. and R. Luka, 1970. "Laboratory Studies of Cement - Stabilized Mine Tailings", CIM Transaction, Vol. LXXIII, pp 204.

25. Barrett J.R., 1973. "Structural Aspects of Cemented Fill Behaviour". Proc. Jubil. Sympo. on Mine Filling, Aug. 1973, pp. 97-104.

26. Gonano L.P., 1975. "In Situ Testing and Size Effect Behaviour of Cemented Mine Fill". Proc. Symp. In-Situ Testing for Design Parameters, Aust. Geomech. Soc., Victoria Group, Melbourne, Nov. 5th, 1975.

27. Braes B.E., 1973. "The Application of Polymeric Flocculants in Underground Backfill at the Zinc Corporation, Limited and New Broken Hill Consolidated Limited". Proc. Jubil. Sympo. on Mine Filling, Aug. 1973, pp. 123 - 128.

28. Scoble M., Piciacchia L. and J.M. Robert, 1987. "In Situ Testing in Underground Backfill Stopes". C.I.M. Bulletin, July 1987, pp. 33 - 38.

29. Thomas E.G., 1973. "A Review of Cementing Agents for Hydraulic Fill". Proc. Jubil. Sympo. on Mine Filling, Aug. 1973, pp. 65 - 75.

30. Aylmer F.L., 1973. "Cement Properties Related to the Behaviour of Cemented Fill". Proc. Jubil. Sympo. on Mine Filling, Aug. 1973, pp. 59 - 63.

31. Douglas E. and Mainwaring P.R., 1985. "Hydration and Pozzolanic Activity of Non Ferrous Slags". The American Ceramic Society Bulletin, Vol. 64, no. 5, May 1985, pp. 700 - 706.

32. Walton T.R., 1986. "Backfill Research at Canada Cement Lafarge". Proc. McGill Backfill Short Course, Nov. 1986.

33. Aitchison, G.D., Kureme, M., and D.R. Willoughby, 1973. "Geomechanics Considerations in Optimizing the Use of Mine Fill - Part A: A Rational Approach to the Design of Fill". Proc. of the Jubilee Symposium on Mine Filling. pp. 25 -33, AIMM, NW. Queensland, Australia.

34. Aitchison, G.D., Kureme, M. and D.R. Willoughby, 1973. "Geomechanics Considerations in Optimizing the Use of Mine Fill - Part B: The Investigation of the Response of Fill as a Structural Component". Proc. of the Jubilee Symposium on Mine Filling. pp 35 - 48, AIMM, NW. Queensland, Australia.

35. Mitchell R.J. and Smith, J.D., 1979. "Mine Backfill Design and Testing", Canadian Institute of Mining and Metallurgy Bull., January 1979.

36. Pariseau, W.G., 1981. "Finite Element Method Applied to Cut and Fill Mining". Proc. Applications of Rock mechanics to Cut and Fill Mining. pp 284 - 292, IMM, Lulea, Sweden.

37. Pariseau, W.G., M.M. McDonald and J.R.M. Hill, 1973. "Support Performance Prediction for Hydraulic Fills". Proc. of the Jubilee Symposium on Mine Filling. pp 213 - 219, AIMM, NW. Queensland, Australia.

38. Borgesson, L., 1981. "Mechanical Properties of Hydraulic Backfill". Proc. Appl. of Rock Mechanics to Cut and Fill Mining. pp 193 - 195, IMM, Lulea, Sweden.

39. Hustrulid, W., D. Moreno, 1981. "Support Capabilities of Fill - A Non - Linear Analysis". Proc. Appl. of Rock Mechanics to Cut and Fill Mining. pp 107 - 118, IMM, Lulea, Sweden.

40. Singh, K.H., 1976. "Cemented Hydraulic Fill in Ground Support". Canadian Institute of Mining and Metallurgy Bull. January, 1976.

41. Corson D.R. and McKay L.M., 1973. "Field Evaluation of Backfill Behaviour in Deep Vein Mines", Jubil. Symp. on Mine Filling, Mount Isa, August 1973, A.I.M.M.

42. Yu Y.S. and N.A. Toews, 1981. "Modelling of 830 Orebody of Copper Cliff South Mine INCO - A Backfill Trial", October 1981. CANMET Report MRP/MRL 81-117 (TR).

43. Hedley D.G.F.,1984. "Utilization of Backfill Support in Longitudinal Cut and Fill Mining", May 1984, CANMET, Divis. Report.

44. Salamon M.D.G., 1974. "Rock Mechanics of Underground Excavations", 3rd Int. Congress Rock Mechanics, Denver, 1974.

45. Salamon M.D.G.,1968. "Two-Dimensional Treatmentof Problems Arising From Mining Tabular Deposits in Isotropic or Transversely Isotropic Ground", Int. J. Rock Mech. Min. Sci., Vol 5, pp 159-185, 1968.

46. Salamon M.D.G., 1984. "Rockburst Hazards and the Fight for the Alleviation in South African Gold Mines",Rock-Burst Prevention and Control, 1984, pp 11-35.

47. Beer G., 1980. "Effects of Stope Fill on Regional Ground Behaviour - Mining Under Fill - Crown Pillar Removal Part 1". University of Queensland, January 1980, Australia.

48. Sandy J.D. et al,1976. "Failure and Subsequent Stabilization of no. 3 Dump, Mufulira Mine, Zambia", IMM Journal, October, 1976, Volume 85, pp A144-62.

49. Arioglu E., 1984. "Design Aspects of Cemented Aggregate Fill Mixes for Tungsten Stoping Operations". January 3, 1984. Mining Science and Technology. pp. 209 - 214.

50. Mitchell, R.J., 1983. "Earth Structures Engineering". Allen and Union Inc., Winchester, Mass.

51. Nantel J. and Lecuyer N., 1983. "Assessment of SlagBackfill Properties for the Nornada Chadbourne Project", Canadian Institute of Mining and Metallurgy Bulletin, January, 1983.

52. Bowles J.E., 1978. "Engineering Properties of Soiland Their Measurement", 1978, McGraw-Hill book Co., Montreal.

53. American Society for Testing and Materials (ASTM), 1964, Committee D-18 on Soils and Rocks for Engineering Purposes, Philadelphia.

54. Zienkiewicz, O.C., Cheung, Y.K., 1966. "Application of the Finite Element Method on Problems of Rock Mechanics", Proc. of the First Congress of the International Society of Rock Mech., pp 661-666, ISRM.

55. Braes, B.E., 1973. "The Application of Polymeric Flocculants in Underground Backfill at The Zinc Corporation, Limited and New Broken Hill Consolidated, Limited". Proc. of the Jubilee Symposium on Mine Filling. pp 123 - 128, AIMM, NW. Queensland, Australia.

56. Hoffner R., 1973. "Mine Fill Research and Investigations at RIT's Division of Mining, Stockholm, Sweden", 1973. Jubillee Symp. on Mine Filling, Mount Isa, Australia, I.M.M.

57. Keren I. and Kainian S.,1983. "Influence of Tailings Particles on Physical and Mechanical Properties of Fill", 1983, Mining with Back Fill Lulea.

58. Lyon G.C., Slaughter P.J. and Kerr M.H.,1973. "The Design and Operation of the Cemented Hydraulic Fill Station", Mount Isa Ltd., Jubillee Symposium on Mine Filling, 1973, Mount Isa, Australia, I.M.M.

59. Thakur P.C., 1973. "The Design of Sand Pump for Optimum Results". Jubillee Symposium on Mine Filling, 1973,Mount Isa, Australia I.M.M.

60. Korfaev S.A.,1961. "Resultsof Investigations in theHydro Transportation of Backfill Material", January 1961, Dept. of Mines and Technical Surveys Mines Branch, Ottawa.

61. De Korompay V., 1974. "Review of Hydraulic Transportation Systems for Mine Backfill, Sept. 1974. EMR, Mines Branch Report 74/118.

62. OliverV.H.R. and Russell F.M., 1973. "The Mufulira Sandplant", Jubillee Symposium on Mine Filling, Mount Isa, August 1973, A.I.M.M.

63. Coates D.F.and YuY.S.,1968. "Analysis of Grading Effects on Hydraulic and Consolidated Fill", November 1968, E M R Report #68/106-LD.

64. Nieminen P. and P. Seppamen, 1983. "The Use of Blast-Furnace Slag and Other By-Products as Binding Agents in Consolidated Backfilling at Outokumpu Oy's Mine". Proc. of the International Symposium on Mining with Backfill, Lulea, June 1983.

65. Manca P.P., Massacci G., Massidda L. and G. Rossi, 1984. "Stabilization of Mill Tailings for Mining With Portland Cement and Fly Ash". I.M.M.,pp. A48 - A54, April 1984.

66. Thomas, E.G., 1973. "Cemented Hydraulic Fill Mix Design as it Applies to Mine Scheduling". Proc. of the Jubilee Symposium on Mine Filling. pp 139 - 145, AIMM, NW. Queensland, Australia.

67. Piciacchia, L., M.J. Scoble and N. Rowlands, 1984. "The Integration of Backfill Non - Linear Behaviour into Finite Element Modelling for Underground Mine Design". Second International Conference - Stability in Underground Mining. pp 363 - 376, AIME, Lexington, Kentucky.

68. Thomas E.G. and Cowling R.,1979."Pozzolanic Behaviour of Ground Mount Isa Mine Slag in Cemented Hydraulic Mine Fill at High Slag/Cement Ratios", Proc. 12th Canadian Rock Mech. Symp. Sudbury, Ontario, 1978, CIM Specical Vol. 19, p 129, 1979.

69. Swan G., 1983. "Laboratory Testing of Mines Selbaie Rock and Fill". CANMET, EMR, Report 83-88 (TR), October, 1983.

70. Mitchell R.J. and Wong B.C.,1982. "Behaviour of Cemented Tailings Sand", March 1982, Canadian Geotechnical Journal.

71. Wayment W.R. and Nicholson D.E.,1965. "Improving Effectiveness of Backfill", Aug., 1965, Mining Congress Journal, pp 28 - 32.

72. Yu Y.S.,1966. "Notes on Hydraulic Backfillings", EMR Div. Report 66/163 - MRL, October 1966.

73. Nicholson, D.E., Busch, R.A., "Earth Pressure at Rest and One-Dimensional Compression in Mine Hydraulic Backfills".

74. Corson, D.R., Dorman, K.R., And R.H. Sprute, 1981. "Improving the Support Characteristics of Hydraulic Fill". Proc. Appl.of Rock Mechanics to Cut and Fill Mining. pp 93 - 99, IMM, Lulea, Sweden.

75. Franklin J.C. et al., 1982. "Radon Emanation From Stopes Backfilled with Cemented Uranium Tailings", U.S.B.M., RI 8664, 1982.

76. De Korompay V., 1977. "Utilization of Chemically Stabilized Fill to Prevent Radon contamination from Radioactive Hydraulic Mine Backfills", 1977. CANMET Divisional Report 77-107 (TR).

77. Stratton-Crawley R. and Agar G.E., 1979. "Multi-Stage Hydrocyclone Circuit Optimization by Computer Simulation", Proc. 11th Ann. Meeting, Can. Min. Process., 1979, Ottawa, pp 98-127.

78. Shama R., G. Chodola and G. Herget, 1981. "Pressure Monitoring of Mine Backfill", CANMET Divisional Report # 81-103(TR), July 1981.

79. Zahary G., H. Zorychta and S. Zaidi, 1972. "Results - Fill Pressure Measurements in a Cut and Fill Stope", CANMET, Internal Report #72/119, September, 1972.

80. Corson, D.R. and Wayment, W.R., "Load-Displacement Measurements in Backfilled Stope of a Deep Vein Mining", USBM, RI 7038.

81. Piciacchia L., 1984. "The Behaviour of Cemented Backfill Employed in Cut and Fill Stoping". M.Eng. Thesis, McGill University, August, 1984.

82. Hergert, G., 1981. "Borehole Dilatometer for Backfill Studies". Division Report MRP/MRL 82-2(TR); CANMET, EMR, Canada.

83. Morrison R.G.K., 1942. "Report on the Rockburst Situation in Ontario Mines". Trans. Can. Inst. Min. Met., XLV, pp. 225 - 272

84. Davidge G.R., 1984. "Microseismic Monitoring at Falconbridge Mine". Proc, of a Canmet - Sponsered Workshop on Monitoring in Canadian Mines, pp. 3 - 18.

85. Oliver P.H., 1985. "Creighton Mine, July 6 1984, Rockburst". Seminar on Rockbursting, Can. Inst. Min. Met. Sudbury.

86. Notley K.R., 1985. "Rock Mechanics Analysis of the Springhill Mine Disaster". Jnl. Min. Sci. Tech., Elsevier, Vol. 1,2 pp. 149 - 163.

87. Vance J.B. and B.W. Schmitke, 1984. " High Frequency Microseismic Monitoring at PCS Mining". Proc. of a Canmet - Sponsered Workshop on Microseismic Monitoring in Canadian Mines, pp. 87 - 102.

88. Bourbonnais J., 1981. "A Research Application of Multi-Channel Microseismic Monitoring to Rock Bursting at the East Malartic Mine in Northwestern Quebec". Proc. of the 3rd. Conf. on Acoustic Emission / Microseismic Activity in Geological Structures and Materials, Penn., 1981.

89. Pakalnis V., 1981. "Strength and Limitations of Microseismic Monitoring for Rockburst Control in Ontario Mines". Proc. of the 3rd. Conf. on Acoustic Emission / Microseismic Activity in Geological Structures and Materials, pp. 549 - 558, Penn., 1981.

90. Johnson H.E., 1984. "A Study of Statistics on Rock Falls in the Ontario Mining Industry During 1960 - 1979". Prof. Dev. Seminar on Rockbolting Practices, Laurentian University, Sudbury.

91. Hedley D.G.F., Roxburgh J.W. and S.N. Muppalaneni, 1984. "A Case History of Rockbursting at Elliot Lake". Canmet MRP/MRL 84-16.

92. Neumann M. and A. Makuch, 1984. "Case Study of Microseismic Monitoring of F-2 Zone at Campbell Red Lake Mines Limited". Proc. of a Canmet - Sponsered Workshop on Microseismic Monitoring in Canadian Mines, pp. 33 - 50.

93. Cook J., 1984. "Notes on Rockbursting at Macassa Mine". Proc. of a Canmet - Sponsered Workshop on Microseismic Monitoring in Canadian Mines, pp. 131 - 134.

94. Herget G., 1980. "Regional Stresses in the Canadian Shield". Proc. 13th. Can. Rock Mech. Symposium, CIM, pp. 9 - 16.

95. Graham C., 1984. Rockburst Seminar. McGill University, Dept. of Mining and Met.

96. Coates D.F., 1965. "Rock Mechanicxs Principles". Mines Branch Monograph 874. Revised 1981.

97. Blake W., 1982. "Destressing to Control Rock Bursting". Underground Mining Methods Handbook, AIME, pp. 1535 -1539.

98. Emere G.T.G., 1984. "Stope Support Technology Development". World Mining Equipment, Jan. 1984, p. 39.

99. Willan J., Scoble M. and V. Pakalnis, 1985. "Destressing Practice in Rockburst - Prone Ground". Proc. 4th Conf. Ground Control in Mining, Univ. W. Virginia.

100. Wagner H., 1984. "Support Requirements For Rockburst Conditions". Proc. 1st. Int. Congress on Rockbursting and Seismicity in Mines. Johannesburg, 1984, pp. 209 - 218.

101. McGarr A., R. Green and S.M. Spottiswoods, 1981. "Strong Ground Motion of Mine Tremors: Some Inplications for Near Source Ground Motion Parameters". Bull. Seism. Soc. Amer., Vol. 71, no. 1, pp. 295 - 319.

102. Barton N. and B. Kjaensli, 1981. "Shear Strength of Rockfill". Proceedings ASCE, vol. 107, no. GT7, July 1981.

103. Wang F.D. and M.C. Sun, 1970. "Slope Stability by Finite Element Stress Analysis and Limiting Equilibrium Method". U.S.B.M., R.I. 7341.

104. DeKorompay V., 1978. "Multi Purpose Tester For Measuring Simultaneously Engineering and Radiation Properties of Radioactive Hydraulic Backfills, Waste Materials and Uranium Ores". Canmet MRP/MRL 78 - 83 (TR).

105. Franklin J.C., R.J. Zawadski, T.O. Meyer and A.L. Hill, 1976. "Data Acquisition System for Radon Monitoring". U.S.B.M. RI 8100.

106. McVey J.R., J.C. Franklin, and D.M. Shaw, 1977. "Portable Instrument Measures Four Ventilation Parameters". Min. Congr. Journal, Vol. 63, No. 4, April 1977, pp. 49 - 52.

107. Borrowman S.R. and P.T. Brooks, 1975. "Radium Removal From Uranium Ores and Mill Tailings". U.S.B.M., RI 8099.

108. Bates R.C. and J.C. Franklin, 1977. "U.S.B.M. Radiation Control Research. Proc. 1st Conf. on Uranium Mining Technology, Reno, Nev., April 24-29, 1977.

109. Franklin J.C., T.O. Meyer and R.C. Bates, 1977. "Barriers for Radon in Uranium Mines". U.S.B.M., RI 8259.

110. Franklin J.C., L.T. Nuzum and A.L. Hill, 1975. "Polymeric Materials for Sealing Radon Gas Into the Walls of Uranium Mines". U.S.B.M., RI 8036.

111. Nicholson D.E. and Wayment W.R., 1963. "Properties of Hydraulic Backfills and Preliminary Compaction Tests". U.S.B.M., RI 6477.

112. Nicholson D.E. and Wayment W.R., 1966. "Vibratory Compaction of Mine Hydraulic Backfills". U.S.B.M., RI 6922.

113. Hazen A., 1911. "Discussion of Dams on Sand Foundations". Trans., Am. Soc. of Civil Eng., vol. 73, p. 199.

114. Terzaghi K. and R.B. Peck, 1967. "Soil Mechanics in Engineering Practice". 2nd edition, New York, Wiley.

115. Shahabi A.A., Das B.M. and A.J. Tarquin, 1984. "An Empirical Relation for Coefficient of Permeability of Sand". Fourth Australia - New Zealand Confer. on Geomechanics, Perth, May 1984.

116. Bates R.C. and W.R. Wayment, 1970. "Laboratory Study of Factors Influencing Waterflow in Mine Backfills". U.S.B.M., RI 7034.

117. Whitman R.V., 1985. "On Liquefaction". Proc. of the 11th Inter. Confer. on Soil Mechanics and Foundation Eng. San Fransisco, 1985, pp. 1923 - 1926.

118. Wayment W.R., Wilhelm G.L. and J.D. Bardill, 1962. "Friction Head Losses of Sand Slurries During Pipeline Transport". U.S.B.M., RI 6065, Part 1.

119. Bardill J.D., Corson D.R. and W.R. Wayment, 1962. "Friction Head Losses of Barite and Limestone Slurries During Pipeline Transport". U.S.B.M., RI 6065, Part 2.

120. Kivisto P.V., 1986. "Bulkhead Design For Backfill". Proc. Backfill Short Course on Mine Backfill Design, McGill University, Montreal, November 24 - 26, 1986.

121. Nantel J., 1980. "Analysis of Bulkhead Failure at Centennial Mine and A Review of Mine Backfill Systems in The Province of Manitoba". Internal Report to The Manitoba Department of Energy and Mines, pp 1-59.

122. Nantel J., 1981. "Design and Installation Procedures of Timber Bulkheads For Fill Containment". Internal Report to the Canadian National Committee on Rock Mechanics : Sub - Committee on Underground Bulkheads and Dams, pp 1-31.

123. Morrision, Hershfield, Burgess and Huggins Ltd., 1978. "Bulkheads and Dams For Mines". Internal Report to the Ontario Ministry of Labour, pp 1-56.

124. Kivisto P.V., 1986. "Anchoring Reinforced Concrete Bulkheads". Proc. Backfill Short Course on Mine Backfill Design, McGill University, Montreal, November 24 - 26, 1986.

125. Garrett W.S. and L.T. Campbell Pitt, 1958. "Tests on an Experimental Underground Bulkhead For High Pressures". Jour. South African Inst. of Mining and Metallurgy, Oct. 1958, pp 123-143.

126. Plitt L.R., 1976. "A Mathematical Model of the Hydrocyclone Classifier". CIM Bull., Dec. 1976, pp 114 - 123.

127. Van Eeckhout E., 1983. "Numerical Modelling of Stiff Backfill in the Coeur d'Alene Mining District". Unpublished.

128. Coulthard M.A., 1980. "Numerical Analysis of Fill Pillar Stability - Three Dimensional Linearly Elastic Finite Element Calculations". Commonwealth Scientific and Industrial Research Organ., Div. of Applied Geomechanics, Technical report No. 97, pp 1-37.

129. Yu Y.S., Toews N.A. and A.S. Wong, 1983. "Mintab User's Guide - A Mining Simulator for Determining the Elastic Response of Strata Surrounding Tabular Mining Excavations". CANMET, Div. Report MRP/MRL 83-25 (TR).

130. Yu Y.S., Toews N.A. and A.S. Wong, 1981. "Implementation of Backfill With the Mintab Program". CANMET, Divisional Report MRP/MRL 81-62 (TR).

131. Yu Y.S. and Toews N.A., 1985. "Sap2d System - An Overview". CANMET, Divisional Report MRP/MRL 85-95 (TR).

132. Toews N.A., Yu Y.S. and A.S. Wong, 1985. "Sap2d Documentation (Vax - 11/750 Version) - 2D Linear Elastic Finite Element Program". CANMET, Divisional Report MRP/MRL 85-35 (TR).

133. Yu Y.S., Toews N.A. and A.S. Wong, 1985. "Sap2D Documentation (Vax - 11/750 Version) - An Interface Program for Finite Element Program Sap2d". CANMET, Divisional Report MRP/MRL 85-34 (TR).

134. Toews N.A., Yu Y.S. and A.S. Wong, 1985. "Meshgen Documentation (Vax - 11/750 Version) - A Mesh Generating Program For Finite Element Analysis of Two Dimensional Structures". CANMET, Divisional Report MRP/MRL 85-32 (TR).

135. Piciacchia L., 1984. "The Behaviour of Cemented Backfill Employed in Cut and Fill Stoping". M.Eng. Thesis, McGill Univeristy, Montreal, Quebec, August 1984.

136. Mitchell R.J., Olsen R.S. and J.D. Smith, 1982. "Model Studies on Tailings Used in Mine Backfill". Canadian Geotechnical Journal, vol. 19, pp. 14 -28, 1982.

137. Wang F.D. and Sun M.C., 1970. "Slope Stability Analysis by the Finite Element Stress Analysis and Limiting Equilibrium Method". U.S.B.M., RI 7341.

138. Hoek E. and J.W. Bray, 1977. "Rock Slope Engineering". Second edition, IMM, London.

139. Hassani F.P., Scoble M.J. and L. Piciacchia, 1985. "The Significance of Cement Content To Hydraulic Backfill Design". Proc. 87th Annual General Meeting of the CIM, Vancouver, B.C., April 21 - 25, 1985.

140. Campbell P.S., 1986. "Underground Mining Backfill Design Practices in Ontario". Presented at the Professional Development Seminar on Mine Backfill Systems, McGill University, Nov. 1986.

141. Beauchamp L., Piciacchia L. and M. Scoble, 1987. " A Review of Cemented Hydraulic and Rock Fill Material Properties". Proc. 1987 AMMQ Ground Control Symposium, Val d'Or, Quebec.

142. Anon, 1987. "General Data on Sigma Mines". Internal Public., Sigma Mines (Quebec) Limited, Val d'Or, Quebec.

143. Hunt G.,1986. "Backfill Support Studies at the Denison Mine, Canada". Proc. Backfill Short Course on Mine Backfill Design, McGill Univer., Mtl., Nov 24 - 26, 1986.

144. Roy M.A., 1985. "Sautage Perimetrique et Controle de Terrain". Proceedings, 1985 AMMQ Ground Control Symposium, Val d'Or, Quebec.

145. Closset M.L.,1985."Controle d'Une Instabilite Dans Un Chantier de Mines Selbaie". Proceedings,1985 AMMQ Ground Control Symp. Val d'Or, Quebec.

146. Hanson D.S.G., 1982. " Geotechnical Analysis to Aid Recovery of North Main Shaft Pillar - Flin Flon Mine". Proceedings, First Inter. Confer. on Stability in Underground Mining, August 1982, Vancouver, B.C.

147. Walker S.D. and Cregheur P., 1978. " The Chadbourne Mine, Noranda, Quebec: A Gold Bearing Breccia". 1978 Noranda Internal Report.

148. Brousseau M.G., 1986. "L'Evolutiondes Differents Systemesde Support de Terrain a la Mine Bousquet". Proceedings, 1986 AMMQ Ground Control Symposium, Val d'Or, Quebec.

149. Cook J.F., McLaughlin B. and G. Brousseau, 1985."Mining Problems at La Mine Bousquet". CIM Bulletin, Jan. 1985, pp. 35 - 40.

150. Robertson P.K., 1986. "In Situ Testing and its Application to Foundation Engineering". Canadian Geotechnical Journal, November 1986, pp. 573 - 594.

151. Wroth C.P., 1984. "The Interpretaion of In Situ Soil Tests". Geotechnique 34(4), pp. 449 - 489.

152. Tavenas F., 1986. "In Situ Testing: Where Are We? Where Should We Go?". Geotechnical News, December 1986, pp. 35 - 38.

153. Schmertmann J.H., 1977. "Use the SPT to measure dynamic soil properties? - Yes, but....! In Dynamic Geotechncial Testing. ASTM, Special Technical Publication 654, pp. 341 - 355.

154. Kovacs W.D., Salomone L.A., and F.Y. Yokel, 1981. " Energy Measurements in the Standard Penetration Test". Building Science Series, National Bureau of Standards (U.S.), No. 135.

155. Andrus R.D., Yund T.L. and R.R. Carter, 1986. "Geotechnical Evaluation of Liquefaction Induced Lateral Spread". Proc. 22nd Annual Symposium on Engineering Geology and Soils Engineering, Thousand Springs Valley, Idaho.

156. Campanella R.G. and P.K. Robertson, 1983. "Flat Plate Dilatometer Testing: Research and Development". Soil Mechanics Series, No. 68, Department of Civil Engineering, and Proc. of 1st International Dilatometer Conference, Edmonton, Alta., University of British Columbia, Vancouver B.C.

157. Jamiolkowski M., Ladd C.C., Germaine J.T. and R. Lancellotta, 1985. "New Developments in Field and Laboratory Testing of Soils: State of The Art Paper". Proc. 11th Inter. Conf. on Soil Mechanics and Foundation Engineering, San Francisco.

158. Piciacchia L. 1986. "Pressuremeter Selection and Use In Underground Environments". Proc. Backfill Short Course on Mine Backfilling, McGill University, Montreal, November 24 - 26 1986.

159. Fahey M. and Randolph F., 1984. "Effects of Disturbance on Parameters Derived From Self-Boring Pressuremeter Tests in Sand". Geotechnique, March 1984, pp. 81 - 97.

160. Withers N.J., Schaap L.H.J. and Dalton C.P., 1986. "The Development of a Full Displacement Pressuremeter". Proc. The Pressuremeter and Its Marine Applications: 2nd Inter. Symp. ASTM STP 950, pp. 38 - 55.

161. Baguelin F., Jezequel J.F. and D.H. Shields, 1978. "The Pressuremeter and Foundation Engineering". Trans Tech Public., Series on Rock and Soil Mechanics. Clausthal, Germany.

162. Anon, 1986. "Pencel Pressuremeter : Instruction Manual". Roctest Limited, St. Lambert, Quebec.

163. Capelle J.F., 1983. "New and Simplified Pressuremeter Apparatus". Proc. Int. Symp. on Recent Developments in Laboratory and Field Tests and Analysis of Geotechnical Problems, Bangkok, Asian Inst. Tech., pp. 159 - 164.

164. Lame G., 1852. "Lecons Sur la Theorie Mathematique de L'elasticite des Corps Solides". Bachelier, Paris, France.

165. Amar S. and J.F. Jezequel, 1972. "Essaia en Place et en Laboratoire sur Sols Coherents: Comparaison des Resultats". Bull. de Liaison des Ponts et Chaussees, No. 58, April - May, 1972, pp. 97 - 108.

166. Anon, 1967. "Interpretation d'un Essai Pressiometrique". Centre d'Etudes Menard, Publication D 31/67, 1967.

167. Felio G.Y. and J.L. Braiud, 1986. "Conventional Parameters From Pressuremeter Test Data: Review of Existing Methods". Proc. The Pressuremeter and Its Marine Applications: 2nd Inter. Symp., ASTM STP 950, pp. 265 - 282.

168. Gambin M., 1977. "Le Pressiometre et la Determination de L'angle de Frottement et de la Cohesion d'un Sol". Internal Report, Geoprojekt, Paris, France, 1977, pp. 1 - 21.

169. Calhoon M., 1970. "Field Testing With the Pressuremeter". Lecture given at the Unviersity of Kansas, U.S.A. (unpublished)

170. Gibson R.E. and W.F. Anderson, 1961. "In Situ Measurement of Soil Properties With the Pressuremeter". Civil Engineering Public Works Review, Vol. 56, No. 658, pp. 615 - 618, May 1961.

171. Palmer, A.C., "Undrained Plane - Strain Expansion of a Cylindrical Cavity in Clay; A Simple Interpertation of the Pressuremeter Test". Geotechnique, Vol. 22, No. 3, 1972. pp. 451-457.

172. Fyffe S., Reid W.M. and J.B. Summers, 1986. "The Push-In Pressuremeter: 5 Years Offshore Experience". Proc. The Pressure meter and Its Marine Applications: 2nd Inter. Symp., ASTM STP 950, pp. 22 - 37.

173. Baguelin F., Jezequel J.F., LeMee E. and A. LeMehaute, 1972. "Expansion of Cylindrical Probes in Cohesive Soils". Jour. of the Soil Mech. and Foundation Division, Nov., 1972, pp. 1128 - 1142.

174. Houlsby G.T., Clarke B.G. and C.P. Wroth, 1986. "Analysis of the Unloading of a Pressuremeter in Sand". Proc. The Pressure-meter and Its Marine Applications: 2nd Inter. Symp., ASTM STP 950, pp. 245 - 262.

175. Anon, 1979. "Standard Test Method for Specific Gravity of Soils". ANSI / ASTM D854 - 58

176. Lowell S., 1979. "Null - Pycnometer Theory and Operating Instructions". Manual, Quantachrome Corp., Syesset, N.Y.

177. Anon,1971. "Standard Test Method of Laboratory Determination of Moisture Content of Soil". ANSI / ASTM D2216 - 71.

178. Anon, 1972. "Standard Test Method for Particle - Size Analysis of Soil". ANSI / ASTM D422-63.

179. Anon, 1982. "Quantitative Analysis for the Scanning Electron Microscope". Manual, Tracor Northern, Rexdale Ontario.

180. Anon, 1978. "Standard Test Method for Moisture - Density Relations of Soils and Soils Aggregate Mixtures Using 5.5 lb. (2.49-kg) Rammer and 12 in.(305 mm) Drop ". ASTM D698 - 78.

181. Anon, 1978. "Standard Test Method for Moisture - Density Relations of Soils and Soils Aggregate Mixtures Using 10 lb. (4.45-kg) Rammer and 18 in.(457 mm) Drop ". ASTM D1557 - 78.

182. Anon, 1979. "Standard Test Method for Compressive Strength of Molded Soil - Cement Cylinders". ANSI / ASTM D1633 - 63.

183. Anon, 1982. " Instruction Manual for LGS - AEM Micromicro Ammeter #ISMLGSAEM-1". Manual (JOEL JSM T-300), Joel Ltd., Tokyo, Japan.

184. Anon, 1982. "TN5000 Series Analyzer - Flex Operating Manual". Manual, Tracor Northern, Rexdale, Ontario.

185. Anon, 1979. "Standard Method for Direct Shear Test of Soils Under Consolidated Drained Conditions". ASTM D3080 - 72.

186. Wray W.K., 1986. "Measuring Engineering Properties of Soil". Bectall Inter. Series in Civil Eng. and Eng. Mechanics. Chapter 11.

187. Anon, 1973. "Suggested Method for the Determination of Shear Strength of Rocks". Journal International Society of Rock Mechanics and Mining Science and Geomechanics.

188. Anon, 1985. "Suggested Method for the Determining the Point Load Index. Journal International Society of Rock Mechanics and Mining Science and Geomechanics. Vol. 22, no 2, pp. 51-60, 1985.

189. Swan G., 1985. "A New Approach to Cemented Backfill Design", CIM Bulletin, Dec., 1985, pp 53 -58.

190. Anon, 1978. "Standard Test Methods for The Bearing Ratio of Laboratory - Compacted Soils". ASTM D1883 -73.

191. Casagrande A., 1975. "Liquefaction And Cyclic Deformation of Sands, A Critical Review". Harvard Soil Mechanics Series 88.

192. Castro G. and S.J. Poulos, 1971. "Factors Affecting Liquefaction and Cyclic Mobility". J. ASCE (103) GT6, pp 501 - 516.

193. Schofield A.N., 1981. "Dynamic and Earthquake Geotechnical Centrefuge Modelling". Proc. Geotech. Earthquake Eng. and Soil Dynamics, St Louis, III, pp. 1081 - 1100.

194. DeRuiter J., 1982. "The Static Cone Penetrometer Test, State of The Art Report". Proc. 2nd European Symposium on Penetration Testing. Amsterdam, May 24 - 27, 1982. pp. 389 - 405.

195. Bieniawski Z. T., 1974. "Estimating the Strength of Rock Materials". Journ. South Afric. Inst. Min. and Met. 74. pp. 312 - 320.

196. Anon, 1974. "Standard Method For Testing For Permeability of Granular Soils (Constant Head)". ASTM D2434-68.

197. Yu T., 1983. "Ground Support With Consolidated Rockfill". CNCRM Sympos. on Underground Support Systems. CIM Sudbury, Ont. pp. 1 - 37.

198. Yu T. and D. Counter, 1983. "Backfill Practice and Technology at Kidd Creek Mines". C.I.M Bull. August, 1983. pp. 56 - 65.

199. Kolsrud B., 1981. "The Nasliden Project - Why, What and How". Proc. Application of Rock Mechanics to Cut and Fill Mining, Lulea, Sweden, pp.137 - 140.

200. Krauland N., 1981. "FEM model of Nasliden Mine - Requirements and Limitations at Start of Project". Proc. Application of Rock Mechanics to Cut and Fill Mining, Lulea, Sweden, pp.141 -144.

201. Jager A.J., Piper P.S. and N.S. Gay, 1987. "Rock Mechanics Aspects in Deep South African Gold Mines". ISRM Congress, Montreal, Que., Canada.

202 Teychenne D.C., Franklin R.E. and H.C. Erntroy, 1975. "Design of Normal Concrete Mixes, HMSO, London.

203. Illston J.M., Dinwoodie J.M. and A.A. Smith, 1979. "Concrete Timber and Metals - The Nature and Behaviour of Structural Materials". VNR Publishing Berkshire, England.

204. Blake W., 1971. "Rockburst Mechanics". Ph.D. Thesis, Colorado School of Mines.

205. Hart R.D., 1981. "Geomechanical Modelling of a Cut and Fill Mining Operation". Proc. Appl. of Rock Mechanics to Cut and Fill Mining. pp 107 - 118, IMM, Lulea, Sweden.

206. Todd D.K., 1967. "Ground Water Hydrology". Wiley & Sons, pp. 44 - 54.

207. Gray D.M., 1973. "Handbook on the Principles of Hydrology". Water Information Center Inc., N.Y., pp. 5.18 - 5.24.

208. Freeze R.A., J.A. Cherry, 1979. "Groundwater". Prentice Hall Inc., N.Y., pp. 26 - 30 and 350 - 351.

209. Anon, 1984. "NWA Statpak - Multi-function Statistics Library Version 3.1". Northwest Analytical Inc, Portland, Oregon.

APPENDIX 1

PHYSICAL DESIGN PARAMETERS AND EQUATIONS

E = Modulus of deformation
ν = Poisson's Ratio
c = Apparent cohesion
t = Filling Time Cycle
S_b = Surface bearing strength
σ_c = Compressive strength
τ = Shear strength
ϕ = Angle of internal friction
σ_3 = Confining stress
α_b = Blasting acceleration
W_s = Weight of fill produced
γ_s = In situ fill density
G = Density of fill solids
Cu = Coefficient of uniformity
K = Permeability Coefficient
K_1 = Permeability required to inhibit liquifaction
K_r = Required permeability
K_f = Fill permeability
e = Void ratio
α_p = Specific surface
$\bar{d}$ = Mean inter - particle distance
p = Fill porosity
V_p = Aggregate volume fraction
U_o = Minimum diameter
U_1 = Maximum diameter
D_{60} = Particle size passing 60% of the material
D_{10} = Particle size passing 10% of the material
γ_o = Ore density
w = Water density
c_v = Cement content by volume
$c\%$ = % Cement content by weight
Pd = Pulp density
V_v = Volume of Voids to be filled
n = Volume of Voids in in situ material
H_w = Height of excess water
H_f = height of settled backfill
V_f = Volume of settled backfill
G_{st} = Specific gravity of tailings
A = Plan drainage area

APPENDIX 1

PHYSICAL DESIGN PARAMETERS AND EQUATIONS

E	=	Modulus of deformation
ν	=	Poisson's Ratio
c	=	Apparent cohesion
t	=	Filling Time Cycle
S_b	=	Surface bearing strength
σ_c	=	Compressive strength
τ	=	Shear strength
ϕ	=	Angle of internal friction
σ_3	=	Confining stress
α_b	=	Blasting acceleration
W_s	=	Weight of fill produced
γ_s	=	In situ fill density
G	=	Density of fill solids
Cu	=	Coefficient of uniformity
K	=	Permeability Coefficient
K_l	=	Permeability required to inhibit liquifaction
K_r	=	Required permeability
K_f	=	Fill permeability
e	=	Void ratio
α_p	=	Specific surface
$\bar{d}$	=	Mean inter - particle distance
p	=	Fill porosity
V_p	=	Aggregate volume fraction
U_o	=	Minimum diameter
U_l	=	Maximum diameter
D_{60}	=	Particle size passing 60% of the material
D_{10}	=	Particle size passing 10% of the material
γ_o	=	Ore density
w	=	Water density
c_v	=	Cement content by volume
c%	=	% Cement content by weight
Pd	=	Pulp density
V_v	=	Volume of Voids to be filled
n	=	Volume of Voids in in situ material
H_w	=	Height of excess water
H_f	=	height of settled backfill
V_f	=	Volume of settled backfill
G_{st}	=	Specific gravity of tailings
A	=	Plan drainage area

[1 - 1]

GRADING

$$Cu = D_{60}/D_{10}$$

$$V_p = 0.6\ (1 - p - c_v/100)$$

$$(N)_i = \int_{u_o}^{u_1} U^i\ f(u)\ du$$

$$\alpha_p = \frac{6\ (N)_2}{(N)_3}$$

determine, $\bar{d}$ from

$$V_p = \left(1 + \frac{1}{2}\bar{d}\ p + \frac{1}{2}\bar{d}^2\ p\ \frac{(N)_1}{(N)_2} + \frac{1}{6}\bar{d}^3\ p\ \frac{(N)_0}{(N)_2}\right) = 1$$

PERCOLATION AND PERMEABILITY

$$e = (G * w / \gamma_s) - 1$$

$$K = D_{10}^2;\ \alpha\ e^2$$

[1 - 2]

WEIGHT OF REQUIRED FILL

$$W_s = \gamma_s * V_v$$

[1 - 3]

REQUIRED WEIGHT OF ADDITIONAL MATERIAL

$$W_R = W_S - W_A * \frac{x}{100}$$

[1 - 4]

PULP DENSITY FROM:

$$\frac{H_w}{H_f} = \frac{V_w}{V_f} = \frac{1-Pd}{Pd} * G_{st} * (1-n) - n$$

Or

$$K \geq \frac{W_s\ \left(\left(\frac{1-Pd}{Pd}\right) * G_{st} * (1-n) - n\right)}{G_{st} * \gamma_w * (1-n) * A}$$

APPENDIX 2

COST PARAMETERS AND EQUATIONS

S_c = Stockpiling cost/tonne of material
T_c = Transportation cost/(tonne * km)
Q_c = Cost of cement/tonne
D_c = Cost of disposal/tonne
R_c = Cost of regrading/tonne
F_c = Cost of flocculants/lb
P_c = Production Costs/tonne of alternate material
T_f = Tonnes of fill produced
S_f = Sheduling of fill production
T_v = Tonnes of material removed from void
V_v = Volume of void
W_s = Weight of fill required
W_a = Total tonnes of available material from plant
W_r = Total tonnes of alternate material required
X = % of W_a which is usable
Y = % of W_s which must be stockpiled
F_a = Flocculant addition (lbs./tonne)
C_t = Total cost of tailings
C_f = Total cost of flocculant
C_r = Total cost of alternate material
C_s = Total cost of stockpiling
C_c = Total cost of cement
C_{tr} = Total cost of transportation
C_d = Total cost of drainage, bulkheads
C_{total} = Total project fill cost
C_{tf} = Cost/tonne of fill
C_{to} = Cost/tonne of ore removal
D = Total transportaion distance (Km)

[2 - 1]

$$C_t = (R_c - D_c) * W_a * X/100$$

[2 - 2]

$$C_f = (F_c * F_a) * (W_a * \frac{(X)}{100} + W_r)$$

$$= F_c * F_a * W_s$$

[2 - 3]

$$C_r = P_c * W_r$$

[2 - 4]

$$C_s = S_c \ (W_r + W_a \frac{(X)}{100}) * Y/100$$

$$= S_c * W_s * Y/100$$

[2 - 5]

$$C_{tr} = T_c \ (W_r + W_a * (X)/100)$$

$$= T_c * W_s * D$$

[2 - 6]

$$C_c = \frac{C\% * W_s * Q_c}{100}$$

[2 - 7]

$$C_{total} = C_T + C_F + C_r + C_s + C_{tr} + C_c + C_d$$

$$C_{tf} = C_{total}/W_s$$

$$C_{to} = C_{tf} * \gamma_o/\gamma_f$$

APPENDIX I

MINE BACKFILL QUESTIONNAIRE
FOR QUEBEC MINES

MINE BACKFILL QUESTIONAIRE

General Information

1. Company Name:

2. Company Correspondant and Phone Number:

3. Mining Method(s) (e.g. 50% cut and fill, 50% blasthole):

4. Type of Mine (e.g. Cu, Ag, etc)

5. Metric Tonnes/Day Mined:

6. Access via shaft ☐ ramp ☐ other ☐ :

7. Kindly describe typical ranges of stoping dimensions.

8. Do you have a resident ground control engineer?
   yes ☐ no ☐

9. If answer to #8 is yes please give name:

10. If ground control modelling techniques are employed, what method(s) are used:

11. Are insitu rock mechanics measurement used as part of the design process?
yes☐ no☐

12. If answer to #11 is yes kindly elaborate on the type of instrumentation used and its purpose.

13. Is backfill of any form used at your mine?
yes☐ no☐

14. Do you plan to use fill in the future? yes☐ no☐

If answer to both questions 13 and 14 are no, there is not need to continue. Thank you for your cooperation, please return questionaire in the self addressed envelope.

Backfill Usage and Handling

15. What type of backfill is being used? (e.g. 700mt/day cemented sandfill and 600mt/day uncemented rockfill)

16. What is the origin of this material? (e.g. tailings, development, quarry etc.):

17. Kindly describe the surface handling of the backfill along with a description of the distribution and placement system at your mine.

18. If more than one type of mining method and more than one type of fill is used please indicate proportioning. (e.g. 50% of cut and fill stopes filled with cemented sand fill, 50% with rockfill.....)

Backfill Properties and Design

19. If backfill is cemented, what cementing agents is (are) used, and in what quantities? (e.g. 100mt/day portland cement, 100mt/day pozzolans etc.):

20. In what proportions are the cementing agents added? (e.g. 3% portland cement and 3% pozzolans):

21. What is the chemical/mineralogical composition of the fill material used?

22. What is the grain size distribution of the material used? (attach graph if available)

23. What is the moisture content of the insitu fill?

24. What is the void ratio of the insitu fill?

25. What percolation rates does your fill(s) typically exhibit?

26. Are these percolation rates attained with the use of flocculants?

yes☐ no☐

27. If answer to #26 is yes, please provide details?

28. What backfill properties are known?
(if known give details)

Shear strength:

Uniaxial compressive strength:

Triaxial compressive strength:

Other:

29. By what means were the properties in #28 determined? (e.g. Soil shear box, plate load test etc.)

30. If modelling is used, is the backfill material regarded as a structural component in your models?
yes☐ no☐

31. If answer to #30 is yes, what properties is the fill being assigned?

32. If answer to #11 is yes, have any backfilled stopes been monitored in the past or are being monitored presently?
yes☐ no☐

33. If insitu fill pressures have been measured, please give details?

34. What do you consider to be the problems associated with backfill design, in order of significance.

1)

2)

3)

4)

Backfill Safety

35. Has bulkhead failure been a problem at your mine?
yes☐ no☐

36. Please provide details of your bulkhead design and any problems related to bulkhead performance?

37. What do you consider to be the prominent safety hazards related to the use of backfill? (e.g. oxygen depletion, slippery surfaces etc)

1)

2)

3)

4)

APPENDIX 4

CALCULATION AND DERIVATION OF DEFORMATION AND STRESS EQUATIONS FOR THEORETICAL PRESSUREMETER STUDIES

$$1 = \left(\frac{x}{a}\right)^2 + \left(\frac{y}{b}\right)^2 + \left(\frac{z}{c}\right)^2, \quad Z = c\sqrt{1 - \left(\frac{x}{a}\right)^2 - \left(\frac{y}{a}\right)^2}$$

In the case of the above deformation geometry:

$$a = b = r_o + \delta$$

then,

$$1 = \left(\frac{x}{a}\right)^2 + \left(\frac{y}{a}\right)^2 + \left(\frac{z}{c}\right)^2, \quad Z = c\sqrt{1 - \left(\frac{x}{a}\right)^2 - \left(\frac{y}{a}\right)^2}$$

We further note that at:

$$x = 0; y = r_o; z = \frac{L}{2}$$

$$1 = 0 + \left(\frac{r_o}{a}\right)^2 + \left(\frac{L}{2c}\right)^2$$

$$\left[1 - \left(\frac{r_o}{a}\right)^2\right] = \frac{L^2}{4c^2} \rightarrow c^2 = \frac{L^2}{4[1 - \left(\frac{r_o}{a}\right)^2]}$$

then,

$$c = \frac{L}{2\sqrt{[1 - \left(\frac{r_o}{a}\right)^2]}}$$

Having determined constants a, b and c defining the ellipsoid, we can now determine the volume of the shaded coordinates.

$$x = r\cos\theta, y = r\sin\theta\ ; Z = z$$

Firstly,

$$z = C\sqrt{1 - \left(\frac{x}{a}\right)^2 - \left(\frac{y}{a}\right)^2}$$

$$z = C\sqrt{1 + \left[-\frac{1}{a^2}\{r^2\cos^2\theta + r^2 sin^2\,\theta\}\right]}$$

$$z = C\sqrt{1 + \left[-\frac{r^2}{a^2}\right]\left[\{\cos^2\theta + sin^2\,\theta\}\right]}$$

$$z = C\sqrt{1 - \frac{r^2}{a^2}}$$

$$V = 2C\int_0^{2\pi} d\theta \int_{r_o}^{r_o + \delta} \left(\sqrt{1 - \frac{r^2}{a^2}}\right) r\,dr$$

$$u = 1 - \frac{r^2}{a^2}$$

$$du = -\frac{2r}{a^2}\,dr$$

$$= -\frac{2a^2c}{2}\int_0^{2\pi} d\theta \int_{1-\frac{r_o^2}{a^2}}^{0} u^{\frac{1}{2}}\,du$$

$$= -a^2 c \int_0^{2\pi} d\theta \int_{1-\frac{r_o^2}{a^2}}^{0} u^{\frac{1}{2}}\, du$$

$$= -\frac{2a^2 c}{3} \int_0^{2\pi} d\theta\, u^{1.5}\Big|_{1-\frac{r_o^2}{a^2}}^{0} = \left[-\frac{2a^2 c}{3}\right]\left[u^{1.5}\Big|_{1-\frac{r_o^2}{a^2}}^{0}\right]\left[\theta\Big|_0^{2\pi}\right]$$

This simplifies to:

$$\textit{Volume of deformation} = \Delta V = -\frac{2a^2 c}{3}\left[0 - \left(1 - \frac{r_o^2}{a^2}\right)^{1.5}\right][2\pi]$$

$$= \frac{4\pi}{3} a^2 c\left[\left(1 - \frac{r_o^2}{a^2}\right)^{1.5}\right]$$

It has already been shown that:

$$a = r_o + \delta\,, \qquad c = \frac{L}{2\left(1 - \left(\frac{r_o}{a}\right)^2\right)^{\frac{1}{2}}}$$

Then,

$$\Delta V = \frac{2\pi L}{3}(r_o + \delta)^2\left(\left[1 - \left(\frac{r_o}{a}\right)^2\right]^{-0.5}\left[1 - \left(\frac{r_o}{a}\right)^2\right]^{1.5}\right)$$

$$\Delta V = \frac{2\pi L}{3} (r_o + \delta)^2 \left(1 - \frac{r_o^2}{a^2}\right)$$

$$\Delta V = \frac{2\pi L}{3} (r_o + \delta)^2 \left(\frac{a^2 - r_o^2}{a^2}\right)$$

$$\Delta V = \frac{2\pi L}{3} \frac{(r_o + \delta)^2}{a^2} \left(a^2 - r_o^2\right)$$

$$\Delta V = \frac{2\pi L}{3} \left((r_o + \delta)^2 - r_o^2 \right) = \frac{2\pi L}{3} \left(r_o^2 + 2 r_o^2 \delta + \delta^2 - r_o^2 \right)$$

$$\Delta V = \frac{2\pi L}{3} \left(2 r_o \delta + \delta^2 \right) \Rightarrow \frac{3\Delta V}{2\pi L} = 2 r_o \delta + \delta^2$$

If, for simplification, we let:

$$K = \frac{3}{2} \frac{\Delta V}{\pi L}$$

then,

$$K = 2 r_o \delta + \delta^2$$

and

$$2 r_o \delta + \delta^2 - K = 0$$

Using the quadratic solution:

$$i.e., \quad \frac{-b \pm \sqrt{b^2 + 4ac}}{2}$$

$$\therefore \delta = \frac{-2r_o \pm 2\sqrt{r_o^2 + 4K}}{2}$$

$$= \frac{-2r_o - 2\sqrt{r_o^2 + K}}{2}$$

$$= \frac{-2r_o + 2\sqrt{r_o^2 + K}}{2}$$

the only physically correct solution.

$$\delta = \frac{-2r_o + 2\sqrt{r_o^2 + K}}{2}$$

$$\delta = \frac{2(r_o^2 + 3/2\ \frac{\Delta V}{\pi L})^{\frac{1}{2}} - 2r_o}{2}, \qquad \delta_{max}\ @\ z = 0\ for given\ \Delta V$$

$$\delta = (r_o^2 + 3/2\ \frac{\Delta V}{\pi L})^{\frac{1}{2}} - r_o \quad = \delta_{max} \tag{1}$$

At this stage, given a particular instrument, i.e. L and r_0 are fixed, we can determine δ (displacement) for any injected volume, ΔV.

Equation 1 illustrates that the final diameter,

$$a = \delta_{max} + r_o = (r_o^2 + 3/2\ \frac{\Delta V}{\pi L})^{\frac{1}{2}}$$

1. In determining ΔV, we assume symmetrical deformation.
2. Also, the deformation relation is applicable only to δmax at z = 0.

   Using points 1 and 2, we can
3. reduce the equation for ellipsoid to z = 0.
4. Express deformations for z = -L/2 to z = L/2 in terms of δ_{max} at z = 0.

Therefore, the initial equation,

$$1 = \left(\frac{x}{a}\right)^2 + \left(\frac{y}{b}\right)^2 + \left(\frac{z}{c}\right)^2$$

reduces to:

$$1 = \left(\frac{y}{a}\right)^2 + \left(\frac{z}{c}\right)^2$$

We also note that the final radius is given by "y".

Therefore, we rearrange this equation in terms of "y":

$$y = a\left[1 - \left(\frac{z}{c}\right)^2\right]^{\frac{1}{2}}$$

Hence, the displacement is given by:

$$\partial(z) = y - r_o = a\left[1 - \left(\frac{z}{c}\right)^2\right]^{\frac{1}{2}} - r_o \qquad (2)$$

We can now expand this equation by substituting a and c:

$$a = r_o + \delta_{max}$$

$$c = \frac{aL}{2\sqrt{a^2 - r_o^2}} \quad at\,\Delta V = 0\,and\,c = \infty$$

$$a^2 = r_o^2 + 2r_o\delta_{max} + \delta_{max}^2$$

The next step is to substitute first c and then a into Equation 2:

$$\delta(z) = a\left[1 - \left(\frac{2\sqrt{a^2 - r_o^2}}{aL}\,Z\right)^2\right]^{\frac{1}{2}} - r_o$$

$$\delta(z) = \frac{a}{aL}\left[a^2L^2 - 4(a^2 - r_o^2)Z^2\right]^{\frac{1}{2}} - r_o$$

$$\delta(z) = \frac{1}{L}\left[r_o^2 + 2r_o\delta_{max} + \delta_{max}^2\right]L^2 - 4(2r_o\delta_{max} + \delta_{max}^2)Z^2\Big]^{\frac{1}{2}} - r_o \qquad (3)$$

$$\delta(z) = \frac{1}{L}\left[\{r_o^2 + 2r_o\delta_{max} + \delta_{max}^2\}L^2 - 4(2r_o\delta_{max} + \delta_{max}^2)Z^2\right]^{\frac{1}{2}} - r_o$$

We have, further seen that:

$$\delta_{max} = (r_o^2 + 3/2\,\frac{\Delta V}{\pi L})^{\frac{1}{2}} - r_o$$

Furthermore,

$$\delta^2_{max} = (r_o^2 + 3/2 \frac{\Delta V}{\pi L}) - 2 r_o (r_o^2 + 3/2 \frac{\Delta V}{\pi L})^{\frac{1}{2}} + r_o^2$$

$$\delta^2_{max} = 3/2 \frac{\Delta V}{\pi L}) - 2 r_o (r_o^2 + 3/2 \frac{\Delta V}{\pi L})^{\frac{1}{2}} + 2r_o^2$$

By substituting δ_{max} and δ_{max}^2 into Equation 3, $\delta(\Delta V,Z)$.

Let's look at simplifying each ofthe terms in Equation 3 separately.

<u>First term</u>

$$r_o + 2 r_o \delta_{max} + \delta^2_{max}$$

$$= r_o^2 + 2r_o [(r_o^2 + 3/2 \frac{\Delta V}{\pi L})^{\frac{1}{2}} - r_o] + 3/2 \frac{\Delta V}{\pi L} - 2r_o (r_o^2 + 3/2 \frac{\Delta V}{\pi L})^{\frac{1}{2}} + 2r_o^2$$

$$= r_o^2 + 2r_o (r_o^2 + 3/2 \frac{\Delta V}{\pi L})^{\frac{1}{2}} - 2 r_o + 3/2 \frac{\Delta V}{\pi L} - 2r_o (r_o^2 + 3/2 \frac{\Delta V}{\pi L})^{\frac{1}{2}} + 2r_o^2$$

$$= 3/2 \frac{\Delta V}{\pi L} + r_o^2 \quad \Rightarrow A$$

$$= 3/2 \frac{\Delta V}{\pi L} - 2r_o \quad \Rightarrow B$$

Second term

$$2\,r_o\,\delta_{max} + \delta_{max}^2 = 2r_o\,[(r_o^2 + 3/2\,\frac{\Delta V}{\pi L})^{\frac{1}{2}} - r_o] + 3/2\,\frac{\Delta V}{\pi L} - 2r_o\,(r_o^2 + 3/2\,\frac{\Delta V}{\pi L})^{\frac{1}{2}}$$

$$2\,r_o\,(r_o^2 + 3/2\,\frac{\Delta V}{\pi L})^{\frac{1}{2}} - 2\,r_o^2 + 3/2\,\frac{\Delta V}{\pi L} - 2r_o\,(r_o^2 + 3/2\,\frac{\Delta V}{\pi L})^{\frac{1}{2}}$$

First term

$$r_o + 2\,r_o\,\delta_{max} + \delta_{max}^2$$

$$= r_o^2 + 2r_o[\,(r_o^2 + 3/2\,\frac{\Delta V}{\pi L})^{\frac{1}{2}} - r_o] + 3/2\,\frac{\Delta V}{\pi L} - 2r_o\,(r_o^2 + 3/2\,\frac{\Delta V}{\pi L})^{\frac{1}{2}} + 2r_o^2$$

$$= r_o^2 + 2r_o\,(r_o^2 + 3/2\,\frac{\Delta V}{\pi L})^{\frac{1}{2}} - 2\,r_o + 3/2\,\frac{\Delta V}{\pi L} - 2r_o\,(r_o^2 + 3/2\,\frac{\Delta V}{\pi L})^{\frac{1}{2}} + 2r_o^2$$

$$= 3/2\,\frac{\Delta V}{\pi L} + r_o^2 \qquad \Rightarrow \quad A$$

Second term

$$2\,r_o\,\delta_{max} + \delta_{max}^2 = 2r_o\,[(r_o^2 + 3/2\,\frac{\Delta V}{\pi L})^{\frac{1}{2}} - r_o] + 3/2\,\frac{\Delta V}{\pi L} - 2r_o\,(r_o^2 + 3/2\,\frac{\Delta V}{\pi L})^{\frac{1}{2}}$$

$$2\,r_o\,(r_o^2 + 3/2\,\frac{\Delta V}{\pi L})^{\frac{1}{2}} - 2\,r_o^2 + 3/2\,\frac{\Delta V}{\pi L} - 2r_o\,(r_o^2 + 3/2\,\frac{\Delta V}{\pi L})^{\frac{1}{2}}$$

$$= 3/2\,\frac{\Delta V}{\pi L} - 2r_o \quad \Rightarrow B$$

Substituting A and B back into Equation 3, we obtain:

$$\delta(\Delta V, Z) = \frac{1}{L}\left[\left(3/2\,\frac{\Delta V}{\pi L} + r_o^2\right)L^2 - 4\left(3/2\,\frac{\Delta V}{\pi L}\right)Z^2\right]^{\frac{1}{2}} - r_o$$

$$\delta(\Delta V, Z) = \frac{1}{L}\left[\left(3/2\,\frac{\Delta V}{\pi L} + r_o^2\right)L^2 - \frac{6\Delta V Z^2}{\pi L}\right]^{\frac{1}{2}} - r_o \qquad (4)$$

The final form of Equation 4 can be simplified by rearranging the terms in the equation and yields the following:

$$\delta(\Delta V, Z) = \frac{1}{L}\left[\left(3/2\,\frac{\Delta V}{\pi L} + (L^2 - 4Z^2)\right) + r_o^2 L^2\right]^{\frac{1}{2}} - r_o \qquad (5)$$

We can verify this equation by checking three conditions: Z = 0, Z = L/2 and ΔV = 0

$$\delta(\Delta V, 0) = \frac{1}{L}\left[3/2\,\frac{\Delta V}{\pi L}(L^2) + r_o^2 L^2\right]^{\frac{1}{2}} - r_o$$

$$= \left[3/2\,\frac{\Delta V}{\pi L} + r_o^2\right]^{\frac{1}{2}} - r_o = \delta_{max}$$

$$\delta(\Delta V, L/2) = \frac{1}{L}\left[3/2\,\frac{\Delta V}{\pi L}\left(L^2 - 4\,\frac{L^2}{4}\right) + r_o^2 L^2\right]^{\frac{1}{2}} - r_o = r_o - r_o = 0$$

$$\delta(0,Z) = \frac{1}{L}\left[3/2\ \frac{0}{\pi L}\ (L^2 - 4Z^2) + r_o^2 L^2\right]^{\frac{1}{2}} - r_o = r_o - r_o = 0$$

A Slight Diversion

One concern in presuremeter testing is the uniformity of loading or straining of the soil being tested. It has been shown by "Briand" that the l/d ratio for mono-cellmar probes should be .> 6.5; this was done experimentally. Now, using Equation 5, we can make theoretical analyses.

If we look at a particular point on the surface of the pressuremeter and compare it with δmax or expansion, we can see the influence of L/d ratio on the difference between the two points. In our example, i.e. δ(ΔV, L/4) - δ(ΔV, 0), in order to obtain constant straining, this difference should approach 0, so we can see for "practical reasons" what L/D ratios would yield satisfactory result.

$$\delta(\Delta V, \frac{L}{4}) = \frac{1}{L}\left[3/2\ \frac{\Delta V}{\pi L}\ (L^2 - 4\ \frac{L^2}{16}) + r_o^2 L^2\right]^{\frac{1}{2}} - r_o$$

$$= \frac{1}{L}\left[3/2\ \frac{\Delta V}{\pi L}\ L^2\ (1 - \tfrac{1}{4}) + r_o^2 L^2\right]^{\frac{1}{2}} - r_o$$

$$= \left[9/8\ \frac{\Delta V}{\pi L} + r_o^2\right]^{\frac{1}{2}} - r_o$$

$$\delta(\Delta V, \frac{L}{4}) - \delta(\Delta V, 0) = (\frac{9}{8}\ \frac{\Delta V}{\pi L} + r_o^2)^{\frac{1}{2}} - r_o - (3/2\ \frac{\Delta V}{\pi L} + r_o^2)^{\frac{1}{2}} + r_o$$

$$= \left(\frac{9}{8}\frac{\Delta V}{\pi L} + r_o^2\right)^{\frac{1}{3}} - \left(3/2\frac{\Delta V}{\pi L} + r_o^2\right)^{\frac{1}{3}}$$

If $n = L/d = L/2r_0$, then $2nr_0 = L$

$$= \left(\frac{9}{8}\frac{\Delta V}{2n\pi r_o} + r_o^2\right)^{\frac{1}{3}} - \left(3/2\frac{\Delta V}{2n\pi r_o} + r_o^2\right)^{\frac{1}{3}}$$

$$= \left(\frac{9\Delta V}{16n\pi r_o} + r_o^2\right)^{\frac{1}{3}} - \left(\frac{3\Delta V}{4n\pi r_o} + r_o^2\right)^{\frac{1}{3}}$$

We find that this principal difference is still dependant on the initial diameter. This is consistent with "Branids" conclusions.

Graphs 1 and 2 show consistency with that which was found by Hartmon, Branid which recommends and L/D ratio in the range of 6.6.

If we look at a particular pressuremeter type, say the "Pencel" which has the following specifications:

$$d = 3.52\ cm \Rightarrow r_o = 1.76\ cm$$

Volume initially 230cc and $r_{interior} = 1.6$ cm

$$230 = (1\ 6)^2\ \Pi\ .\ L$$

$$\Rightarrow L = \frac{230}{(1\ 6)^2\ \pi} = 28.60$$

Hence L/D ratio = 28.60/3.52 = 8.12, which is above that which is recommended by Hurtman, Branid.

Given the pressuremeter parameters, we can simplify Equation 5,first by putting everything in terms of L/D ratio $\Rightarrow L = 2nr_0$

$$\delta(\Delta V, Z) = \frac{1}{2nr_o}\left[\frac{3}{4}\frac{\Delta V}{nr_o}\left(4n^2r_o^2 - 4z^2\right)\right| + n\,n^2r_o^4\Big|^{\frac{1}{2}} - r_o$$

Equation 5 in terms of L/D(n) equation:

$$\delta(\Delta V, Z) = \frac{1}{n\,r_o}\left[\frac{3}{4}\frac{\Delta V}{nr_o}\left(n^2r_o^2 - z^2\right)\right| + n^2r_o^4\Big|^{\frac{1}{2}} - r_o$$

The relevant values for the pencel are:

n = 6.7144 and ro = 3.52

This one in particular is shown in Figures 3 and 4.

After some expansion, we have

$$r^2 - (r_o + \delta)^2 - (r - y)^2 - r_o^2$$

$$r - (r^2 - r_o^2 - 2r_o\delta + \delta^2 + r_o^2)^{\frac{1}{2}} = y$$

$$r - (r^2 - 2r_o\delta - \delta^2)^{\frac{1}{2}} = y$$

$$r - [r^2 - \delta\ (2 + \delta\ )]^{\frac{1}{2}} = y$$

Then the circumferencial strain:

$$e_\theta = \frac{y}{r-y} = \frac{r - [r^2 - \delta(2 + \delta)]^{\frac{1}{2}}}{[r^2 - \delta(2 + \delta)]^{\frac{1}{2}}}$$

$$= -1 + r\,[r^2 - \delta(2 + \delta)]^{-\frac{1}{2}}$$

$$e_\theta = -1 + [1 - \delta(\frac{2+\delta}{r^2})]^{-\frac{1}{2}}$$

$$e_\theta = [1 - \delta(\frac{2+\delta}{r^2})]^{-\frac{1}{2}} - 1 \qquad (6a)$$

Also,

$$(1 + e_o)(1 + e_r) = 1$$

then,

$$e_r = \frac{1}{1 + e_\theta} - 1 = [1 - \delta(\frac{2+\delta}{r^2})]^{\frac{1}{2}} - 1 \qquad (6b)$$

We have already seen however that $\delta(\Delta V,Z)$, hence:

$$e_\theta(\Delta V,Z) = [1 - \delta\ (\Delta V,Z)(\frac{2 + \delta\ (\Delta V,Z)}{r^2})]^{-\frac{1}{2}} - 1 \qquad (7)$$

and

$$e_r(\Delta V,Z) = [1 - \delta\ (\Delta V,Z)(\frac{2 + \delta\ (\Delta V,Z)}{r^2})]^{\frac{1}{2}} - 1 \qquad (8)$$

where

$$\delta\ (\Delta V,Z) = = \frac{1}{L}\left[3/2\ \frac{\Delta V}{\pi L}\ (L^2 - 4Z^2) + r_o^2 L^2\right]^{\frac{1}{2}} - r_o$$

This was defined as Equation 5 previously. The equations developd by Palmer were done so for the tricellur type probe as such they are not a function of 'Z' the complex. I has been shown by Palmer that:

$$stress\ gradient \Rightarrow [\sigma_r - \sigma_\theta] = \phi(e_\theta)$$

Equilibrium equation:

$$= \frac{Cy^2 - C + Dy^2 + Dy + Ey^2 - Ey}{y\,(y-1)\,(y+1)}$$

$$1 = (C + D + E)y^2 + (D - E)y - C$$

$$C + D + E = 0 \rightarrow E + E = 1 \rightarrow E = \frac{1}{2}$$

$$\frac{r d\sigma_r}{dr} = \sigma_\theta - \sigma_r = -\phi(e_\theta)$$

Furthermore,

$$\frac{d\sigma_r}{dr} = -\frac{1}{r}\phi(e_\theta)$$

and

$$d\sigma_r = -\int \frac{1}{r}\phi(e_\theta)\, dr$$

The result of this integral becomes:

$$\phi(\delta) = \delta(1+\delta)(2+\delta)\psi'(\delta) \tag{9}$$

where δ is given by Equation 5 as:

$$\delta\ (\Delta V, Z) = = \frac{1}{L}\left[3/2\ \frac{\Delta V}{\pi L}(L^2 - 4Z^2) + r_o^2 L^2\right]^{\frac{1}{2}} - r_o$$

If we consider a particular "mono-cellular" instrument (i.e., we fix ro and L) and consider a particular horizon across the instrument, we can defien two constants. If we let:

$$A = \frac{3(L^2 - 4Z^2)}{2\pi L^3}\ ;\ B = r_o$$

Equation 5 becomes:

$$\delta(\Delta V) = [A\Delta V + B^2]^{\frac{1}{2}} - B$$

$$\delta^2 = A\Delta V + B^2 - 2B[A\Delta V + B^2]^{\frac{1}{2}} + B^2$$

$$\frac{(\delta + B)^2 - B^2}{A} = \Delta V$$

From Equation 7,

$$e_\theta(\Delta V) = \left[[1 - \frac{\delta(2 + \delta)}{r^2}\right]^{-\frac{1}{2}} - 1$$

$$= \left[[1 - \frac{(2\delta + \delta^2)}{r^2}\right]^{-\frac{1}{2}} - 1$$

$$\psi(\delta) - \alpha_n = \int_{r_o + \delta}^{\infty} \frac{1}{r} \phi\,[-1 + \left[[1 - \frac{(2\delta + \delta^2)}{r^2}\right]^{-\frac{1}{2}}\, dr$$

We must make substitutions throughout:

$$let\, x = [-1 + \left[[1 - \frac{(2\delta + \delta^2)}{r^2}\right]^{-\frac{1}{2}}$$

$$(x+1)^2 = \frac{1}{\left[1 - \frac{(2\delta + \delta^2)}{r^2}\right]}$$

$$(x+1)^2 - (x+1)^2 \frac{(2\delta + \delta^2)}{r^2} = 1$$

$$(x+1)^2 - 1 = (x+1)^2 \frac{(2\delta + \delta^2)}{r^2}$$

$$r^2 = \frac{(x+1)^2 (2\delta + \delta^2)}{(x+1)^2 - 1}$$

$$r = \left[\frac{(x+1)^2 (2\delta + \delta^2)}{(x+1)^2 - 1}\right]^{\frac{1}{2}}$$

$$r^3 = \left[\frac{(x+1)^2 (2\delta + \delta^2)}{(x+1)^2 - 1}\right]^{3/2}$$

$$x = -1 + \left[1 - \frac{(2\delta + \delta^2)}{r^2}\right]^{-\frac{1}{2}}$$

$$dx = -\frac{1}{2}\left[\left[1 - \frac{(2\delta + \delta^2)}{r^2}\right]^{-3/2}\left[\frac{2(2\delta + \delta^2)}{r^3}\right]\right] dr$$

$$dx = -\left[1 - \frac{(2\delta + \delta^2)}{\frac{(x+1)^2(2\delta + \delta^2)}{(x+1)^2 - 1}}\right]^{-3/2}\left[\frac{(2\delta + \delta^2)}{\left[\frac{(x+1)^2(2\delta + \delta^2)}{(x+1)^2 - 1}\right]^{3/2}}\right] dr$$

$$dx = \left[1 - \frac{(x+1)^2 - 1}{(x+1)^2}\right]^{-3/2}\left[\frac{(x+1)^2(2\delta + \delta^2)}{(x+1)^2 - 1}\right]^{-3/2}(2\delta + \delta^2)\, dr$$

$$dx = \left[\frac{(x+1)^2 - (x+1)^2 + 1}{(x+1)^2}\right]^{-3/2}\left[\frac{(x+1)^2(2\delta + \delta^2)}{(x+1)^2 - 1}\right]^{-3/2}(2\delta + \delta^2)\, dr$$

$$= \left[\frac{(2\delta + \delta^2)}{(x+1)^2 - 1}\right]^{-3/2}(2\delta + \delta^2)\, dr$$

$$= \left[\frac{1}{(x+1)^2 - 1}\right]^{-3/2}(2\delta + \delta^2)^{-\frac{1}{2}}\, dr$$

$$= \frac{1}{[(x+1)^2 - 1]^{-3/2}}\ (2\delta + \delta^2)^{-\frac{1}{2}}\, dr$$

$$= [(x+1)^2 - 1]^{-3/2}\ (2\delta + \delta^2)^{-\frac{1}{2}}\, dr$$

$$[(x+1)^2-1][(x+1)^2-1]^{\frac{1}{2}}\ (2\delta+\delta^2)^{-\frac{1}{2}}\,dr$$

$$=[(x+1)^2-1](x+1)\left[\frac{(x+1)^2-1}{(x+1)^2\ (2\delta+\delta^2)}\right]^{\frac{1}{2}}\quad dr$$

$$=\left[(x+1)^2-1](x+1)\right]\frac{1}{r}\quad dr$$

$$=\left[(x^2+2x+1-1)\ (x+1)\right]\frac{1}{r}\quad dr$$

$$dx=\left[x(x+2)\ (x+1)\right]\frac{1}{r}\quad dr$$

The integral requires the integration. Boundaries to be redefined as well.

$$\psi(\delta)-\sigma_h=\int_0^{\delta}\frac{1}{x(x+2)\ (x+1)}\,\phi(x)\,dx$$

It follows that:

$$\psi'(\delta)=\frac{1}{\delta(\delta+2)\ (\delta+1)}\,\phi(\delta)$$

and

$$\phi(\delta) = \delta(\delta + 2)(\delta + 1)\psi'(\delta)$$

This is identical to Equation 9 which was found by Palmer Palmer further found that by expressing δ in terms of volume injected, i.e.

$$\delta = (1 - \Delta V/V)^{-\frac{1}{3}} - 1 \ (in\ case\ tri-cellular\ probe)$$

He found that

$$\delta(\delta + 1)(\delta + 2) = \frac{2}{d[log\ (\Delta V/V]}$$

This was done so that if

$$f(x) = \delta(\delta + 1)(\delta + 2)$$

then we seek a function g(x) such that:

$$f(x) = \frac{1}{g'(x)} \rightarrow g'(x) = \frac{1}{f(x)}$$

and hence,

$$g'(x) = \int \frac{1}{f(x)} \qquad (10)$$

We have already shown that

$$\delta\ (\Delta V,Z) = = \frac{1}{L}\left[3/2\ \frac{\Delta V}{\pi L}\ (L^2 - 4Z^2) + r_o^2 L^2\right]^{\frac{1}{2}} - r_o$$

This can be expanded to:

$$\delta\ (\Delta V,Z) = = \left[3/2\ \frac{\Delta V}{\pi L^3}\ L^2 - 3/2\ \frac{\Delta V}{\pi L^3}\ 4Z^2) + r_o^2 L^2\right]^{\frac{1}{2}} - r_o$$

If we define three constants: (each of which can be defined by instrument line):

$$A = \frac{3}{2\pi L}\ .B = \frac{-6}{\pi L^3}\ .C = r_o^2 L^2 \qquad (11)$$

$$\delta(\Delta V, Z) = [A\Delta V + B\Delta V Z^2 + C]^{\frac{1}{2}} - r_o$$

$$= [\ \Delta V\ (A + BZ^2) + C\ ]^{\frac{1}{2}} - r_o$$

We can make a further simplification by rendering Equation 11 independant of Z, i.e. letting:

$$D = A + BZ^2$$

Then,

$$\delta(\Delta V) = [D\Delta V + C]^{\frac{1}{2}} - r_o$$

First, we simplify

$$\delta(\delta + 1)(\delta + 2)$$

$$\delta = [D\Delta V + C]^{\frac{1}{3}} - r_o$$

$$\delta^2 = [D\Delta V + C] - 2r_o[D\Delta V + C]^{\frac{1}{3}} + r_o^2$$

$$\delta^3 = [D\Delta V + C]^{3/2} - 3r_o[D\Delta V + C] + 3r_o^2[D\Delta V + C]^{\frac{1}{3}} - r_o^3$$

$$\delta(\delta + 1)(\delta + 2) = (\delta^2 + \delta)(\delta + 2) = \delta^3 + 3\delta^2 + 2\delta$$

$$= [D\Delta V + C]^{3/2} - 3r_o[D\Delta V + C] + 3r_o^2[D\Delta V + C]^{\frac{1}{3}} - r_o^3$$

$$+ 3[D\Delta V + C] - 6r_o[D\Delta V + C]^{\frac{1}{3}} + 3r_o^2 + 2[D\Delta V + C]^{\frac{1}{3}} - 2r_o^2$$

$$[D\Delta V + C]^{3/2} + 3(1 - r_o)[D\Delta V + C] + [3r_o^2 - 6r_o + 2][D\Delta V + C]^{\frac{1}{3}} - [r_o^3 - 3r_o^2 + 2r_o]$$

Then we have:

$$[D\Delta V + C]^{3/2} + E[D\Delta V + C] + F[D\Delta V + C]^{\frac{1}{3}} + G \qquad (12)$$

$$E = 3\,(1 - r_o)\,;\; F = [3r_o^2 - 6r_o + 2],\; G = -[r_o^3 - 3r_o^2 + 2r_o]$$

If we now go back to Equation 10, we find that

$$g(x) = \int \frac{1}{f(x)}$$

where f(x) is defined by Equation 12.

$$g(x) = \int \frac{1}{[D\Delta V + C]^{3/2} + E[D\Delta V + C] + F[D\Delta V + C]^{\frac{1}{2}} + G}\, d(\Delta V)$$

$$Let\;\; u = D\Delta V + C$$

$$du = D\, d(\Delta V)$$

$$g(x) = \frac{1}{D}\int \frac{1}{u^{3/2} + Eu + Fu^{\frac{1}{2}} + G}\, du$$

$$g(x) = \frac{1}{D}\int \frac{1}{u^{3/2} + Eu + Fu^{\frac{1}{2}} + G}\left[\frac{u^{\frac{1}{2}}}{u^{\frac{1}{2}}}\right] du$$

$$Let\; x = u^{\frac{1}{2}},\; x^2 = u$$

$$dx = \frac{1}{2}u^{-\frac{1}{2}}\, du$$

$$g(x) = \frac{2}{D}\int \frac{x}{x^3 + Ex^2 + Fx + G}\,dx$$

We must first simplify

$$x^3 + Ex^2 + Fx + G$$

Let us first make the substitution y = x - e/3; the equation above reduces to:

$$y^3 = ay + b$$

where

$$a = \frac{1}{3}(3F - E^2);\ b = \frac{1}{27}(2E^3 - 9EF + 27G)$$

where E, F, and G have been previously defined as:

$$E = 3(1 - r_o);\ F = (3r_o^2 - 6r_o + 2),\ G = -(r_o^3 - 3r_o^2 + 2r_o)$$

Then a becomes:

$$a = \frac{1}{3}(9r_o^2 - 18r_o + 6 - [9\{1 - 2r_o + r_o^2\}])$$

$$= \frac{1}{3}(9r_o^2 - 18\,r_o + 6 - 9 + 18r_o - 9r_o^2)$$

$$a = -1$$

$$b = \frac{1}{27}(2\ \ 27\,(1 - r_o)(1 - 2r_o + r_o^2) - 9(3[1 - r_o][3r_o^2 - 6r_o + 2])$$

$$+ 27\,(-r_o^3 + 3r_o^2 - 2r_o))$$

$$= \frac{1}{27}[54 - 162r_o + 162\,r_o^2 - 54r_o^3 + 81r_o^3 - 243r_o^2 + 216r_o - 54$$

$$- 27r_o^3 + 81r_o^2 - 54r_o$$

$$b = 0$$

Then:

$$x^3 + Ex^2 + Fx + G$$

$$= y^3 - y$$

Then

$$g(x) = g(y) = \frac{2}{D}\int \frac{y + \frac{E}{3}}{y(y-1)(y+1)}\,dy$$

$$= \frac{2}{D}\int \frac{y\,dy}{y(y-1)(y+1)} + \frac{E}{3}\int \frac{1}{y(y-1)(y+1)}\,dy$$

We must first solve each of these by partial fraction.

Therefore, the first integral:

$$\frac{1}{(y-1)(y+1)} = \frac{A}{(y-1)} + \frac{B}{(y+1)}$$

$$= \frac{Ay + A + By - B}{(y-1)(y+1)}$$

Then

$$1 = (A + B)y + (A + B)$$

Then,

$$A + B = 0 \rightarrow A = -B \text{ and } A - B = 1$$

Incorporating the two equations:

$$-2B = 1 \rightarrow B = -\frac{1}{2}$$

$$Then \quad A = \frac{1}{2}$$

The second integral becomes:

$$\frac{1}{y(y-1)(y+1)} = \frac{C}{y} + \frac{D}{(y-1)} + \frac{E}{(y+1)}$$

$$D - E = 0 \rightarrow D = E, \; D = \frac{1}{2}$$

$$-C = 1 \rightarrow C = -1$$

Thus the integral:

$$= \frac{2}{D}\left[\int \frac{dy}{(y-1)(y+1)} + \frac{E}{3}\int \frac{dy}{y(y-1)(y+1)}\right]$$

$$= \frac{2}{D}\left[\frac{1}{2}\int \frac{dy}{(y-1)} - \frac{1}{2}\int \frac{dy}{(y+1)} + \frac{E}{3}\left\{-\int \frac{dy}{y} + \frac{1}{2}\int \frac{dy}{(y-1)}\right] + \frac{1}{2}\int \frac{dy}{(y+1)}\right\}\Bigg|$$

$$= \frac{2}{D}\left[\frac{1}{2}ln\left(\frac{y-1}{y+1}\right) + \frac{E}{3}\left\{-ln\, y + \frac{1}{2}\, ln[(y-1)(y+1)]\right\}\right]$$

$$= \frac{2}{D}\left[\frac{1}{2} ln\left(\frac{y-1}{y+1}\right) + \frac{E}{3}\left\{ -\frac{1}{2} ln\, y + \frac{1}{2} ln[(y-1)(y+1)]\right\}\right]$$

$$= \frac{2}{D}\left[\frac{1}{2} ln\left(\frac{y-1}{y+1}\right) + \frac{E}{6} ln\left\{ \frac{(y-1)(y+1)}{y}\right\}\right]$$

$$\frac{1}{D} ln\left(\frac{y-1}{y+1}\right) + \frac{E}{3D} ln\left\{ \frac{(y-1)(y+1)}{y}\right\}\Bigg] \tag{13}$$

We now have to make some back substitutions. First,

$$y = x - \frac{E}{3}$$

Back-substitute.

Equation 13 becomes:

$$\frac{1}{D} ln\left(\frac{x-\frac{E}{3}-1}{x-\frac{E}{3}+1}\right) + \frac{E}{3D} ln\left\{ \frac{(x-\frac{E}{3}-1)(x-\frac{E}{3}+1)}{x-\frac{E}{3}}\right\}\Bigg] \tag{14}$$

$$\frac{1}{D} ln\left(\frac{3x-E-3}{3x-E+3}\right) + \frac{E}{3D} ln\left\{ \frac{(3x-E-3)(3x-E+3)}{3(3x-E)}\right\}\Bigg]$$

Then we back substitute

$$x = u^{\frac{1}{3}} \; and \; u = D\;\Delta V + C$$

$$\frac{1}{D}\,ln\left(\frac{3(D\;\Delta V + C)^{\frac{1}{3}} - E - 3}{3(D\;\Delta V + C)^{\frac{1}{3}} - E + 3}\right) + \frac{E}{3D}\;ln\left\{\frac{(3(D\;\Delta V + C)^{\frac{1}{3}} - E - 3)\,(3(D\;\Delta V + C)^{\frac{1}{3}} - E + 3)}{3(3(D\;\Delta V + C)^{\frac{1}{3}} - E)}\right\}\Bigg|$$

$$g\,(\Delta V, Z) = \frac{1}{D}\,ln\left(\frac{3(D\;\Delta V + C)^{\frac{1}{3}} - E - 3}{3(D\;\Delta V + C)^{\frac{1}{3}} - E + 3}\right)$$

$$+\;\frac{E}{3D}\;ln\left\{\frac{(3(D\;\Delta V + C)^{\frac{1}{3}} - E - 3)\,(3(D\;\Delta V + C)^{\frac{1}{3}} - E + 3)}{3(3(D\;\Delta V + C)^{\frac{1}{3}} - E)}\right\}\Bigg| \qquad (15)$$

$$D = A + BZ^2; A = \frac{3}{2\pi L}, B = \frac{-6}{\pi L^3}$$

$$D = \frac{3}{2\pi L} - \frac{6}{\pi L^3}Z^2$$

$$C = r_o^2 L^2$$

$$E = 3\,(1 - r_o)$$

Then:

$$\phi(\Delta V, Z) = \frac{d\psi}{dg(\Delta V, Z)}$$

where g(ΔV, Z) is given by Equation 13

g(ΔV, Z) can be simplified for individual instrument, concentration on the Pencel, where:

$$r_o = 1.76\ cm, L = 28.6\ cm$$

$$D = 0167 - 0000816Z^2 = \frac{167 - 816Z^2}{10{,}000}$$

$$C = 2533.7$$

$$E = -2.28$$

Also,

$$3[D\Delta V + C]^{\frac{1}{3}} = \left[\frac{167 - .816Z^2}{5773.5}\Delta V + 4388\ 5 \right]^{\frac{1}{3}}$$

Equation 15 becomes:

$$g(\Delta V, Z) = \frac{10{,}000}{167 - .816Z^2} ln\left(\frac{\left[\left(\frac{167 - 816Z^2}{5773.5}\Delta V + 4388\ 5 \right)^{\frac{1}{3}} - .72 \right]}{\left(\frac{167 - .816Z^2}{5773\ 5}\Delta V + 4388\ 5 \right)^{\frac{1}{3}} + 5\ 28} \right) \qquad (16)$$

$$-\frac{7600}{167-.816Z^2}\ln\frac{\left[\left(\frac{167-.816Z^2}{5773.5}\Delta V+4388.5\right)^{\frac{1}{2}}-.72\right]\left[\left(\frac{167-816Z^2}{5773\,5}\Delta V+4388\,5\right)^{\frac{1}{2}}+5\,28\right]}{\left(\frac{167-.816Z^2}{5773\,5}+4388\,5\right)^{\frac{1}{2}}+6\,84}$$

Lastly,

$$\Phi_{Pencel}(\Delta V, Z)=\frac{d\psi}{dg_p(\Delta V, Z)}$$

where $g_p(\Delta V,Z)$ is defined by Equation 16.

We also note that if ψ is the measured pressure, we can see that ψ as a function of Z is dependant on the deformation. We have have already found $\delta(\Delta V,Z)$

$$\psi_r=\frac{\psi\left(r_o^2+\frac{3}{2}\frac{\Delta V}{\pi L}\right)^{\frac{1}{2}}}{\frac{1}{L}\left[\left(r_o^2+\frac{3}{2}\frac{\Delta V}{\pi L}\right)L^2-\frac{6\Delta VZ^2}{\pi L}\right]^{\frac{1}{2}}} \tag{17}$$

then

$$\phi(\Delta V, Z)=\frac{d\psi}{dg_p(\Delta V, Z)}$$

ψr can be further simplified for a specific instrument:

$$\psi_r = \frac{\psi\,(16.6 + .089\,\Delta V)^{\frac{1}{2}}}{\left[(2533.7 + 13.65\,\Delta V) - 067\Delta V Z^2\right]^{\frac{1}{2}}} \tag{18}$$

Houlsby found:

$$\frac{\psi}{\sigma_r} = \left[\frac{r_o}{r_1}\right]^{N-1} \tag{19}$$

where

$$N = \frac{1 - \sin\phi}{1 + \sin\phi} \rightarrow \phi = \text{angle of internal friction}$$

We substitute Equation 17 into Equation 19

$$\frac{\psi_r}{\sigma_r} = \left[\frac{r_o}{r_1}\right]^{N-1} \tag{20}$$

This implies

$$\psi_r \left[\frac{r_o}{r_1}\right]^{1-N} = \sigma_r$$

and that σ_r is not only dependant on ϕ measured but also on ΔV and Z which figure in Equation 17.

If Equation 18 is inserted into Equation 19, we have a version of Equation 20 which is particular to thge pencel pressuremeter.

APPENDIX E

SCANNING ELECTRON MICROSCOPE DATA
FOR MINERALOGICAL INVESTIGATIONS

TN-5500 TRACOR NORTHERN CANADA WED 22-OCT-86 12:54

Cursor: 0.000keV = 0 ROI (21) 0 100:10 240

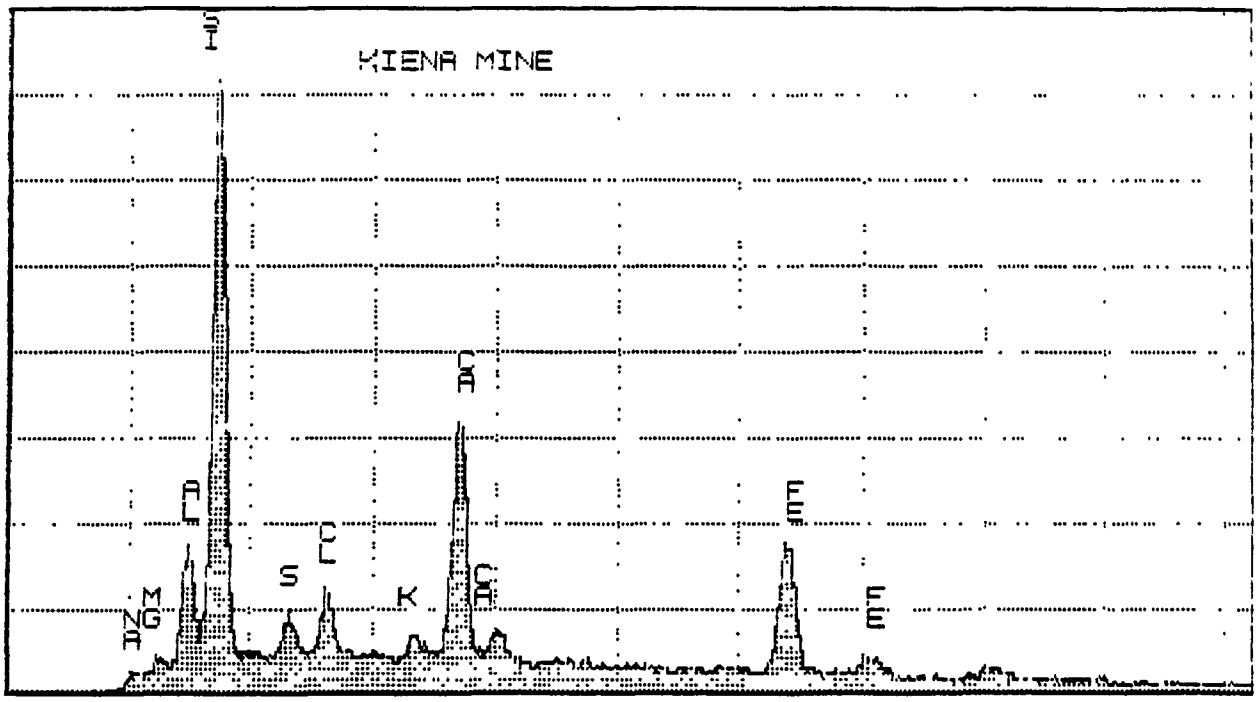

0.000 VFS = 2048 10 240

20 EXEC(6-E) DATA LABEL

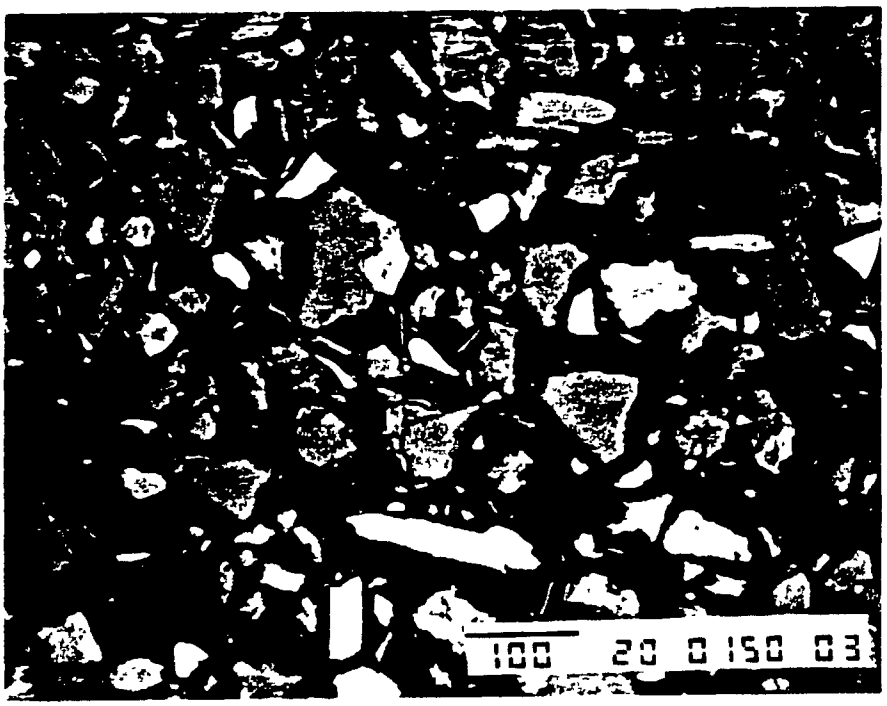

TN-5500 TRACOR NORTHERN CANADA FRI 24-OCT-86 09:49

Cursor: 0 300keV = 0 ROI (T) 0 000:10 240=130995

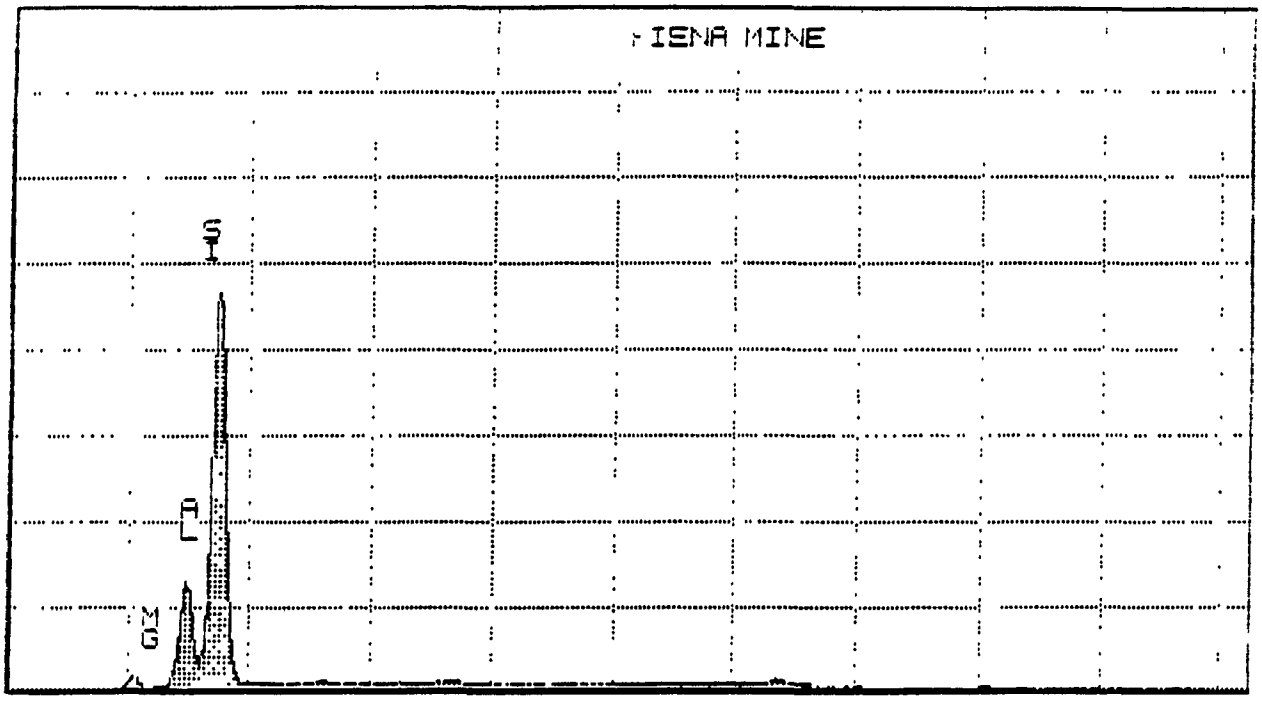

0 000 VFS = 16384 10 240

20 E/EC(6-E) DATA LABEL

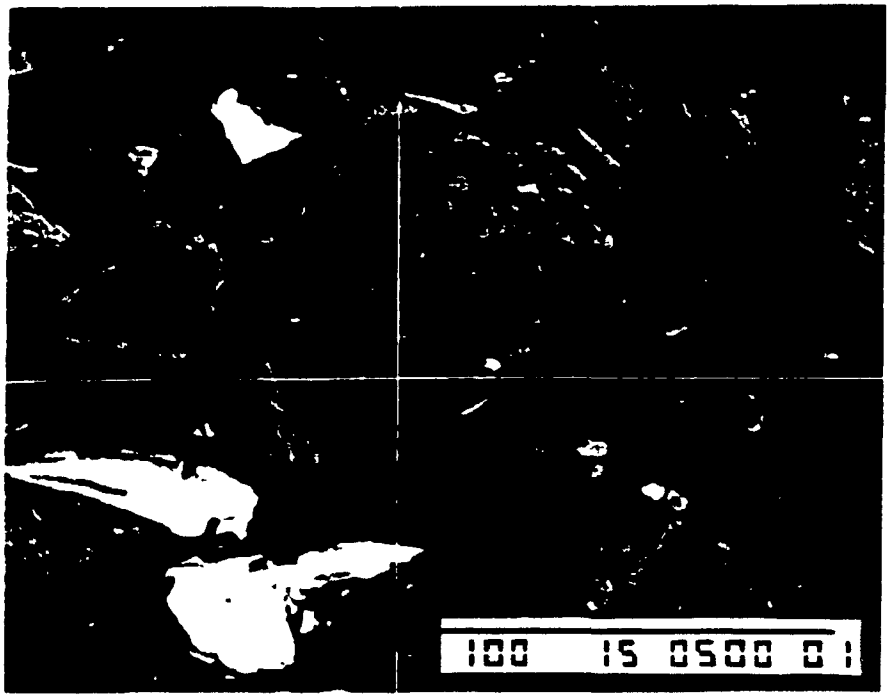

TN-2500 TRACOR NORTHERN CANADA FRI 24-OCT-86 09:40

Cursor: 0 000keV = 0 ROI (7) 0 000:10 240=207568

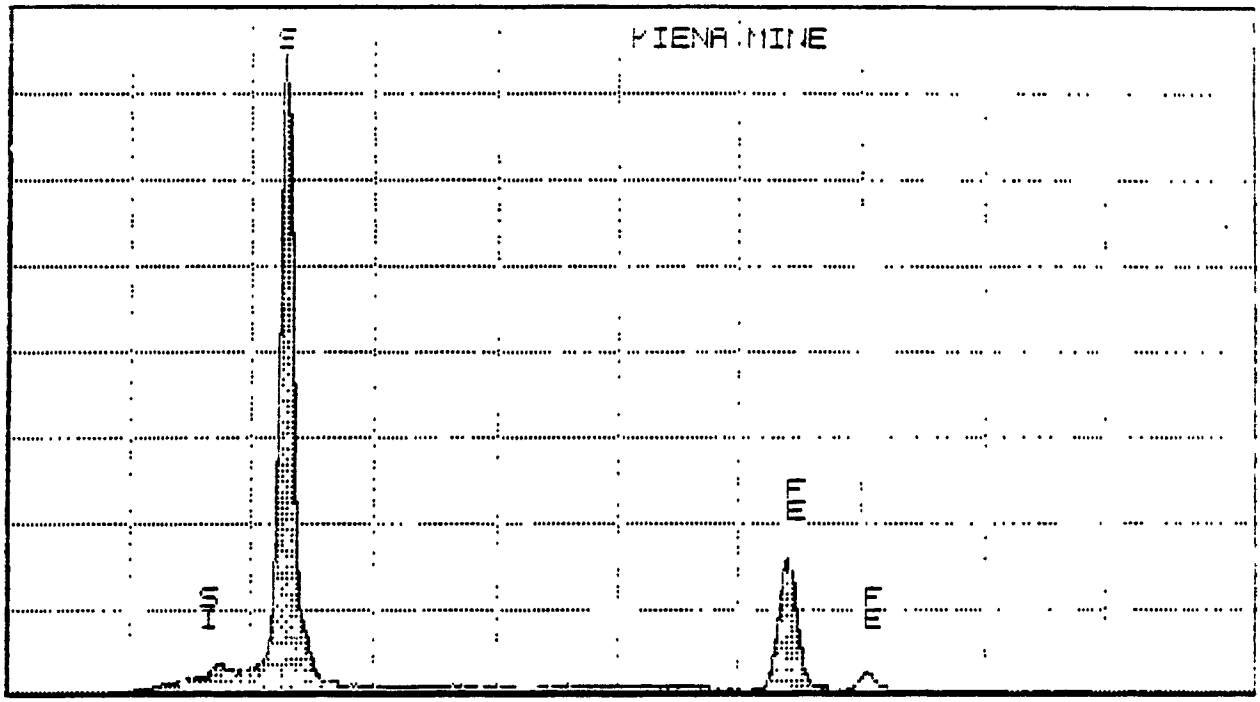

0 000 VFS = 16384 10 240

20 EXEC(6-E) DATA LABEL

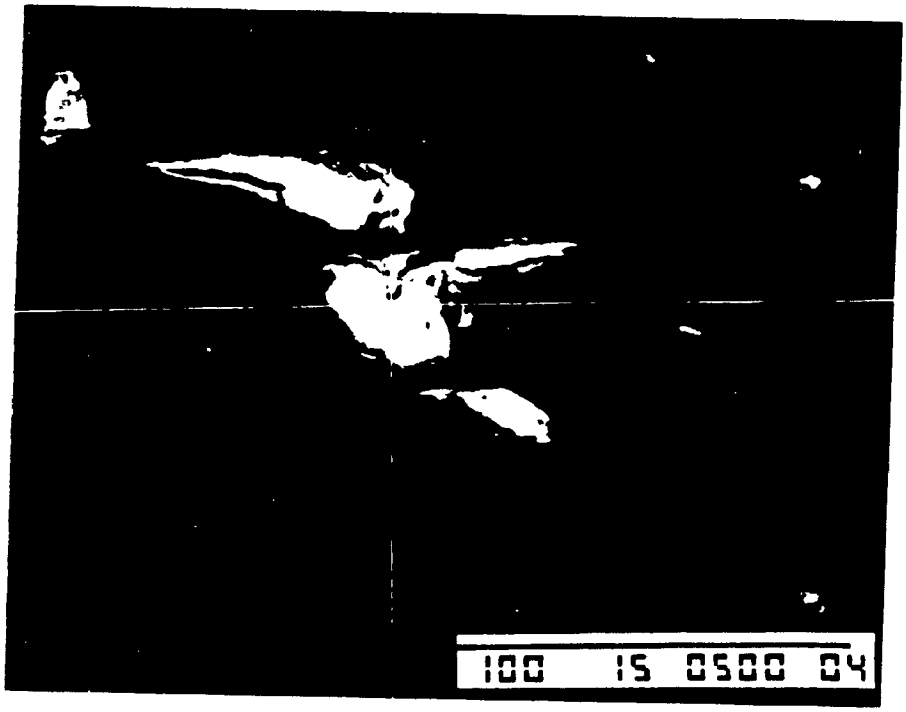

TN-5500 TRACOR NORTHERN CANADA FRI 24-OCT-86 06:02

Cursor: 0 000keV = 0 ROI CT: 0 000:10 240=69784

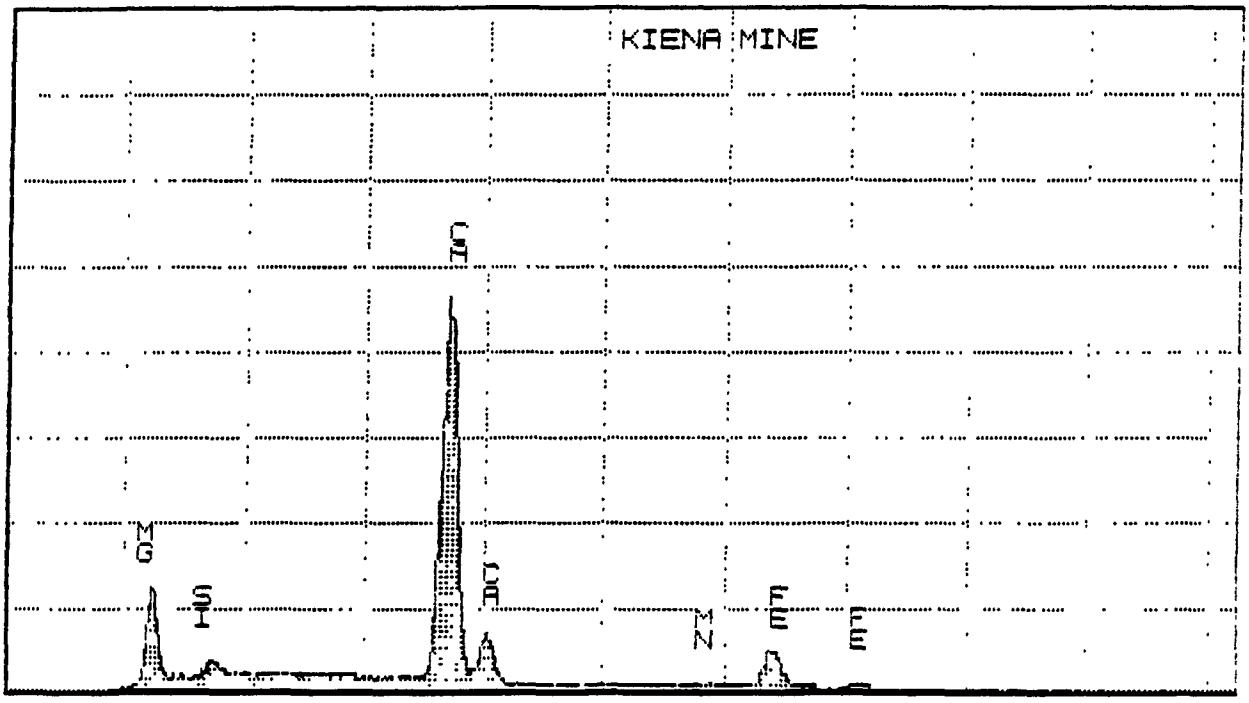

0 000 VFS = 8192 10 240

20 EXEC(6-E) DATA LABEL

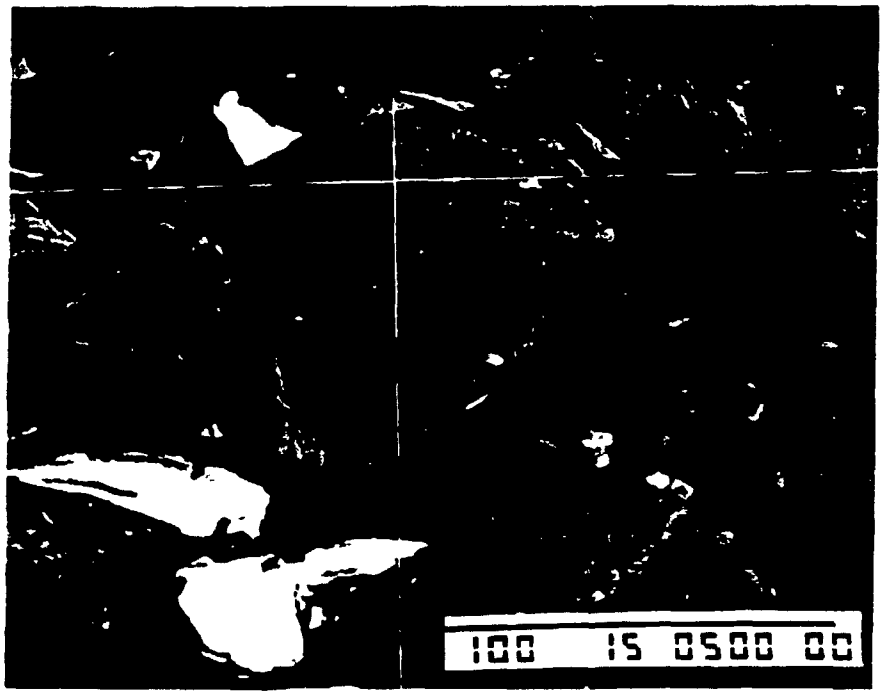

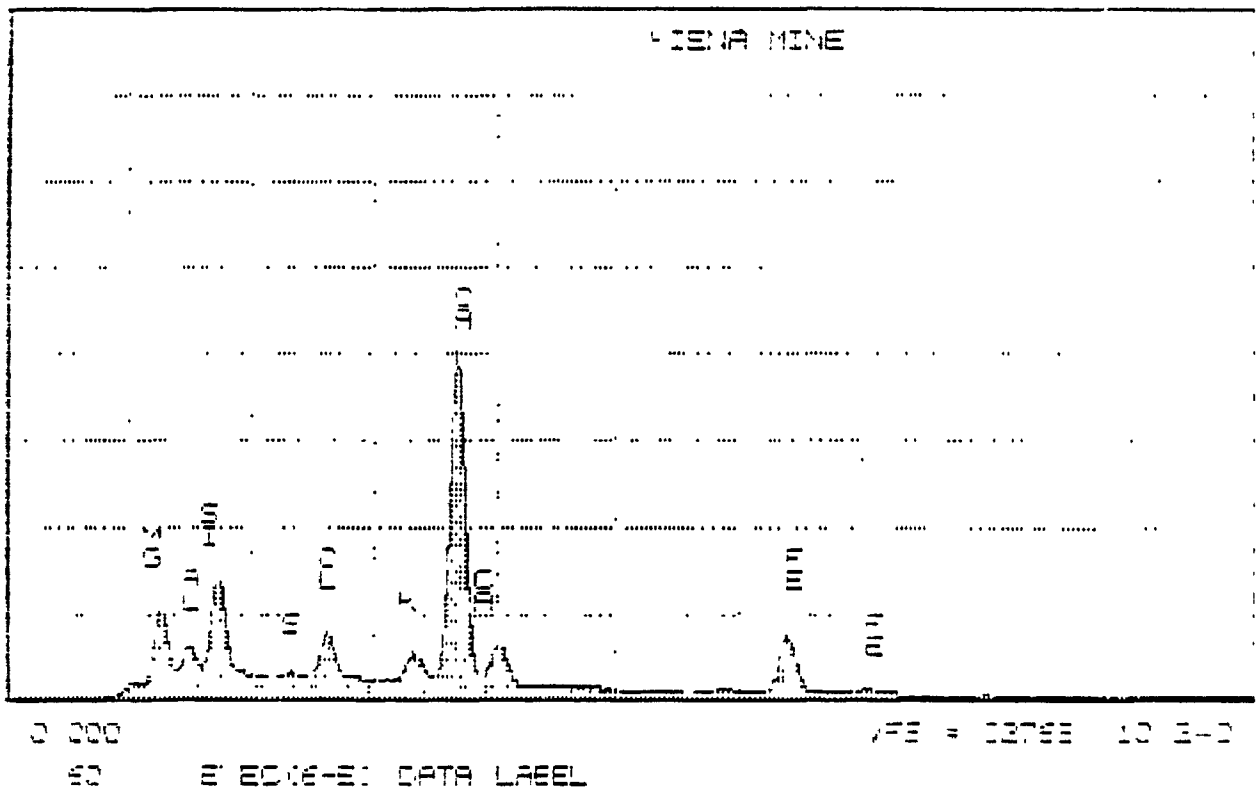
VIENA MINE
0.000
60

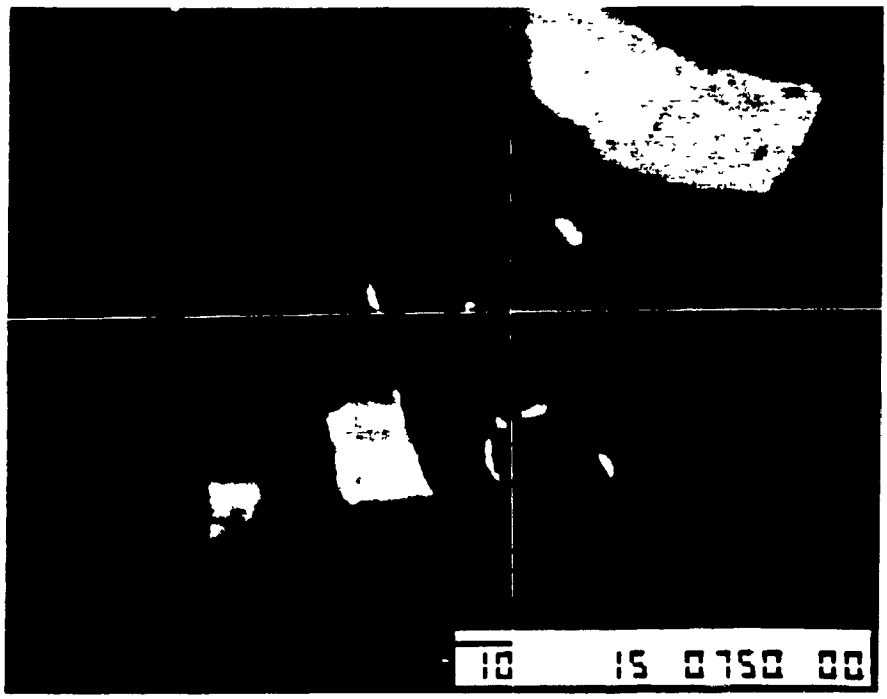
10 15 0750 00

TN-5500 TRACOR NORTHERN CANADA WED 22-OCT-86 11:26

Cursor: 0 000keV = 0 ROI (21) 0 100:10 240

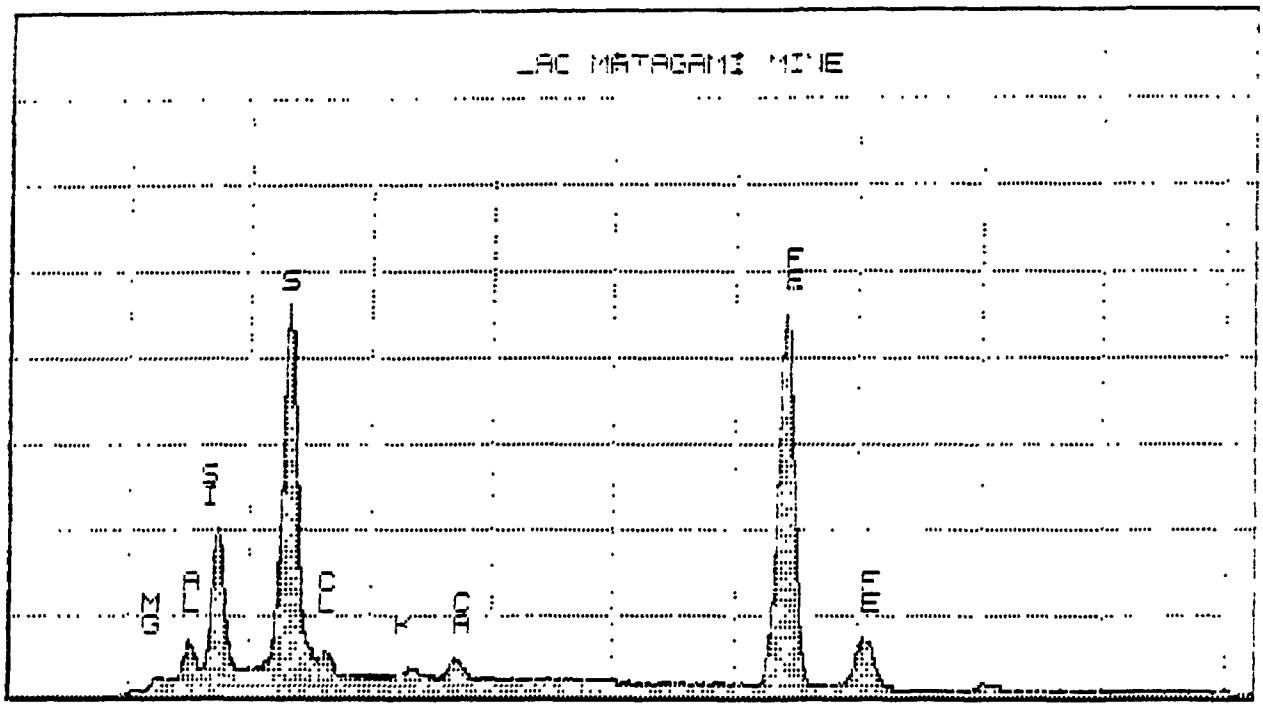

0 000 VFS = 8192 10 240

60 EXEC(6-E) DATA LABEL

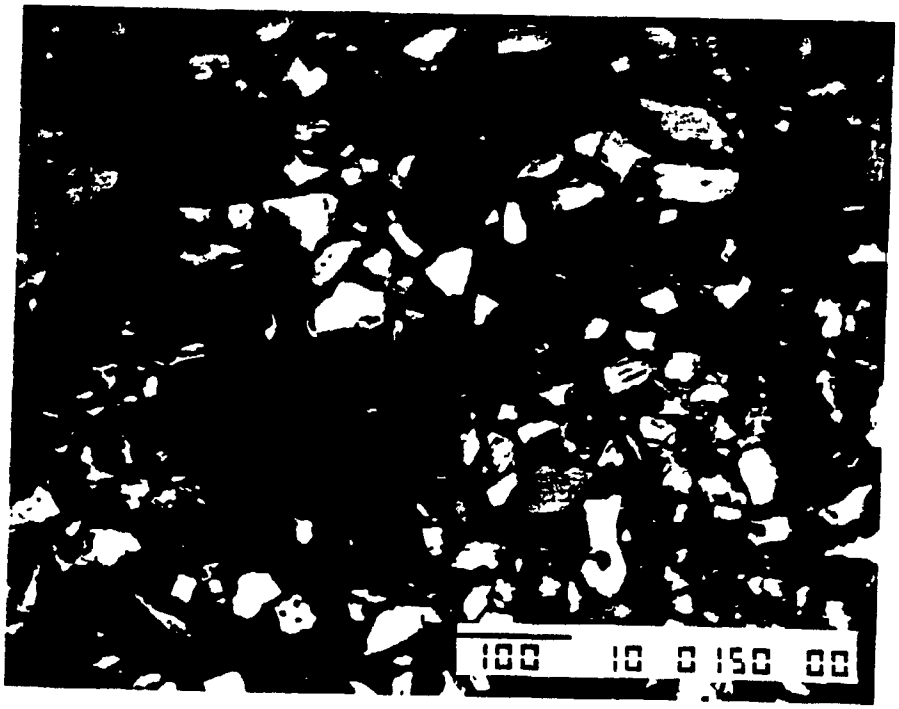

TN-5500 TRACOR NORTHERN CANADA WED 22-OCT-86 11:40

Cursor: 0.000keV = 0 ROI (21) 0 100:10.240

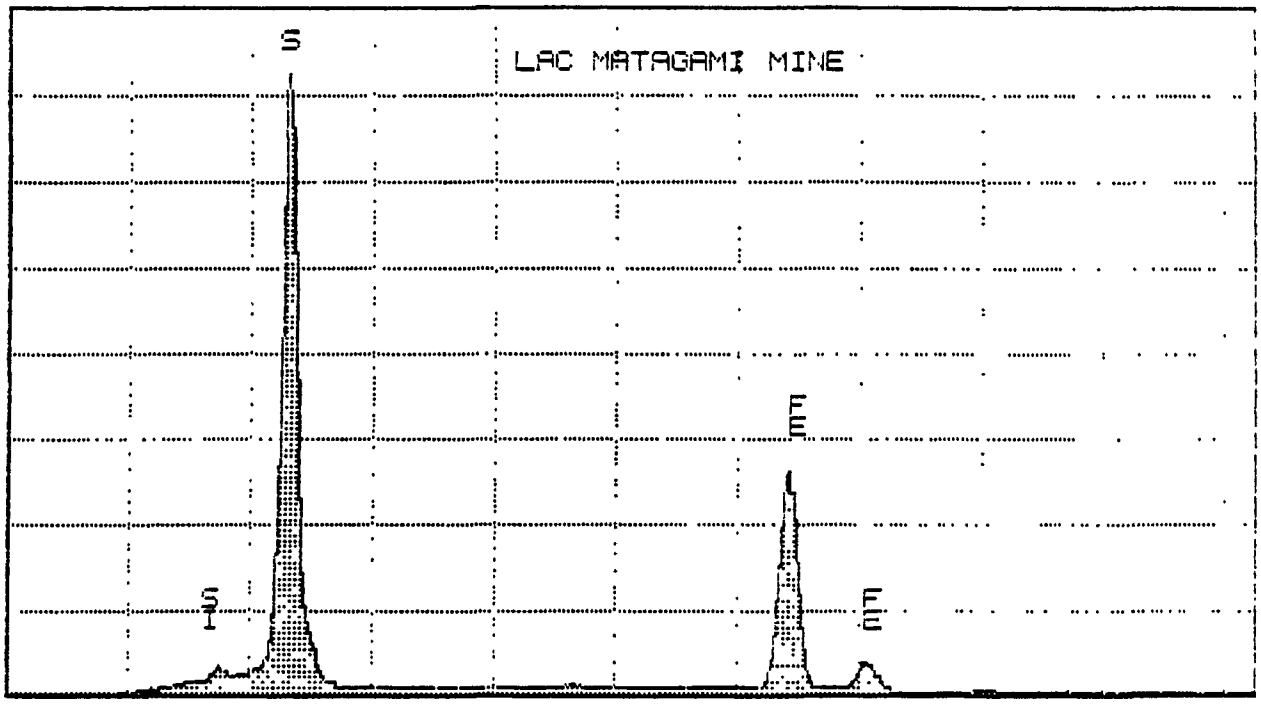

0.000 VFS = 16384 10.240

EXEC(6-E) DATA LABEL 30

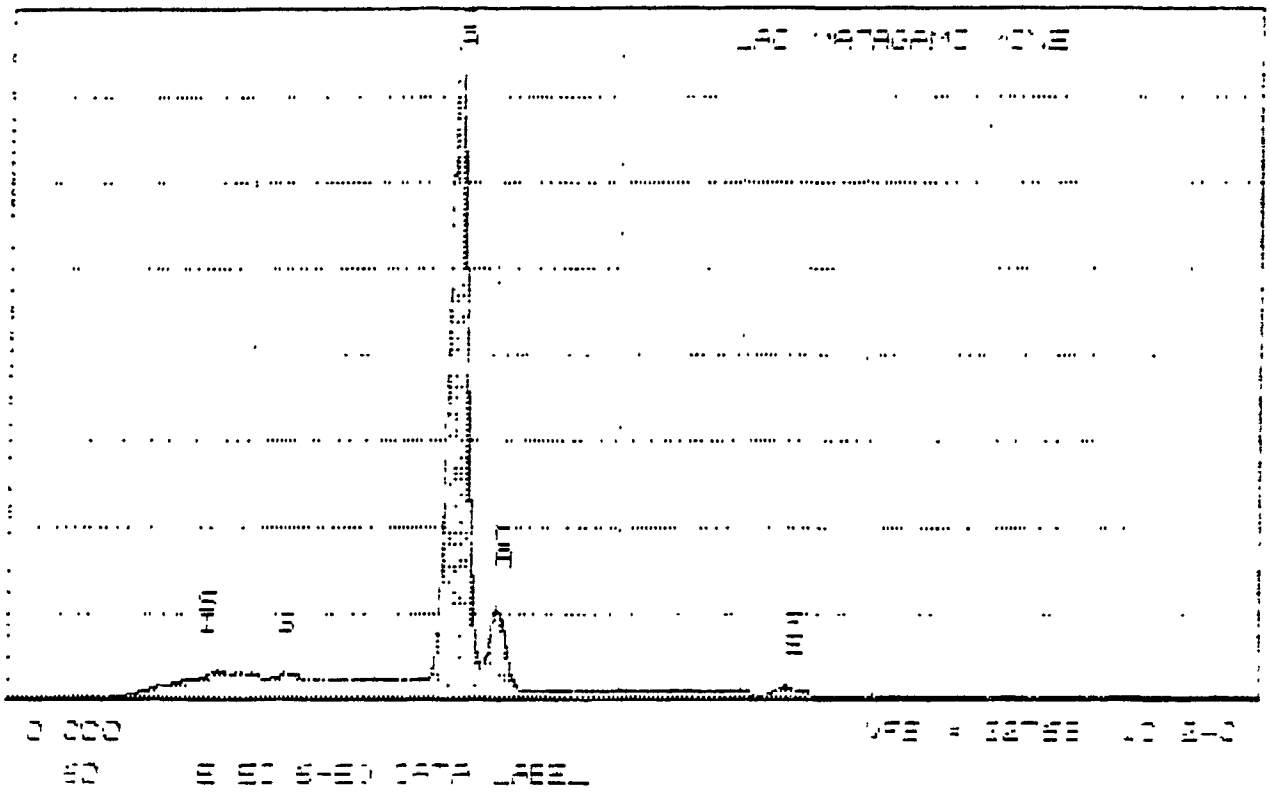

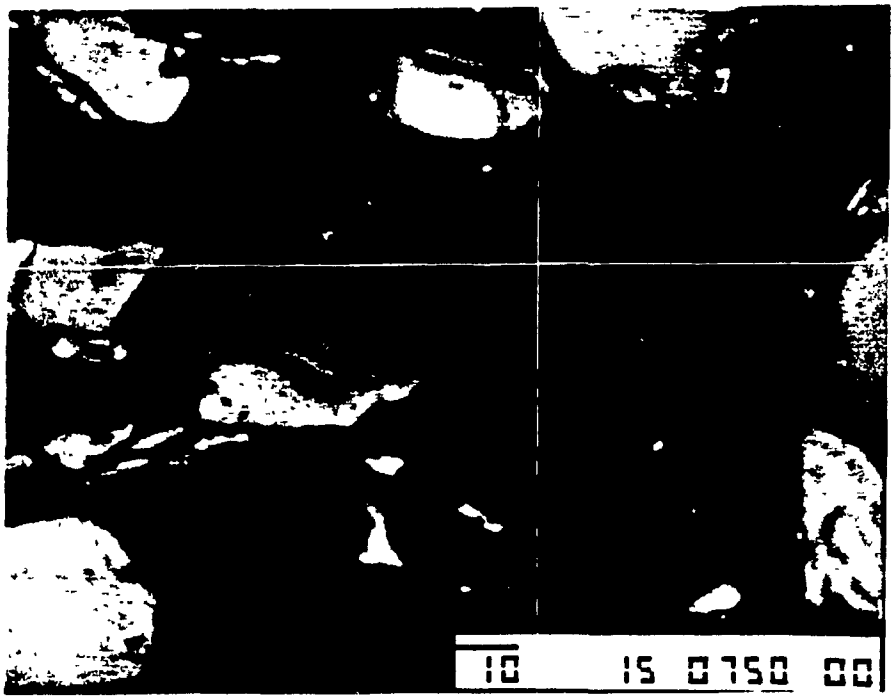
10 15 0750 00

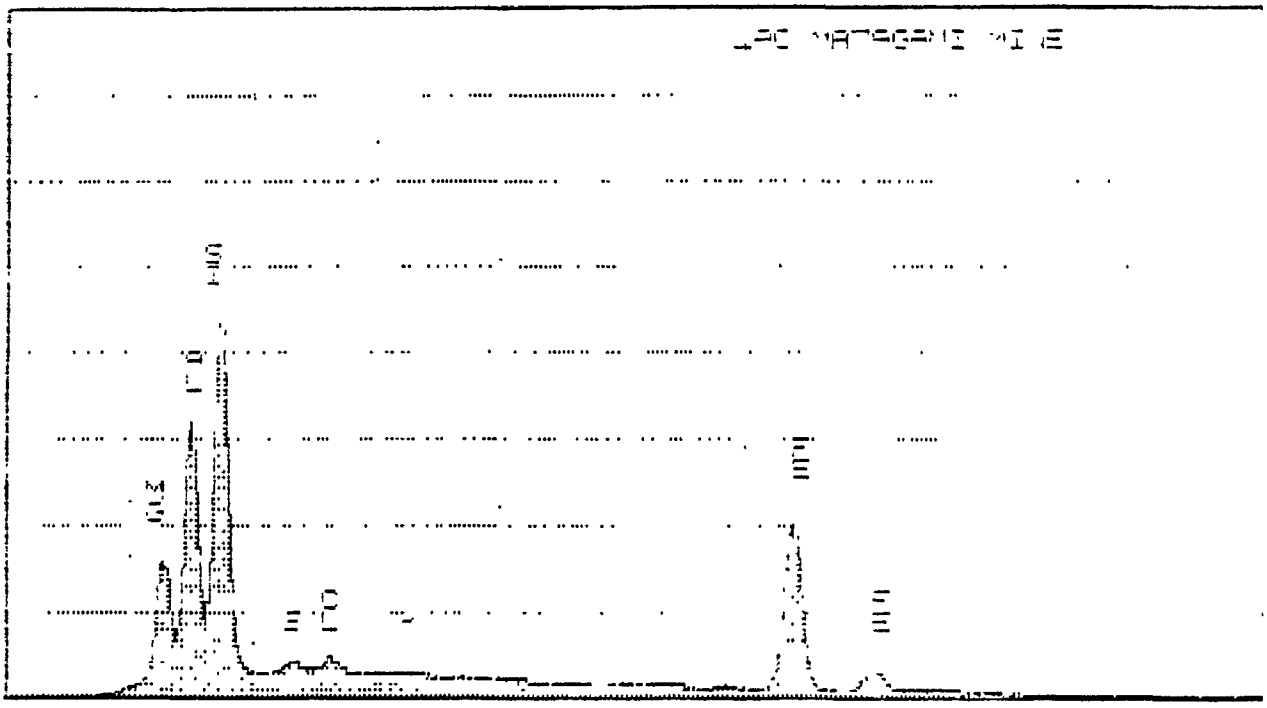

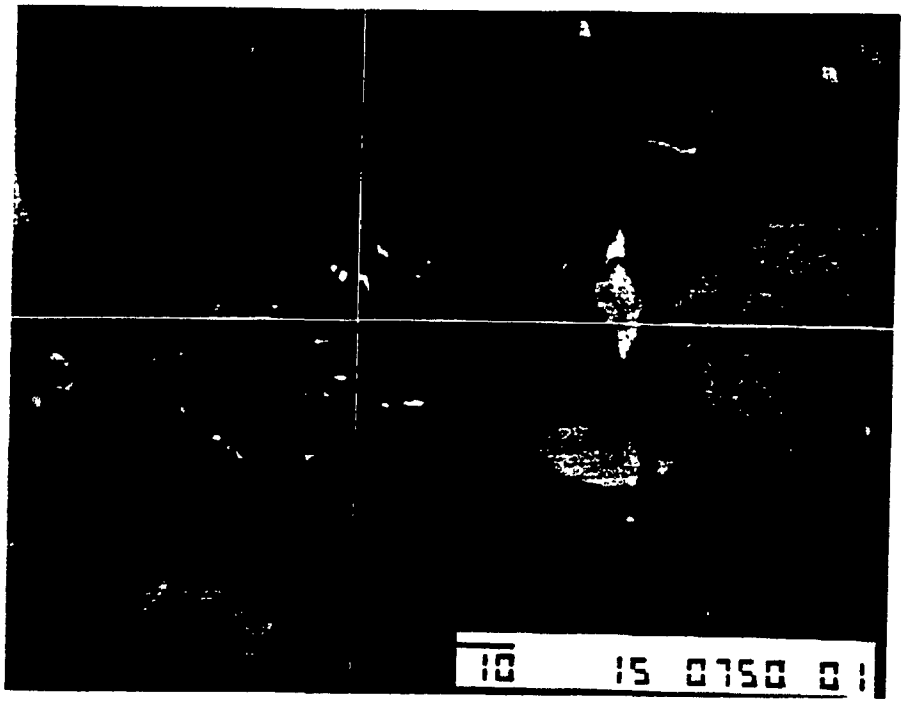
10 15 0750 01

TN-5500 TRACOR NORTHERN CANADA WED 22-OCT-86 11:51

Cursor: 0 000keV = 0 ROI (21) 0 100:10 240

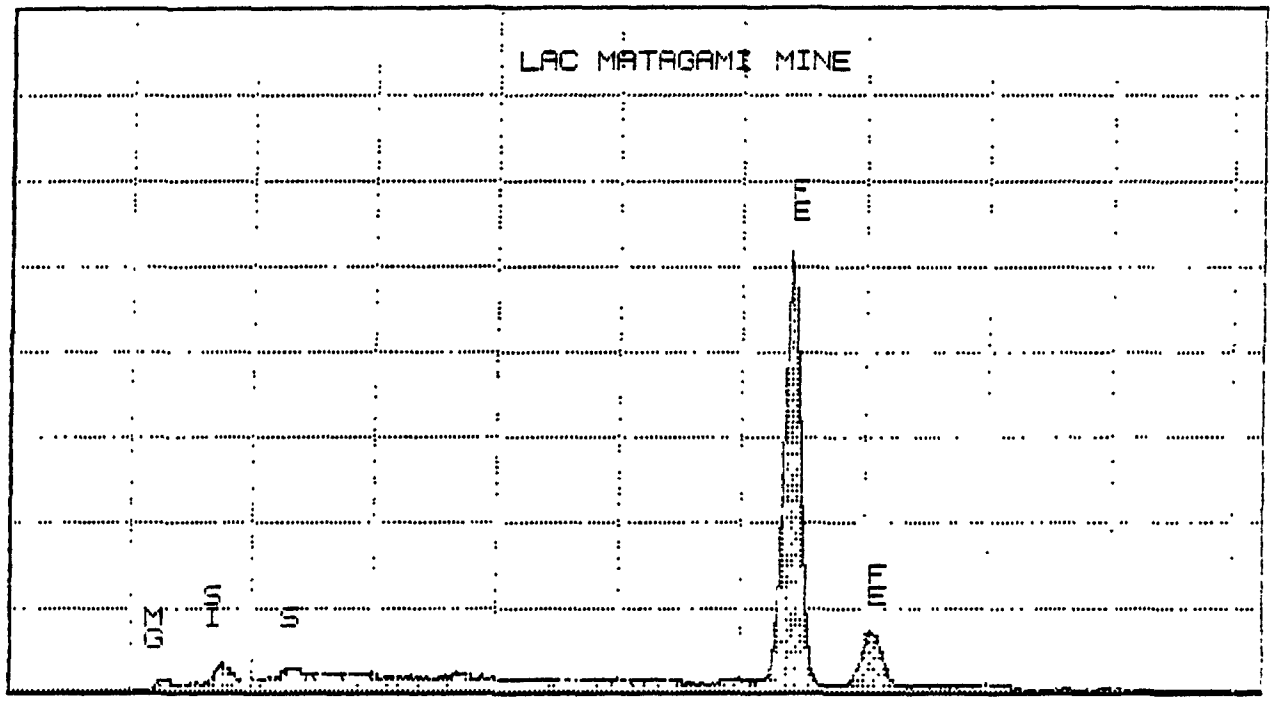

0.000 VFS = 0192 10.240

20 EXEC(6-E) DATA LABEL

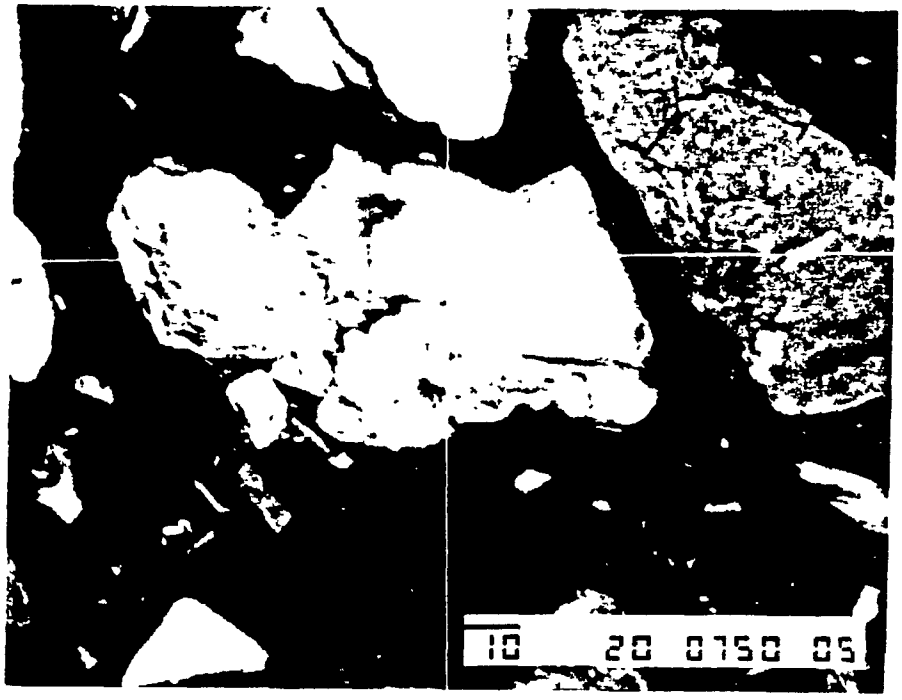

TN-5500 TRACOR NORTHERN CANADA WED 22-OCT-86 12:24

Cursor: 0 000keV = 0 ROI (21) 0 100:10 240

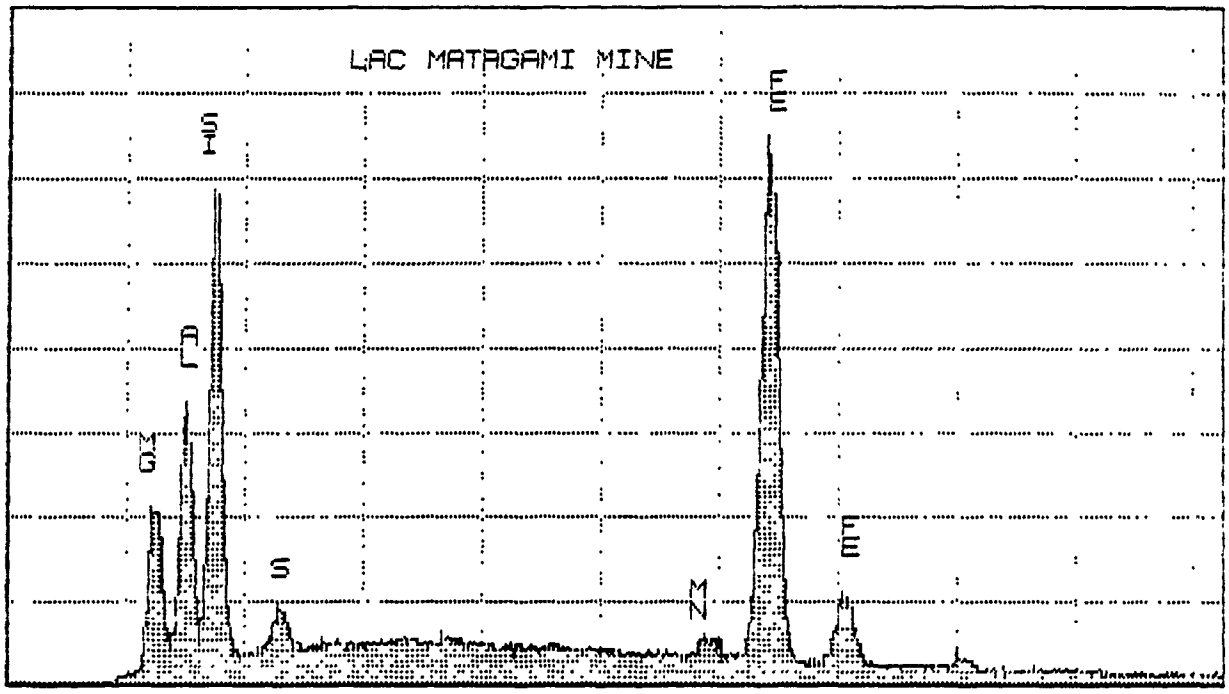

0 000 VFS = 2048 10 240

20 EXEC(6-E) DATA LABEL

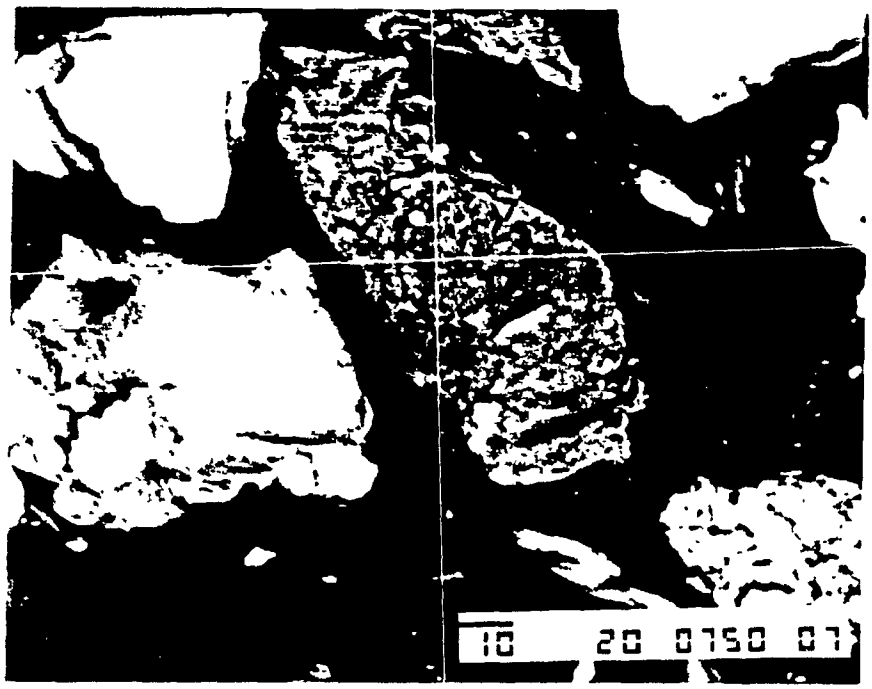

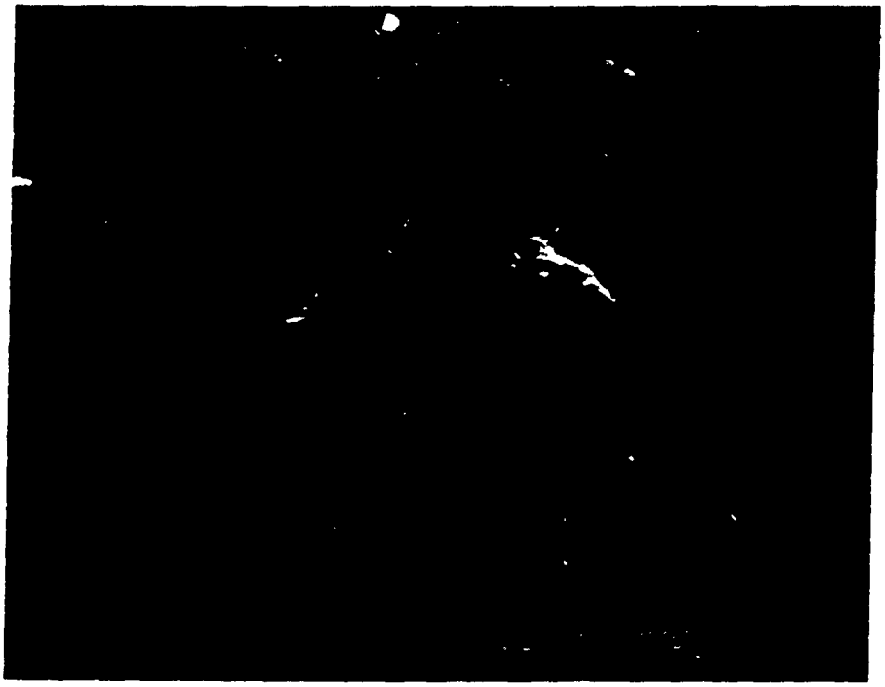

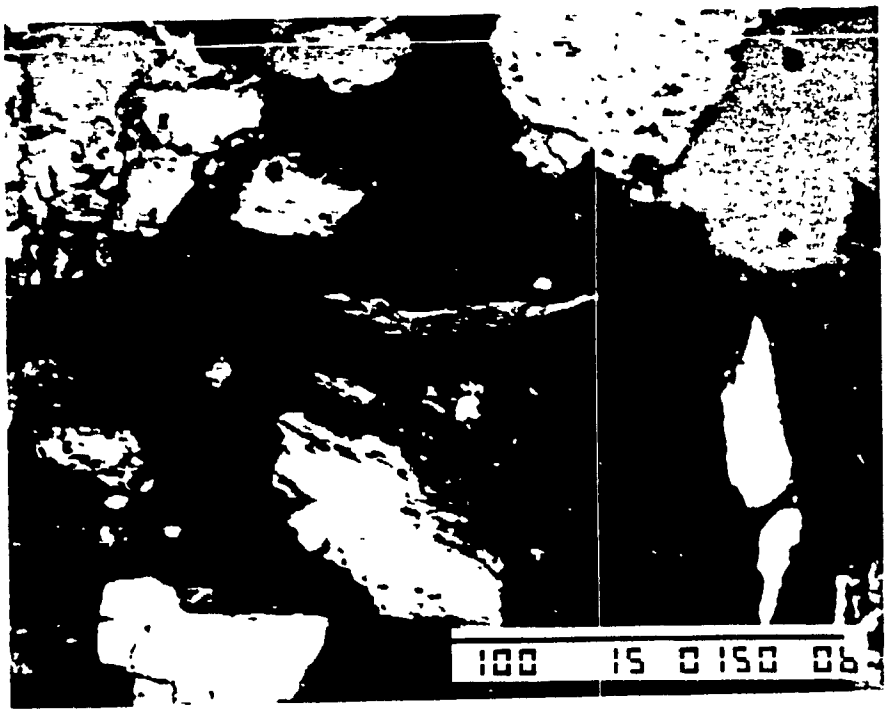
100 15 0150 06

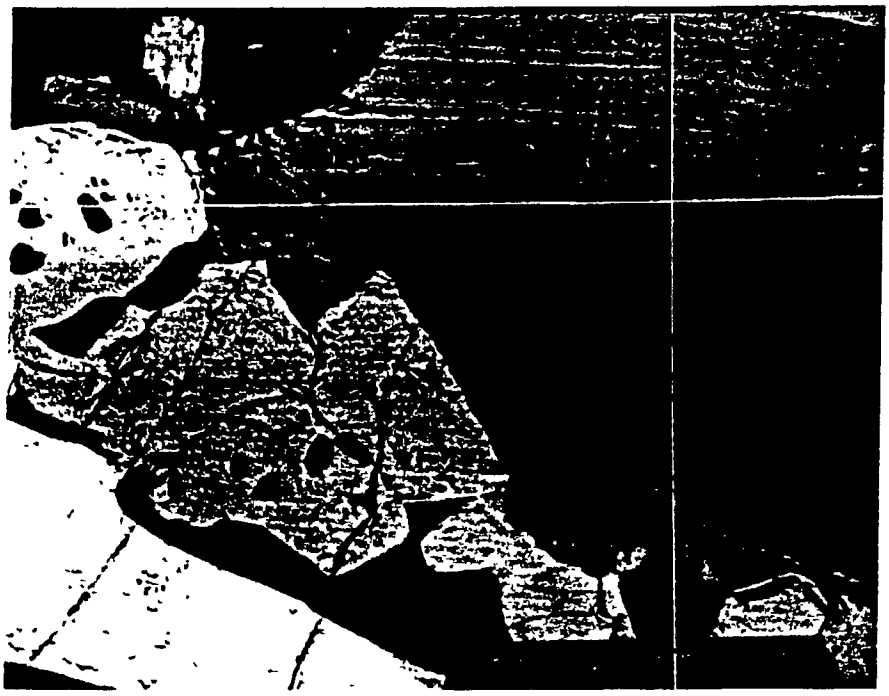

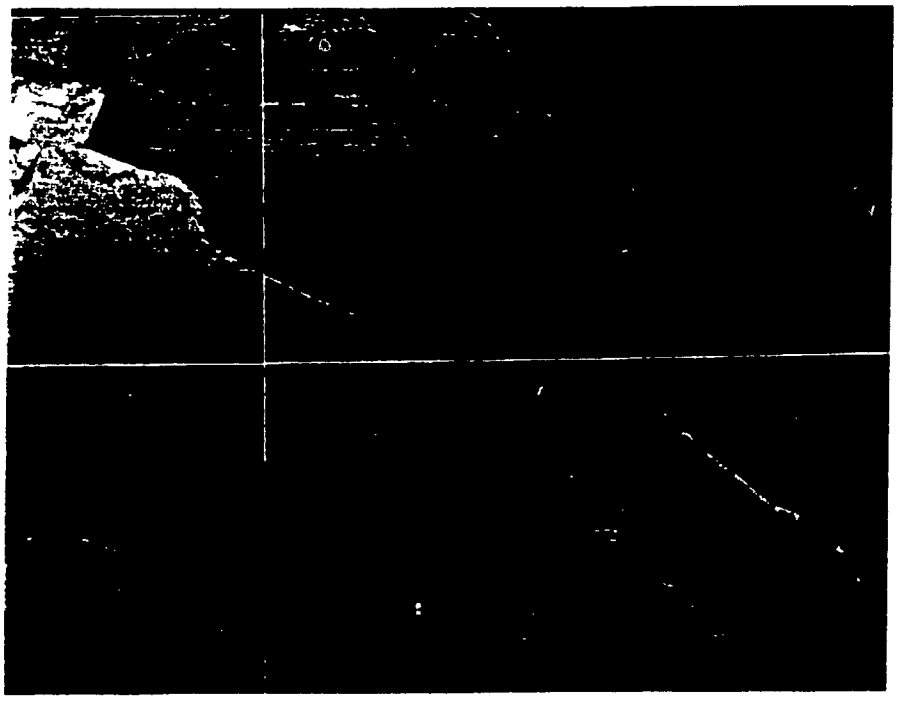

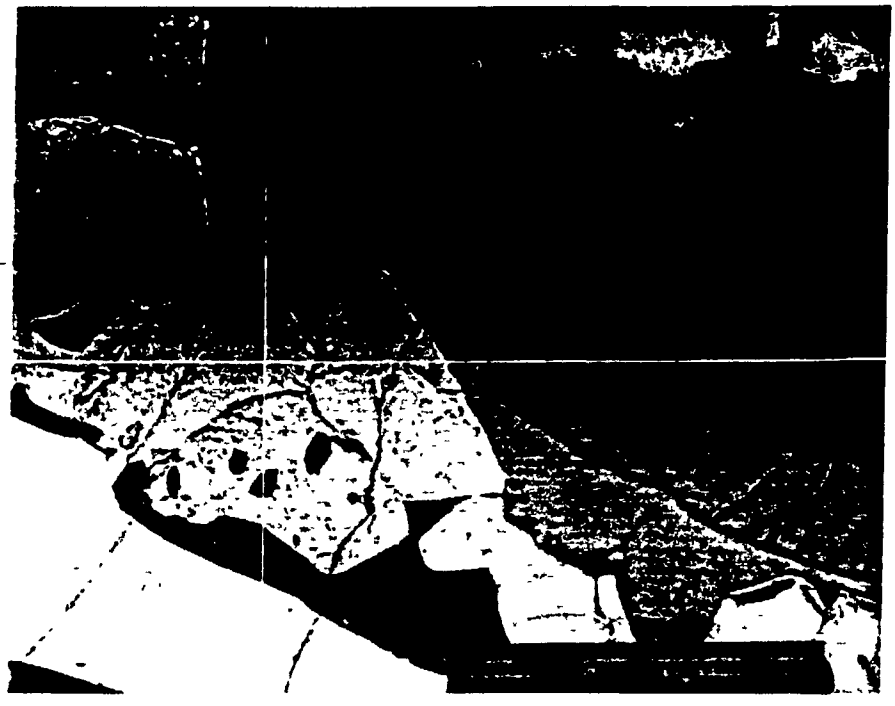

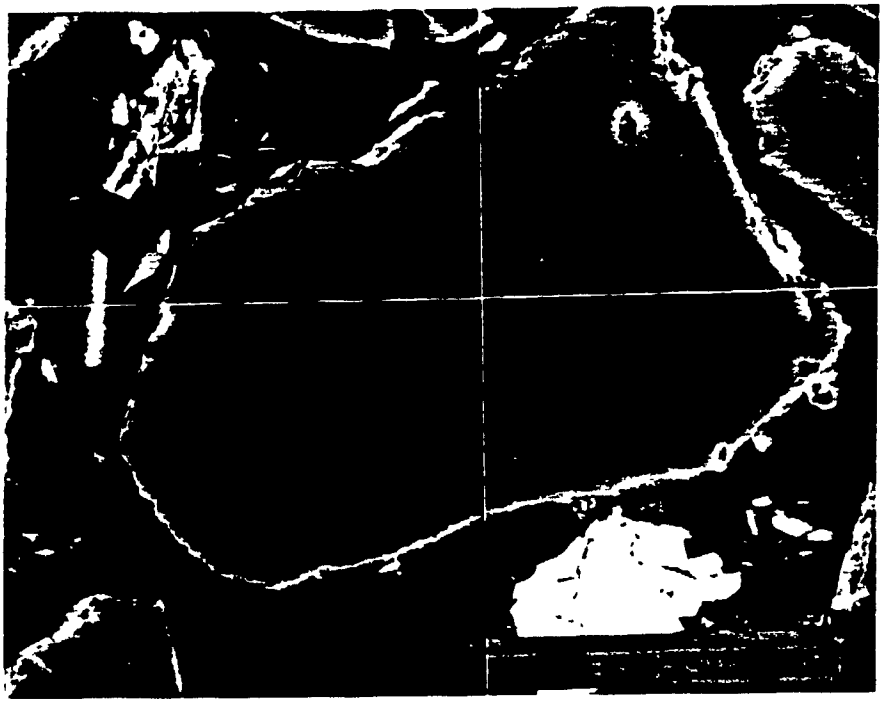

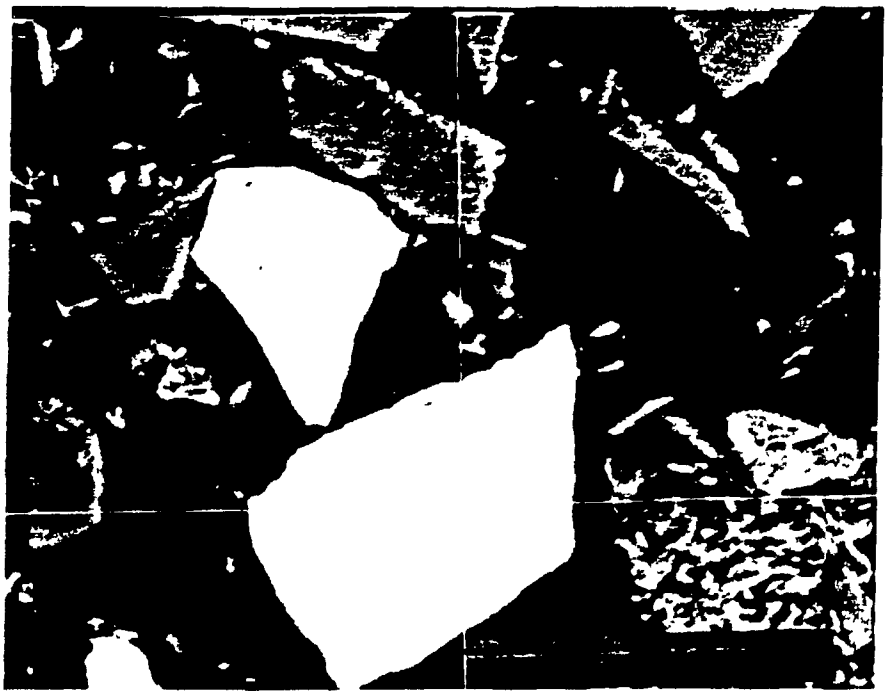

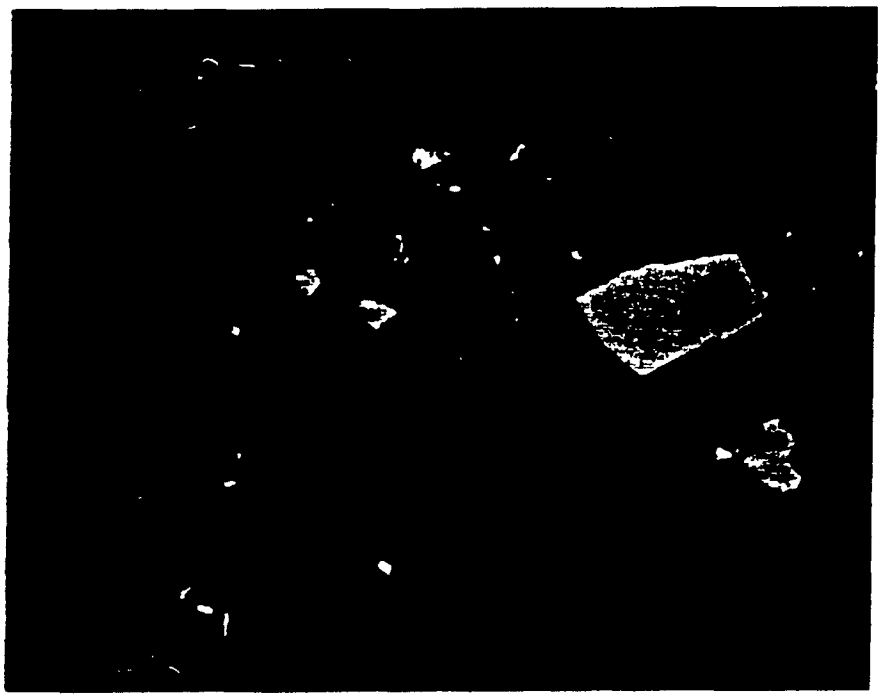

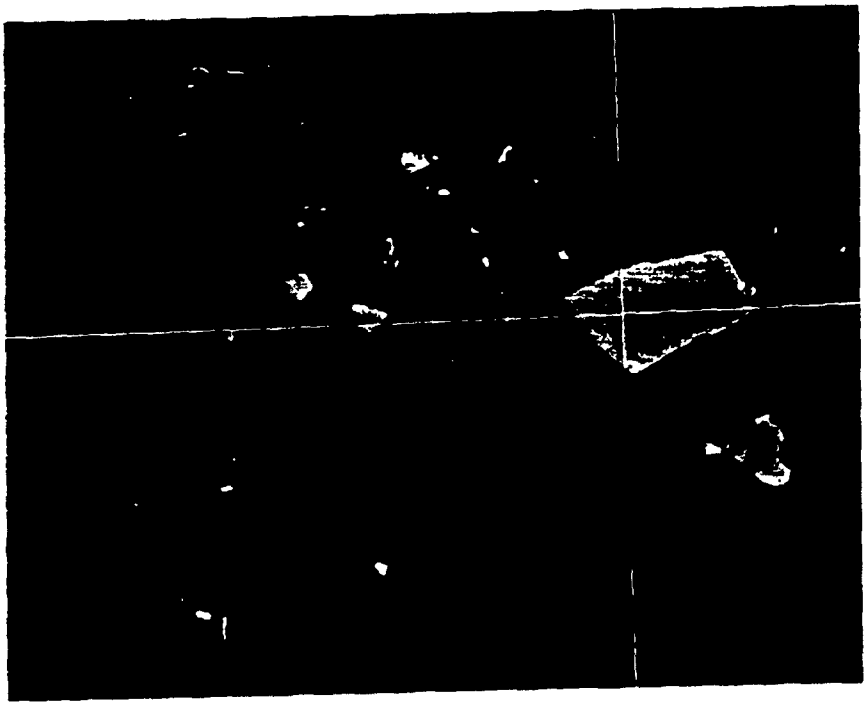

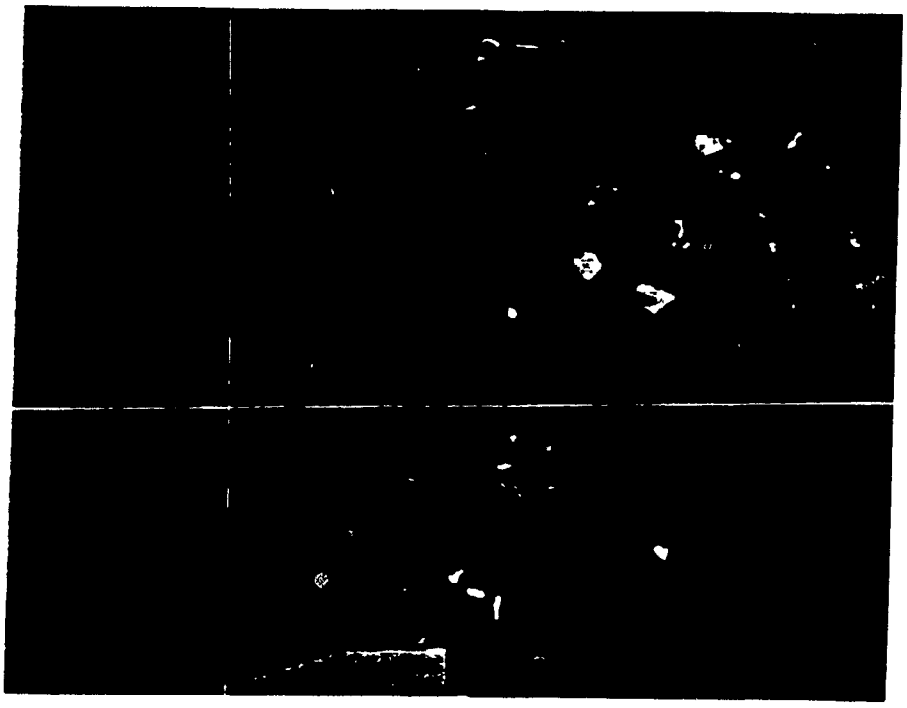

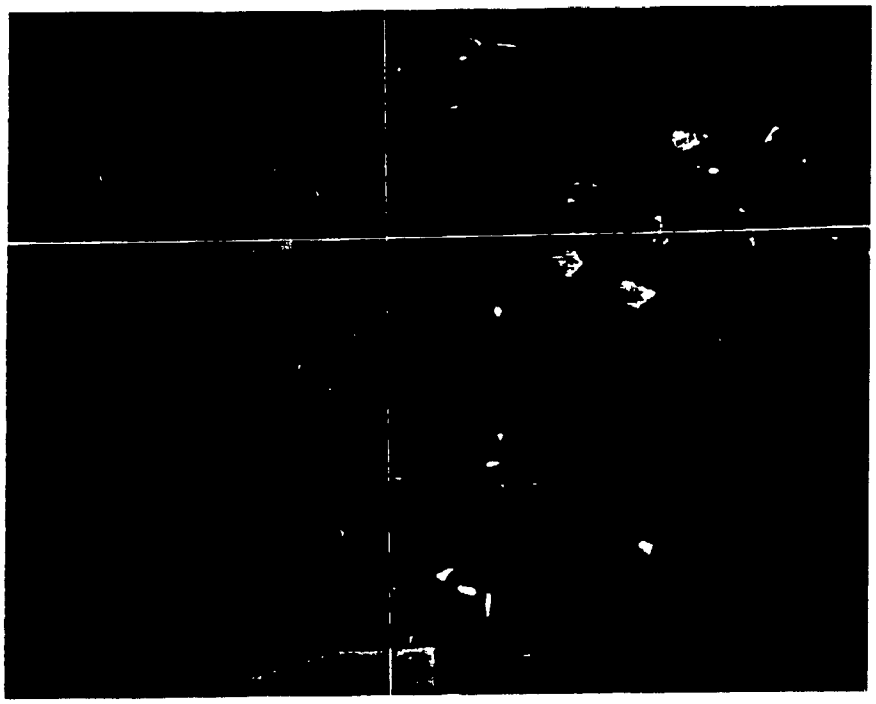

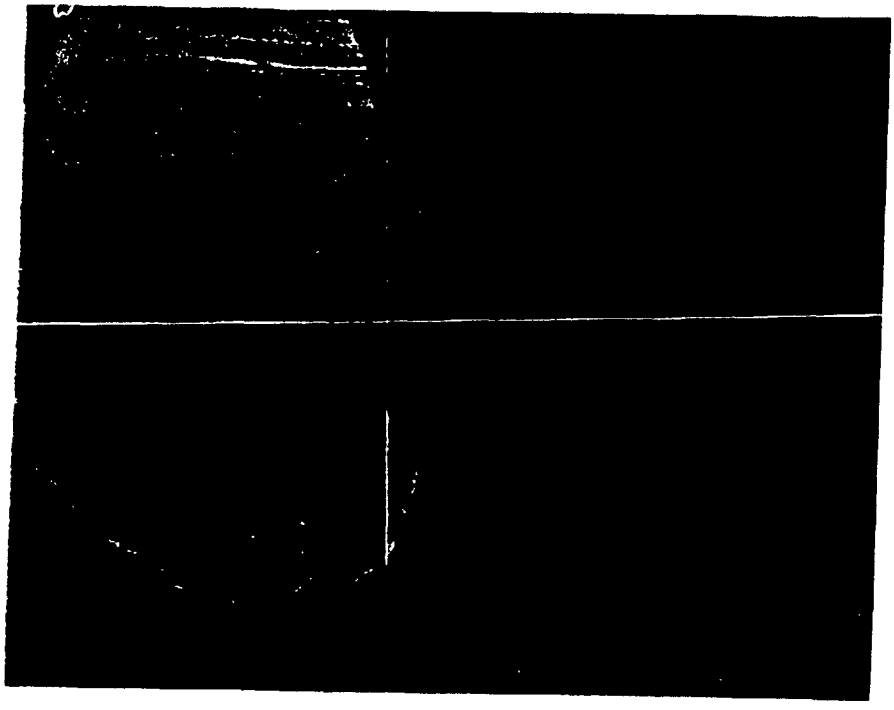

TN-5500 TRACOR NORTHERN CANADA FRI 24-OCT-86 09:05

Cursor: 0.000keV = 0 ROI CT: 0 200:10 240=1911140

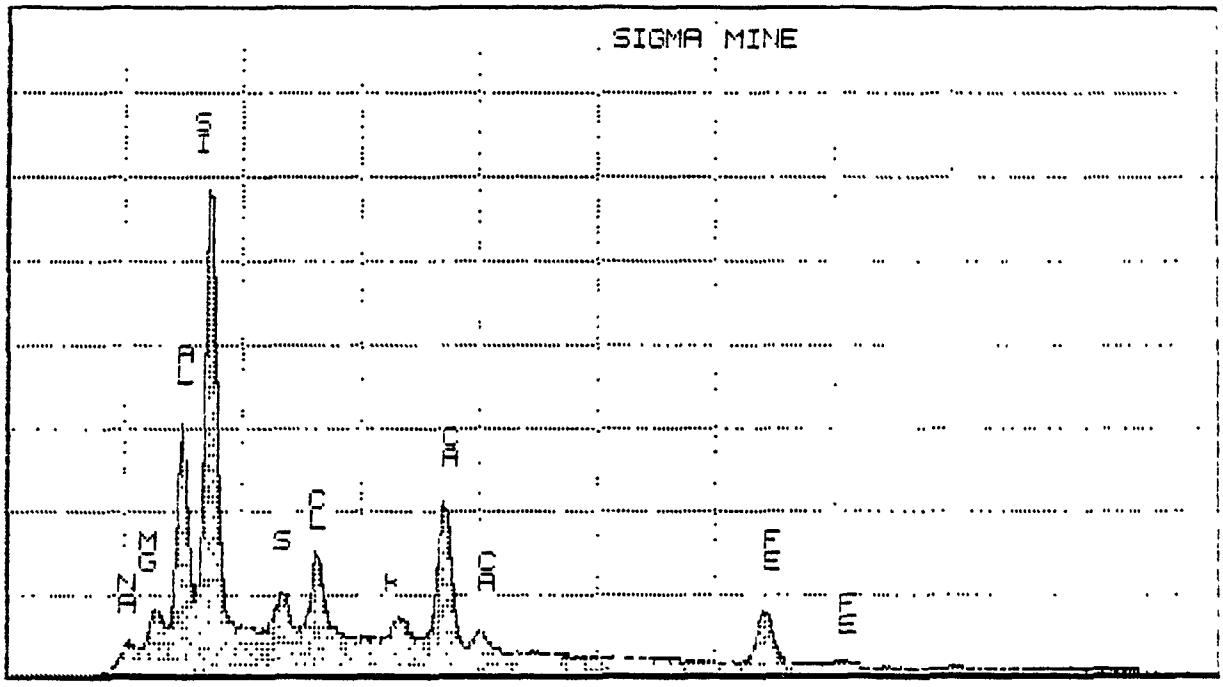

0.000 VFS = 8192 10.240

20 EXEC(6-E) DATA LABEL

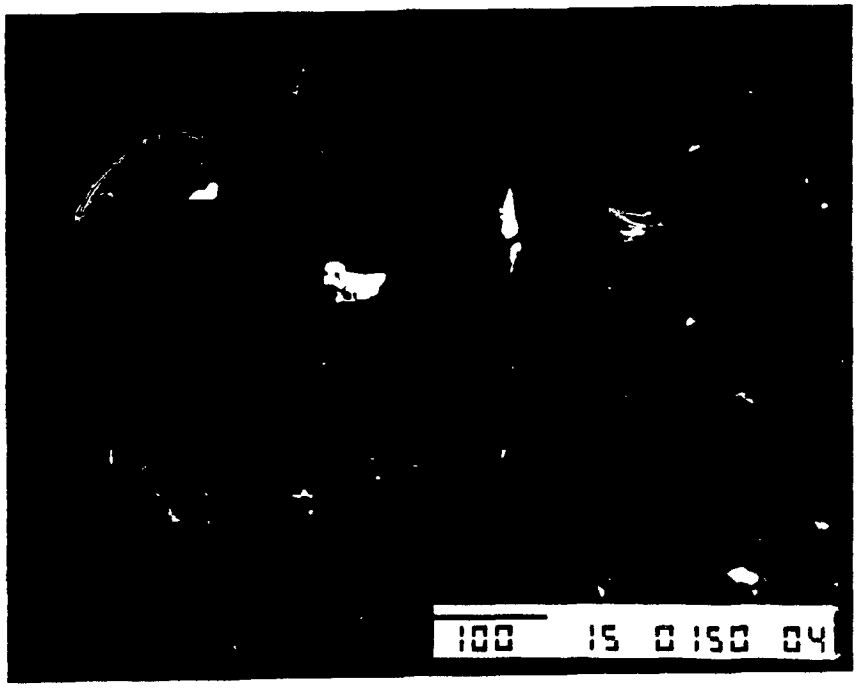

TN-5500 TRACOR NORTHERN CANADA FRI 24-OCT-86 10:05

Cursor: 0 000keV = 0 ROI (7) 0 000:10.240=115362

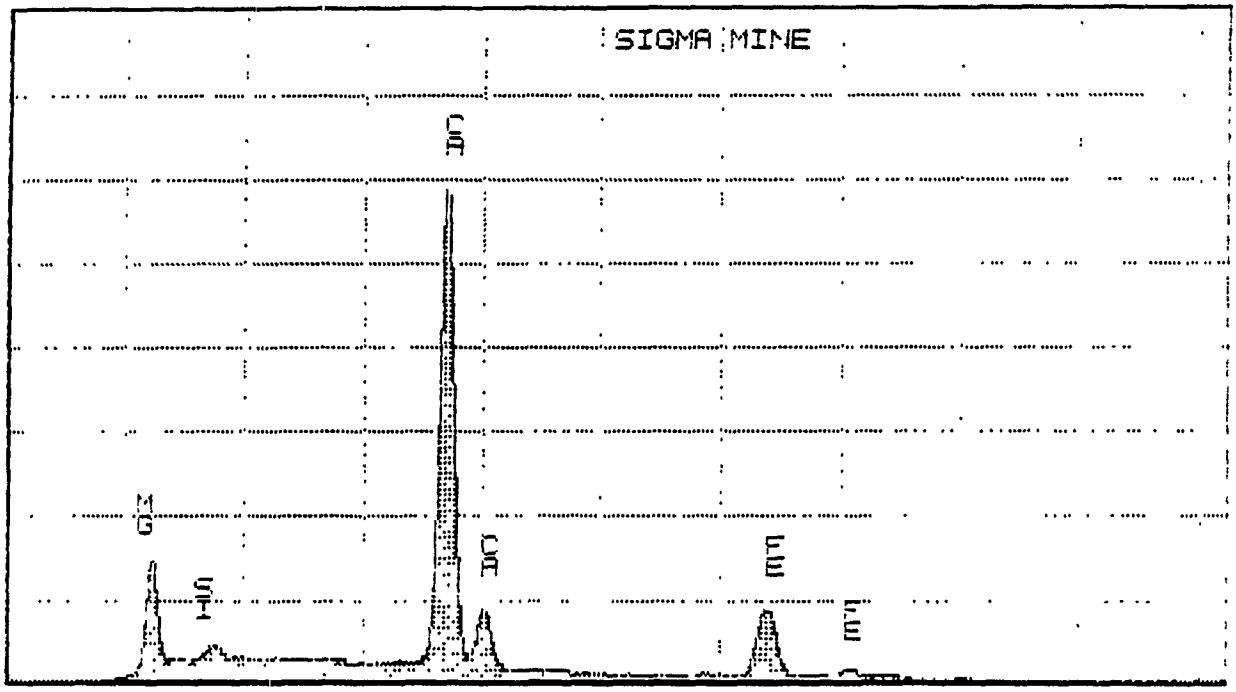

0 000 VFS = 8192 10 240

30 EXEC(6-E) DATA LABEL

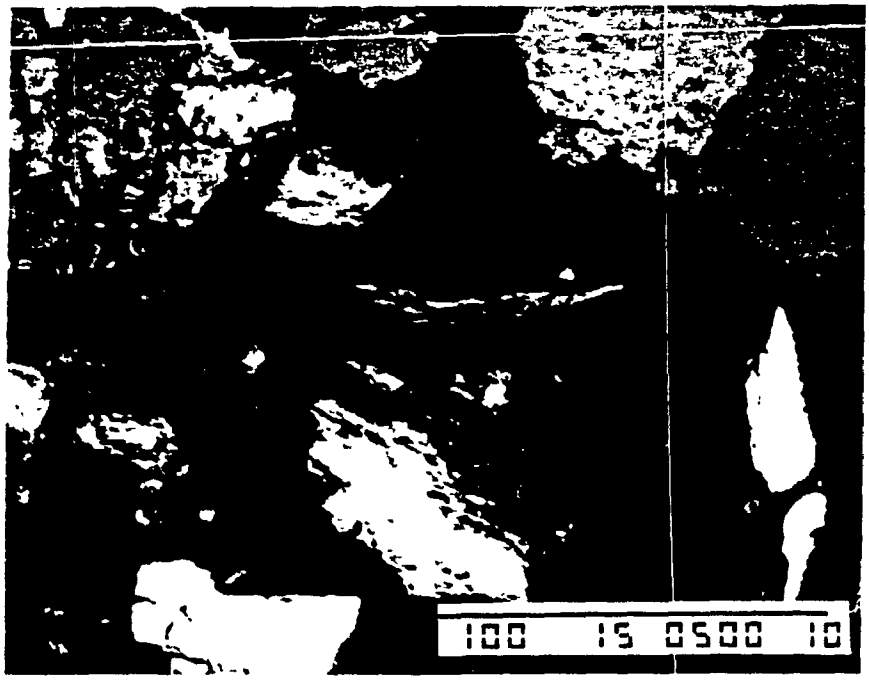

TN-5500 TRACOR NORTHERN CANADA FRI 24-OCT-86 09:50

Cursor: 0.000keV = 0 POI (T) 0 000:10.240=46C2T3

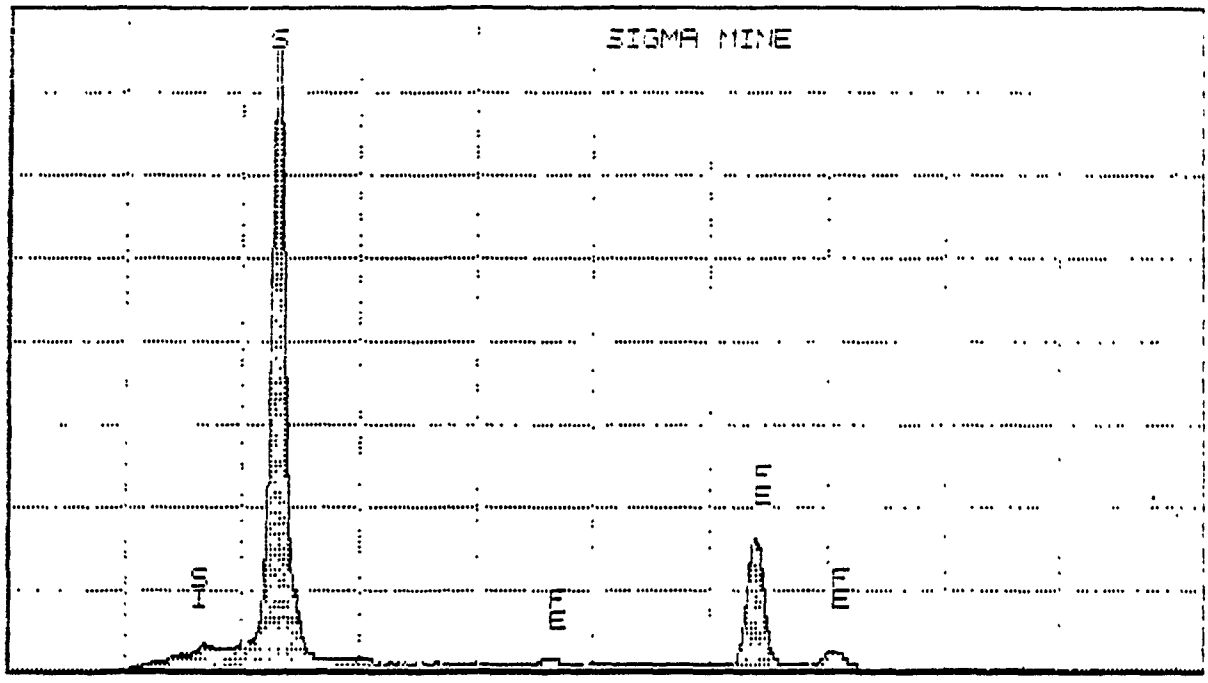

0 000 VFS = 12762 10 240

EXEC(S-E) DATA LABEL 20

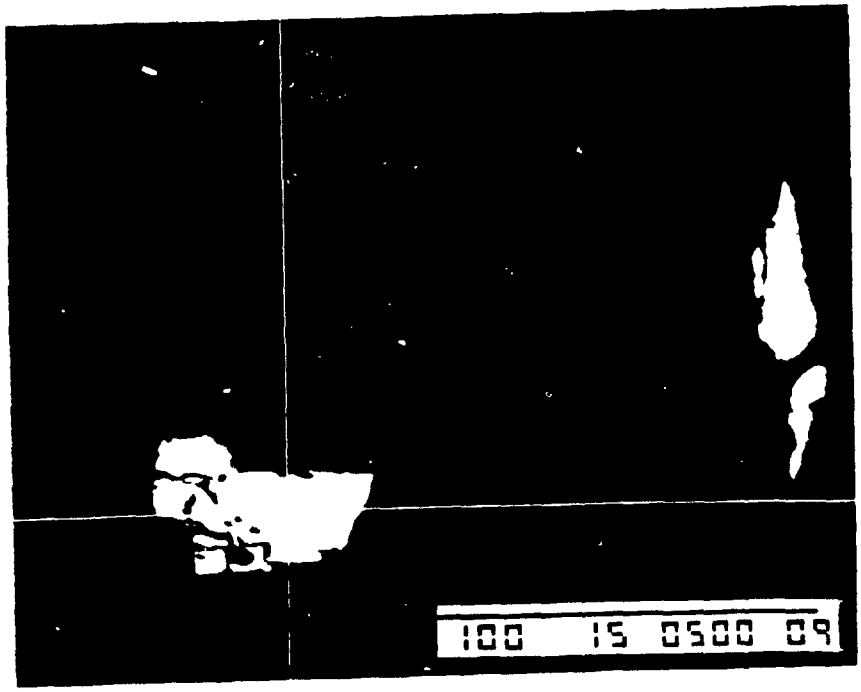

TN-5500 TRACOR NORTHERN CANADA FRI 24-OCT-86 09:46

Cursor: 0 000keV = 0 ROI (T) 0 000:10 240=250186

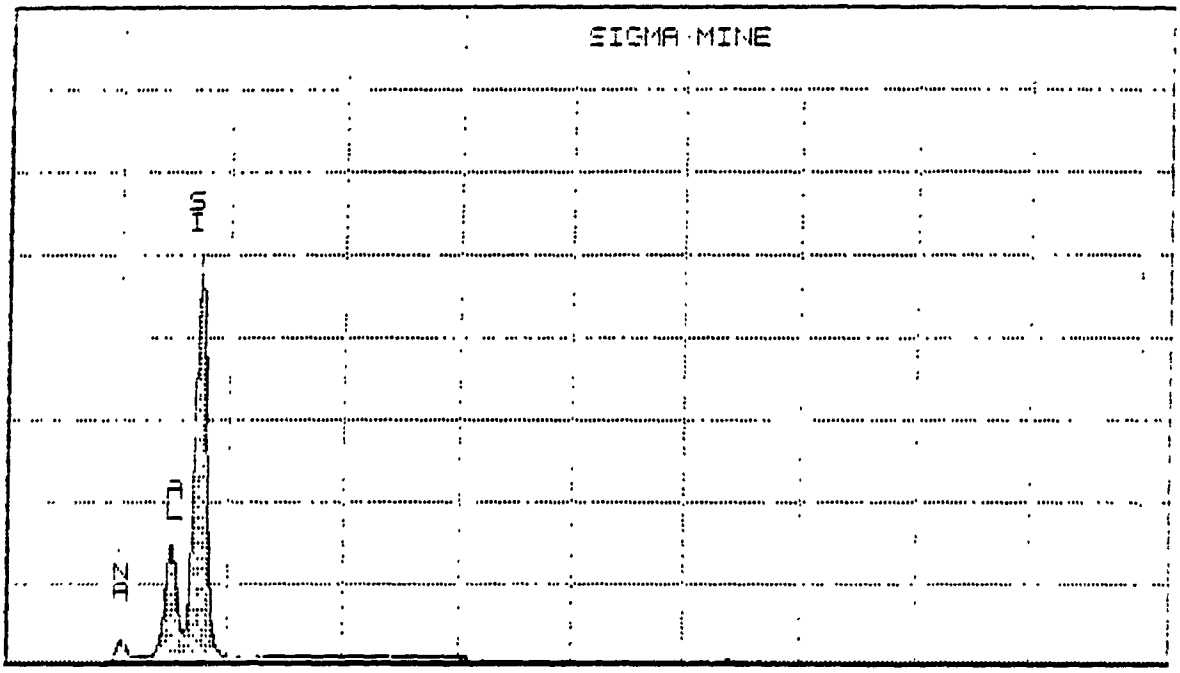

0 000 VFS = 32768 10 240

30 EXEC(S-E) DATA LABEL

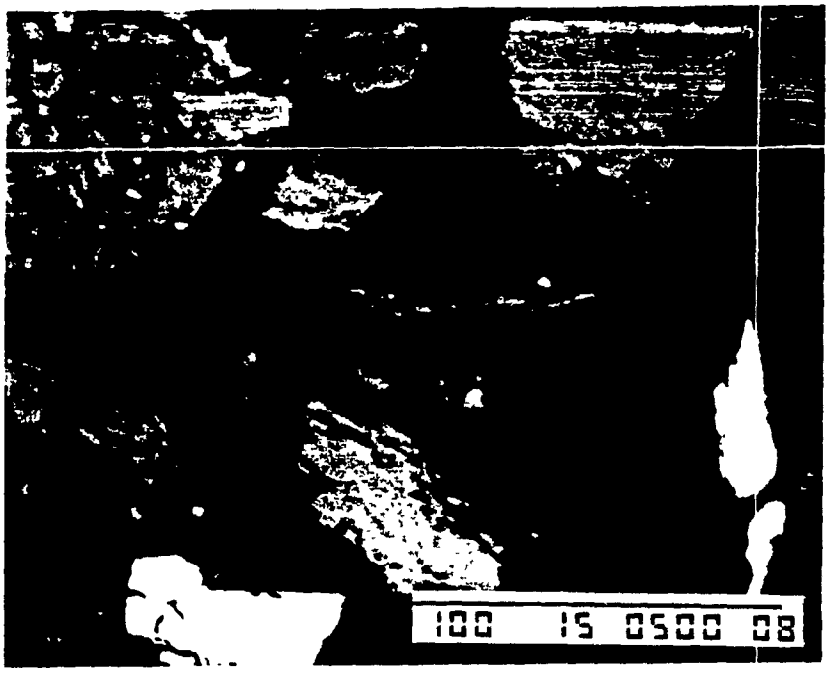

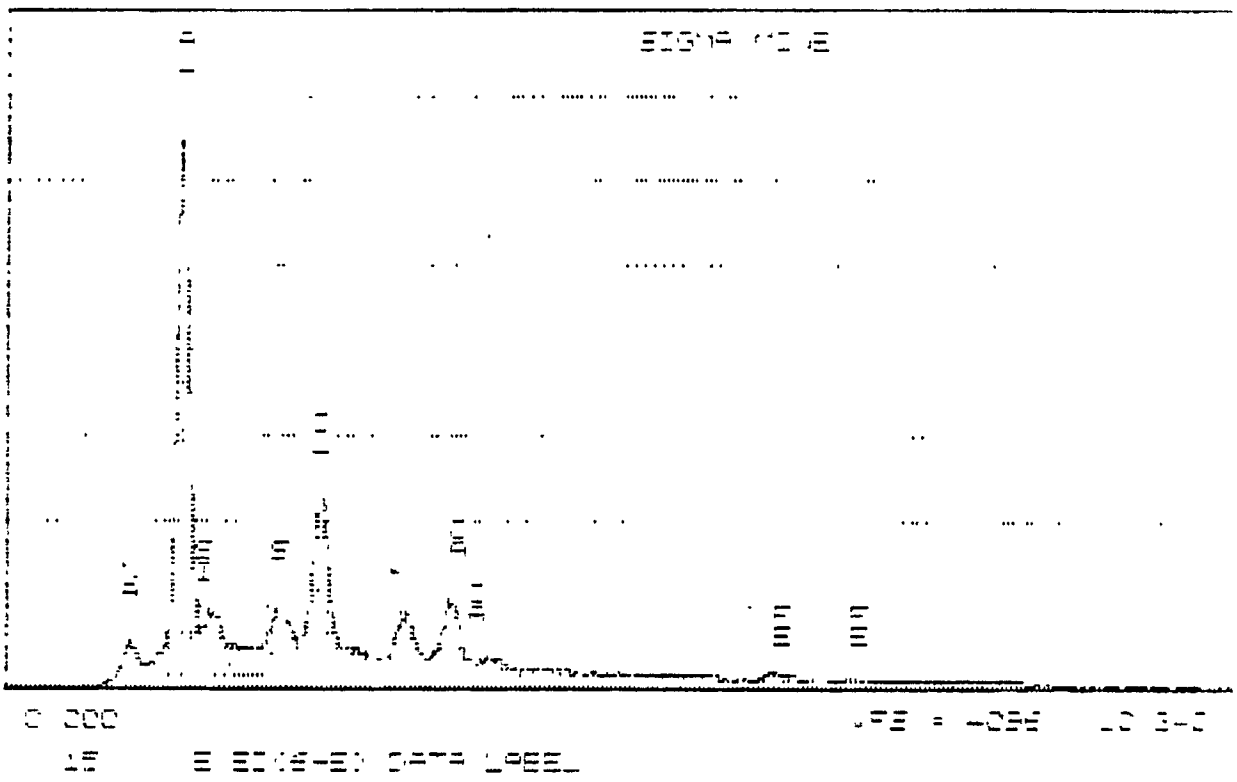

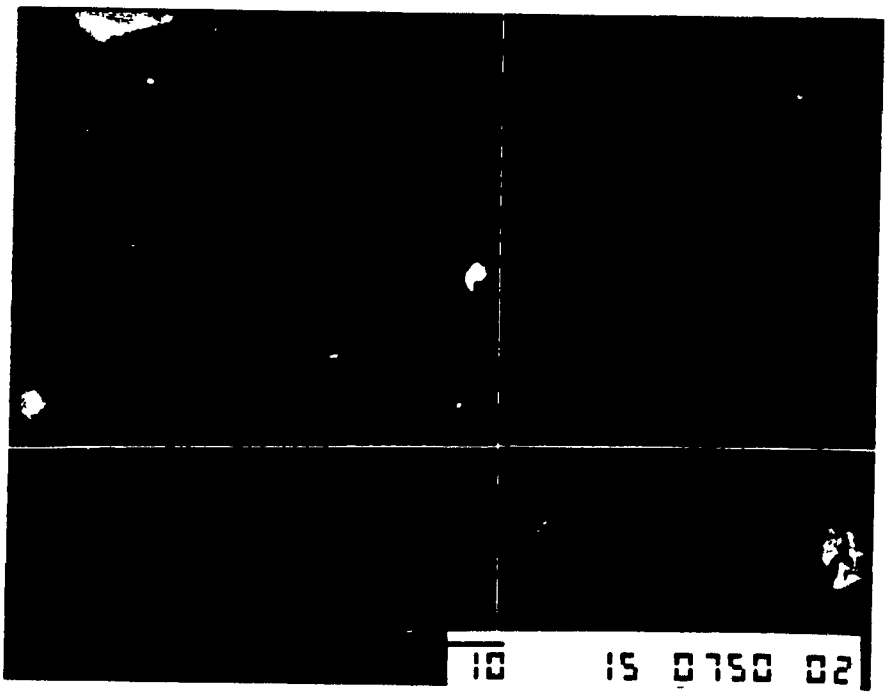
10 15 0750 02

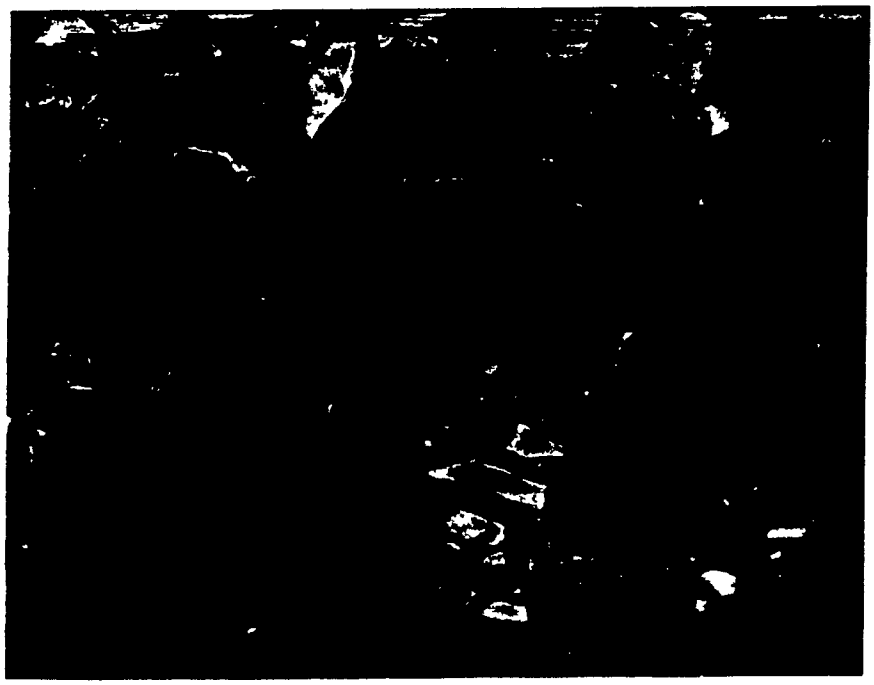

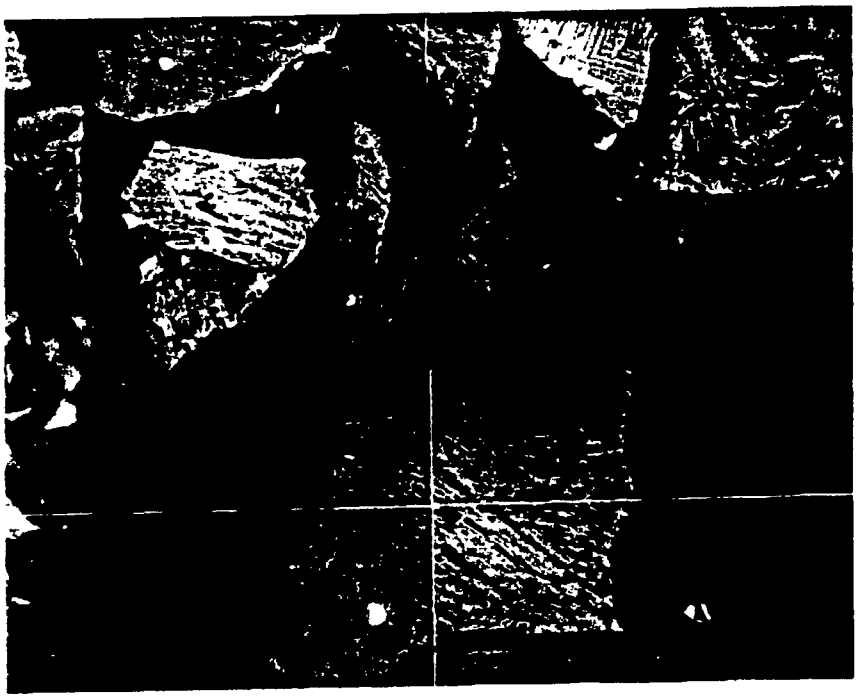

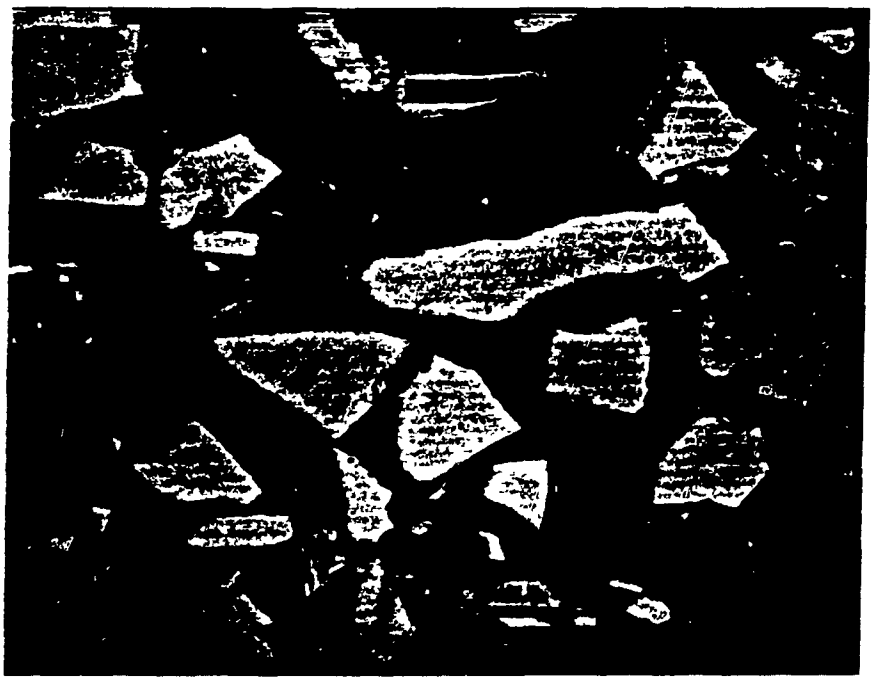

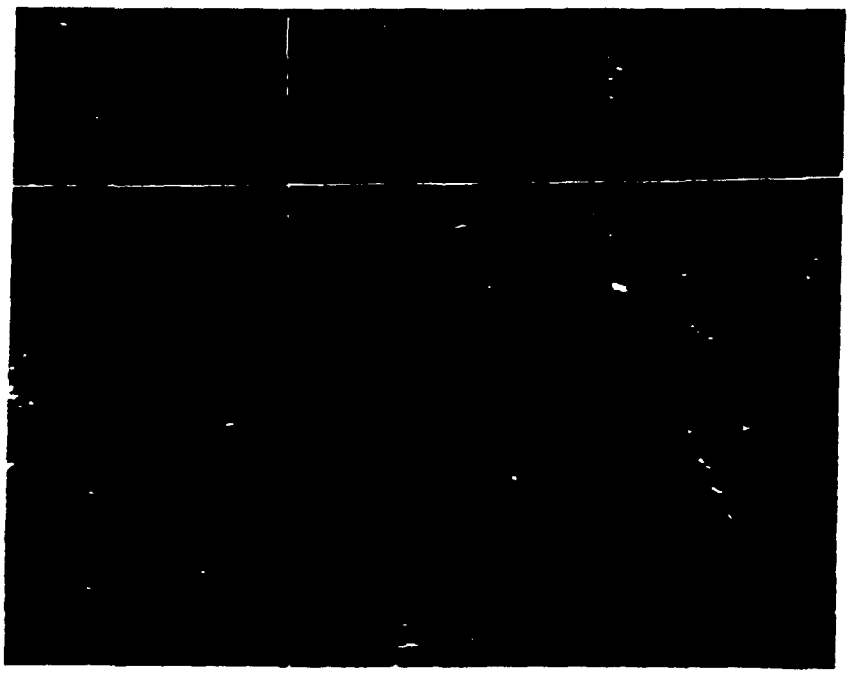

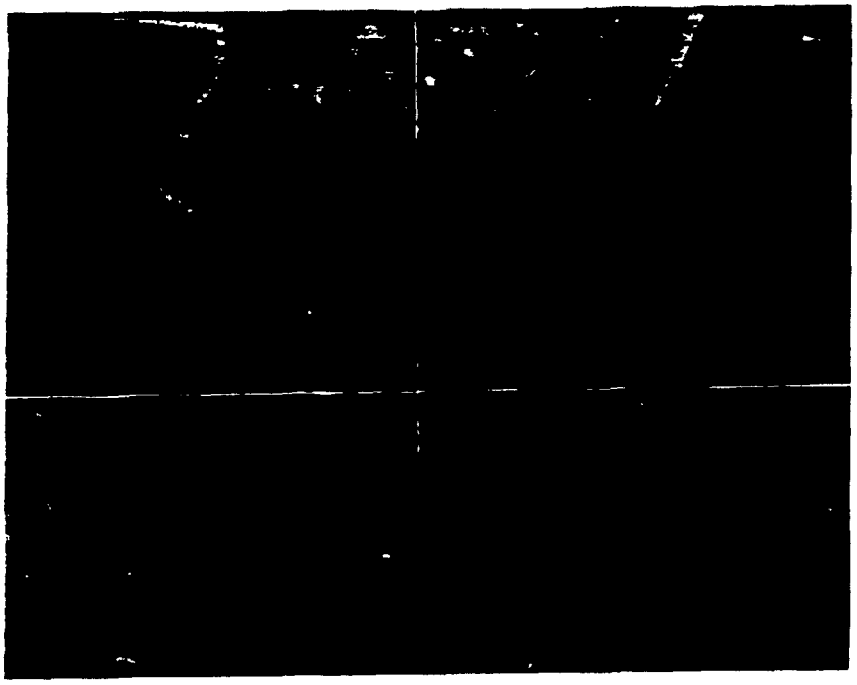

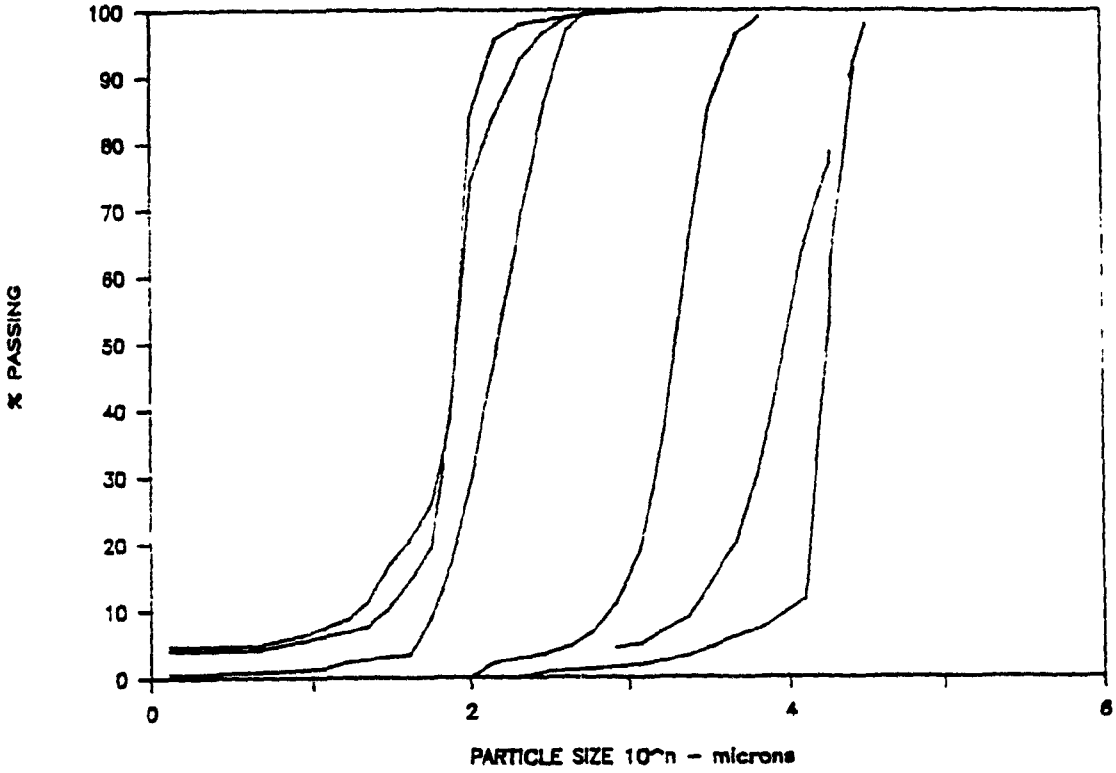
100
90
80
70
60
50
40
30
20
10
0
% PASSING
0
2
4
6
PARTICLE SIZE 10^n – microns

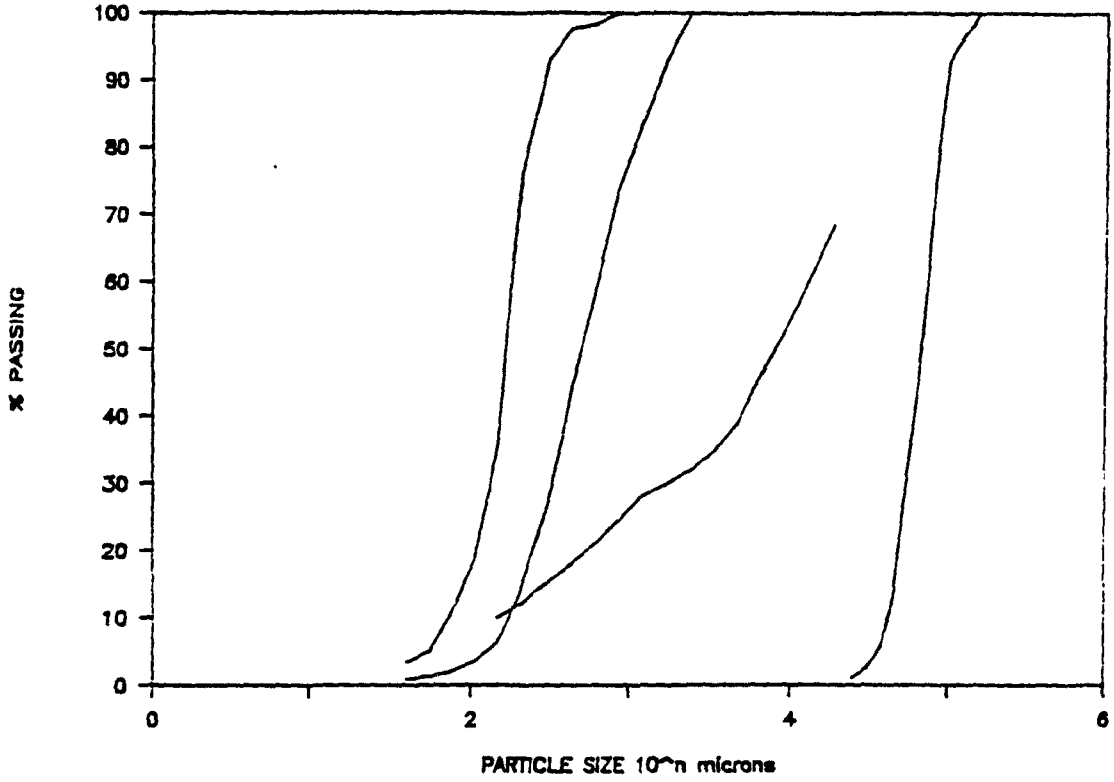
100
90
80
70
60
50
40
30
20
10
0
% PASSING
0
2
4
6
PARTICLE SIZE 10^n microns

BOUSQUET ROCKFILL

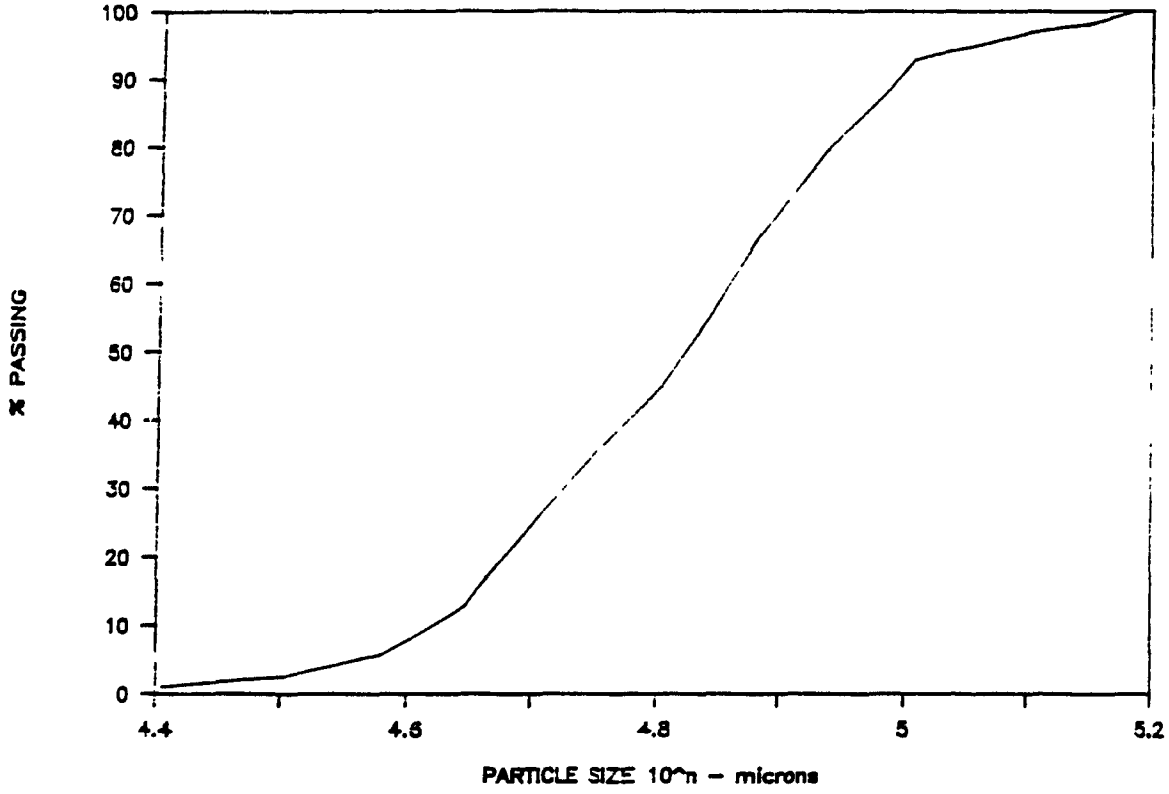

CHADBOURNE BACKFILL

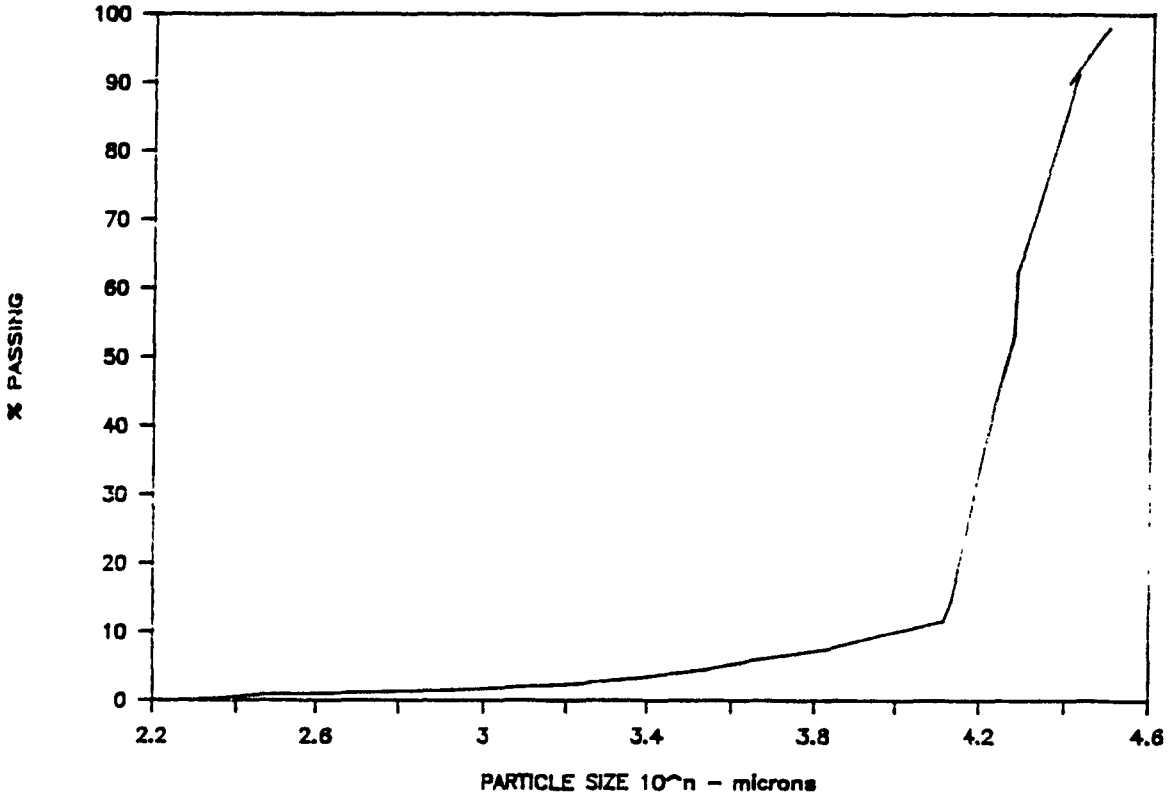

DENISON CLASSIFIED

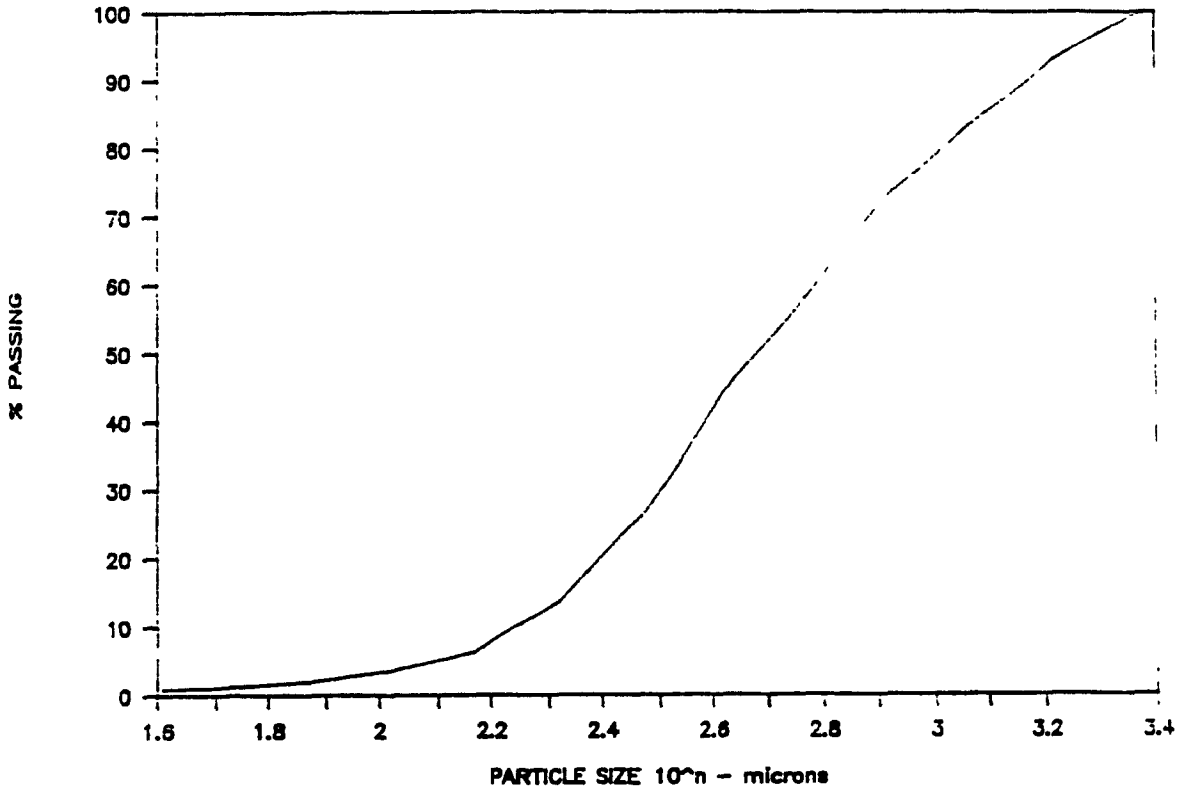

DENISON UNCLASSIFIED

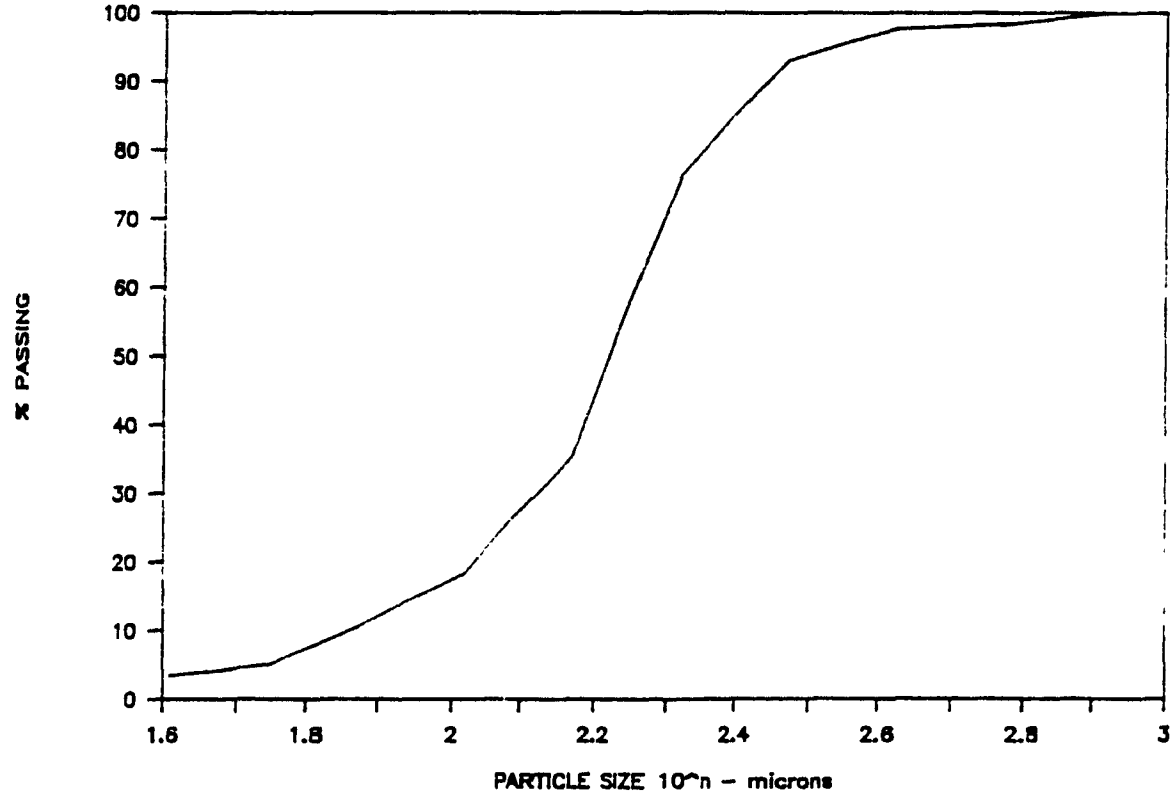

KIENA BACKFILL

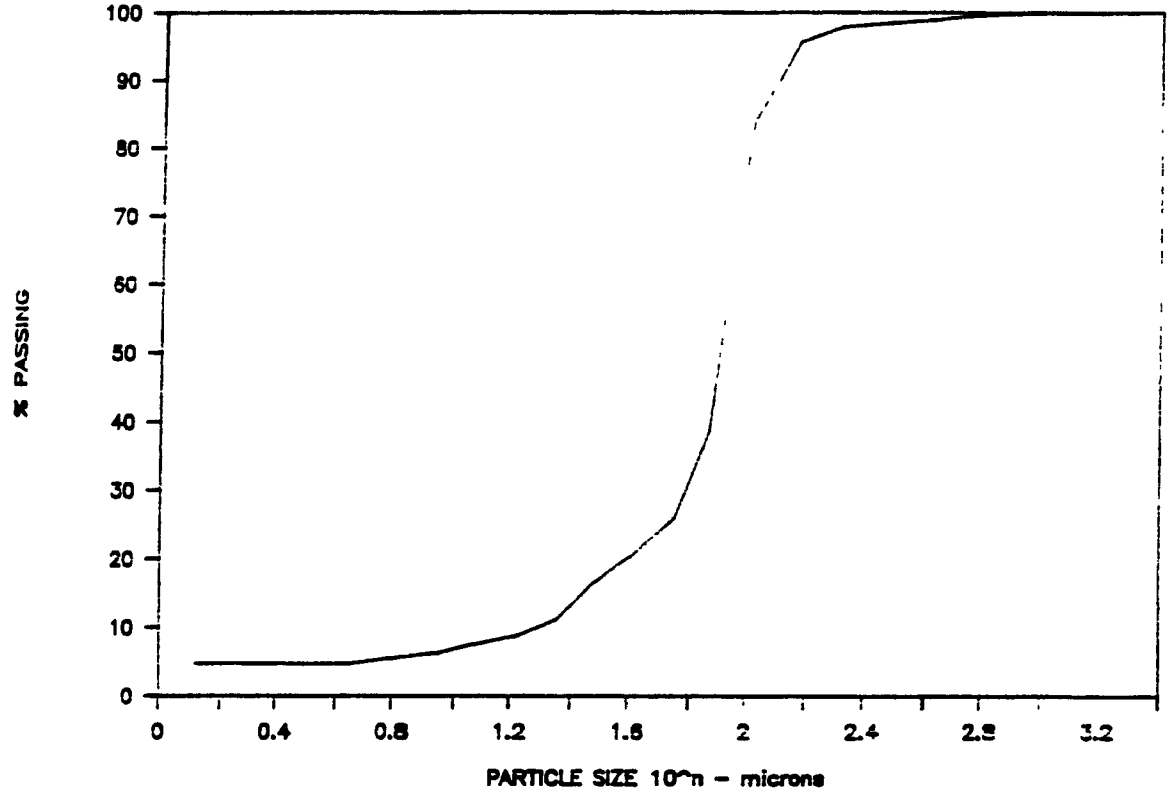

LAC MATAGAMI BACKFILL

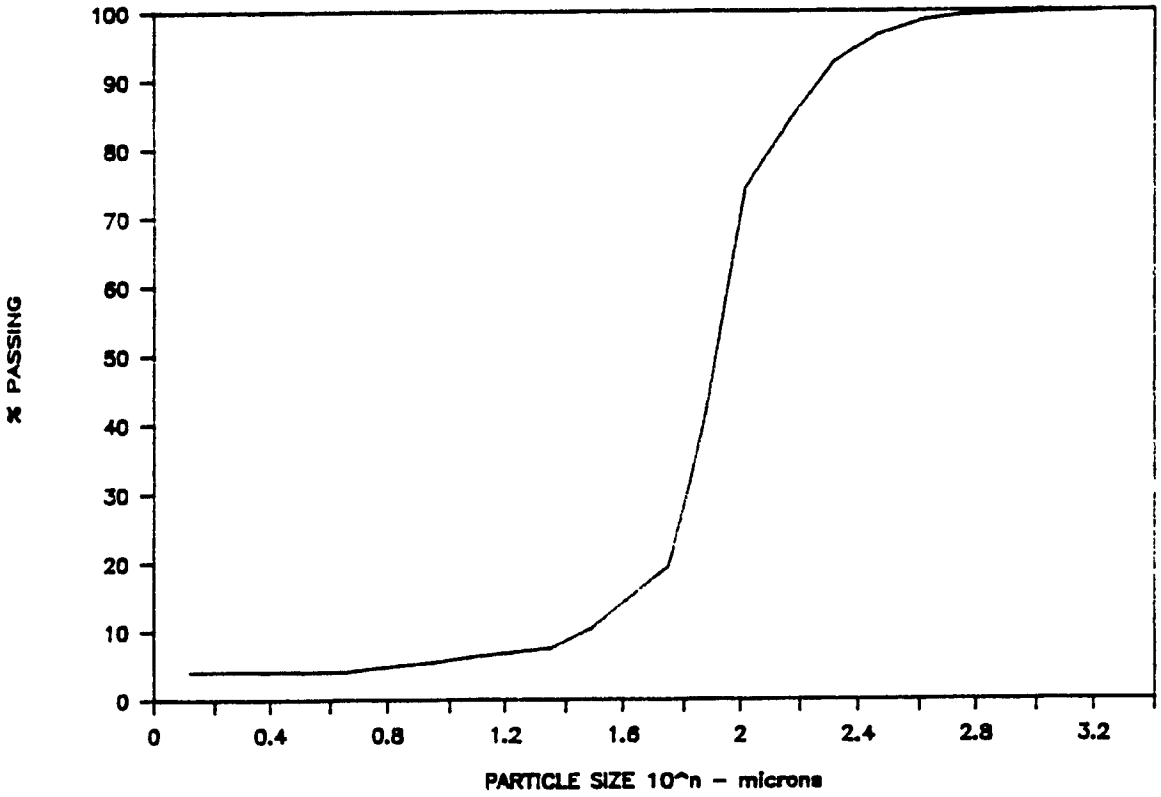

REMNOR BACKFILL

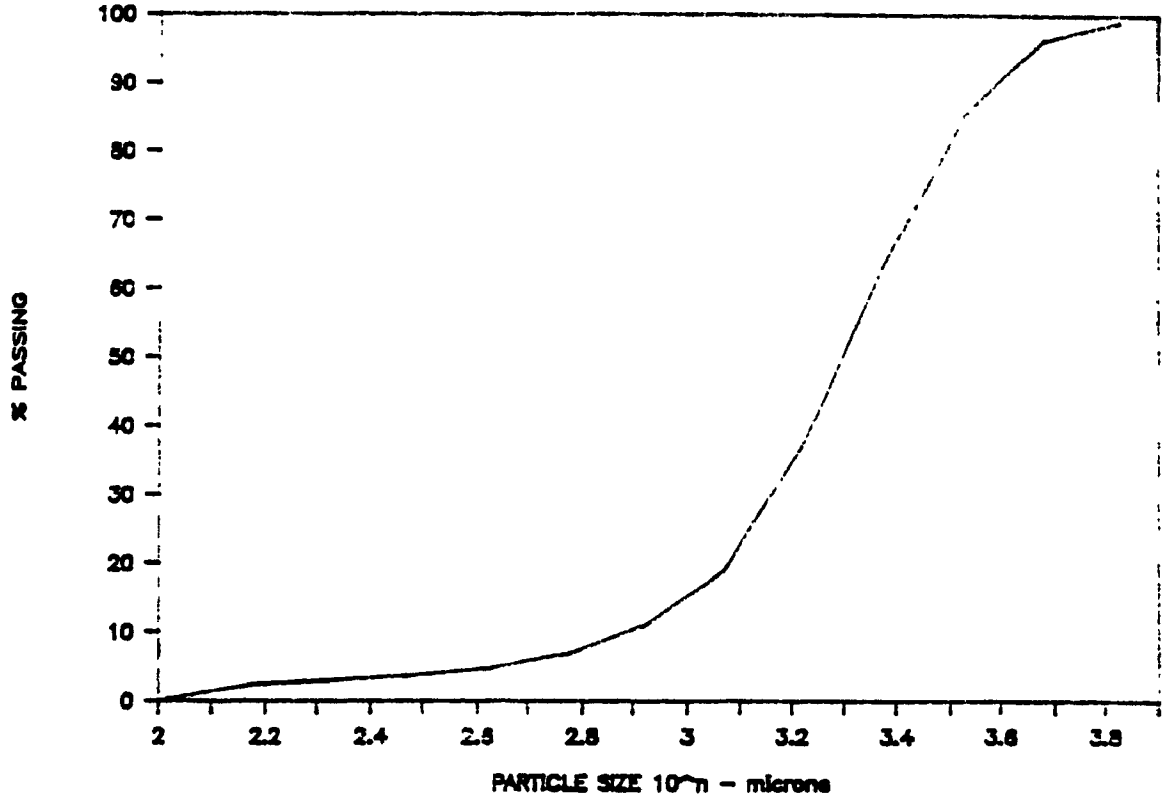

SELBAIE ROCKFILL

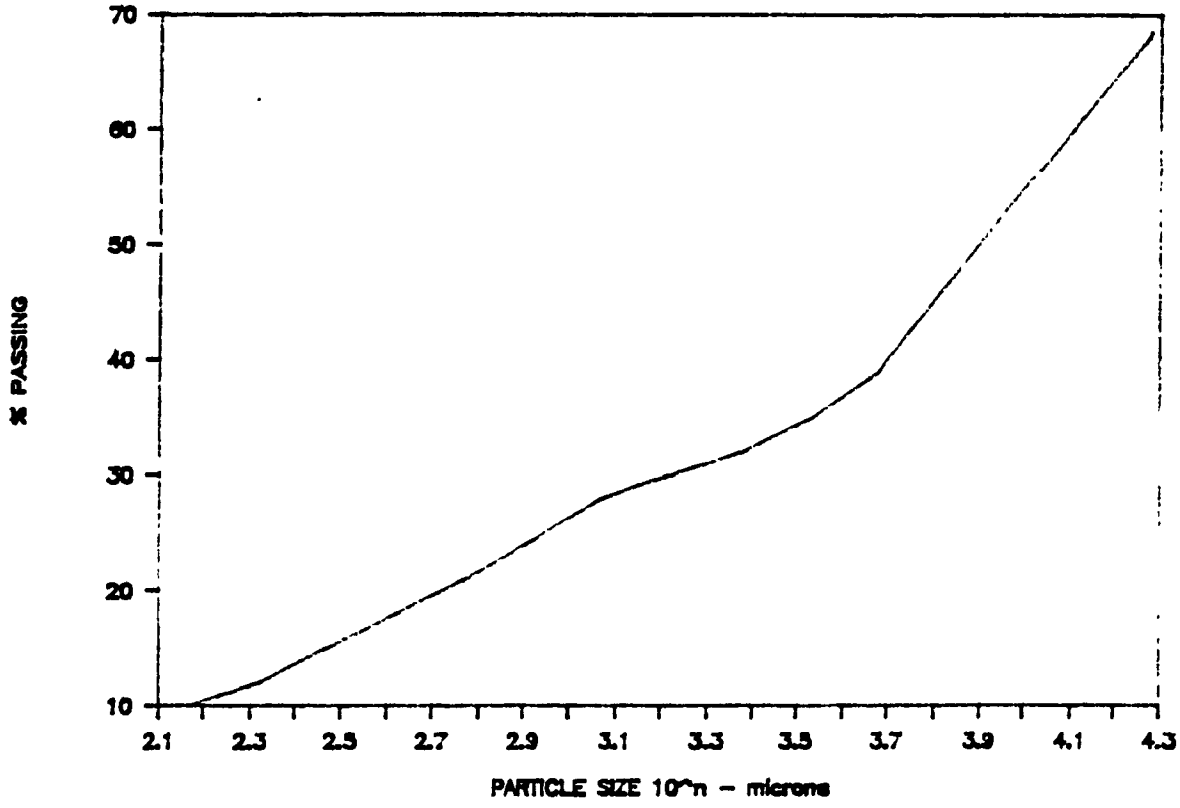

SIGMA BACKFILL

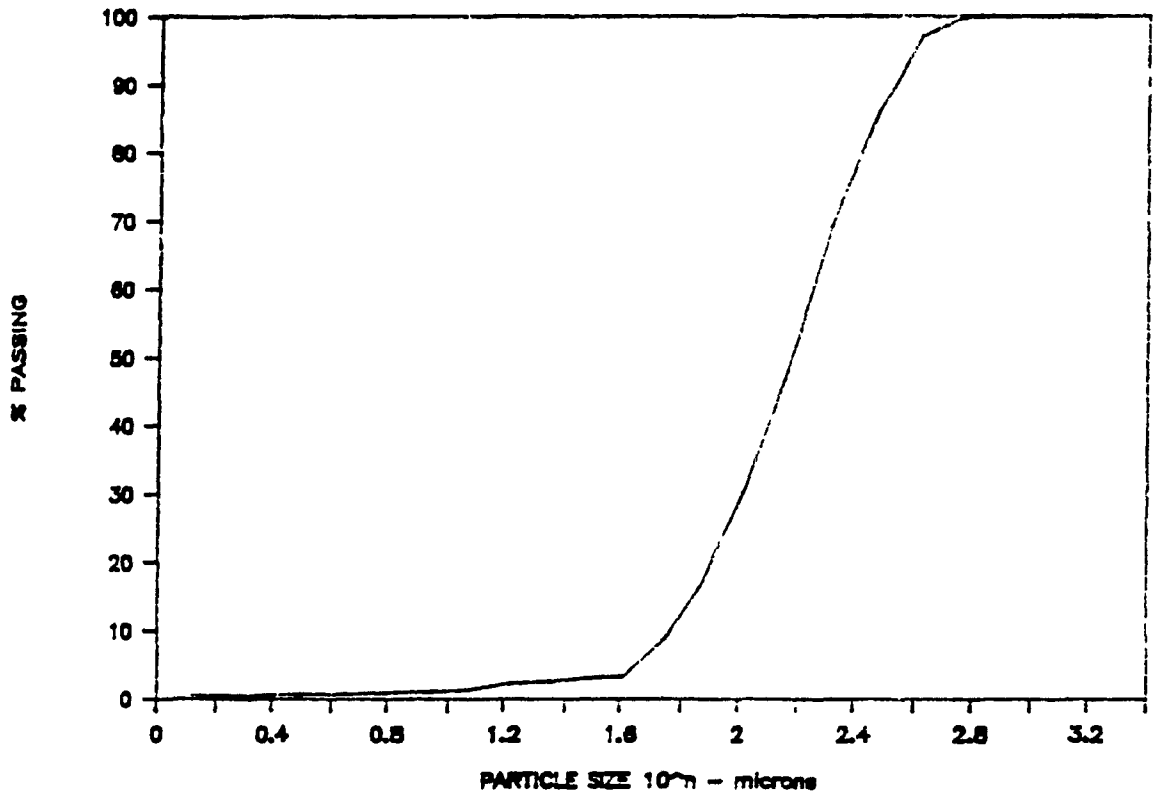

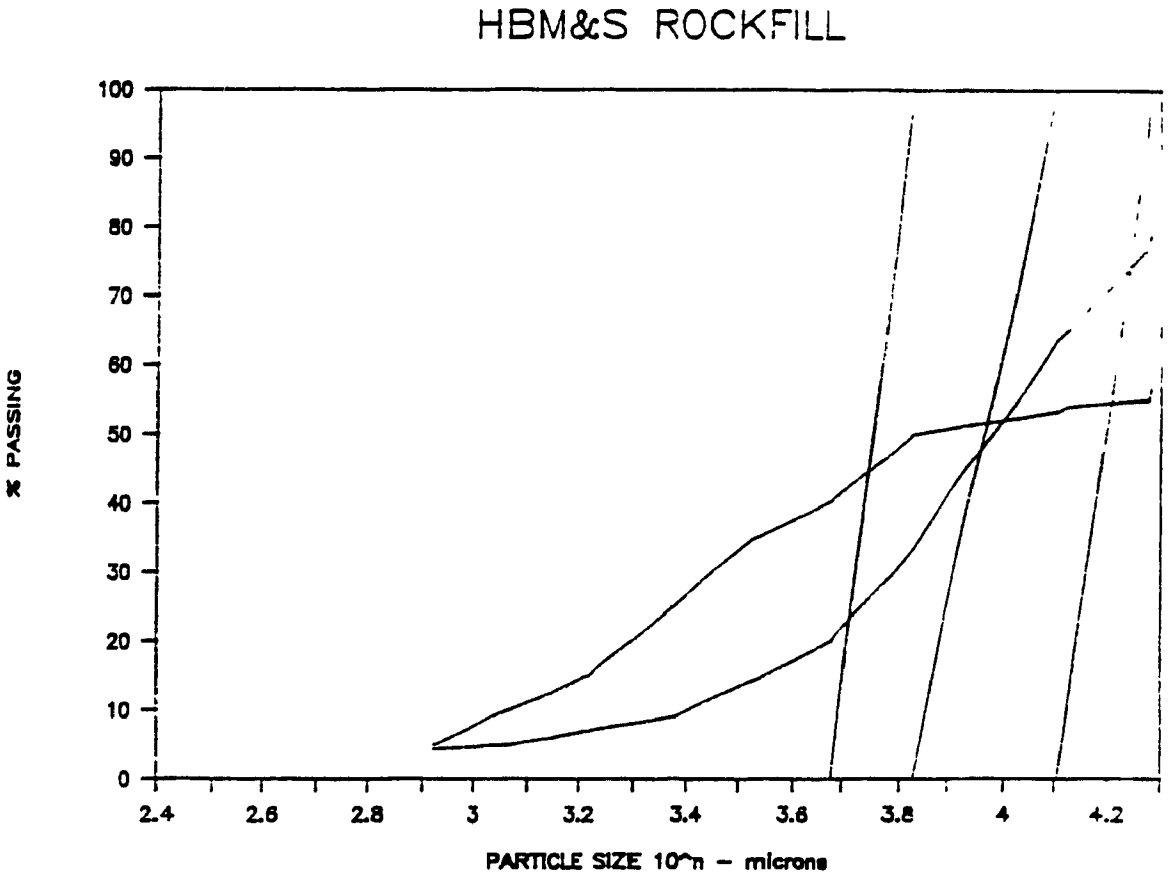
HBM&S ROCKFILL
% PASSING
100
90
80
70
60
50
40
30
20
10
0
2.4
2.6
2.8
3
3.2
3.4
3.6
3.8
4
4.2
PARTICLE SIZE 10^n – microns

HBM&S ROCKFILL

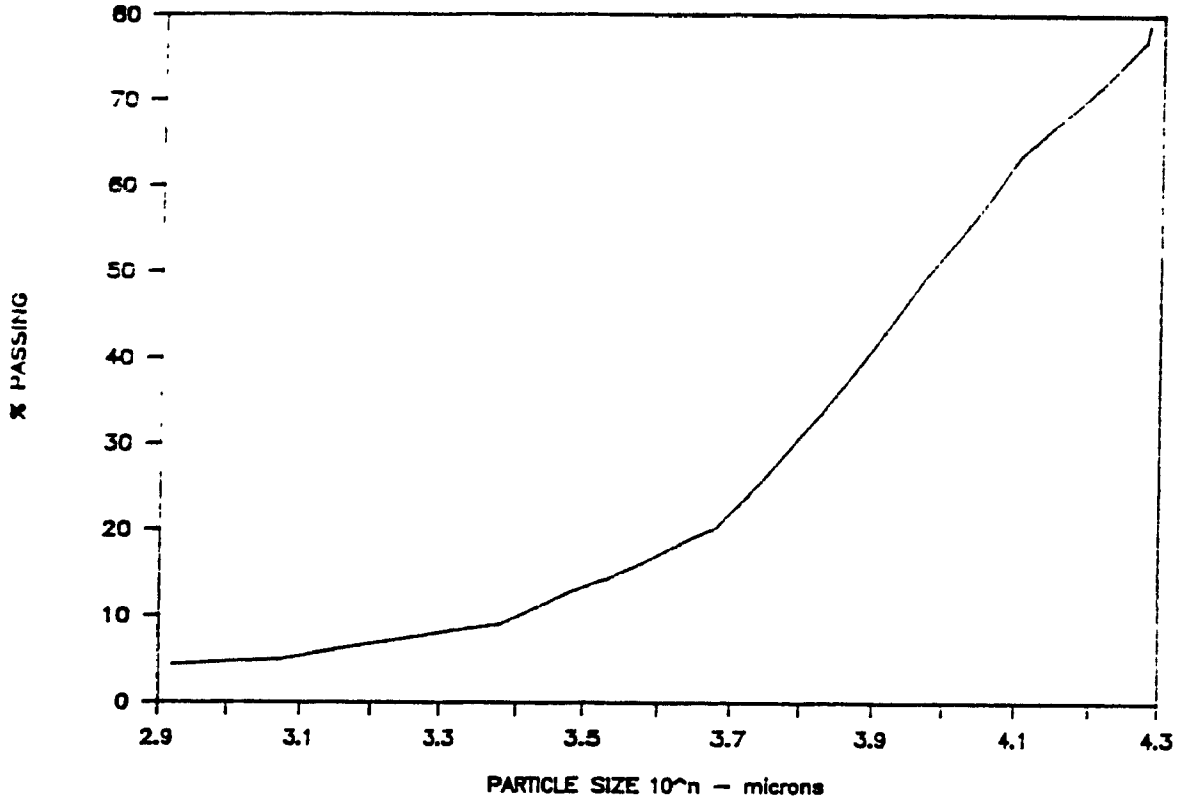

HBM&S ROCKFILL

ARTIFICIAL COMBINATION

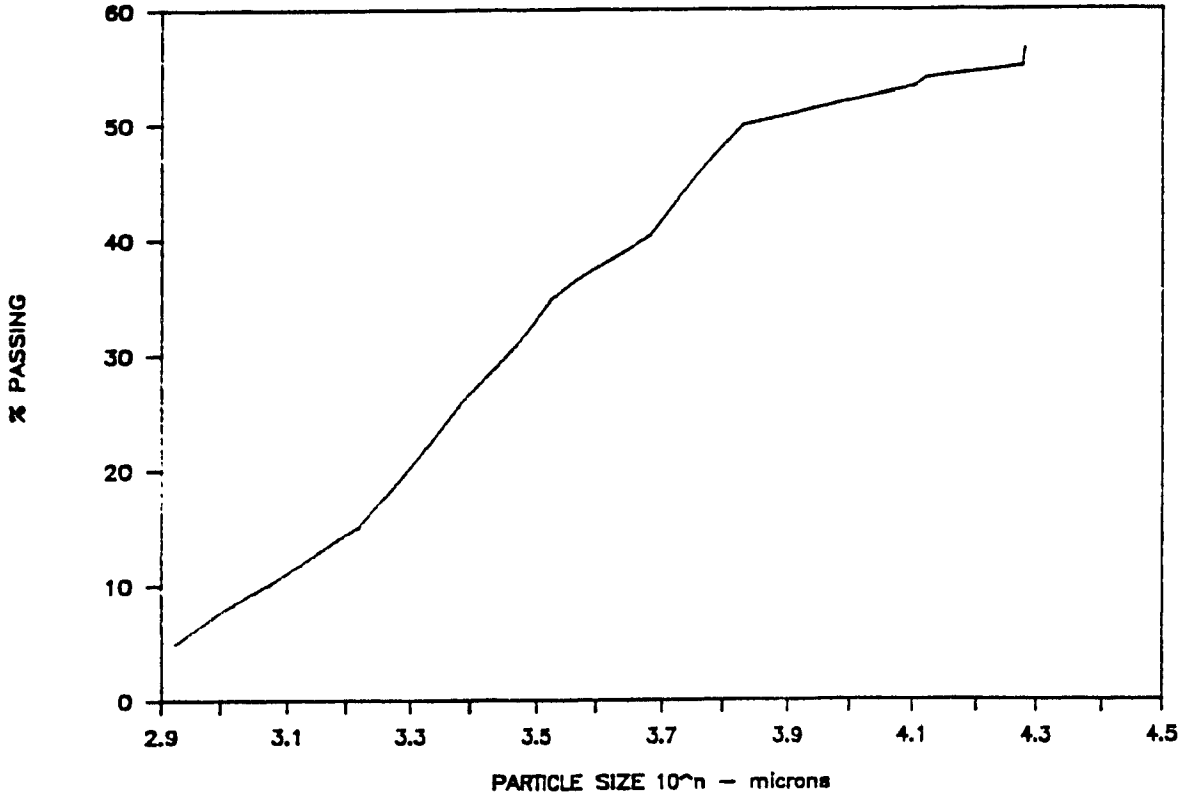

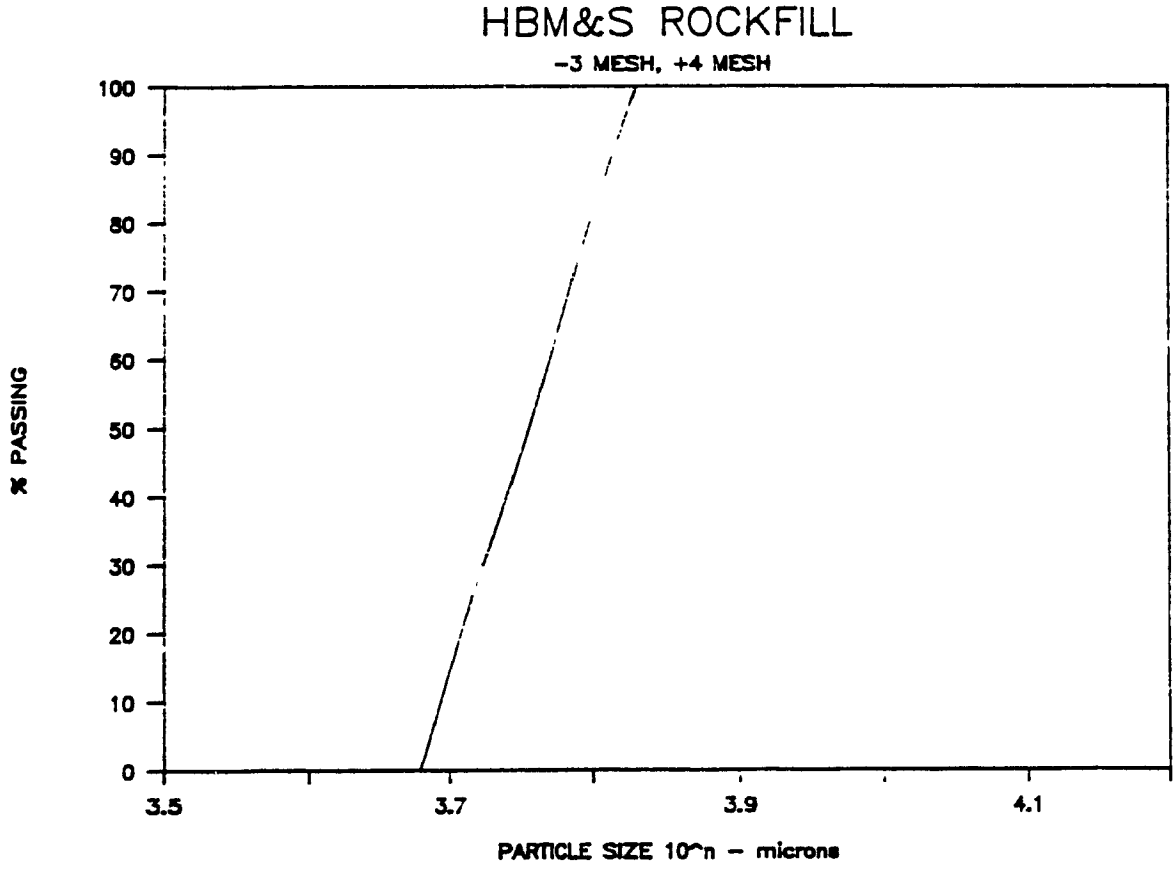
HBM&S ROCKFILL
-3 MESH, +4 MESH
% PASSING
100
90
80
70
60
50
40
30
20
10
0
3.5
3.7
3.9
4.1
PARTICLE SIZE 10^n - microns

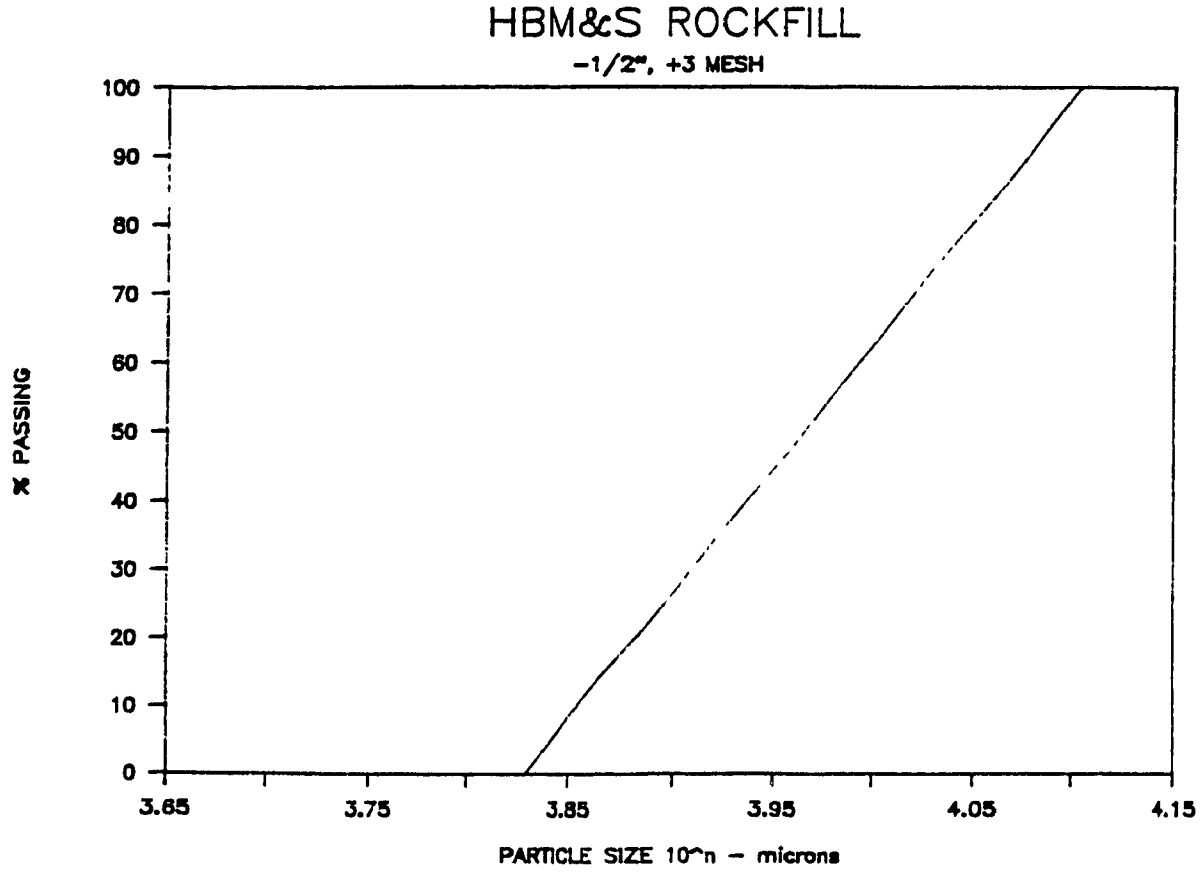
HBM&S ROCKFILL
-1/2", +3 MESH
% PASSING
100
90
80
70
60
50
40
30
20
10
0
3.65
3.75
3.85
3.95
4.05
4.15
PARTICLE SIZE 10^n - microns

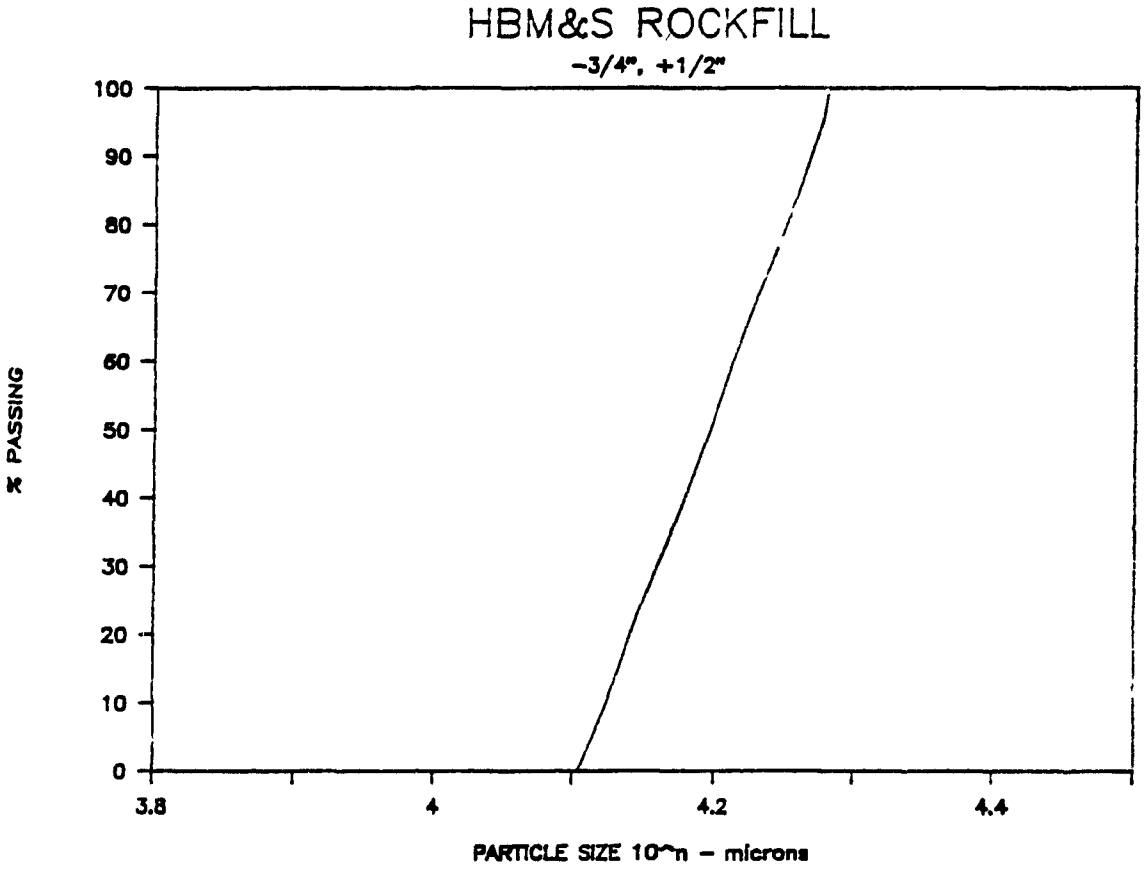
HBM&S ROCKFILL
-3/4", +1/2"
100
90
80
70
60
50
40
30
20
10
0
% PASSING
3.8
4
4.2
4.4
PARTICLE SIZE 10^n - microns

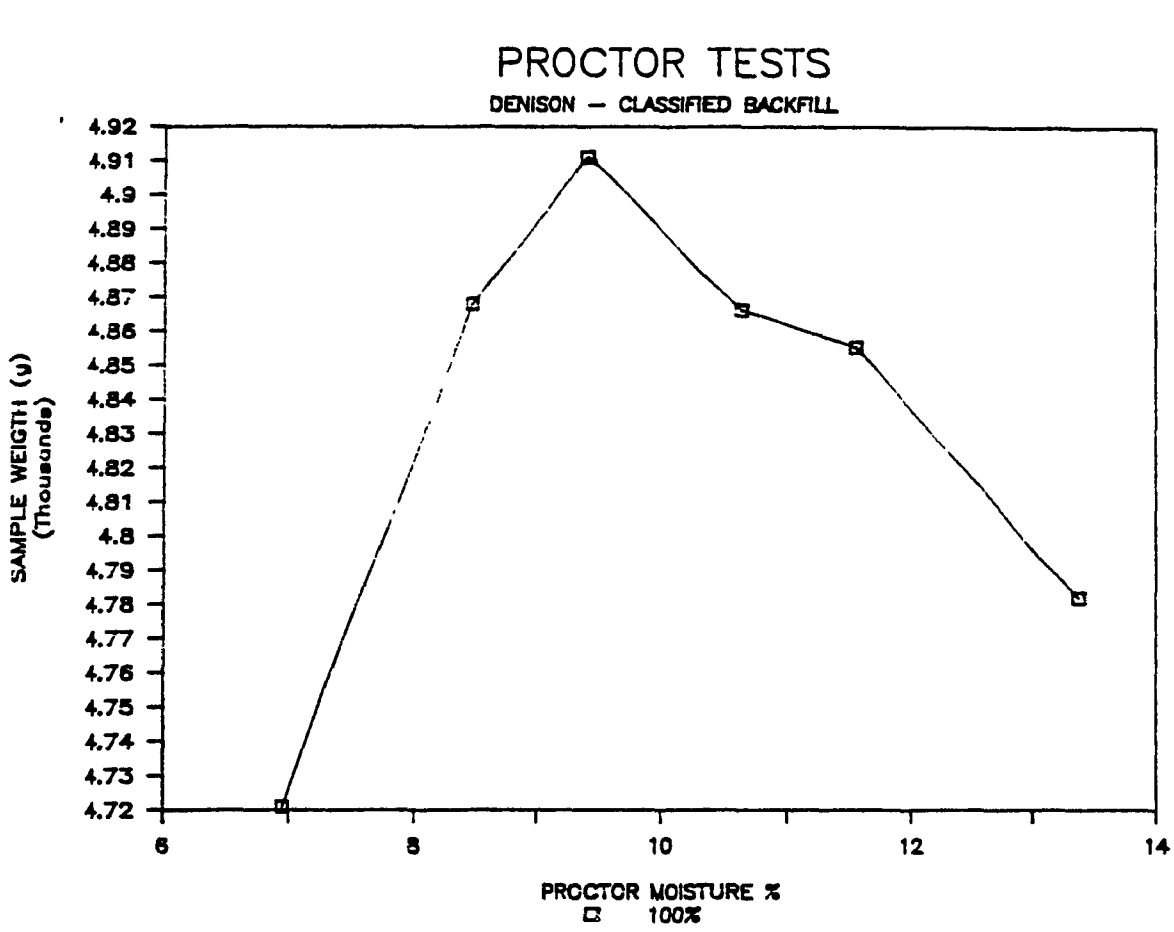
PROCTOR TESTS
DENISON – CLASSIFIED BACKFILL
SAMPLE WEIGHT (g)
(Thousands)
4.92
4.91
4.9
4.89
4.88
4.87
4.86
4.85
4.84
4.83
4.82
4.81
4.8
4.79
4.78
4.77
4.76
4.75
4.74
4.73
4.72
6
8
10
12
14
PROCTOR MOISTURE %
100%

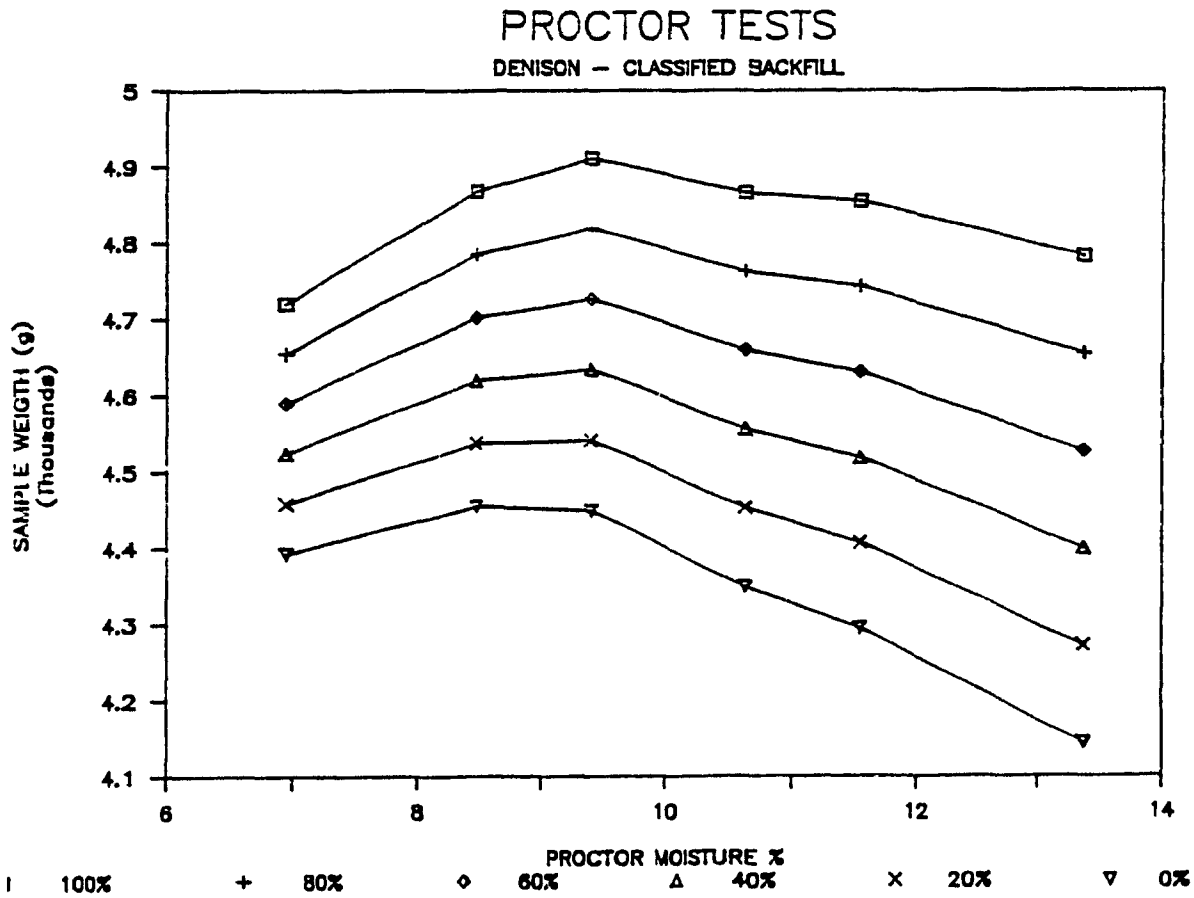
PROCTOR TESTS
DENISON – CLASSIFIED BACKFILL
SAMPLE WEIGHT (g)
(Thousands)
5
4.9
4.8
4.7
4.6
4.5
4.4
4.3
4.2
4.1
6
8
10
12
14
PROCTOR MOISTURE %
100%
80%
60%
40%
20%
0%

PROCTOR TESTS

DENISON – UNCLASSIFIED BACKFILL

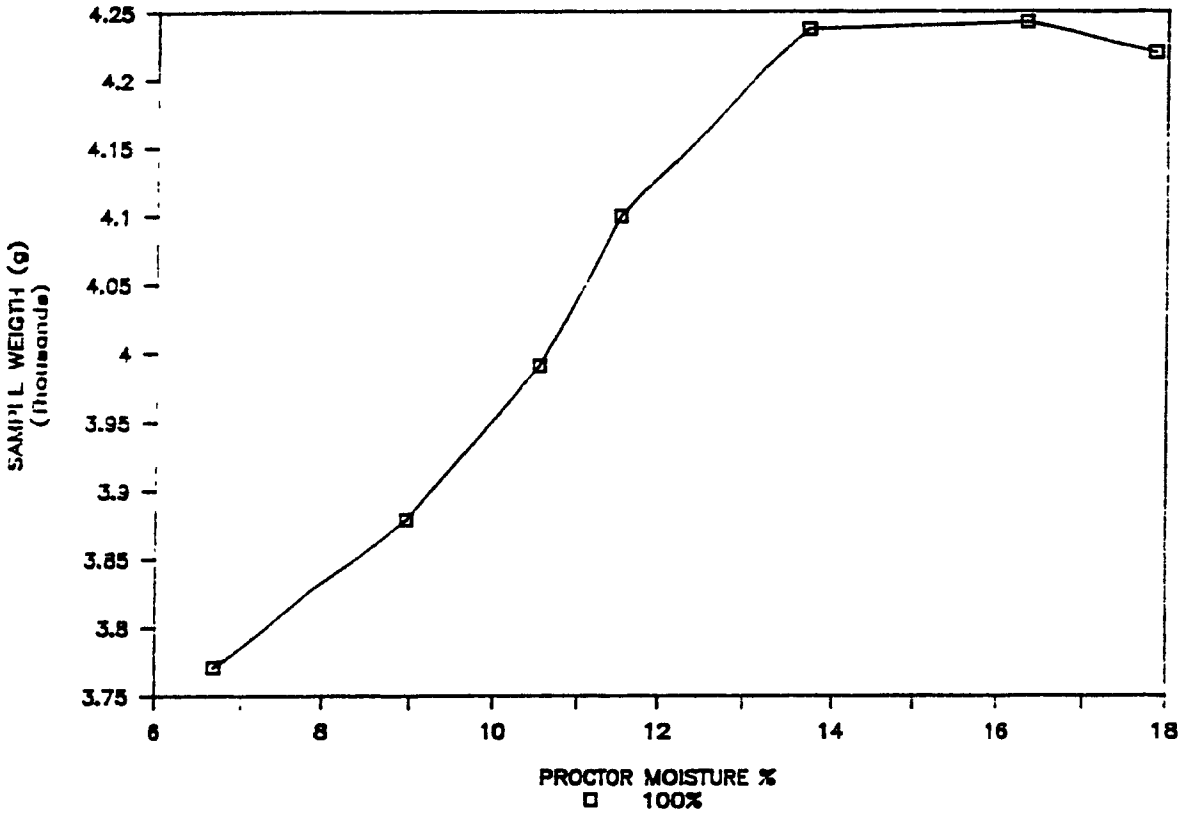

PROCTOR TESTS

DENISON – UNCLASSIFIED BACKFILL

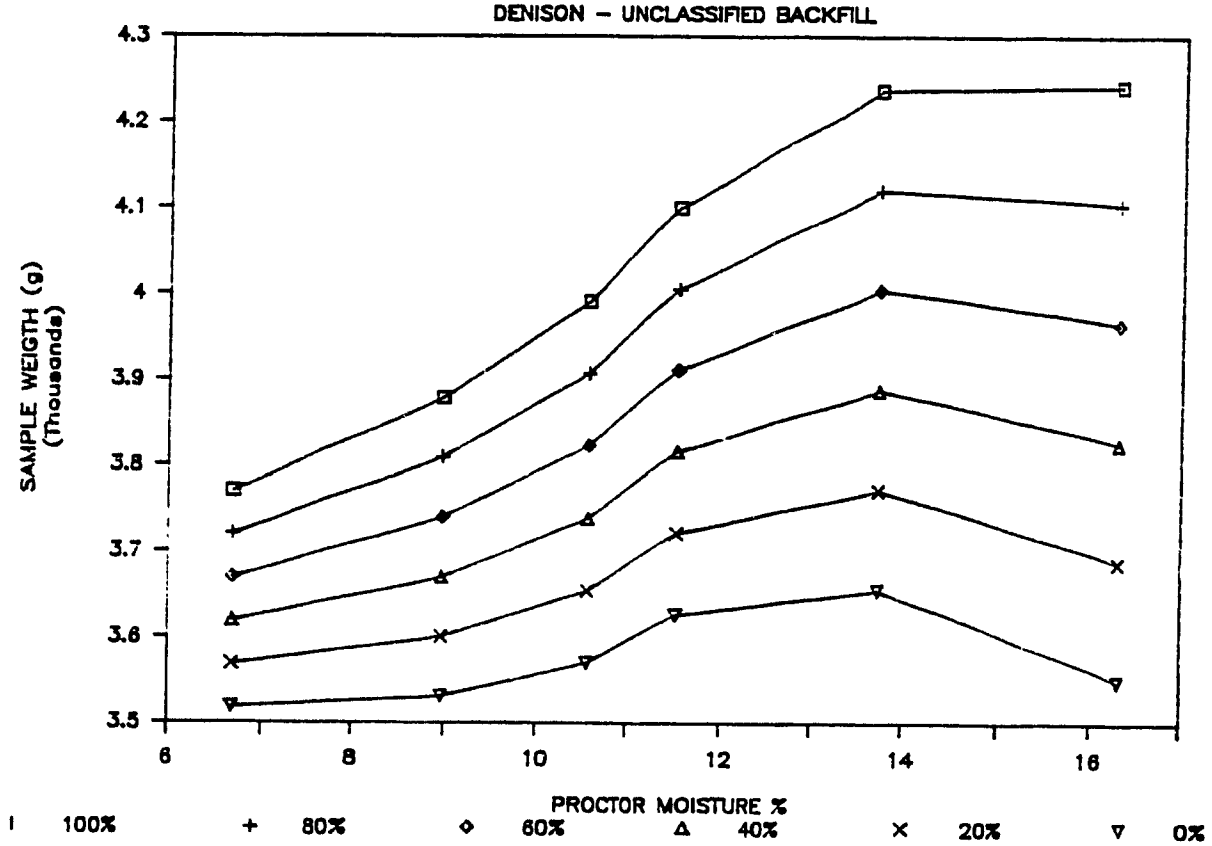

PROCTOR TESTS

KIENA MINE

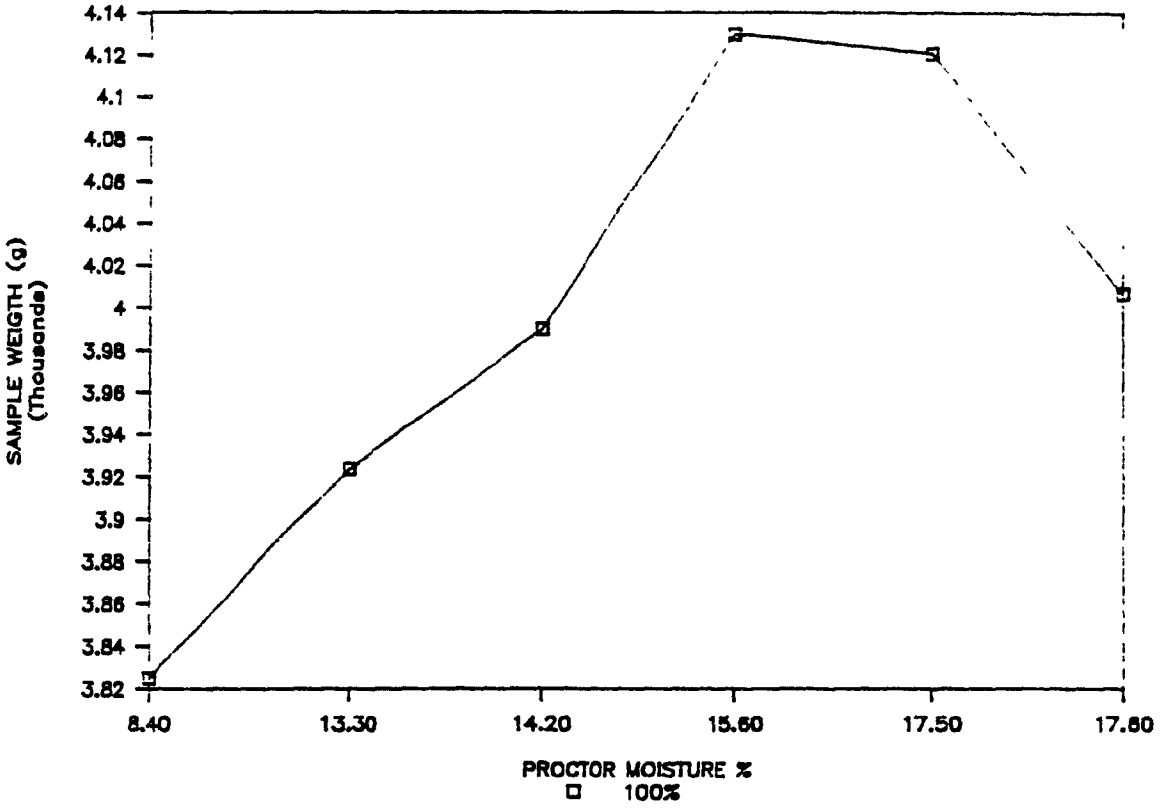

PROCTOR TESTS

KIENA MINE

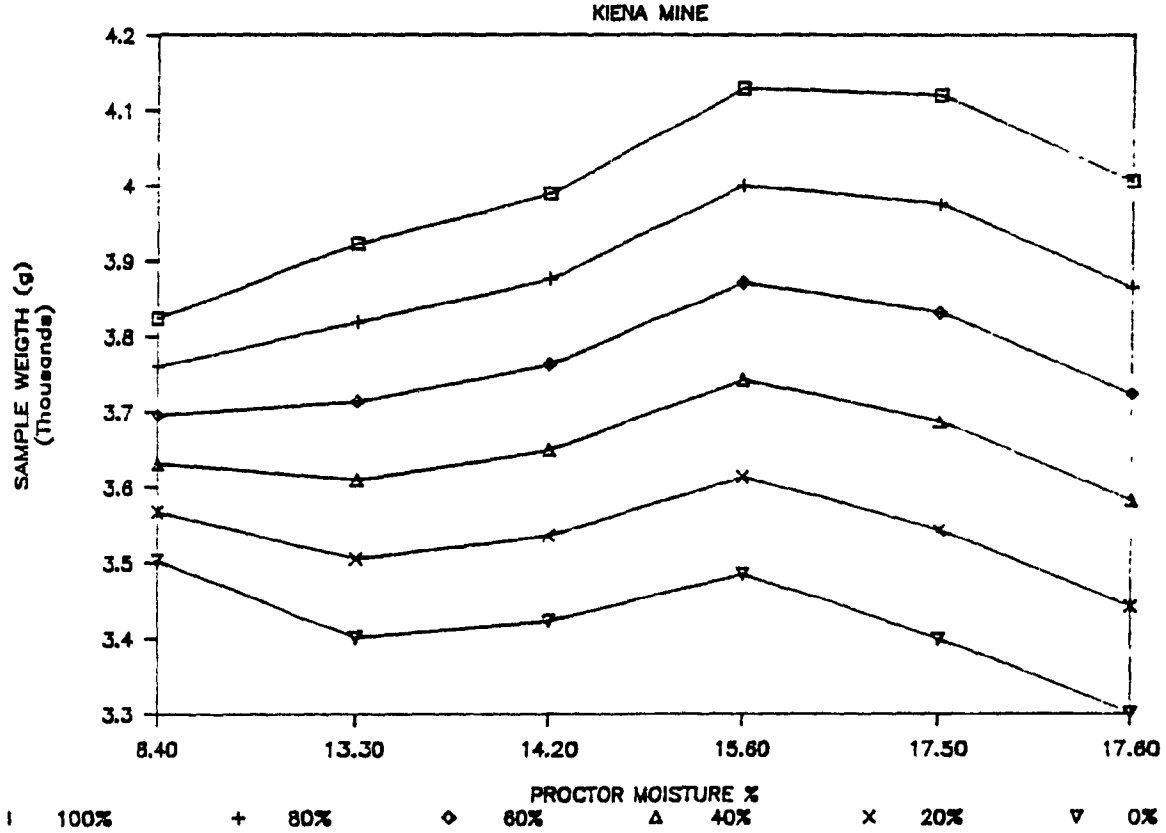

PROCTOR TESTS

LAC MATAGAMI MINE

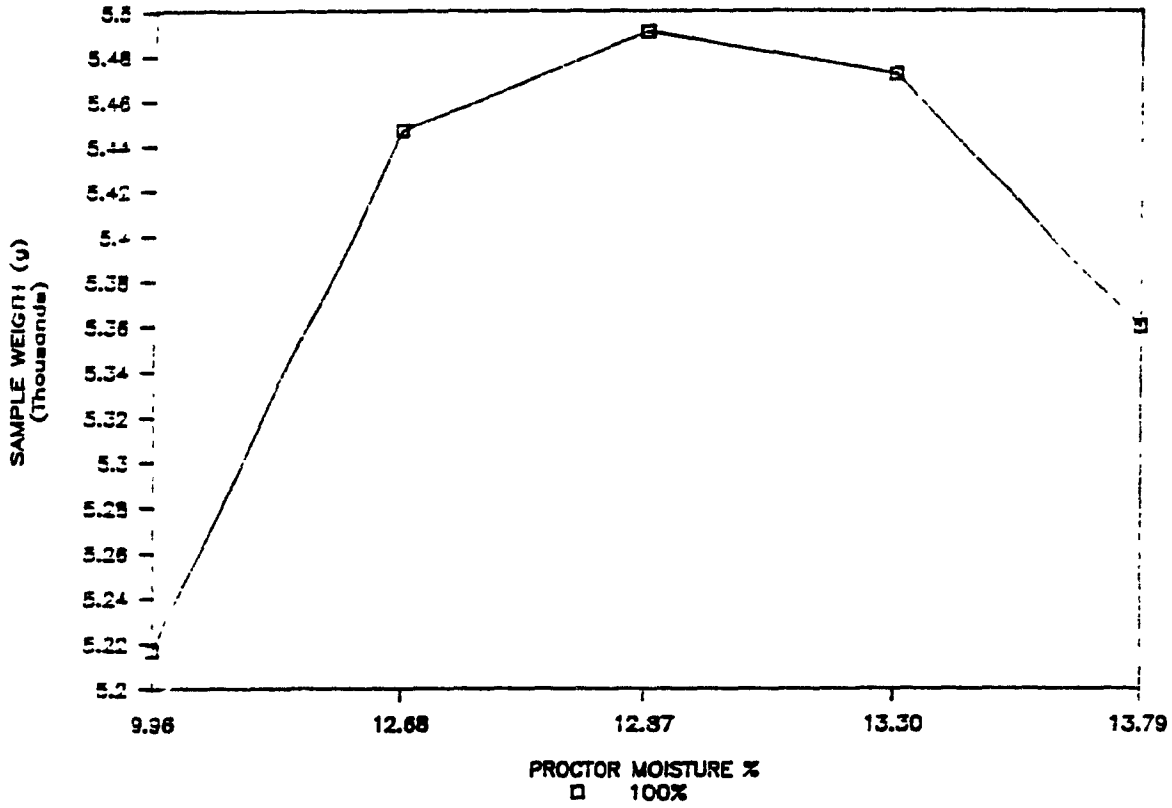

PROCTOR TESTS

LAC MATAGAMI MINE

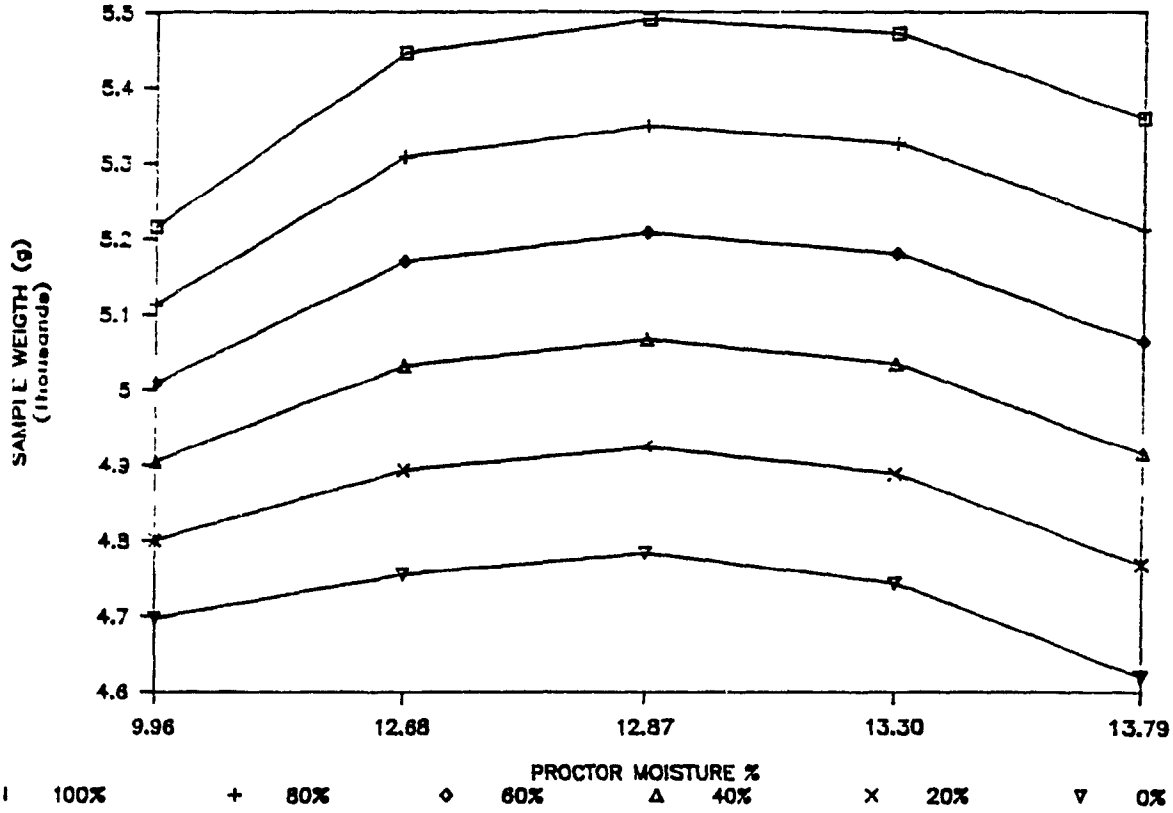

SIGMA MINES

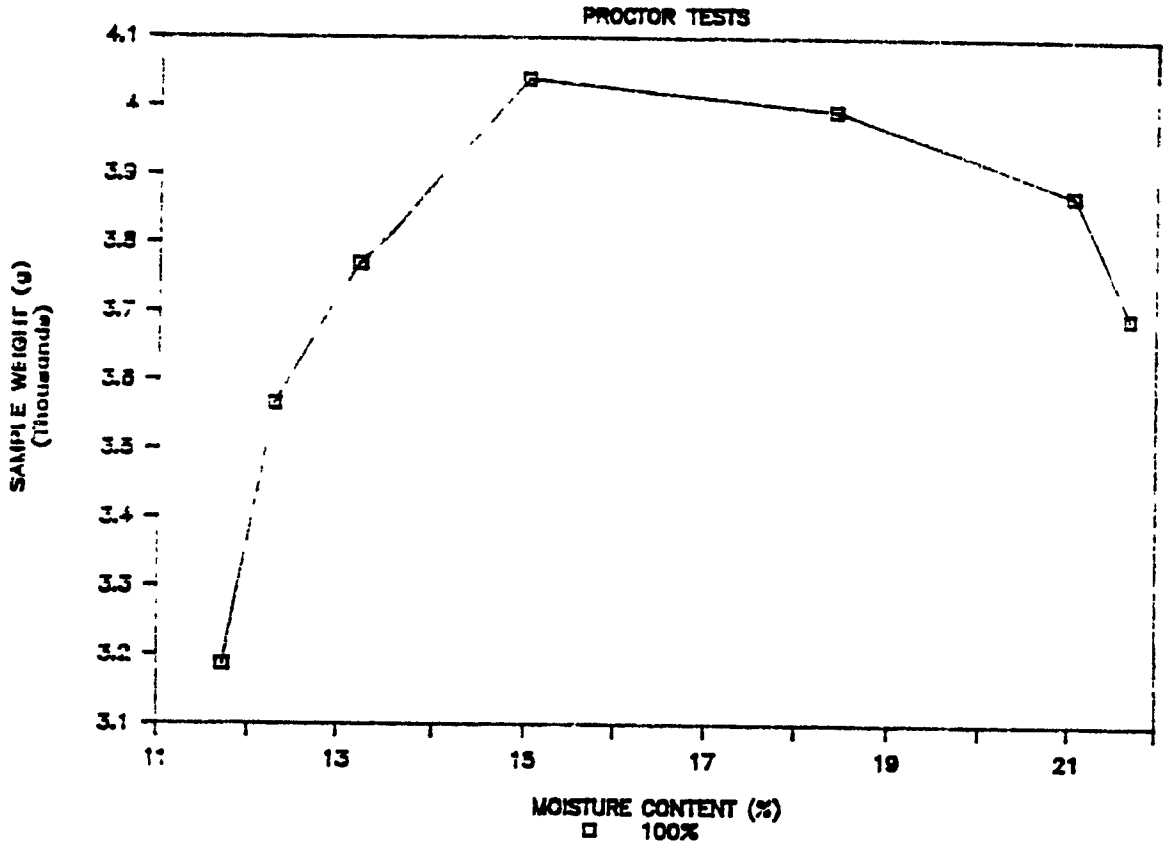

SIGMA MINES

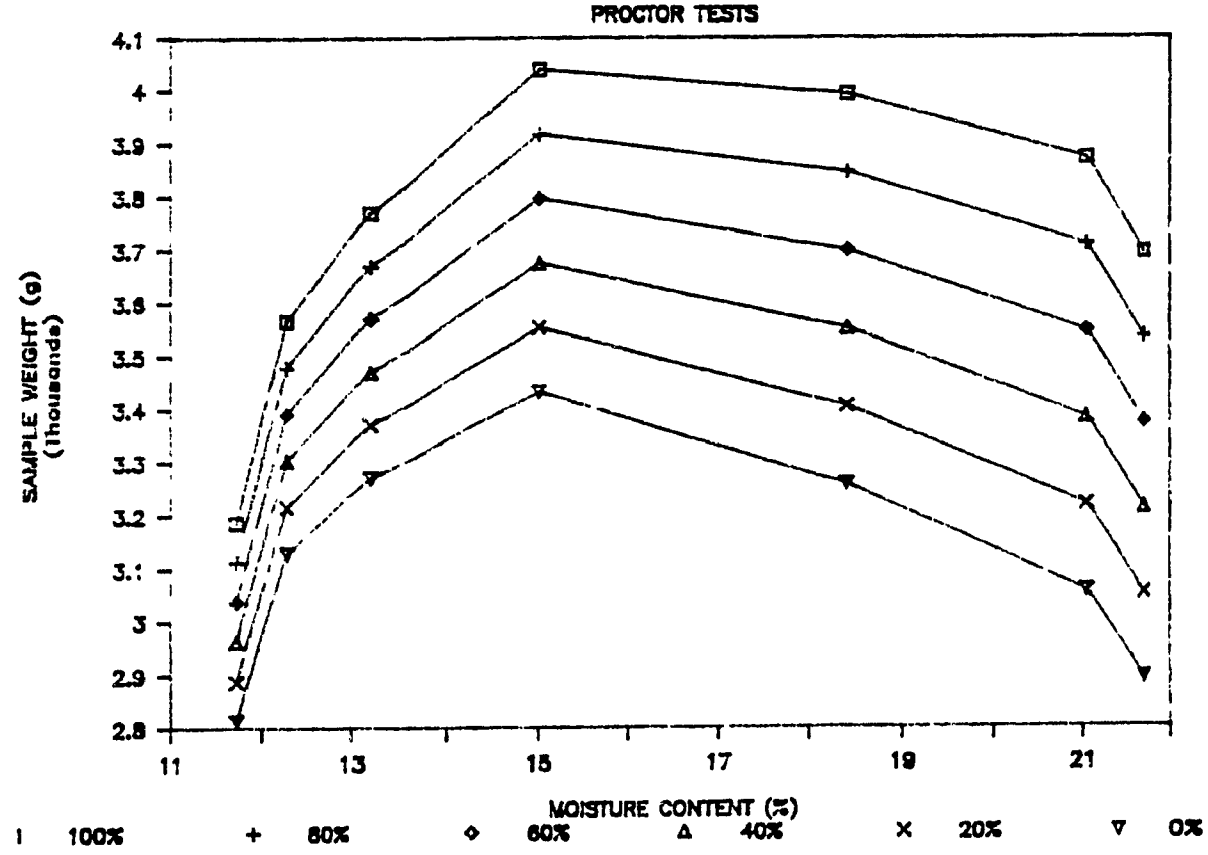

APPENDIX E

SUMMARIZED SAMPLE PROPERTIES DATA

APPENDIX 8

MINE LOCATION	DRY DENSITY	MOISTURE CONTENT %	VOID RATIO	POROSITY %
SIGMA				
A100	1.50	18.24	.73	42.20
B100	1.51	11.79	.72	41.86
E100	1.52	15.67	.71	41.52
E50	1.45	7.51	.79	44.13
B35	1.43	4.25	.82	45.05
A45	1.43	8.19	.82	45.05
E20	1.44	3.15	.81	44.75
B5	1.45	2.01	.79	44.13
A5	1.43	1.16	.82	45.05
LAC MATAGAMI				
B100	2.19	9.43	.63	38.65
E100	2.13	12.32	.44	30.56
A100	2.19	12.21	.63	38.65
E50	2.17	4.67	.65	39.39
A50	2.28	1.31	.57	36.31
B60	2.20	4.79	.62	38.27
A5	2.15	2.89	.66	39.76
E5	2.21	.12	.62	38.27
B5	2.15	.063	.66	39.76
DENISON CLS.				
A100	2.06	10.73	.31	23.66
E100	1.95	7.91	.38	27.54
B100	1.92	6.72	.41	29.08
A50	2.07	5.07	.30	23.08
B50	1.99	2.32	.36	26.47
E50	1.98	3.16	.36	26.47
A5	2.08	1.57	.30	23.08
B5	1.99	.77	.36	26.47
E5	2.00	.96	.35	25.93
DENISON UNC.				
A100	1.70	15.78	.59	37.11
E100	1.67	14.09	.62	38.27
B100	1.62	12.03	.67	40.12
A60	1.71	10.66	.58	36.71
B80	1.65	9.38	.64	39.02
E50	1.67	7.27	.62	38.27
A20	1.74	3.18	.55	35.48
E5	1.67	1.55	.62	38.27
B20	1.63	2.92	.66	39.76

MINE LOCATION	DRY DENSITY	MOISTURE CONTENT %	VOID RATIO	POROSITY %
HBM&S INSITU				
NO VIBRATION	2.22	-	.57	36.31
15 SEC. VIB.	2.34	-	.49	32.89
30 SEC. VIB.	2.43	-	.43	30.07
60 SEC. VIB.	2.68	-	.30	23.08
HBM&S COMBO #1				
NO VIBTATION	1.78	-	.96	48.98
15 SEC. VIB.	1.98	-	.76	43.18
30 SEC. VIB.	2.10	-	.66	39.76
60 SEC. VIB.	2.21	-	.57	36.31
HBM&S +3/4				
NO VIBRATION	.97	-	2.59	72.14
15 SEC. VIB.	1.07	-	2.25	69.23
30 SEC. VIB.	1.14	-	2.05	67.21
60 SEC. VIB.	1.25	-	1.78	64.03
HBM&S -3/4, +1/2				
NO VIBRATION	1.41	-	1.47	59.51
15 SEC. VIB.	1.47	-	1.37	57.81
30 SEC. VIB.	1.51	-	1.30	56.52
60 SEC. VIB.	1.65	-	1.11	52.61
HBM&S -1/2, +3 mesh				
NO VIBRATION	1.32	-	1.64	62.12
15 SEC. VIB.	1.37	-	1.54	60.63
30 SEC. VIB.	1.47	-	1.37	57.81
60 SEC. VIB.	1.53	-	1.27	55.95
HBM&S -3 mesh, +4 mesh				
NO VIBRATION	1.63	-	1.13	53.05
15 SEC. VIB.	1.75	-	.99	49.75
30 SEC. VIB.	1.85	-	.88	46.81
60 SEC. VIB.	2.05	-	.70	41.18
CHADBOURNE	2.11	-	.62	38.27
SELBAIE	1.77	-	.69	40.83
BOUSQUET	1.27	-	1.17	53.92

APPENDIX 9

[illegible] FIELD PRESSUREMETER [illegible]

Campbell Red Lake — Corrected Data

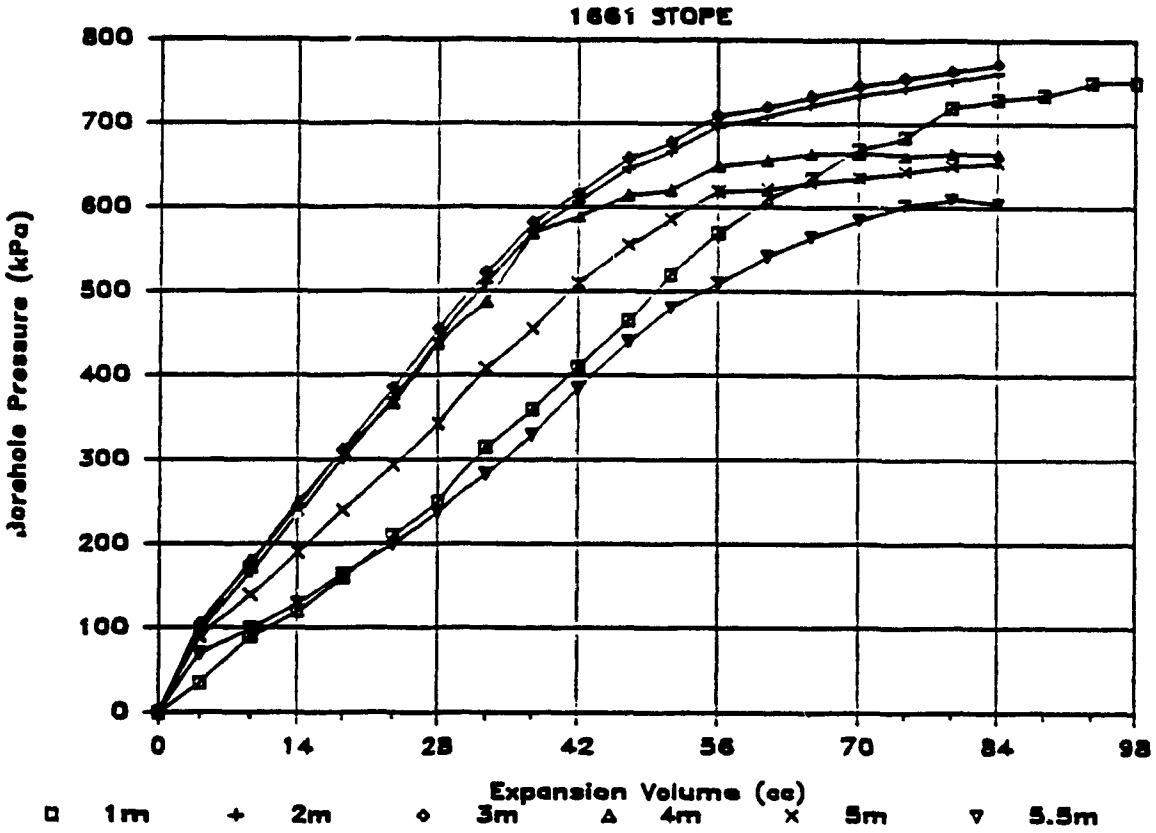

Campbell Red Lake — Corrected Data

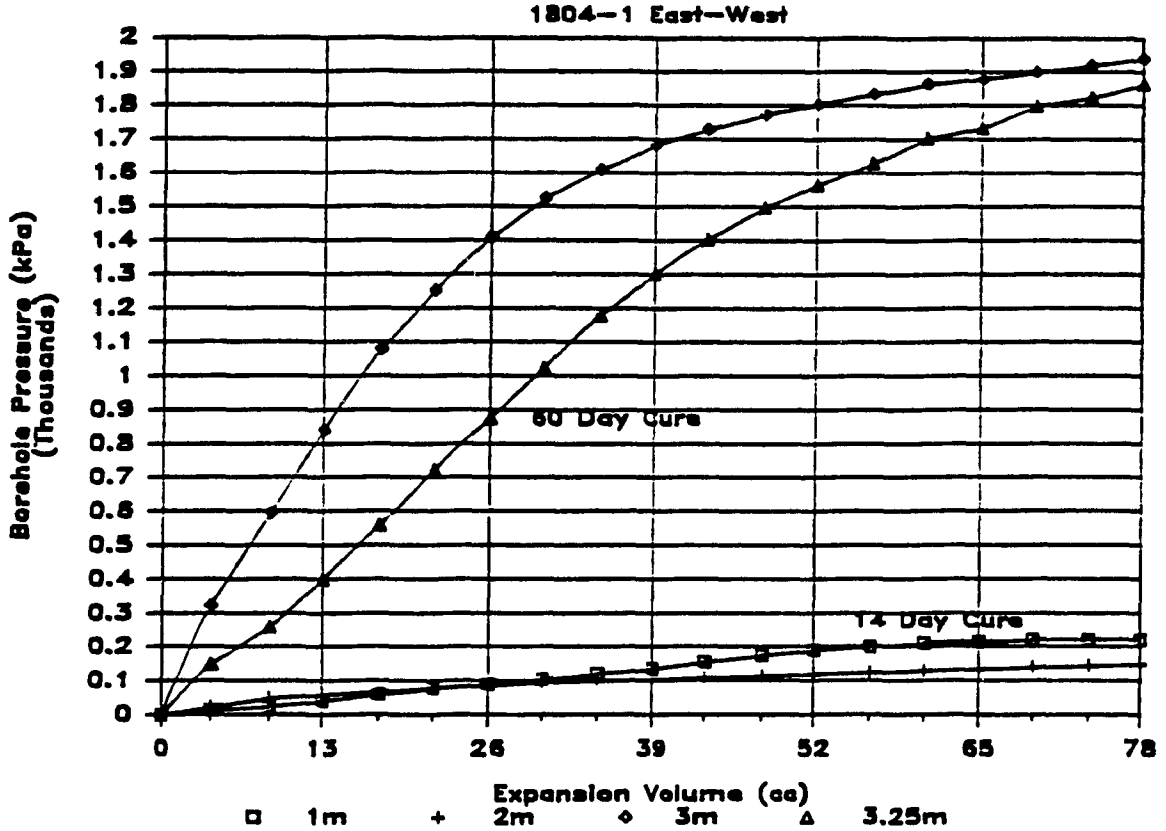

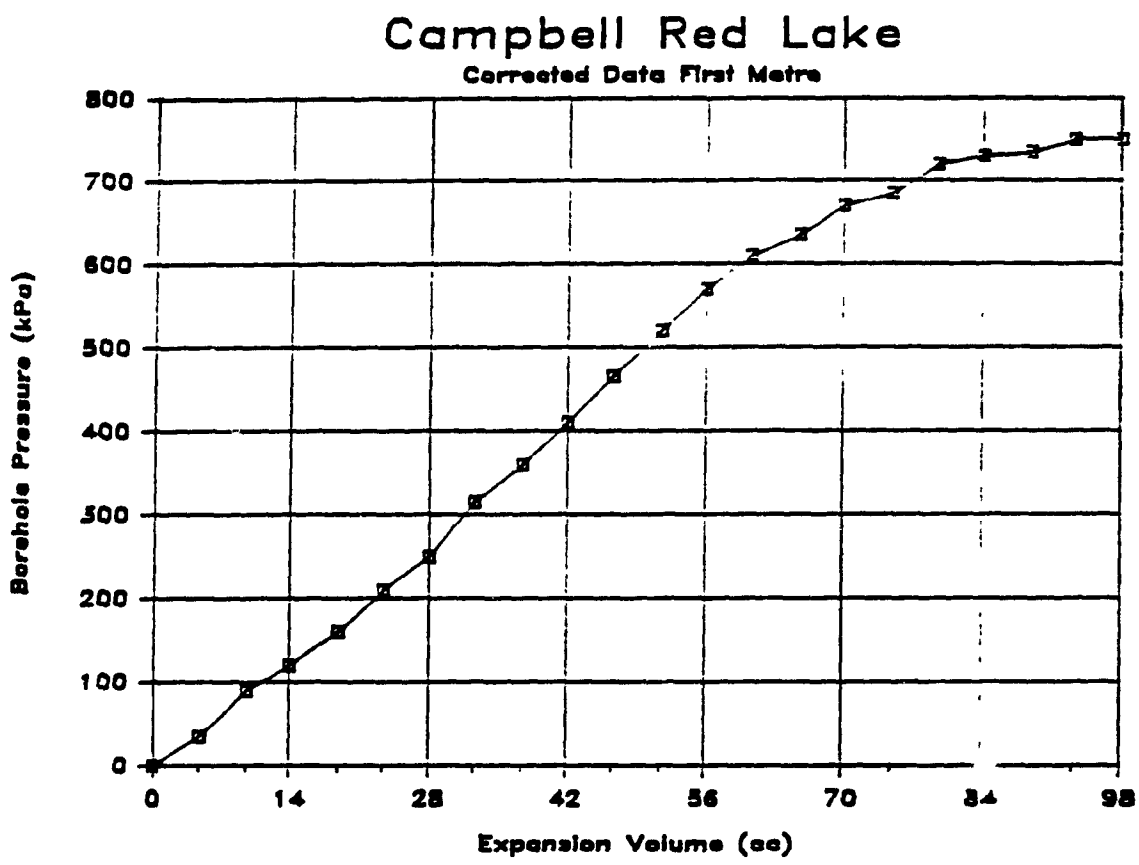
Campbell Red Lake
Corrected Data First Metre
Borehole Pressure (kPa)
800
700
600
500
400
300
200
100
0
0
14
28
42
56
70
84
98
Expansion Volume (cc)

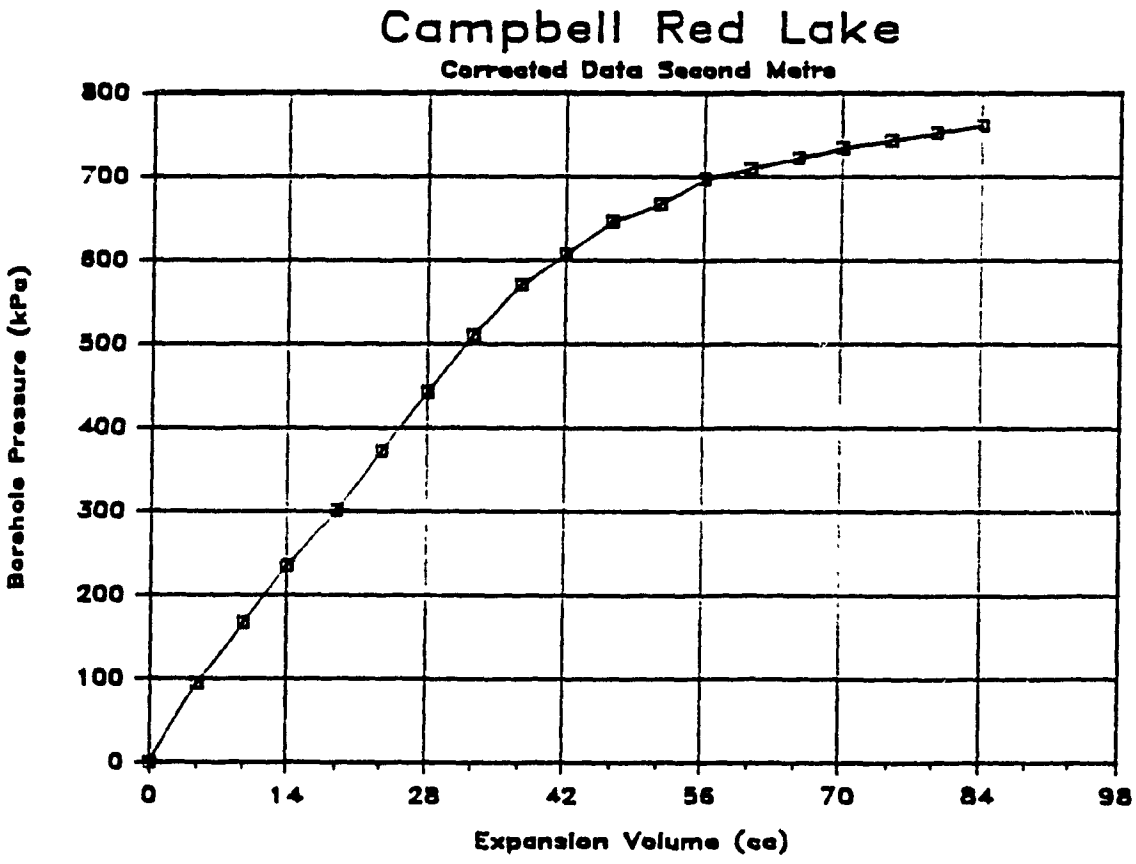
Campbell Red Lake
Corrected Data Second Metre
Borehole Pressure (kPa)
800
700
600
500
400
300
200
100
0
0
14
28
42
56
70
84
98
Expansion Volume (cc)

Campbell Red Lake

Corrected Data Third Metre

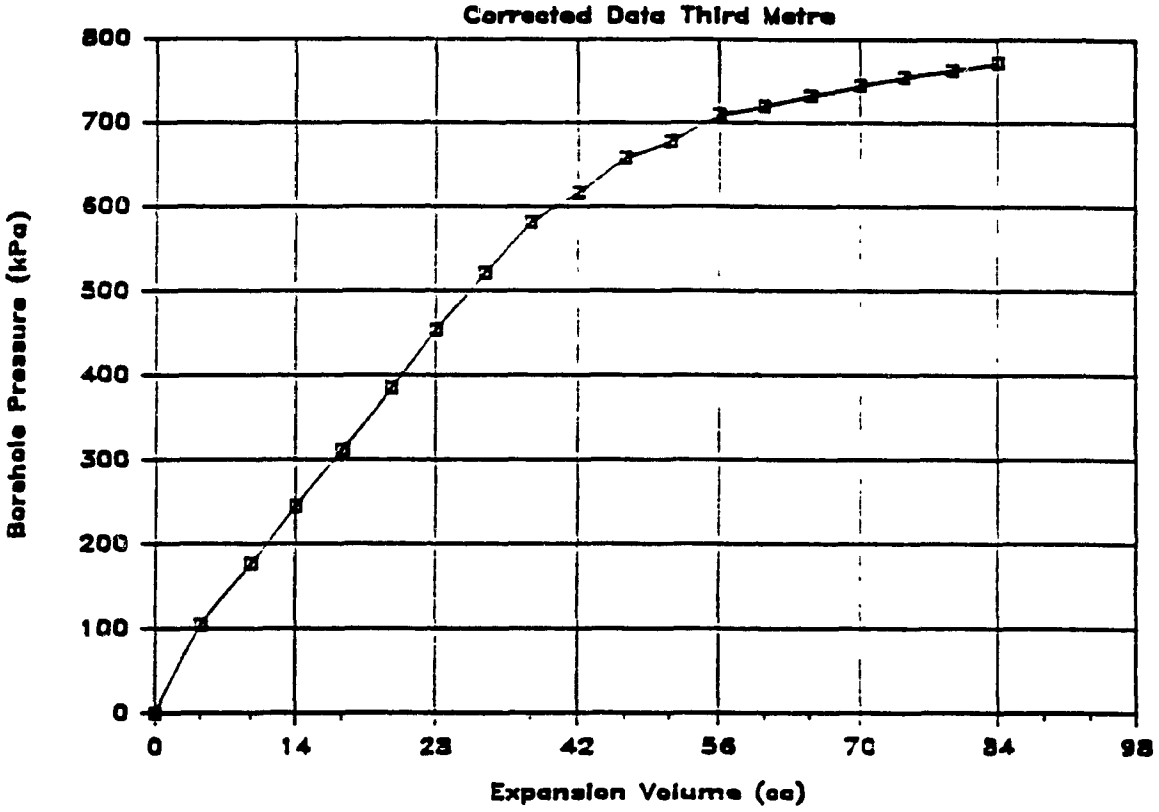

Campbell Red Lake

Corrected Data Fourth Metre

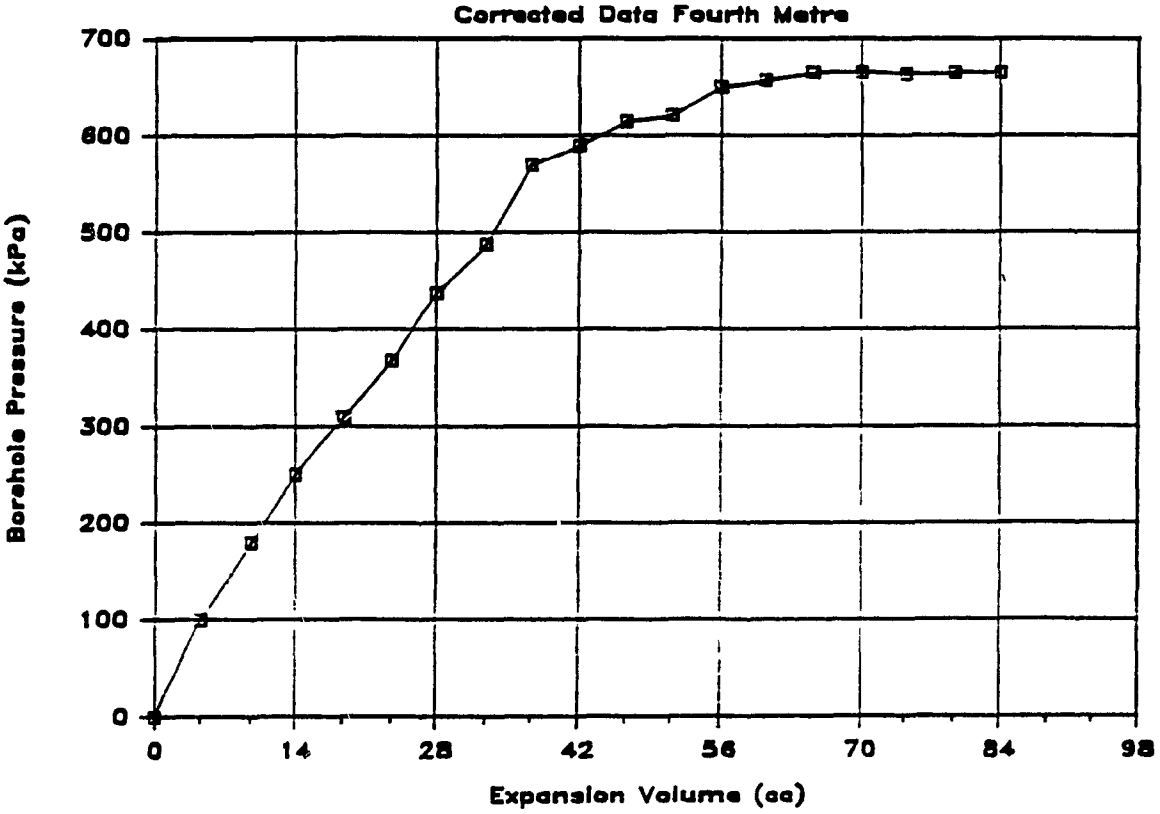

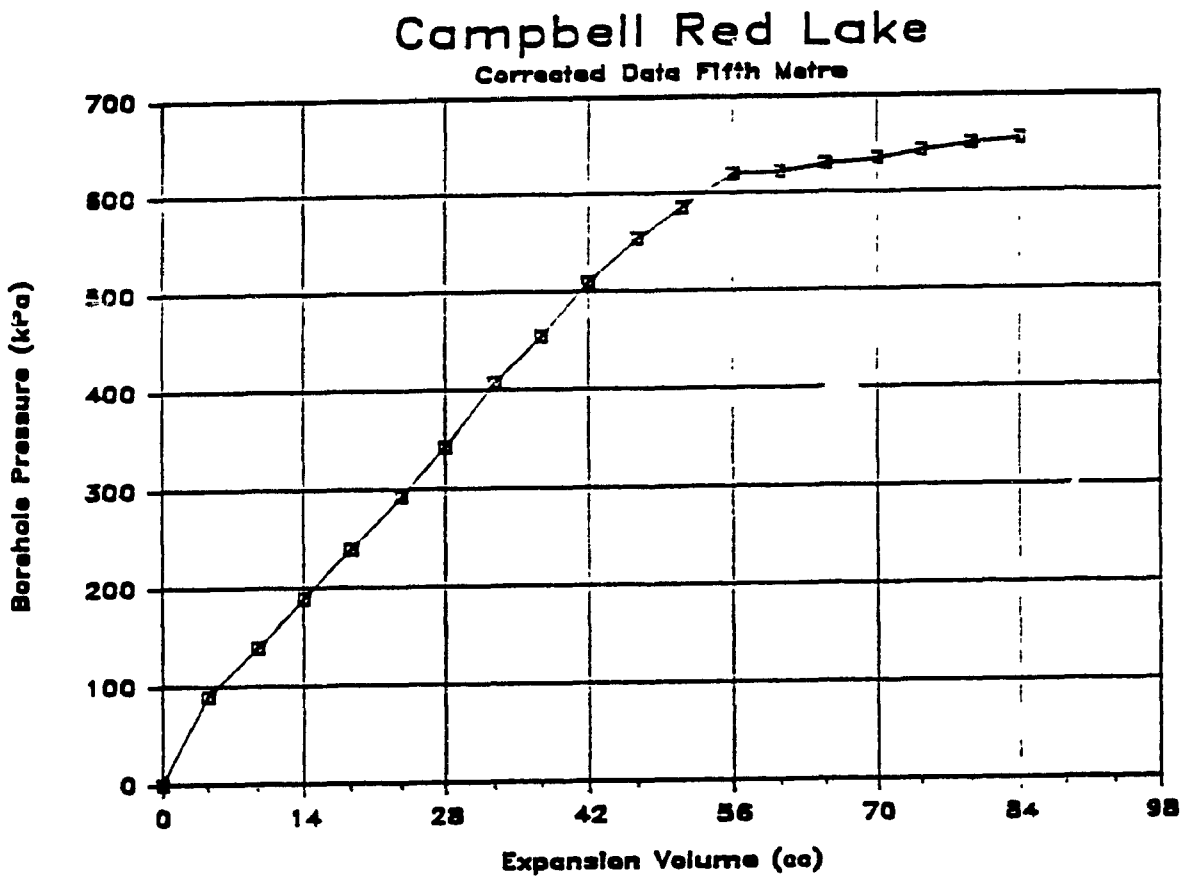
Campbell Red Lake
Corrected Data Fifth Metre
Borehole Pressure (kPa)
700
600
500
400
300
200
100
0
0
14
28
42
56
70
84
98
Expansion Volume (cc)

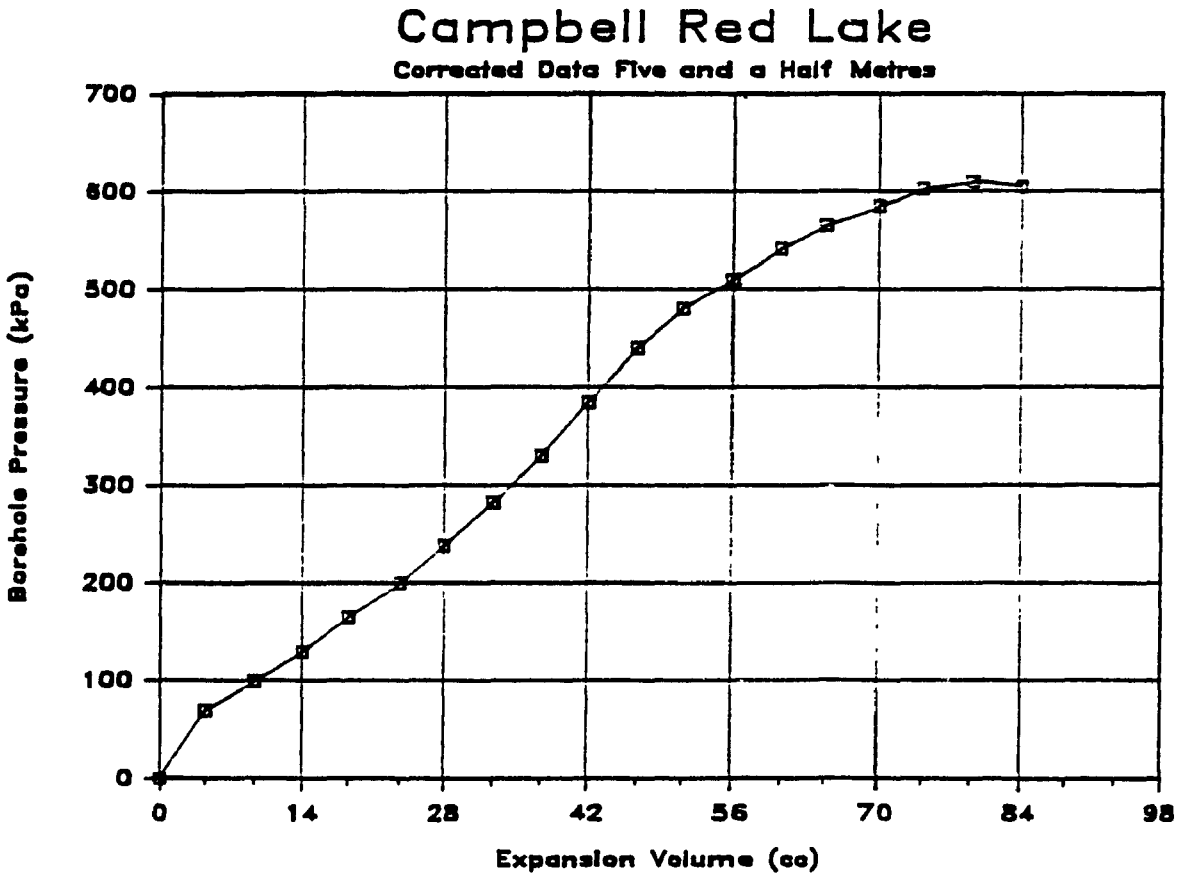
Campbell Red Lake
Corrected Data Five and a Half Metres
Borehole Pressure (kPa)
700
600
500
400
300
200
100
0
0
14
28
42
56
70
84
98
Expansion Volume (cc)

Campbell Red Lake — Corrected Data

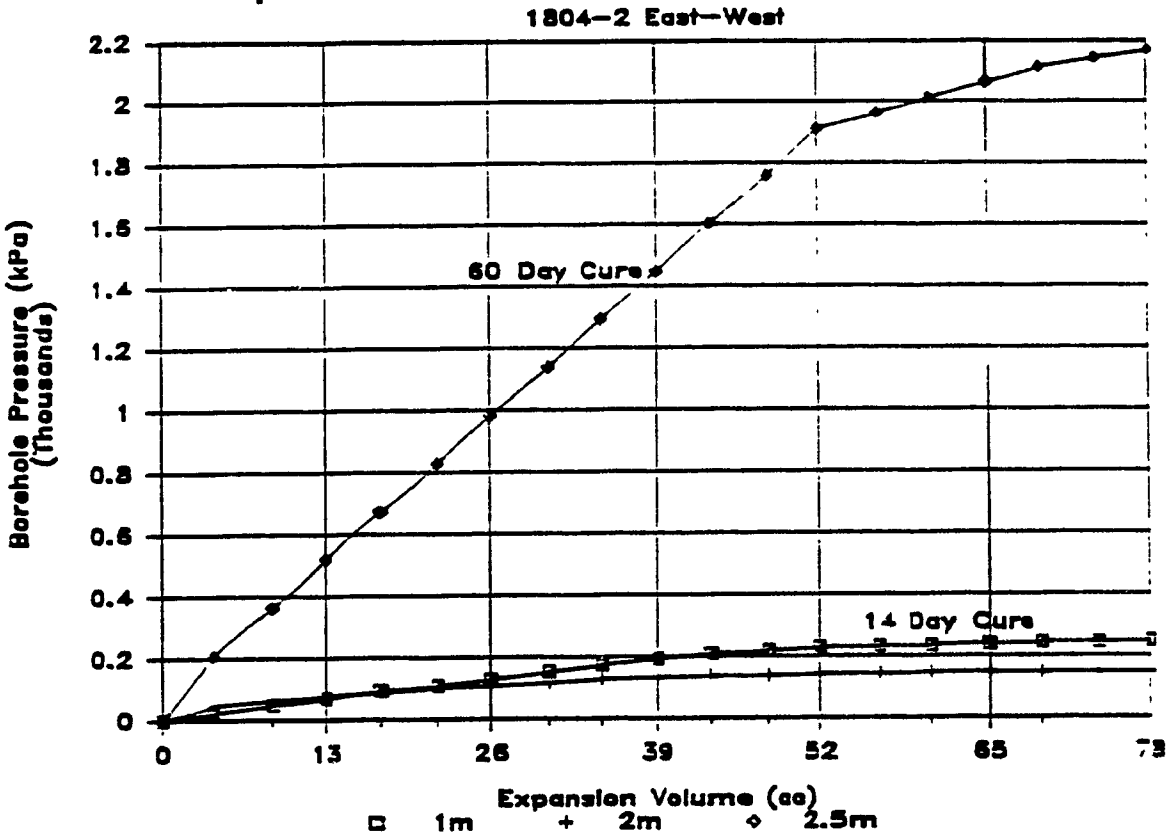

Campbell Red Lake — Corrected Dcta

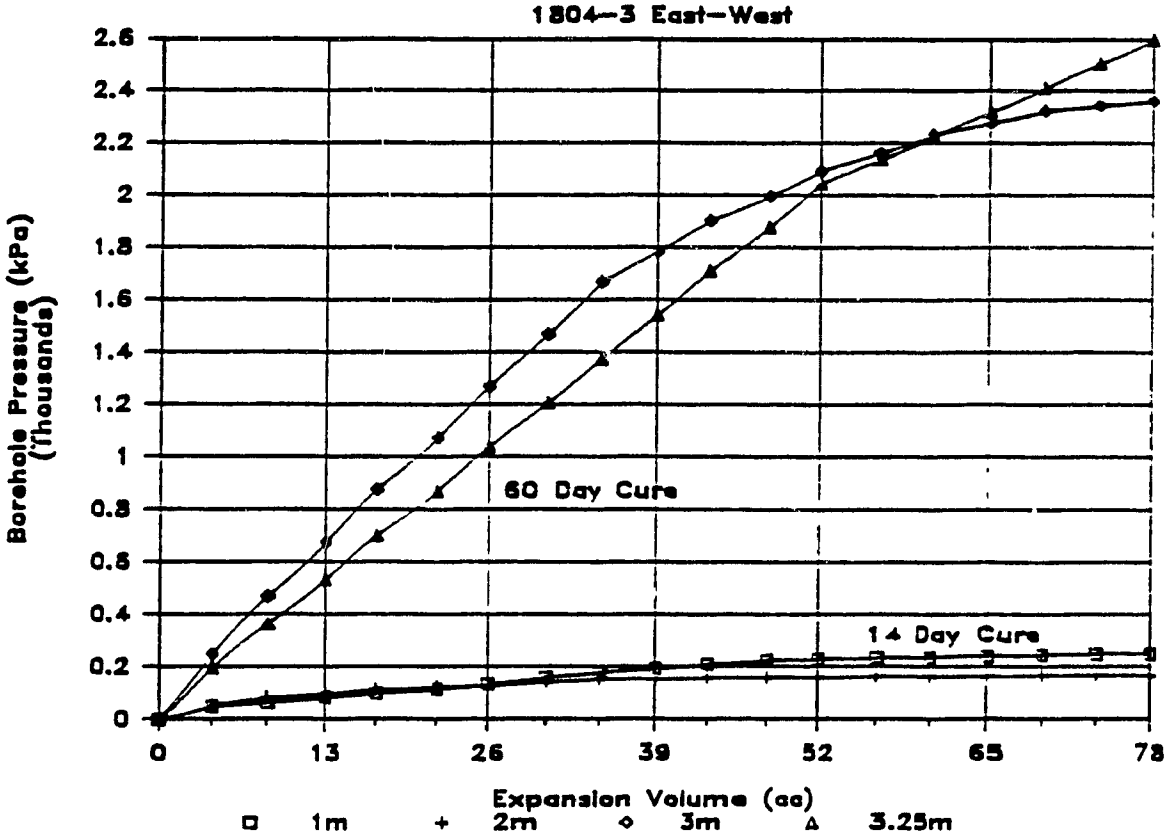

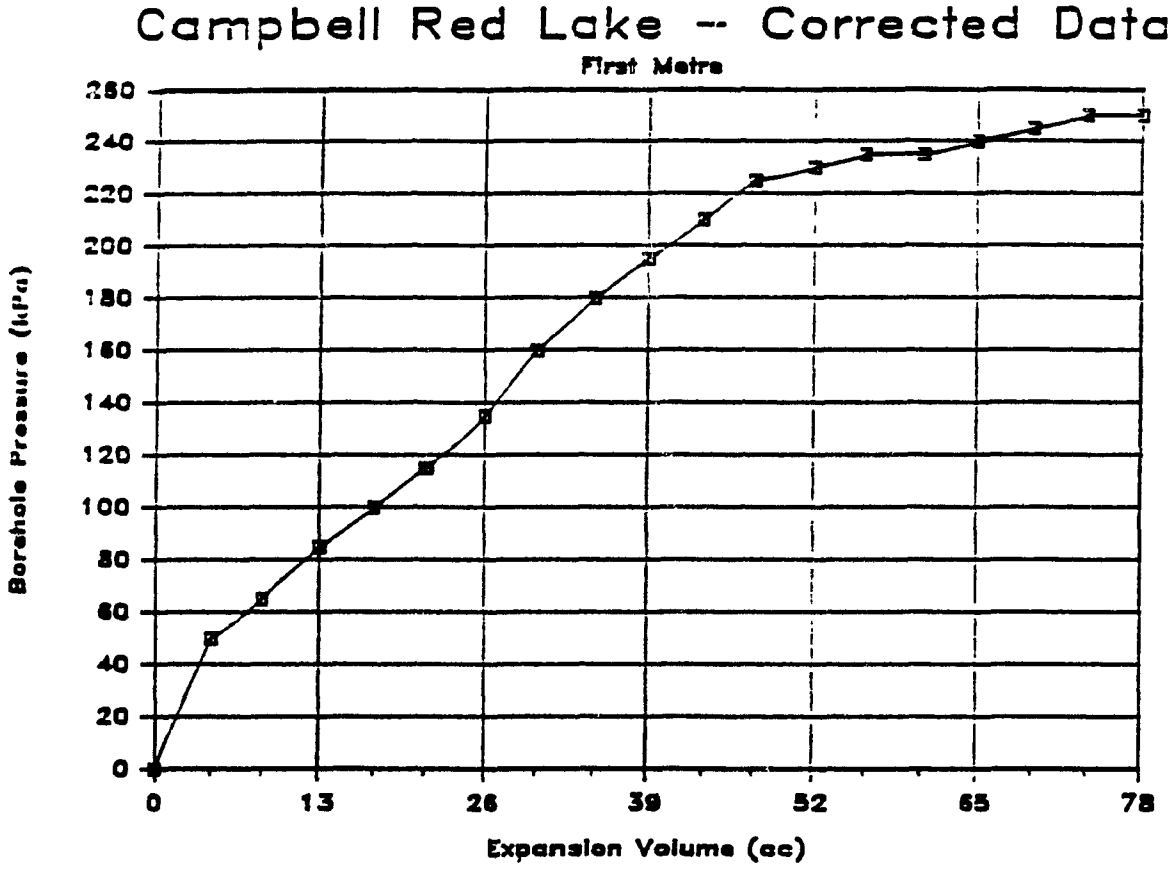
Campbell Red Lake -- Corrected Data
First Metre
Borehole Pressure (kPa)
260
240
220
200
180
160
140
120
100
80
60
40
20
0
0
13
26
39
52
65
78
Expansion Volume (cc)

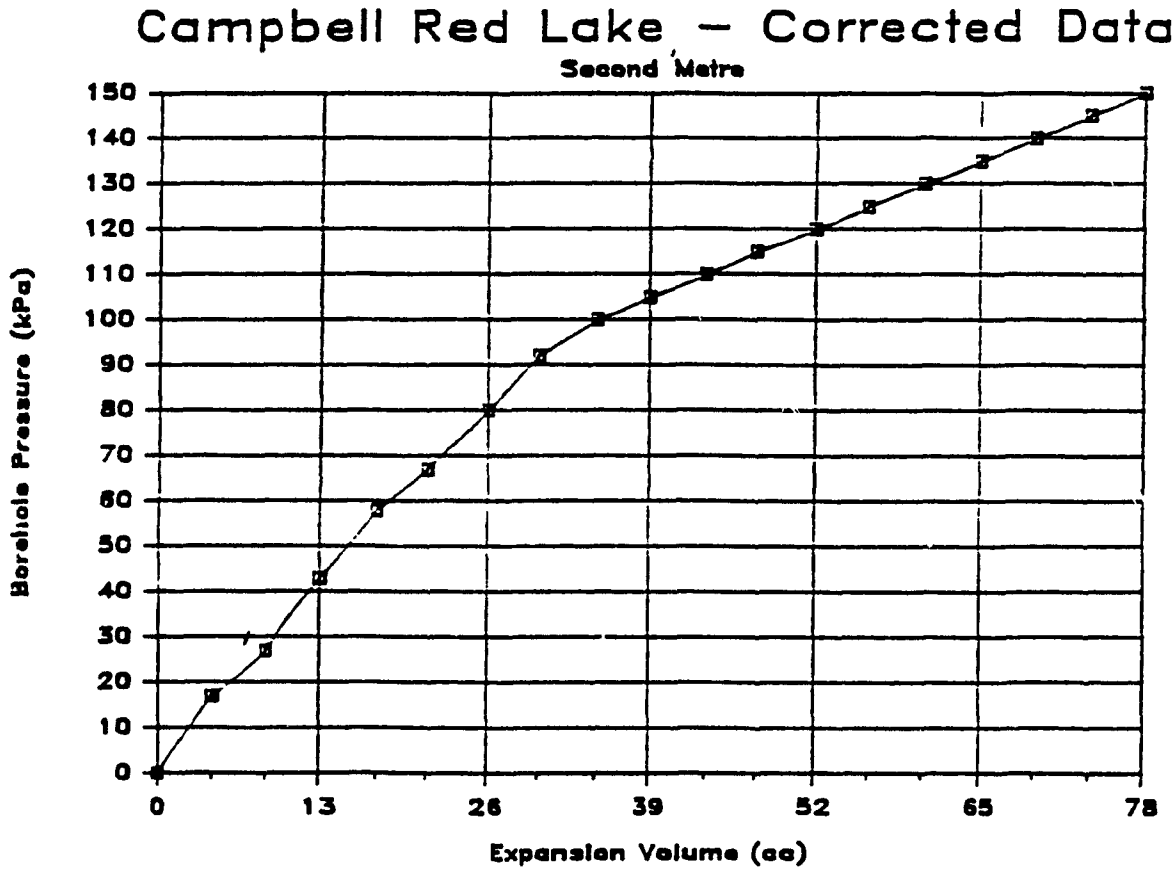
Campbell Red Lake – Corrected Data
Second Metre
Borehole Pressure (kPa)
150
140
130
120
110
100
90
80
70
60
50
40
30
20
10
0
0
13
26
39
52
65
78
Expansion Volume (cc)

Campbell Red Lake – Corrected Data

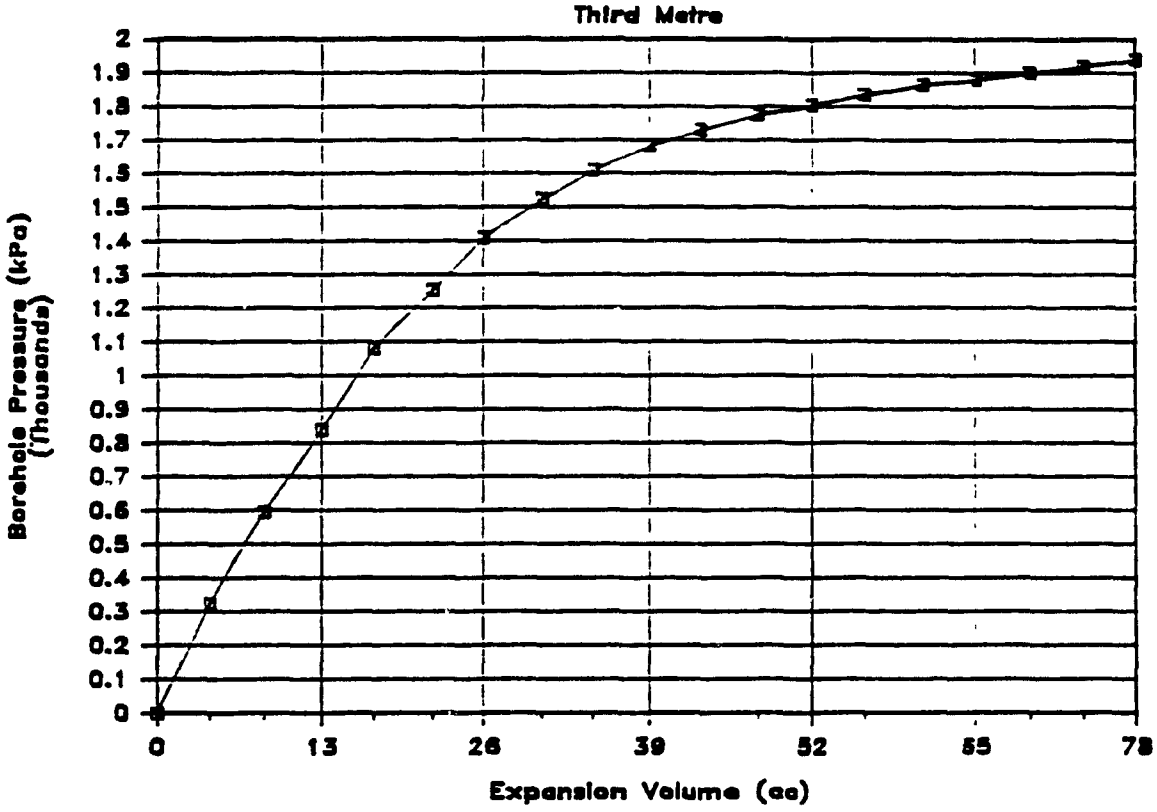

Campbell Red Lake – Corrected Data

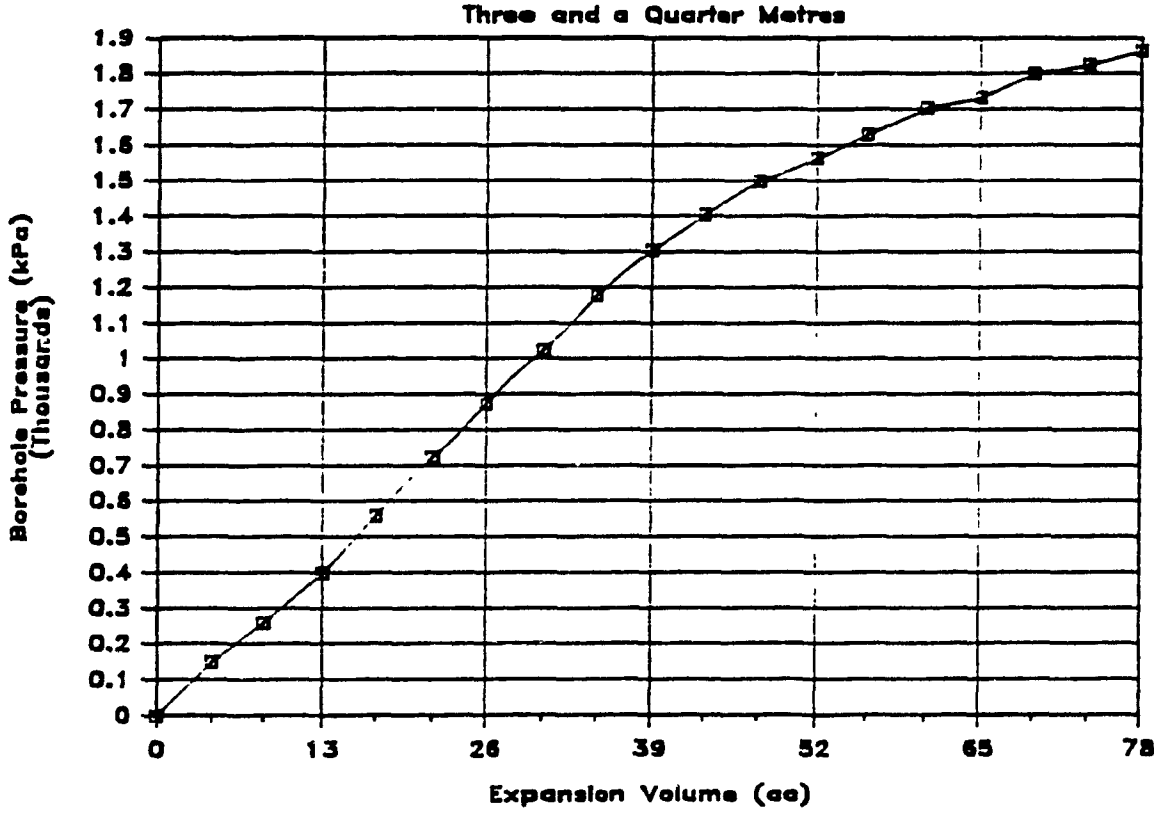

Campbell Red Lake – Corrected Data

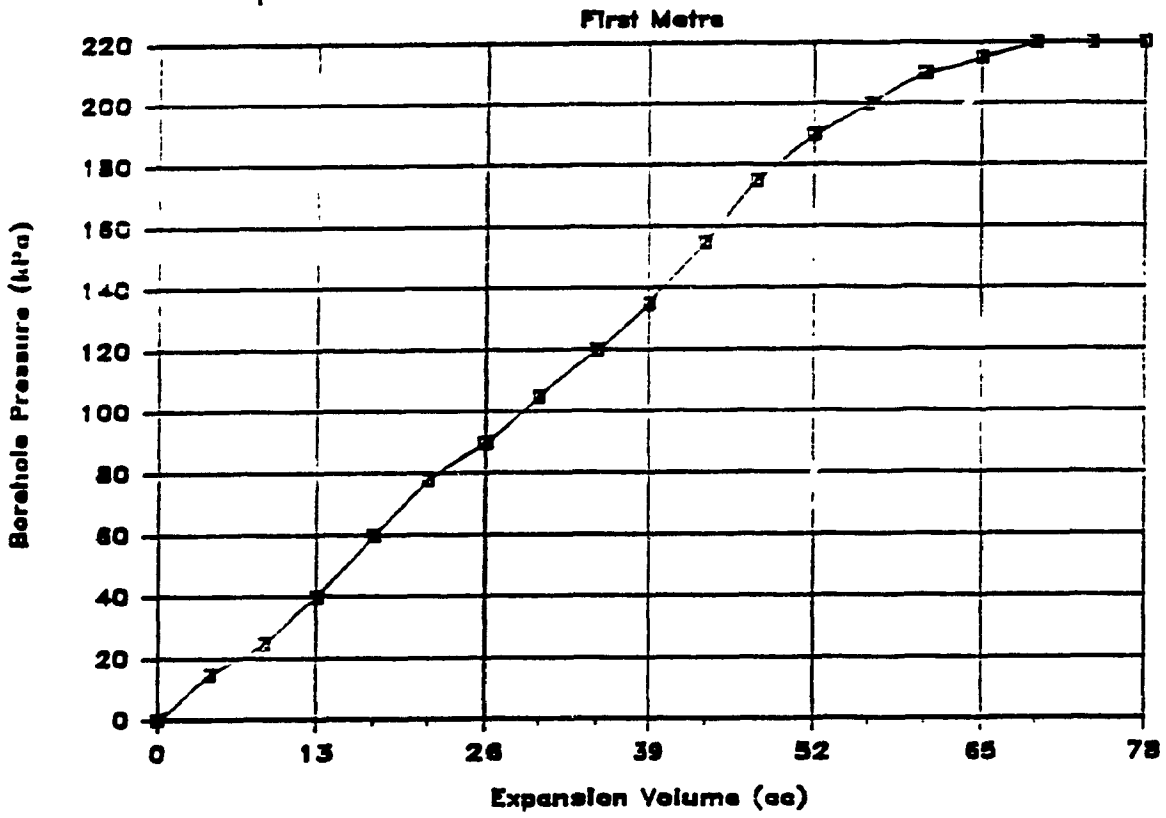

Campbell Red Lake – Corrected Data

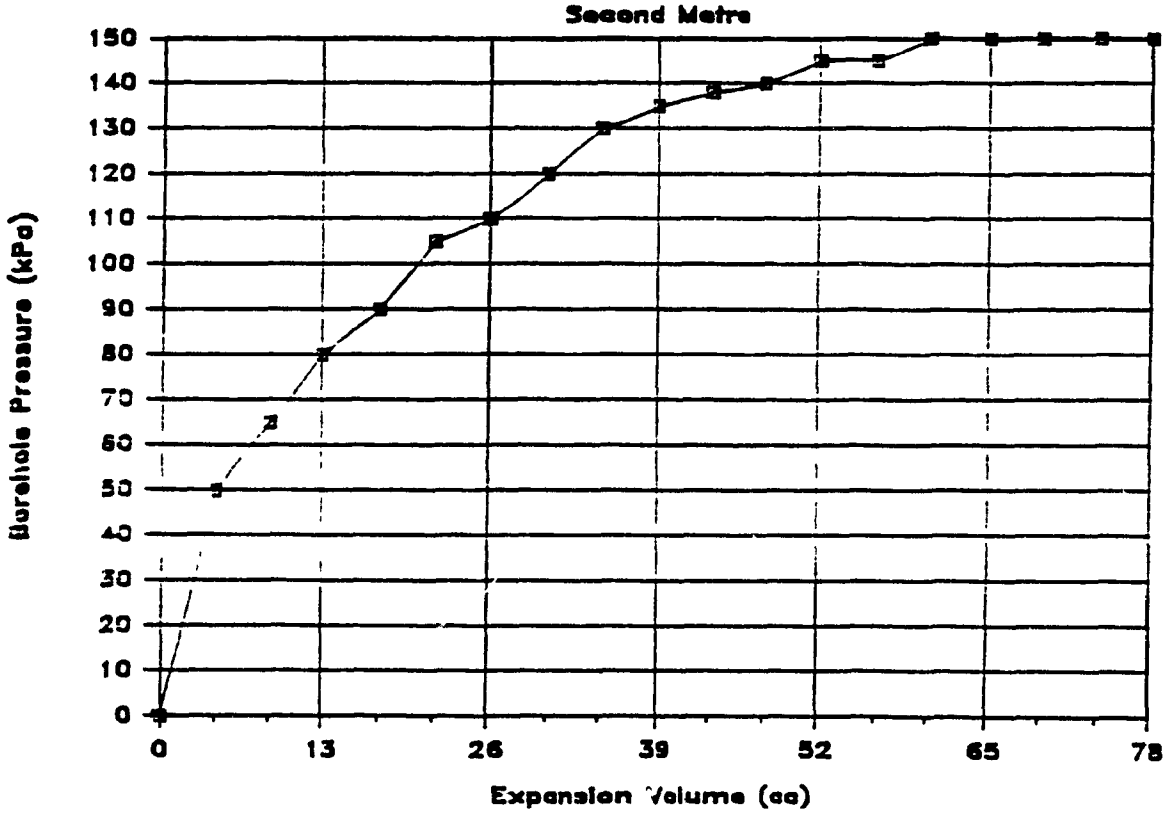

Campbell Red Lake – Corrected Data

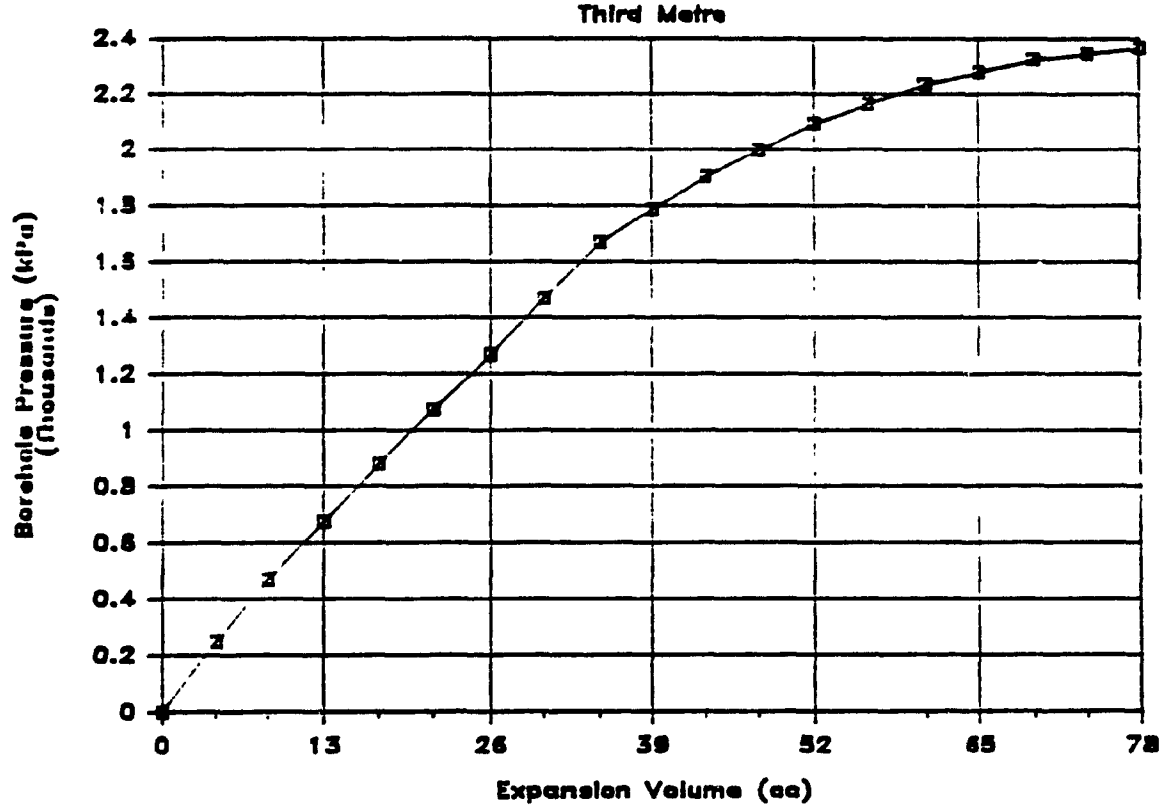

Campbell Red Lake – Corrected Data

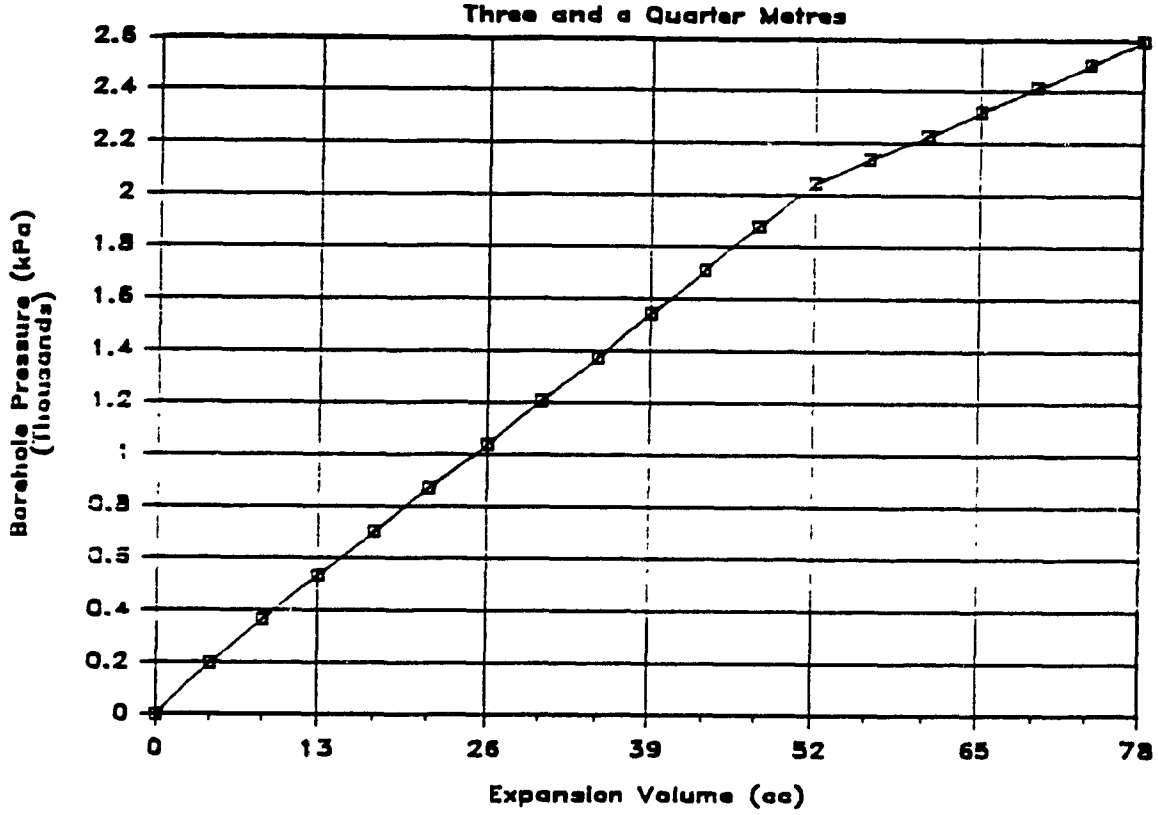

Campbell Red Lake – Corrected Data

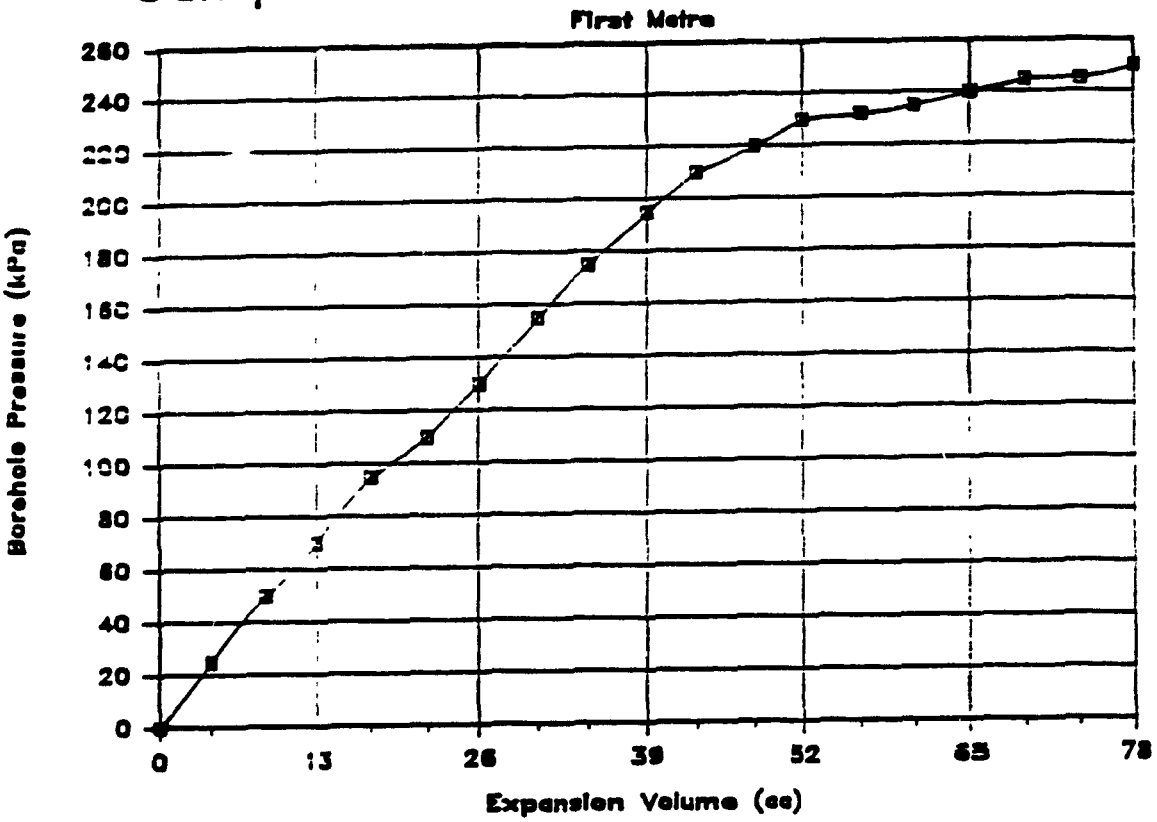

Campbell Red Lake – Corrected Data

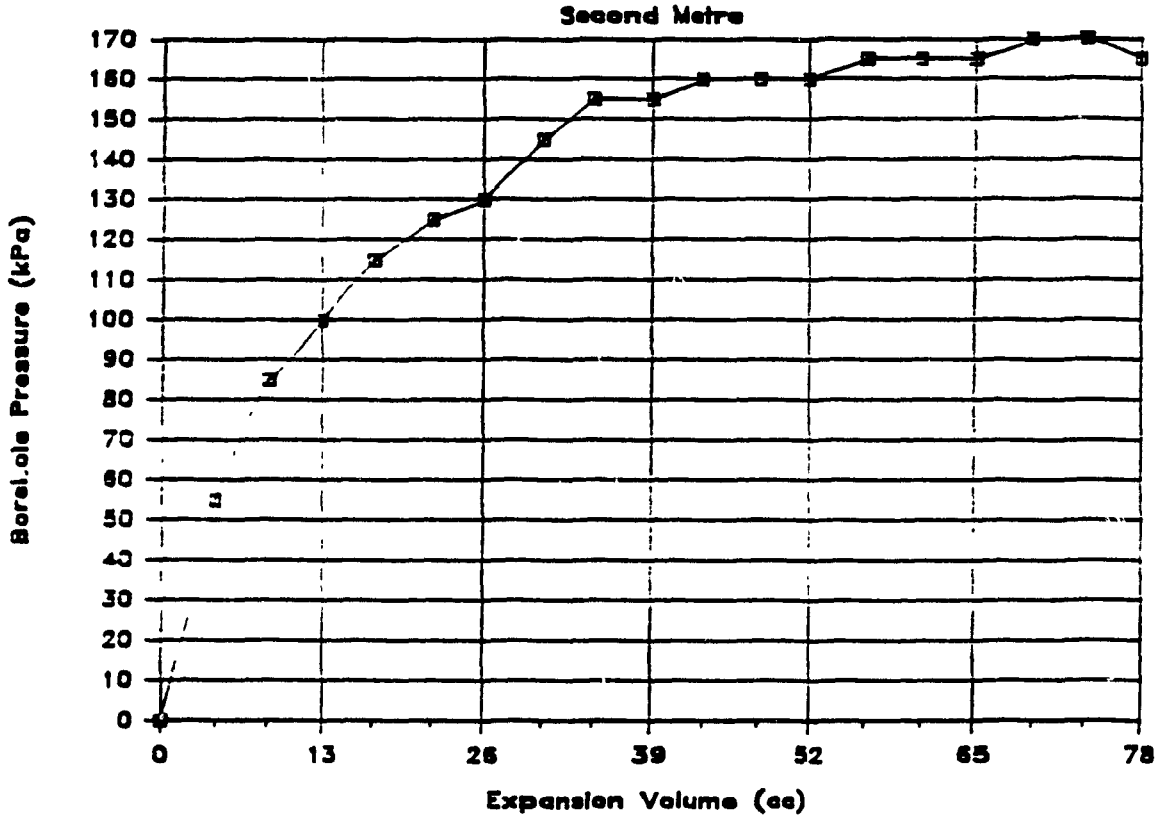

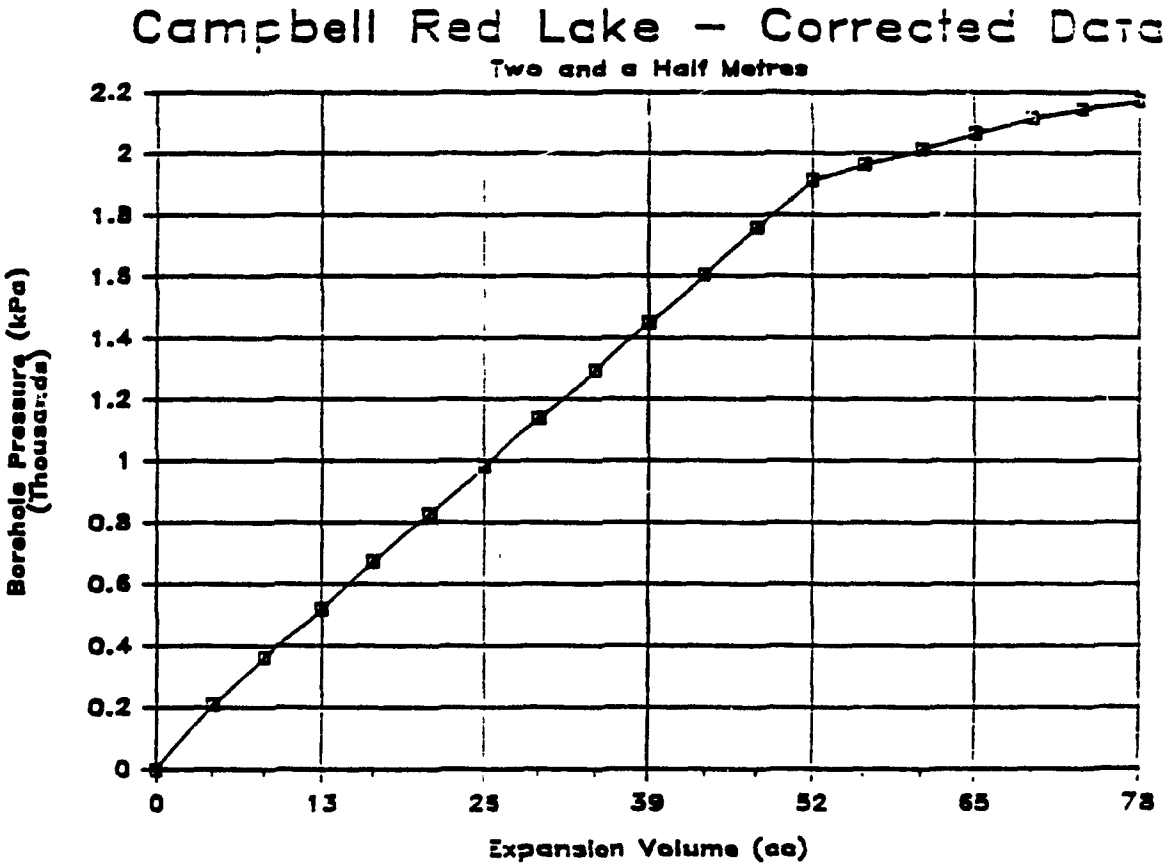
Campbell Red Lake – Corrected Data
Two and a Half Metres
Borehole Pressure (kPa)
(Thousands)
2.2
2
1.8
1.6
1.4
1.2
1
0.8
0.6
0.4
0.2
0
0
13
26
39
52
65
78
Expansion Volume (cc)

Chadbourne Surface Location

Corrected Data

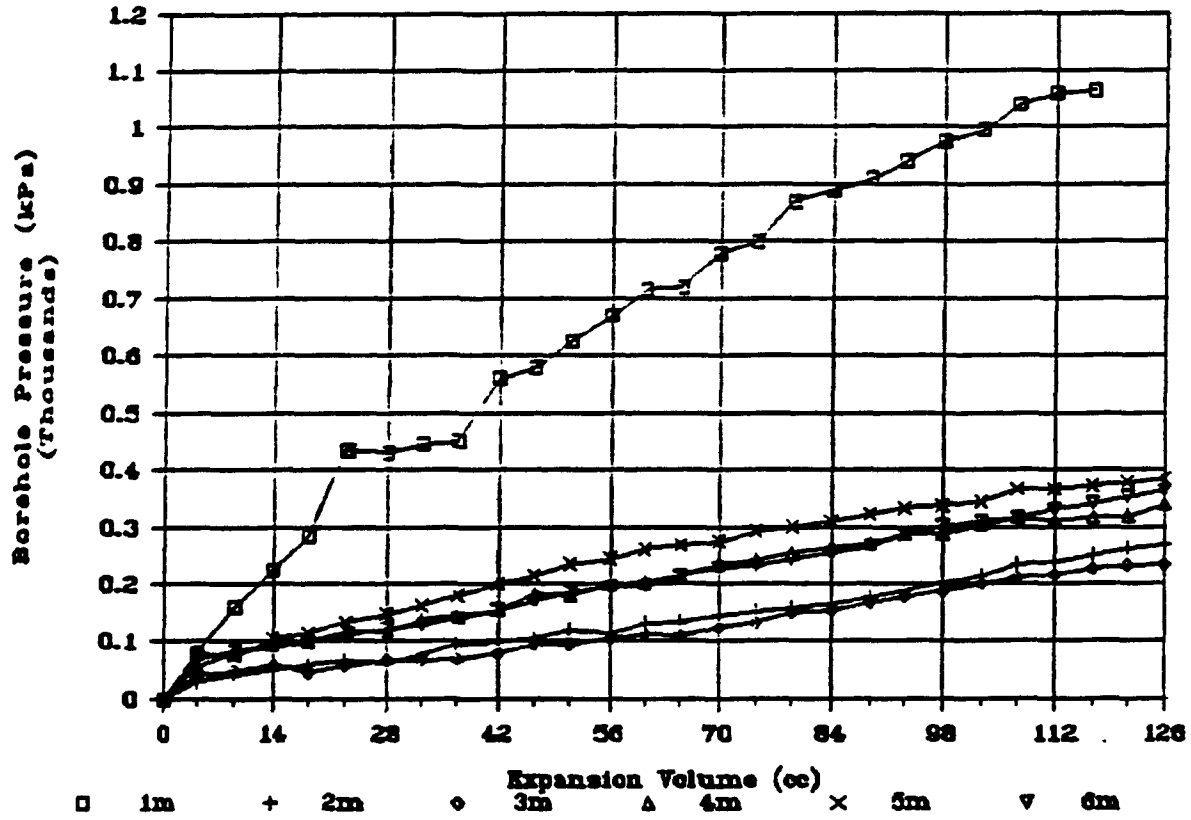

Chadbourne Surface Location

Corrected Data

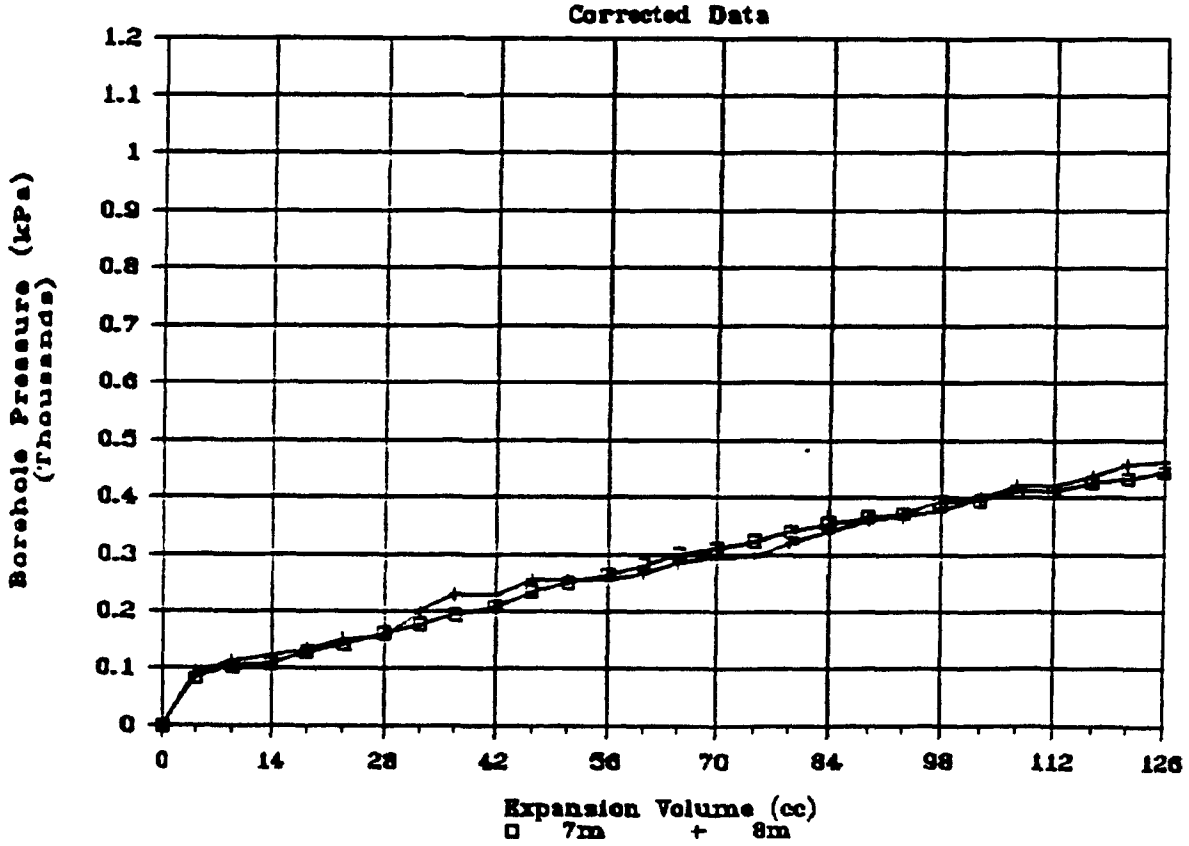

Chadbourne Surface Location

Corrected Data First Metre

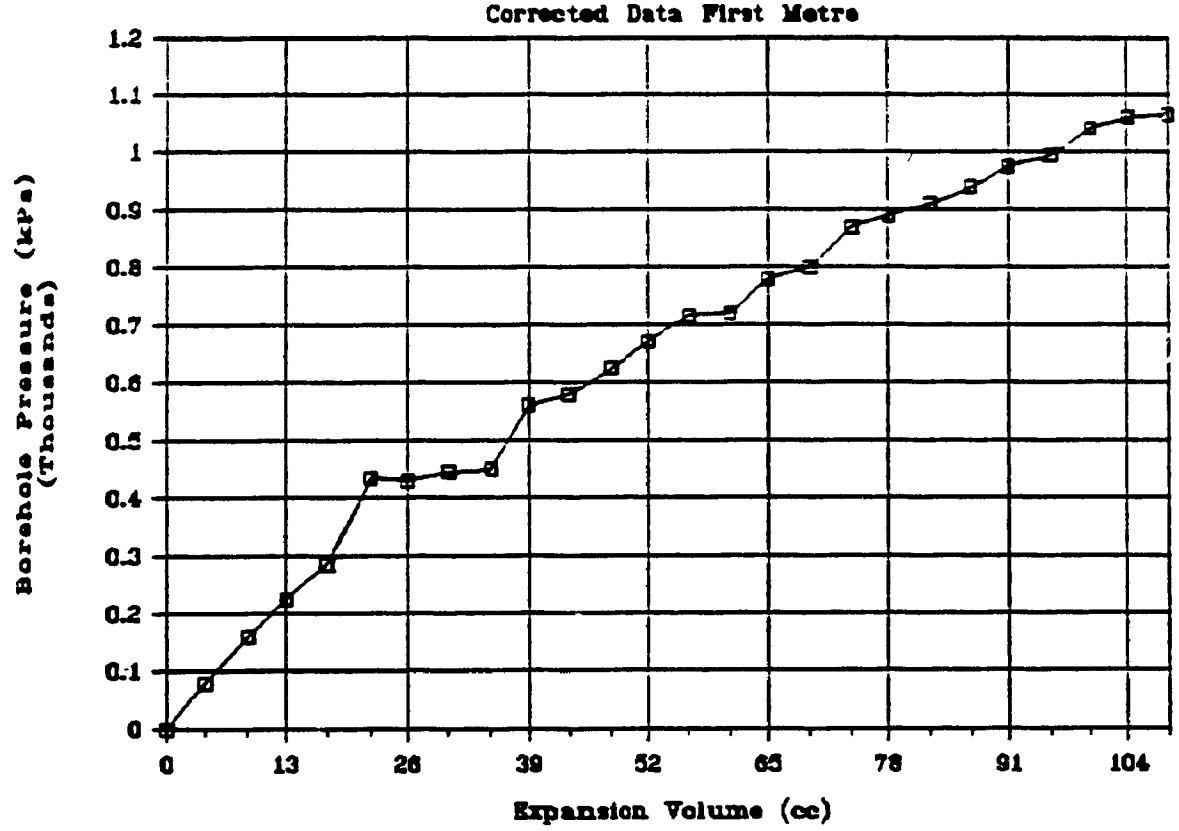

Chadbourne Surface Location

Corrected Data Second Metre

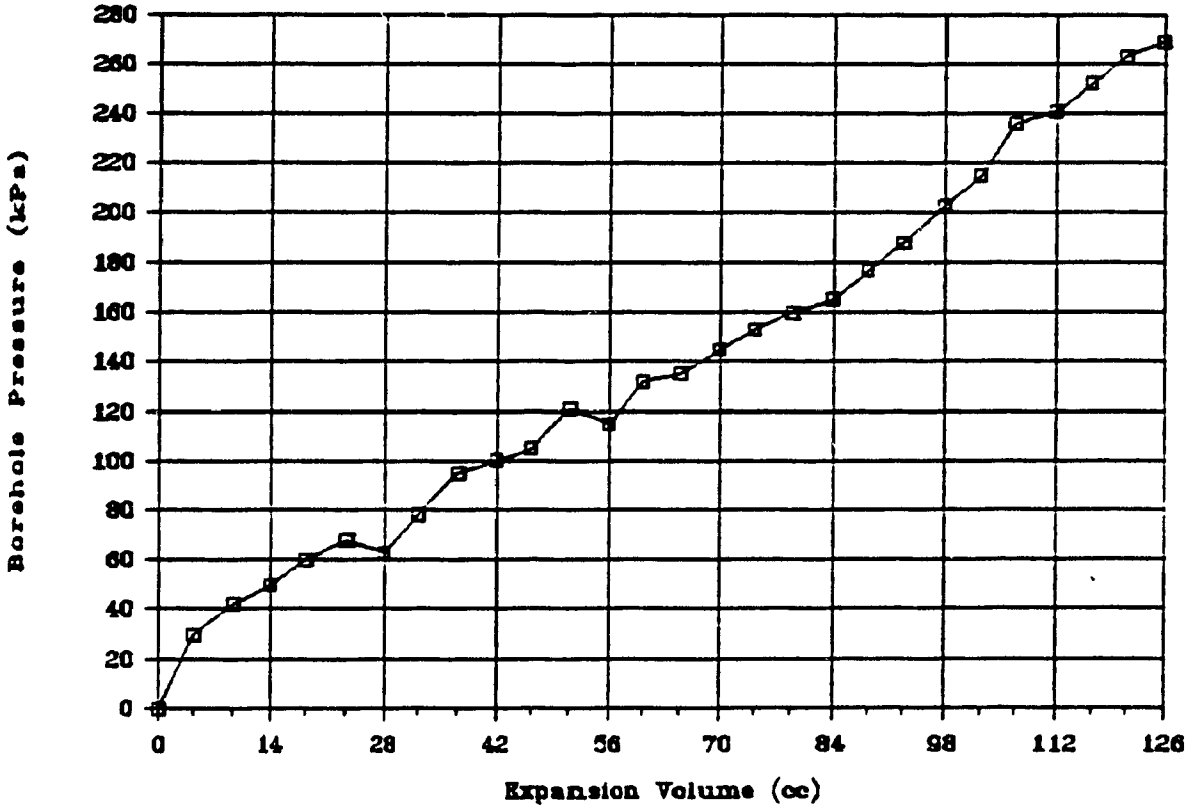

Chadbourne Surface Location

Corrected Data Third Metre

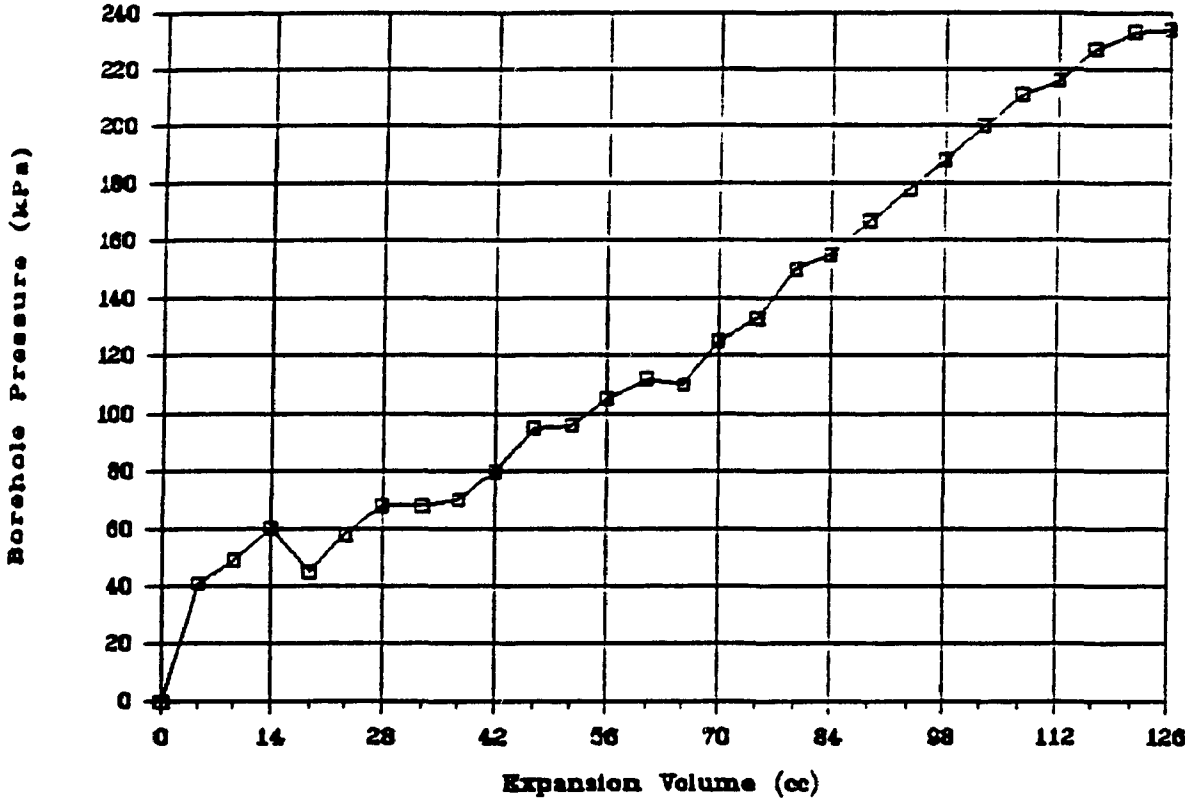

Chadbourne Surface Location

Corrected Data Fourth Metre

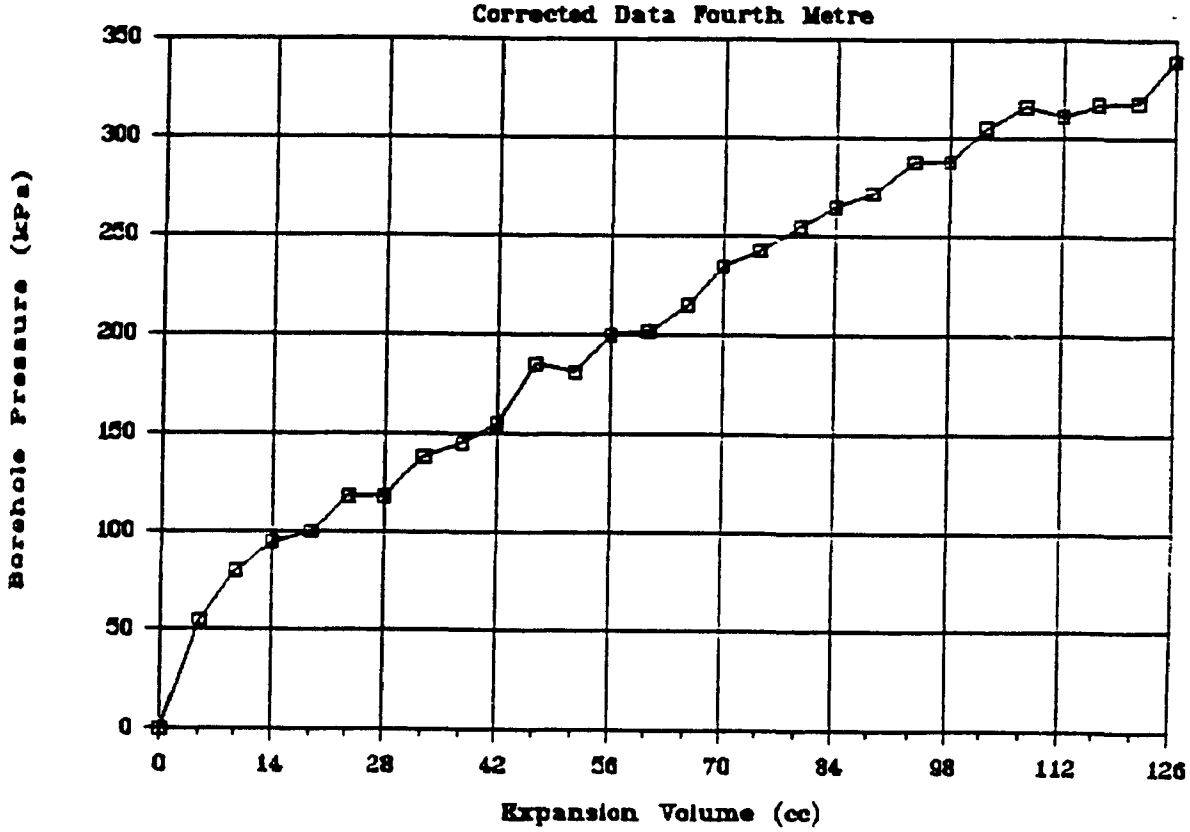

Chadbourne Surface Location

Corrected Data Fifth Metre

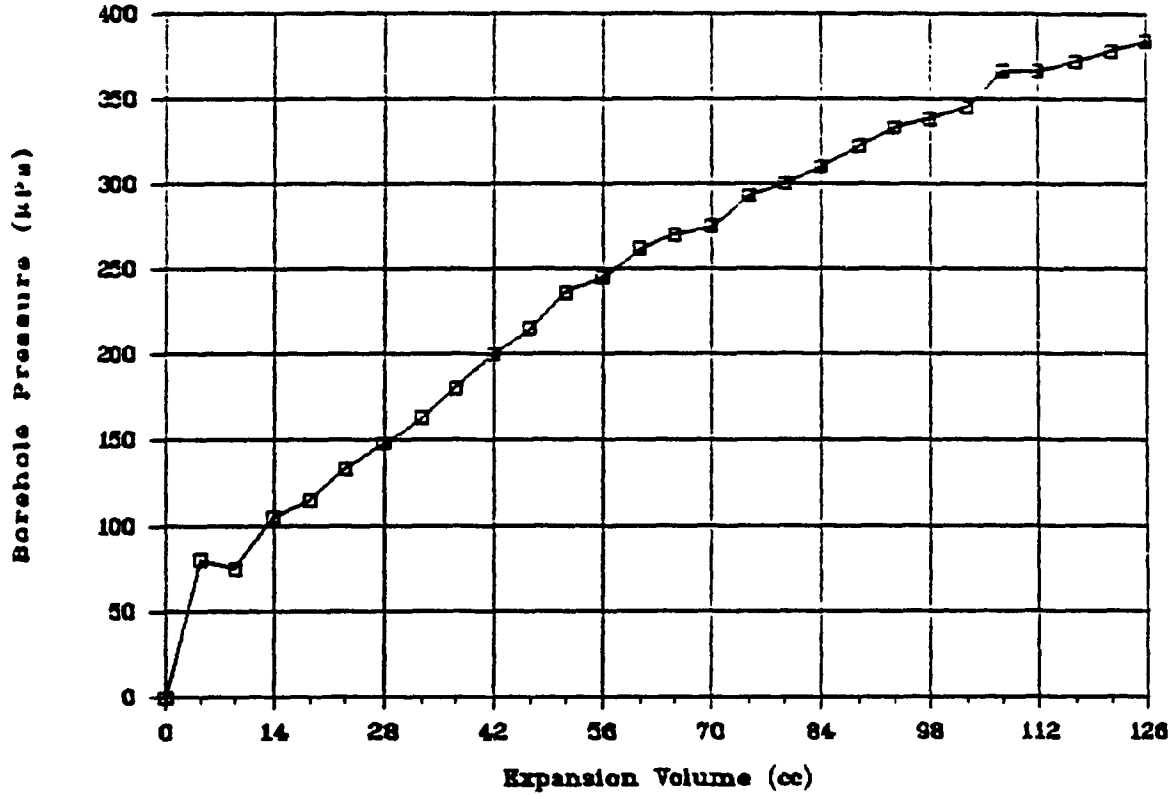

Chadbourne Surface Location

Corrected Data Sixth Metre

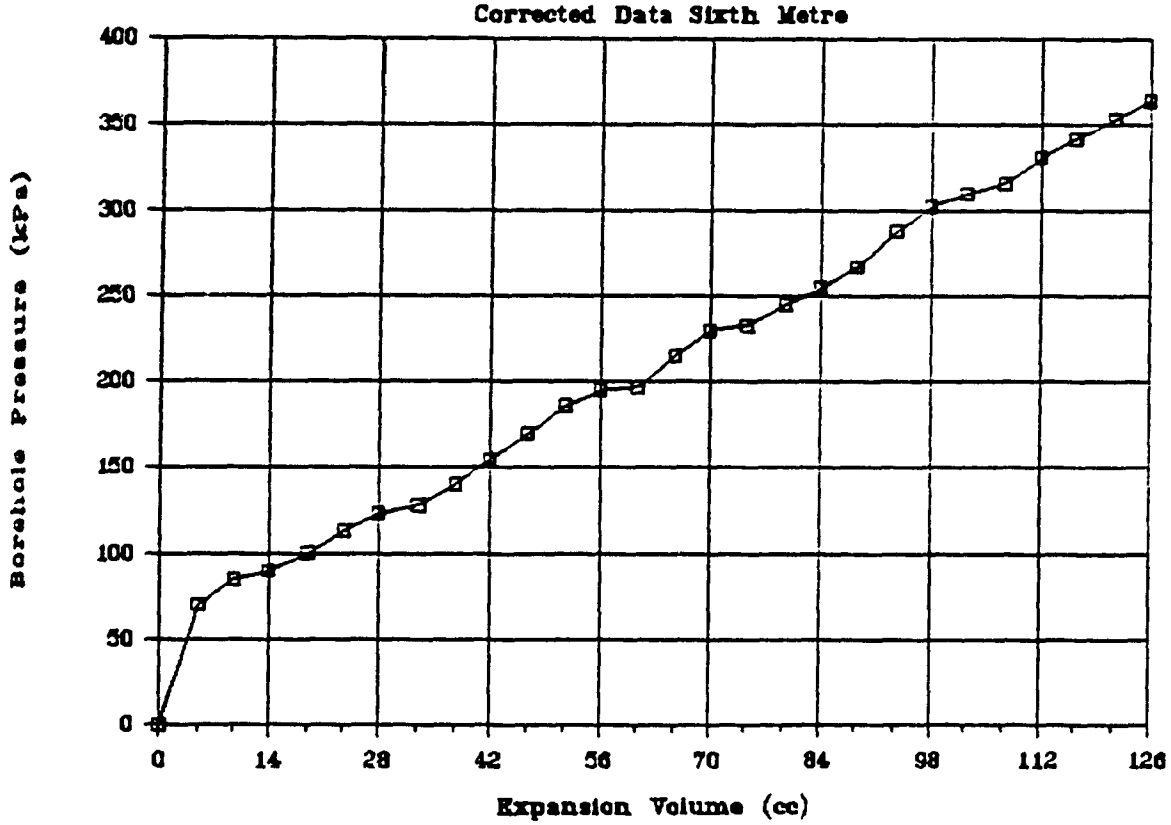

Chadbourne Surface Location

Corrected Data Seventh Metre

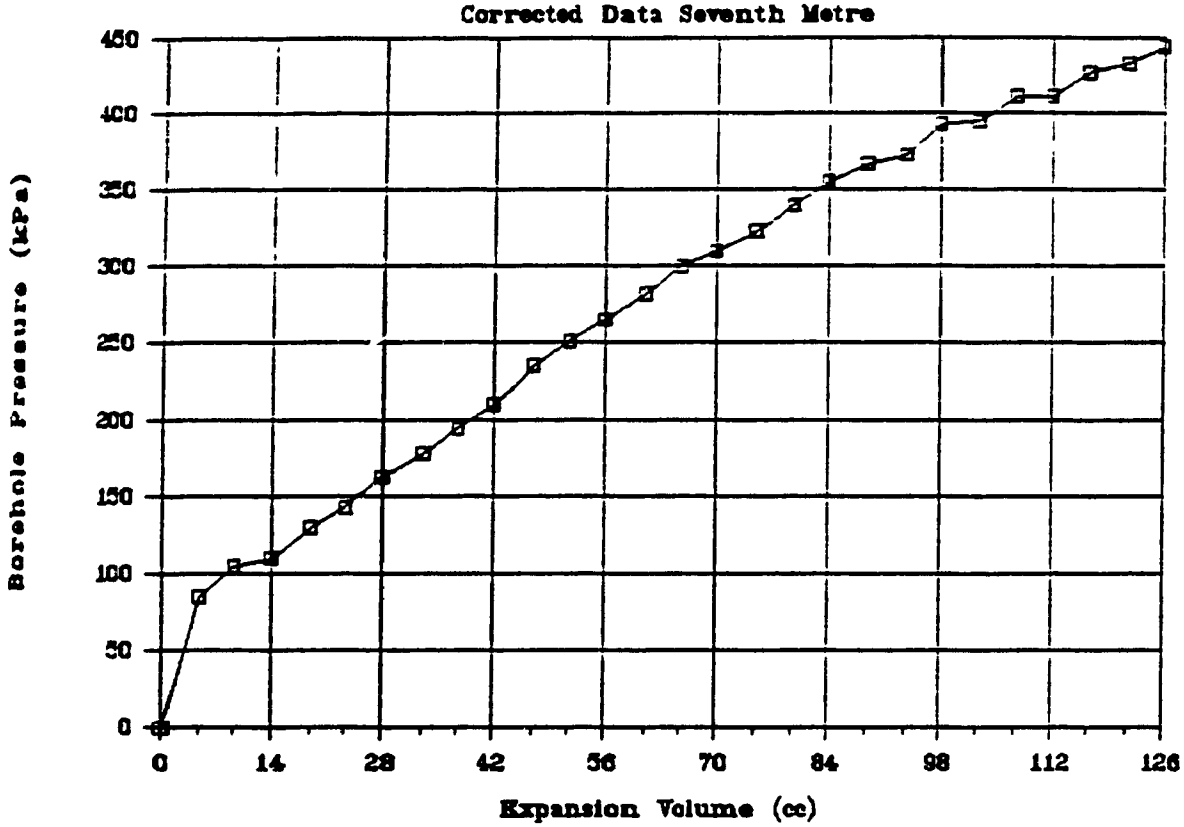

Chadbourne Surface Location

Corrected Data Eighth Metre

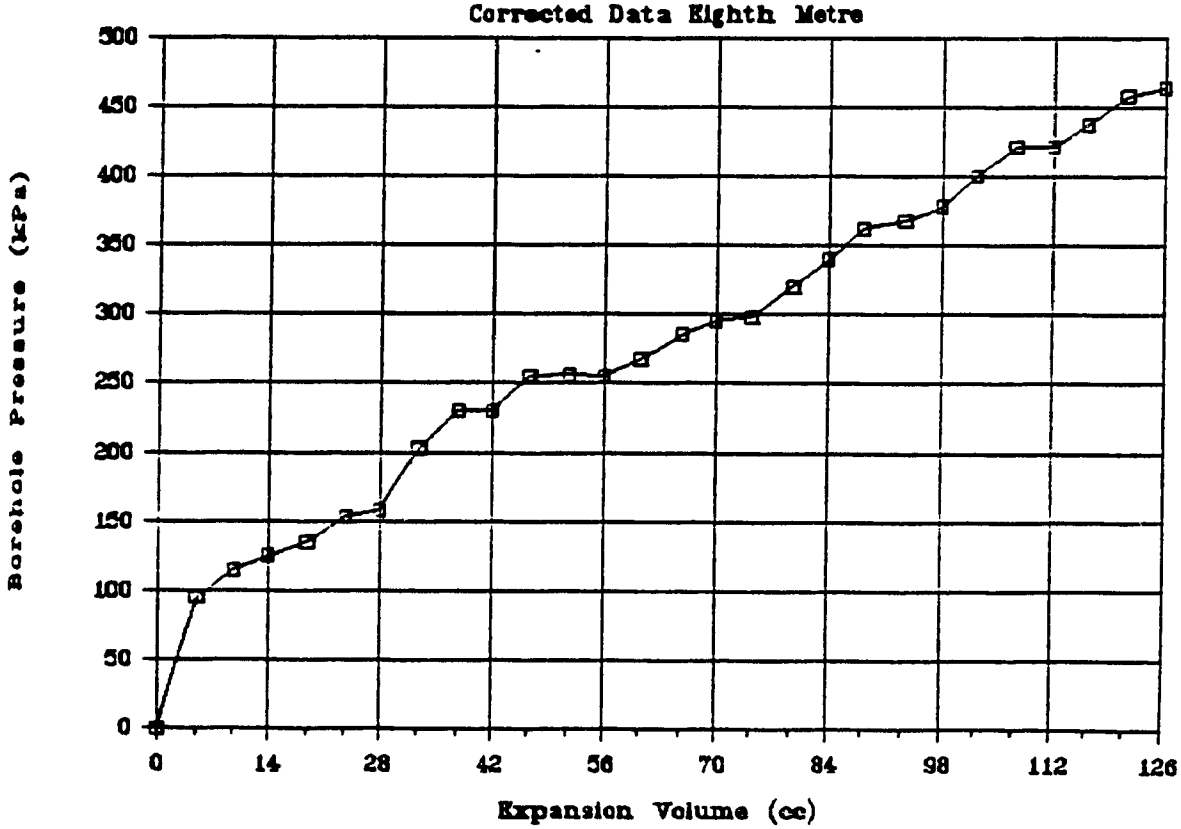

Chadbourne 4a North - West

Corrected Data

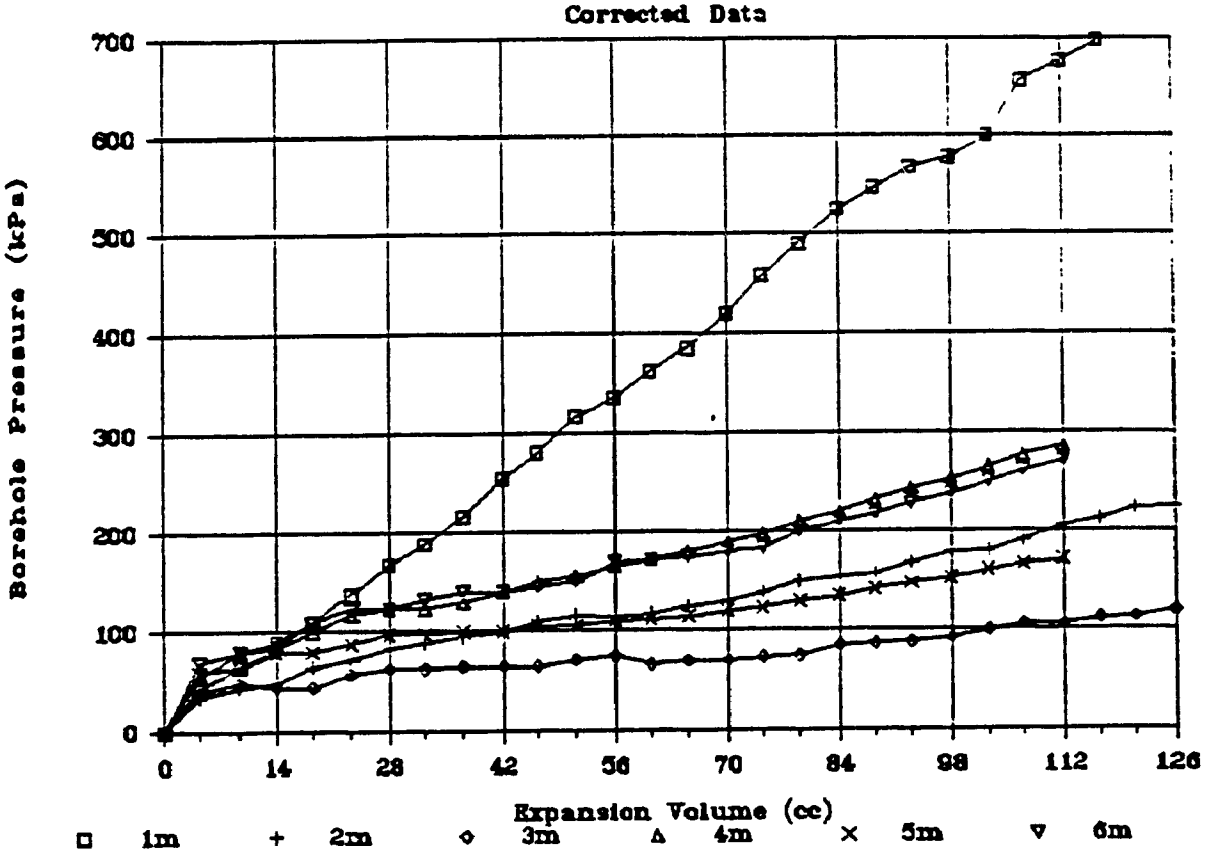

Chadbourne 4a North - West

Corrected Data

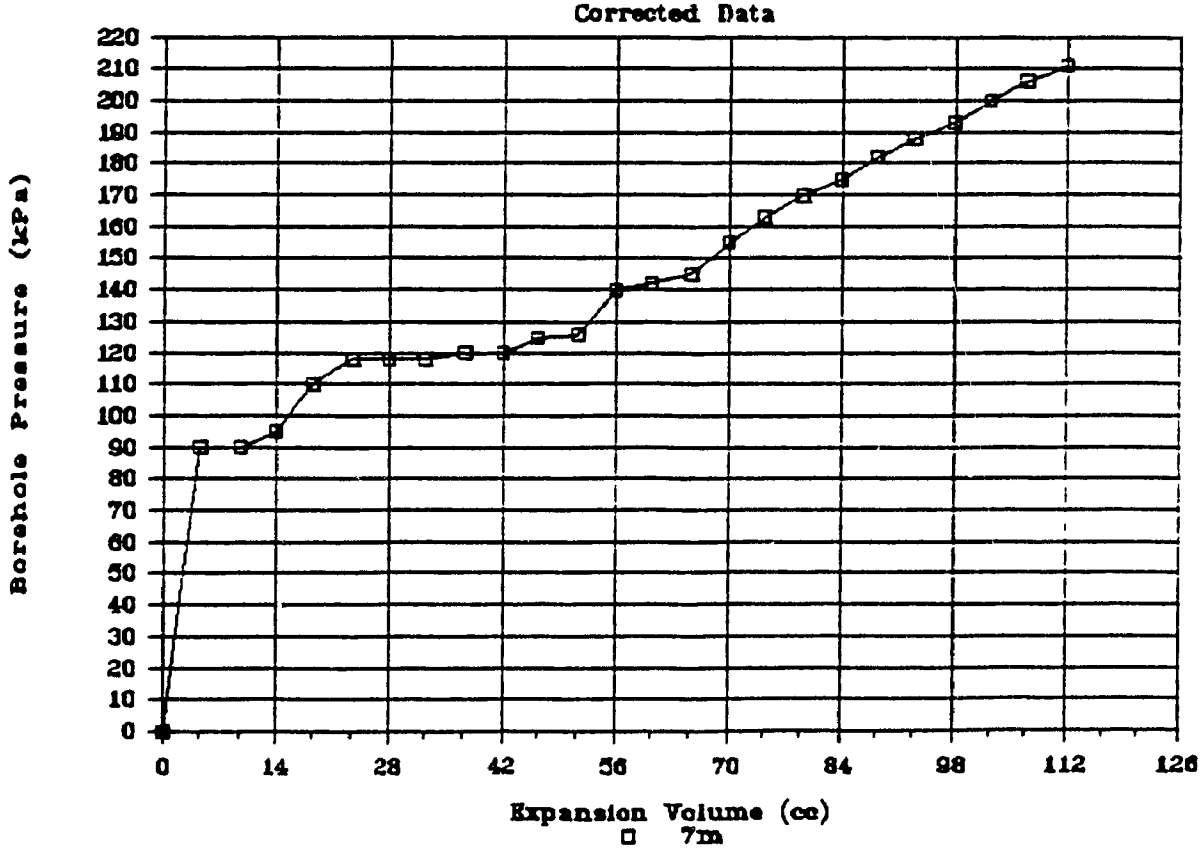

Chadbourne 4a North - West

Corrected Data First Metre

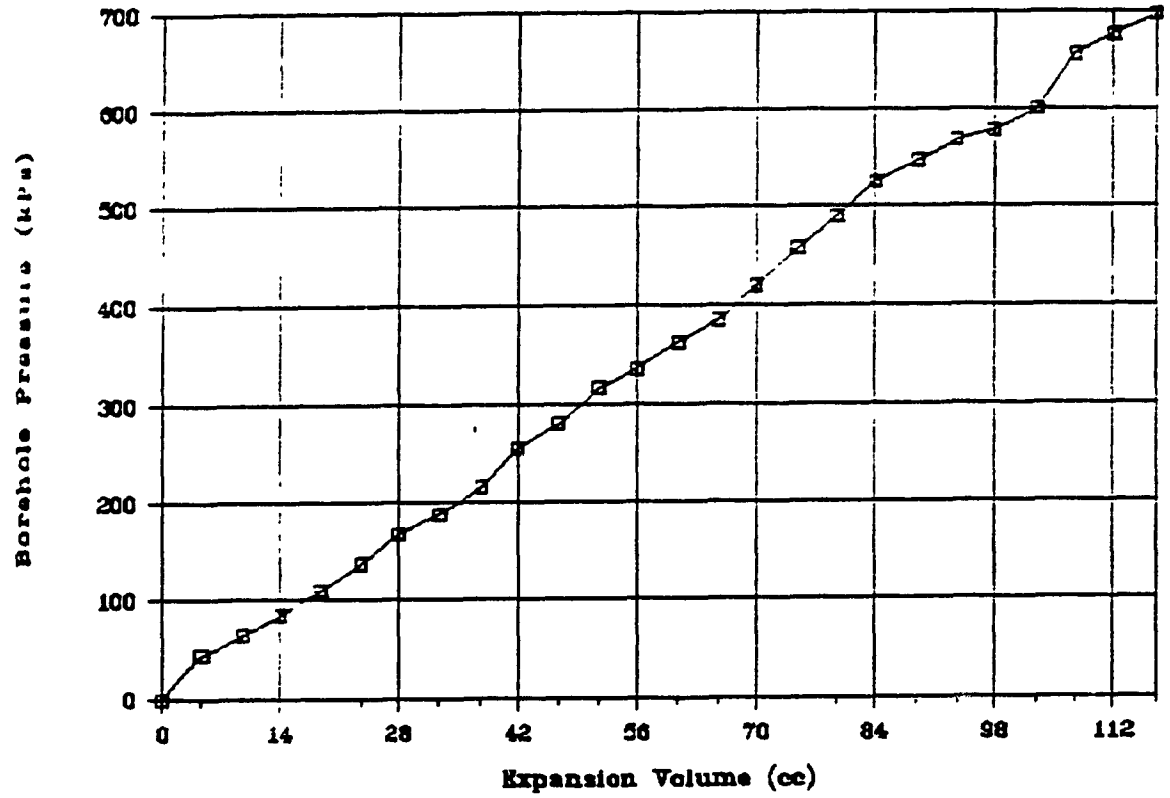

Chadbourne 4a North - West

Corrected Data Second Metre

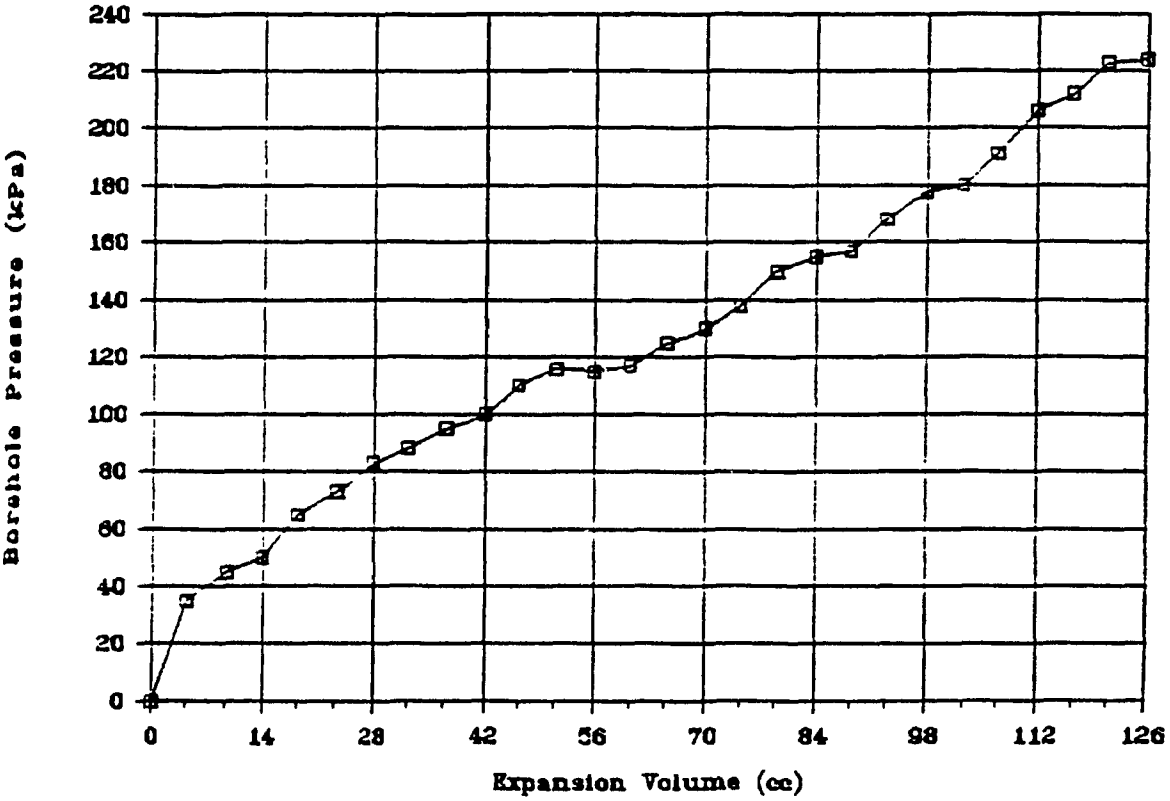

Chadbourne 4a North - West

Corrected Data Third Metre

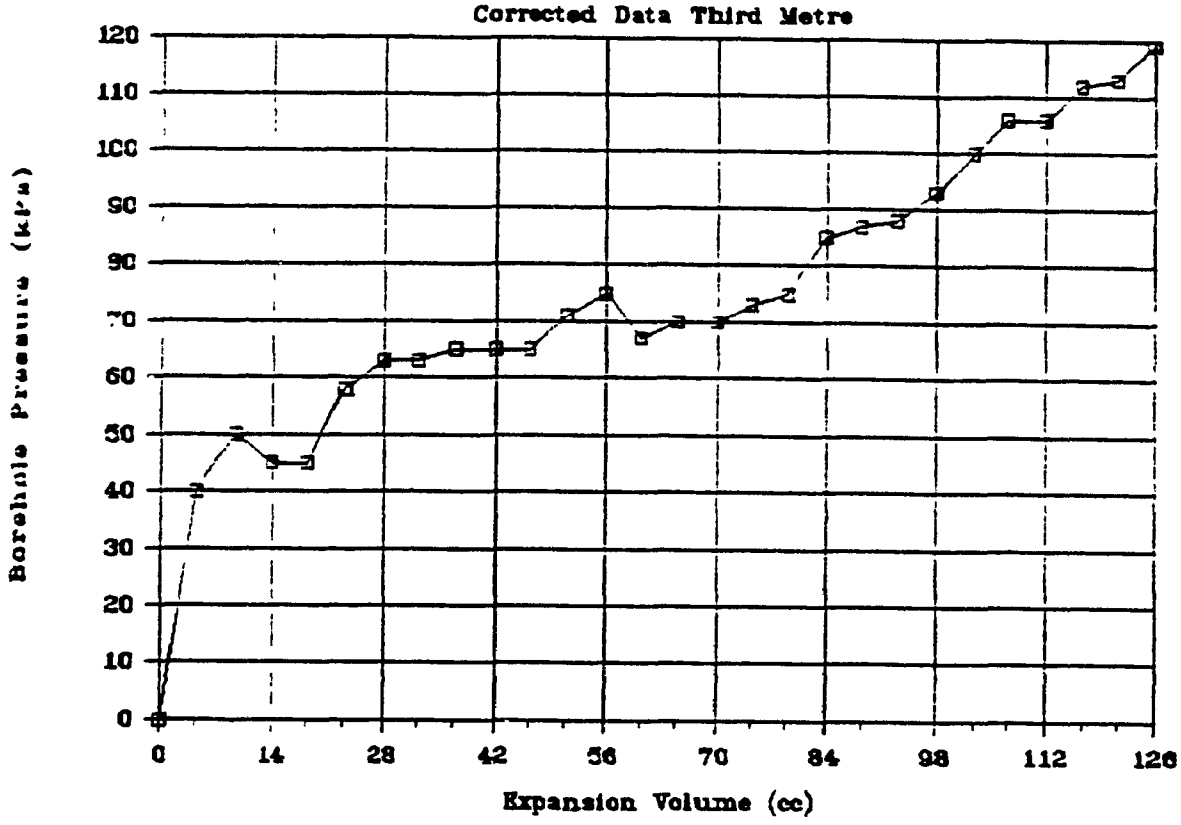

Chadbourne 4a North - West

Corrected Data Fourth Metre

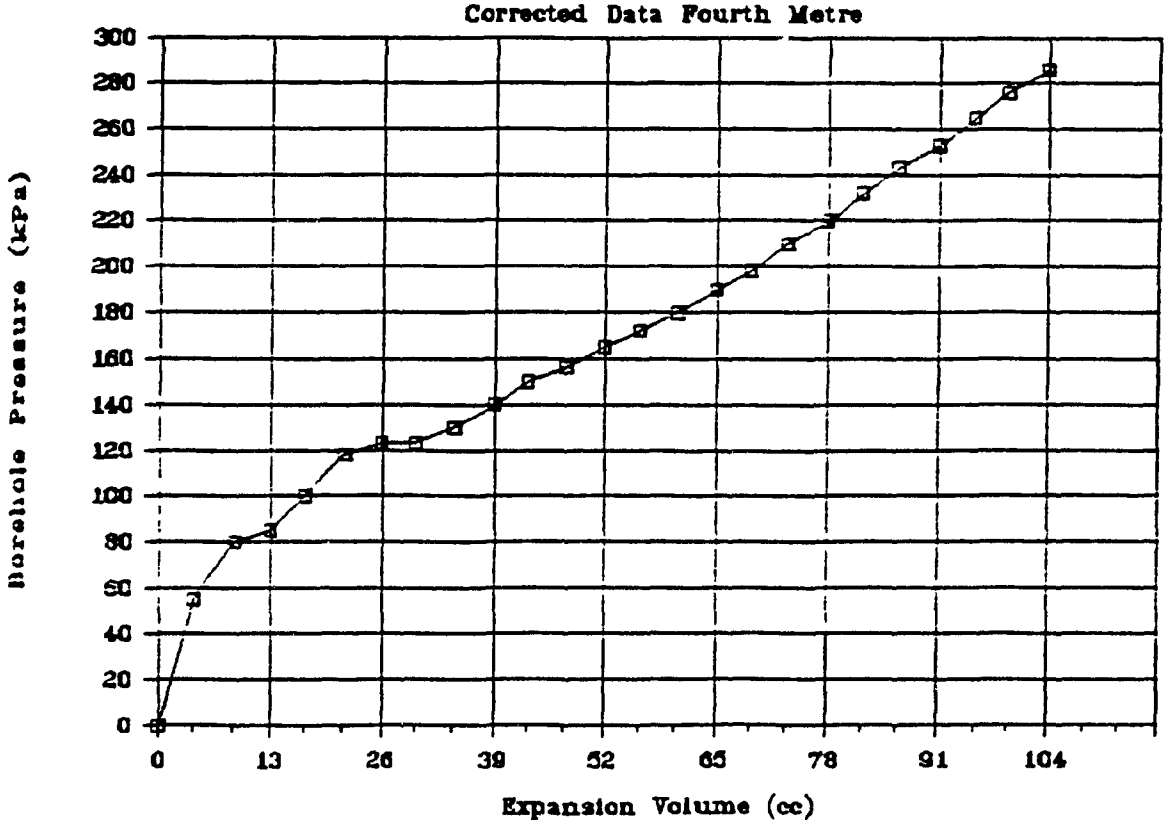

Chadbourne 4a North - West

Corrected Data Fifth Metre

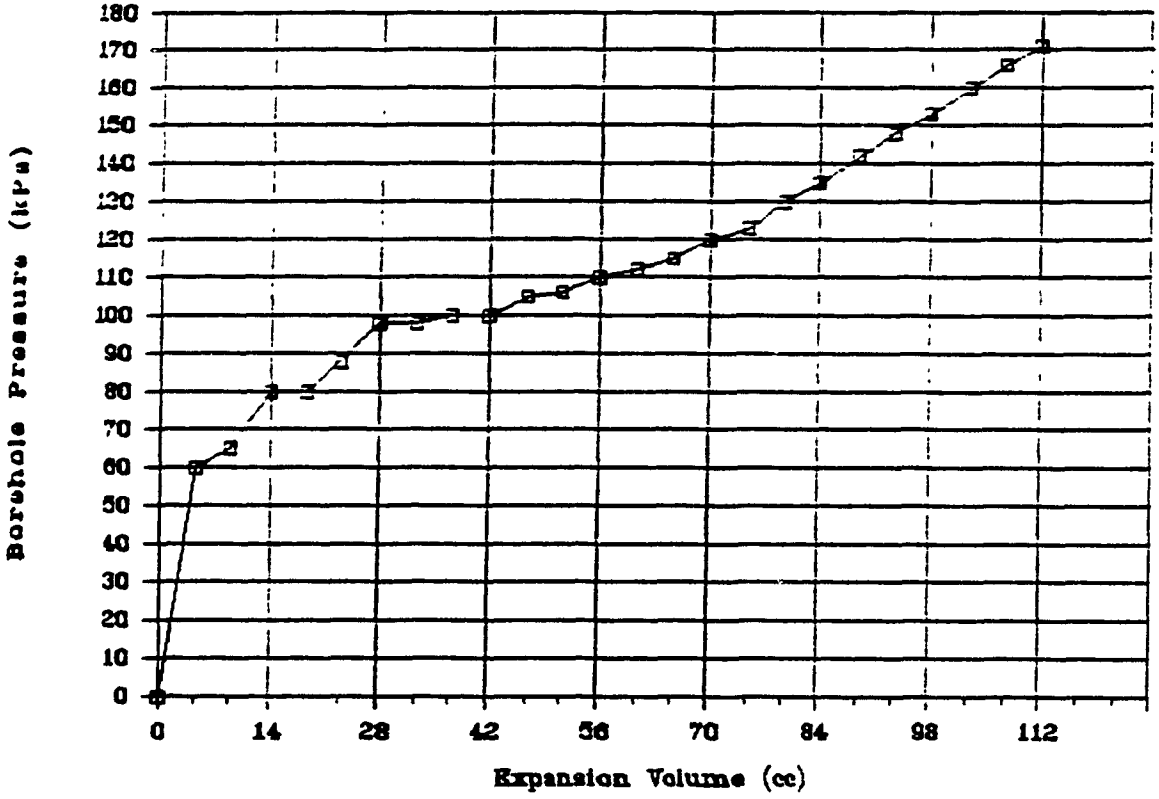

Chadbourne 4a North - West

Corrected Data Sixth Metre

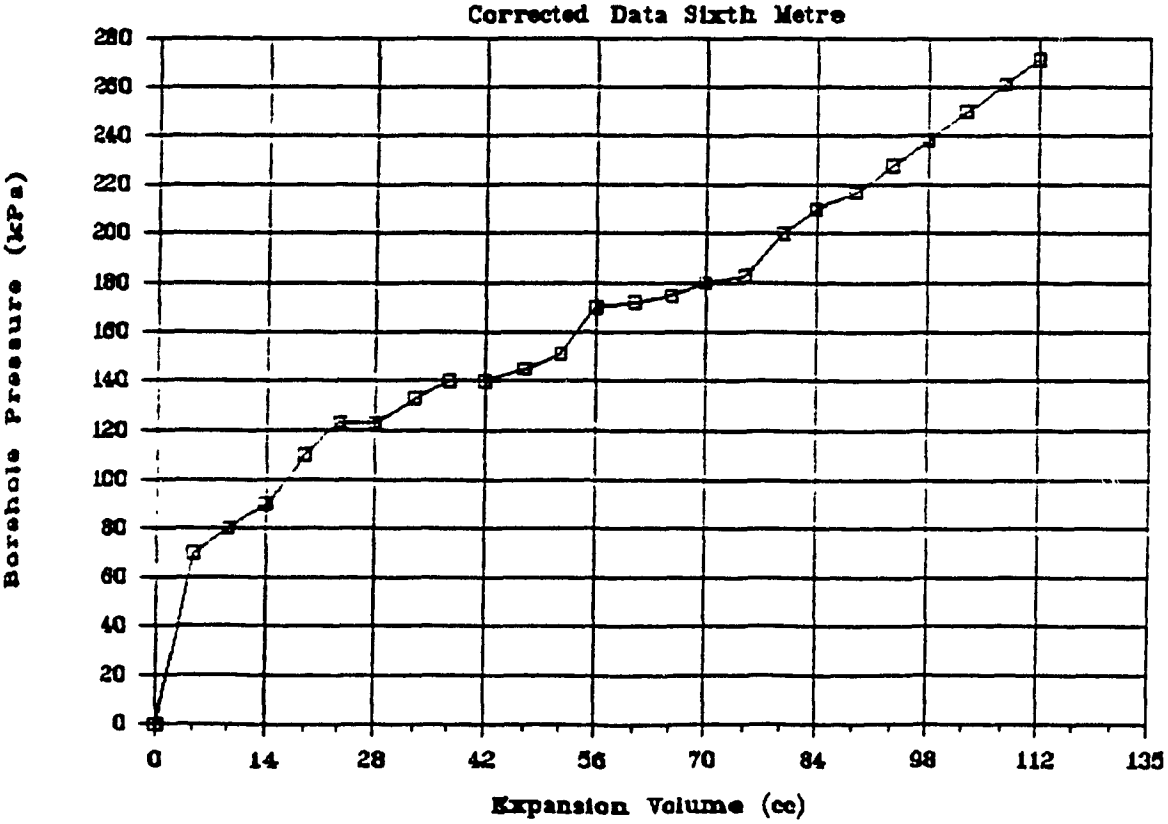

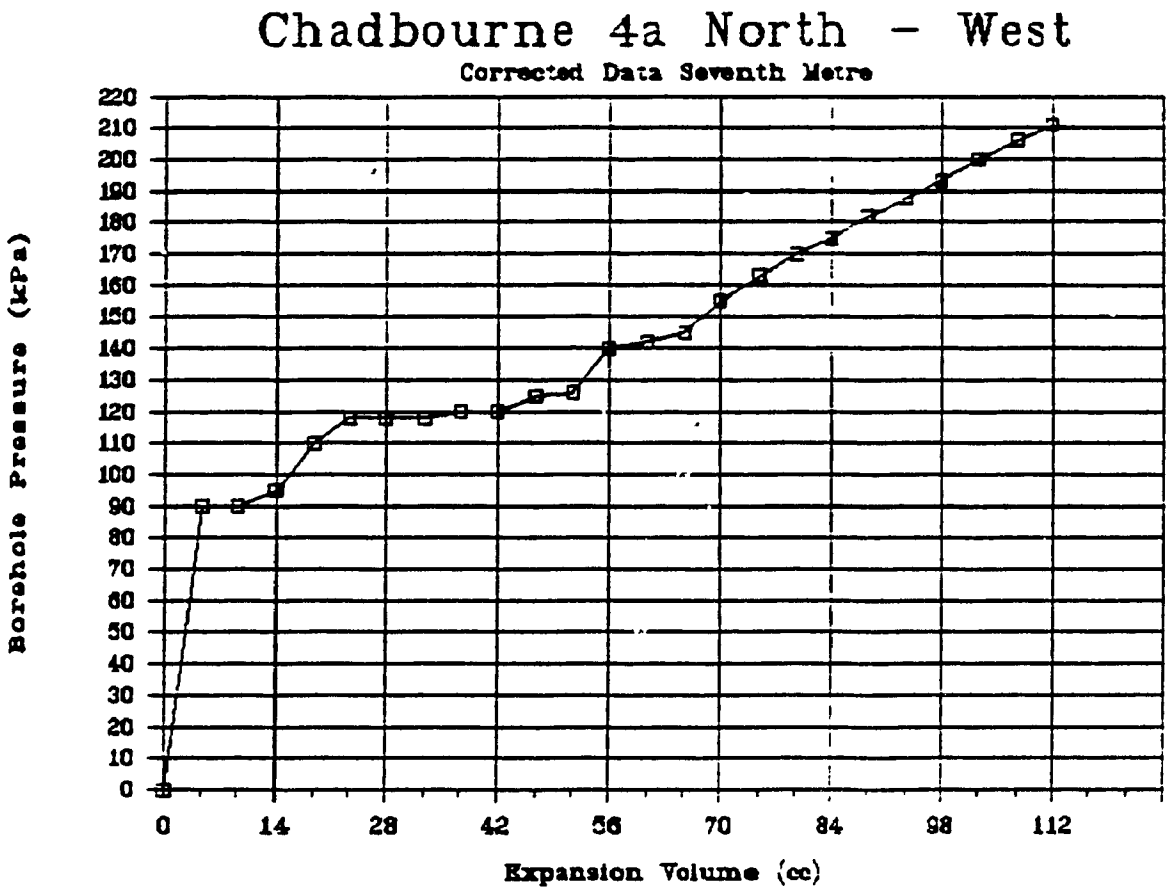
Chadbourne 4a North - West
Corrected Data Seventh Metre
Borehole Pressure (kPa)
220
210
200
190
180
170
160
150
140
130
120
110
100
90
80
70
60
50
40
30
20
10
0
0
14
28
42
56
70
84
98
112
Expansion Volume (cc)

Chadbourne 4c Stope

Corrected Data

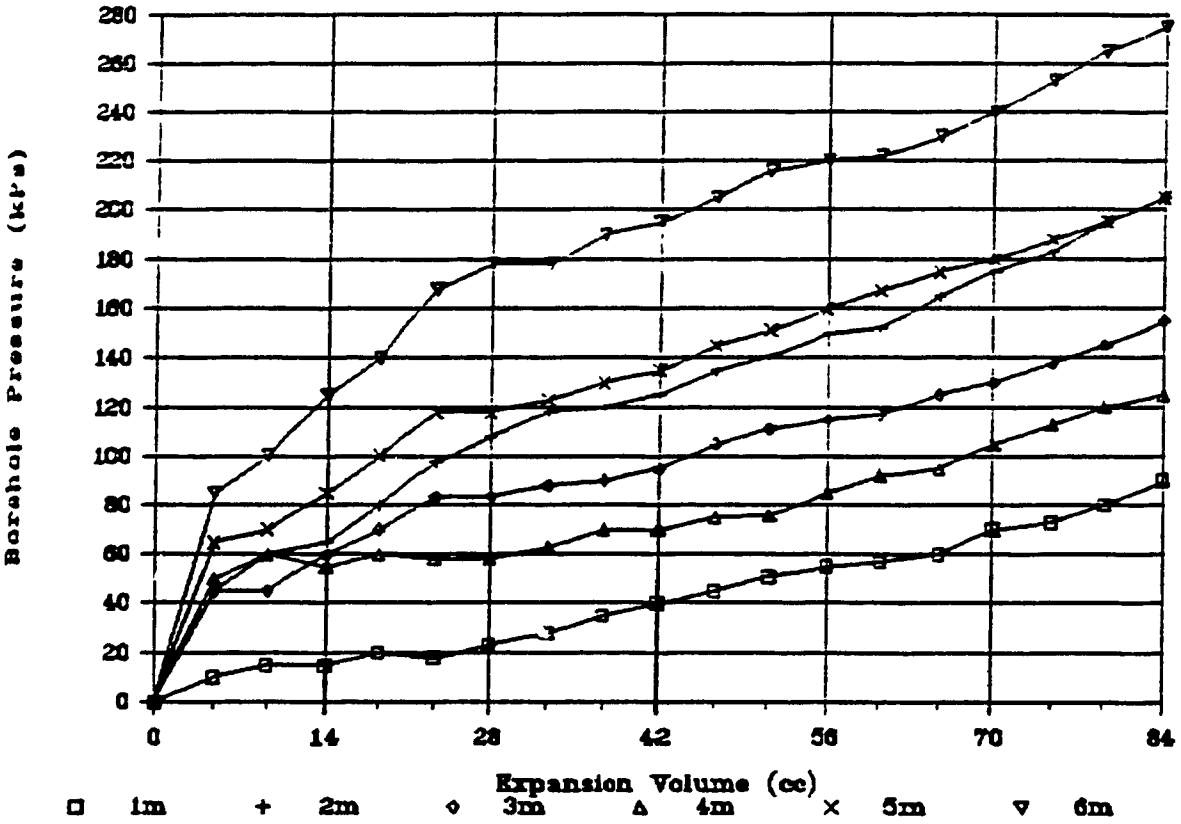

Chadbourne 4c Stope

Corrected Data

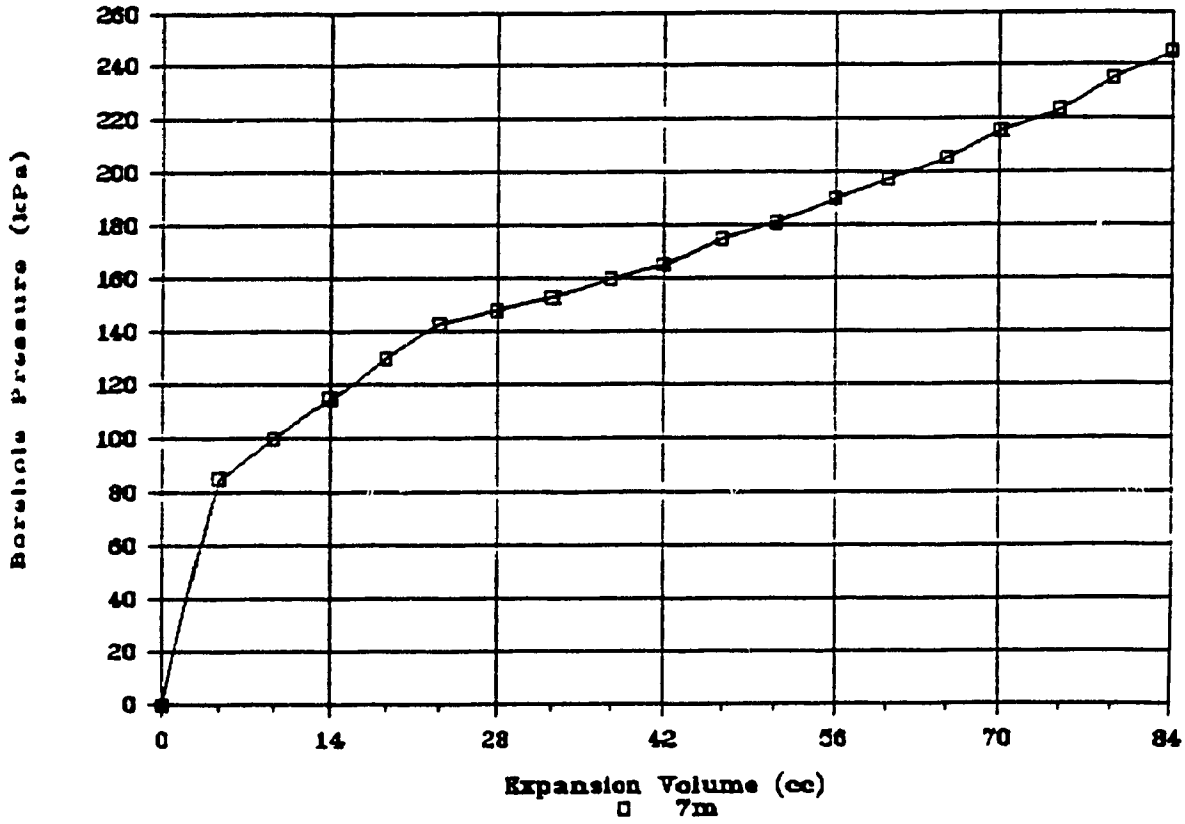

Chadbourne 4c Stope

Corrected Data First Metre

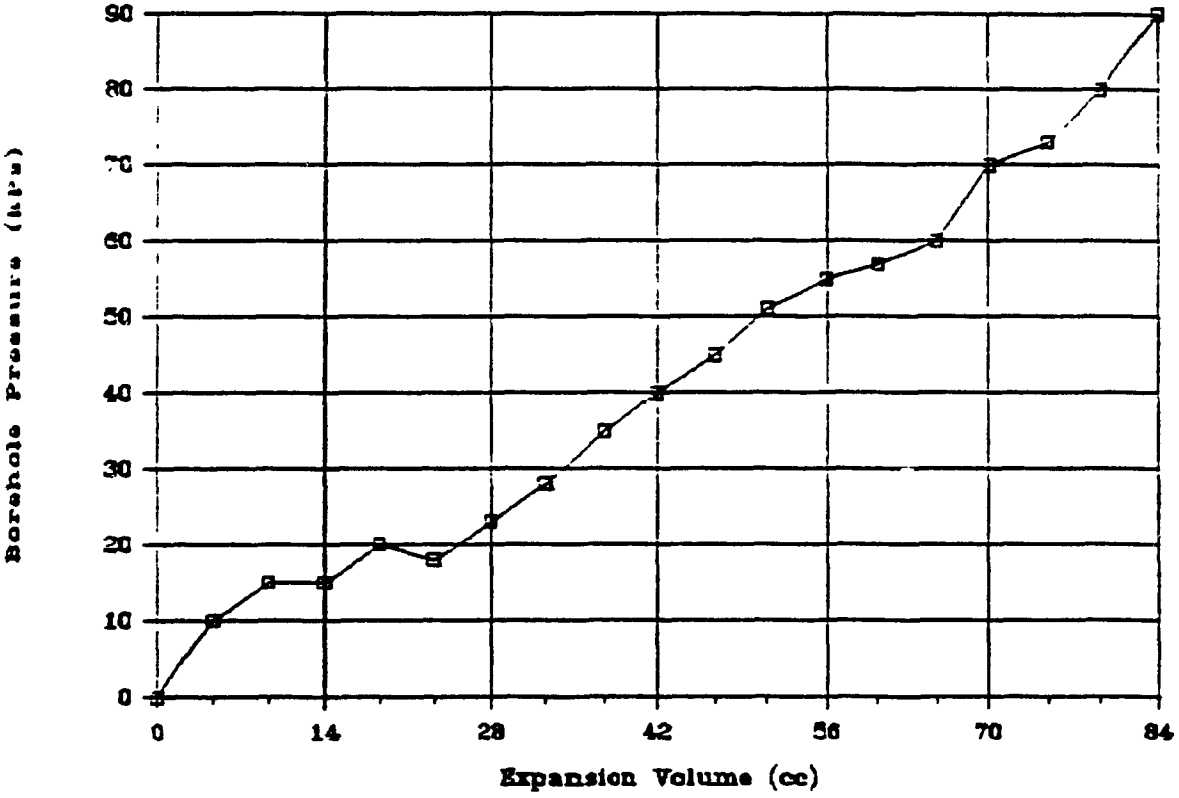

Chadbourne 4c Stope

Corrected Data Second Metre

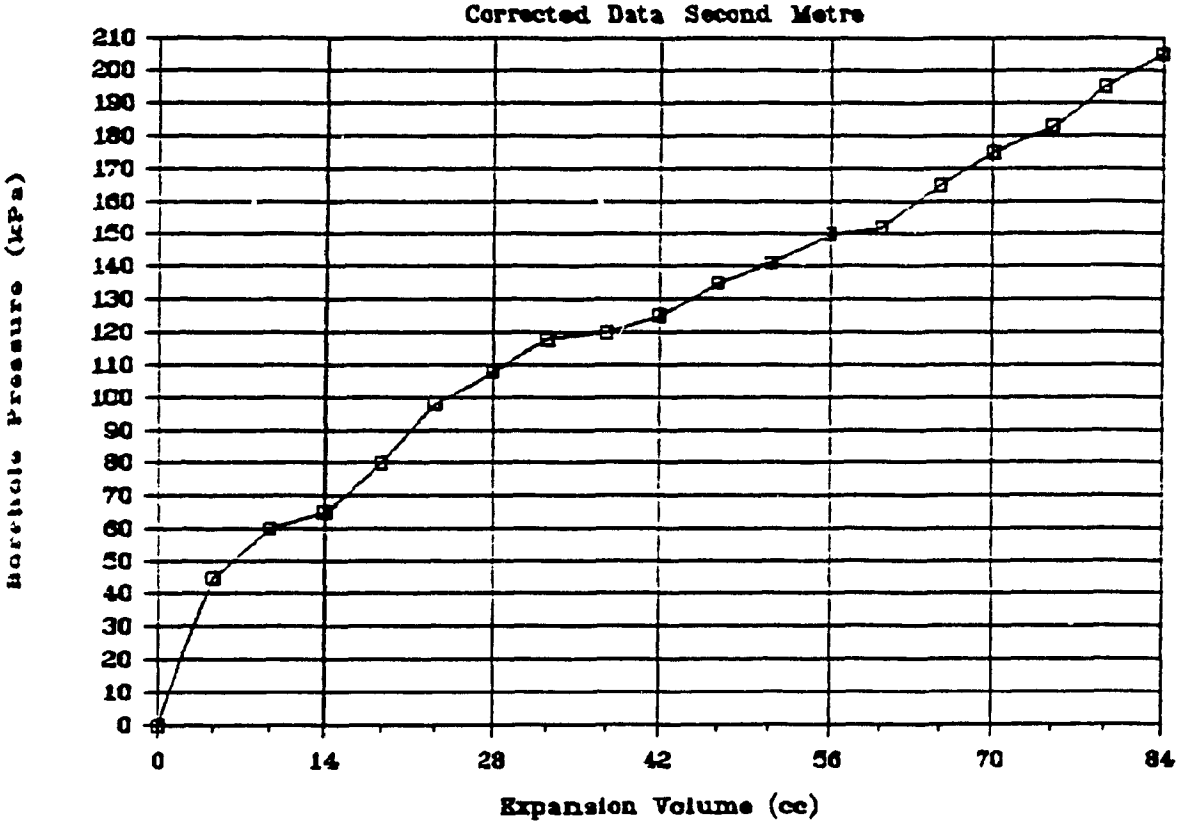

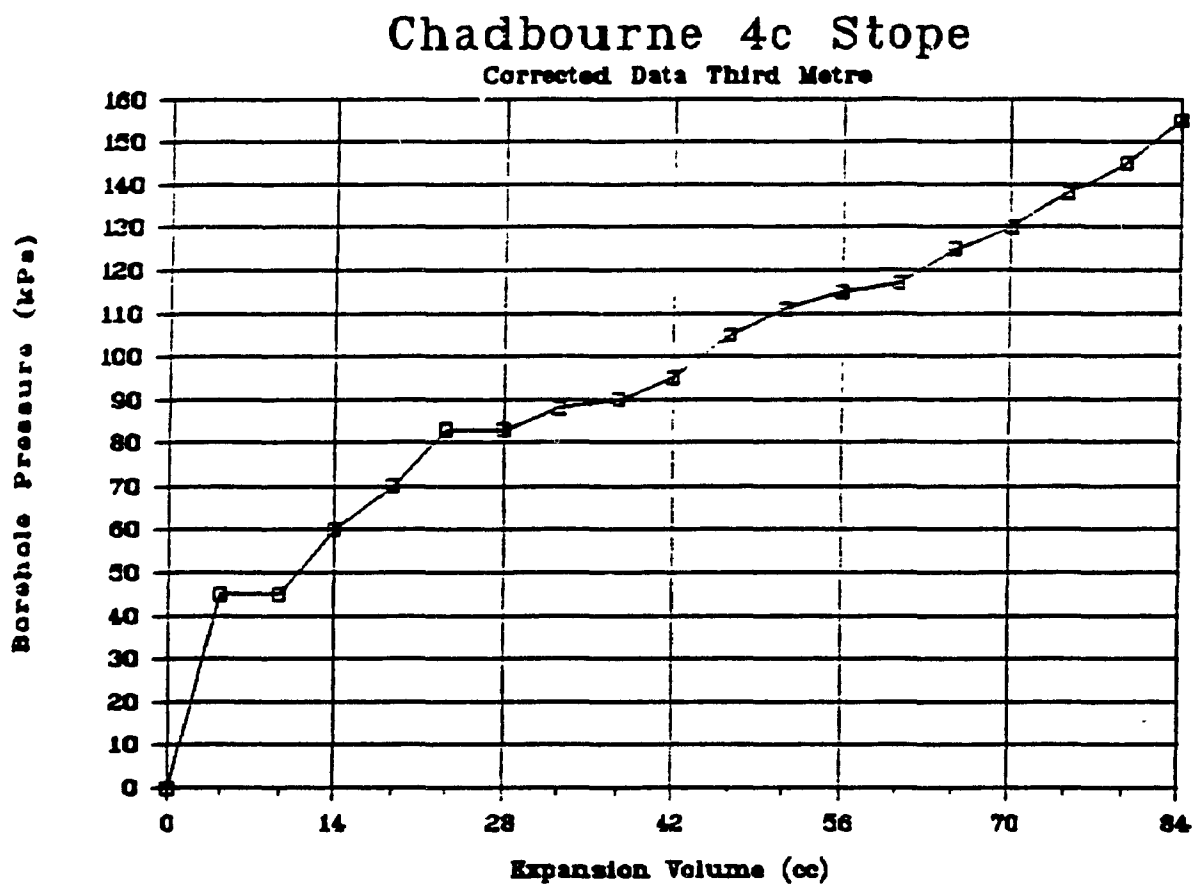
Chadbourne 4c Stope
Corrected Data Third Metre
Borehole Pressure (kPa)
160
150
140
130
120
110
100
90
80
70
60
50
40
30
20
10
0
0
14
28
42
56
70
84
Expansion Volume (cc)

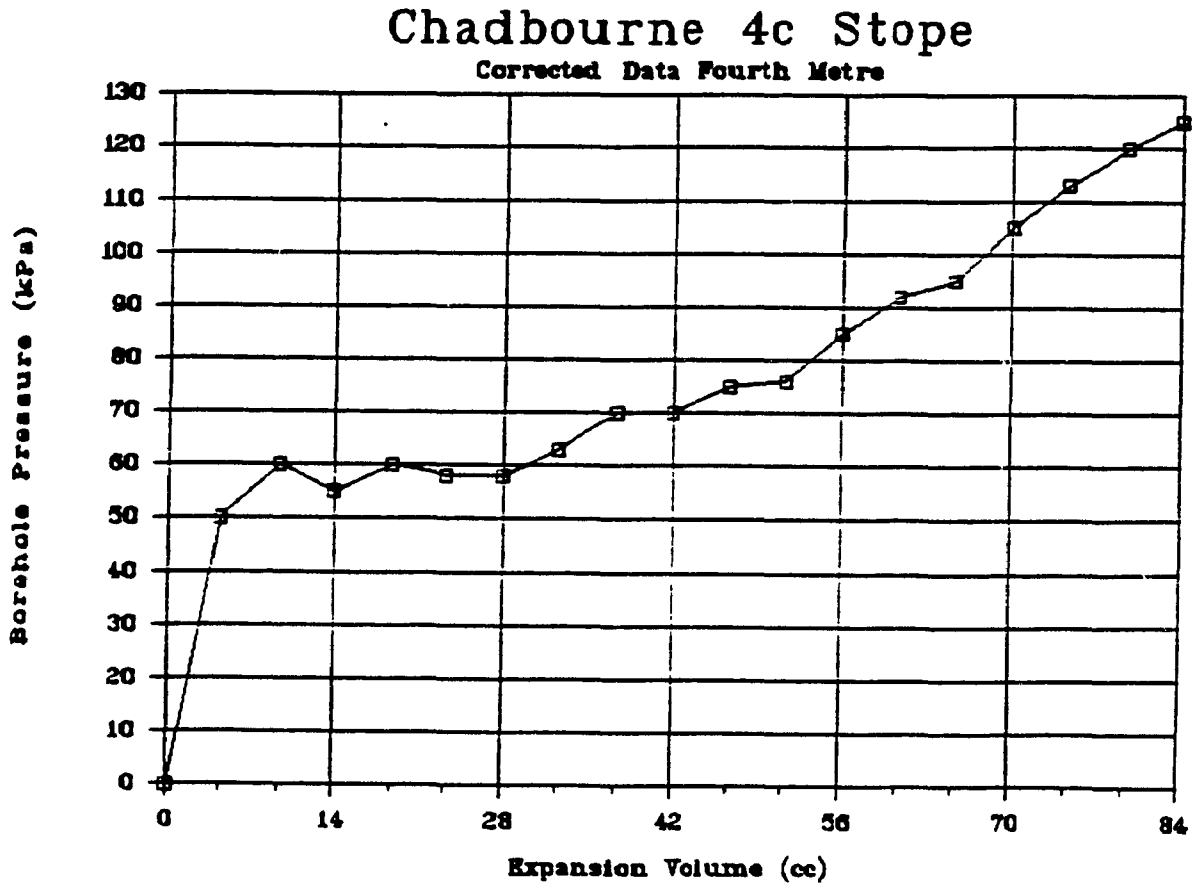
Chadbourne 4c Stope
Corrected Data Fourth Metre
Borehole Pressure (kPa)
130
120
110
100
90
80
70
60
50
40
30
20
10
0
0
14
28
42
56
70
84
Expansion Volume (cc)

Chadbourne 4c Stope

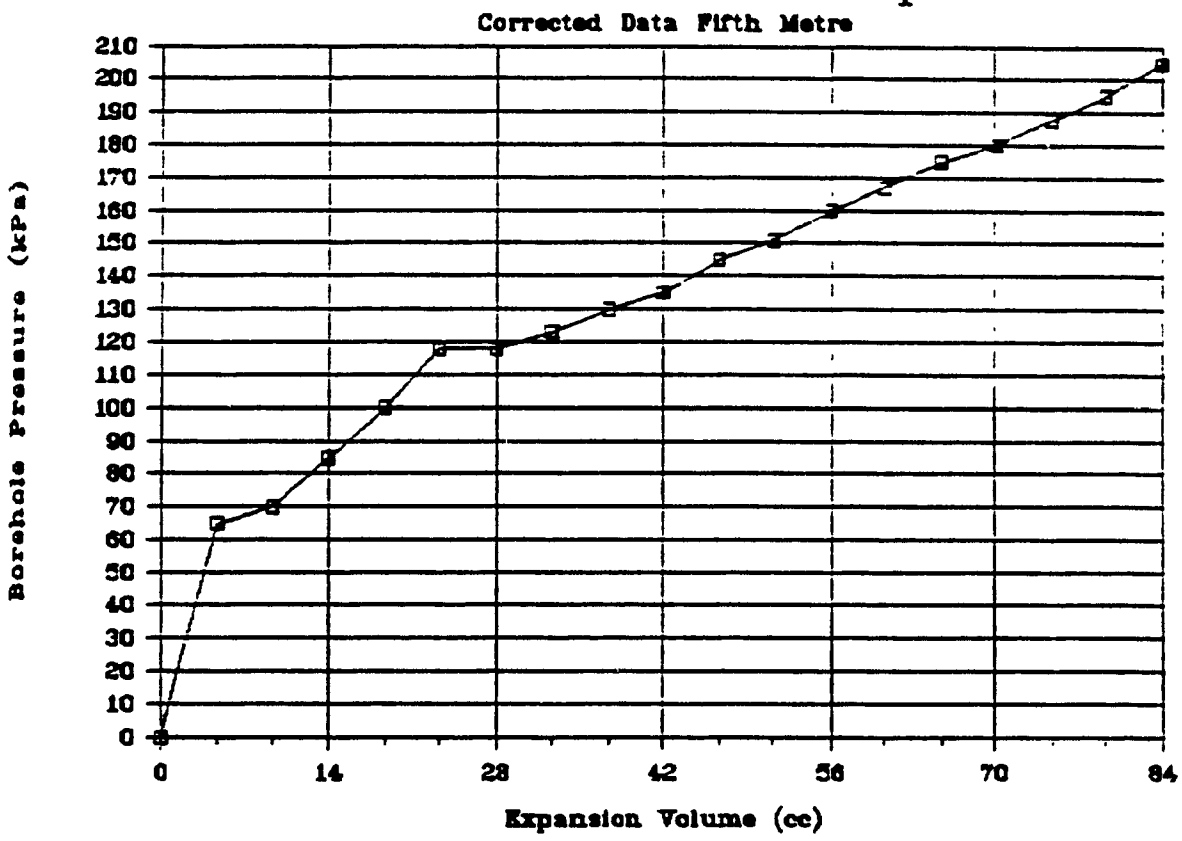

Chadbourne 4c Stope

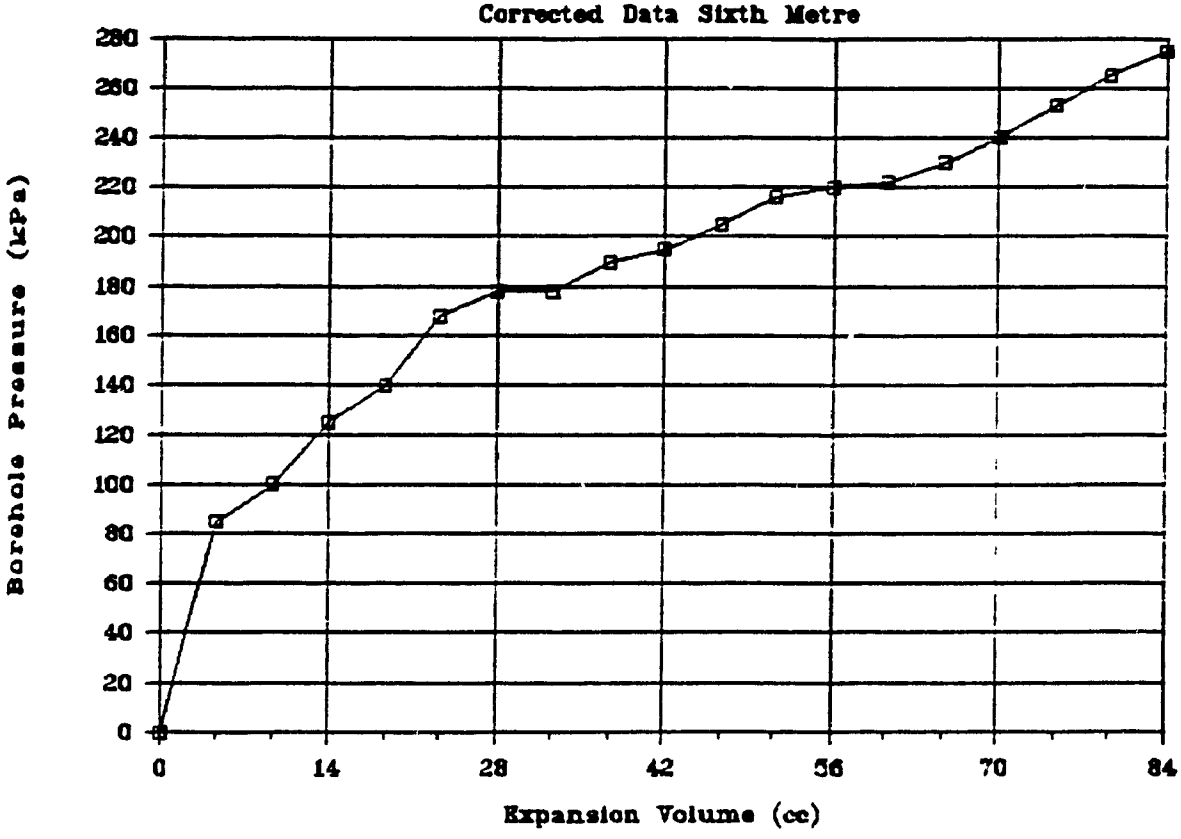

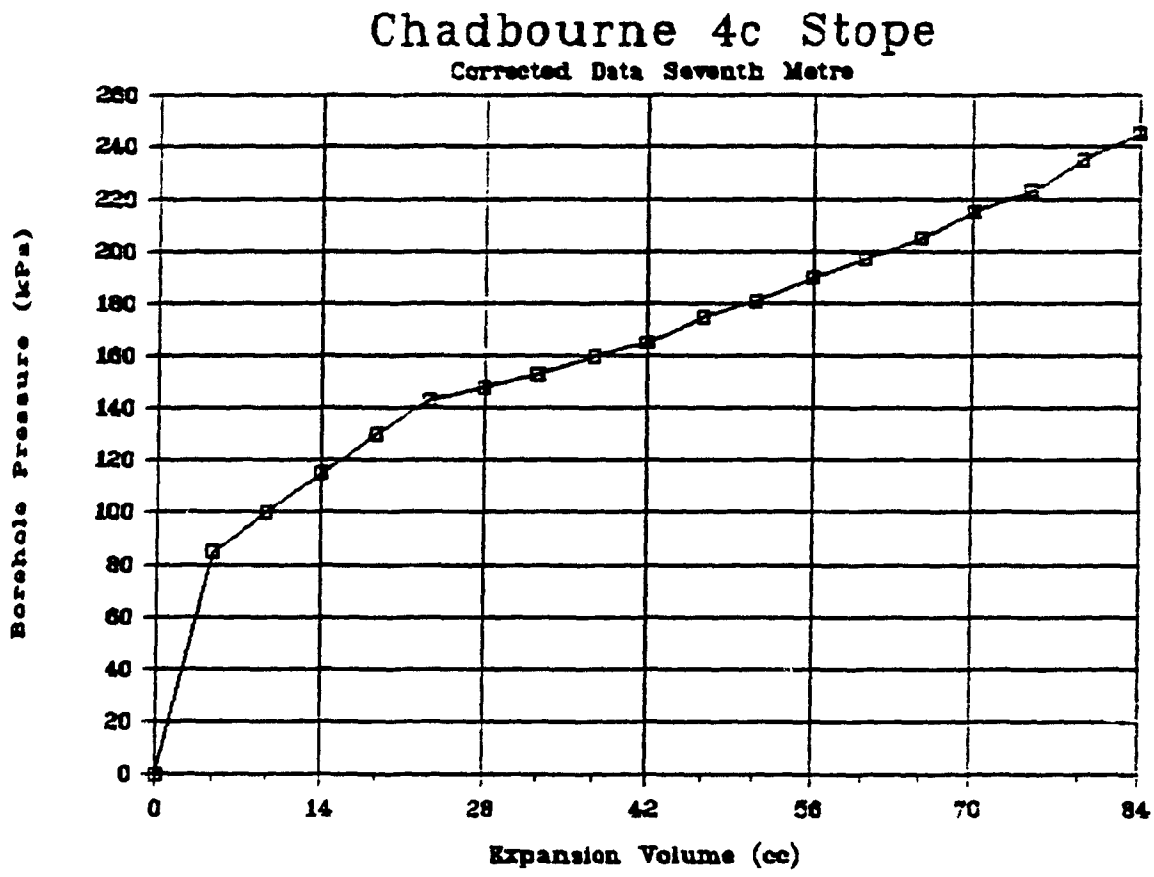
Chadbourne 4c Stope
Corrected Data Seventh Metre
Borehole Pressure (kPa)
260
240
220
200
180
160
140
120
100
80
60
40
20
0
0
14
28
42
56
70
84
Expansion Volume (cc)

Denison - Corrected Data

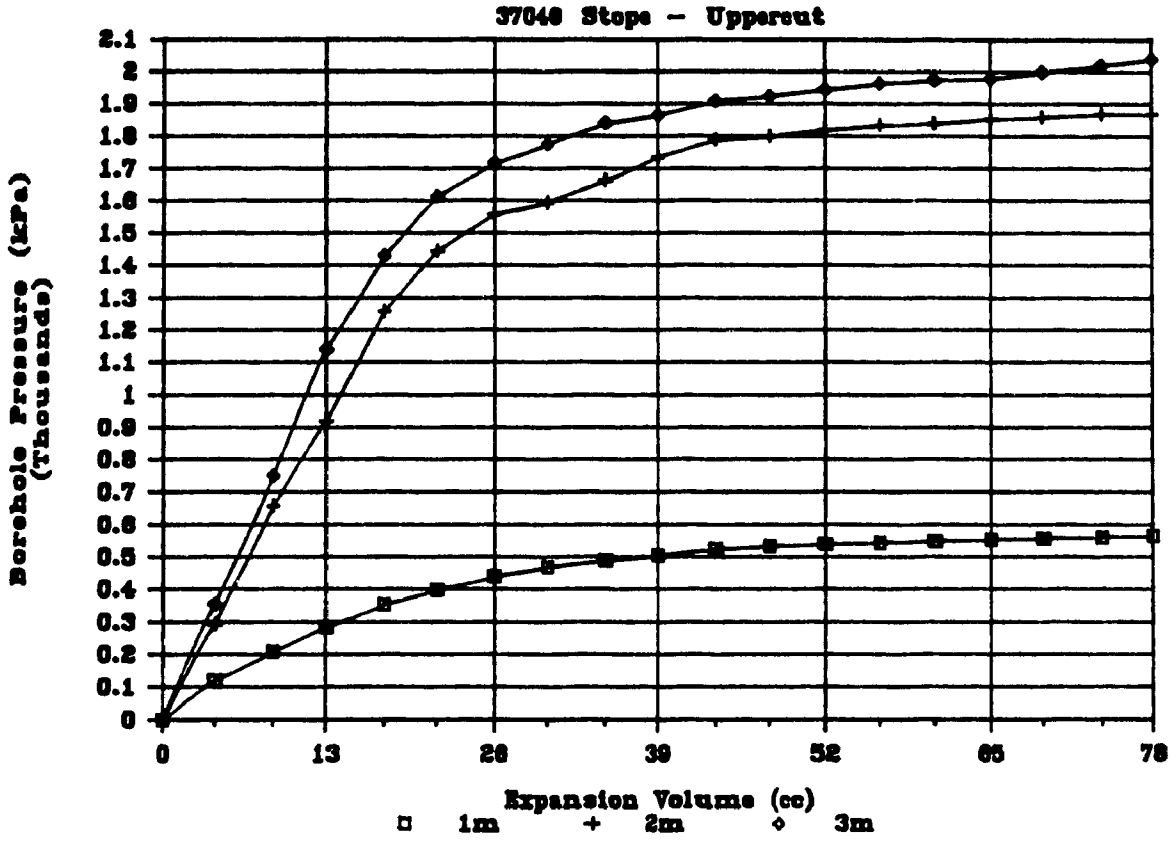

Denison - Corrected Data

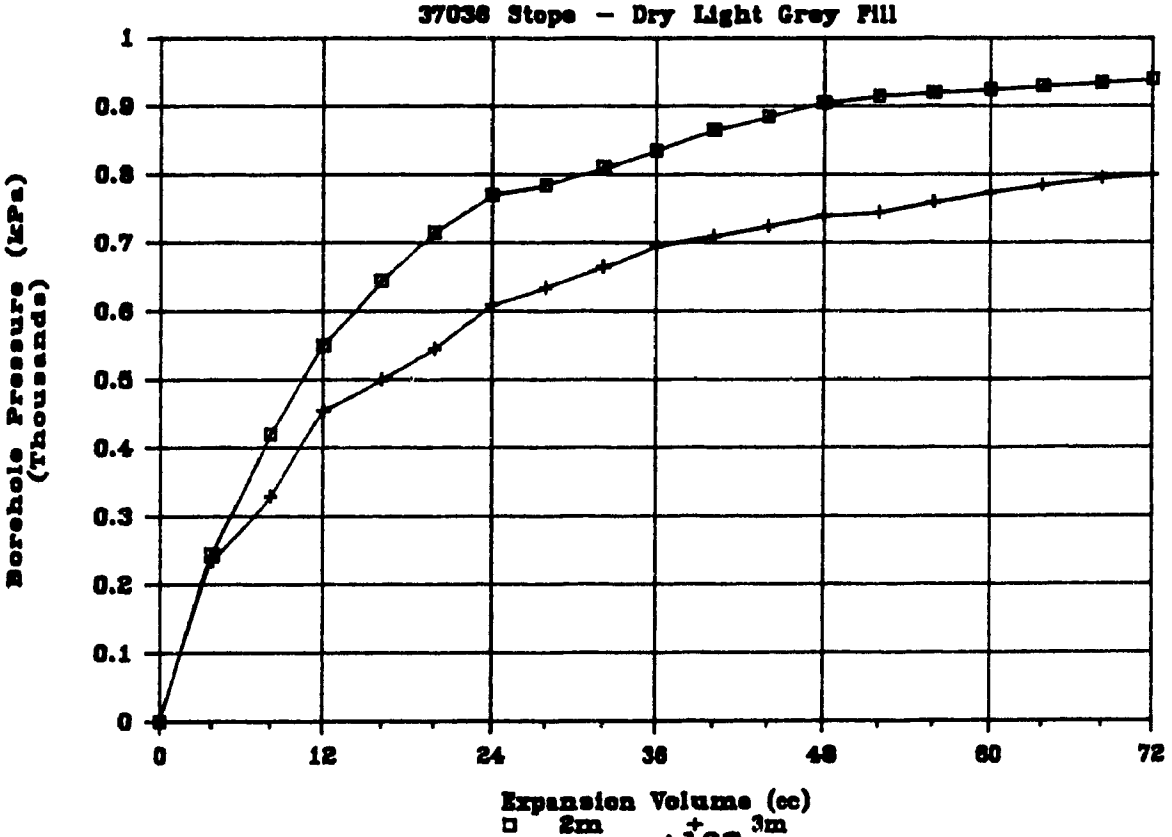

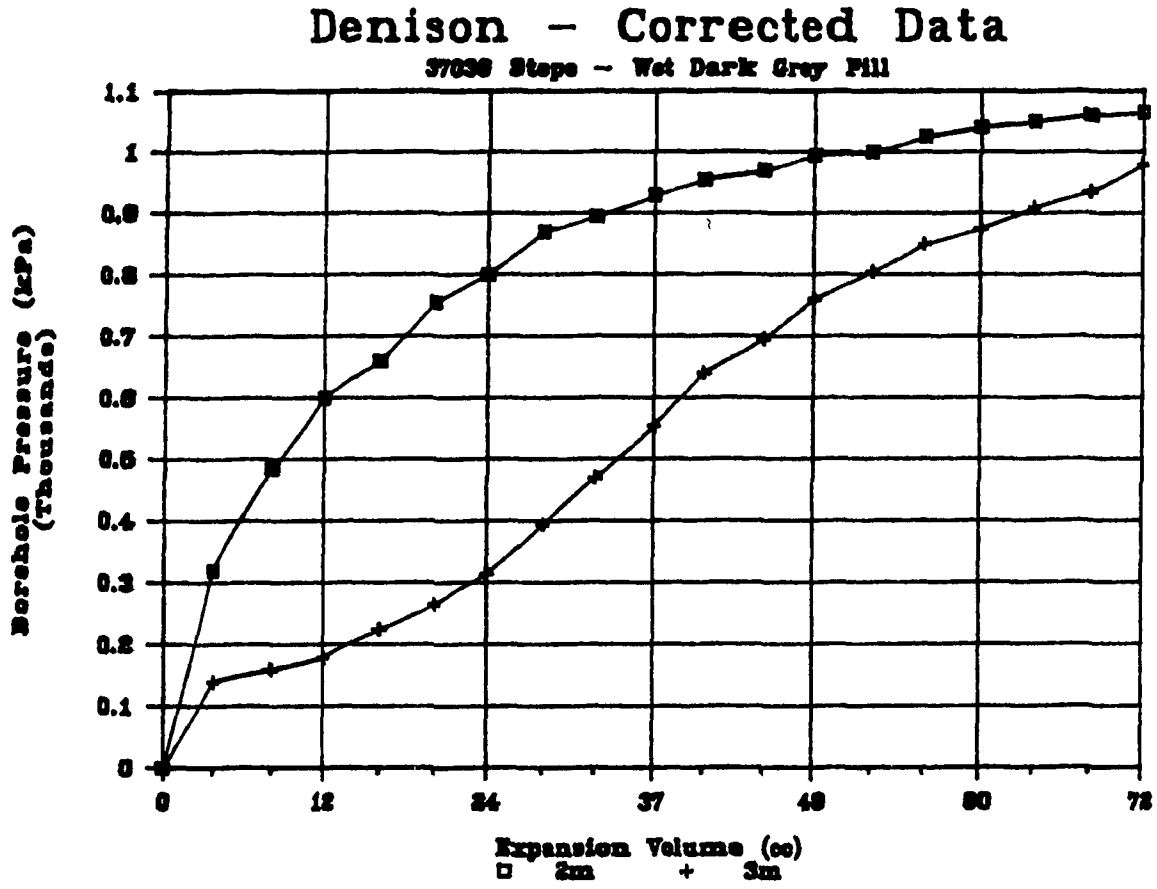
Denison - Corrected Data
37038 Stope - Wet Dark Grey Fill
Borehole Pressure (kPa)
(Thousands)
1.1
1
0.9
0.8
0.7
0.6
0.5
0.4
0.3
0.2
0.1
0
0
12
24
37
49
60
72
Expansion Volume (cc)
2m
3m

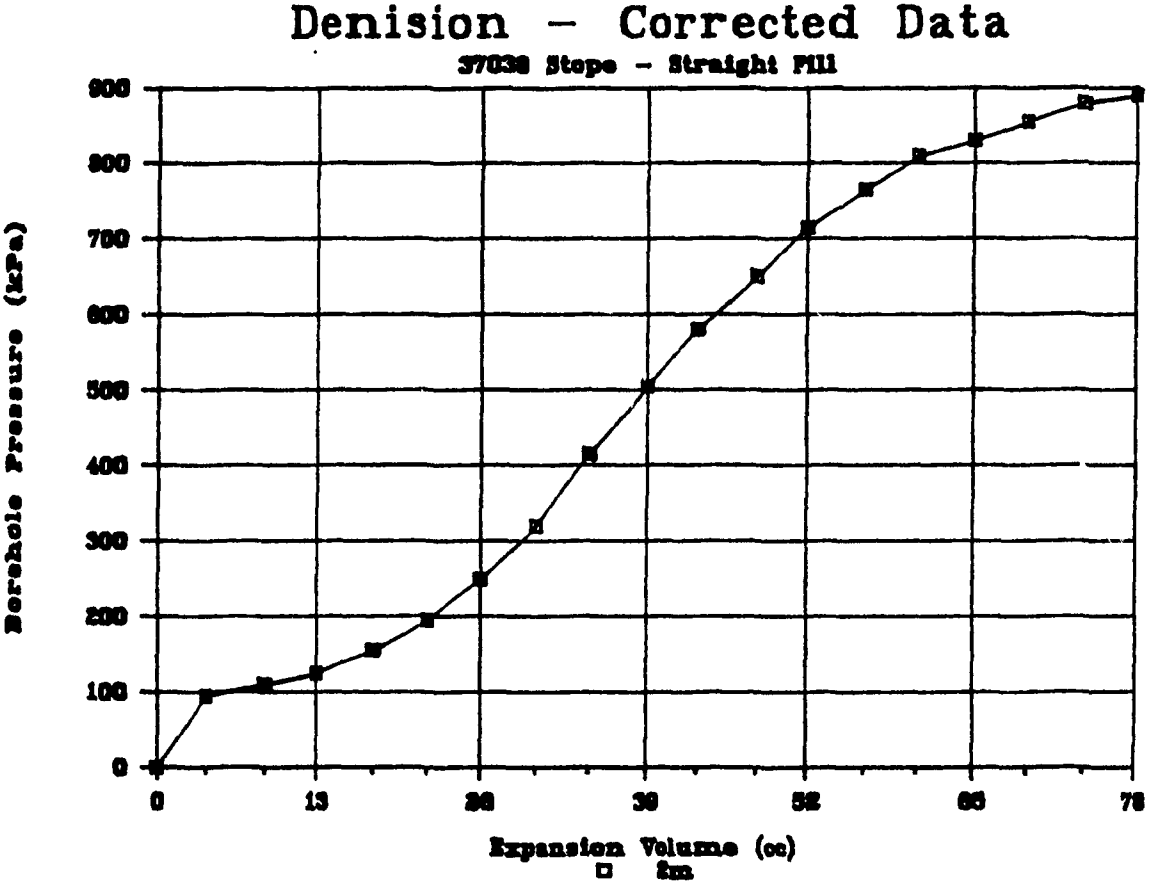
Denision - Corrected Data
37038 Stope - Straight Fill
Borehole Pressure (kPa)
900
800
700
600
500
400
300
200
100
0
0
13
26
39
52
65
78
Expansion Volume (cc)
2m

Denison – Corrected Data

37046 Stope – Bulkhead

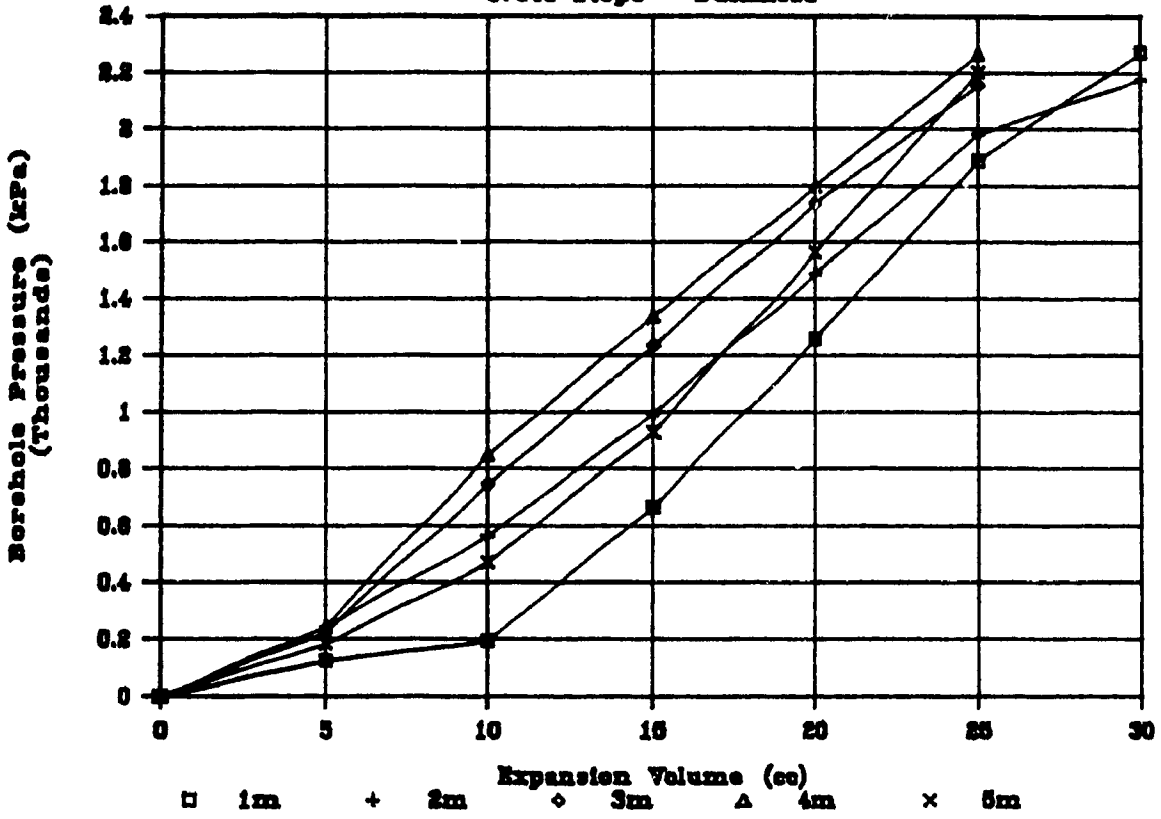

Denison – Corrected Data

First Metre

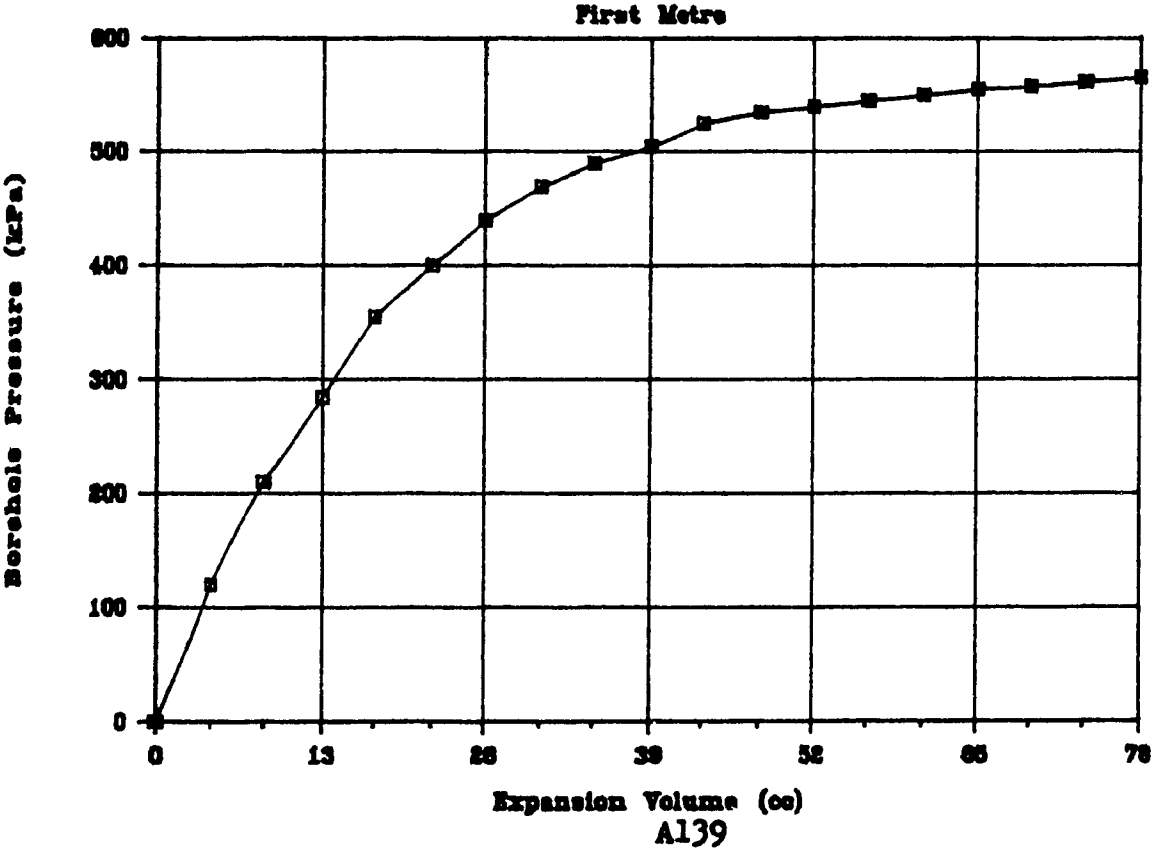

Denison – Corrected Data

Second Metre

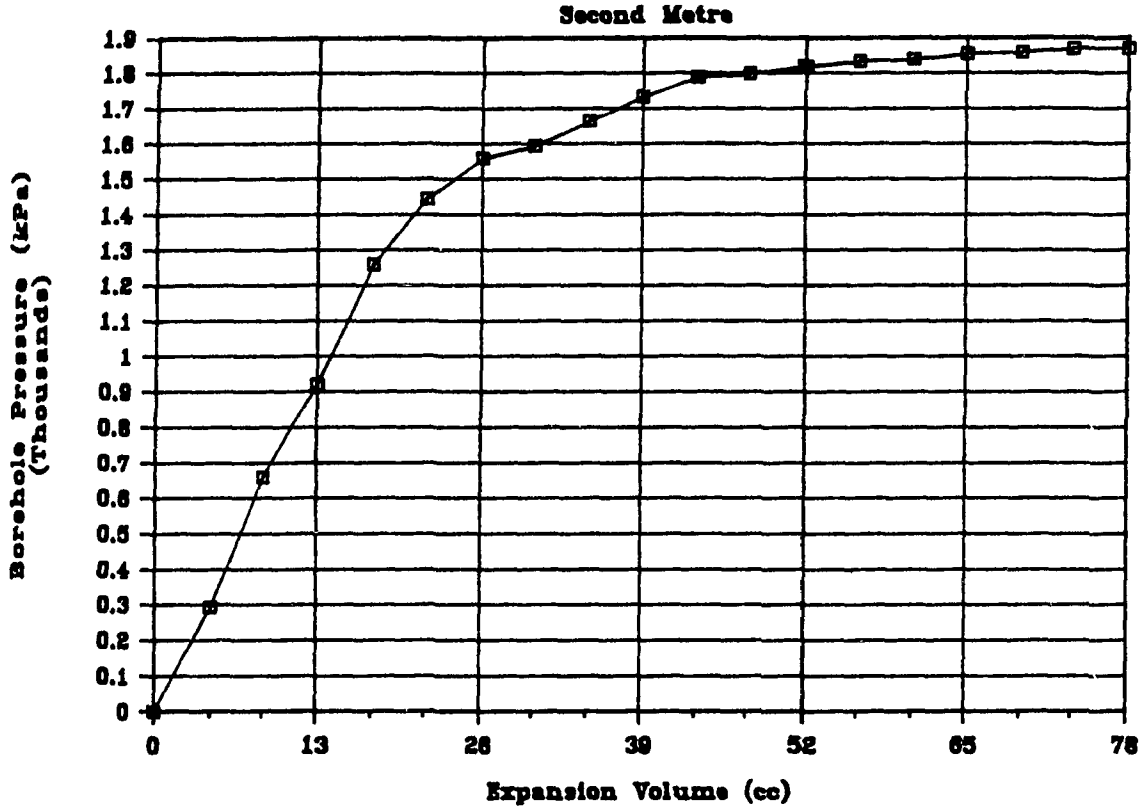

Denison – Corrected Data

Third Metre

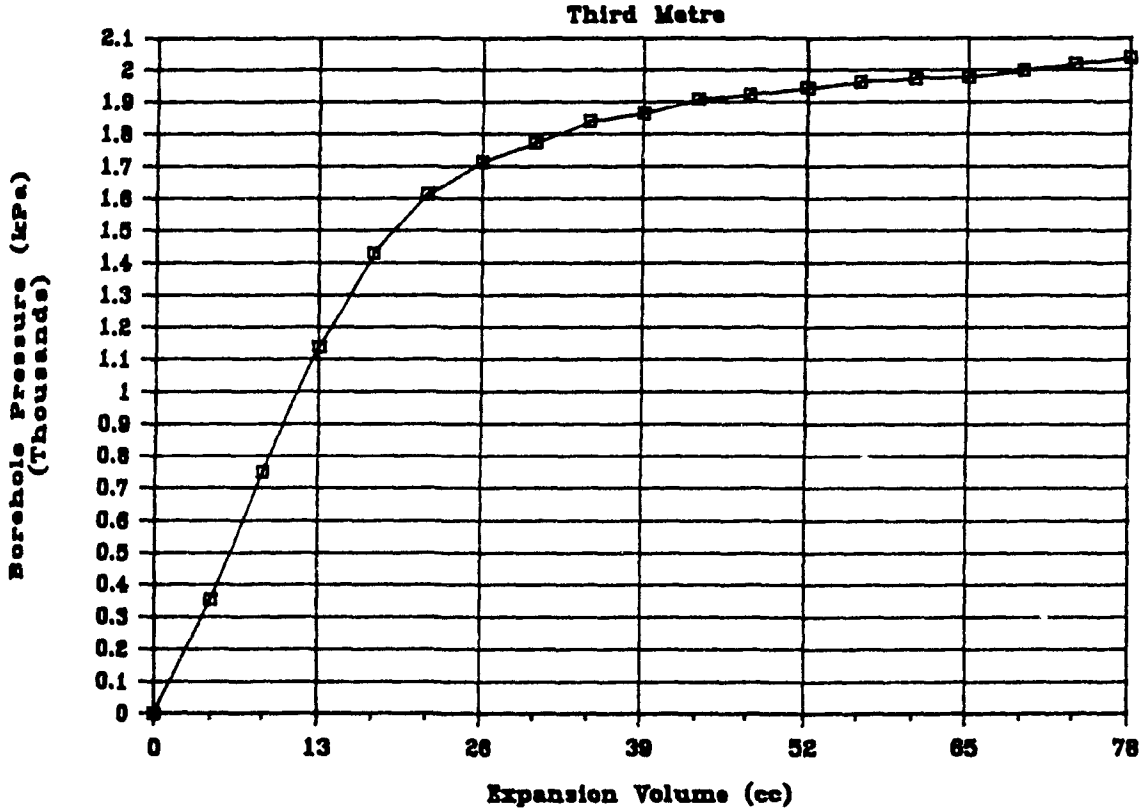

Denison - Corrected Data

Second Metre

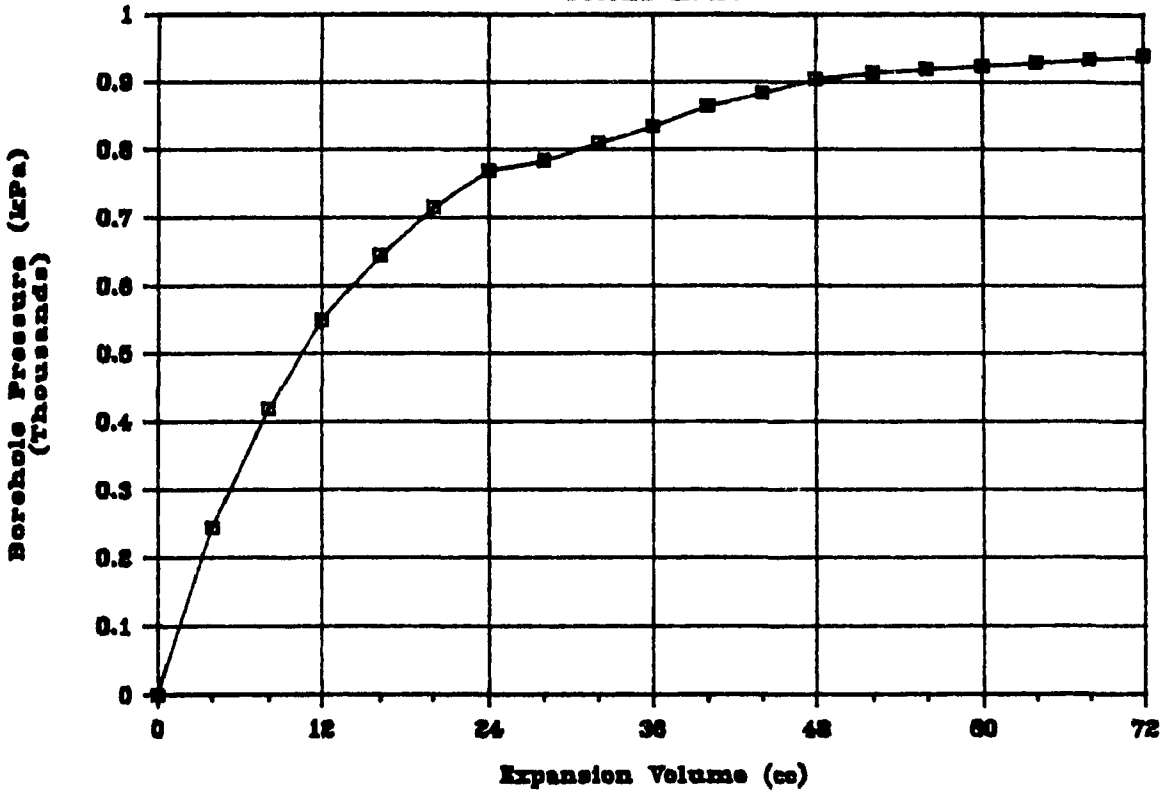

Denison - Corrected Data

Third Metre

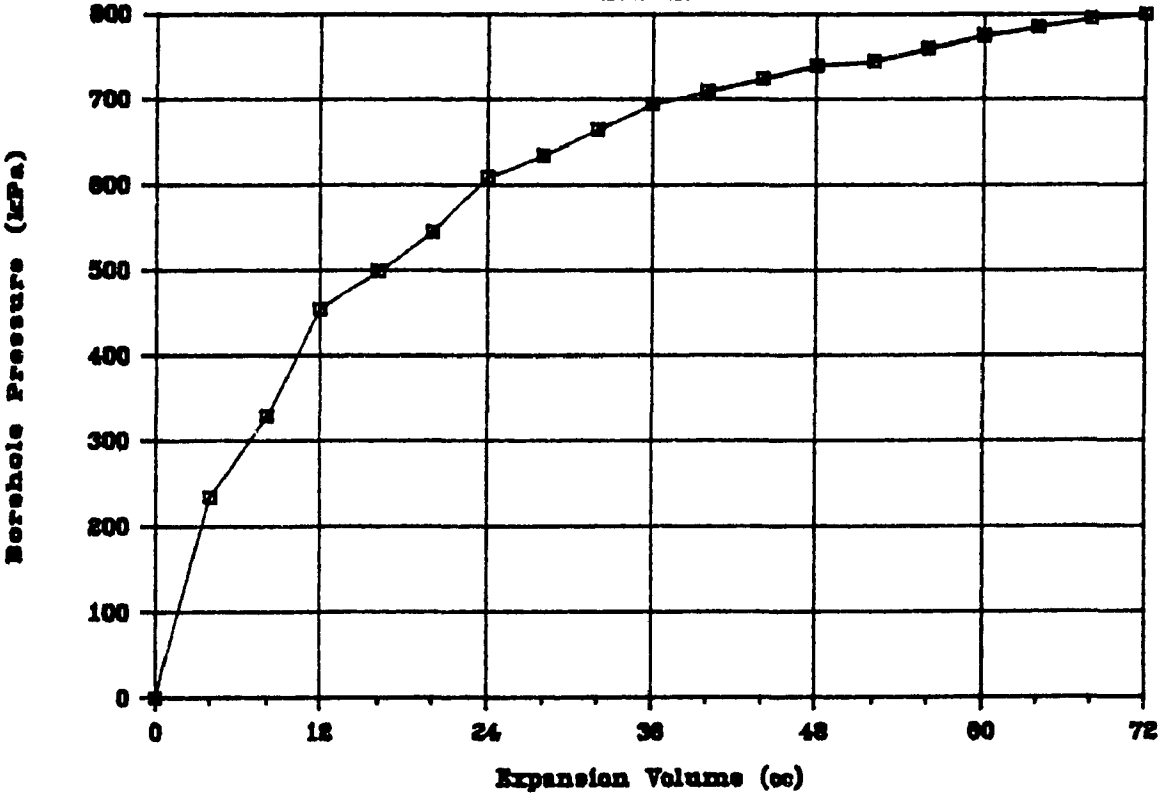

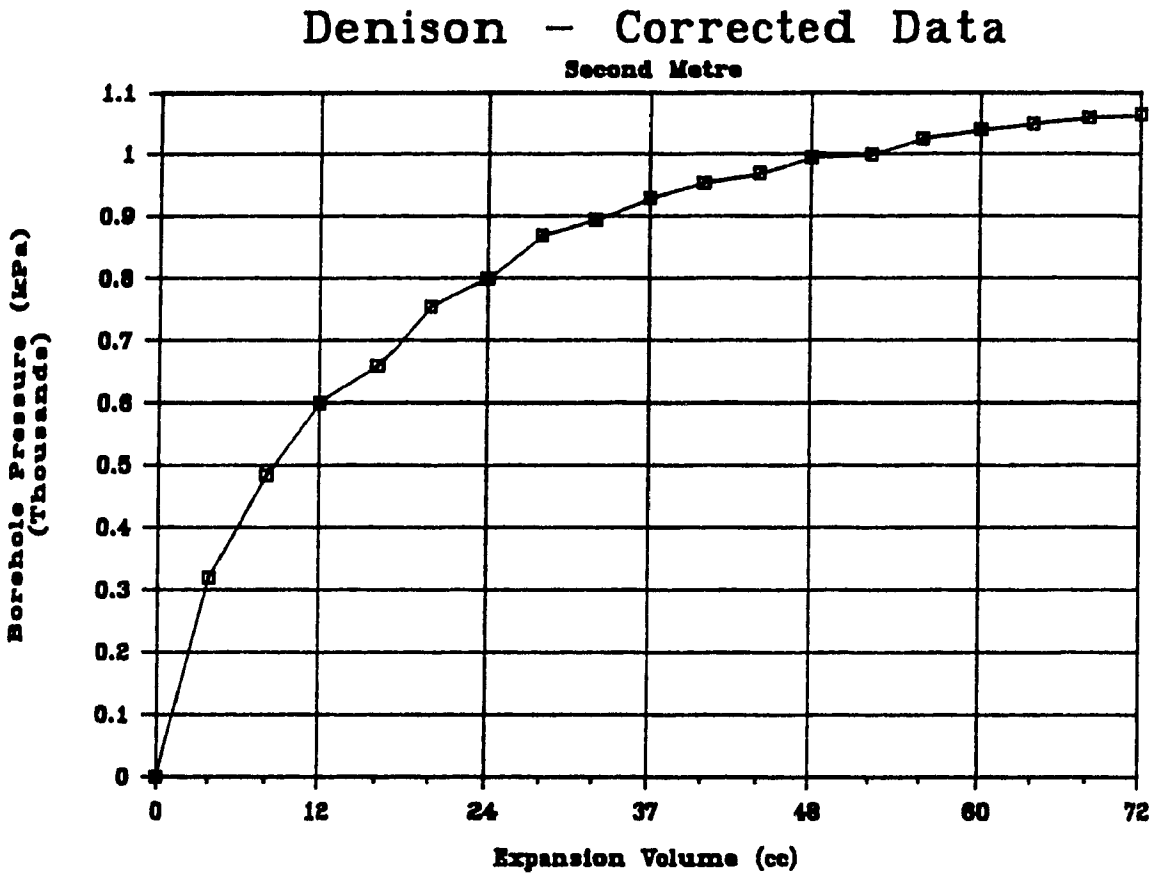
Denison - Corrected Data
Second Metre
Borehole Pressure (kPa)
(Thousands)
1.1
1
0.9
0.8
0.7
0.6
0.5
0.4
0.3
0.2
0.1
0
0
12
24
37
48
60
72
Expansion Volume (cc)

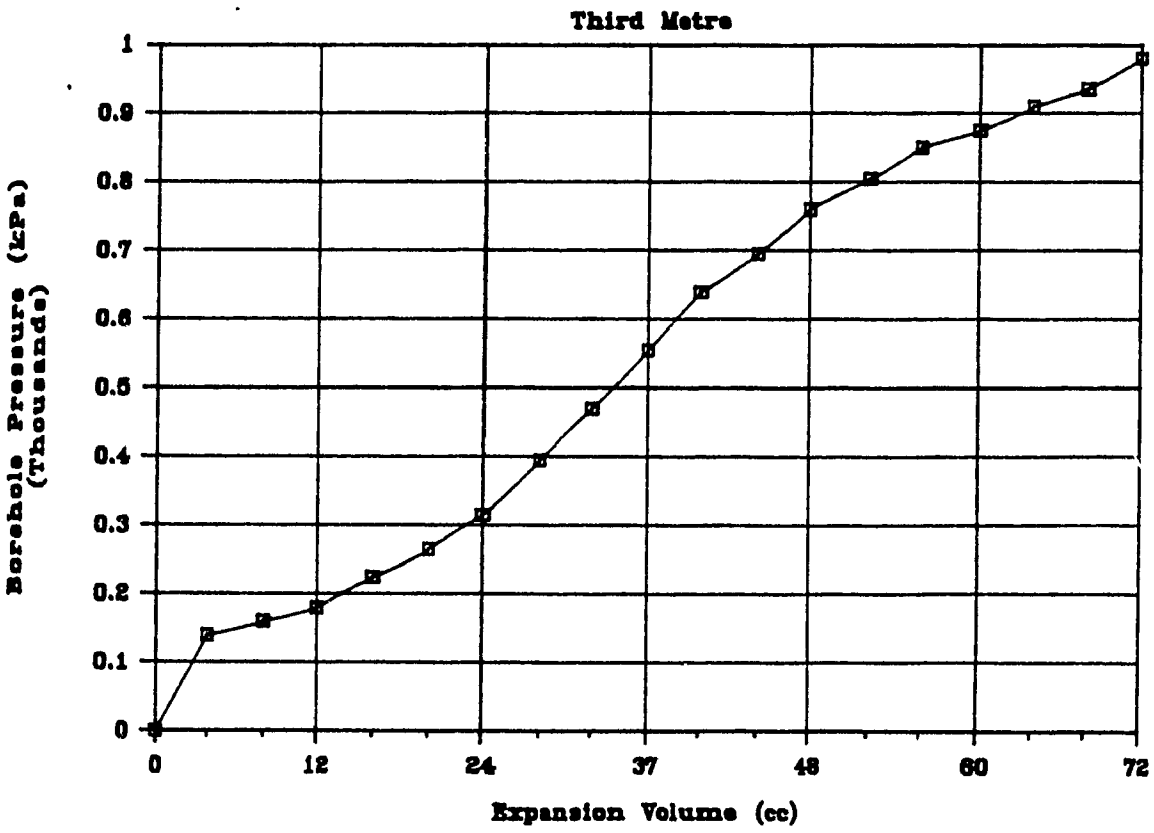
Denison - Corrected Data
Third Metre
Borehole Pressure (kPa)
(Thousands)
1
0.9
0.8
0.7
0.6
0.5
0.4
0.3
0.2
0.1
0
0
12
24
37
48
60
72
Expansion Volume (cc)

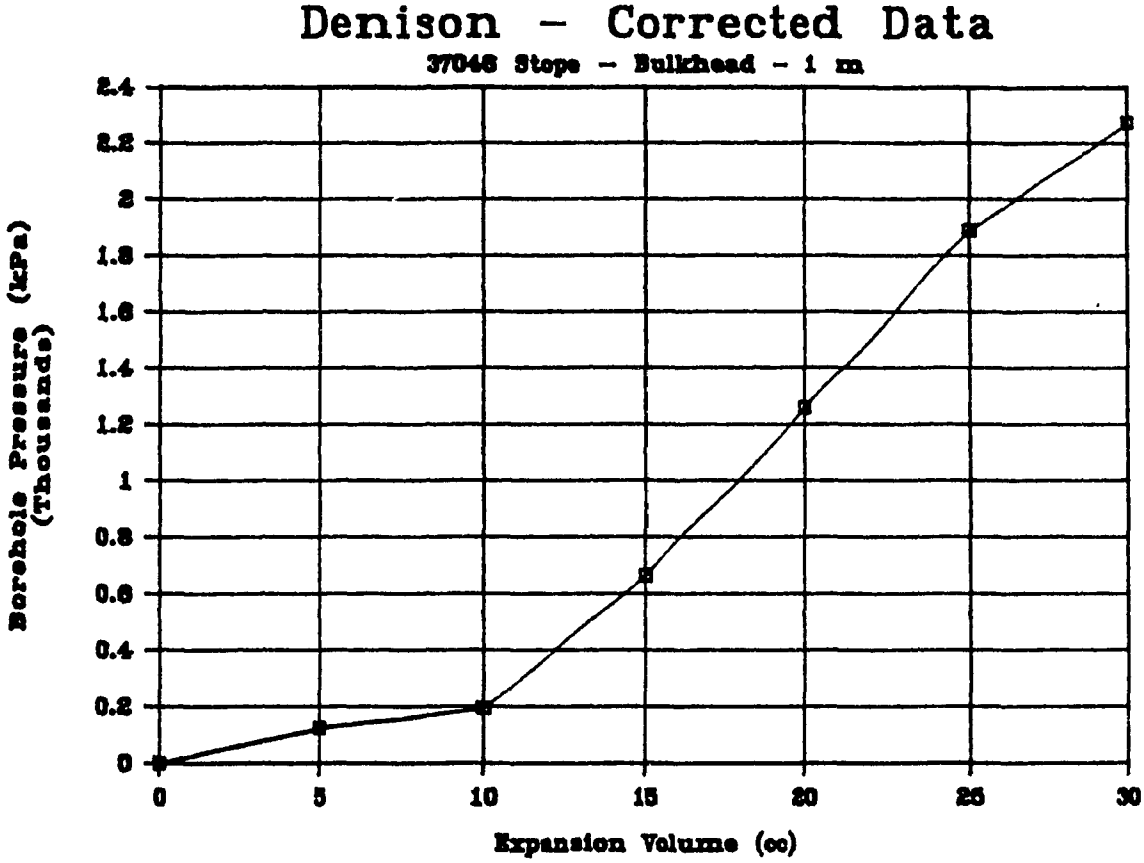
Denison - Corrected Data
37046 Stope - Bulkhead - 1 m
Borehole Pressure (kPa)
(Thousands)
2.4
2.2
2
1.8
1.6
1.4
1.2
1
0.8
0.6
0.4
0.2
0
0
5
10
15
20
25
30
Expansion Volume (cc)

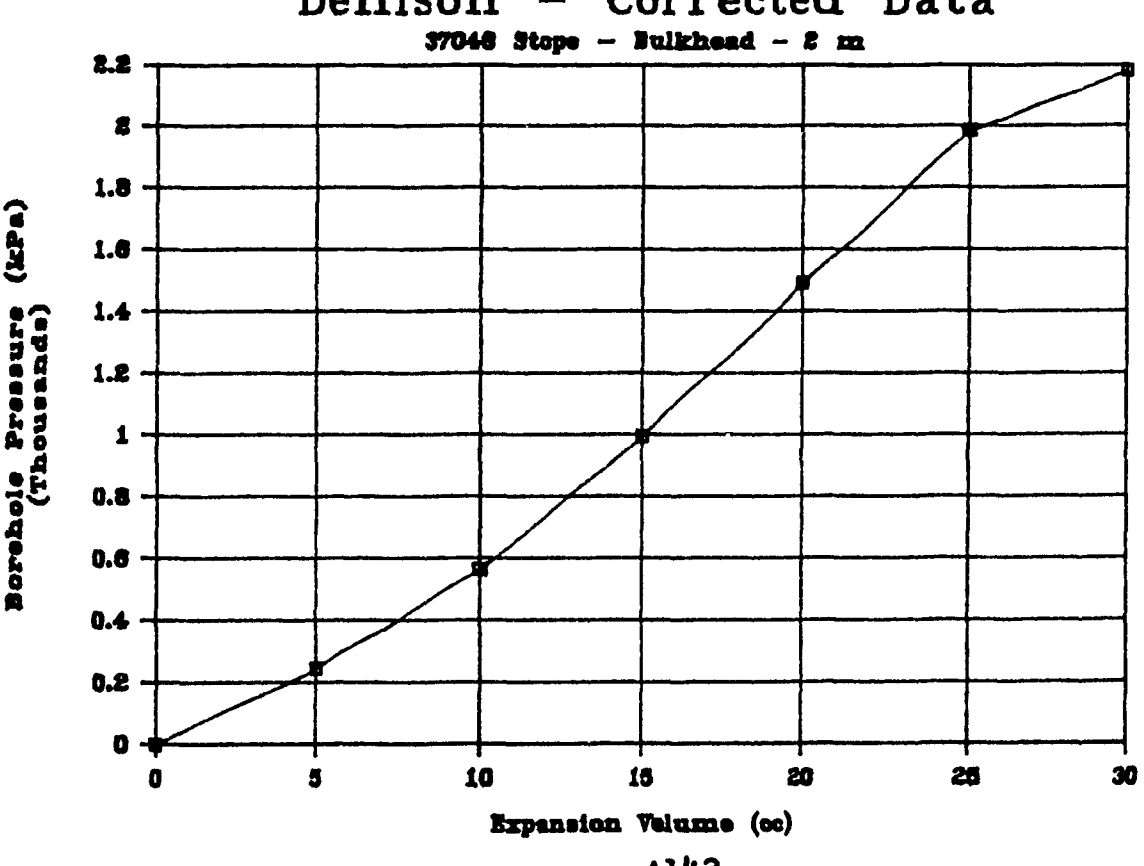
Denison - Corrected Data
37046 Stope - Bulkhead - 2 m
Borehole Pressure (kPa)
(Thousands)
2.2
2
1.8
1.6
1.4
1.2
1
0.8
0.6
0.4
0.2
0
0
5
10
15
20
25
30
Expansion Volume (cc)

Denison – Corrected Data

37046 Stope – Bulkhead – 3 m

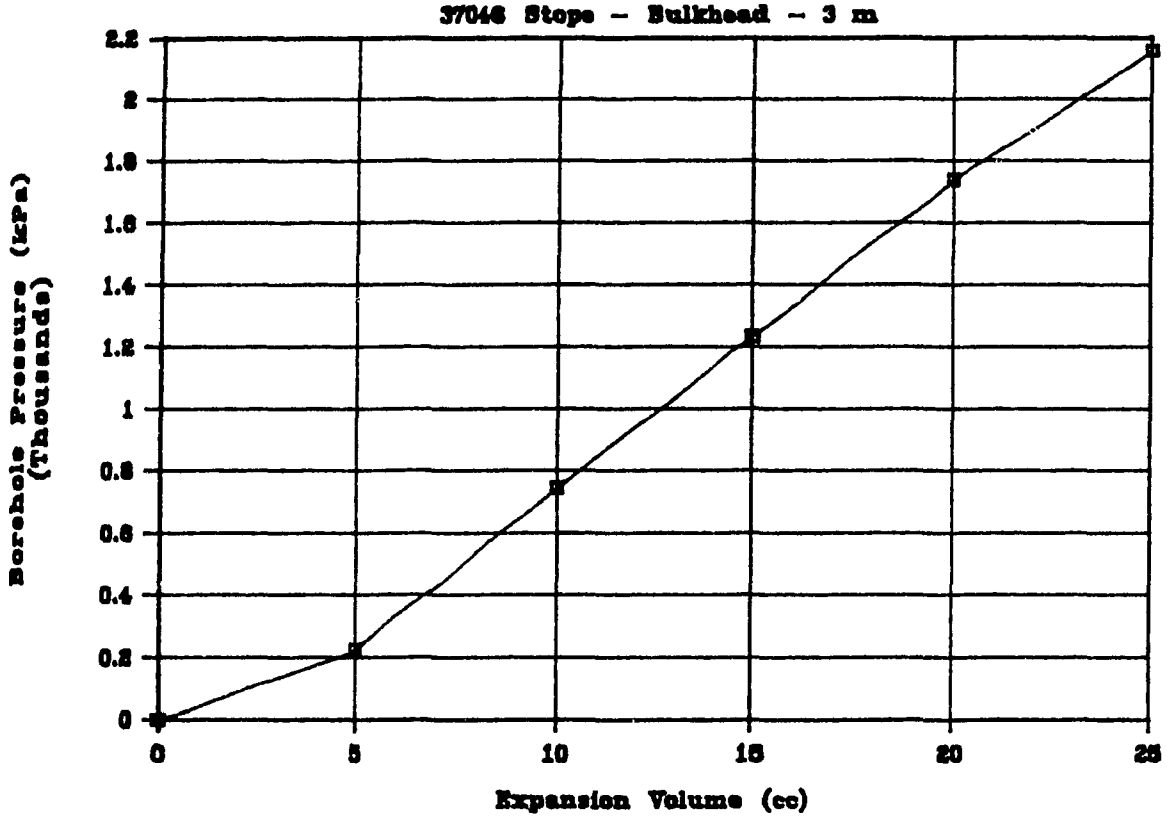

Denison – Corrected Data

37046 Stope – Bulkhead – 4 m

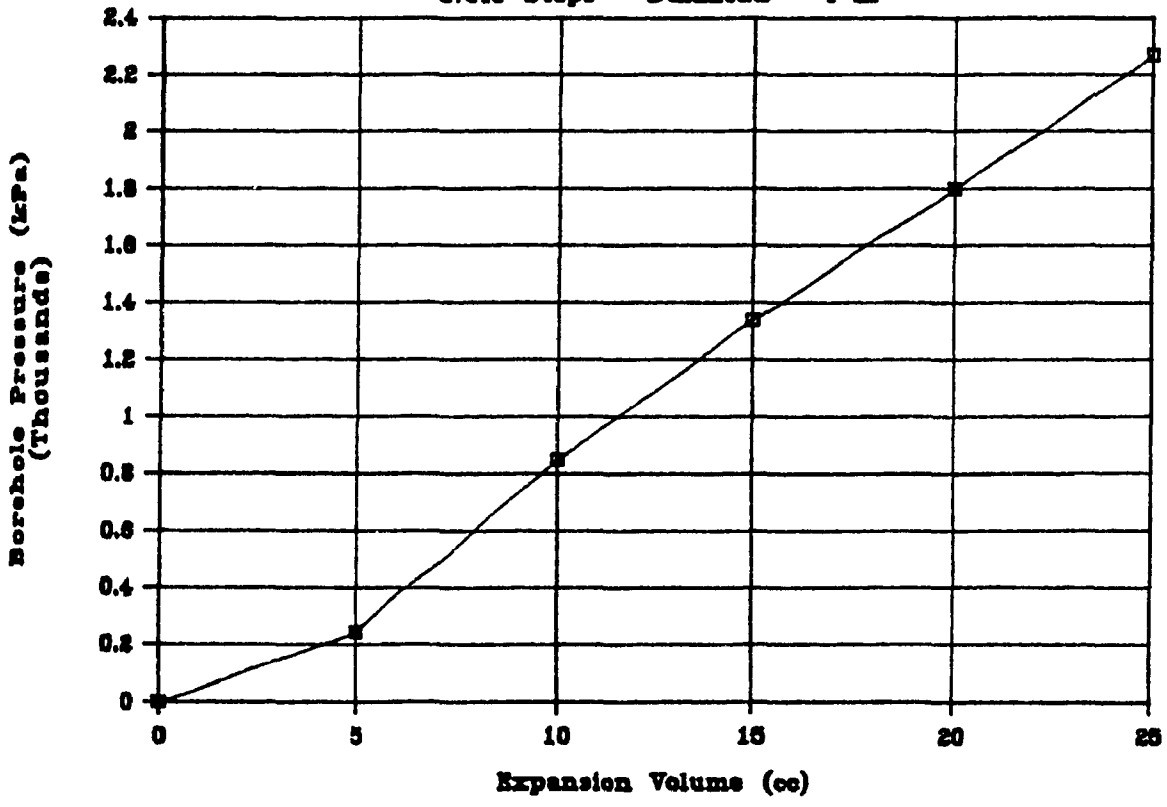

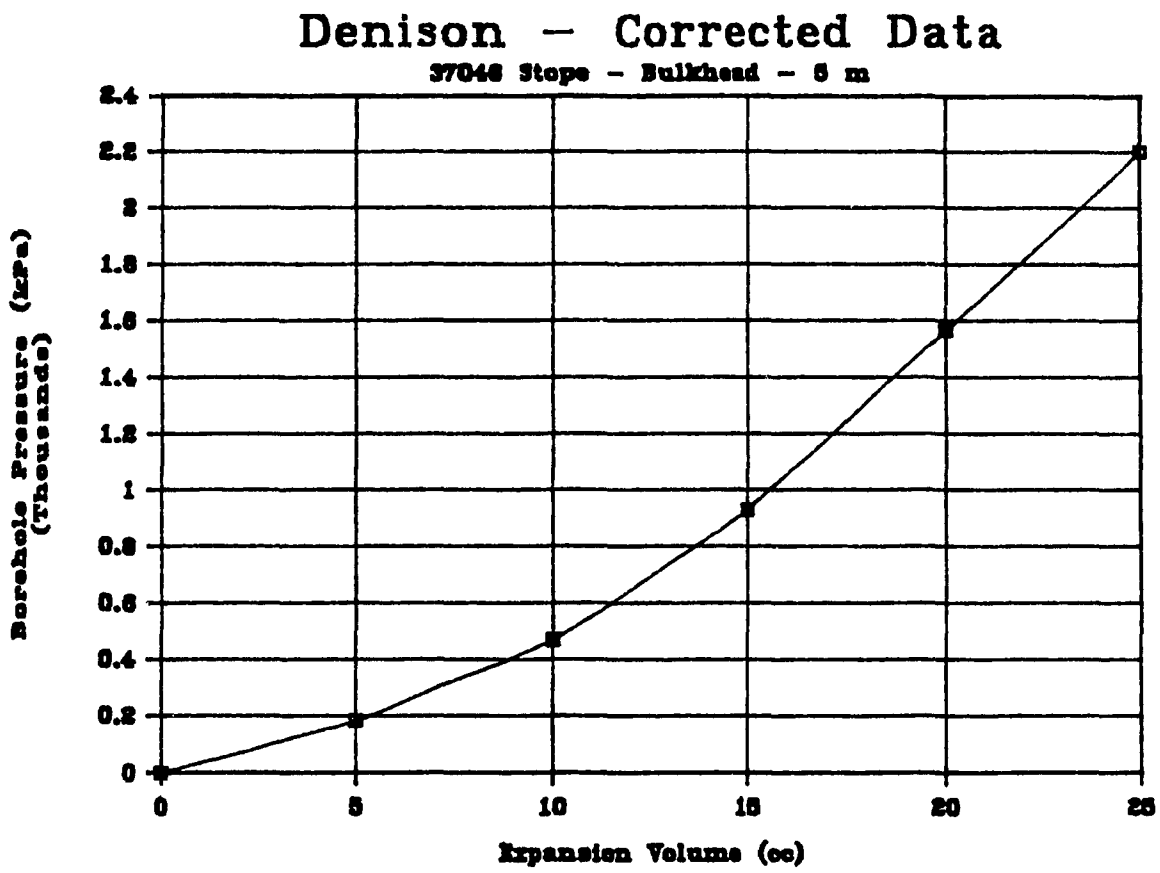
Denison – Corrected Data
37048 Stope – Bulkhead – 5 m
Borehole Pressure (kPa)
(Thousands)
2.4
2.2
2
1.8
1.6
1.4
1.2
1
0.8
0.6
0.4
0.2
0
0
5
10
15
20
25
Expansion Volume (cc)

Kiena Level 21 – 20:1 Sand : Cement

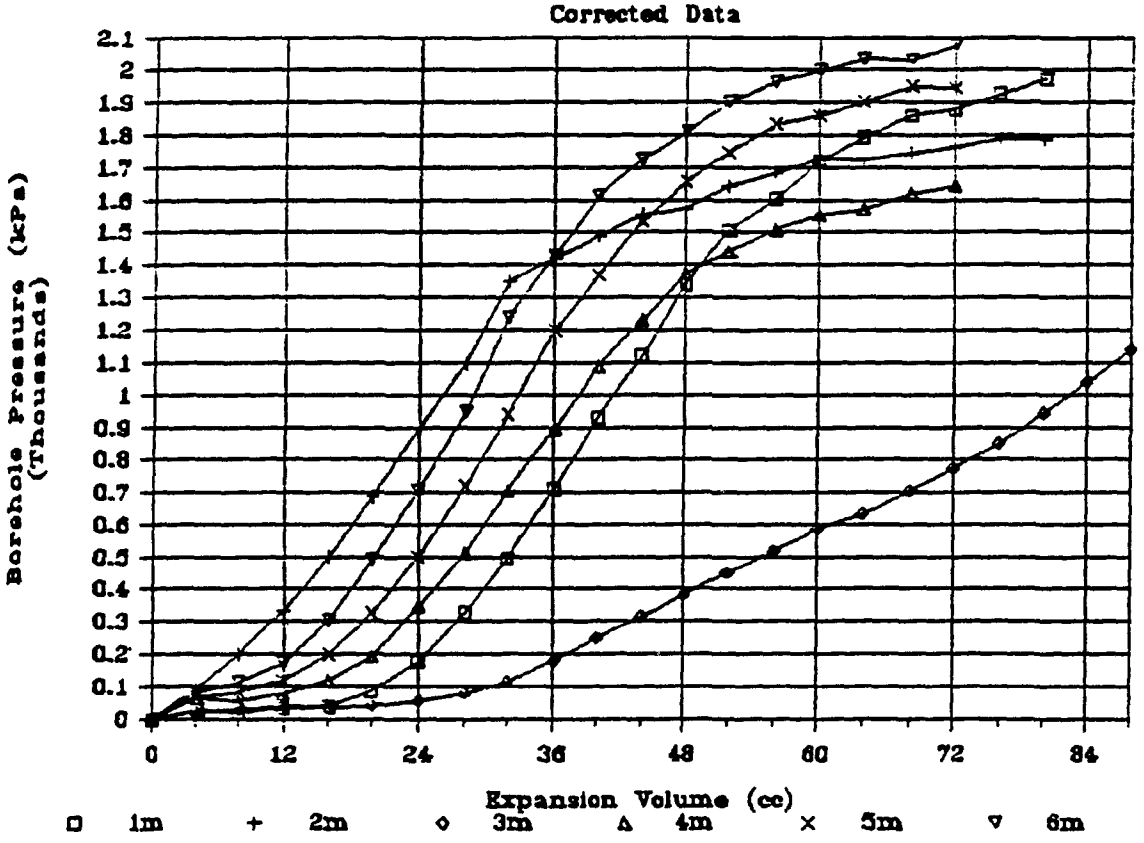

Kiena Level 21

Corrected Data First Metre

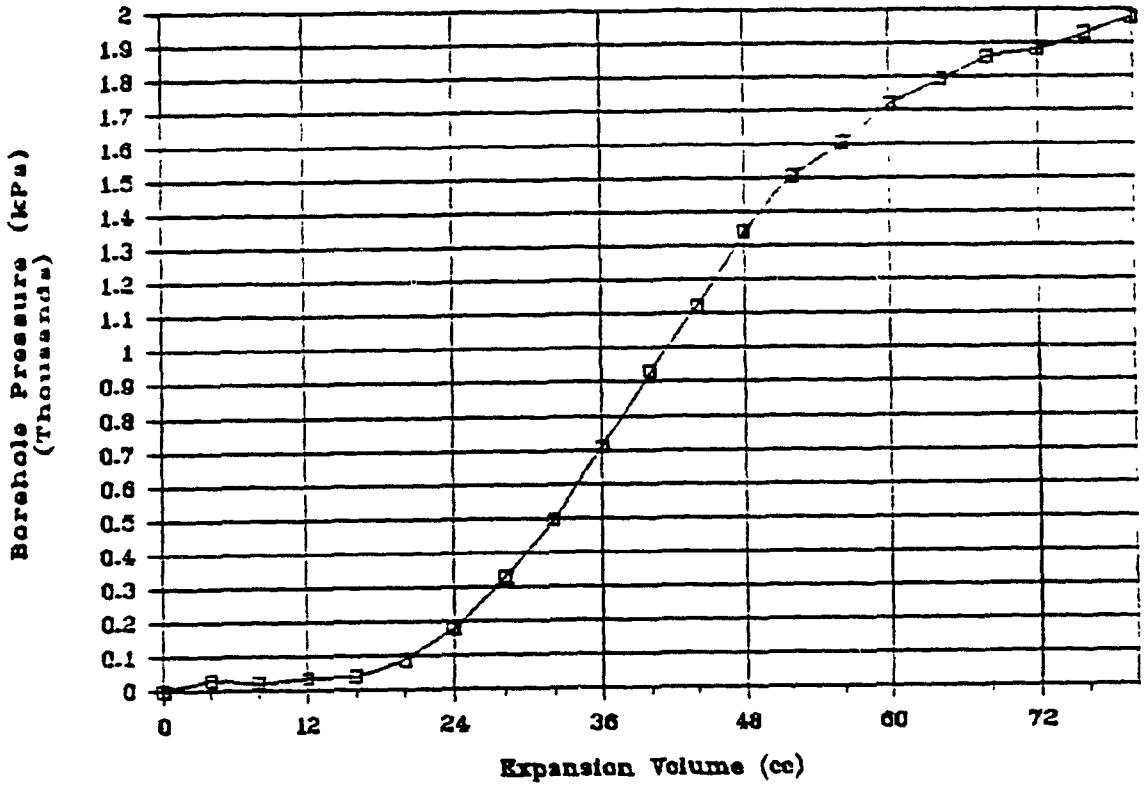

Kiena Level 21

Corrected Data Second Metre

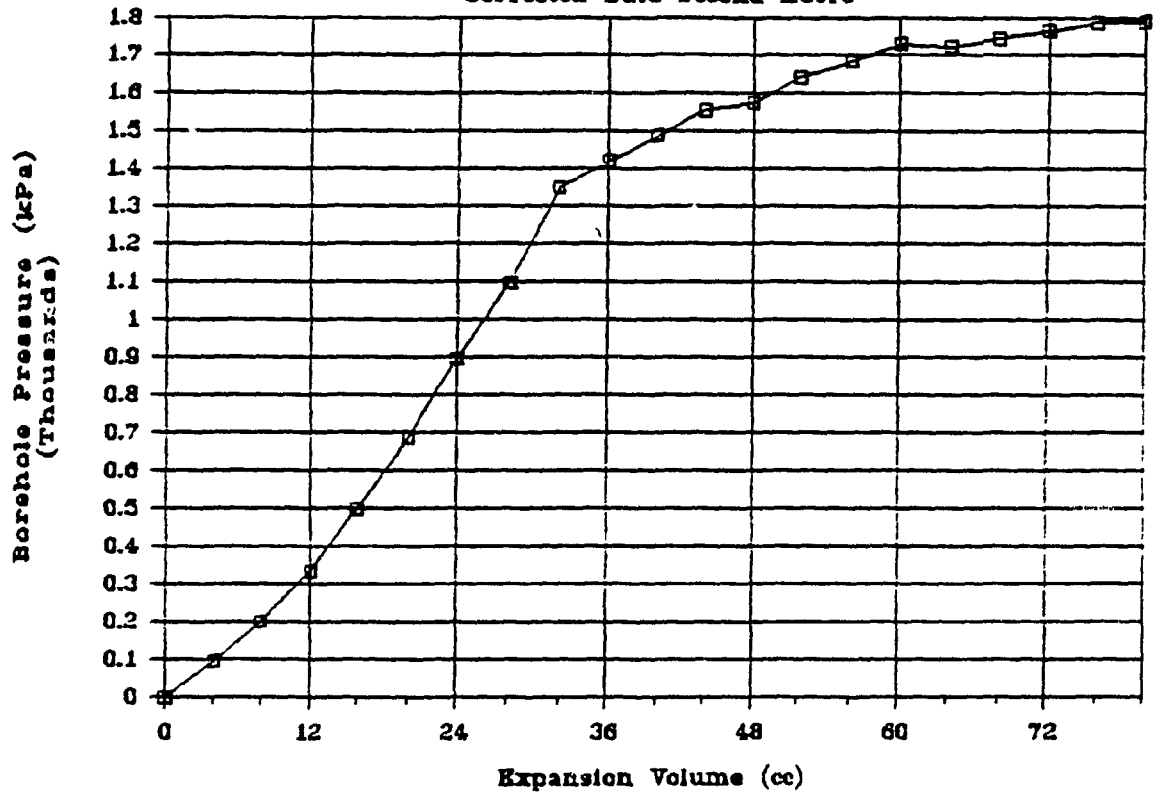

Kiena Level 21

Corrected Data Third Metre

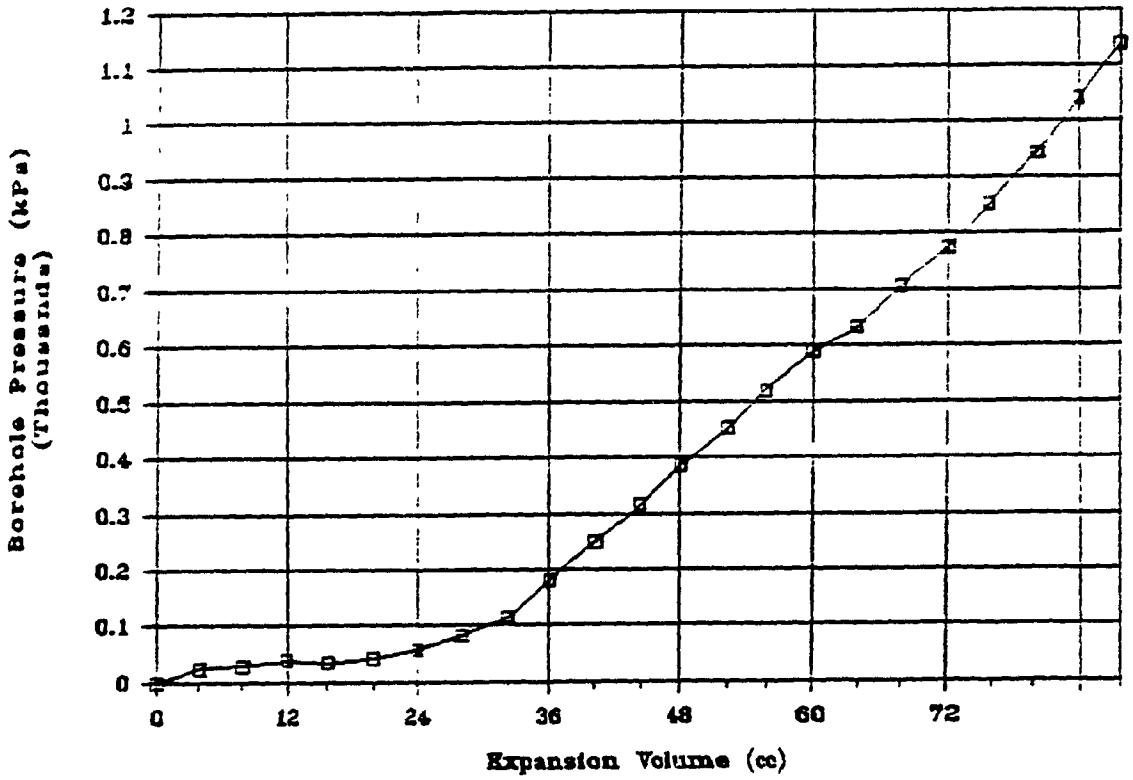

Kiena Level 21

Corrected Data Fourth Metre

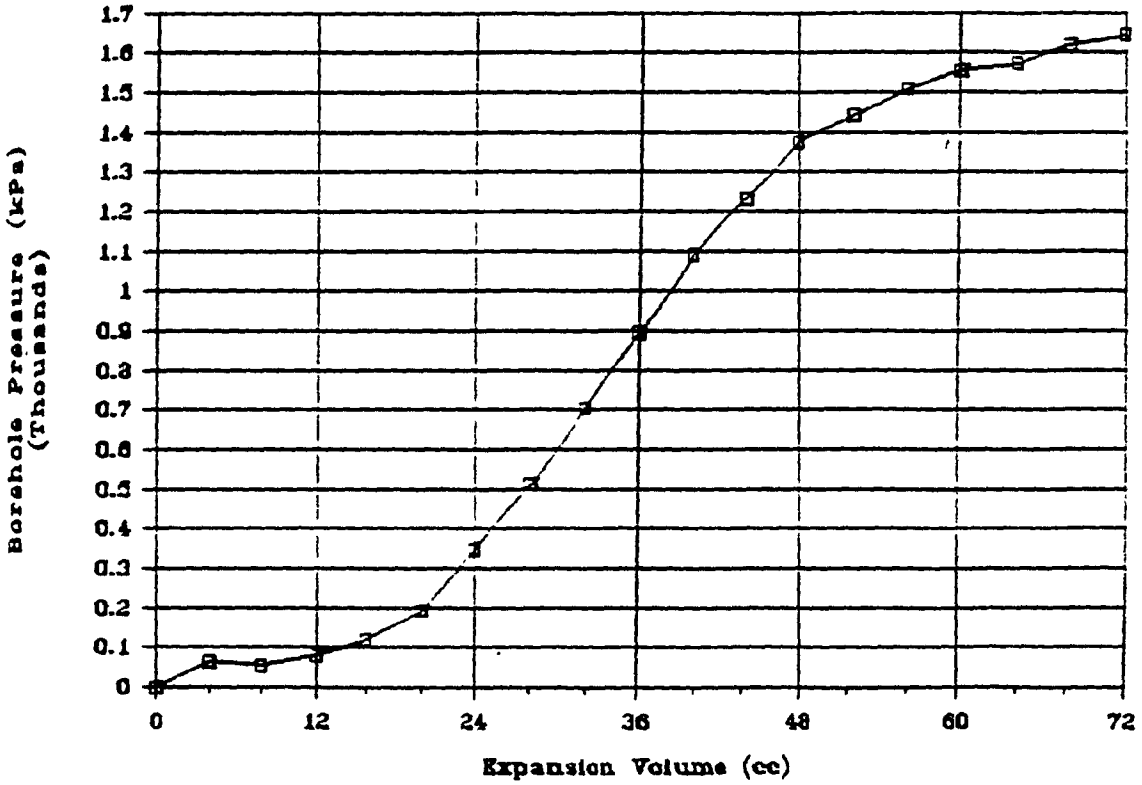

Kiena Level 21

Corrected Data Fifth Metre

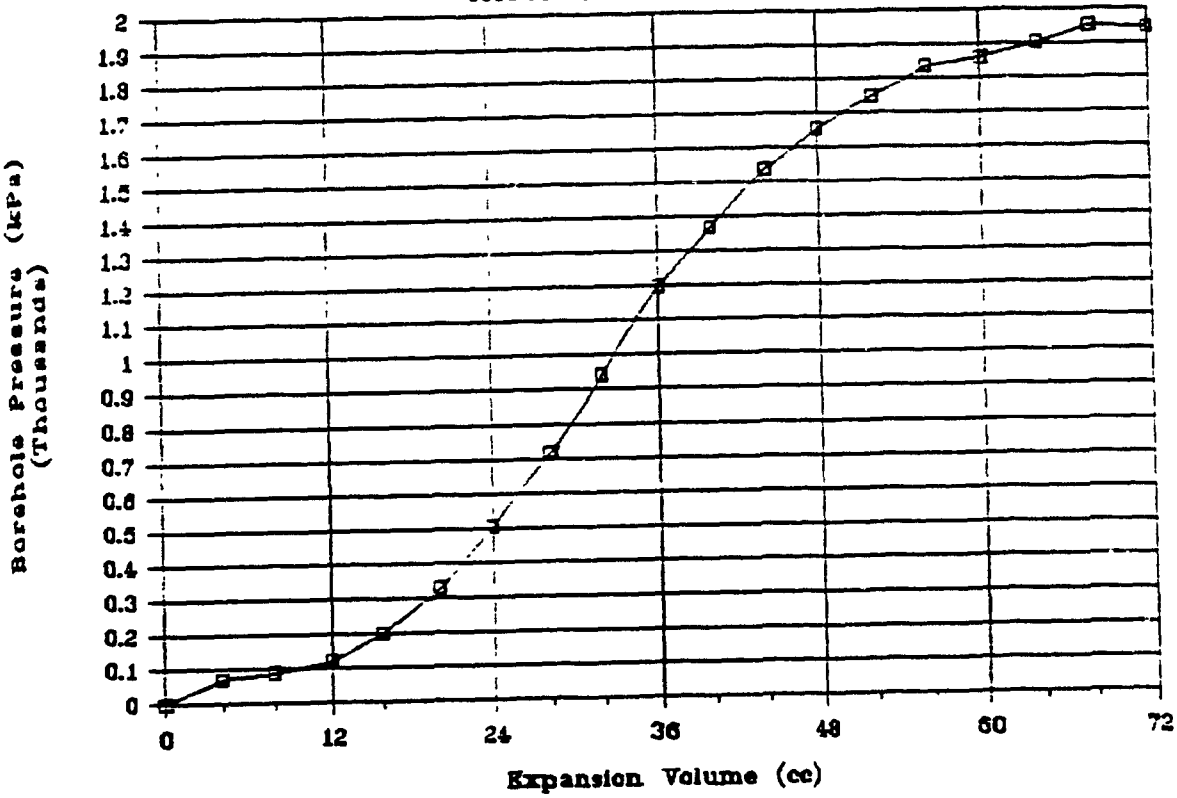

Kiena Level 21

Corrected Data Sixth Metre

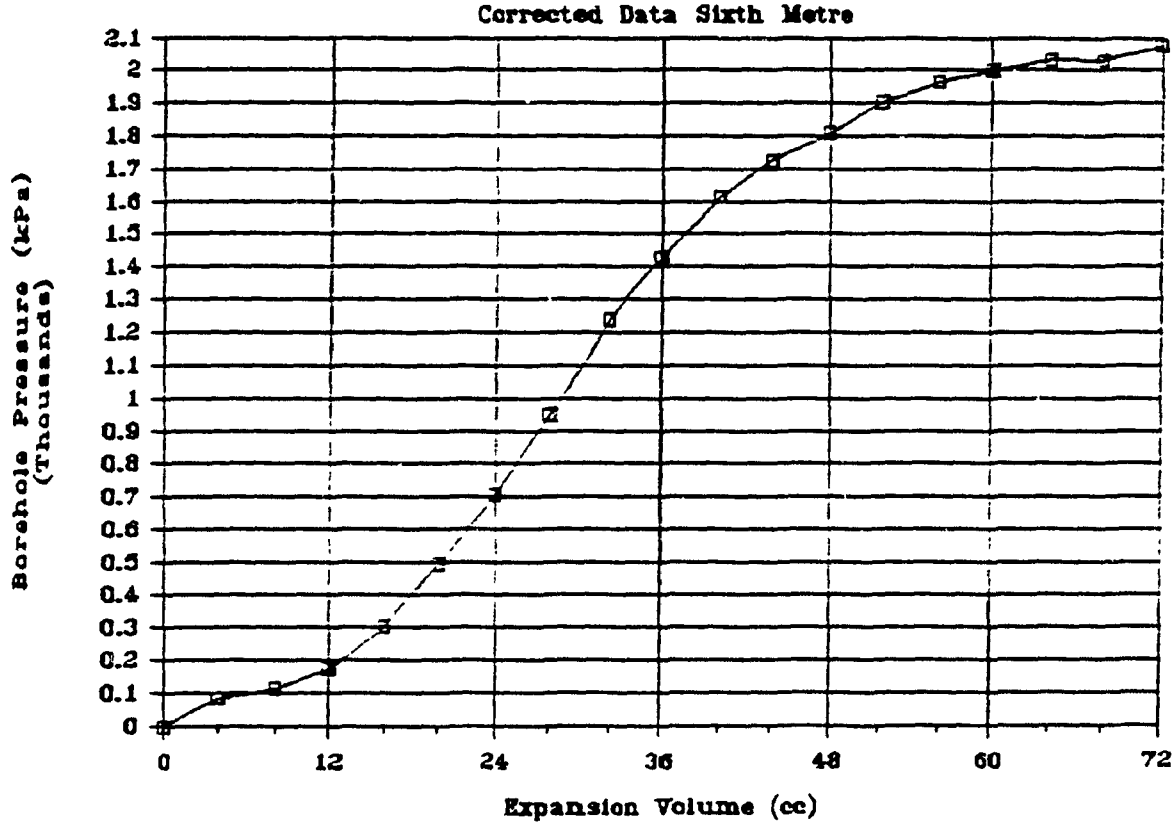

Kiena Location #1 — Corrected Data

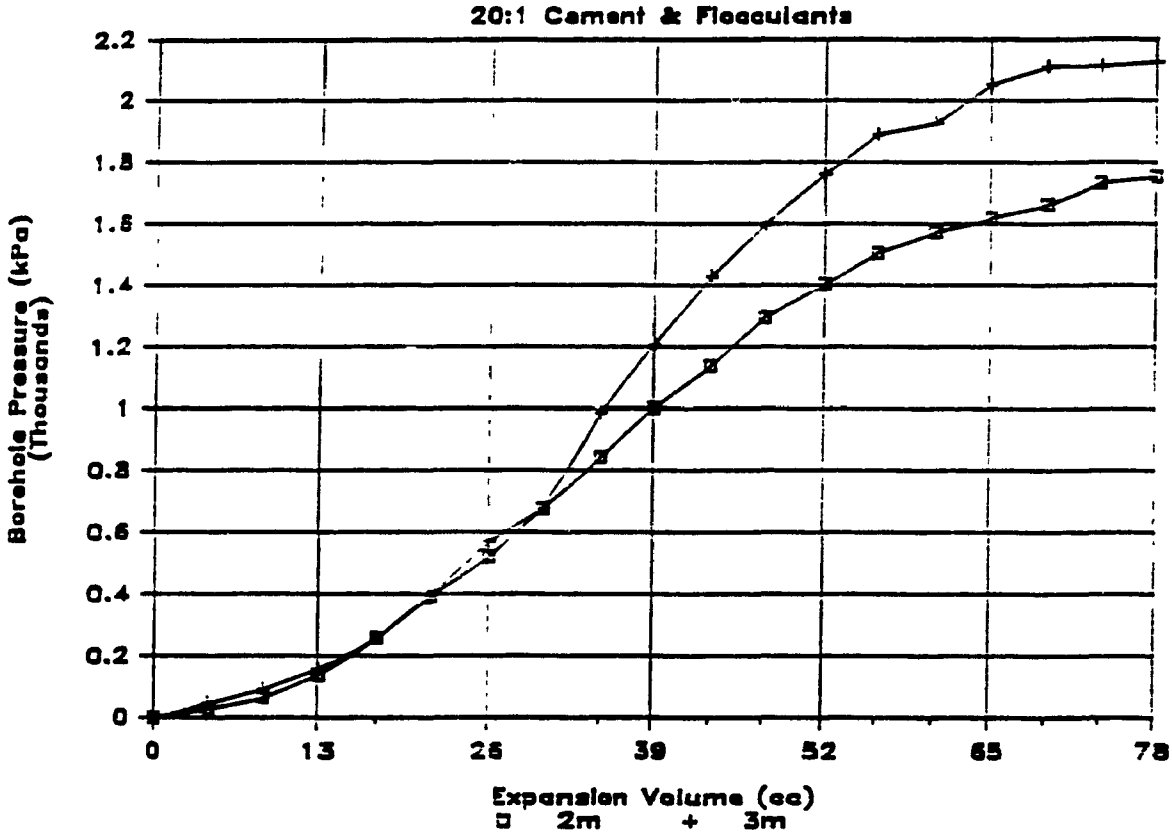

Kiena Location #1 — Corrected Data

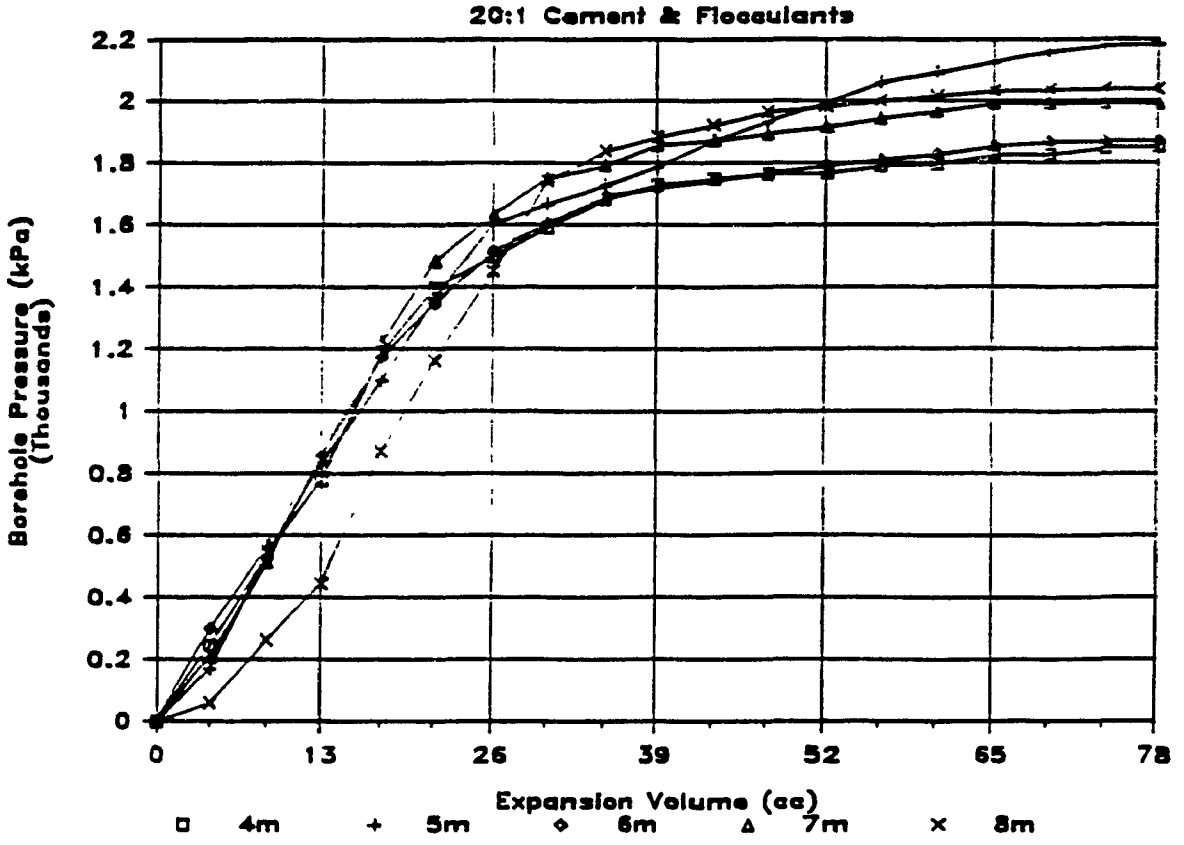

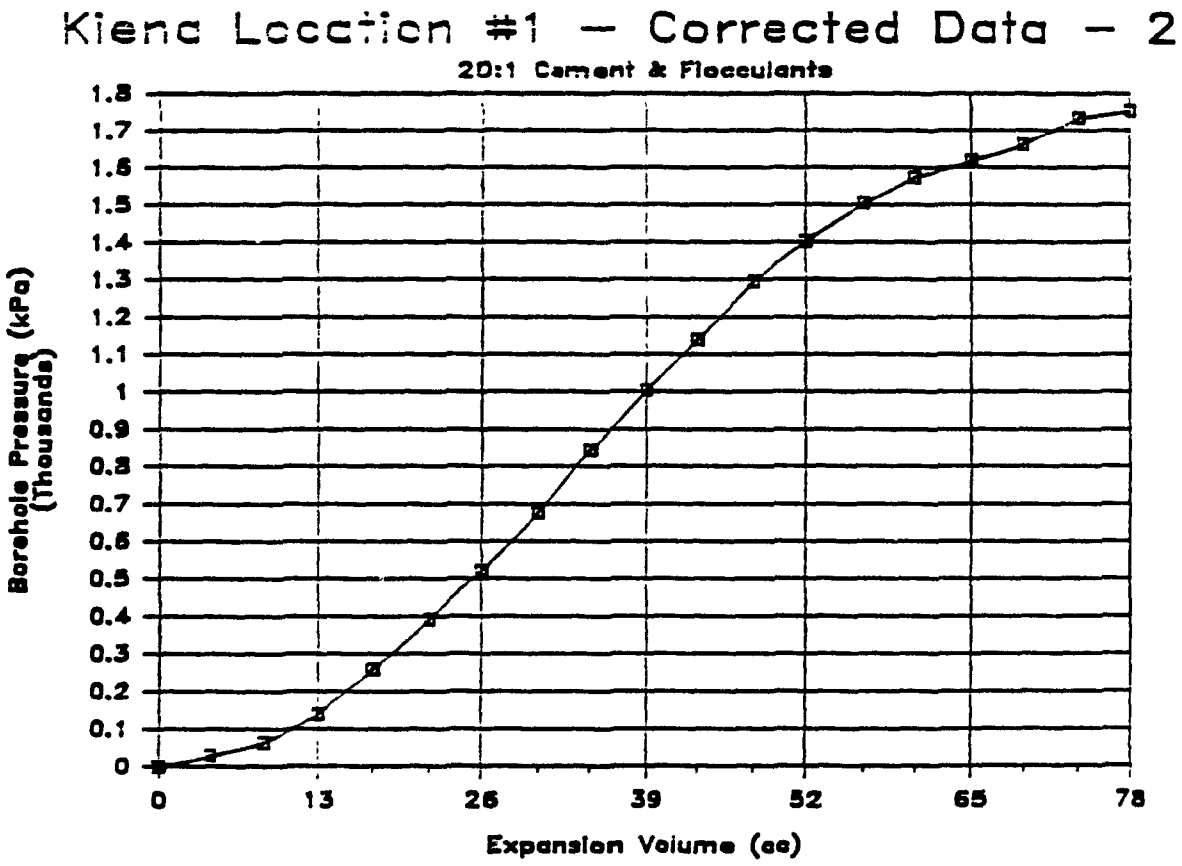
Kiena Location #1 — Corrected Data — 2
20:1 Cement & Flocculants
Borehole Pressure (kPa) (Thousands)
1.8
1.7
1.6
1.5
1.4
1.3
1.2
1.1
1
0.9
0.8
0.7
0.6
0.5
0.4
0.3
0.2
0.1
0
0
13
26
39
52
65
78
Expansion Volume (cc)

Kiena Location #1 — Corrected Data — 3

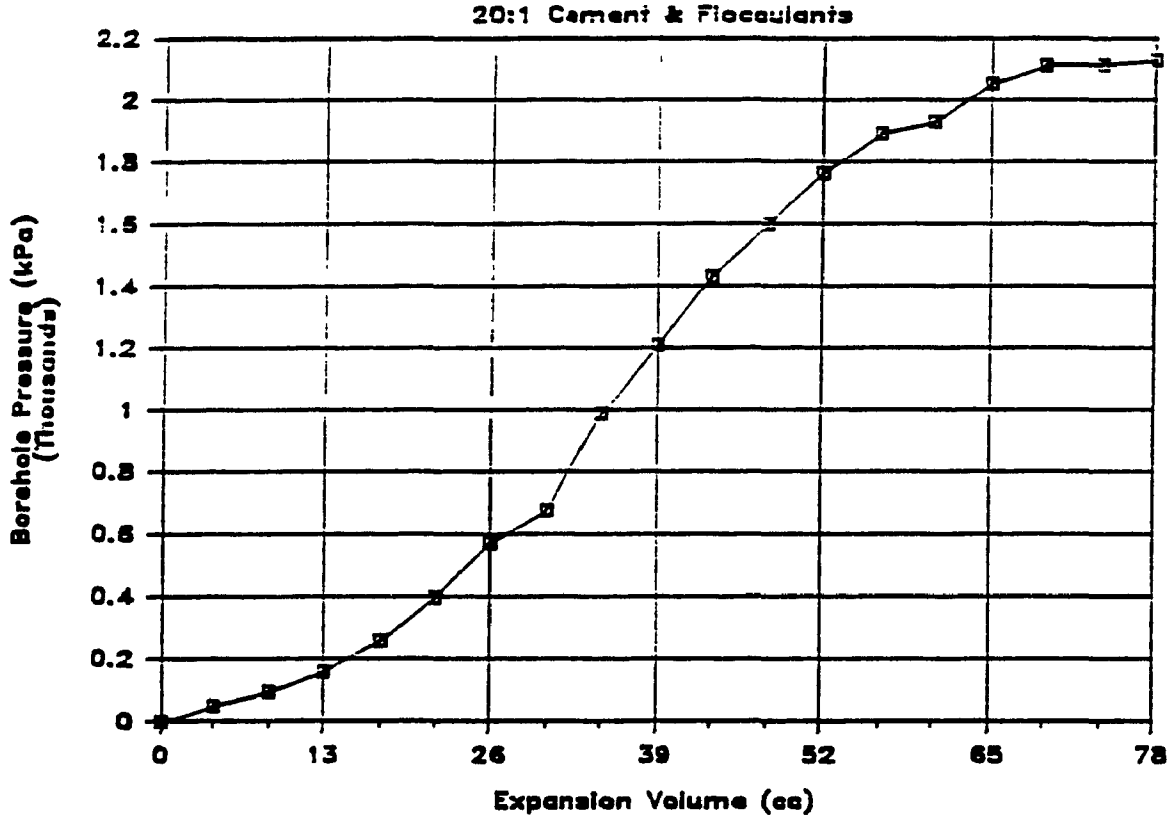

Kiena Location #1 — Corrected Data — 4

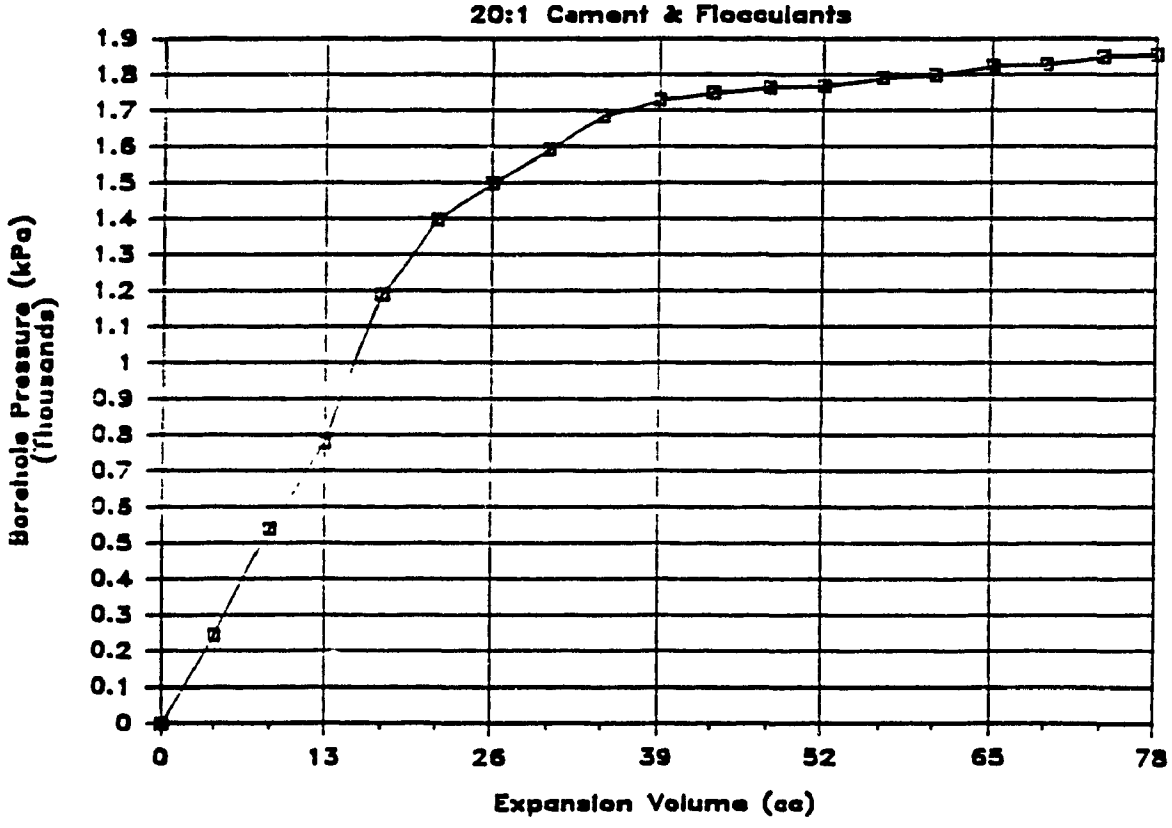

Kiena Location #1 — Corrected Data — 5

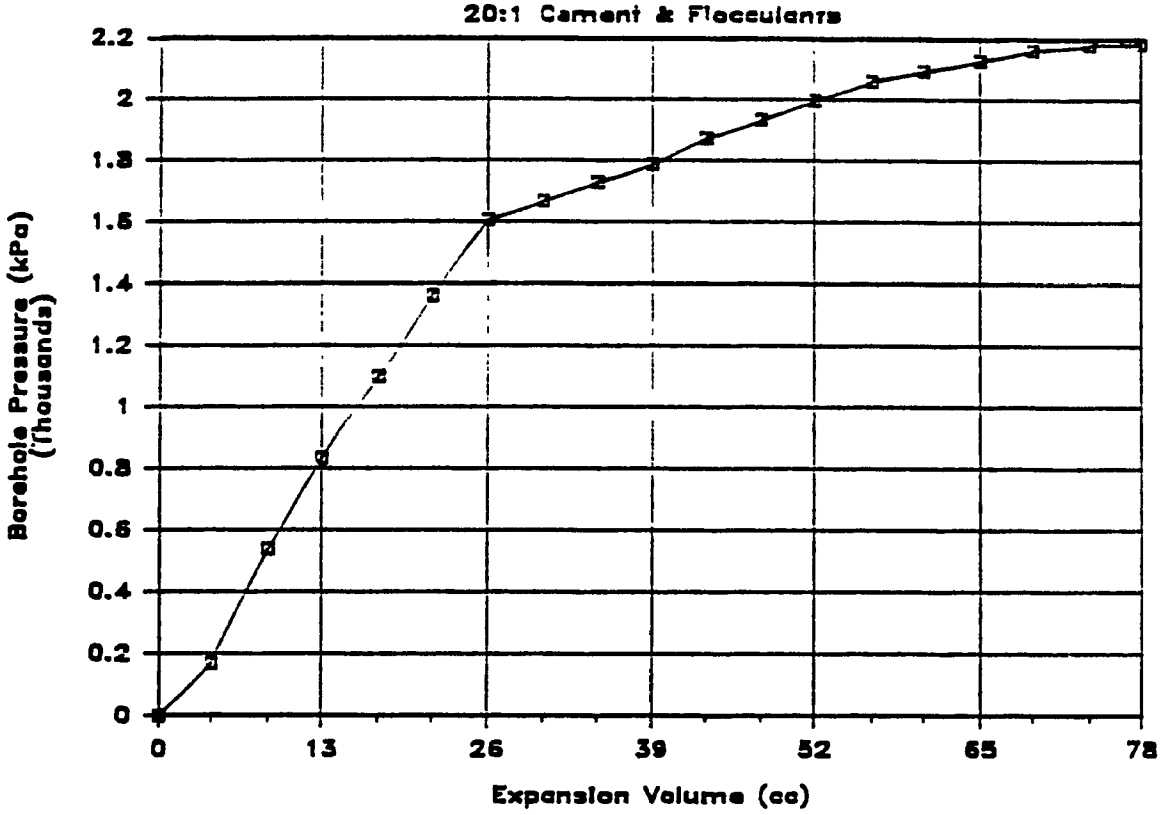

Kiena Location #1 — Corrected Data — 6

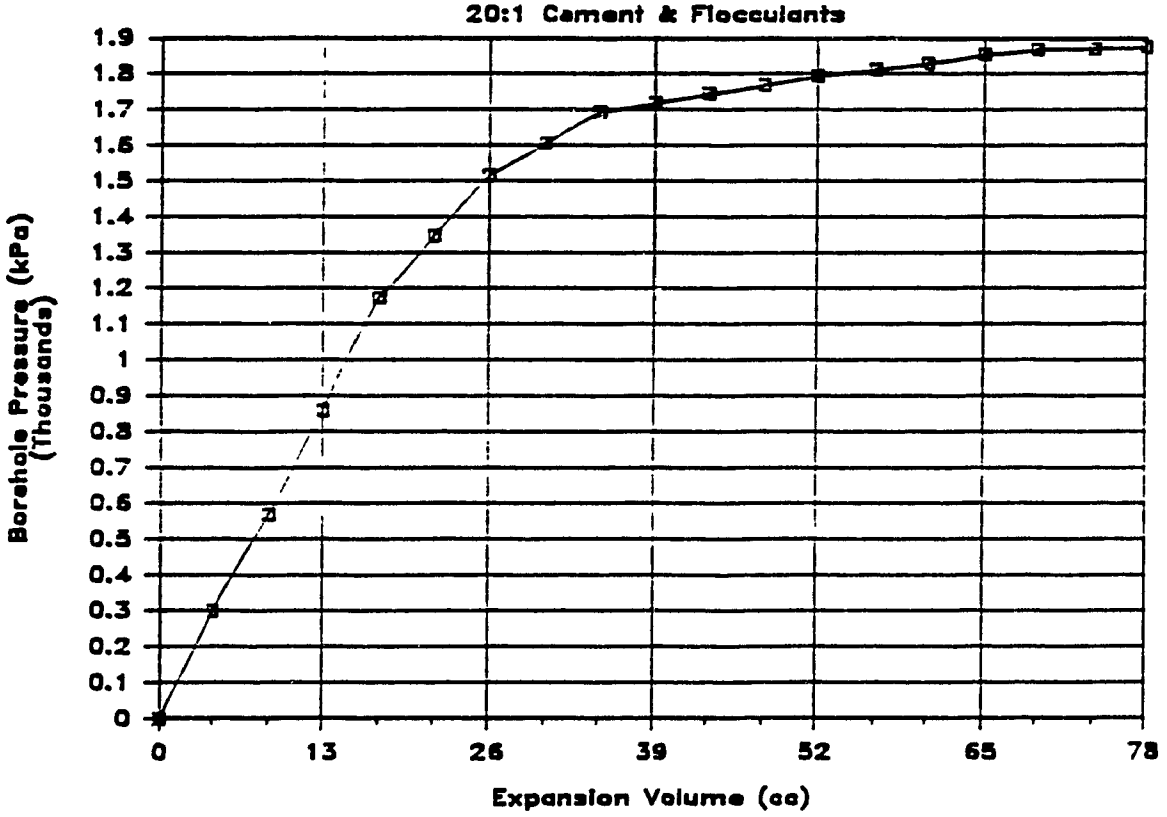

Kiena Location #1 — Corrected Data — 7

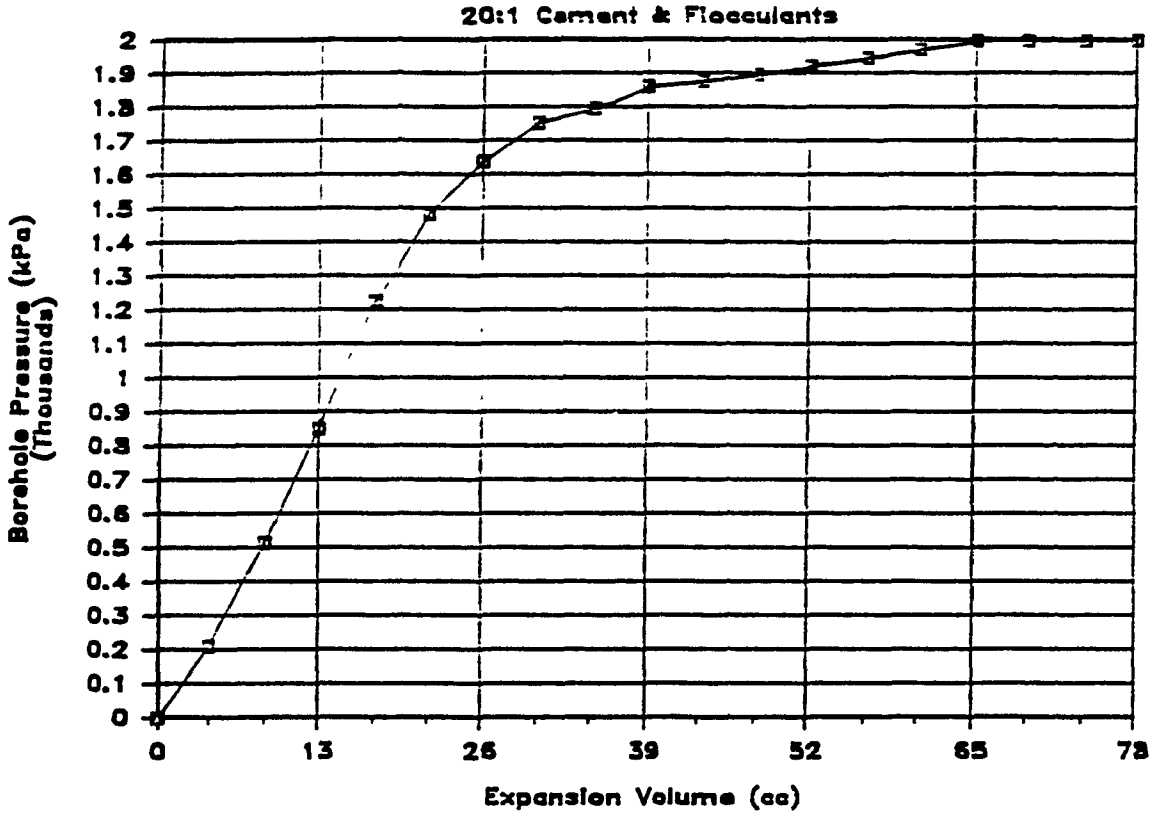

Kiena Location #1 — Corrected Data — 8

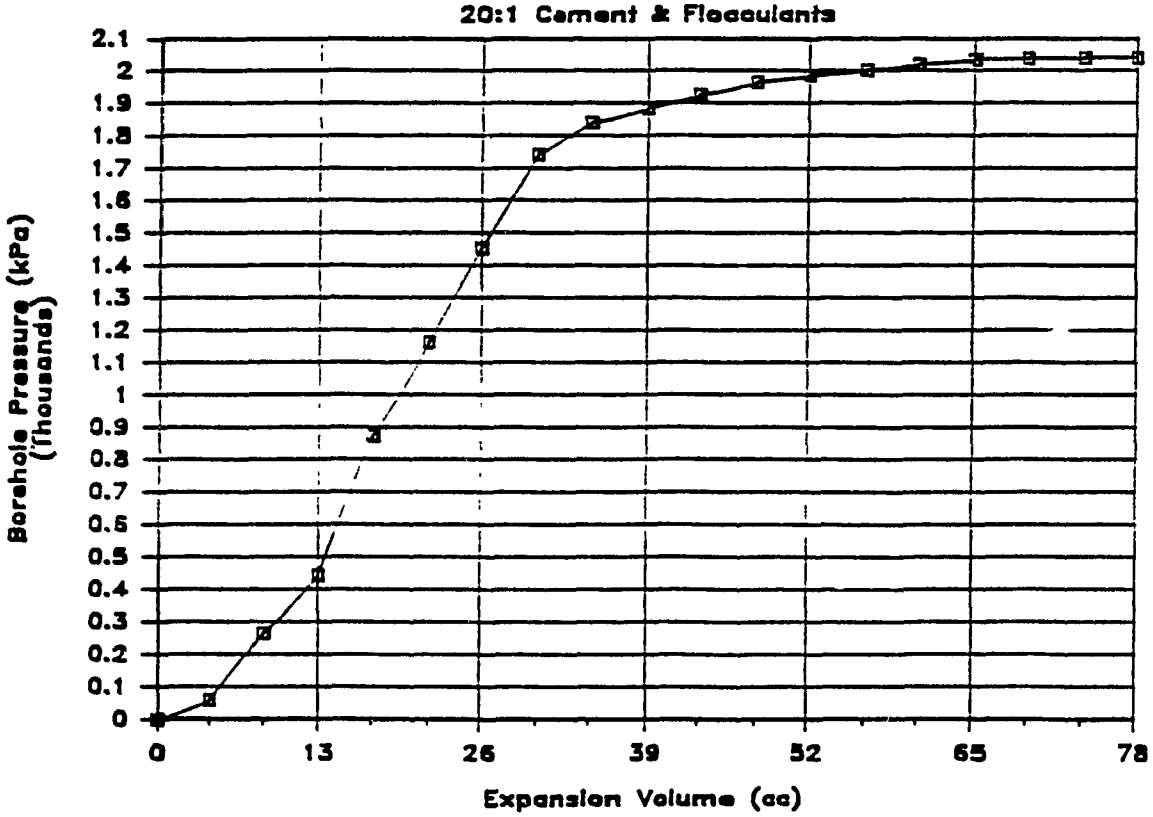

Kiena Location #2 – Corrected Data

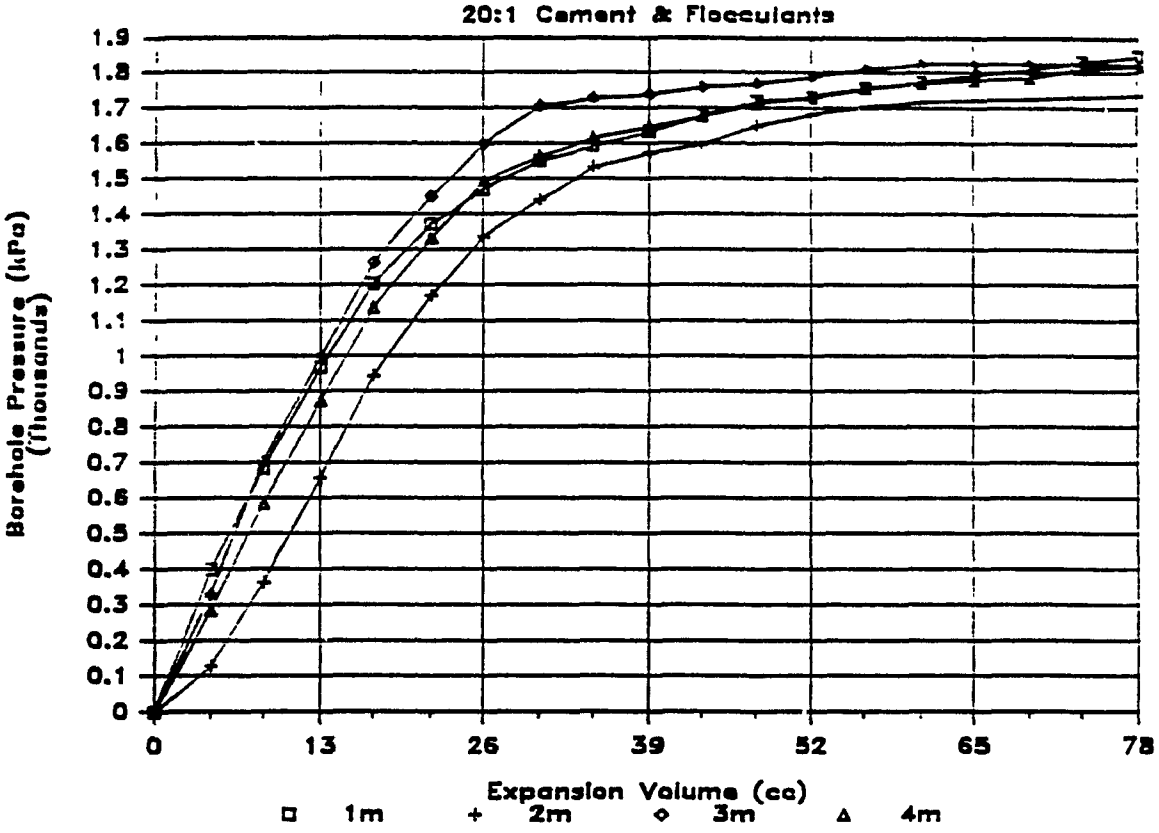

Kiena Location #2 – Corrected Data – 1

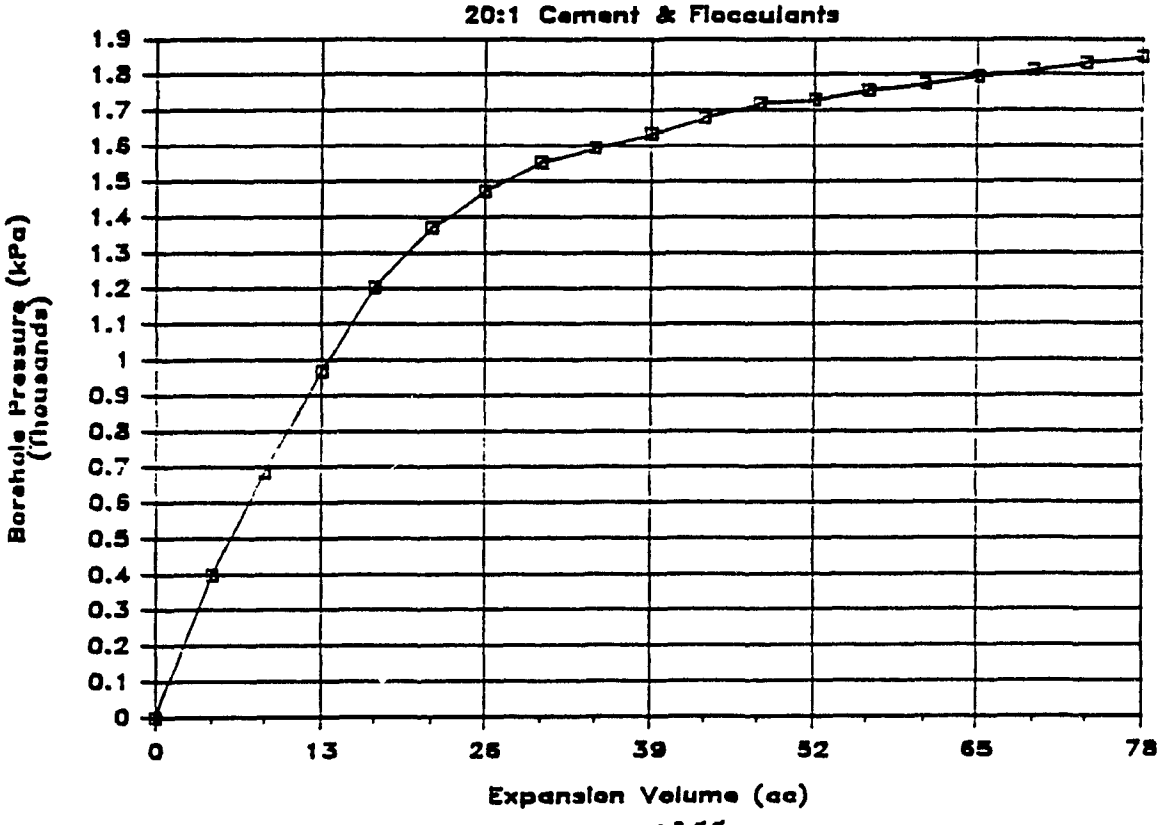

Kiena Location #2 – Corrected Data – 2

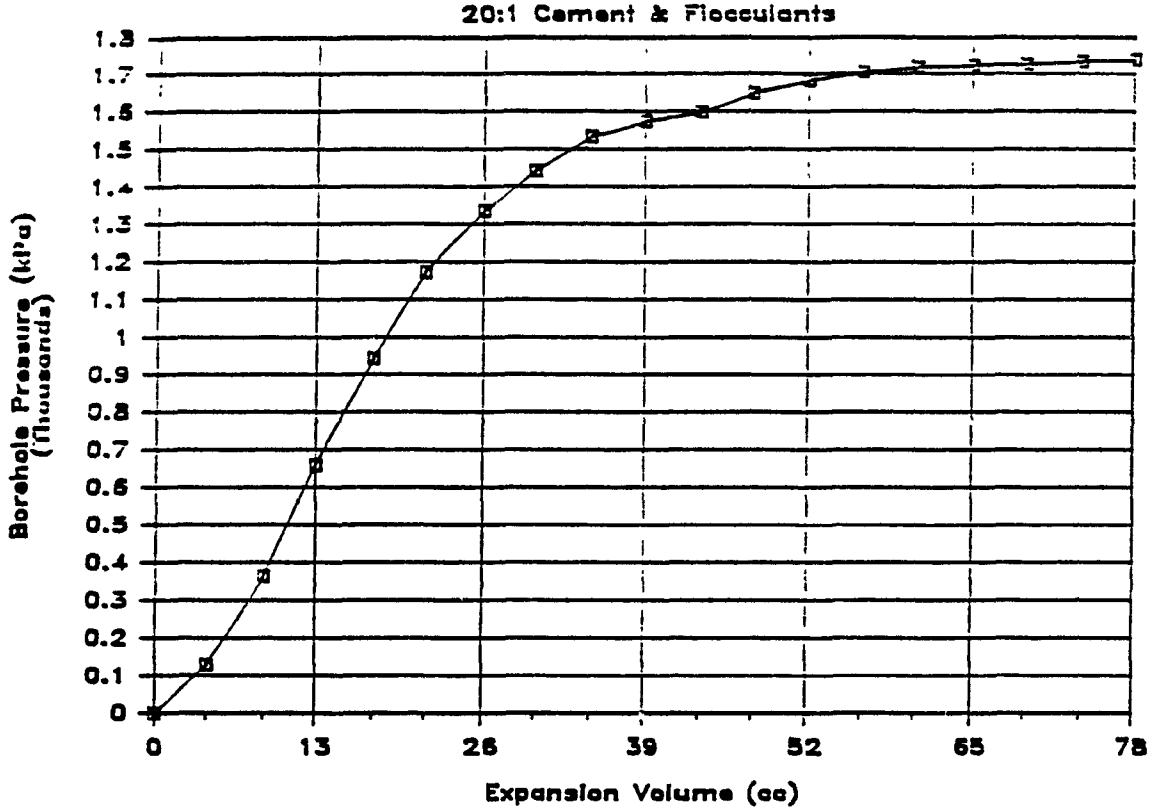

Kiena Location #2 – Corrected Data – 3

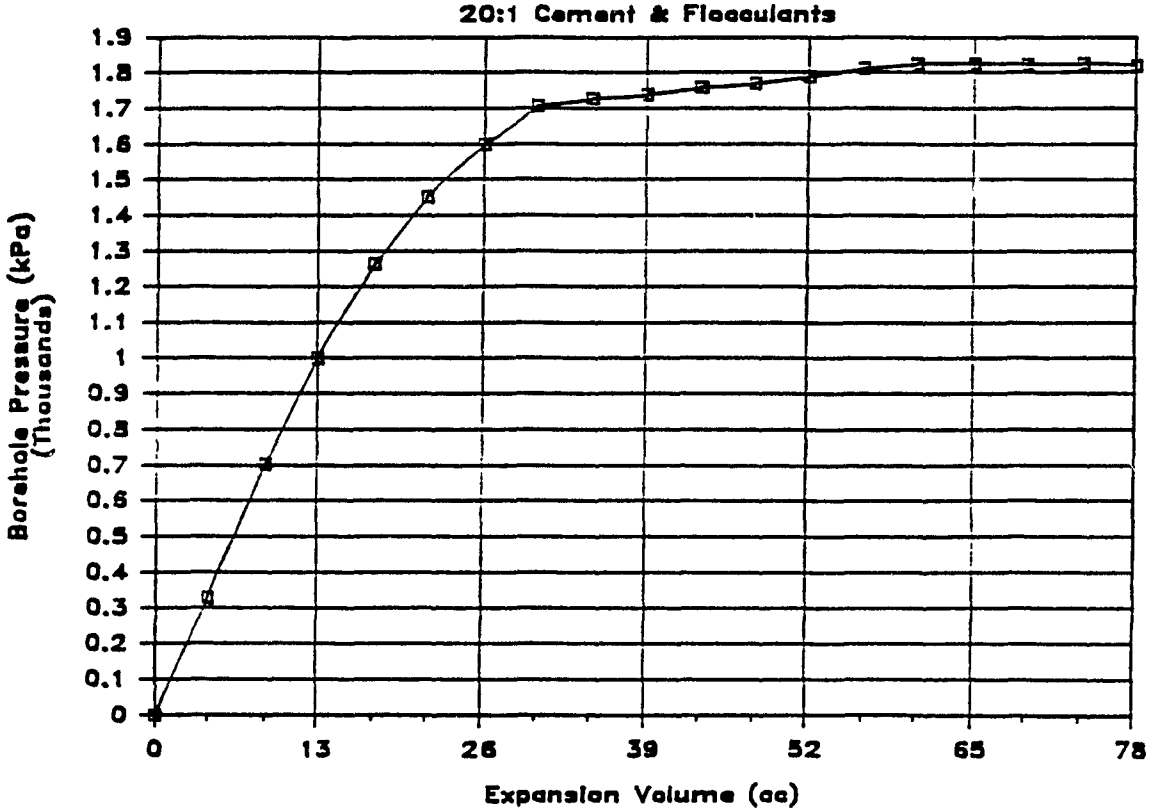

Kiena Location #2 – Corrected Data – 4

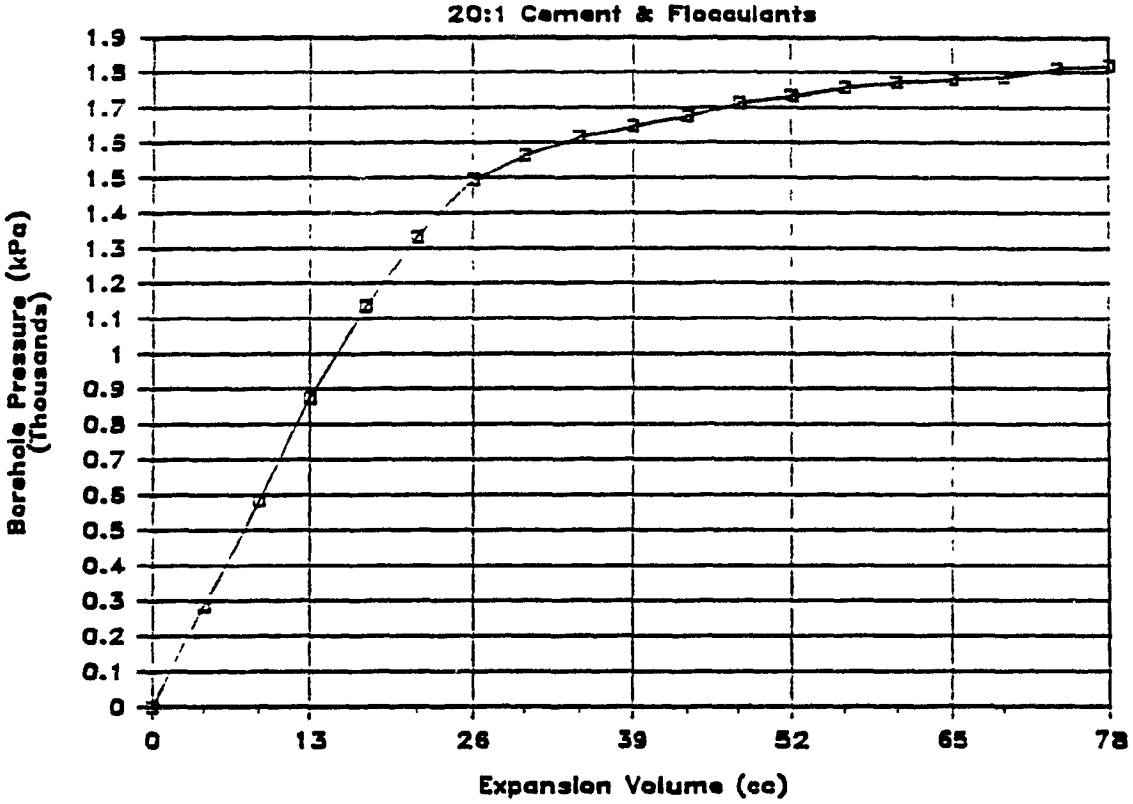

Lac Matagami - Corrected Data

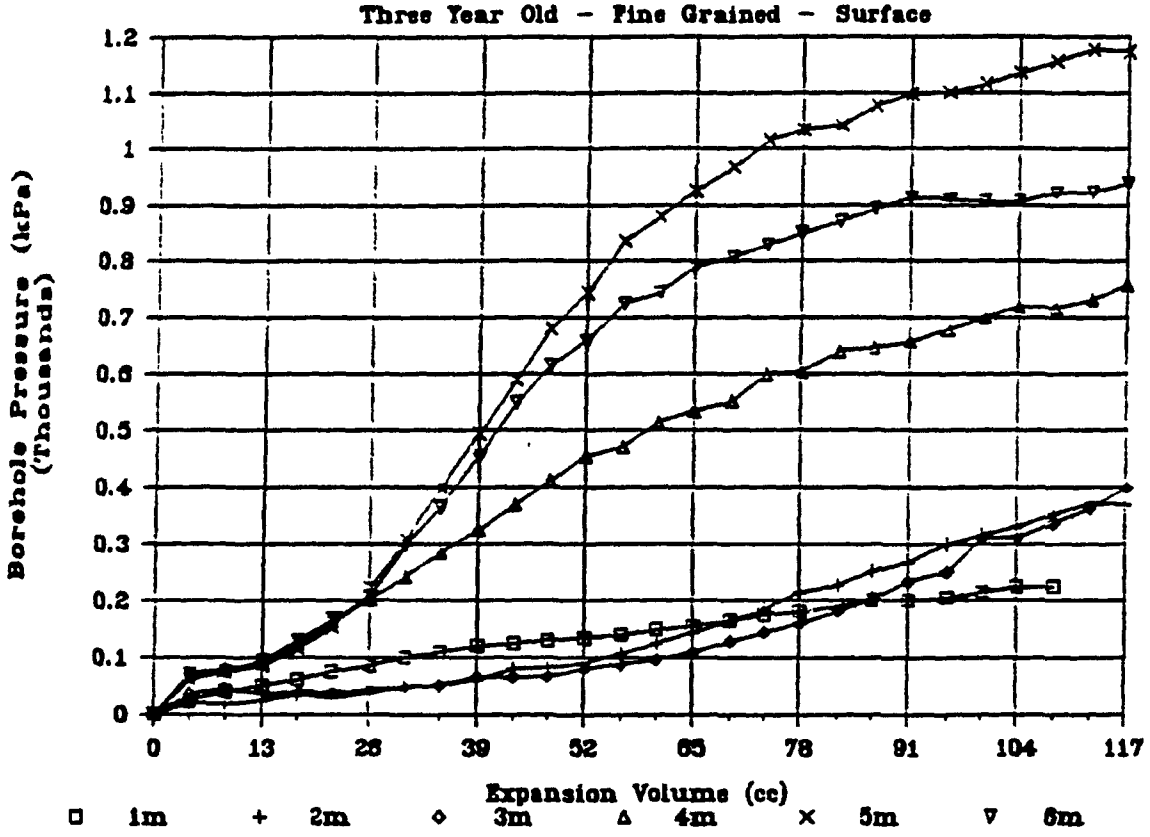

Lac Matagami - Corrected Data

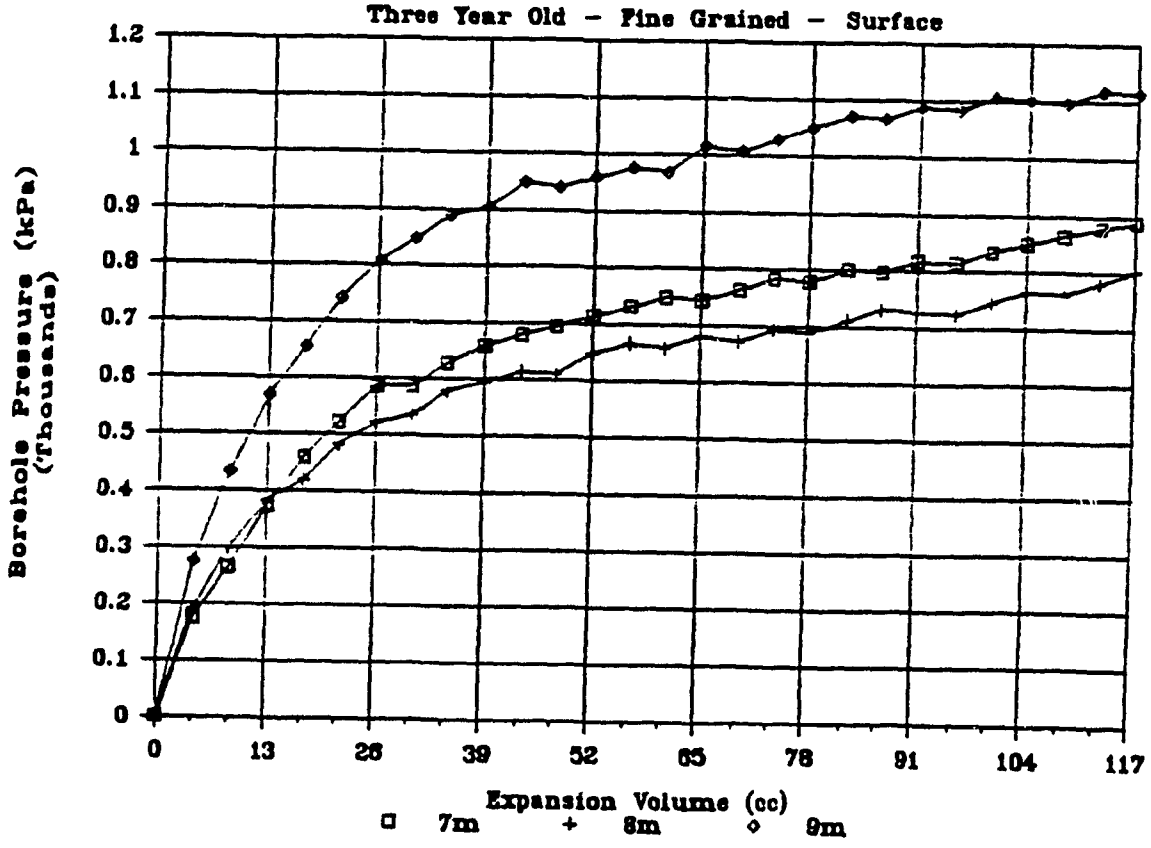

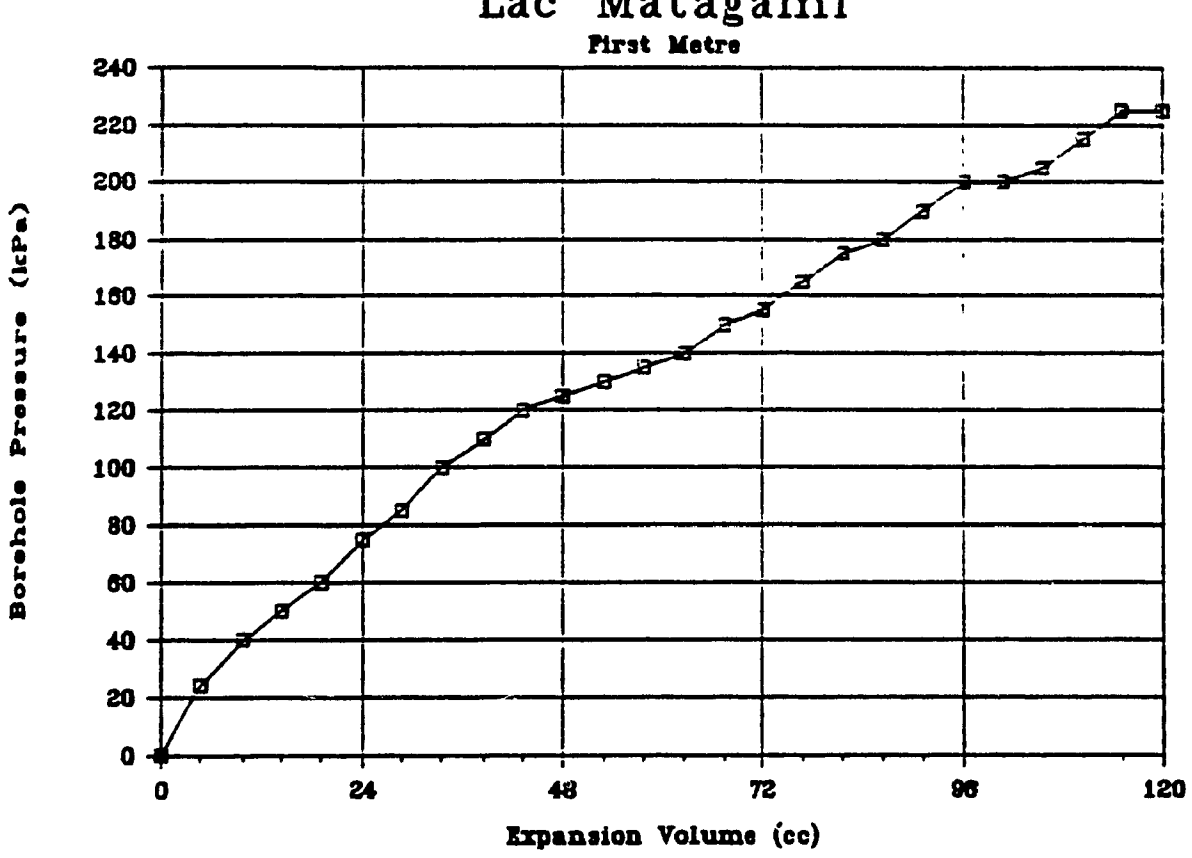
Lac Matagami
First Metre
Borehole Pressure (kPa)
240
220
200
180
160
140
120
100
80
60
40
20
0
0
24
48
72
96
120
Expansion Volume (cc)

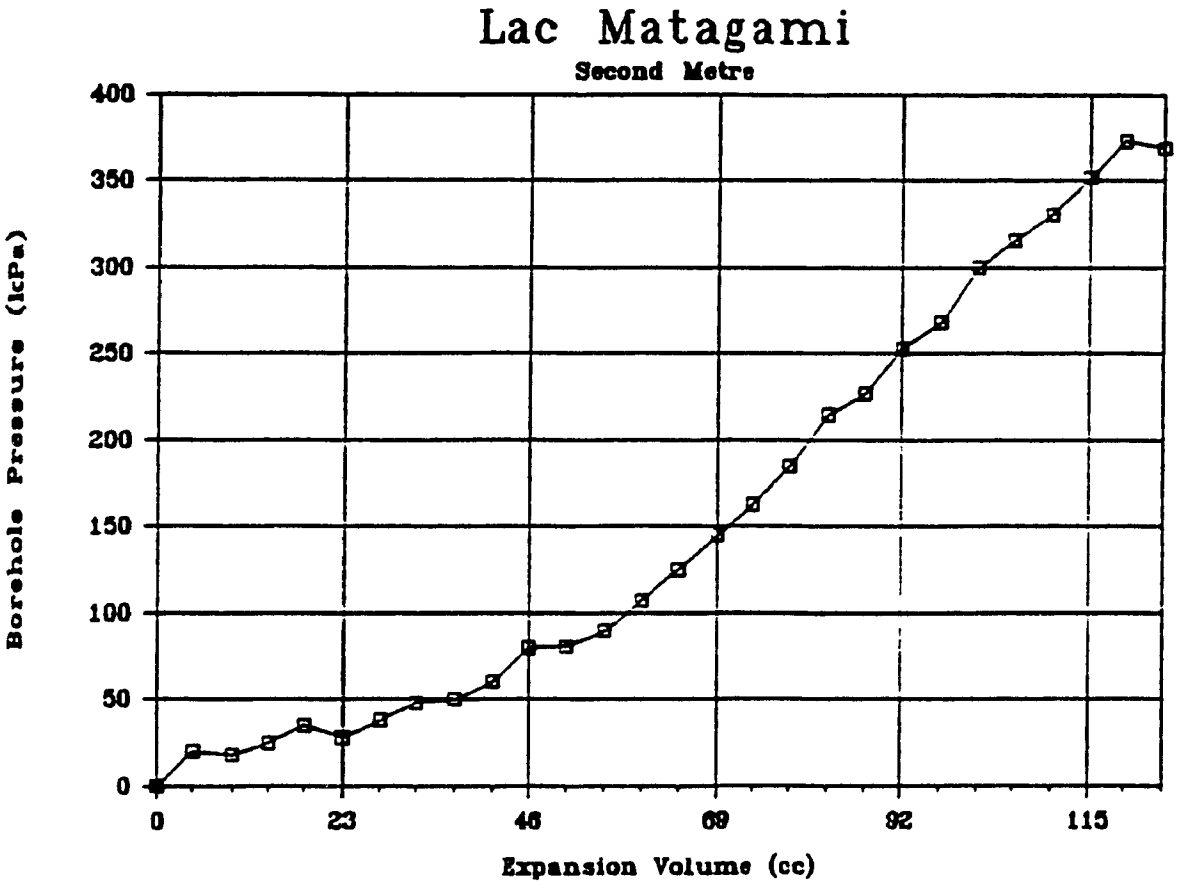
Lac Matagami
Second Metre
Borehole Pressure (kPa)
400
350
300
250
200
150
100
50
0
0
23
46
69
92
115
Expansion Volume (cc)

Lac Matagami

Third Metre

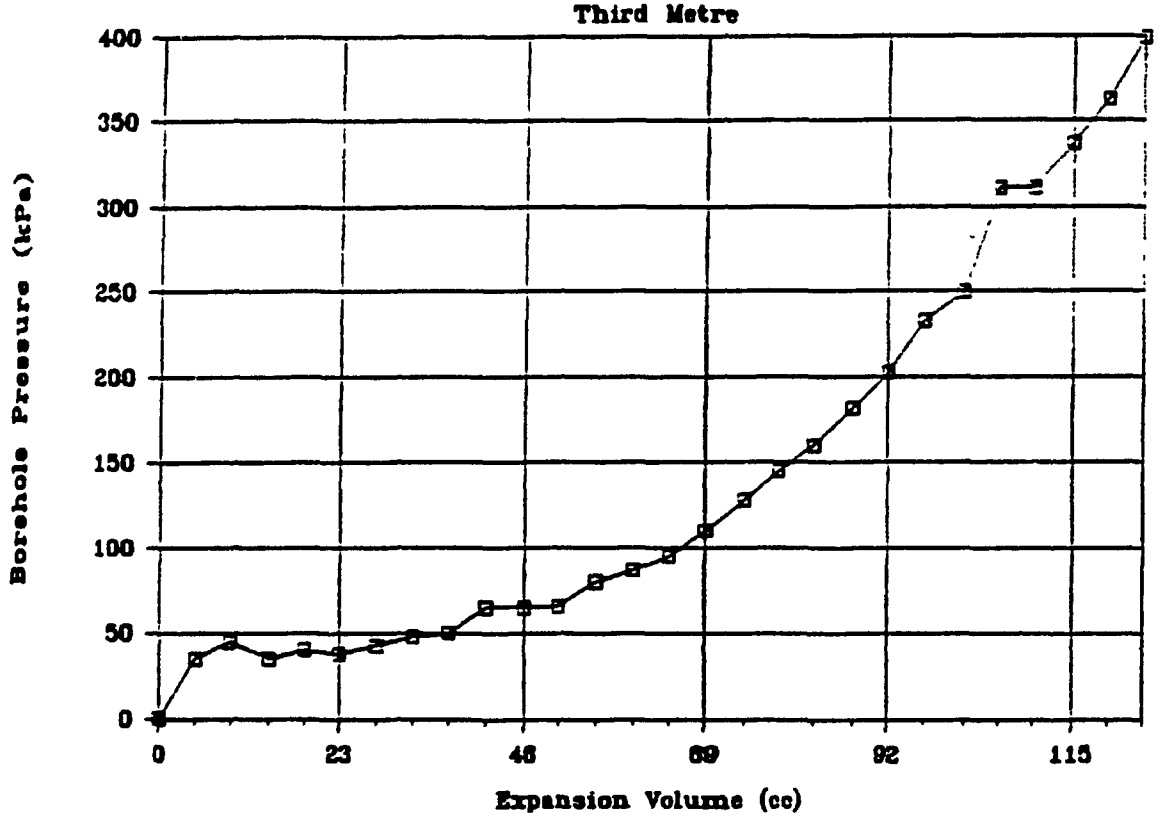

Lac Matagami

Fourth Metre

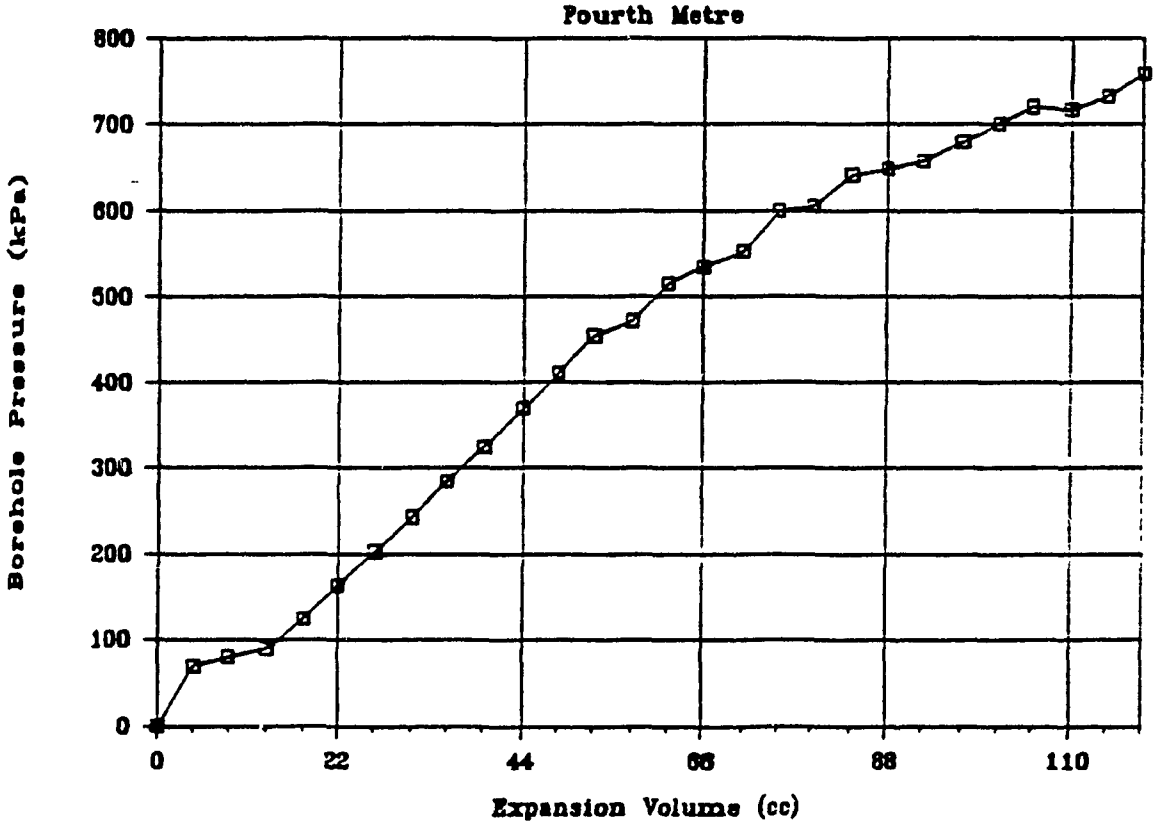

Lac Matagami

Fifth Metre

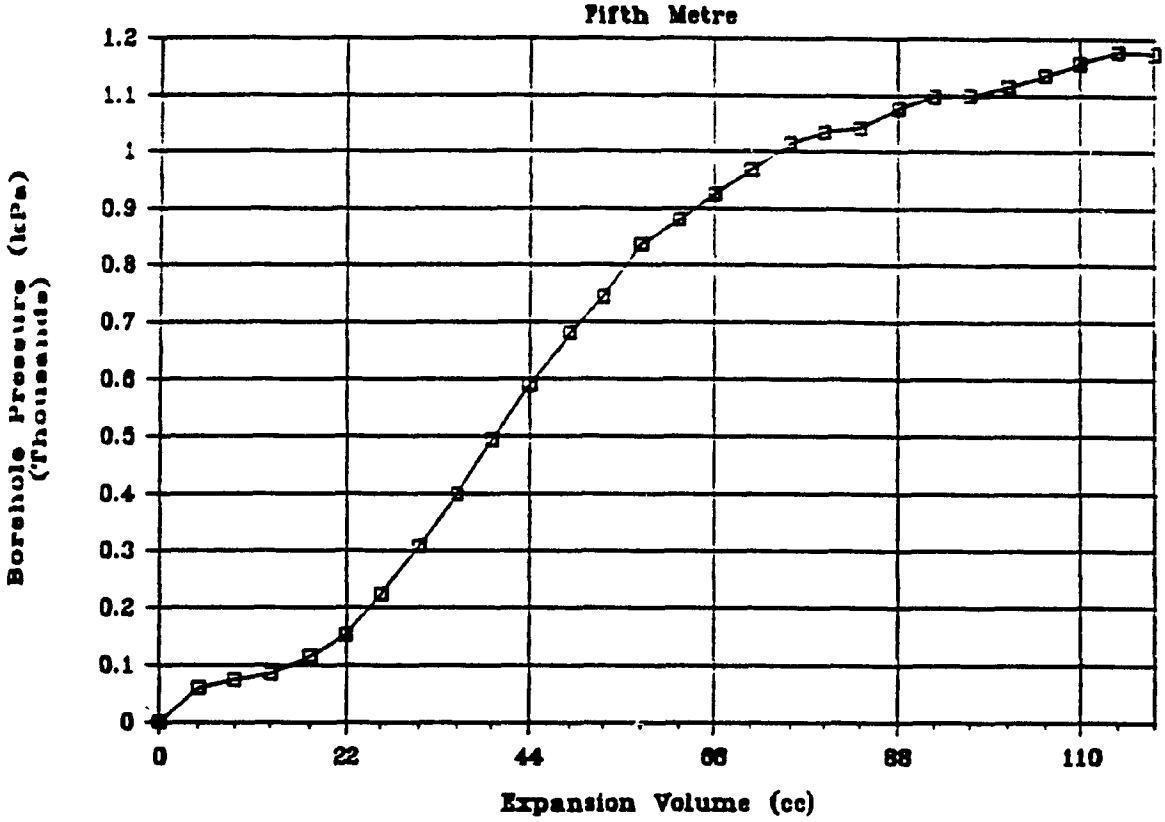

Lac Matagami

Sixth Metre

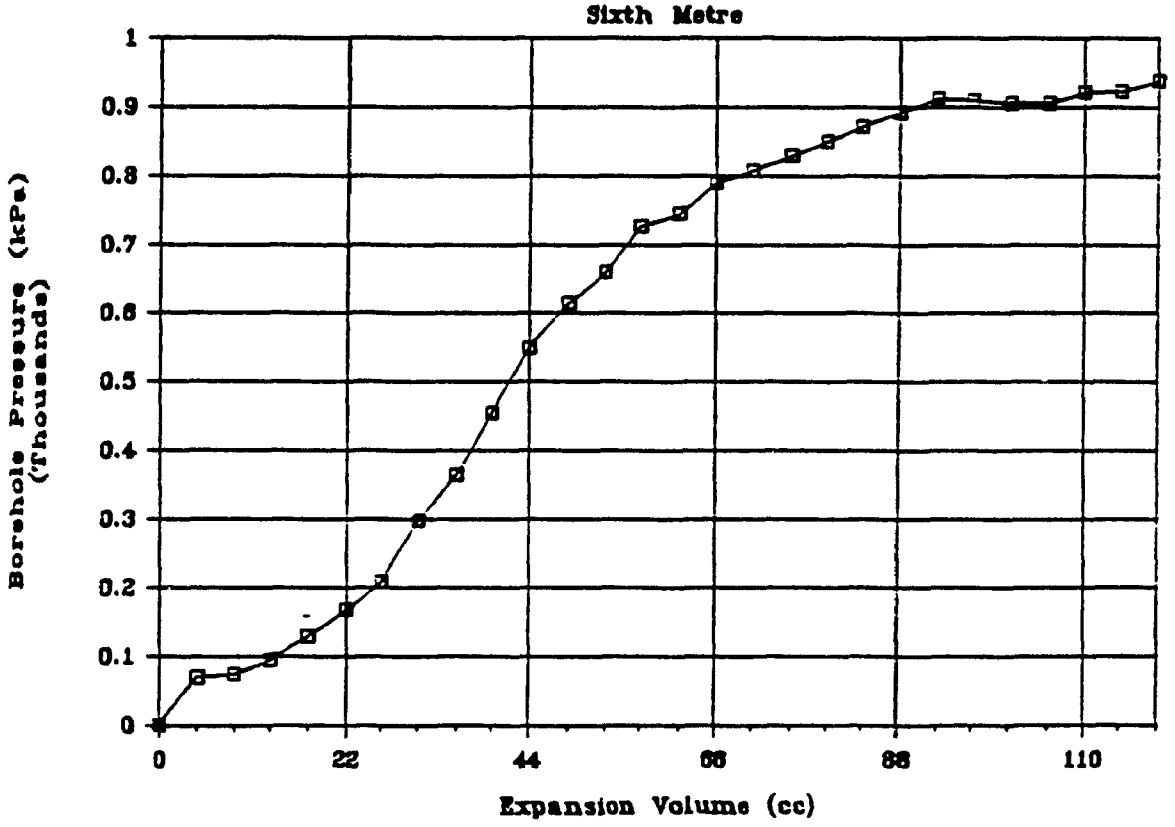

Lac Matagami

Seventh Metre

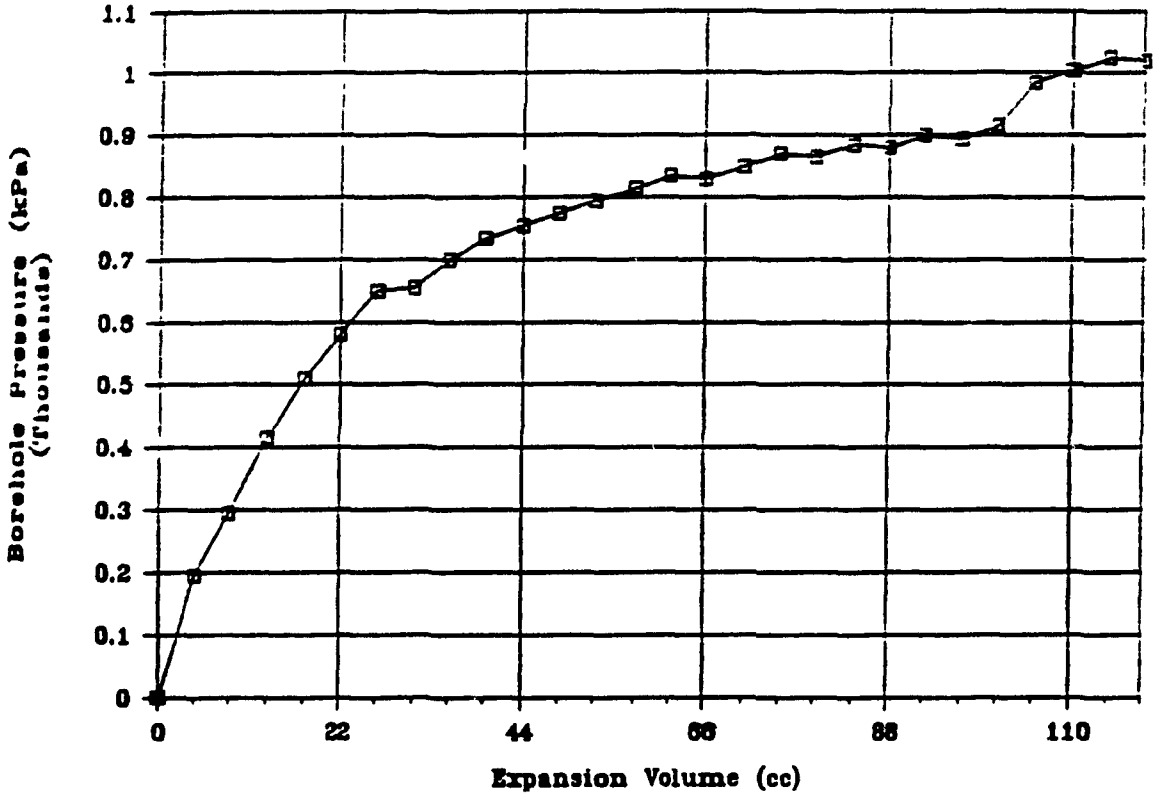

Lac Matagami

Eighth Metre

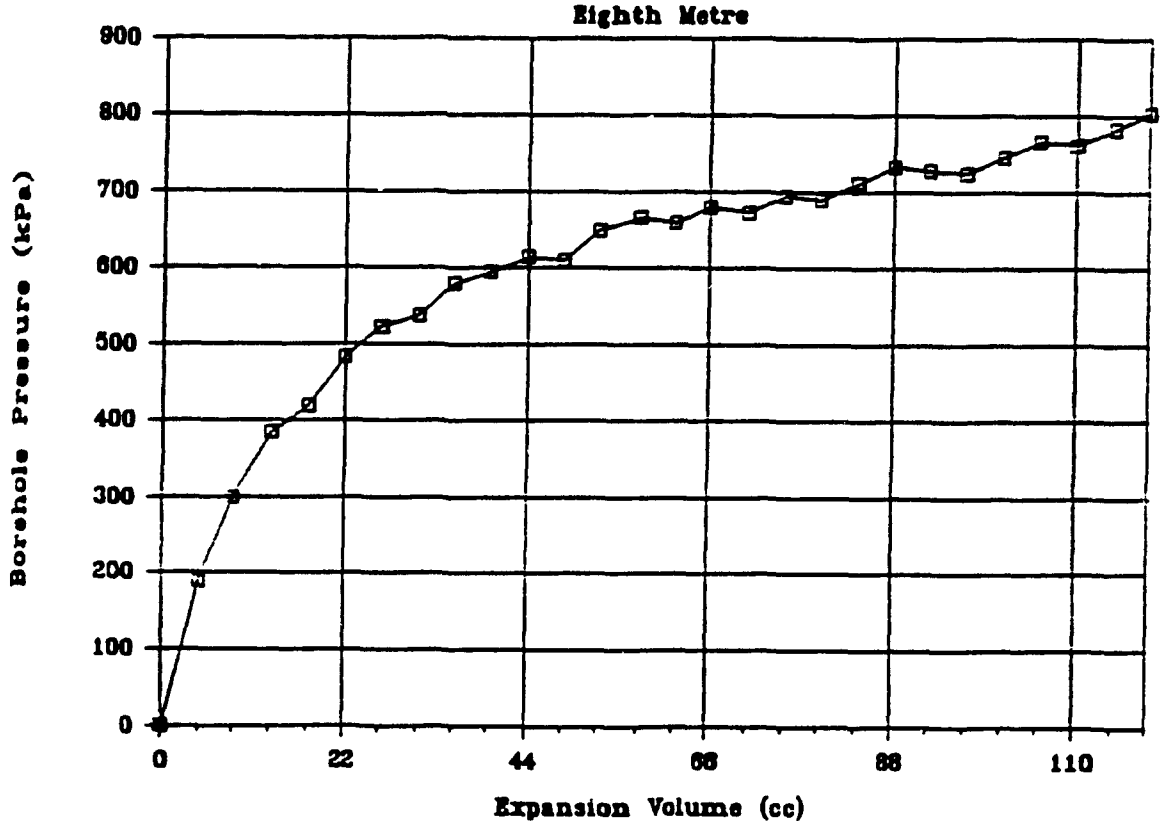

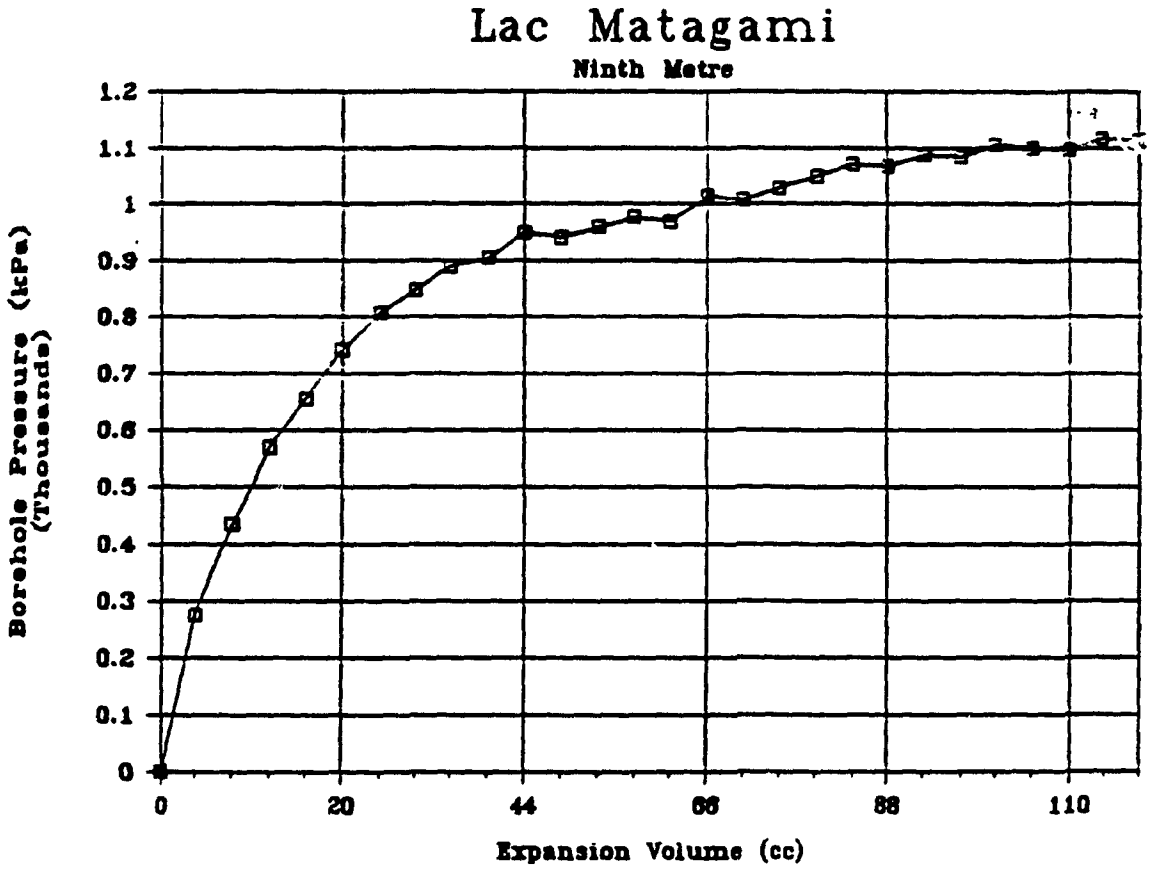
Lac Matagami
Ninth Metre
Borehole Pressure (kPa)
(Thousands)
1.2
1.1
1
0.9
0.8
0.7
0.6
0.5
0.4
0.3
0.2
0.1
0
0
20
44
66
88
110
Expansion Volume (cc)

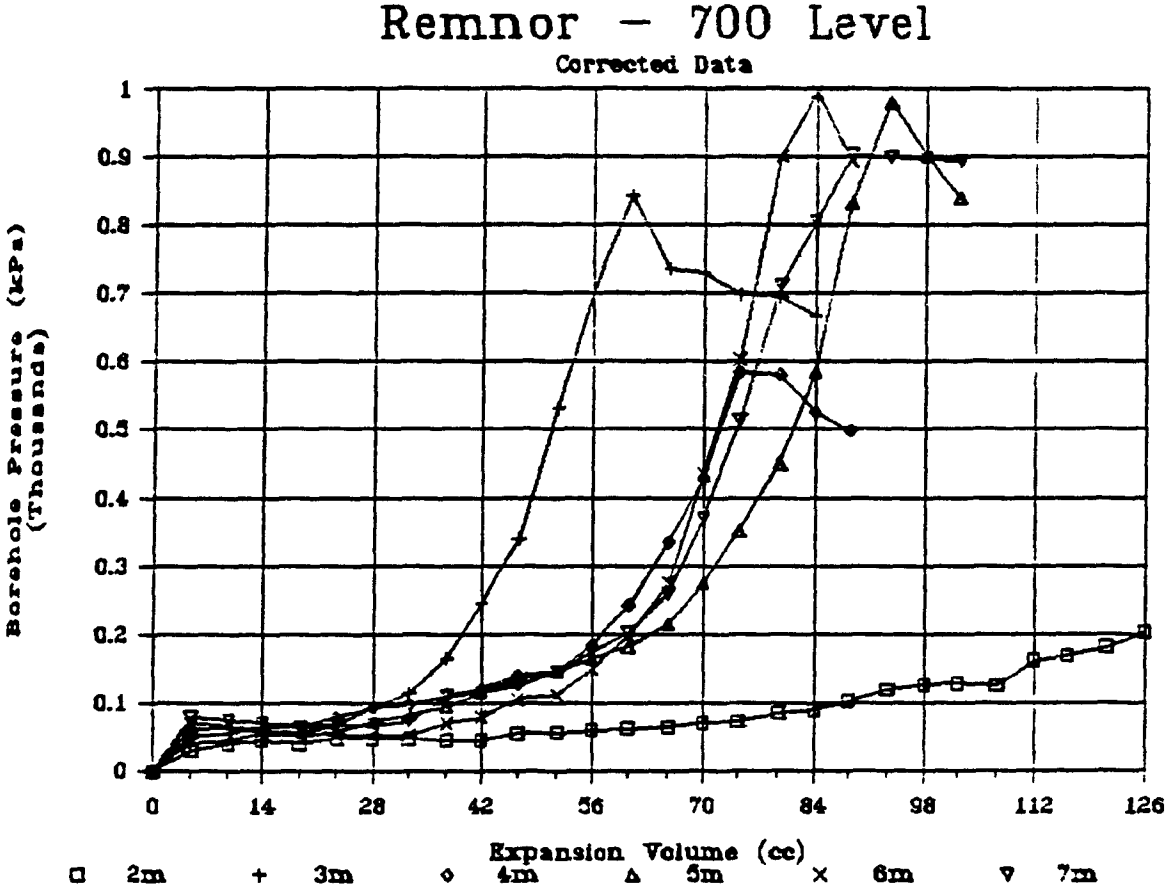
Remnor – 700 Level
Corrected Data
Borehole Pressure (kPa)
(Thousands)
1
0.9
0.8
0.7
0.6
0.5
0.4
0.3
0.2
0.1
0
0
14
28
42
56
70
84
98
112
126
Expansion Volume (cc)
2m
3m
4m
5m
6m
7m

Remnor - 700 Level

Corrected Data Second Metre

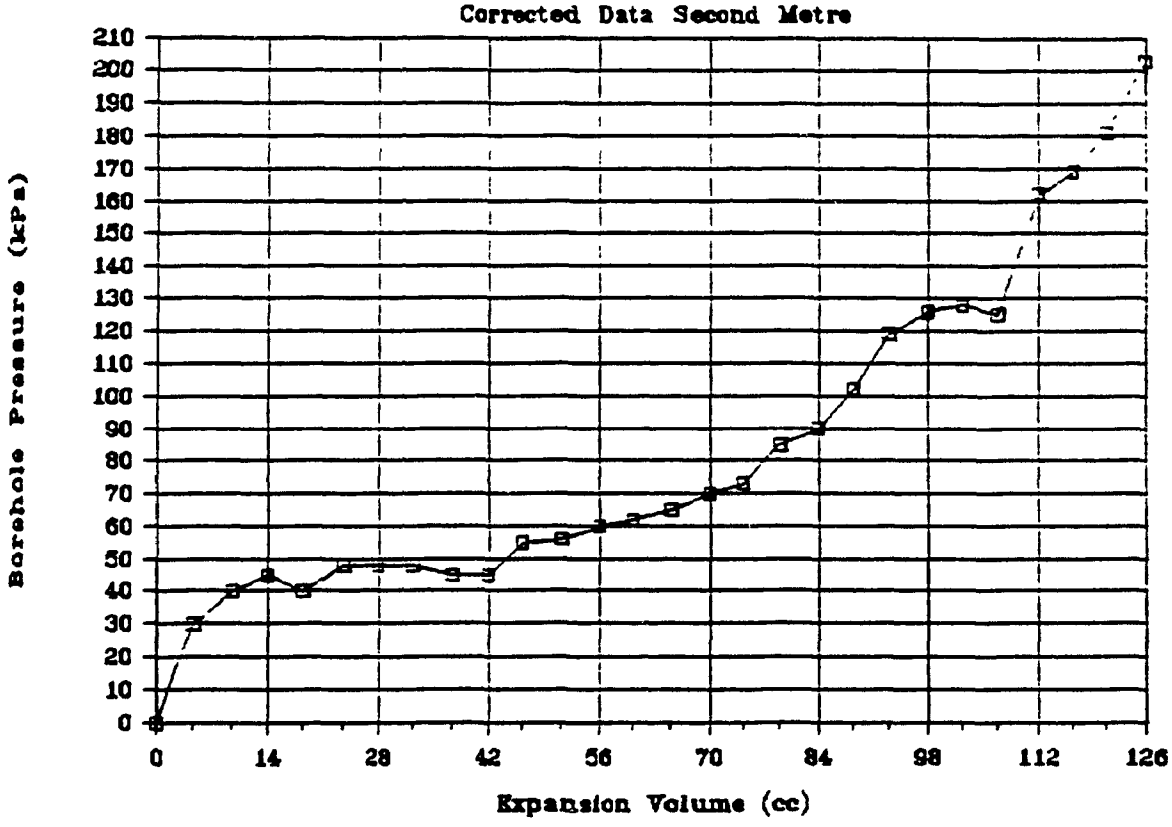

Remnor - 700 Level

Corrected Data Third Metre

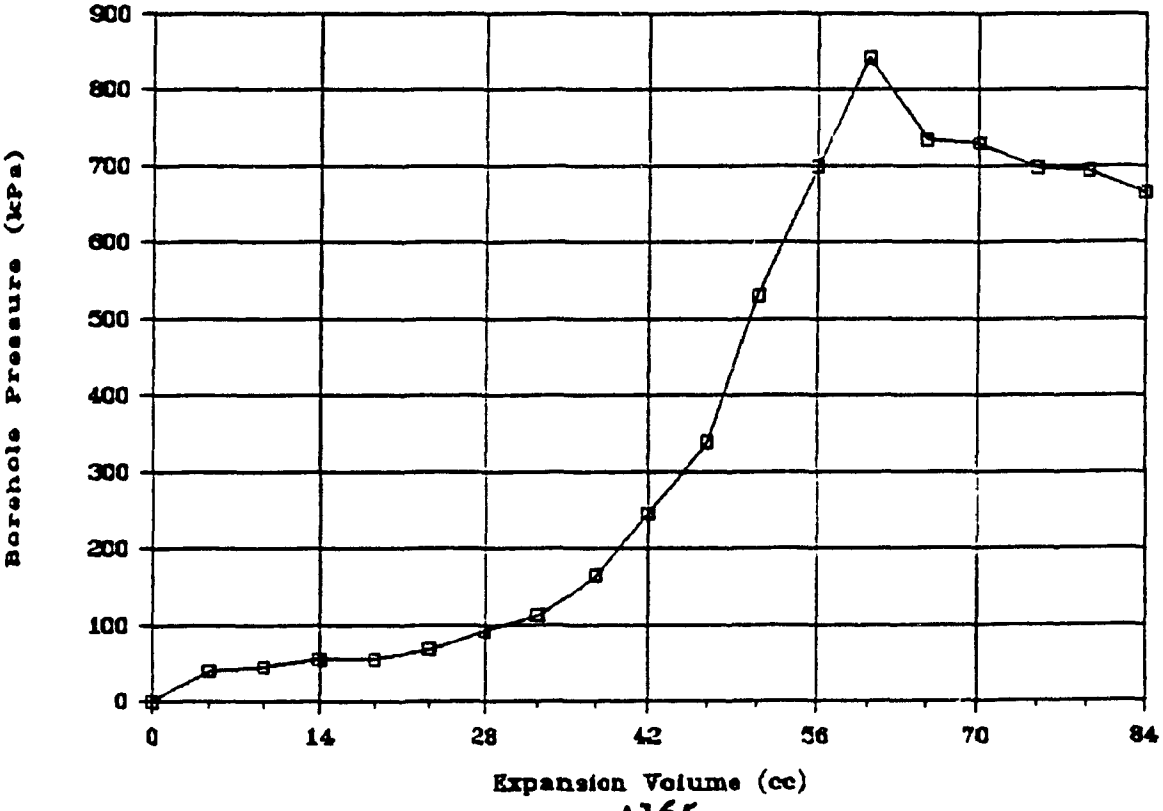

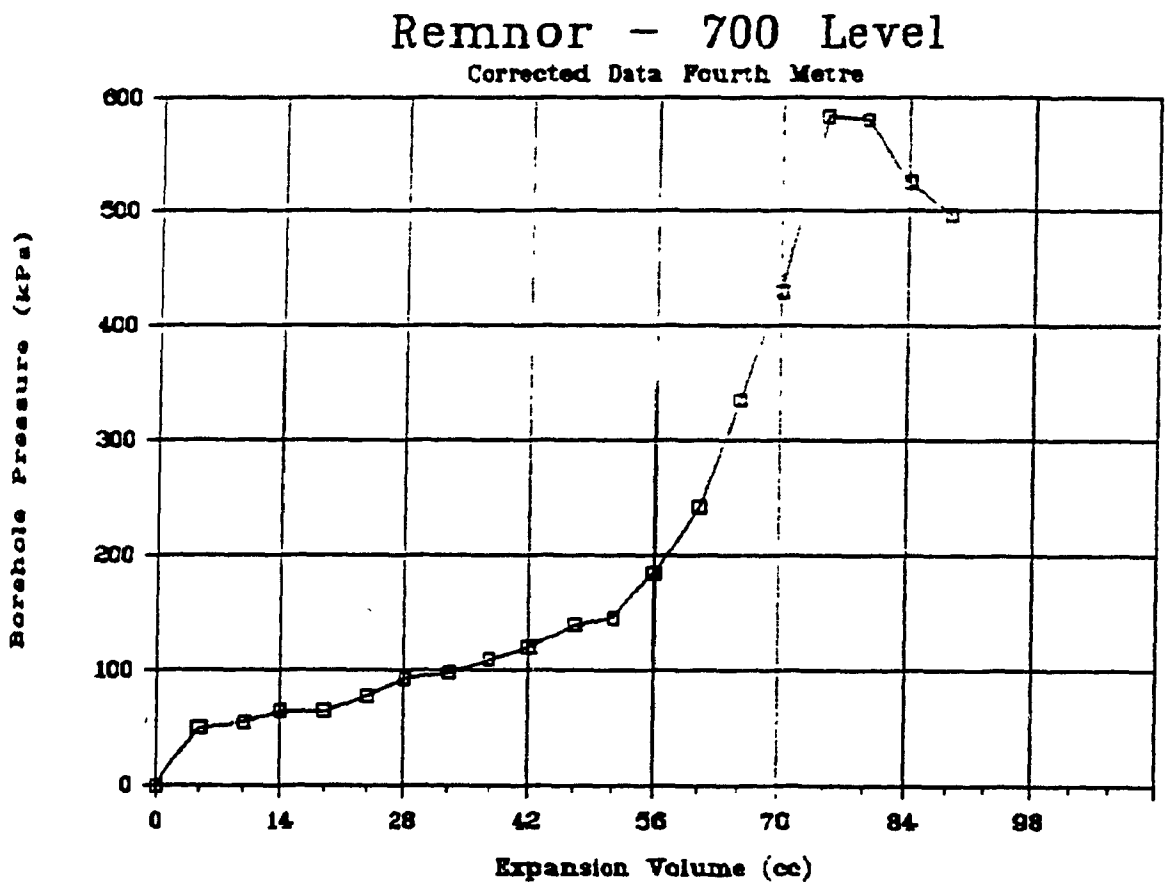
Remnor - 700 Level
Corrected Data Fourth Metre
Borehole Pressure (kPa)
600
500
400
300
200
100
0
0
14
28
42
56
70
84
98
Expansion Volume (cc)

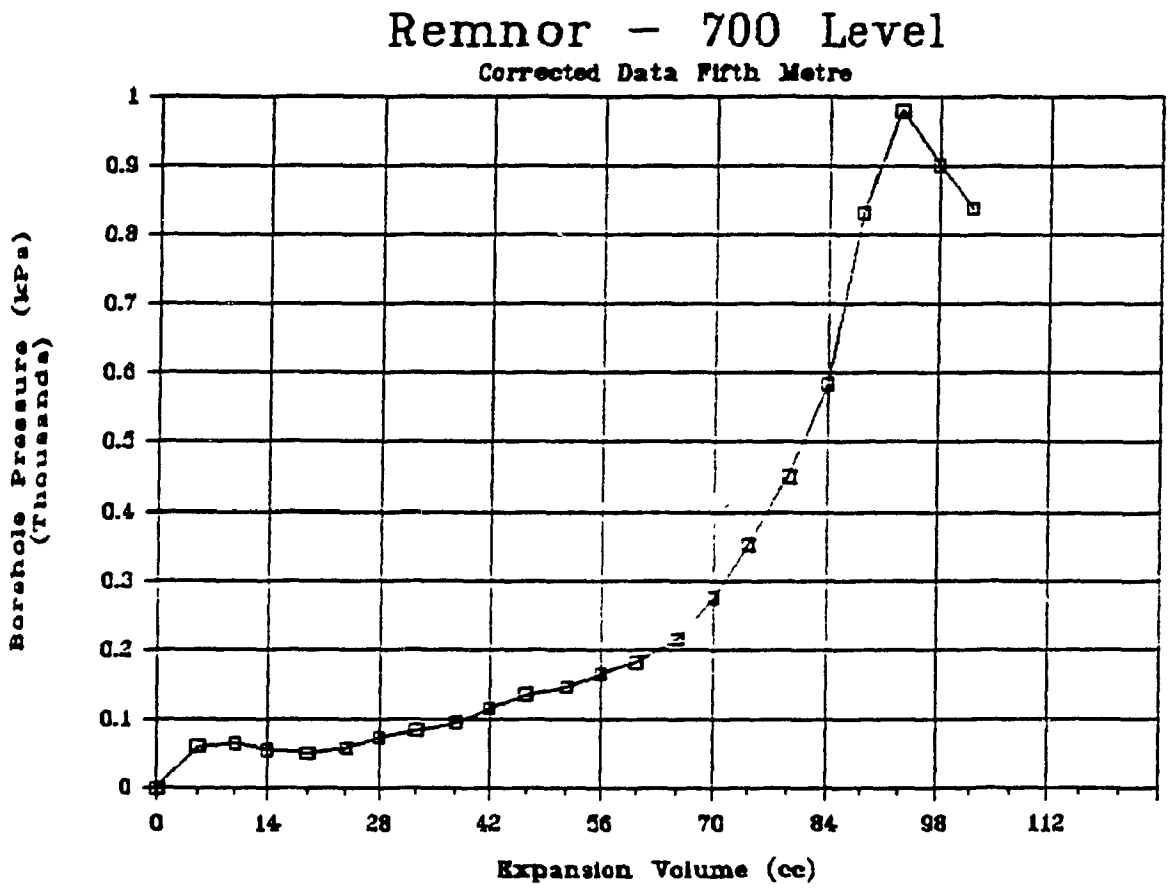
Remnor - 700 Level
Corrected Data Fifth Metre
Borehole Pressure (kPa) (Thousands)
1
0.9
0.8
0.7
0.6
0.5
0.4
0.3
0.2
0.1
0
0
14
28
42
56
70
84
98
112
Expansion Volume (cc)

Remnor - 700 Levels

Corrected Data Sixth Metre

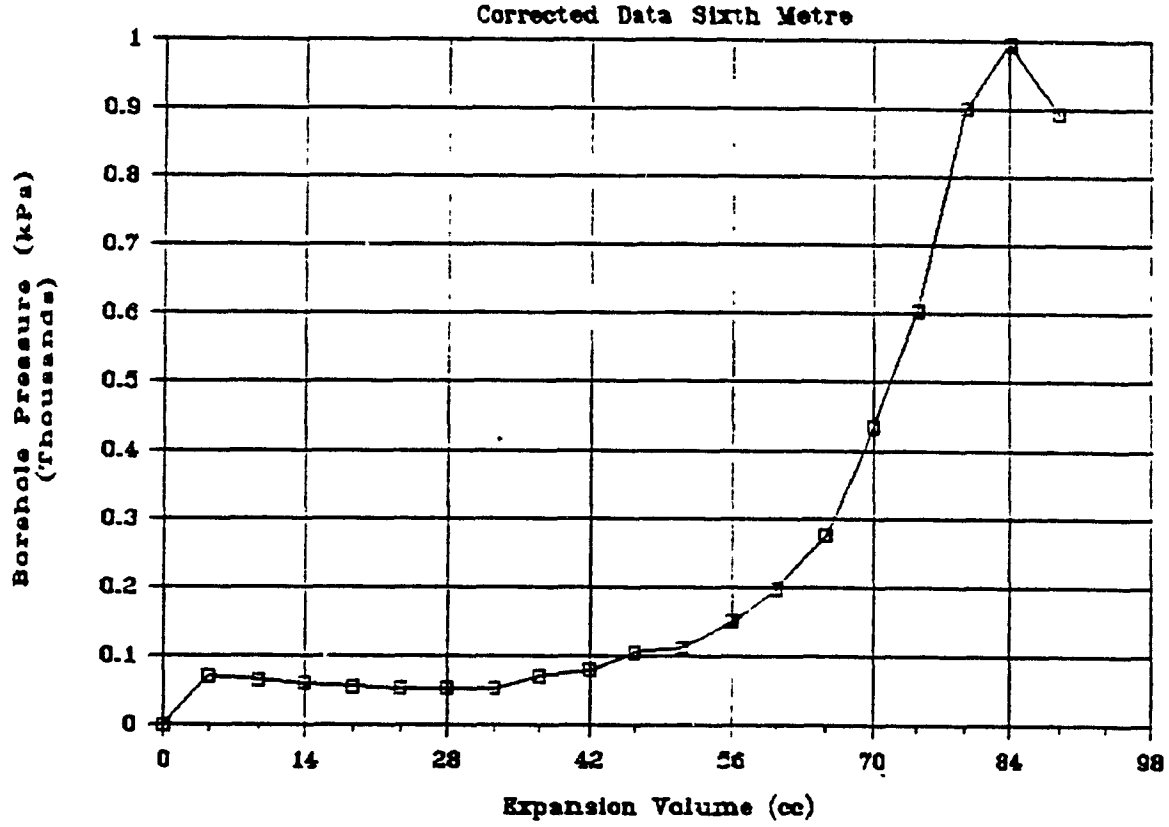

Remnor - 700 Level

Corrected Data Seventh Metre

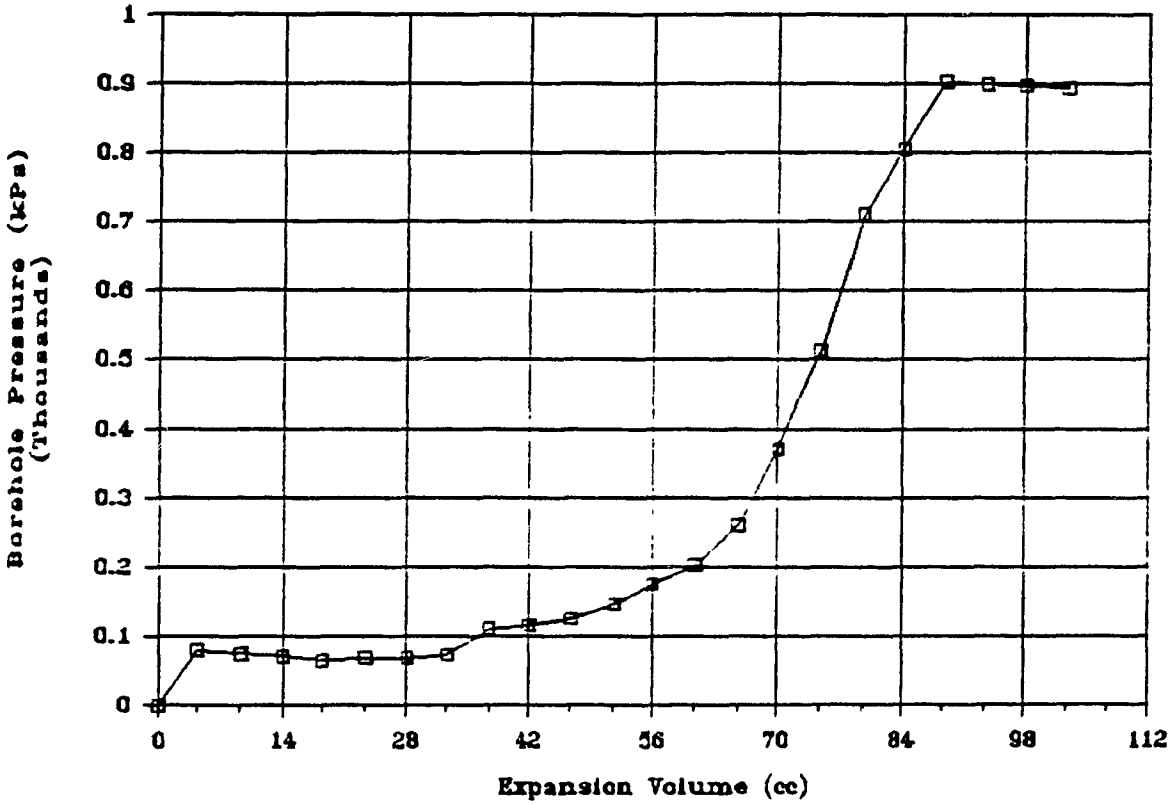

Sigma 1400 Level Breakthrough

Corrected Data

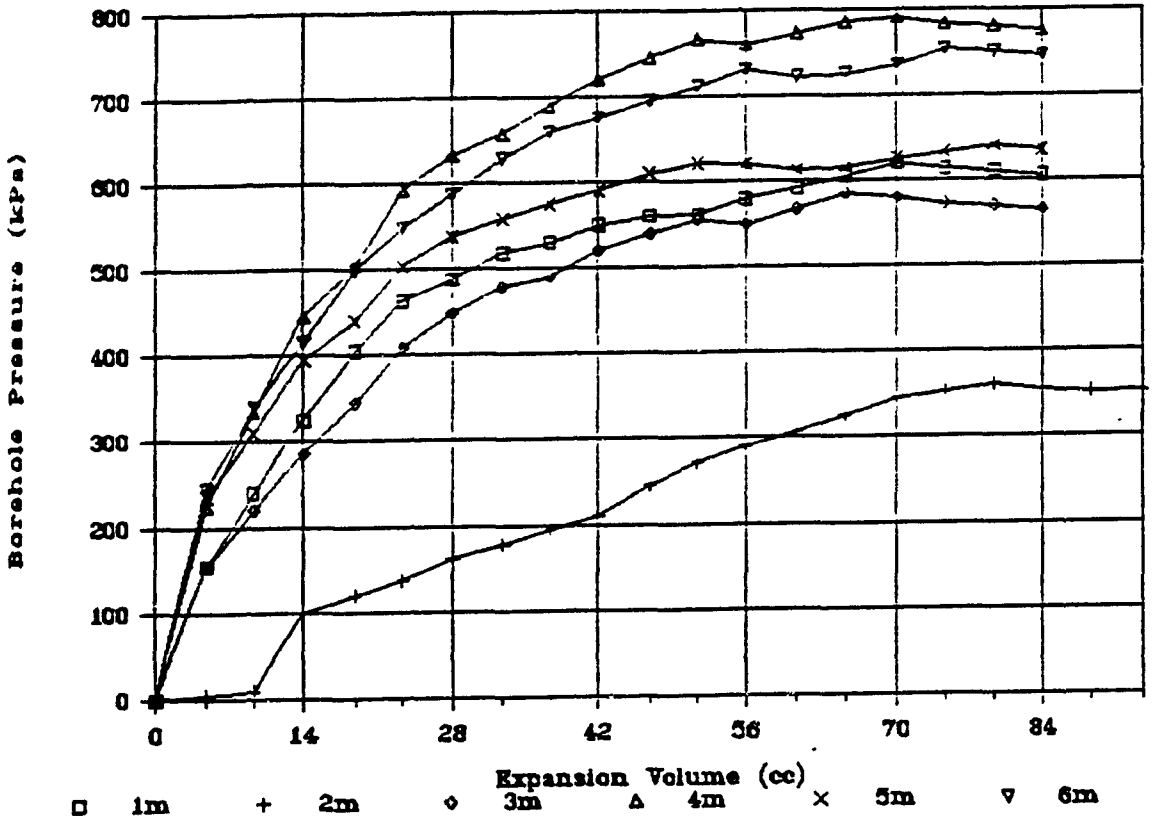

Sigma 1400 Level Breakthrough

Corrected Data

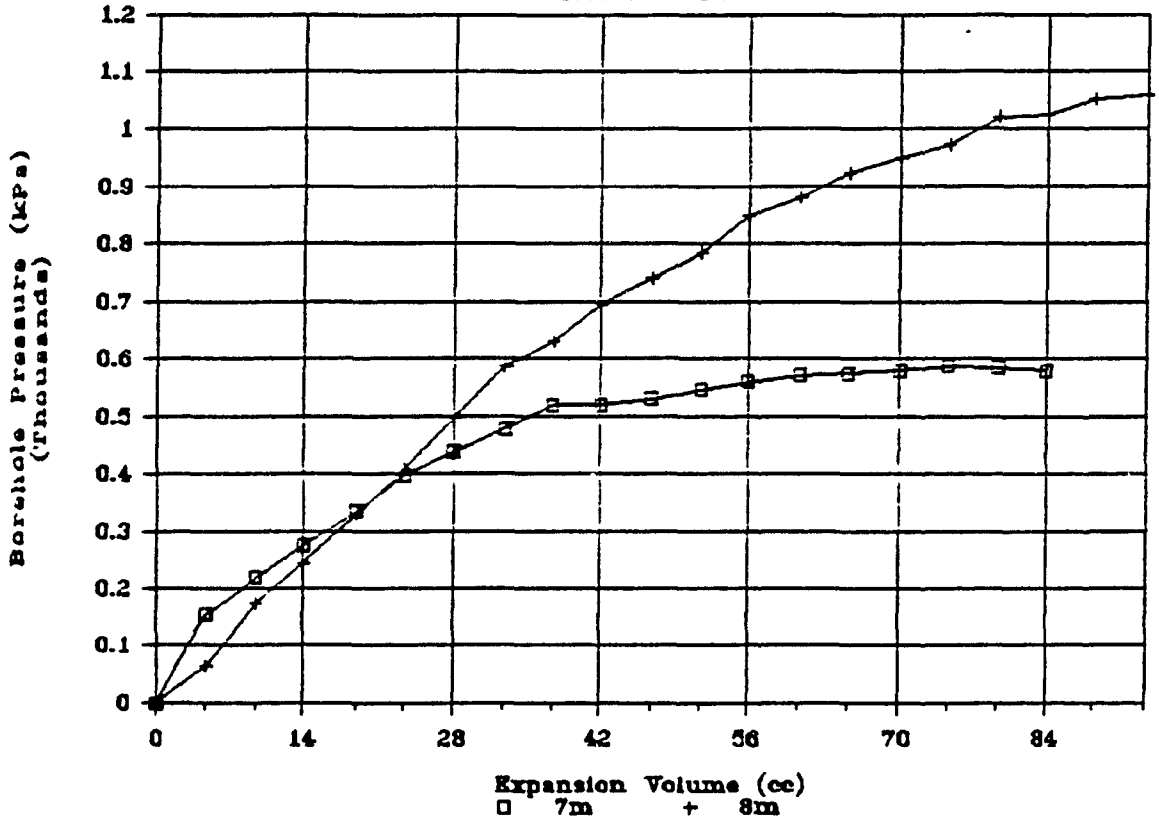

Sigma 1400 Level Breakthrough

Corrected Data First Metre

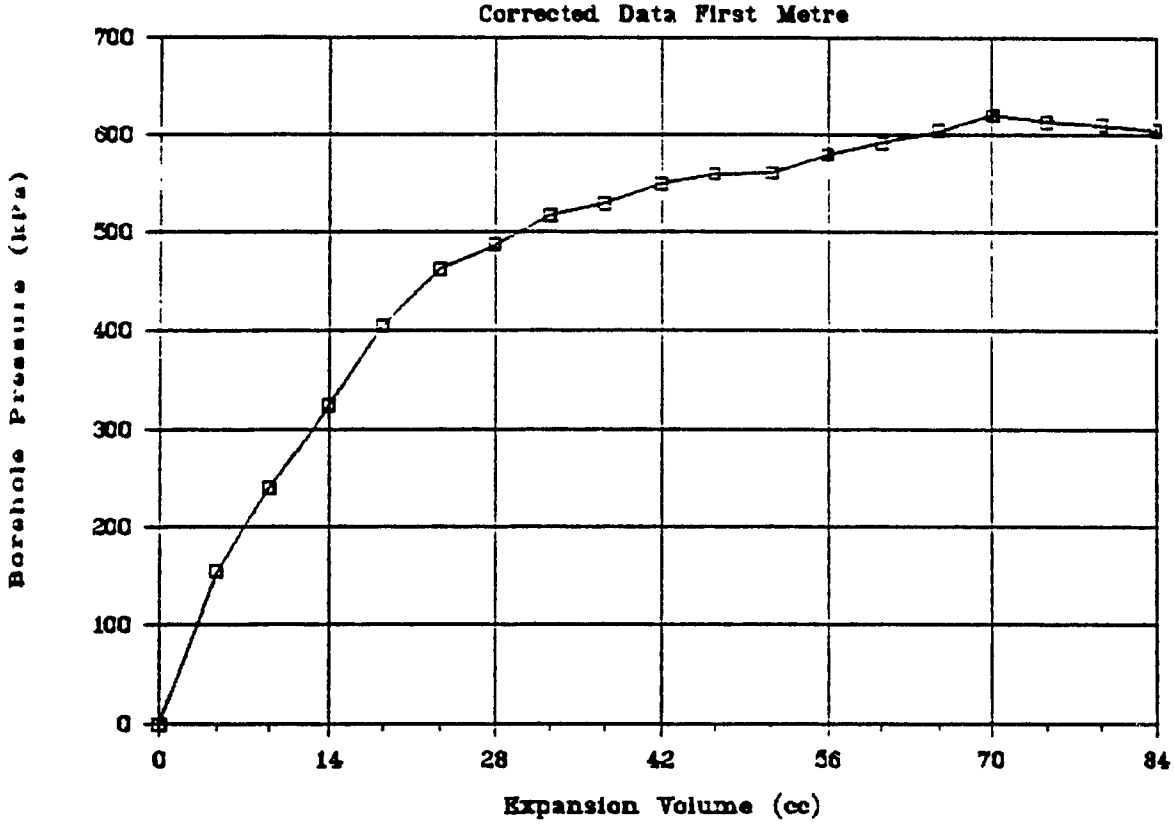

Sigma 1400 Level Breakthrough

Corrected Data Second Metre

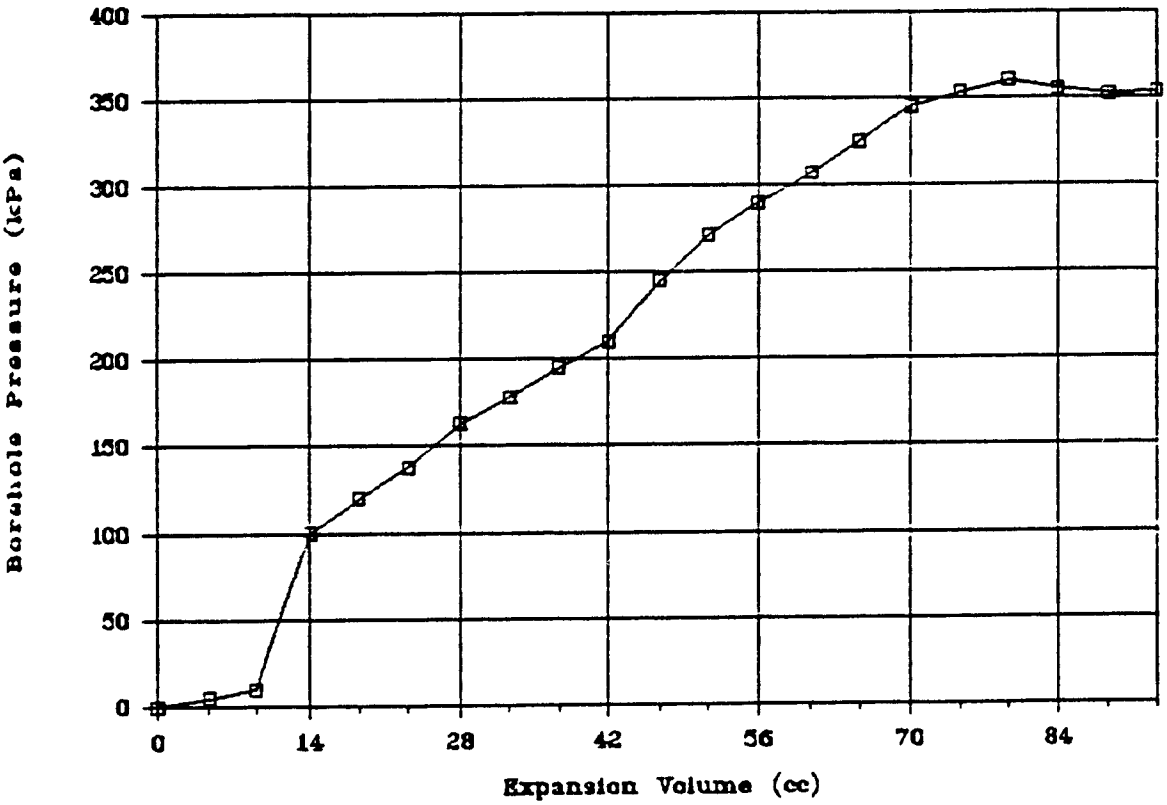

Sigma 1400 Level Breakthrough

Corrected Data Third Metre

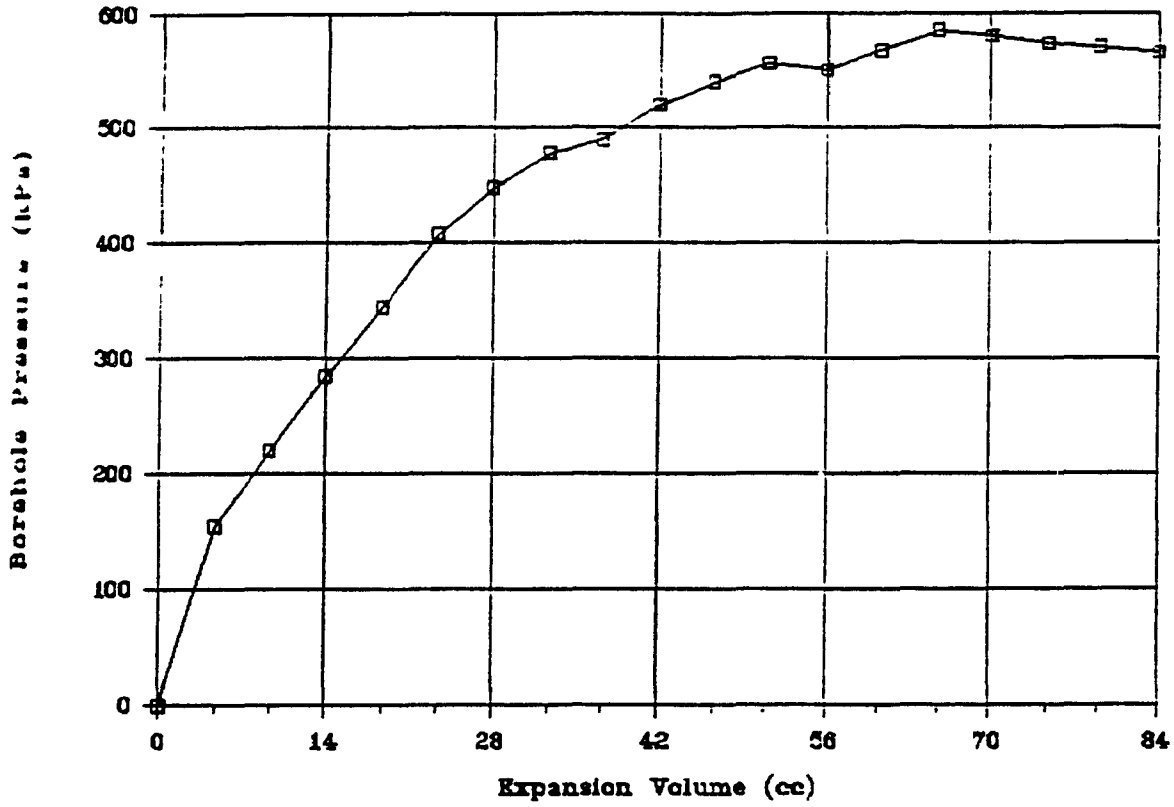

Sigma 1400 Level Breakthrough

Corrected Data Fourth Metre

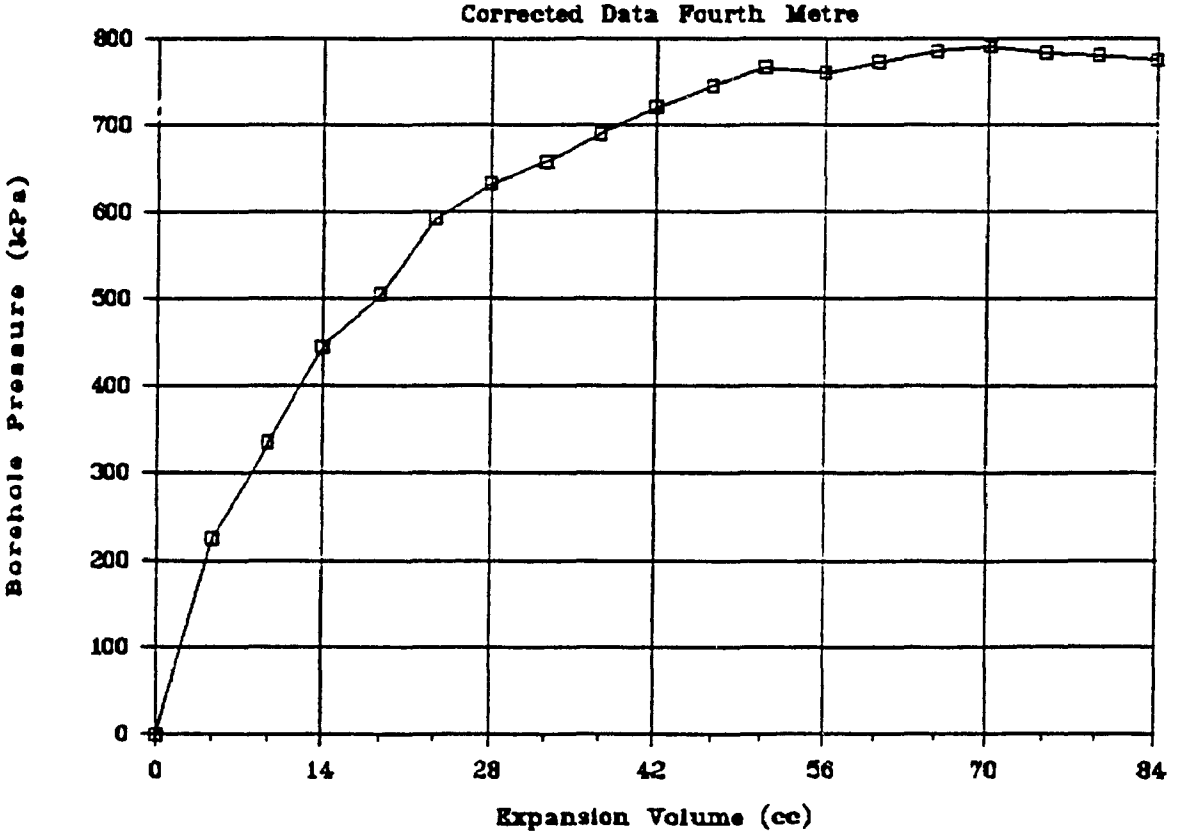

Sigma 1400 Level Breakthrough

Corrected Data Fifth Metre

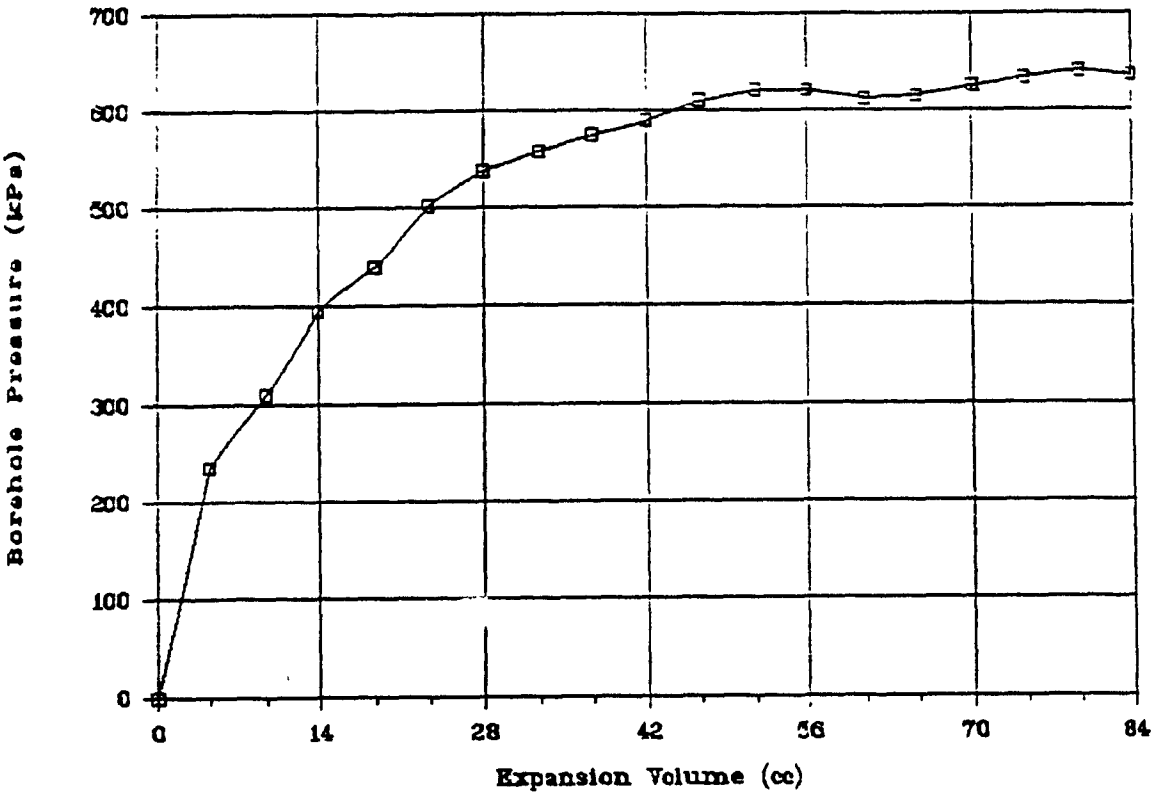

Sigma 1400 Level Breakthrough

Corrected Data Sixth Metre

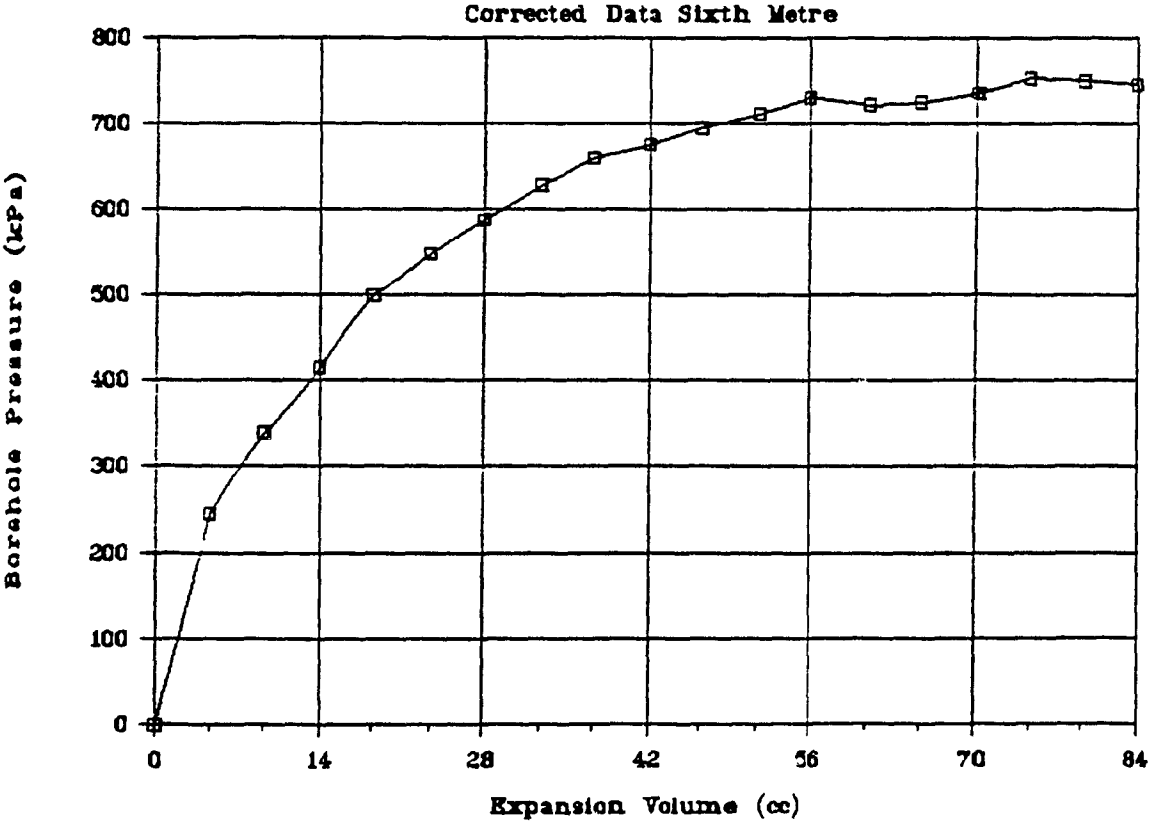

Sigma 1400 Level Breakthrough

Corrected Data Seventh Metre

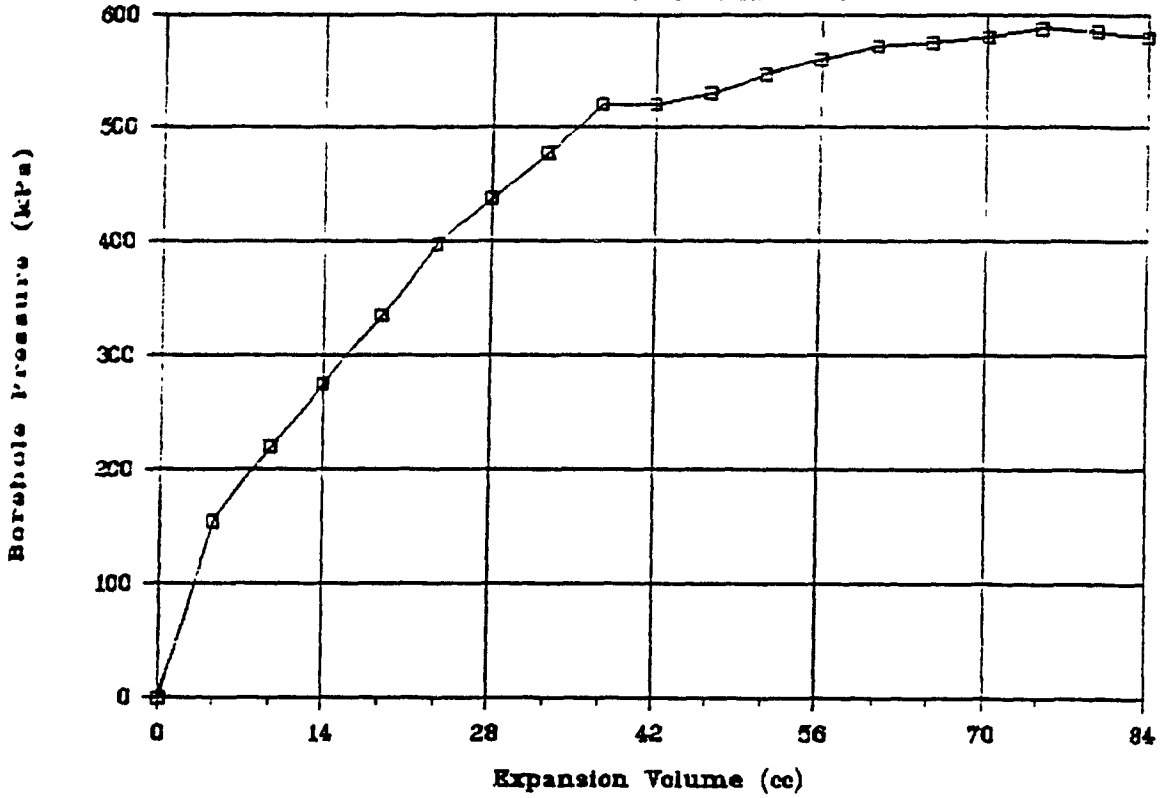

Sigma 1400 Level Breakthrough

Corrected Data Eighth Metre

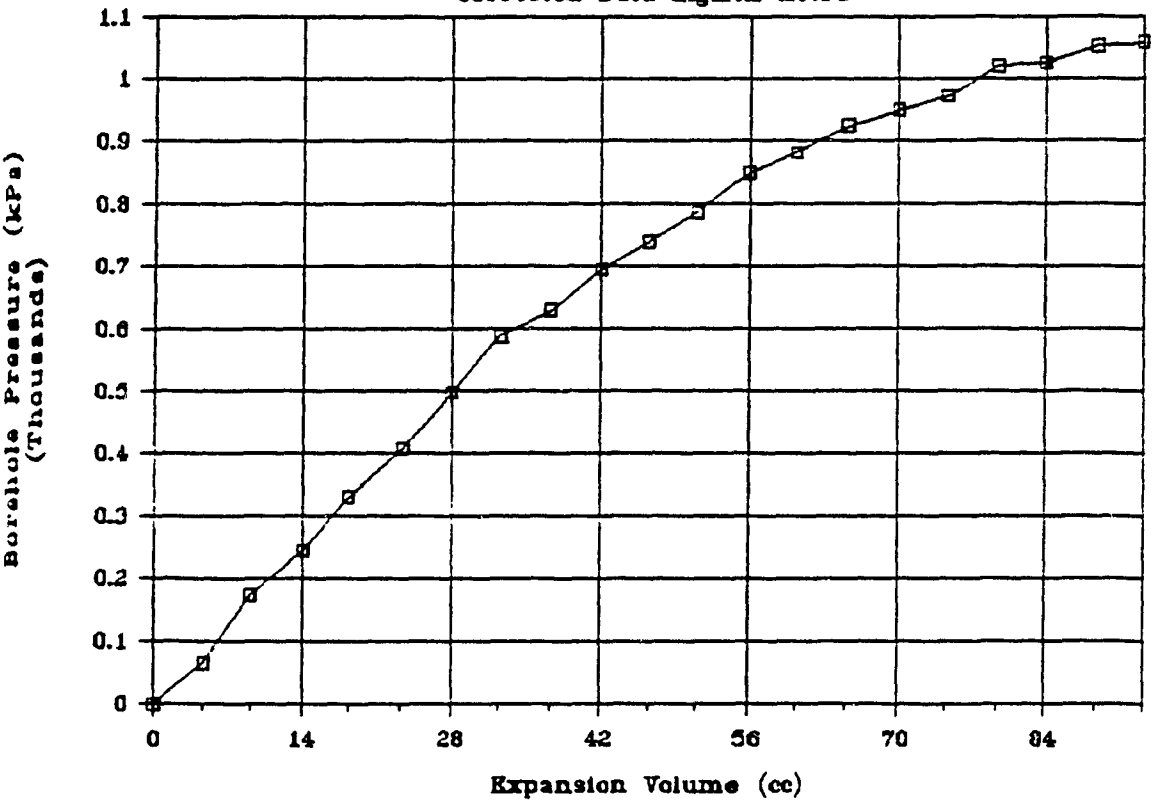

COMPARISON OF

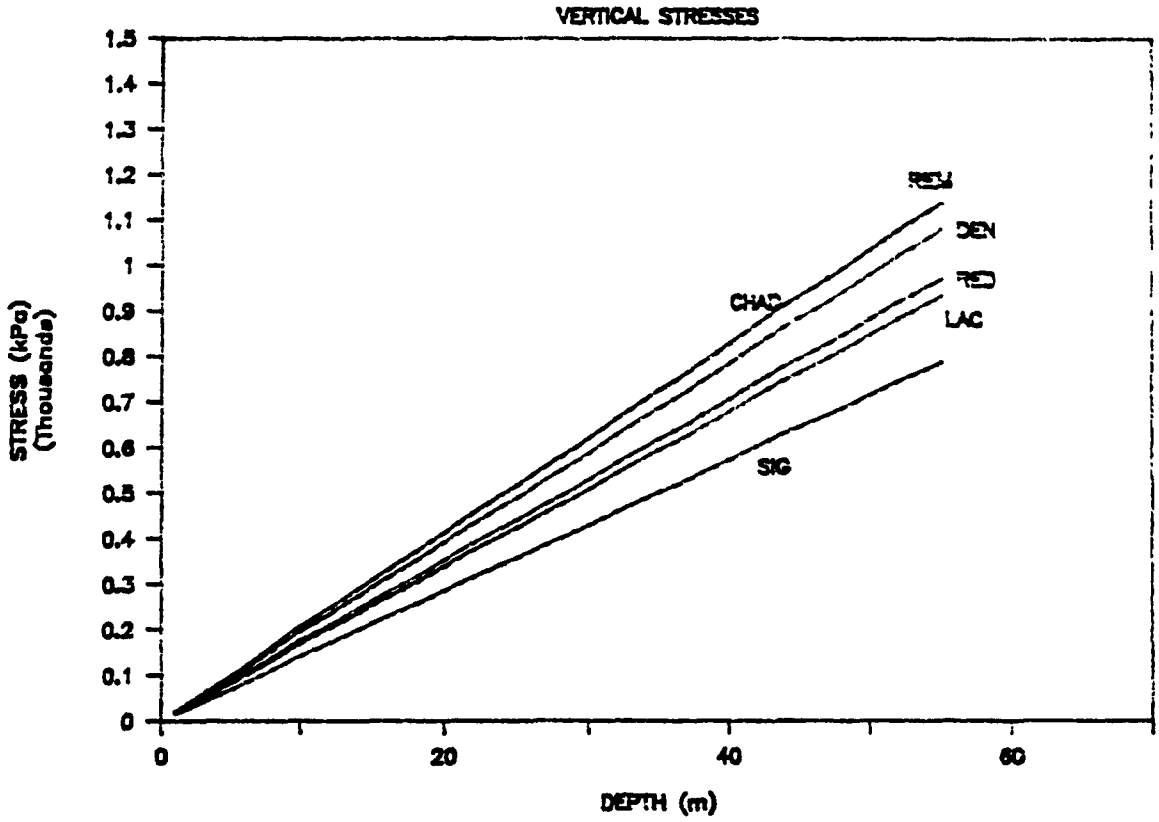

COMPARISON OF

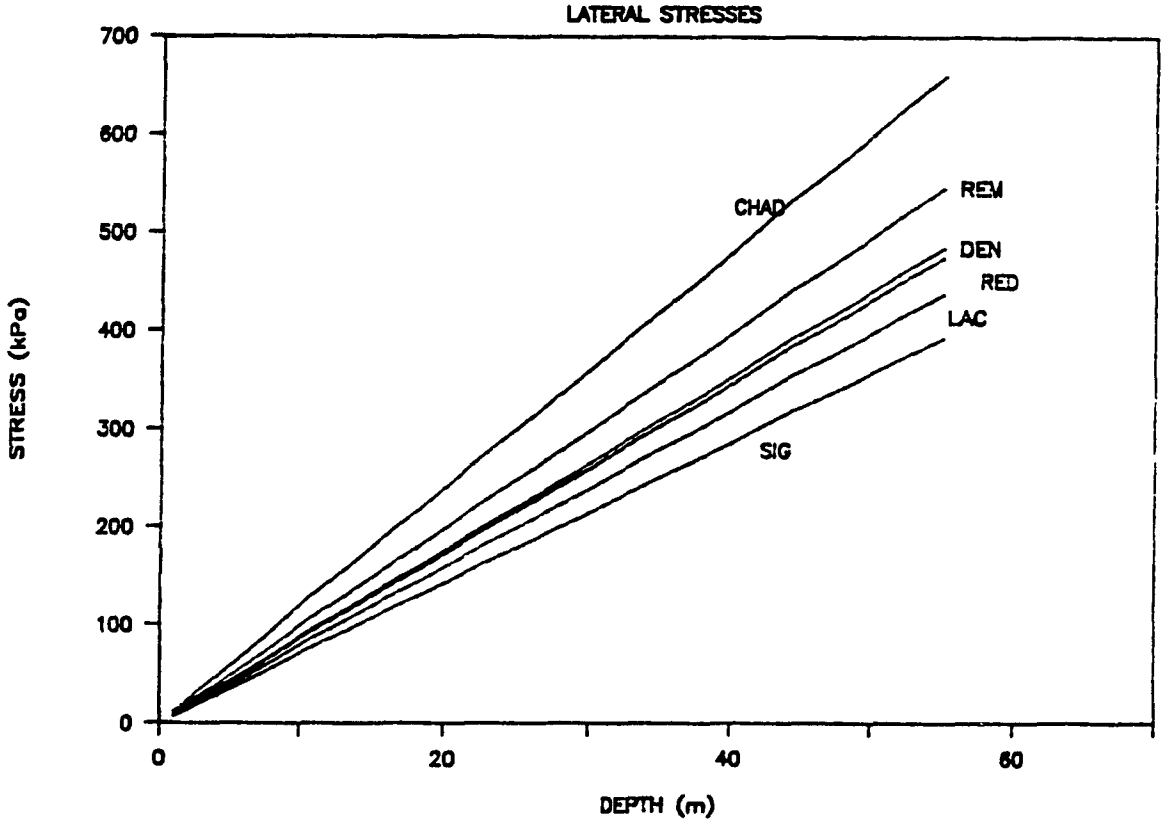

CHADBOURNE

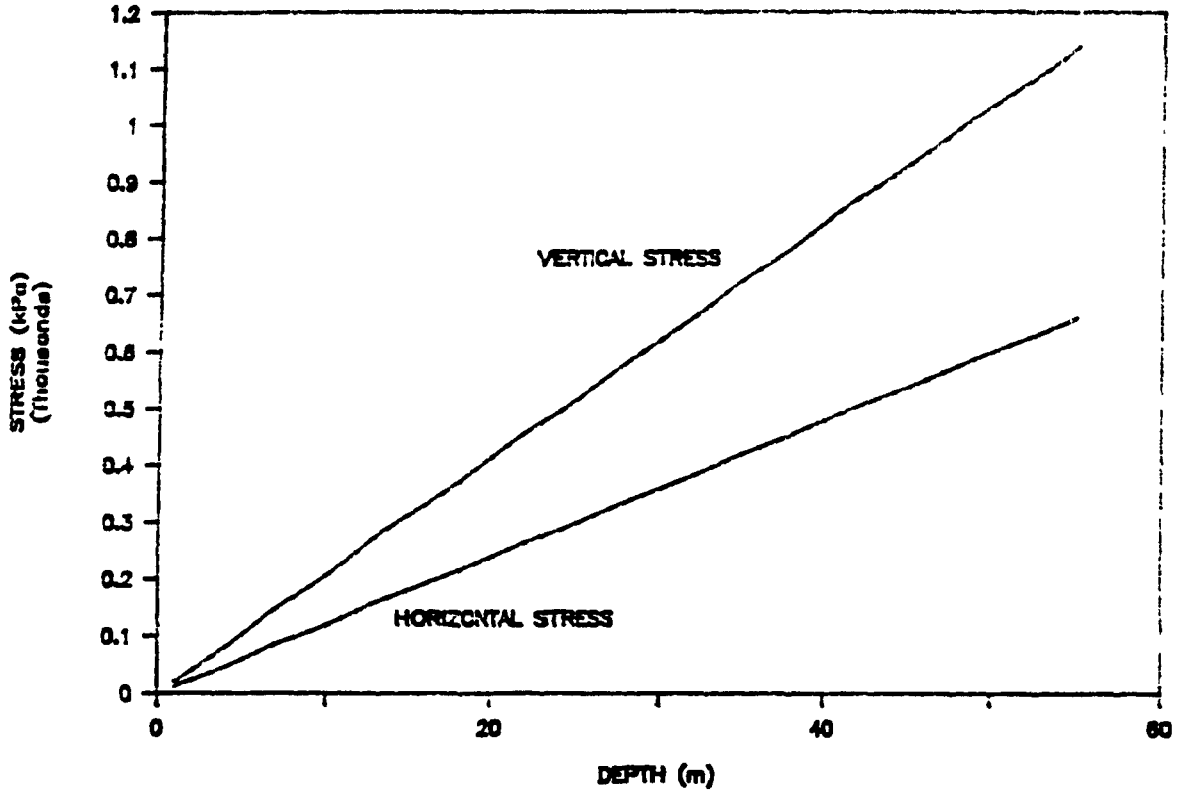

DENISON

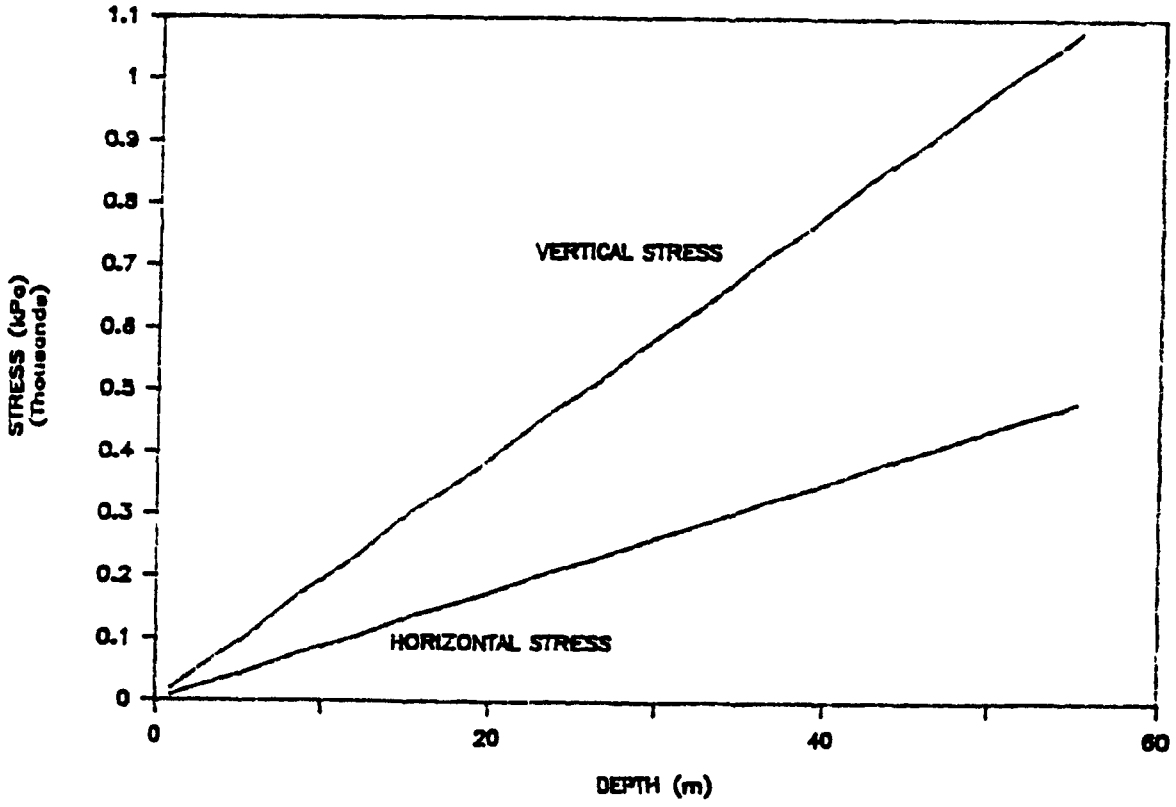

KIENA

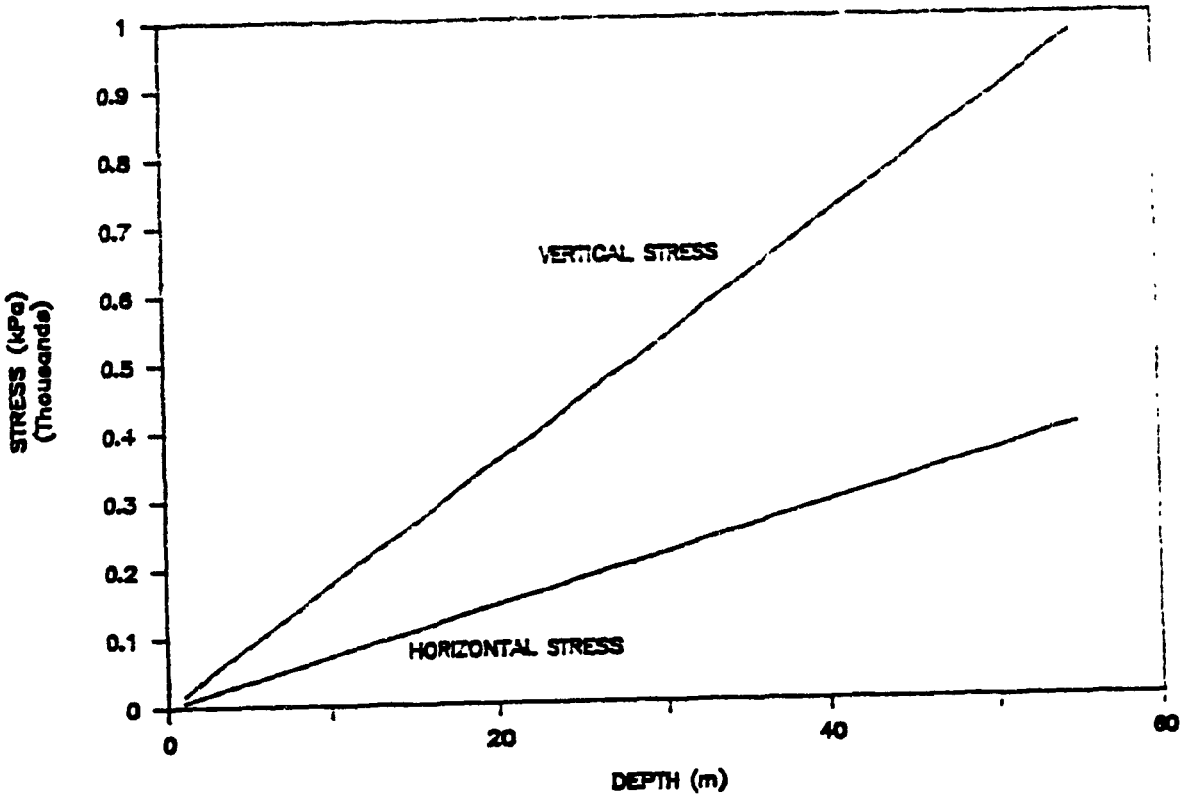

LAC MATAGAMI

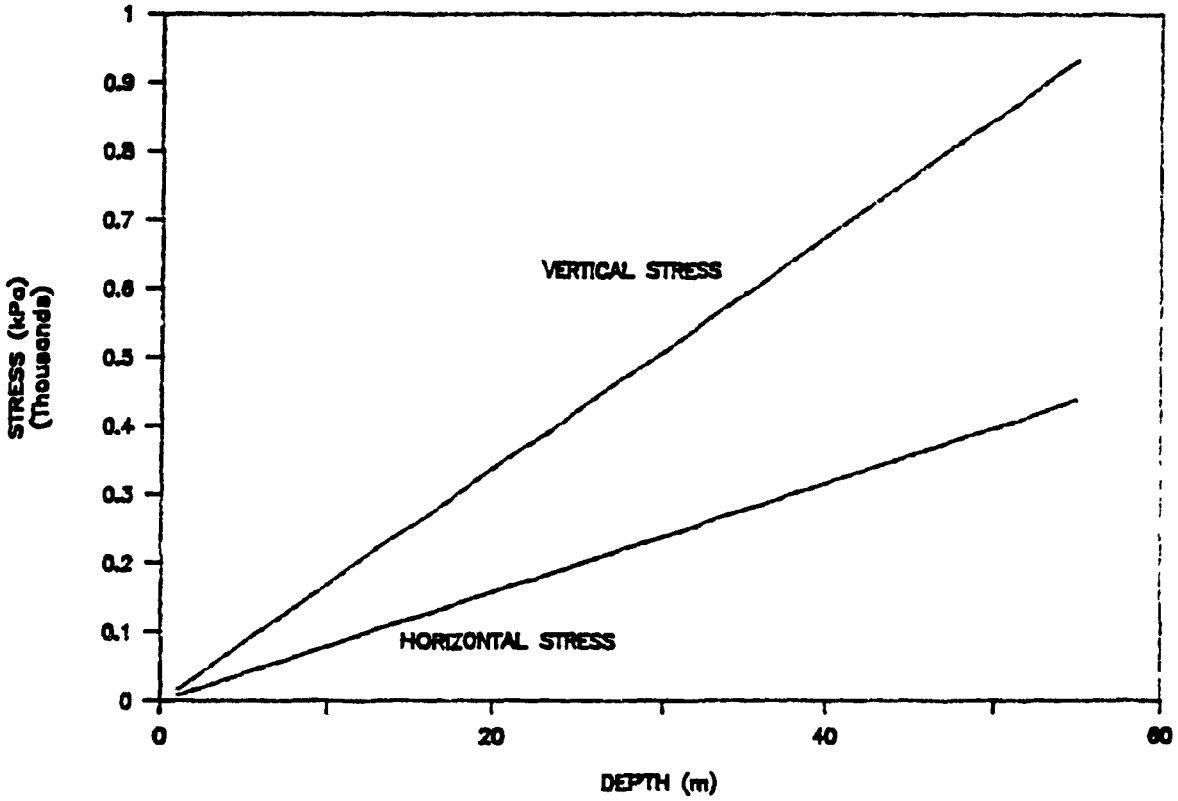

REDLAKE 1661

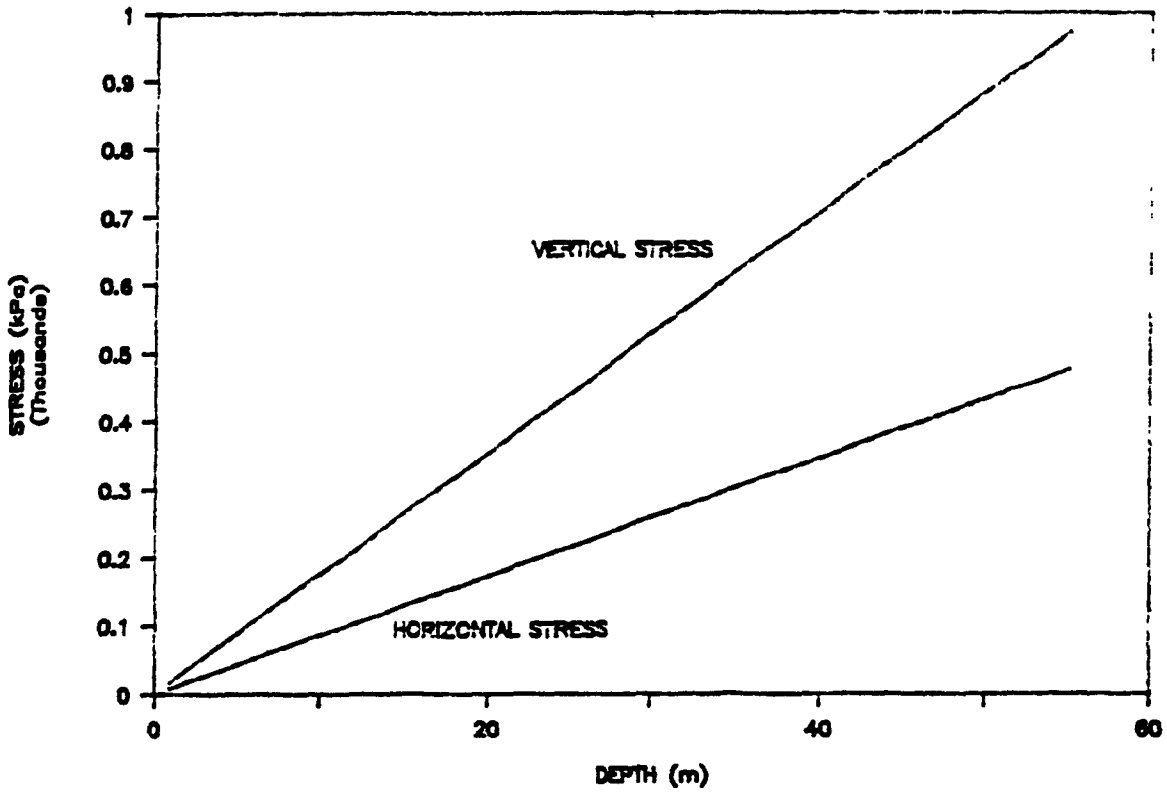

REDLAKE 1804 14D

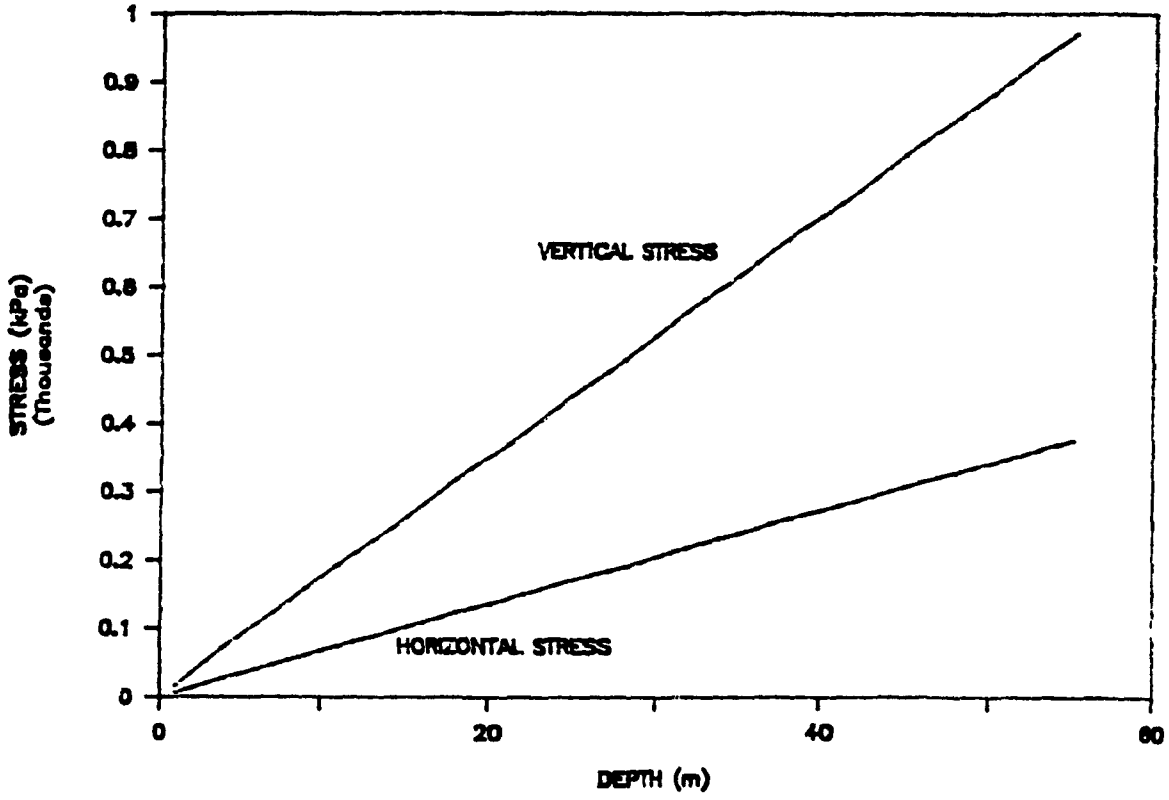

REDLAKE 1804 60D

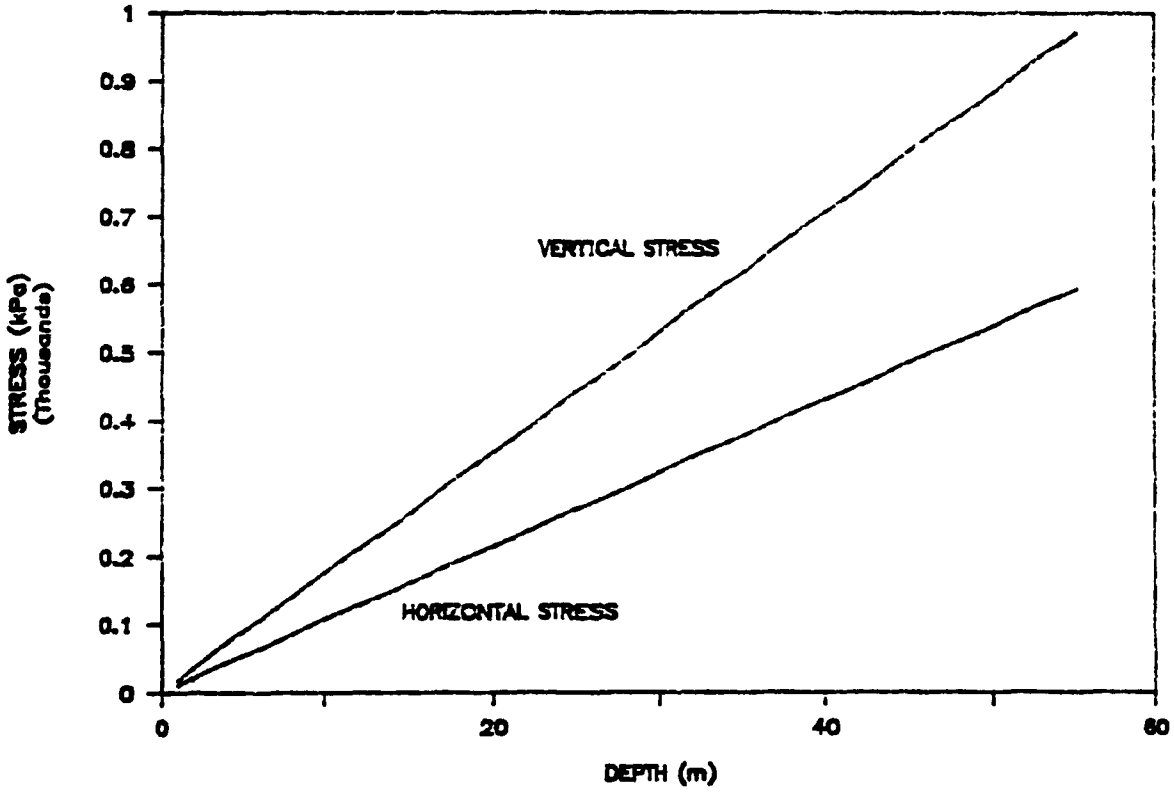

SIGMA

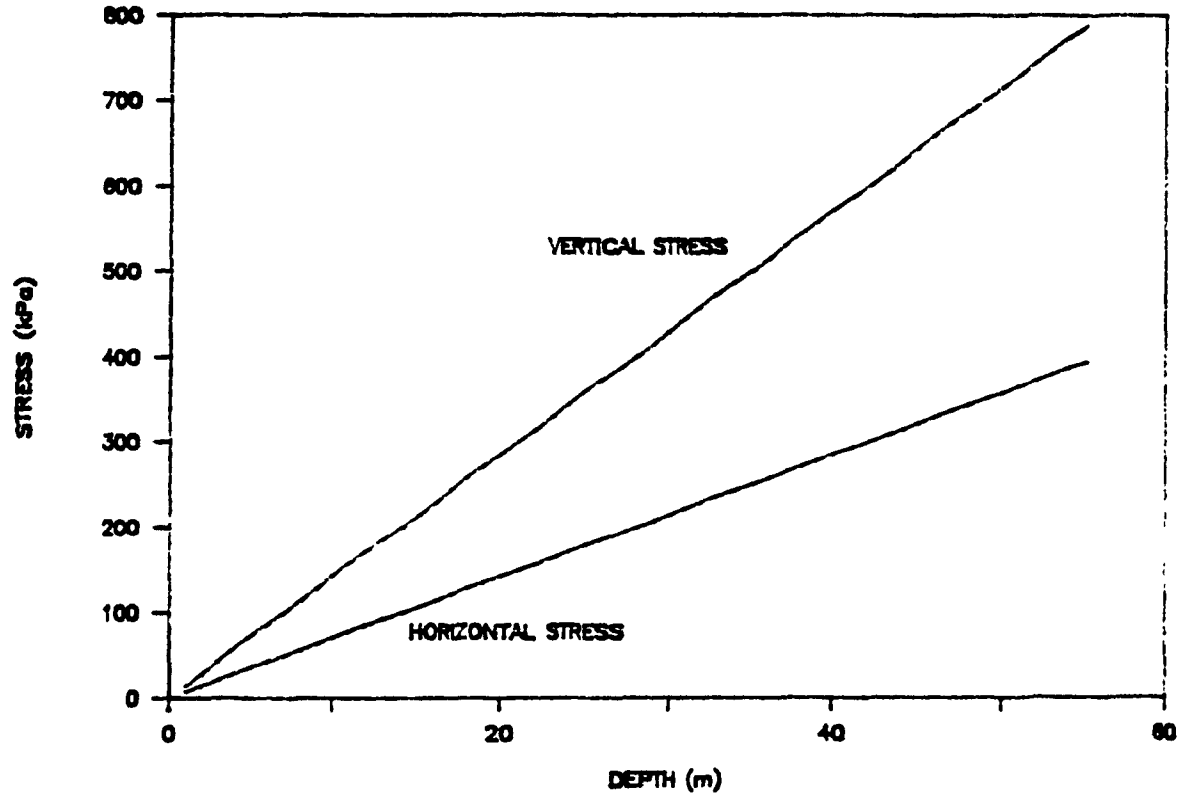

REMNOR

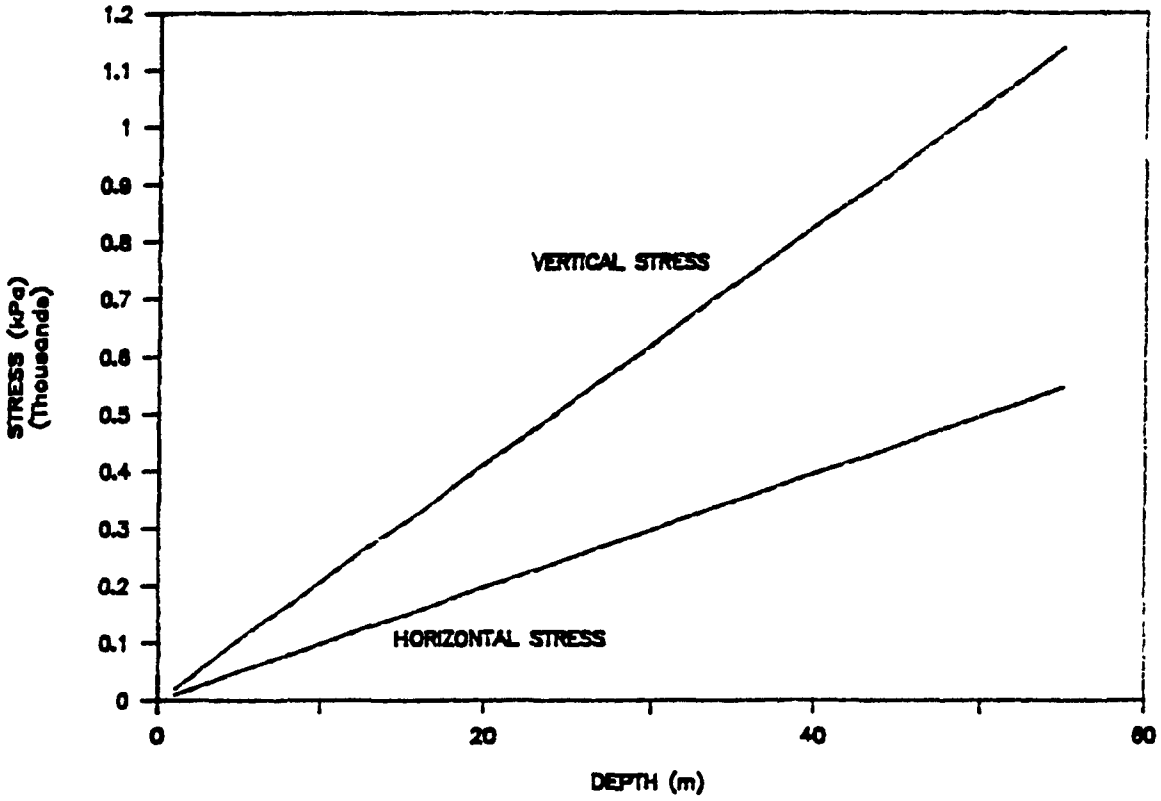
1.2
1.1
1
0.9
0.8
0.7
0.6
0.5
0.4
0.3
0.2
0.1
0
STRESS (kPa)
(Thousands)
VERTICAL STRESS
HORIZONTAL STRESS
0
20
40
60
DEPTH (m)

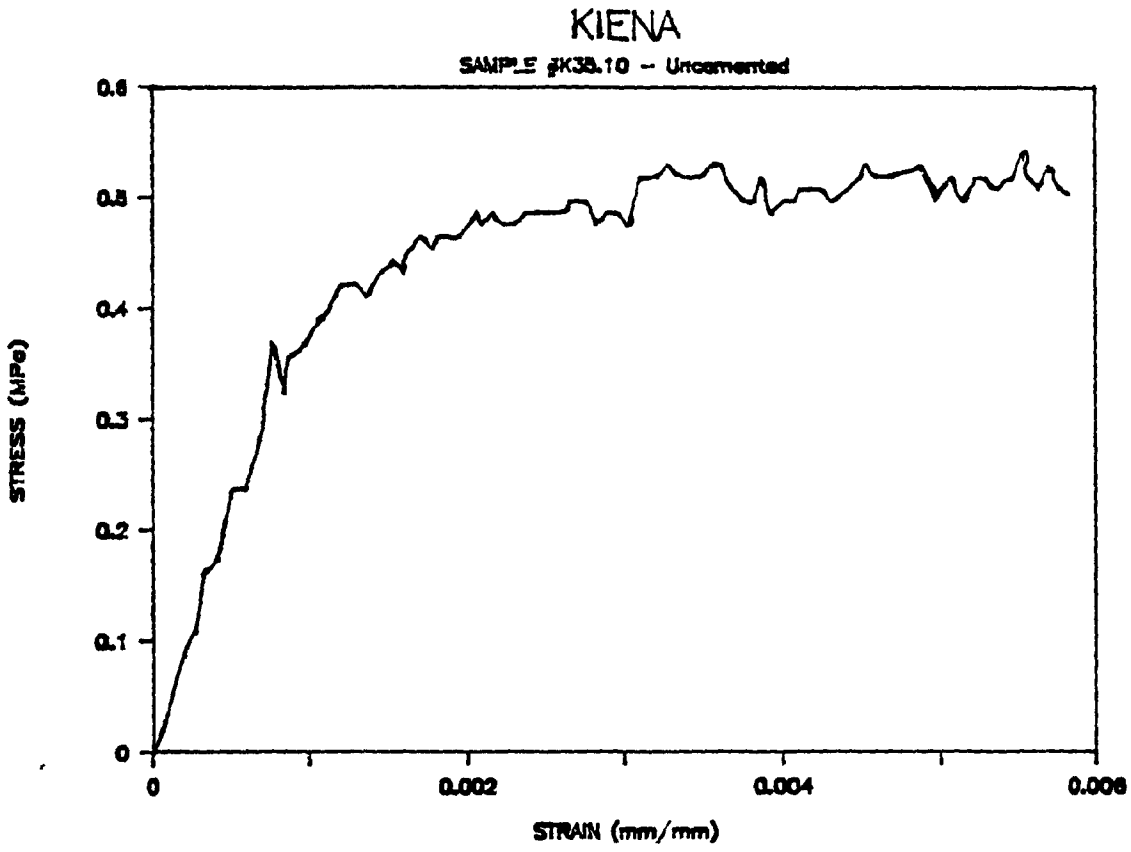
KIENA
SAMPLE #K35.10 – Uncemented
STRESS (MPa)
0.6
0.5
0.4
0.3
0.2
0.1
0
0
0.002
0.004
0.006
STRAIN (mm/mm)

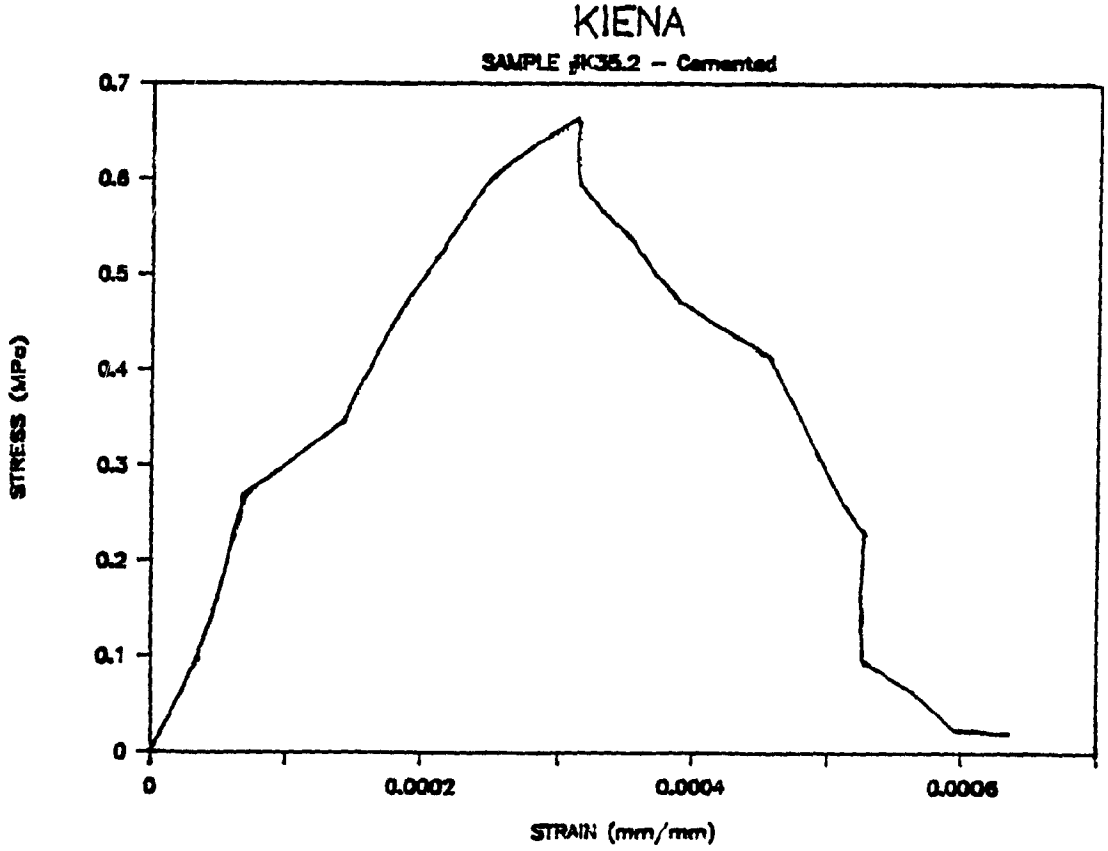
KIENA
SAMPLE #K35.2 – Cemented
STRESS (MPa)
0.7
0.6
0.5
0.4
0.3
0.2
0.1
0
0
0.0002
0.0004
0.0006
STRAIN (mm/mm)

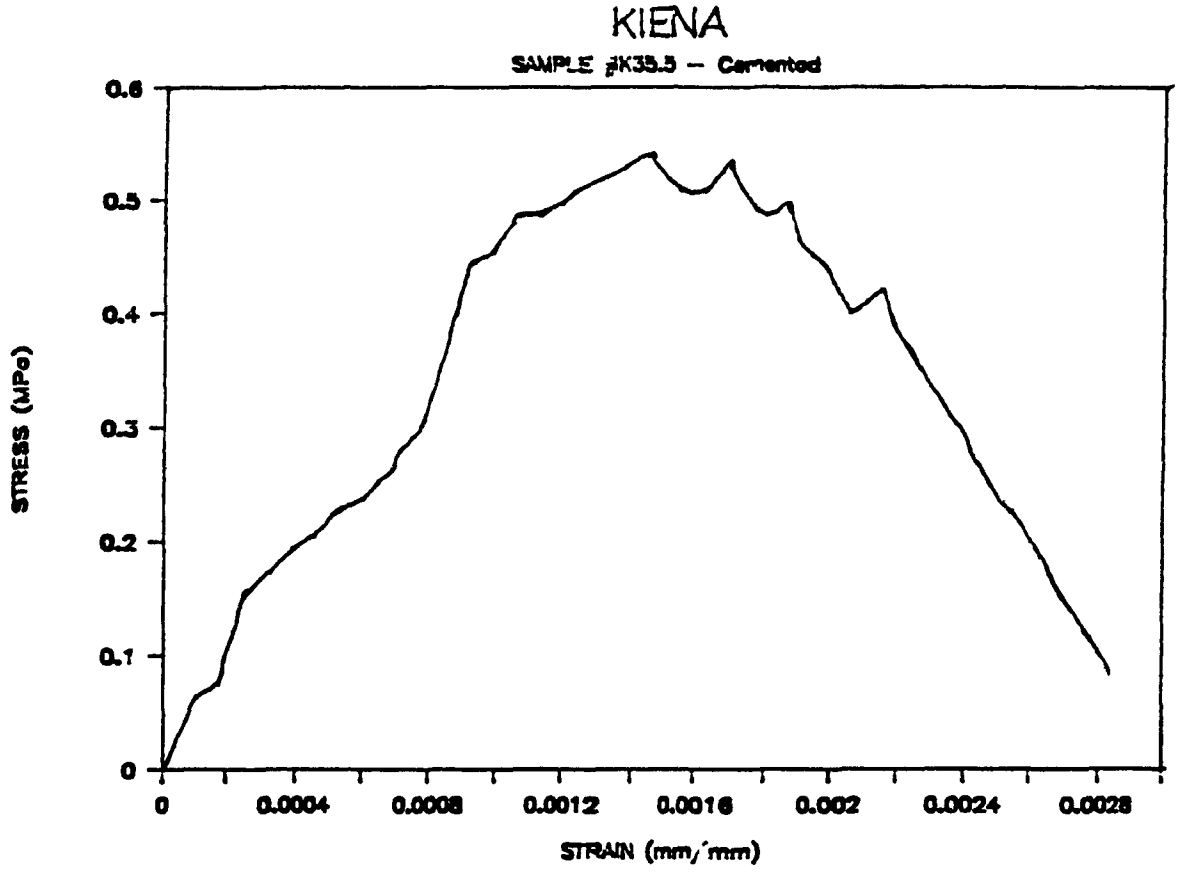
KIENA
SAMPLE #K35.5 – Cemented
STRESS (MPa)
0.6
0.5
0.4
0.3
0.2
0.1
0
0
0.0004
0.0008
0.0012
0.0016
0.002
0.0024
0.0028
STRAIN (mm/mm)

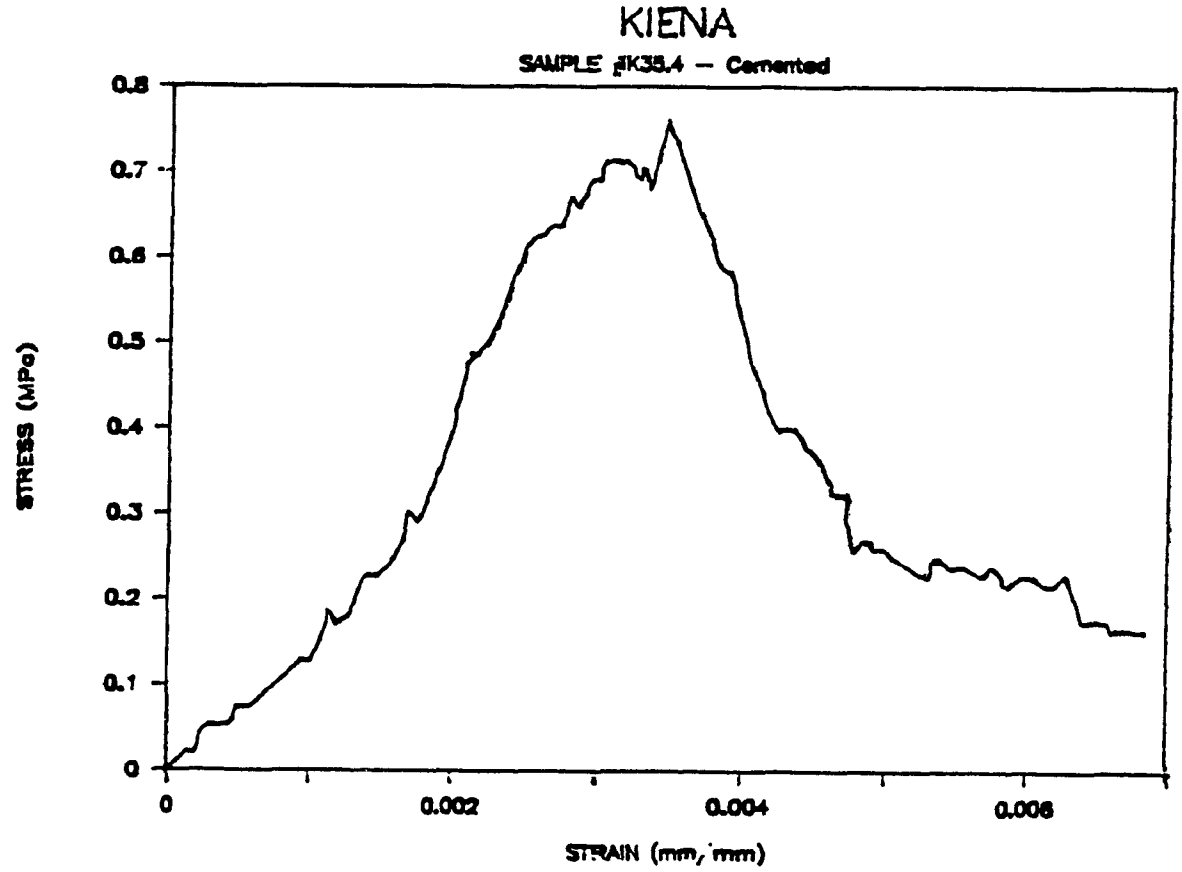
KIENA
SAMPLE #K35.4 – Cemented
STRESS (MPa)
0.8
0.7
0.6
0.5
0.4
0.3
0.2
0.1
0
0
0.002
0.004
0.006
STRAIN (mm/mm)

KIENA

SAMPLE #K35.6 – Cemented

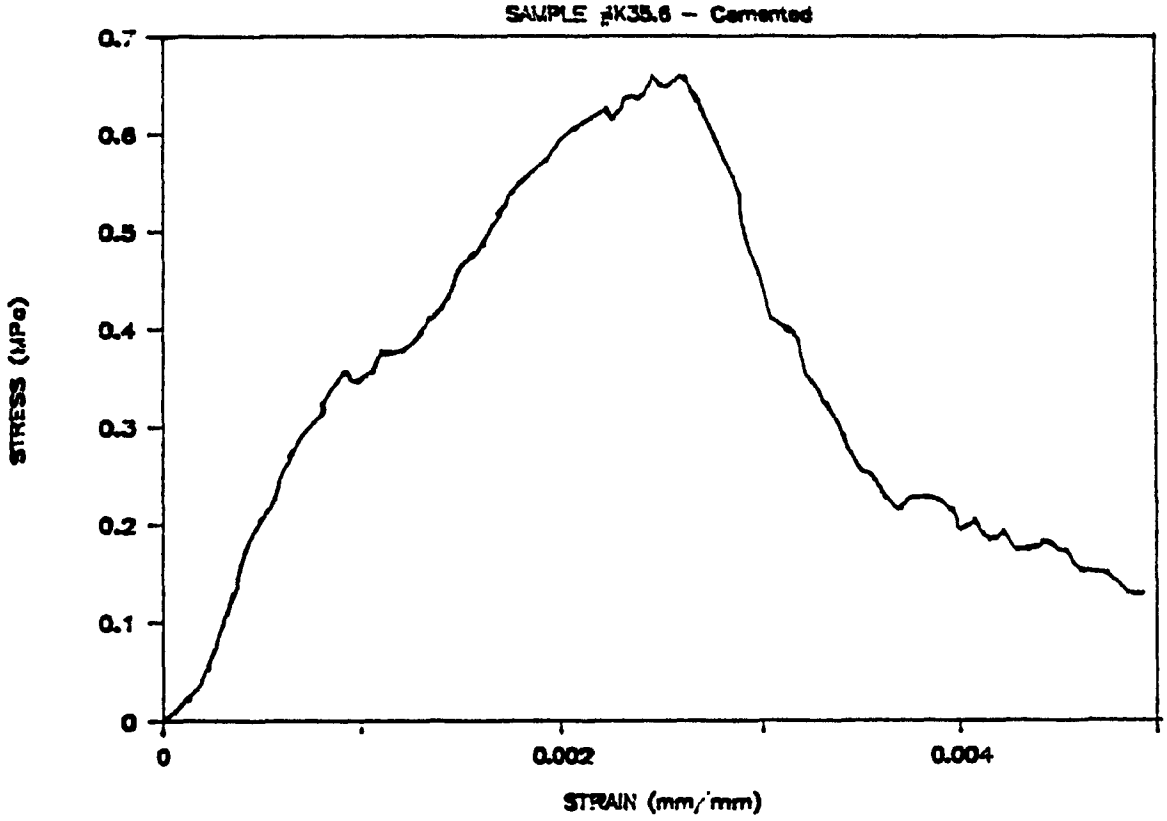

KIENA

SAMPLE #K35.7 – Cemented

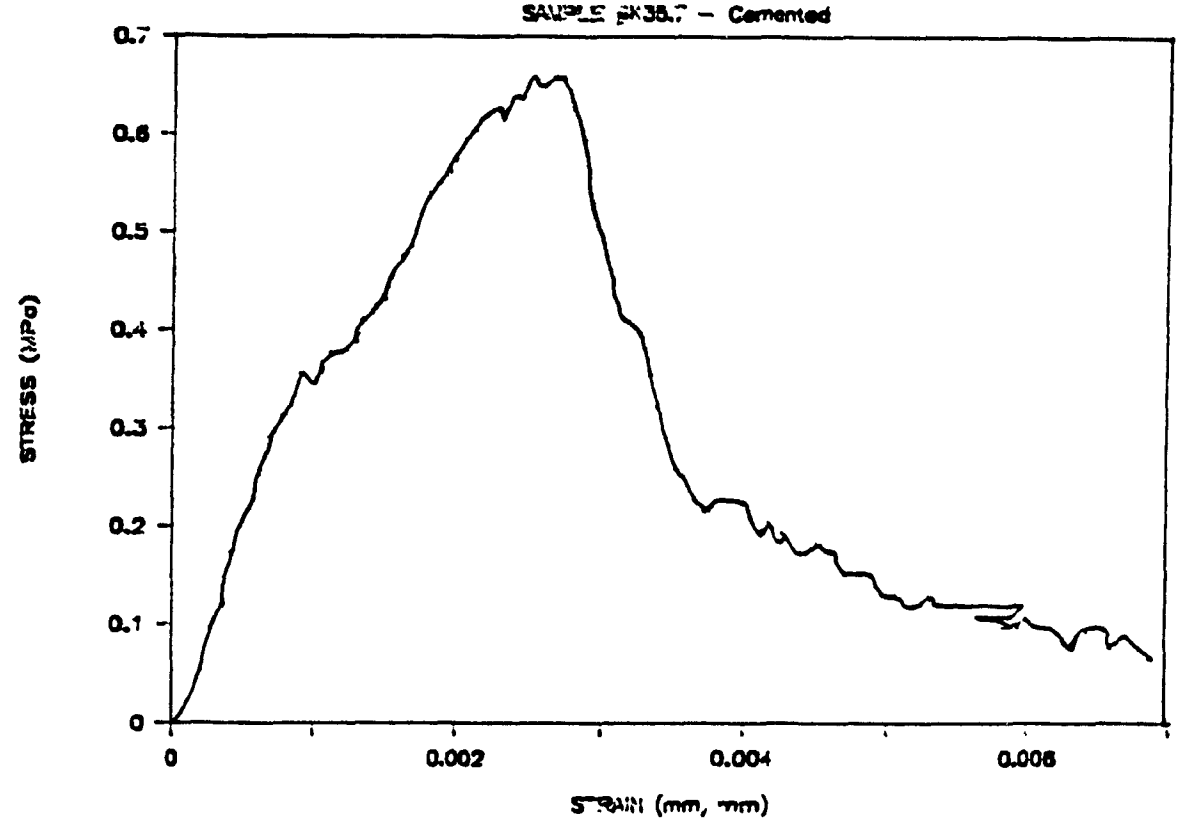

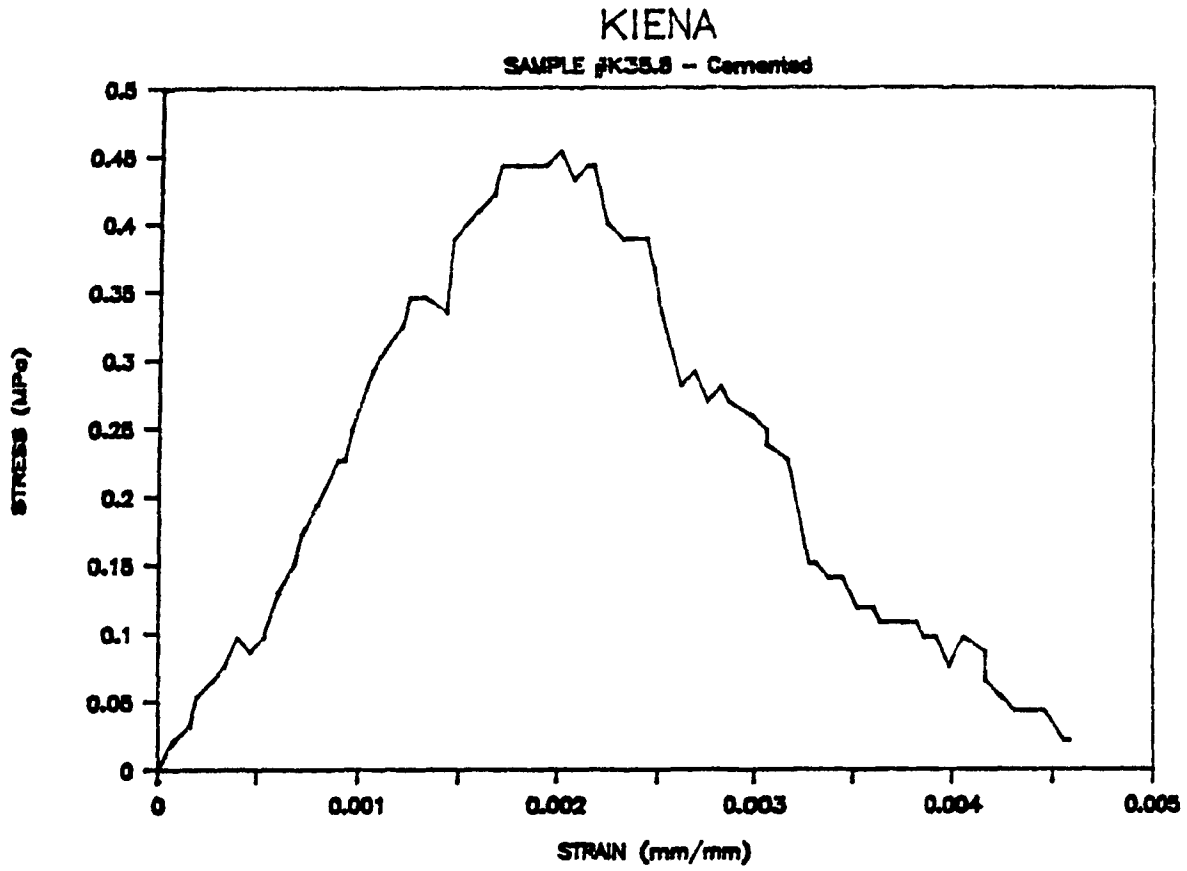
KIENA
SAMPLE #K35.8 – Cemented
STRESS (MPa)
0.5
0.45
0.4
0.35
0.3
0.25
0.2
0.15
0.1
0.05
0
0
0.001
0.002
0.003
0.004
0.005
STRAIN (mm/mm)

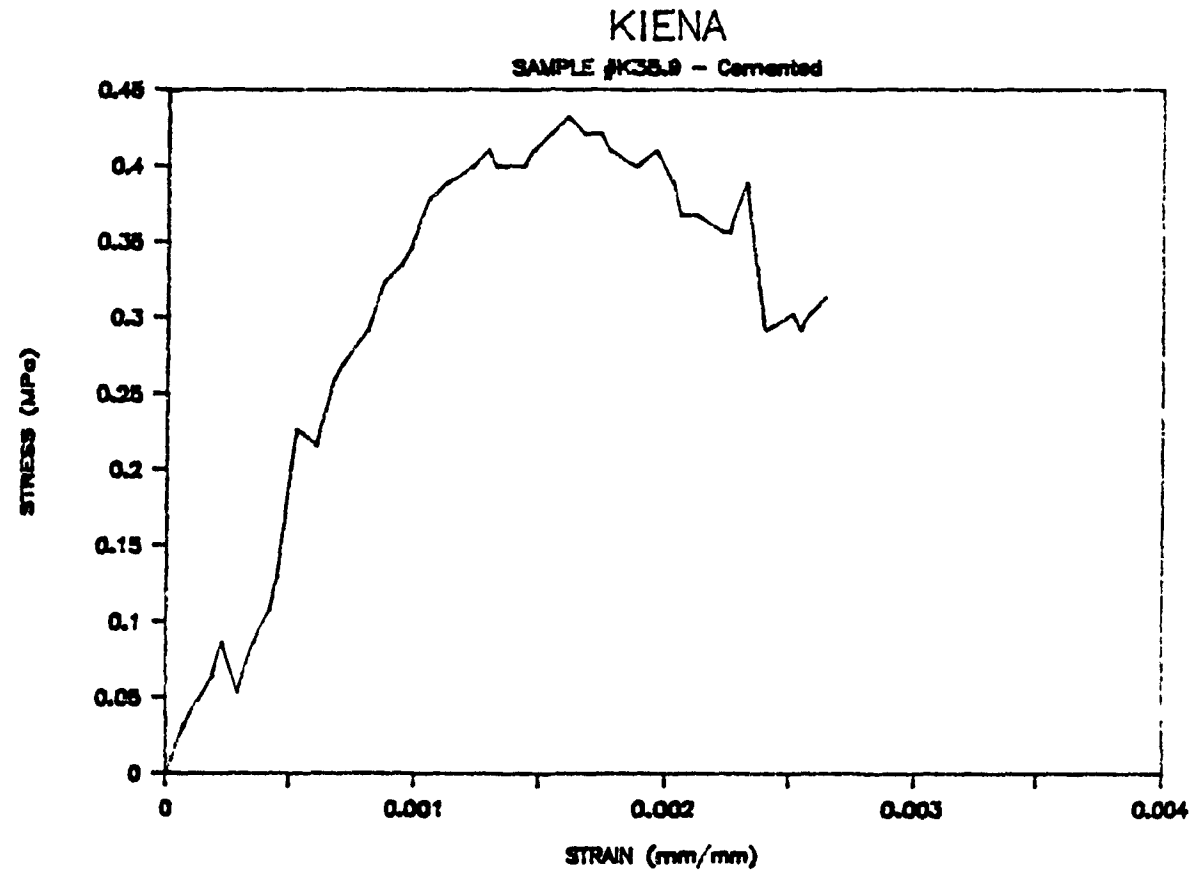
KIENA
SAMPLE #K35.9 – Cemented
STRESS (MPa)
0.45
0.4
0.35
0.3
0.25
0.2
0.15
0.1
0.05
0
0
0.001
0.002
0.003
0.004
STRAIN (mm/mm)

KIENA

SAMPLE K42.1

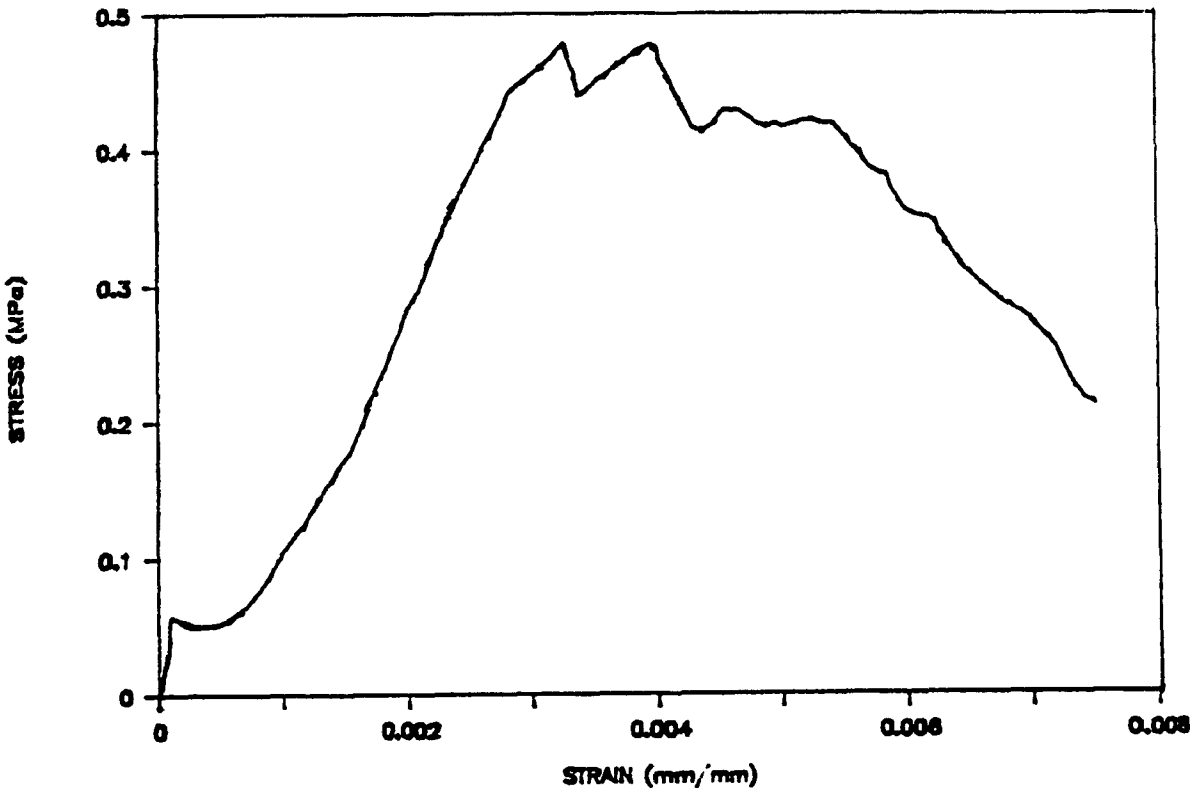

KIENA

SAMPLE K42.3

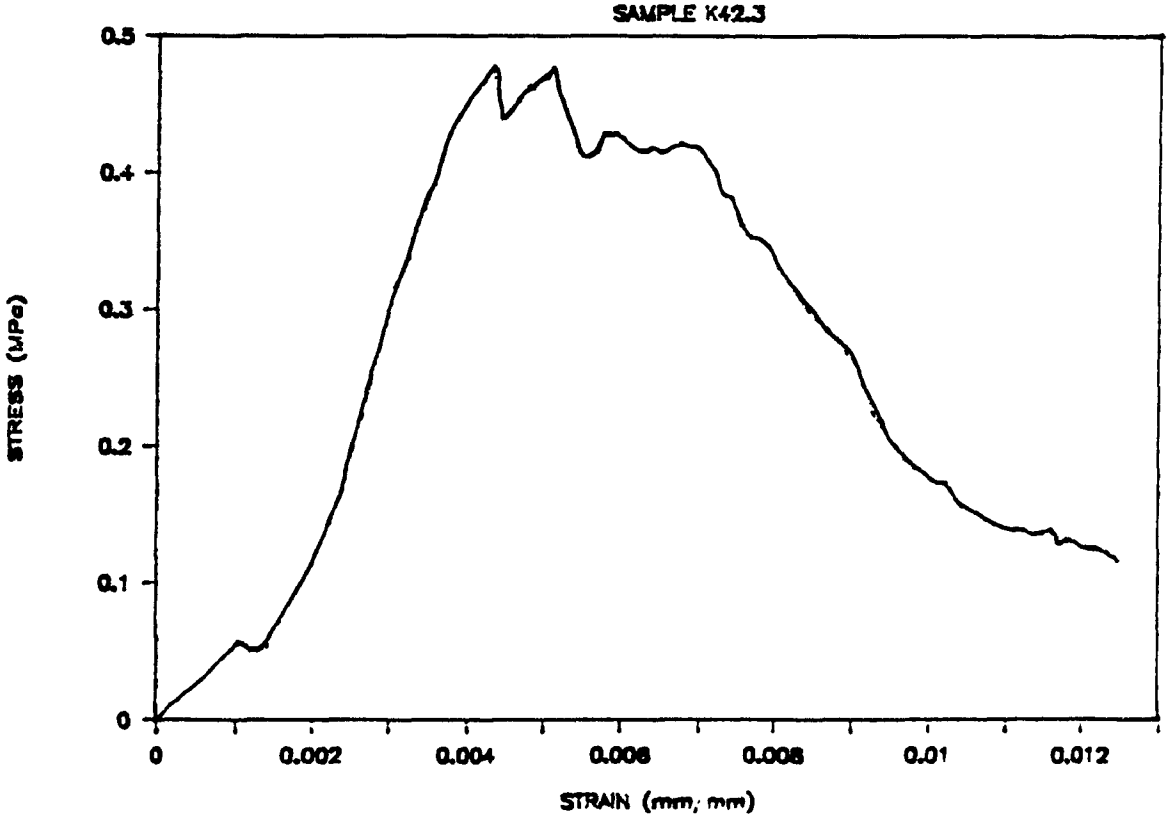

KIENA

SAMPLE K42.4

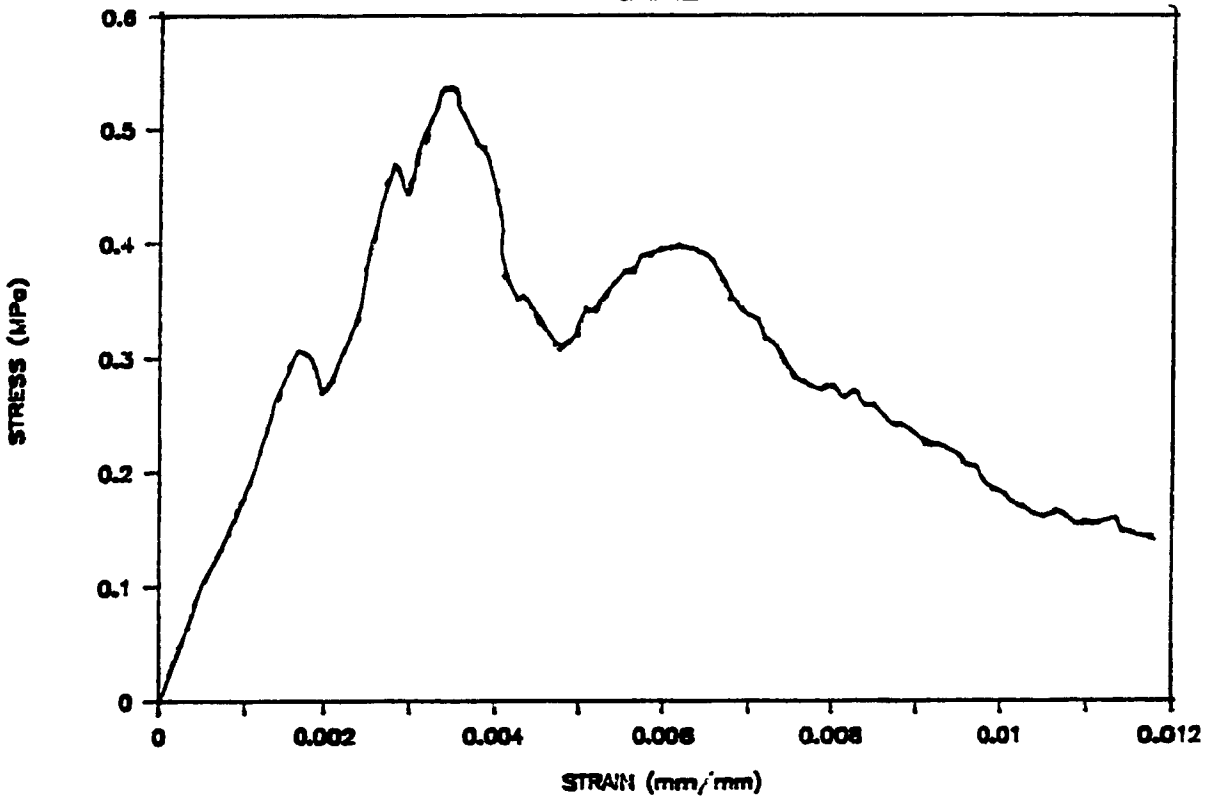

KIENA

SAMPLE K42.5

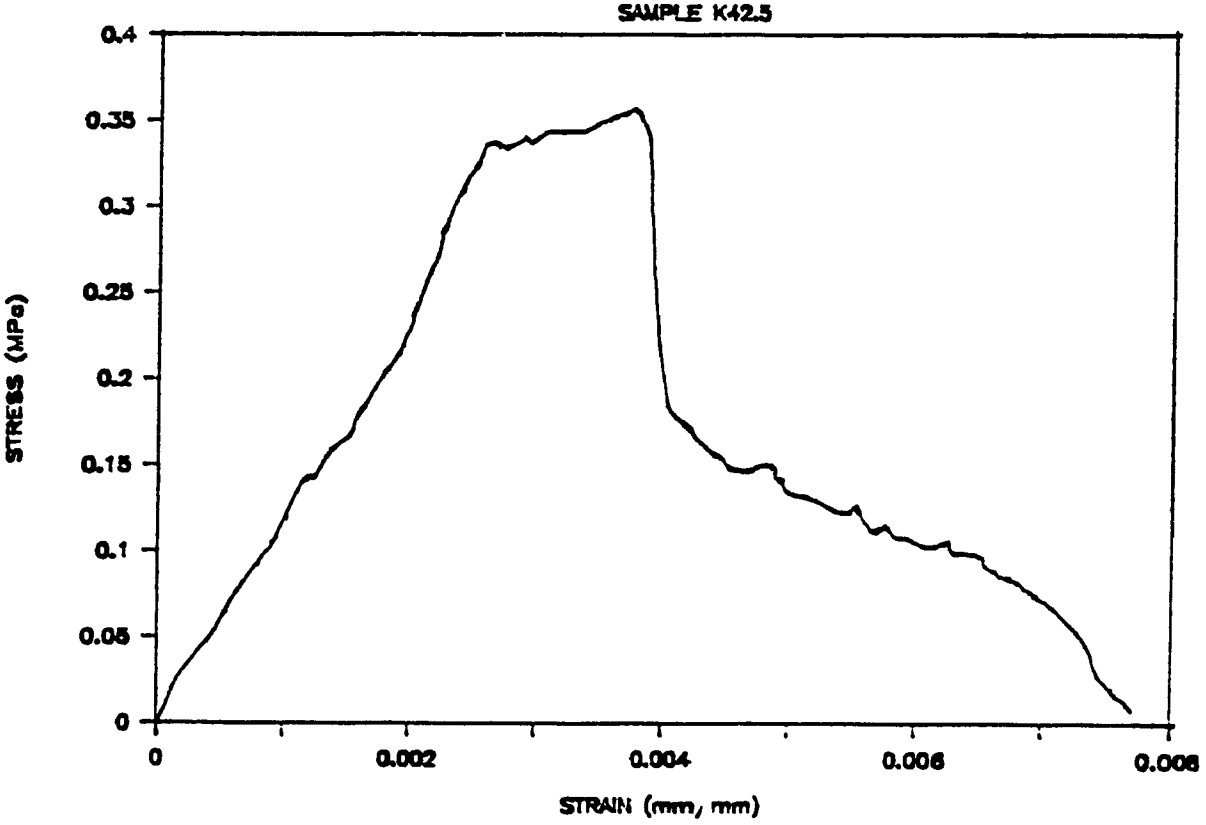

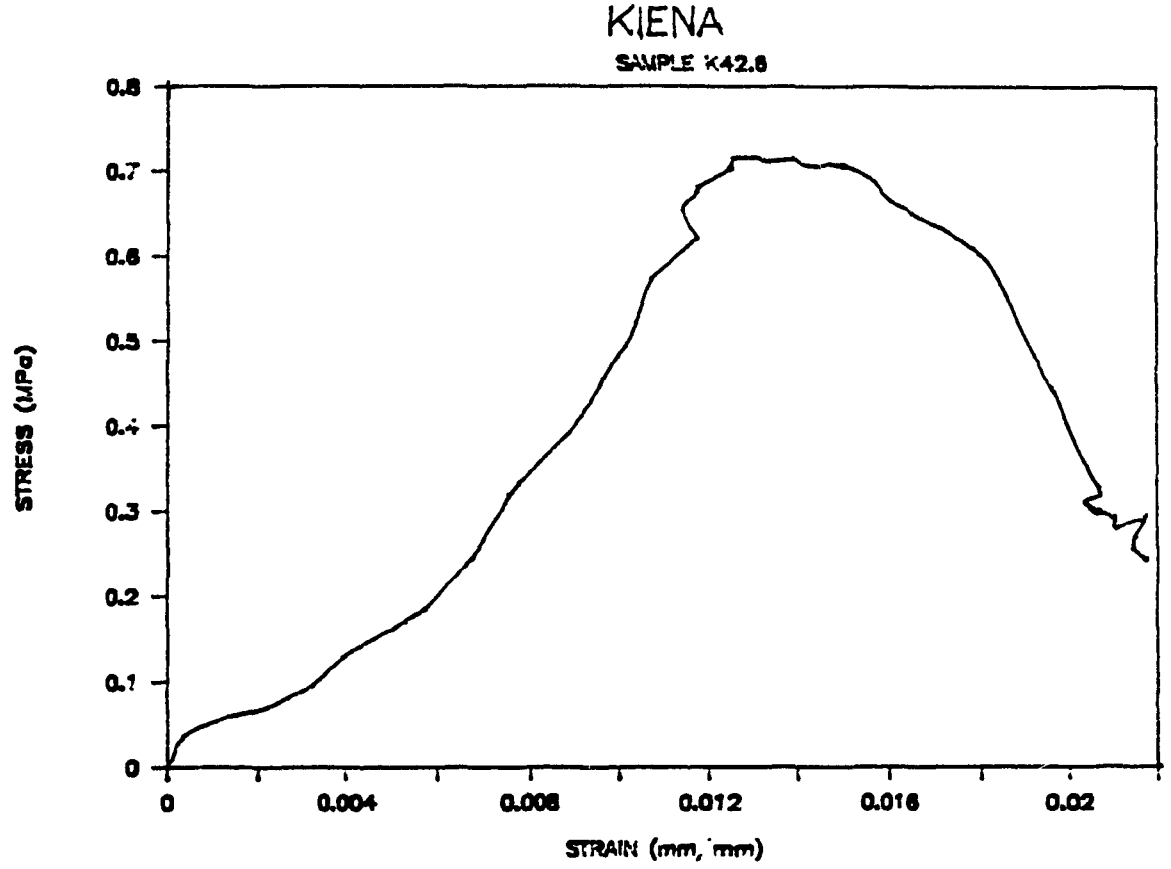
KIENA
SAMPLE K42.6
STRESS (MPa)
0.8
0.7
0.6
0.5
0.4
0.3
0.2
0.1
0
0
0.004
0.008
0.012
0.016
0.02
STRAIN (mm, mm)

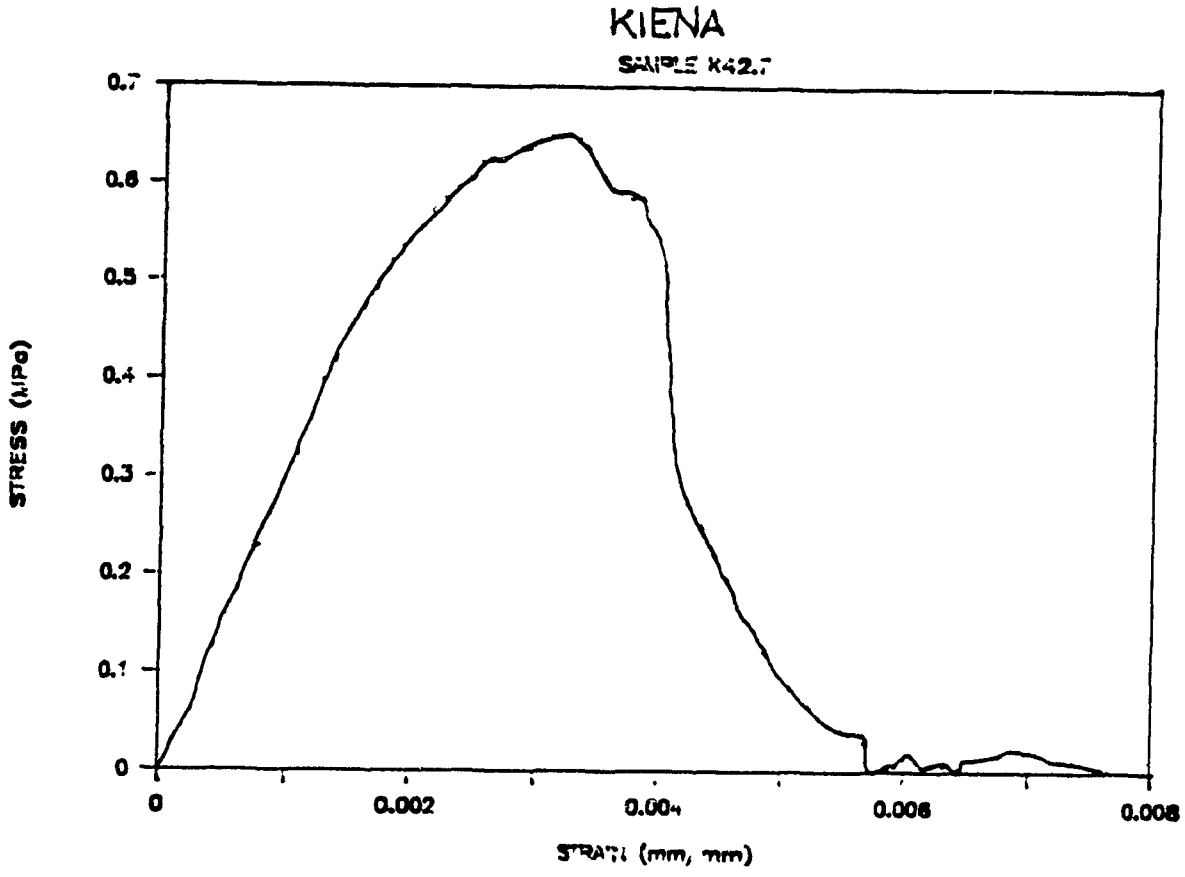
KIENA
SAMPLE K42.7
STRESS (MPa)
0.7
0.6
0.5
0.4
0.3
0.2
0.1
0
0
0.002
0.004
0.006
0.008
STRAIN (mm, mm)

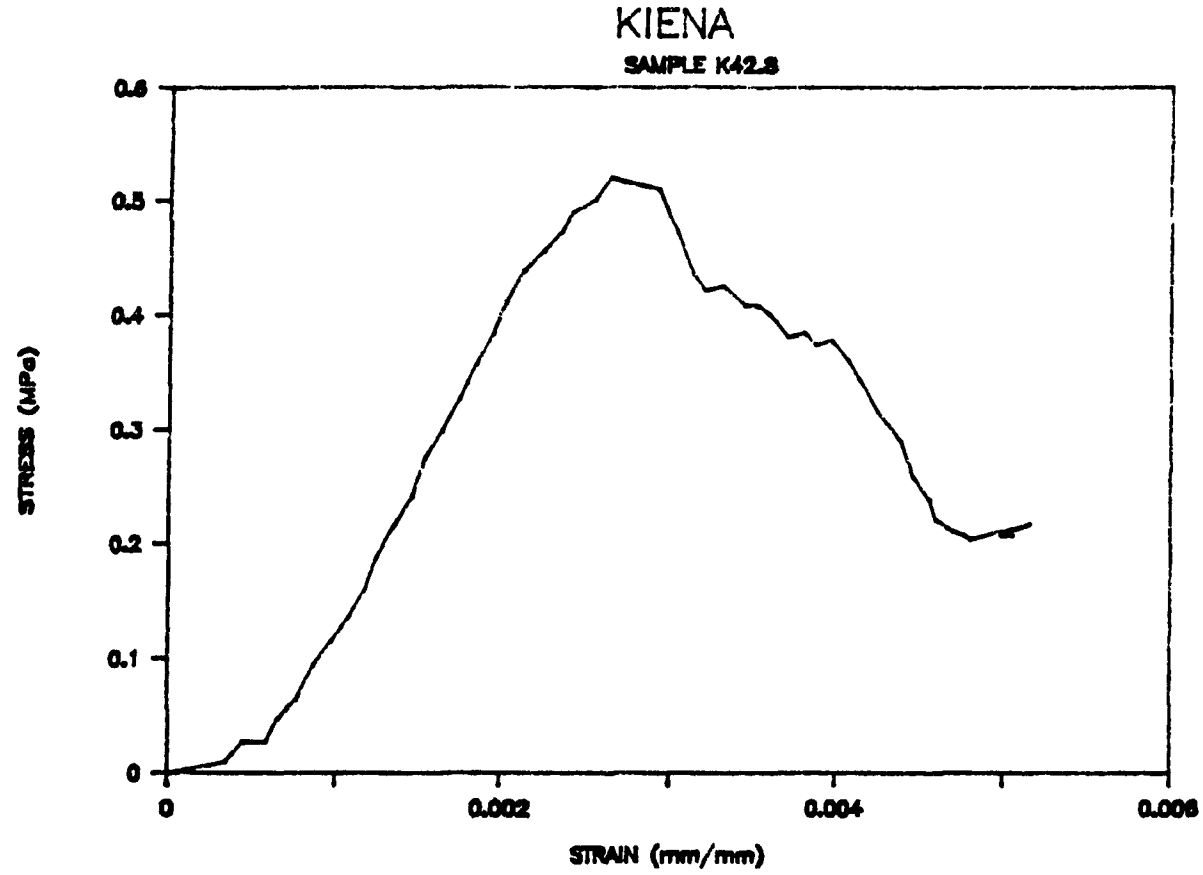
KIENA
SAMPLE K42.8
STRESS (MPa)
0.6
0.5
0.4
0.3
0.2
0.1
0
0
0.002
0.004
0.006
STRAIN (mm/mm)

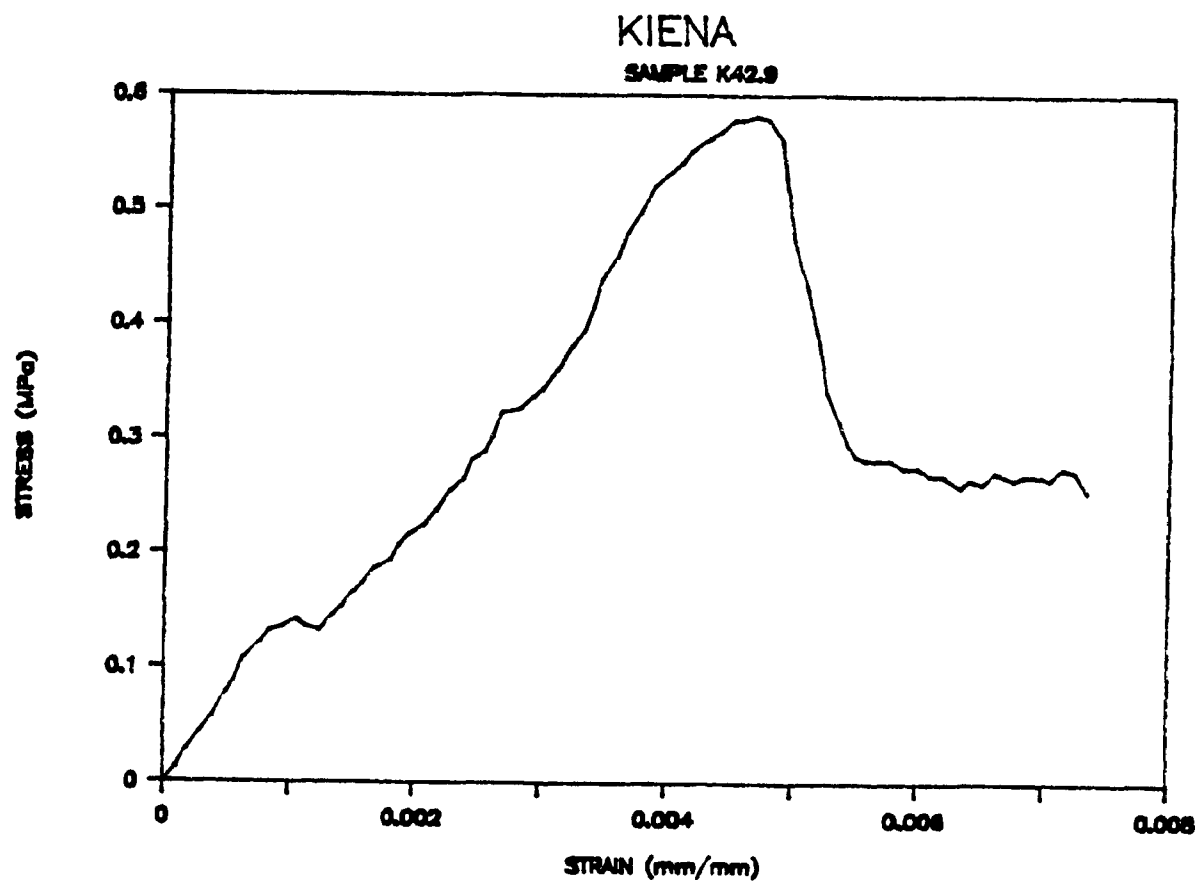
KIENA
SAMPLE K42.9
STRESS (MPa)
0.6
0.5
0.4
0.3
0.2
0.1
0
0
0.002
0.004
0.006
0.008
STRAIN (mm/mm)

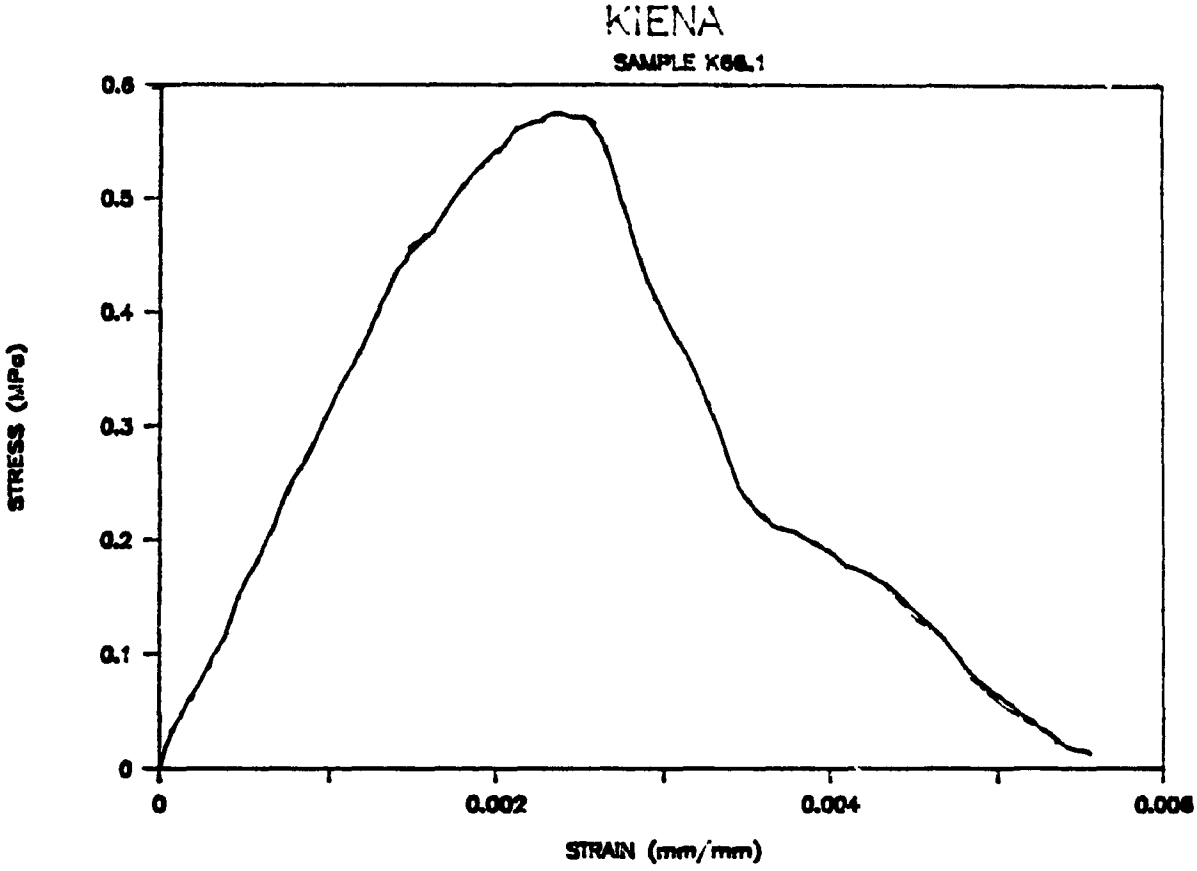
KIENA
SAMPLE K66.1
STRESS (MPa)
0.6
0.5
0.4
0.3
0.2
0.1
0
0
0.002
0.004
0.006
STRAIN (mm/mm)

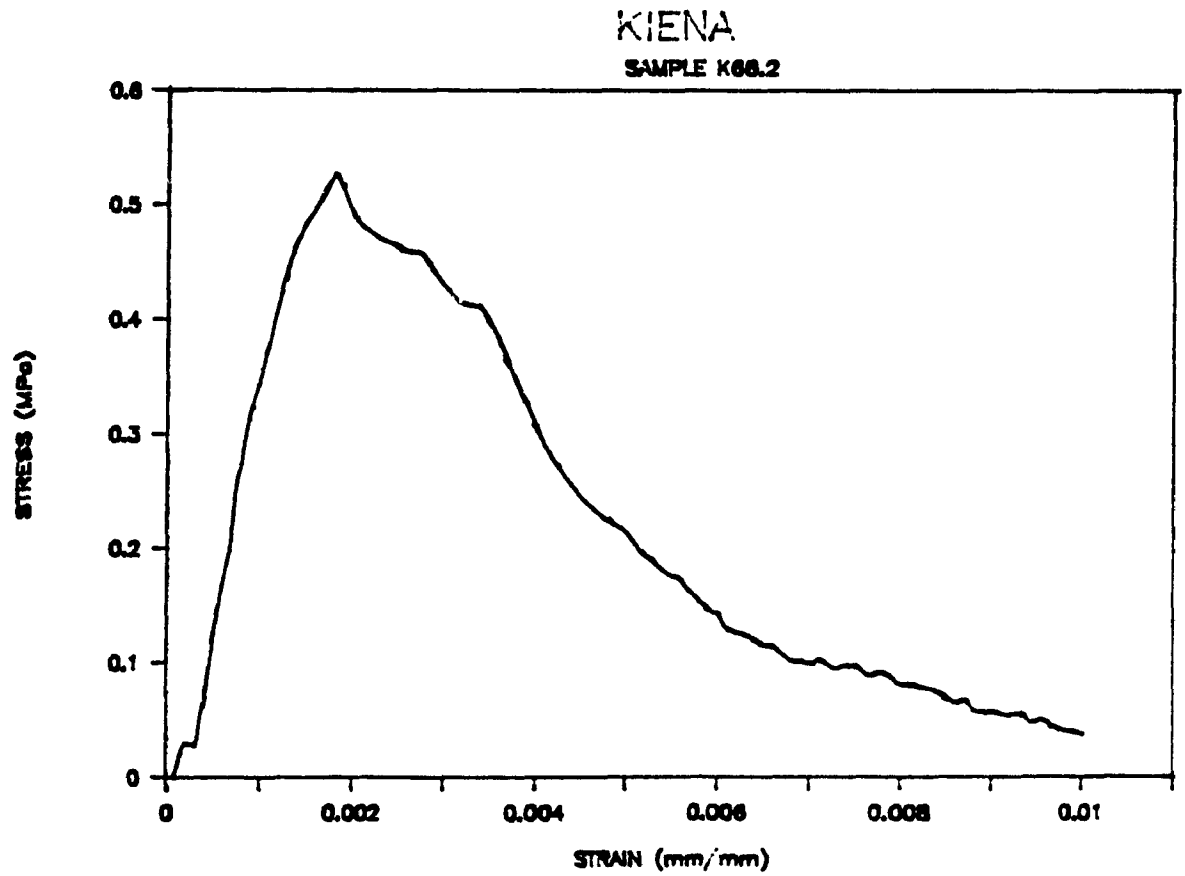
KIENA
SAMPLE K66.2
STRESS (MPa)
0.6
0.5
0.4
0.3
0.2
0.1
0
0
0.002
0.004
0.006
0.008
0.01
STRAIN (mm/mm)

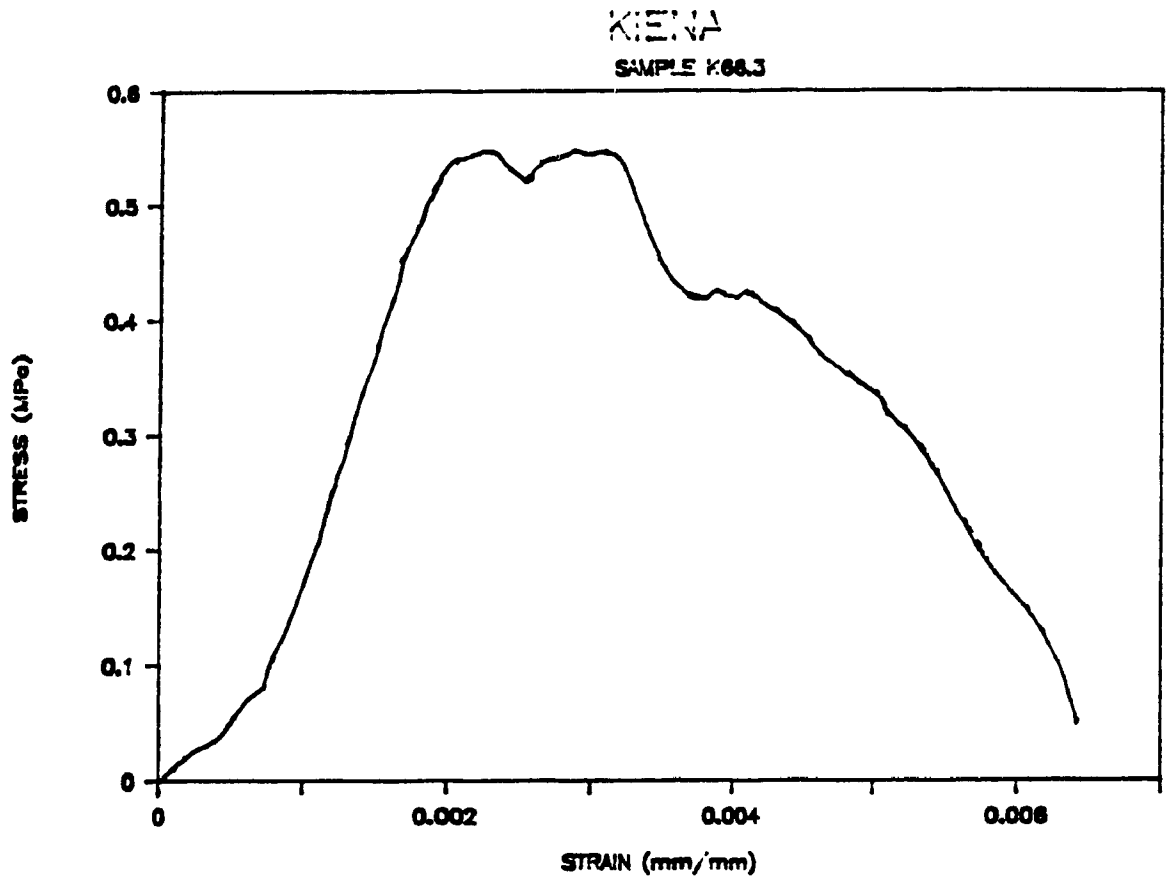
KIENA
SAMPLE K66.3
STRESS (MPa)
0.6
0.5
0.4
0.3
0.2
0.1
0
0
0.002
0.004
0.006
STRAIN (mm/mm)

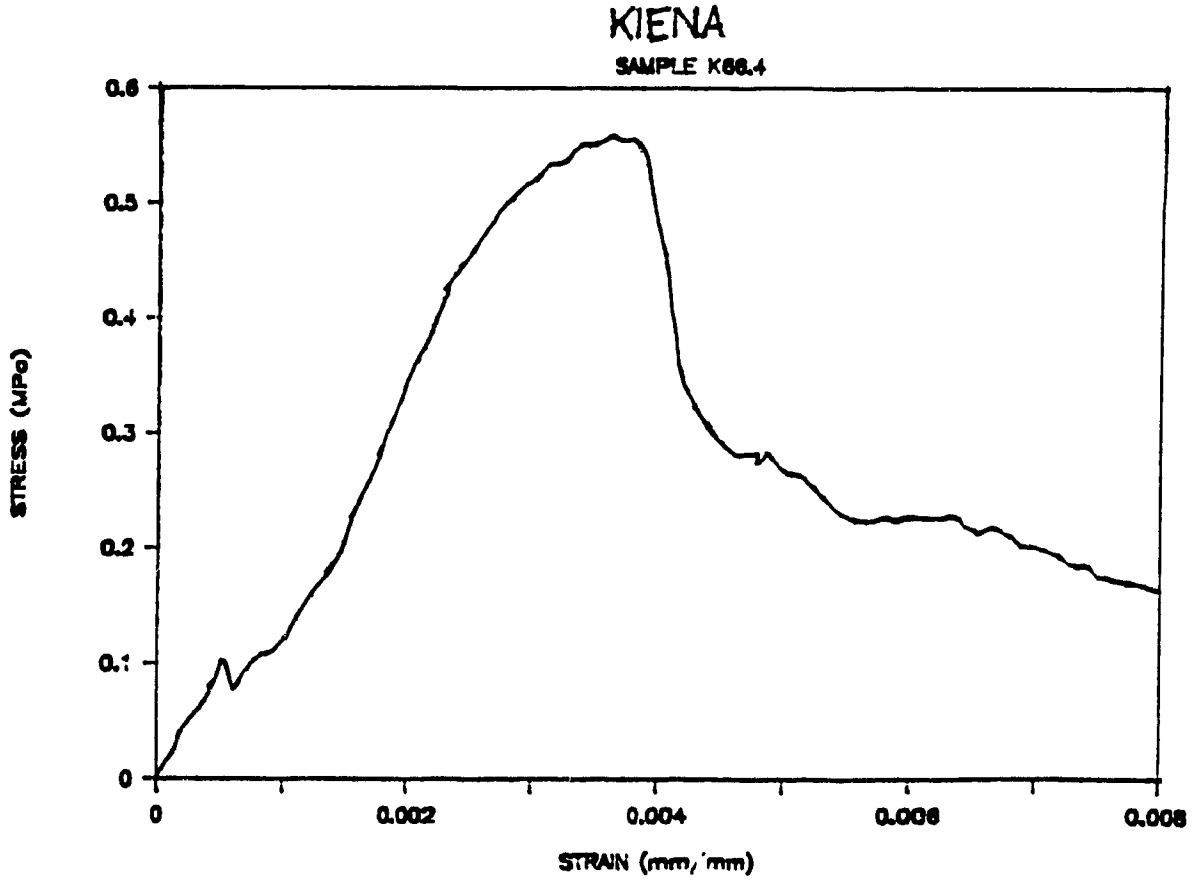
KIENA
SAMPLE K66.4
STRESS (MPa)
0.6
0.5
0.4
0.3
0.2
0.1
0
0
0.002
0.004
0.006
0.008
STRAIN (mm/mm)

KIENA

SAMPLE K66.5

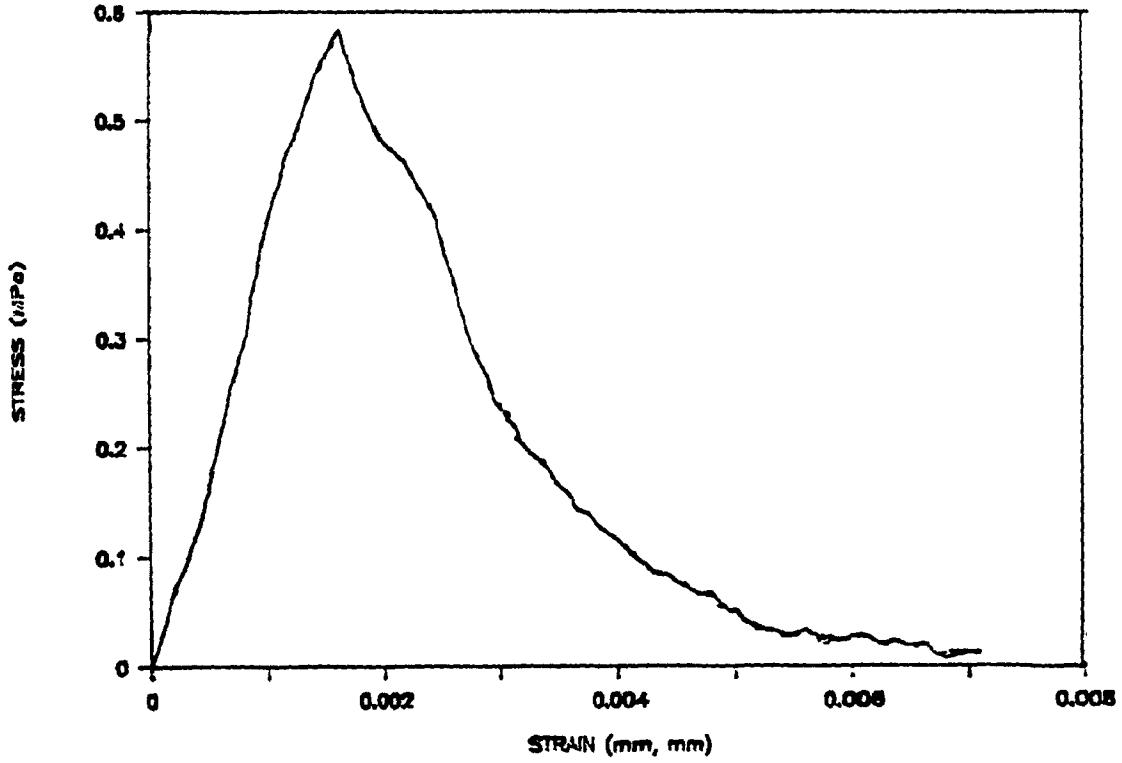

KIENA

SAMPLE K66.6

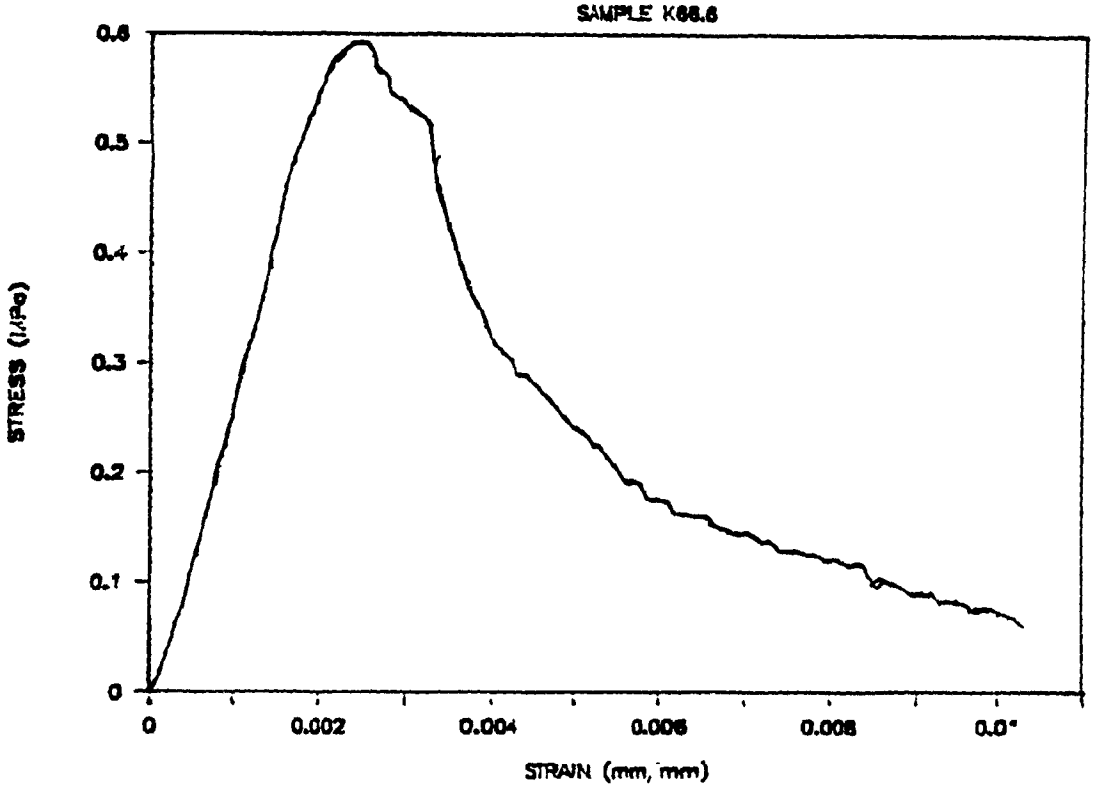

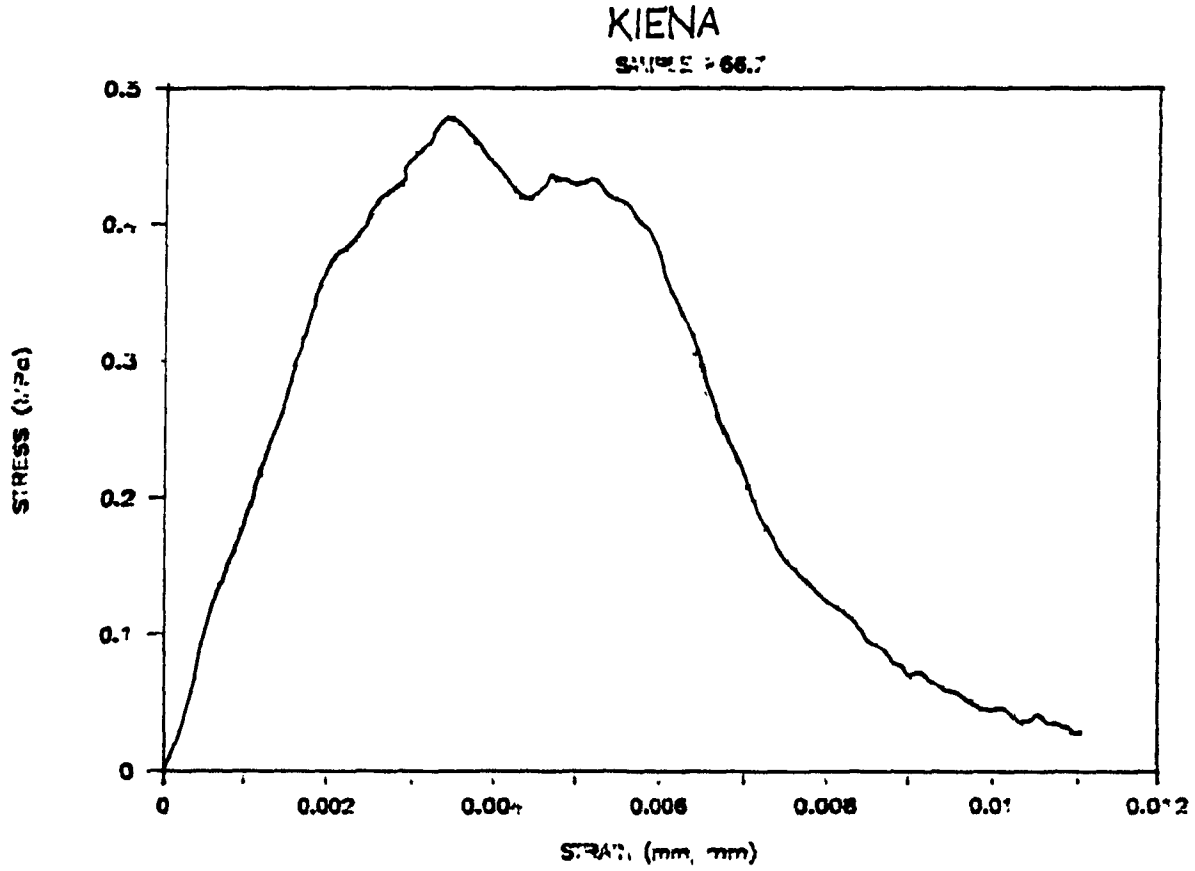
KIENA
0.5
0.4
0.3
0.2
0.1
0
0
0.002
0.004
0.006
0.008
0.01
0.012

KIENA

SAMPLE K67.1

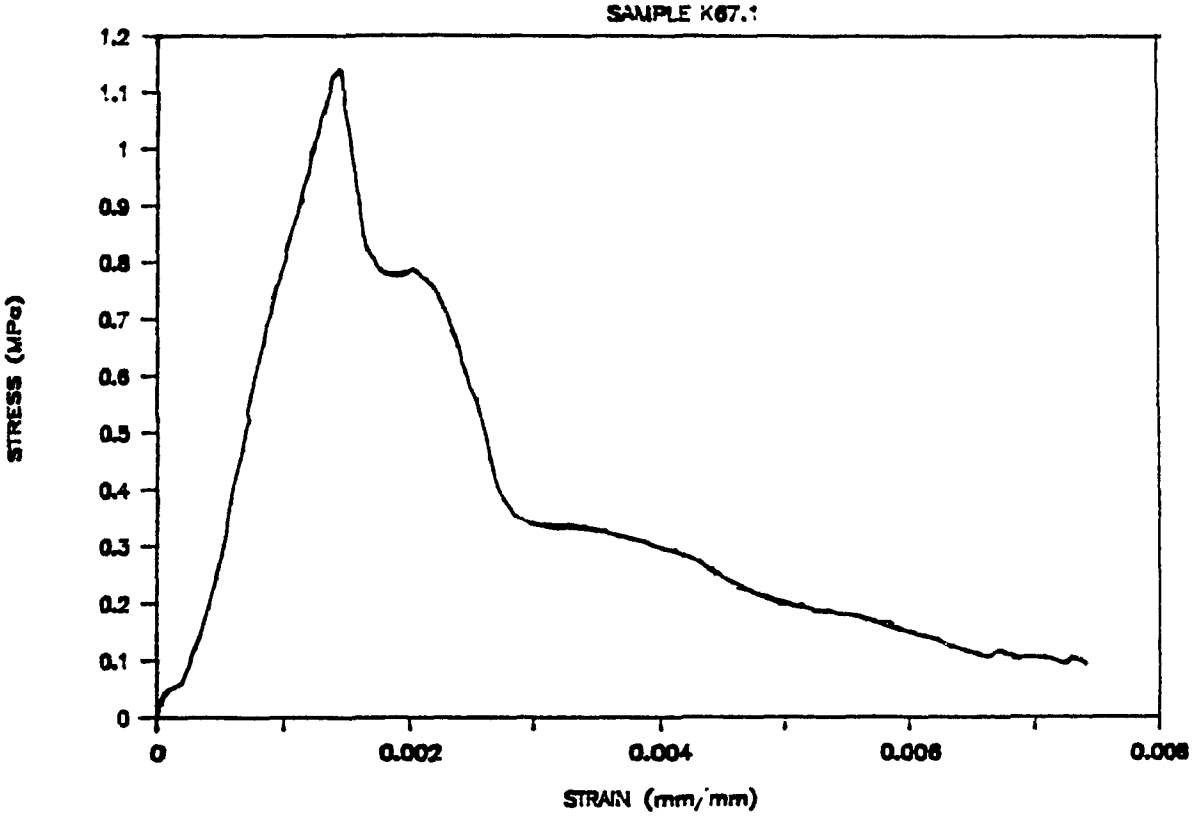

KIENA

SAMPLE K67.2

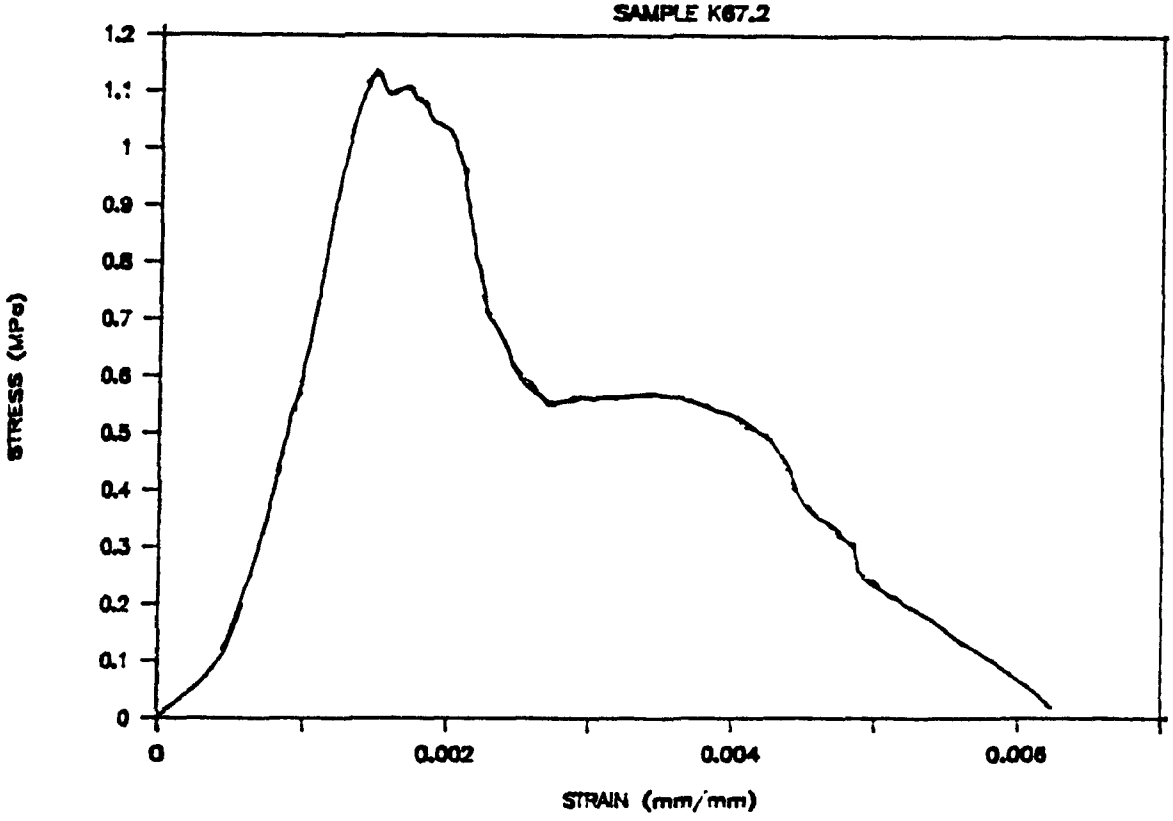

KIENA

SAMPLE K67.3

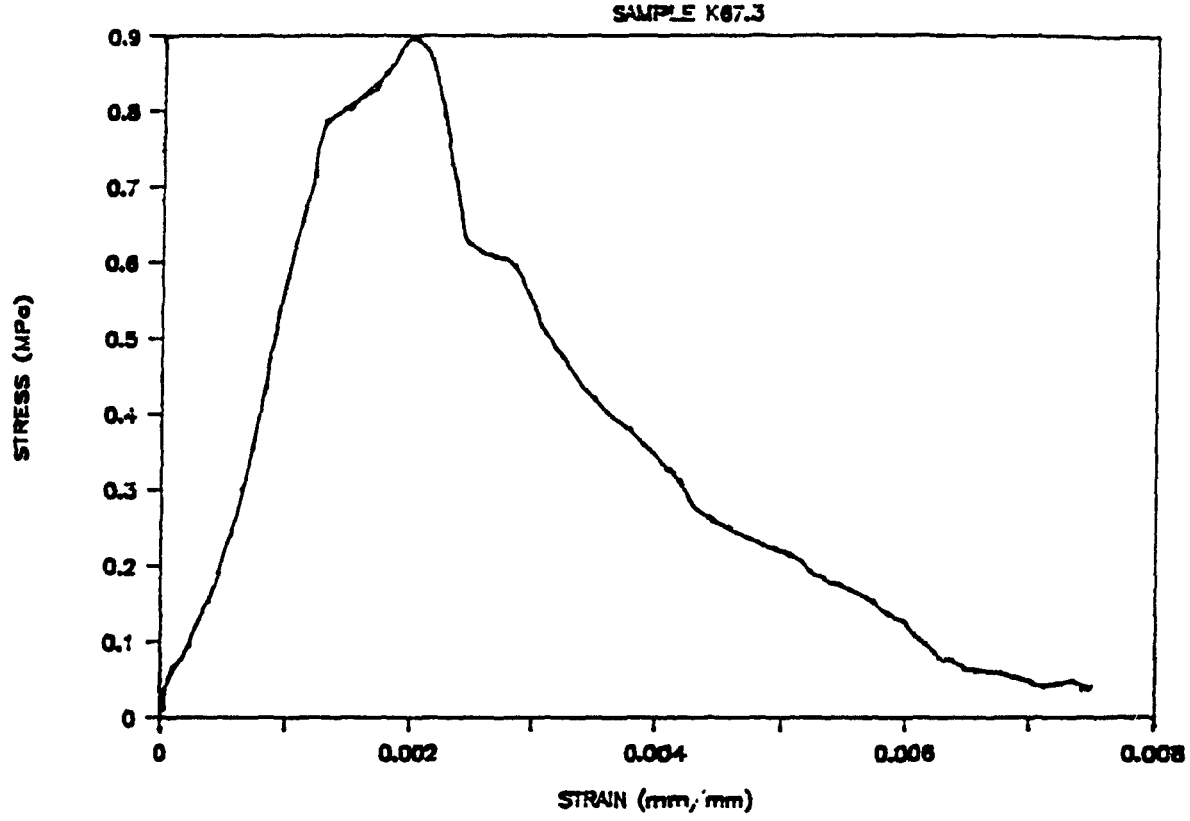

KIENA

SAMPLE K67.4

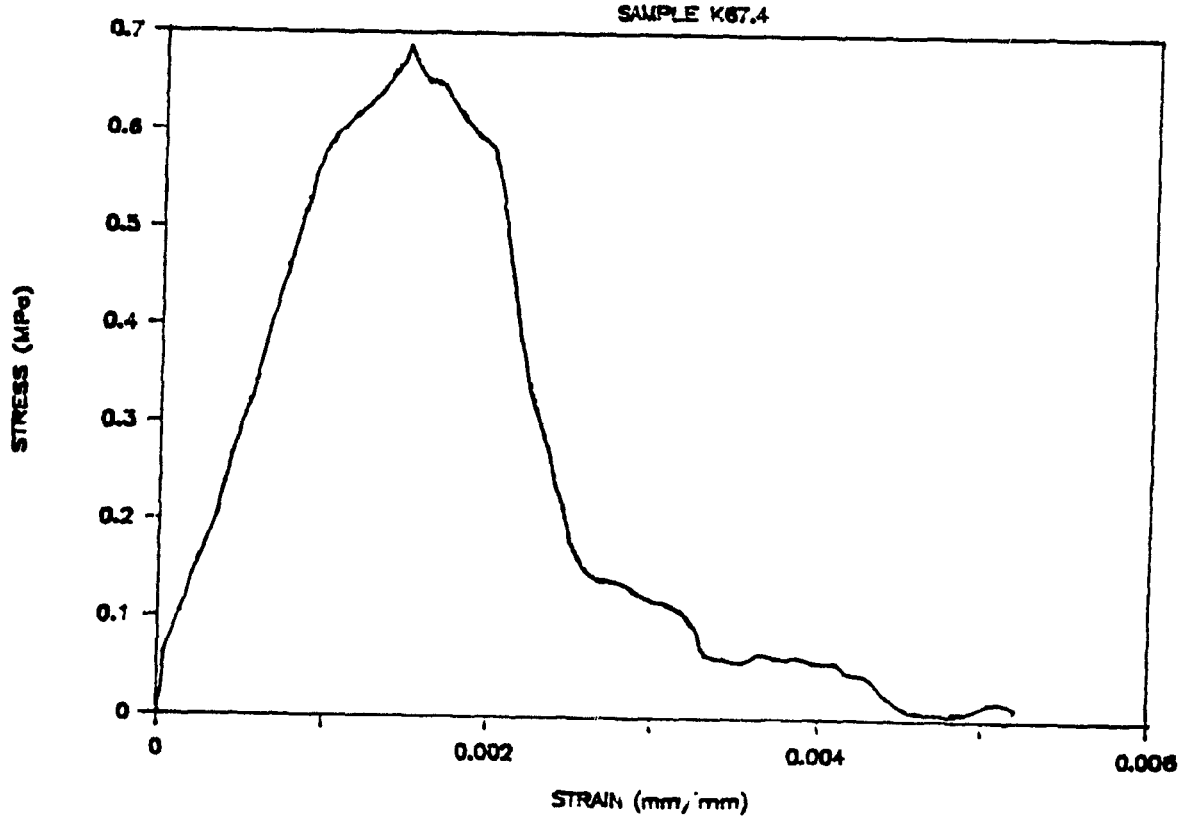

KIENA

SAMPLE K67.5

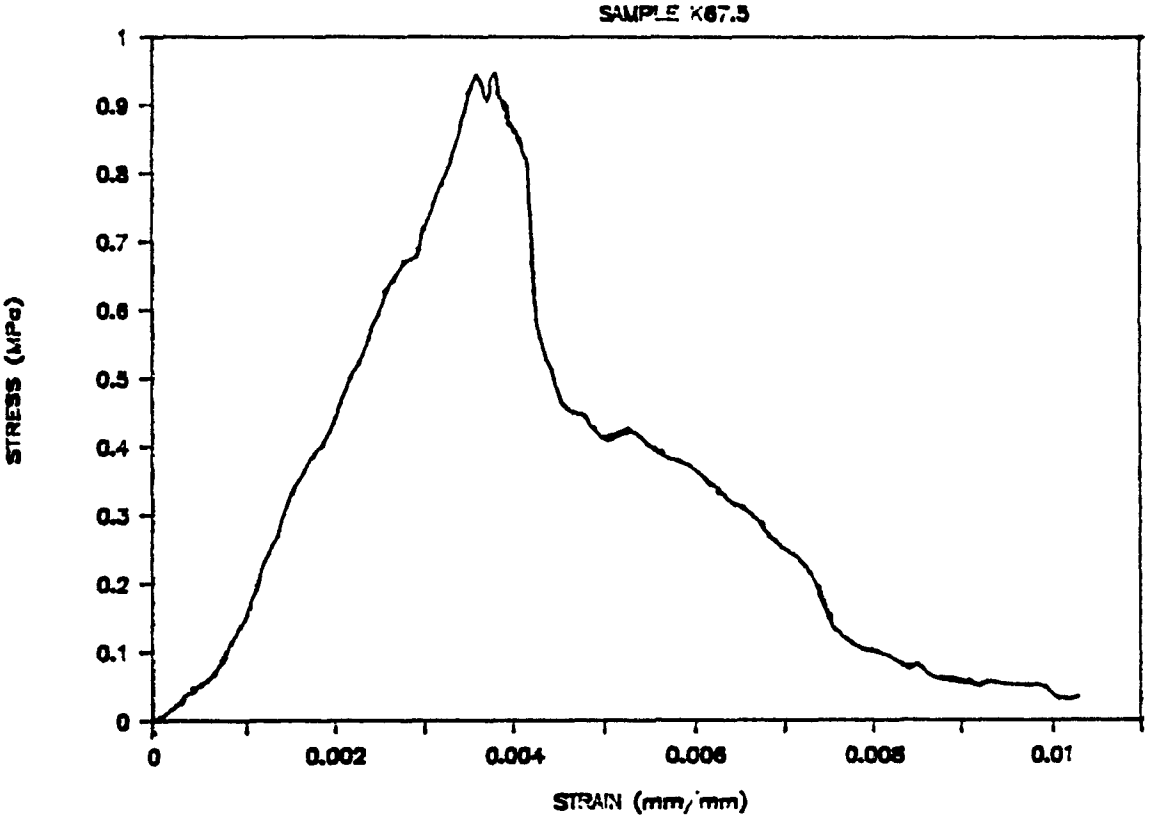

KIENA

SAMPLE K67.6

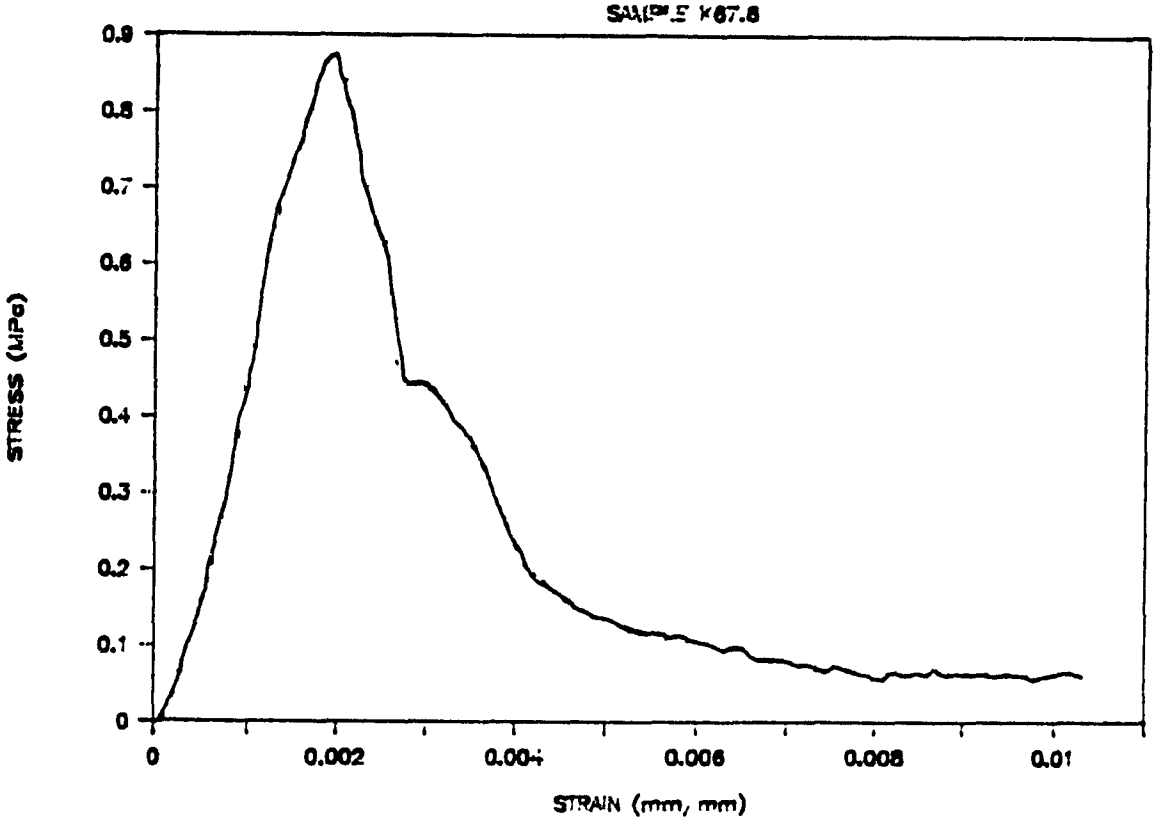

KIENA

SAMPLE K87.7

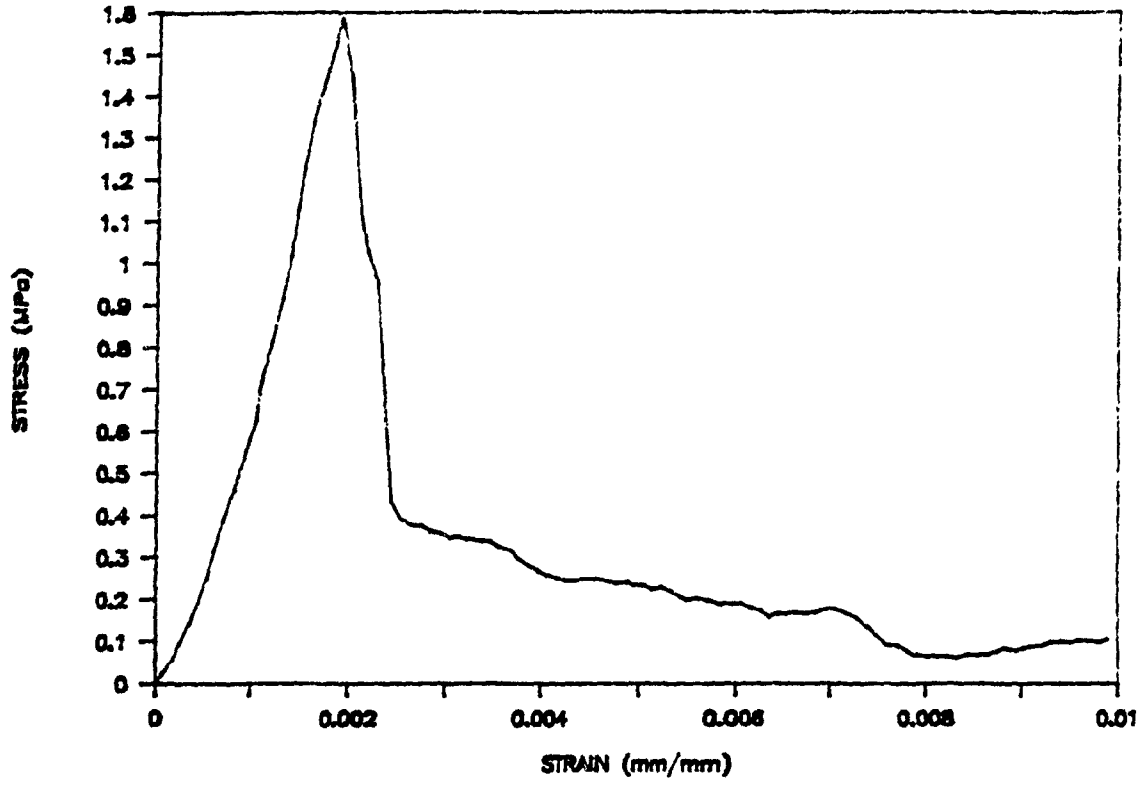

KIENA

SAMPLE K87.8

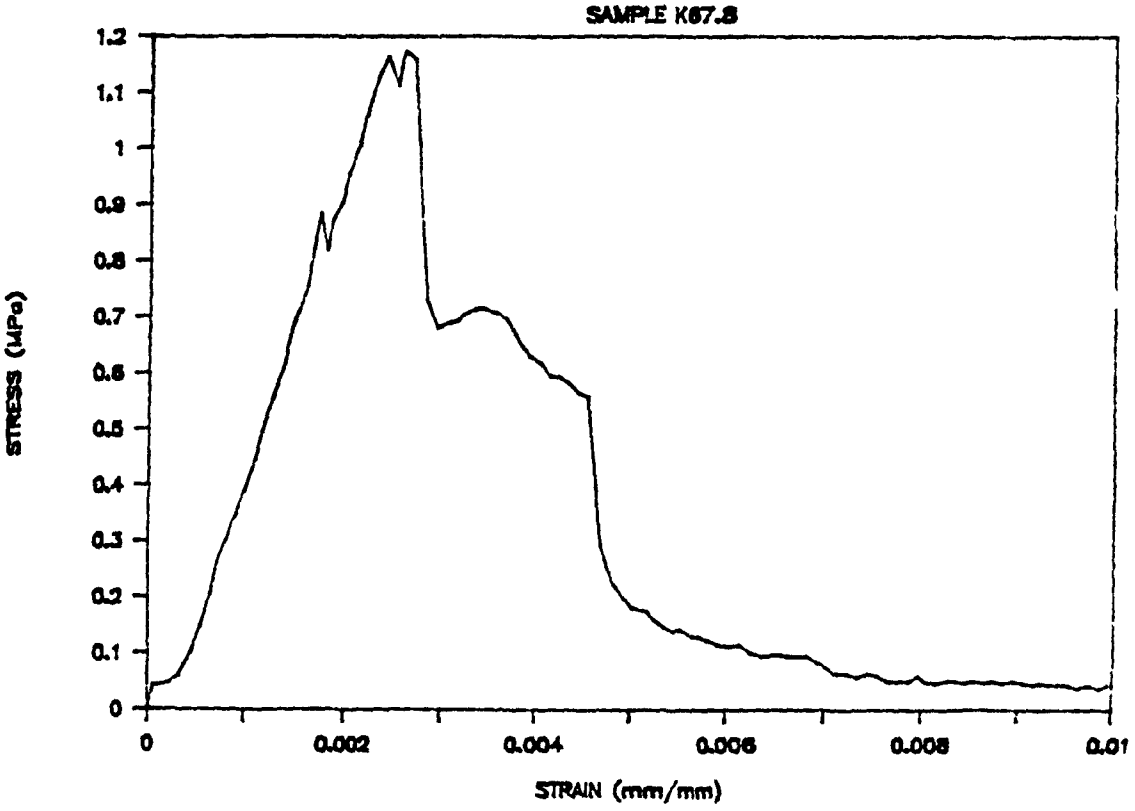

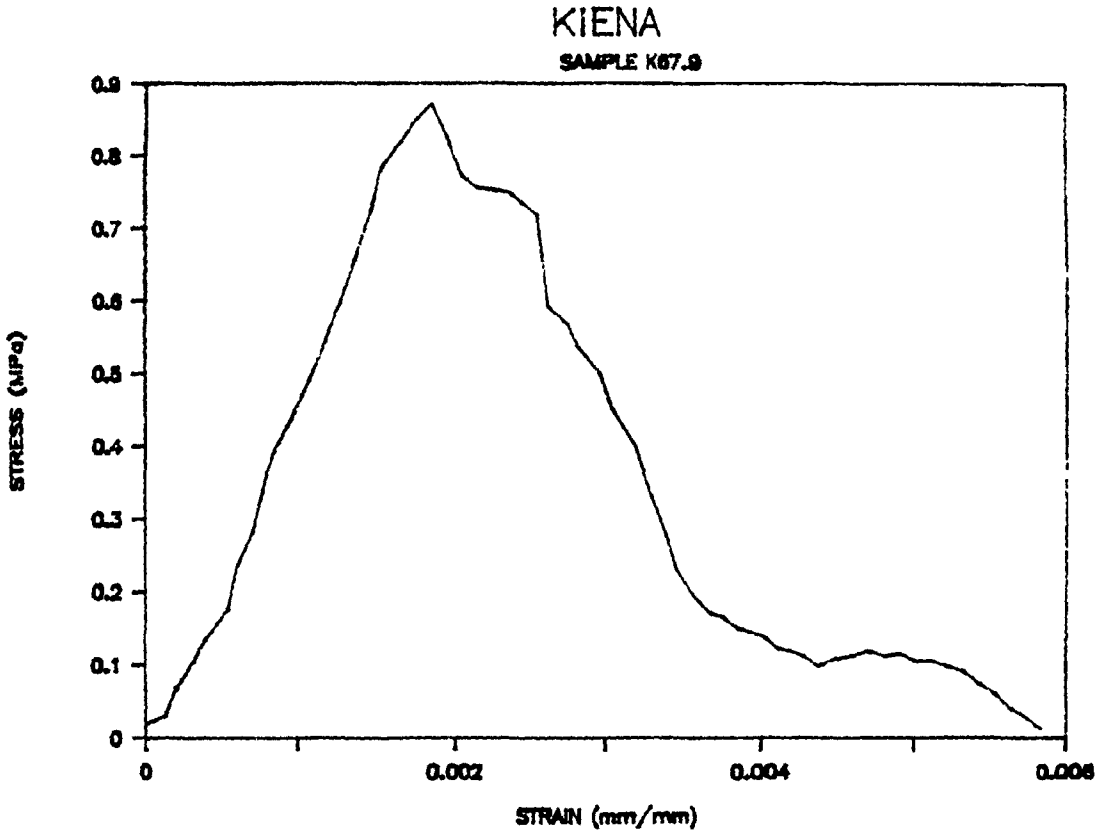
KIENA
SAMPLE K87.9
STRESS (MPa)
0.9
0.8
0.7
0.6
0.5
0.4
0.3
0.2
0.1
0
0
0.002
0.004
0.006
STRAIN (mm/mm)

LAC MATAGAMI

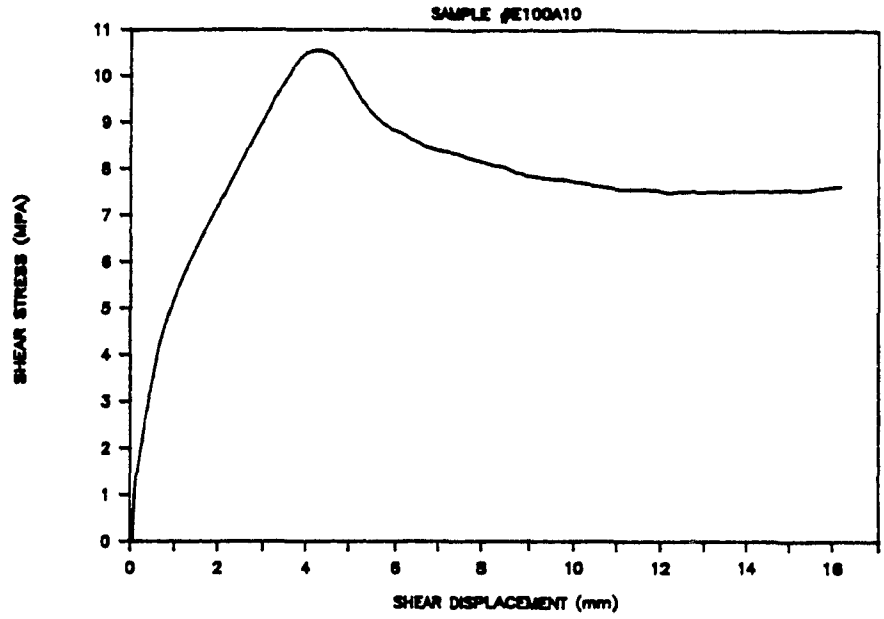

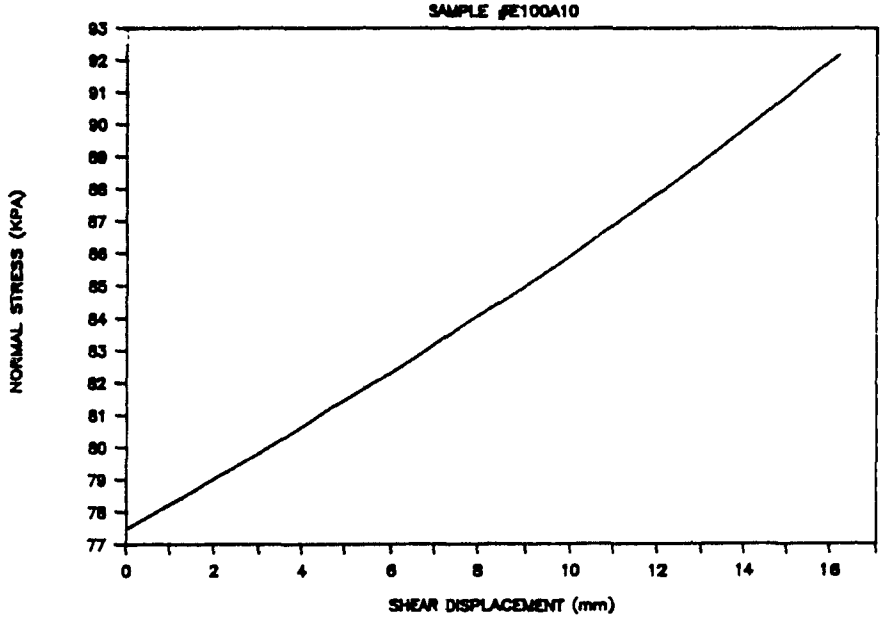

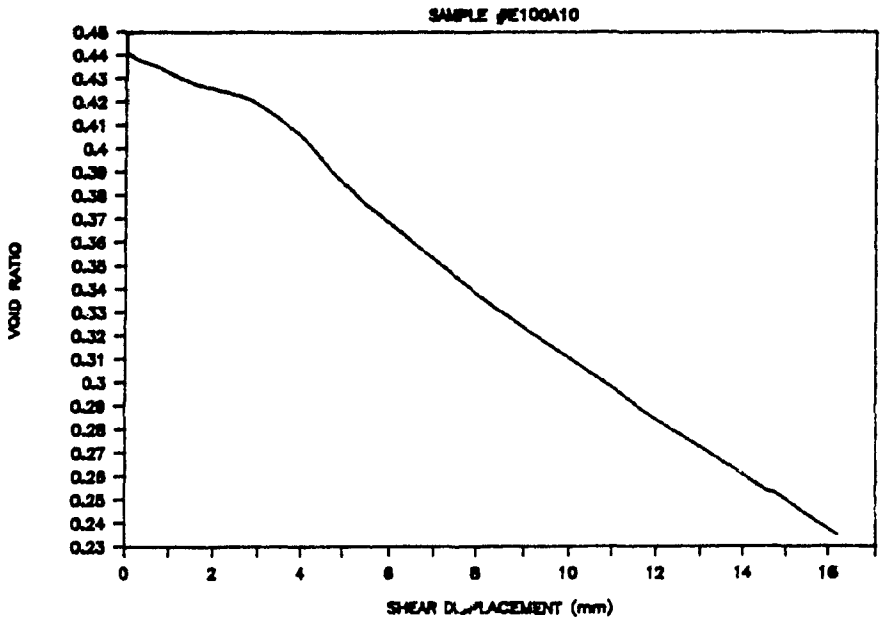

LAC MATAGAMI

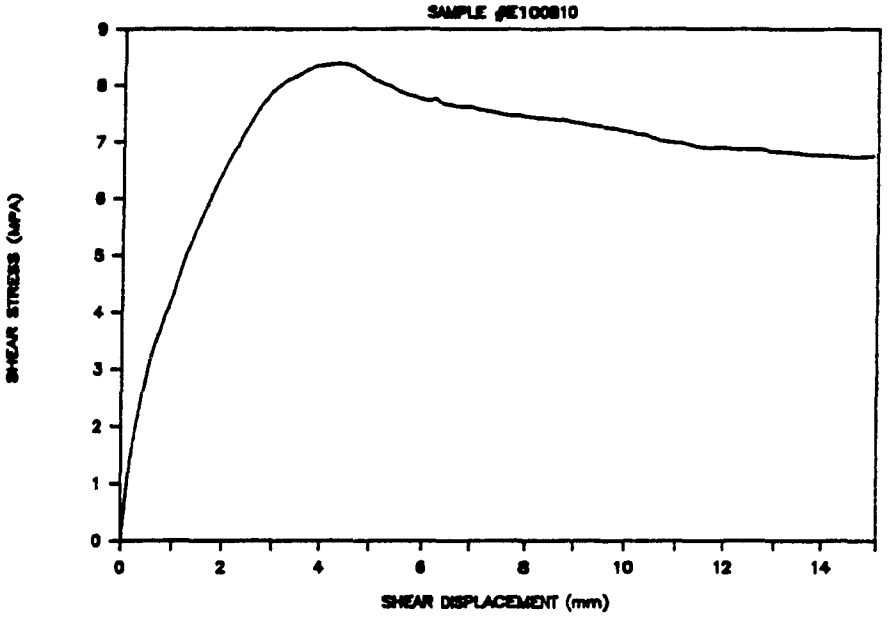

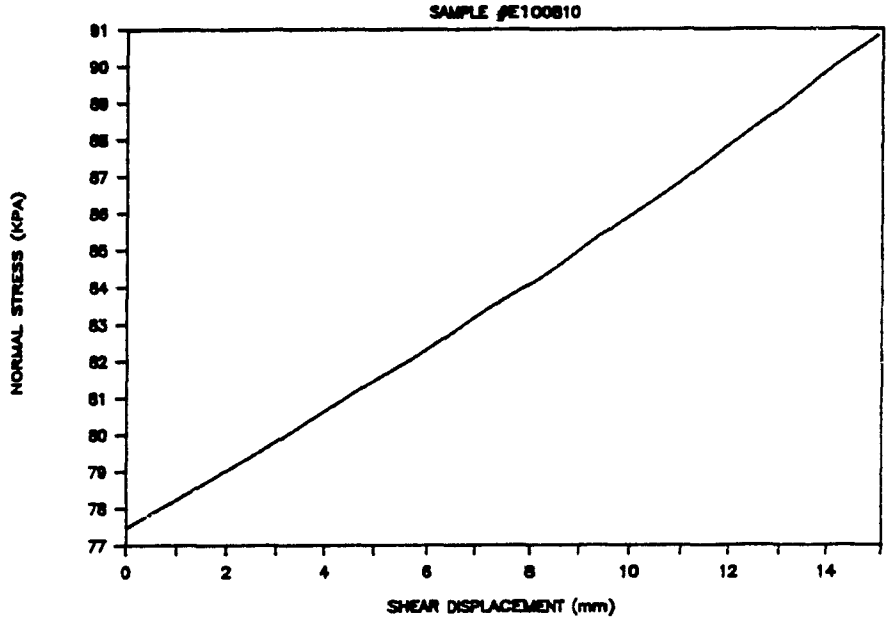

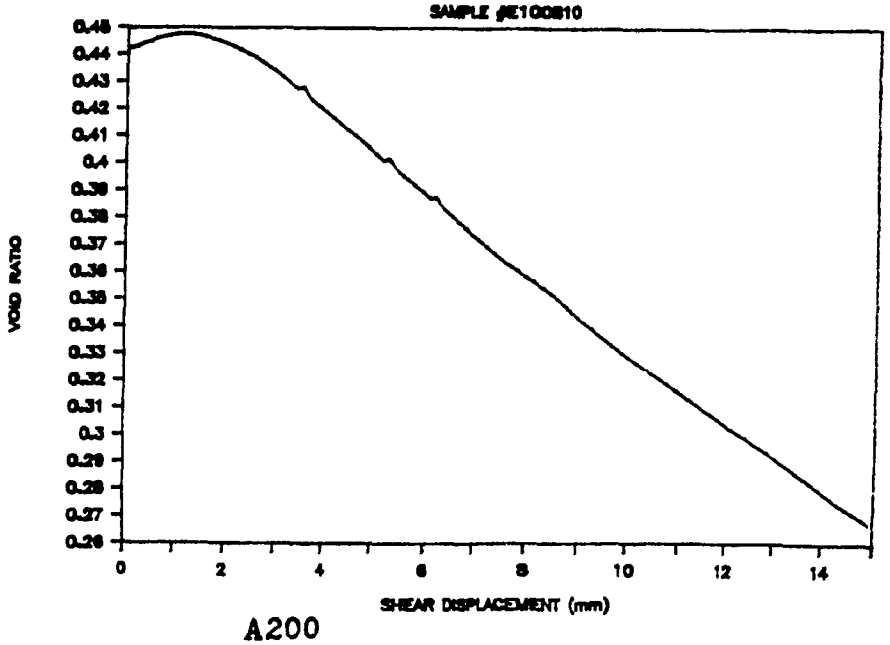

LAC MATAGAMI

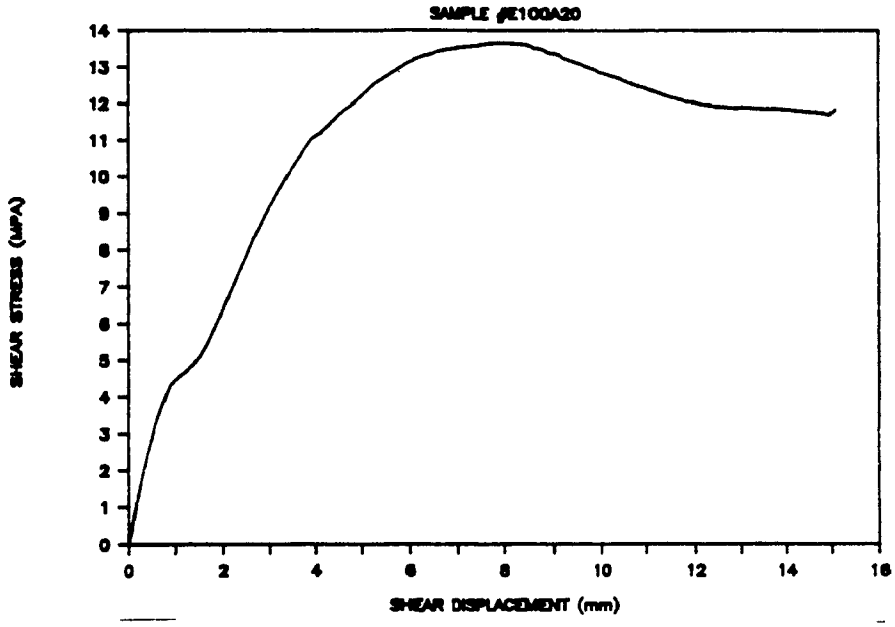

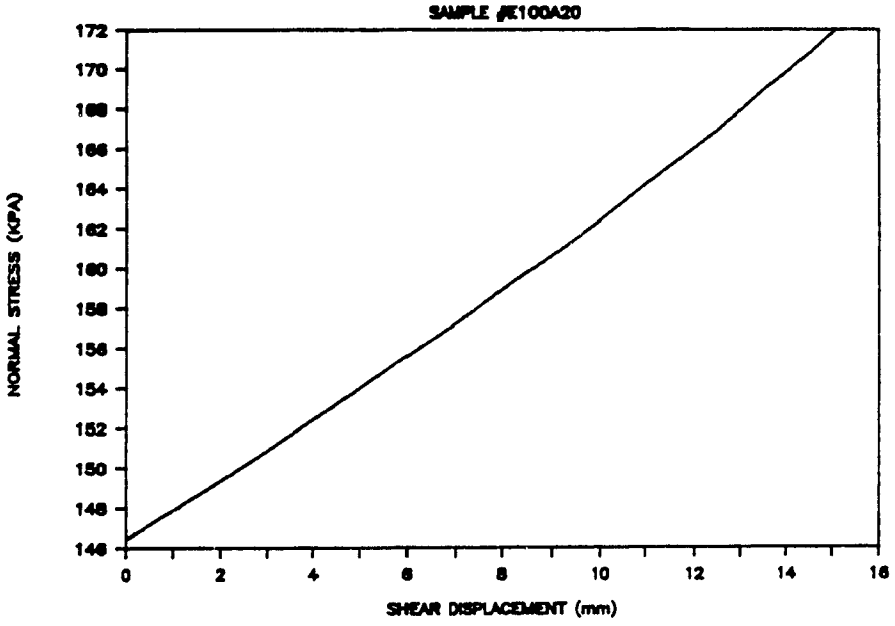

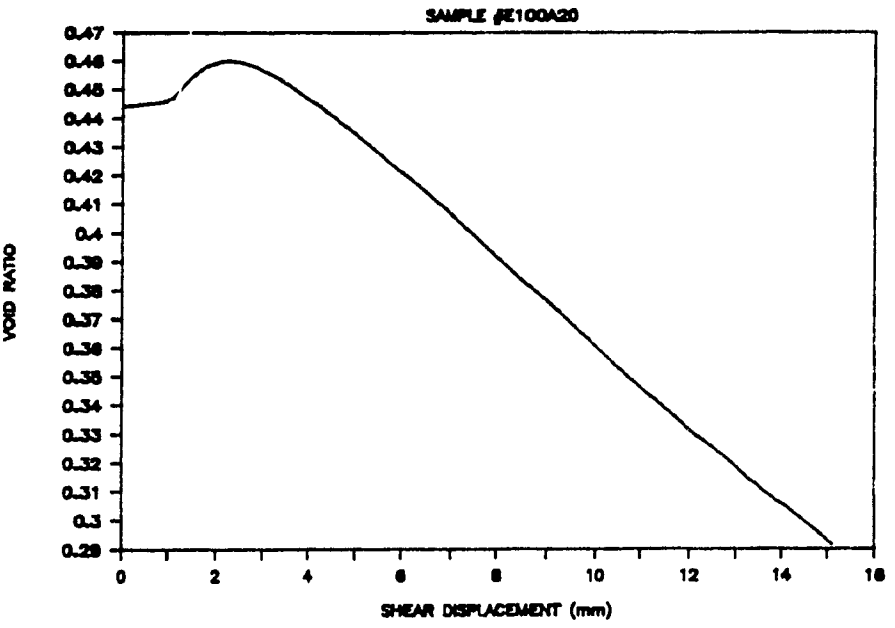

LAC MATAGAMI

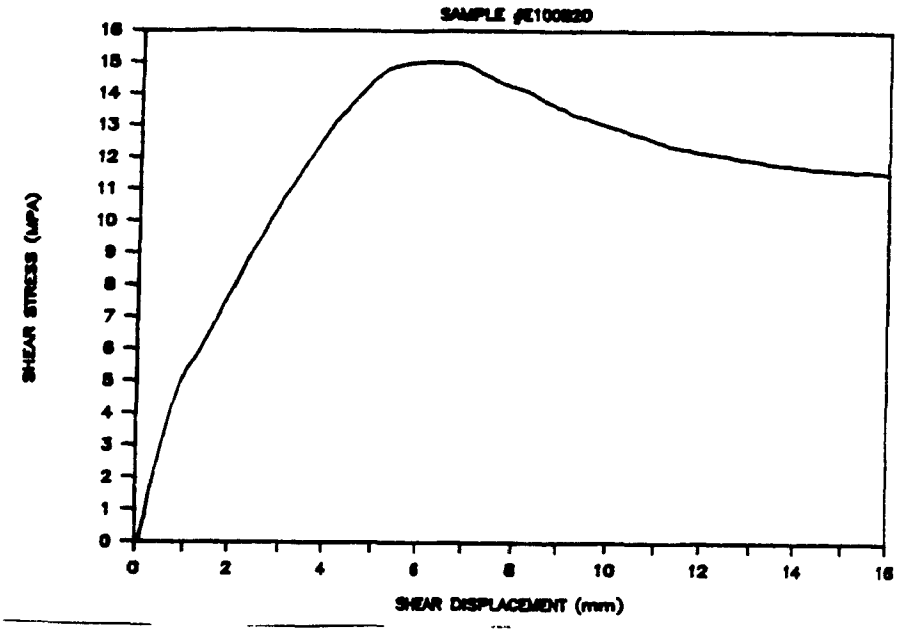

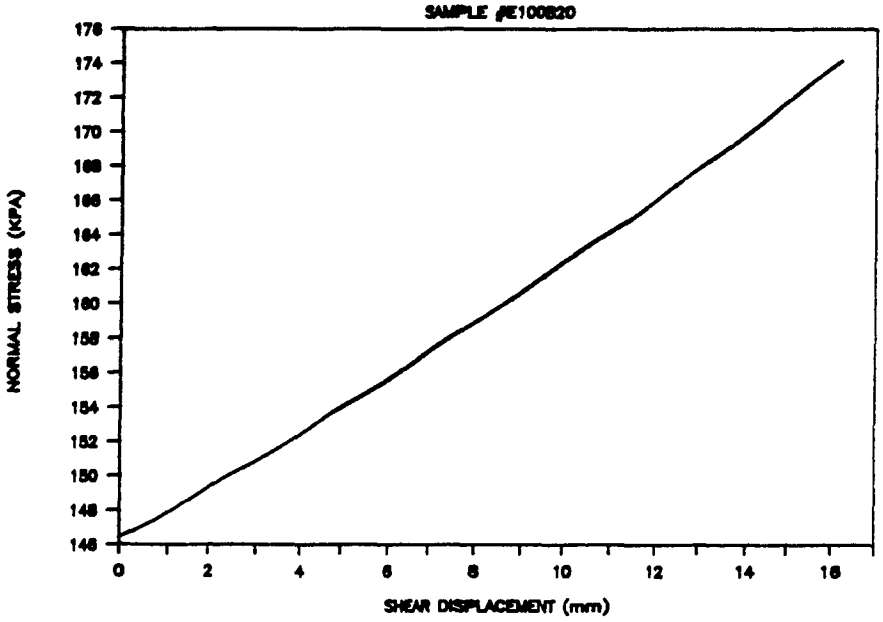

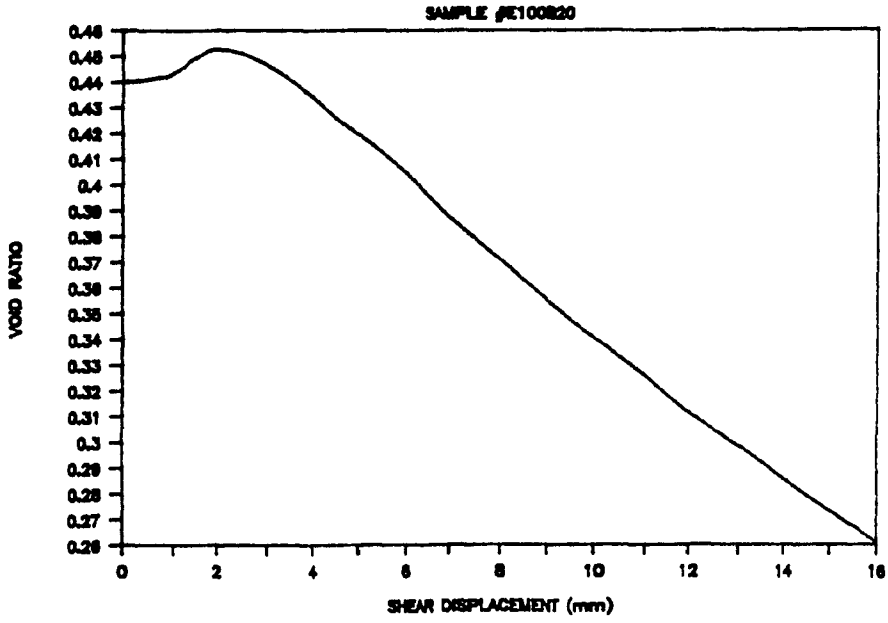

LAC MATAGAMI

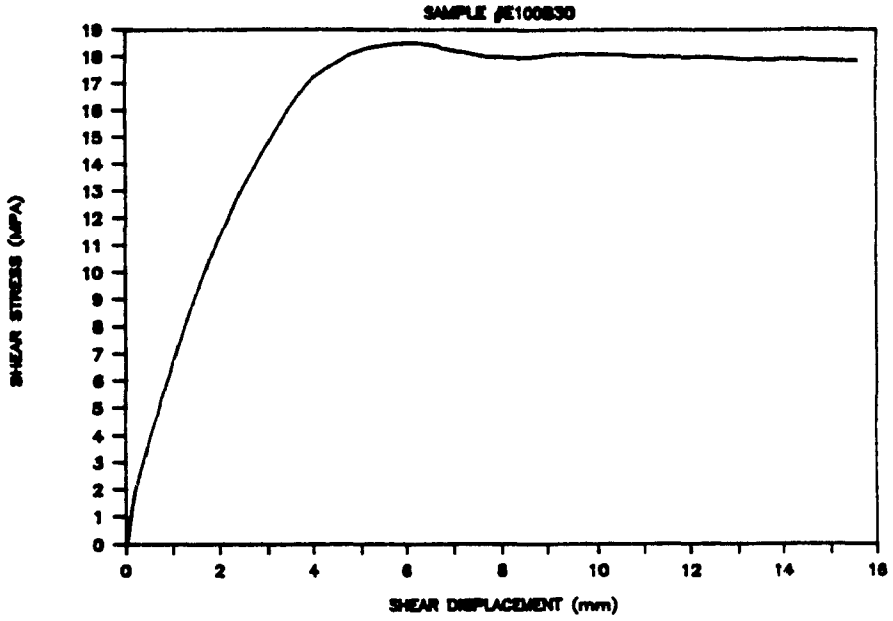

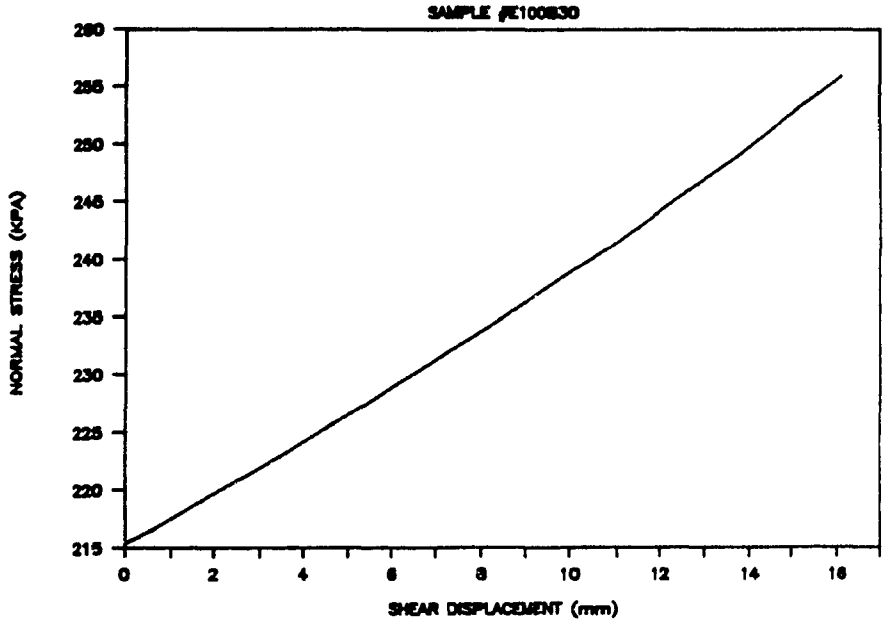

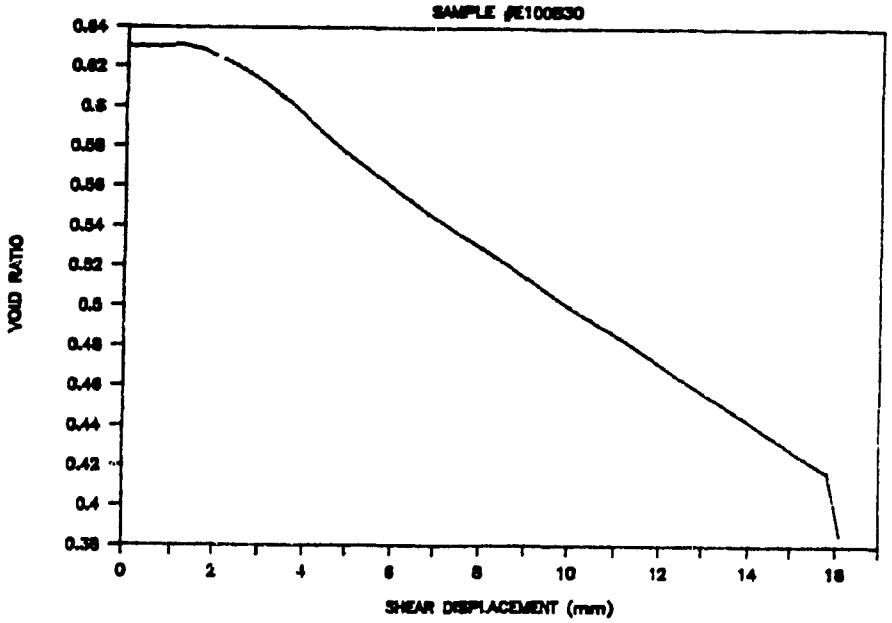

LAC MATAGAMI

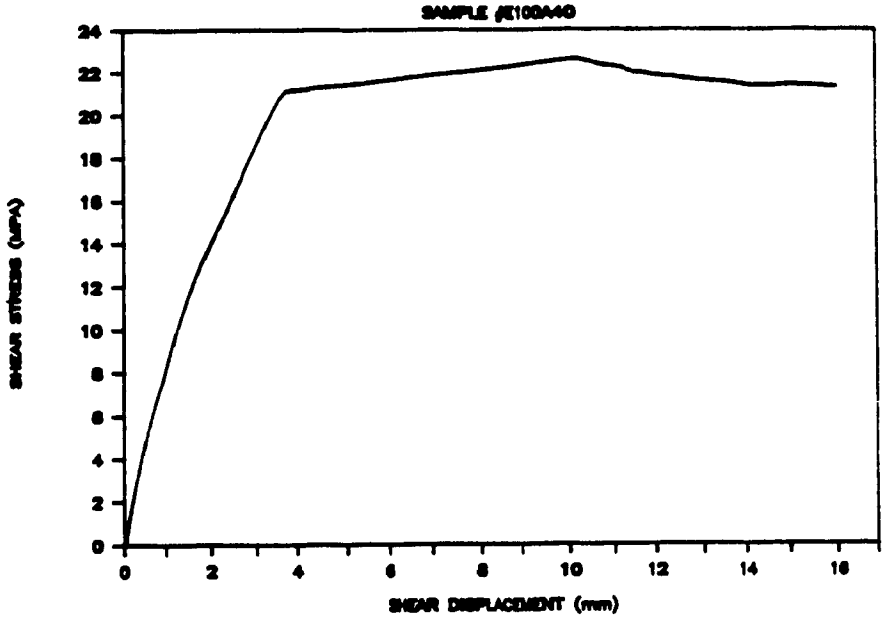

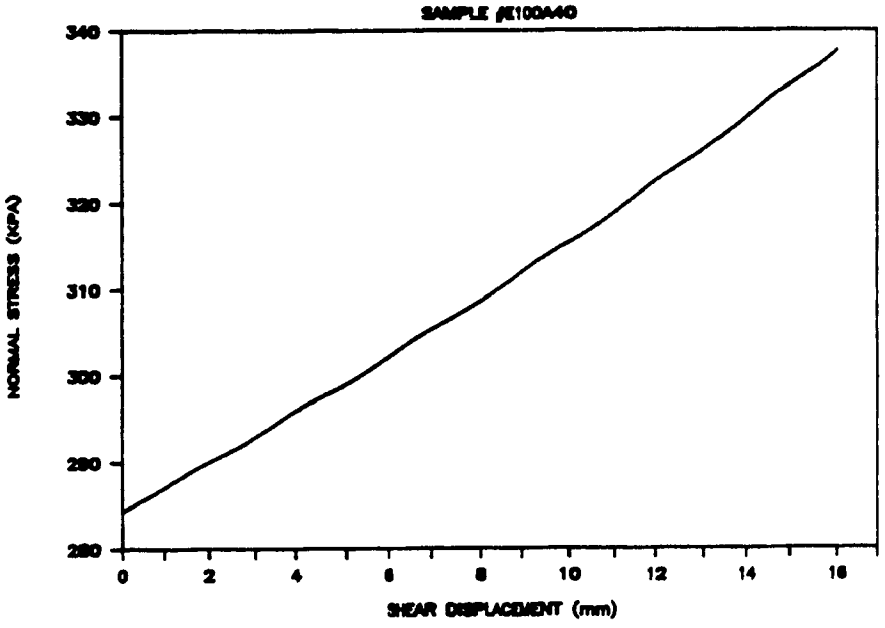

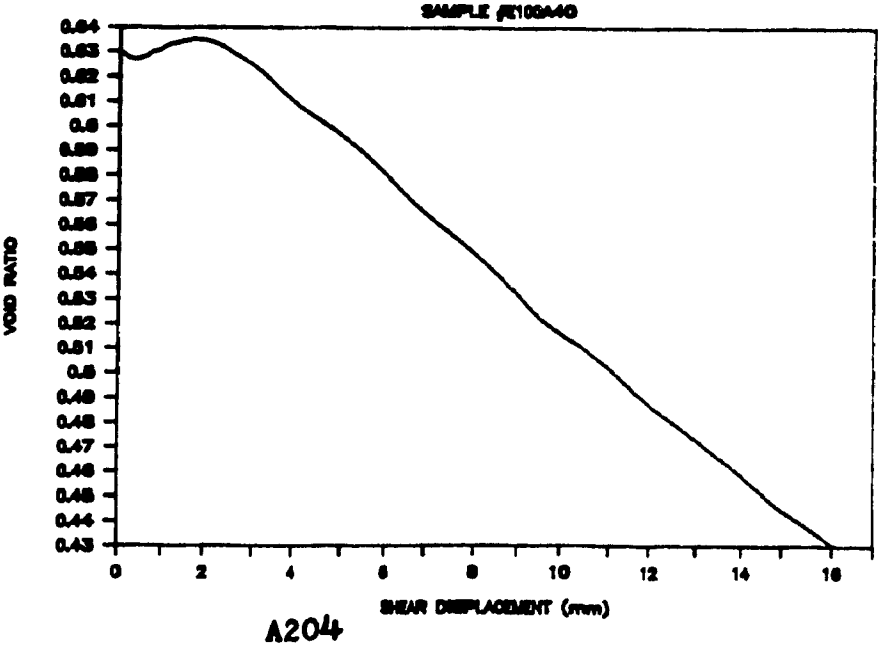

LAC MATAGAMI

SAMPLE gA100A10

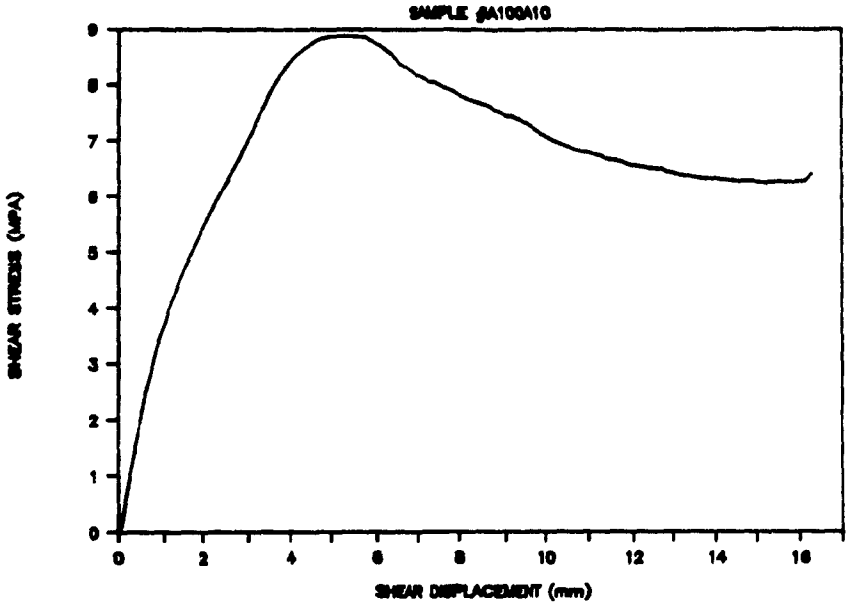

SAMPLE gA100A10

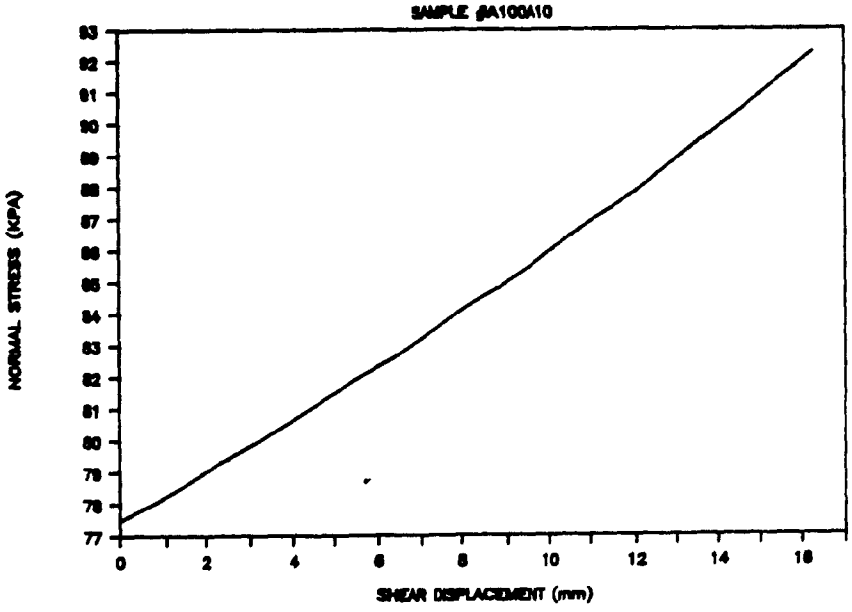

SAMPLE gA100A10

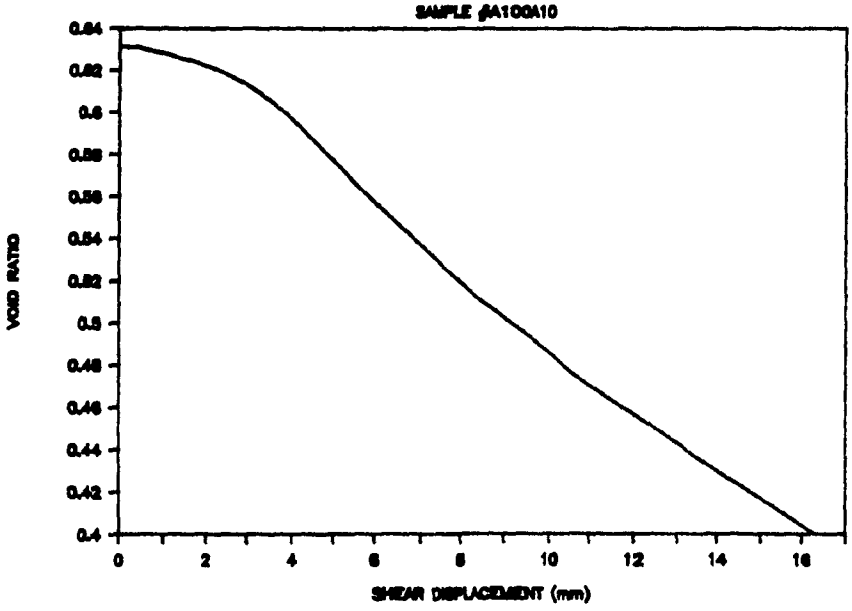

LAC MATAGAMI

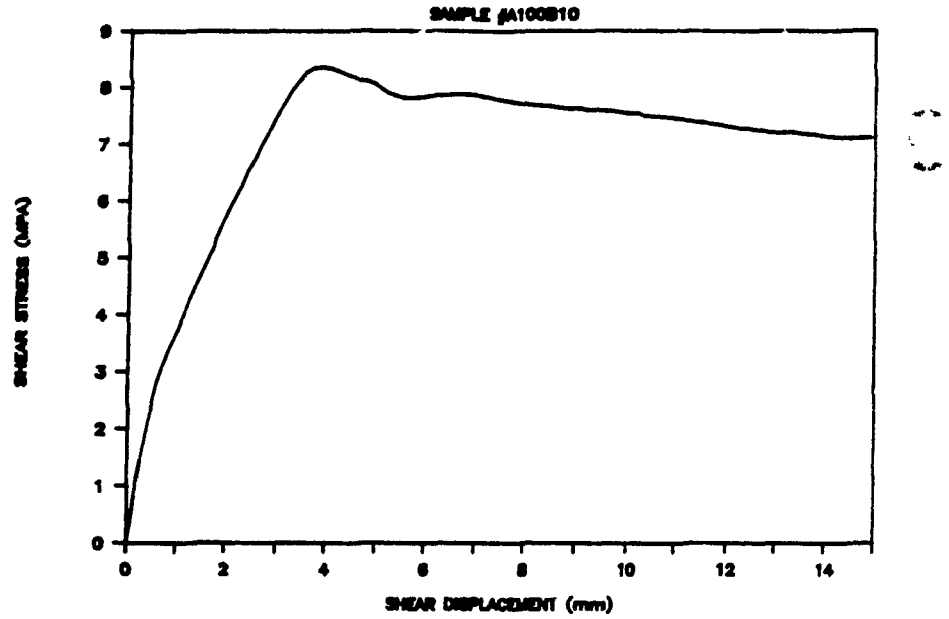

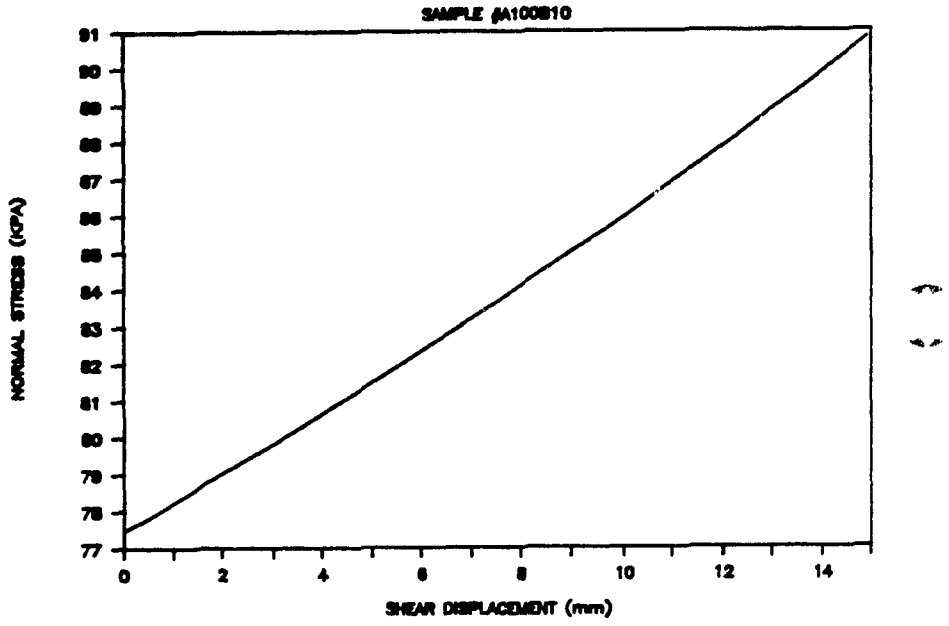

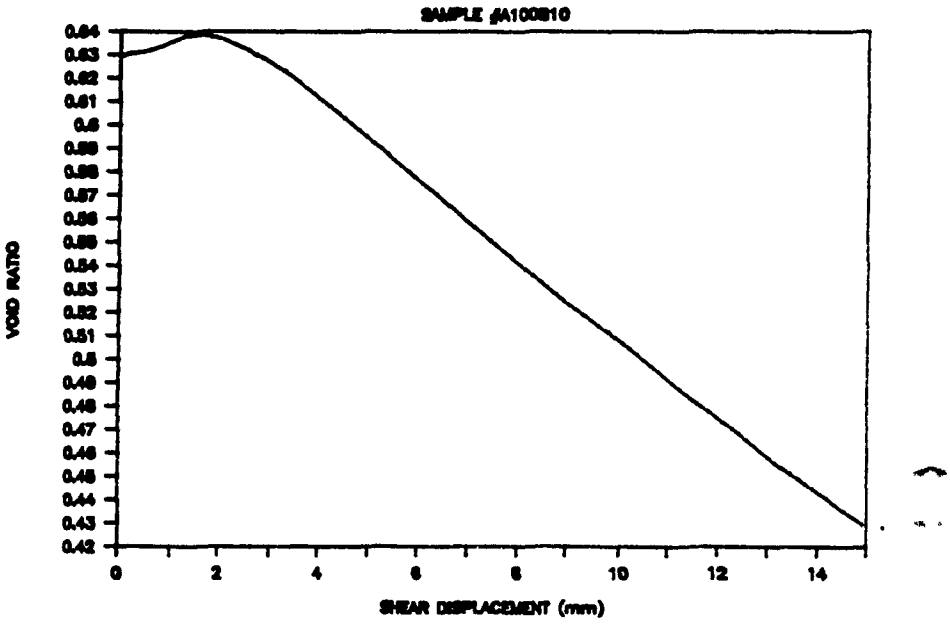

LAC MATAGAMI

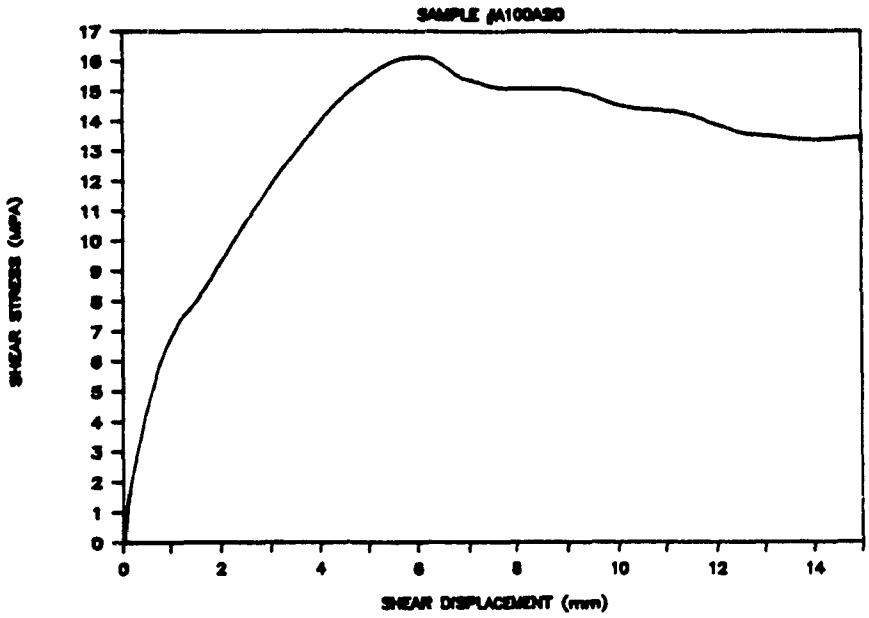

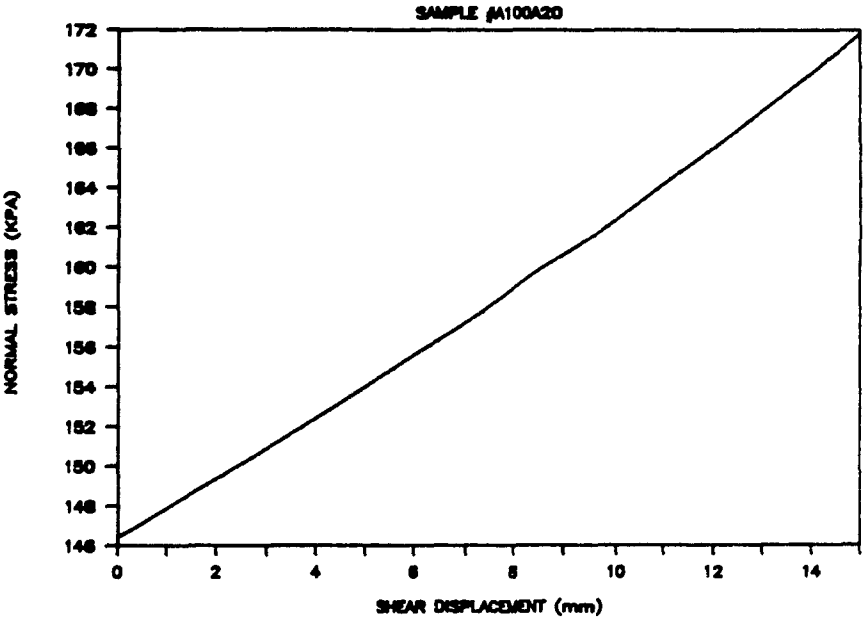

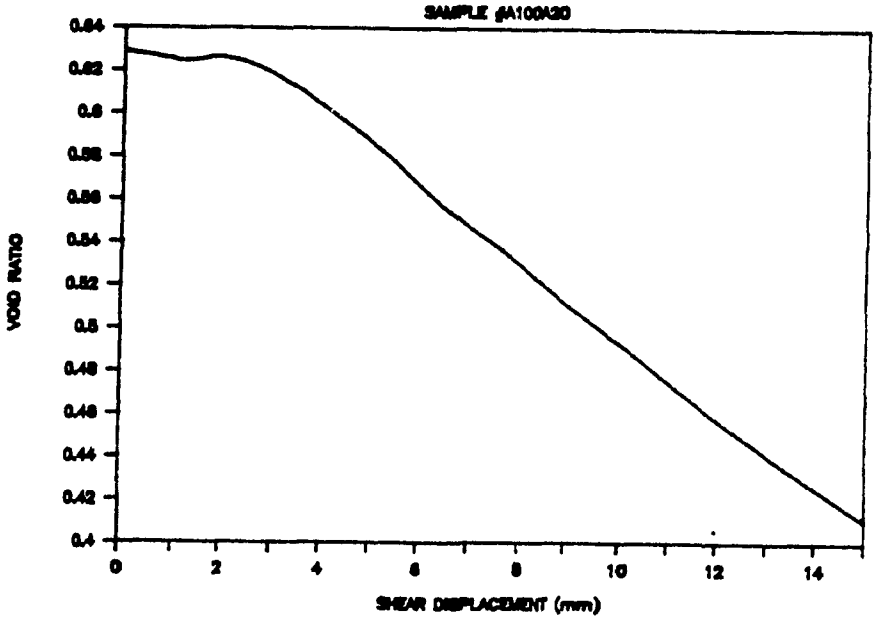

LAC MATAGAMI

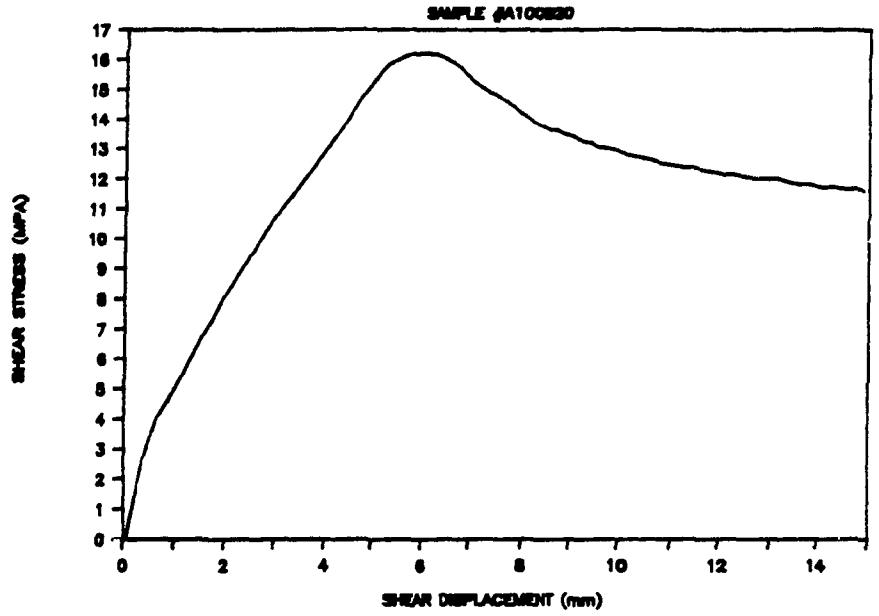

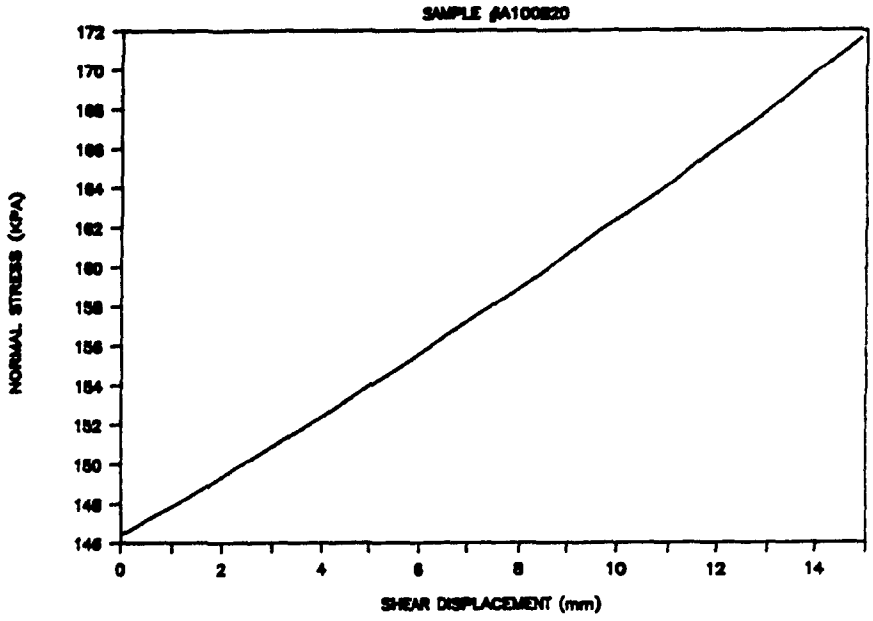

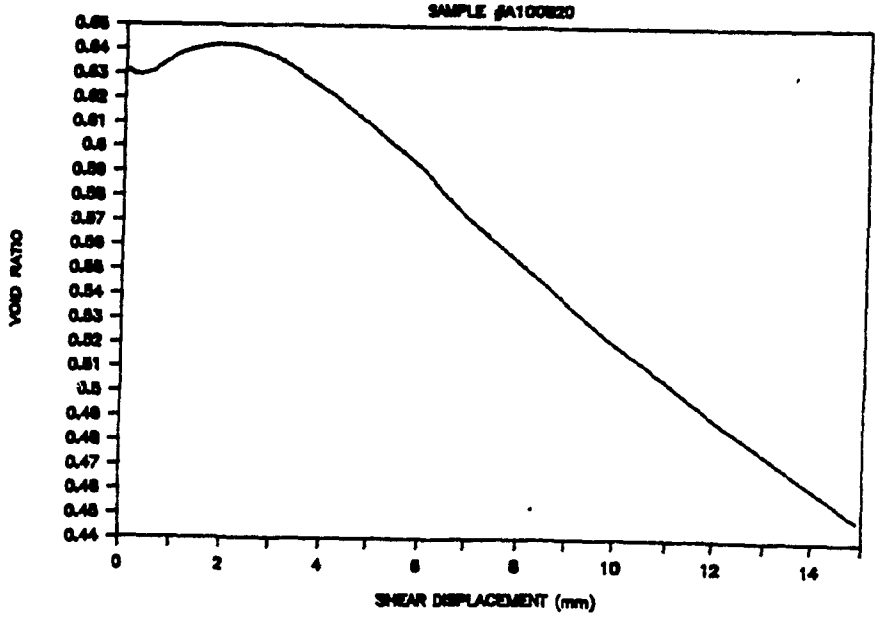

LAC MATAGAMI

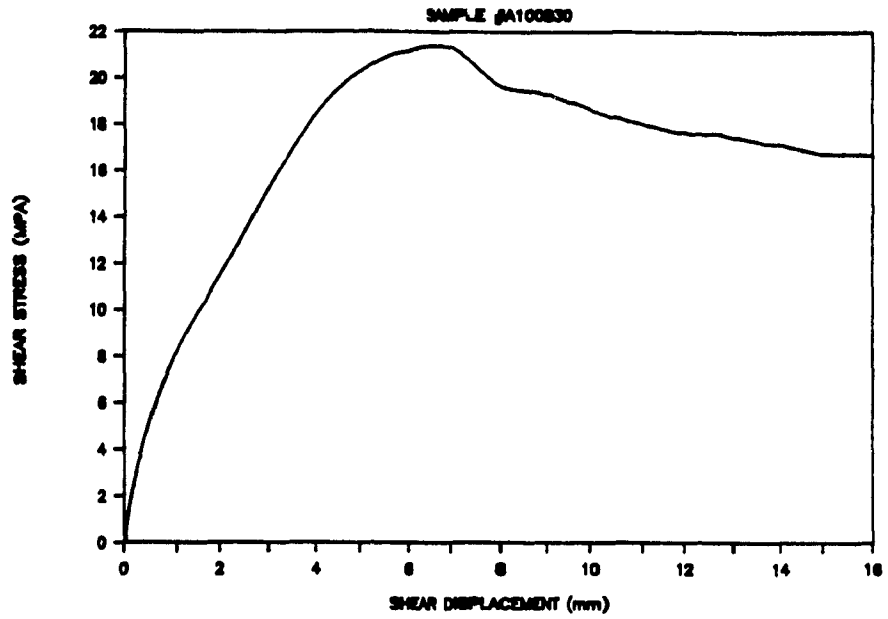

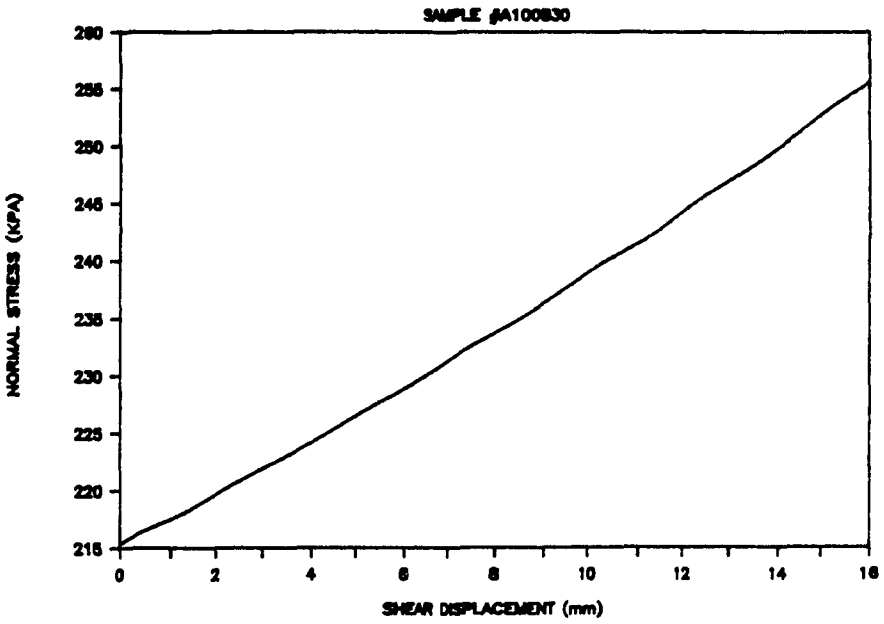

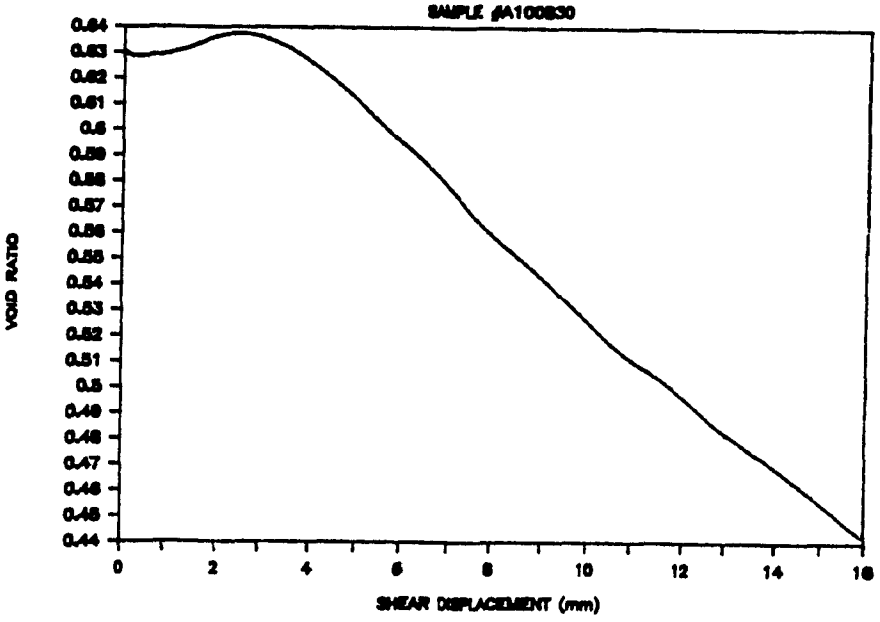

LAC MATAGAMI

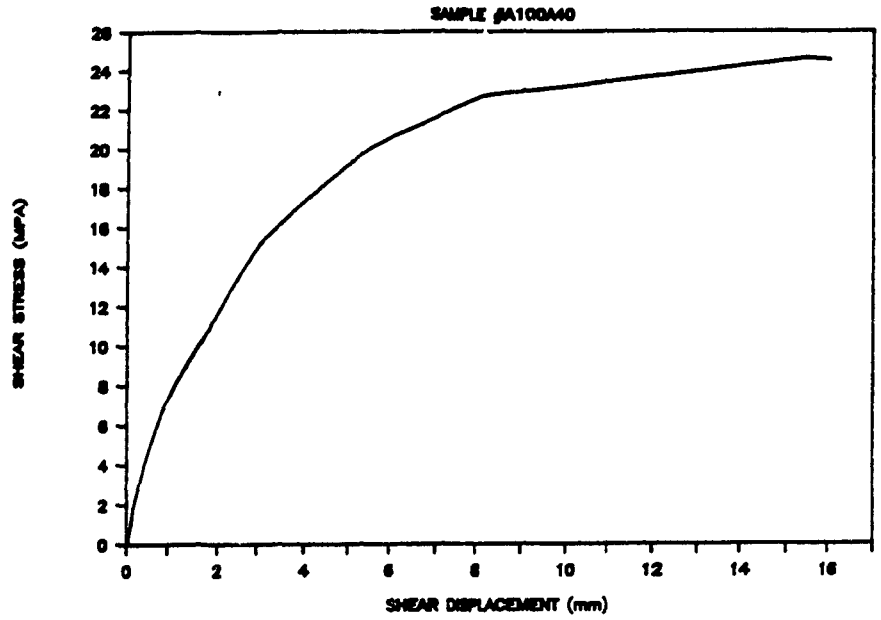

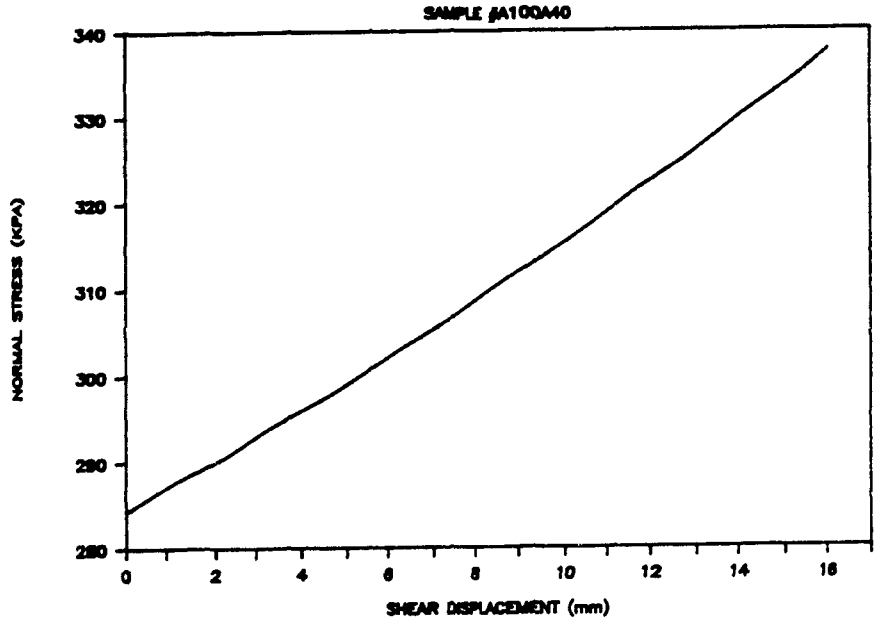

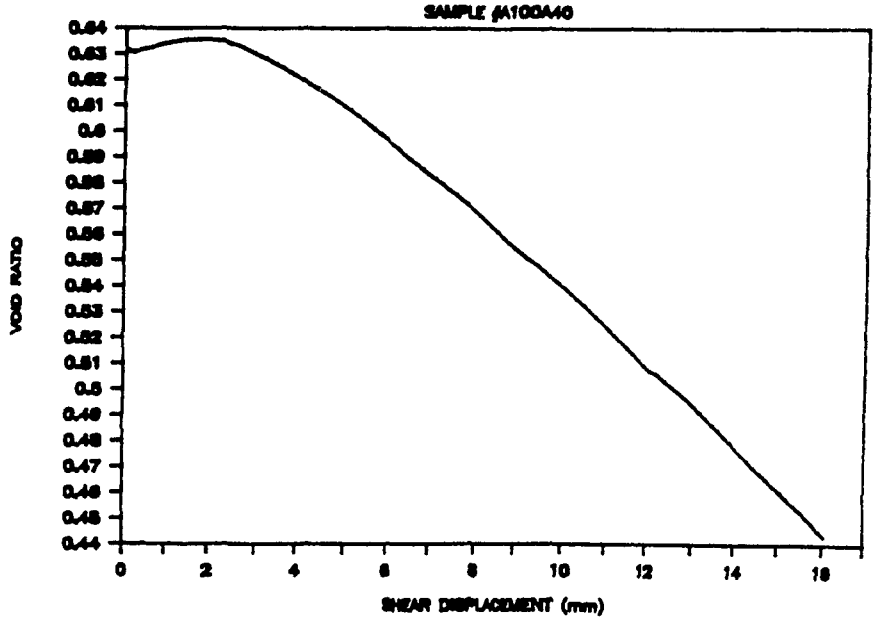

LAC MATAGAMI

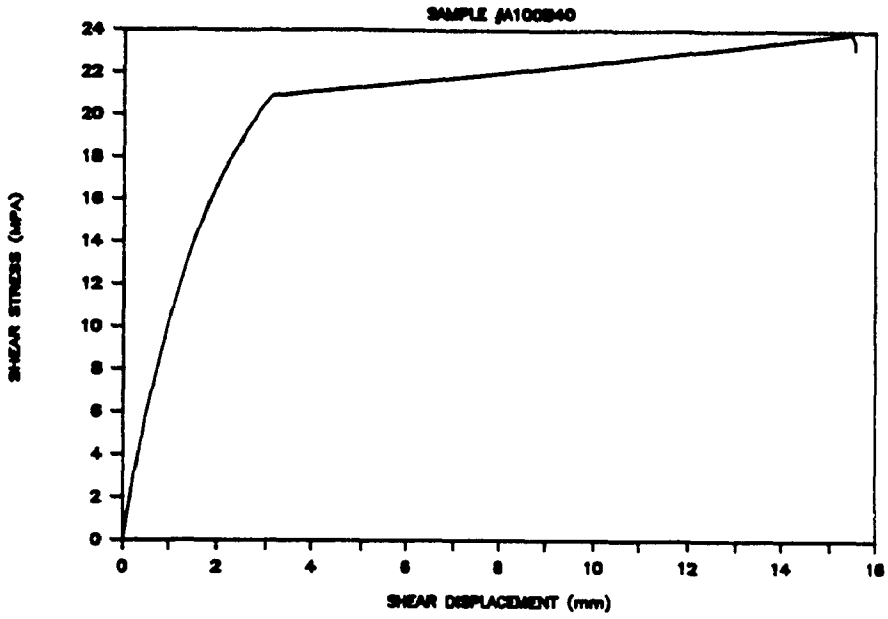

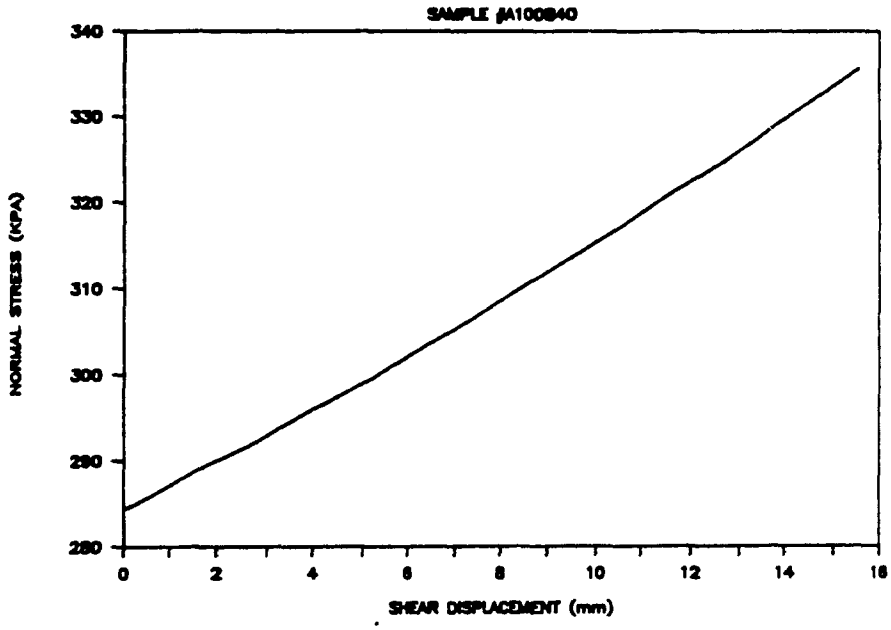

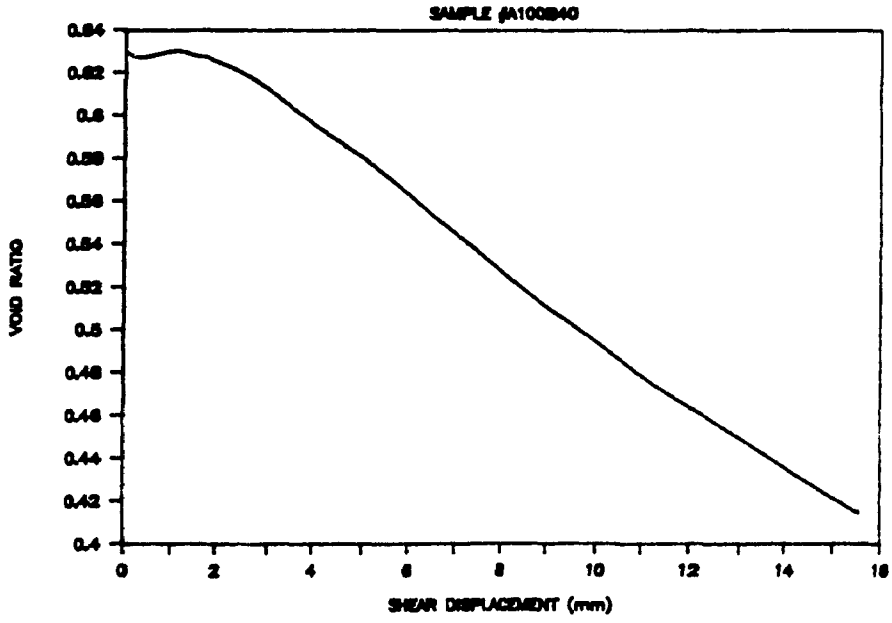

LAC MATAGAMI

SAMPLE #B100A10

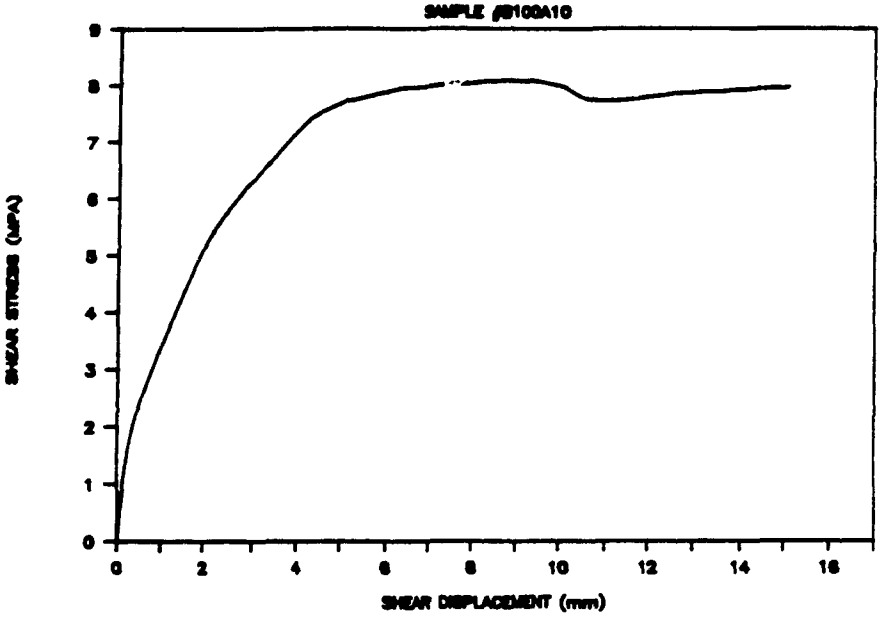

SAMPLE #B100A10

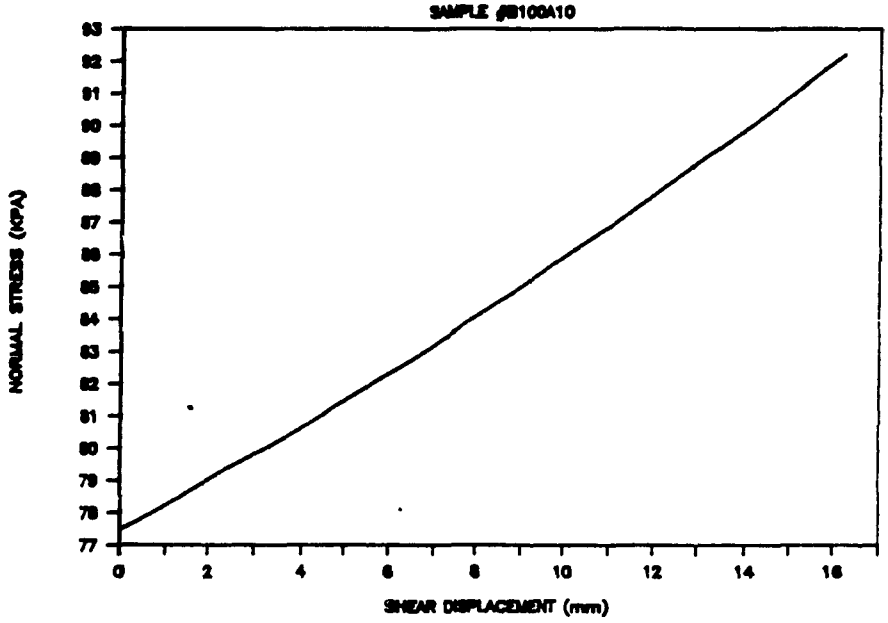

SAMPLE #B100A10

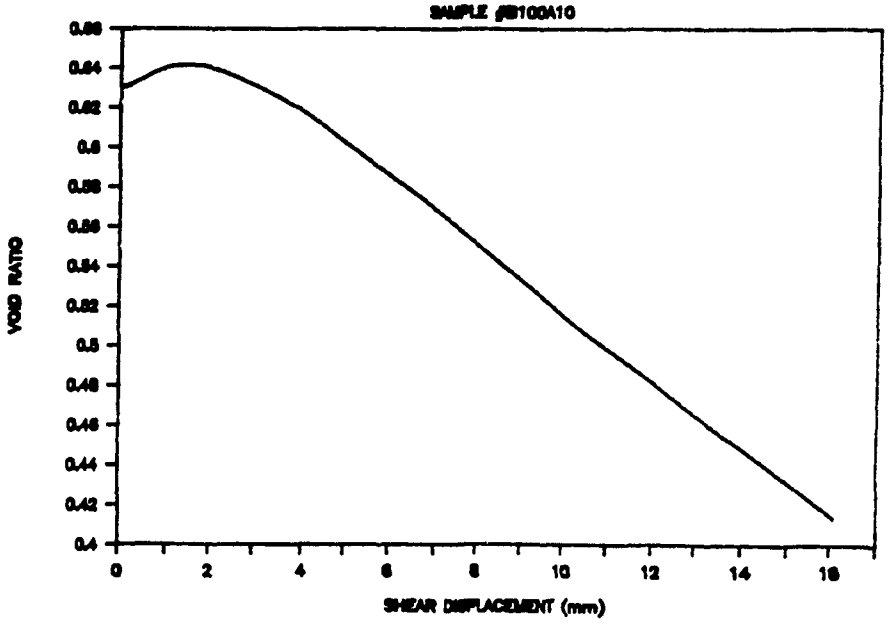

LAC MATAGAMI

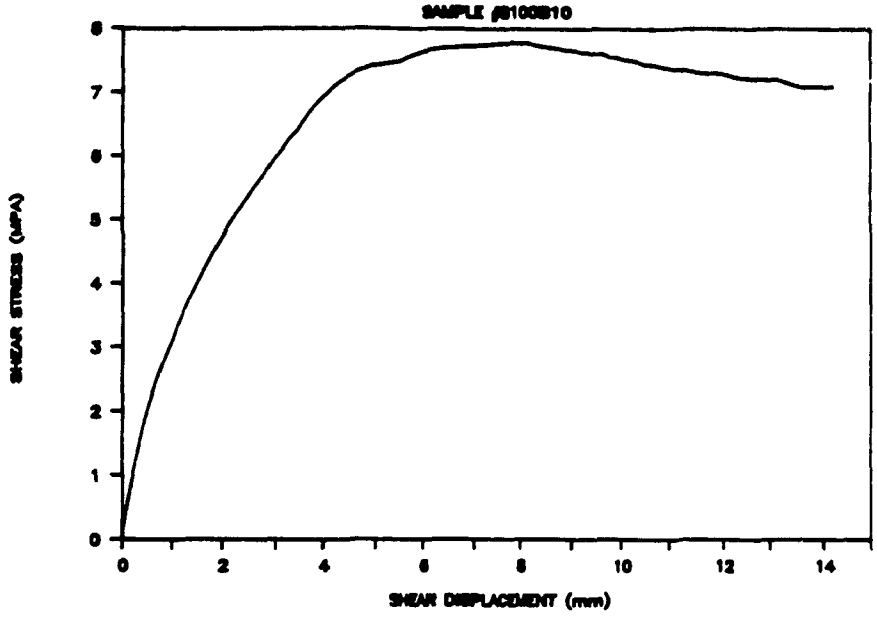

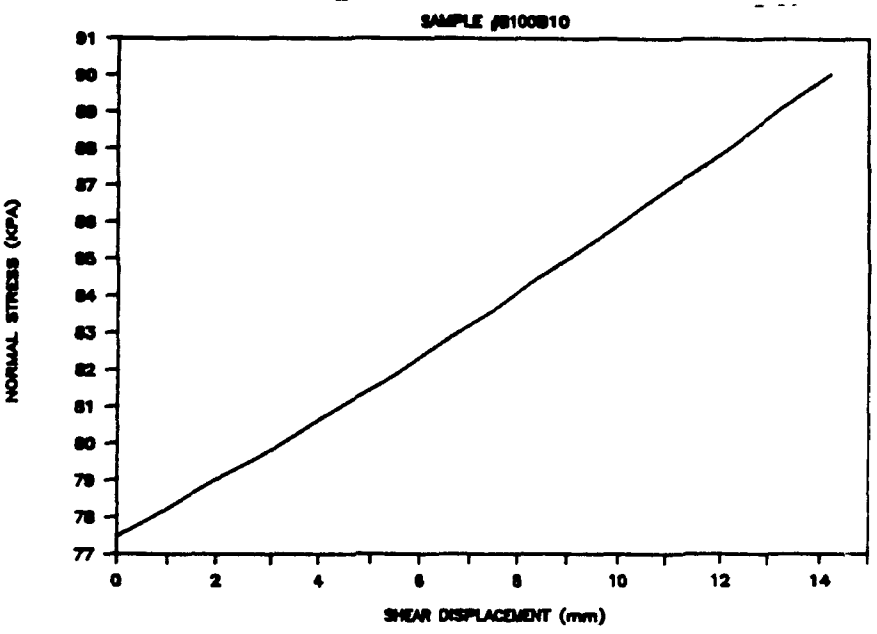

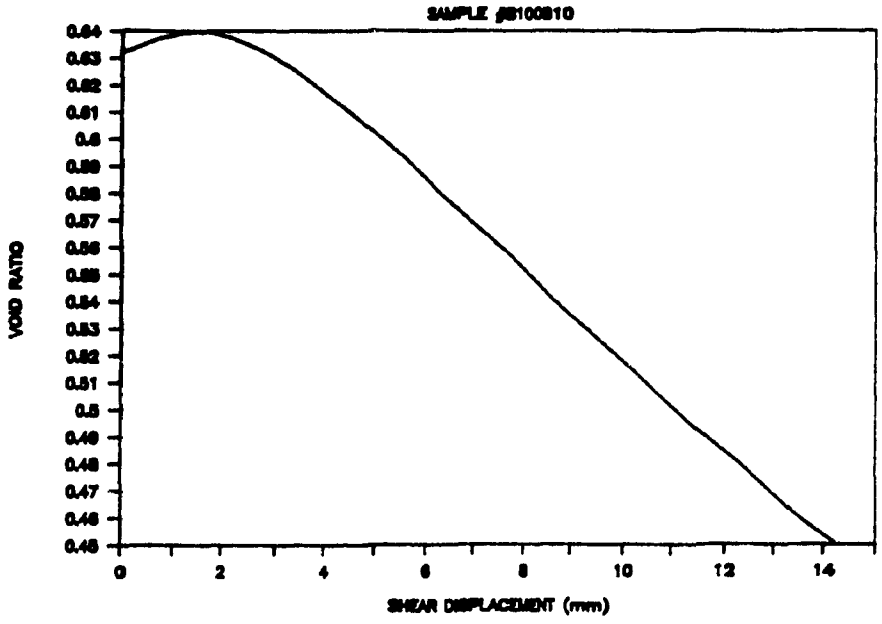

LAC MATAGAMI

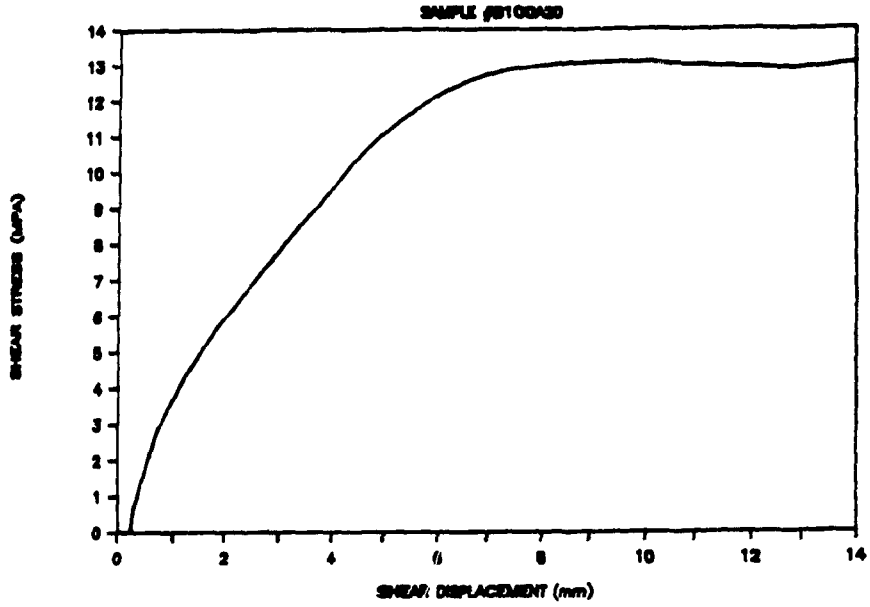

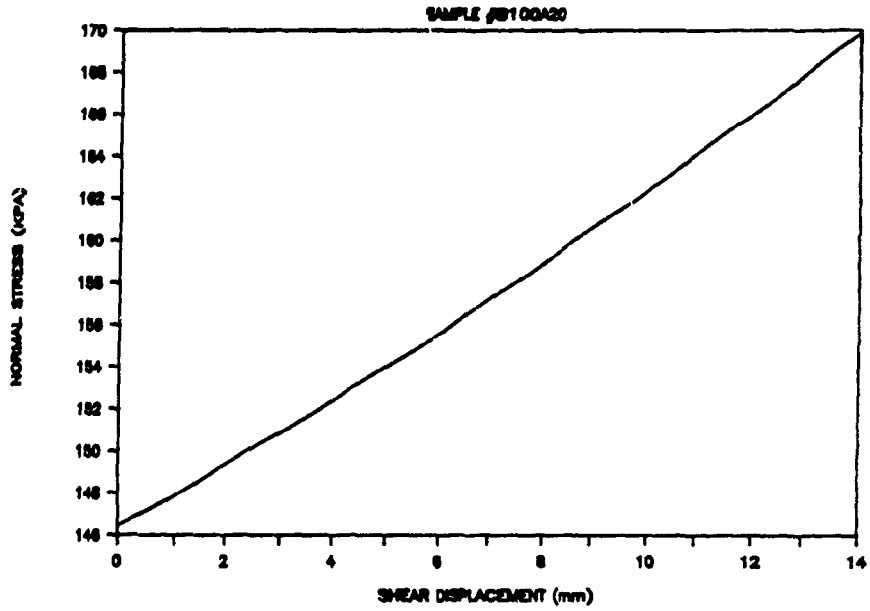

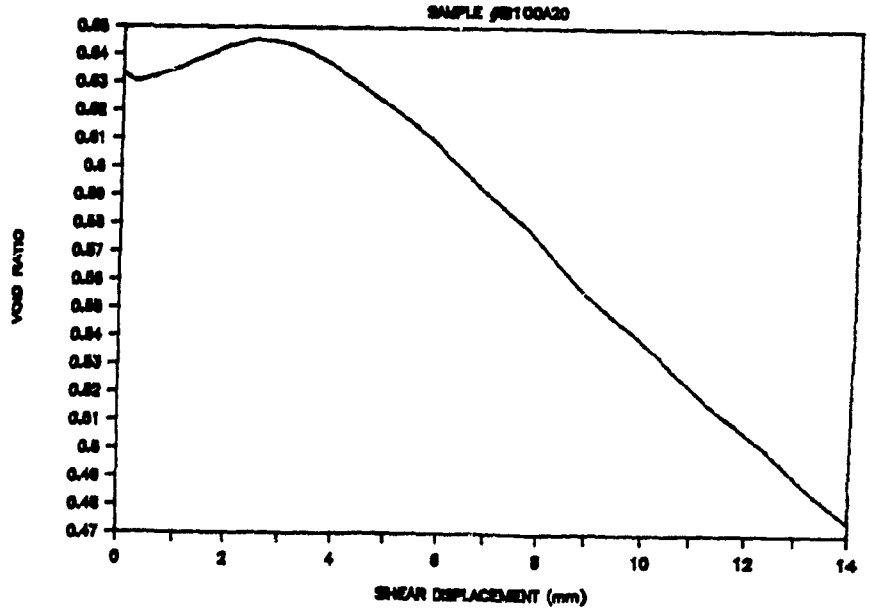

LAC MATAGAMI

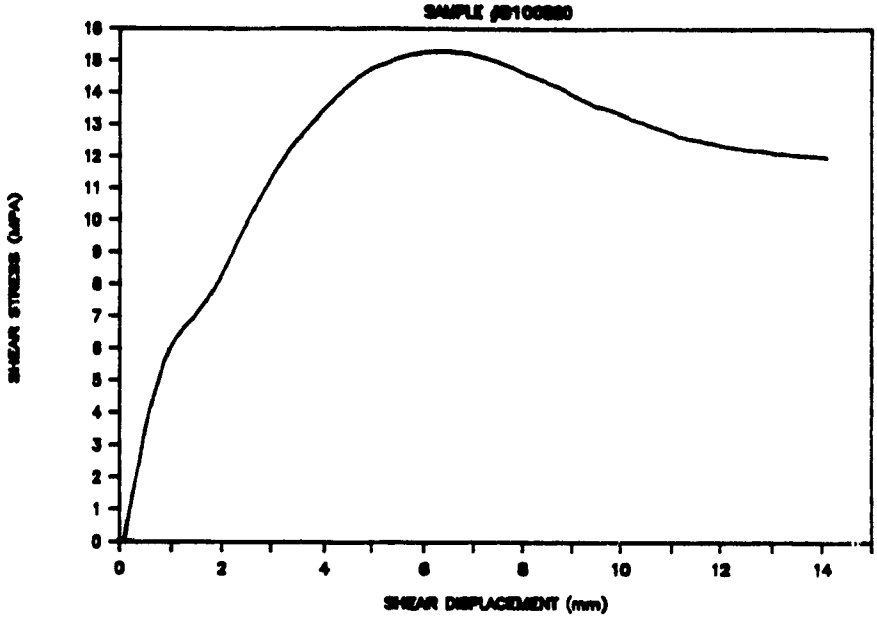

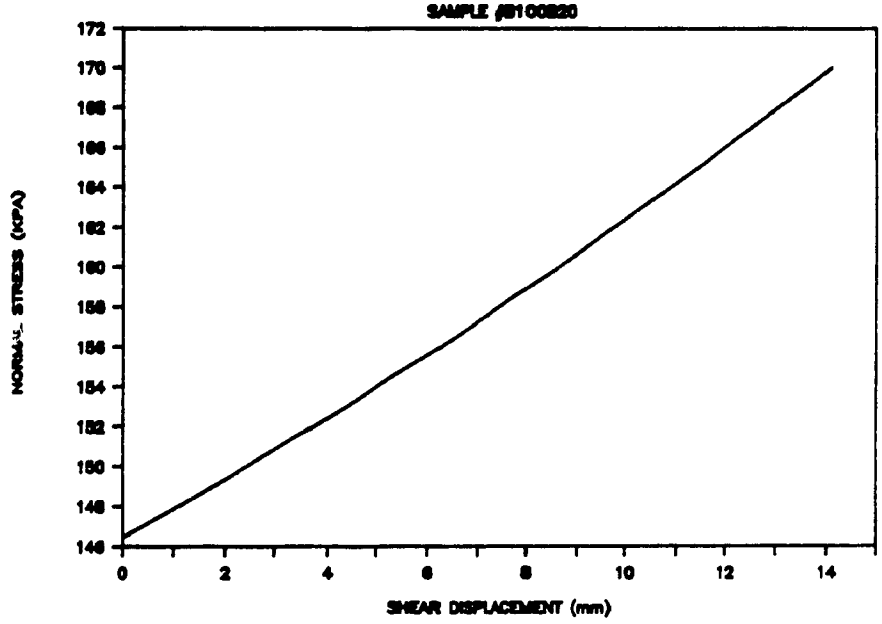

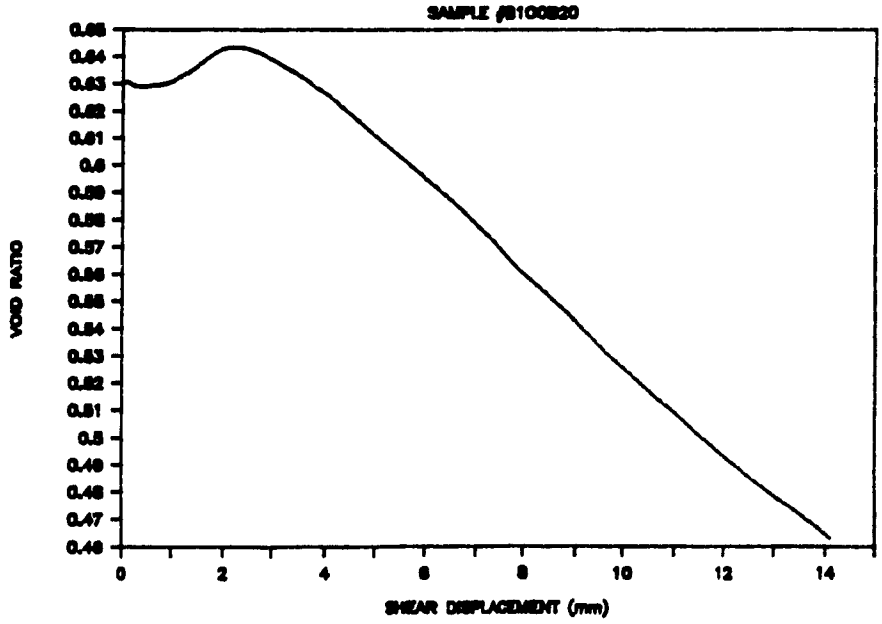

LAC MATAGAMI

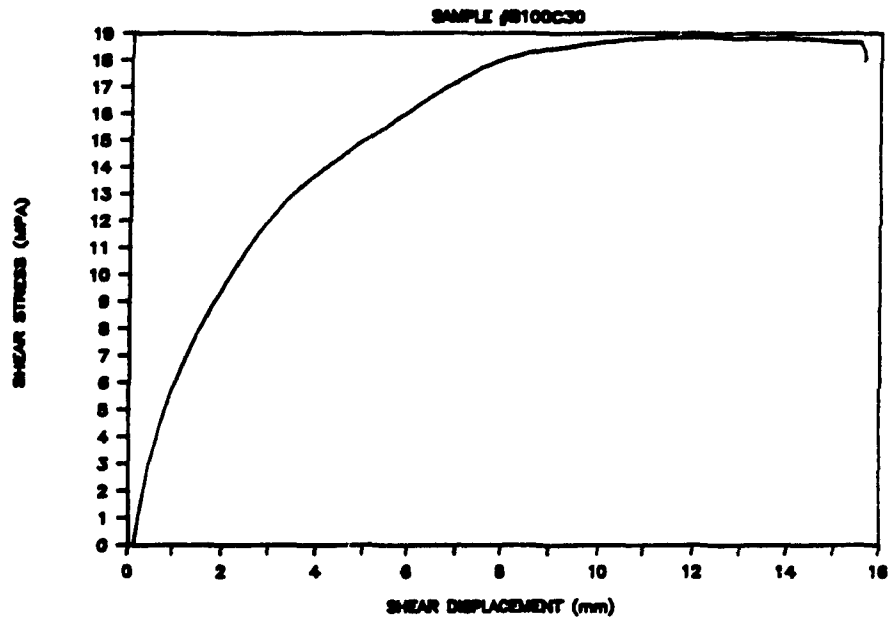

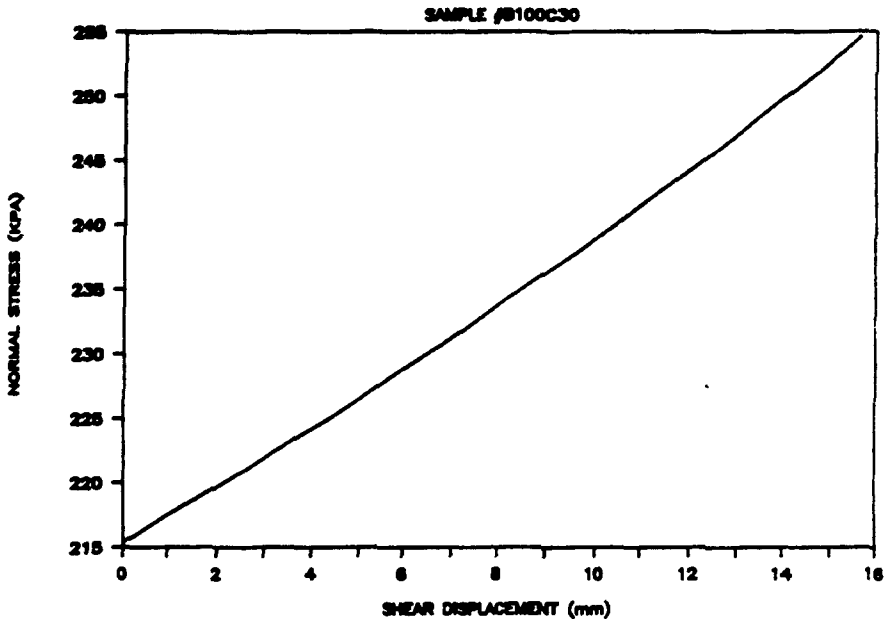

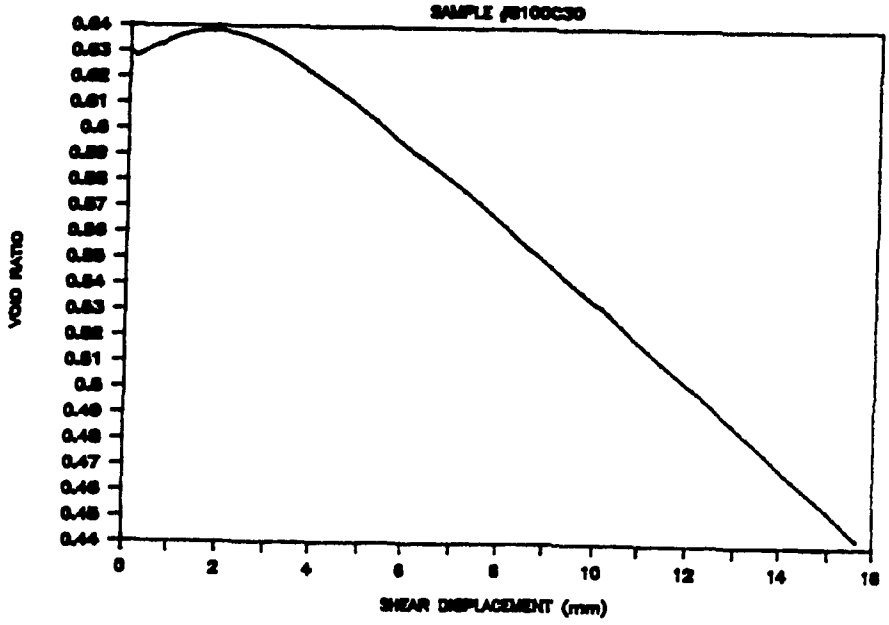

LAC MATAGAMI

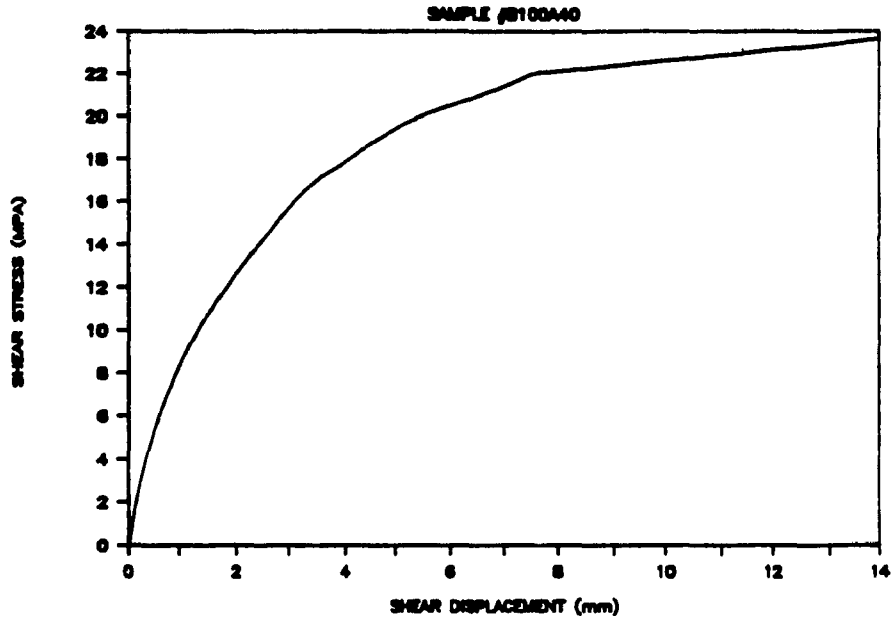

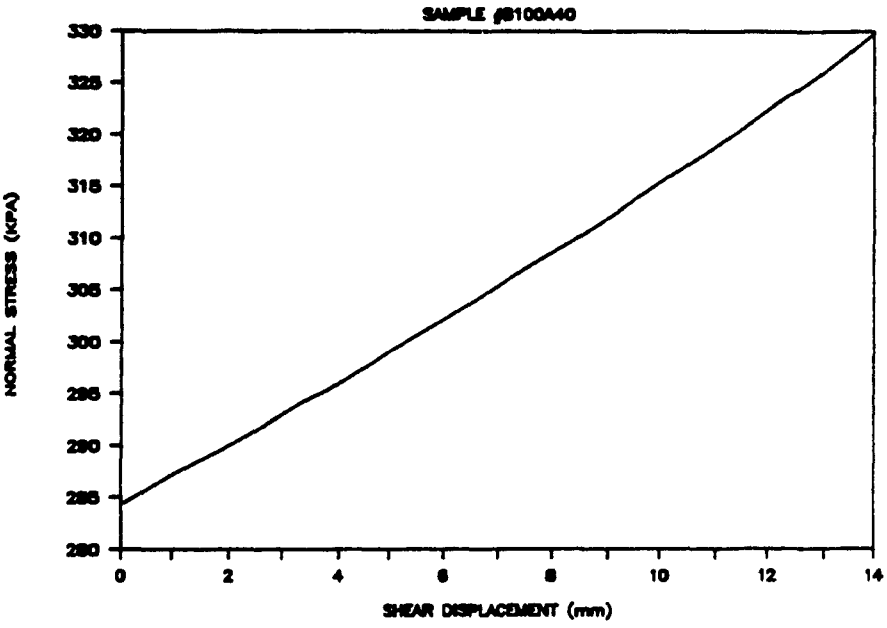

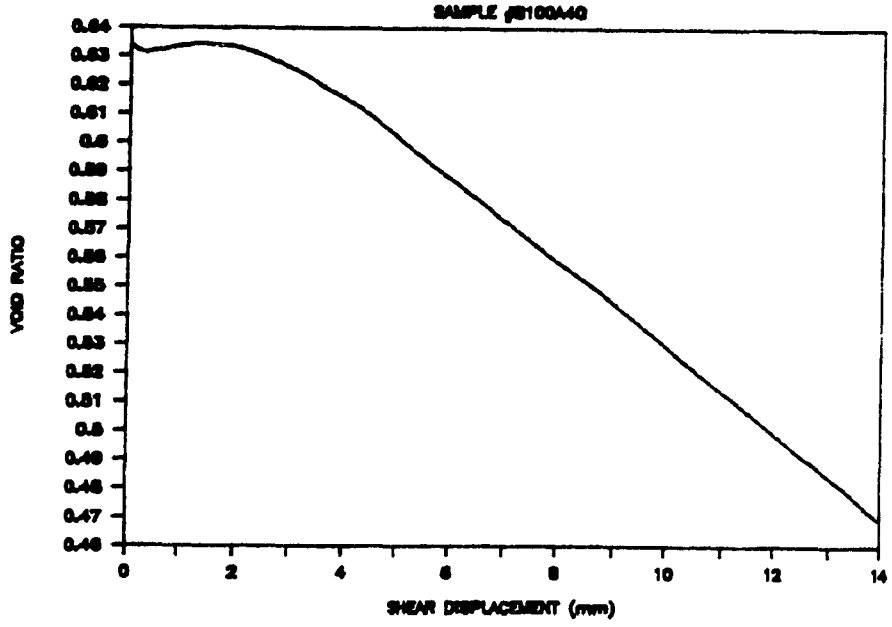

LAC MATAGAMI

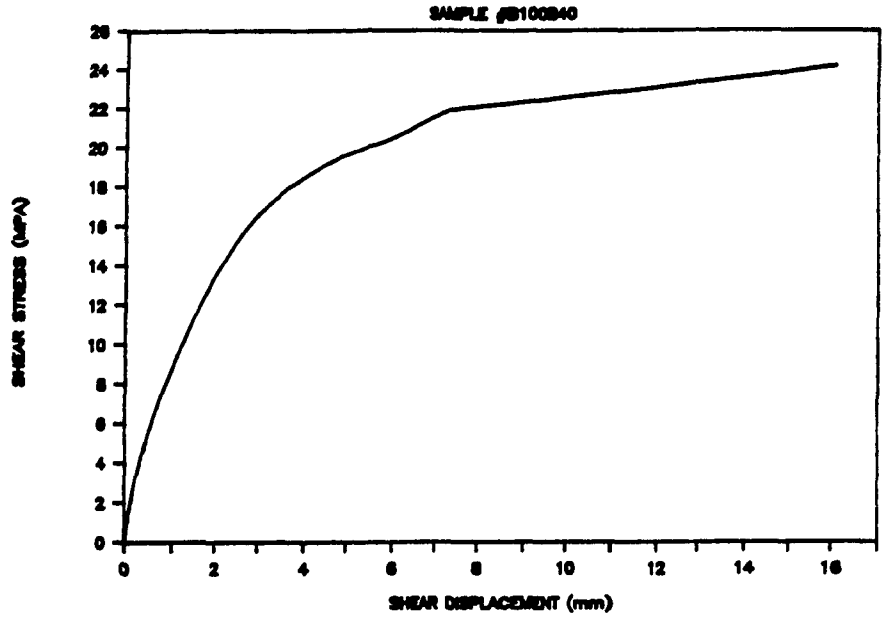

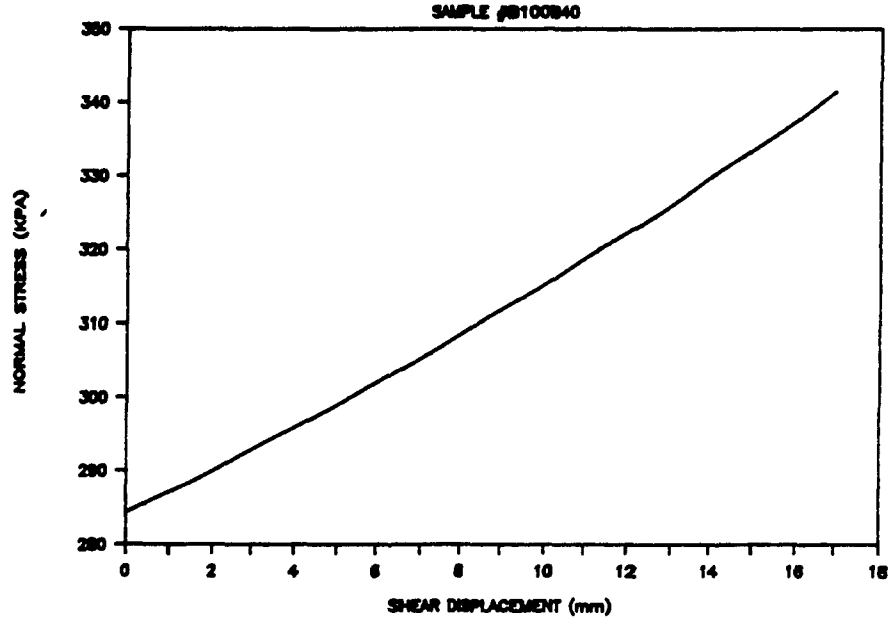

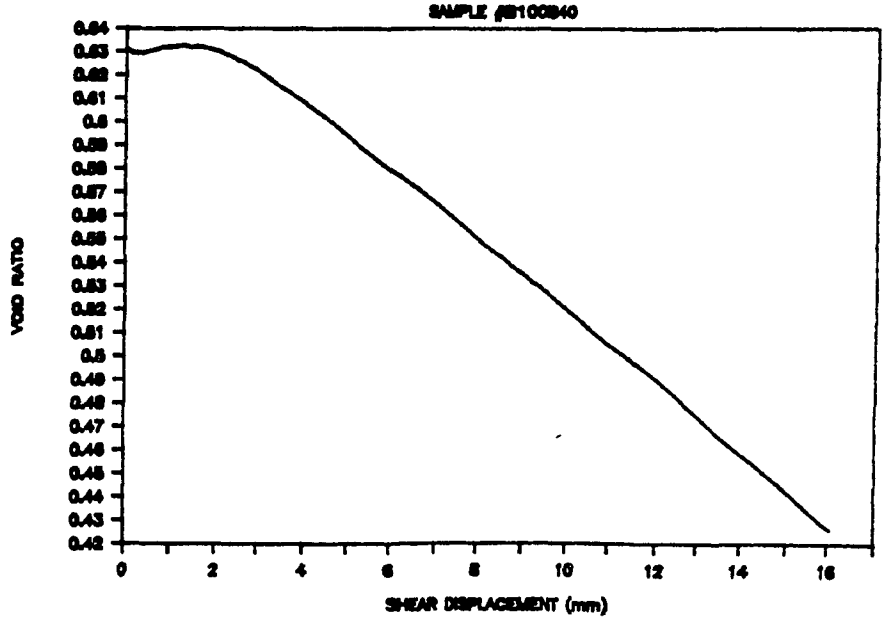

LAC MATAGAMI

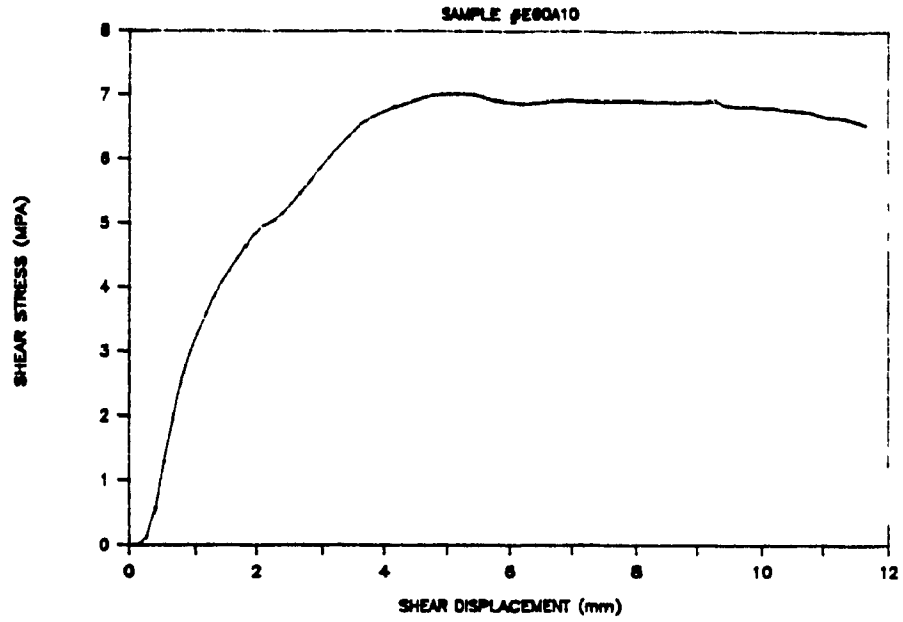

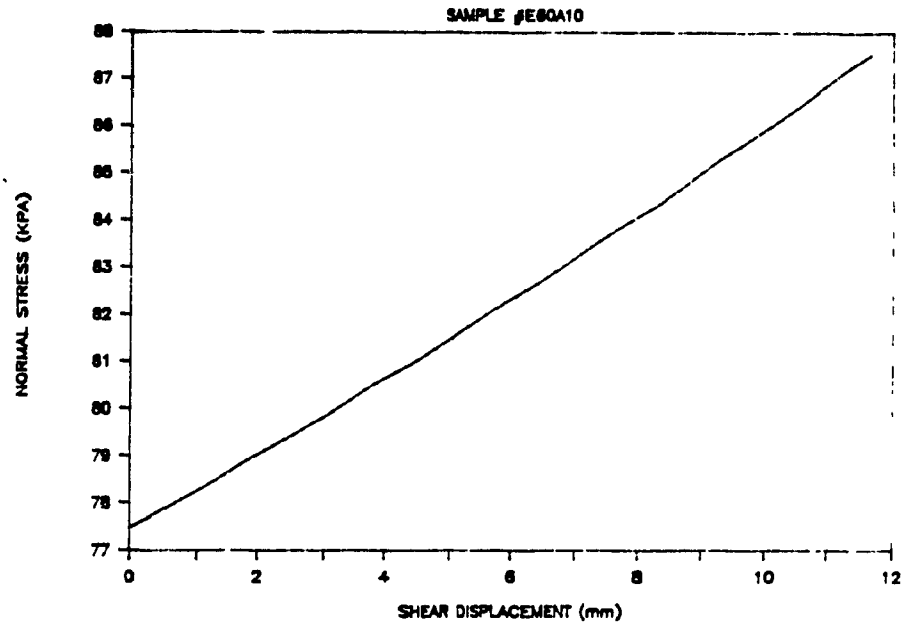

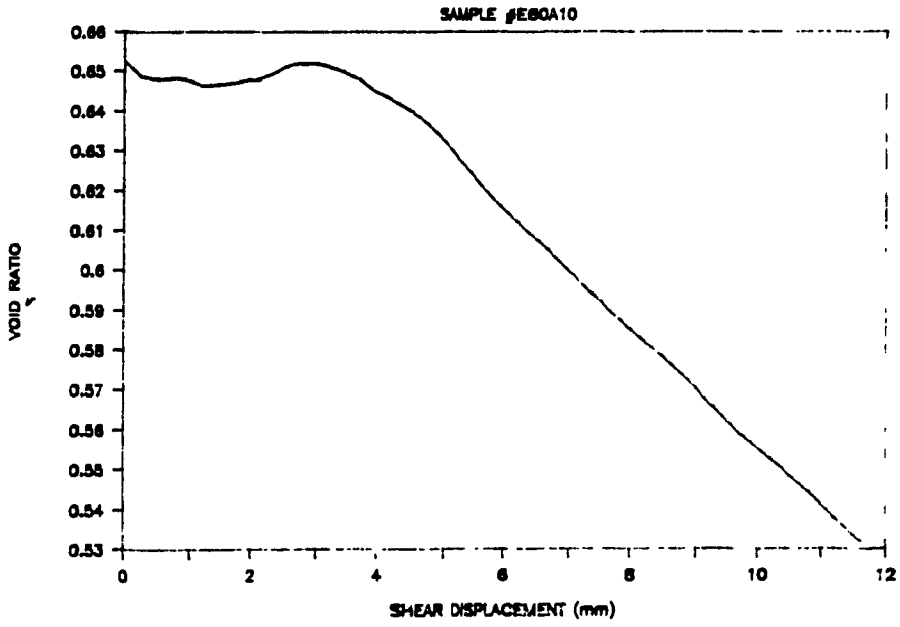

LAC MATAGAMI

SAMPLE #E60B10

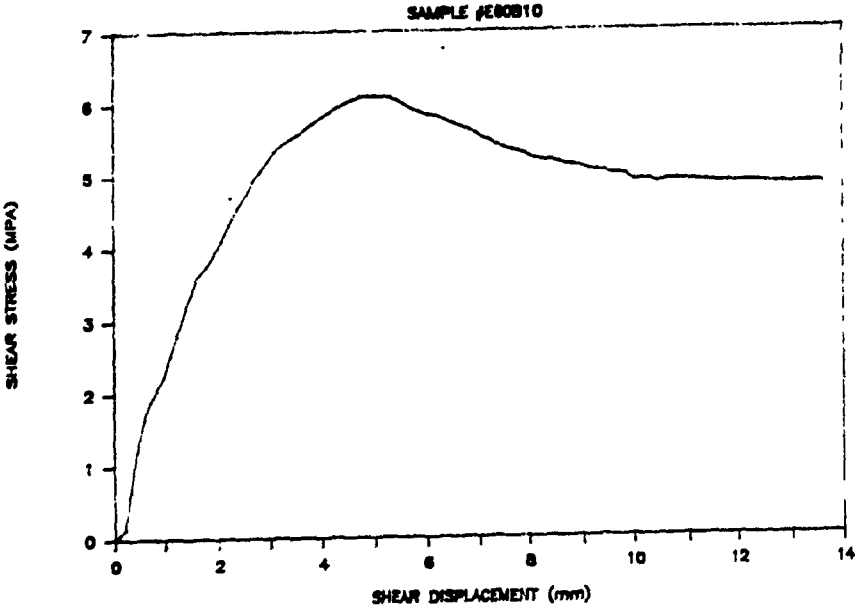

SAMPLE #E60B10

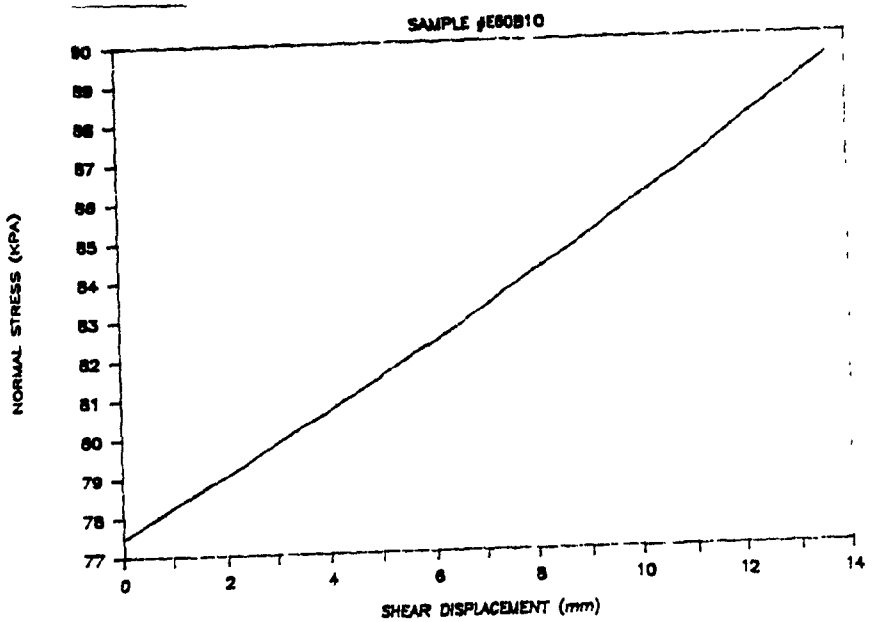

SAMPLE #E60B10

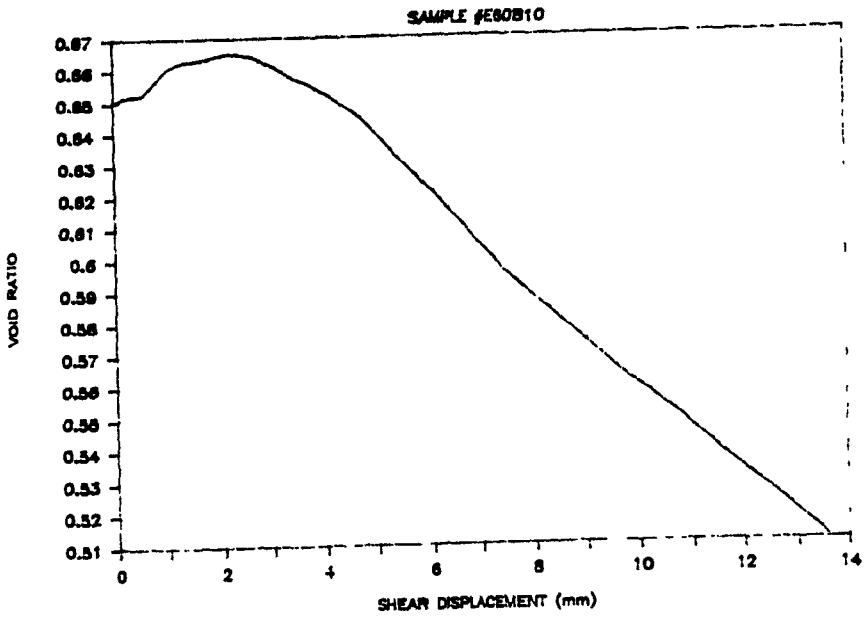

LAC MATAGAMI

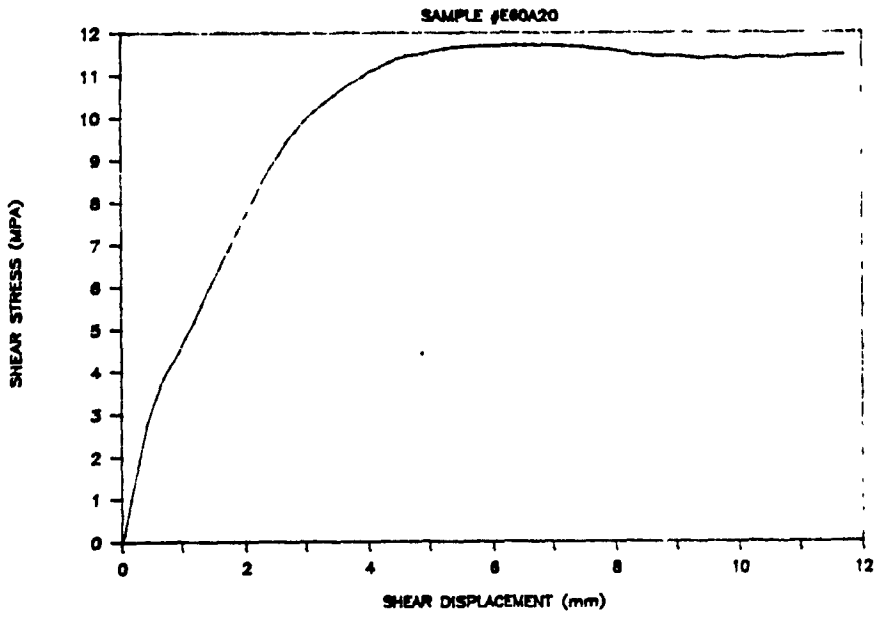

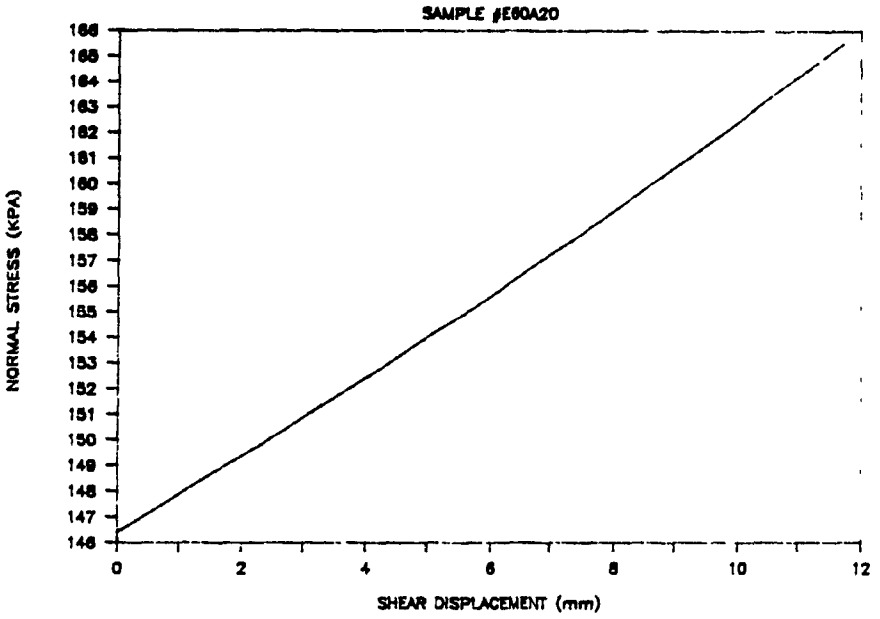

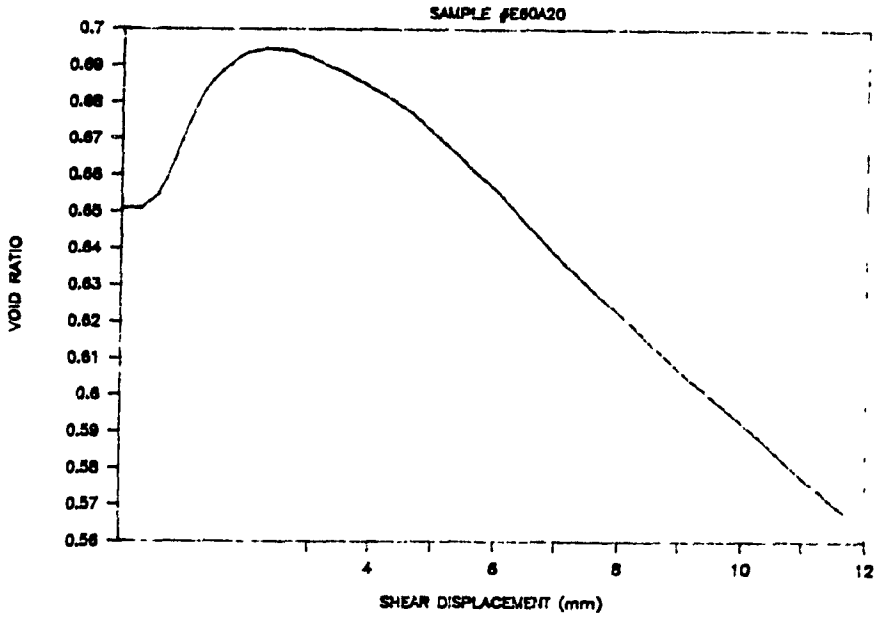

LAC MATAGAMI

SAMPLE #E60820

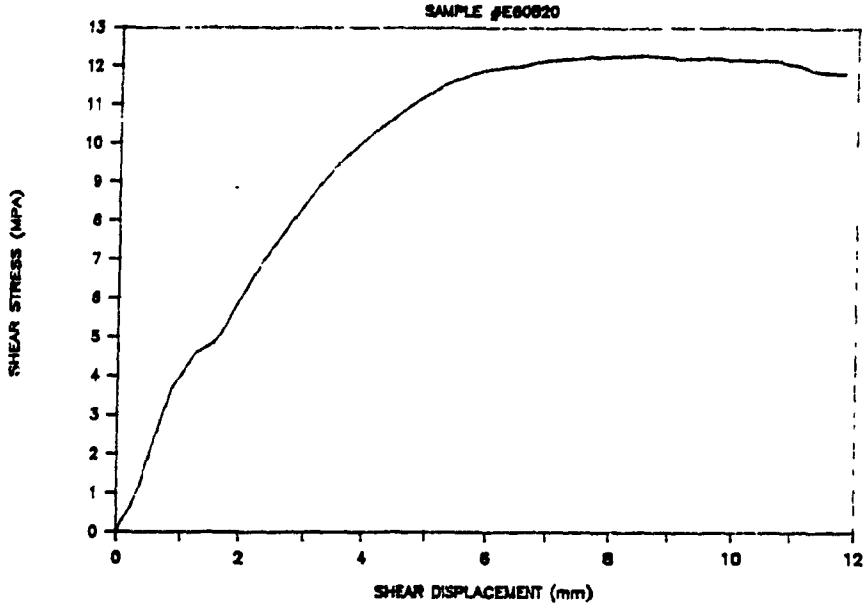

SAMPLE #E60820

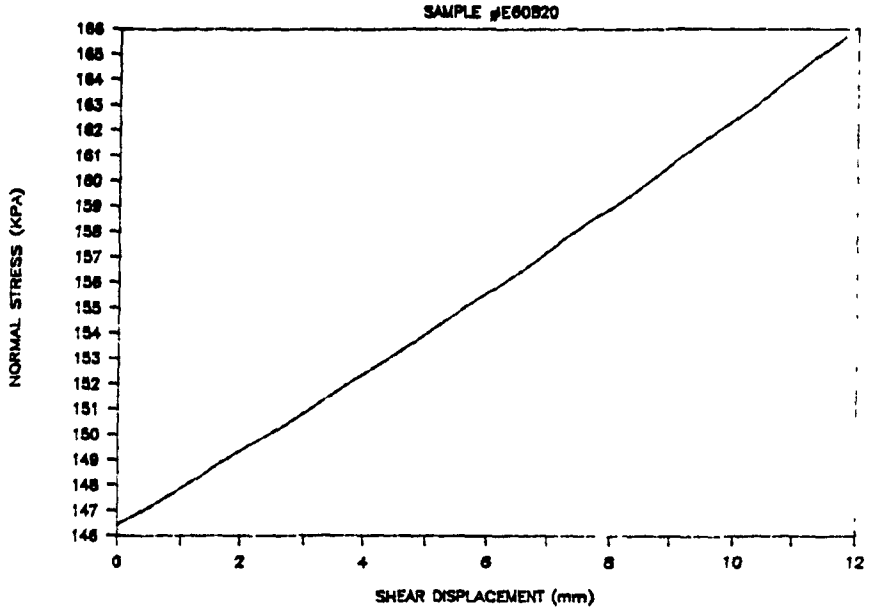

SAMPLE #E60820

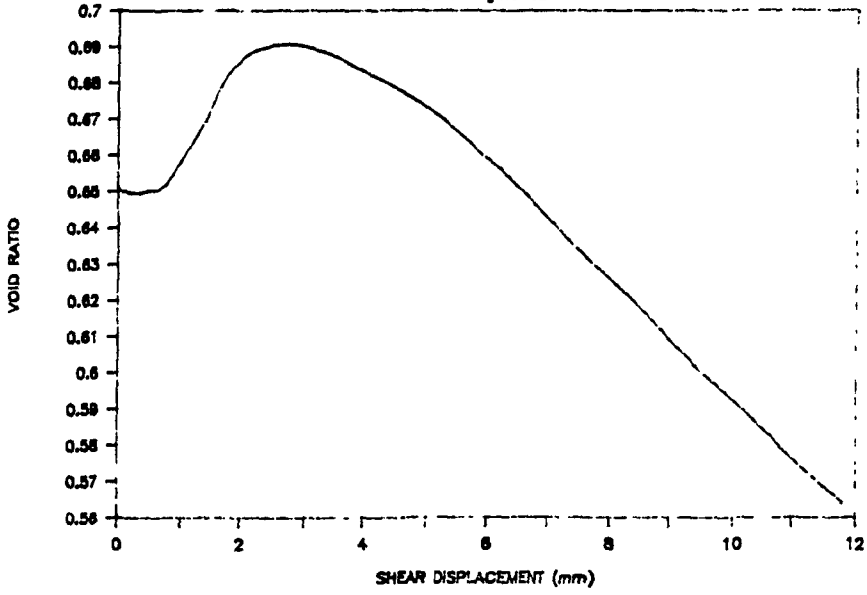

LAC MATAGAMI

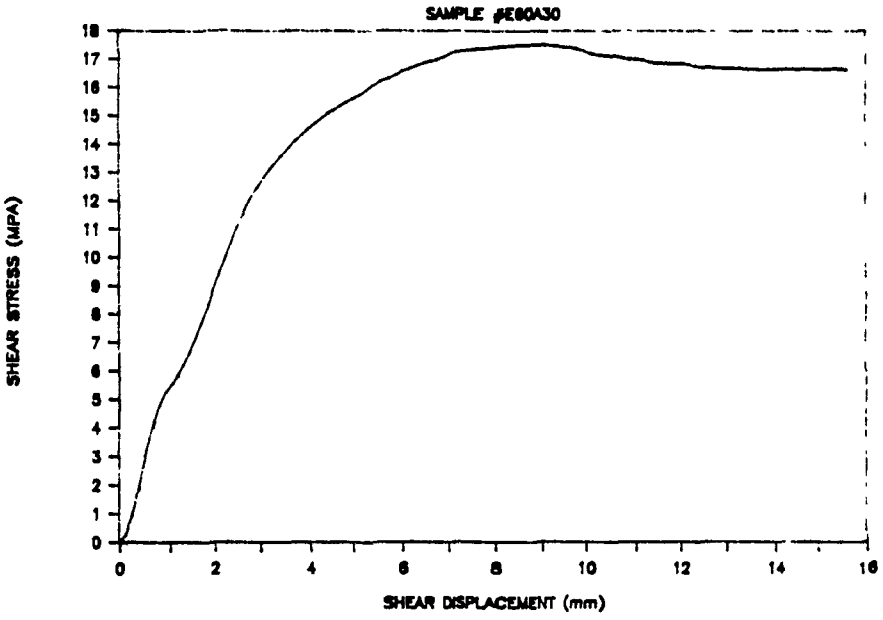

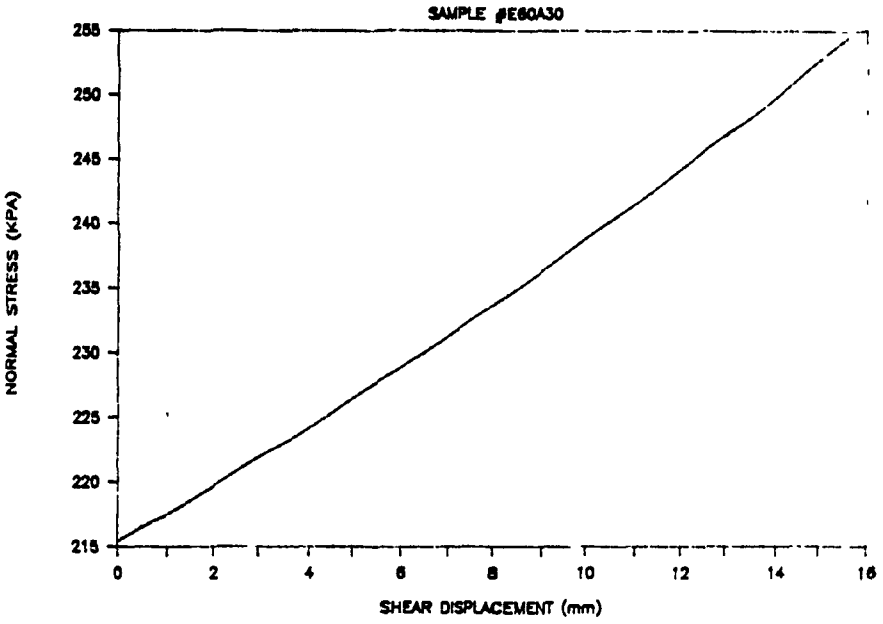

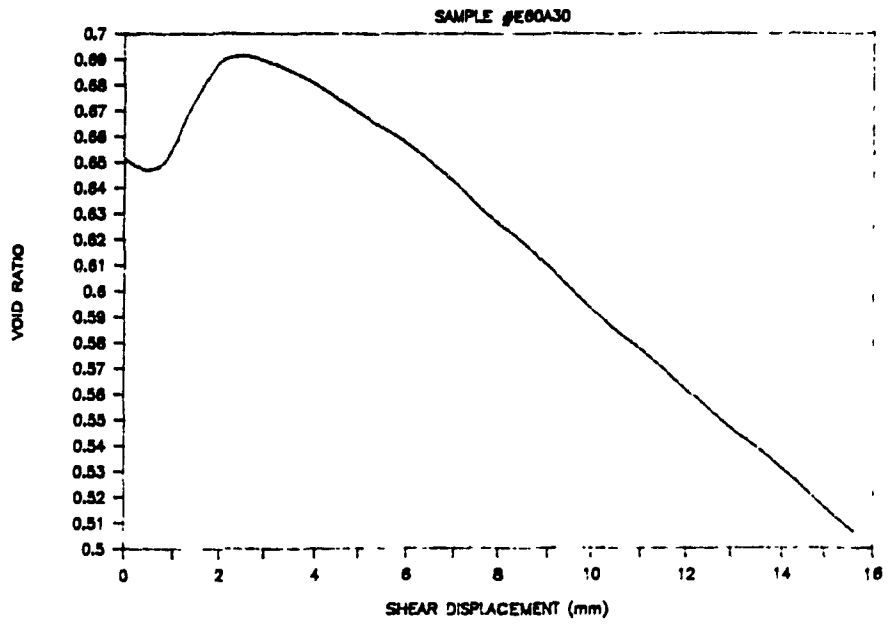

LAC MATAGAMI

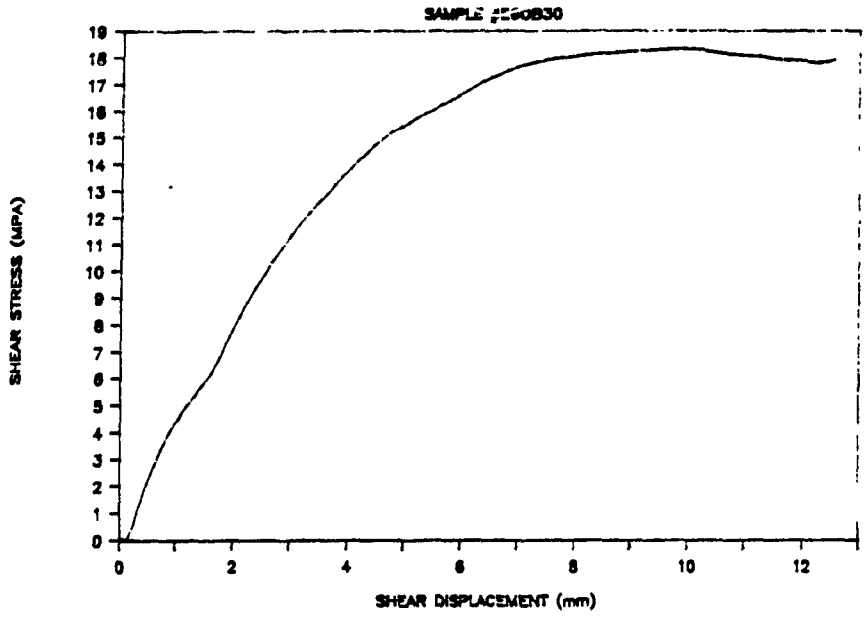

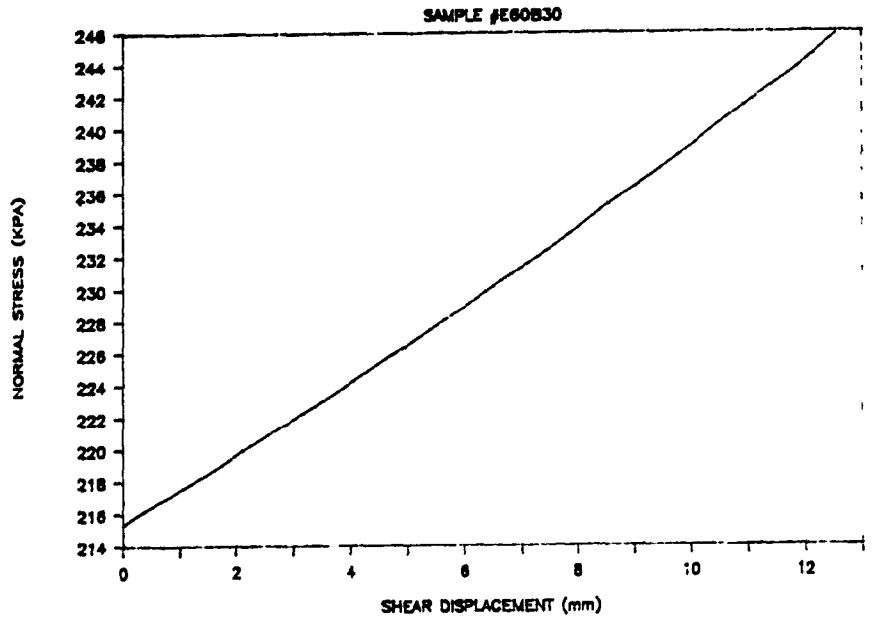

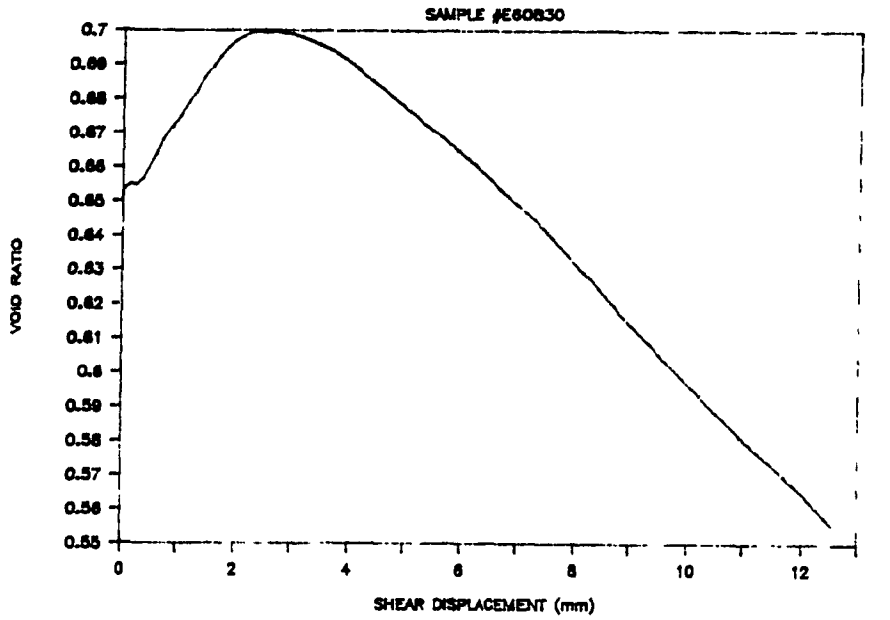

LAC MATAGAMI

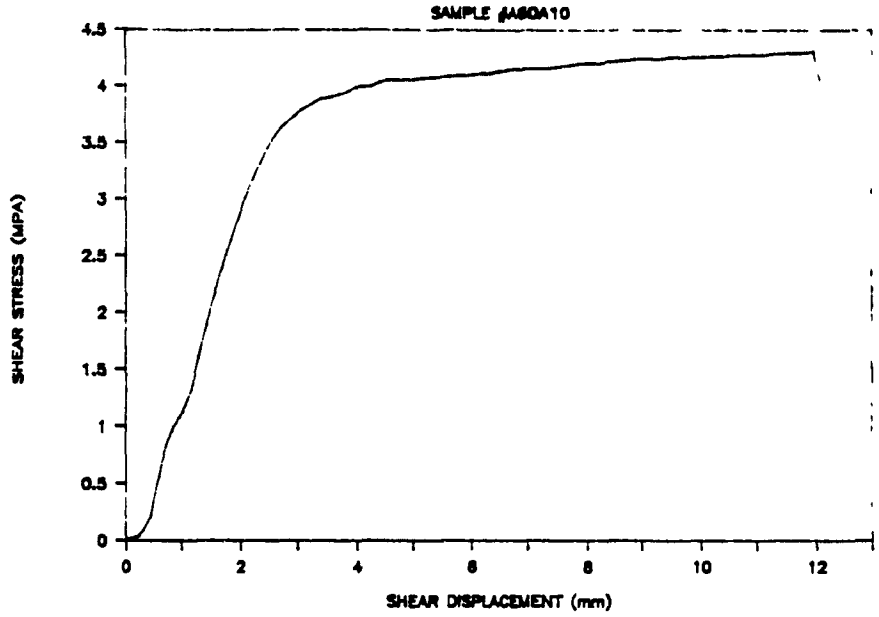

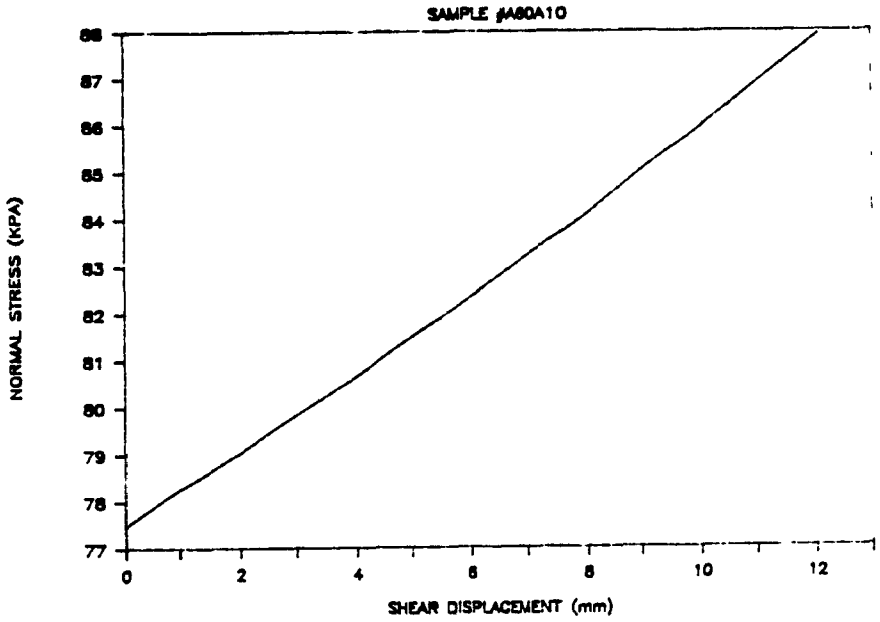

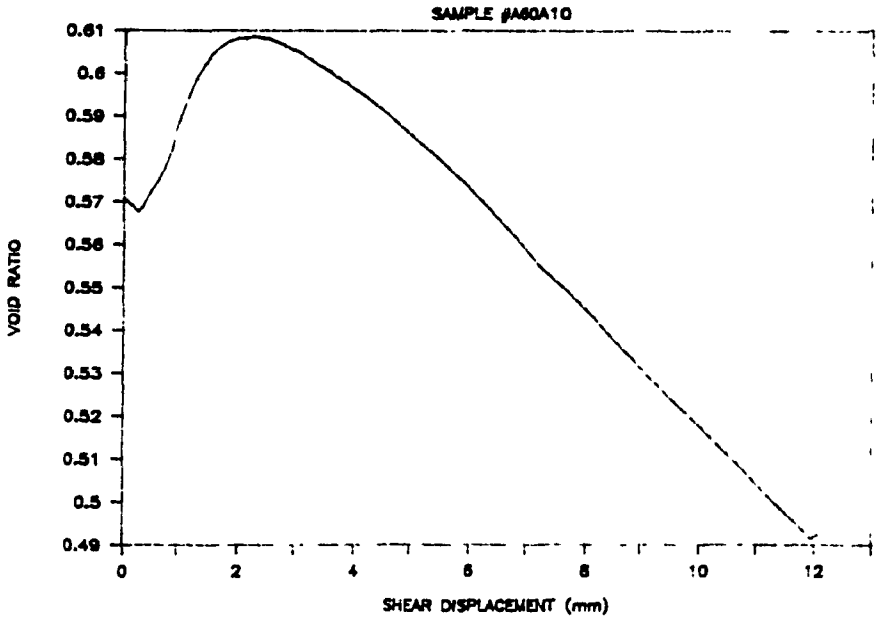

LAC MATAGAMI

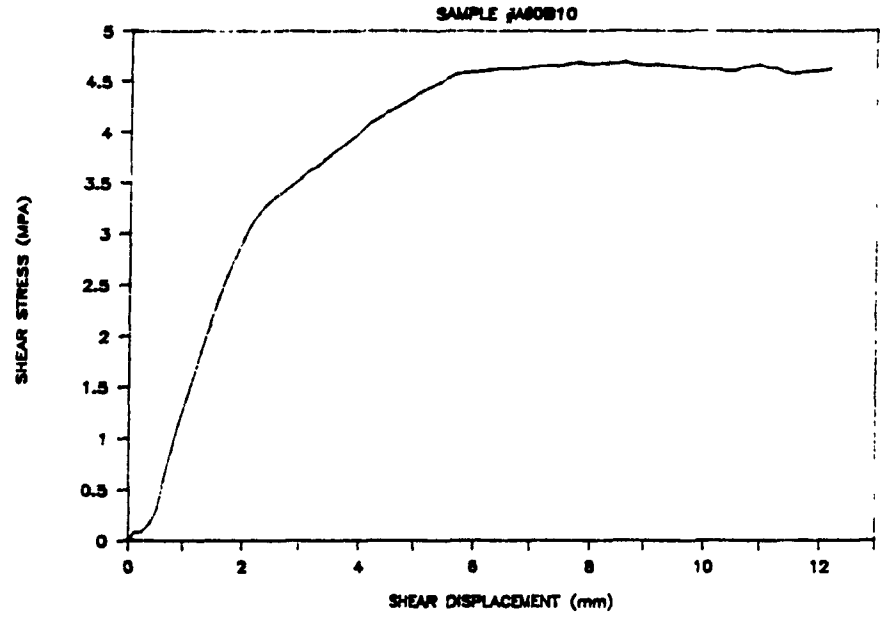

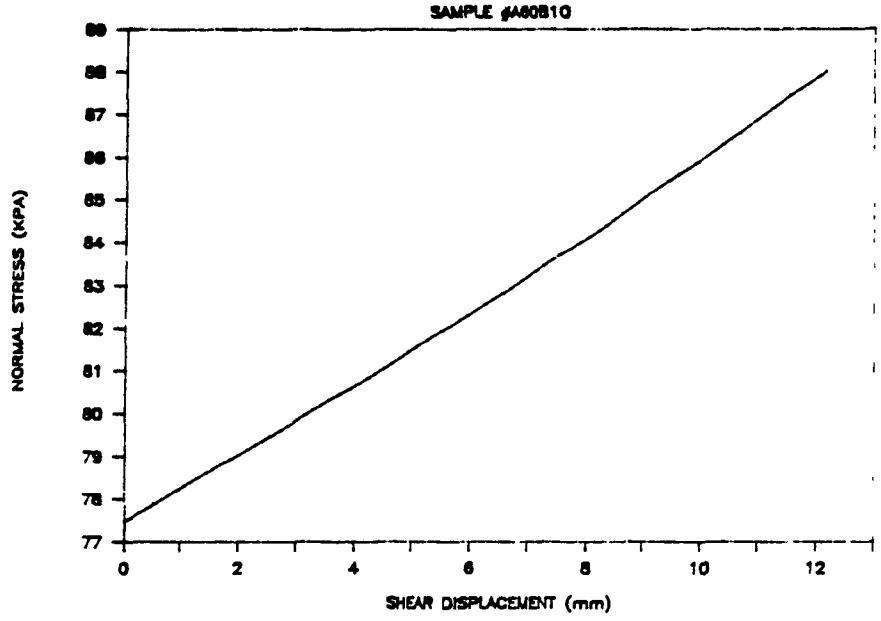

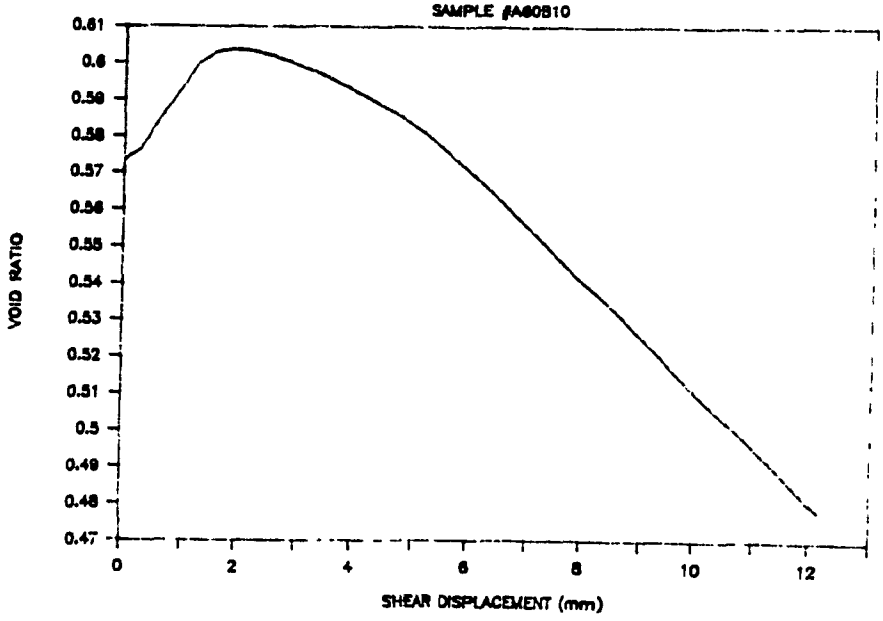

LAC MATAGAMI

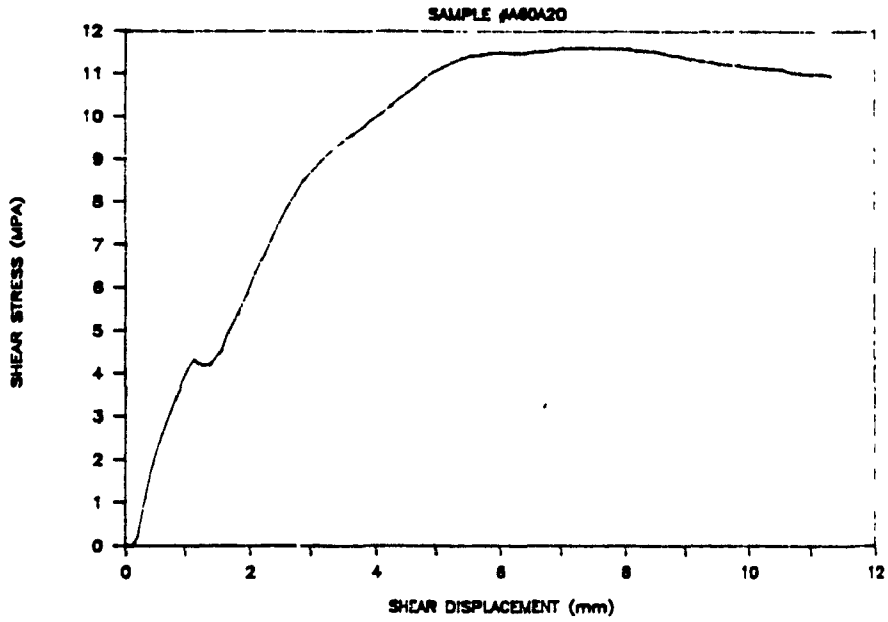

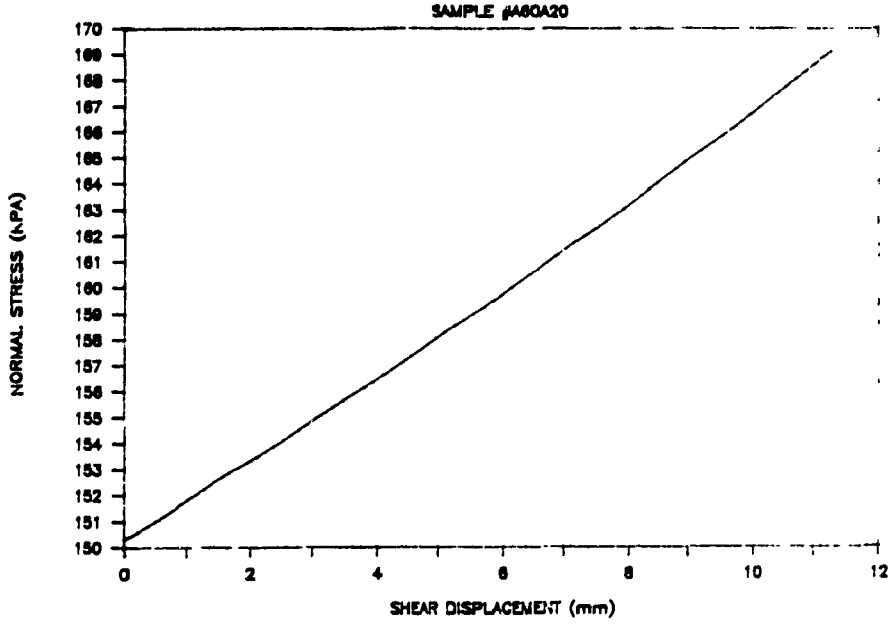

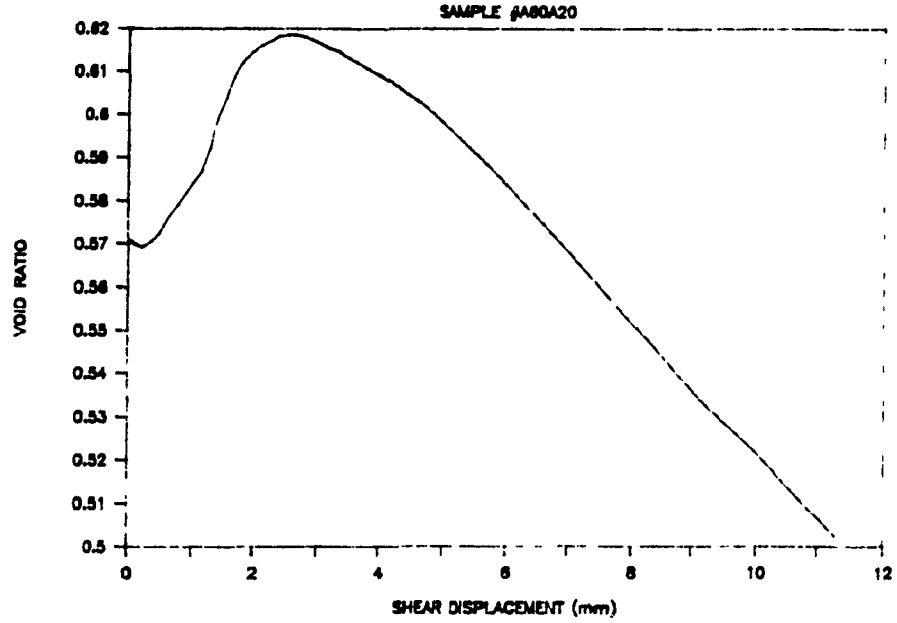

LAC MATAGAMI

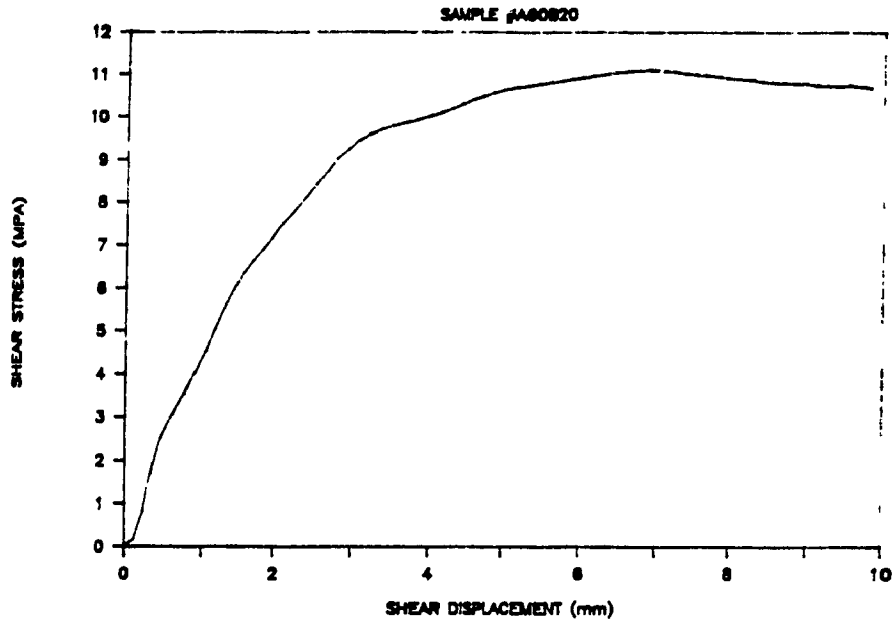

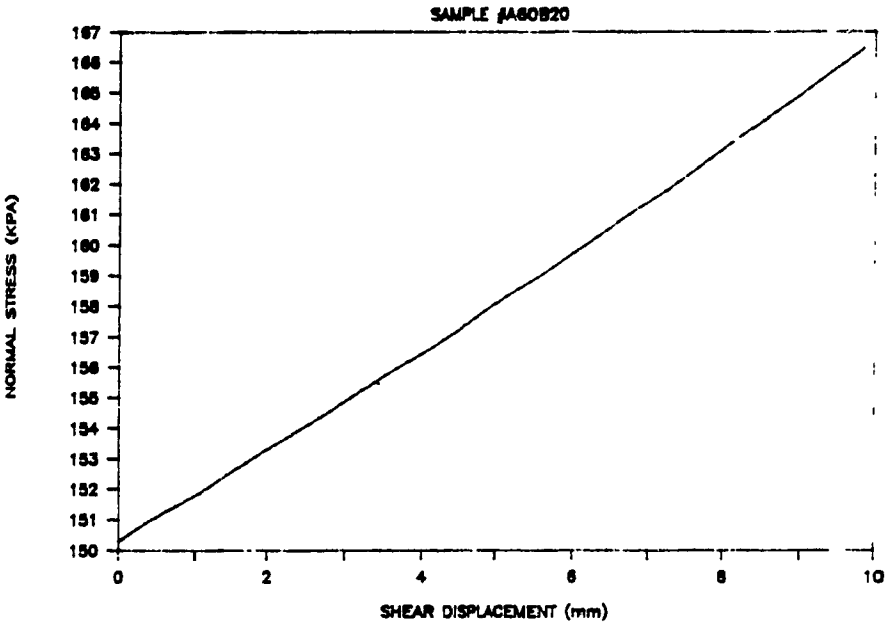

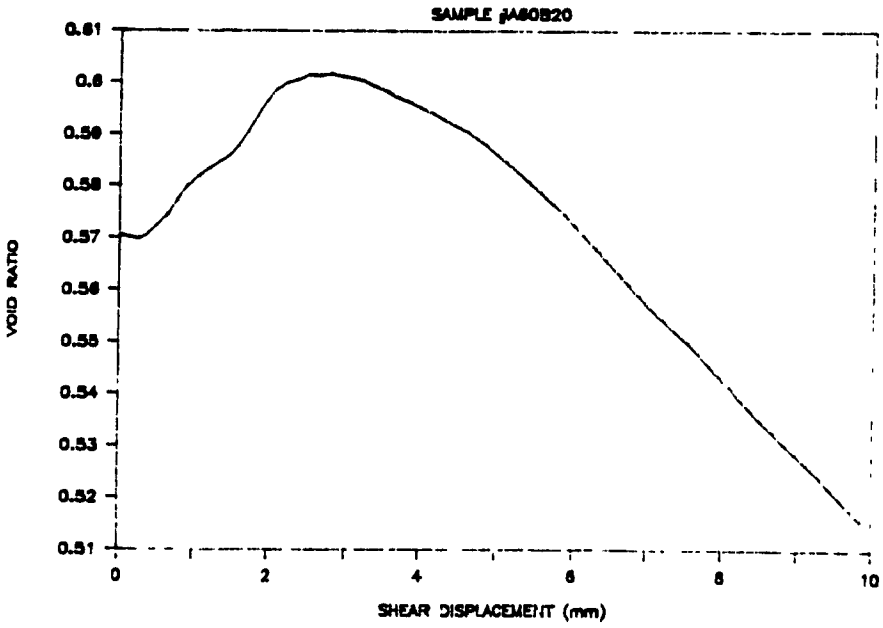

LAC MATAGAMI

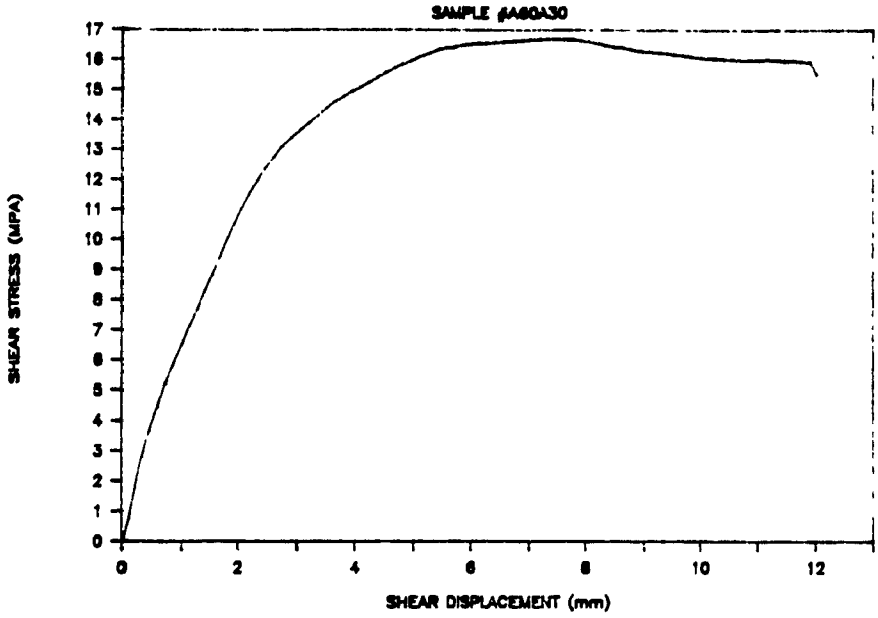

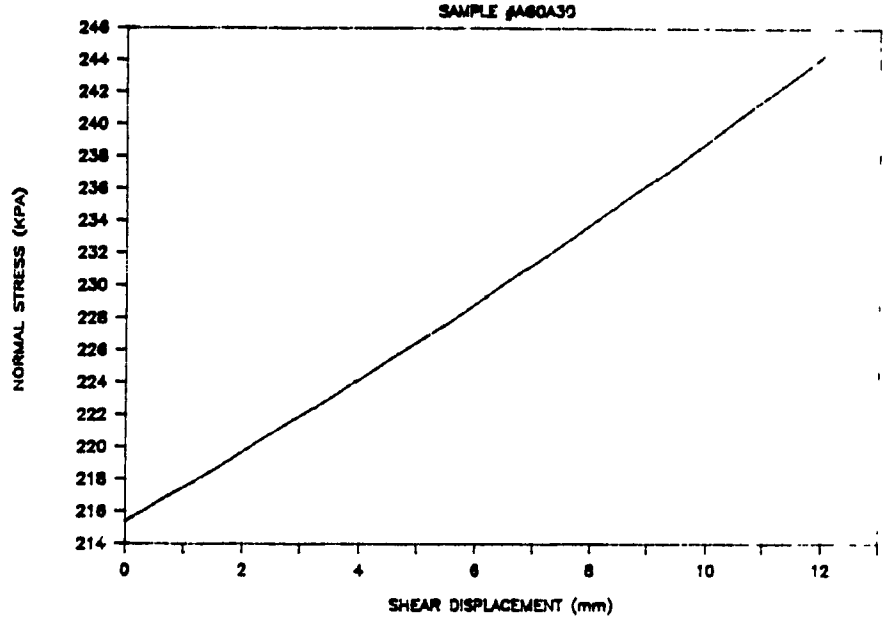

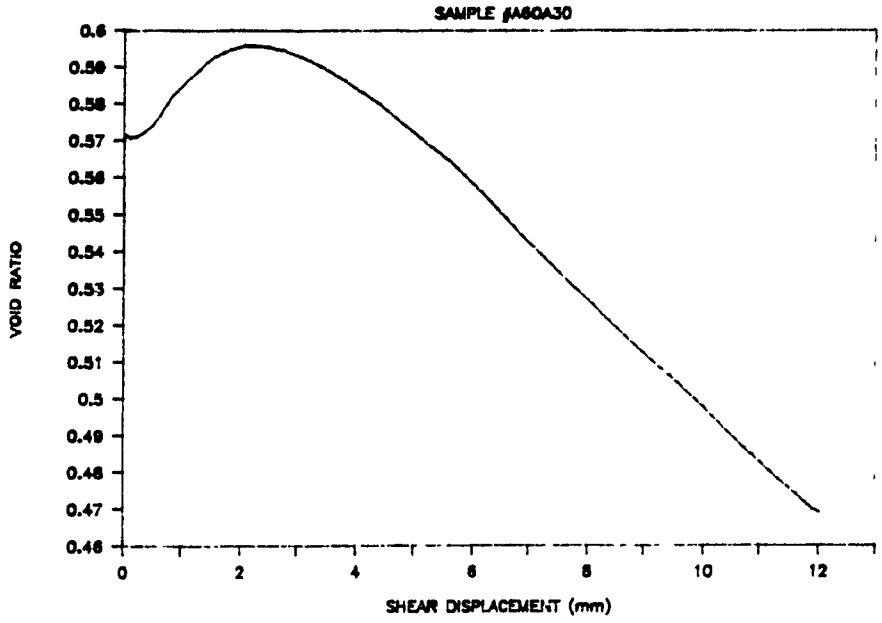

LAC MATAGAMI

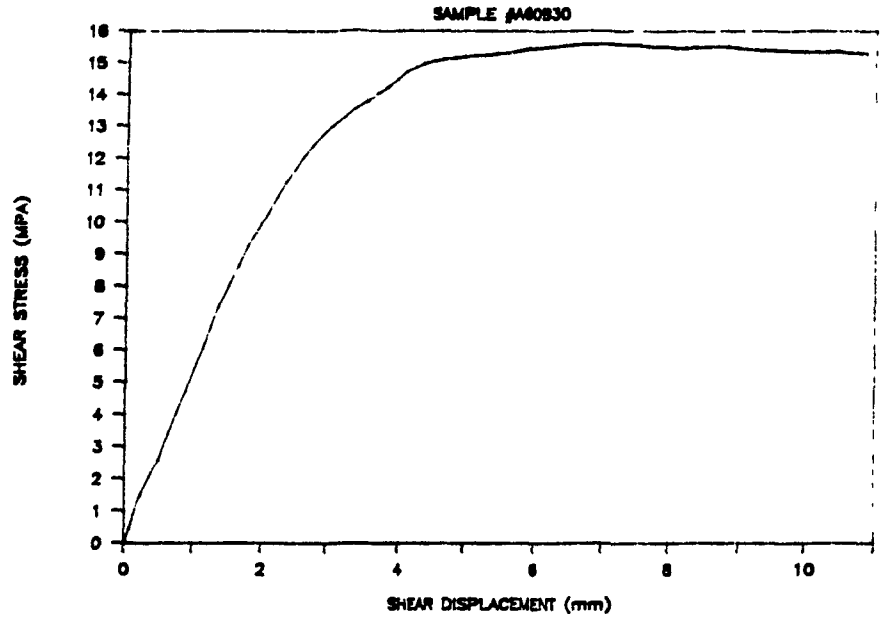

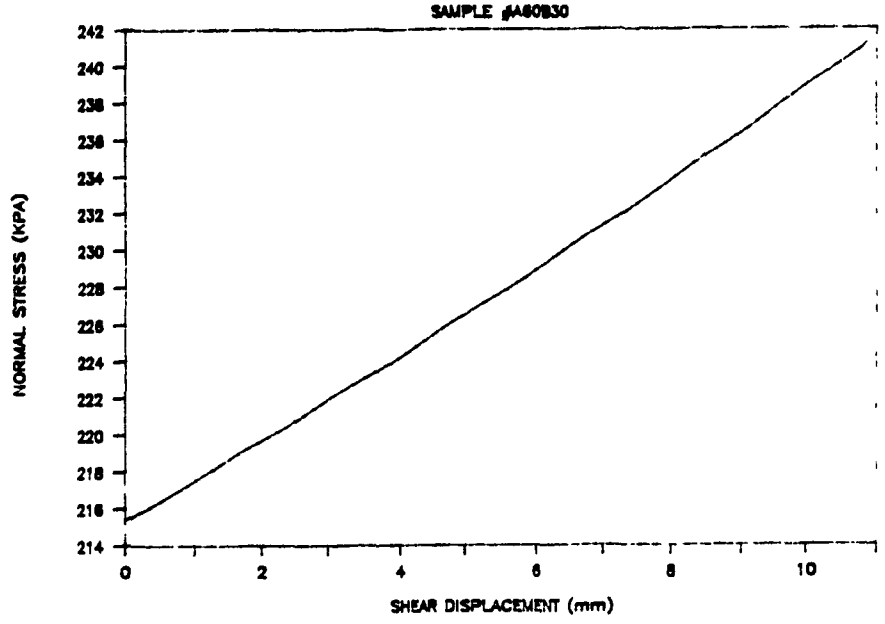

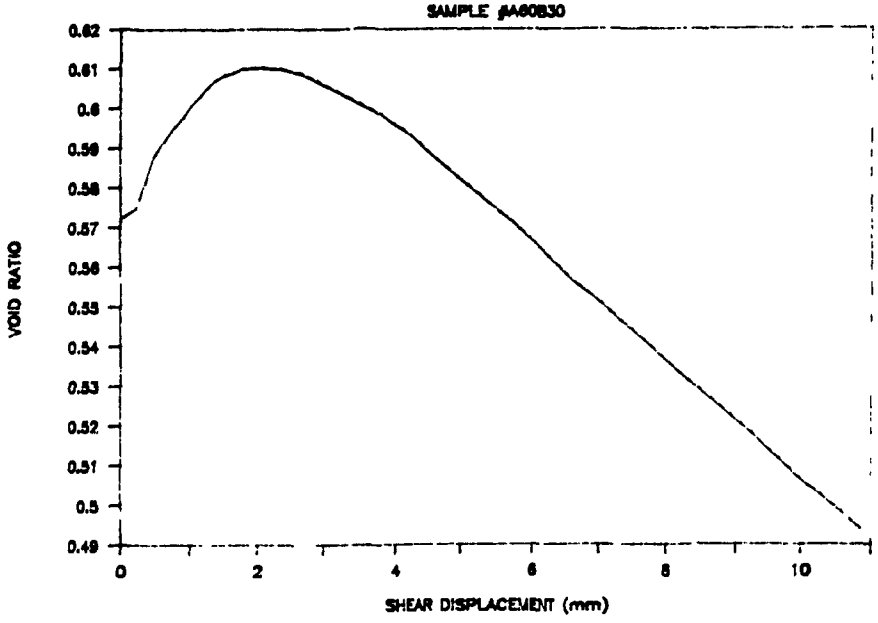

LAC MATAGAMI

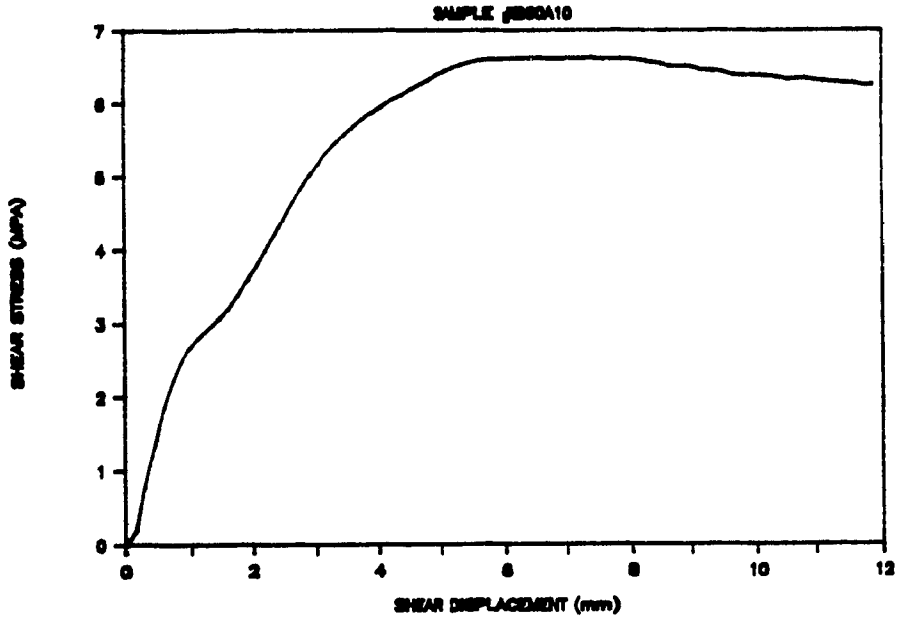

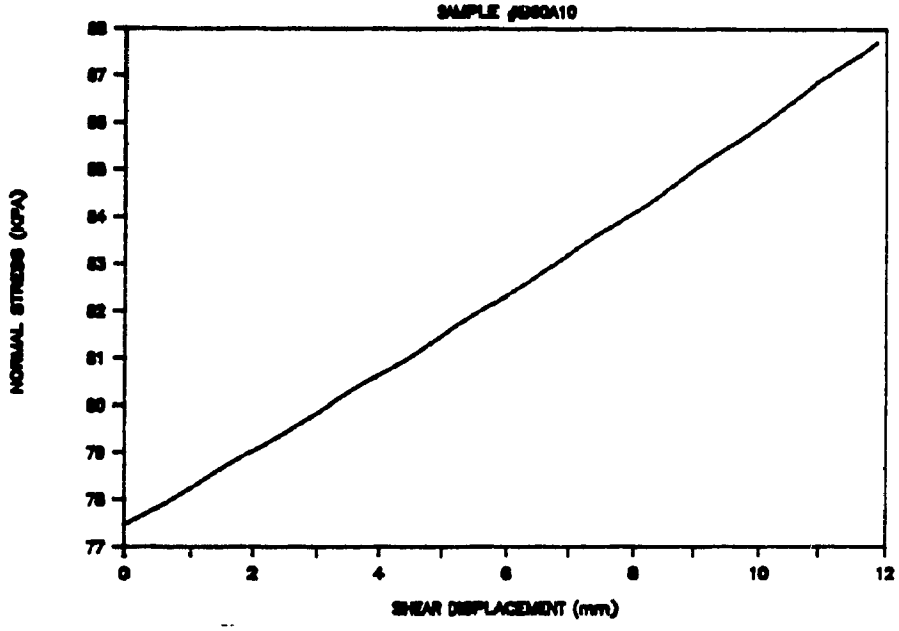

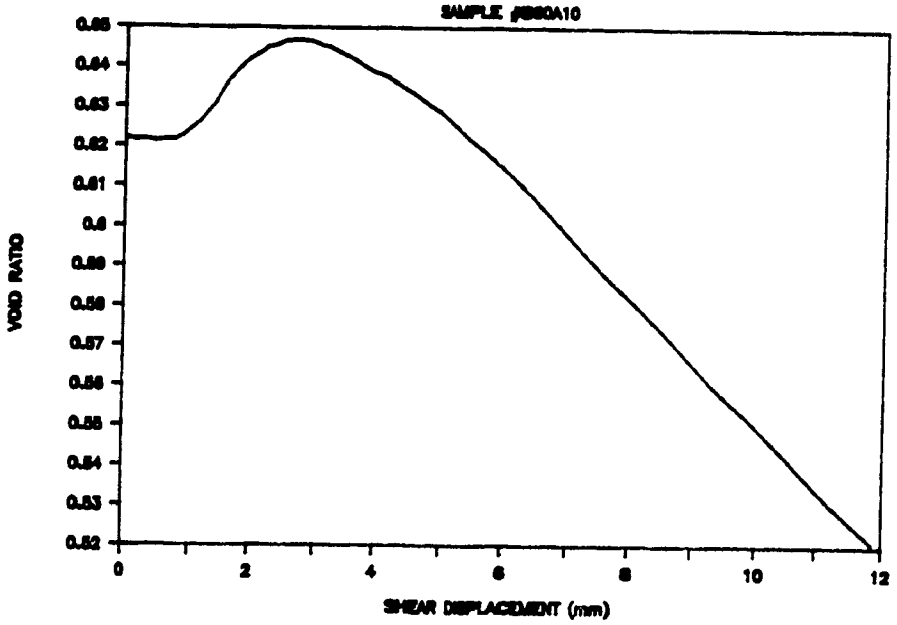

LAC MATAGAMI

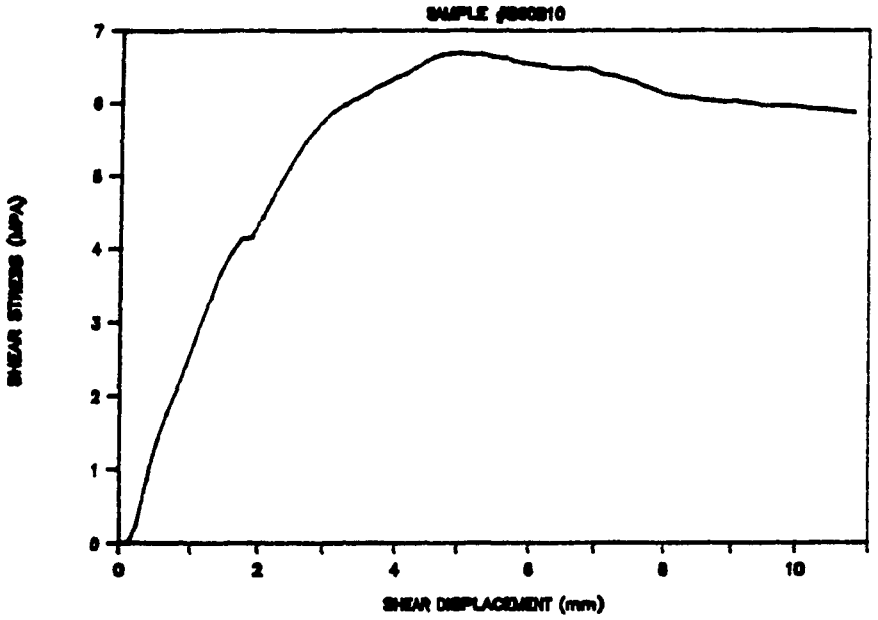

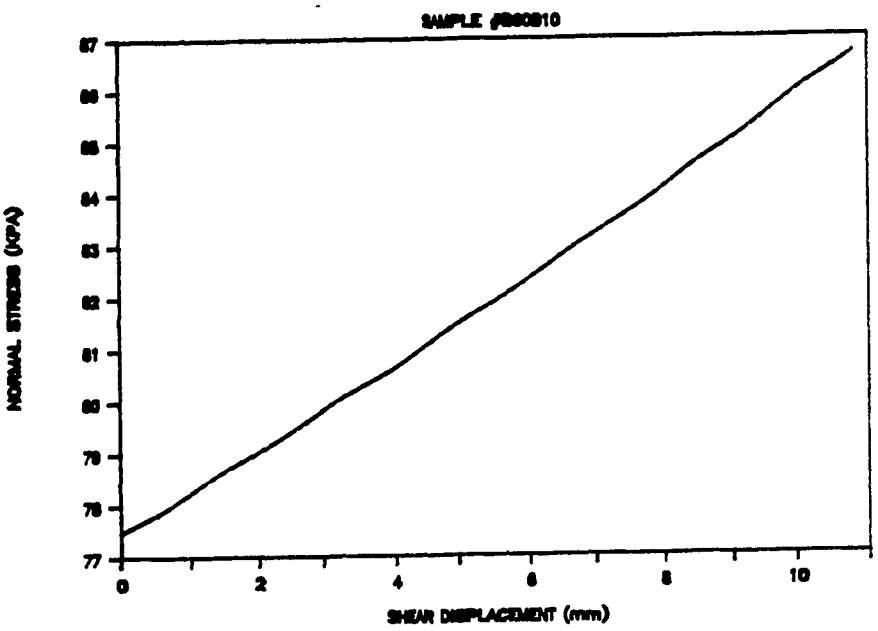

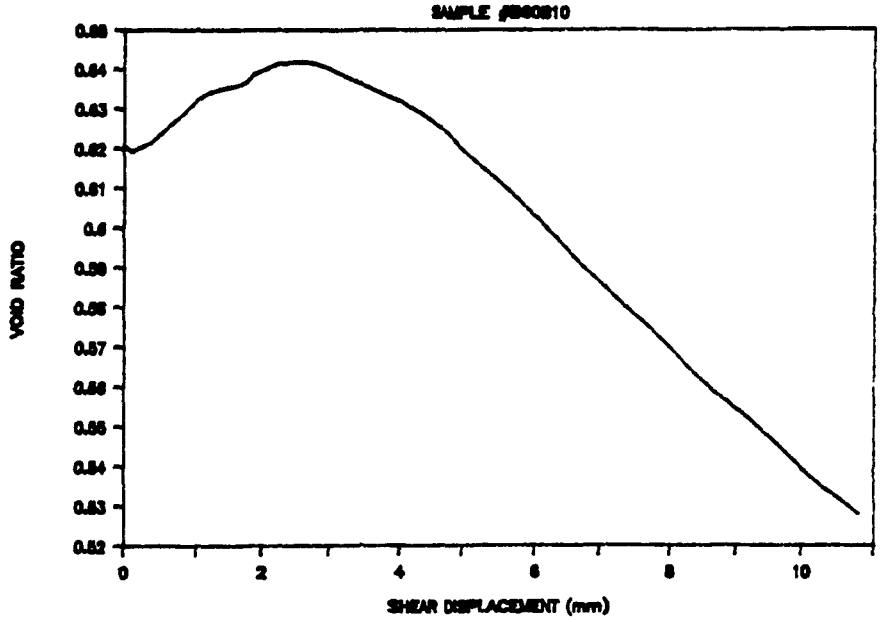

LAC MATAGAMI

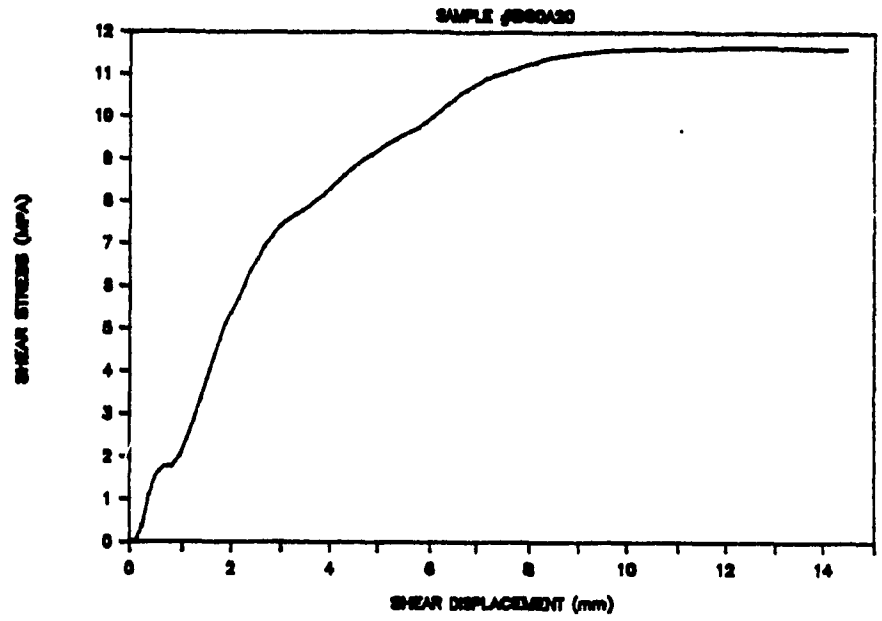

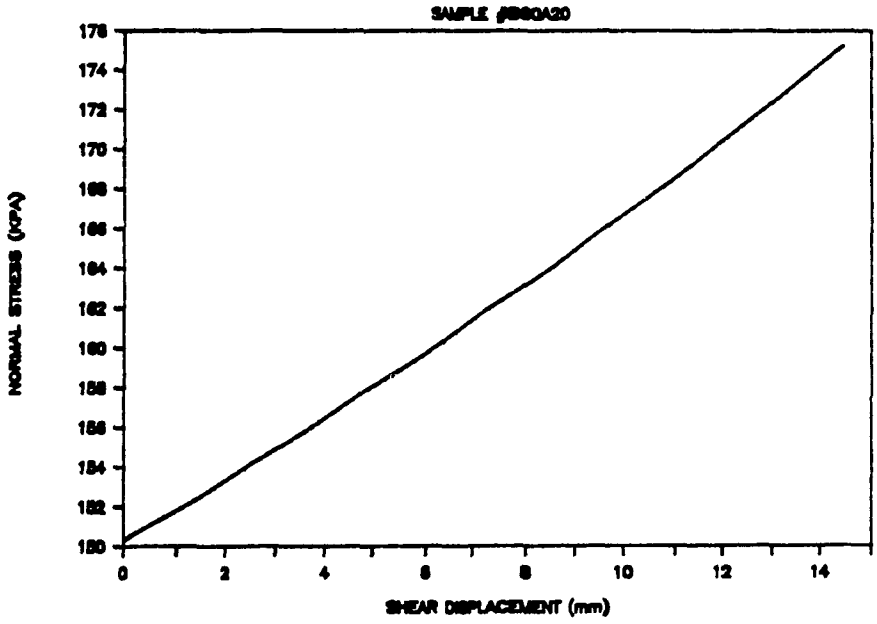

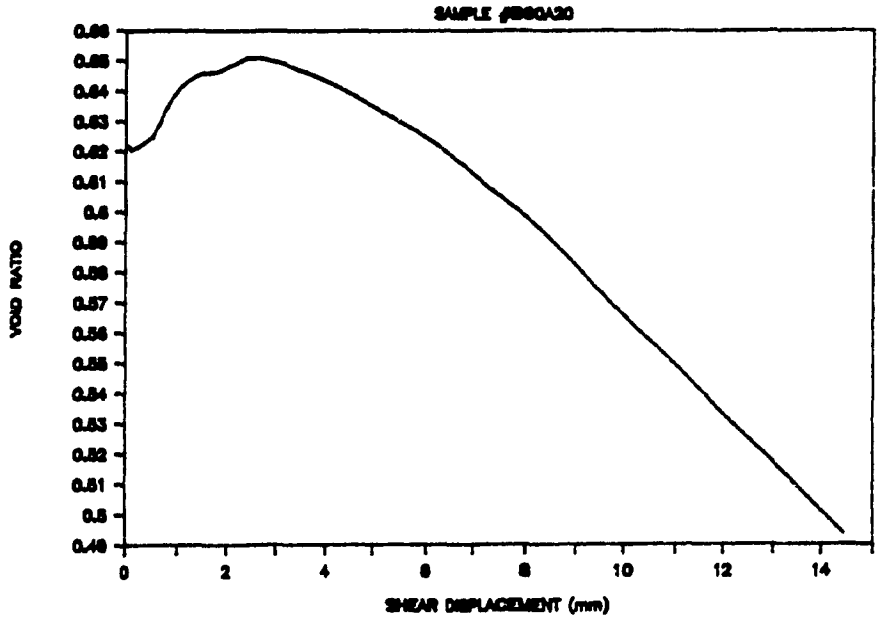

LAC MATAGAMI

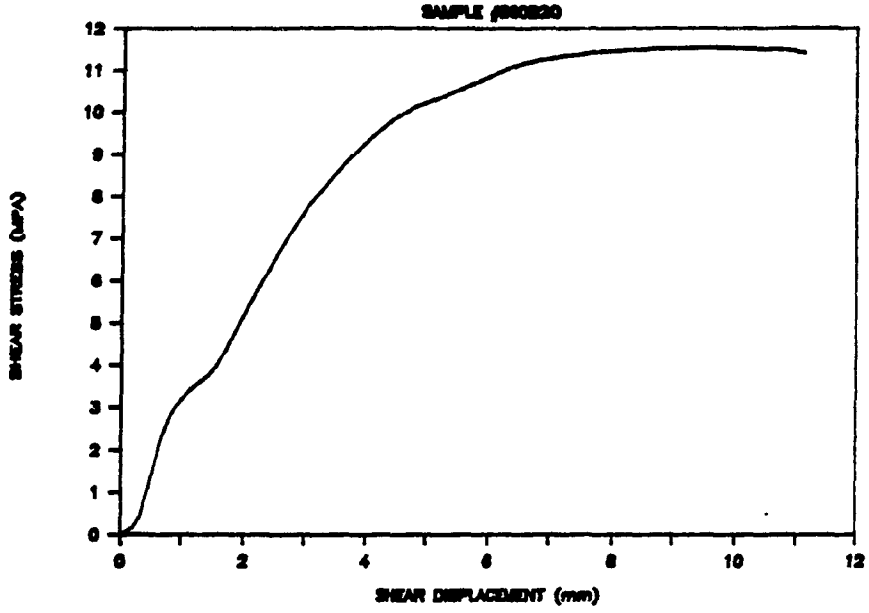

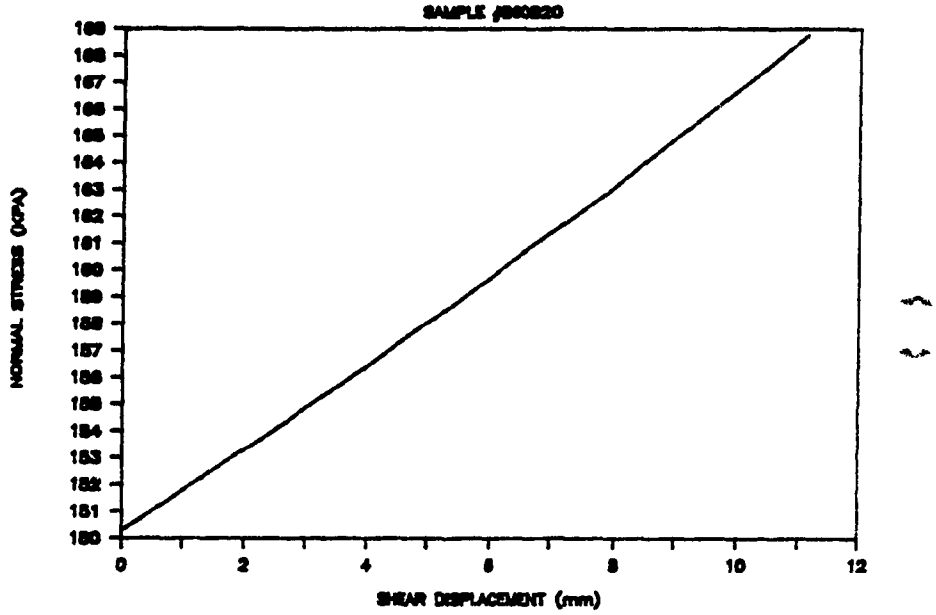

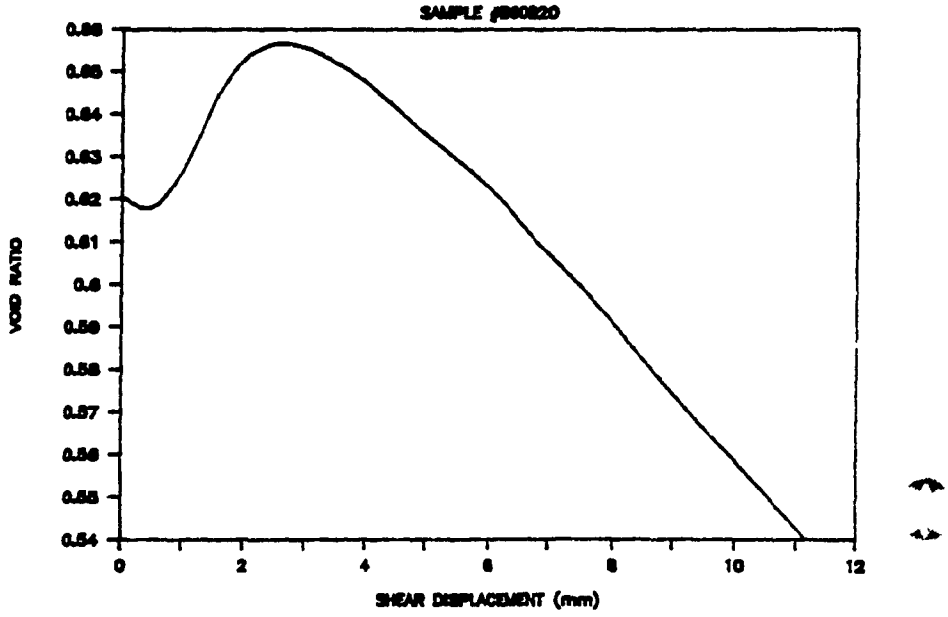

LAC MATAGAMI

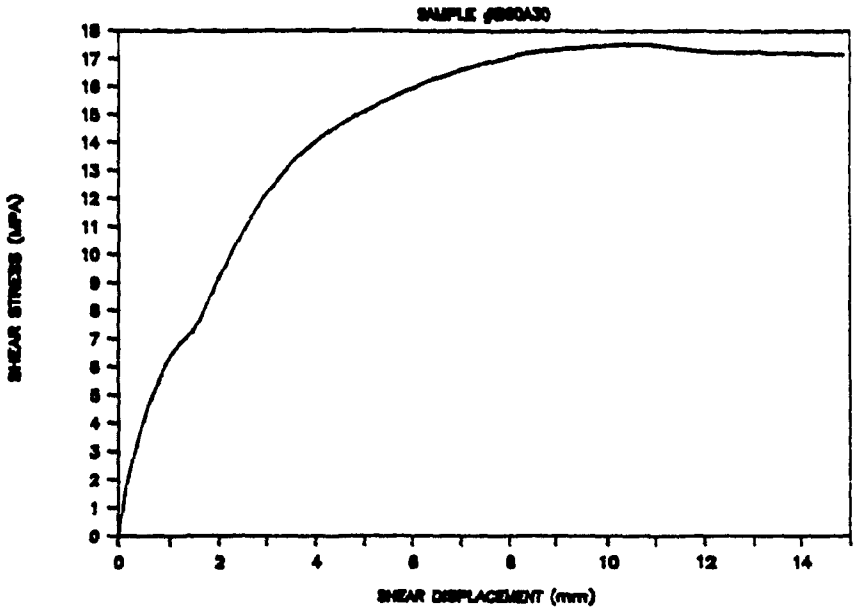

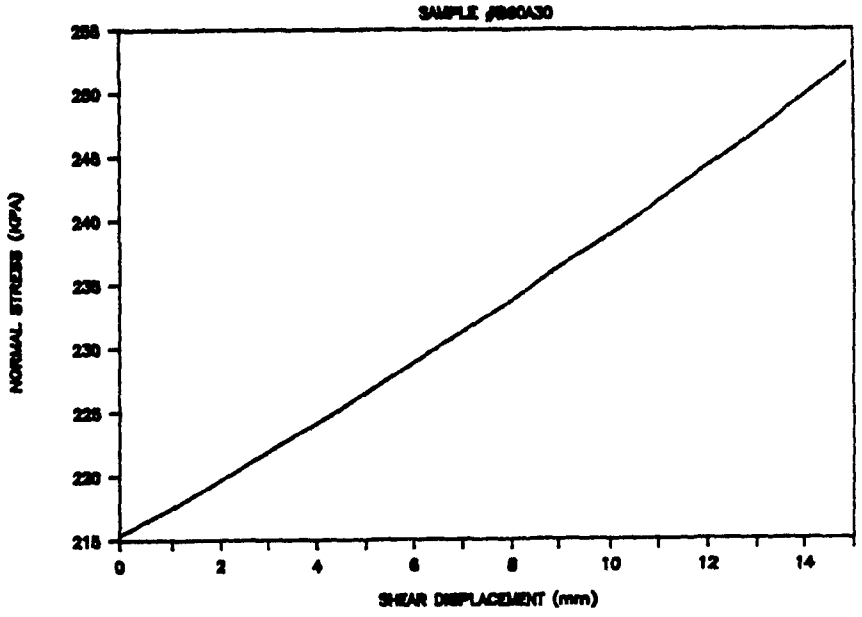

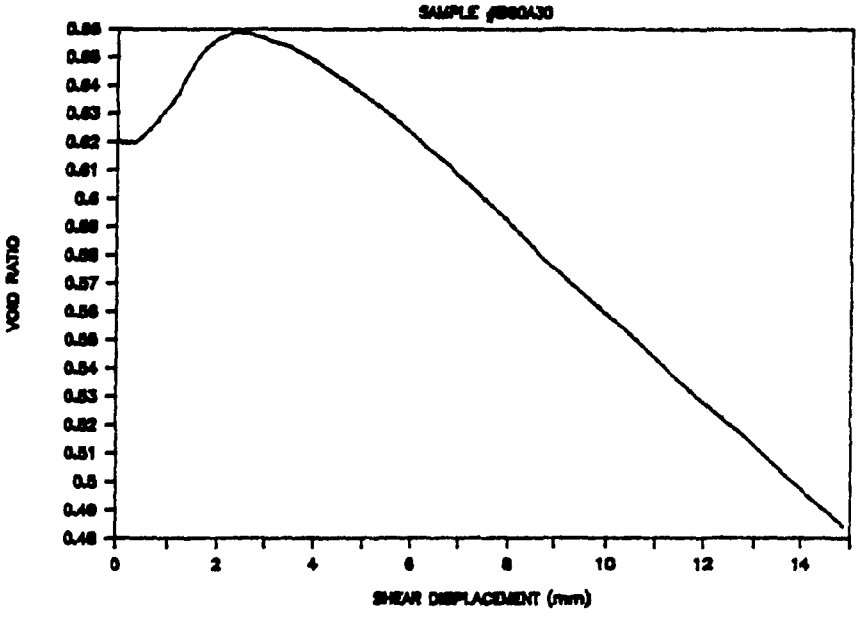

LAC MATAGAMI

SAMPLE #B60B30

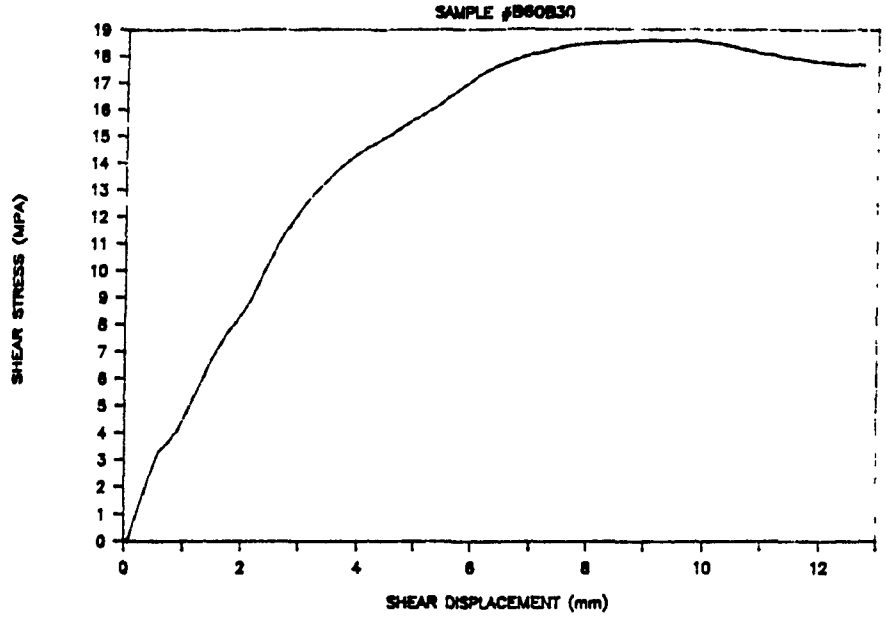

SAMPLE #B60B30

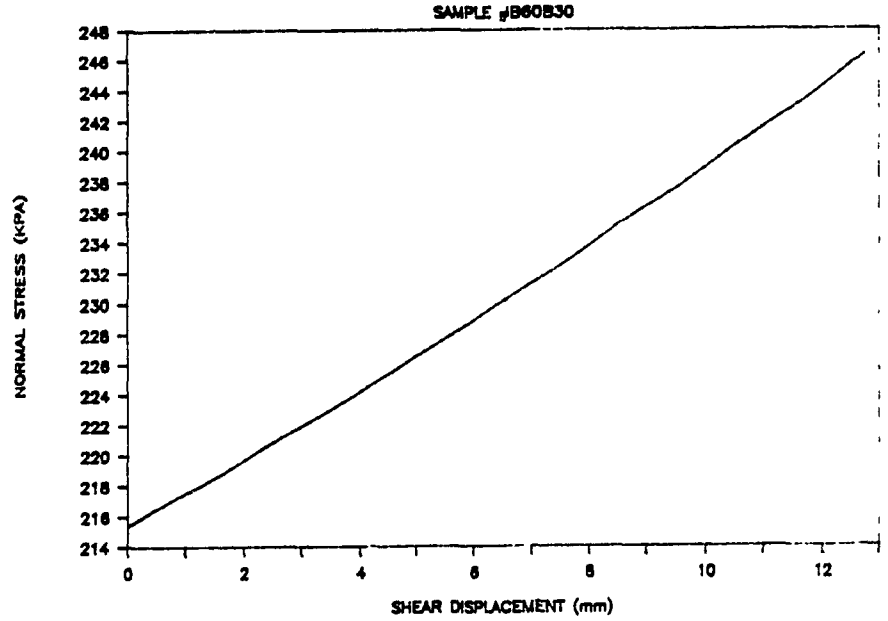

SAMPLE #B60B30

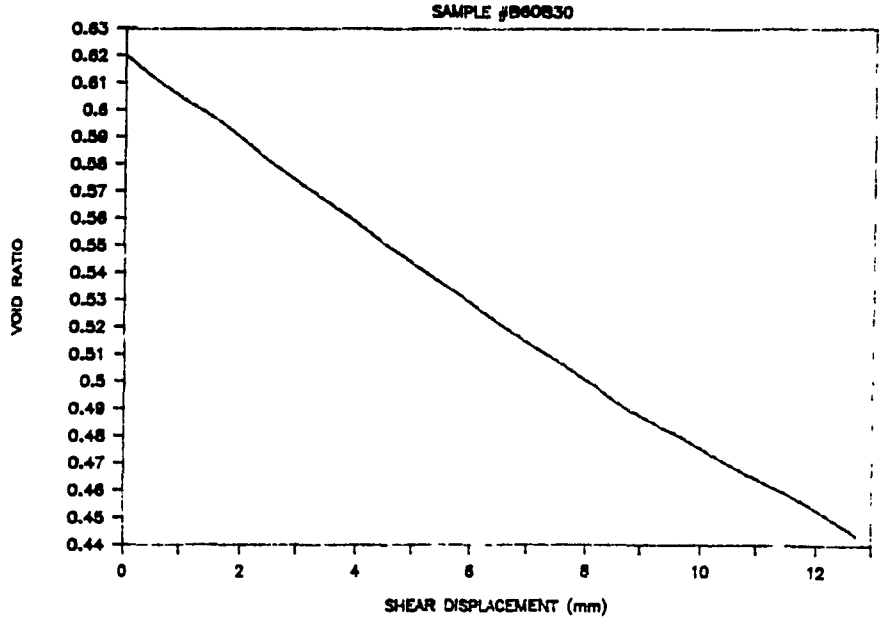

LAC MATAGAMI

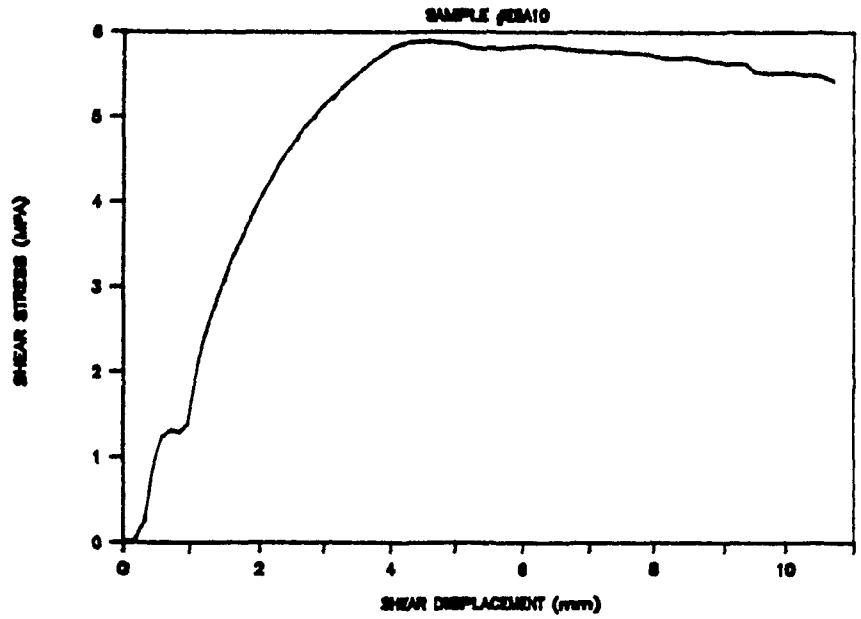

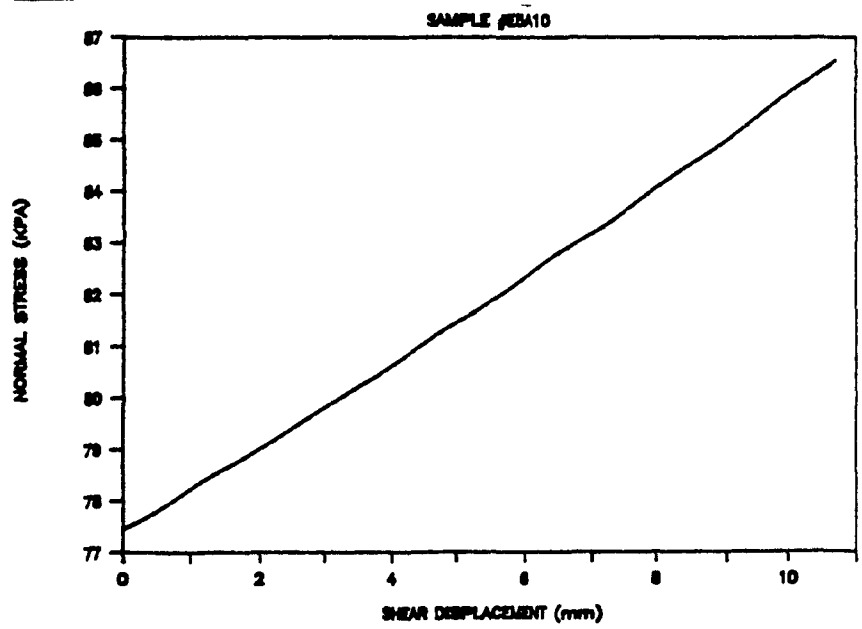

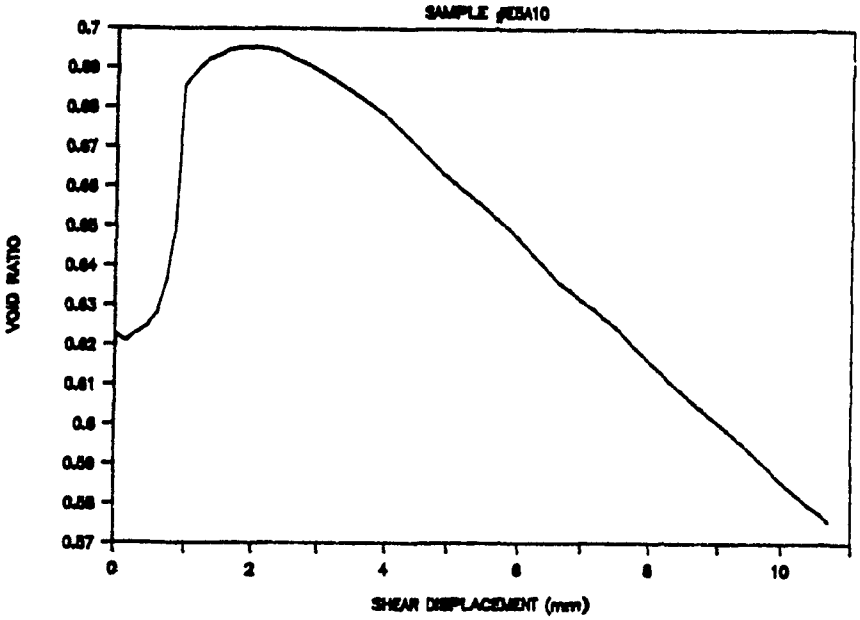

LAC MATAGAMI

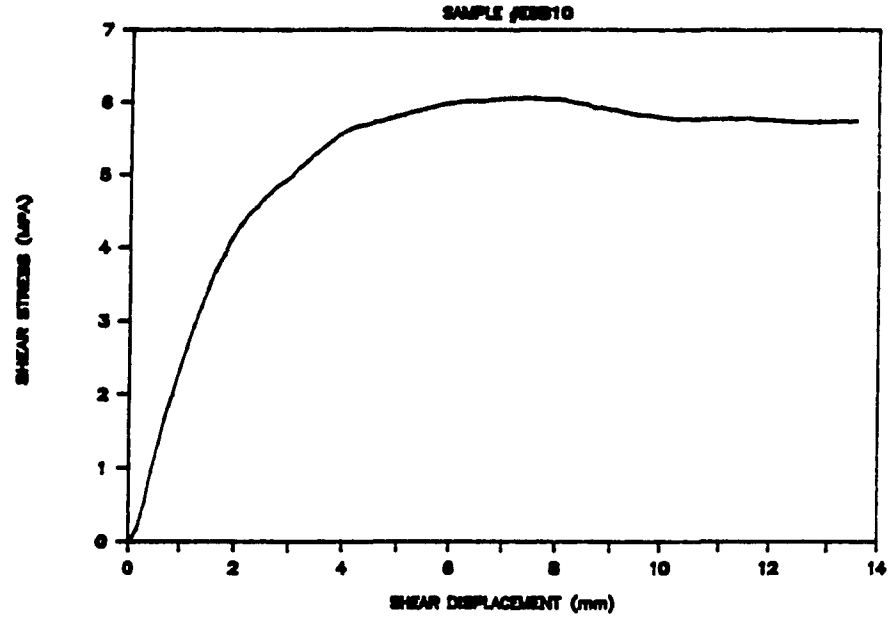

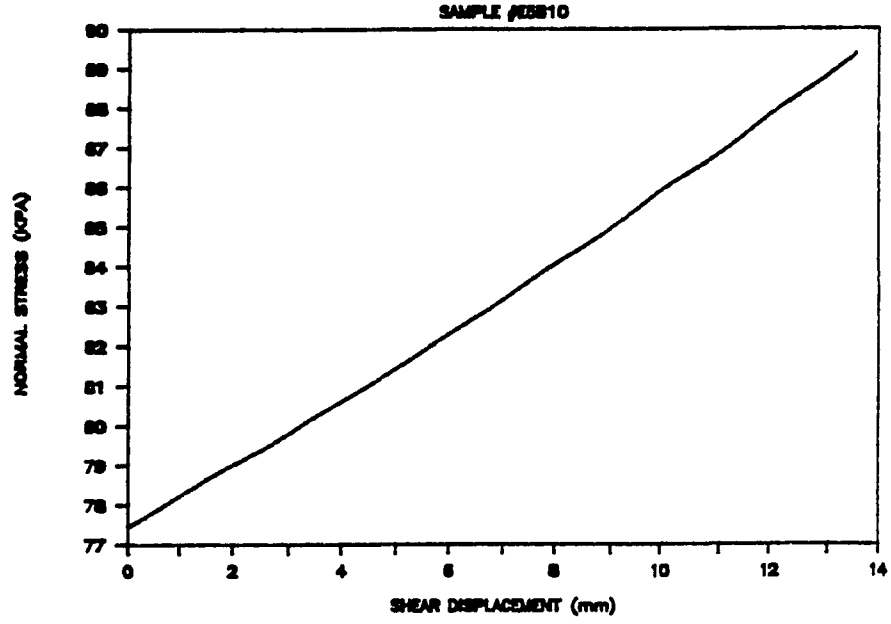

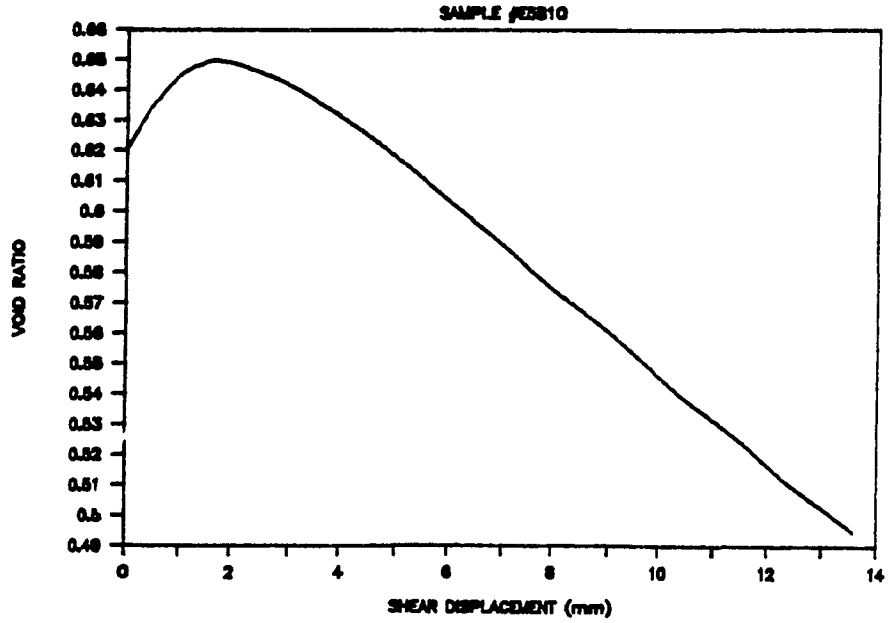

LAC MATAGAMI

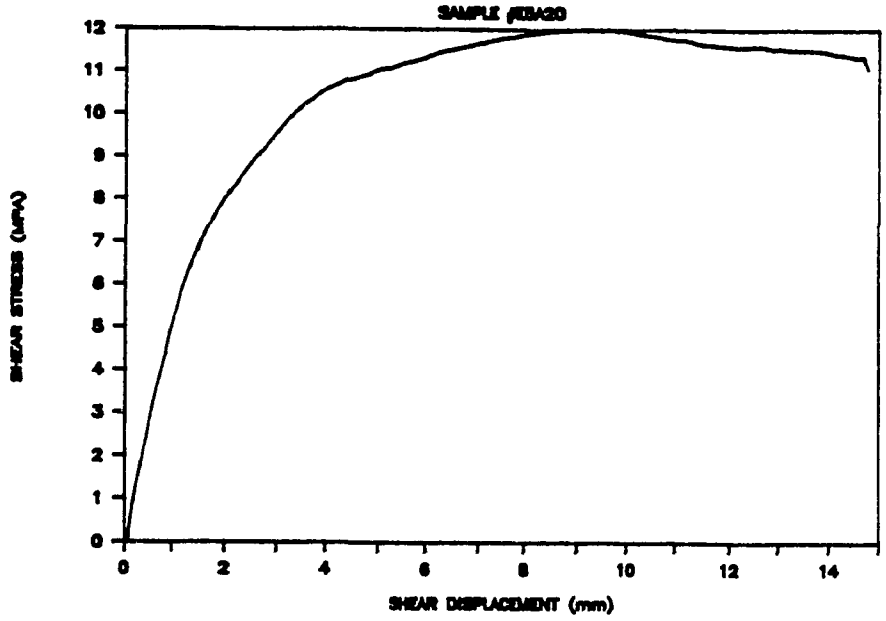

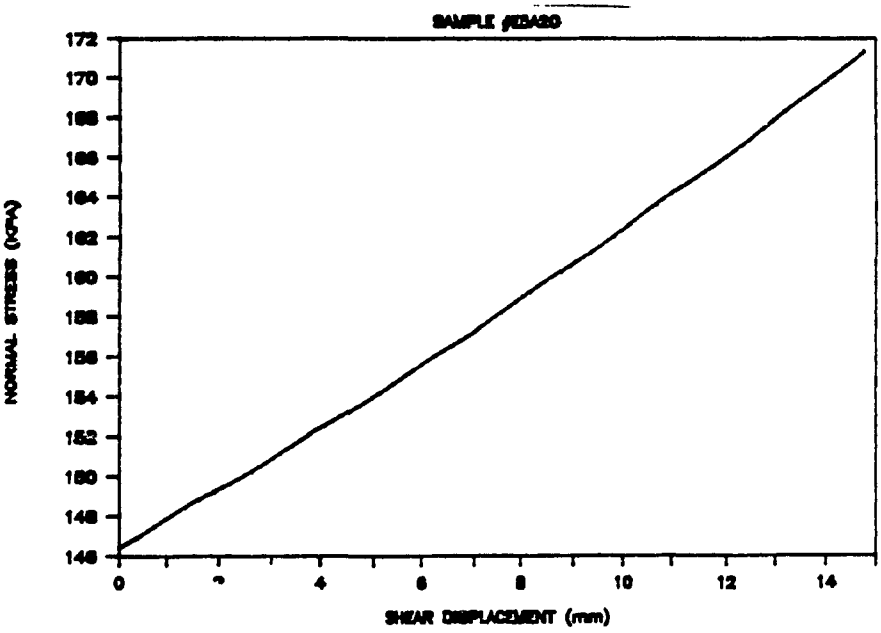

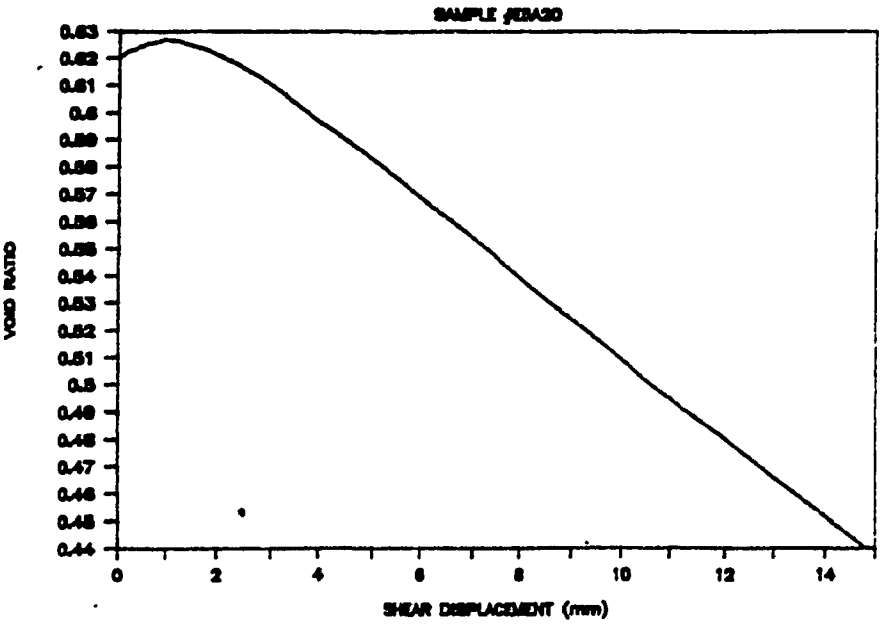

LAC MATAGAMI

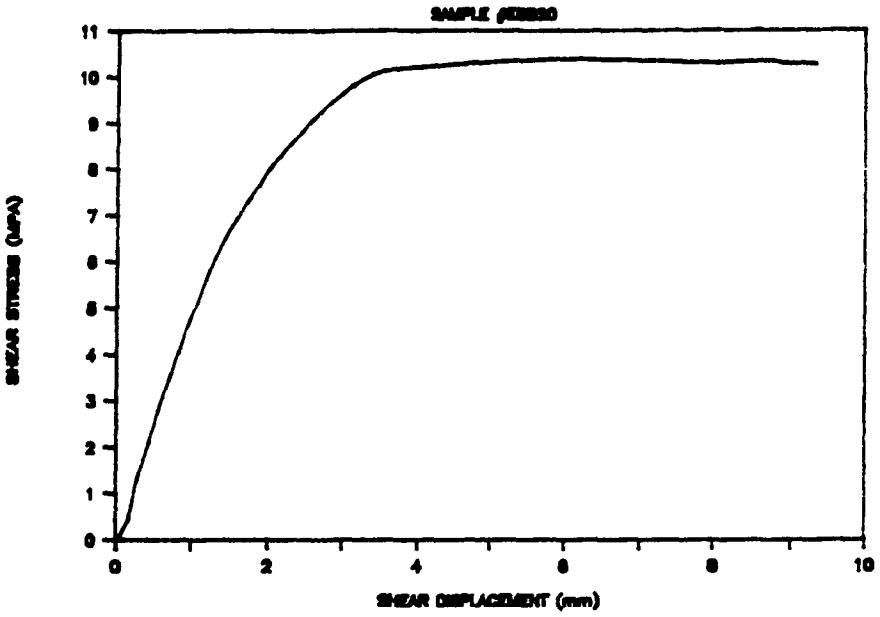

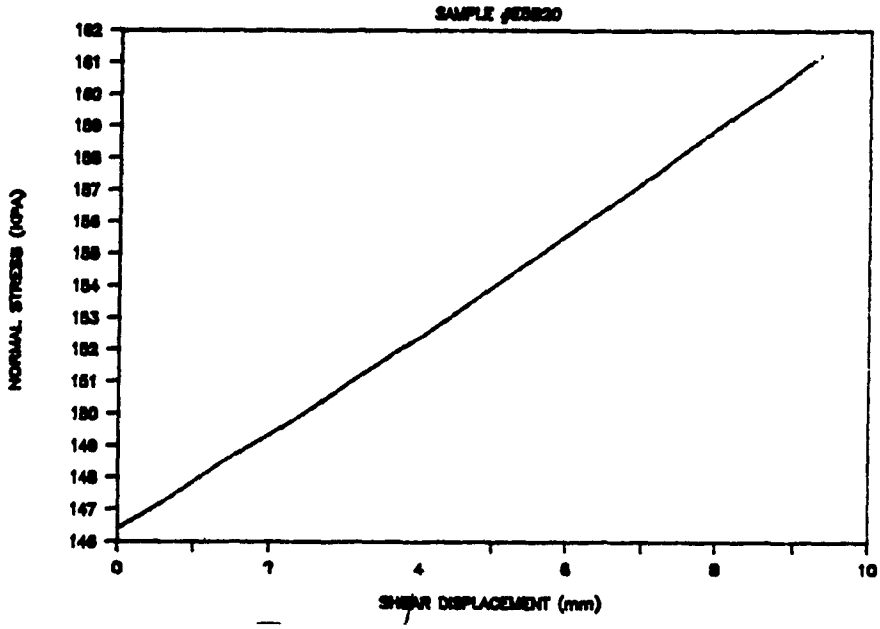

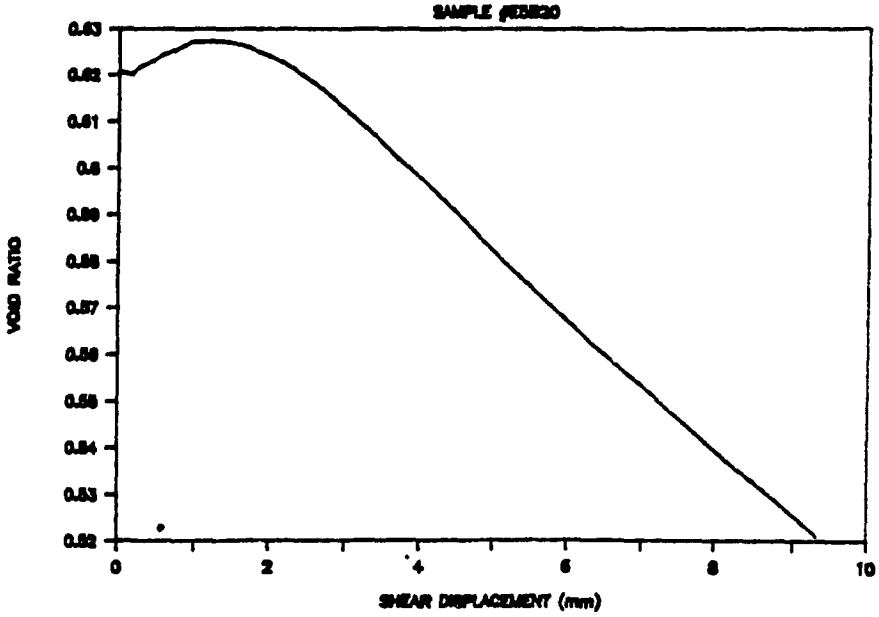

LAC MATAGAMI

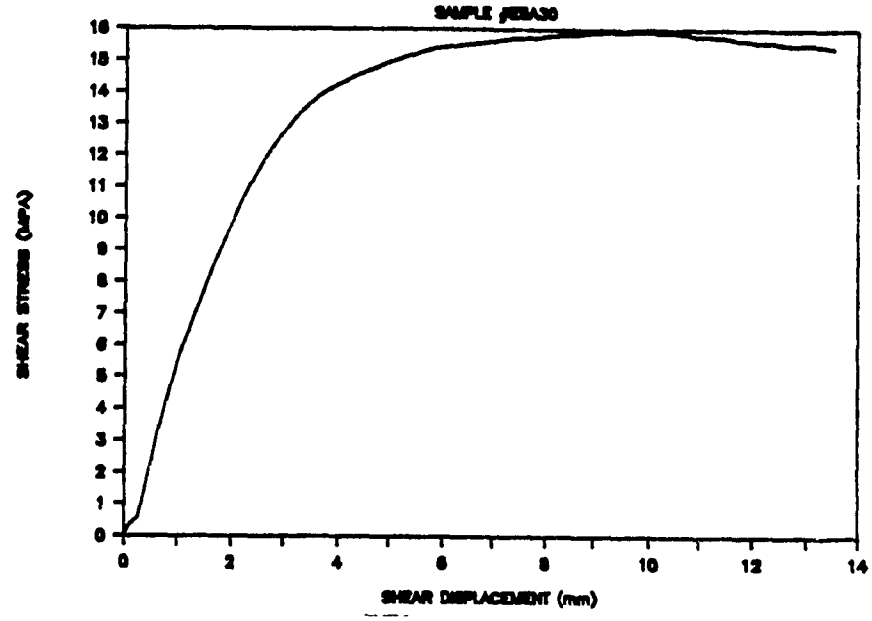

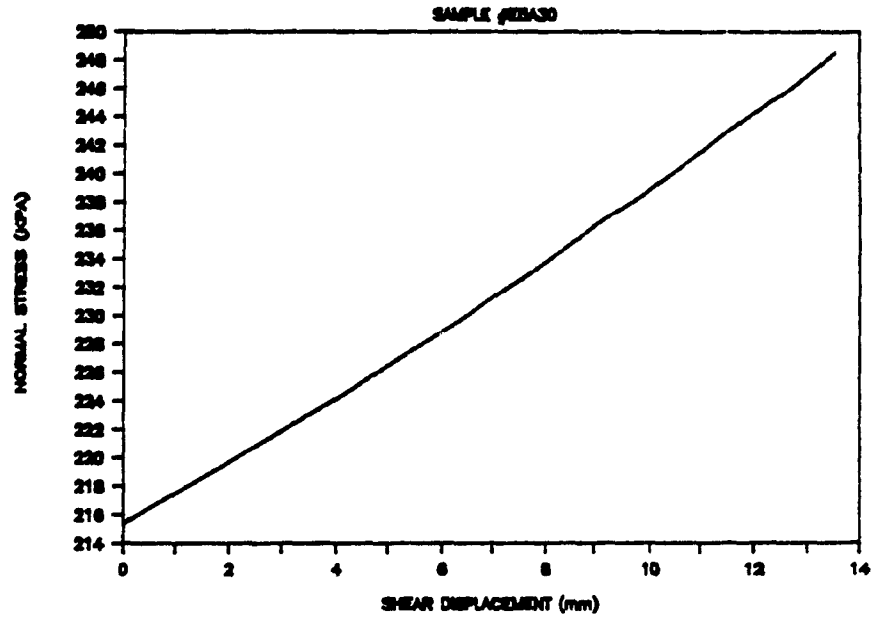

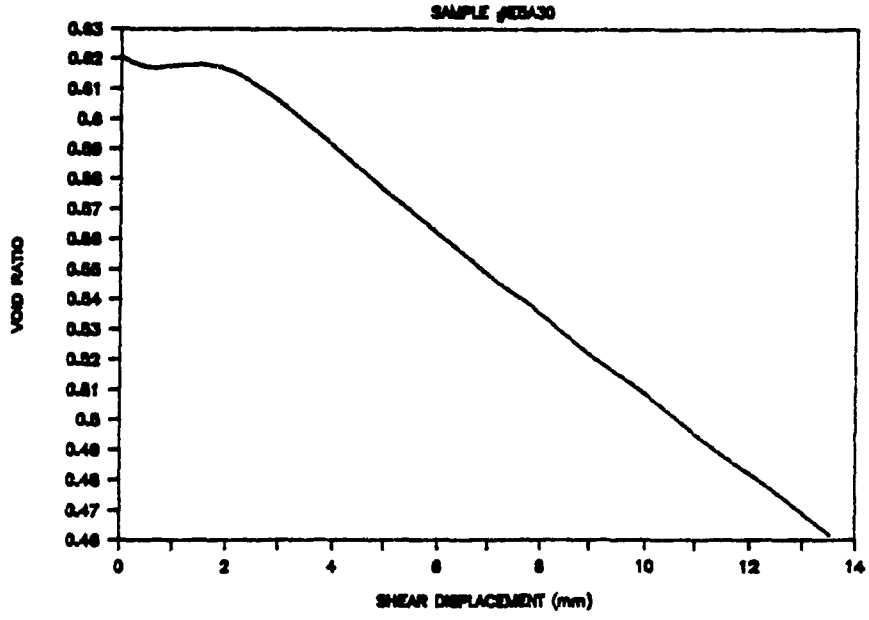

LAC MATAGAMI

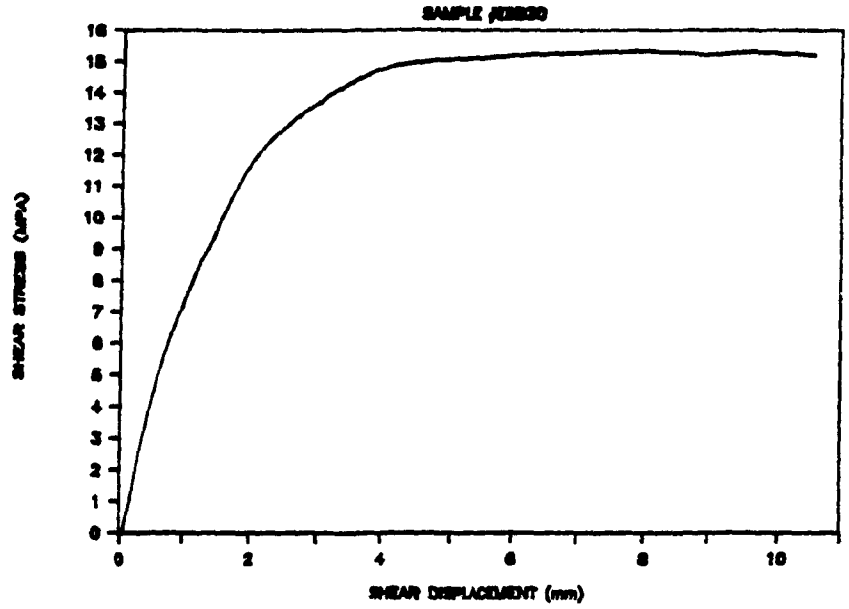

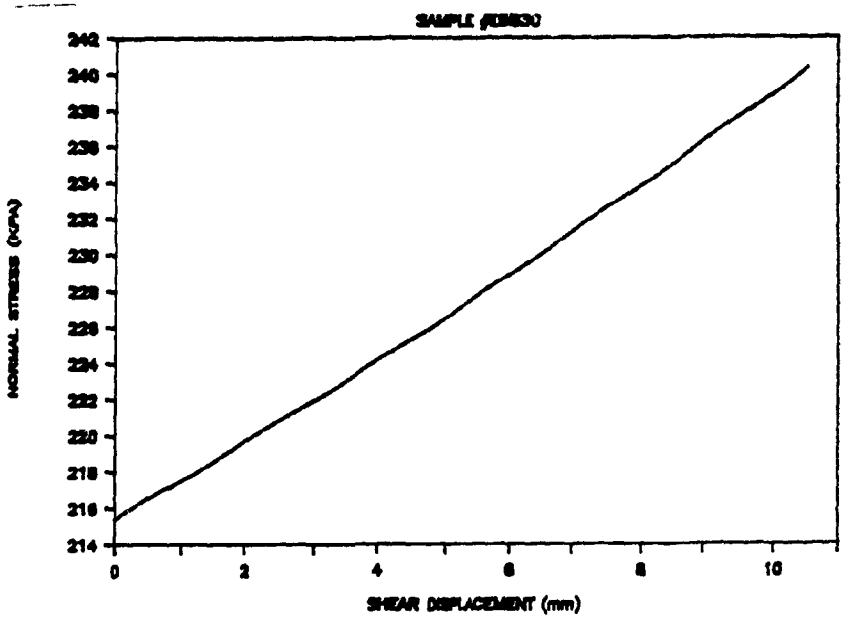

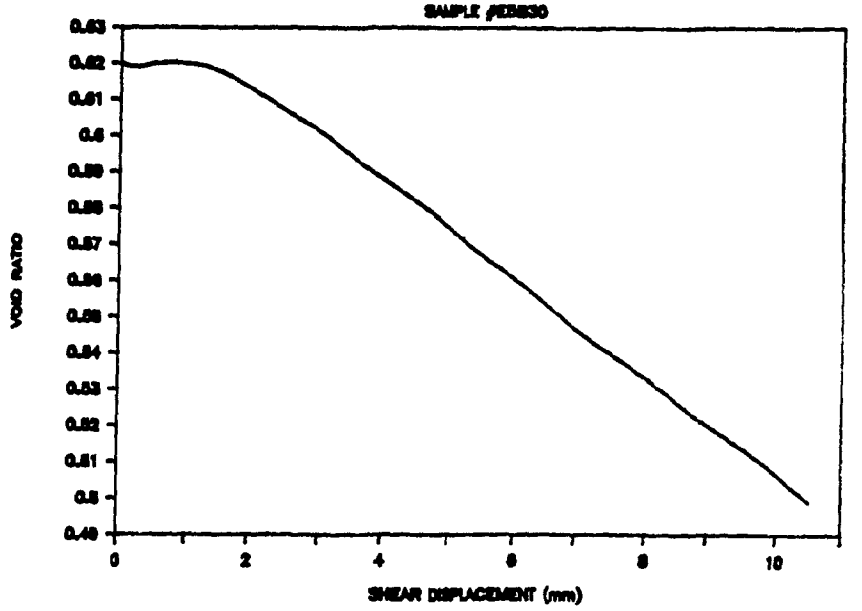

LAC MATAGAMI

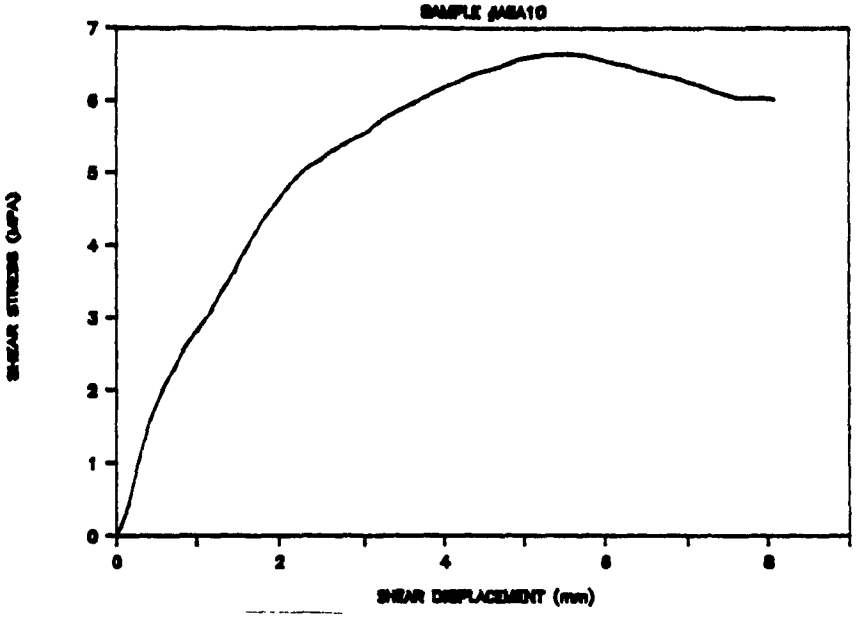

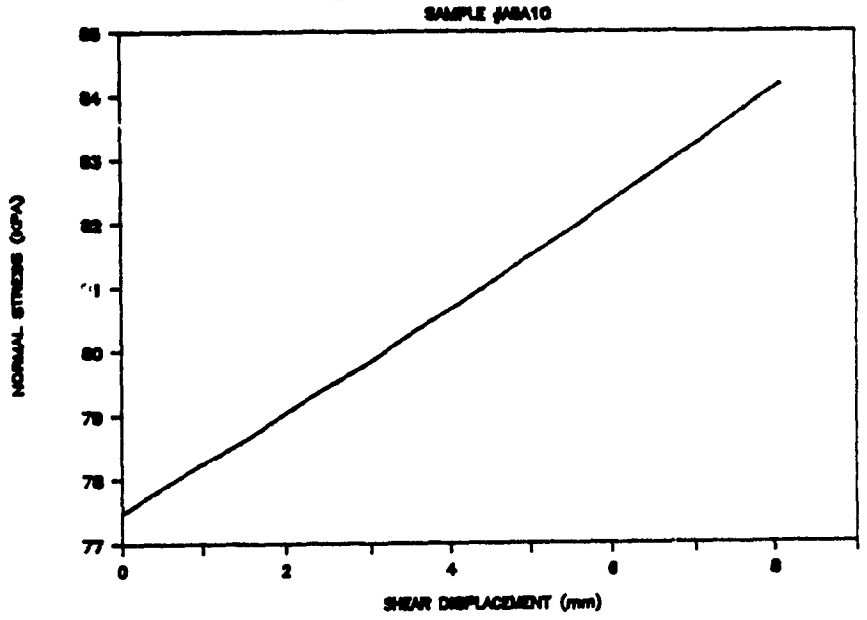

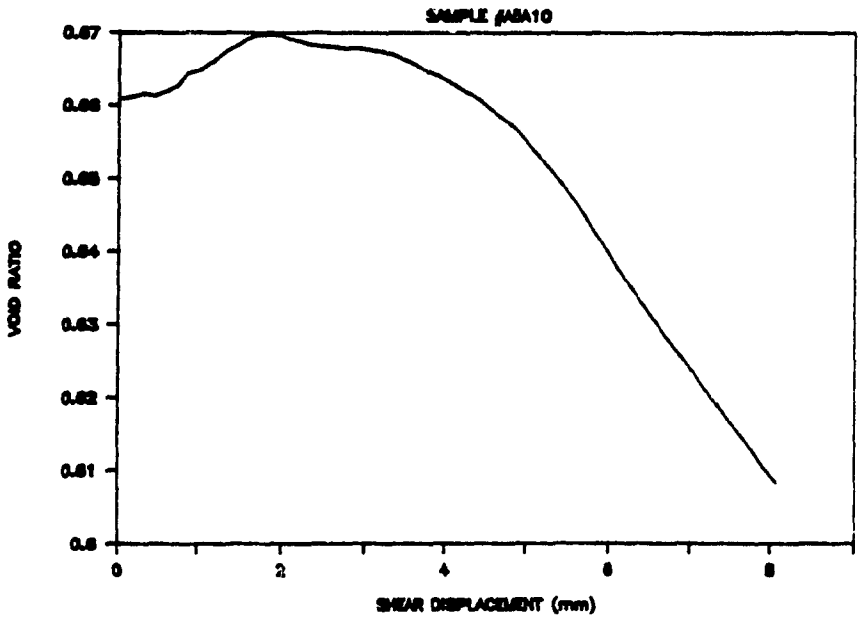

LAC MATAGAMI

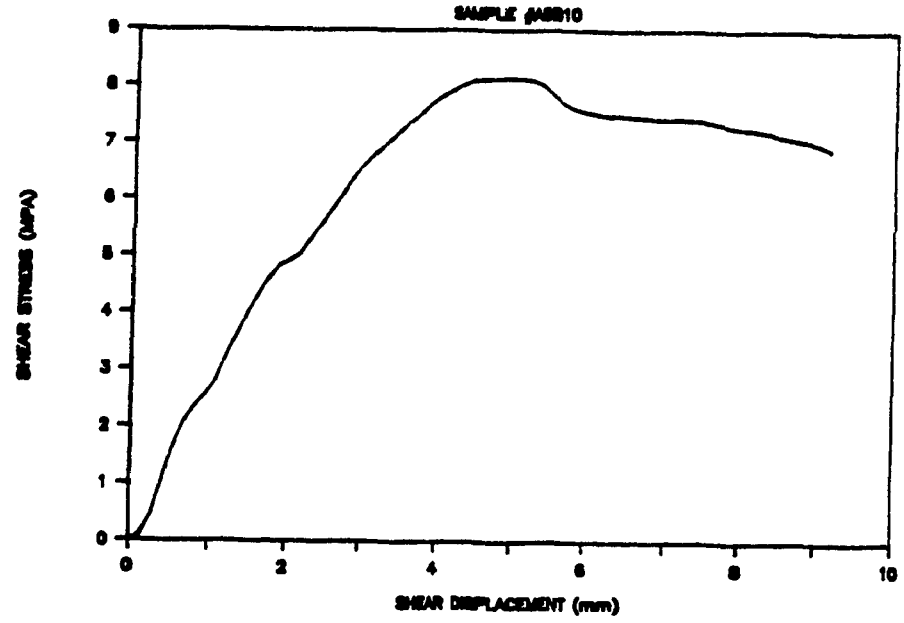

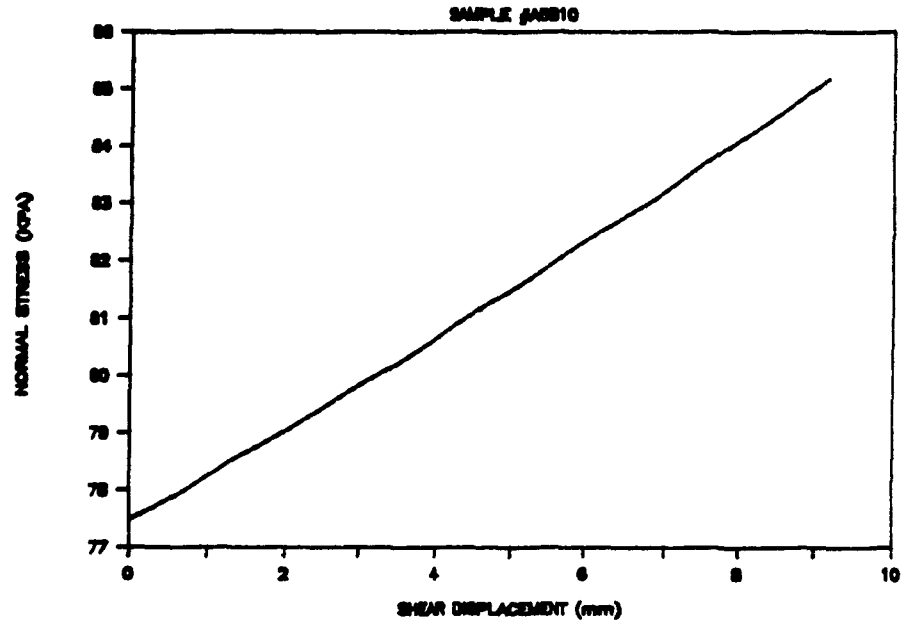

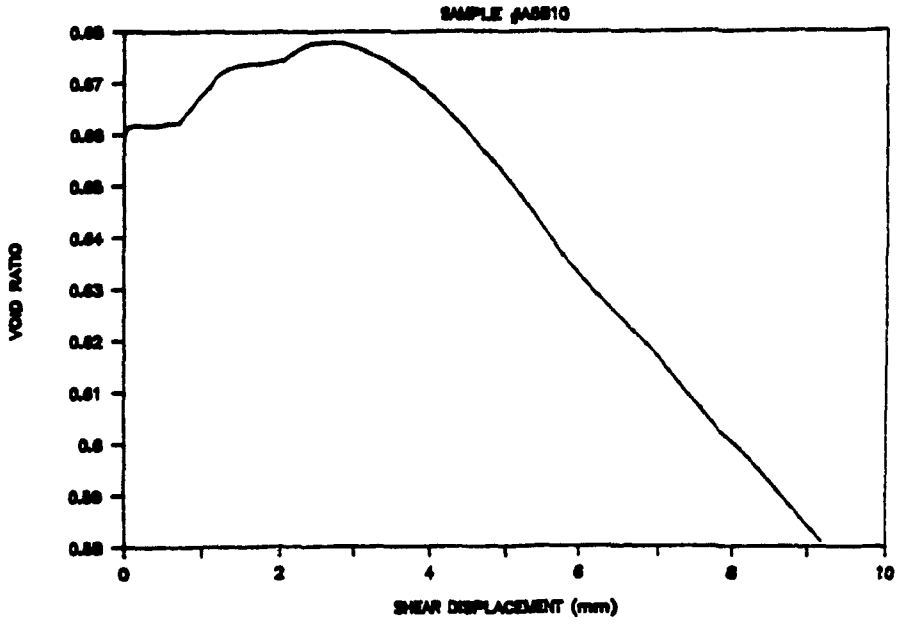

LAC MATAGAMI

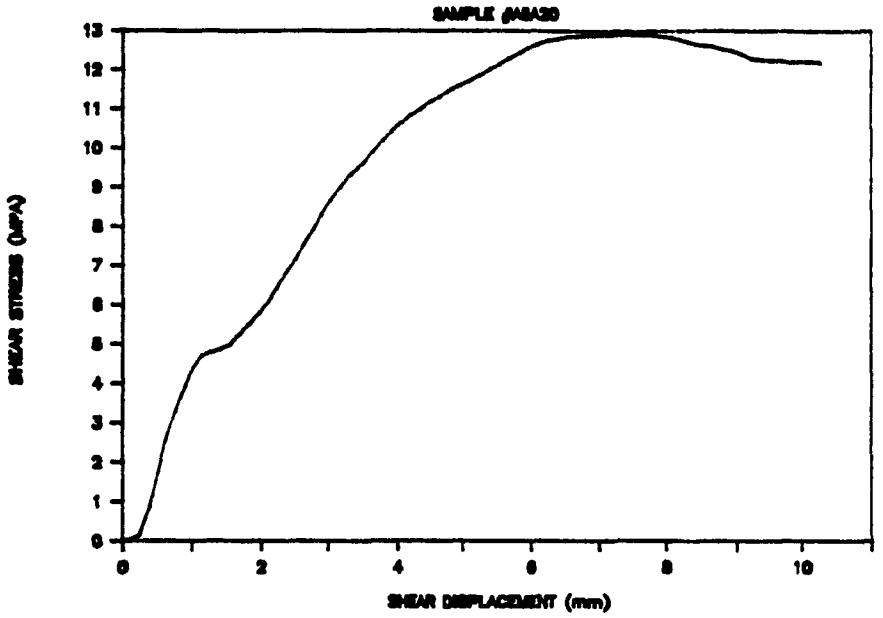

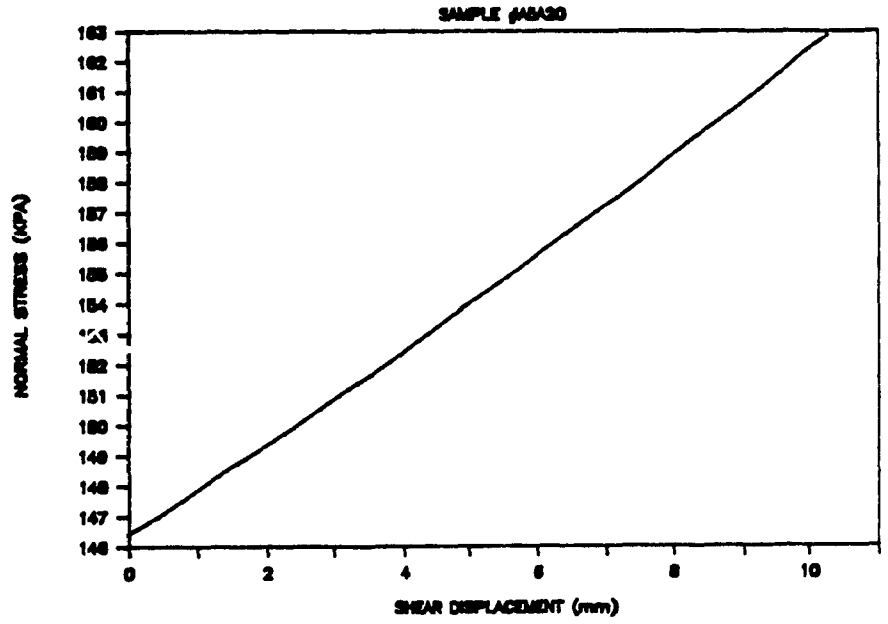

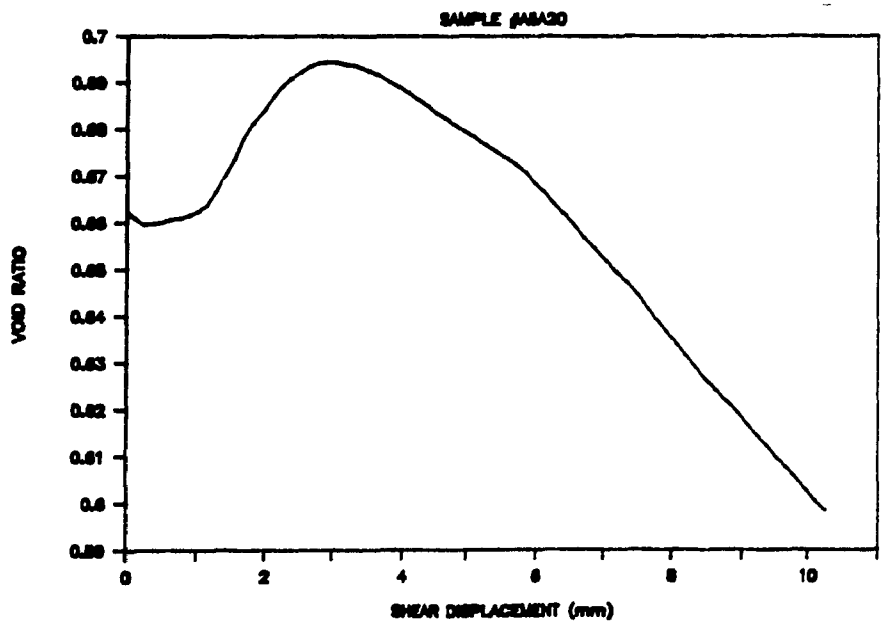

LAC MATAGAMI

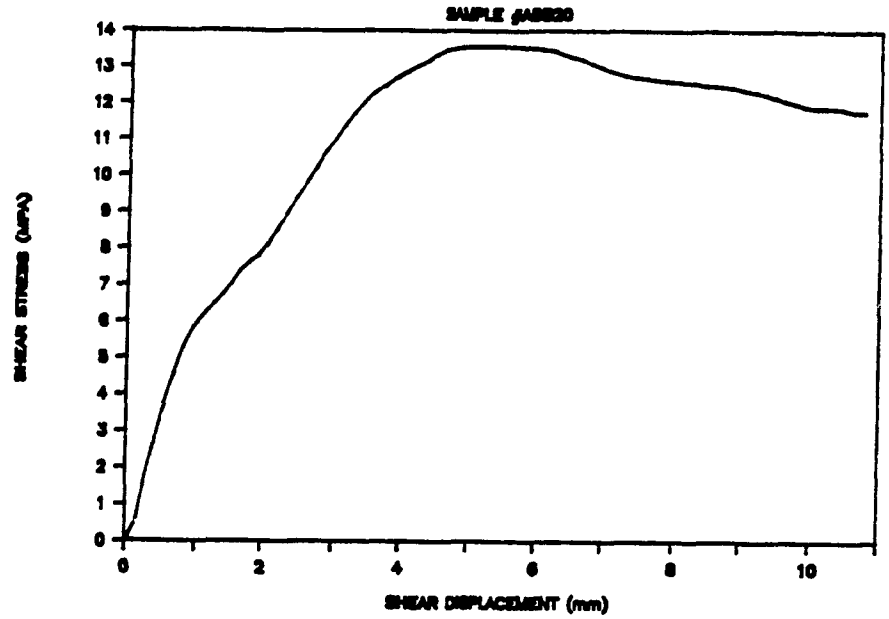

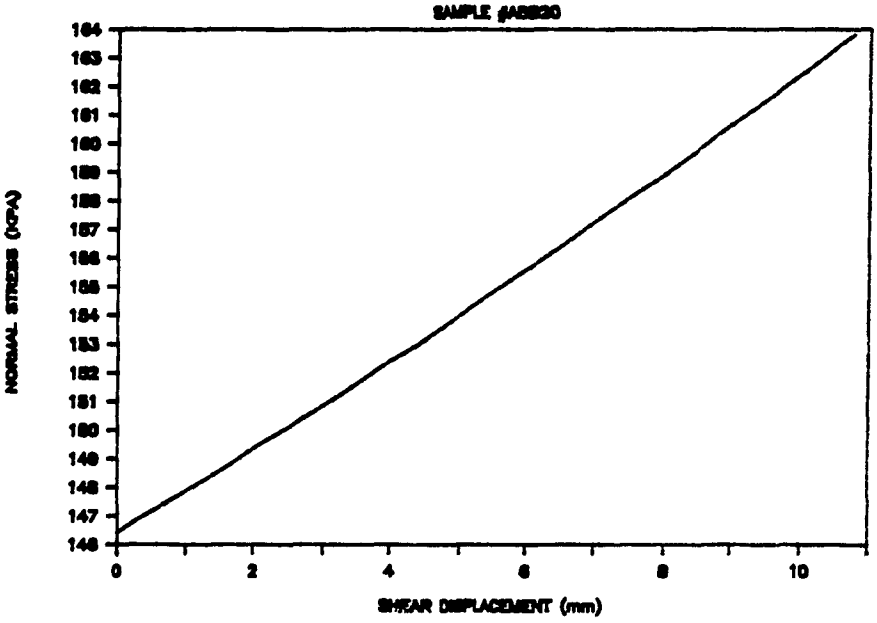

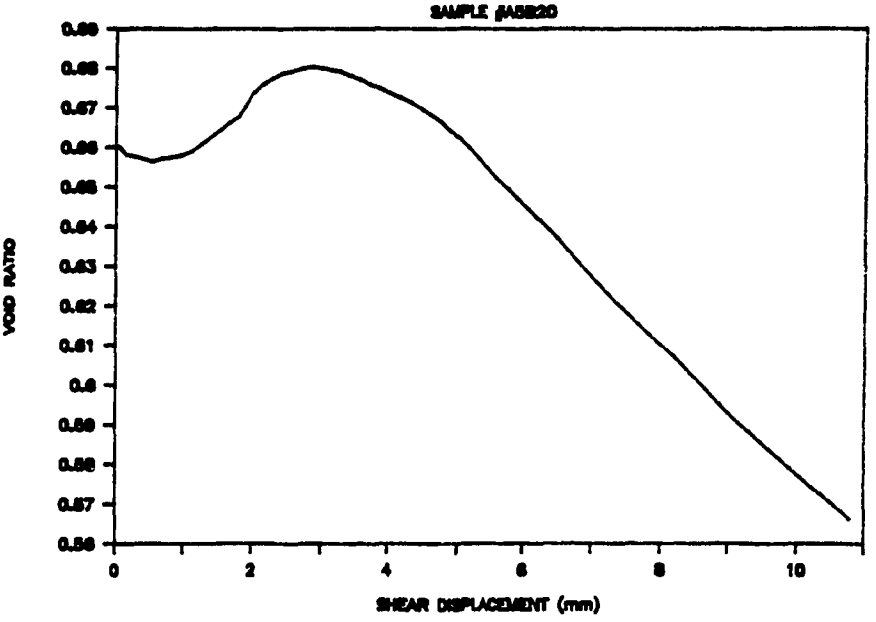

LAC MATAGAMI

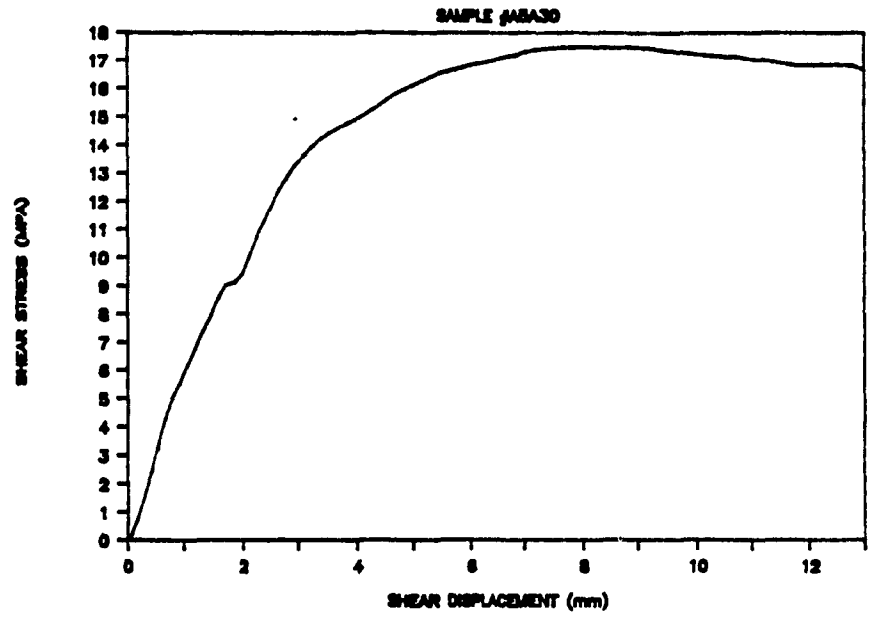

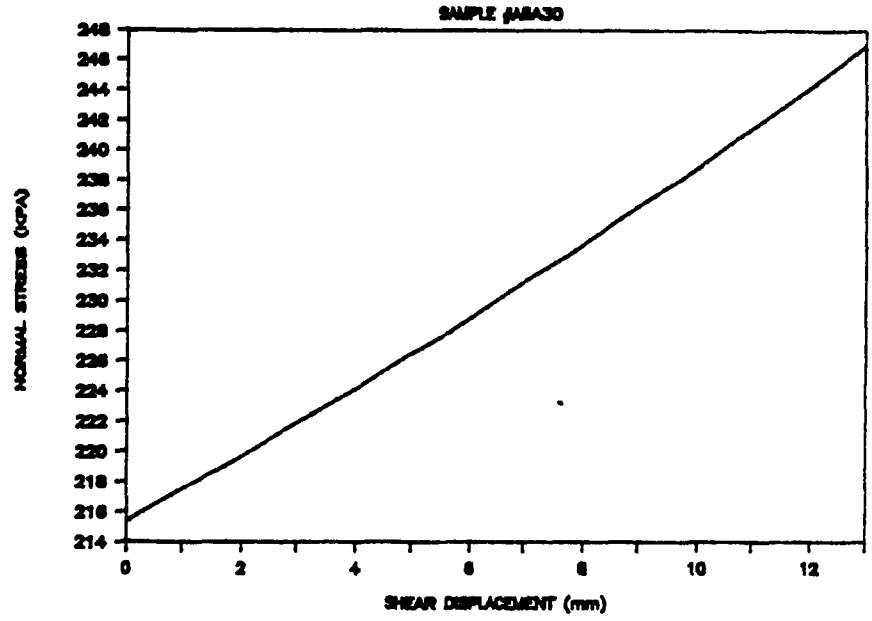

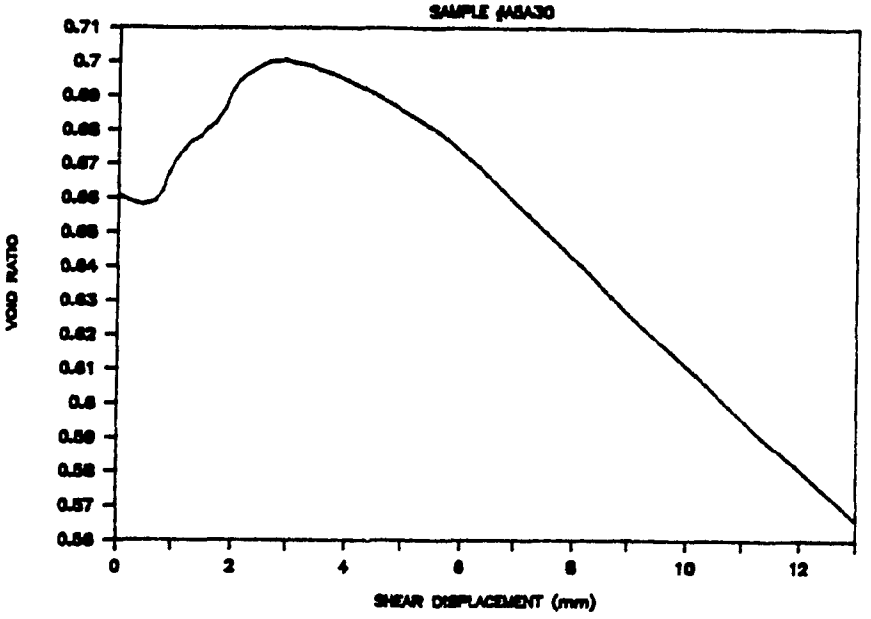

LAC MATAGAMI

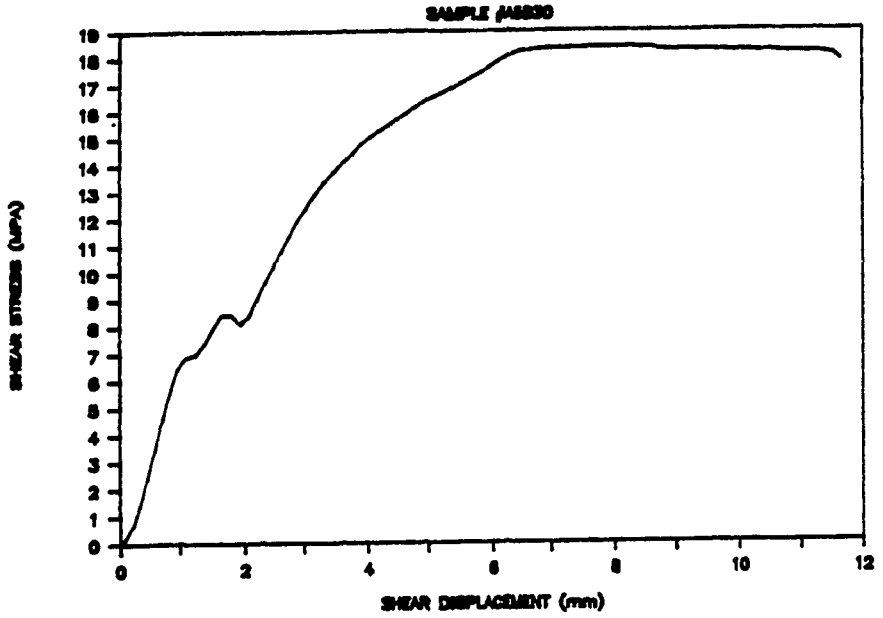

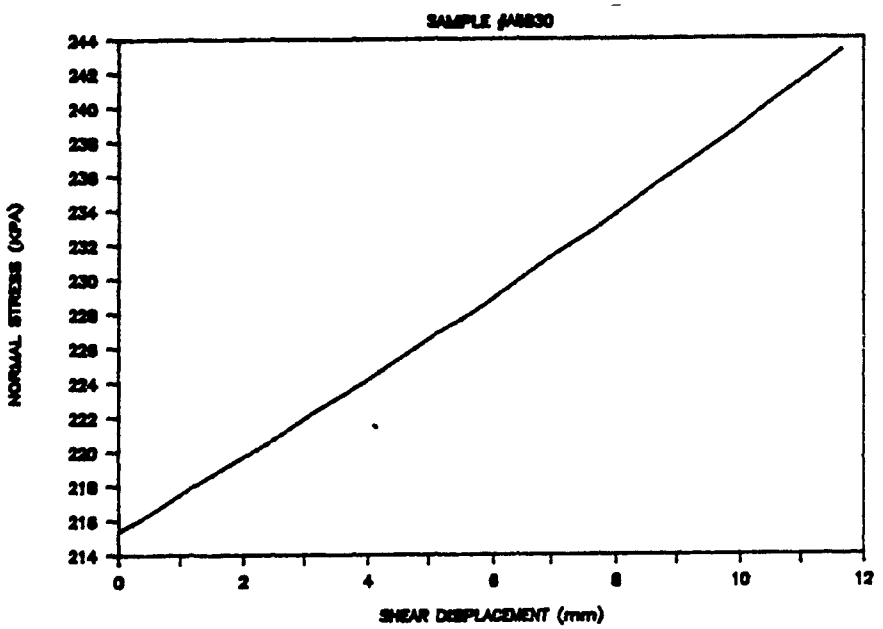

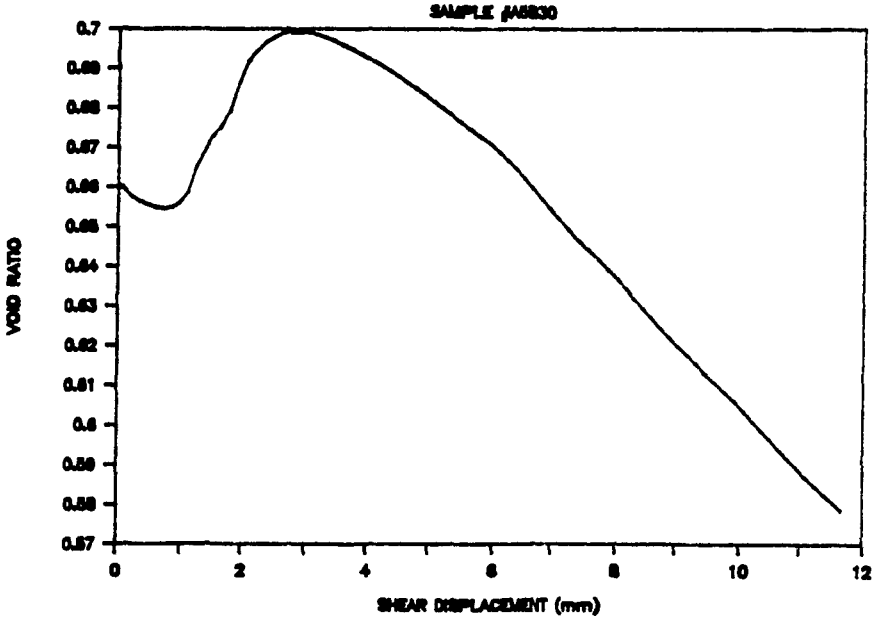

LAC MATAGAMI

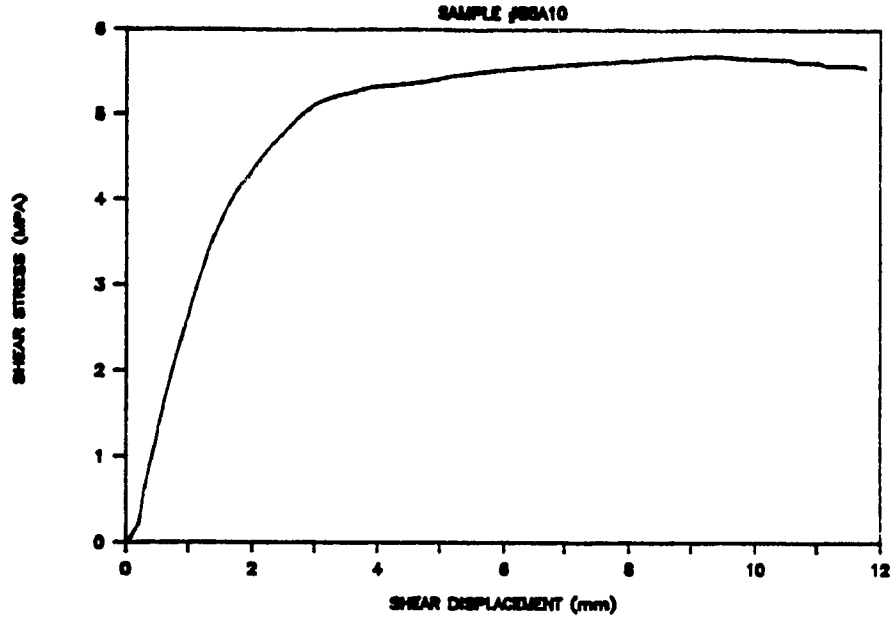

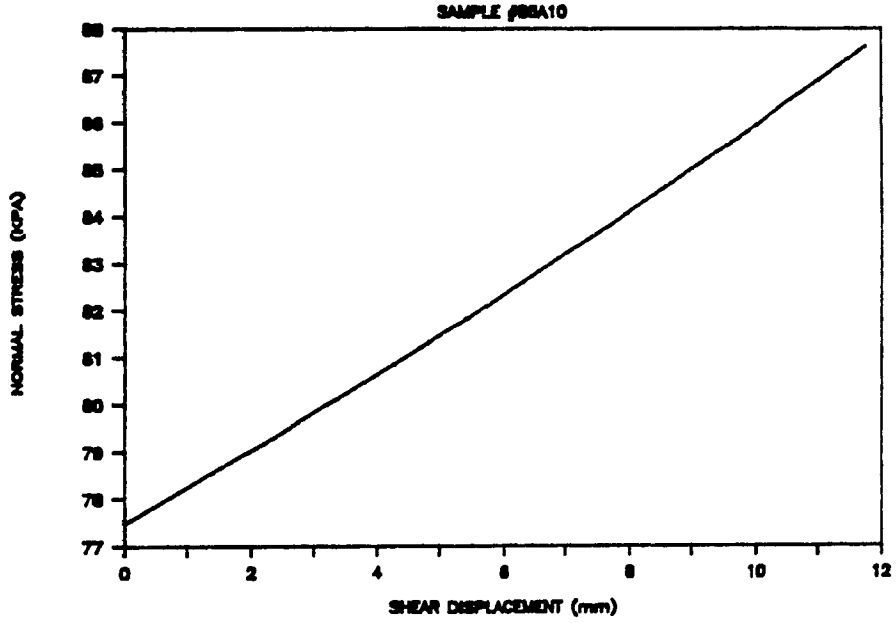

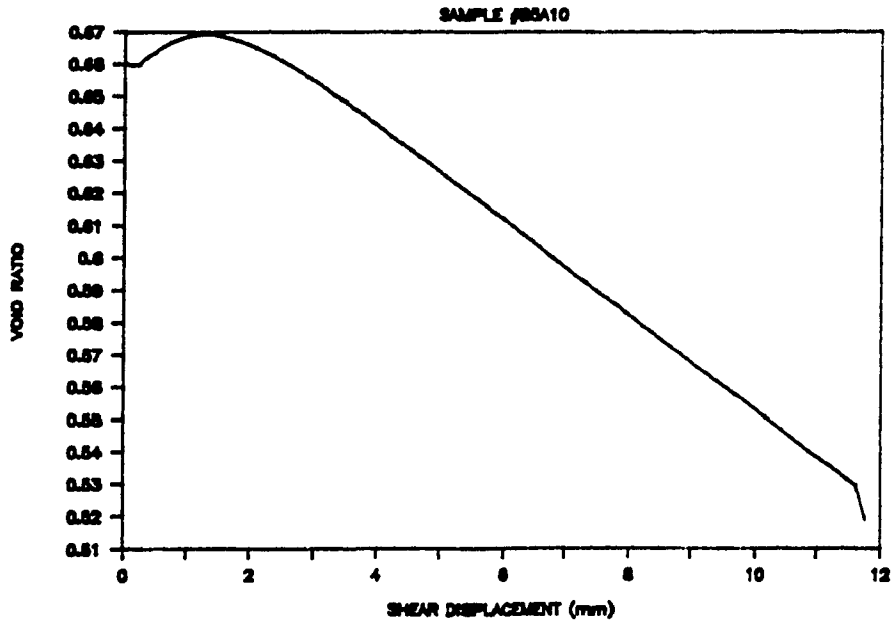

LAC MATAGAMI

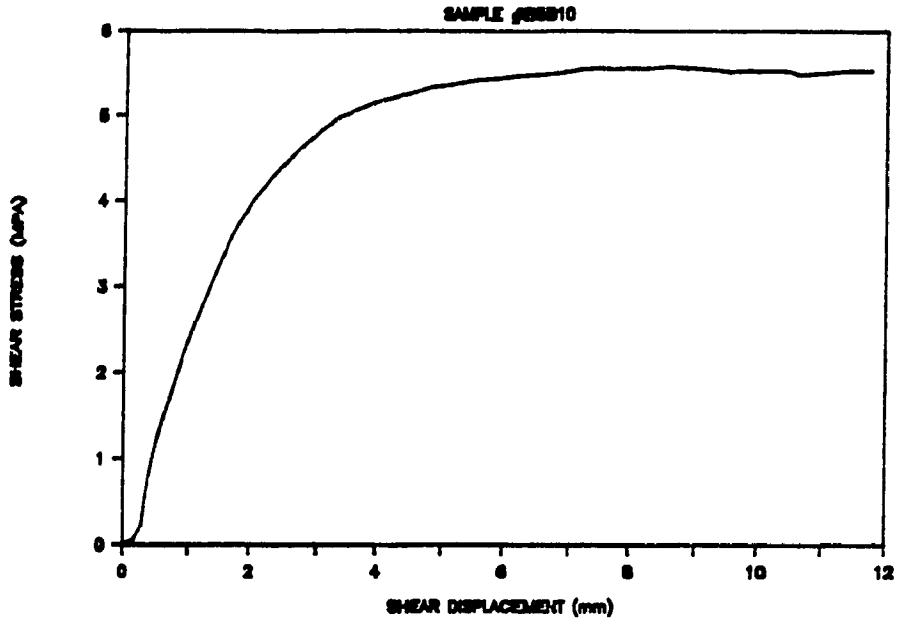

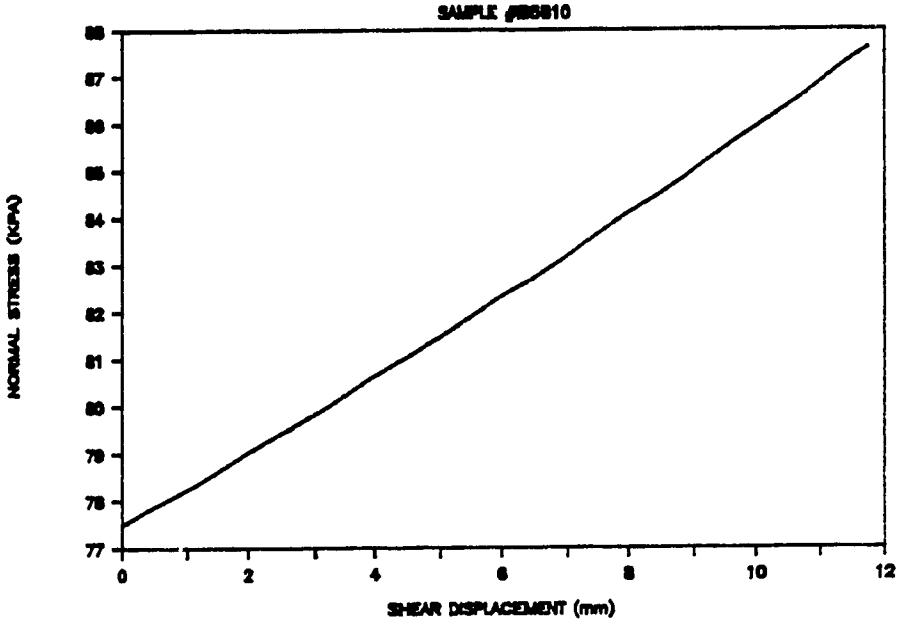

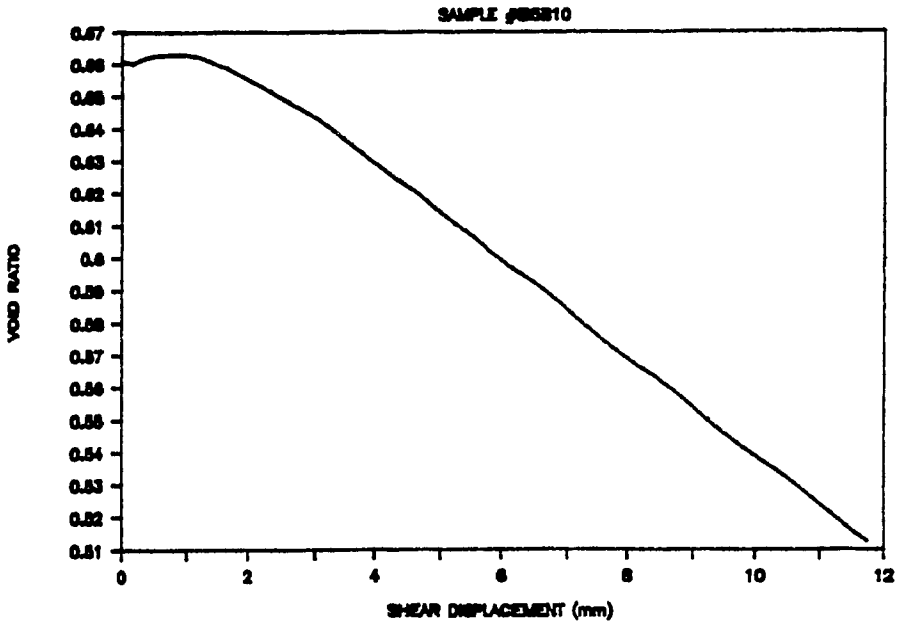

LAC MATAGAMI

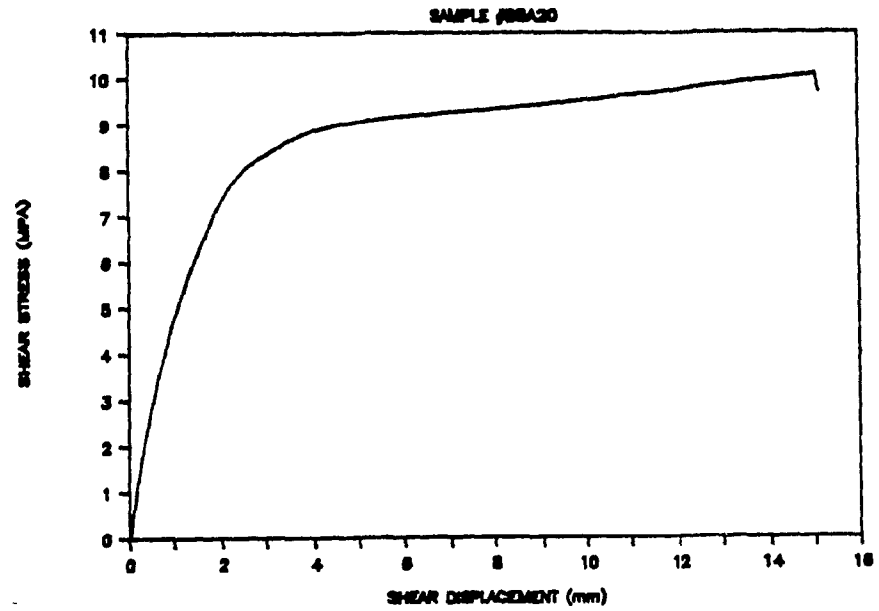

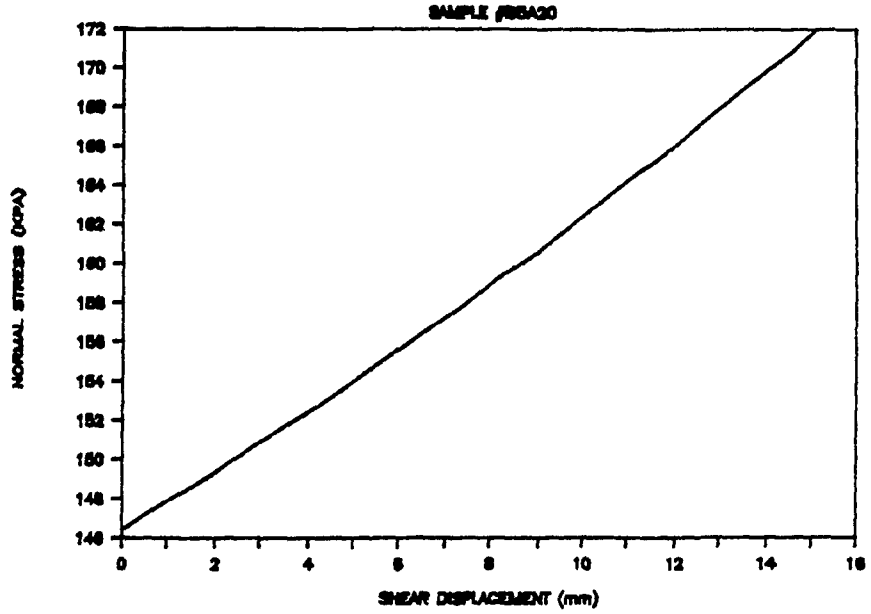

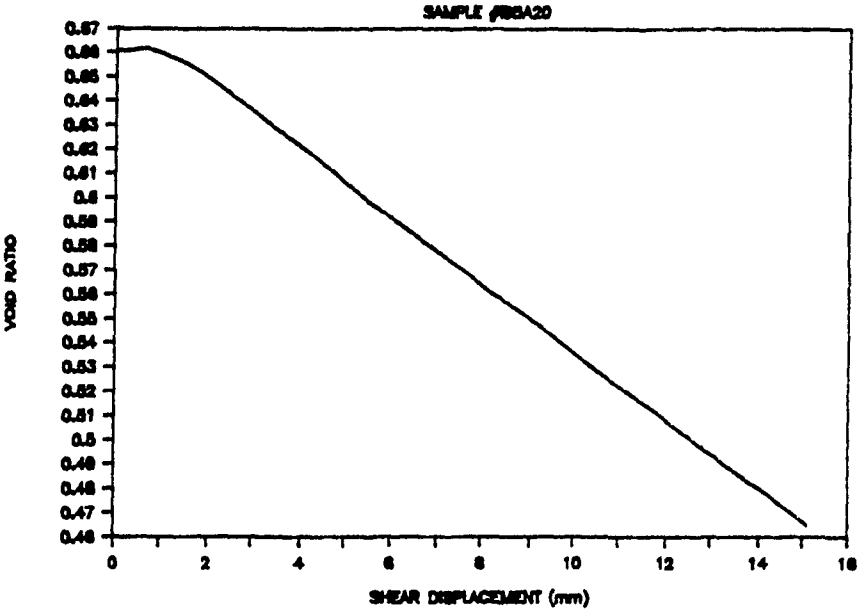

LAC MATAGAMI

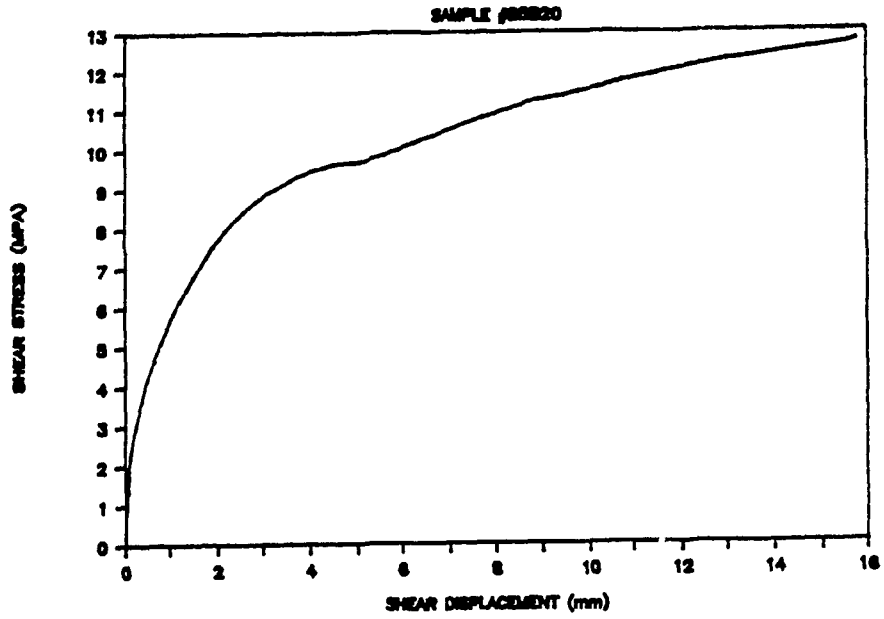

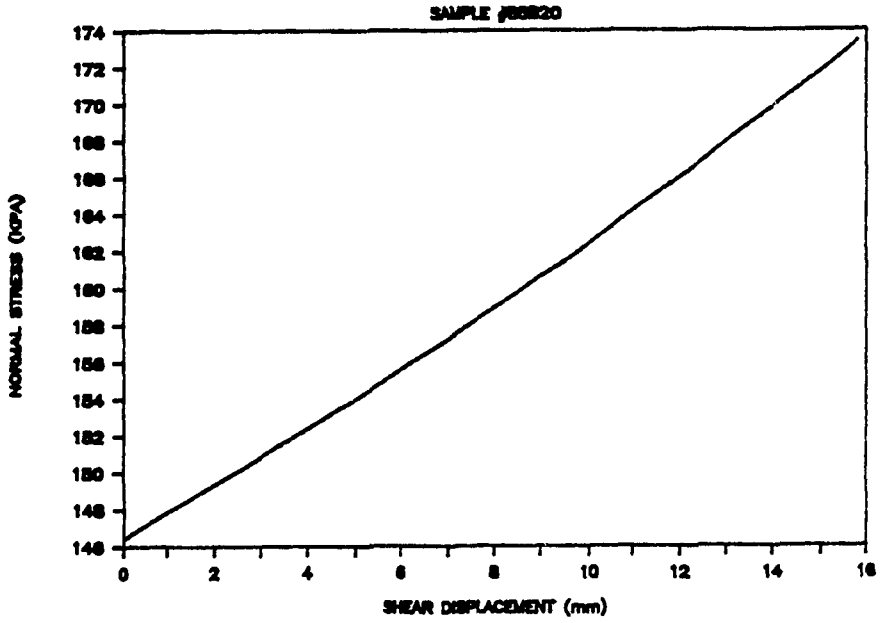

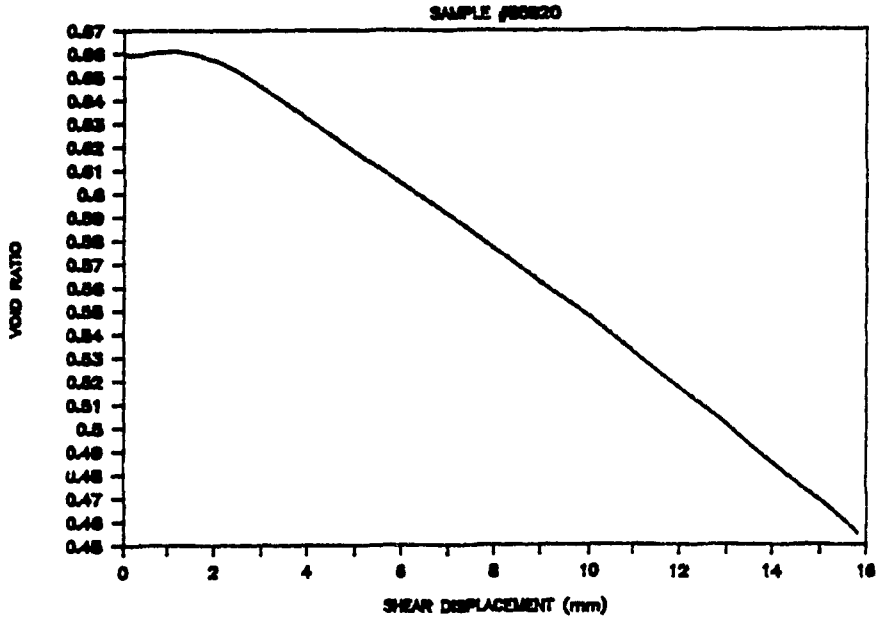

LAC MATAGAMI

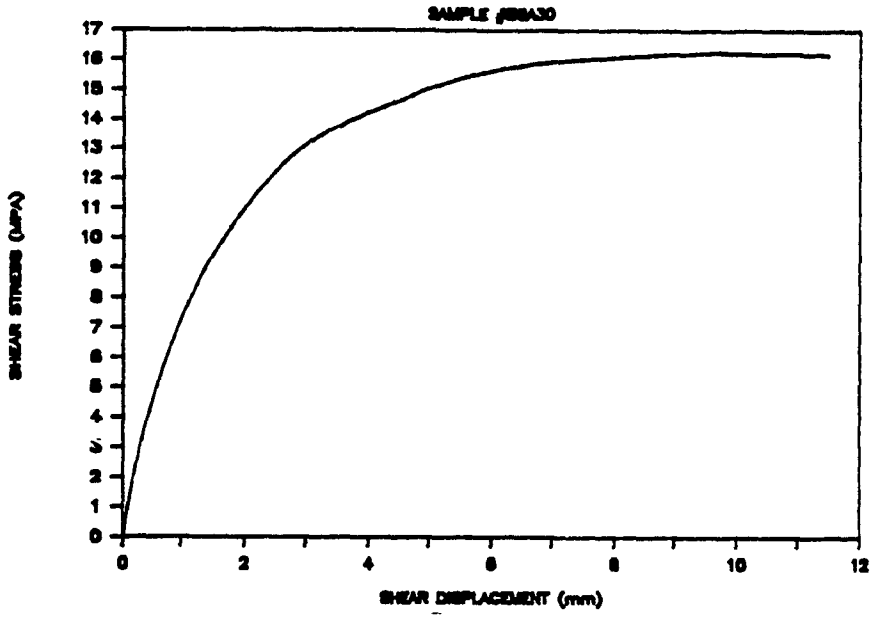

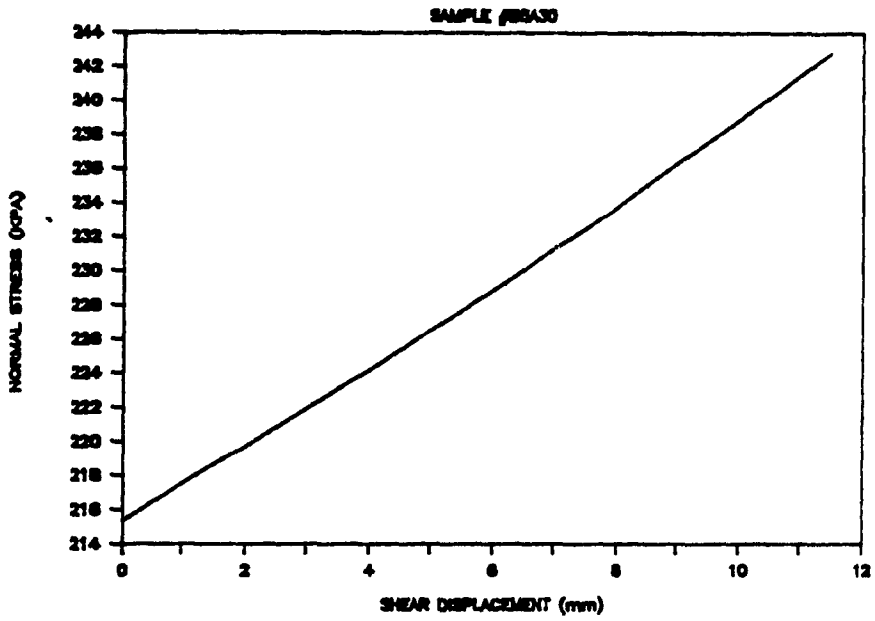

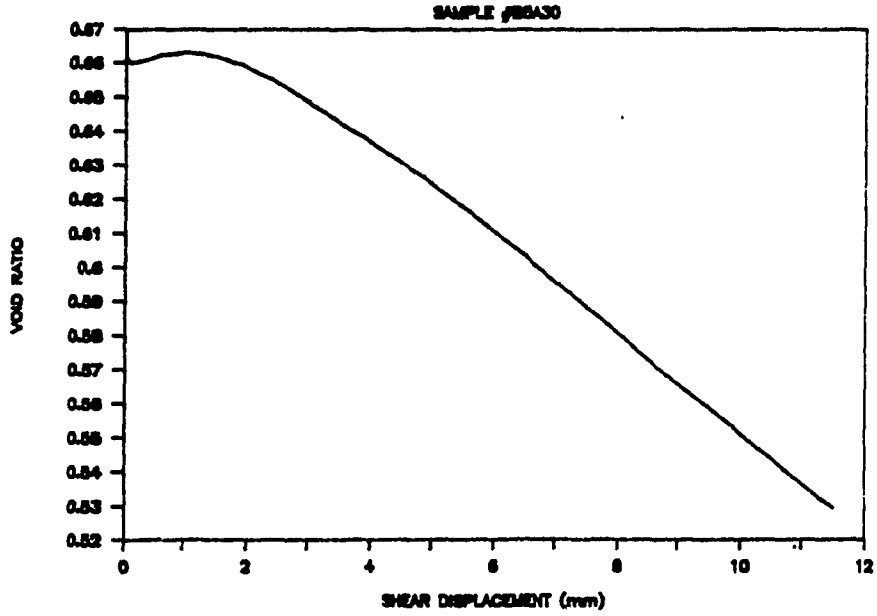

LAC MATAGAMI

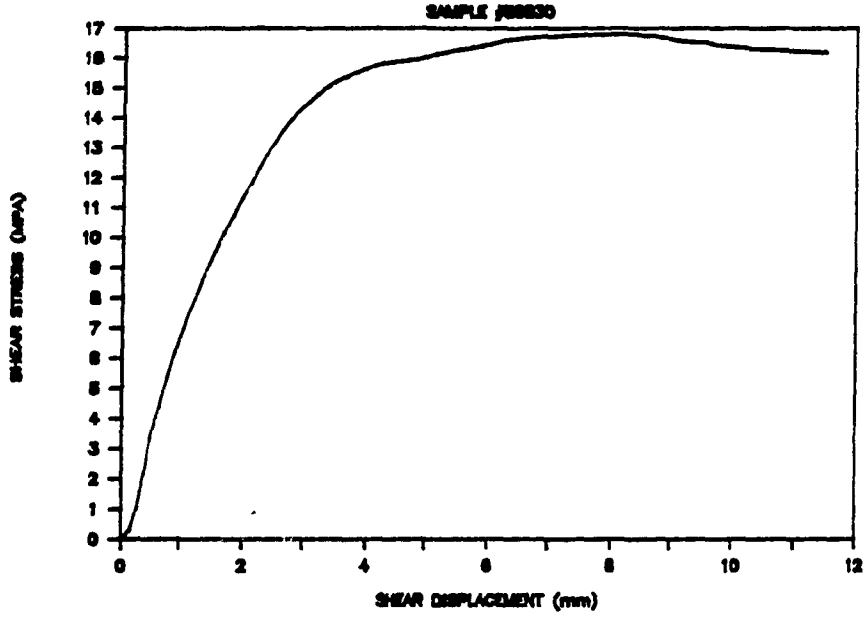

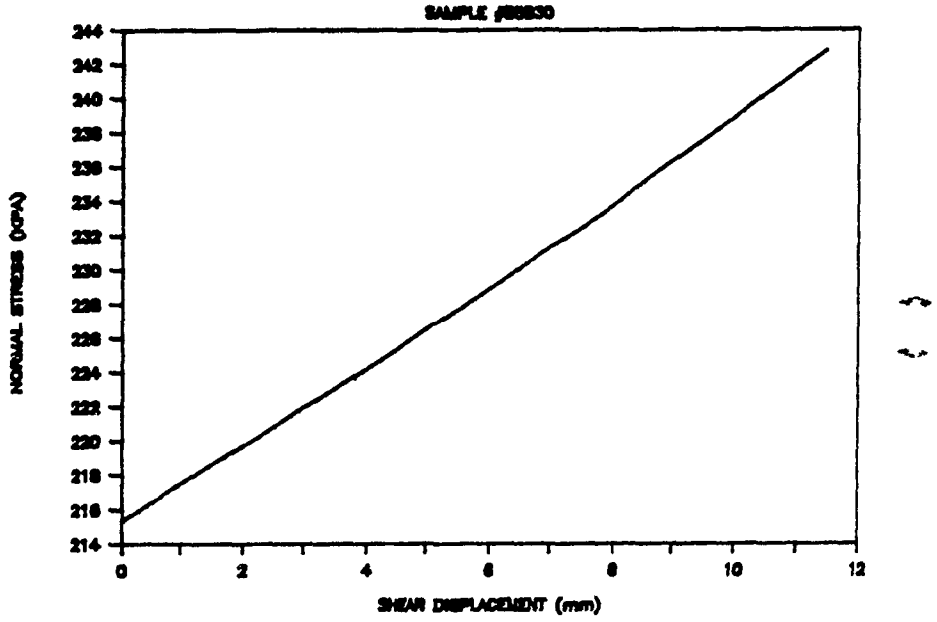

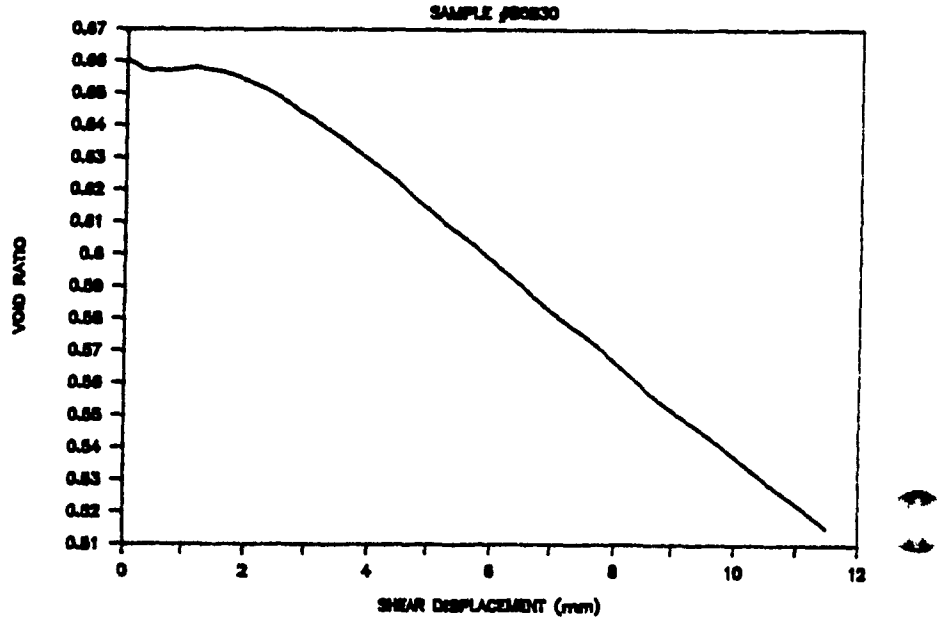

SIGMA GOLD

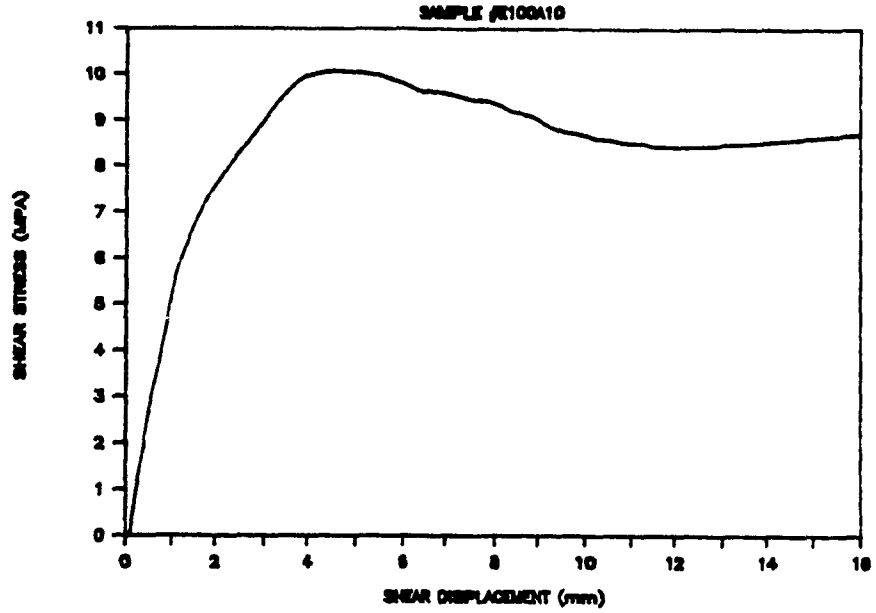
SAMPLE #E100A10
SHEAR STRESS (MPa)
SHEAR DISPLACEMENT (mm)

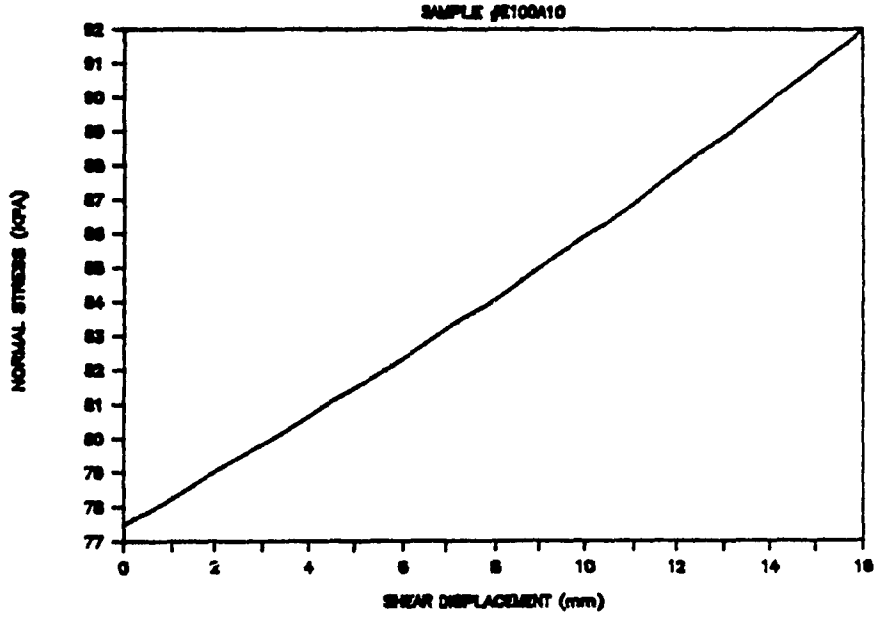
SAMPLE #E100A10
NORMAL STRESS (kPa)
SHEAR DISPLACEMENT (mm)

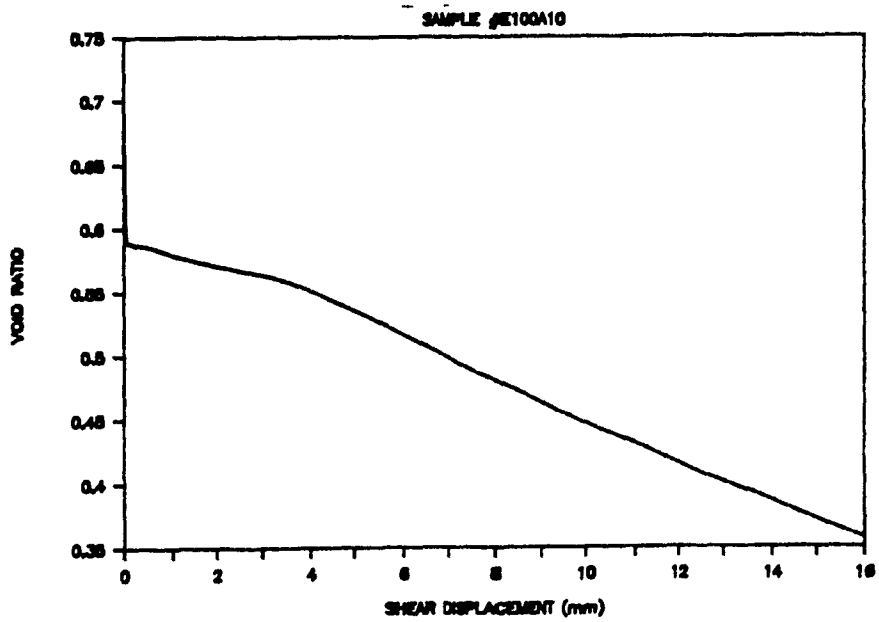
SAMPLE #E100A10
VOID RATIO
SHEAR DISPLACEMENT (mm)

SIGMA GOLD

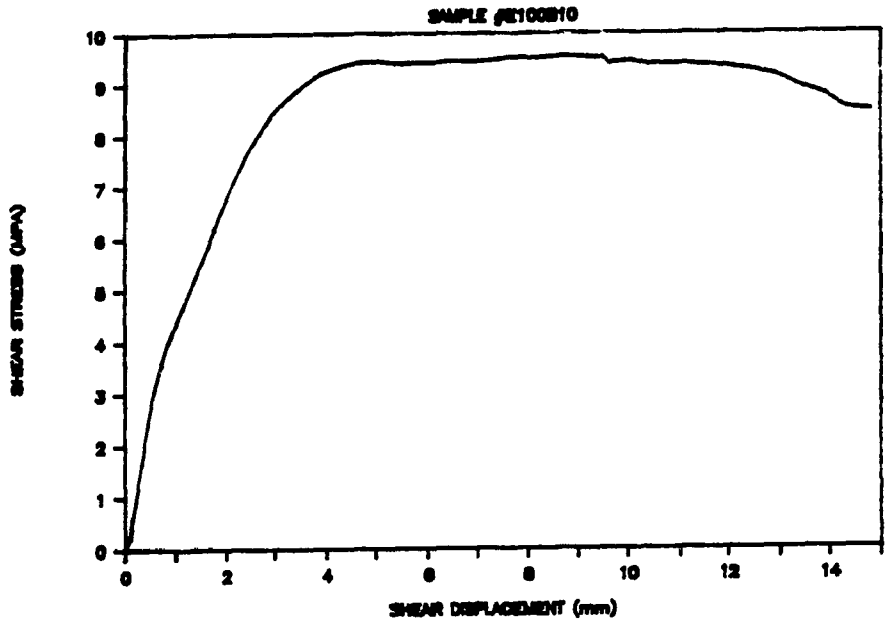
SAMPLE #E100810
SHEAR STRESS (kPA)
SHEAR DISPLACEMENT (mm)

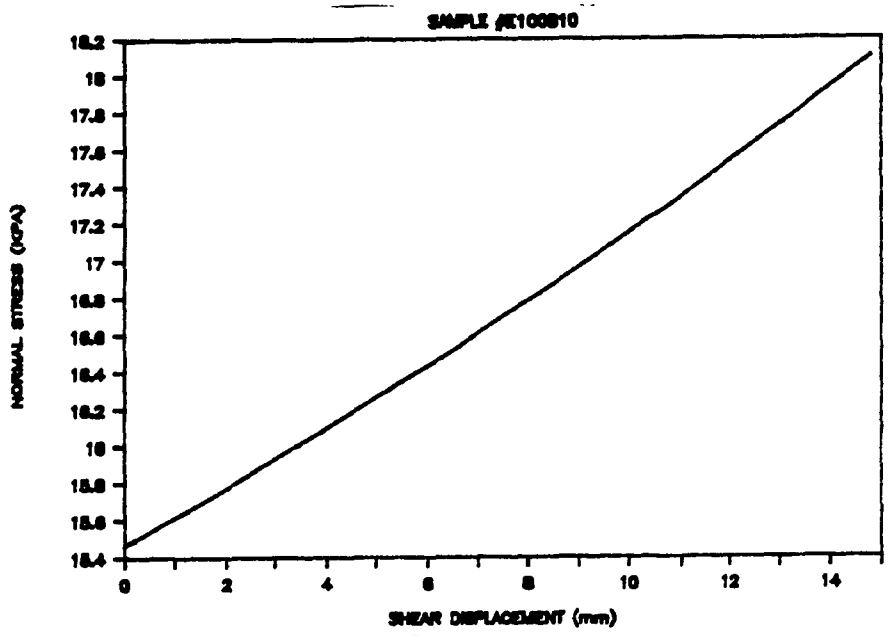
SAMPLE #E100810
NORMAL STRESS (kPA)
SHEAR DISPLACEMENT (mm)

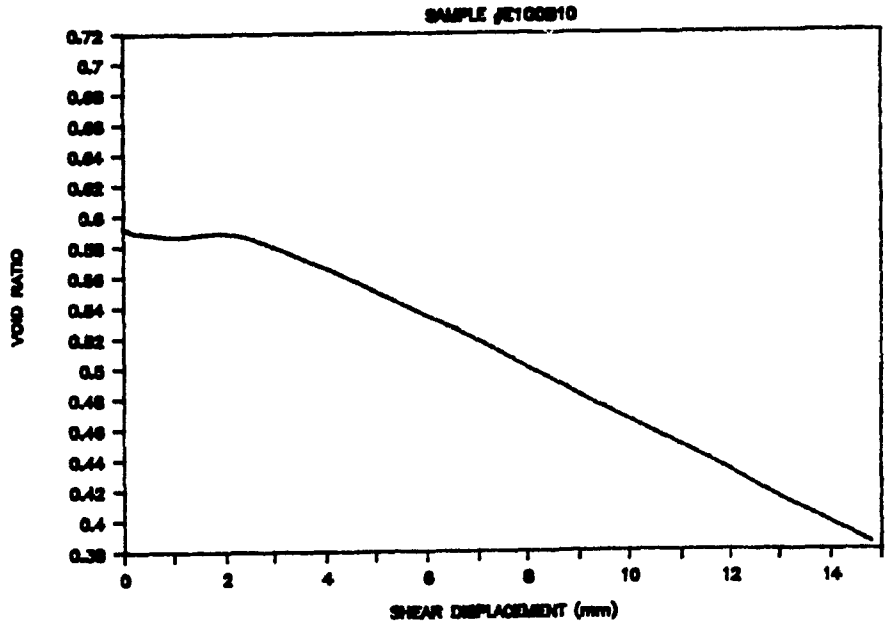
SAMPLE #E100810
VOID RATIO
SHEAR DISPLACEMENT (mm)

SIGMA GOLD

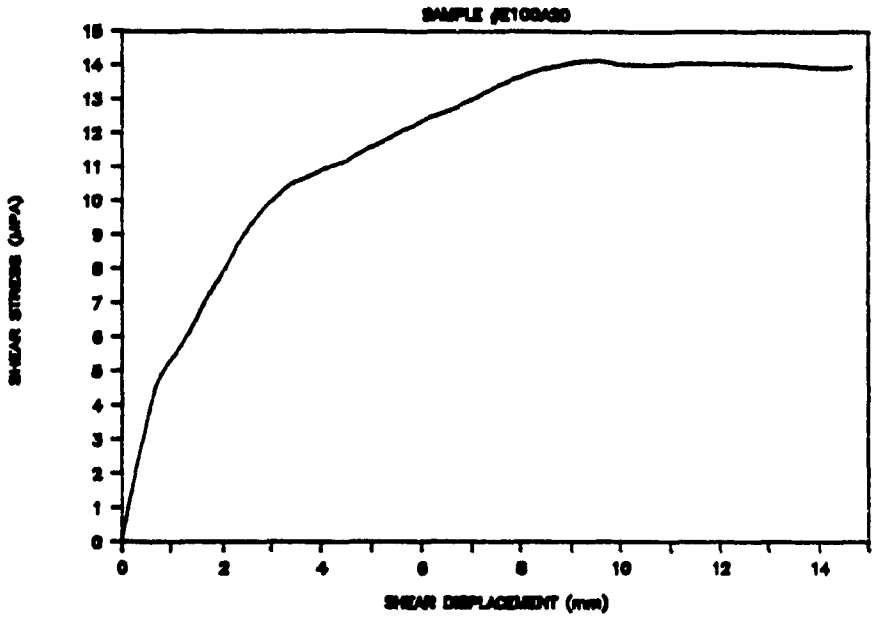
SHEAR STRESS (MPA)
SHEAR DISPLACEMENT (mm)

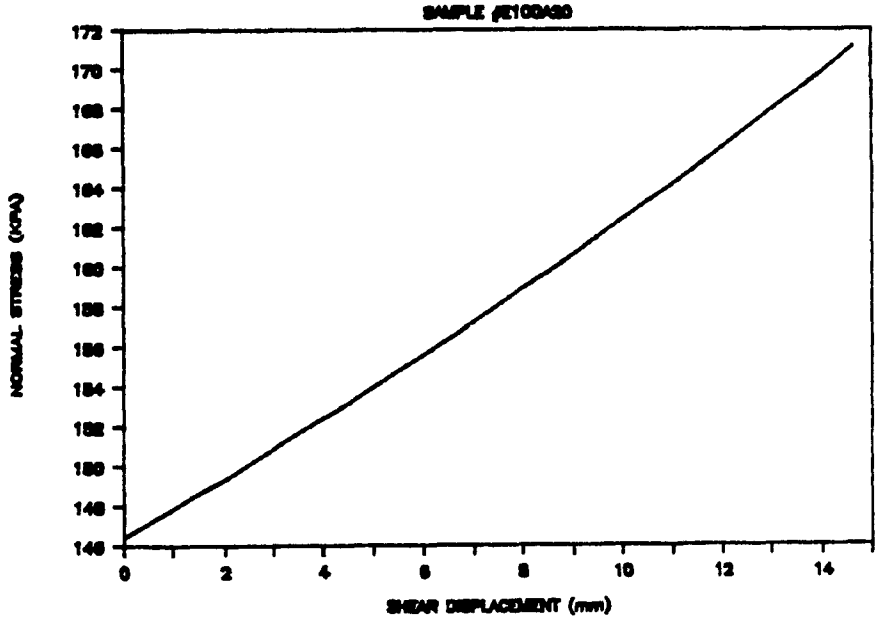
NORMAL STRESS (KPA)
SHEAR DISPLACEMENT (mm)

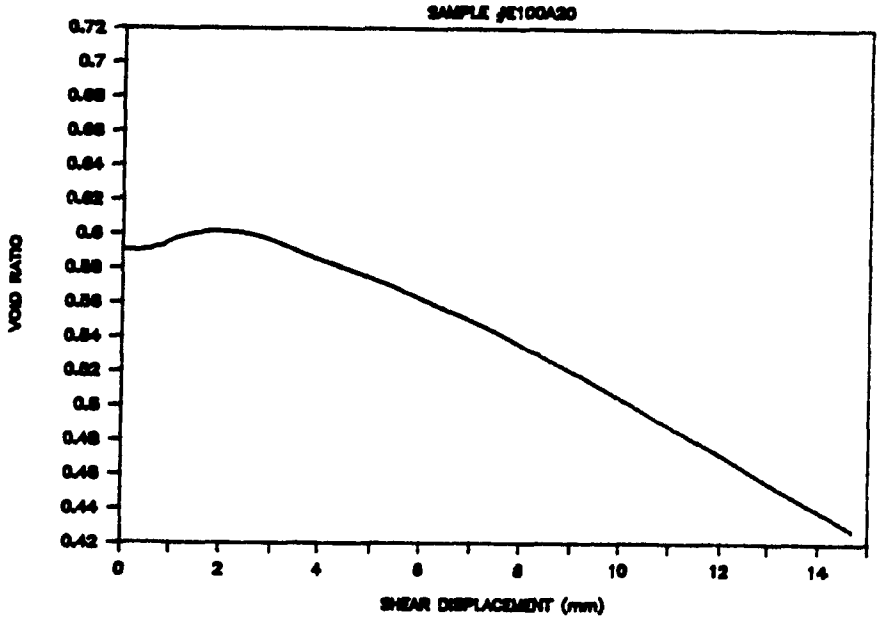
VOID RATIO
SHEAR DISPLACEMENT (mm)

SIGMA GOLD

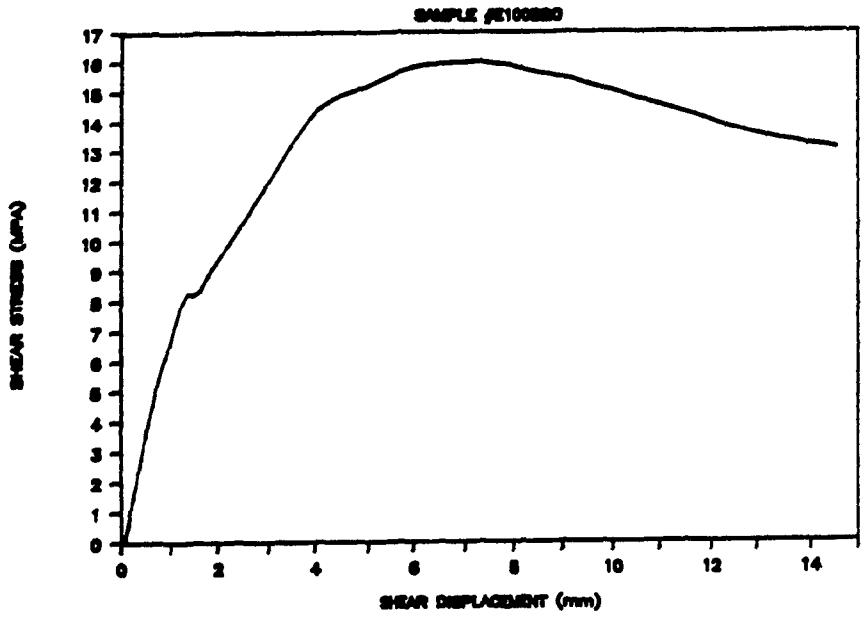
SHEAR STRESS (MPA)
SHEAR DISPLACEMENT (mm)

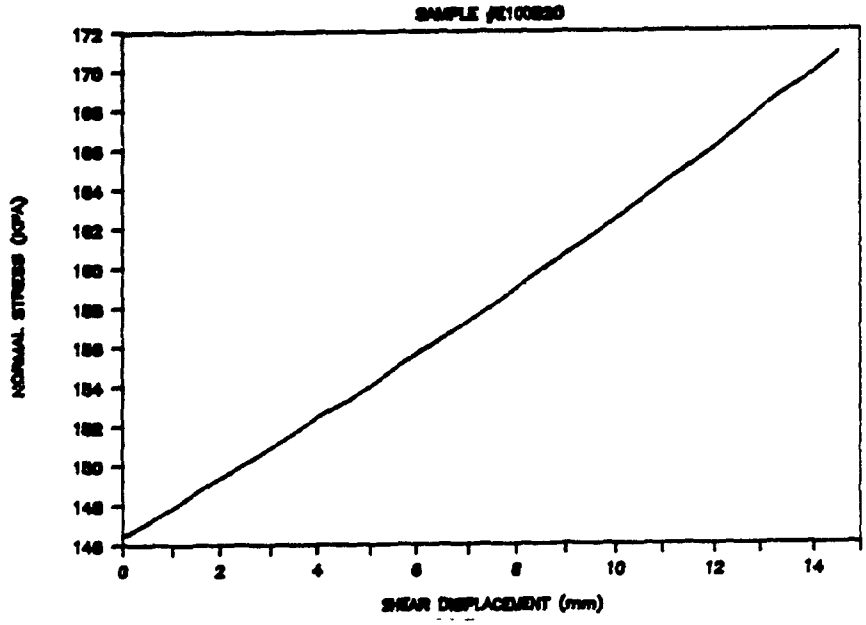
NORMAL STRESS (KPA)
SHEAR DISPLACEMENT (mm)

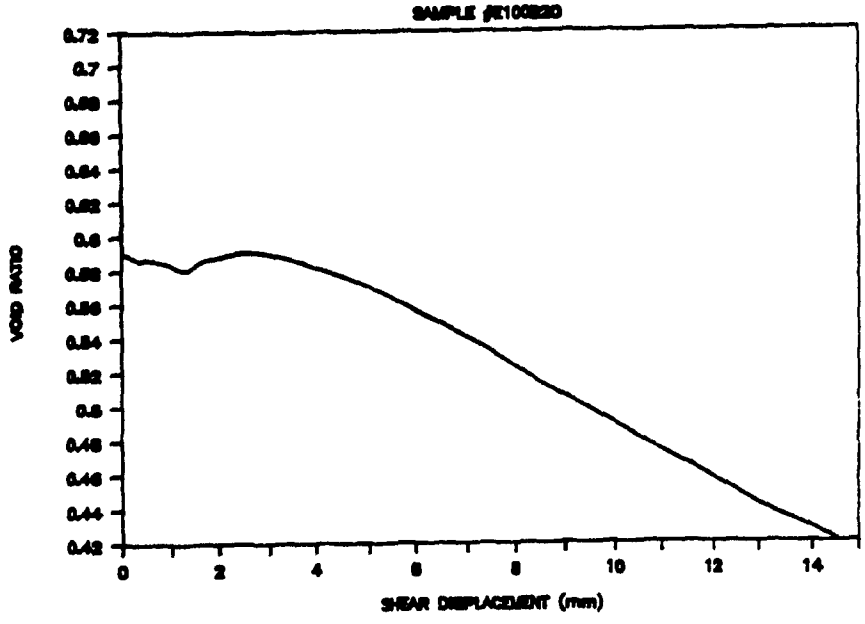
VOID RATIO
SHEAR DISPLACEMENT (mm)

SIGMA GOLD

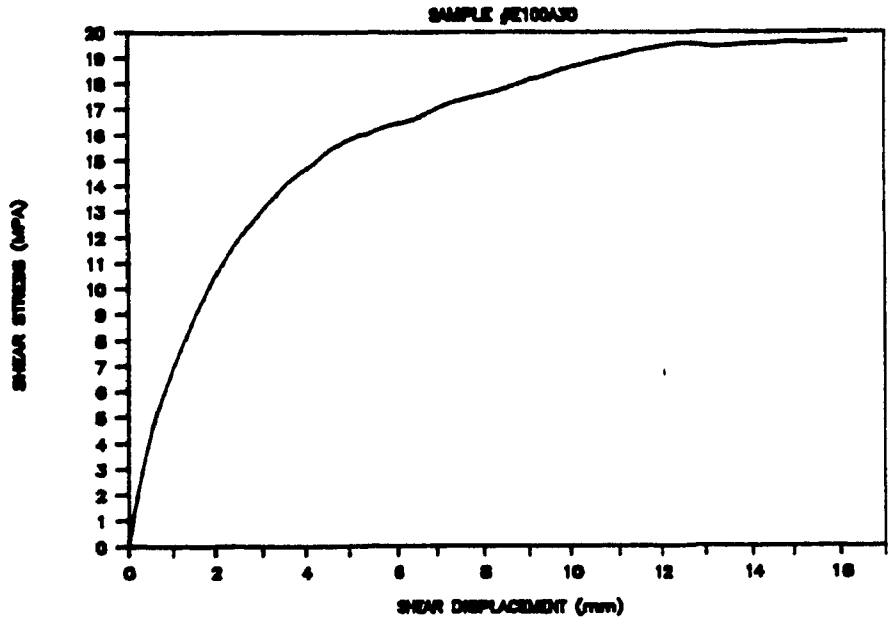
SAMPLE @E100A30
SHEAR STRESS (MPA)
SHEAR DISPLACEMENT (mm)

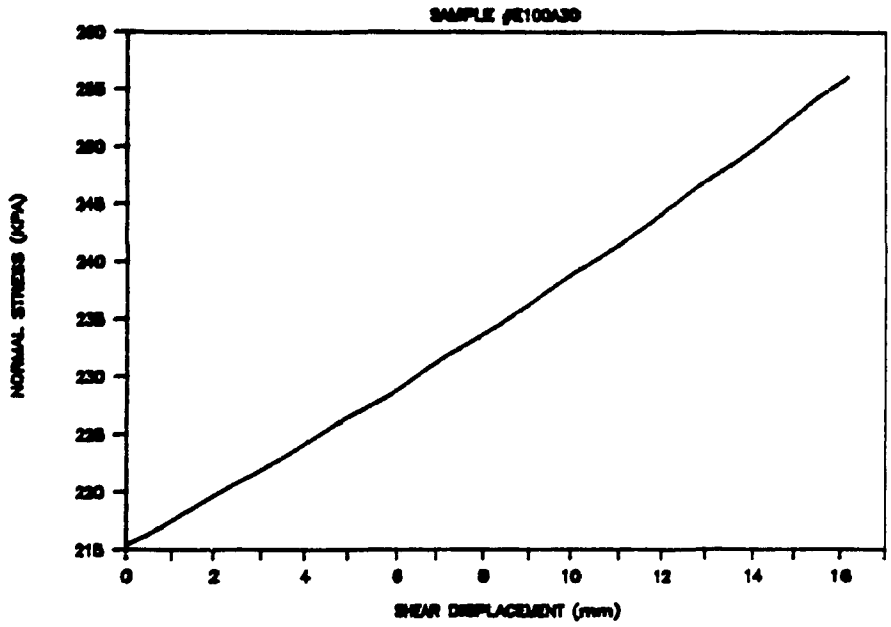
SAMPLE @E100A30
NORMAL STRESS (KPA)
SHEAR DISPLACEMENT (mm)

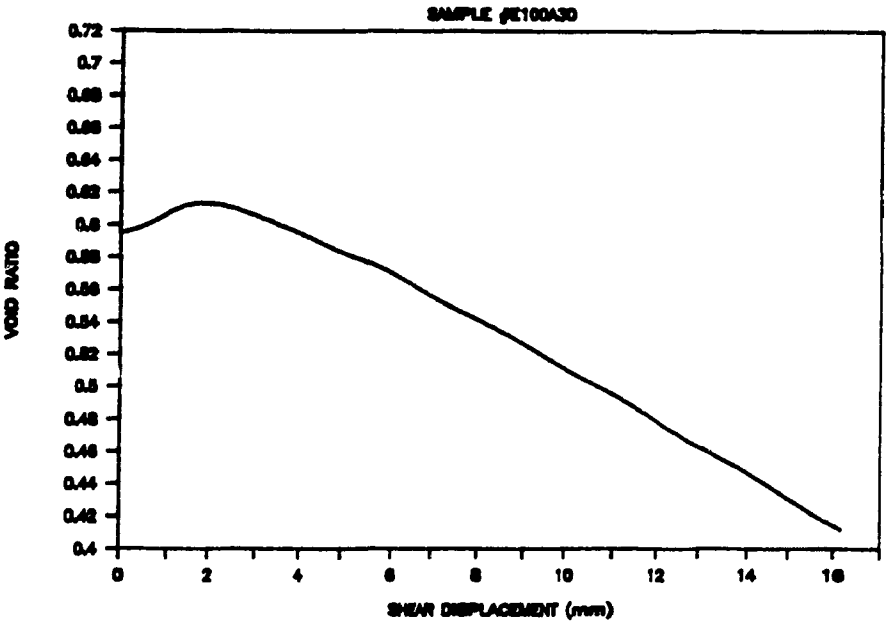
SAMPLE @E100A30
VOID RATIO
SHEAR DISPLACEMENT (mm)

SIGMA GOLD

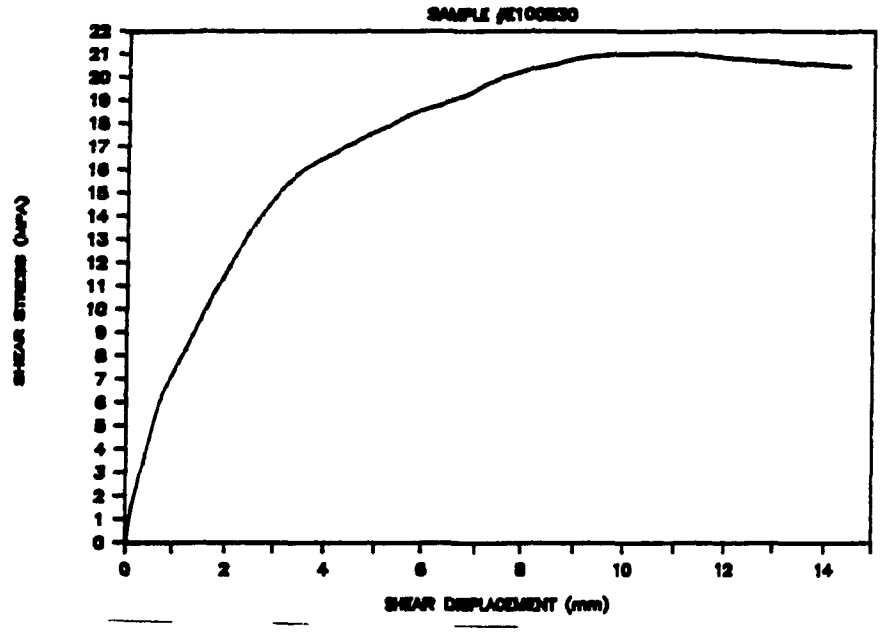
SAMPLE #E100830
SHEAR STRESS (MPA)
SHEAR DISPLACEMENT (mm)

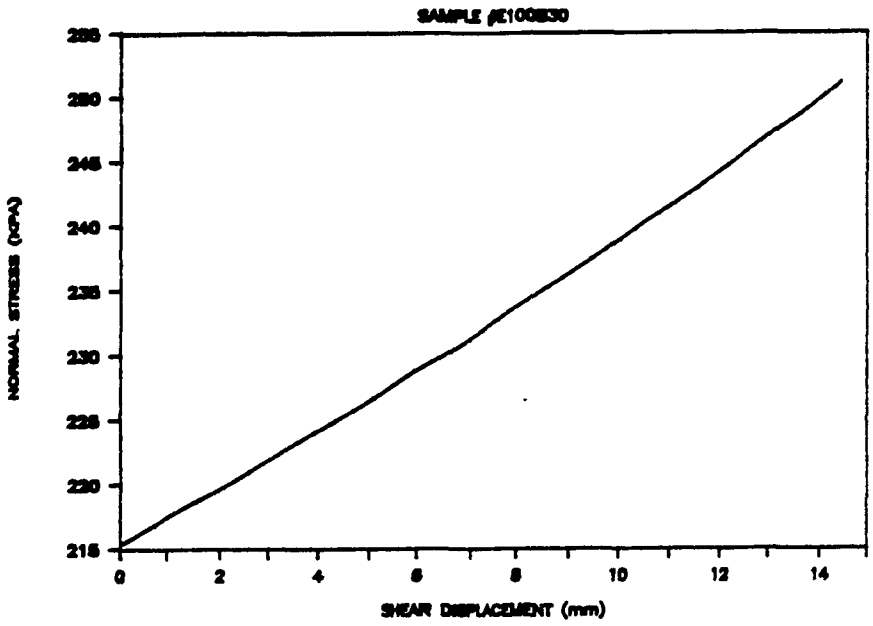
SAMPLE #E100830
NORMAL STRESS (KPA)
SHEAR DISPLACEMENT (mm)

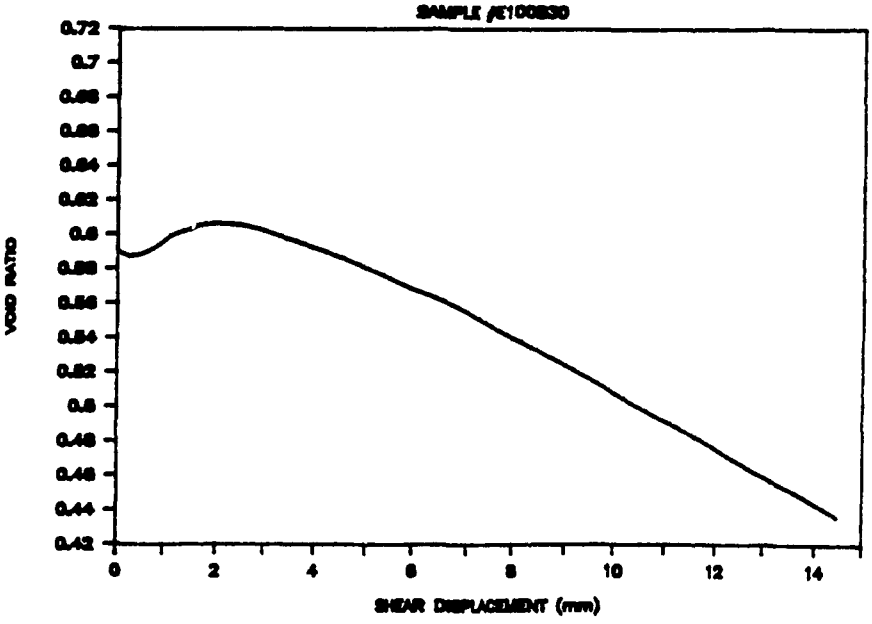
SAMPLE #E100830
VOID RATIO
SHEAR DISPLACEMENT (mm)

SIGMA GOLD

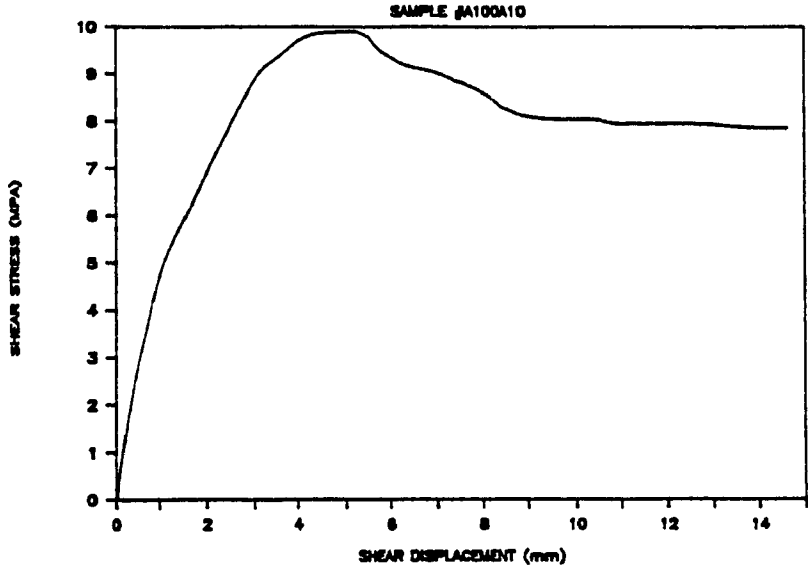
SAMPLE #A100A10
SHEAR STRESS (MPA)
SHEAR DISPLACEMENT (mm)

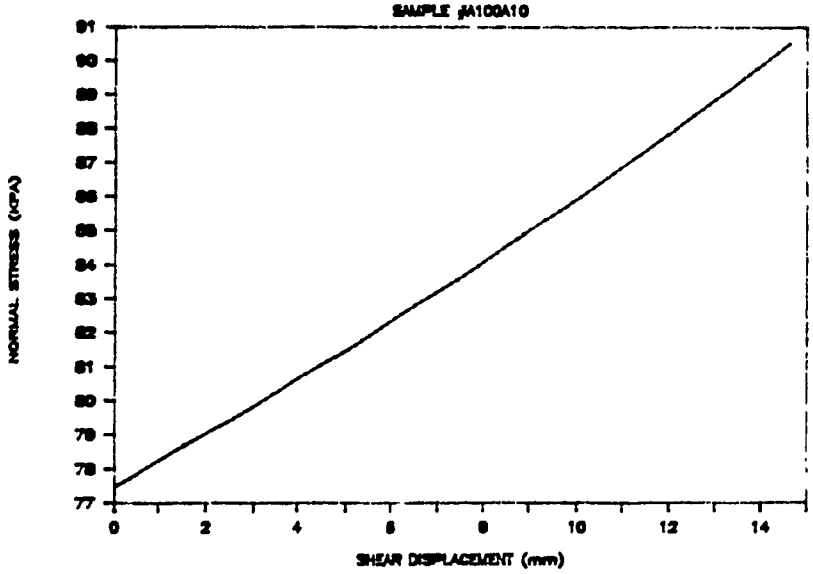
SAMPLE #A100A10
NORMAL STRESS (KPA)
SHEAR DISPLACEMENT (mm)

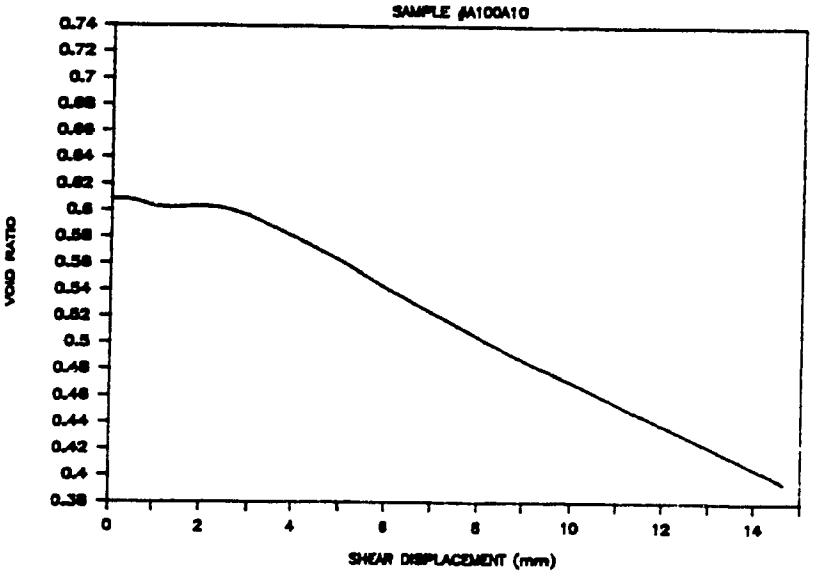
SAMPLE #A100A10
VOID RATIO
SHEAR DISPLACEMENT (mm)

SIGMA GOLD

SAMPLE #A100810

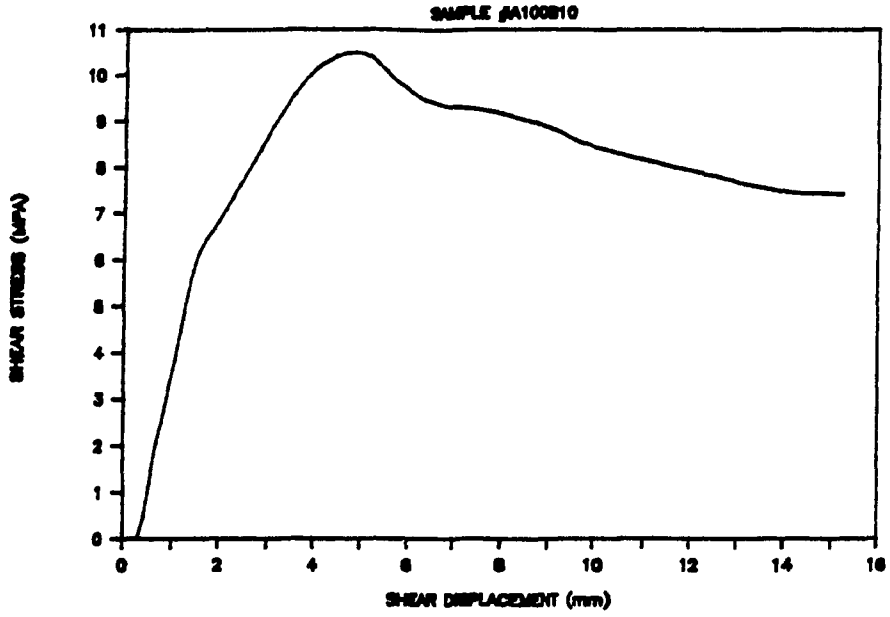

SAMPLE #A100810

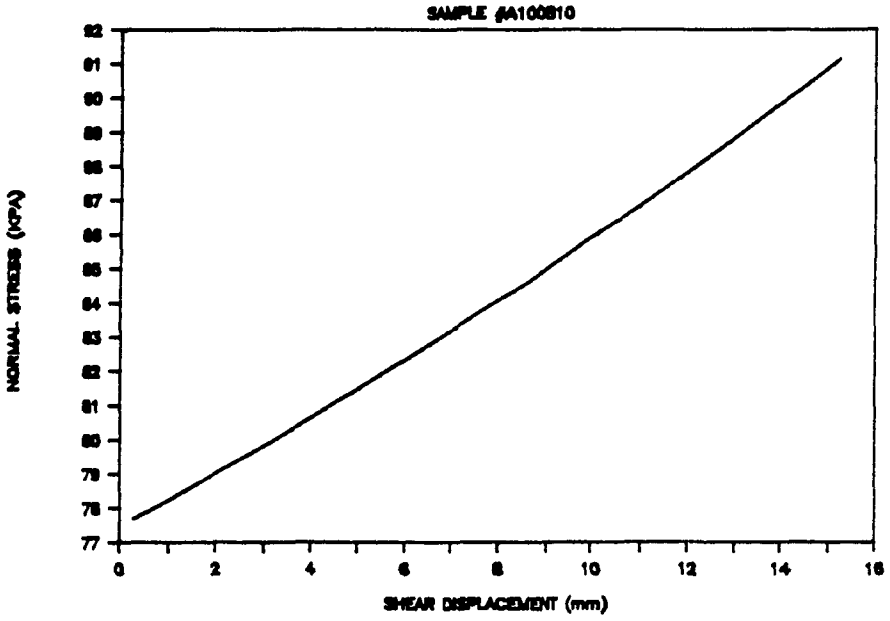

SAMPLE #A100810

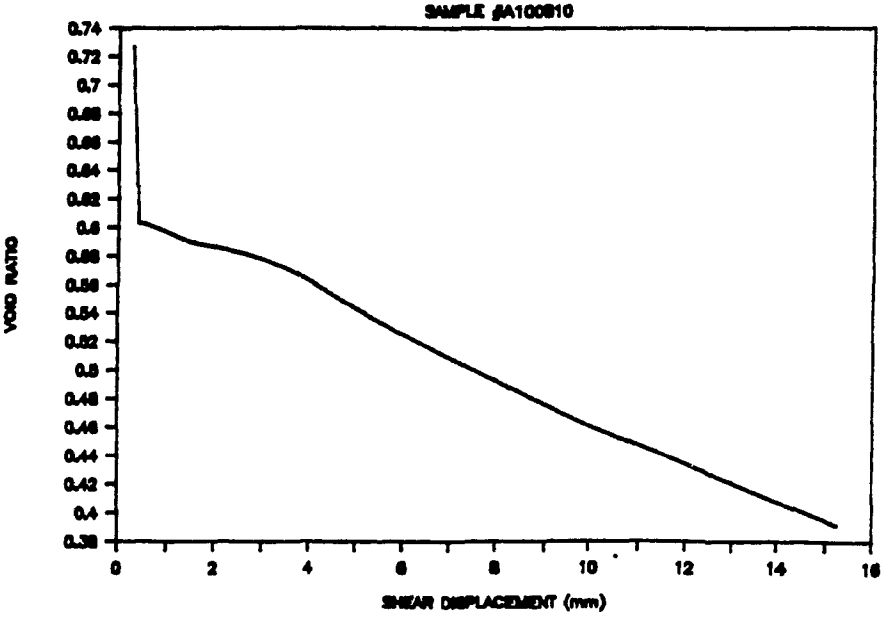

SIGMA GOLD

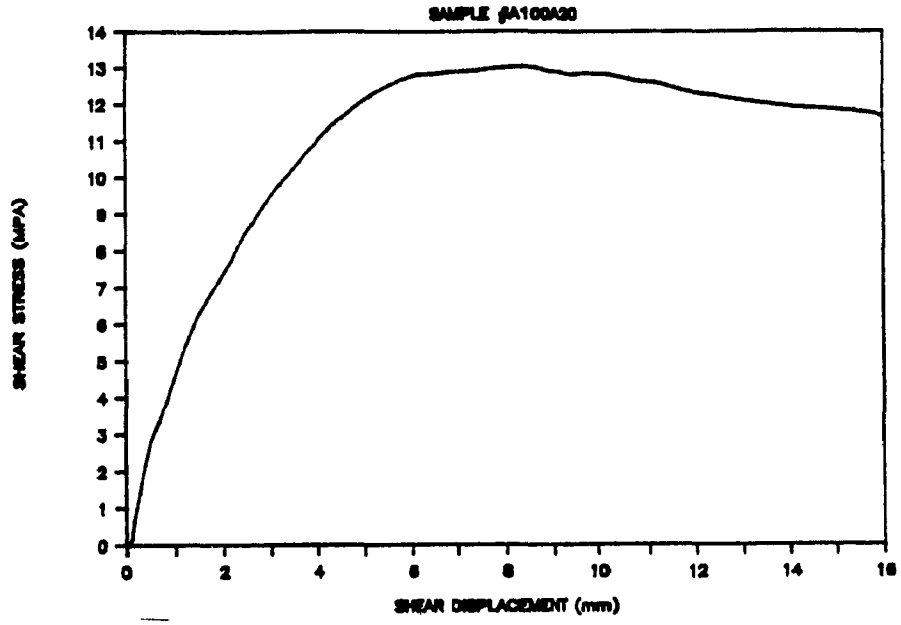
SAMPLE #A100A20
SHEAR STRESS (MPA)
SHEAR DISPLACEMENT (mm)

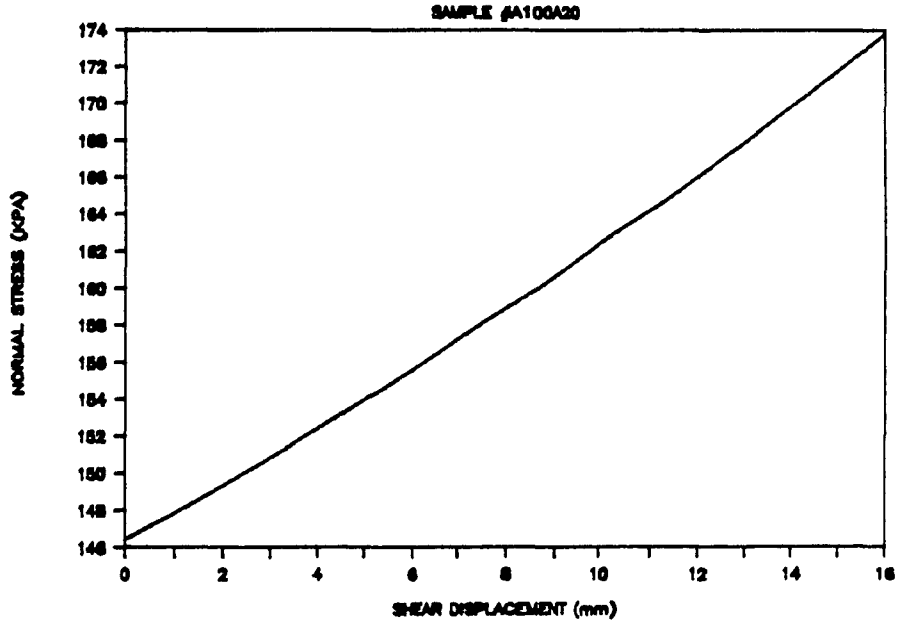
SAMPLE #A100A20
NORMAL STRESS (KPA)
SHEAR DISPLACEMENT (mm)

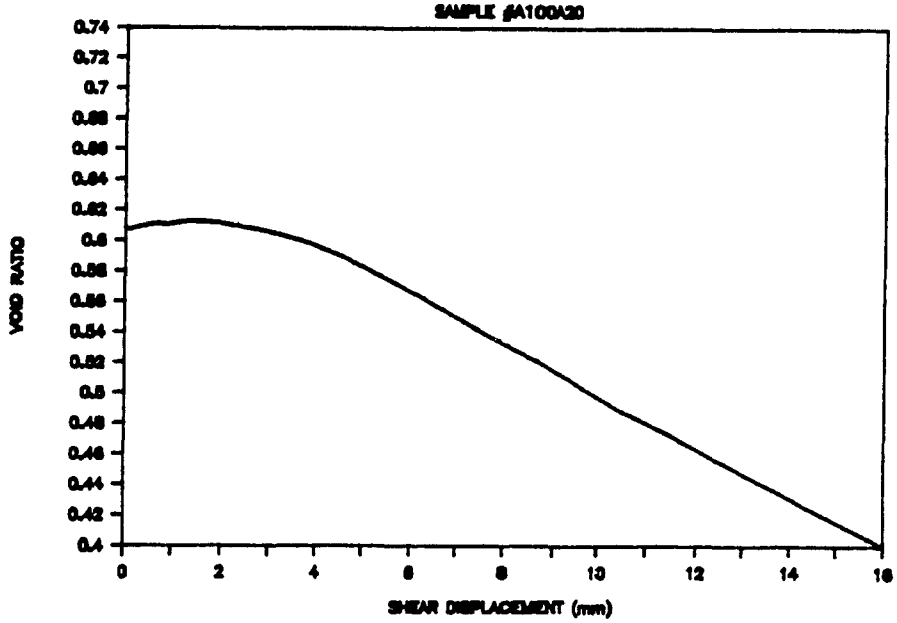
SAMPLE #A100A20
VOID RATIO
SHEAR DISPLACEMENT (mm)

SIGMA GOLD

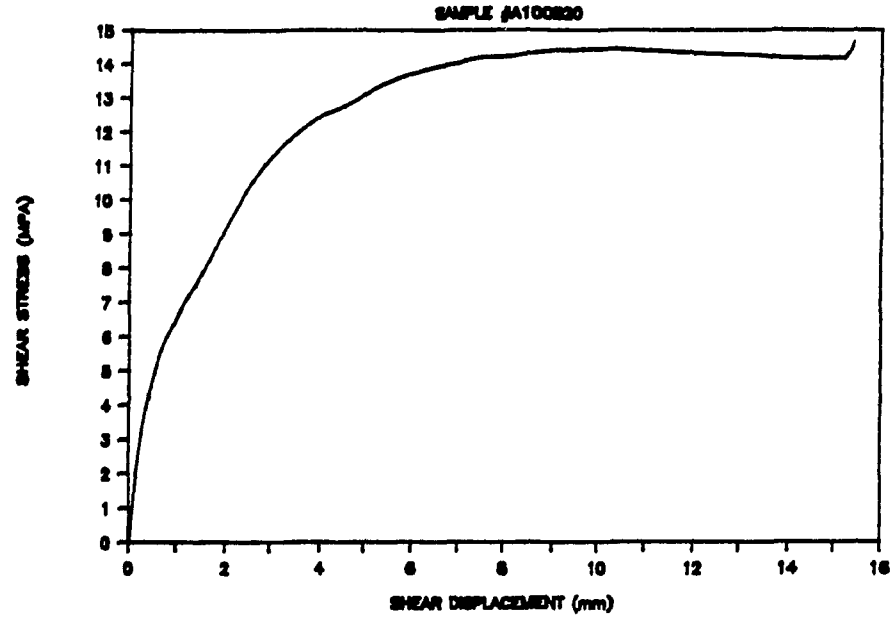
SAMPLE #A100820
SHEAR STRESS (MPA)
SHEAR DISPLACEMENT (mm)

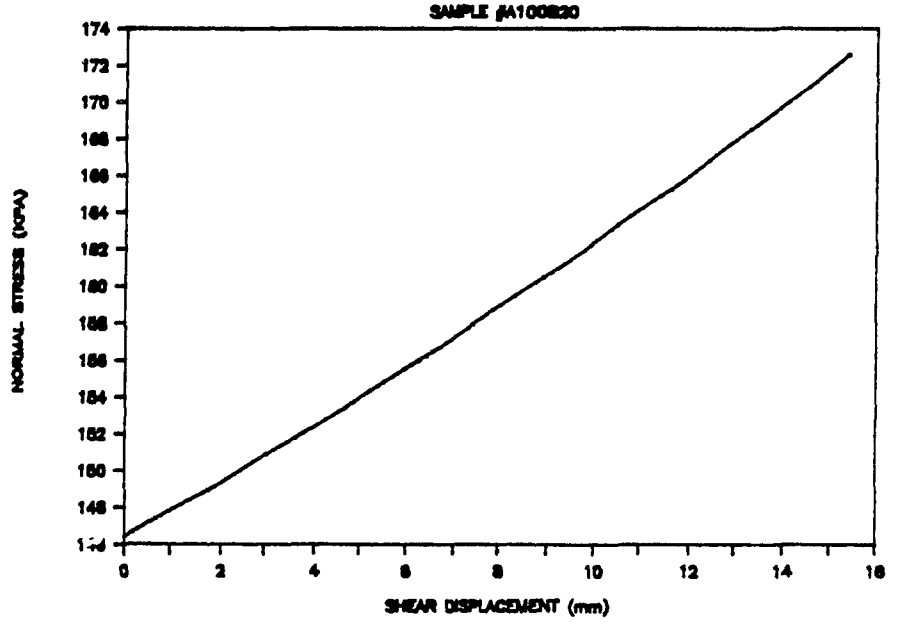
SAMPLE #A100820
NORMAL STRESS (KPA)
SHEAR DISPLACEMENT (mm)

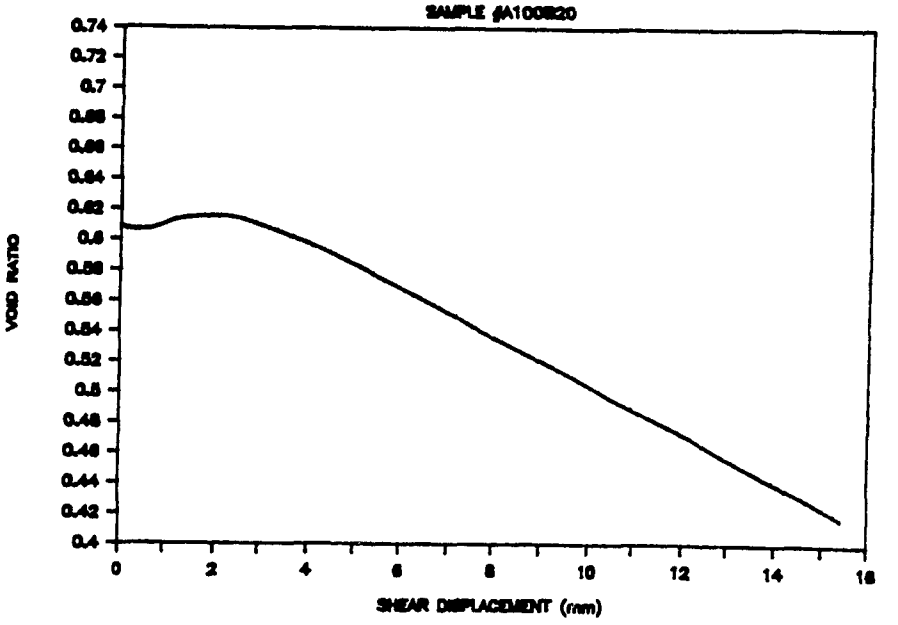
SAMPLE #A100820
VOID RATIO
SHEAR DISPLACEMENT (mm)

SIGMA GOLD

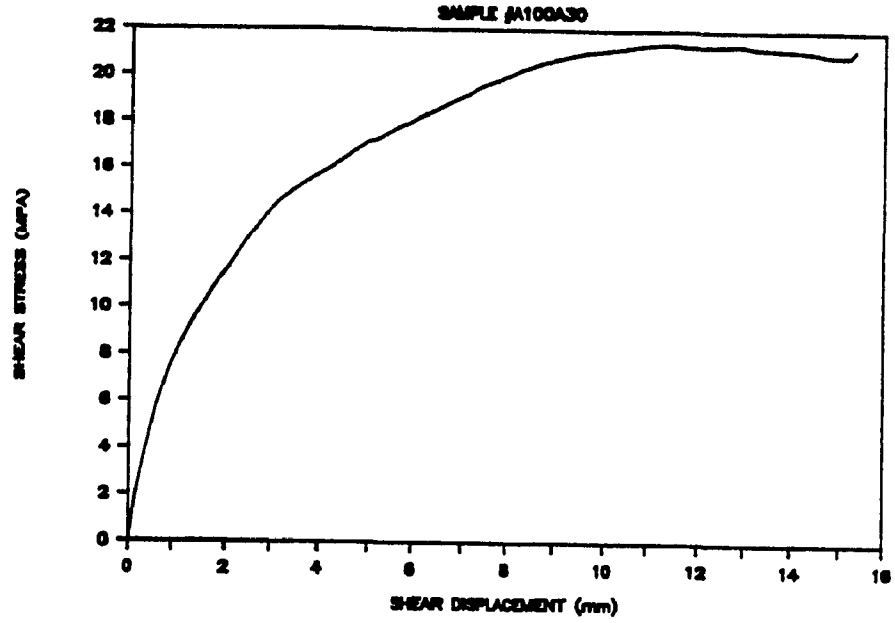
SAMPLE #A100A30
SHEAR STRESS (MPA)
SHEAR DISPLACEMENT (mm)

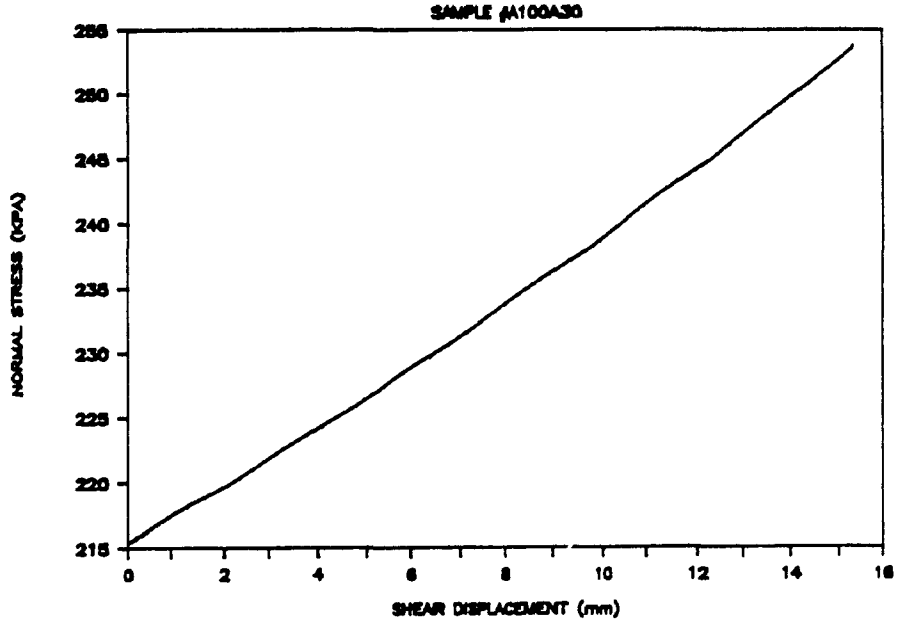
SAMPLE #A100A30
NORMAL STRESS (KPA)
SHEAR DISPLACEMENT (mm)

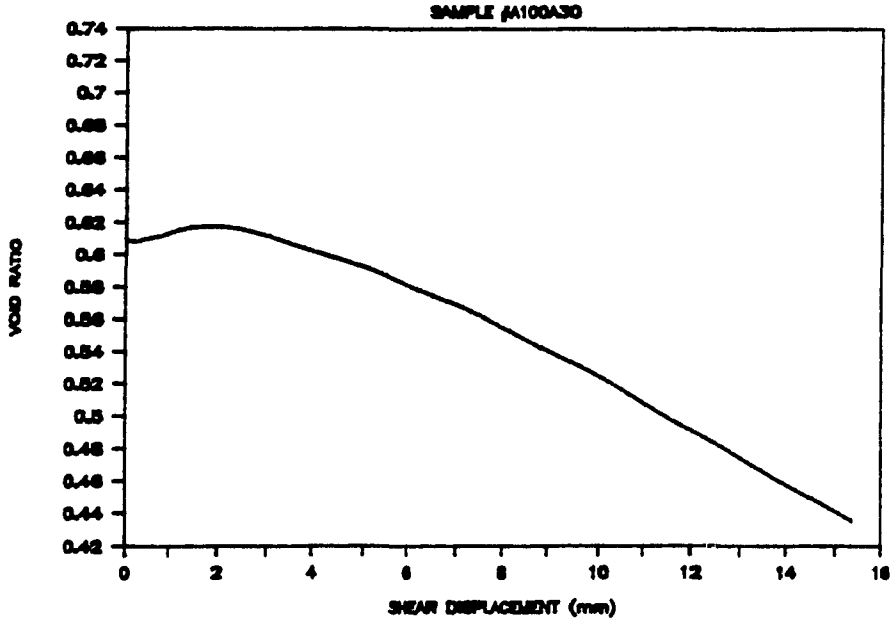
SAMPLE #A100A30
VOID RATIO
SHEAR DISPLACEMENT (mm)

SIGMA GOLD

SAMPLE #A100830

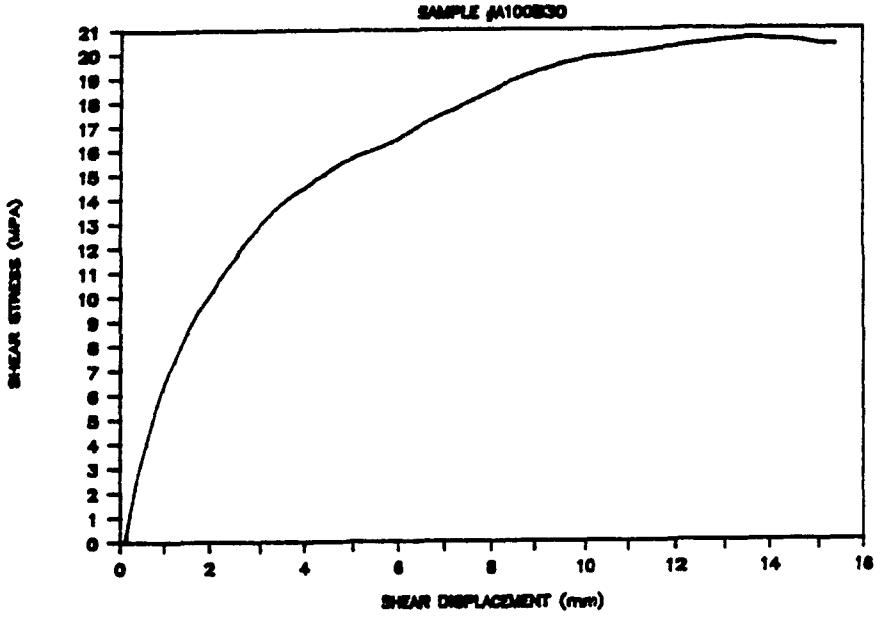

SAMPLE #A100830

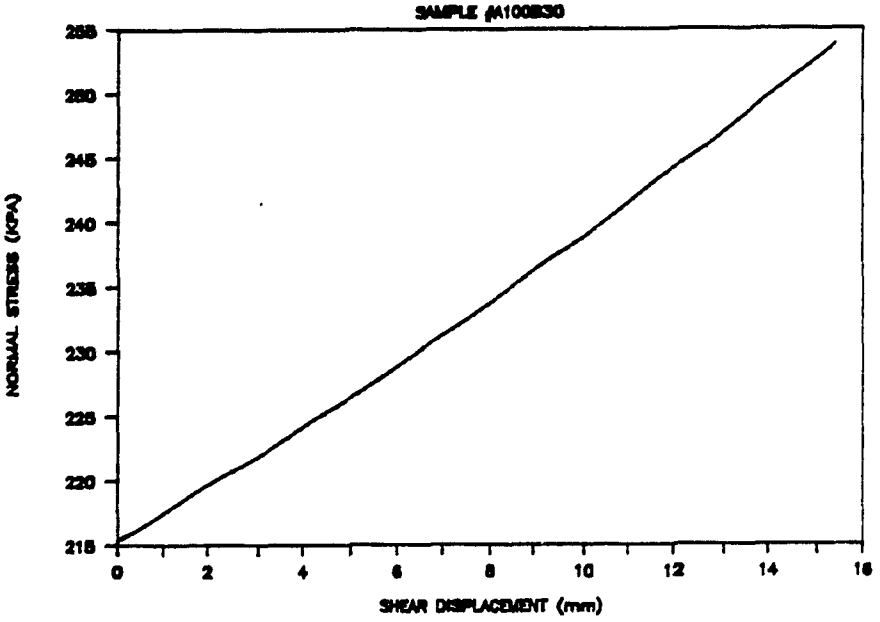

SAMPLE #A100830

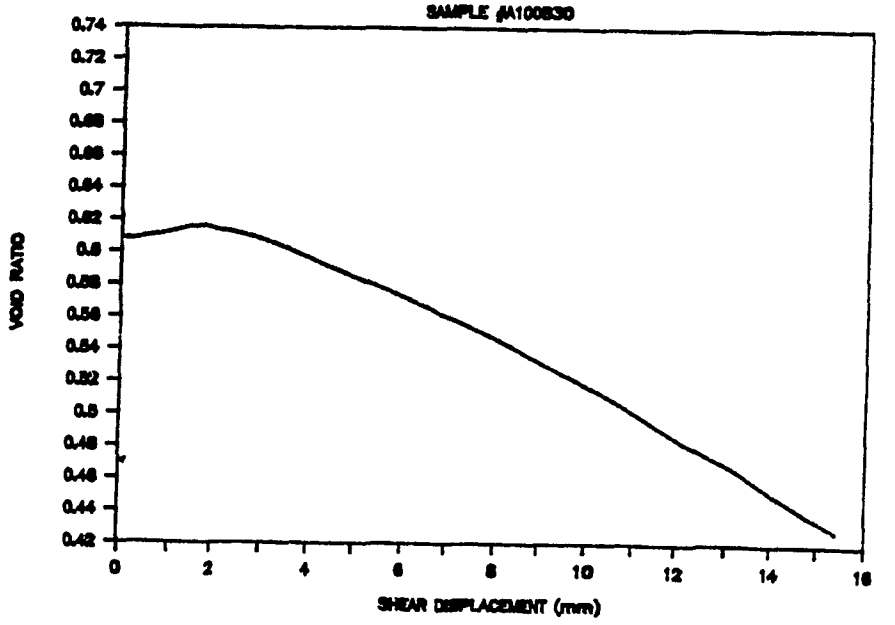

SIGMA GOLD

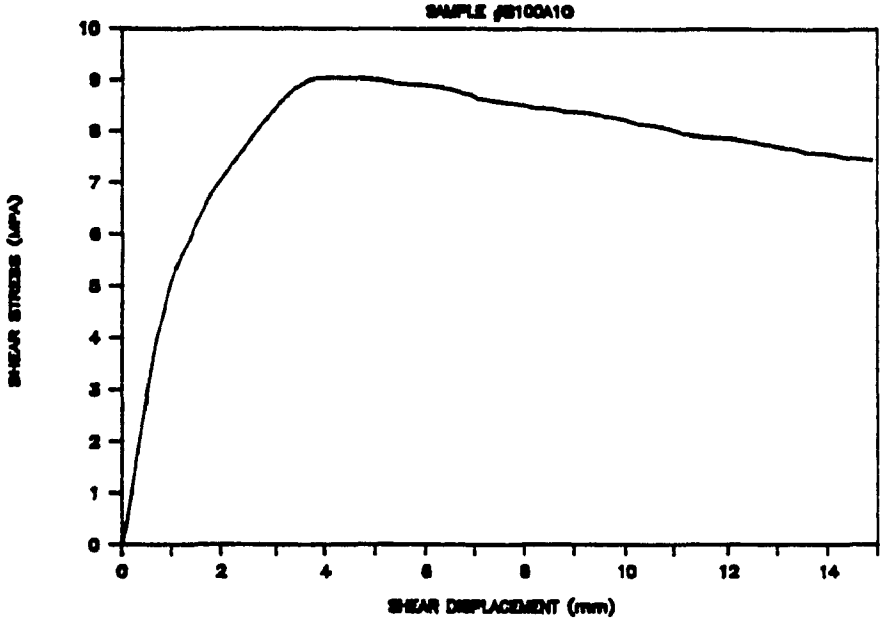
SAMPLE #S100A1G
SHEAR STRESS (MPA)
SHEAR DISPLACEMENT (mm)

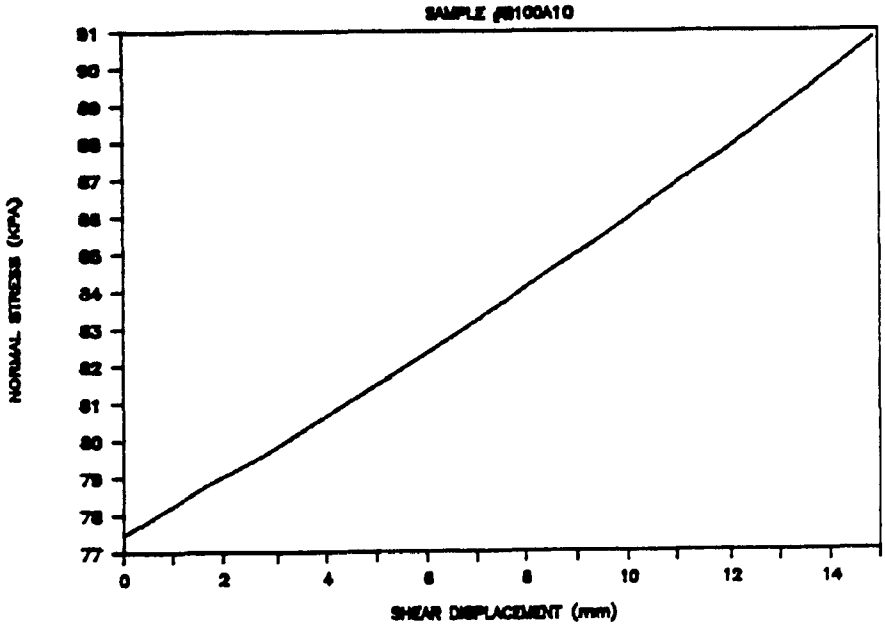
SAMPLE #S100A1G
NORMAL STRESS (KPA)
SHEAR DISPLACEMENT (mm)

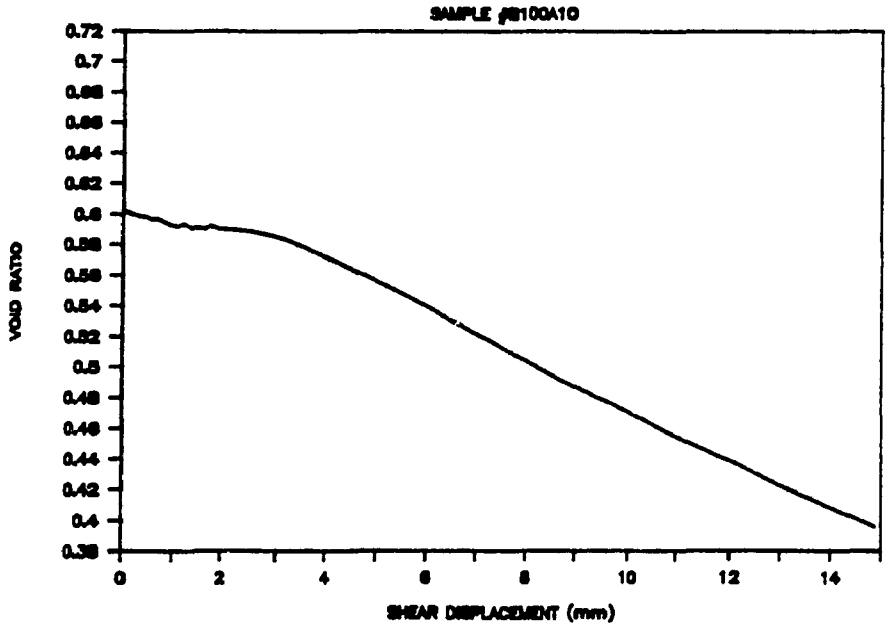
SAMPLE #S100A1G
VOID RATIO
SHEAR DISPLACEMENT (mm)

SIGMA GOLD

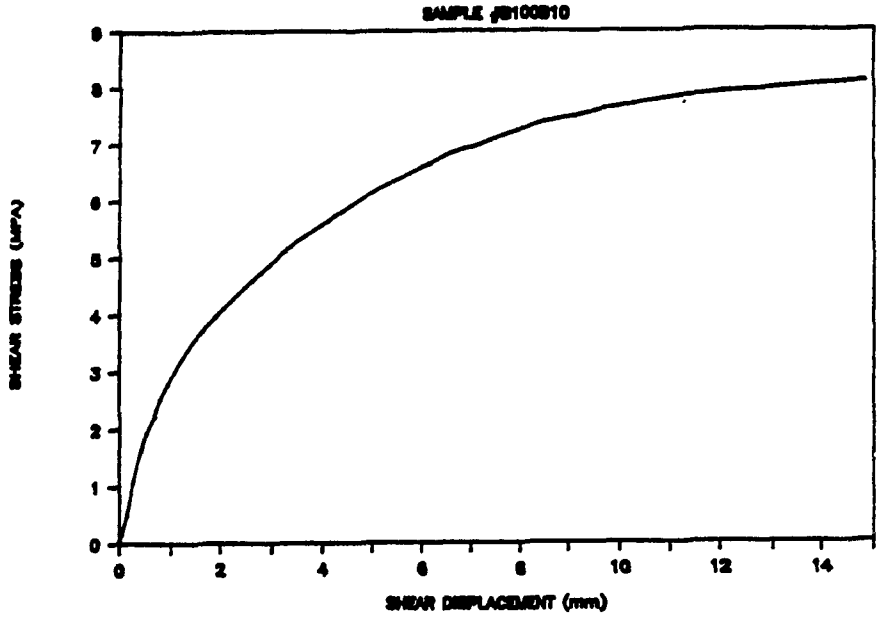
SAMPLE @B100B10
SHEAR STRESS (MPA)
0
1
2
3
4
5
6
7
8
0
2
4
6
8
10
12
14
SHEAR DISPLACEMENT (mm)

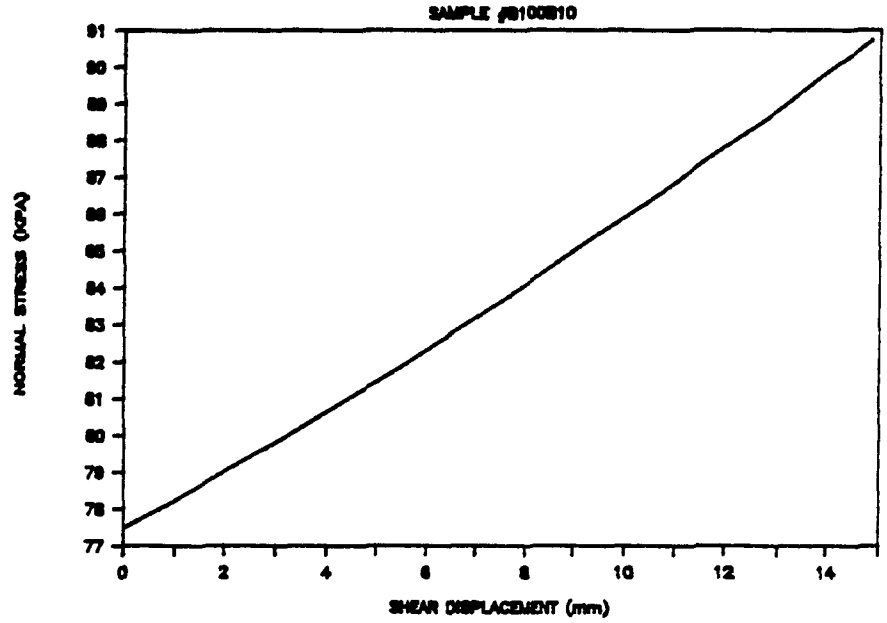
SAMPLE @B100B10
NORMAL STRESS (KPA)
77
78
79
80
81
82
83
84
85
86
87
88
89
90
91
0
2
4
6
8
10
12
14
SHEAR DISPLACEMENT (mm)

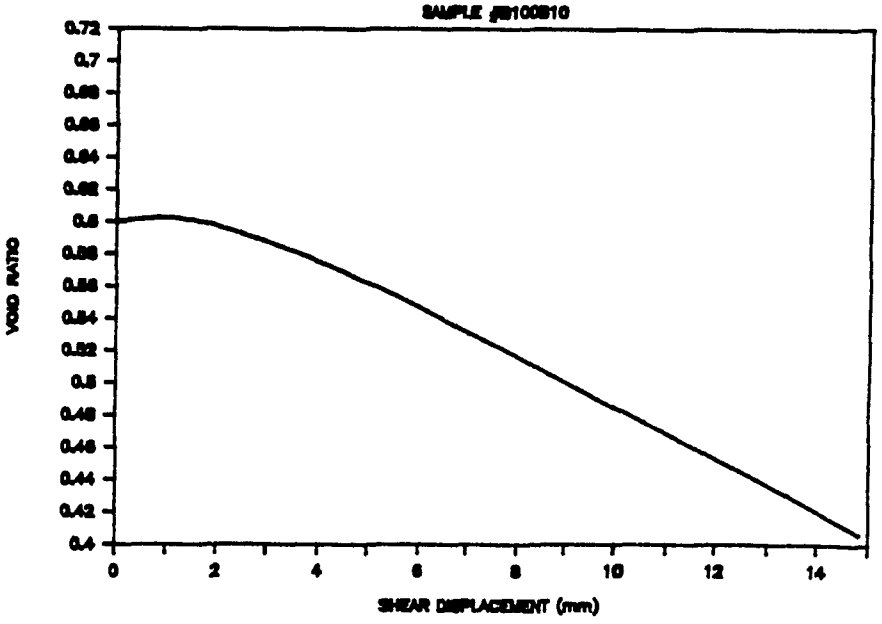
SAMPLE @B100B10
VOID RATIO
0.4
0.42
0.44
0.46
0.48
0.5
0.52
0.54
0.56
0.58
0.6
0.62
0.64
0.66
0.68
0.7
0.72
0
2
4
6
8
10
12
14
SHEAR DISPLACEMENT (mm)

SIGMA GOLD

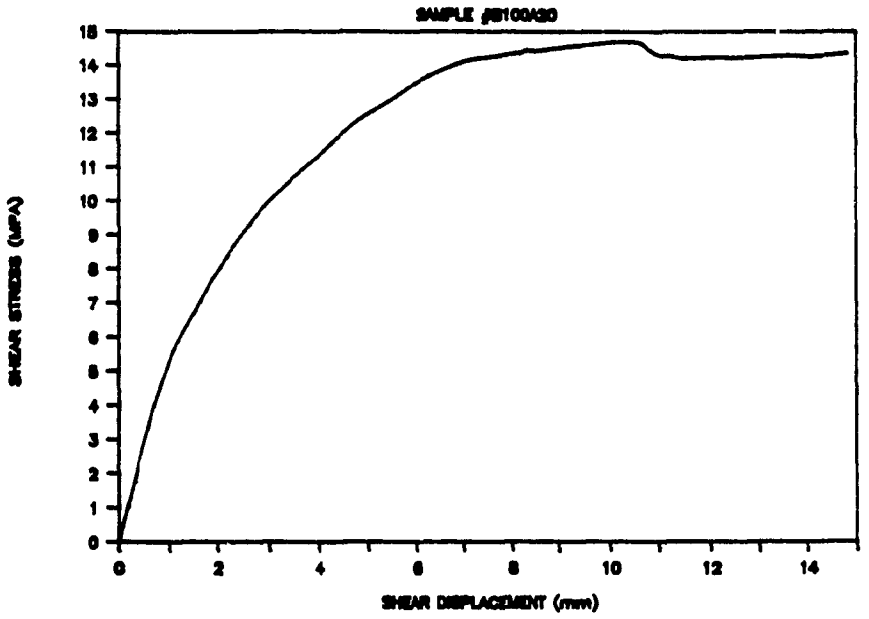
SAMPLE @B100A30
SHEAR STRESS (MPA)
SHEAR DISPLACEMENT (mm)

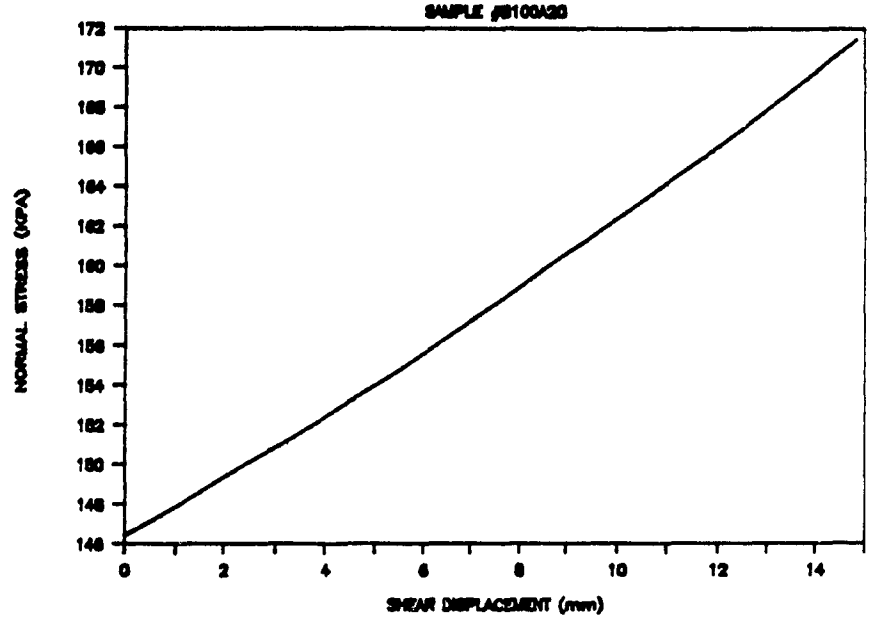
SAMPLE @B100A30
NORMAL STRESS (KPA)
SHEAR DISPLACEMENT (mm)

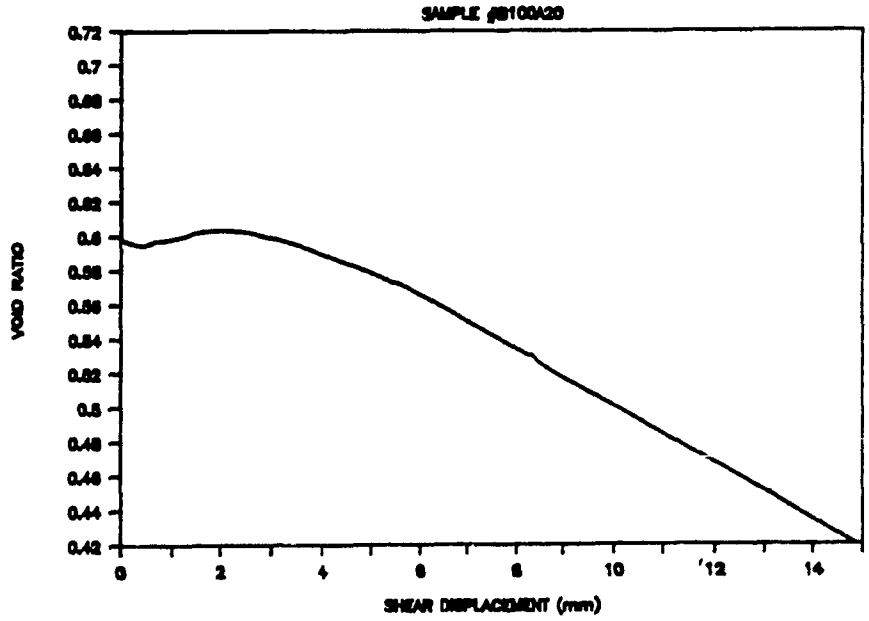
SAMPLE @B100A30
VOID RATIO
SHEAR DISPLACEMENT (mm)

SIGMA GOLD

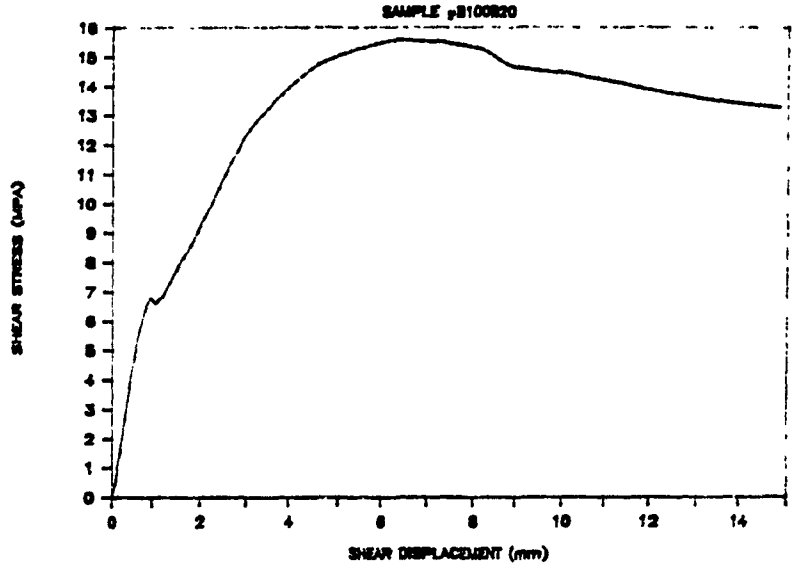
SAMPLE #B100820
SHEAR STRESS (MPA)
SHEAR DISPLACEMENT (mm)

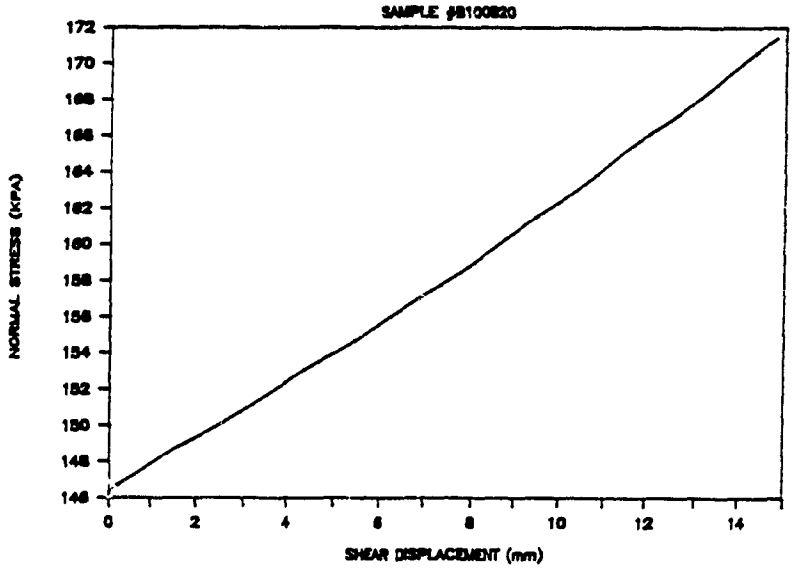
SAMPLE #B100820
NORMAL STRESS (KPA)
SHEAR DISPLACEMENT (mm)

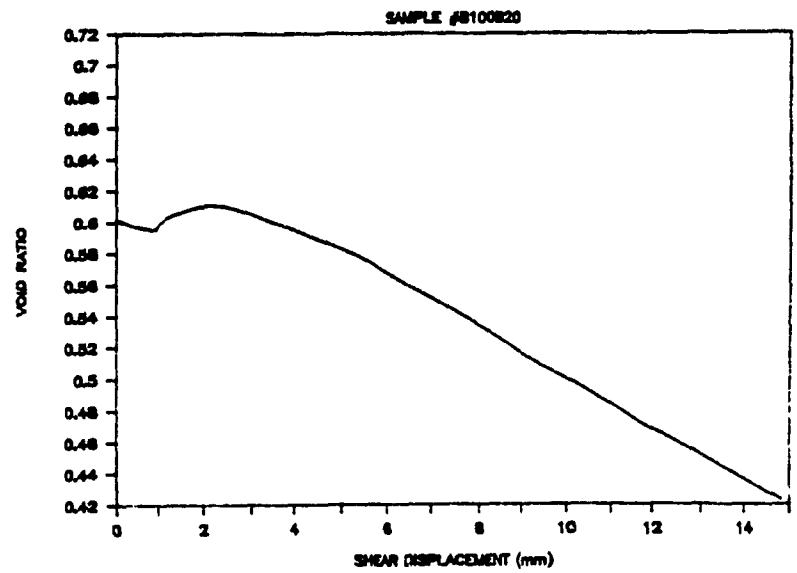
SAMPLE #B100820
VOID RATIO
SHEAR DISPLACEMENT (mm)

SIGMA GOLD

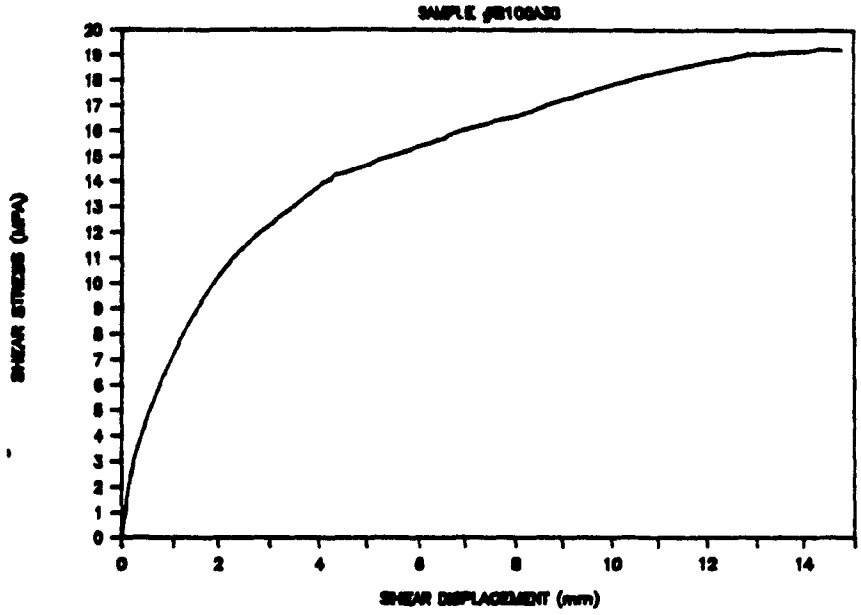
SAMPLE @B100A30
SHEAR STRESS (MPA)
SHEAR DISPLACEMENT (mm)

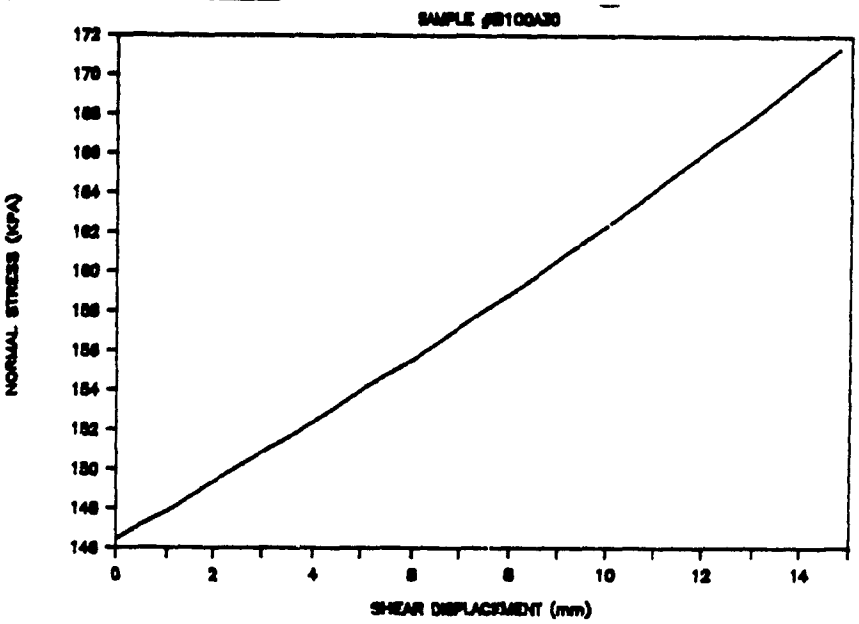
SAMPLE @B100A30
NORMAL STRESS (KPA)
SHEAR DISPLACEMENT (mm)

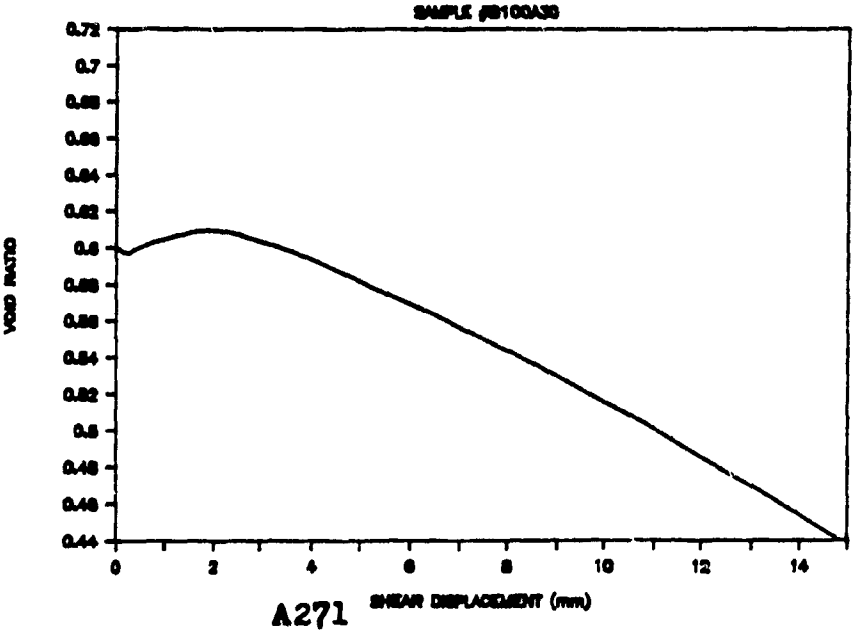
SAMPLE @B100A30
VOID RATIO
SHEAR DISPLACEMENT (mm)

SIGMA GOLD

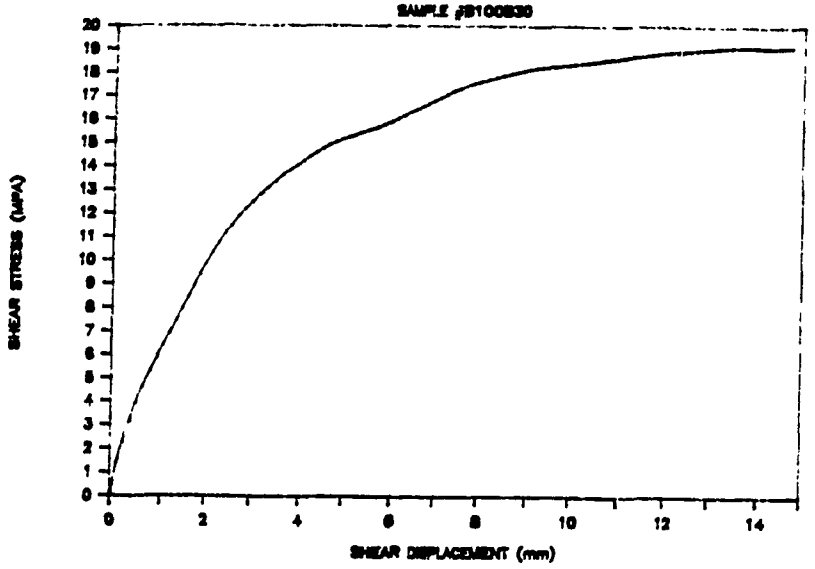
SAMPLE #B100830
SHEAR STRESS (MPA)
SHEAR DISPLACEMENT (mm)

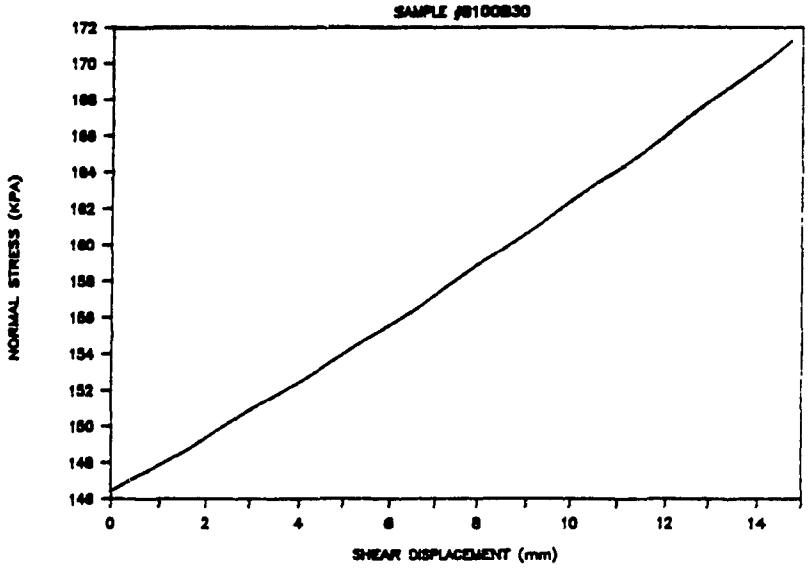
SAMPLE #B100830
NORMAL STRESS (KPA)
SHEAR DISPLACEMENT (mm)

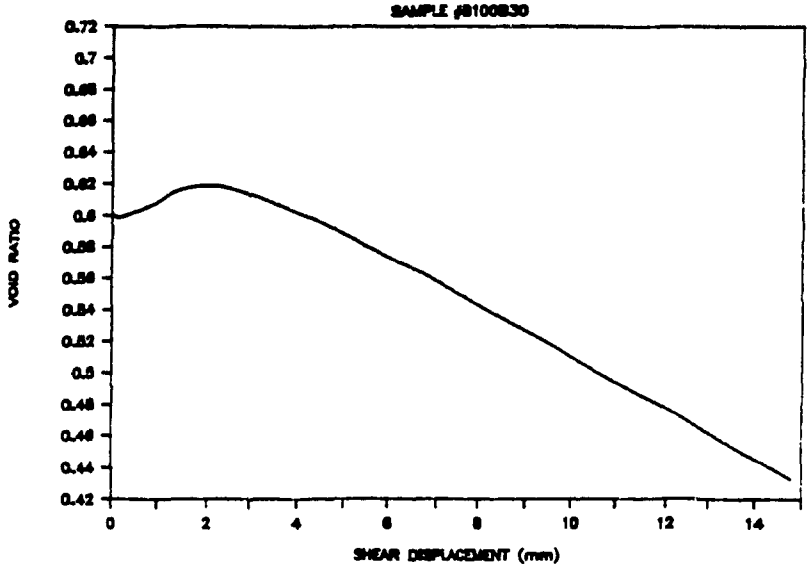
SAMPLE #B100830
VOID RATIO
SHEAR DISPLACEMENT (mm)

SIGMA GOLD

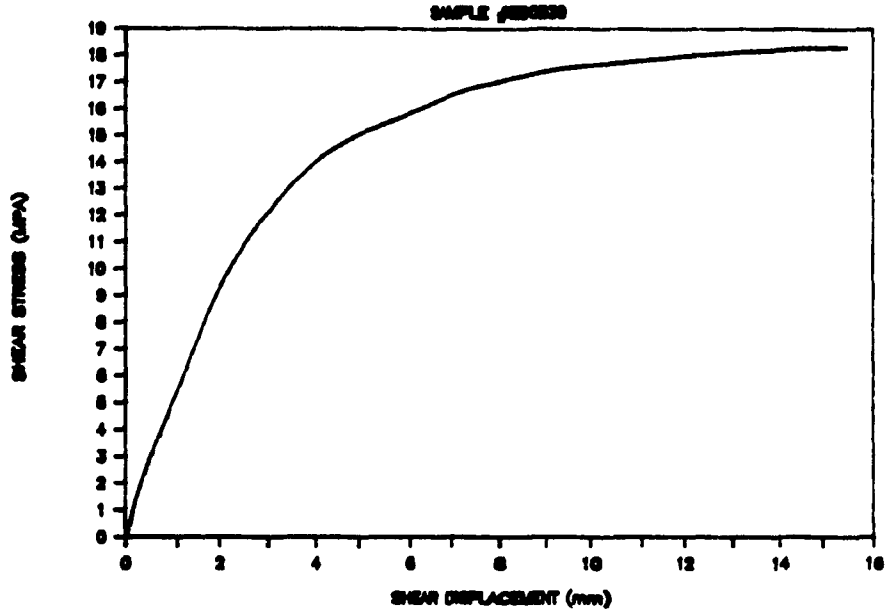
SHEAR STRESS (kPa)
SHEAR DISPLACEMENT (mm)

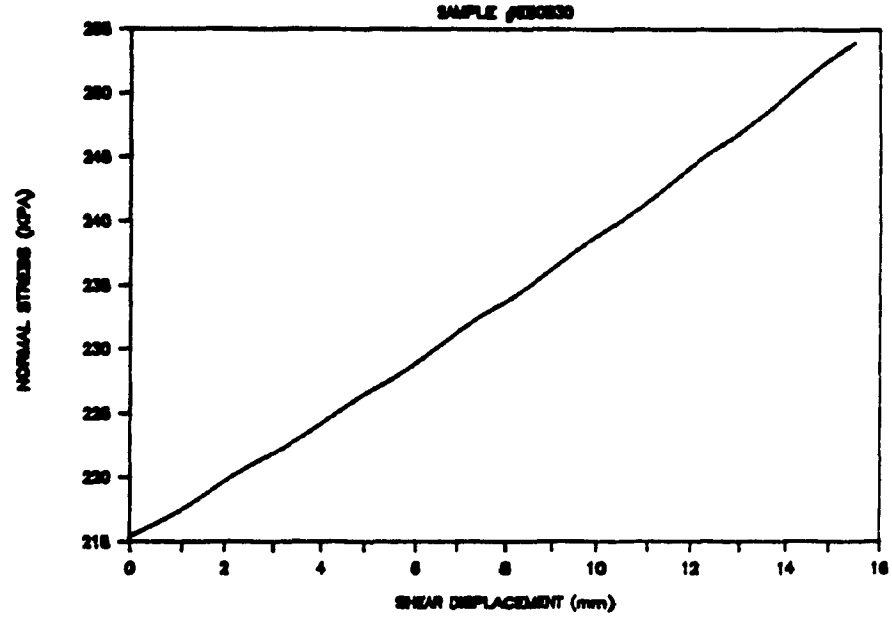
NORMAL STRESS (kPa)
SHEAR DISPLACEMENT (mm)

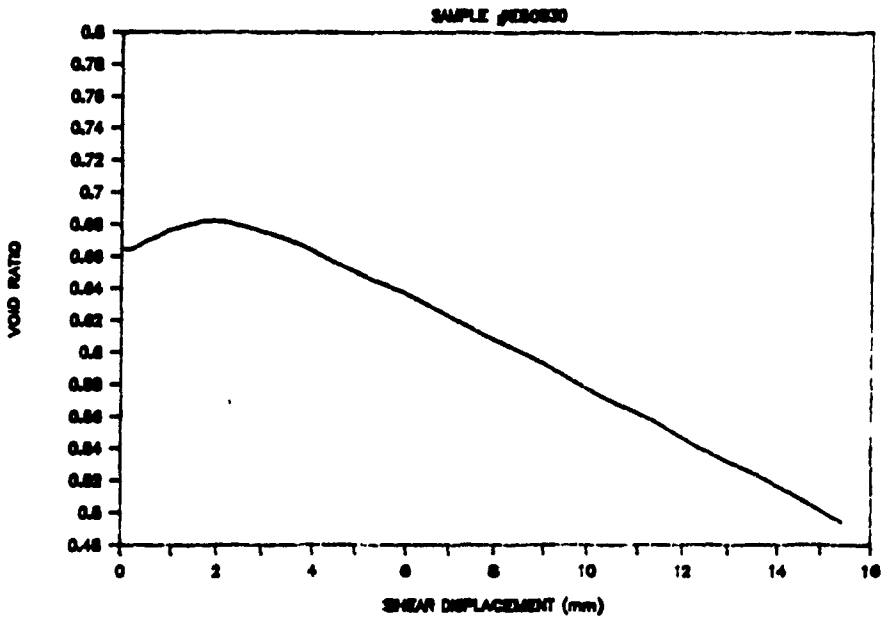
VOID RATIO
SHEAR DISPLACEMENT (mm)

SIGMA GOLD

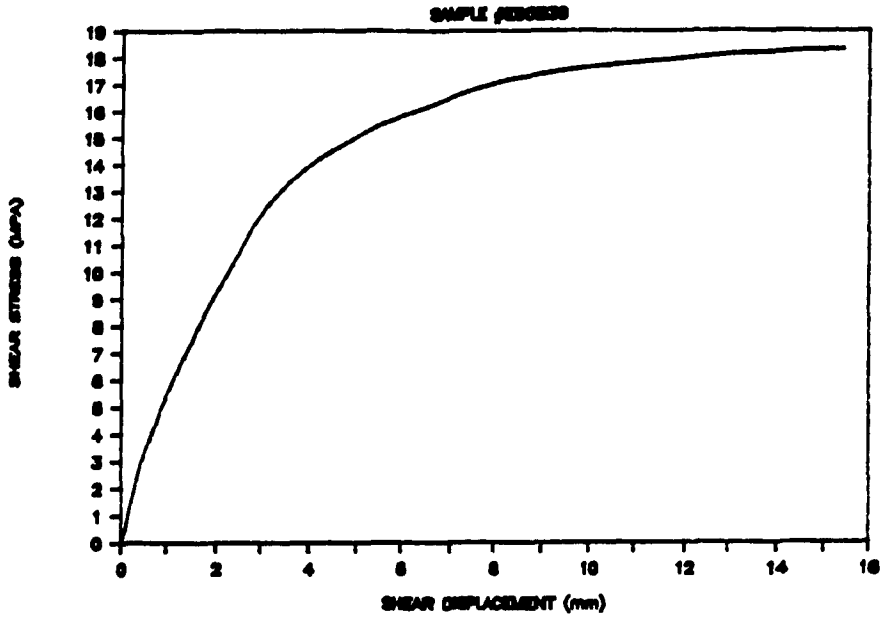
SHEAR STRESS (MPA)
SHEAR DISPLACEMENT (mm)

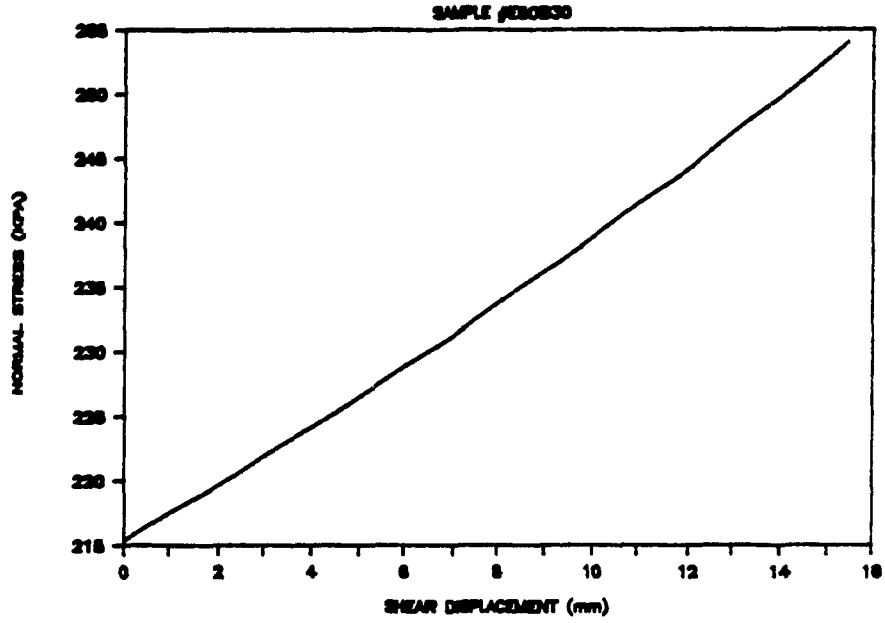
NORMAL STRESS (KPA)
SHEAR DISPLACEMENT (mm)

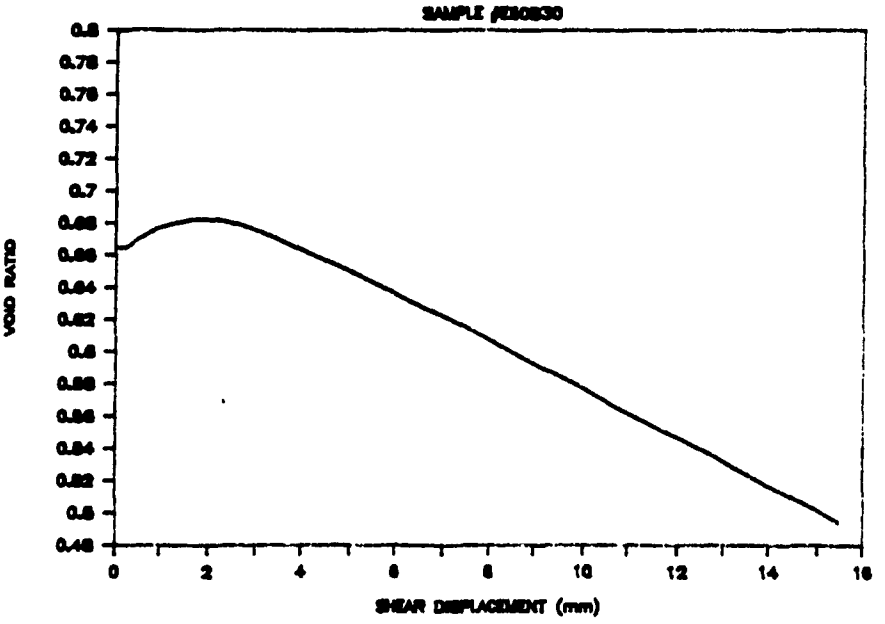
VOID RATIO
SHEAR DISPLACEMENT (mm)

SIGMA GOLD

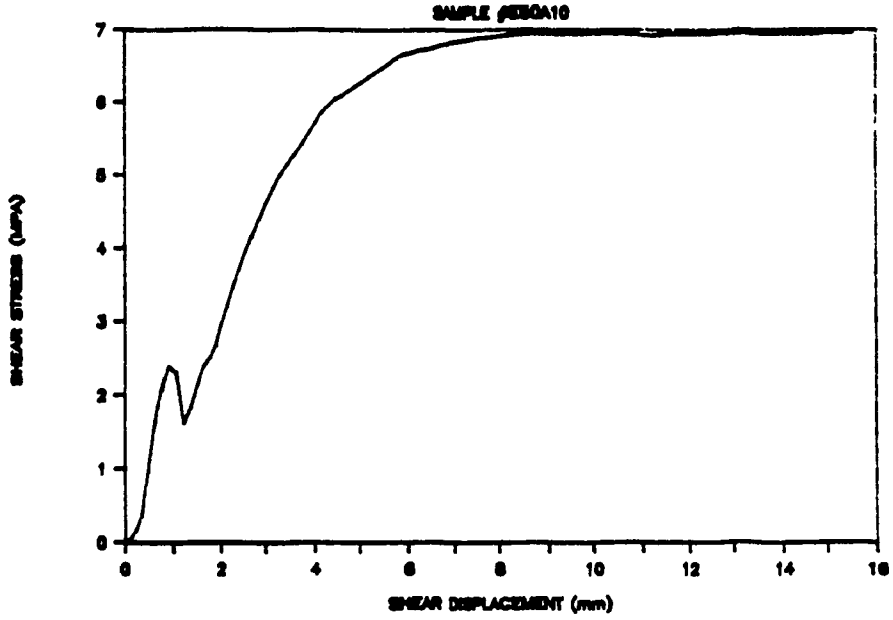
SAMPLE @EBOA10
SHEAR STRESS (MPA)
SHEAR DISPLACEMENT (mm)

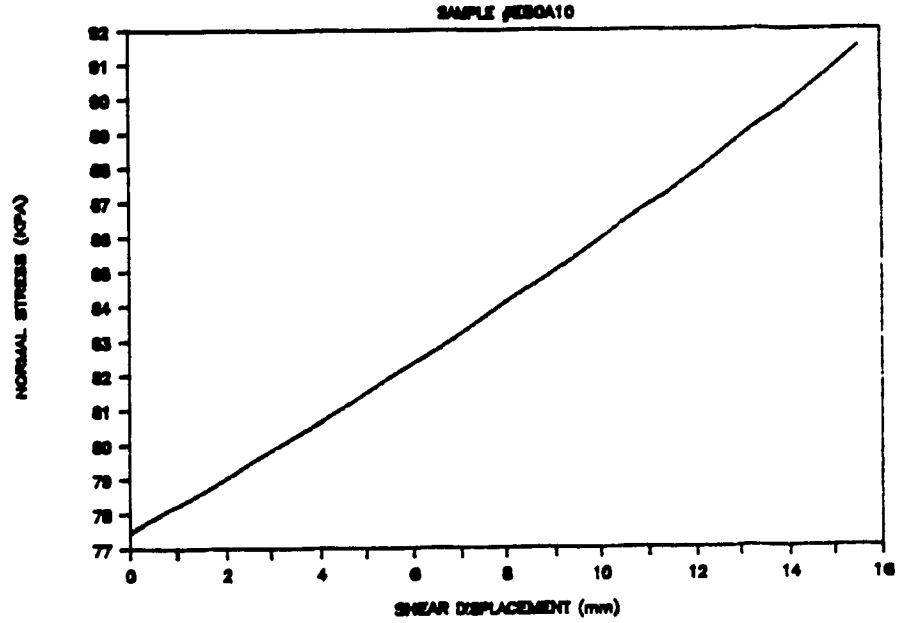
SAMPLE @EBOA10
NORMAL STRESS (KPA)
SHEAR DISPLACEMENT (mm)

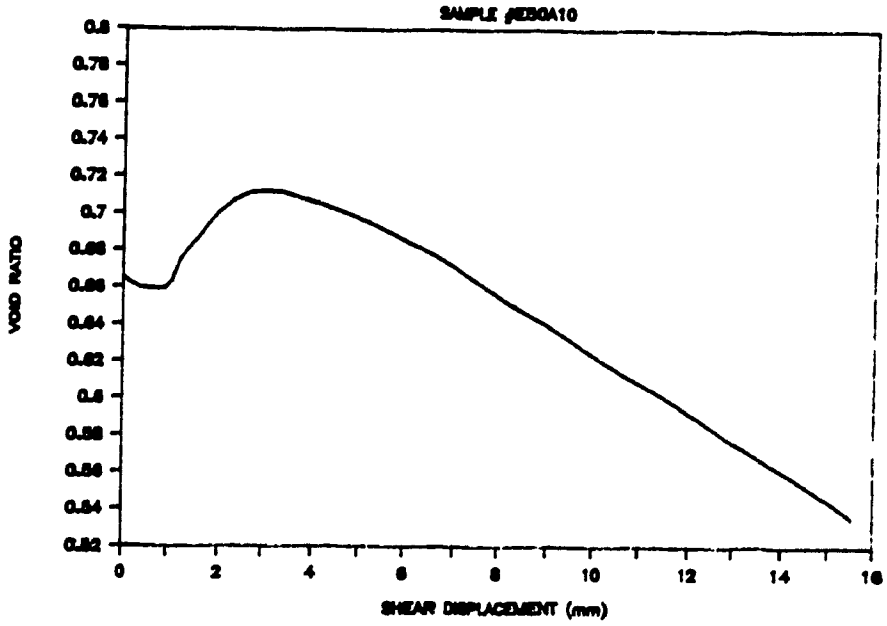
SAMPLE @EBOA10
VOID RATIO
SHEAR DISPLACEMENT (mm)

SIGMA GOLD

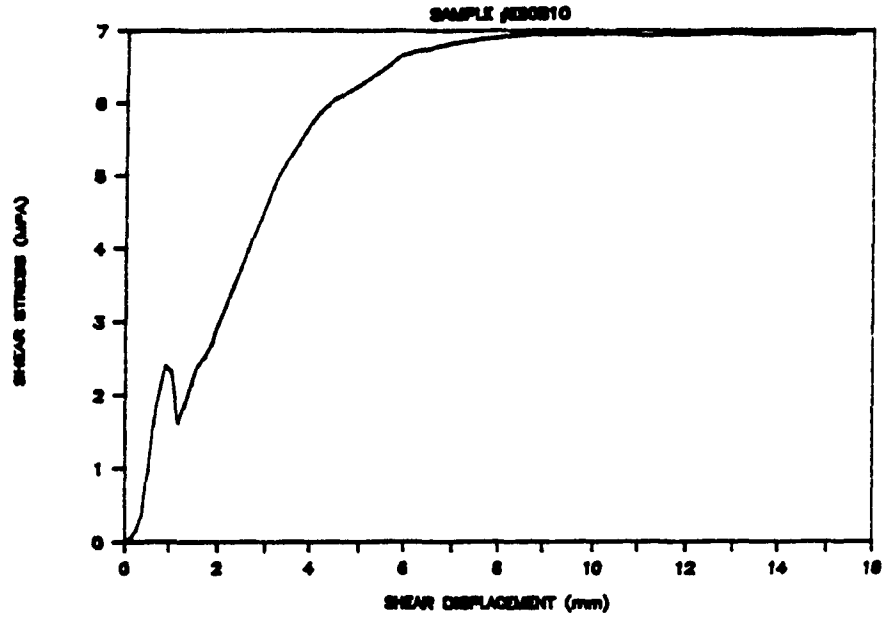
SHEAR STRESS (MPA)
SHEAR DISPLACEMENT (mm)

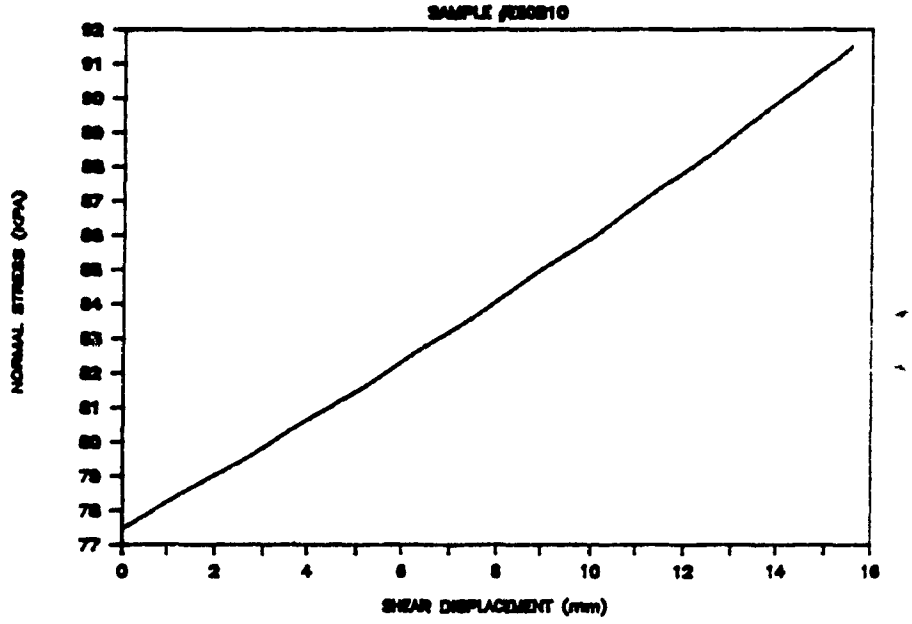
NORMAL STRESS (KPA)
SHEAR DISPLACEMENT (mm)

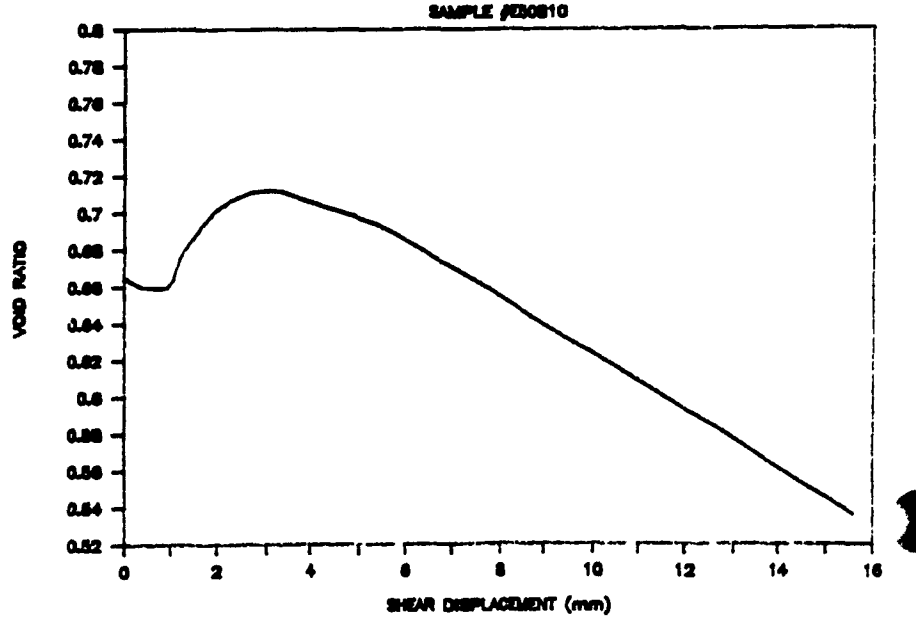
VOID RATIO
SHEAR DISPLACEMENT (mm)

SIGMA GOLD

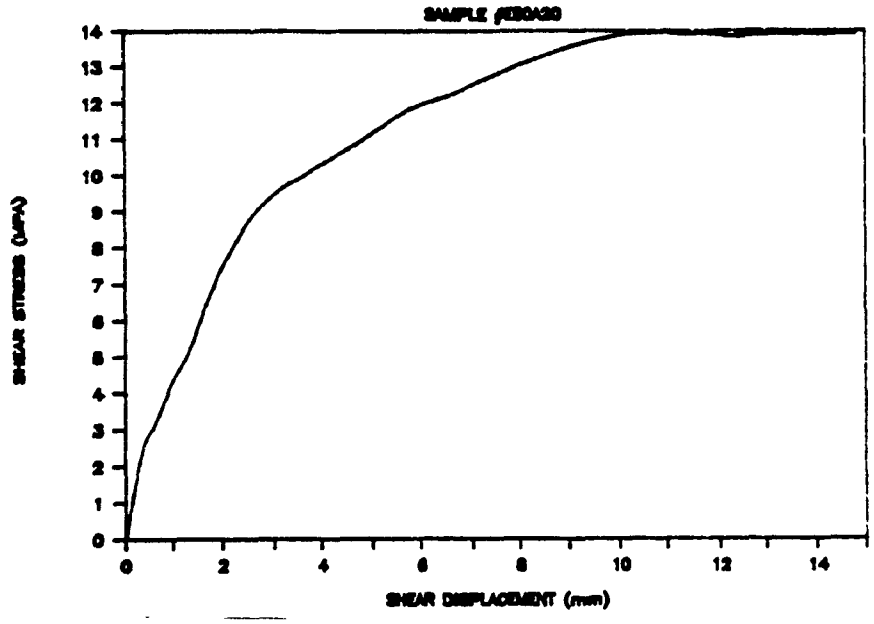
SAMPLE JE80A20
SHEAR STRESS (MPA)
SHEAR DISPLACEMENT (mm)

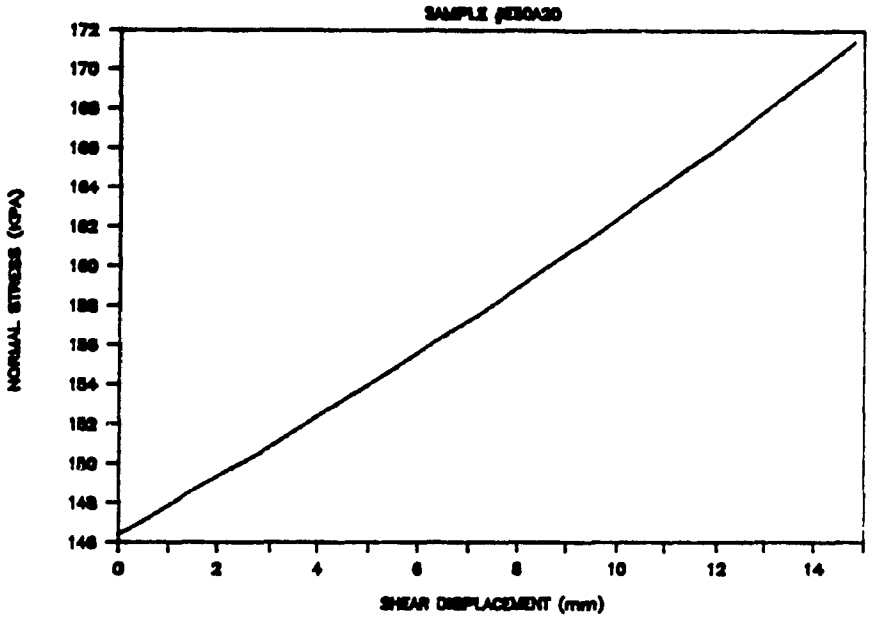
SAMPLE JE80A20
NORMAL STRESS (KPA)
SHEAR DISPLACEMENT (mm)

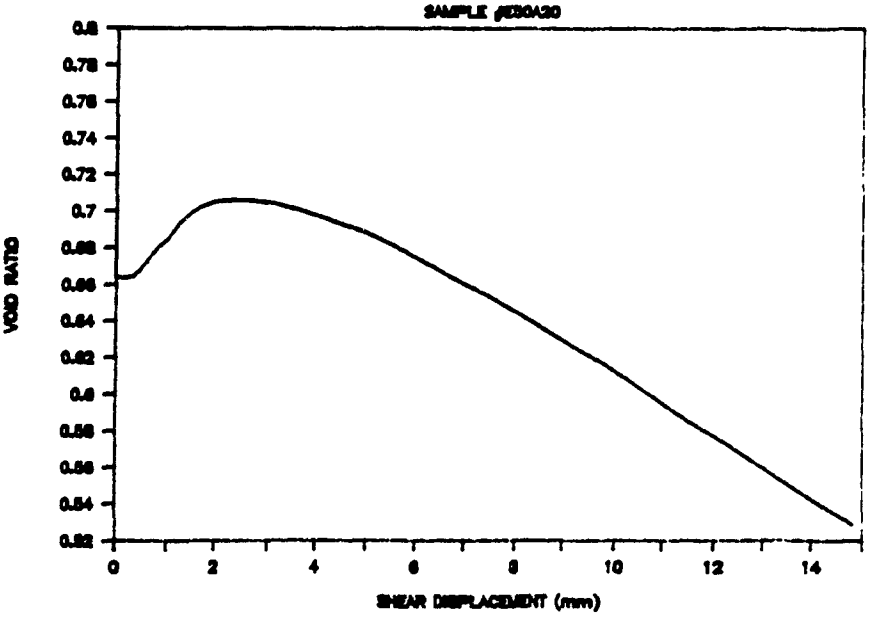
SAMPLE JE80A20
VOID RATIO
SHEAR DISPLACEMENT (mm)

SIGMA GOLD

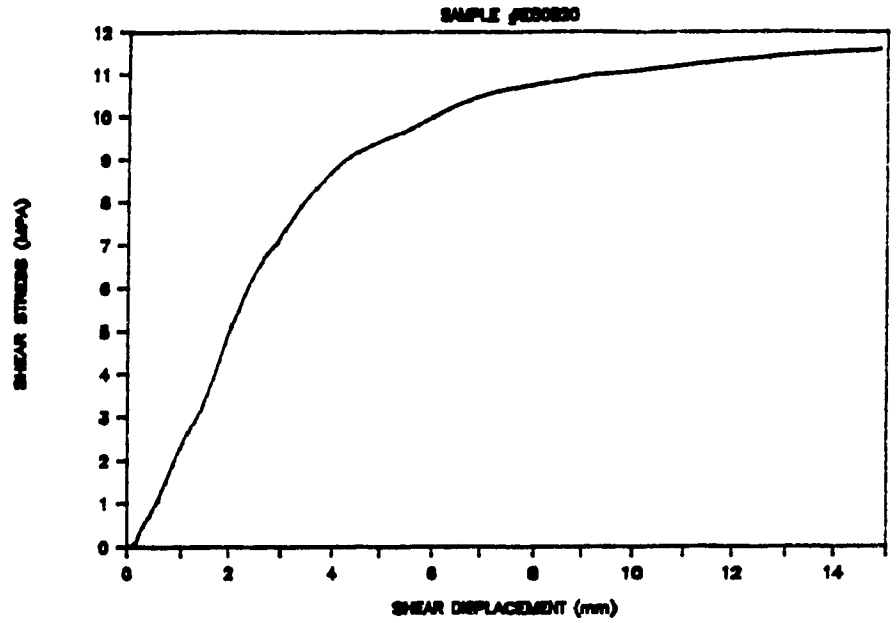
SAMPLE #E50820
SHEAR STRESS (MPA)
SHEAR DISPLACEMENT (mm)

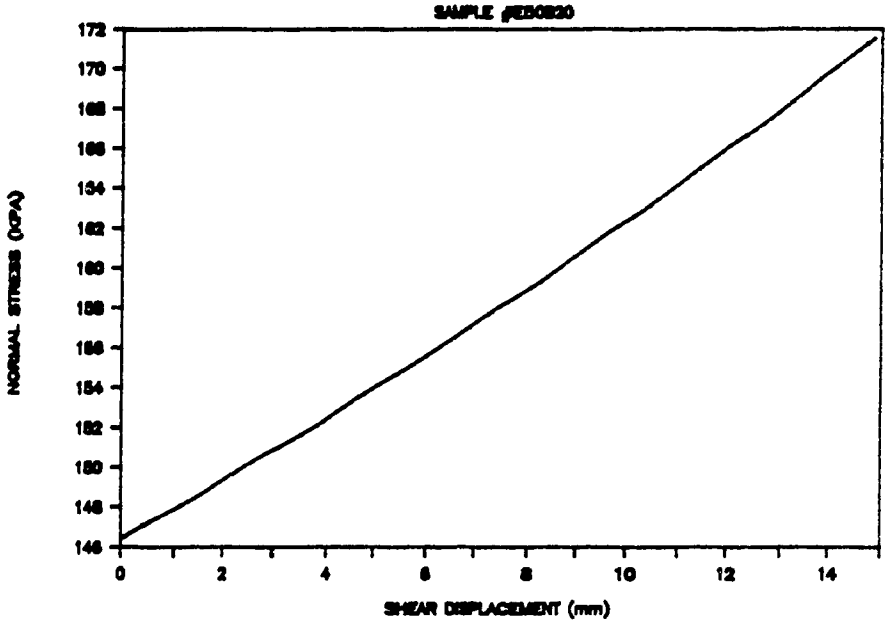
SAMPLE #E50820
NORMAL STRESS (KPA)
SHEAR DISPLACEMENT (mm)

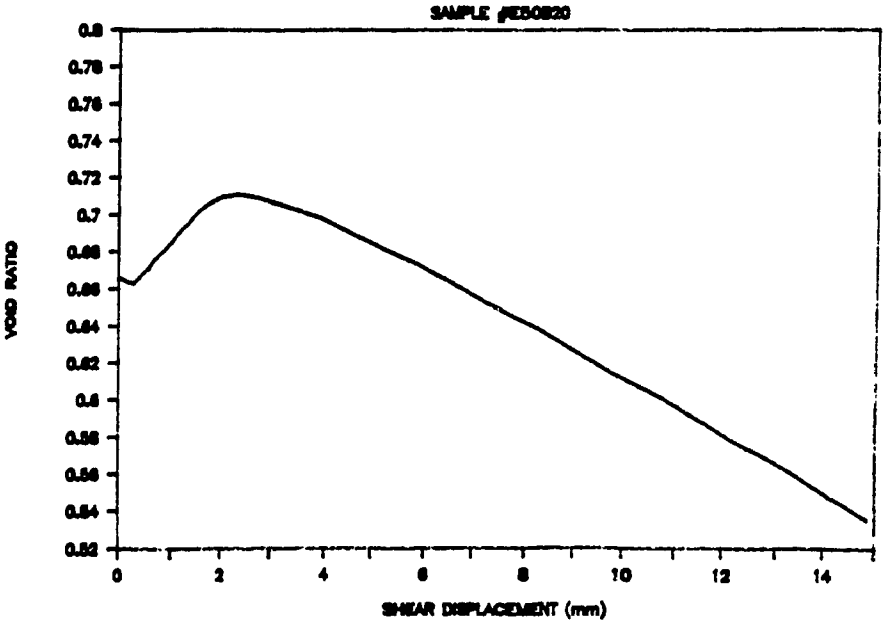
SAMPLE #E50820
VOID RATIO
SHEAR DISPLACEMENT (mm)

SIGMA GOLD

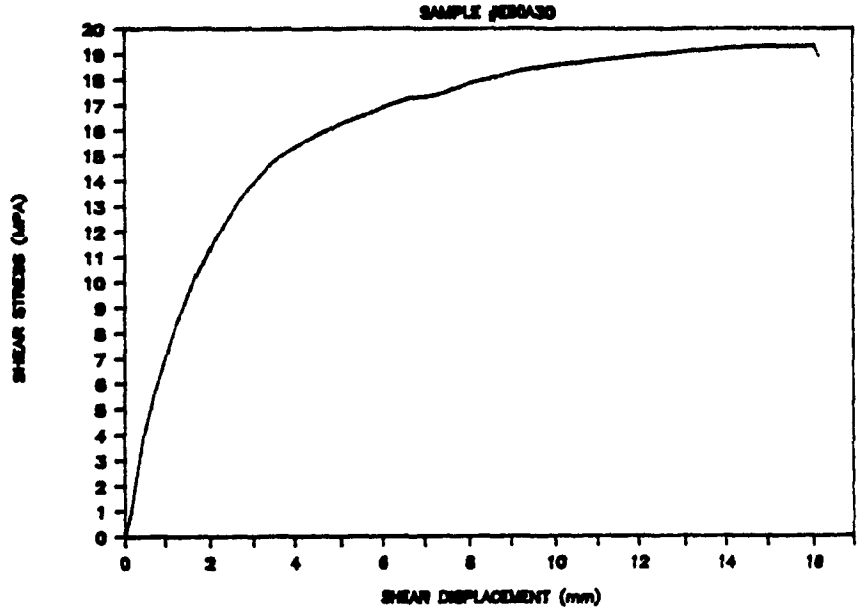
SAMPLE #EB0A30
SHEAR STRESS (MPA)
SHEAR DISPLACEMENT (mm)

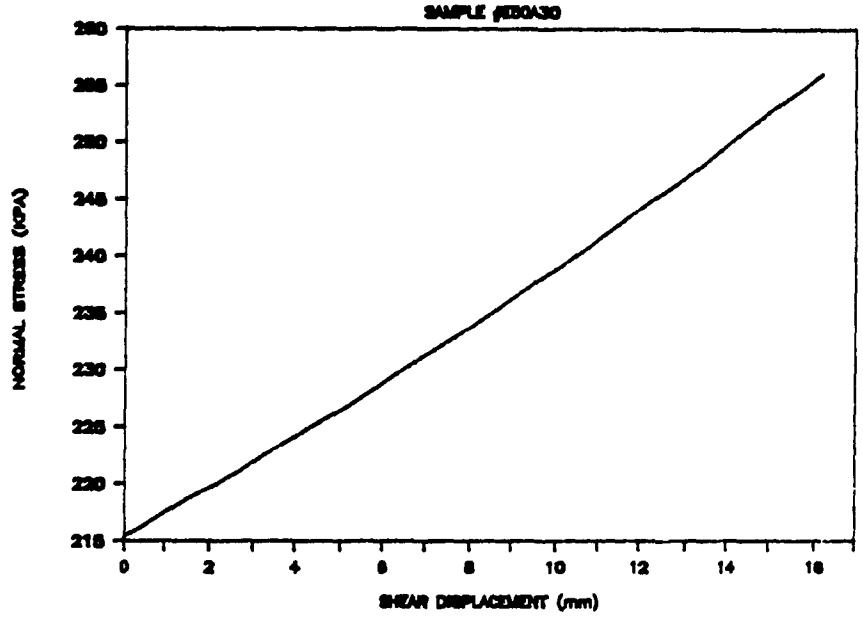
SAMPLE #EB0A30
NORMAL STRESS (KPA)
SHEAR DISPLACEMENT (mm)

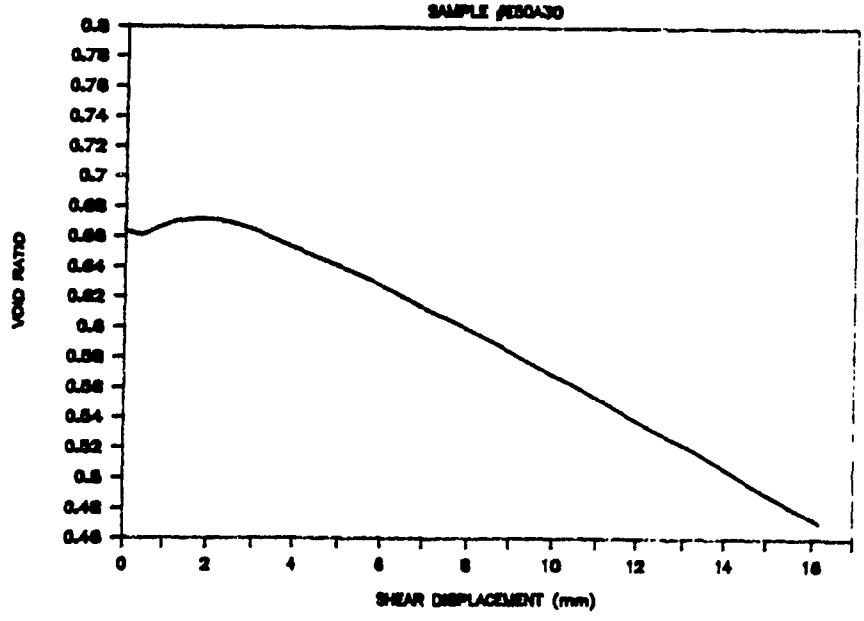
SAMPLE #EB0A30
VOID RATIO
SHEAR DISPLACEMENT (mm)

SIGMA GOLD

SAMPLE #A46A10

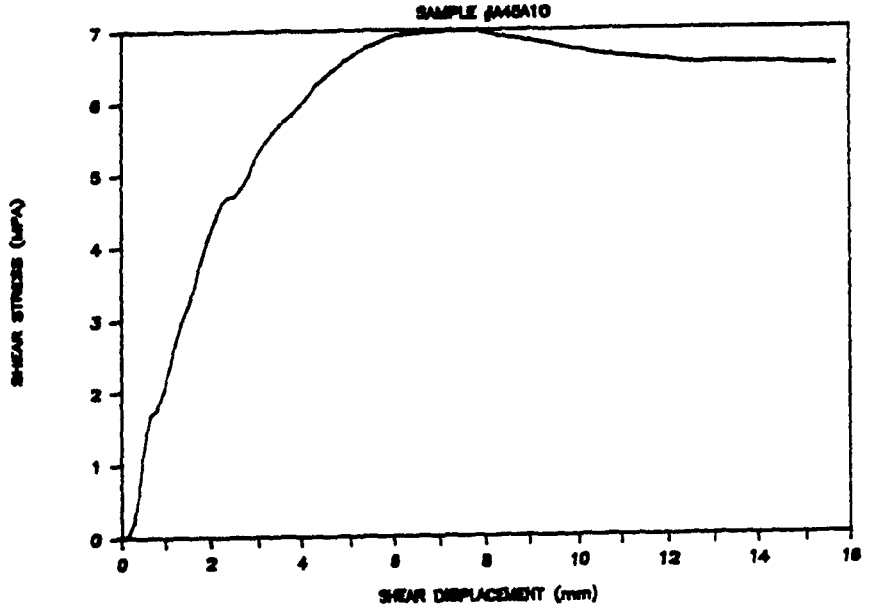

SAMPLE #A46A10

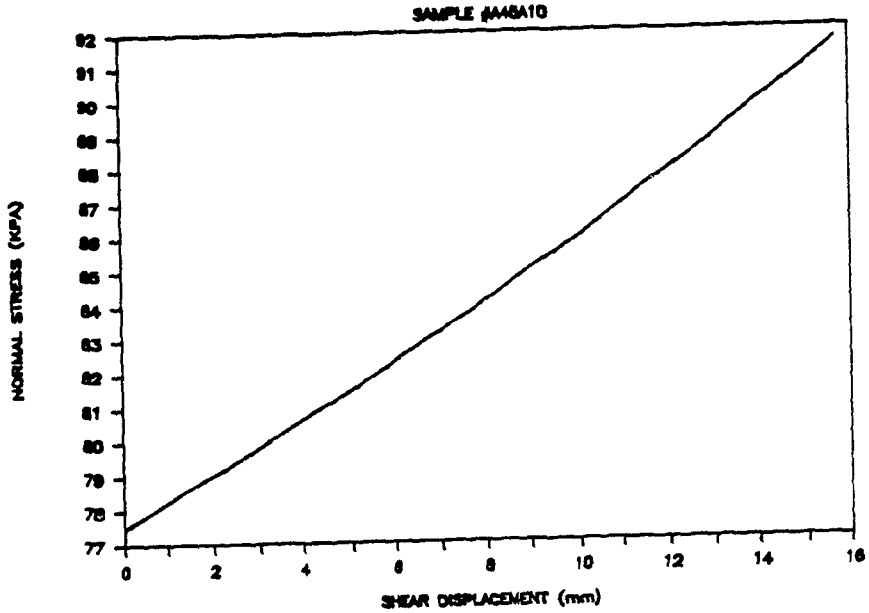

SAMPLE #A46A10

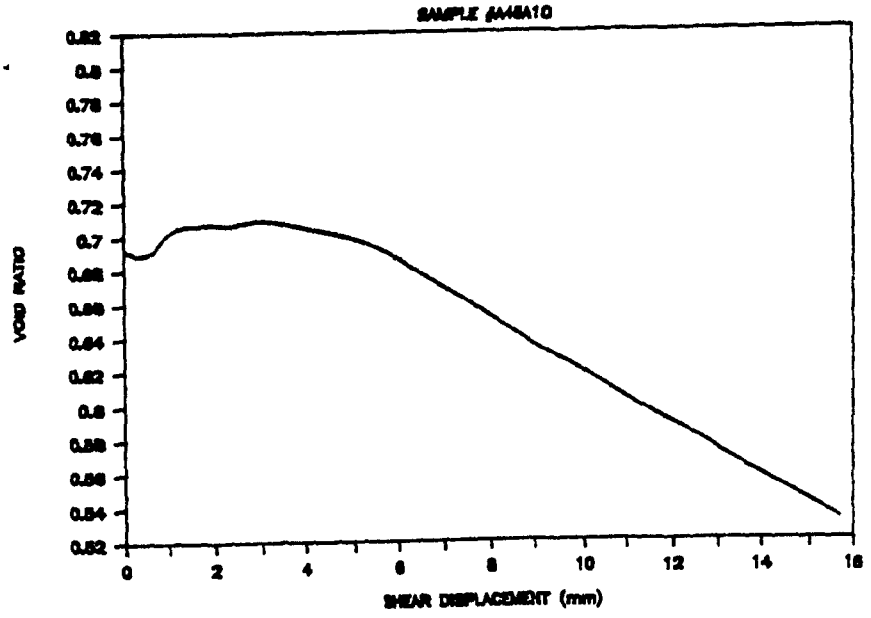

SIGMA GOLD

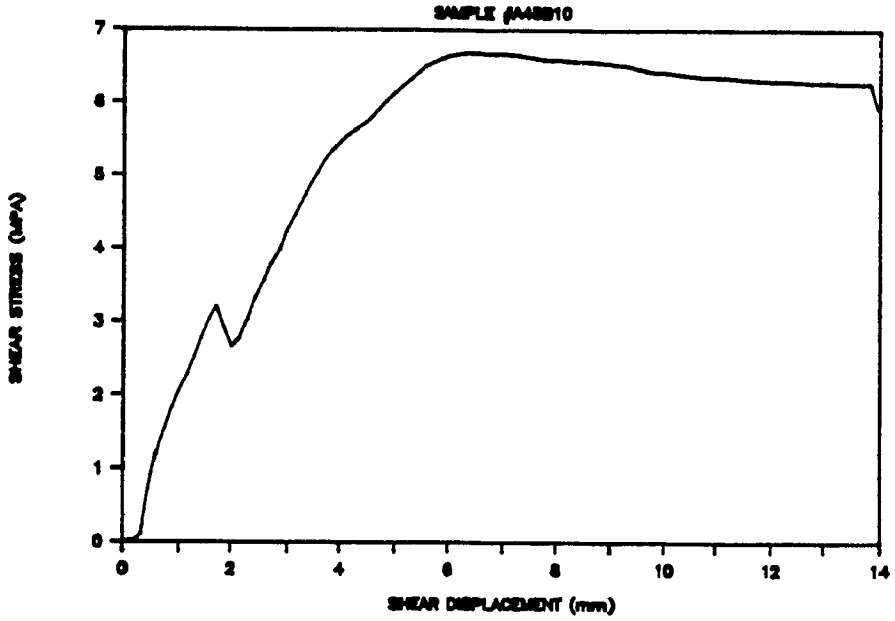
SAMPLE @A45B10
SHEAR STRESS (MPA)
SHEAR DISPLACEMENT (mm)

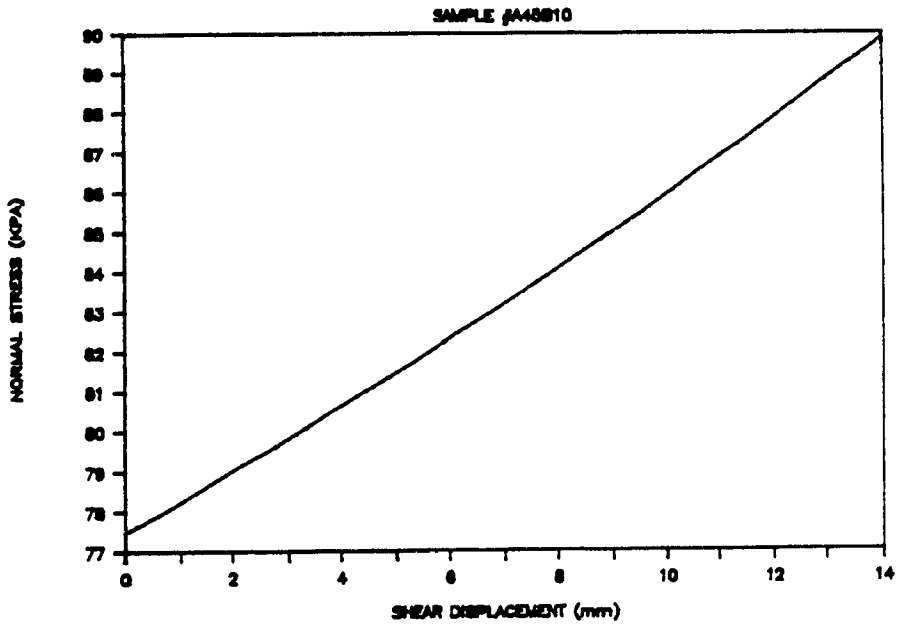
SAMPLE @A45B10
NORMAL STRESS (KPA)
SHEAR DISPLACEMENT (mm)

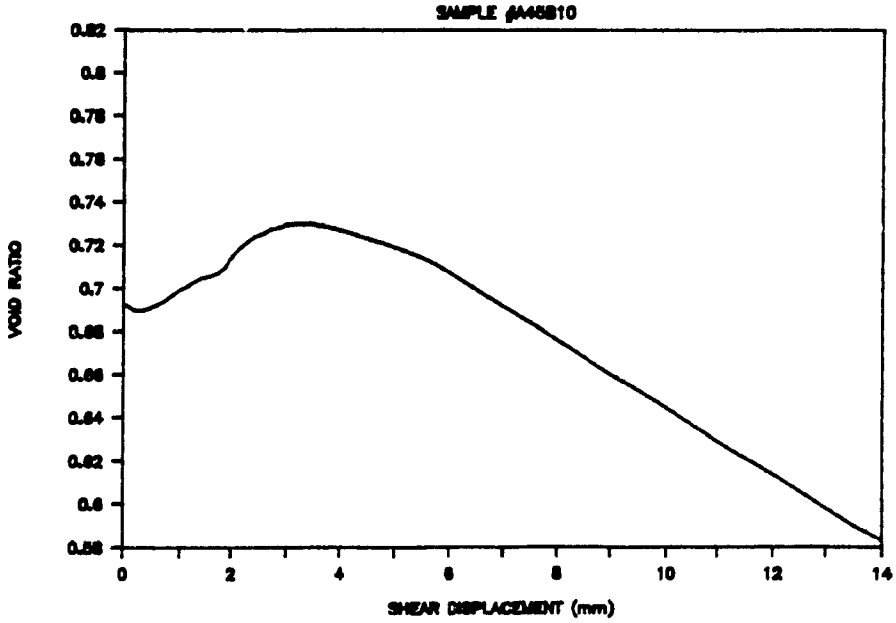
SAMPLE @A45B10
VOID RATIO
SHEAR DISPLACEMENT (mm)

SIGMA GOLD

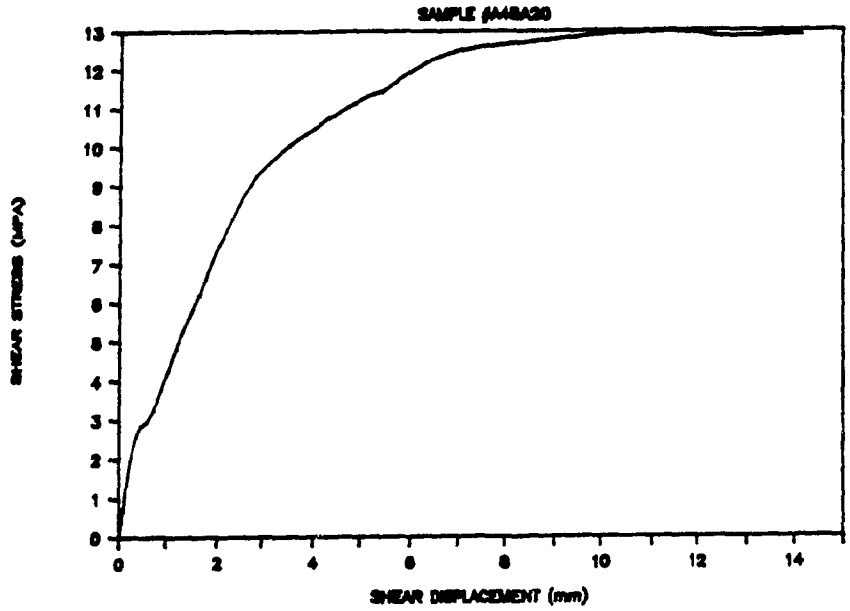
SAMPLE @A46A20
SHEAR STRESS (MPA)
SHEAR DISPLACEMENT (mm)

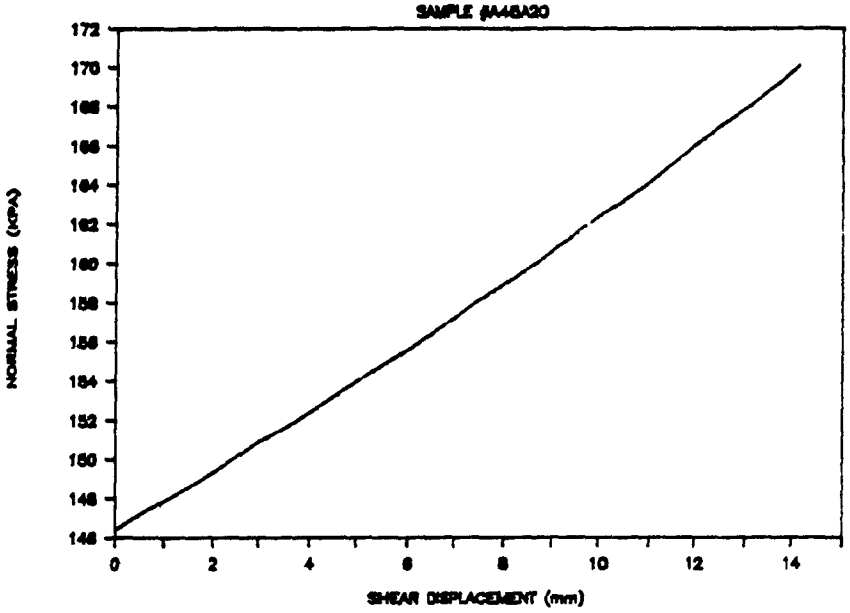
SAMPLE @A46A20
NORMAL STRESS (KPA)
SHEAR DISPLACEMENT (mm)

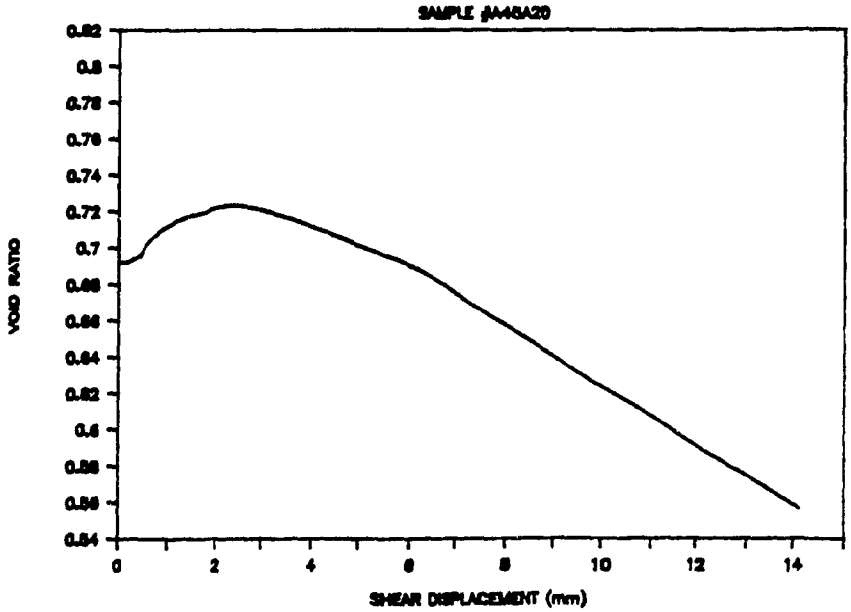
SAMPLE @A46A20
VOID RATIO
SHEAR DISPLACEMENT (mm)

SIGMA GOLD

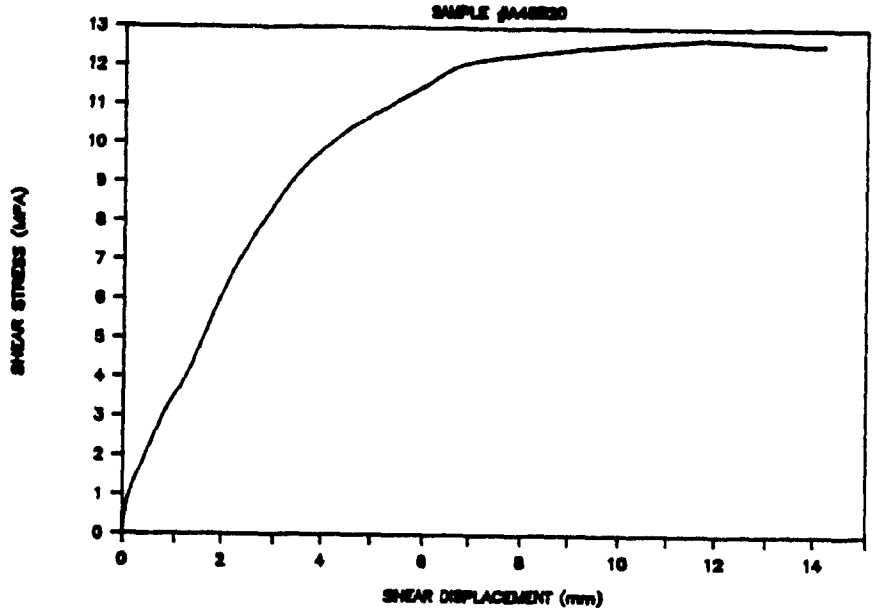
SAMPLE @A46820
SHEAR STRESS (MPA)
SHEAR DISPLACEMENT (mm)

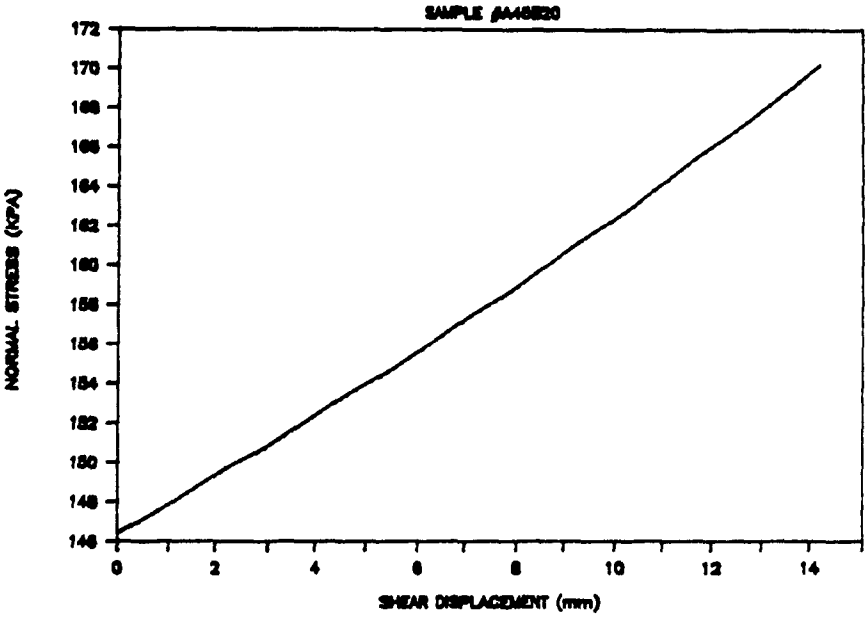
SAMPLE @A46820
NORMAL STRESS (KPA)
SHEAR DISPLACEMENT (mm)

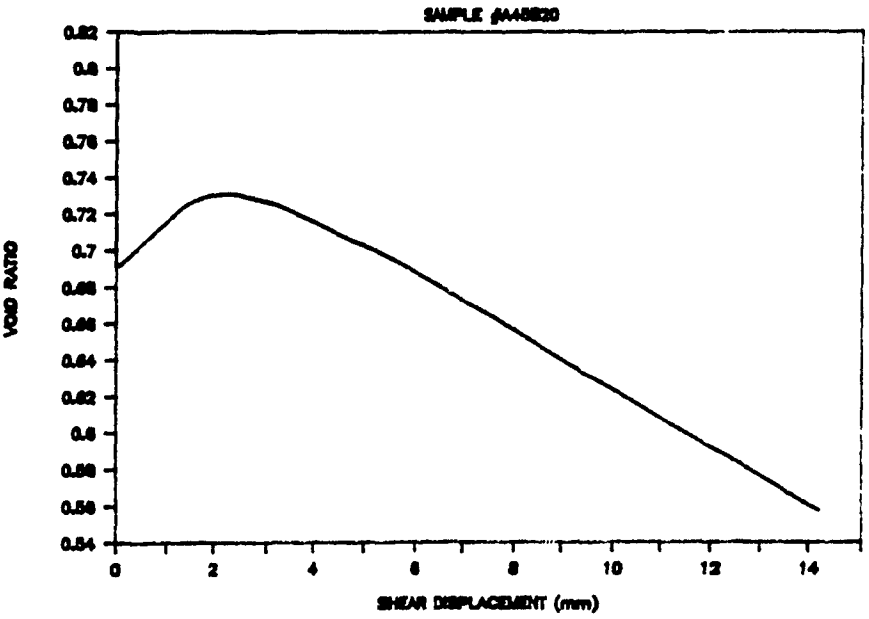
SAMPLE @A46820
VOID RATIO
SHEAR DISPLACEMENT (mm)

SIGMA GOLD

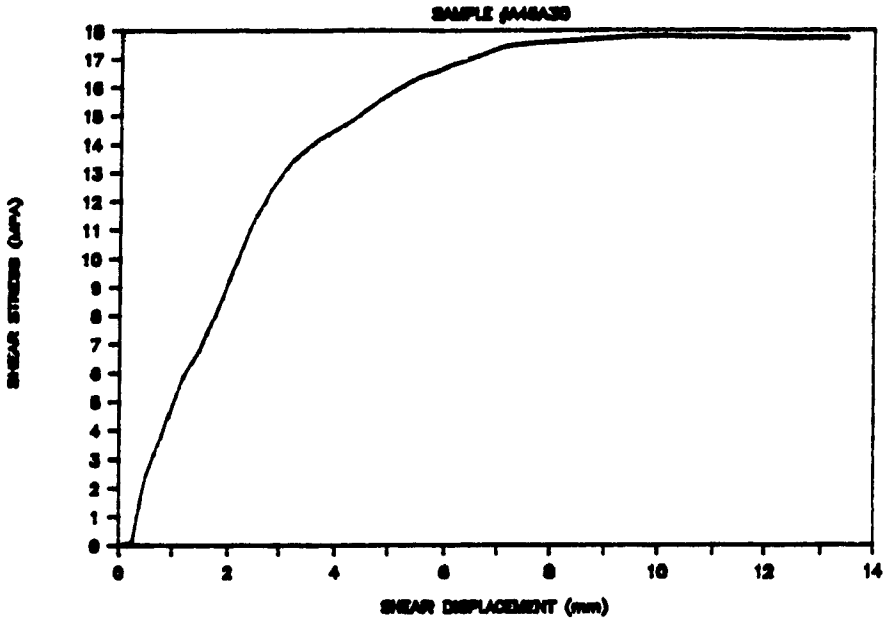
SAMPLE #A46A30
SHEAR STRESS (MPA)
SHEAR DISPLACEMENT (mm)

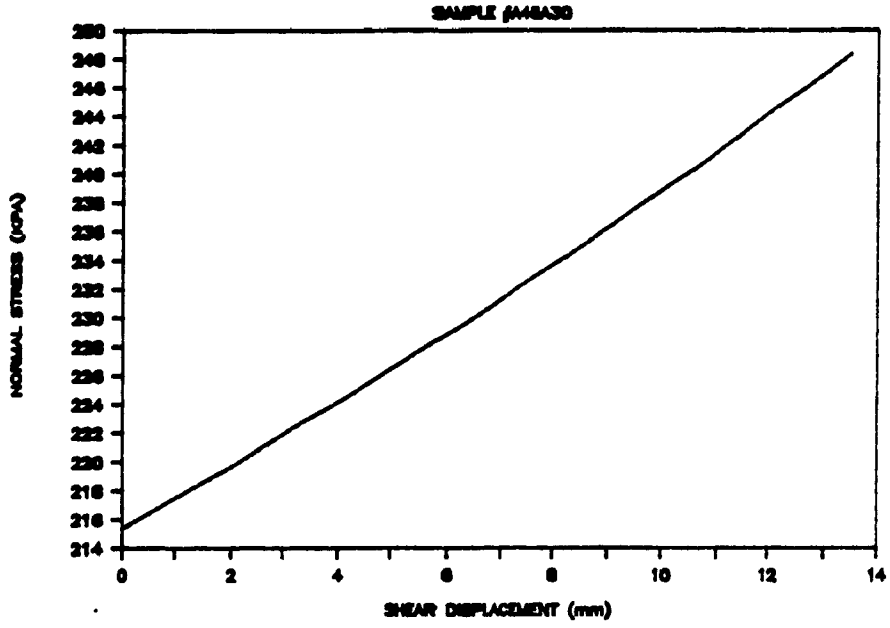
SAMPLE #A46A30
NORMAL STRESS (KPA)
SHEAR DISPLACEMENT (mm)

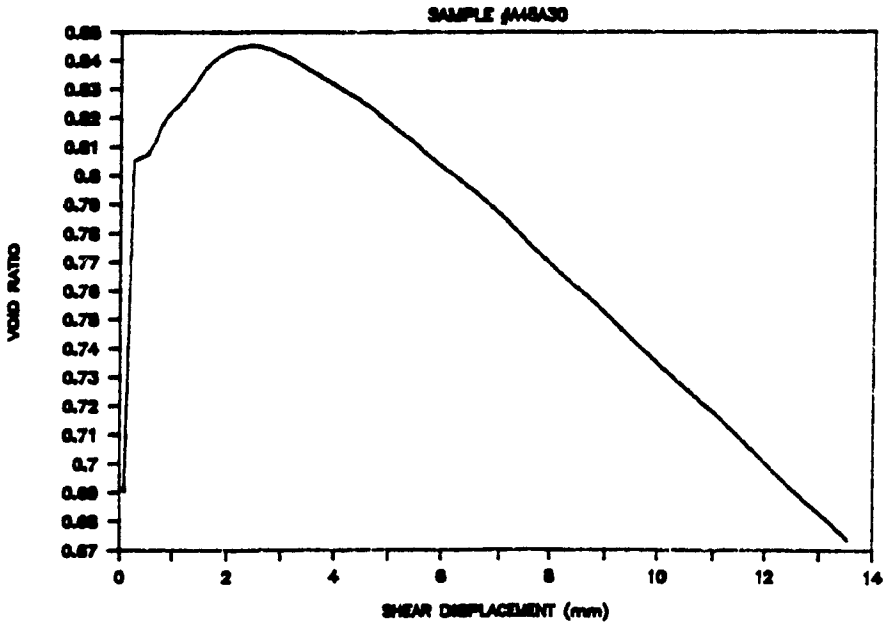
SAMPLE #A46A30
VOID RATIO
SHEAR DISPLACEMENT (mm)

SIGMA GOLD

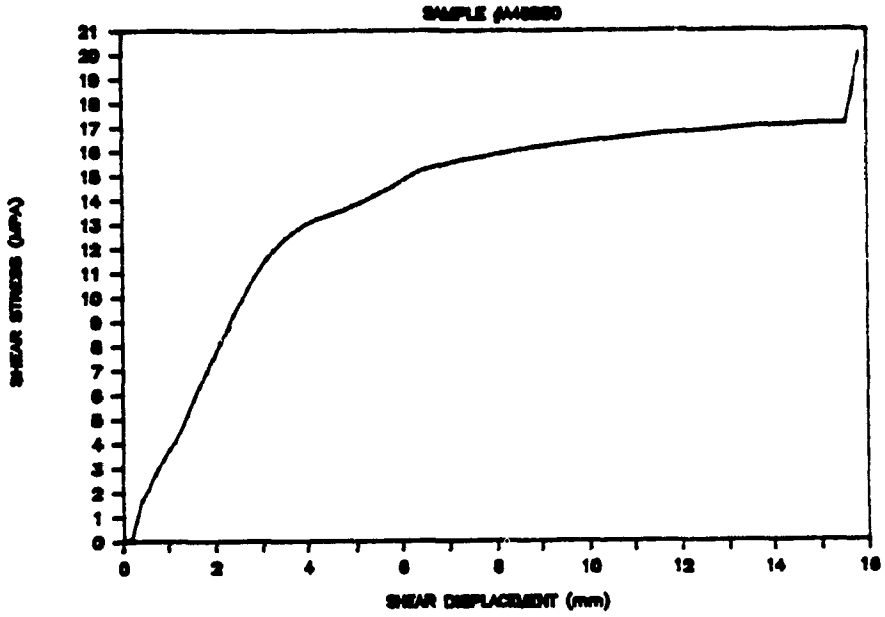
SHEAR STRESS (MPA)
SHEAR DISPLACEMENT (mm)

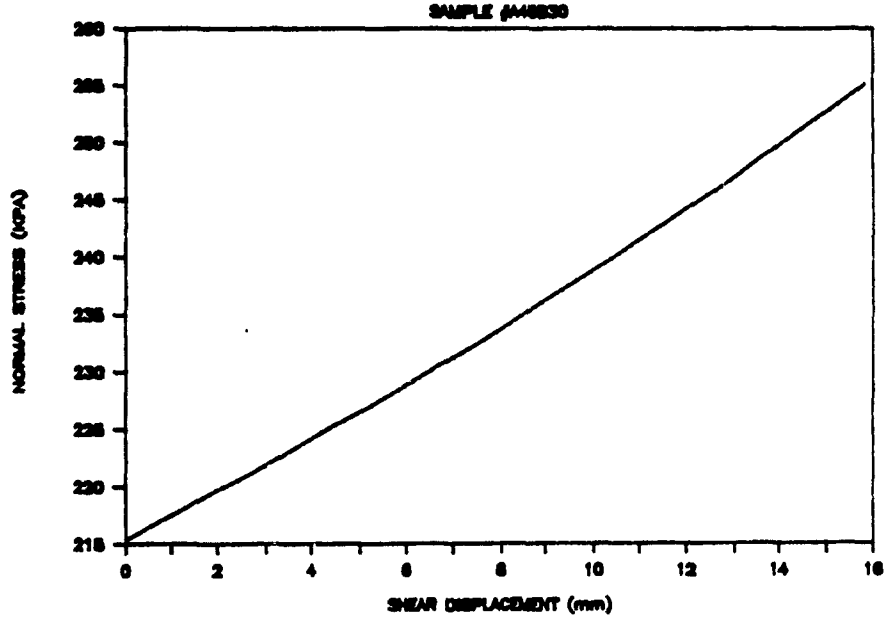
NORMAL STRESS (KPA)
SHEAR DISPLACEMENT (mm)

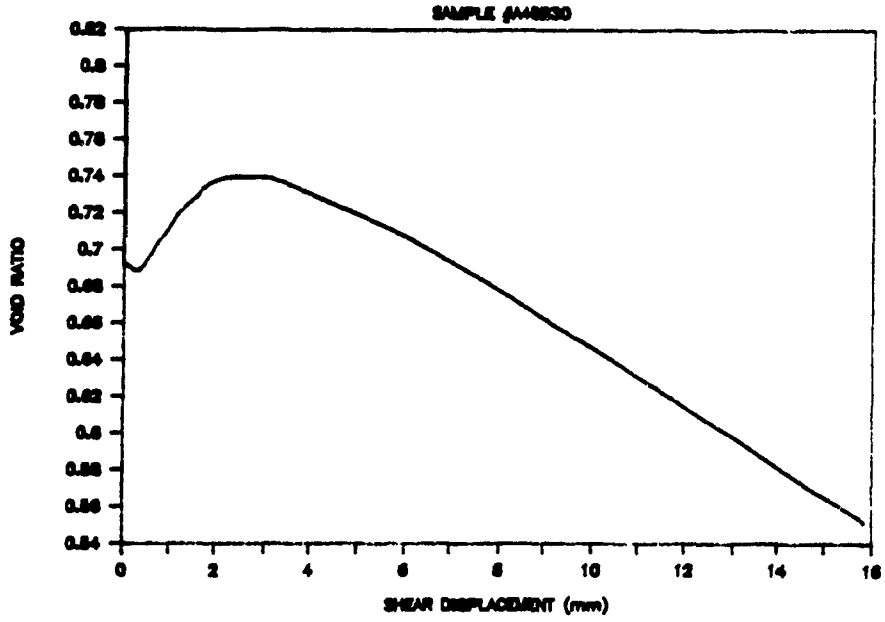
VOID RATIO
SHEAR DISPLACEMENT (mm)

SIGMA GOLD

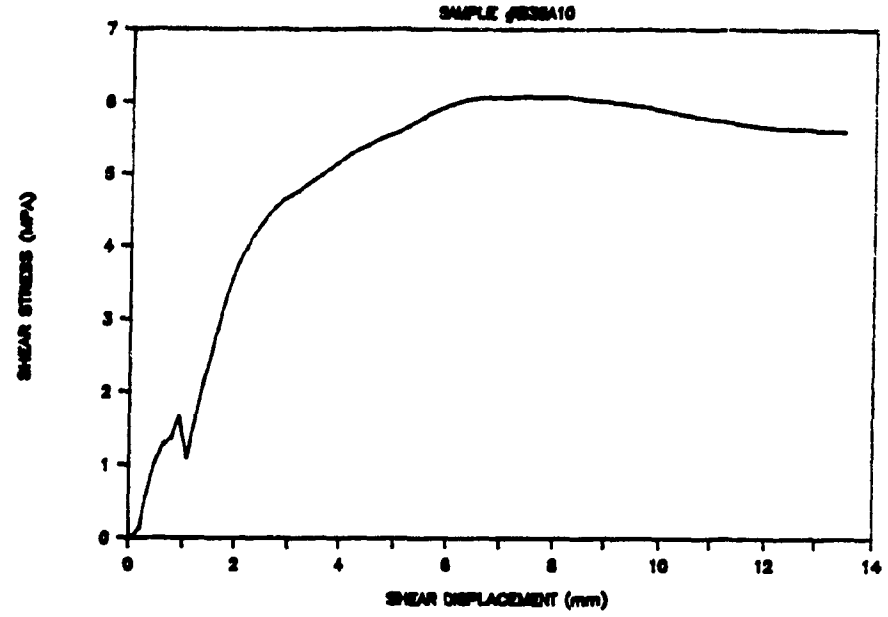
SHEAR STRESS (MPA)
SHEAR DISPLACEMENT (mm)

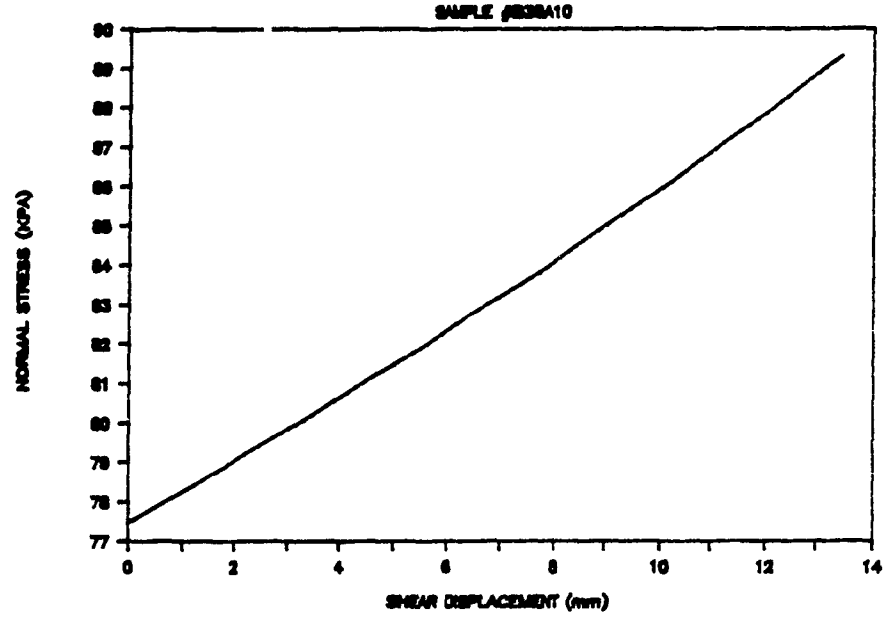
NORMAL STRESS (KPA)
SHEAR DISPLACEMENT (mm)

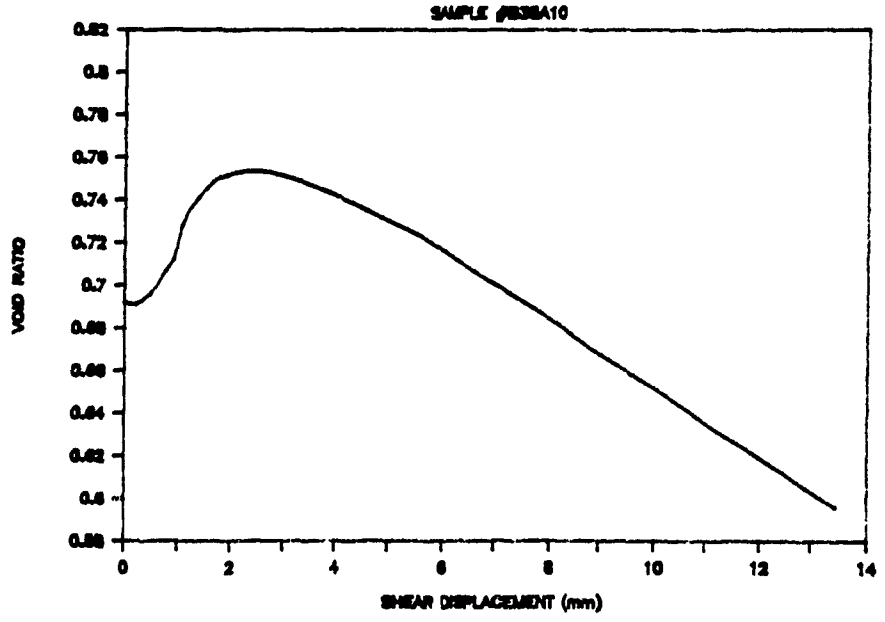
VOID RATIO
SHEAR DISPLACEMENT (mm)

SIGMA GOLD

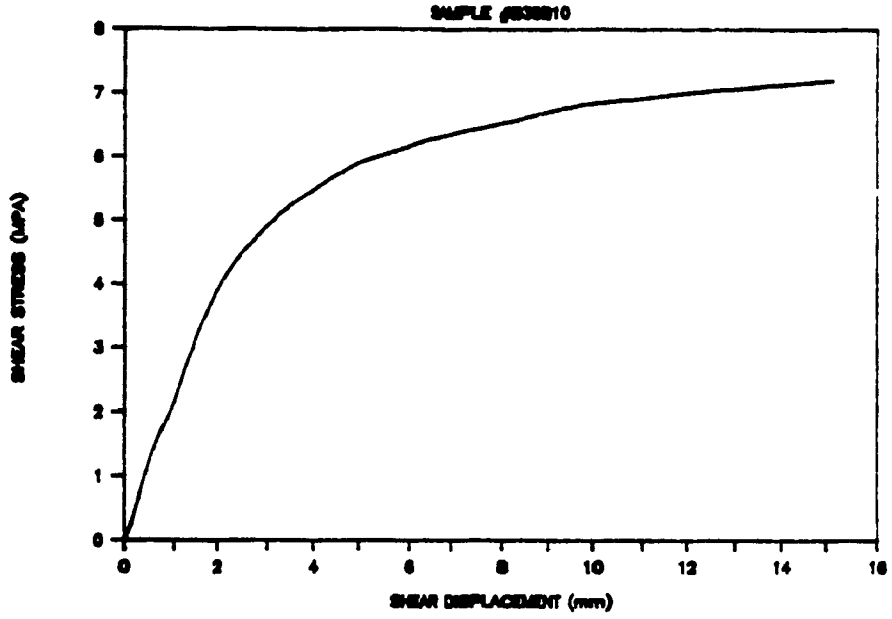
SHEAR STRESS (MPA)
SHEAR DISPLACEMENT (mm)

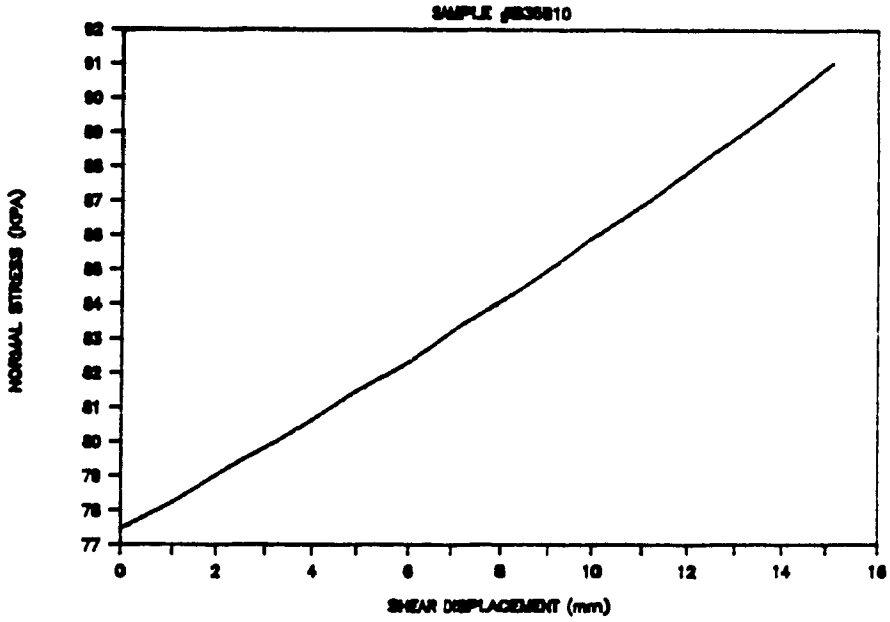
NORMAL STRESS (KPA)
SHEAR DISPLACEMENT (mm)

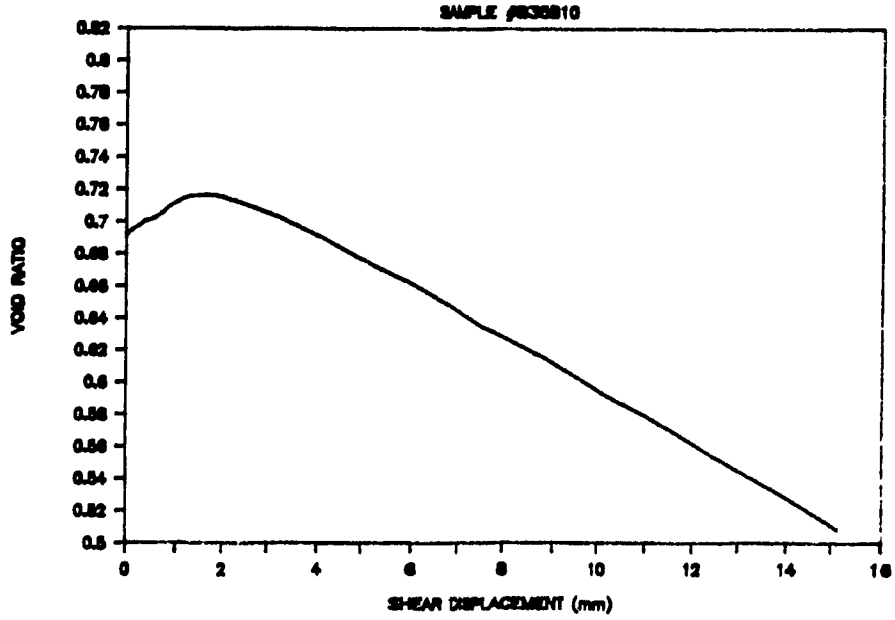
VOID RATIO
SHEAR DISPLACEMENT (mm)

SIGMA GOLD

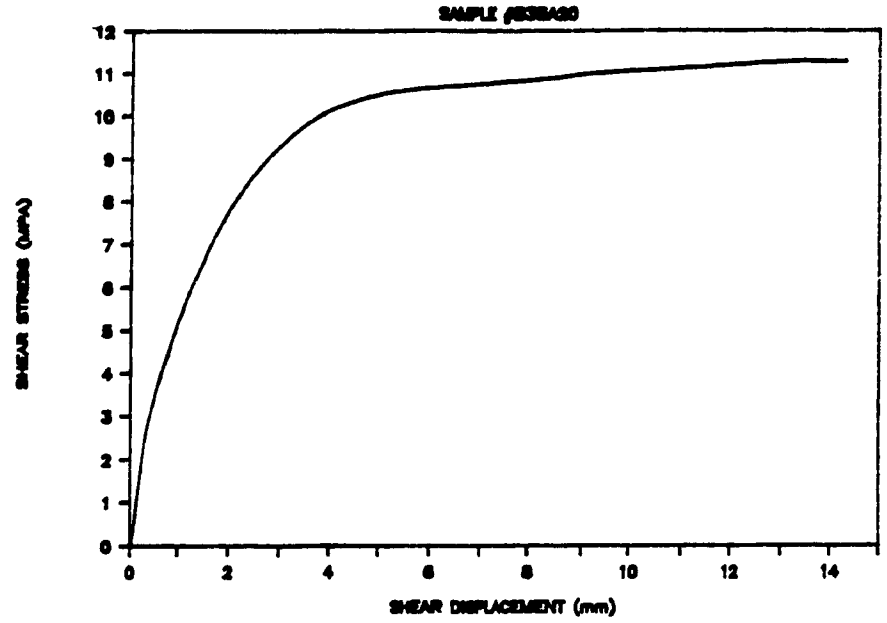
SHEAR STRESS (MPA)
SHEAR DISPLACEMENT (mm)

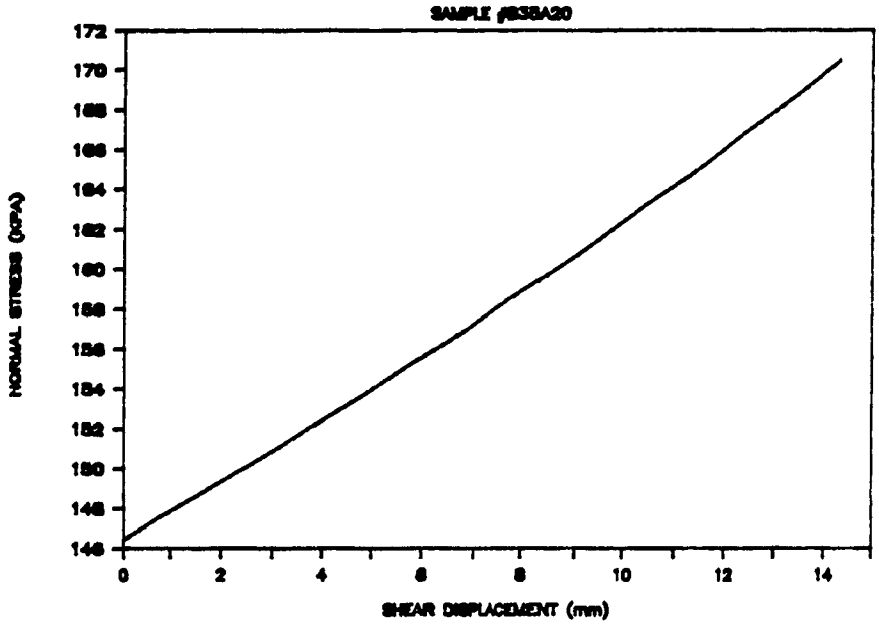
NORMAL STRESS (KPA)
SHEAR DISPLACEMENT (mm)

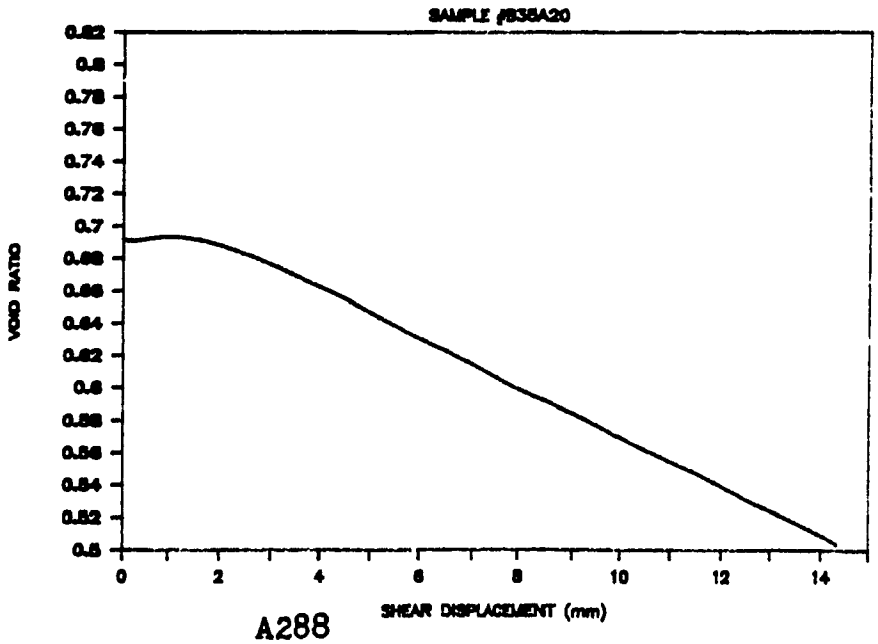
VOID RATIO
SHEAR DISPLACEMENT (mm)

SIGMA GOLD

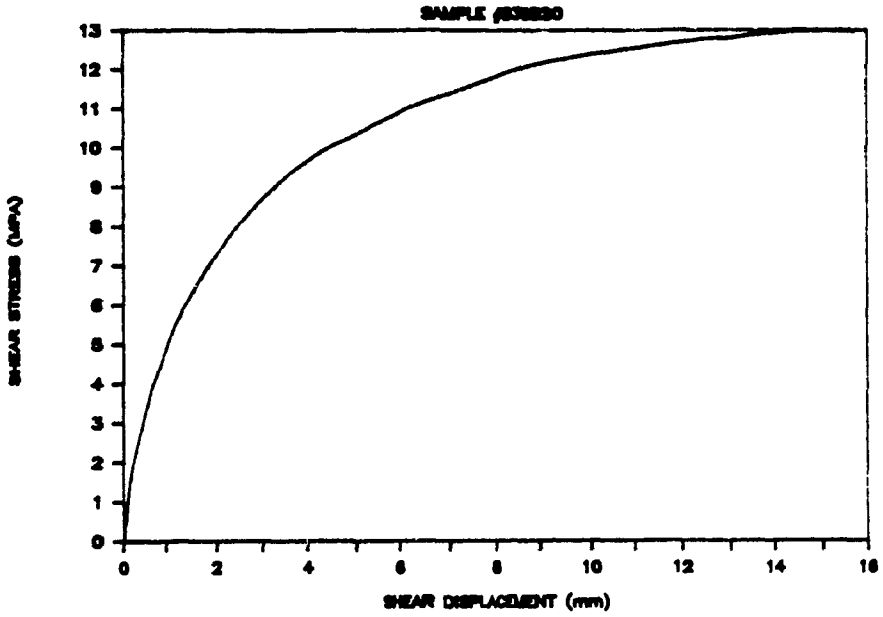
SHEAR STRESS (MPA)
SHEAR DISPLACEMENT (mm)

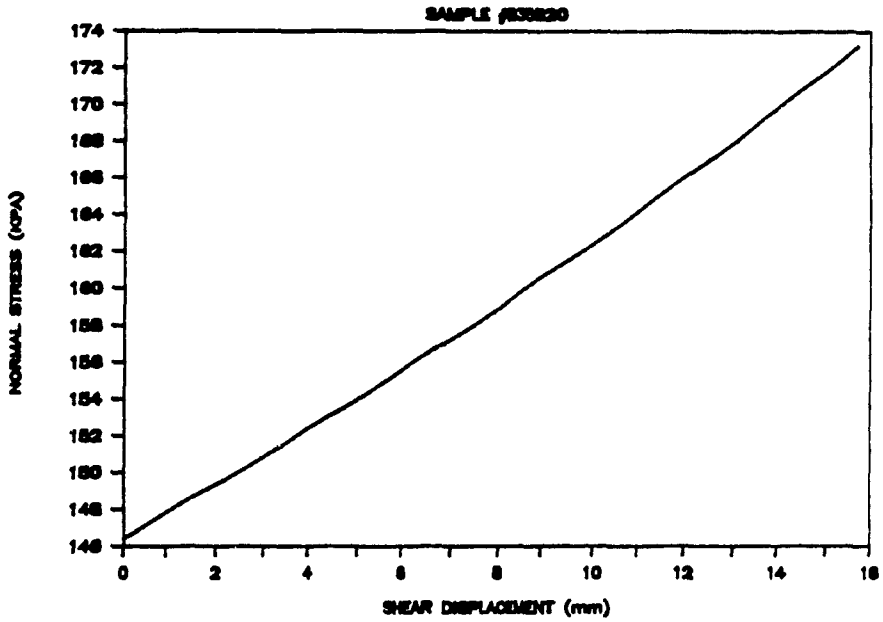
NORMAL STRESS (KPA)
SHEAR DISPLACEMENT (mm)

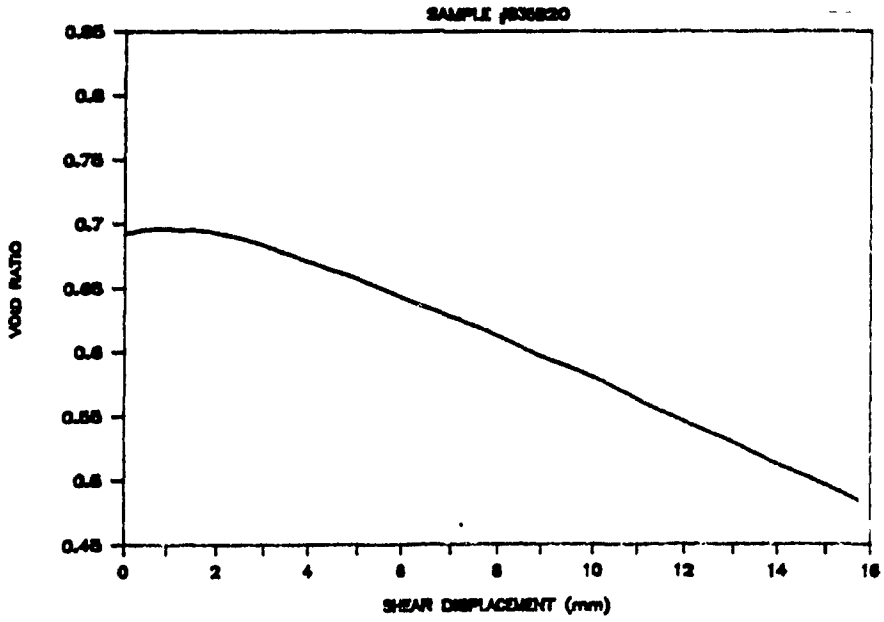
VOID RATIO
SHEAR DISPLACEMENT (mm)

SIGMA GOLD

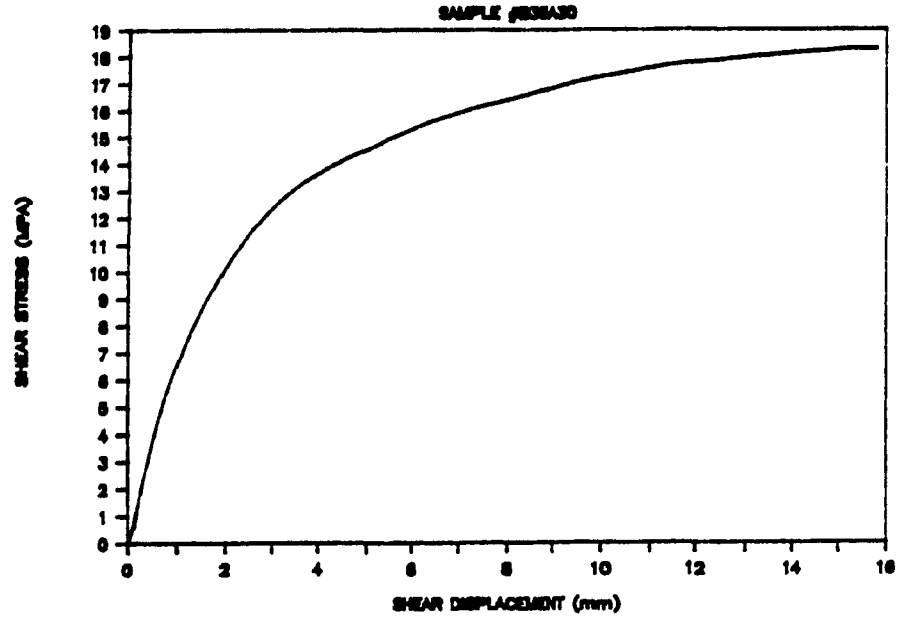
SAMPLE @B36A30
SHEAR STRESS (MPA)
SHEAR DISPLACEMENT (mm)

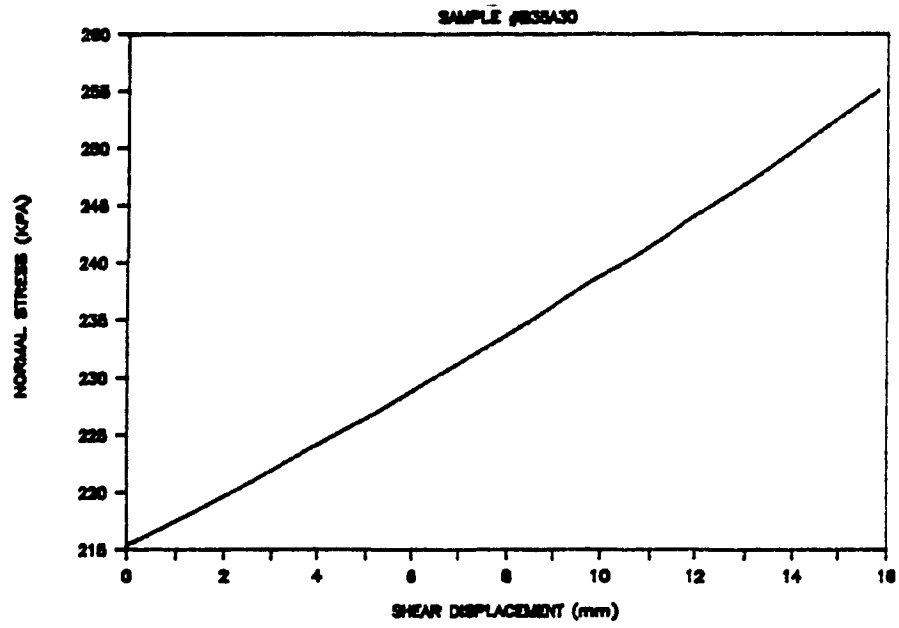
SAMPLE @B36A30
NORMAL STRESS (KPA)
SHEAR DISPLACEMENT (mm)

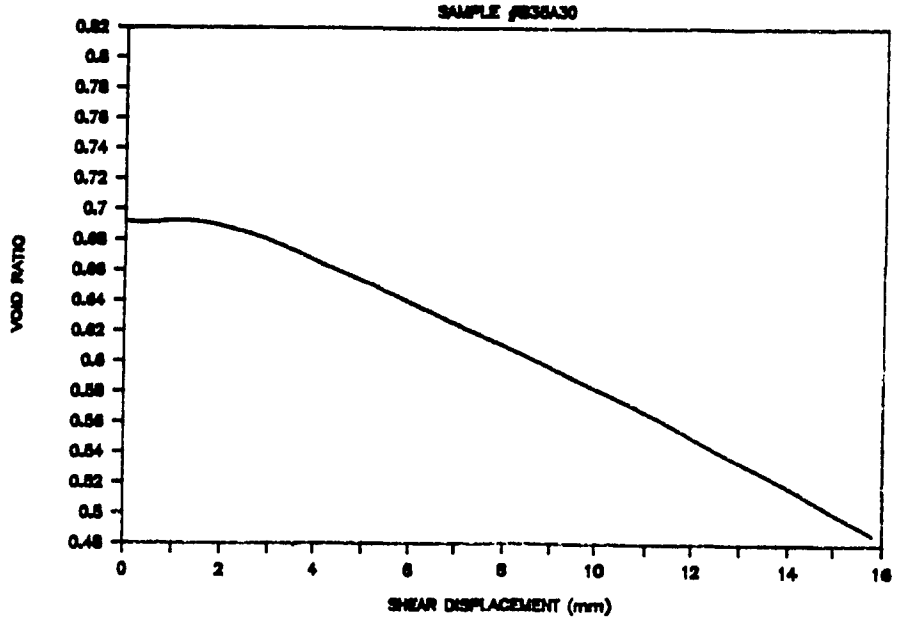
SAMPLE @B36A30
VOID RATIO
SHEAR DISPLACEMENT (mm)

SIGMA GOLD

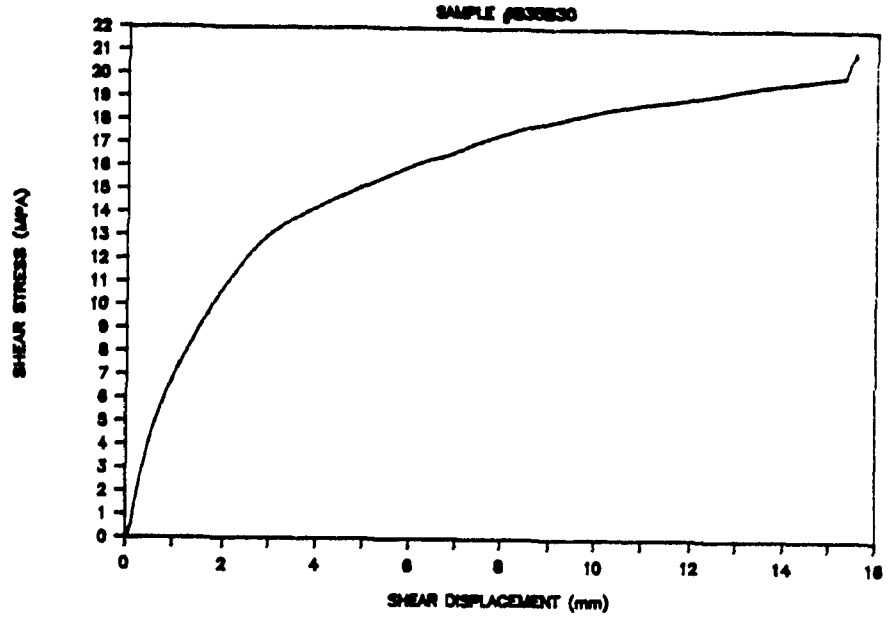
SAMPLE #B35B30
SHEAR STRESS (MPA)
SHEAR DISPLACEMENT (mm)

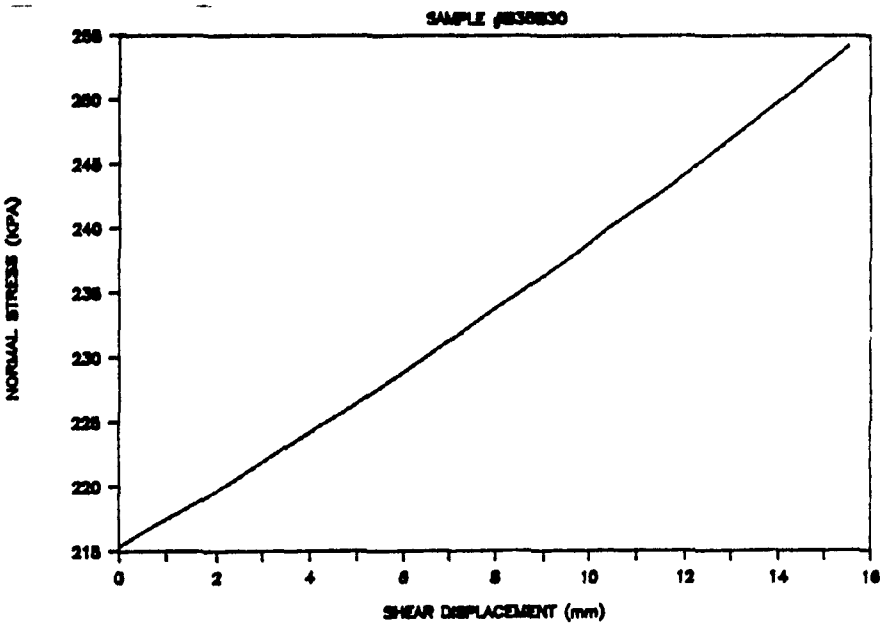
SAMPLE #B35B30
NORMAL STRESS (KPA)
SHEAR DISPLACEMENT (mm)

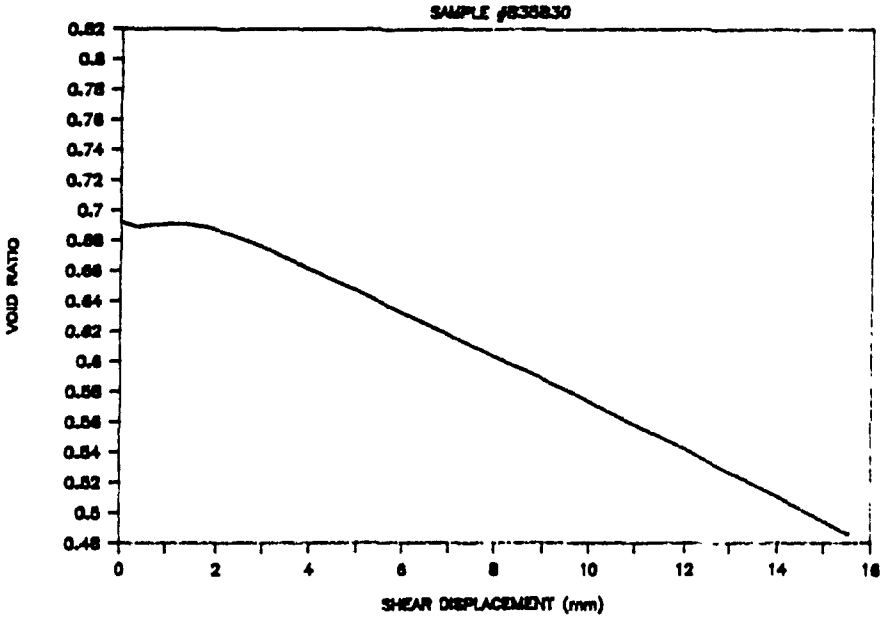
SAMPLE #B35B30
VOID RATIO
SHEAR DISPLACEMENT (mm)

SIGMA GOLD

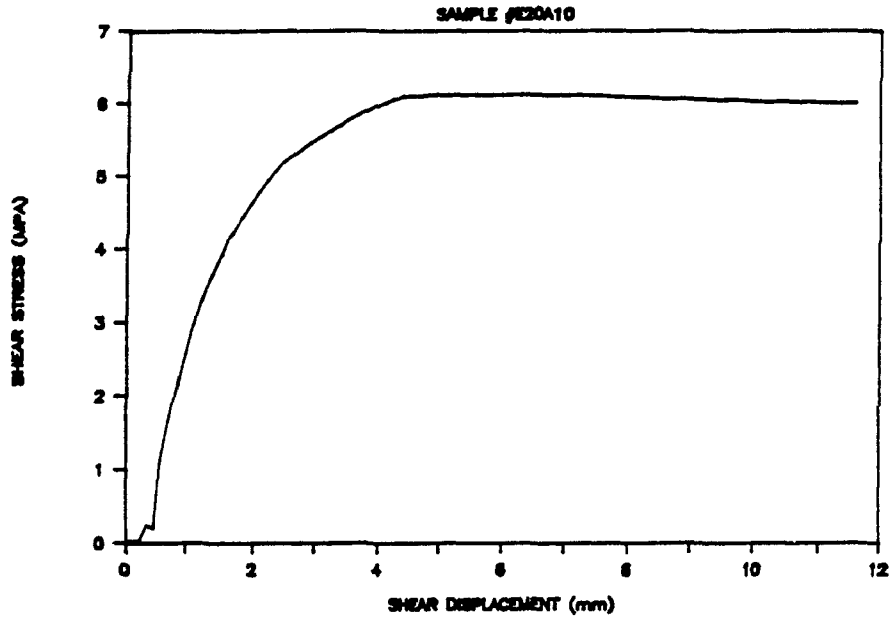
SAMPLE #E20A10
SHEAR STRESS (MPA)
SHEAR DISPLACEMENT (mm)

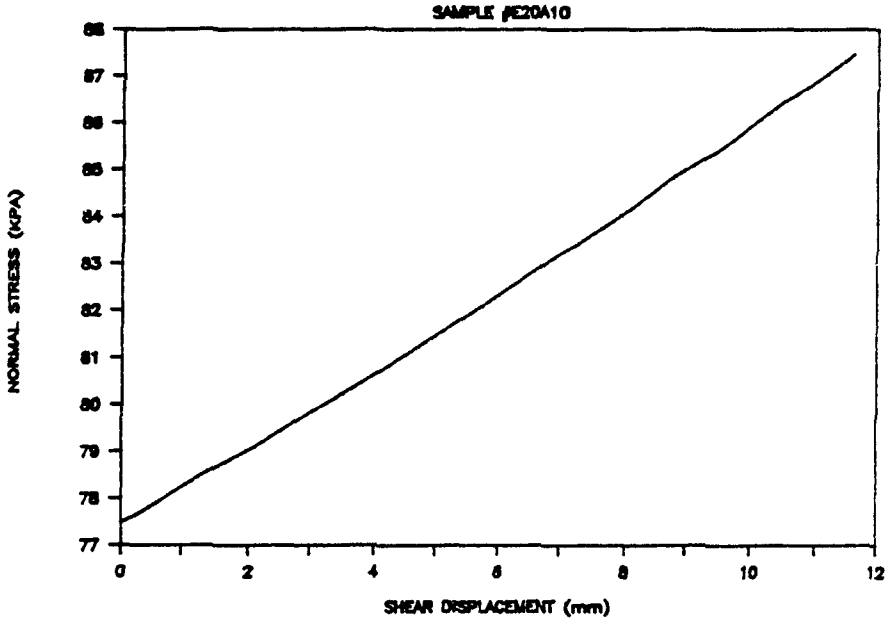
SAMPLE #E20A10
NORMAL STRESS (KPA)
SHEAR DISPLACEMENT (mm)

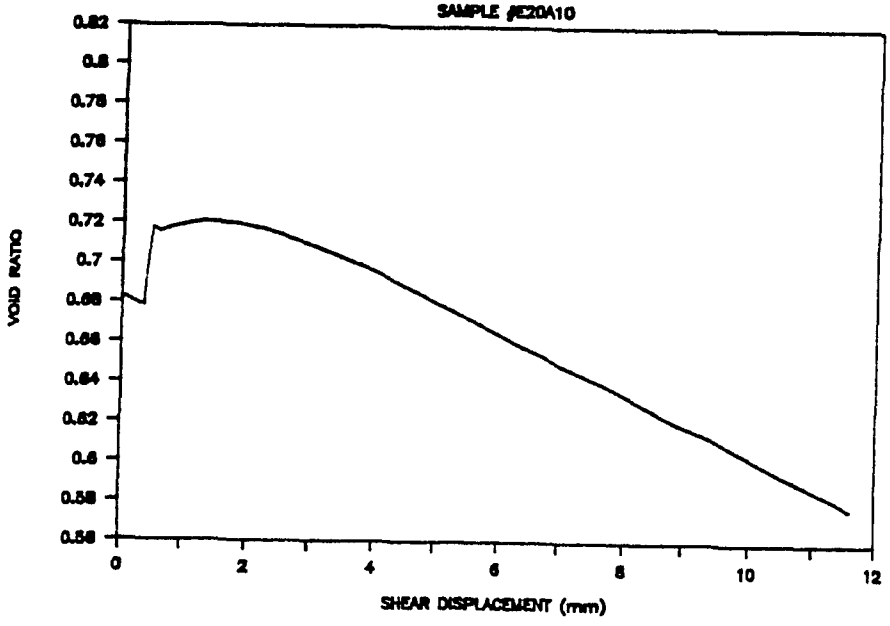
SAMPLE #E20A10
VOID RATIO
SHEAR DISPLACEMENT (mm)

SIGMA GOLD

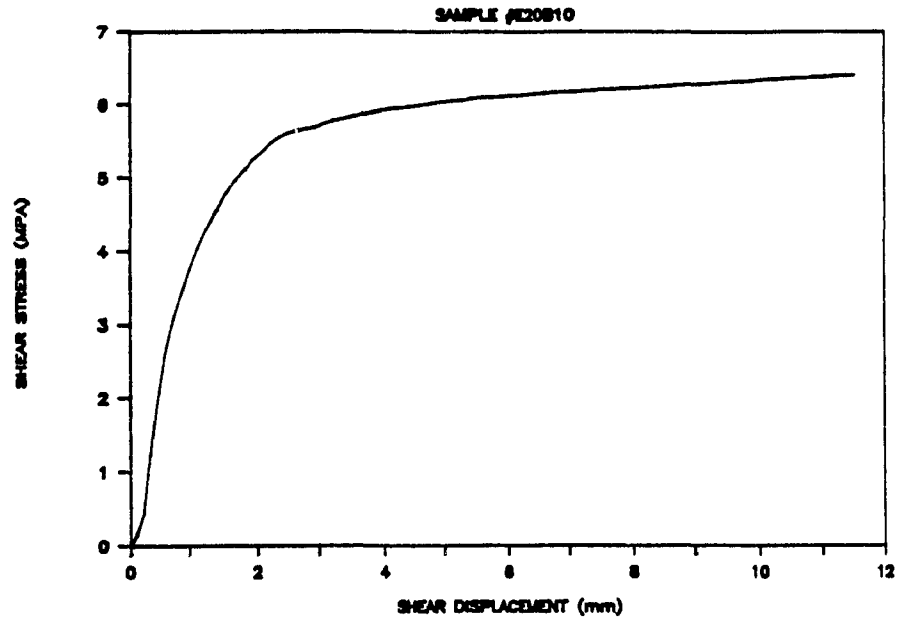
SAMPLE @E20B10
SHEAR STRESS (MPA)
0
1
2
3
4
5
6
7
0
2
4
6
8
10
12
SHEAR DISPLACEMENT (mm)

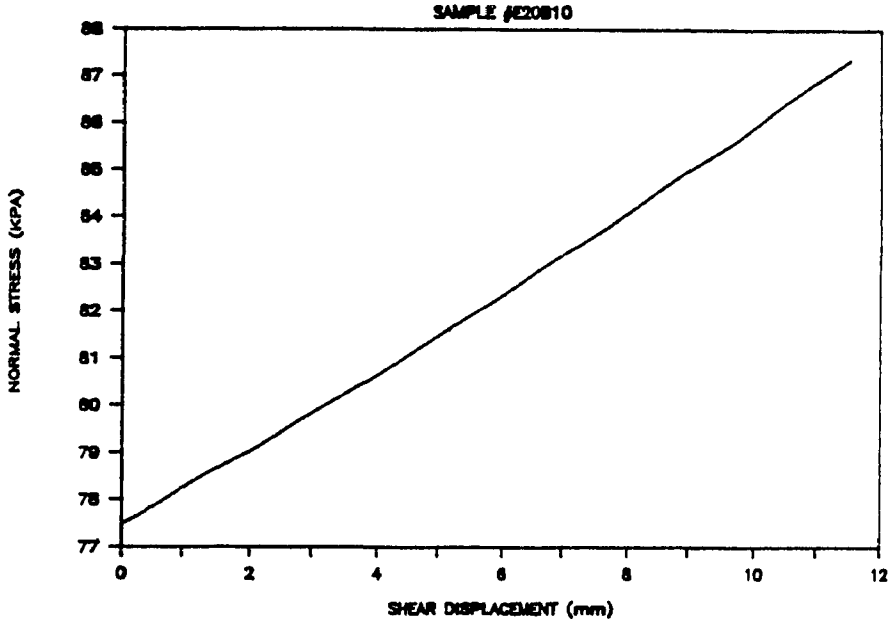
SAMPLE @E20B10
NORMAL STRESS (KPA)
77
78
79
80
81
82
83
84
85
86
87
88
0
2
4
6
8
10
12
SHEAR DISPLACEMENT (mm)

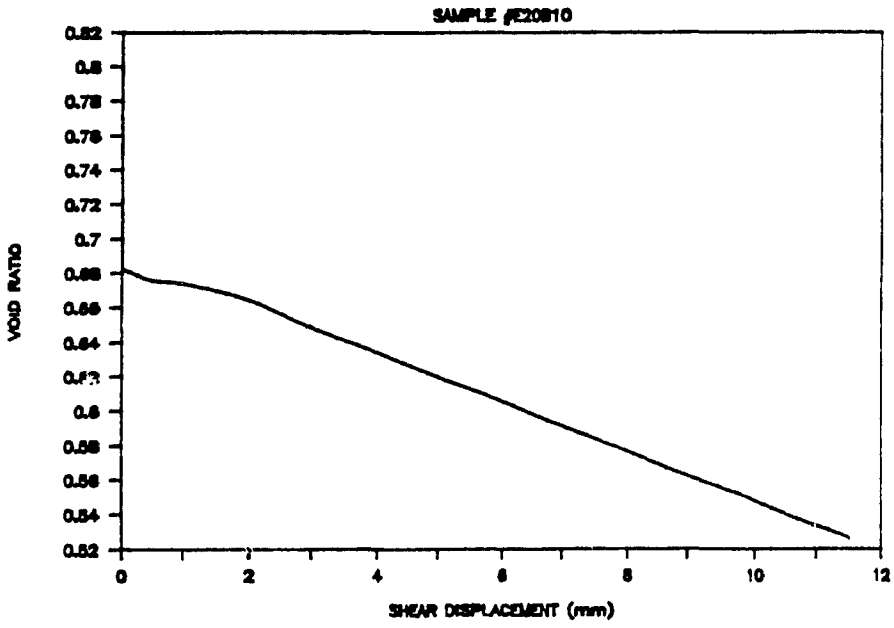
SAMPLE @E20B10
VOID RATIO
0.52
0.54
0.56
0.58
0.6
0.64
0.66
0.68
0.7
0.72
0.74
0.76
0.78
0.8
0.82
0
2
4
6
8
10
12
SHEAR DISPLACEMENT (mm)

SIGMA GOLD

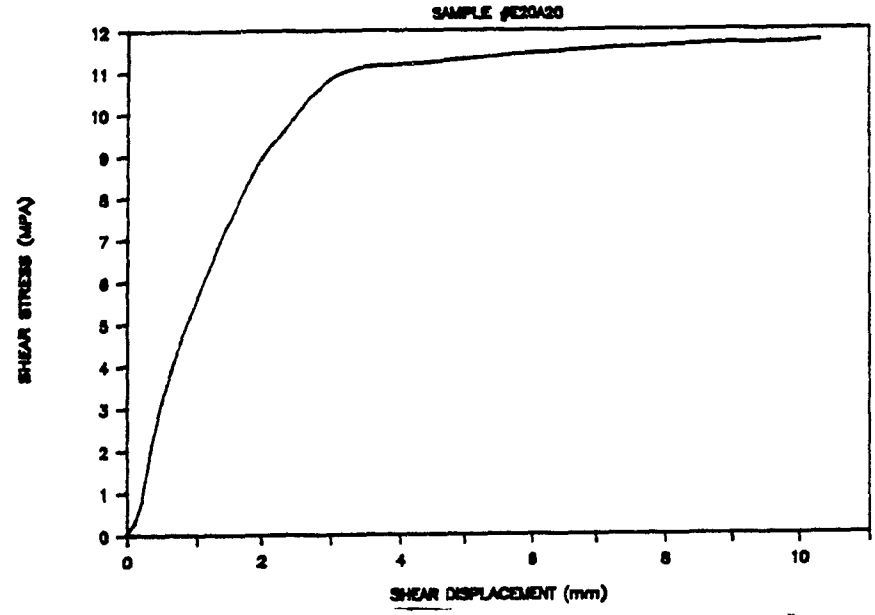
SAMPLE @E20A20
SHEAR STRESS (MPA)
SHEAR DISPLACEMENT (mm)

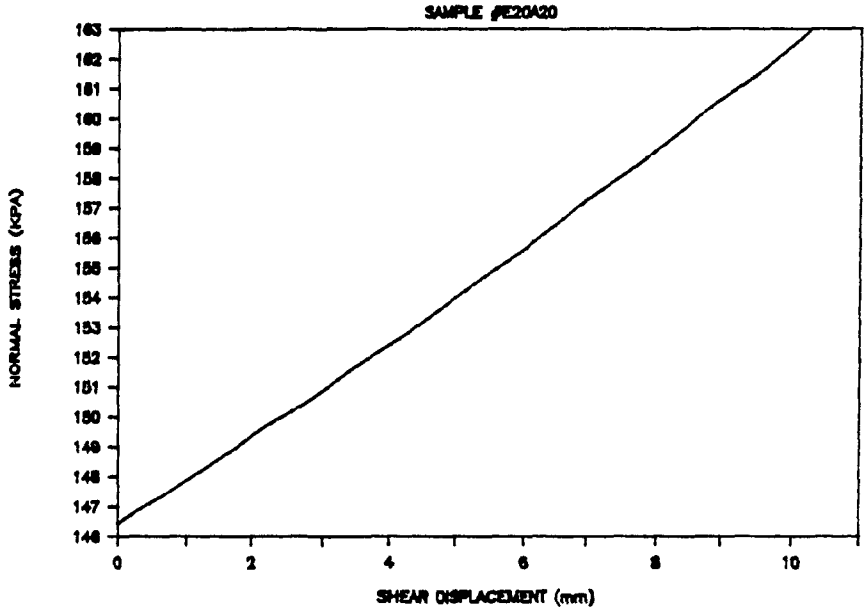
SAMPLE @E20A20
NORMAL STRESS (KPA)
SHEAR DISPLACEMENT (mm)

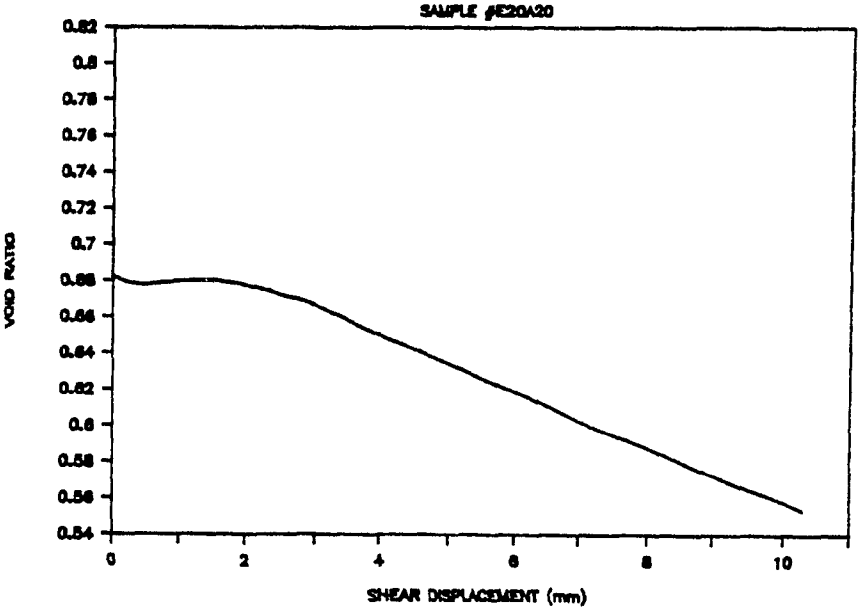
SAMPLE @E20A20
VOID RATIO
SHEAR DISPLACEMENT (mm)

SIGMA GOLD

SAMPLE #E20820

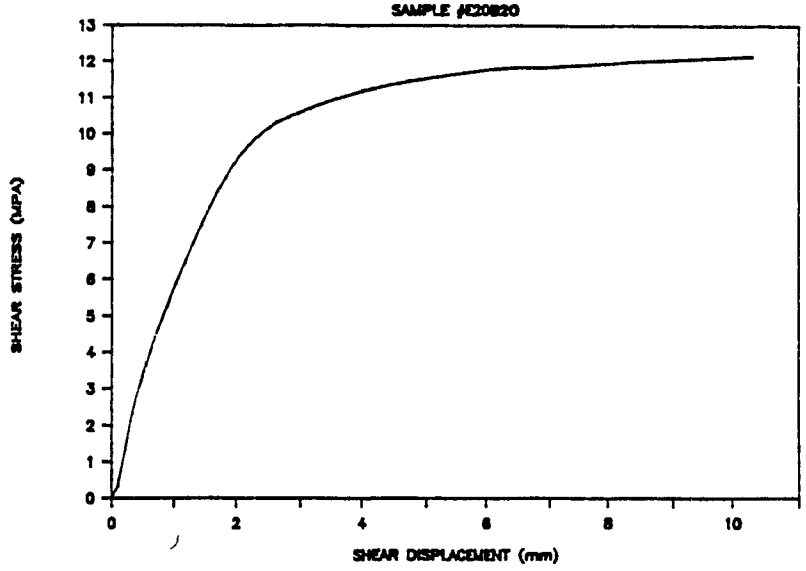

SAMPLE #E20820

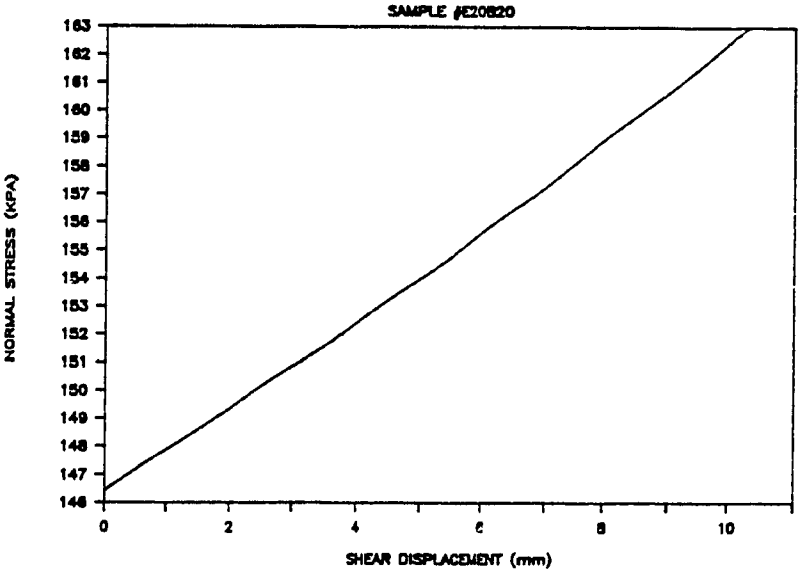

SAMPLE #E20820

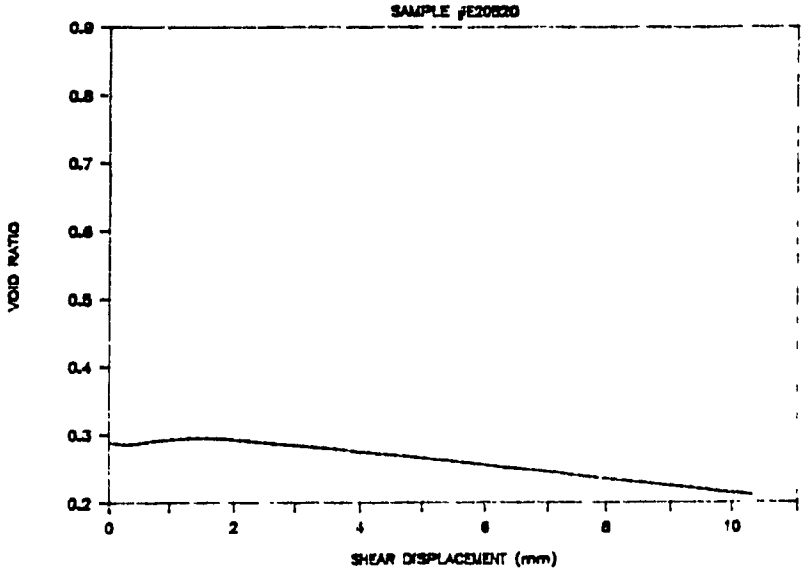

SIGMA GOLD

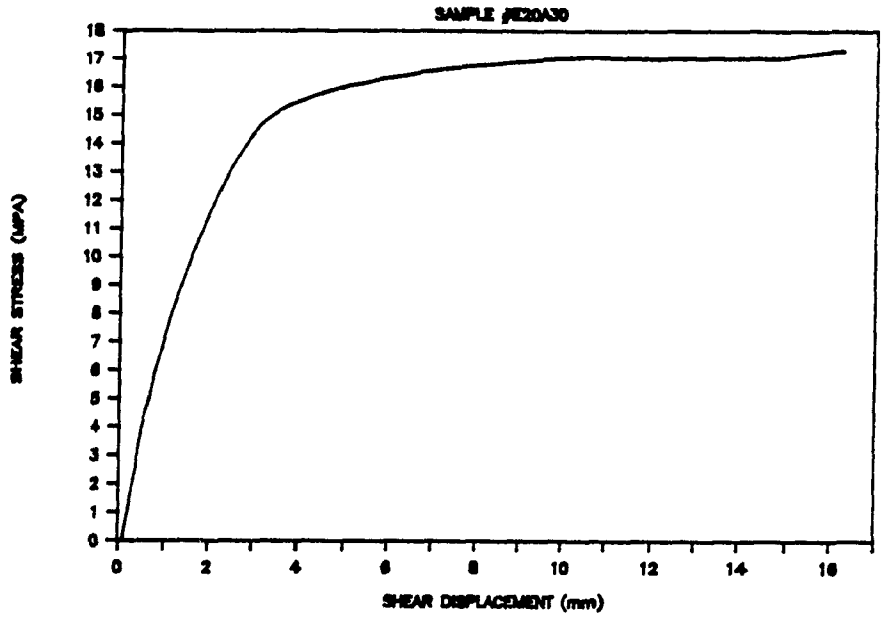
SAMPLE #E20A30
SHEAR STRESS (MPA)
SHEAR DISPLACEMENT (mm)

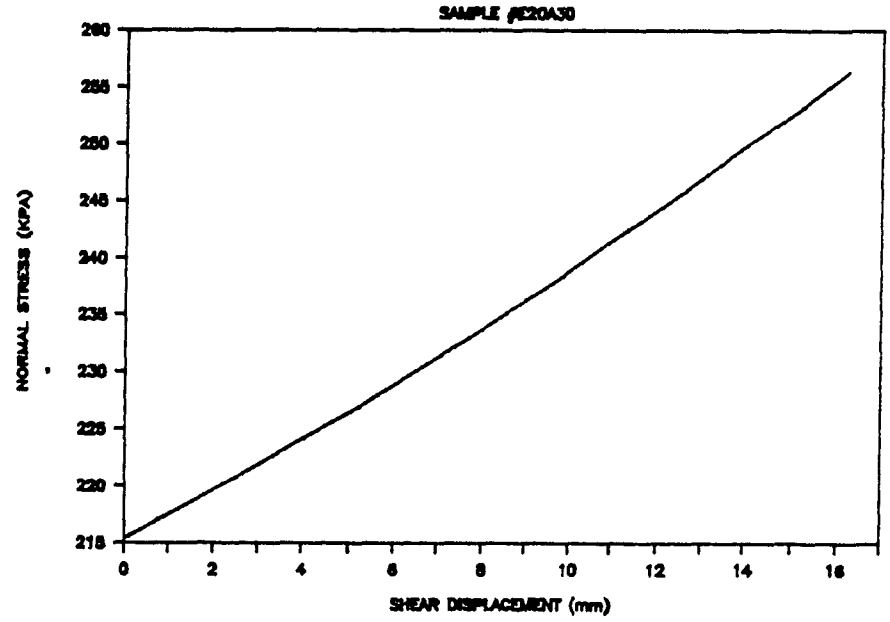
SAMPLE #E20A30
NORMAL STRESS (KPA)
SHEAR DISPLACEMENT (mm)

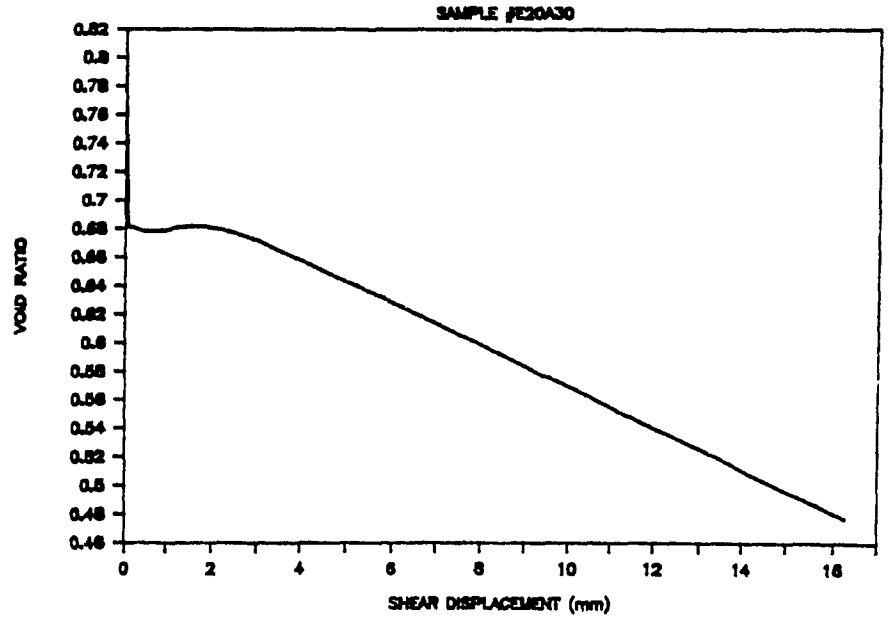
SAMPLE #E20A30
VOID RATIO
SHEAR DISPLACEMENT (mm)

SIGMA GOLD

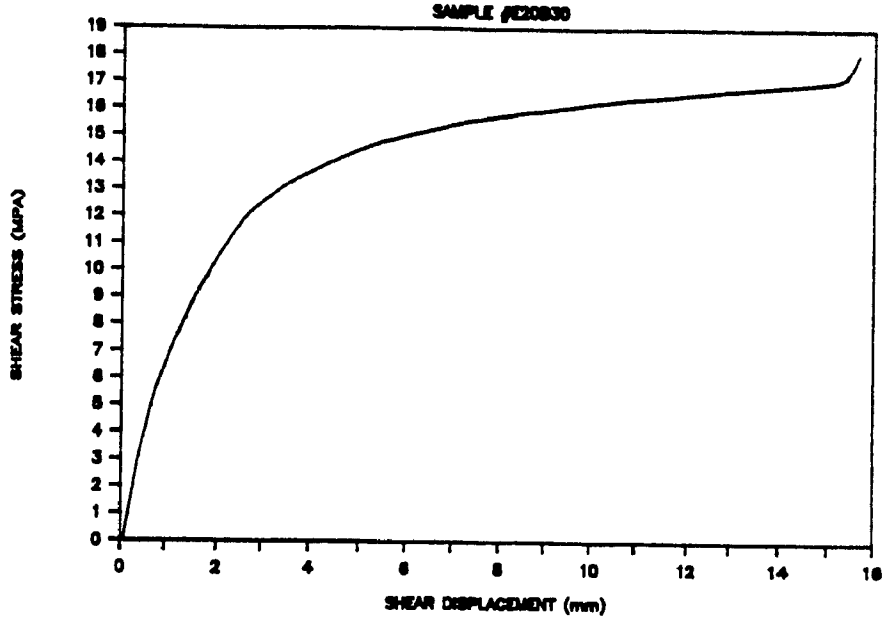
SAMPLE #E20830
SHEAR STRESS (MPA)
SHEAR DISPLACEMENT (mm)

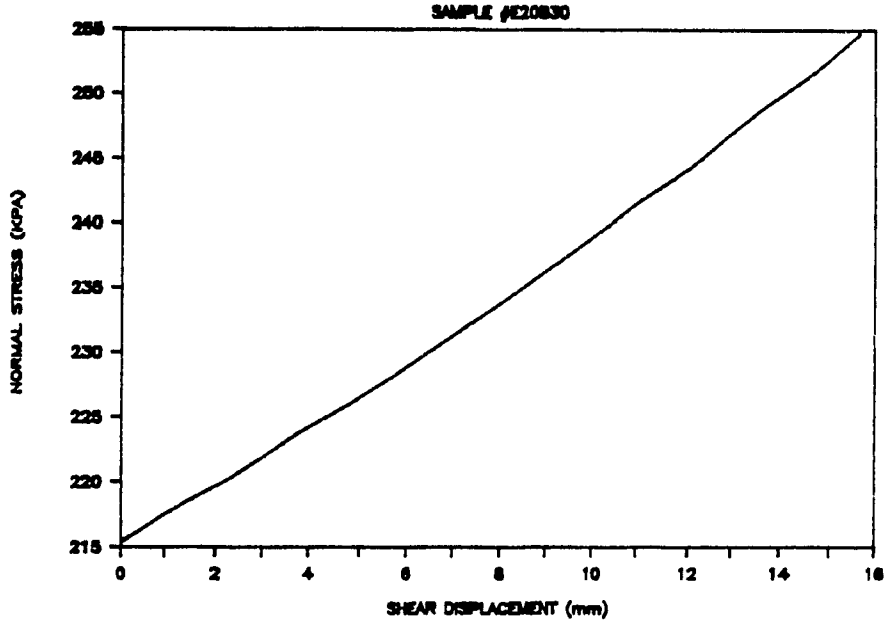
SAMPLE #E20830
NORMAL STRESS (KPA)
SHEAR DISPLACEMENT (mm)

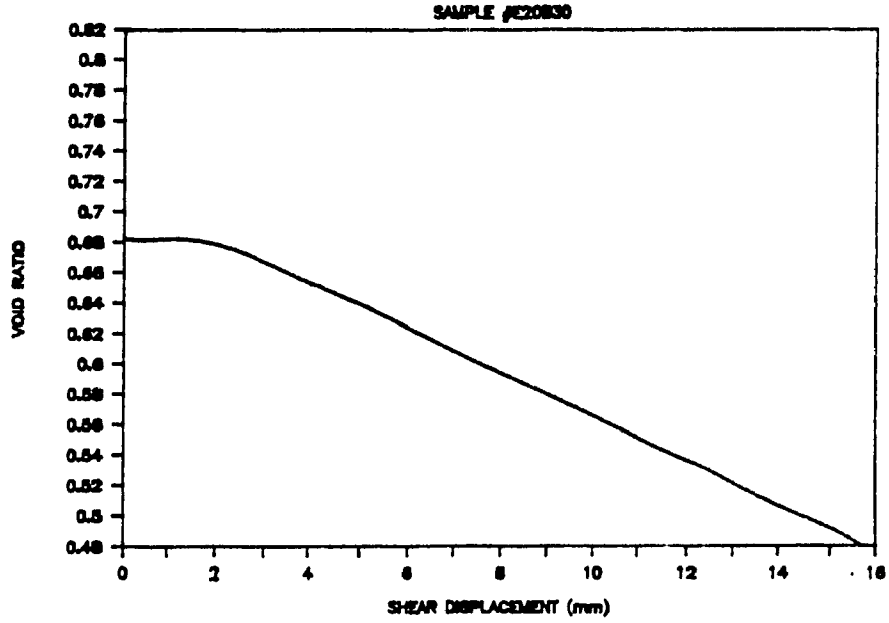
SAMPLE #E20830
VOID RATIO
SHEAR DISPLACEMENT (mm)

SIGMA GOLD

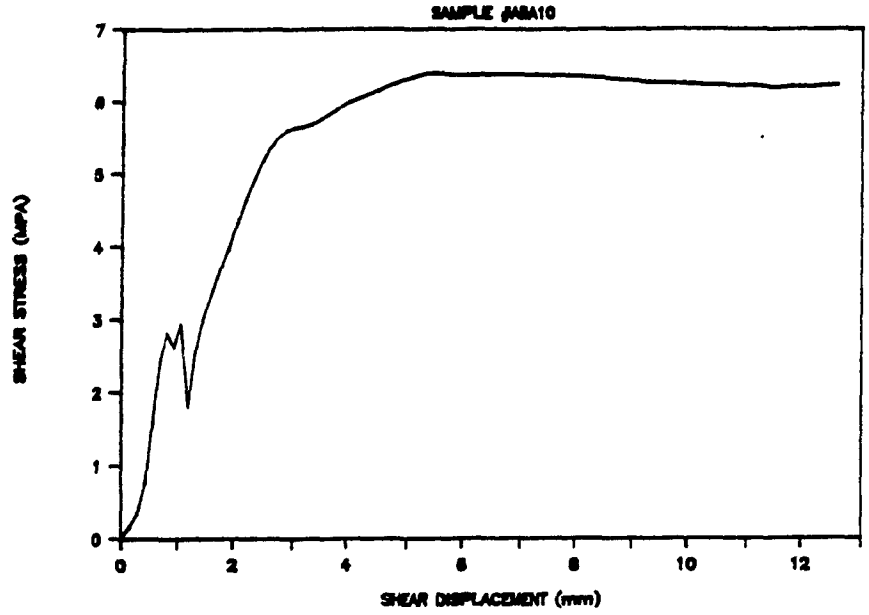
SAMPLE #A5A10
SHEAR STRESS (MPA)
SHEAR DISPLACEMENT (mm)

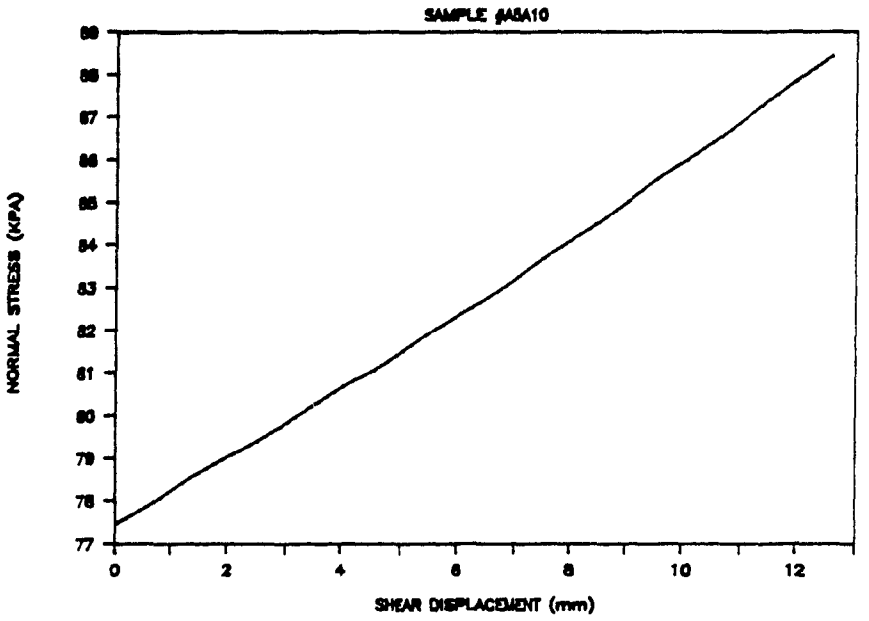
SAMPLE #A5A10
NORMAL STRESS (KPA)
SHEAR DISPLACEMENT (mm)

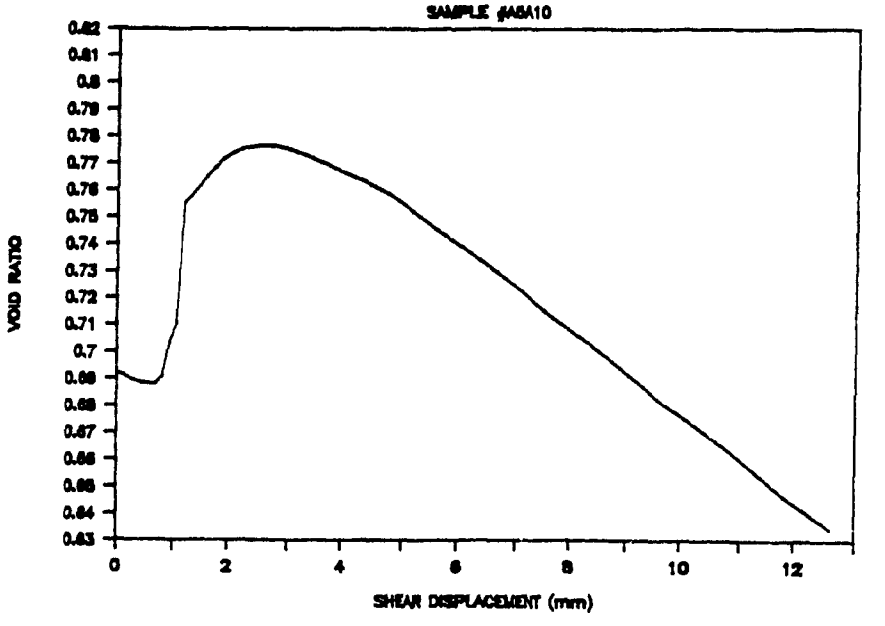
SAMPLE #A5A10
VOID RATIO
SHEAR DISPLACEMENT (mm)

SIGMA GOLD

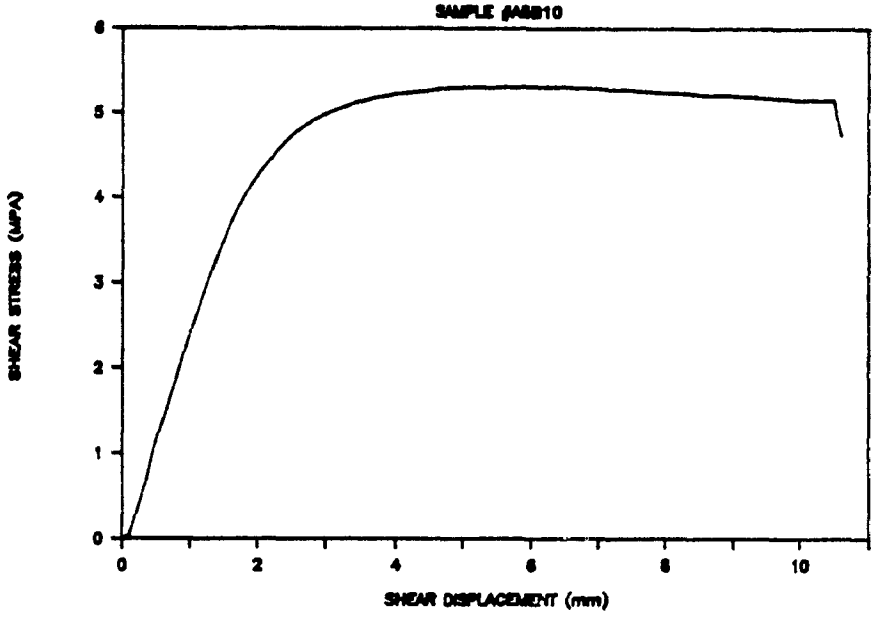
SAMPLE #A5B10
SHEAR STRESS (MPA)
0
1
2
3
4
5
6
0
2
4
6
8
10
SHEAR DISPLACEMENT (mm)

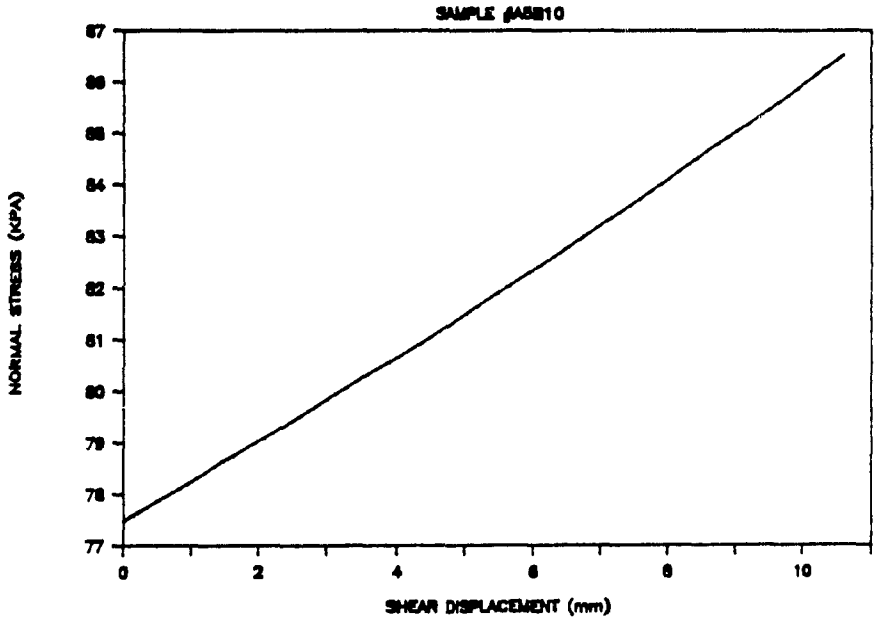
SAMPLE #A5B10
NORMAL STRESS (KPA)
77
78
79
80
81
82
83
84
85
86
87
0
2
4
6
8
10
SHEAR DISPLACEMENT (mm)

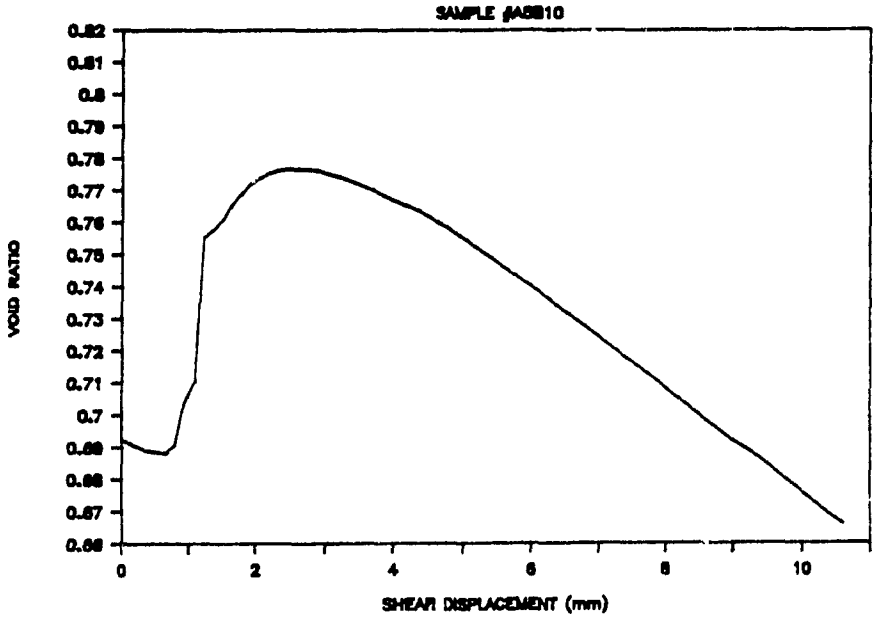
SAMPLE #A5B10
VOID RATIO
0.7
0.71
0.72
0.73
0.74
0.75
0.76
0.77
0.78
0.79
0.8
0.81
0.82
0
2
4
6
8
10
SHEAR DISPLACEMENT (mm)

SIGMA GOLD

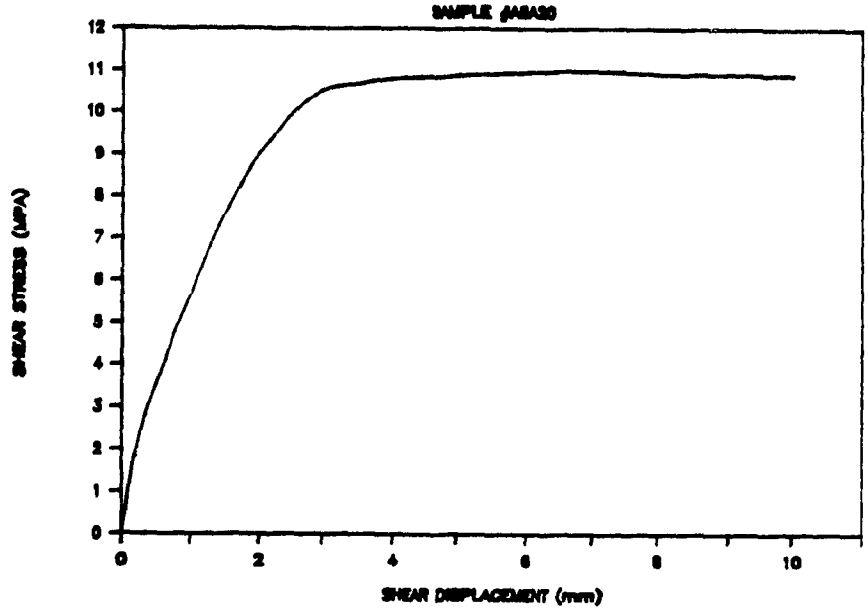
SAMPLE @ASA30
SHEAR STRESS (MPA)
SHEAR DISPLACEMENT (mm)

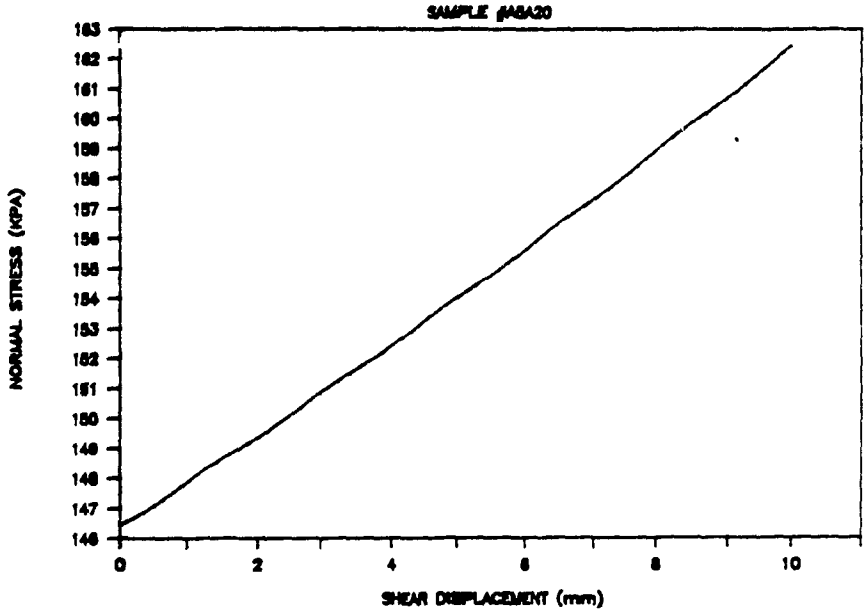
SAMPLE @ASA30
NORMAL STRESS (KPA)
SHEAR DISPLACEMENT (mm)

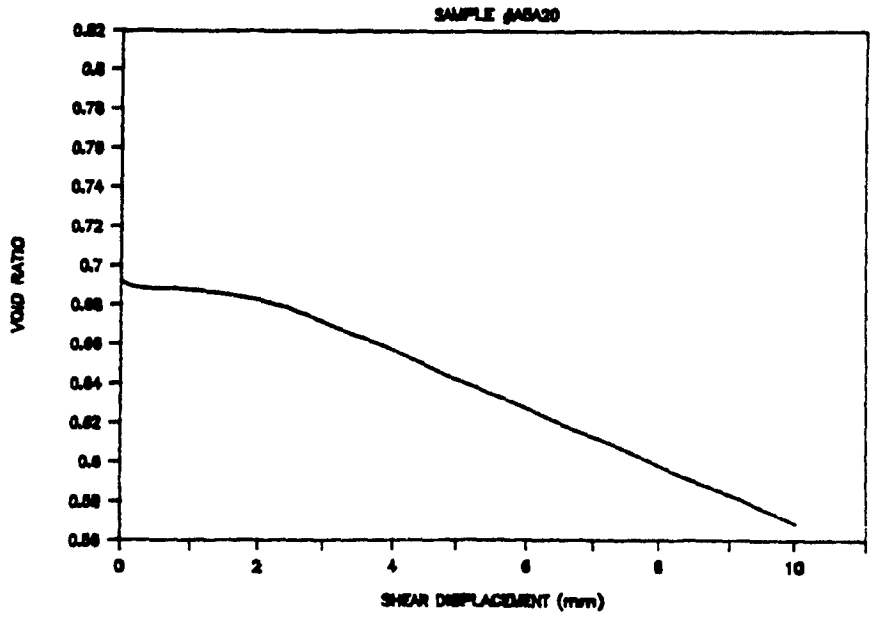
SAMPLE @ASA30
VOID RATIO
SHEAR DISPLACEMENT (mm)

SIGMA GOLD

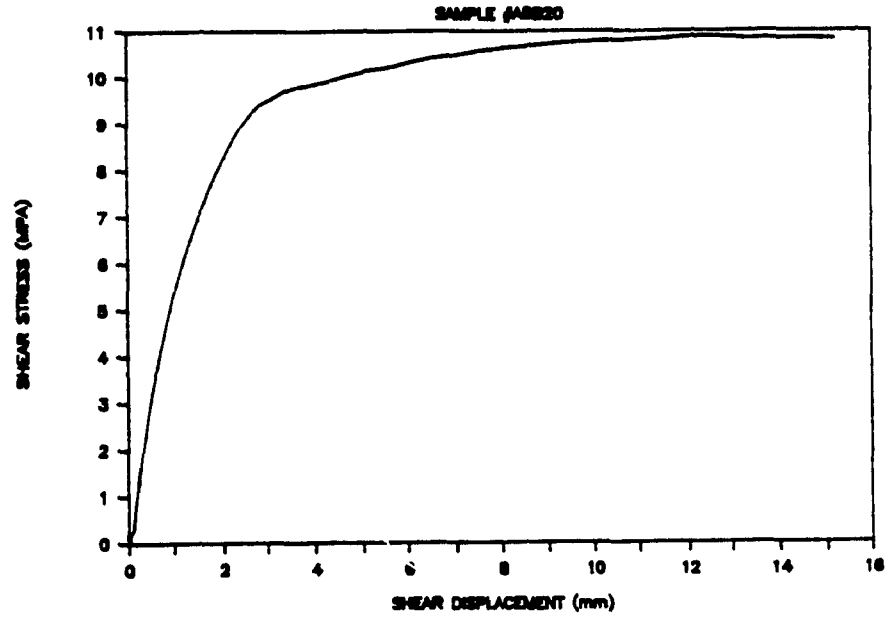
SAMPLE @ABE20
SHEAR STRESS (MPA)
SHEAR DISPLACEMENT (mm)

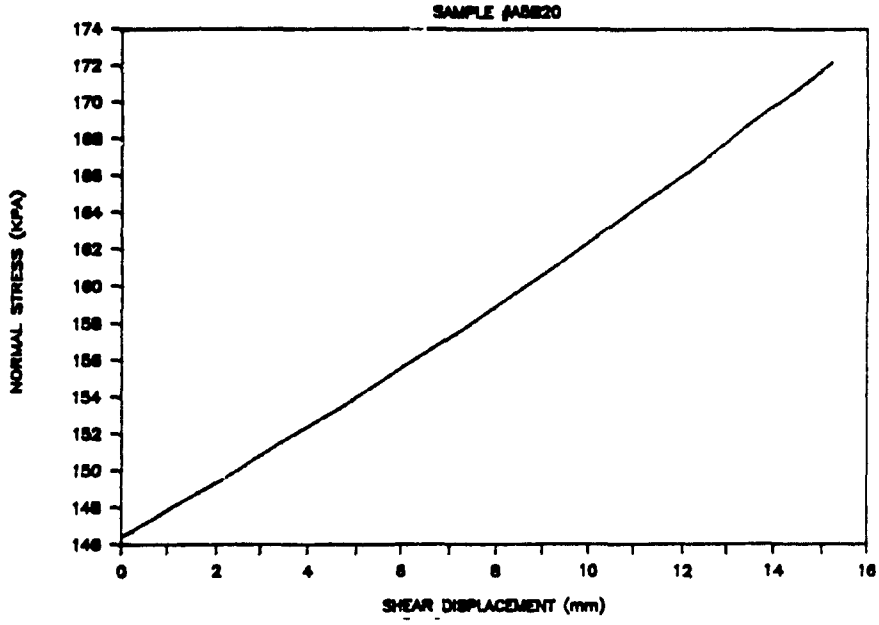
SAMPLE @ABE20
NORMAL STRESS (KPA)
SHEAR DISPLACEMENT (mm)

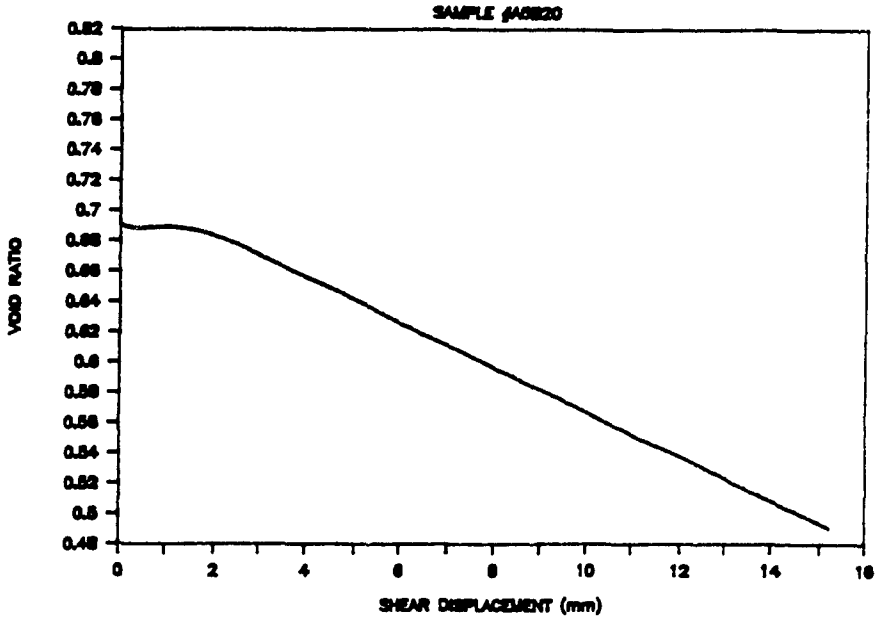
SAMPLE @ABE20
VOID RATIO
SHEAR DISPLACEMENT (mm)

SIGMA GOLD

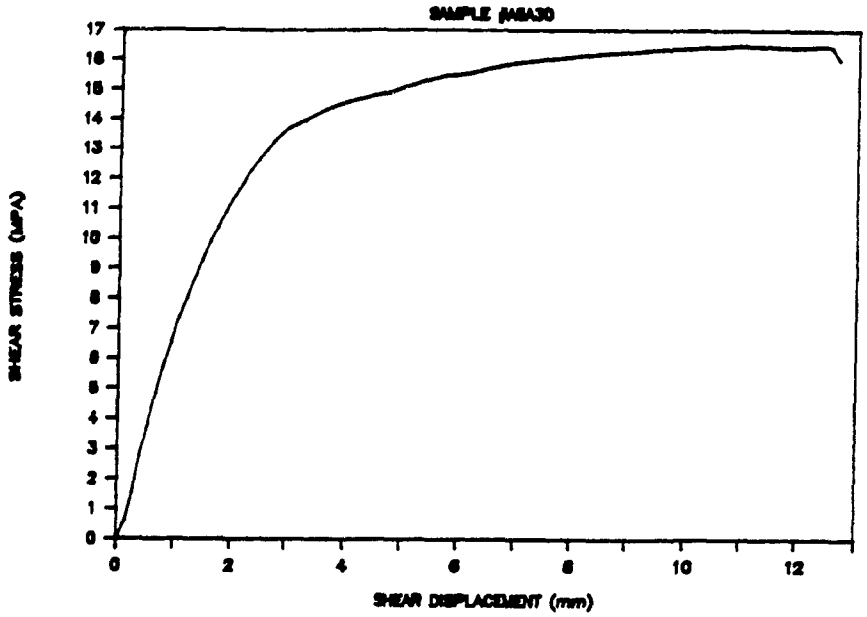
SAMPLE @ABA30
SHEAR STRESS (MPA)
SHEAR DISPLACEMENT (mm)

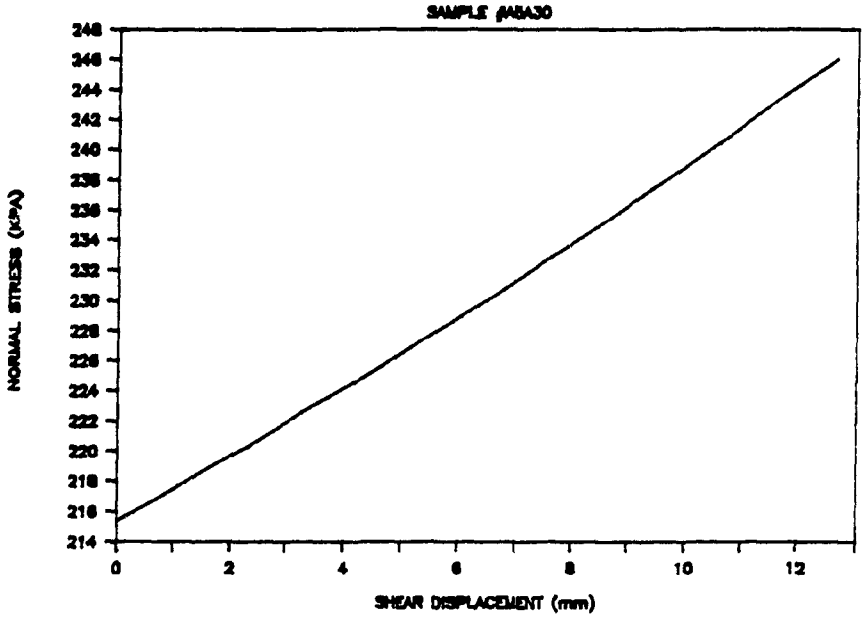
SAMPLE @ABA30
NORMAL STRESS (kPA)
SHEAR DISPLACEMENT (mm)

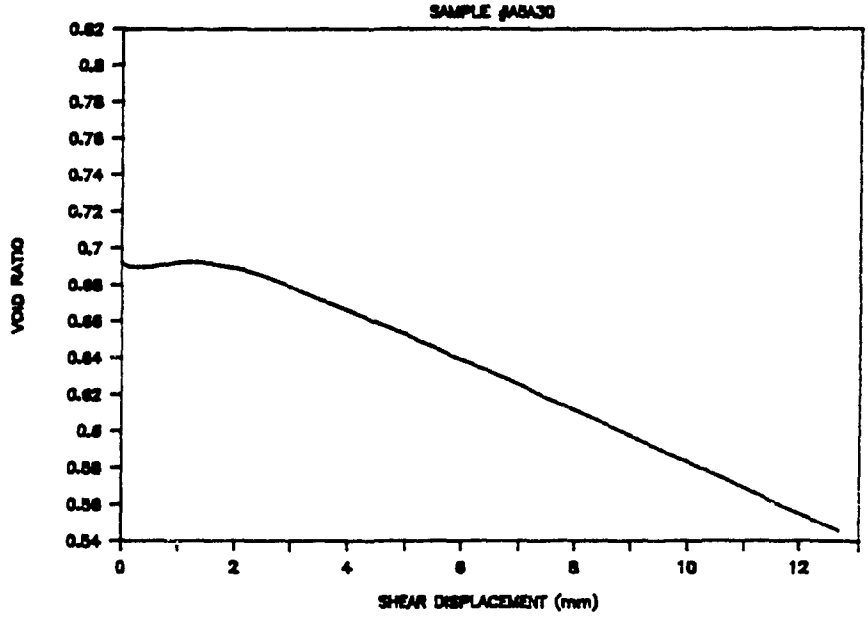
SAMPLE @ABA30
VOID RATIO
SHEAR DISPLACEMENT (mm)

SIGMA GOLD

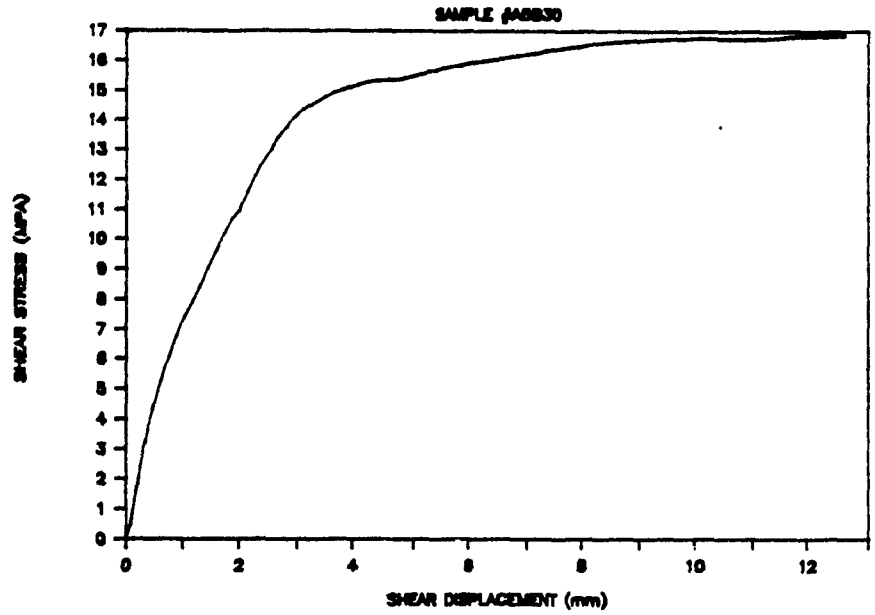
SAMPLE @A6B30
SHEAR STRESS (MPA)
SHEAR DISPLACEMENT (mm)

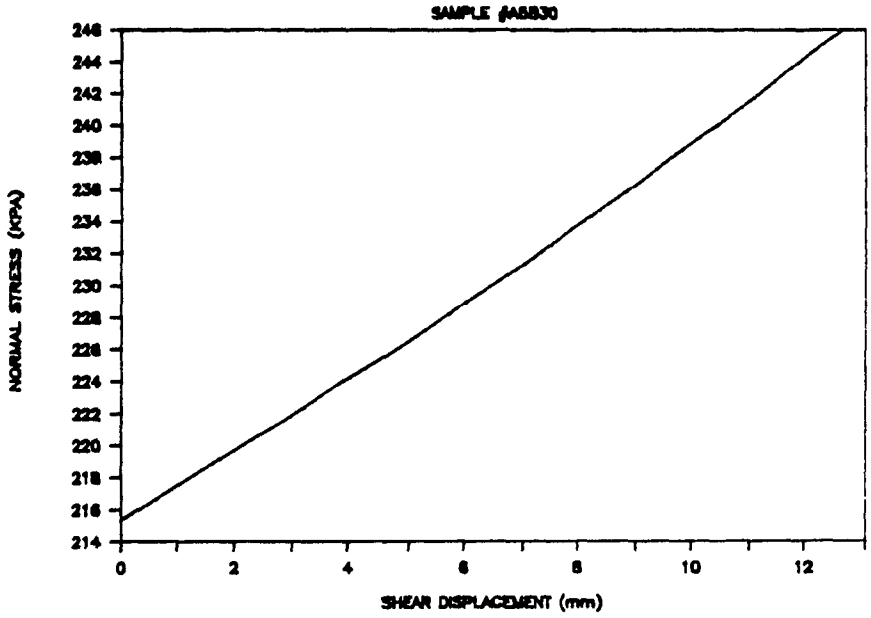
SAMPLE @A6B30
NORMAL STRESS (KPA)
SHEAR DISPLACEMENT (mm)

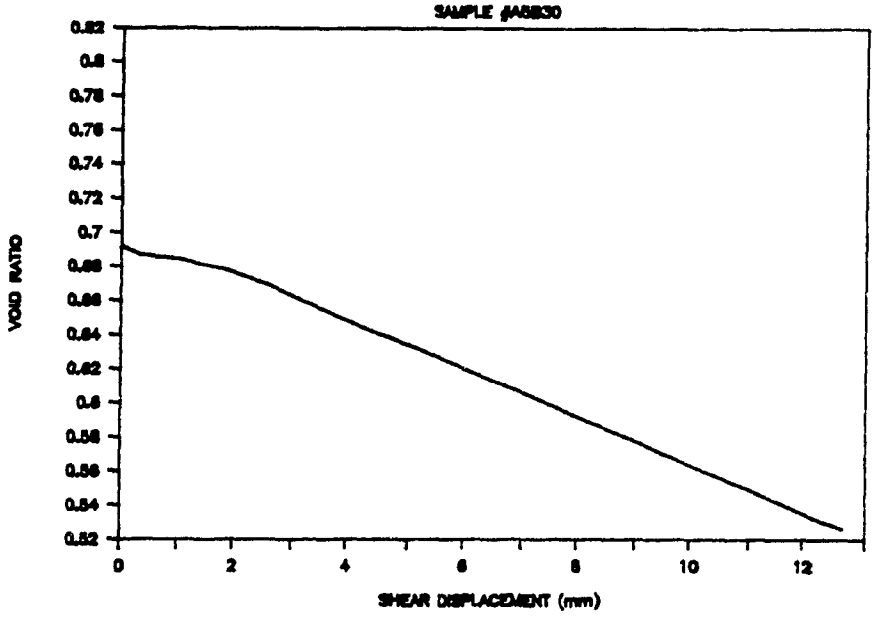
SAMPLE @A6B30
VOID RATIO
SHEAR DISPLACEMENT (mm)

SIGMA GOLD

SAMPLE #85A10

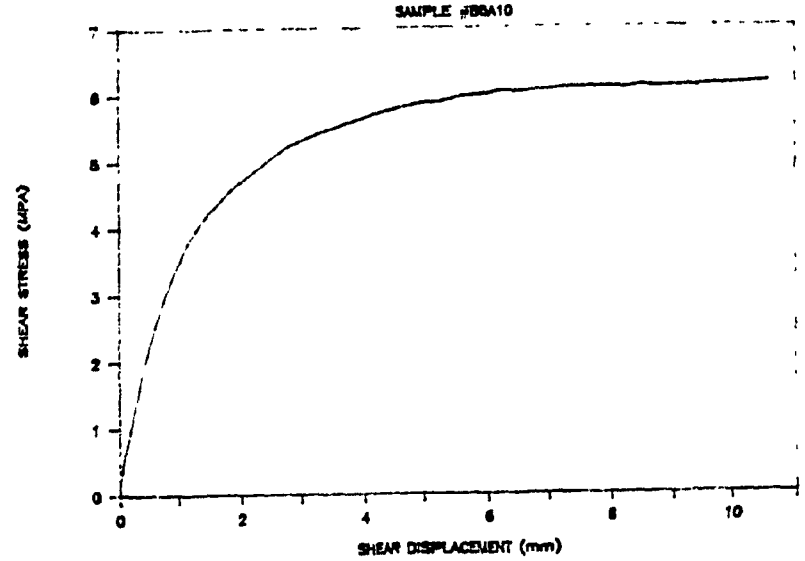

SAMPLE #85A10

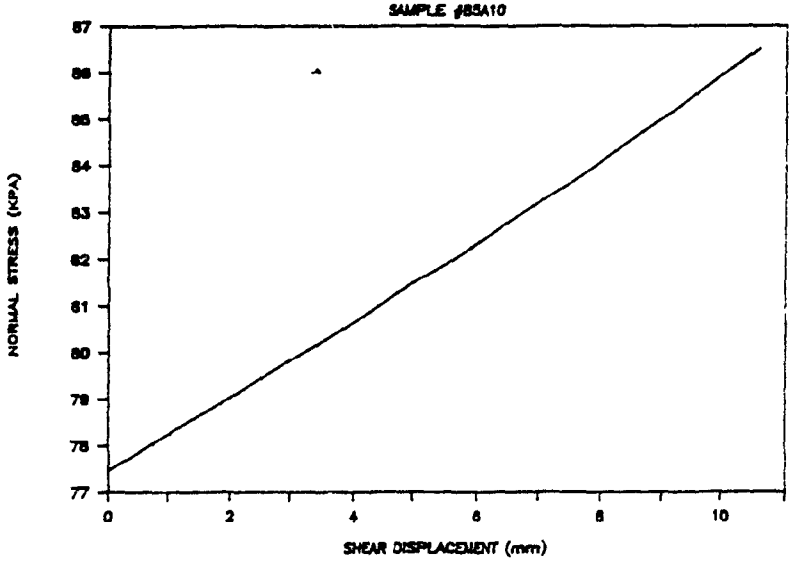

SAMPLE #85A10

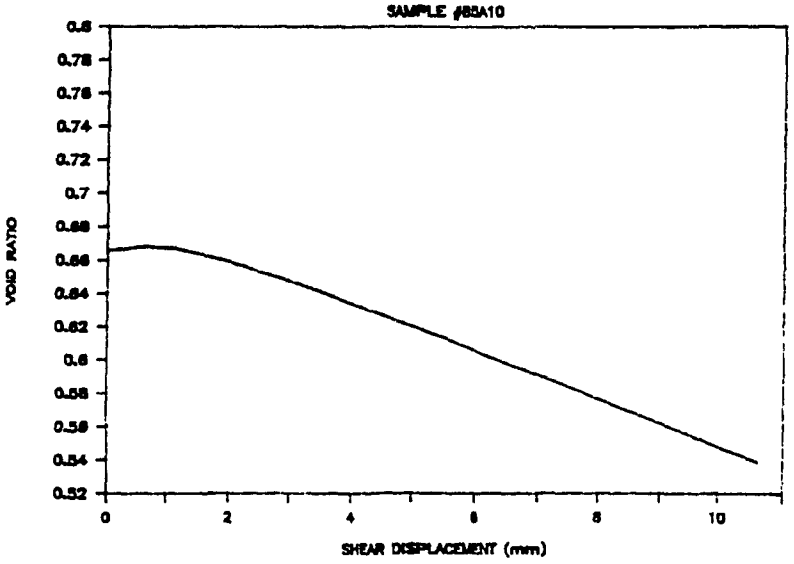

SIGMA GOLD

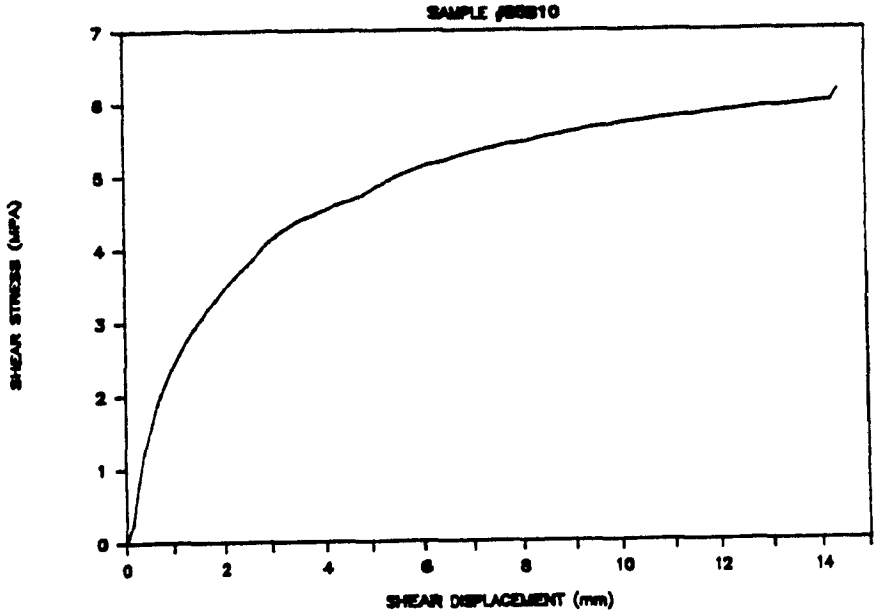
SAMPLE #BSB10
SHEAR STRESS (MPA)
SHEAR DISPLACEMENT (mm)

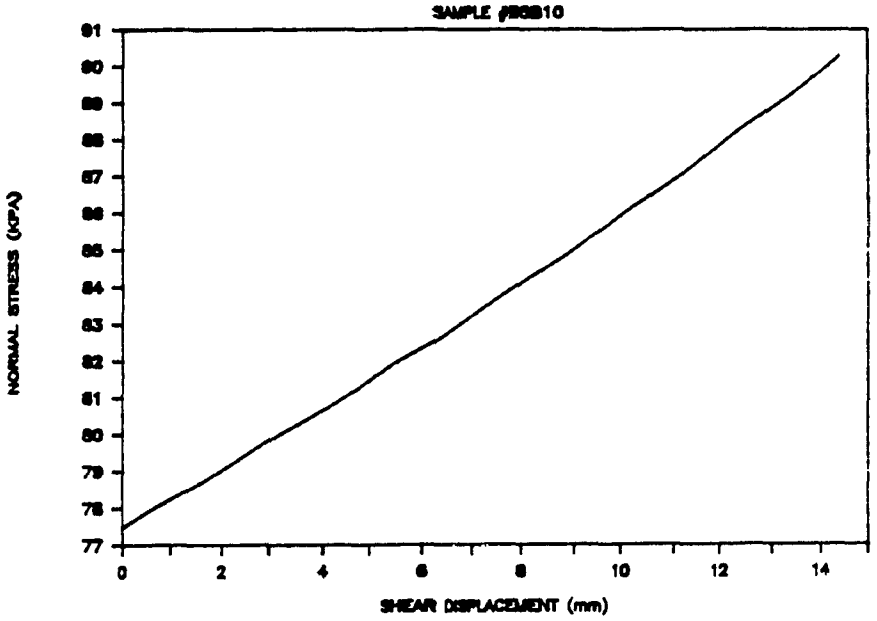
SAMPLE #BSB10
NORMAL STRESS (KPA)
SHEAR DISPLACEMENT (mm)

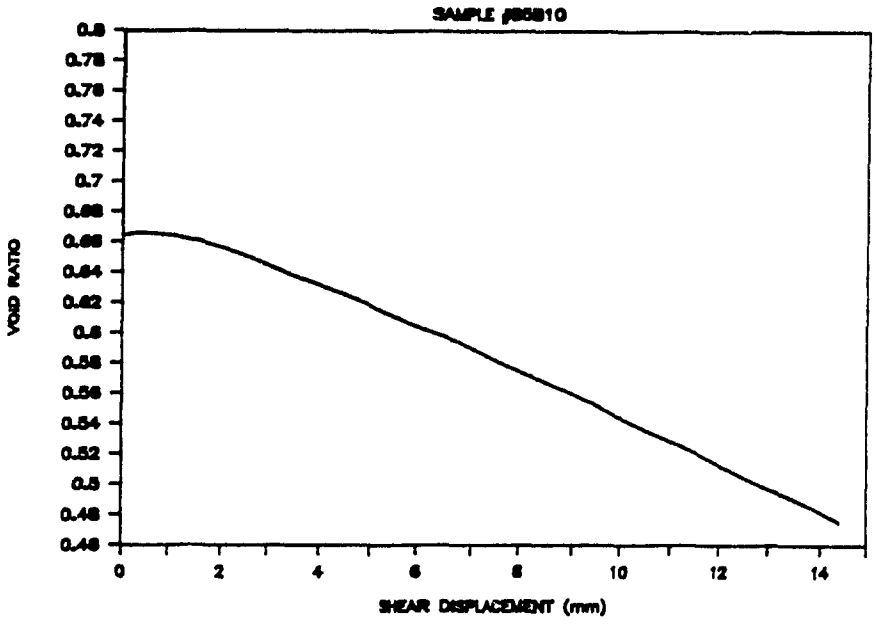
SAMPLE #BSB10
VOID RATIO
SHEAR DISPLACEMENT (mm)

SIGMA GOLD

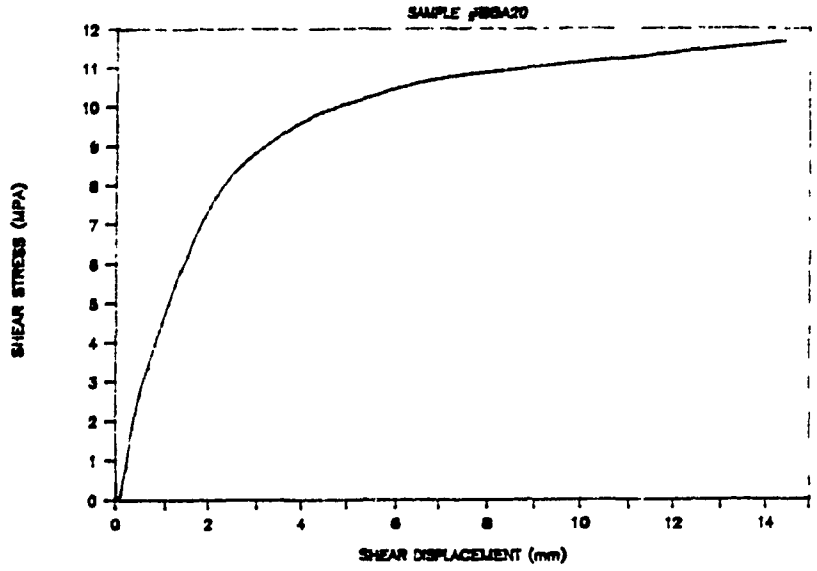
SAMPLE #BBA20
SHEAR STRESS (MPA)
SHEAR DISPLACEMENT (mm)

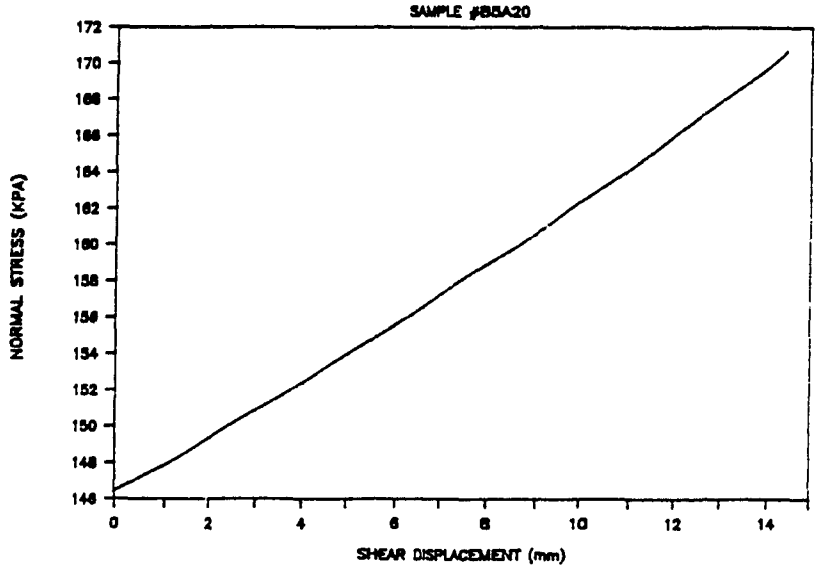
SAMPLE #BBA20
NORMAL STRESS (KPA)
SHEAR DISPLACEMENT (mm)

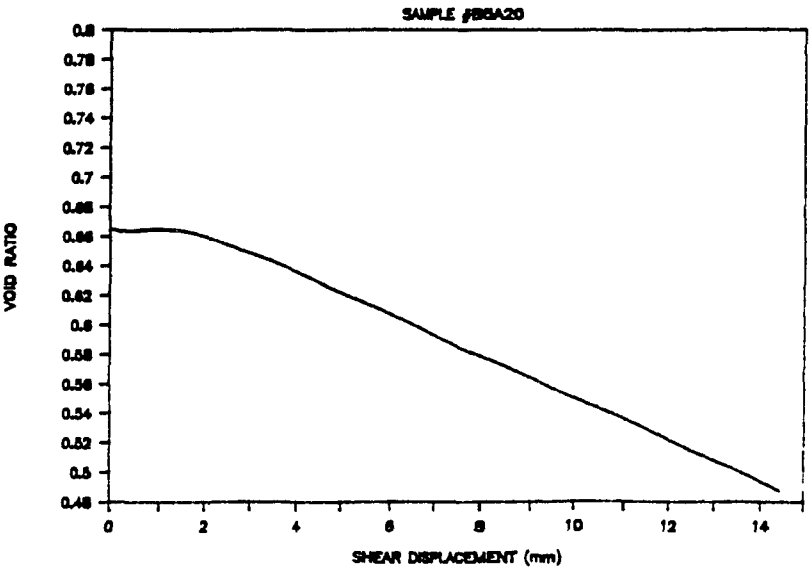
SAMPLE #BBA20
VOID RATIO
SHEAR DISPLACEMENT (mm)

SIGMA GOLD

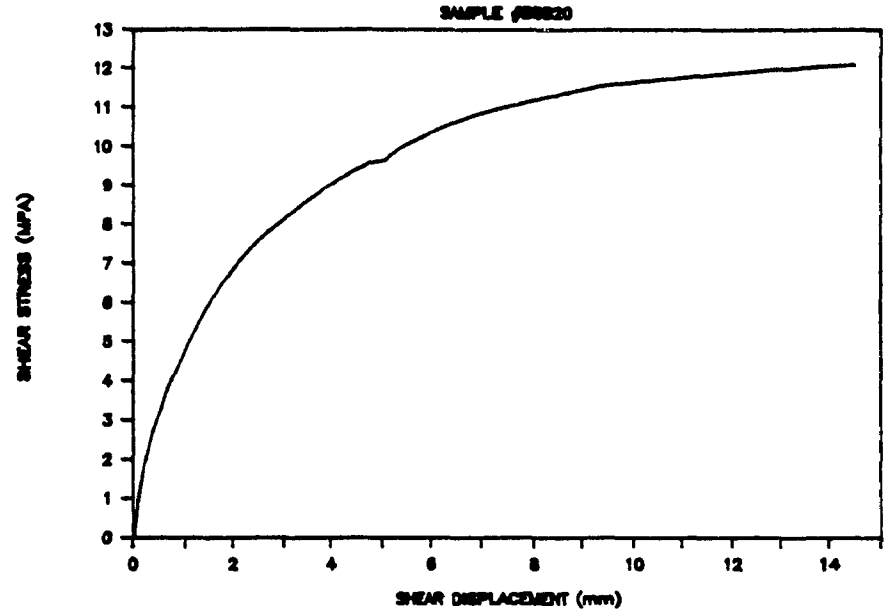
SAMPLE #BB820
SHEAR STRESS (MPA)
0
1
2
3
4
5
6
7
8
9
10
11
12
13
0
2
4
6
8
10
12
14
SHEAR DISPLACEMENT (mm)

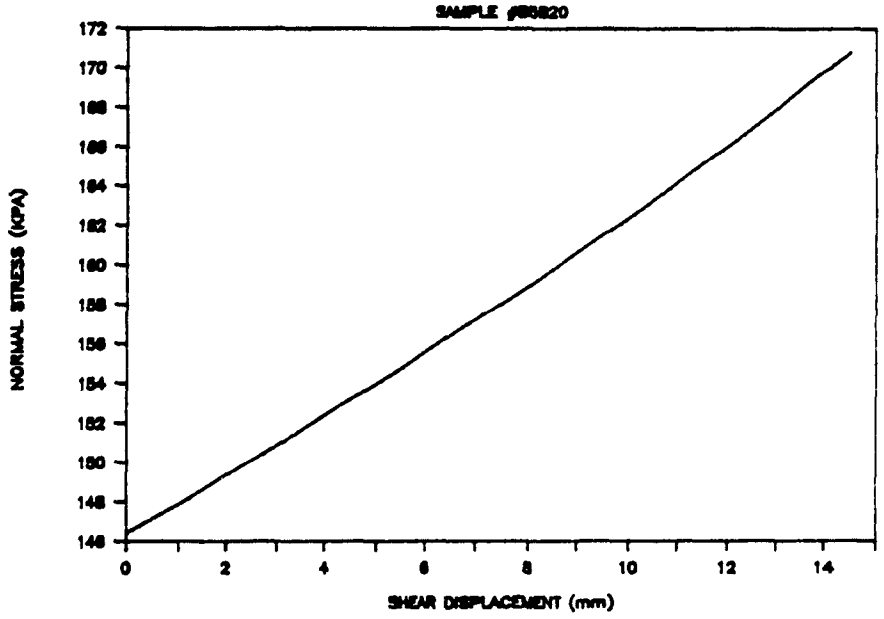
SAMPLE #BB820
NORMAL STRESS (KPA)
148
150
152
154
156
158
160
162
164
166
168
170
172
0
2
4
6
8
10
12
14
SHEAR DISPLACEMENT (mm)

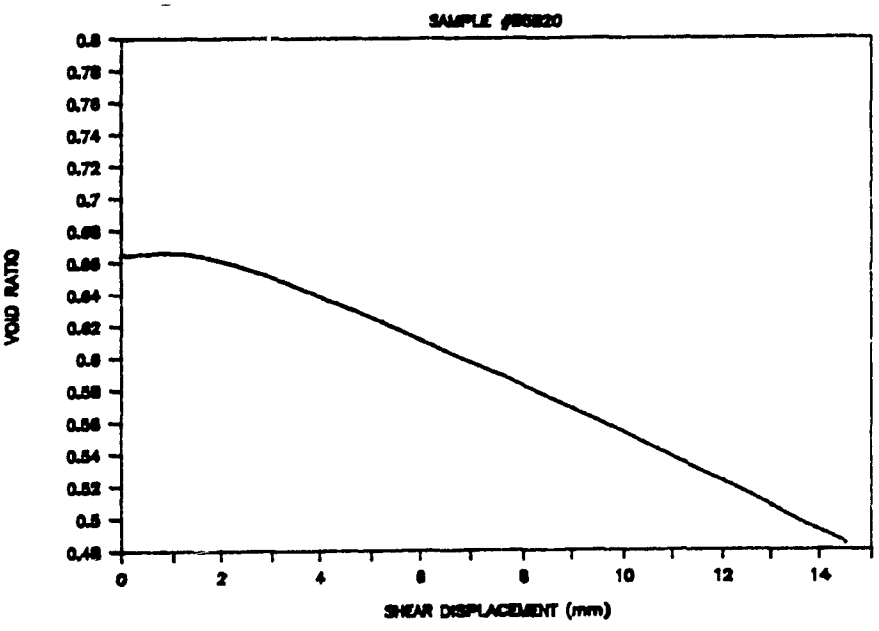
SAMPLE #BB820
VOID RATIO
0.48
0.5
0.52
0.54
0.56
0.58
0.6
0.62
0.64
0.66
0.68
0.7
0.72
0.74
0.76
0.78
0.8
0
2
4
6
8
10
12
14
SHEAR DISPLACEMENT (mm)

SIGMA GOLD

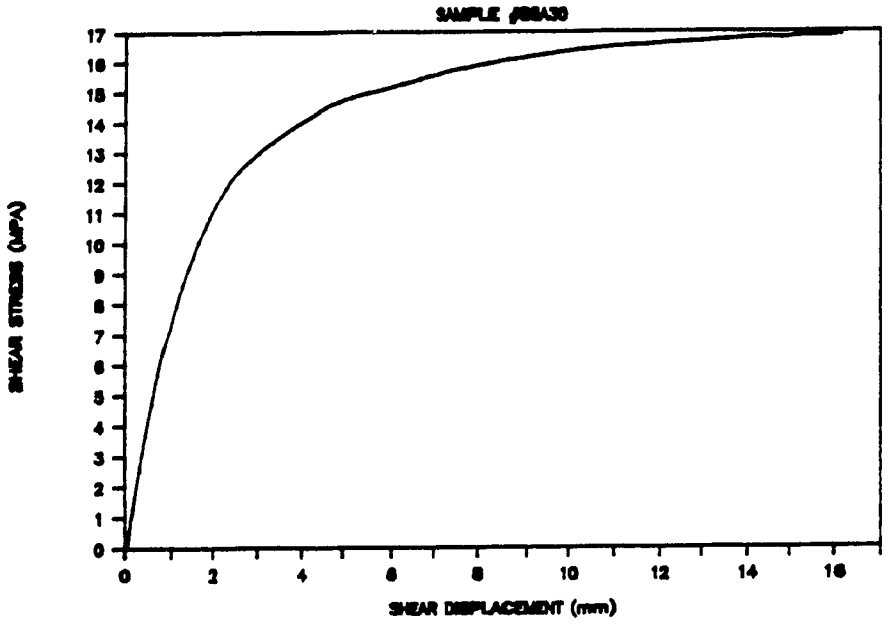
SAMPLE @BSA30
SHEAR STRESS (MPA)
SHEAR DISPLACEMENT (mm)

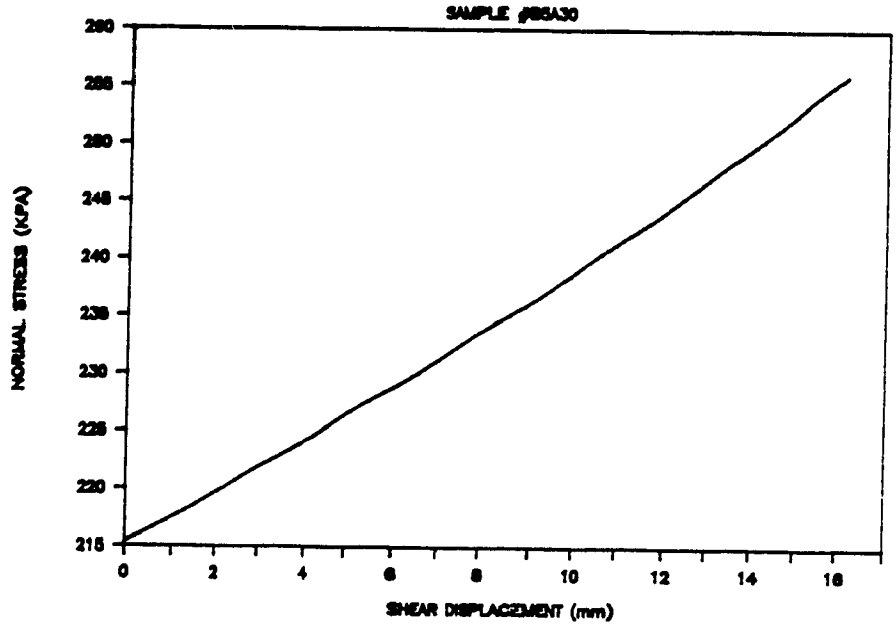
SAMPLE @BSA30
NORMAL STRESS (KPA)
SHEAR DISPLACEMENT (mm)

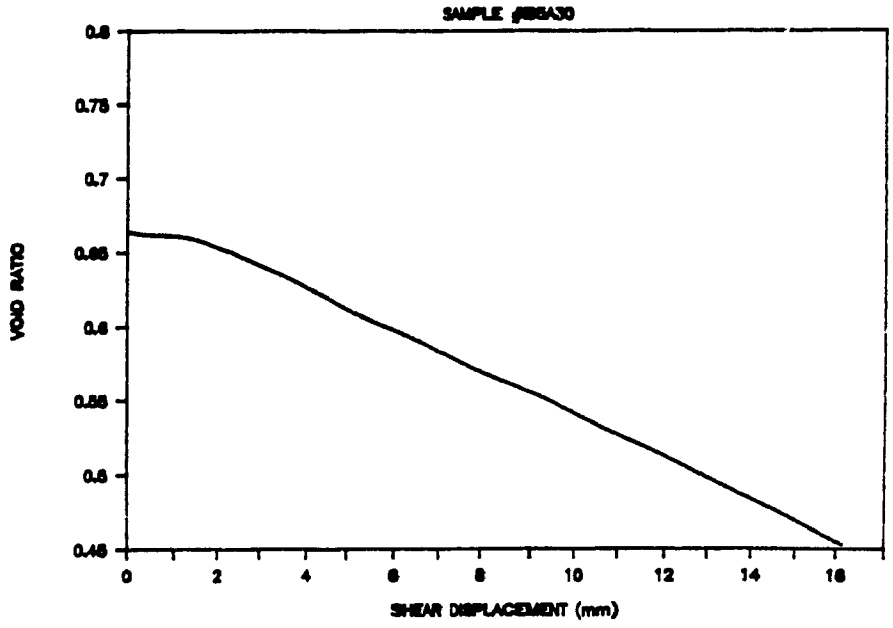
SAMPLE @BSA30
VOID RATIO
SHEAR DISPLACEMENT (mm)

SIGMA GOLD

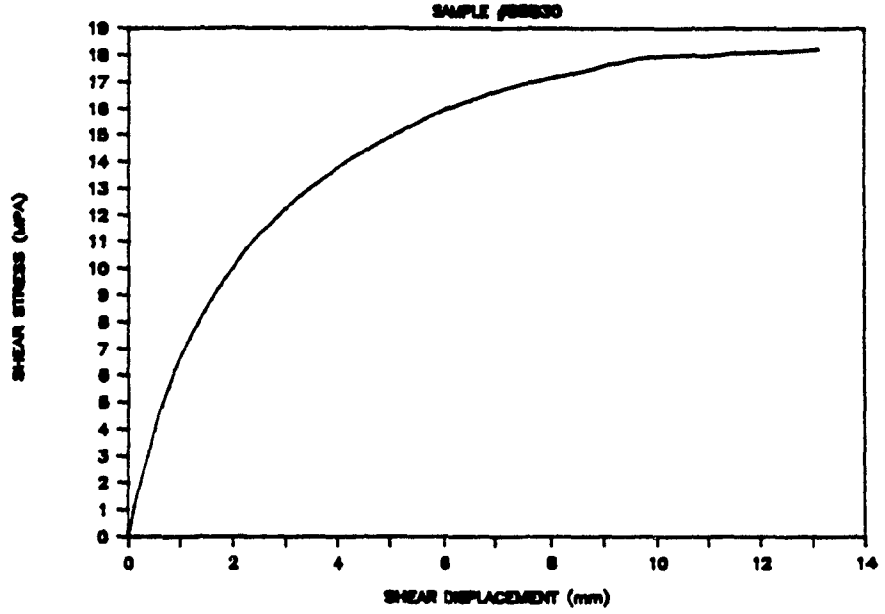
SAMPLE #88830
SHEAR STRESS (MPA)
SHEAR DISPLACEMENT (mm)

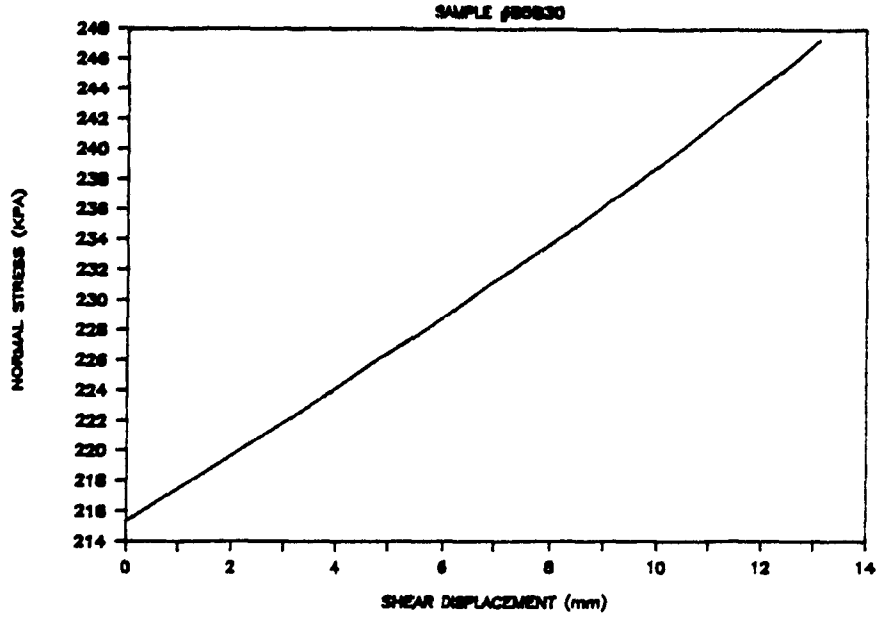
SAMPLE #88830
NORMAL STRESS (KPA)
SHEAR DISPLACEMENT (mm)

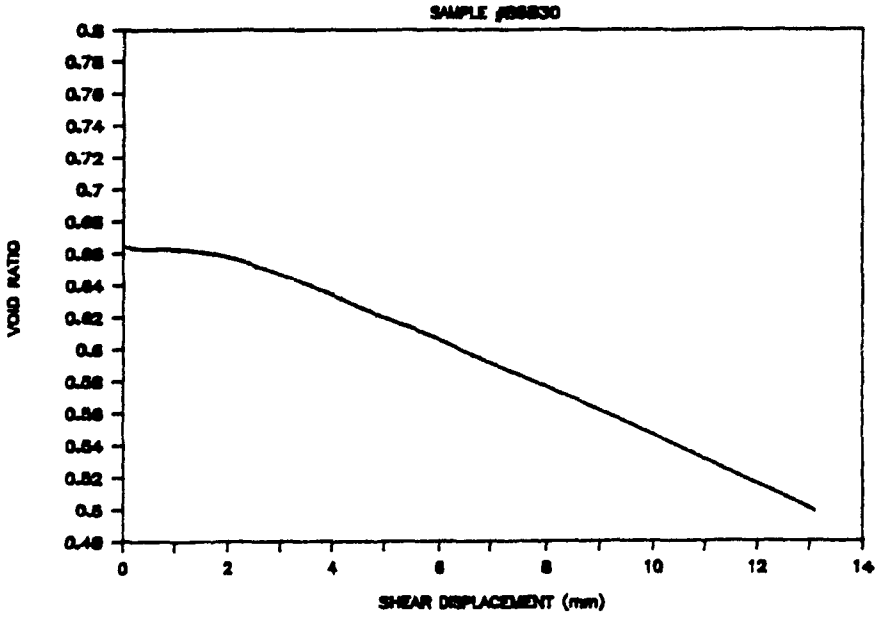
SAMPLE #88830
VOID RATIO
SHEAR DISPLACEMENT (mm)

DENISON

SAMPLE #E100A10 – A

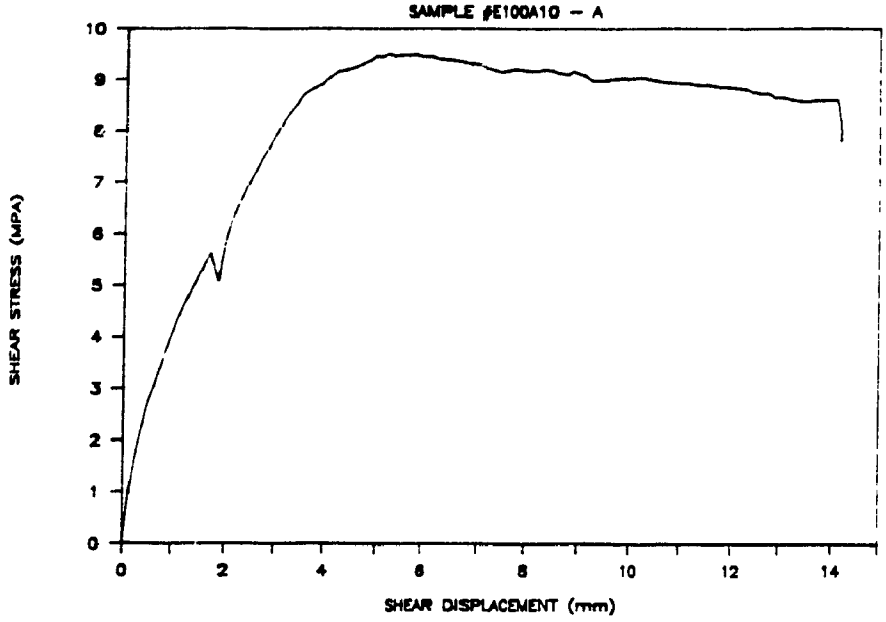

SAMPLE #E100A10 – A

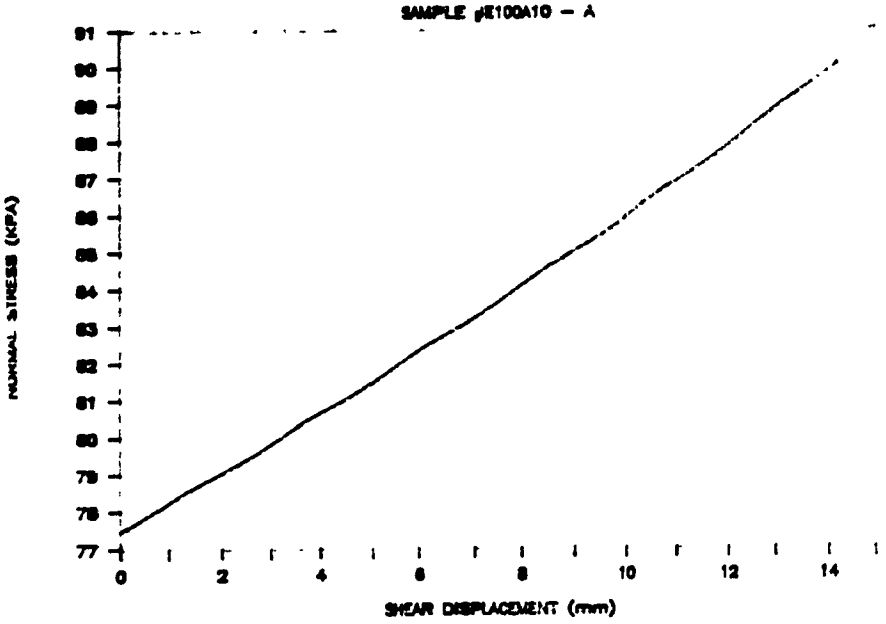

SAMPLE #E100A10 – A

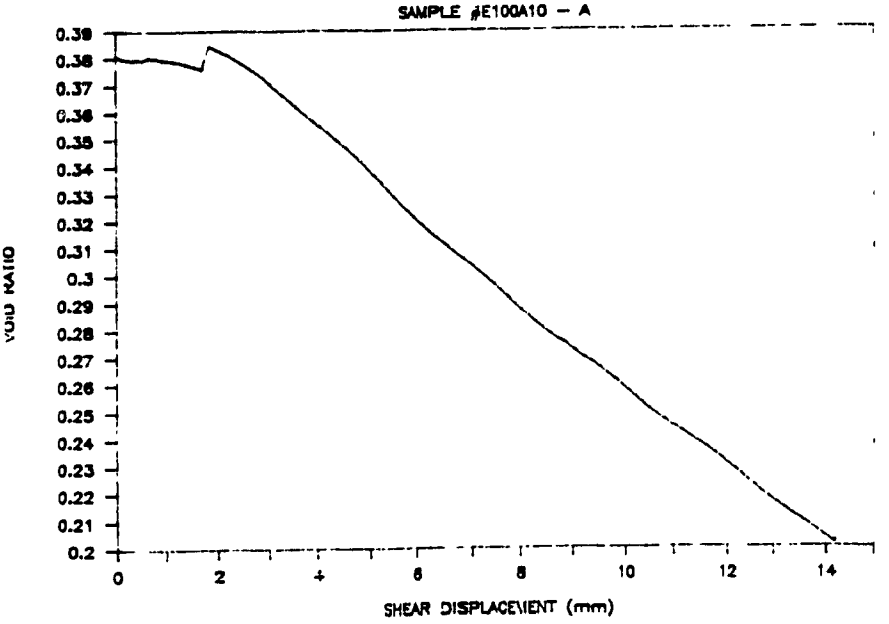

DENISON

SAMPLE #E100B10 – A

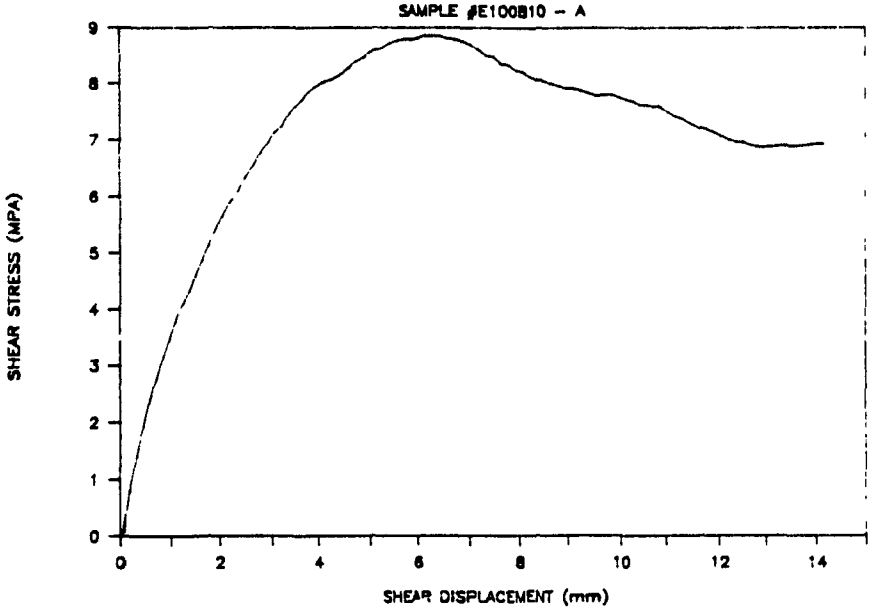

SAMPLE #E100B10 – A

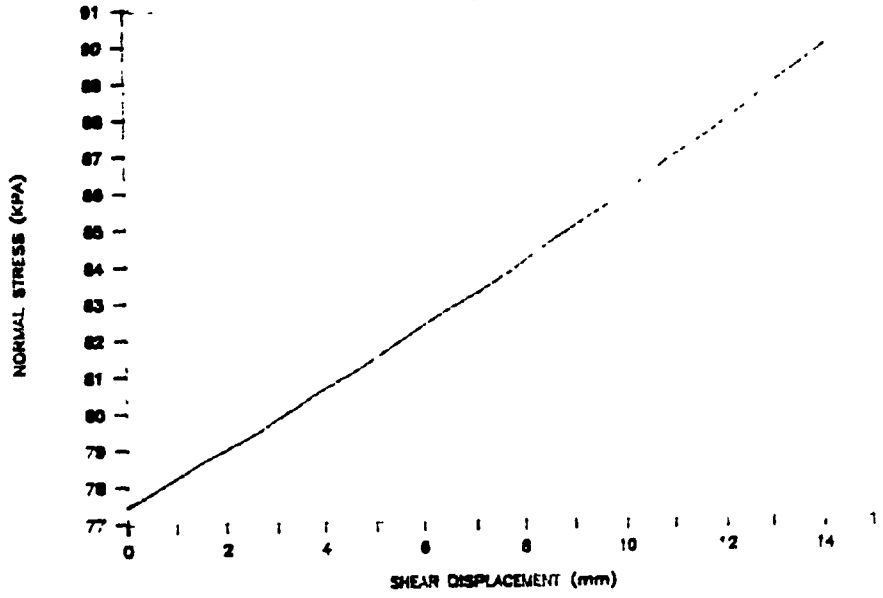

SAMPLE #E100B10 – A

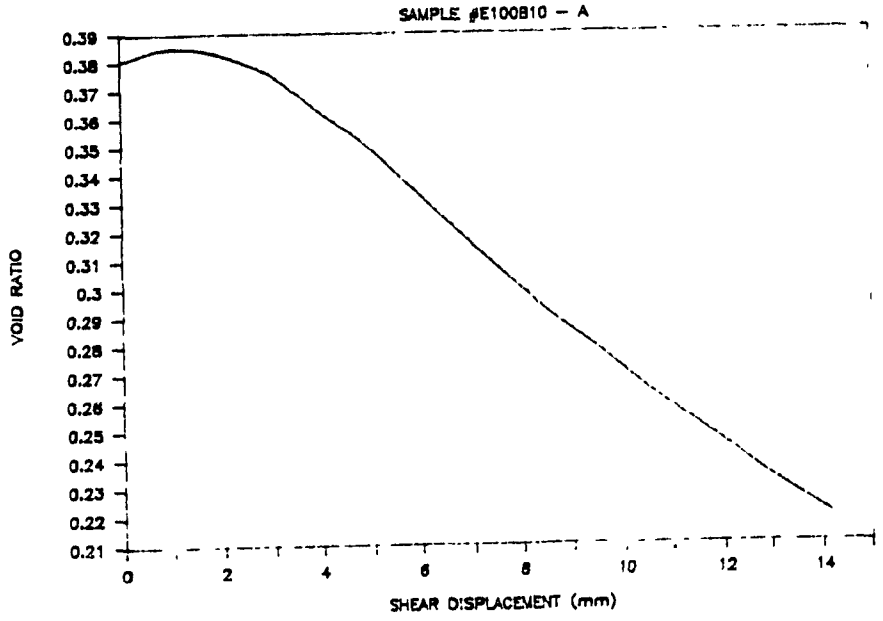

DENISON

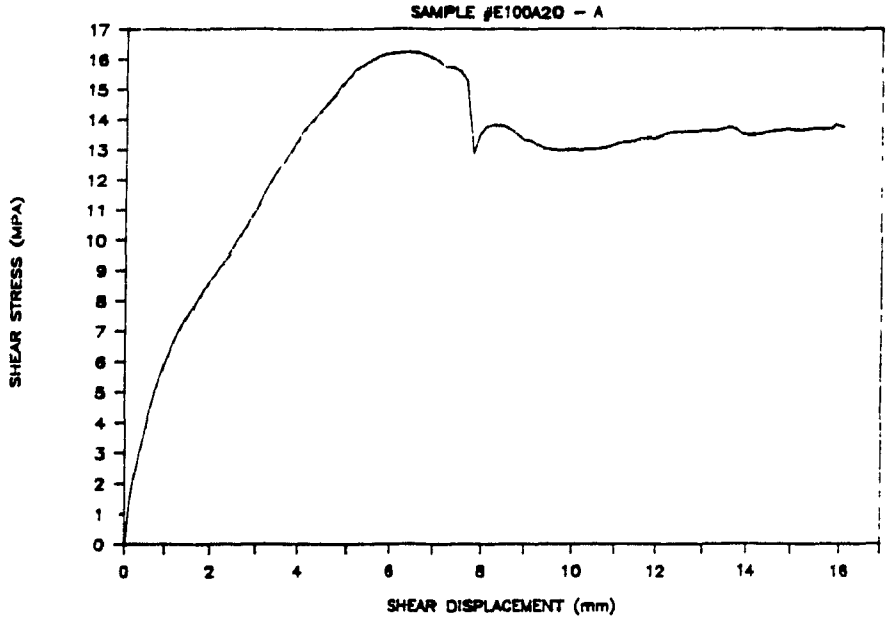
SAMPLE #E100A20 – A
SHEAR STRESS (MPA)
SHEAR DISPLACEMENT (mm)

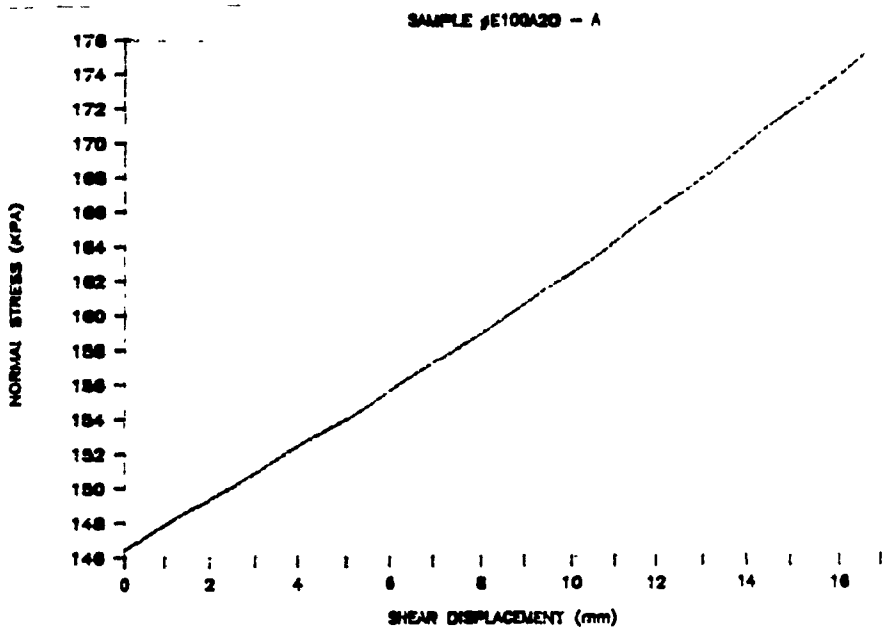
SAMPLE #E100A20 – A
NORMAL STRESS (KPA)
SHEAR DISPLACEMENT (mm)

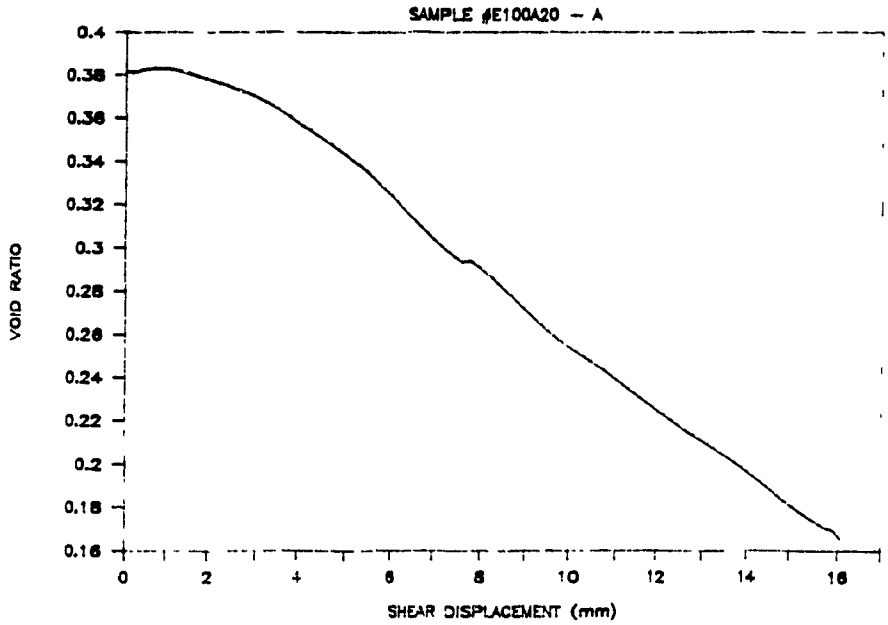
SAMPLE #E100A20 – A
VOID RATIO
SHEAR DISPLACEMENT (mm)

DENISON

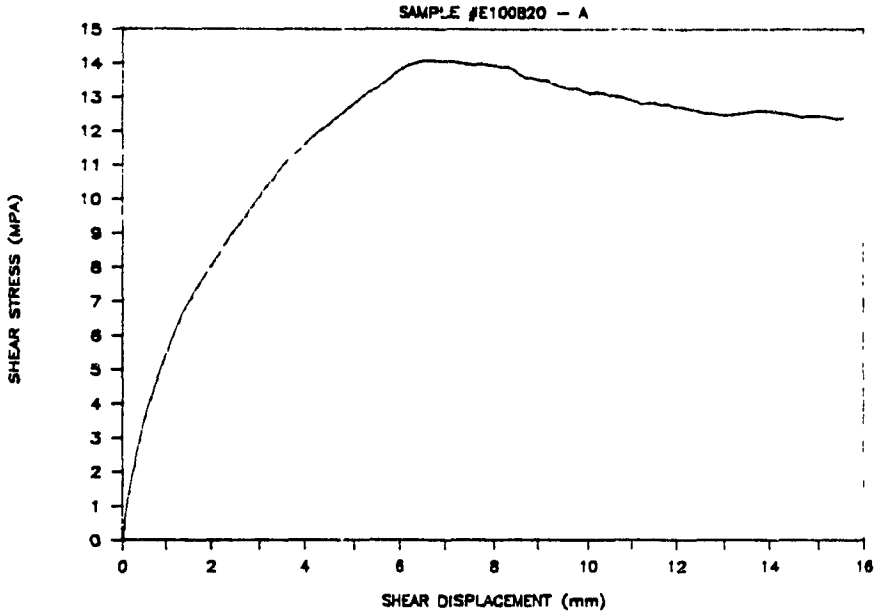
SAMPLE #E100820 – A
SHEAR STRESS (MPA)
SHEAR DISPLACEMENT (mm)

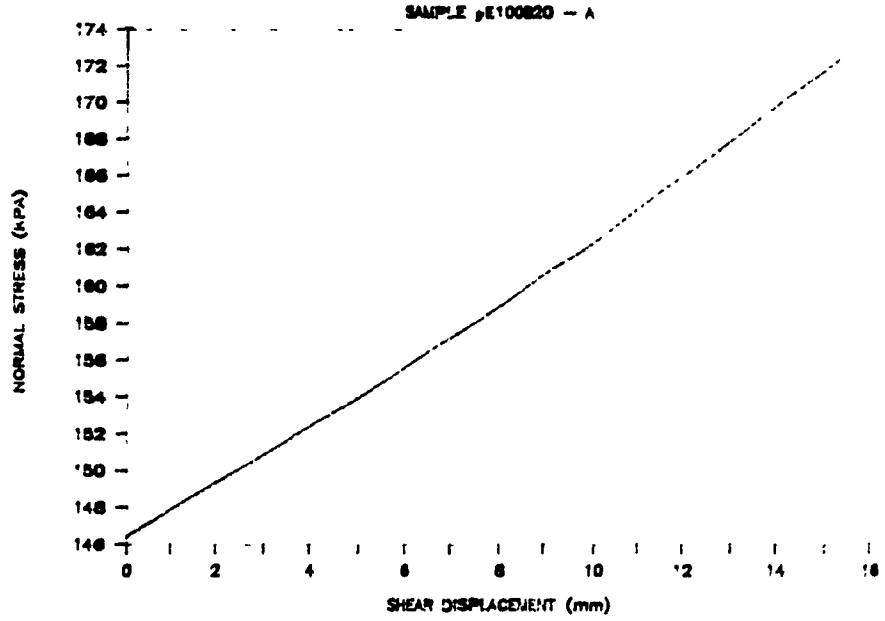
SAMPLE #E100820 – A
NORMAL STRESS (kPA)
SHEAR DISPLACEMENT (mm)

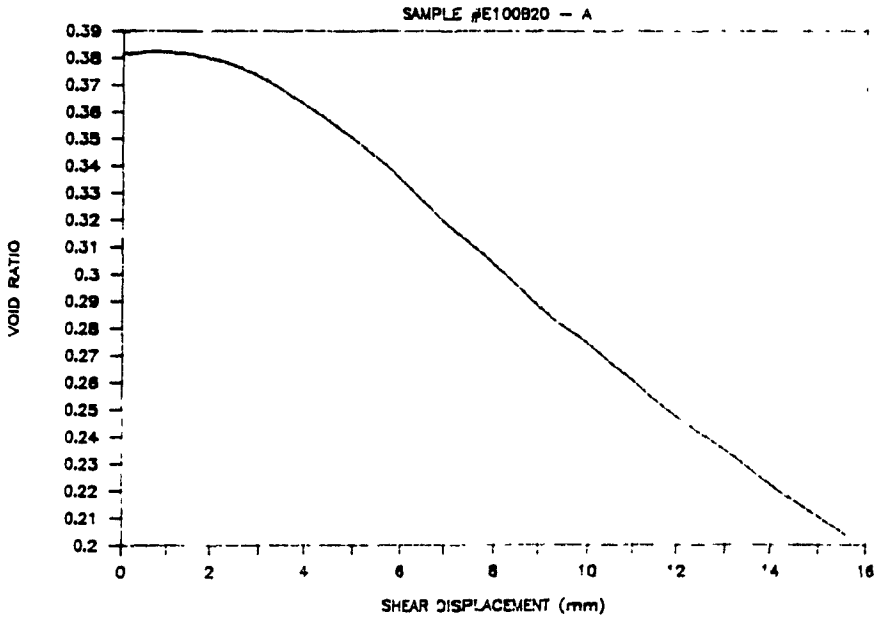
SAMPLE #E100820 – A
VOID RATIO
SHEAR DISPLACEMENT (mm)

DENISON

SAMPLE #E100A30 – A

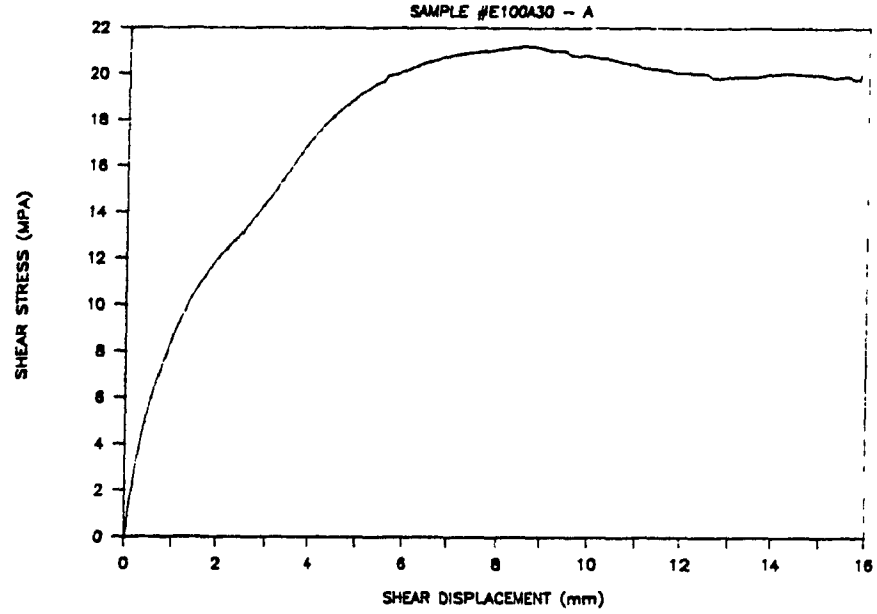

SAMPLE #E100A30 – A

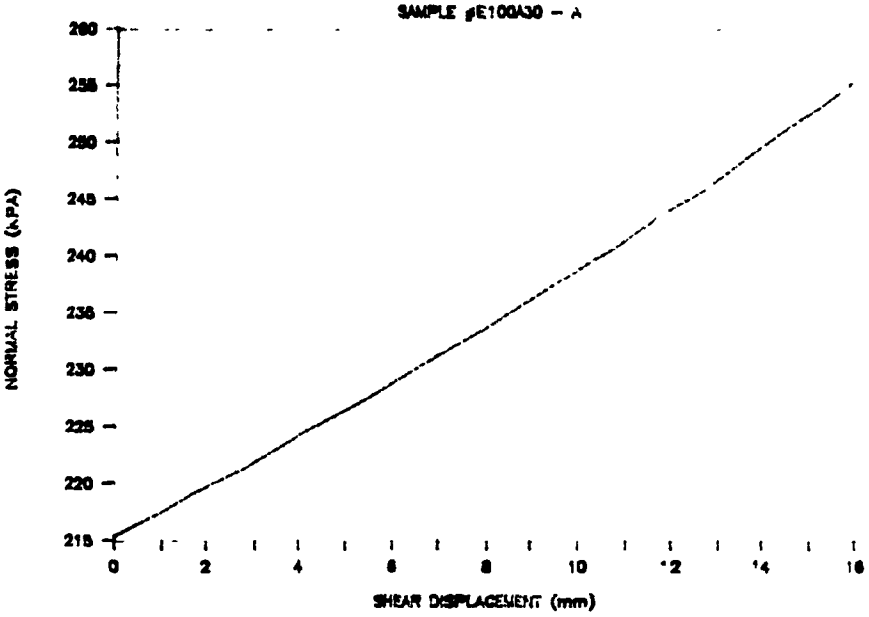

SAMPLE #E100A30 – A

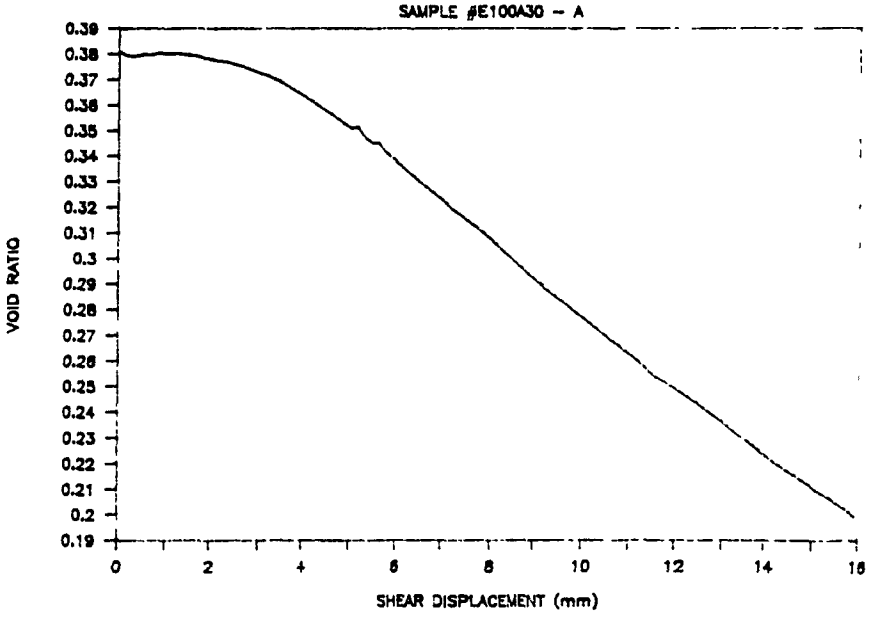

DENISON

SAMPLE #E100B30 - A

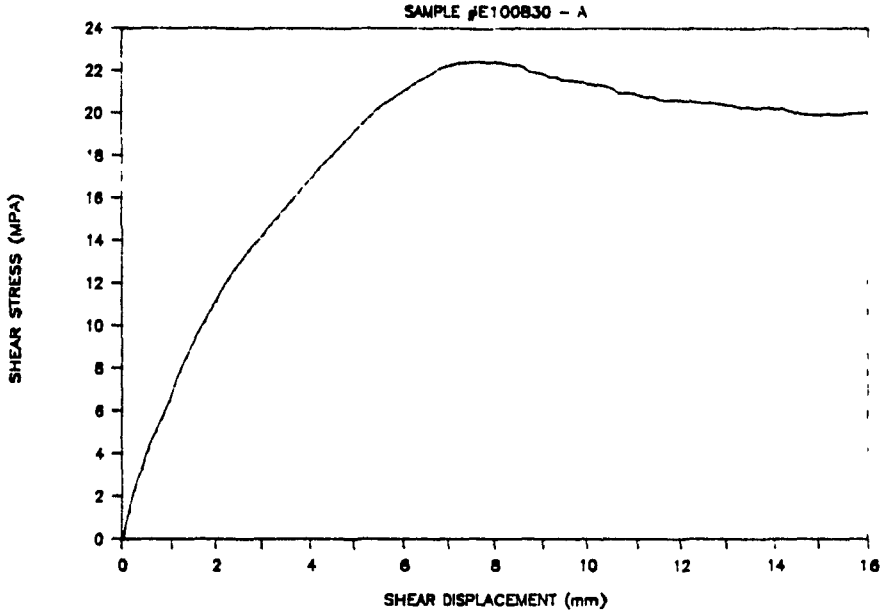

SAMPLE #E100B30 - A

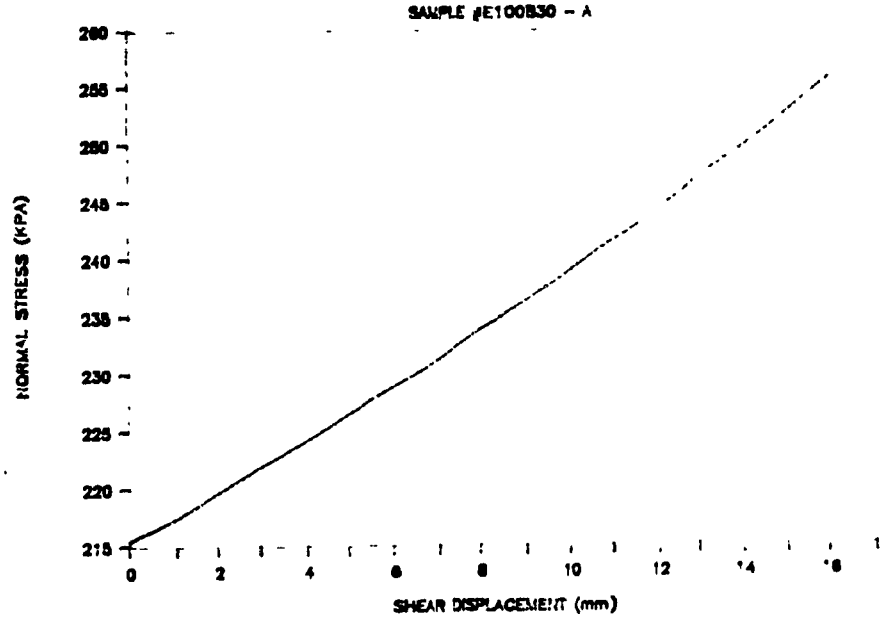

SAMPLE #E100B30 - A

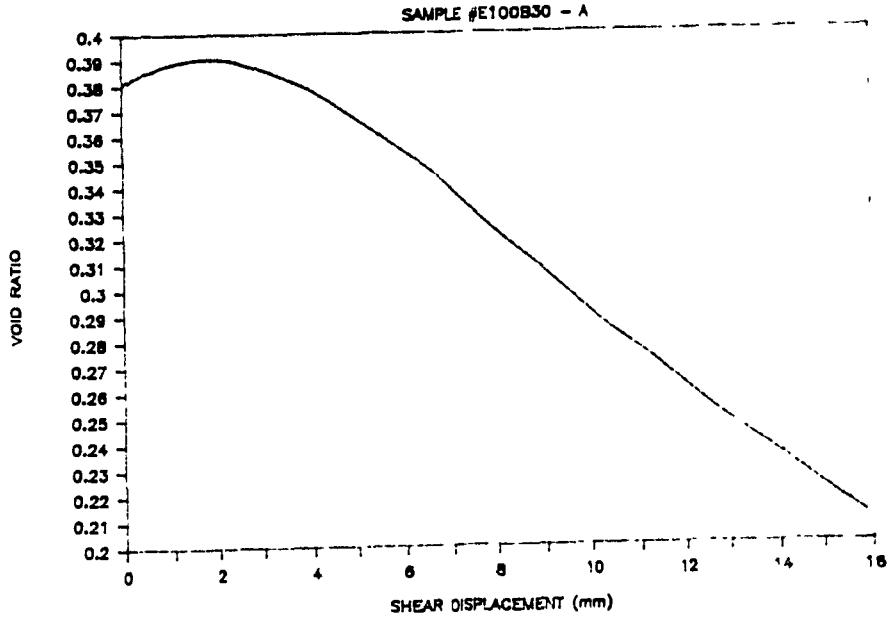

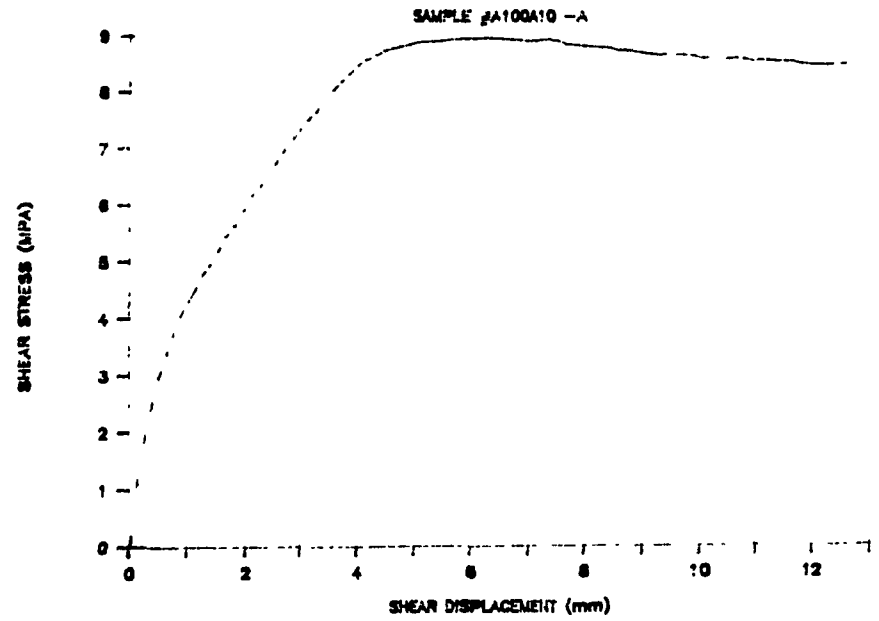
SAMPLE #A100A10 -A
SHEAR STRESS (MPA)
0
1
2
3
4
5
6
7
8
9
0
2
4
6
8
10
12
SHEAR DISPLACEMENT (mm)

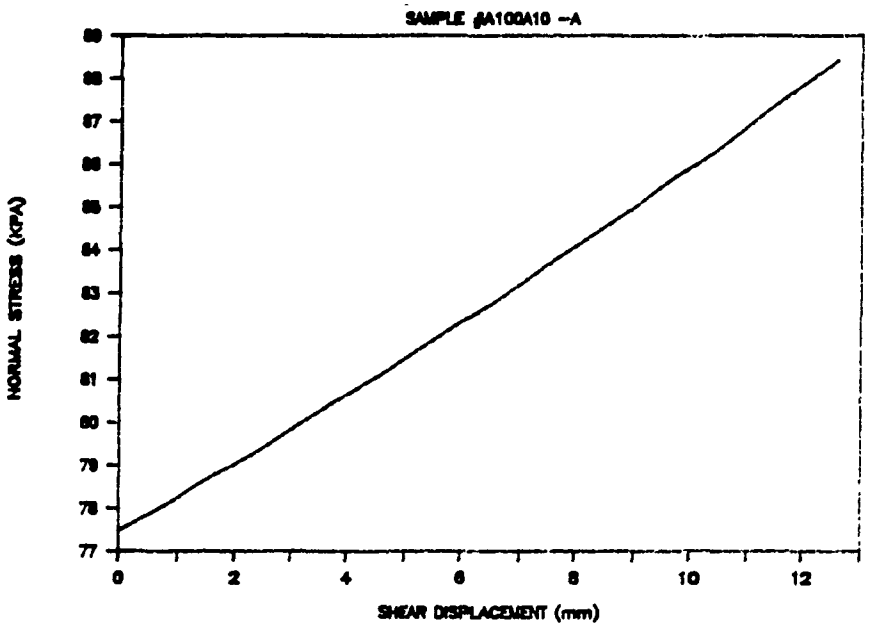
SAMPLE #A100A10 -A
NORMAL STRESS (KPA)
77
78
79
80
81
82
83
84
85
86
87
88
89
0
2
4
6
8
10
12
SHEAR DISPLACEMENT (mm)

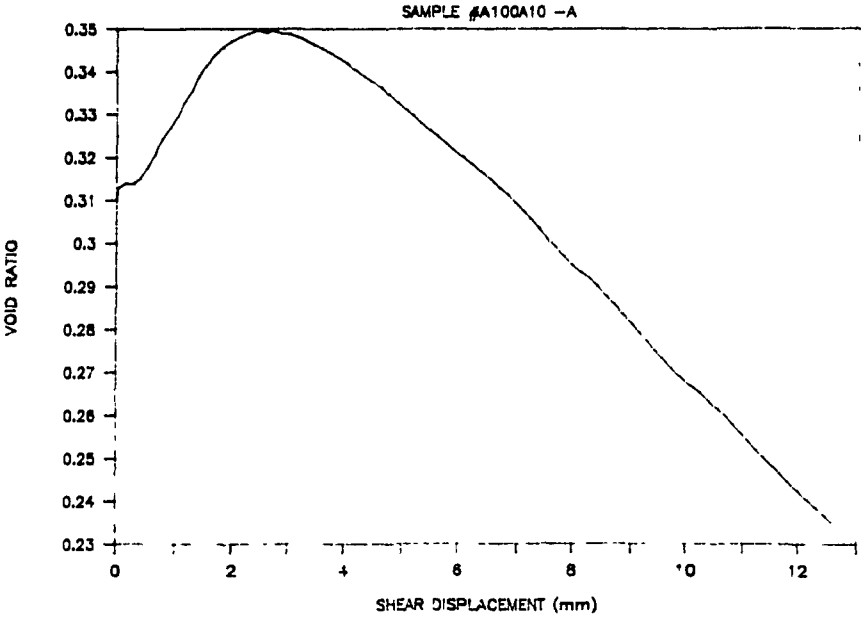
SAMPLE #A100A10 -A
VOID RATIO
0.23
0.24
0.25
0.26
0.27
0.28
0.29
0.3
0.31
0.32
0.33
0.34
0.35
0
2
4
6
8
10
12
SHEAR DISPLACEMENT (mm)

DENISON

SAMPLE #A100B10 – A

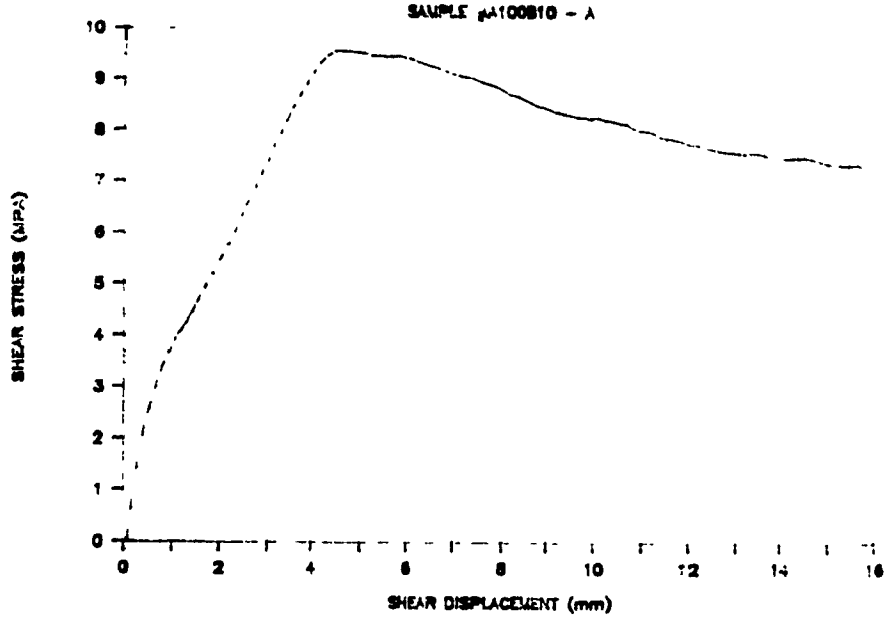

SAMPLE #A100B10 – A

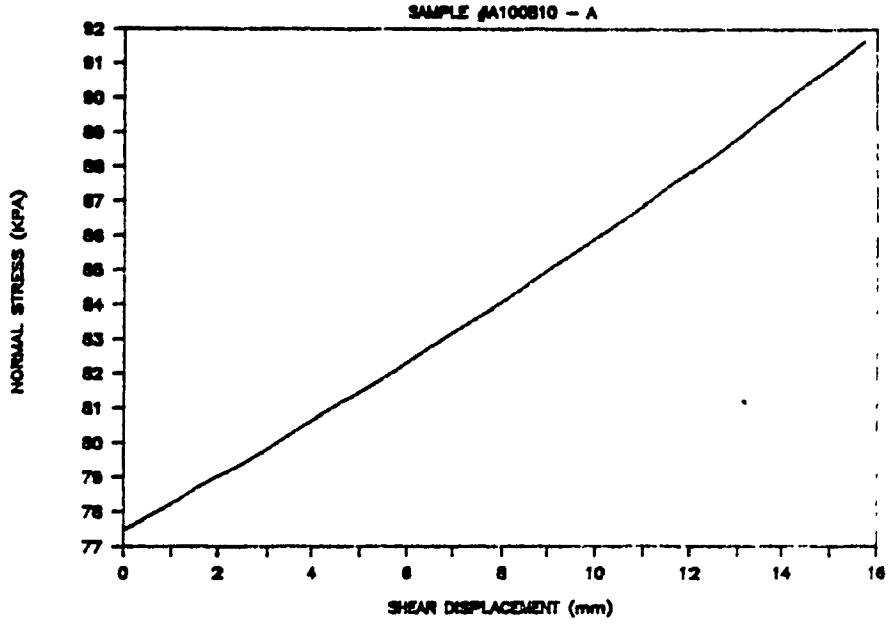

SAMPLE #A100B10 – A

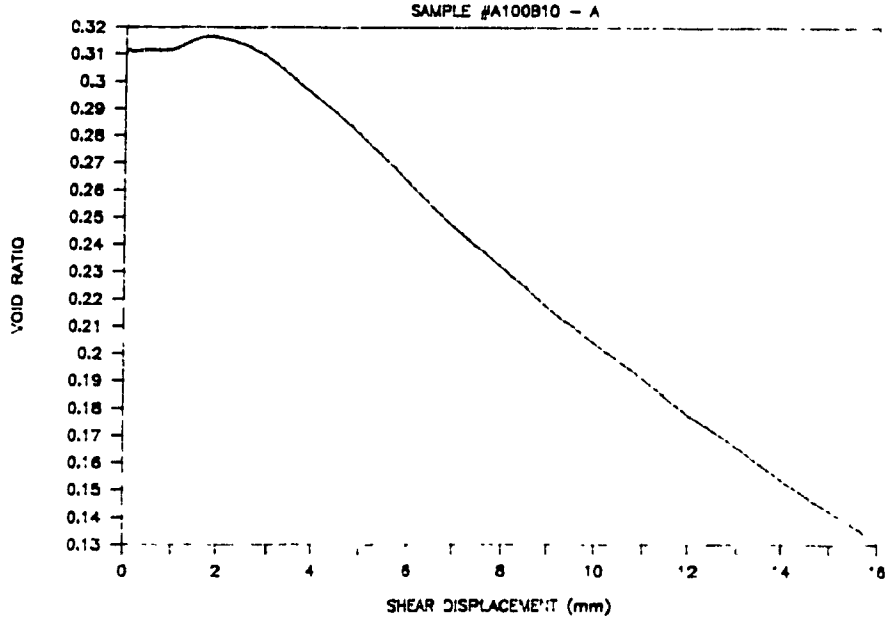

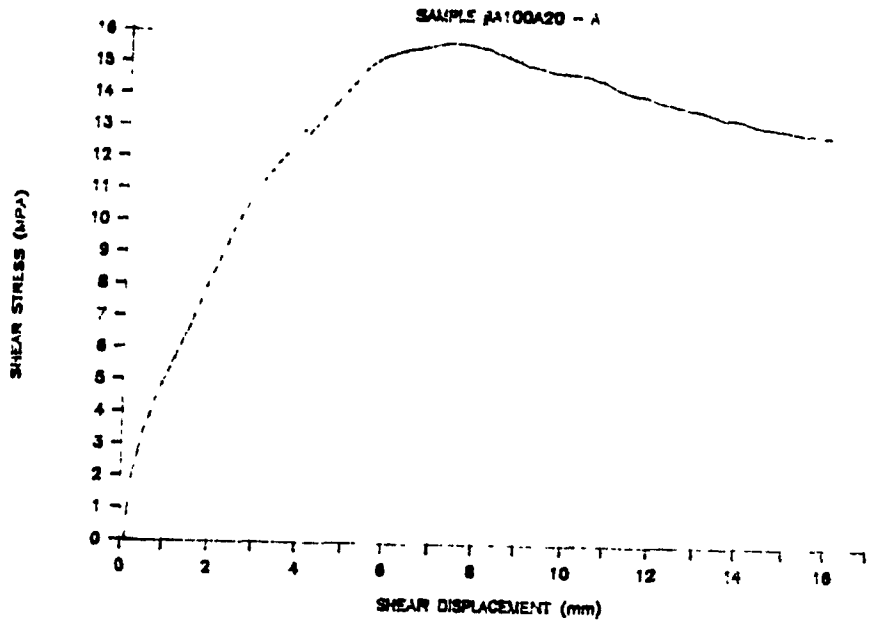
SAMPLE #A100A20 – A
SHEAR STRESS (MPA)
SHEAR DISPLACEMENT (mm)

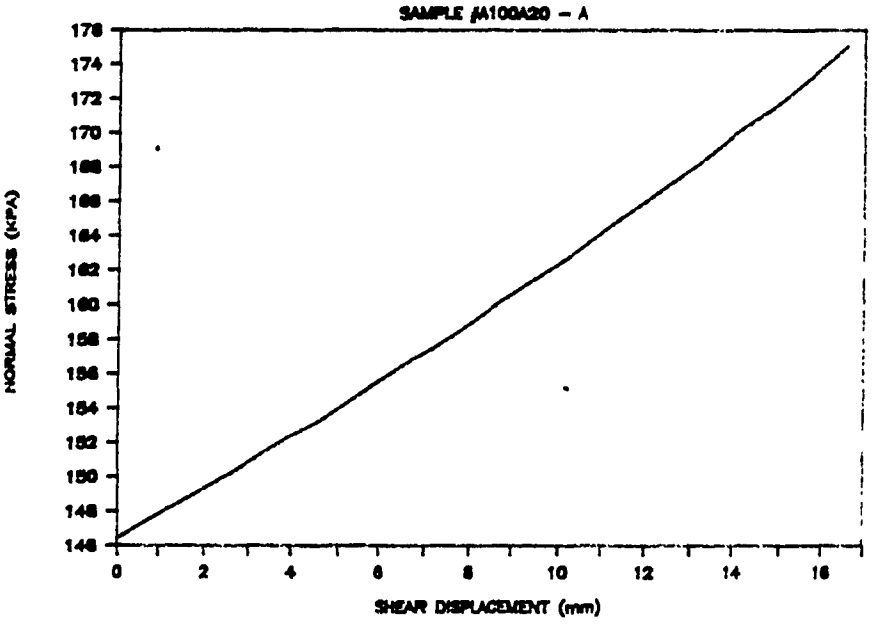
SAMPLE #A100A20 – A
NORMAL STRESS (KPA)
SHEAR DISPLACEMENT (mm)

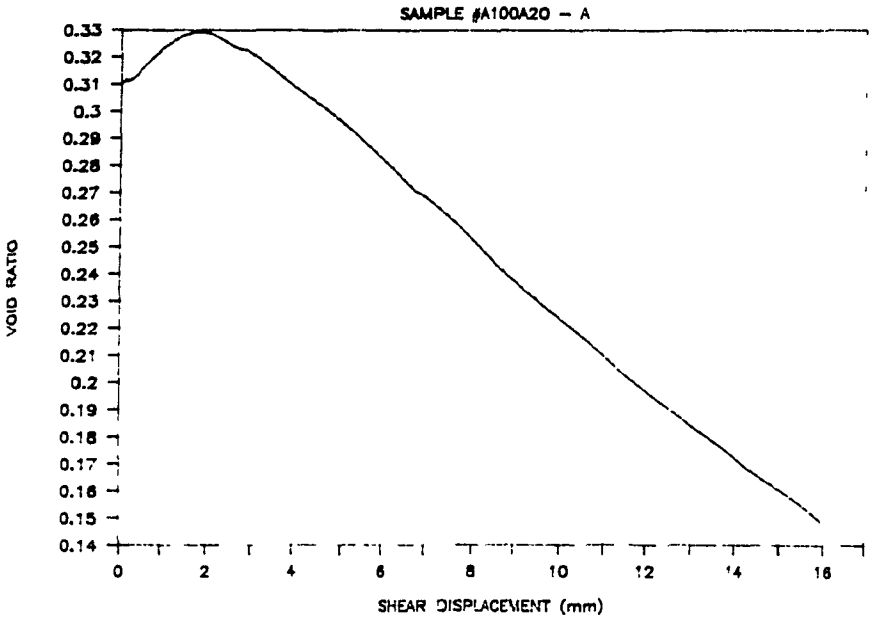
SAMPLE #A100A20 – A
VOID RATIO
SHEAR DISPLACEMENT (mm)

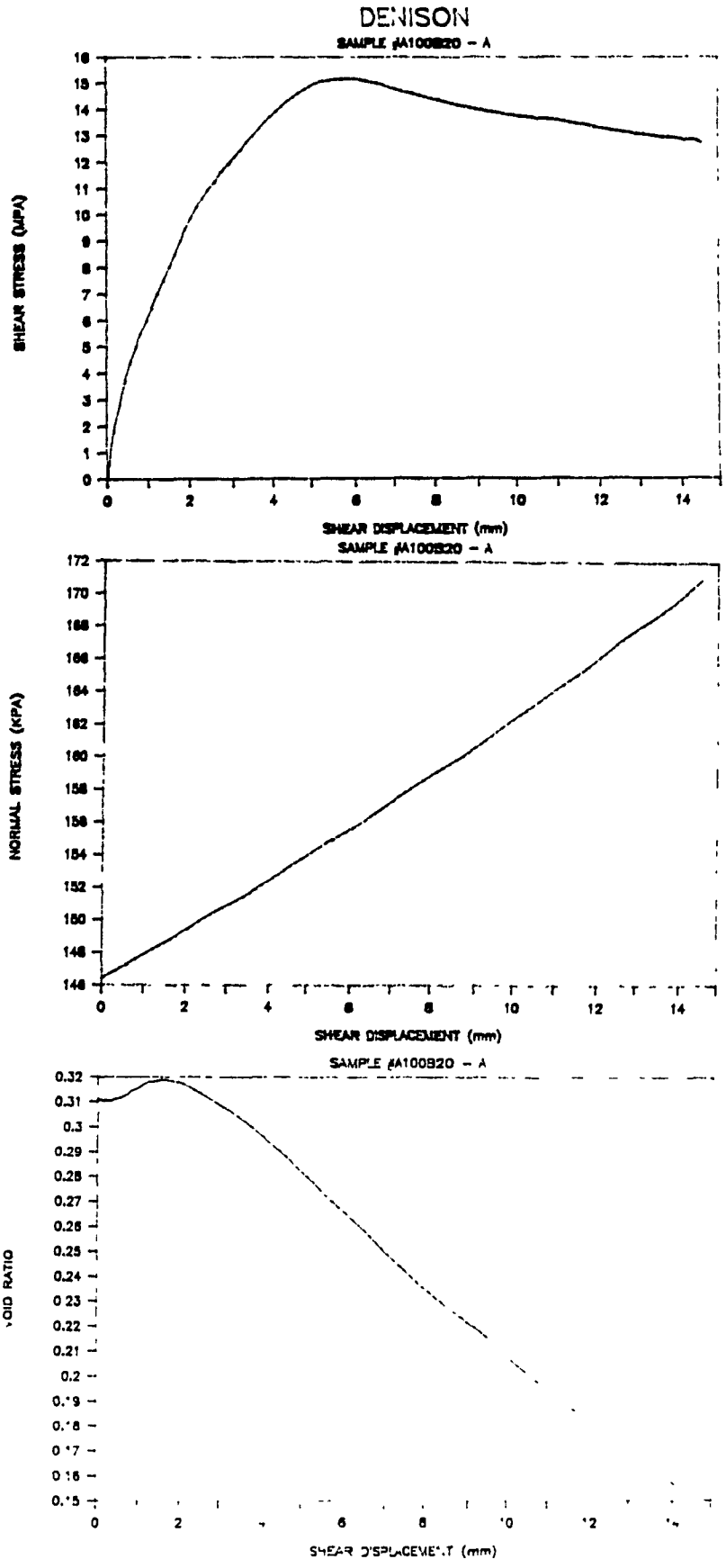
DENISON
SAMPLE #A100S20 - A
SHEAR STRESS (MPA)
SHEAR DISPLACEMENT (mm)
SAMPLE #A100S20 - A
NORMAL STRESS (KPA)
SHEAR DISPLACEMENT (mm)
SAMPLE #A100S20 - A
VOID RATIO
SHEAR DISPLACEMENT (mm)

SAMPLE #A100A30 – A

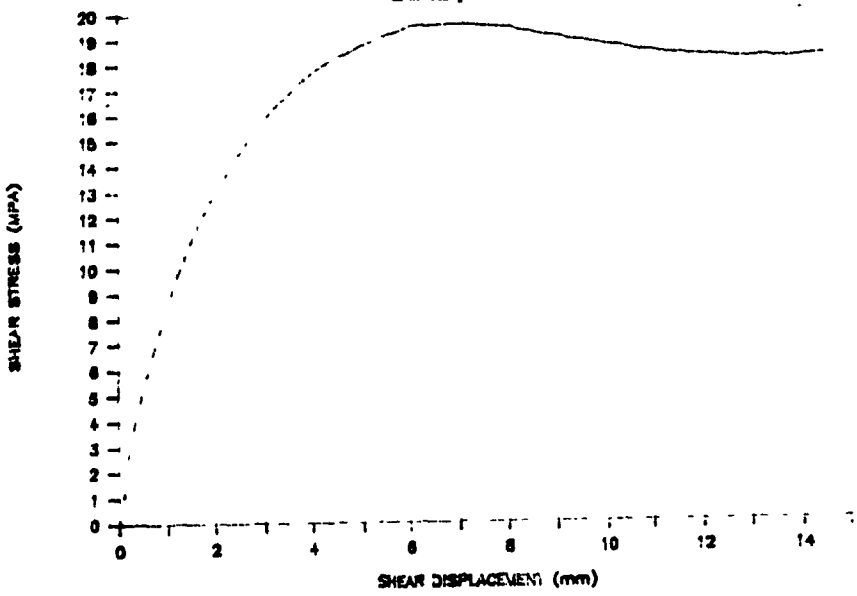

SAMPLE #A100A30 – A

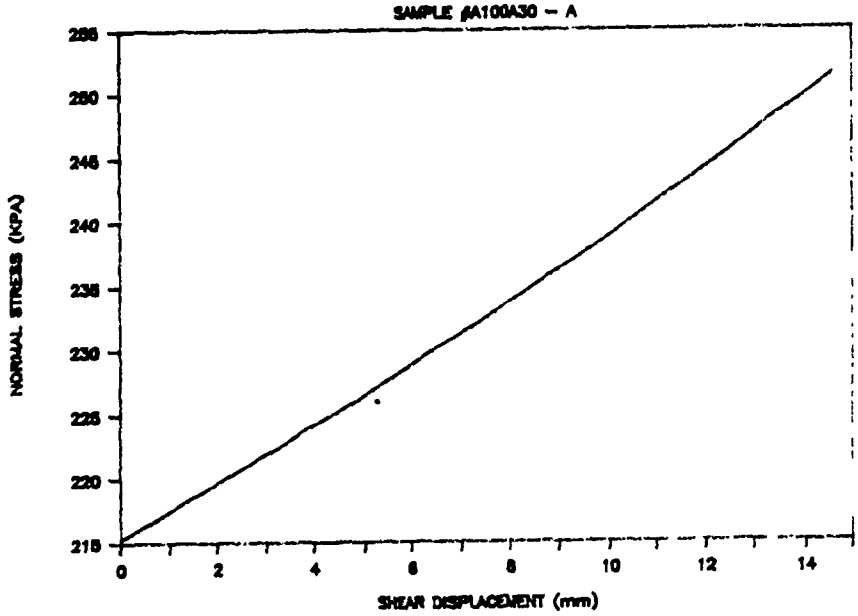

SAMPLE #A100A30 – A

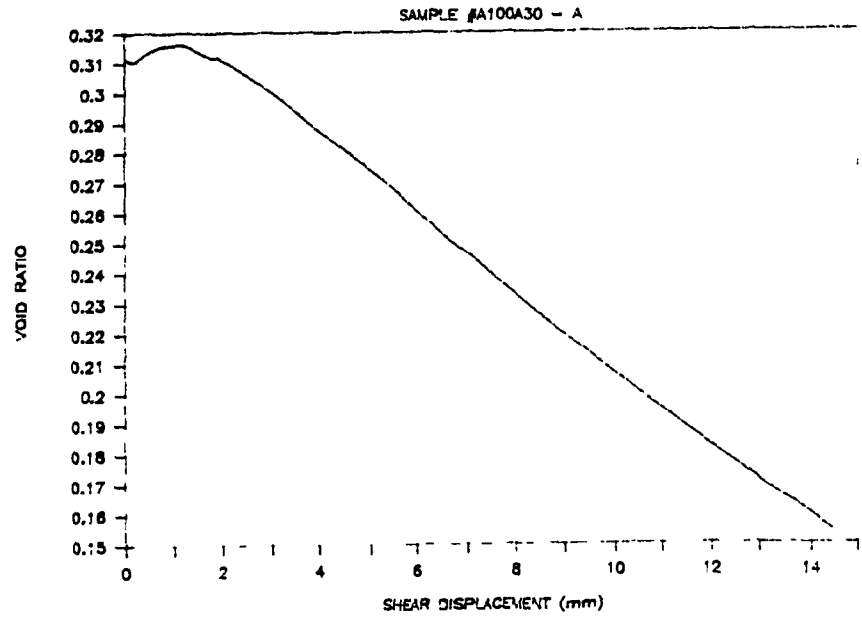

DENISON

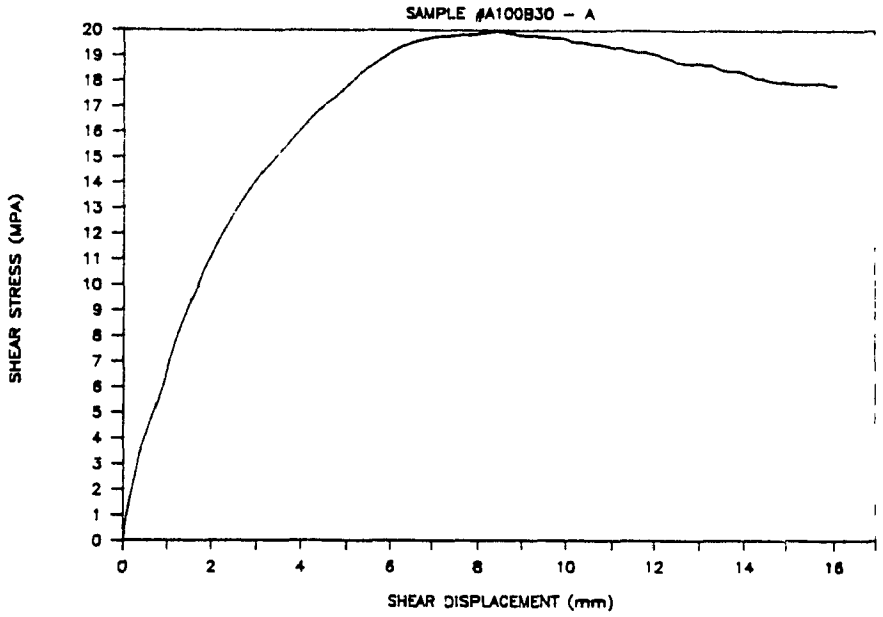
SAMPLE #A100B30 - A
SHEAR STRESS (MPA)
SHEAR DISPLACEMENT (mm)

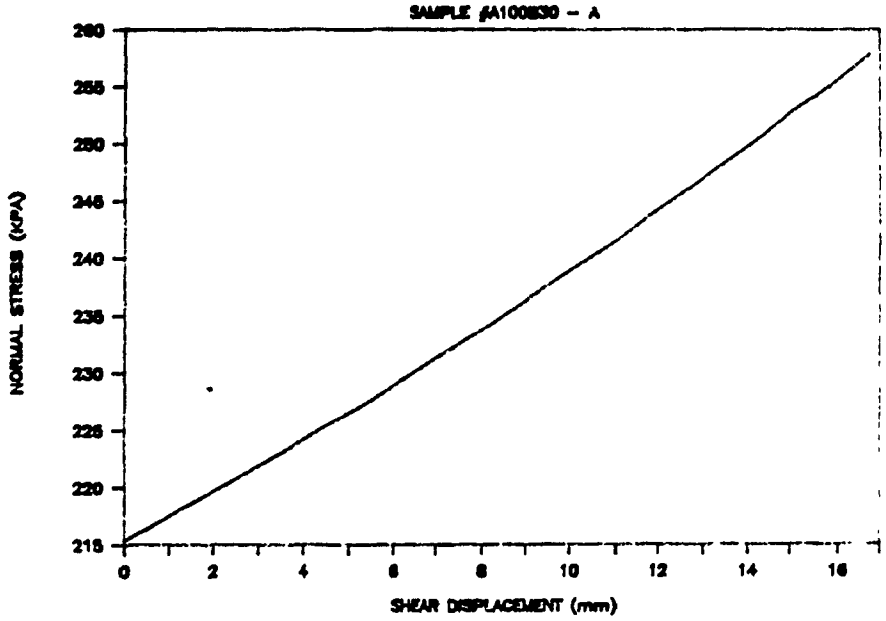
SAMPLE #A100B30 - A
NORMAL STRESS (KPA)
SHEAR DISPLACEMENT (mm)

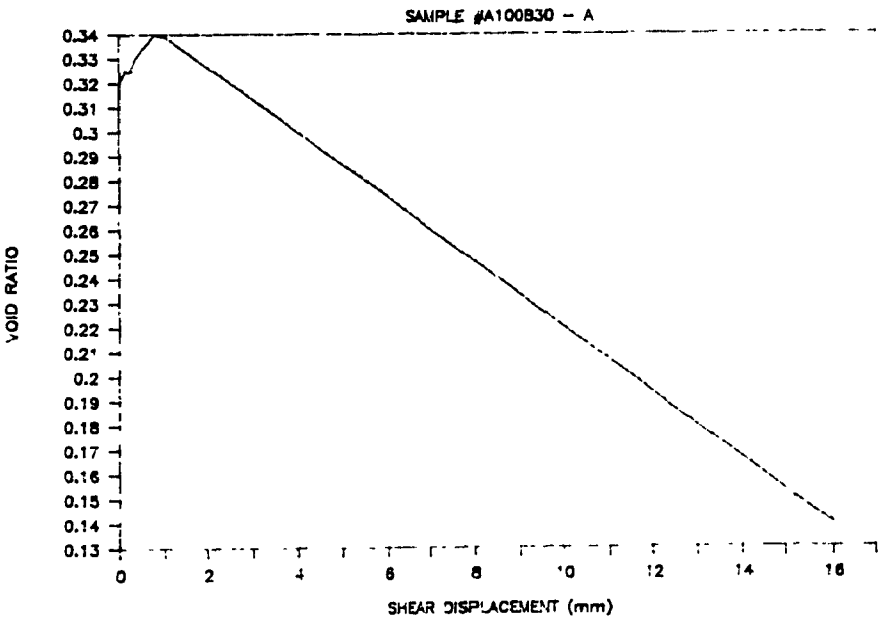
SAMPLE #A100B30 - A
VOID RATIO
SHEAR DISPLACEMENT (mm)

DENISON

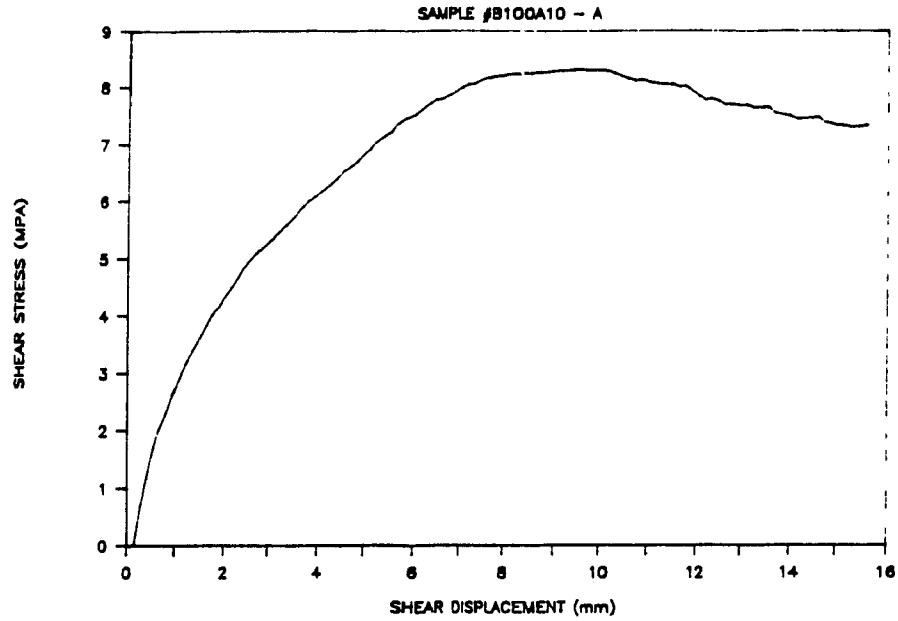
SAMPLE #B100A10 – A
SHEAR STRESS (MPA)
SHEAR DISPLACEMENT (mm)

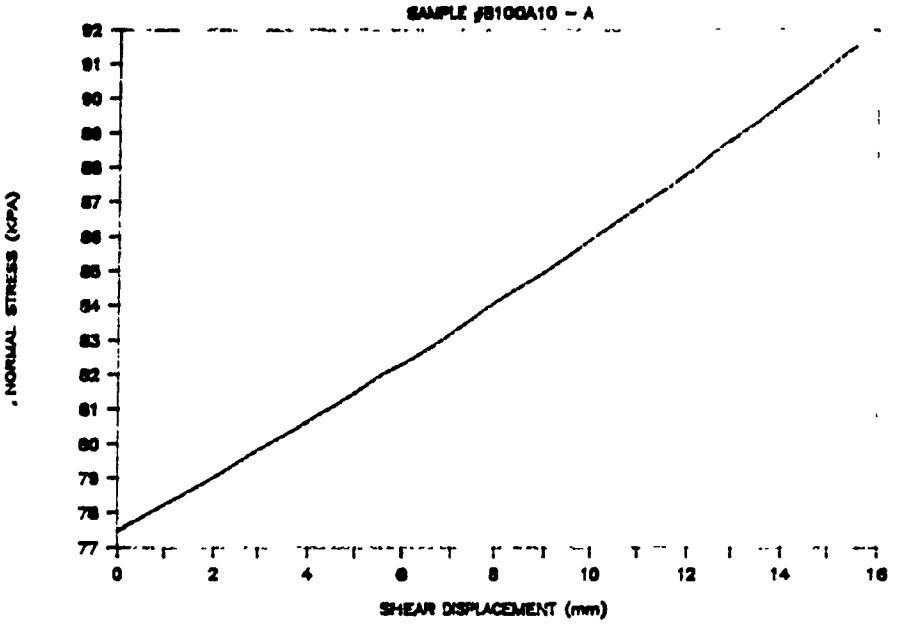
SAMPLE #B100A10 – A
NORMAL STRESS (KPA)
SHEAR DISPLACEMENT (mm)

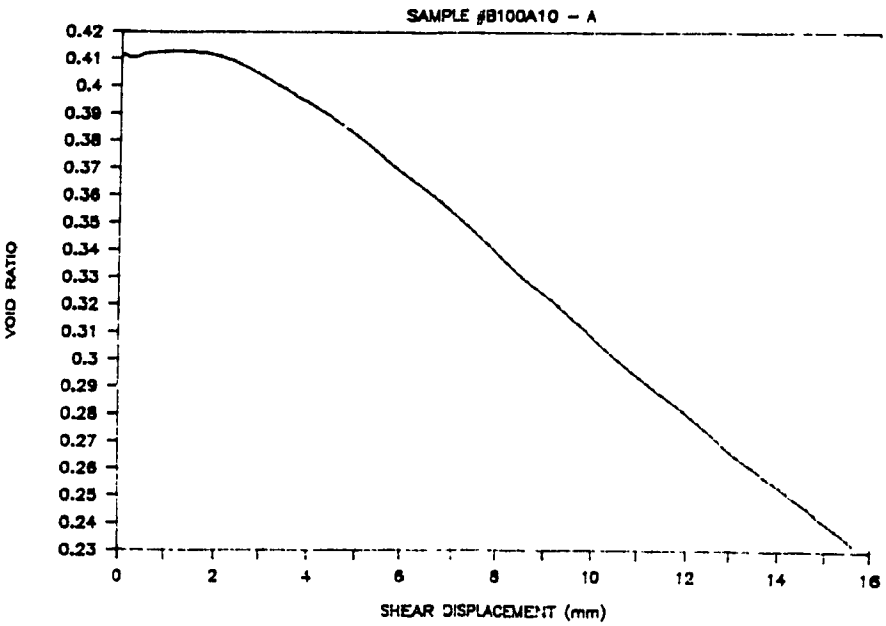
SAMPLE #B100A10 – A
VOID RATIO
SHEAR DISPLACEMENT (mm)

DENISON

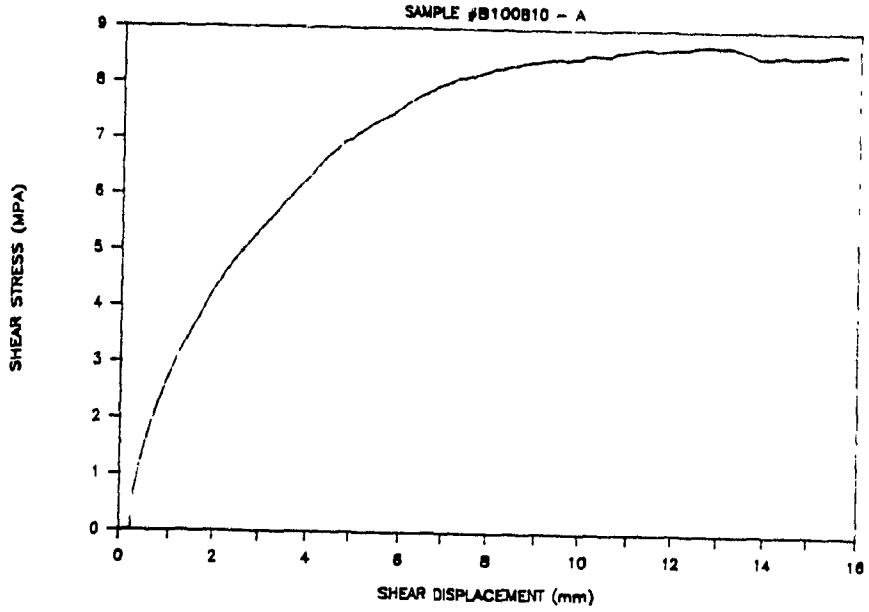
SAMPLE #B100B10 – A
SHEAR STRESS (MPA)
SHEAR DISPLACEMENT (mm)

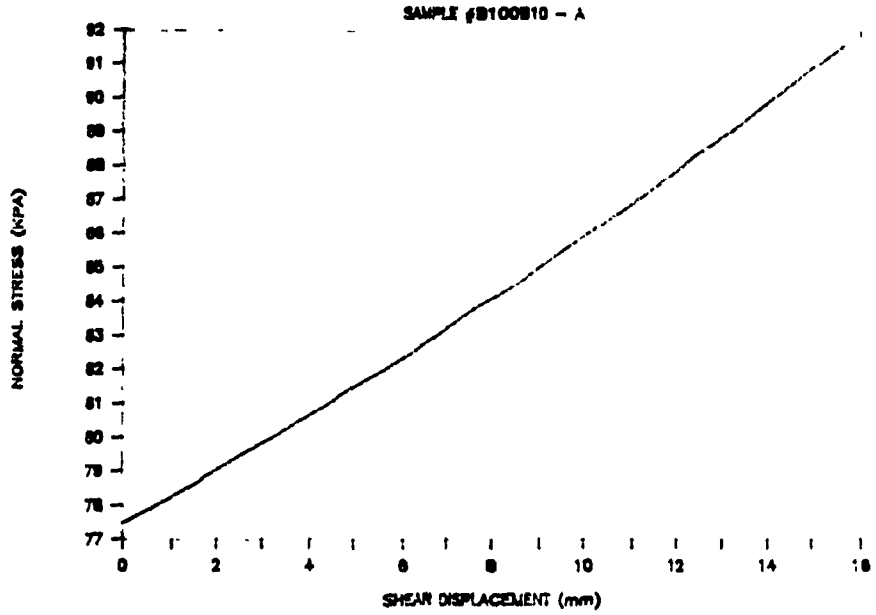
SAMPLE #B100B10 – A
NORMAL STRESS (KPA)
SHEAR DISPLACEMENT (mm)

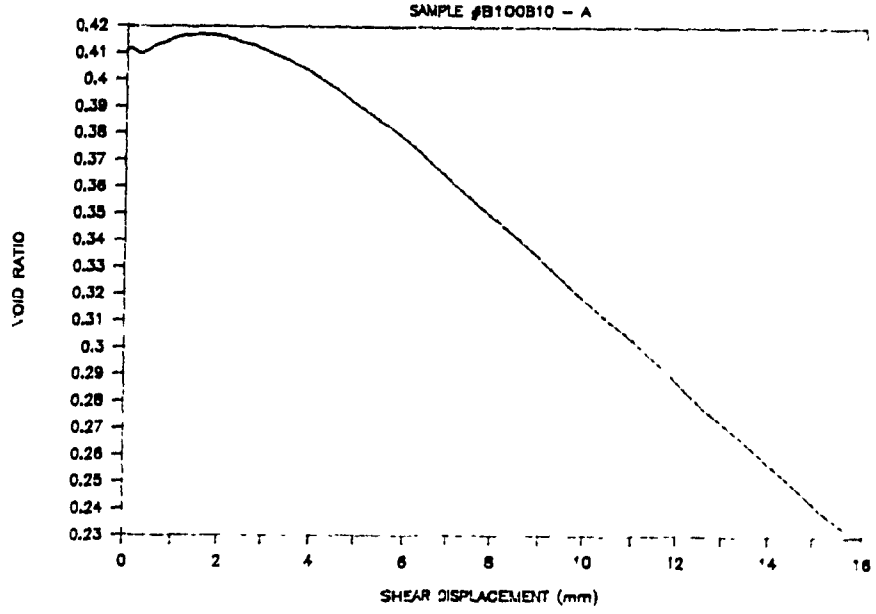
SAMPLE #B100B10 – A
VOID RATIO
SHEAR DISPLACEMENT (mm)

DENISON

SAMPLE #B100A20 – A

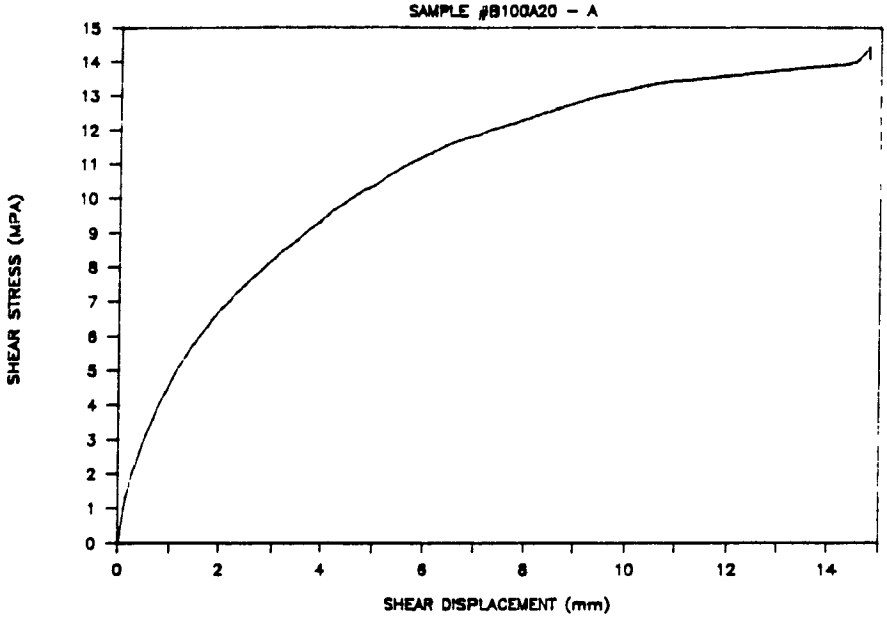

SAMPLE #B100A20 – A

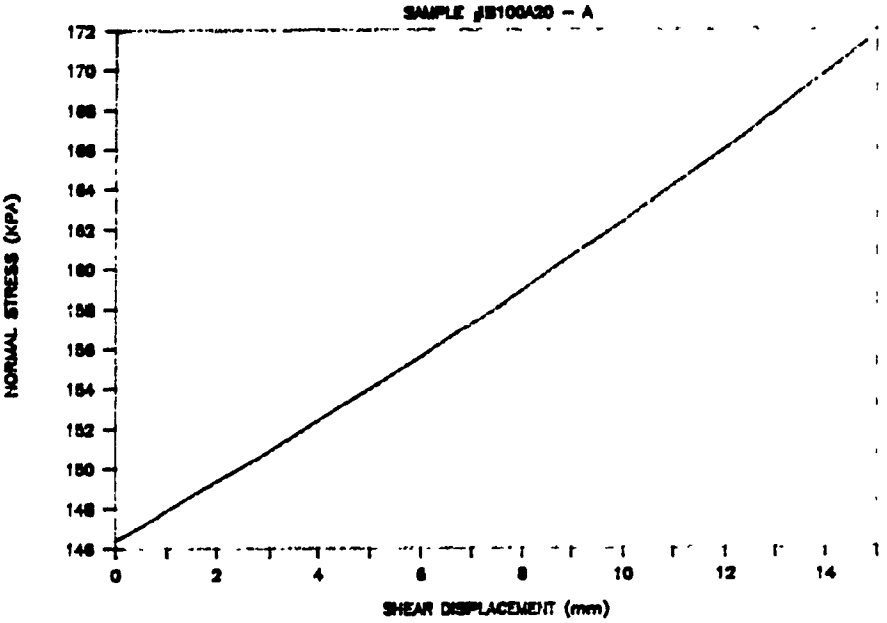

SAMPLE #B100A20 – A

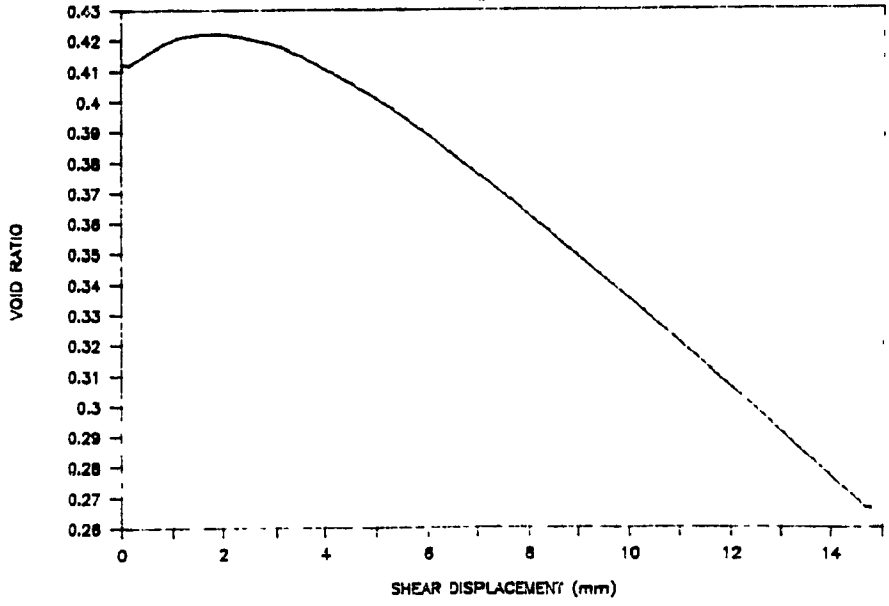

DENISON

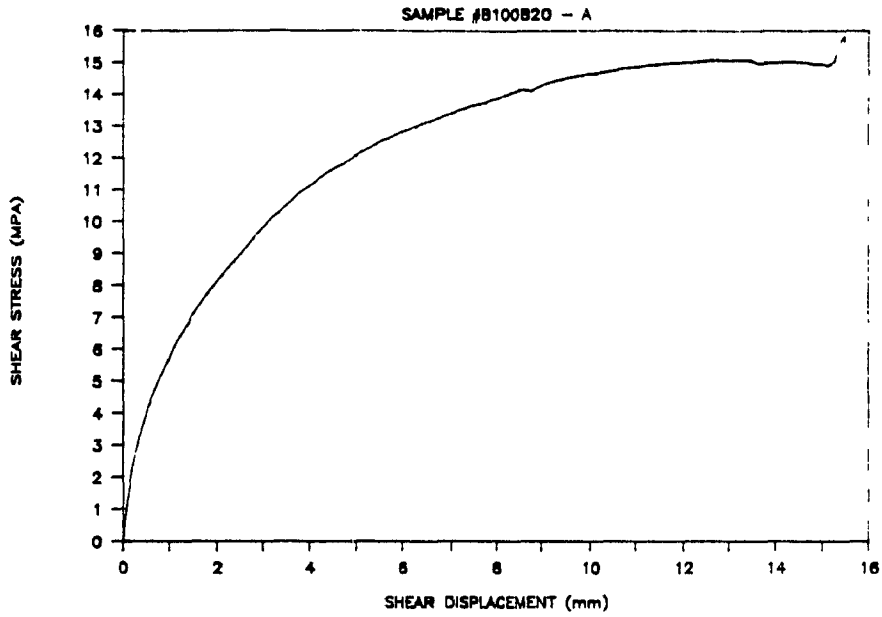
SAMPLE #B100B2O – A
SHEAR STRESS (MPA)
SHEAR DISPLACEMENT (mm)

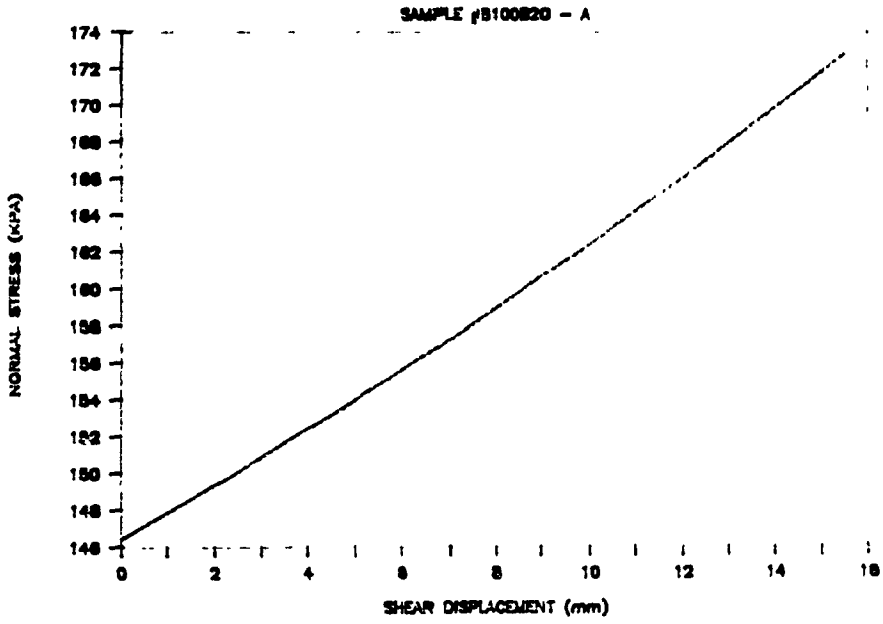
SAMPLE #B100B2O – A
NORMAL STRESS (kPA)
SHEAR DISPLACEMENT (mm)

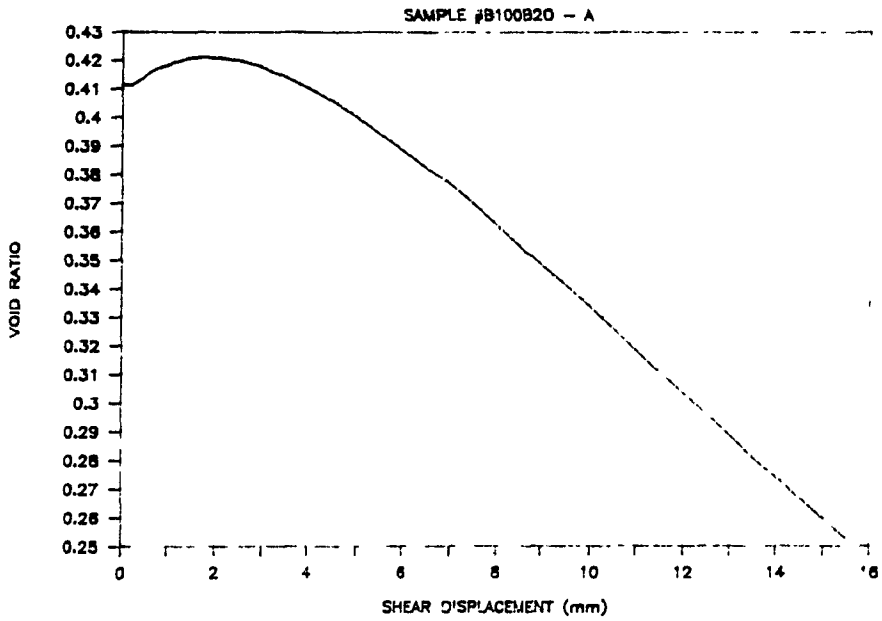
SAMPLE #B100B2O – A
VOID RATIO
SHEAR DISPLACEMENT (mm)

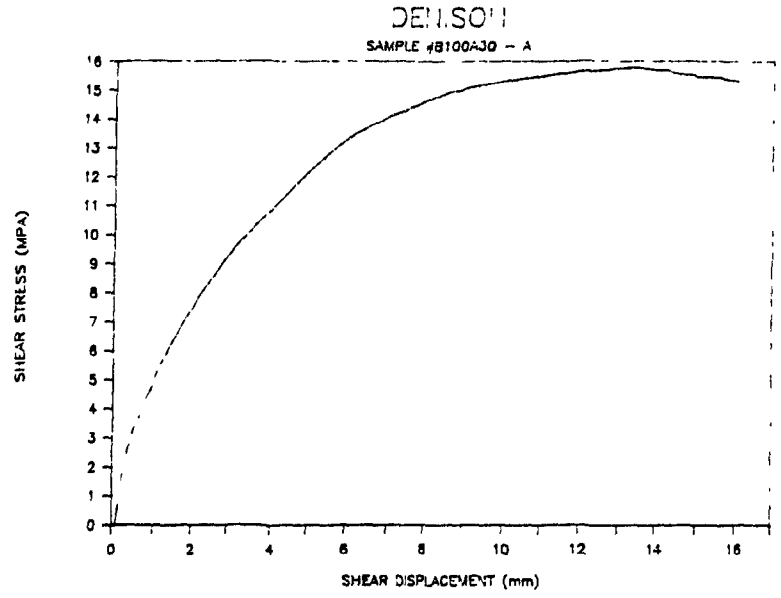
DENISON
SAMPLE #B100A30 – A
SHEAR STRESS (MPA)
SHEAR DISPLACEMENT (mm)

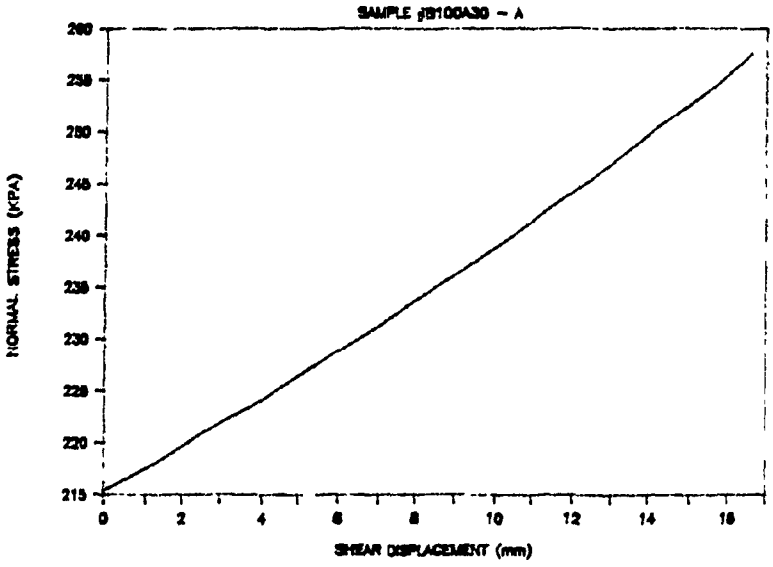
SAMPLE #B100A30 – A
NORMAL STRESS (KPA)
SHEAR DISPLACEMENT (mm)

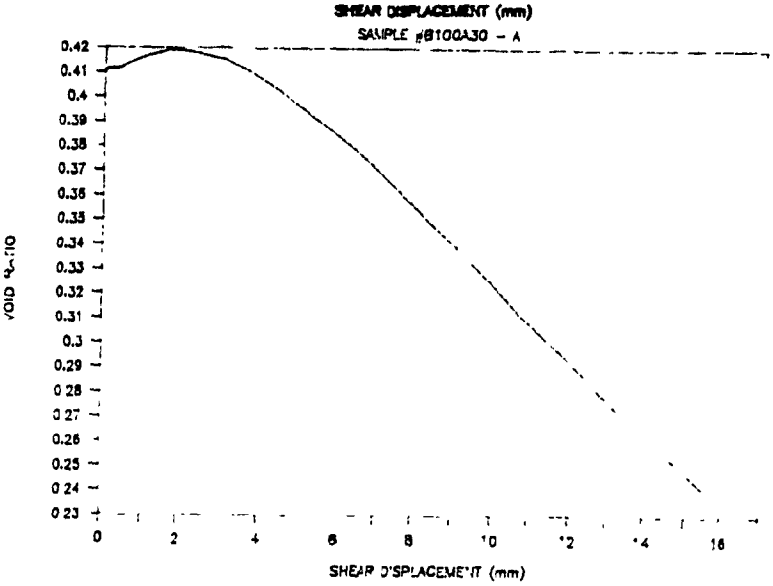
SAMPLE #B100A30 – A
SHEAR DISPLACEMENT (mm)

DENISON

SAMPLE #B100B30 - A

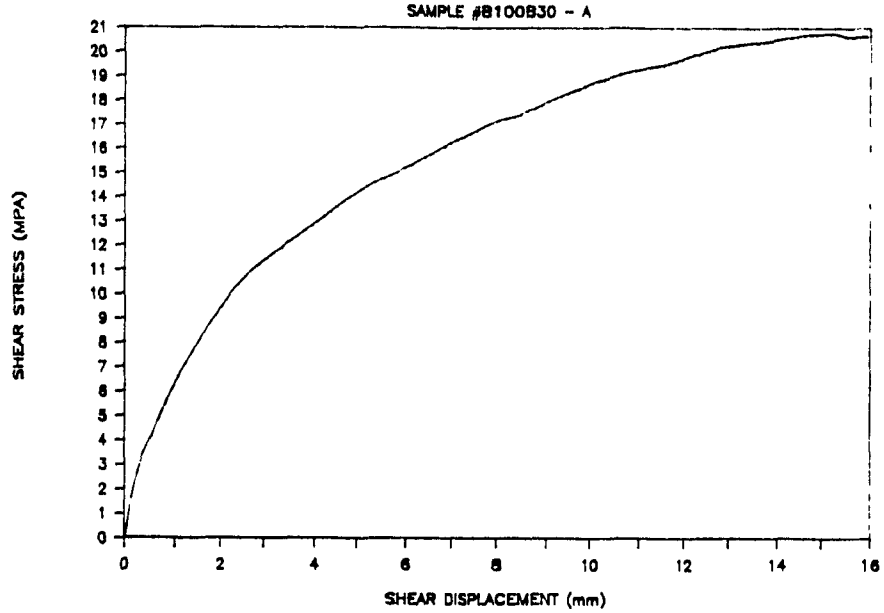

SAMPLE #B100B30 - A

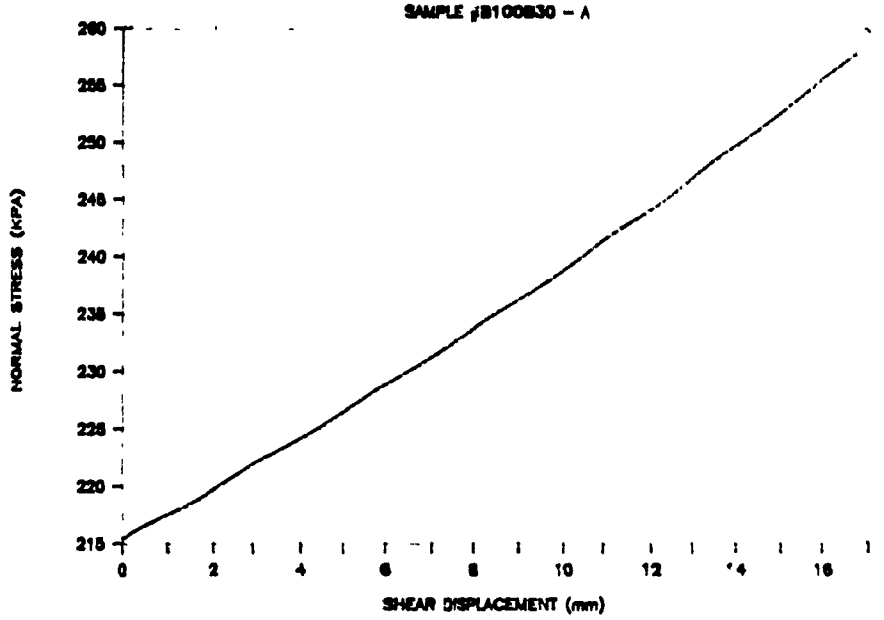

SAMPLE #B100B30 - A

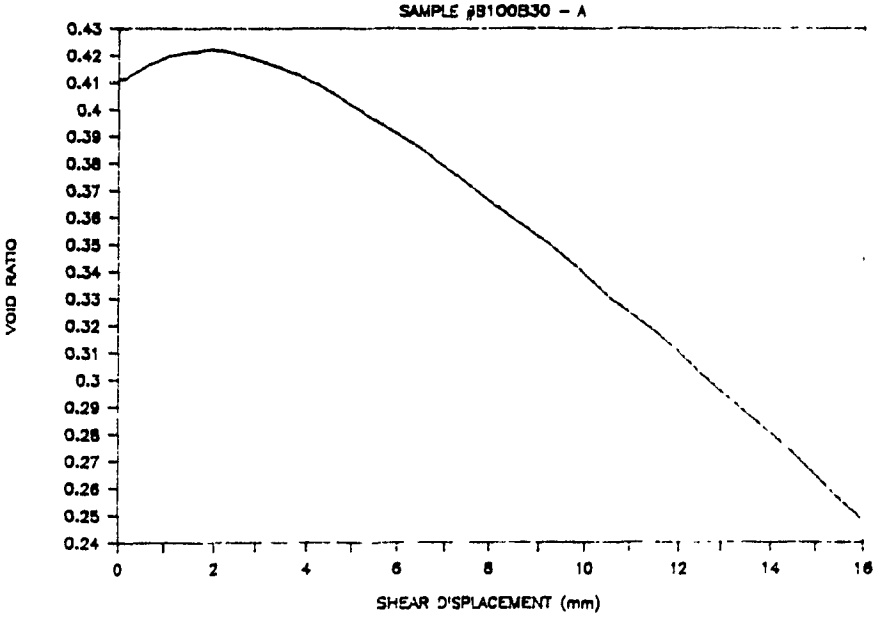

DENISON

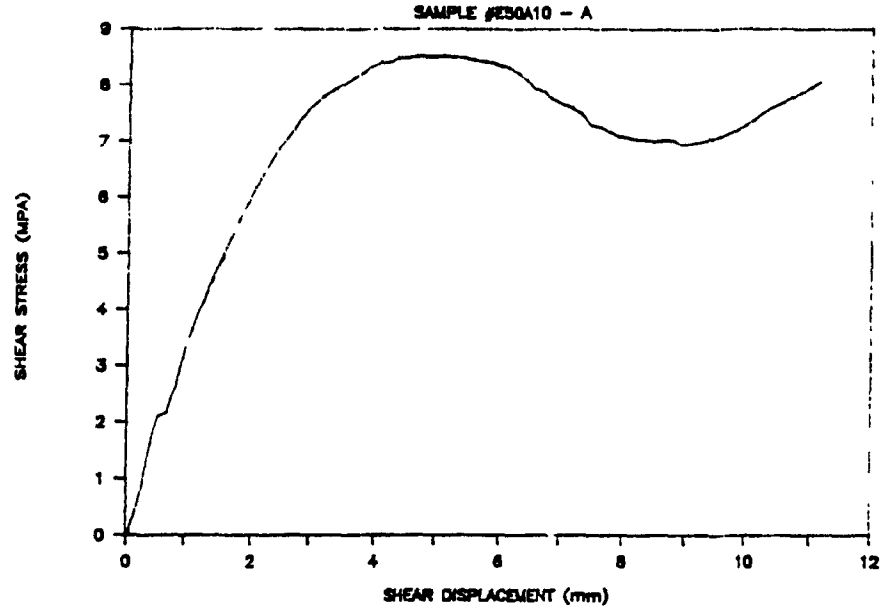
SAMPLE #E50A10 – A
SHEAR STRESS (MPA)
0
1
2
3
4
5
6
7
8
9
0
2
4
6
8
10
12
SHEAR DISPLACEMENT (mm)

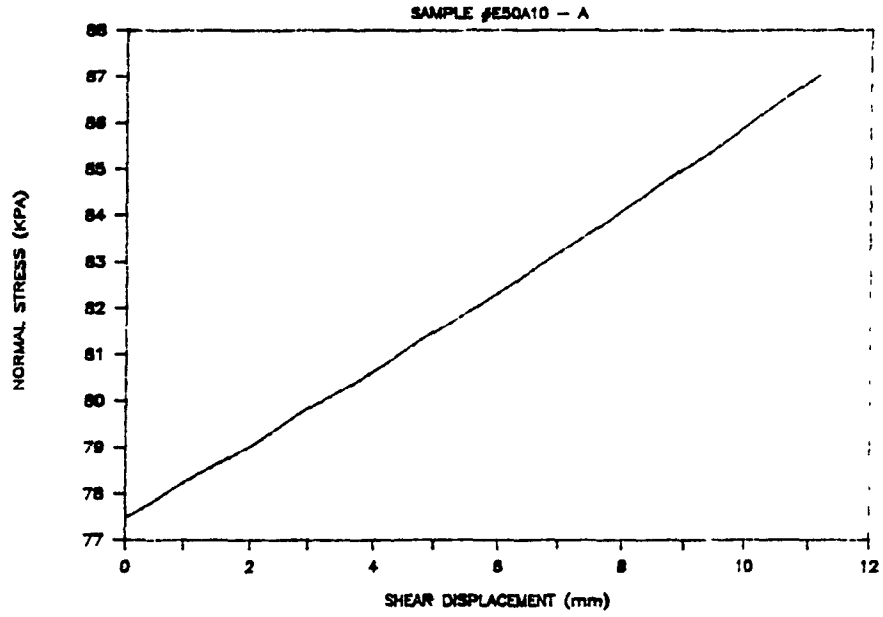
SAMPLE #E50A10 – A
NORMAL STRESS (KPA)
77
78
79
80
81
82
83
84
85
86
87
0
2
4
6
8
10
12
SHEAR DISPLACEMENT (mm)

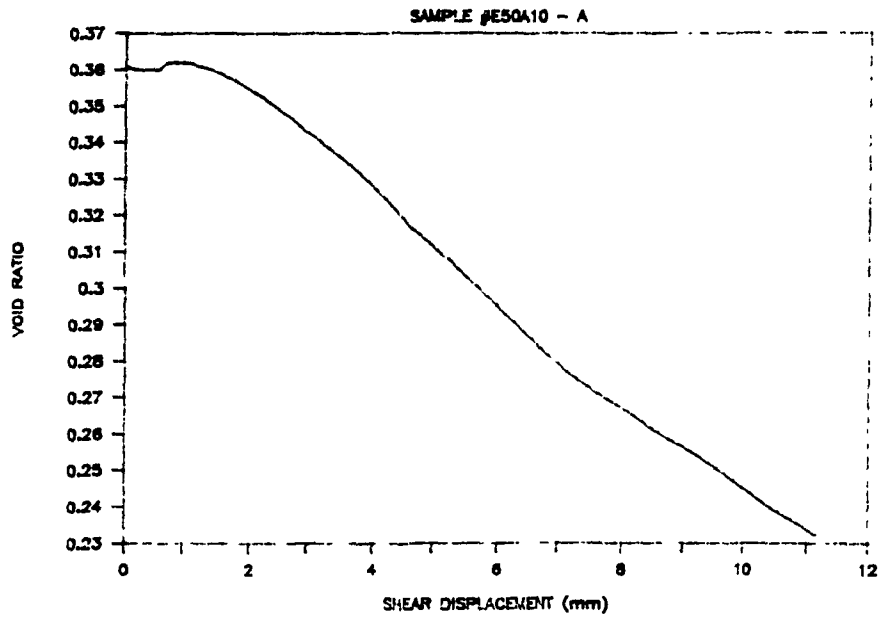
SAMPLE #E50A10 – A
VOID RATIO
0.23
0.24
0.25
0.26
0.27
0.28
0.29
0.3
0.31
0.32
0.33
0.34
0.35
0.36
0.37
0
2
4
6
8
10
12
SHEAR DISPLACEMENT (mm)

DENISON

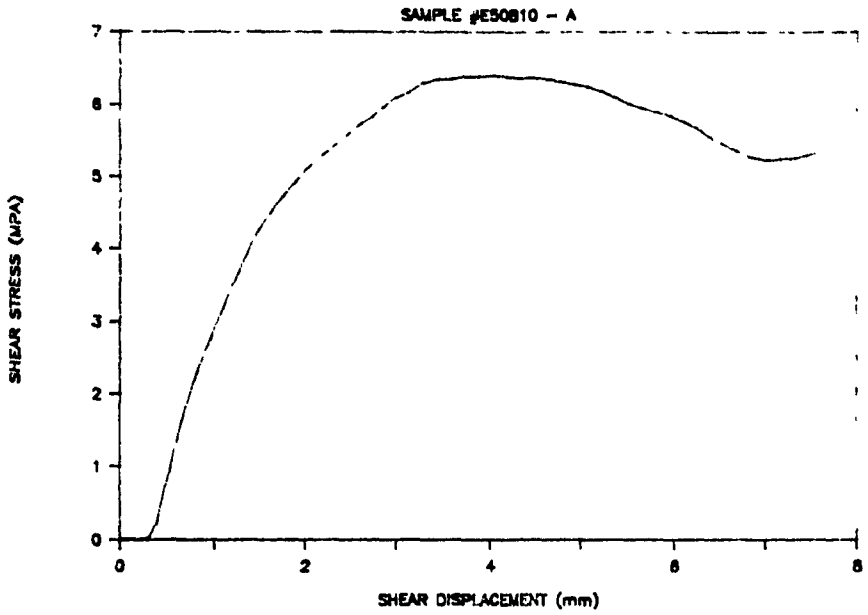
SAMPLE #E50B10 – A
SHEAR STRESS (MPA)
0
1
2
3
4
5
6
7
0
2
4
6
8
SHEAR DISPLACEMENT (mm)

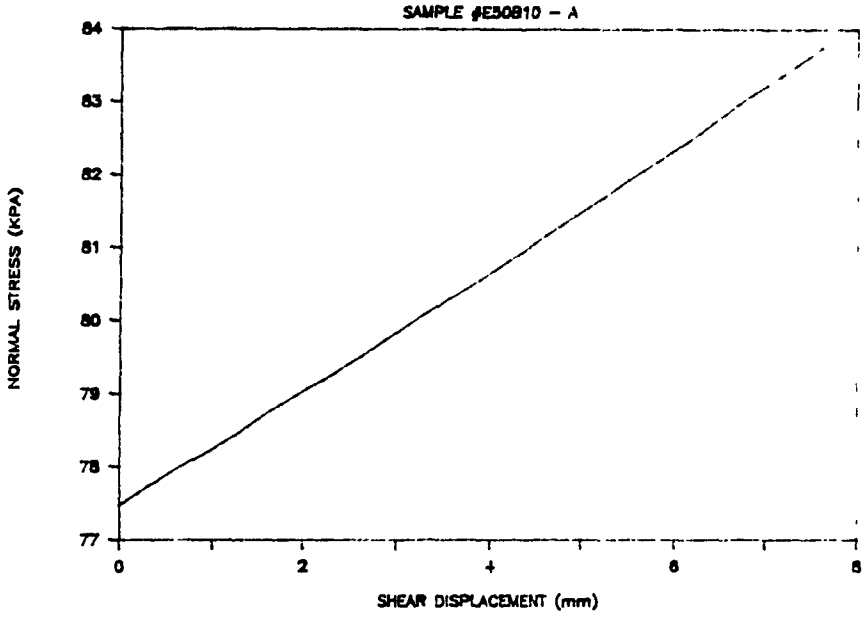
SAMPLE #E50B10 – A
NORMAL STRESS (KPA)
77
78
79
80
81
82
83
84
0
2
4
6
8
SHEAR DISPLACEMENT (mm)

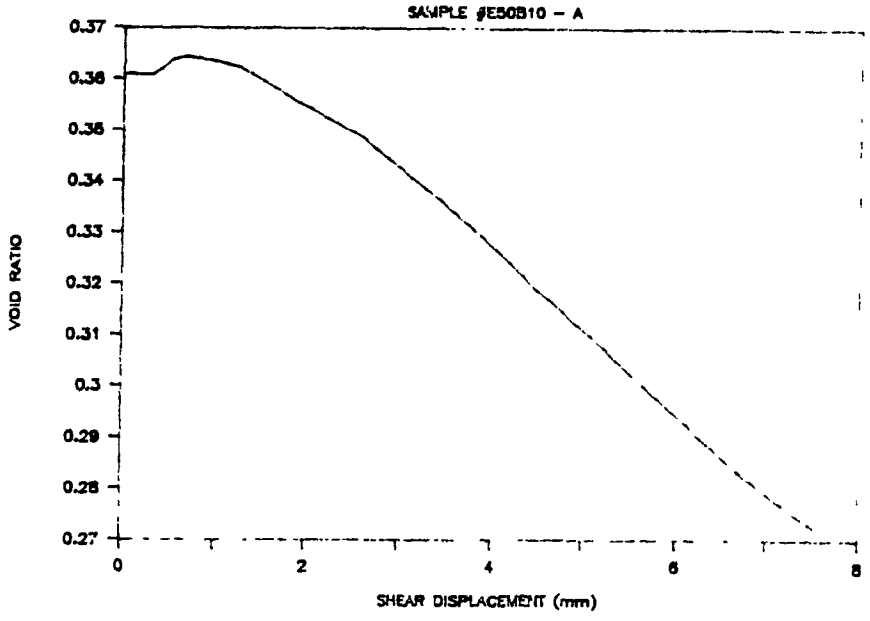
SAMPLE #E50B10 – A
VOID RATIO
0.27
0.28
0.29
0.3
0.31
0.32
0.33
0.34
0.35
0.36
0.37
0
2
4
6
8
SHEAR DISPLACEMENT (mm)

DENISON

SAMPLE #E50A20 – A

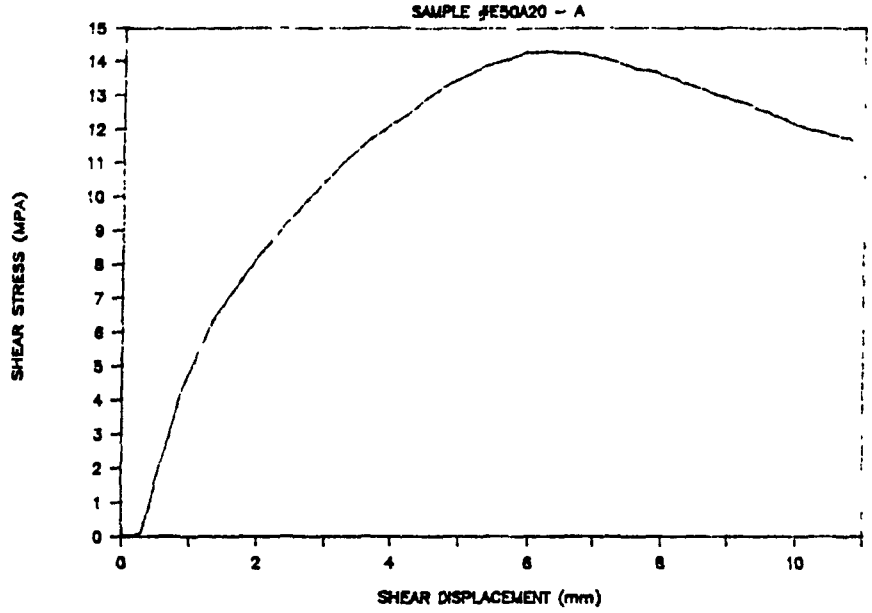

SAMPLE #E50A20 – A

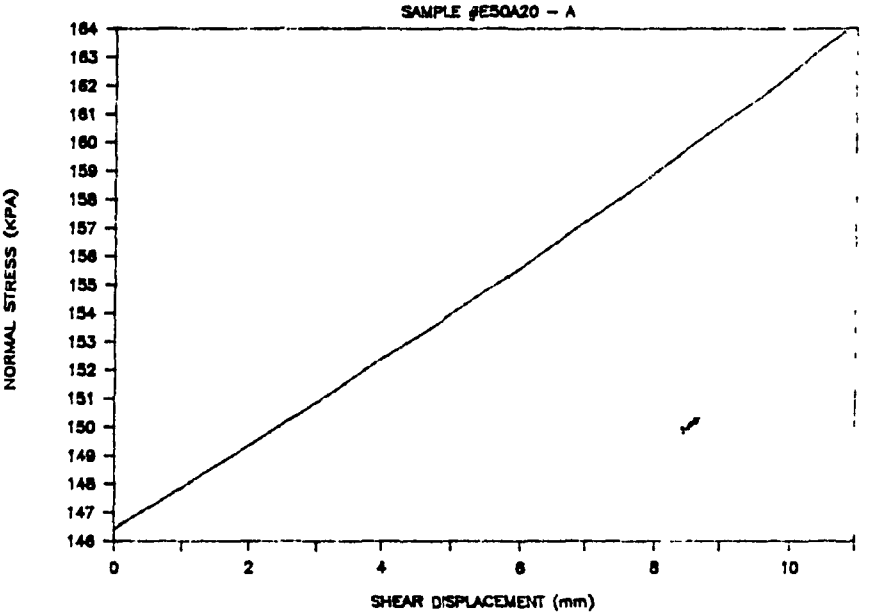

SAMPLE #E50A20 – A

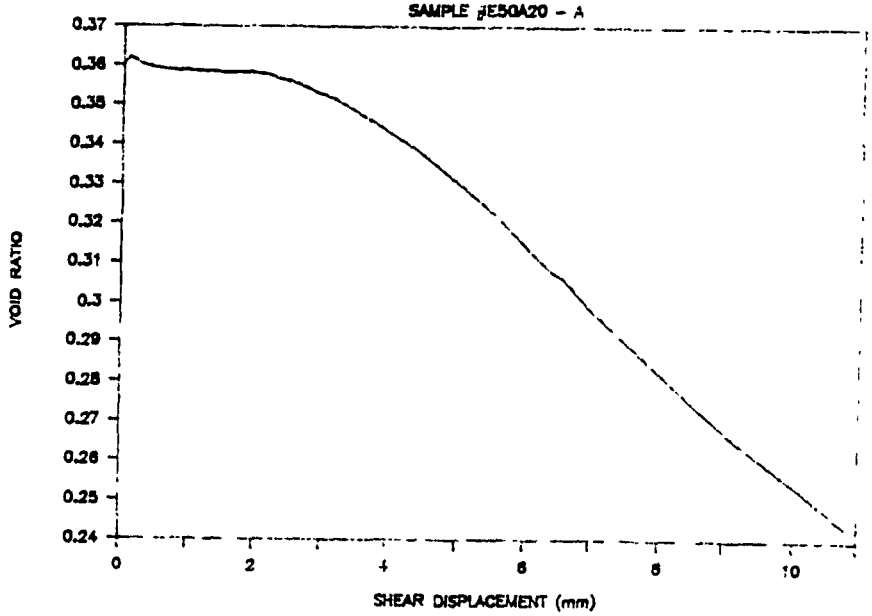

DENISON

SAMPLE #E50B20 – A

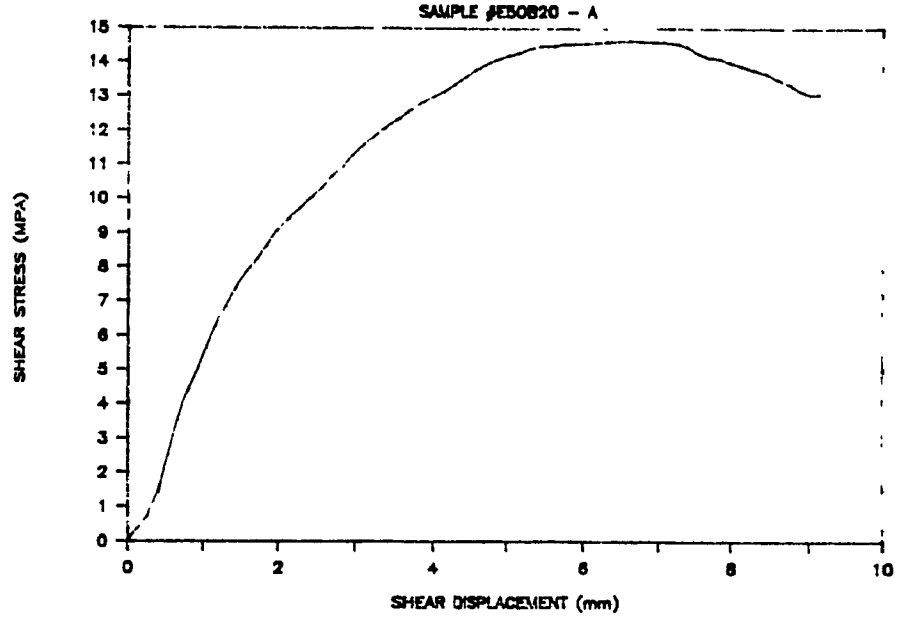

SAMPLE #E50B20 – A

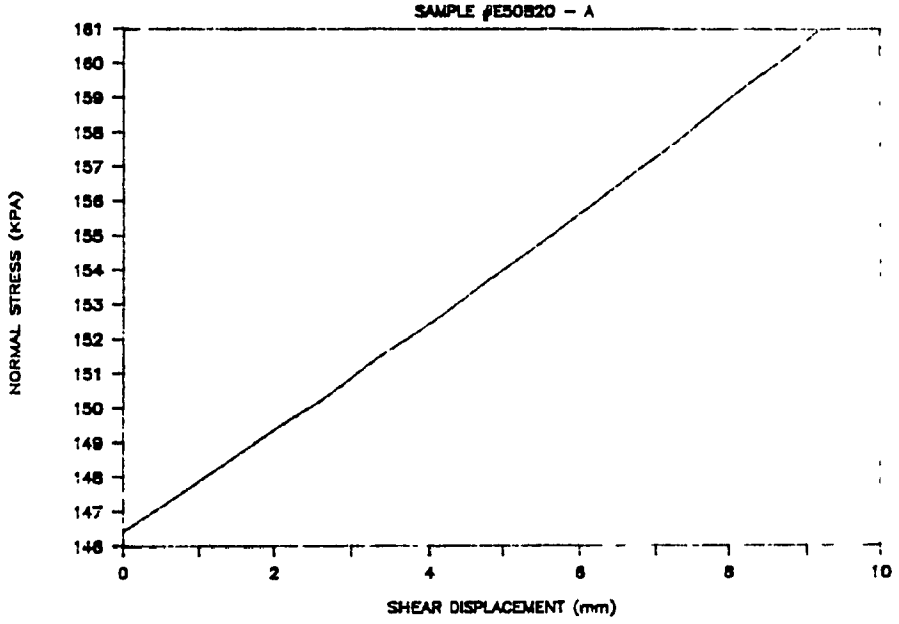

SAMPLE #E50B20 – A

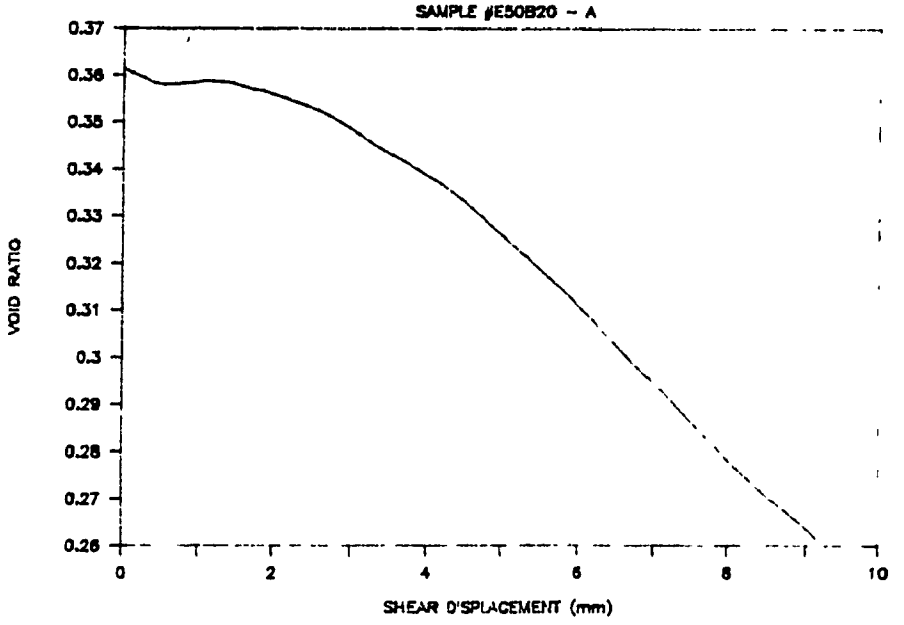

DENISON

SAMPLE #E50A30 – A

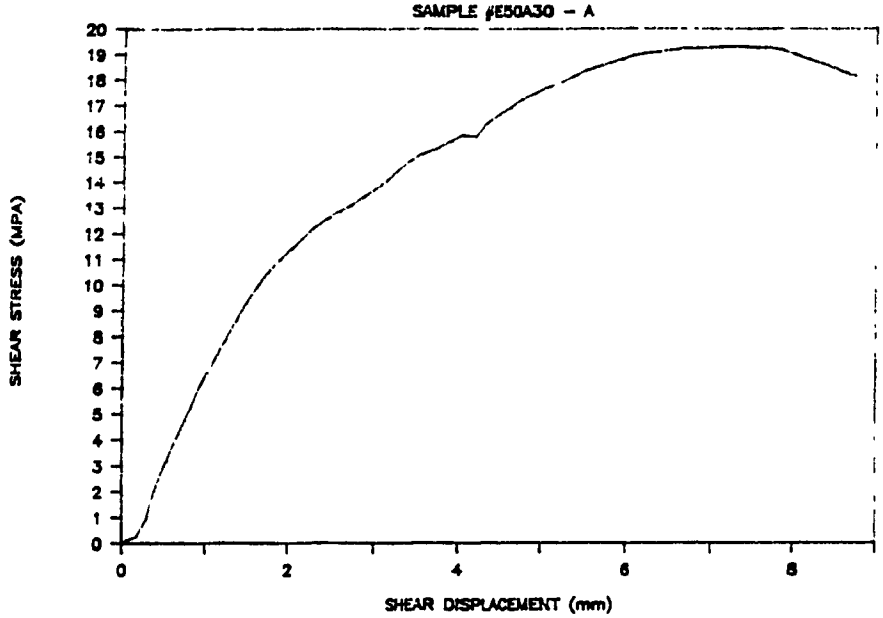

SAMPLE #E50A30 – A

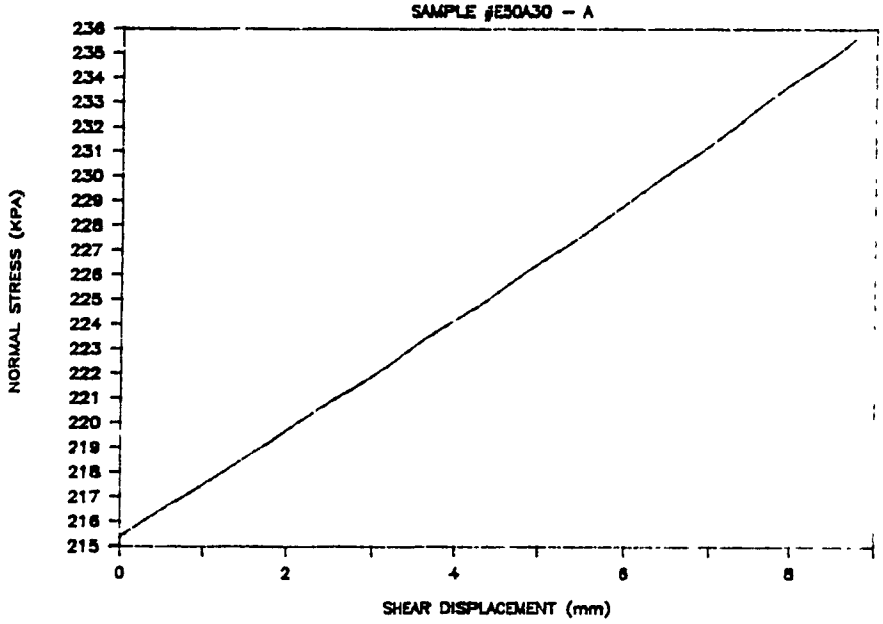

SAMPLE #E50A30 – A

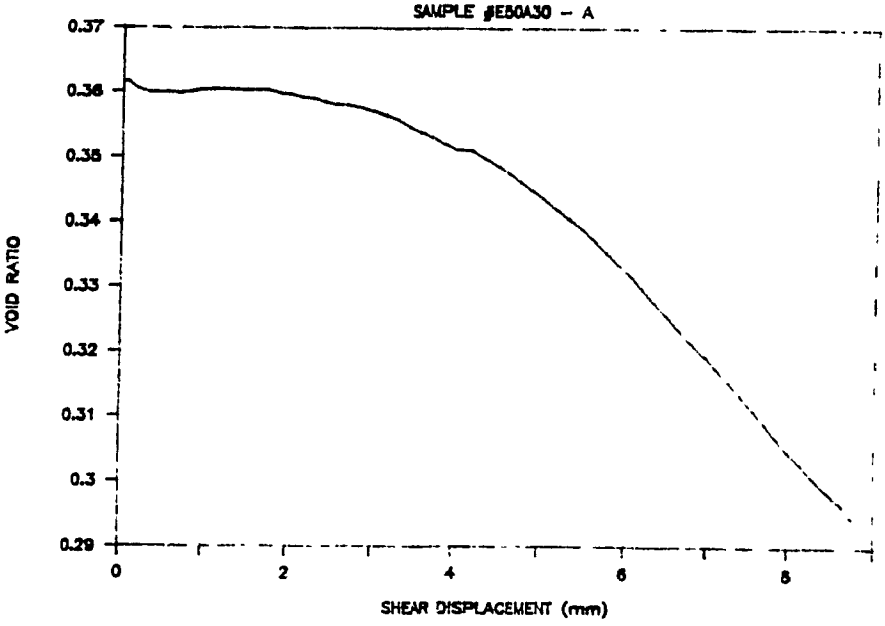

DENISON

SAMPLE #E50830 – A

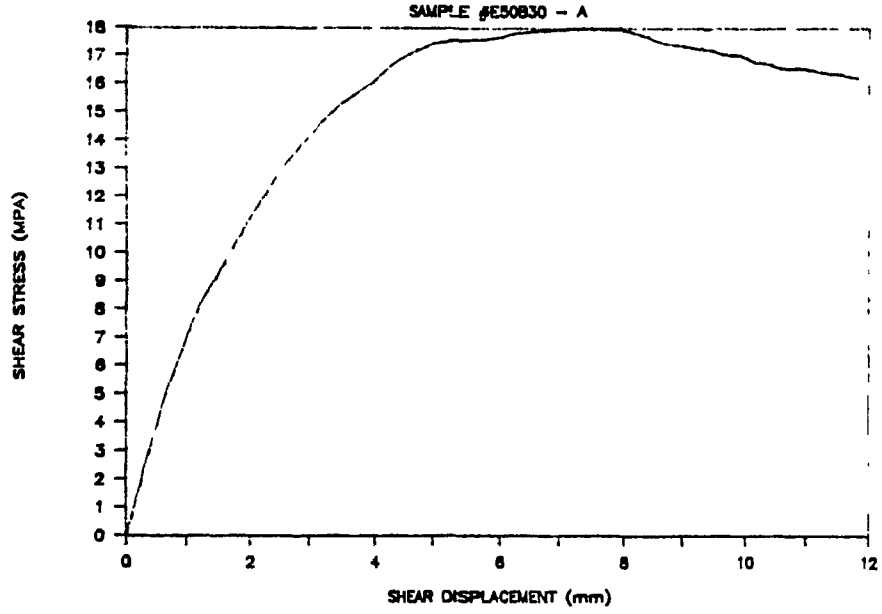

SAMPLE #E50830 – A

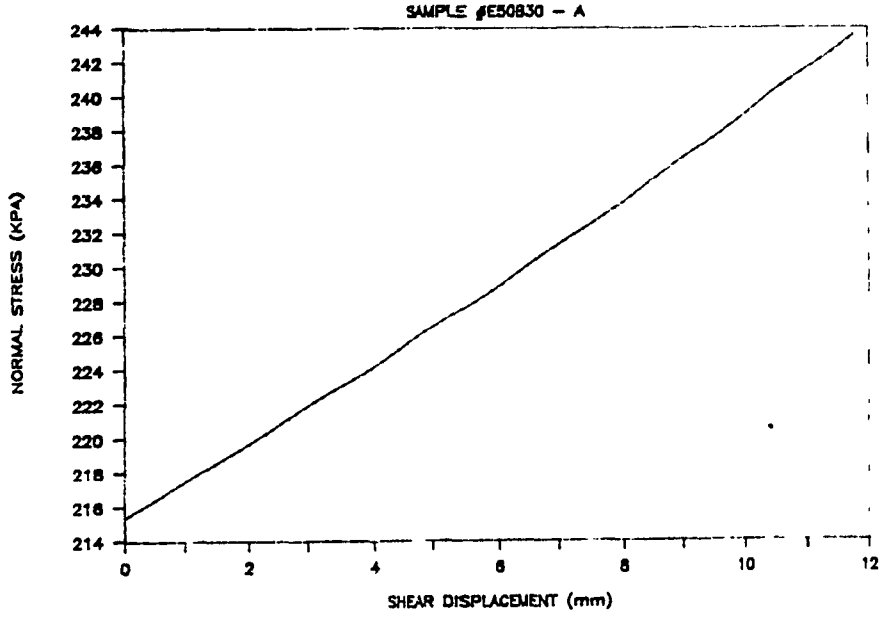

SAMPLE #E50830 – A

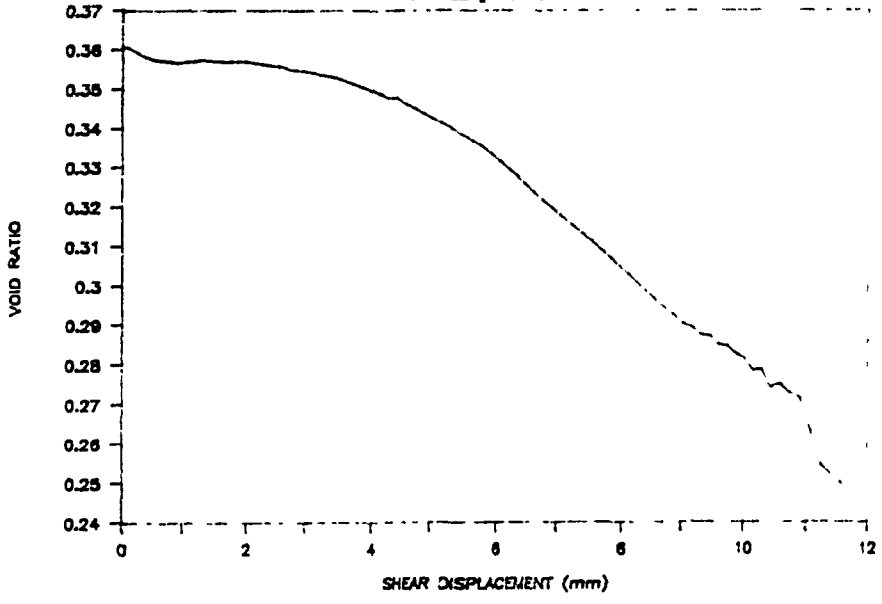

DENISON

SAMPLE #A50A10 – A

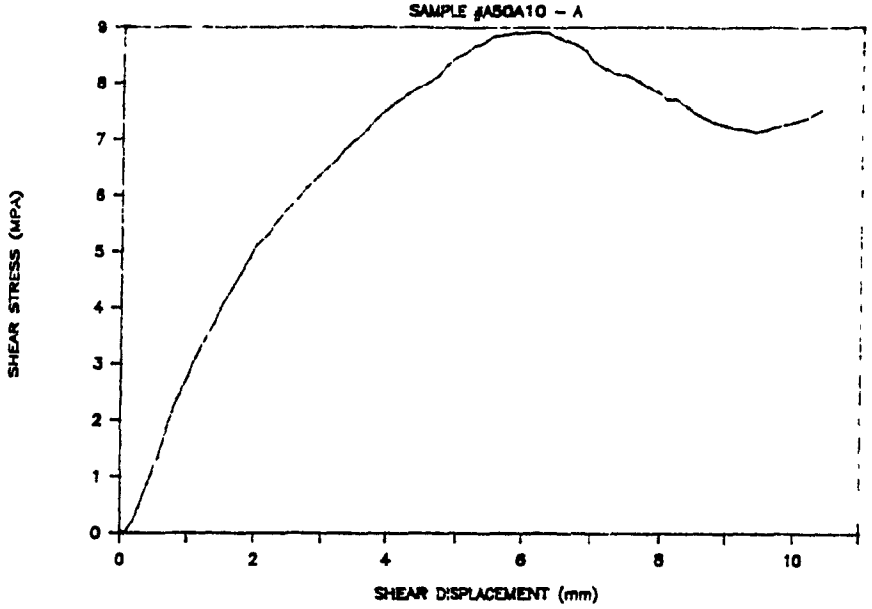

SAMPLE #A50A10 – A

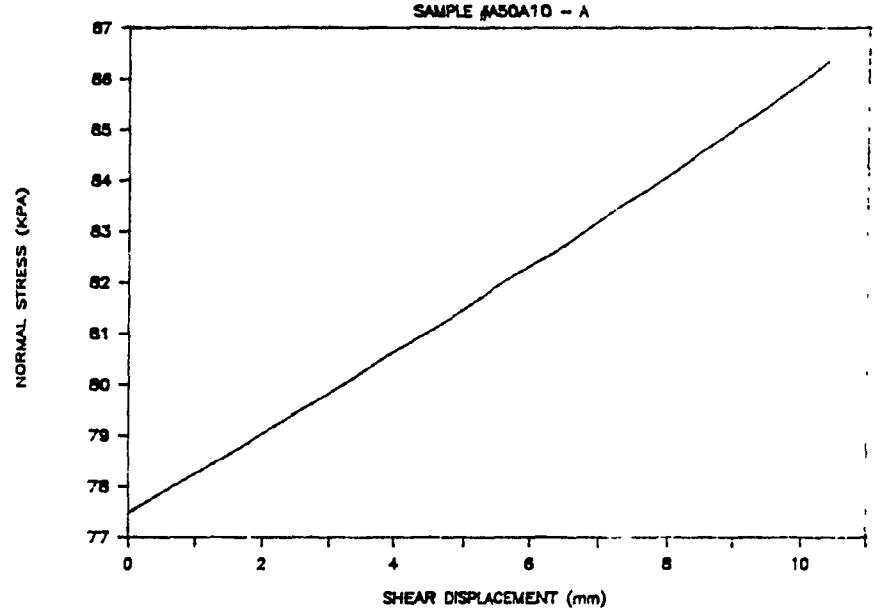

SAMPLE #A50A10 – A

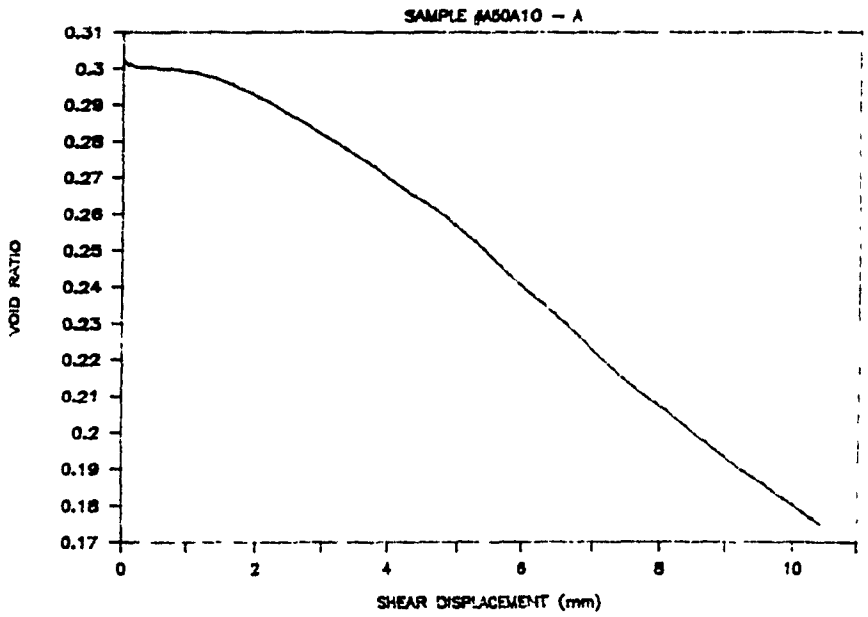

DENISON

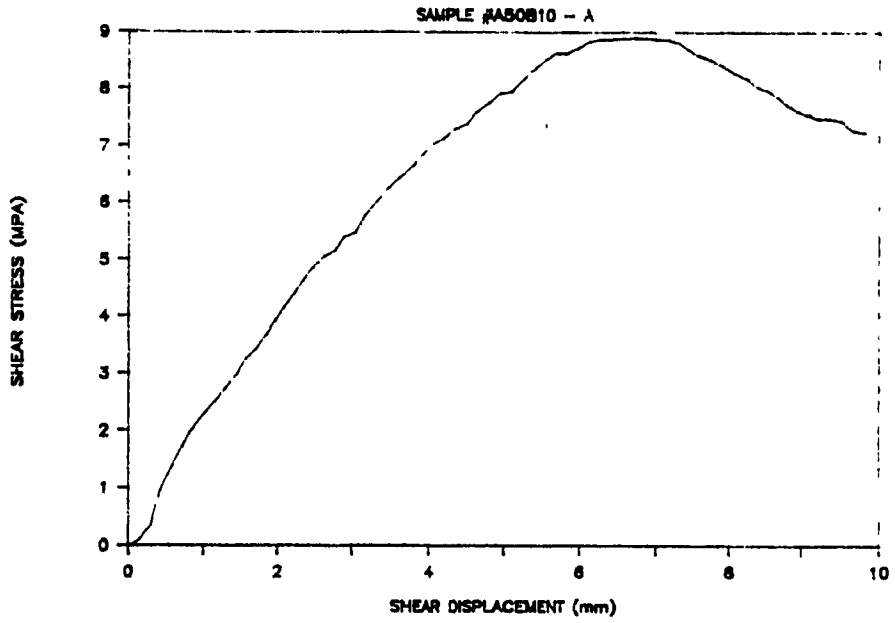
SAMPLE #A50B10 - A
SHEAR STRESS (MPA)
0
1
2
3
4
5
6
7
8
9
0
2
4
6
8
10
SHEAR DISPLACEMENT (mm)

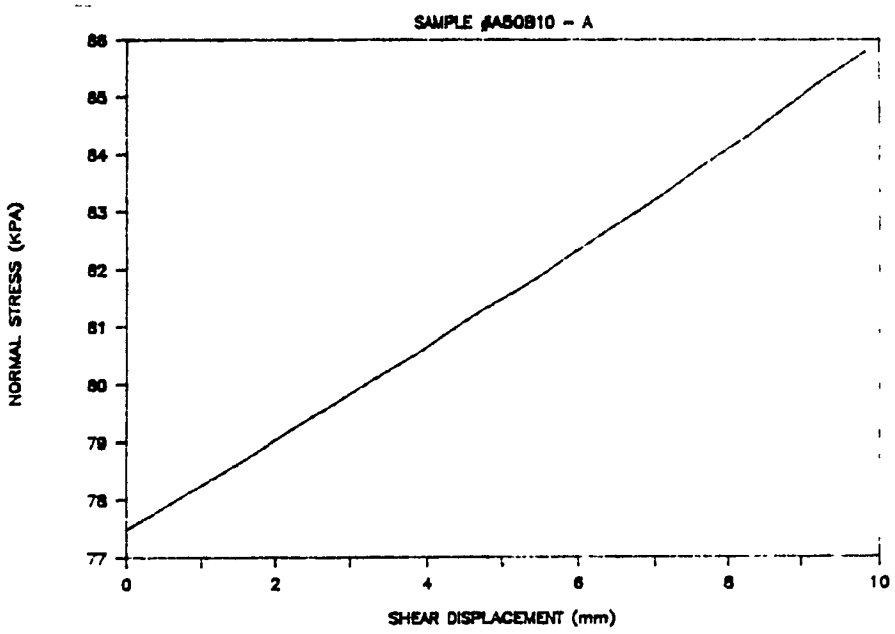
SAMPLE #A50B10 - A
NORMAL STRESS (KPA)
77
78
79
80
81
82
83
84
85
86
0
2
4
6
8
10
SHEAR DISPLACEMENT (mm)

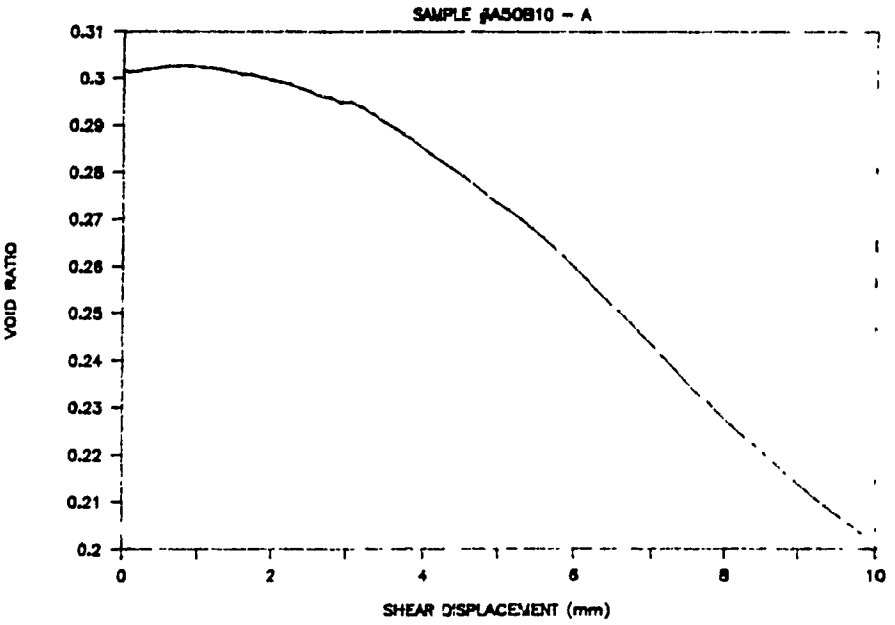
SAMPLE #A50B10 - A
VOID RATIO
0.2
0.21
0.22
0.23
0.24
0.25
0.26
0.27
0.28
0.29
0.3
0.31
0
2
4
6
8
10
SHEAR DISPLACEMENT (mm)

DENISON

SAMPLE #A50A20 – A

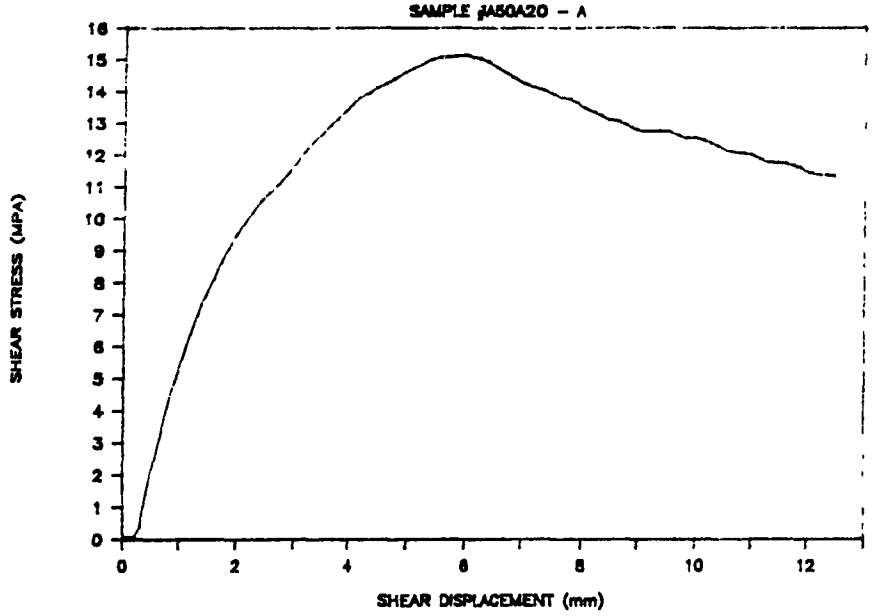

SAMPLE #A50A20 – A

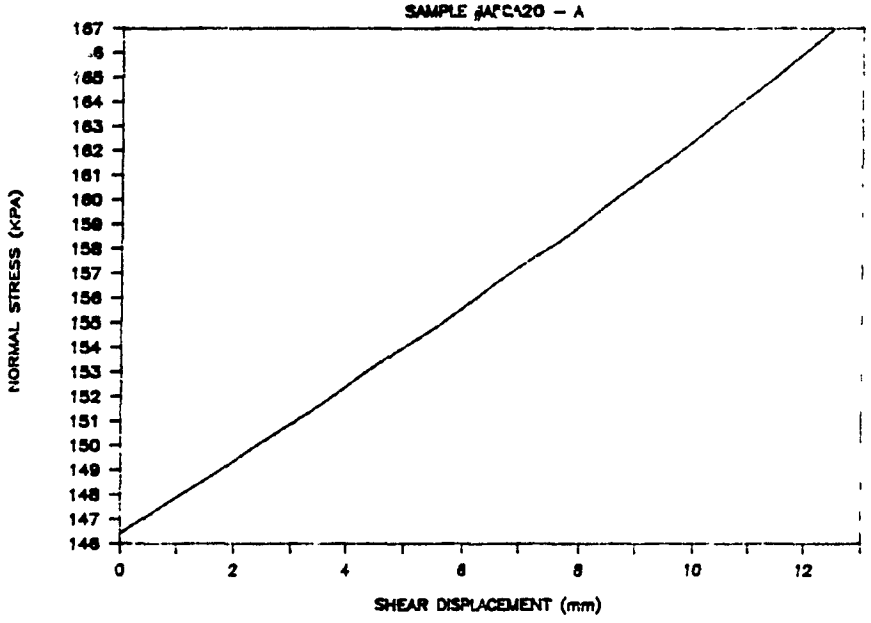

SAMPLE #A50A20 – A

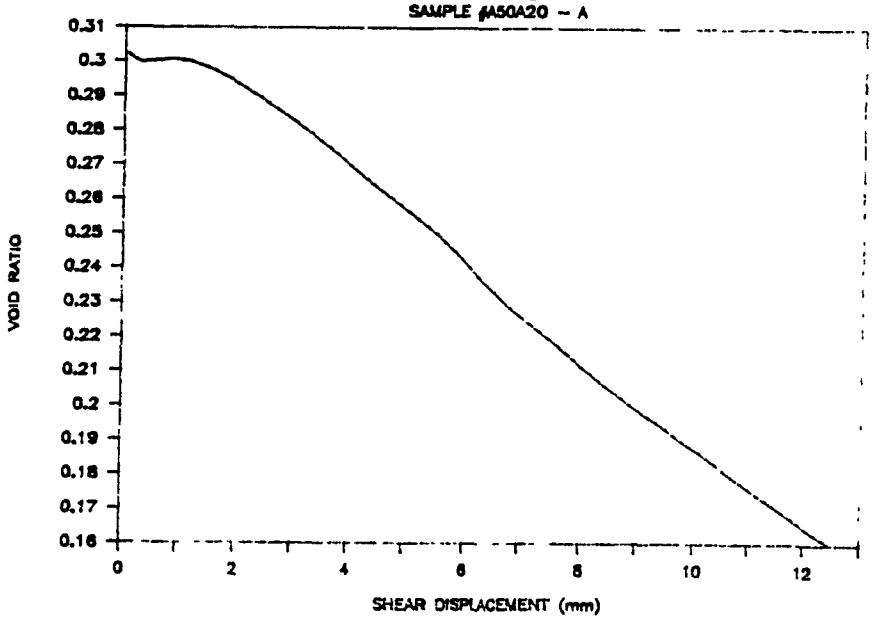

DENISON

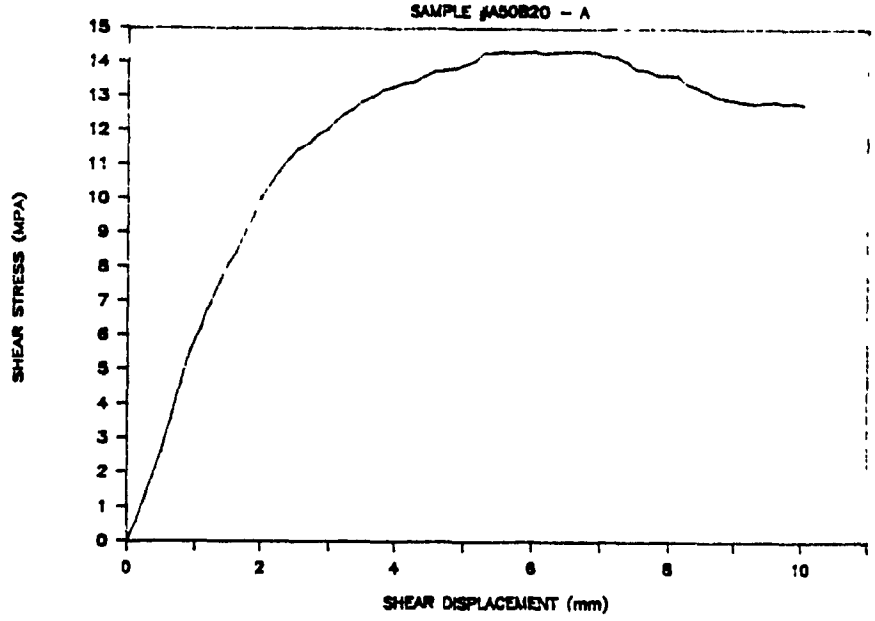
SAMPLE #A50820 – A
SHEAR STRESS (MPA)
SHEAR DISPLACEMENT (mm)

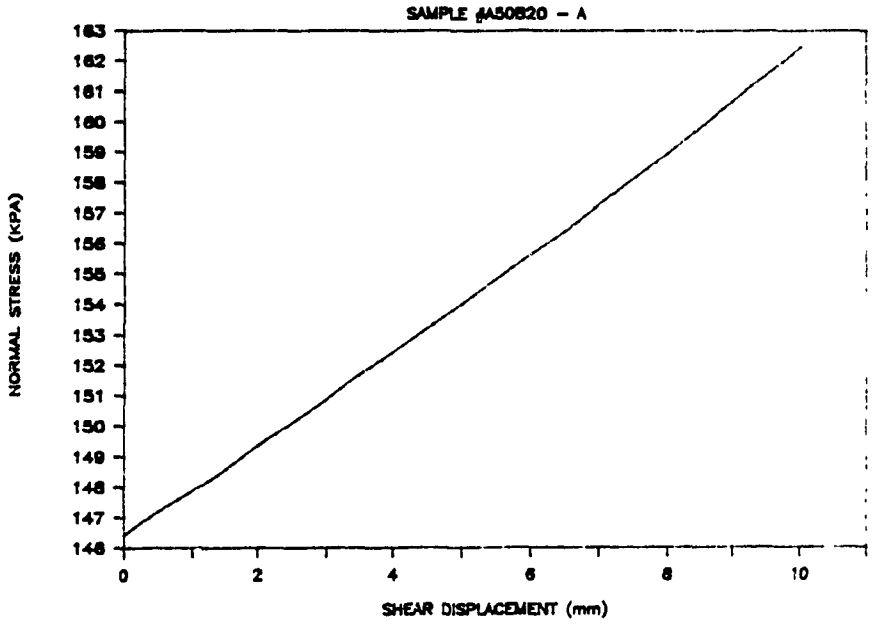
SAMPLE #A50820 – A
NORMAL STRESS (KPA)
SHEAR DISPLACEMENT (mm)

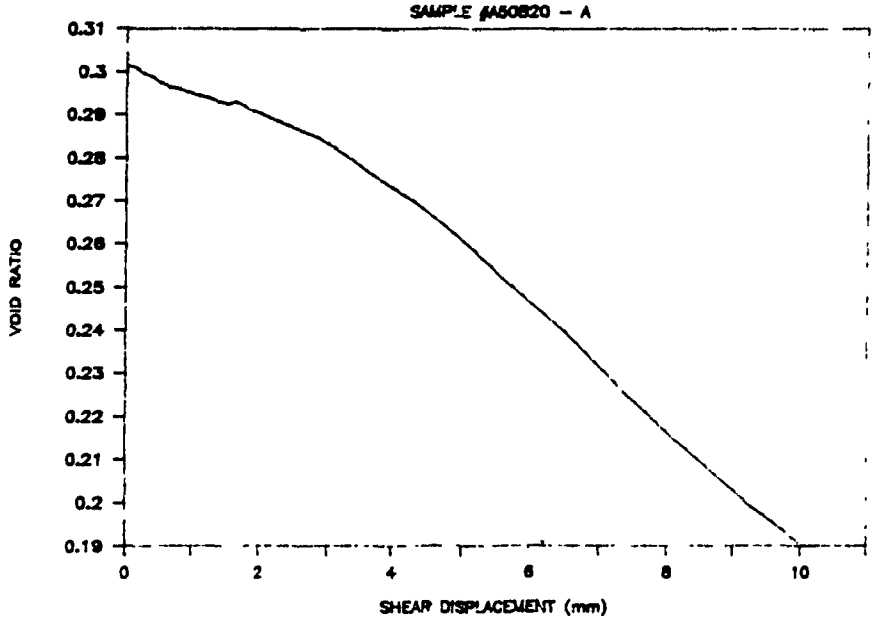
SAMPLE #A50820 – A
VOID RATIO
SHEAR DISPLACEMENT (mm)

DENISON

SAMPLE #A50A30 – A

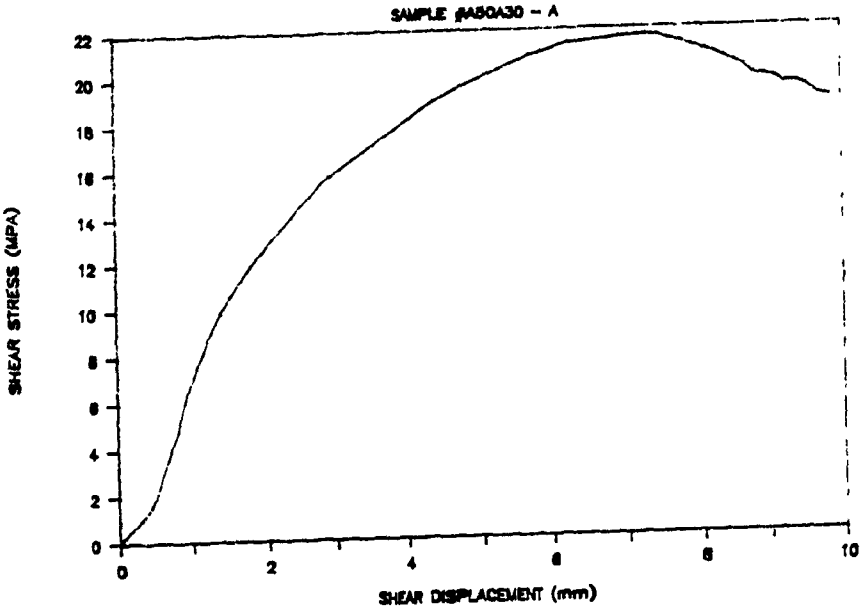

SAMPLE #A50A30 – A

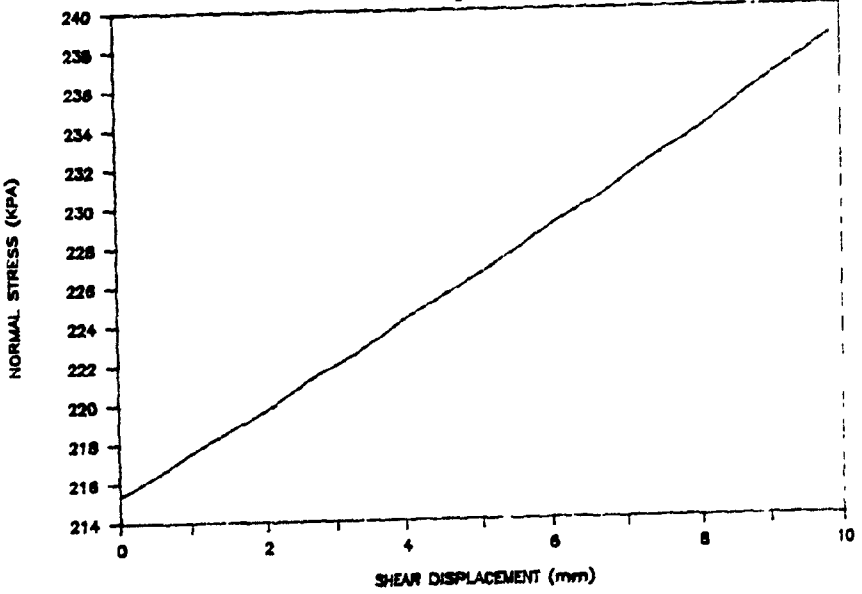

SAMPLE #A50A30 – A

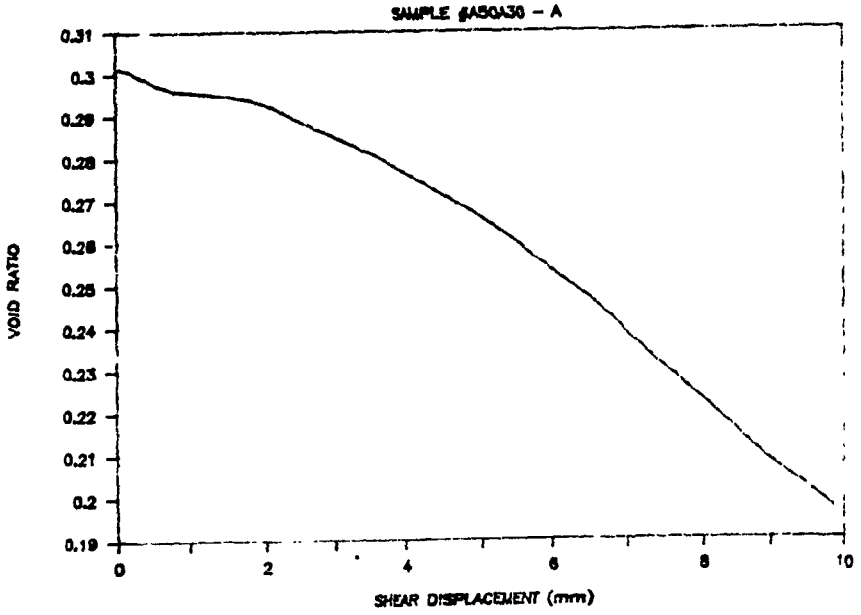

DENISON

SAMPLE #A50830 - A

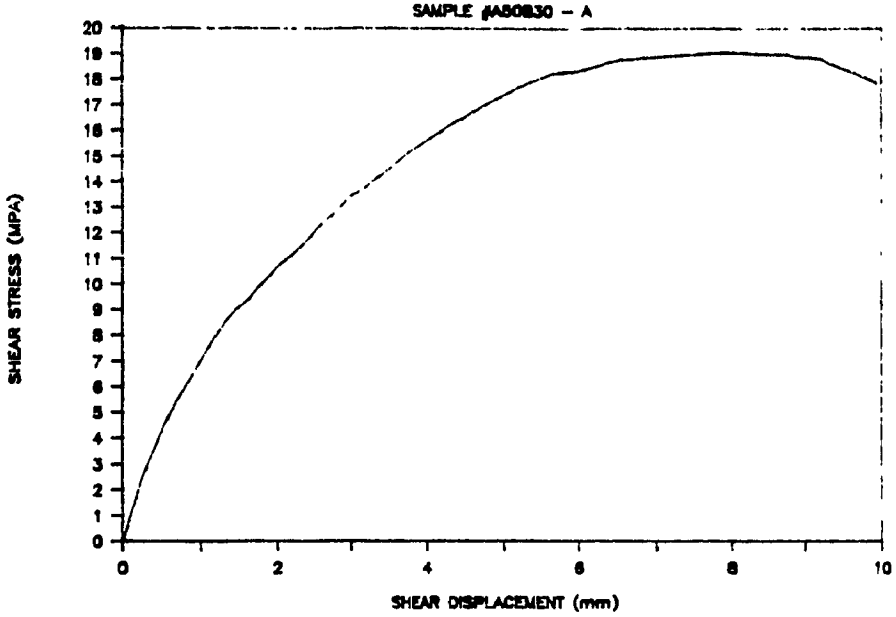

SAMPLE #A50830 - A

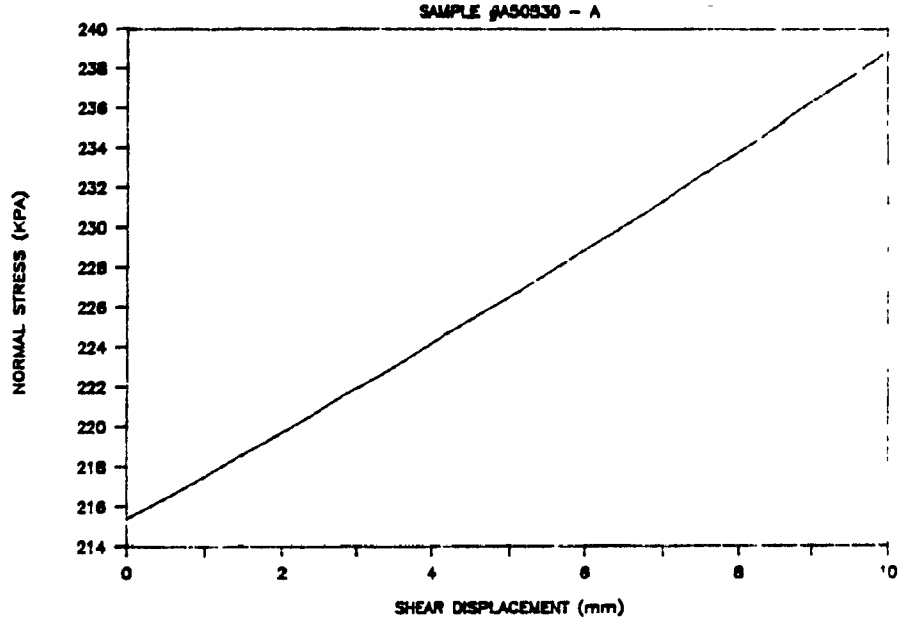

SAMPLE #A50830 - A

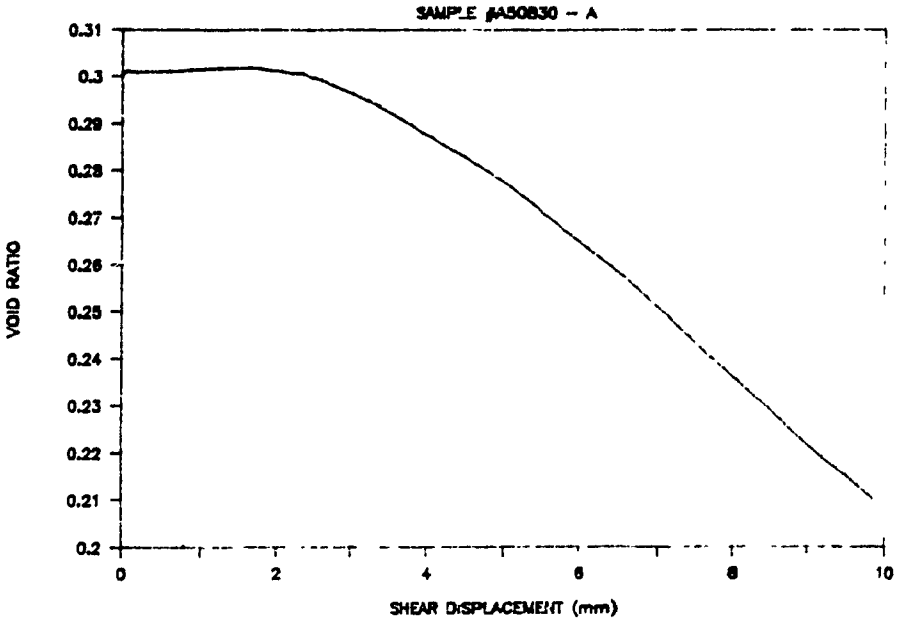

DENISON

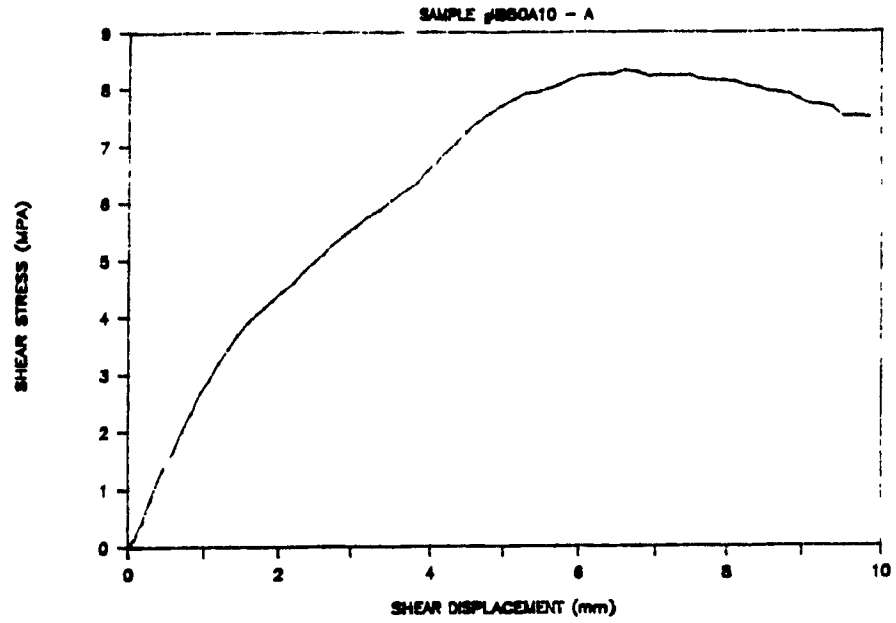
SAMPLE #BSOA10 – A
SHEAR STRESS (MPA)
0
1
2
3
4
5
6
7
8
9
0
2
4
6
8
10
SHEAR DISPLACEMENT (mm)

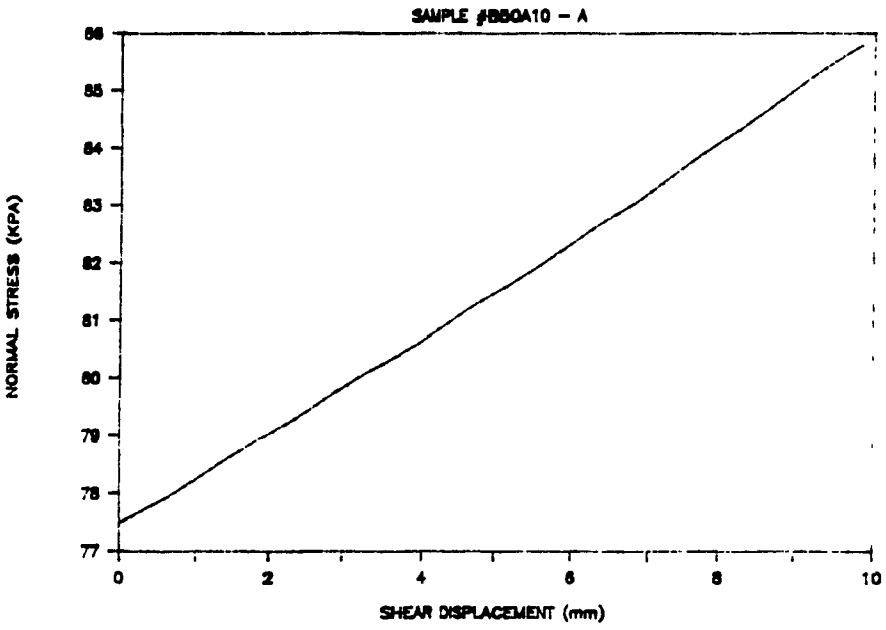
SAMPLE #BSOA10 – A
NORMAL STRESS (KPA)
77
78
79
80
81
82
83
84
85
86
0
2
4
6
8
10
SHEAR DISPLACEMENT (mm)

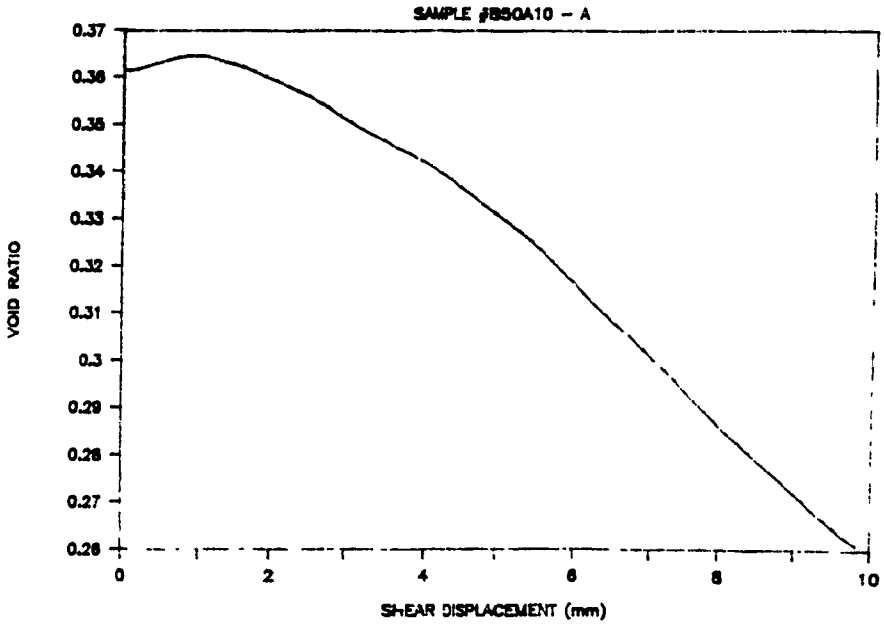
SAMPLE #BSOA10 – A
VOID RATIO
0.26
0.27
0.28
0.29
0.3
0.31
0.32
0.33
0.34
0.35
0.36
0.37
0
2
4
6
8
10
SHEAR DISPLACEMENT (mm)

DENISON

SAMPLE #B60B10 – A

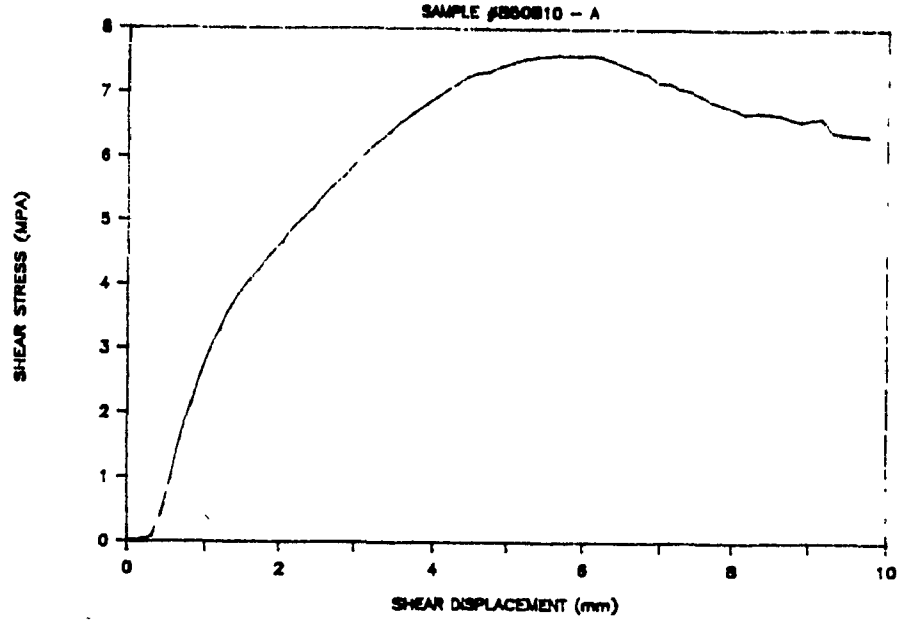

SAMPLE #B60B10 – A

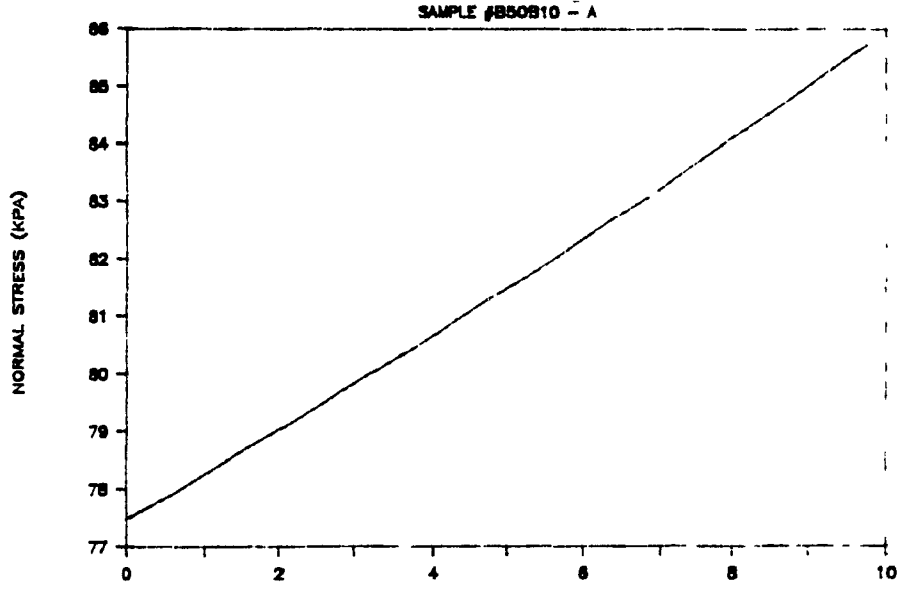

SAMPLE #B60B10 – A

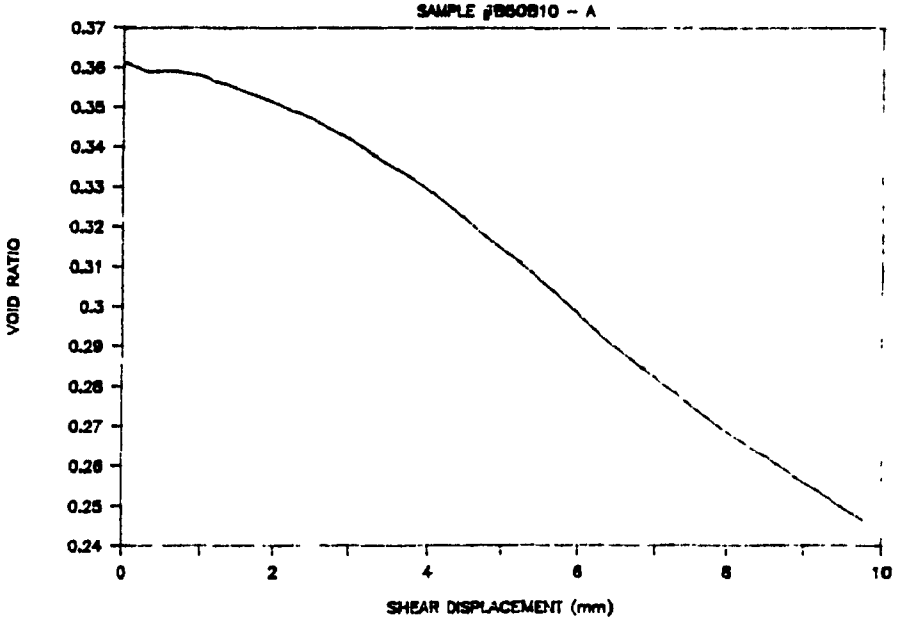

DENISON

SAMPLE #B50A20 – A

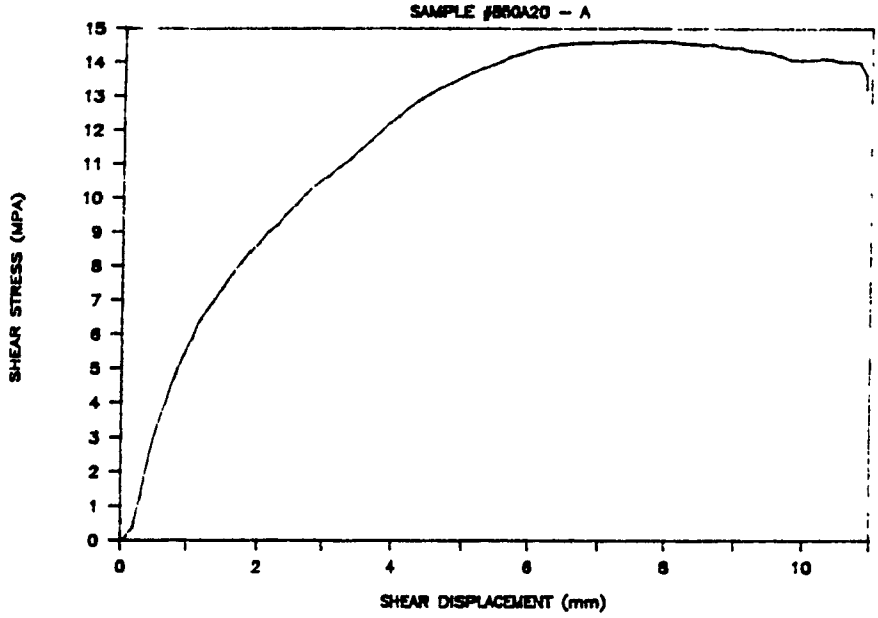

SAMPLE #B50A20 – A

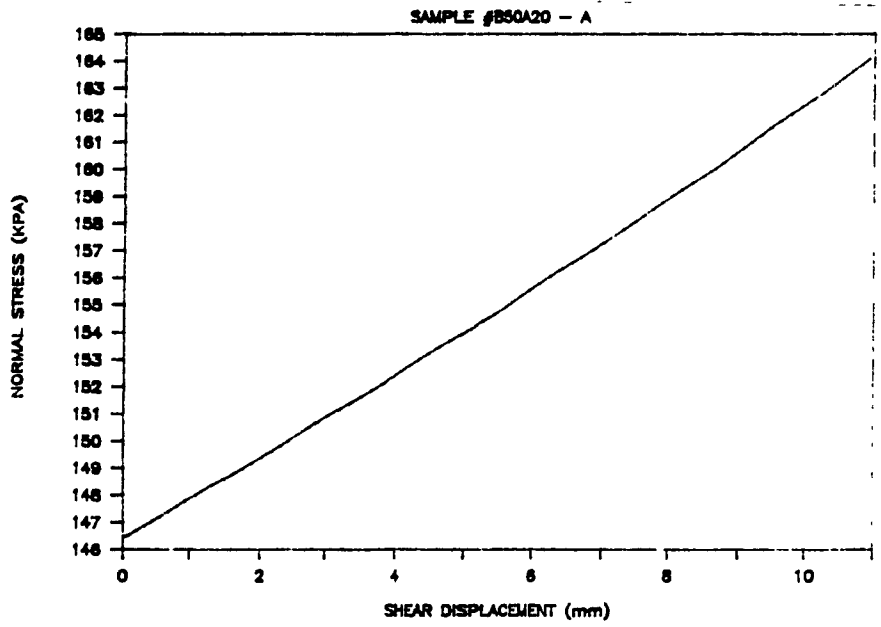

SAMPLE #B50A20 – A

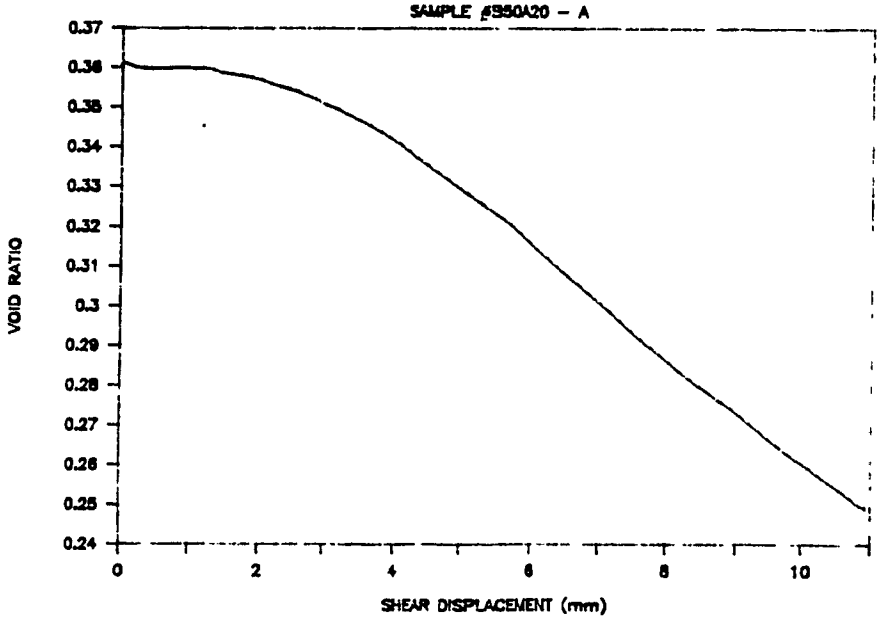

DENISON

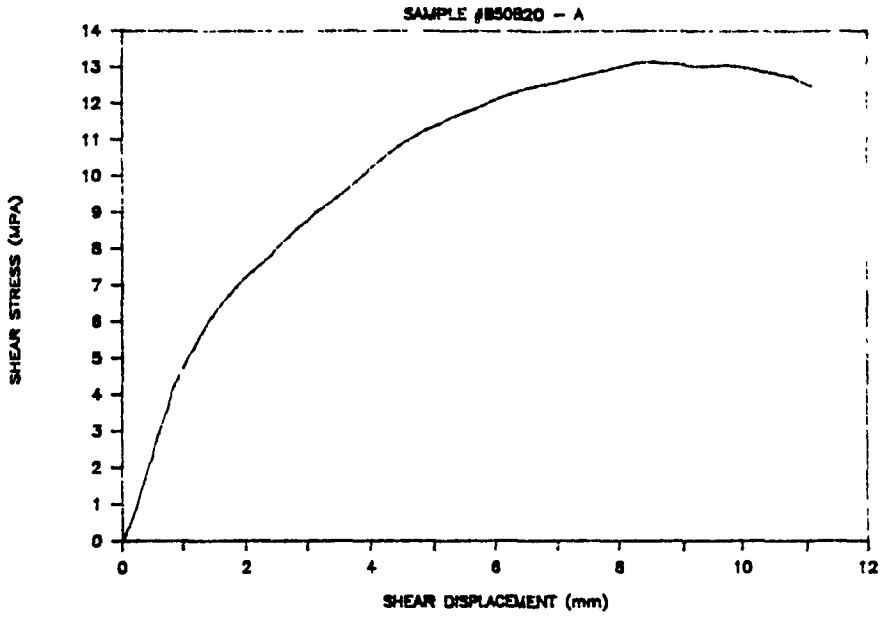
SAMPLE #850820 – A
SHEAR STRESS (MPA)
SHEAR DISPLACEMENT (mm)

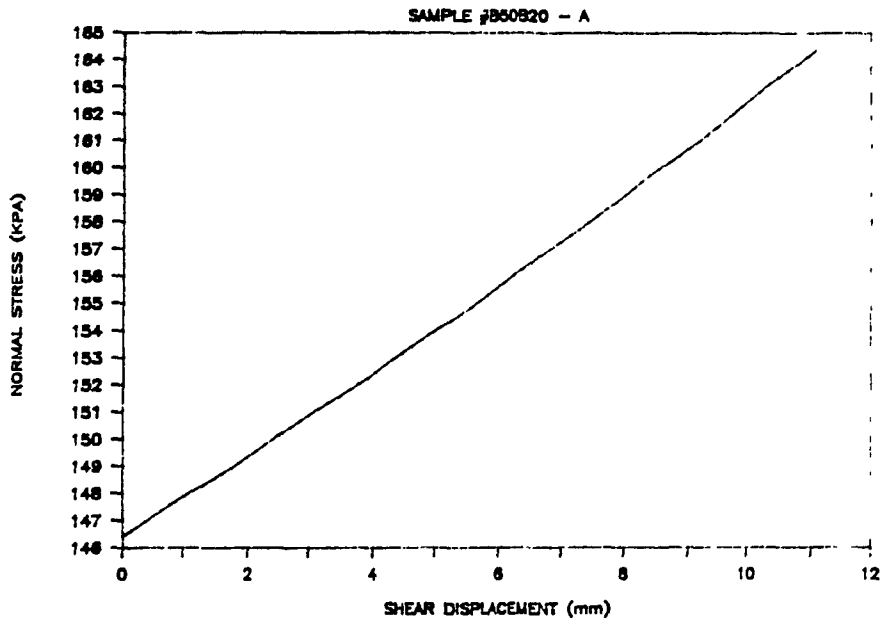
SAMPLE #850820 – A
NORMAL STRESS (KPA)
SHEAR DISPLACEMENT (mm)

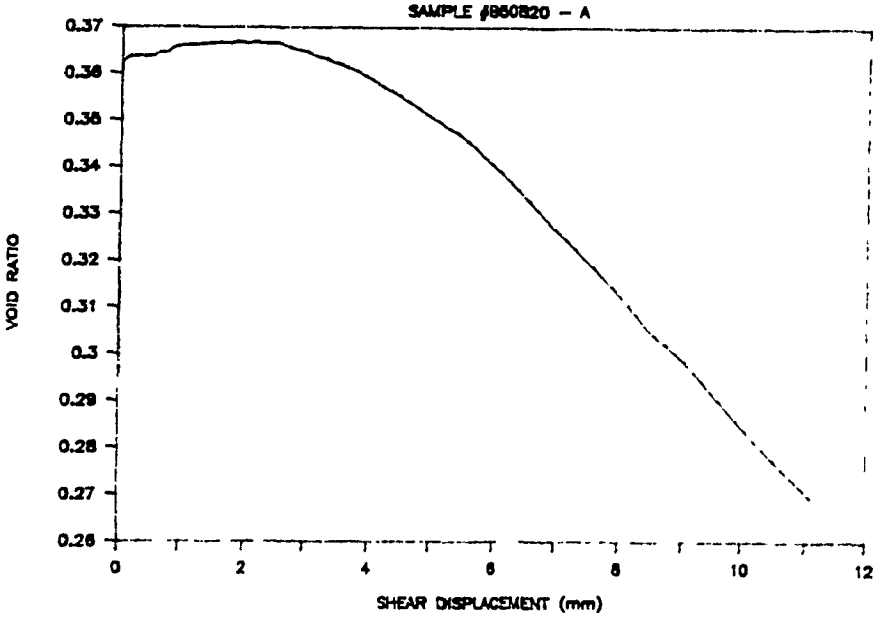
SAMPLE #850820 – A
VOID RATIO
SHEAR DISPLACEMENT (mm)

DENISON

SAMPLE #B50A30 – A

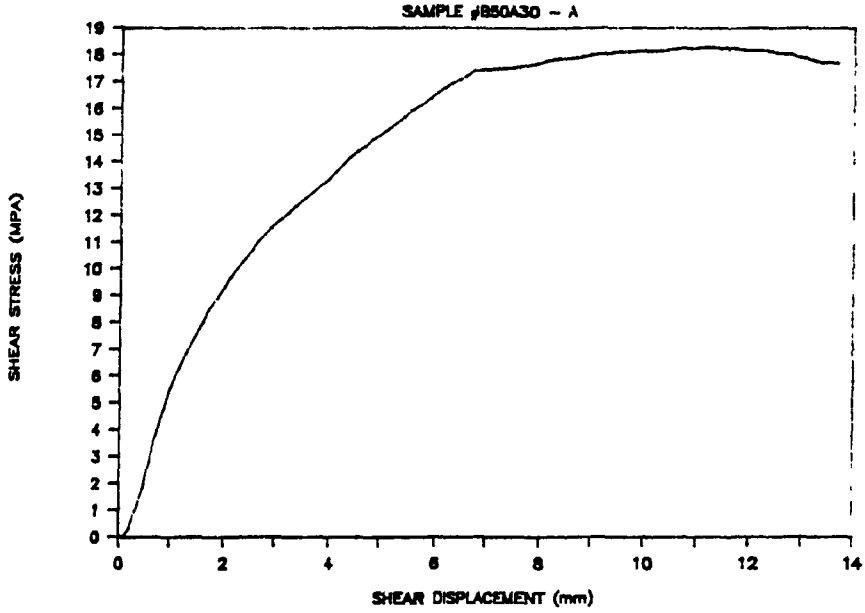

SAMPLE #B50A30 – A

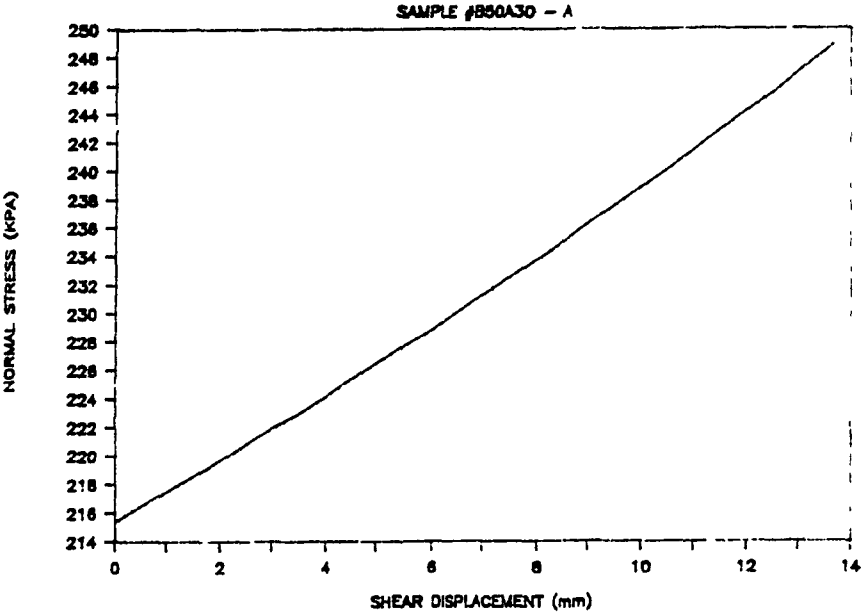

SAMPLE #B50A30 – A

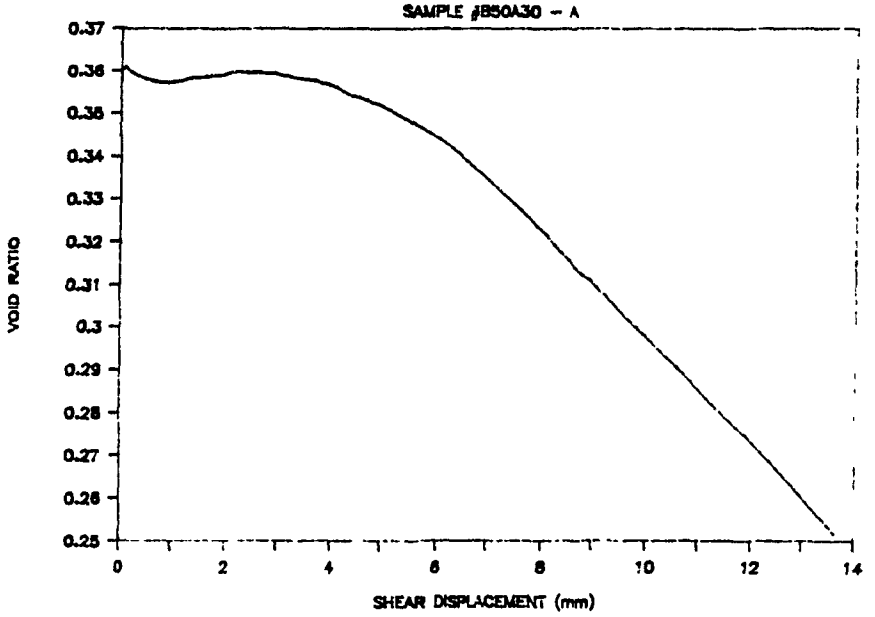

A344

DENISON

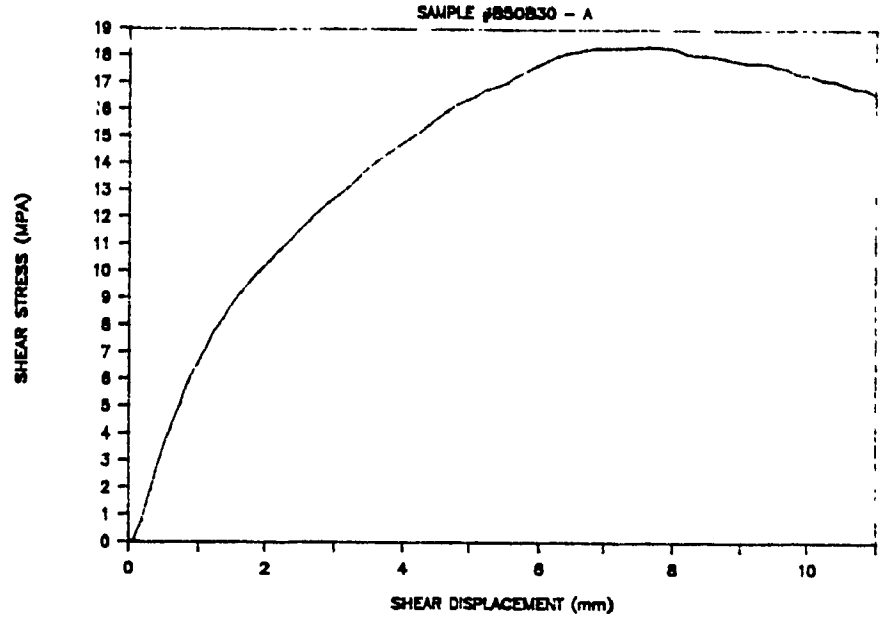
SAMPLE #B50B30 - A
SHEAR STRESS (MPA)
SHEAR DISPLACEMENT (mm)

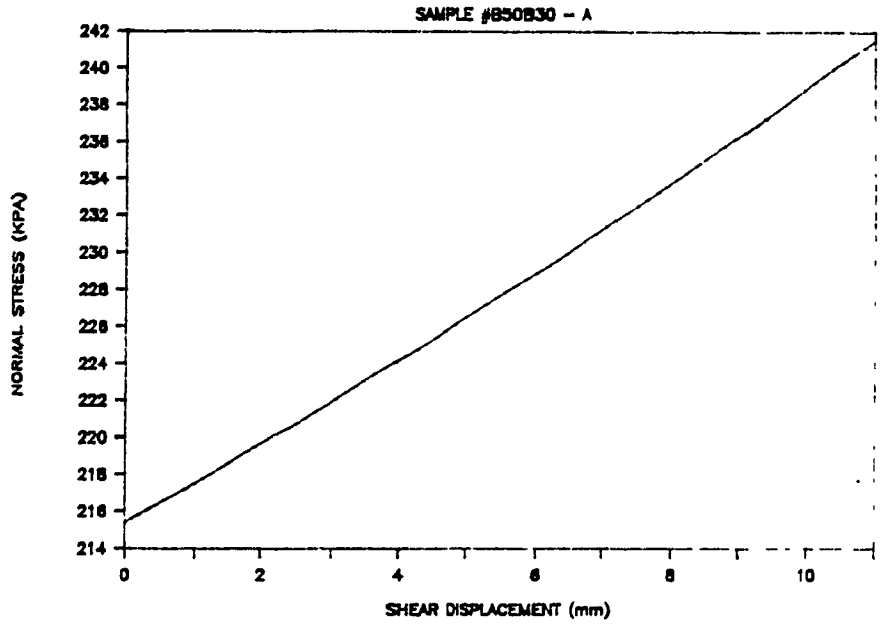
SAMPLE #B50B30 - A
NORMAL STRESS (KPA)
SHEAR DISPLACEMENT (mm)

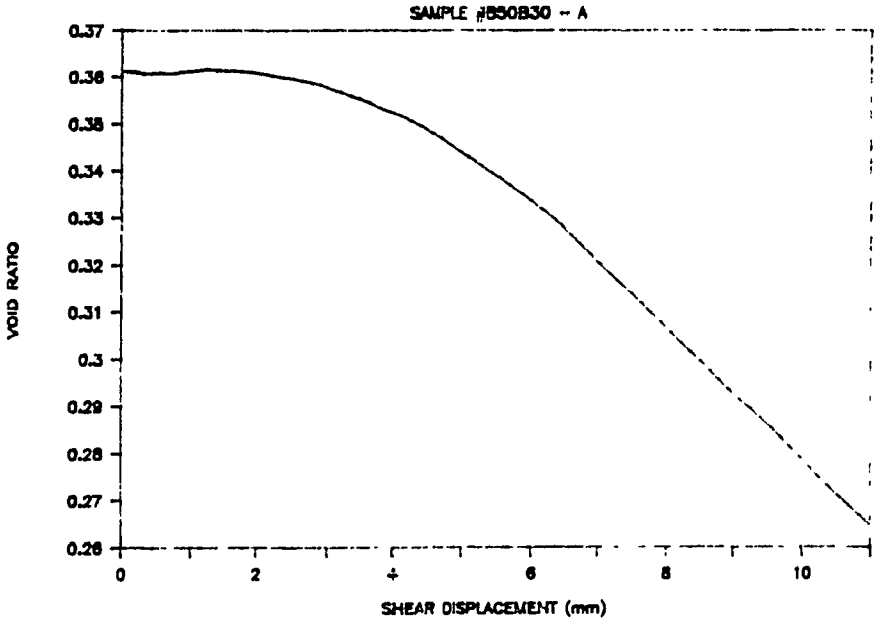
SAMPLE #B50B30 - A
VOID RATIO
SHEAR DISPLACEMENT (mm)

DENISON

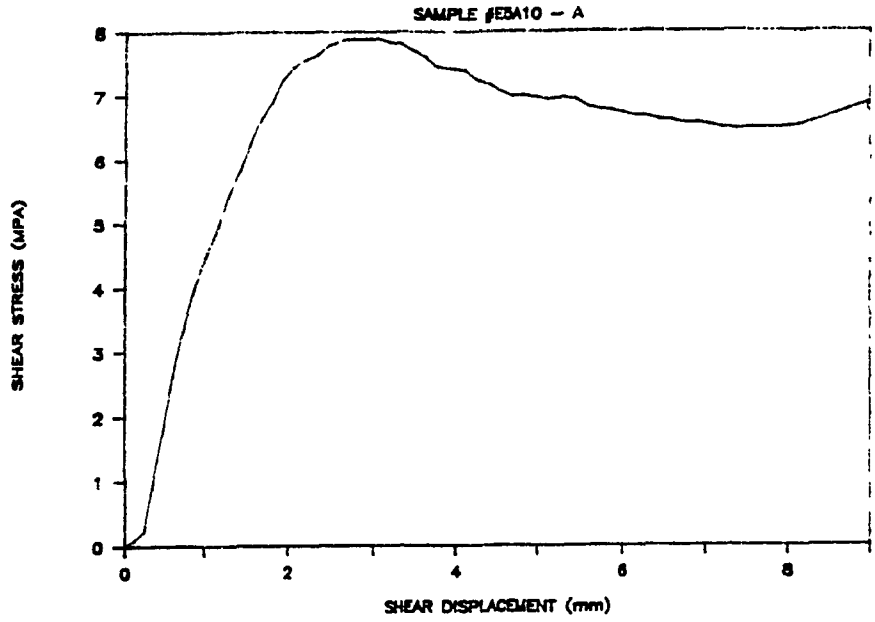
SAMPLE #E5A10 – A
SHEAR STRESS (MPA)
0
1
2
3
4
5
6
7
8
0
2
4
6
8
SHEAR DISPLACEMENT (mm)

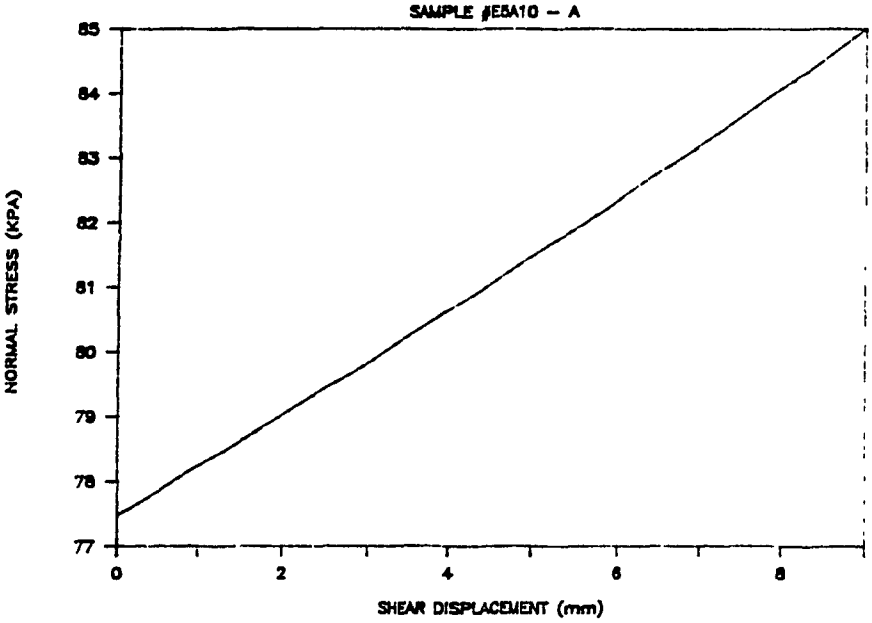
SAMPLE #E5A10 – A
NORMAL STRESS (KPA)
77
78
79
80
81
82
83
84
85
0
2
4
6
8
SHEAR DISPLACEMENT (mm)

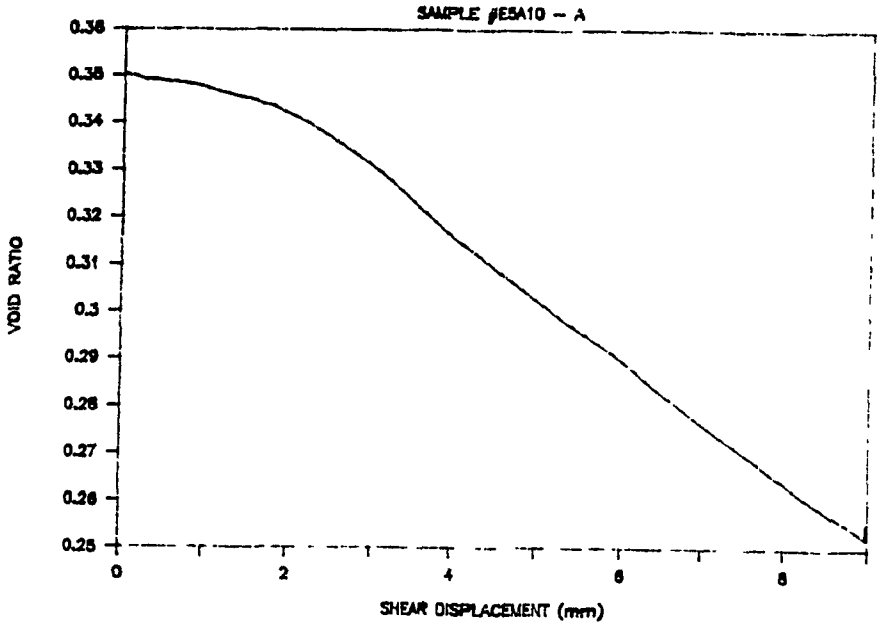
SAMPLE #E5A10 – A
VOID RATIO
0.25
0.26
0.27
0.28
0.29
0.3
0.31
0.32
0.33
0.34
0.35
0.36
0
2
4
6
8
SHEAR DISPLACEMENT (mm)

DENISON

SAMPLE #E5810 – A

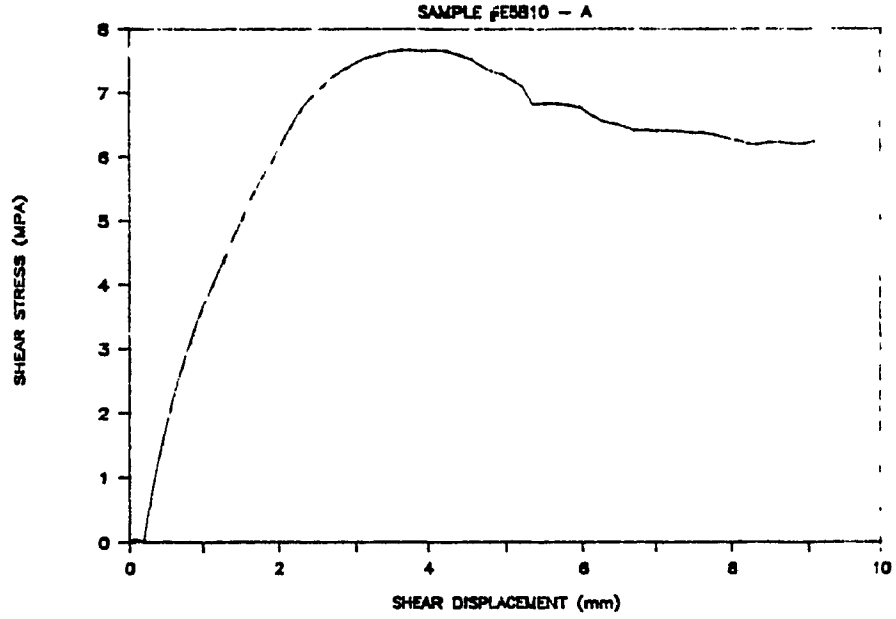

SAMPLE #E5810 – A

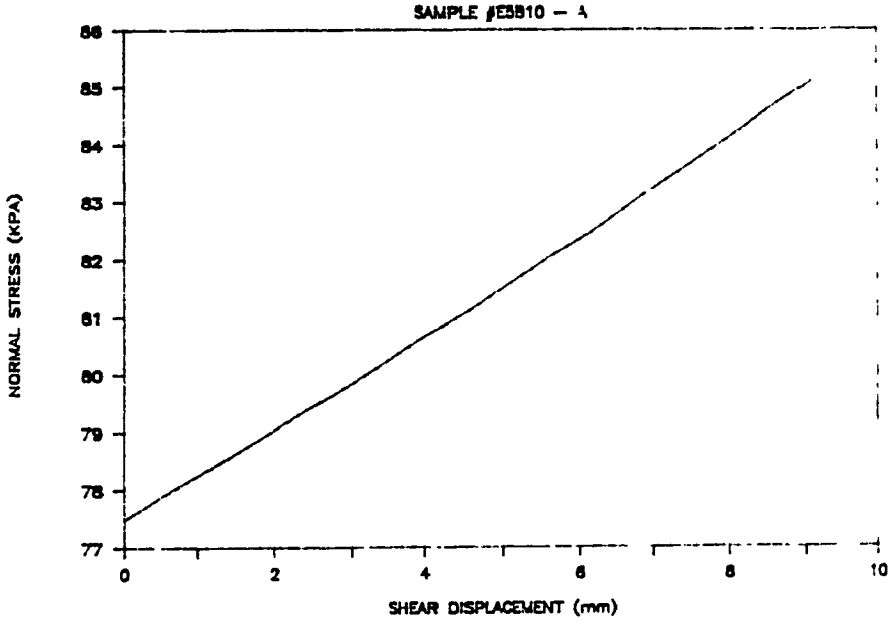

SAMPLE #E5810 – A

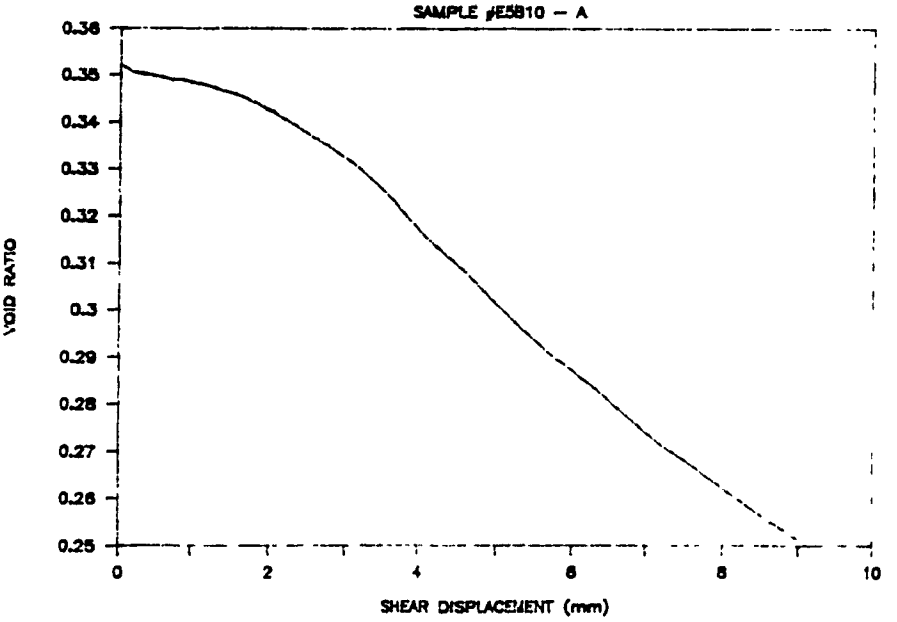

DENISON

SAMPLE #E5A20 – A

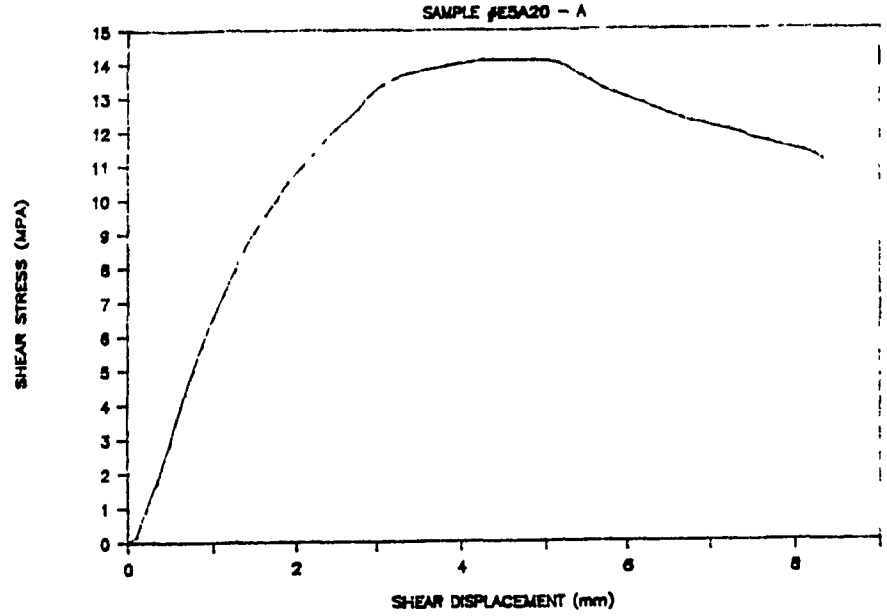

SAMPLE #E5A20 – A

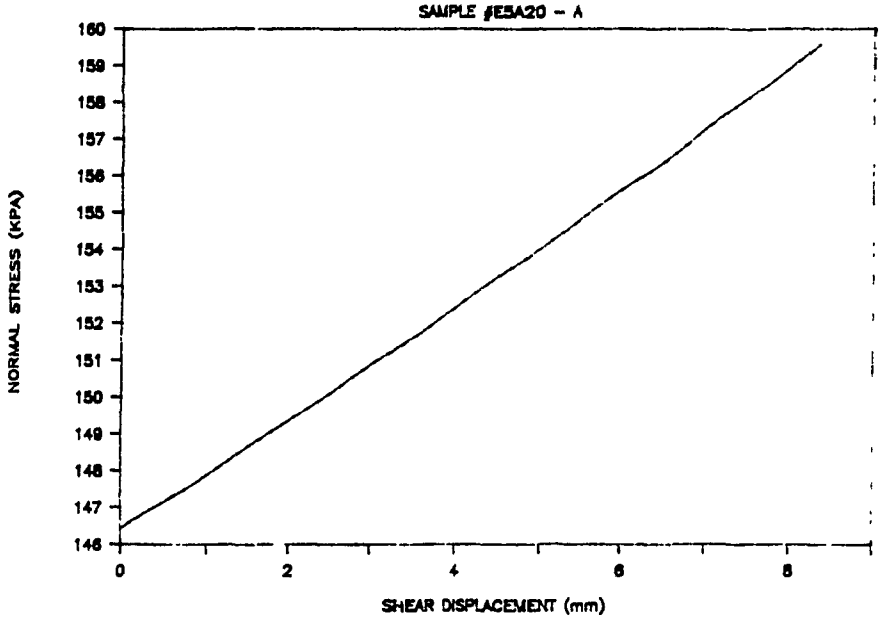

SAMPLE #E5A20 – A

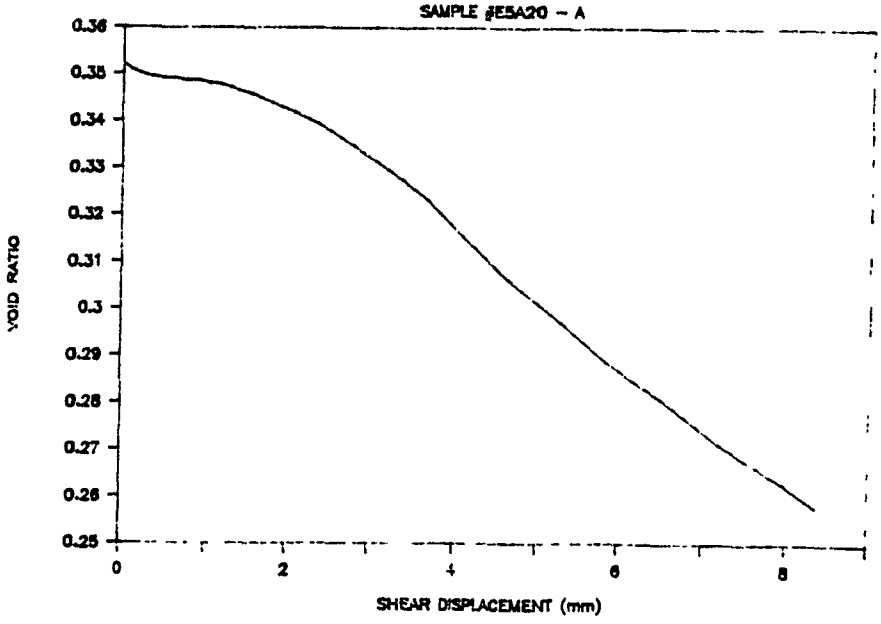

DENISON

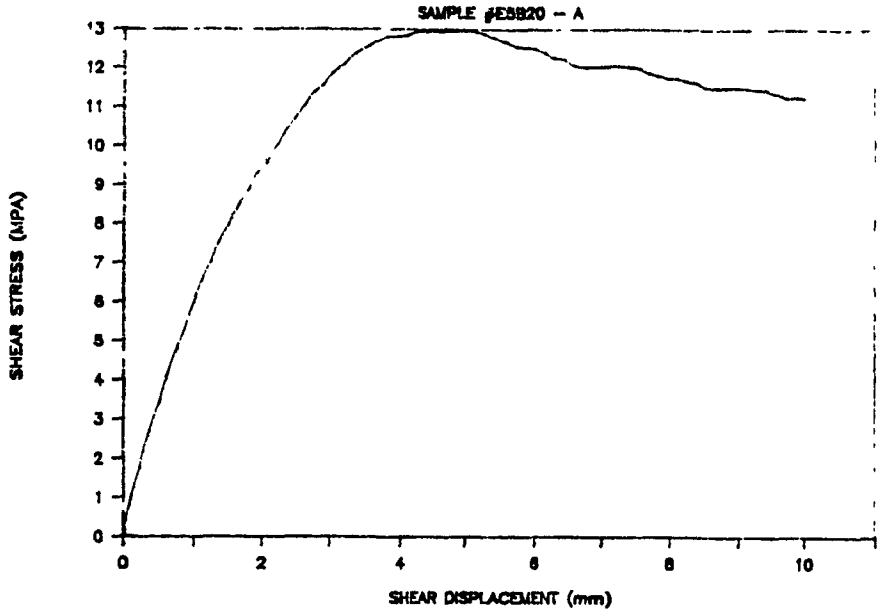
SAMPLE #E5820 – A
SHEAR STRESS (MPA)
SHEAR DISPLACEMENT (mm)

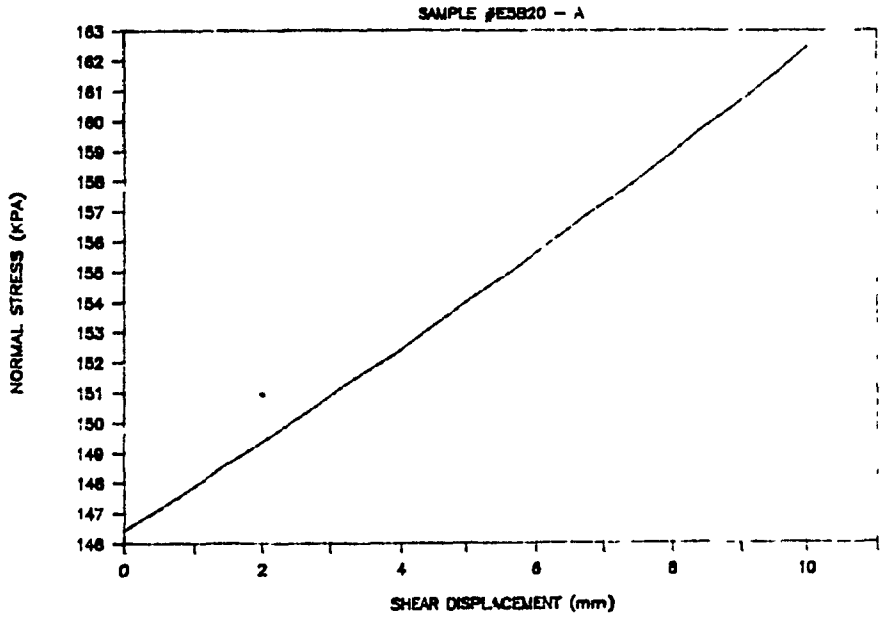
SAMPLE #E5820 – A
NORMAL STRESS (KPA)
SHEAR DISPLACEMENT (mm)

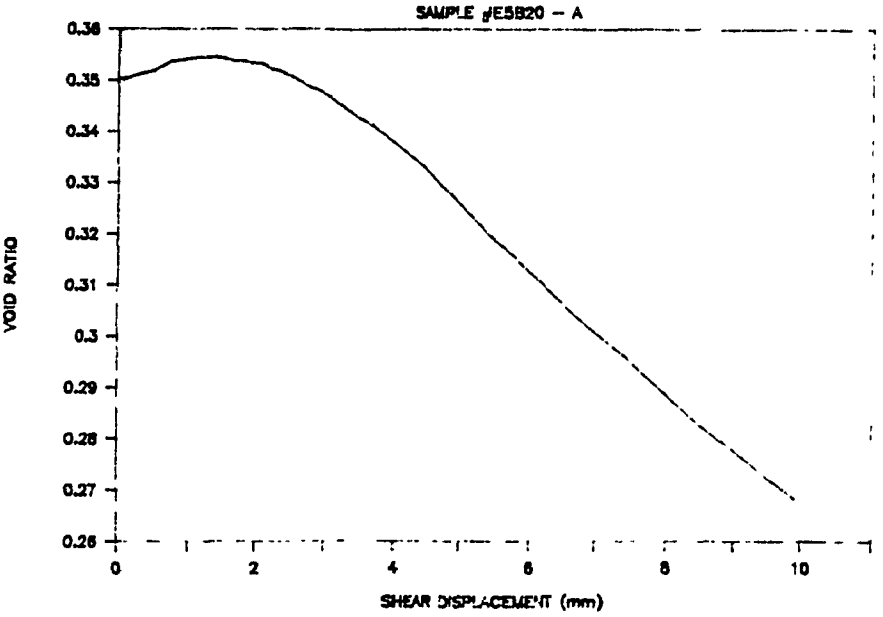
SAMPLE #E5820 – A
VOID RATIO
SHEAR DISPLACEMENT (mm)

DENISON

SAMPLE #E5A30 – A

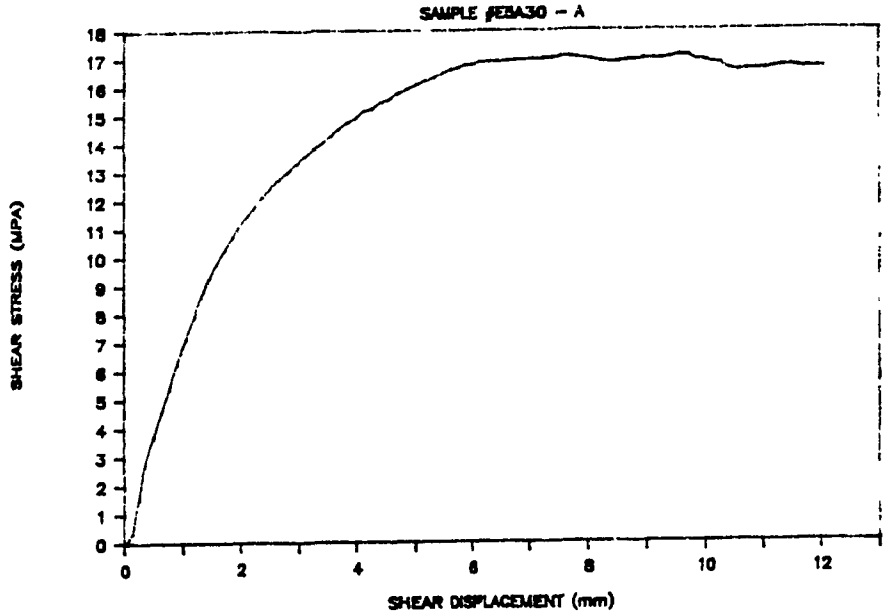

SAMPLE #E5A30 – A

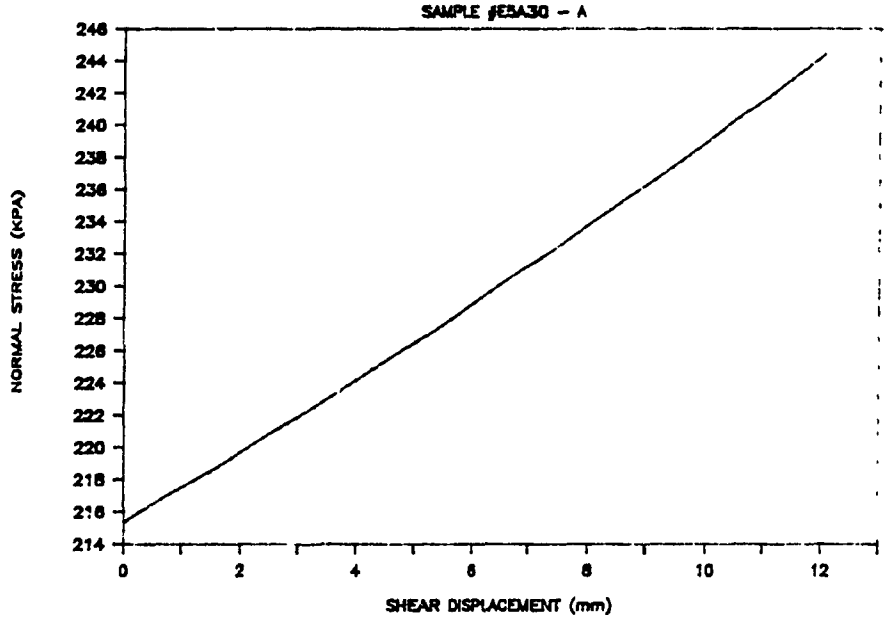

SAMPLE #E5A30 – A

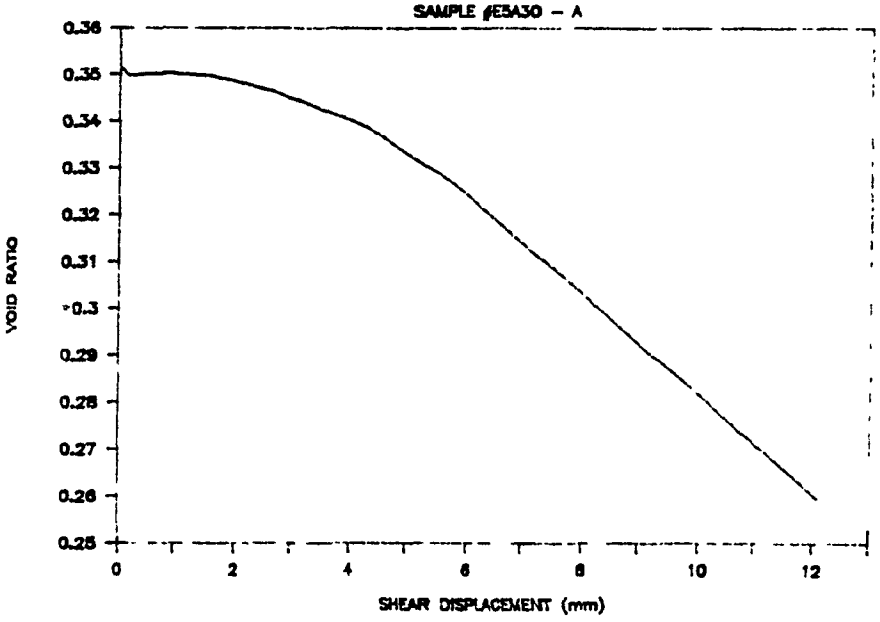

DENISON

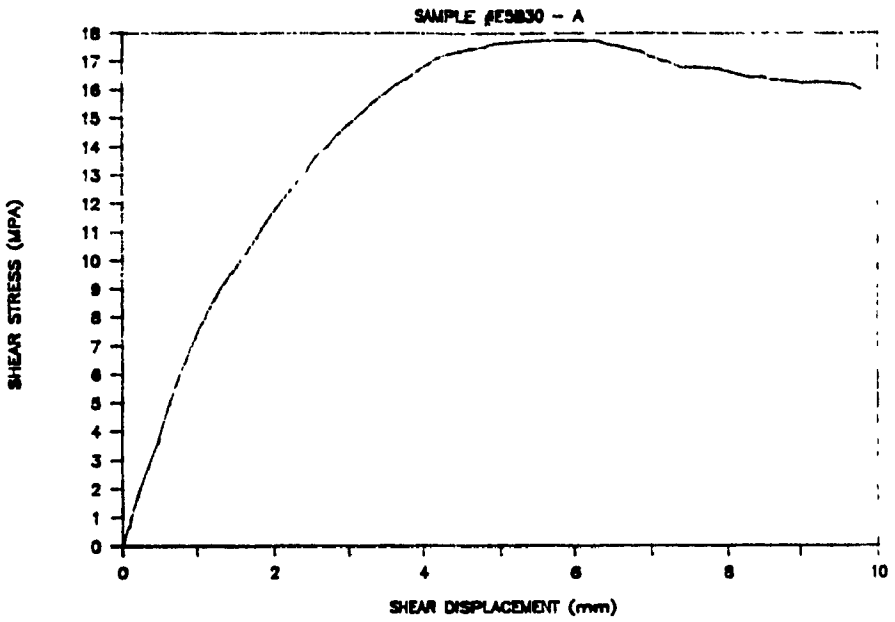
SAMPLE #E5B30 - A
SHEAR STRESS (MPA)
SHEAR DISPLACEMENT (mm)

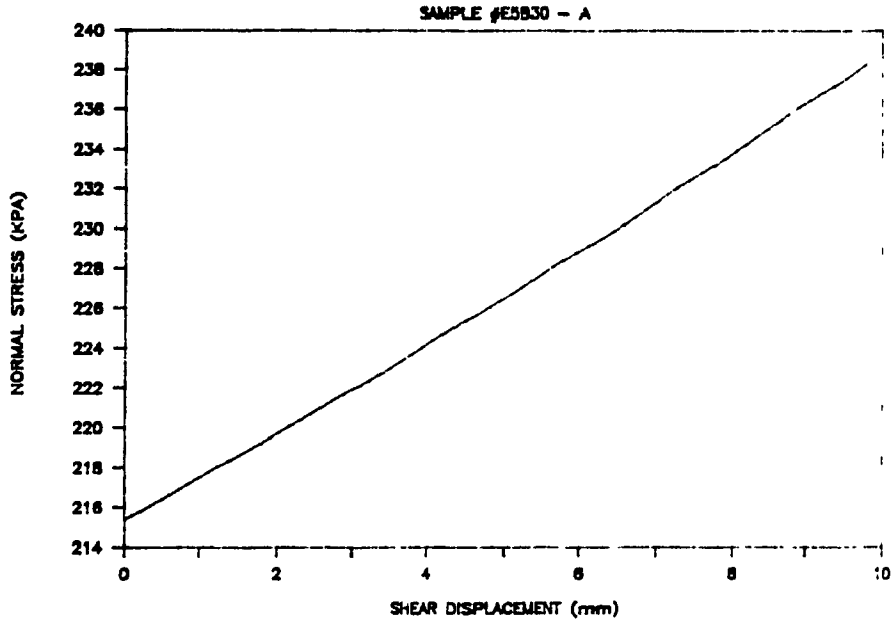
SAMPLE #E5B30 - A
NORMAL STRESS (KPA)
SHEAR DISPLACEMENT (mm)

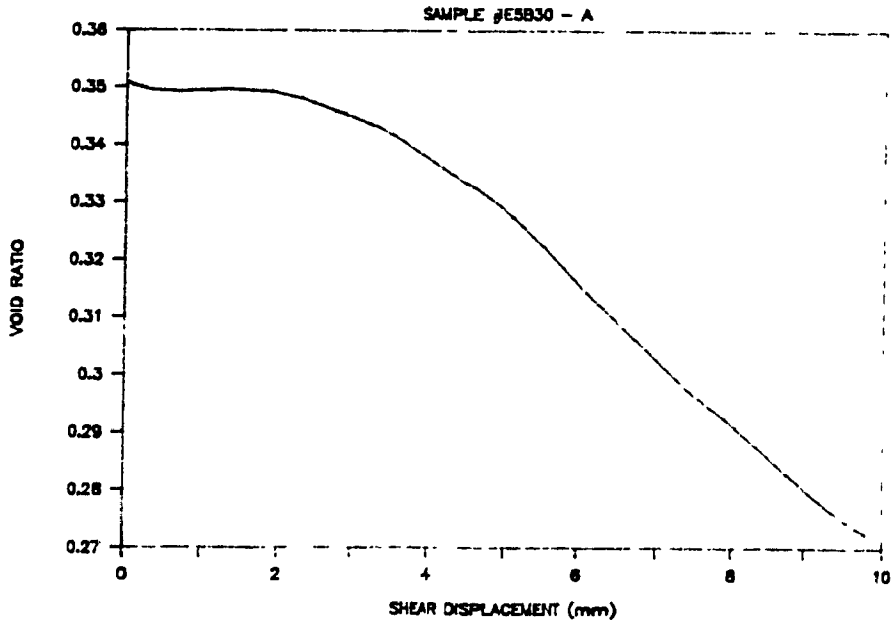
SAMPLE #E5B30 - A
VOID RATIO
SHEAR DISPLACEMENT (mm)

DENISON

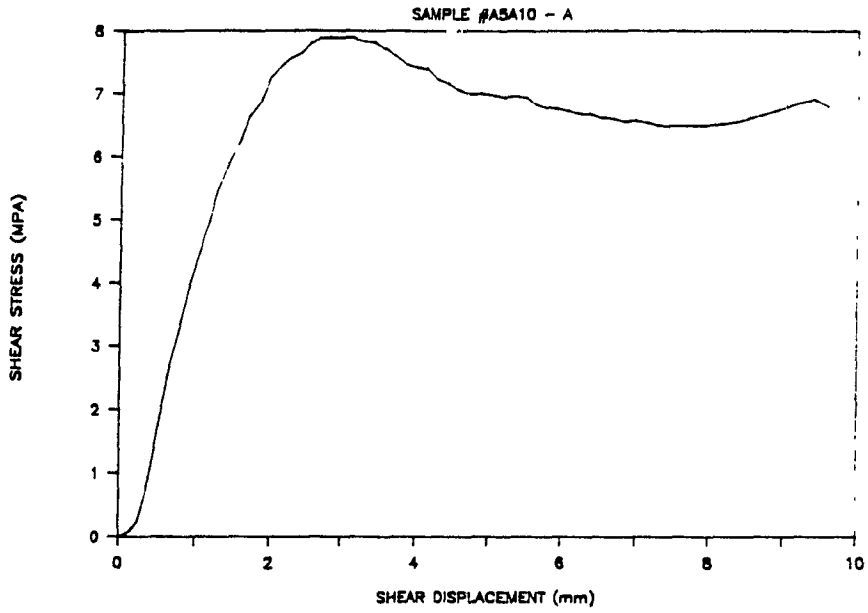
SAMPLE #A5A10 - A
SHEAR STRESS (MPA)
0
1
2
3
4
5
6
7
8
0
2
4
6
8
10
SHEAR DISPLACEMENT (mm)

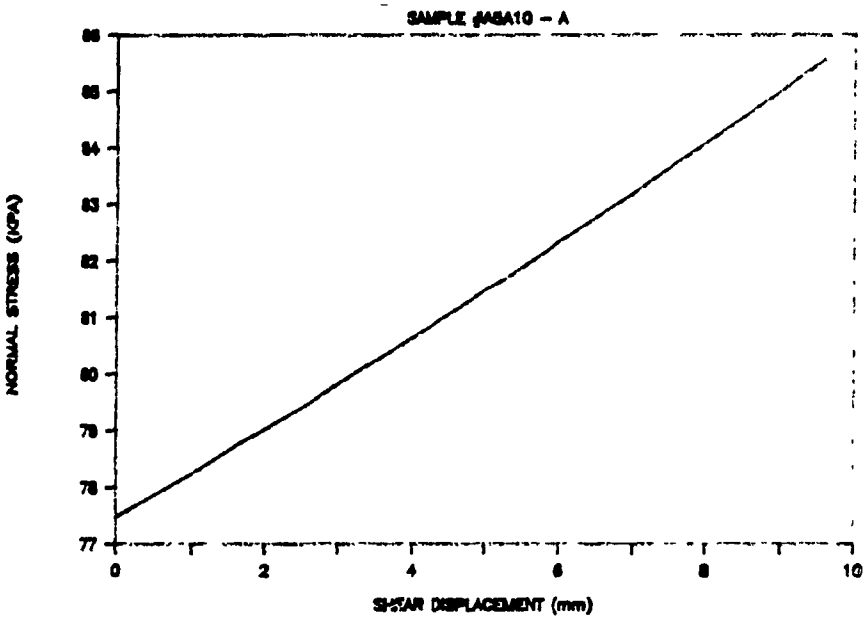
SAMPLE #A5A10 - A
NORMAL STRESS (KPA)
77
78
79
80
81
82
83
84
85
86
0
2
4
6
8
10
SHEAR DISPLACEMENT (mm)

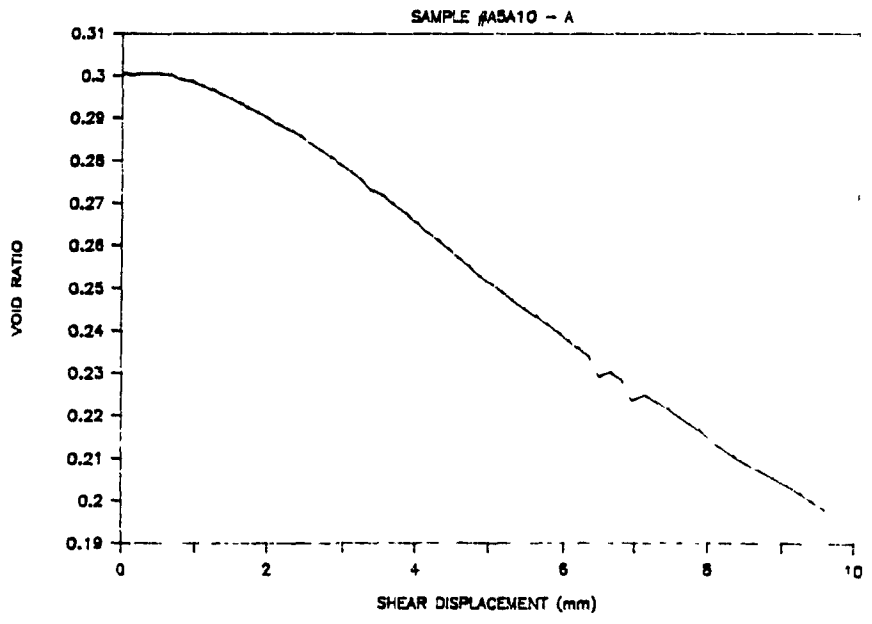
SAMPLE #A5A10 - A
VOID RATIO
0.19
0.2
0.21
0.22
0.23
0.24
0.25
0.26
0.27
0.28
0.29
0.3
0.31
0
2
4
6
8
10
SHEAR DISPLACEMENT (mm)

DENISON

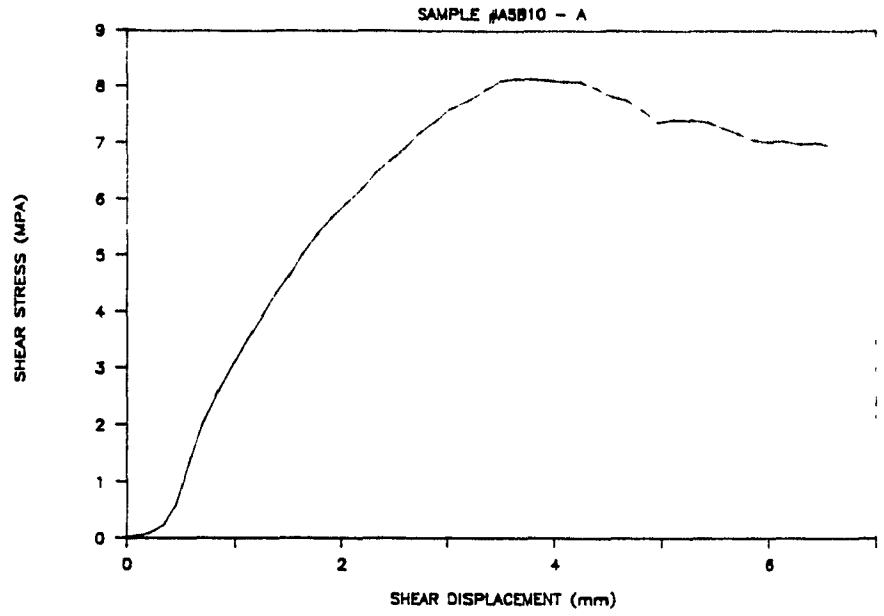
SAMPLE #A5B10 - A
SHEAR STRESS (MPA)
9
8
7
6
5
4
3
2
1
0
0
2
4
6
SHEAR DISPLACEMENT (mm)

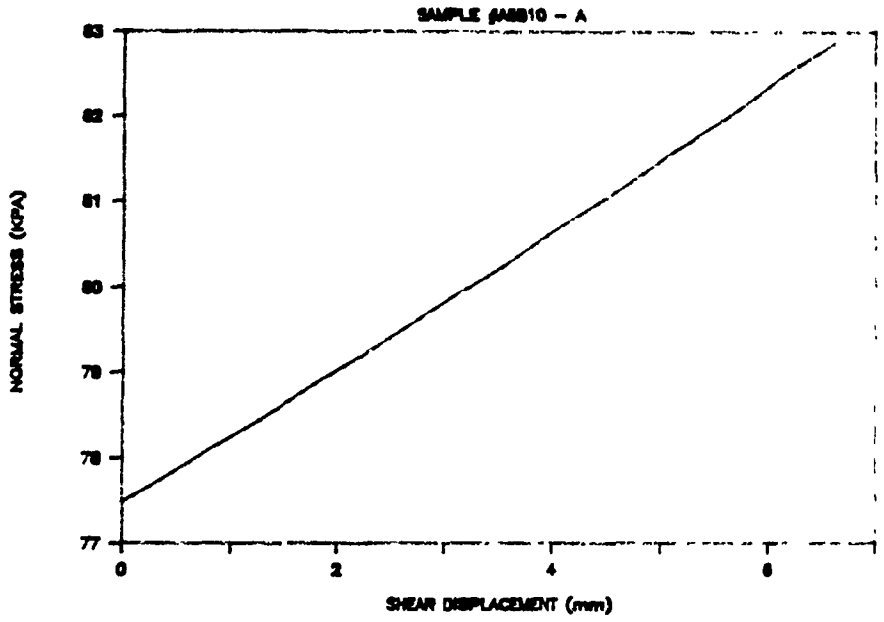
SAMPLE #A5B10 - A
NORMAL STRESS (KPA)
83
82
81
80
79
78
77
0
2
4
6
SHEAR DISPLACEMENT (mm)

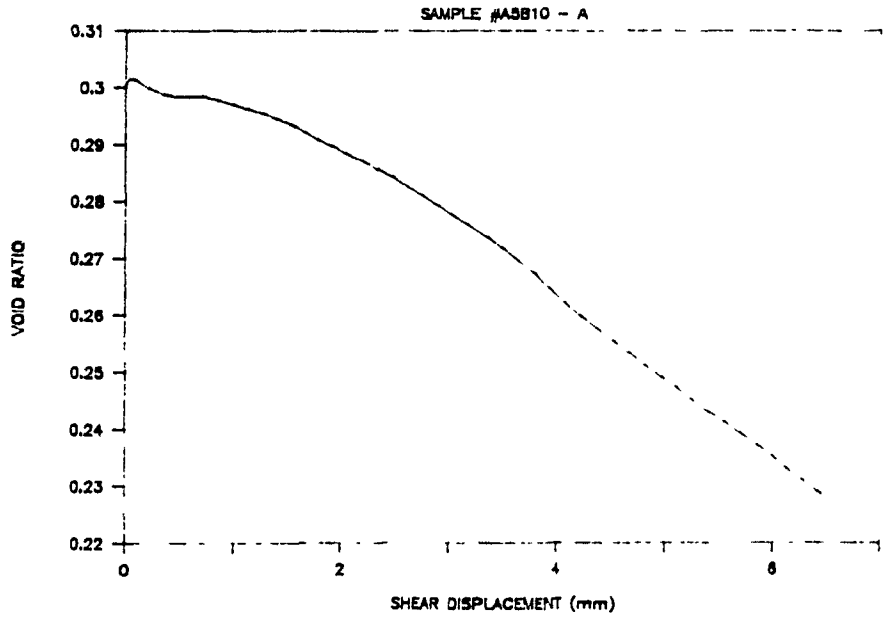
SAMPLE #A5B10 - A
VOID RATIO
0.31
0.3
0.29
0.28
0.27
0.26
0.25
0.24
0.23
0.22
0
2
4
6
SHEAR DISPLACEMENT (mm)

DENISON

SAMPLE #A5A20 – A

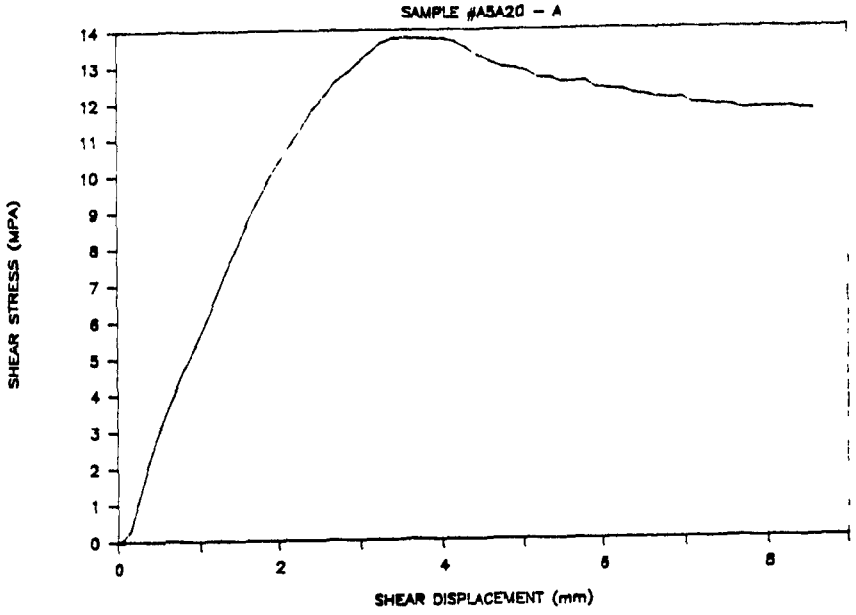

SAMPLE #A5A20 – A

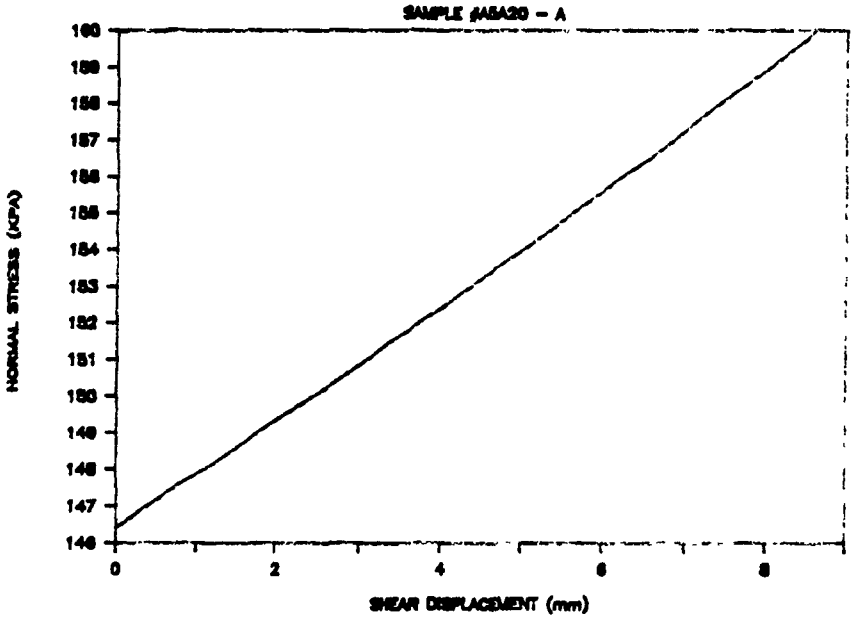

SAMPLE #A5A20 – A

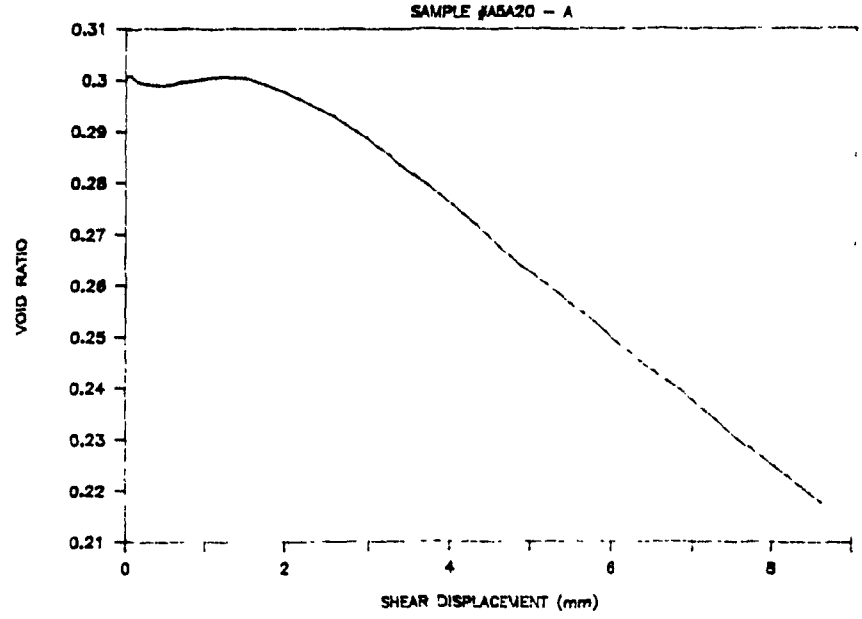

DENISON

SAMPLE #A5B20 - A

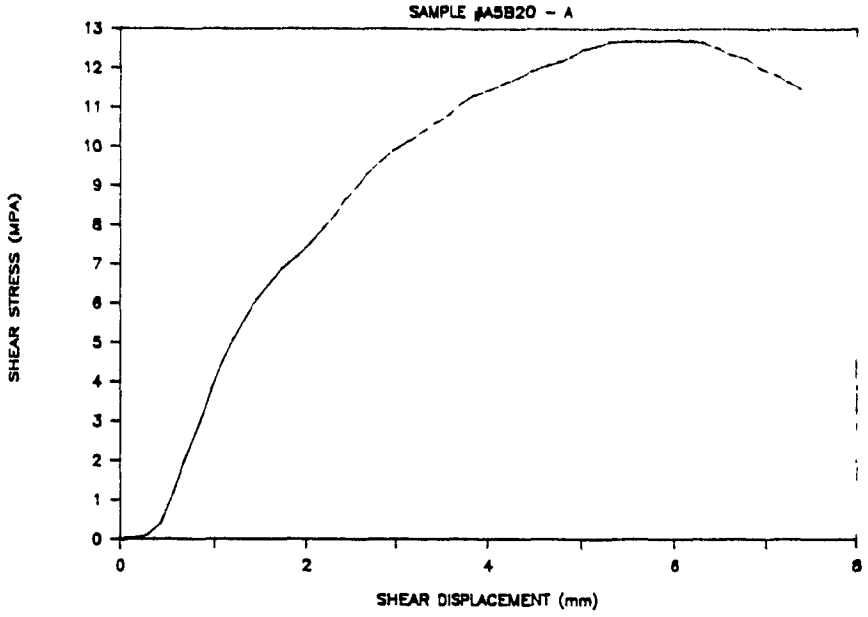

SAMPLE #A5B20 - A

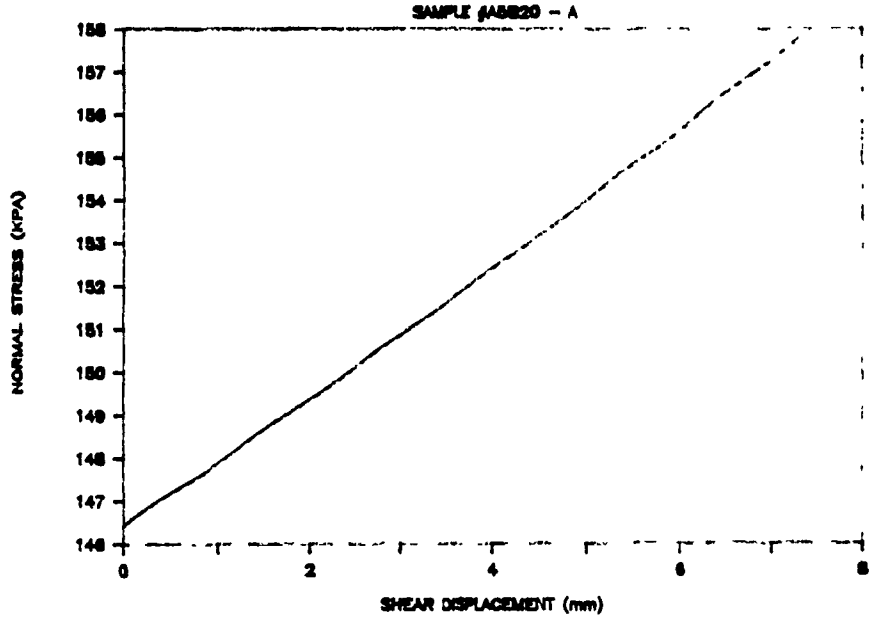

SAMPLE #A5B20 - A

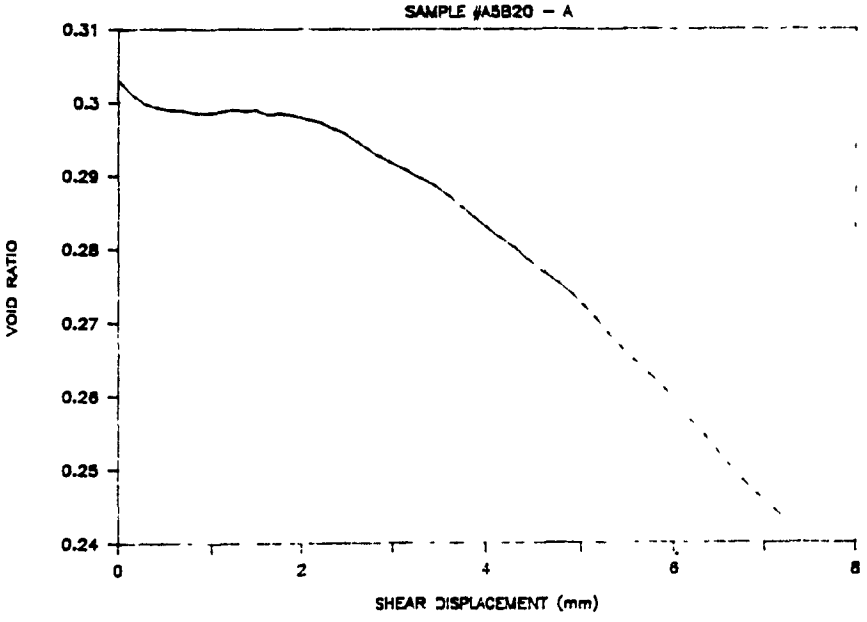

DENISON

SAMPLE #A5A30 – A

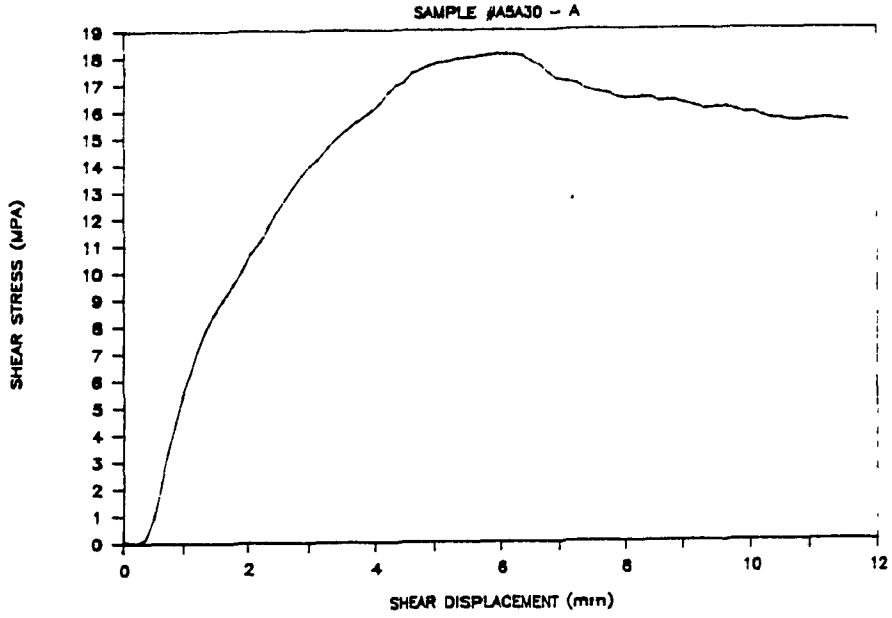

SAMPLE #A5A30 – A

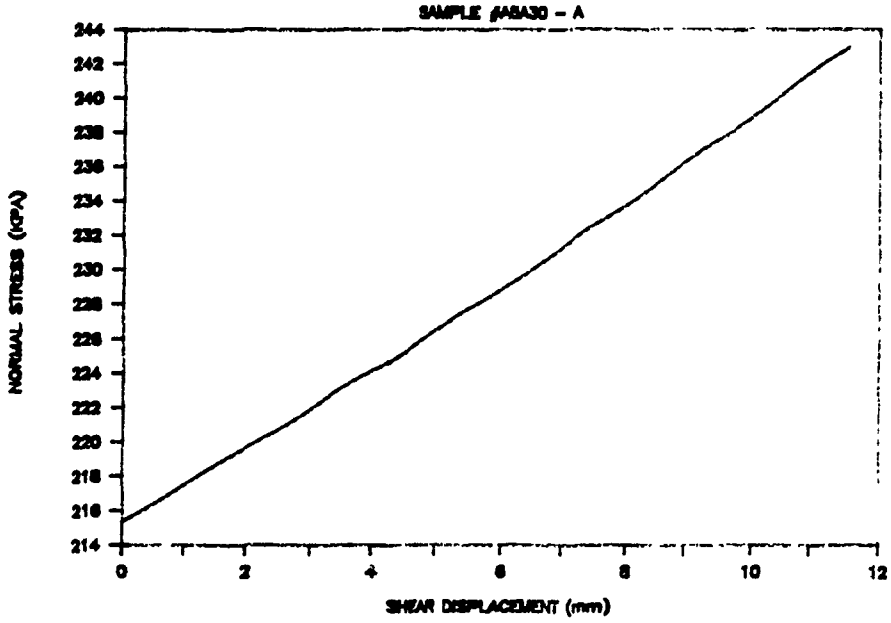

SAMPLE #A5A30 – A

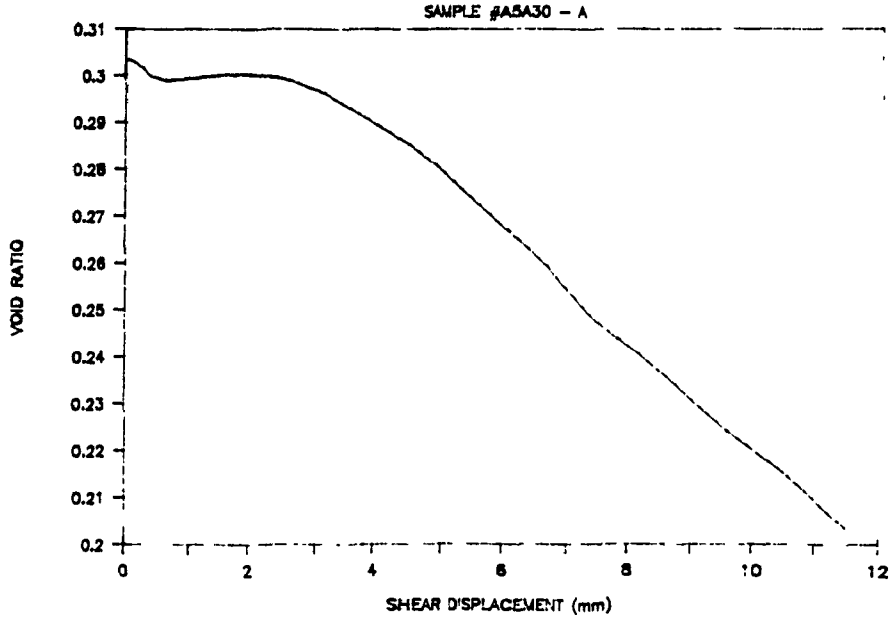

DENISON

SAMPLE #A5B30 – A

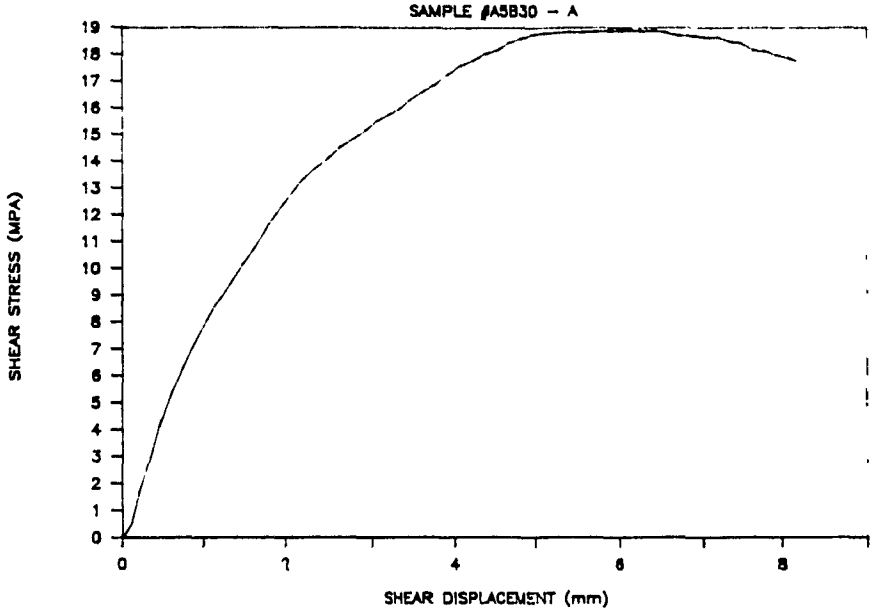

SAMPLE #A5B30 – A

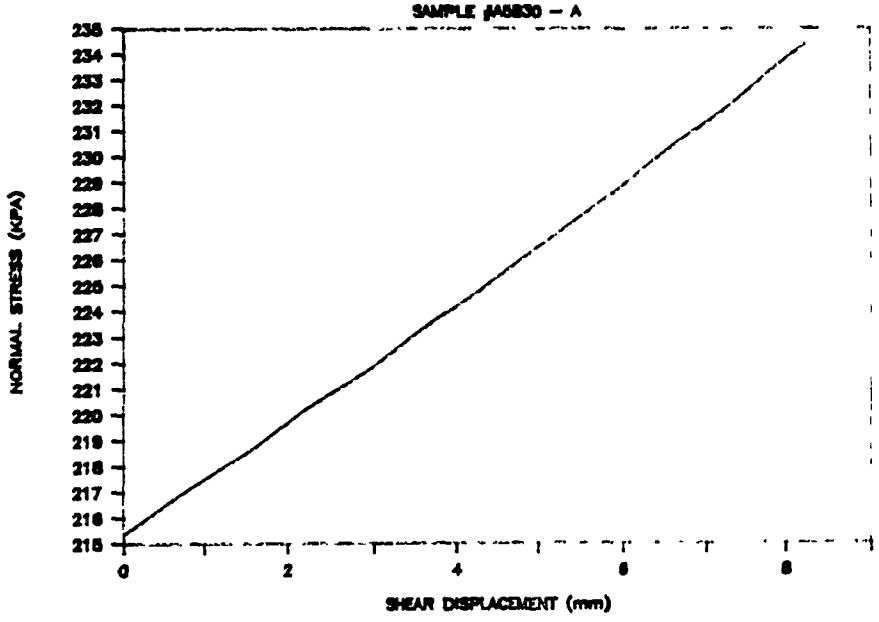

SAMPLE #A5B30 – A

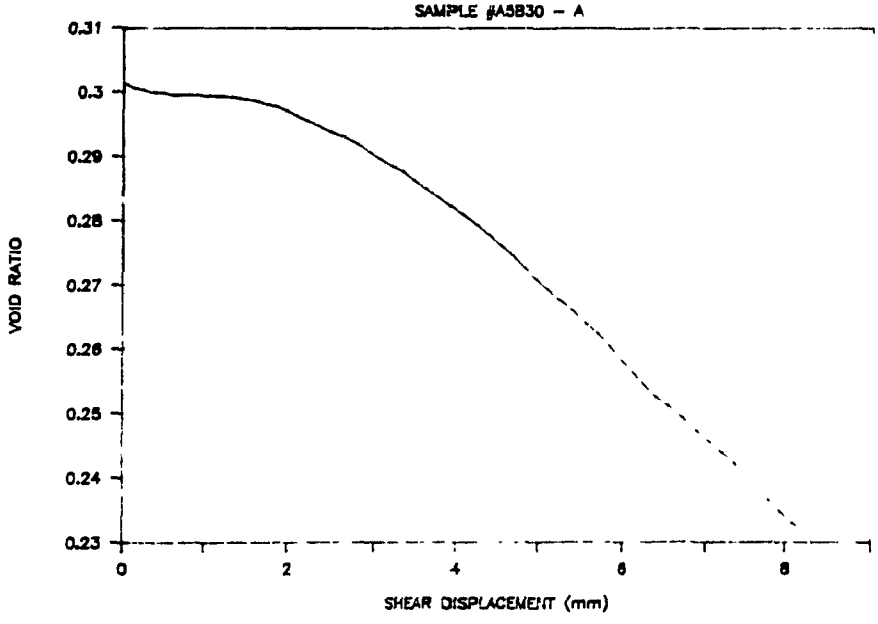

DENISON

SAMPLE #88A10 – A

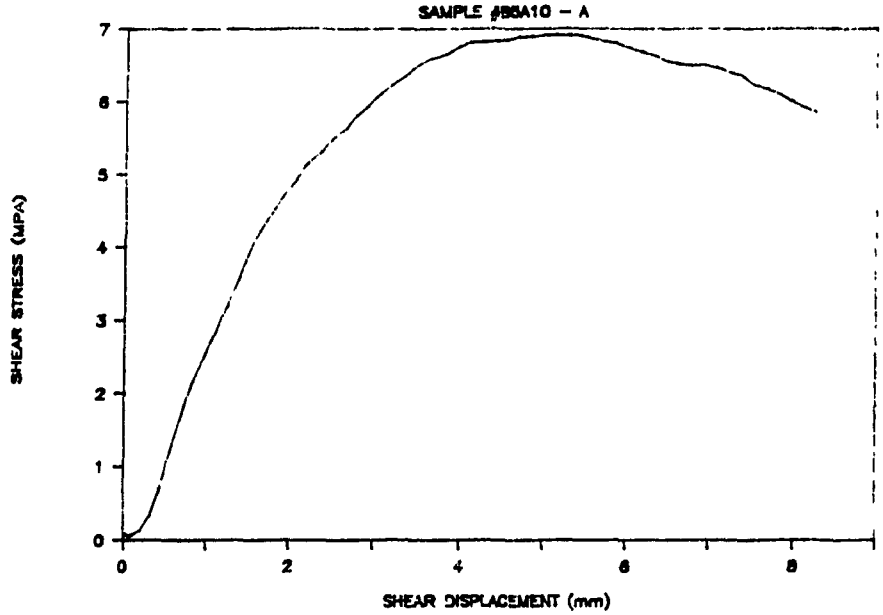

SAMPLE #88A10 – A

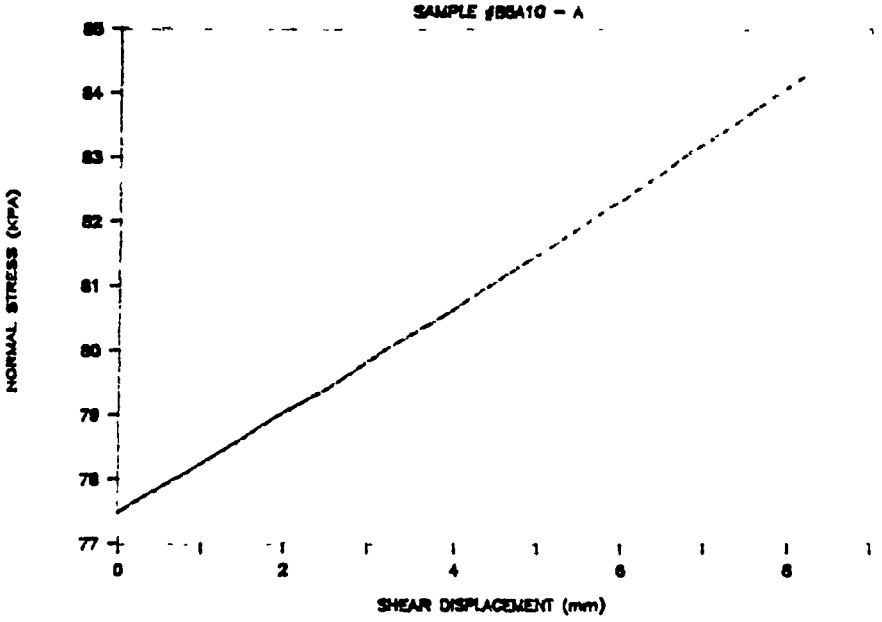

SAMPLE #88A10 – A

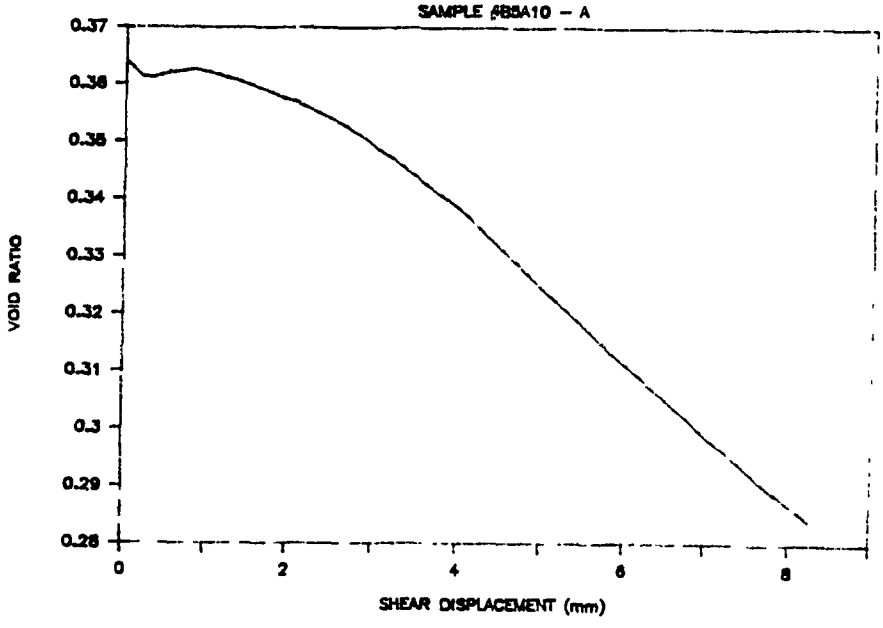

DENISON

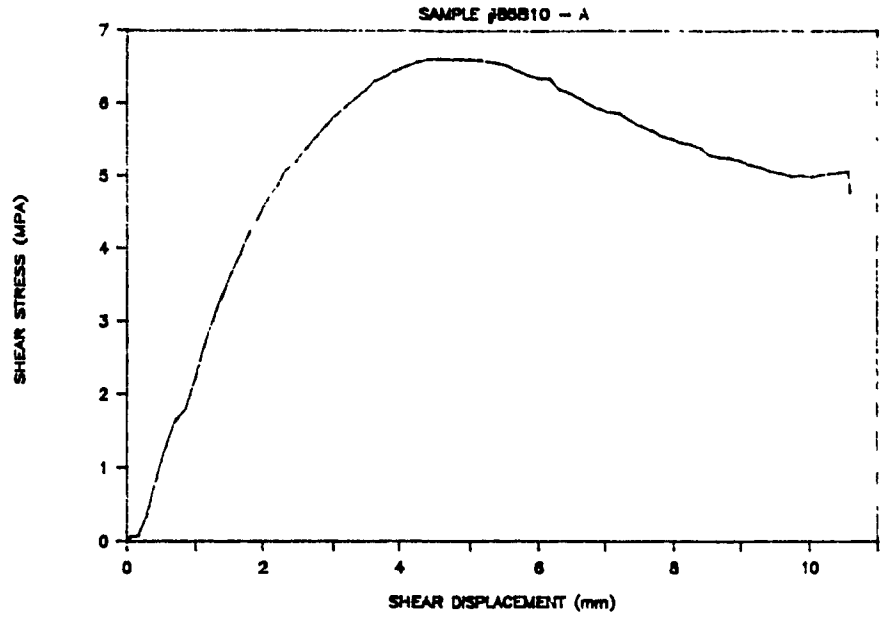
SAMPLE #B5B10 – A
SHEAR STRESS (MPA)
SHEAR DISPLACEMENT (mm)
0
1
2
3
4
5
6
7
0
2
4
6
8
10

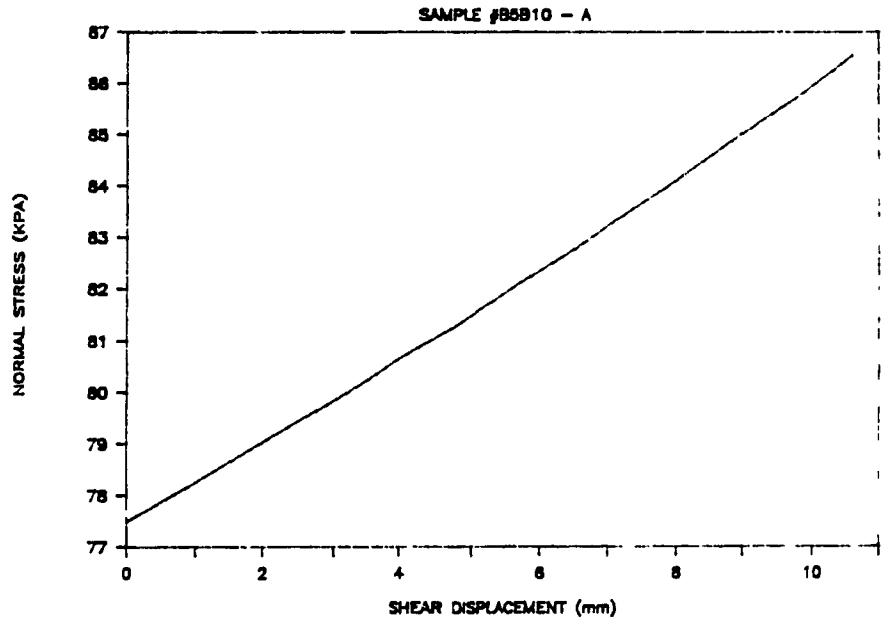
SAMPLE #B5B10 – A
NORMAL STRESS (KPA)
SHEAR DISPLACEMENT (mm)
77
78
79
80
81
82
83
84
85
86
87
0
2
4
6
8
10

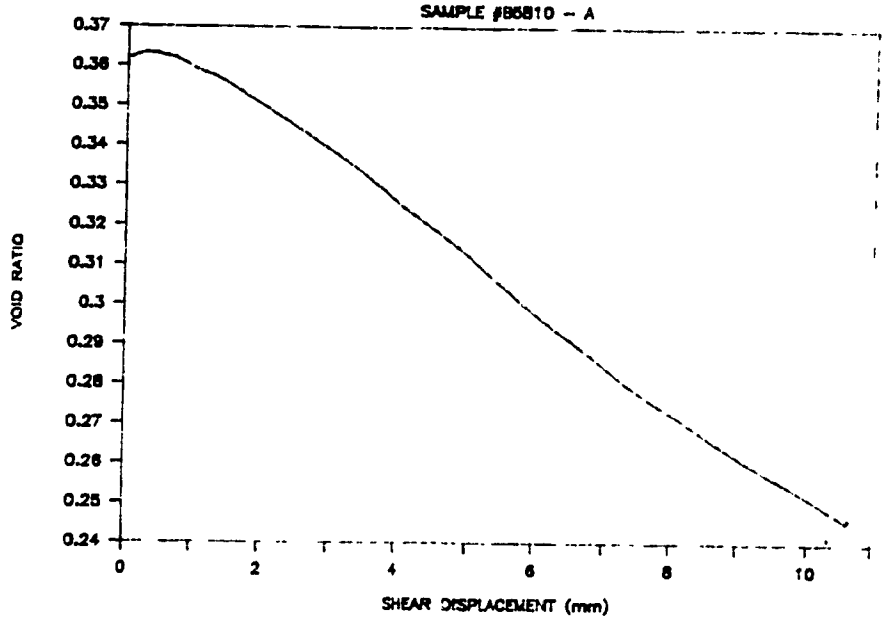
SAMPLE #B5B10 – A
VOID RATIO
SHEAR DISPLACEMENT (mm)
0.24
0.25
0.26
0.27
0.28
0.29
0.3
0.31
0.32
0.33
0.34
0.35
0.36
0.37
0
2
4
6
8
10

DENISON

SAMPLE #B6A20 – A

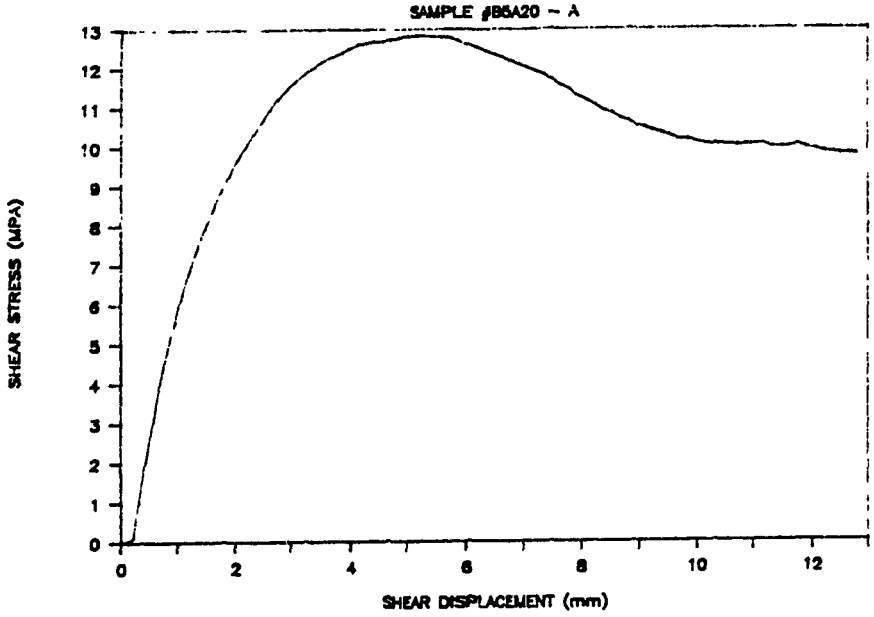

SAMPLE #B6A20 – A

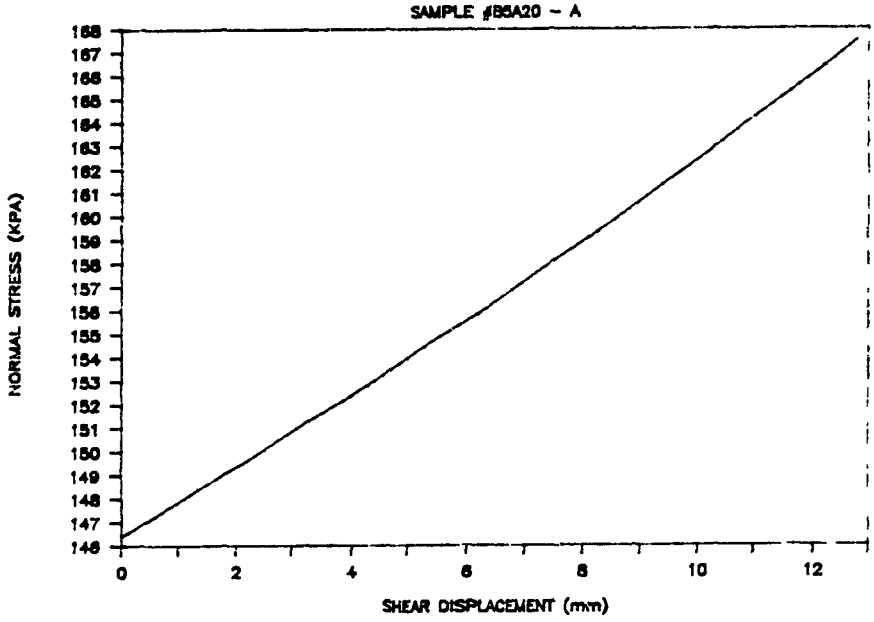

SAMPLE #B6A20 – A

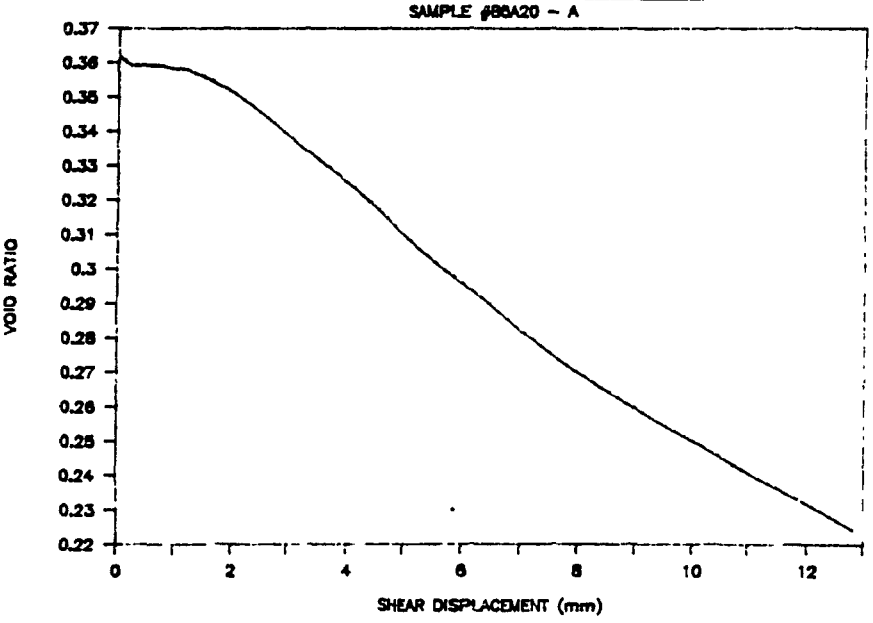

DENISON

SAMPLE #B5820 – A

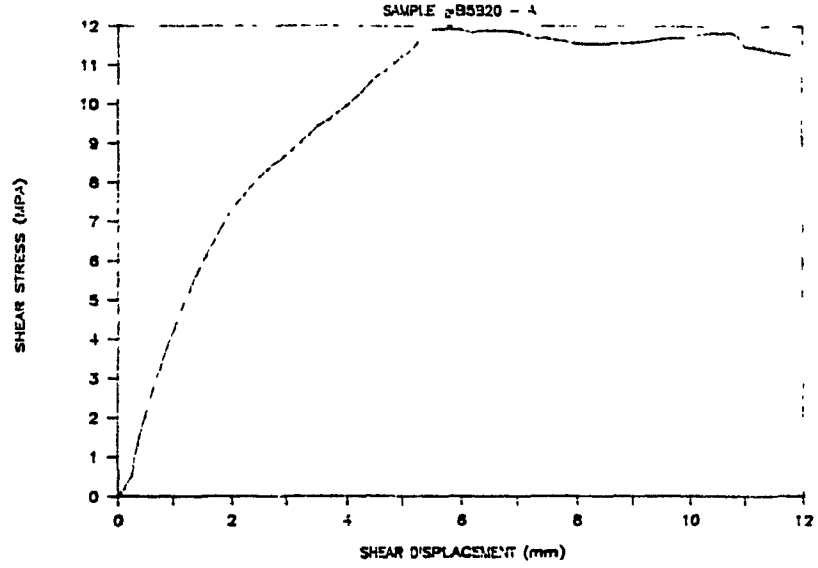

SAMPLE #B5820 – A

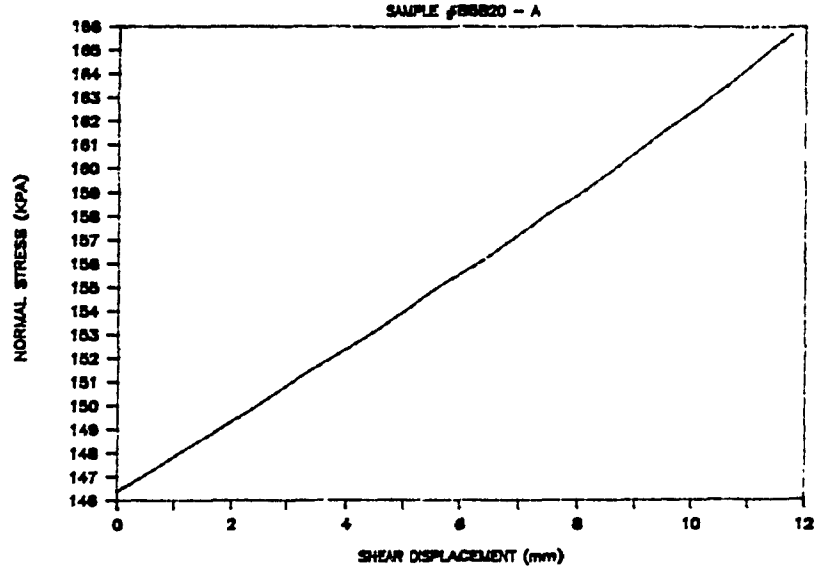

SAMPLE #B5820 – A

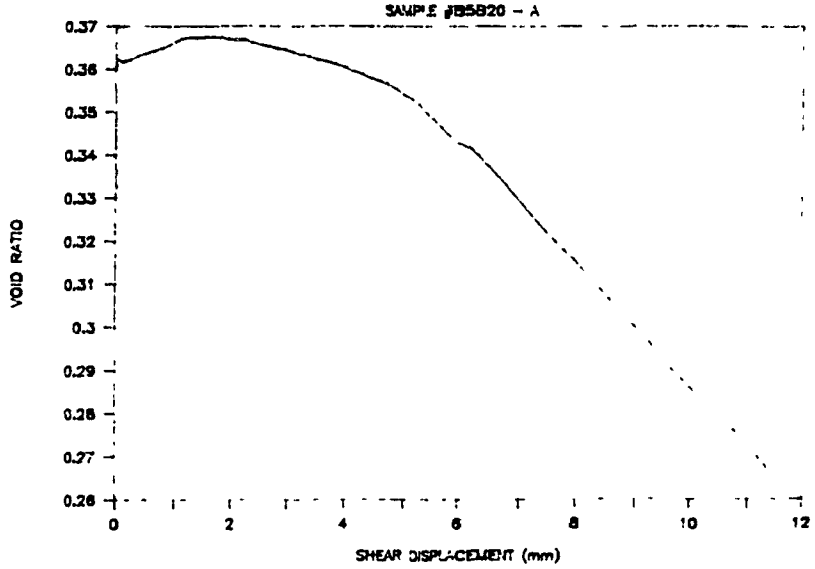

DENISON

SAMPLE #85A30 – A

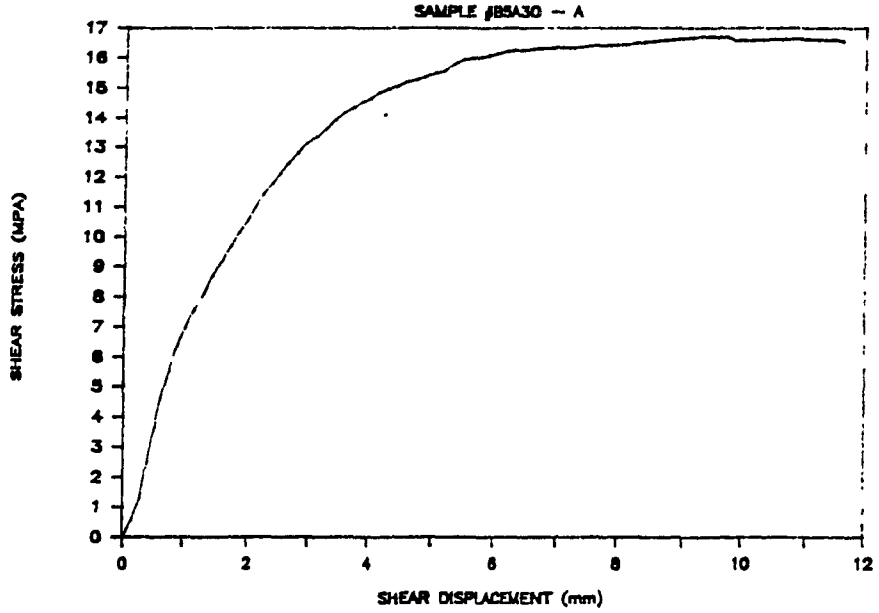

SAMPLE #85A30 – A

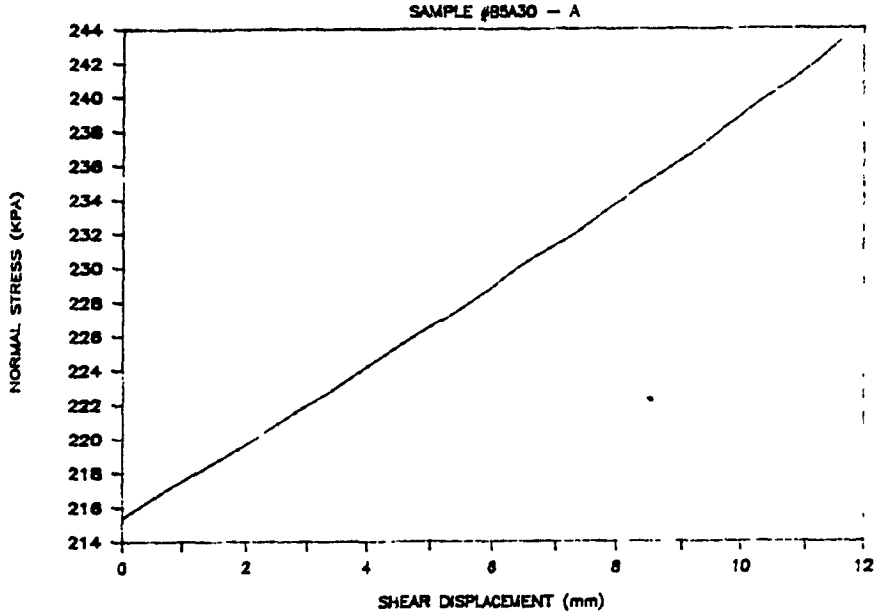

SAMPLE #85A30 – A

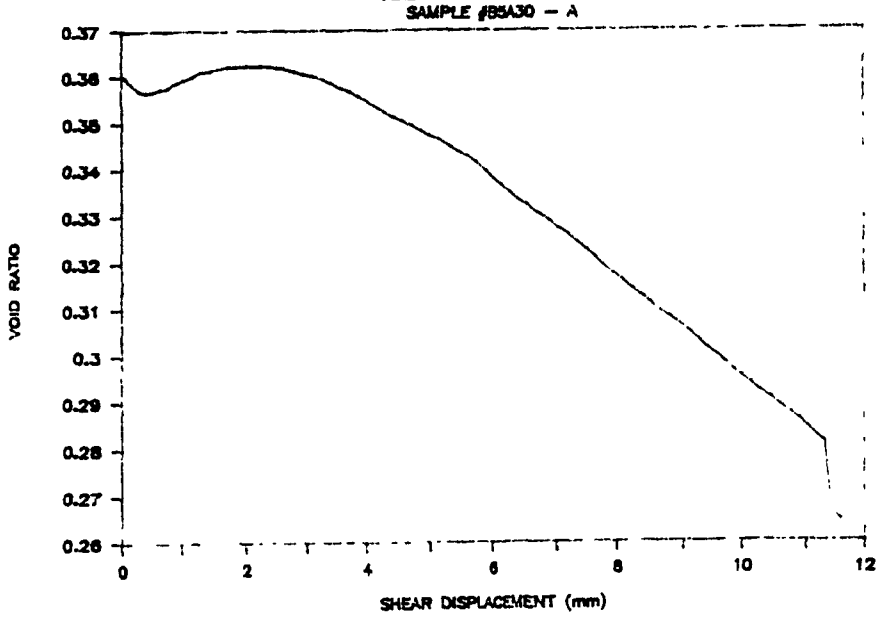

DENISON

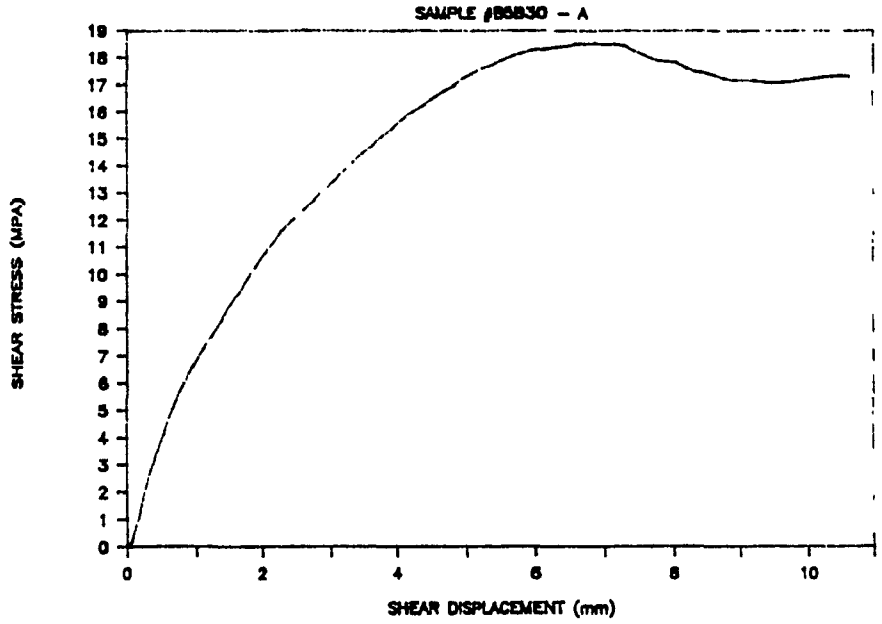
SAMPLE #B5830 – A
SHEAR STRESS (MPA)
0
1
2
3
4
5
6
7
8
9
10
11
12
13
14
15
16
17
18
19
0
2
4
6
8
10
SHEAR DISPLACEMENT (mm)

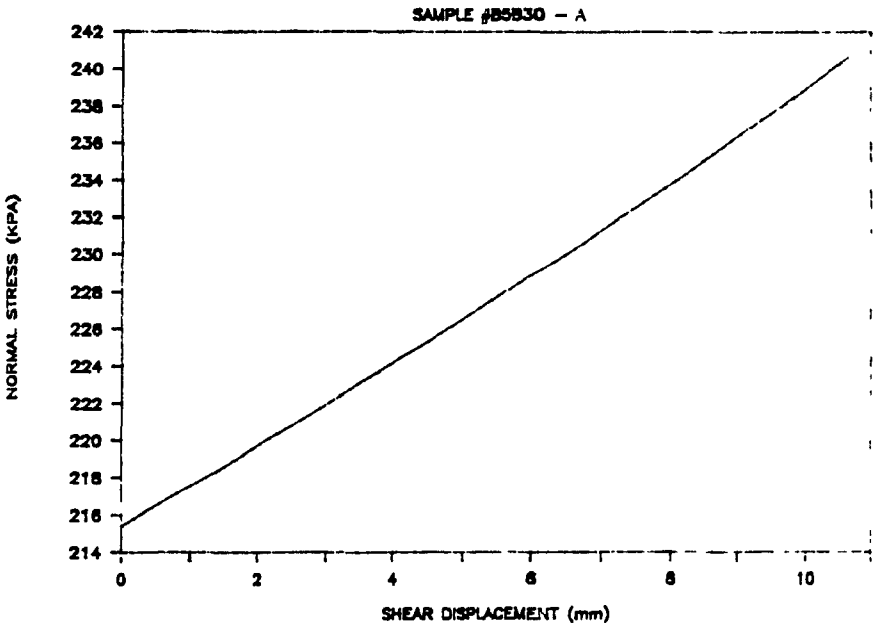
SAMPLE #B5830 – A
NORMAL STRESS (KPA)
214
216
218
220
222
224
226
228
230
232
234
236
238
240
242
0
2
4
6
8
10
SHEAR DISPLACEMENT (mm)

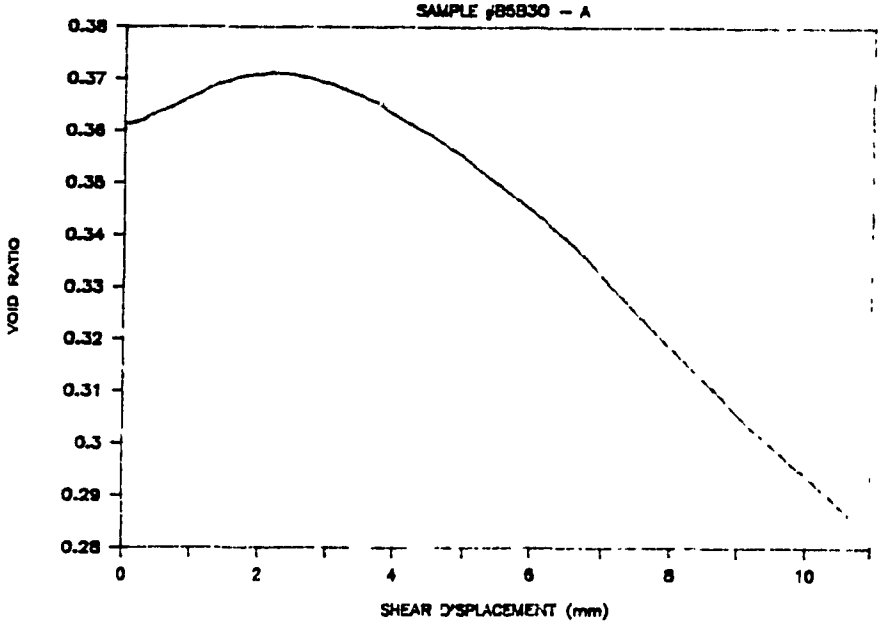
SAMPLE #B5830 – A
VOID RATIO
0.28
0.29
0.3
0.31
0.32
0.33
0.34
0.35
0.36
0.37
0.38
0
2
4
6
8
10
SHEAR DISPLACEMENT (mm)

DENISON

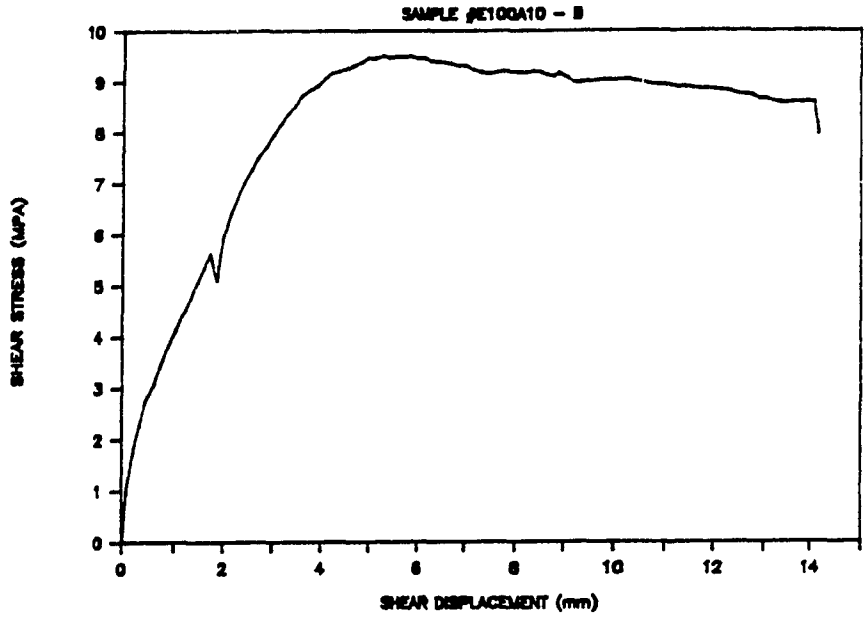
SAMPLE #E100A10 - B
SHEAR STRESS (MPA)
SHEAR DISPLACEMENT (mm)

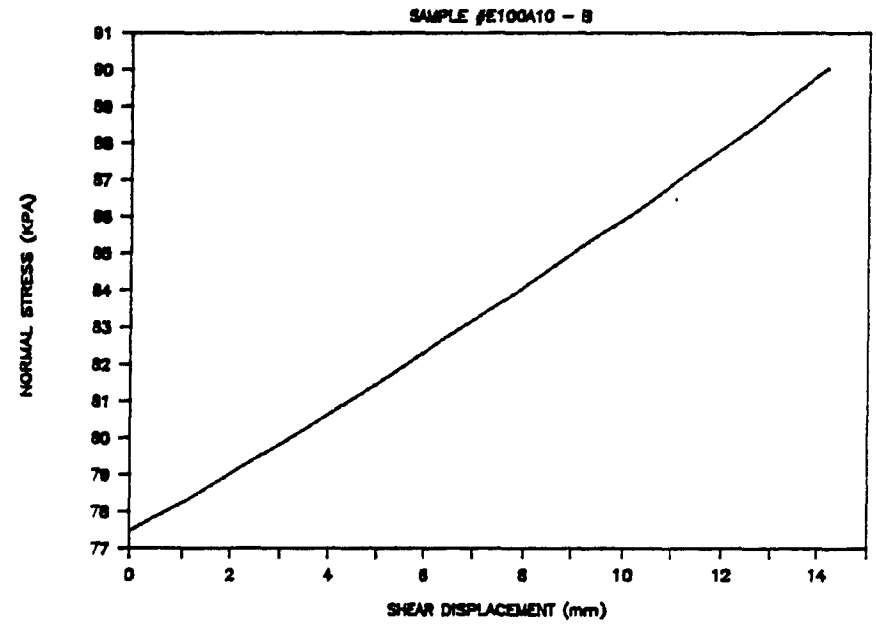
SAMPLE #E100A10 - B
NORMAL STRESS (KPA)
SHEAR DISPLACEMENT (mm)

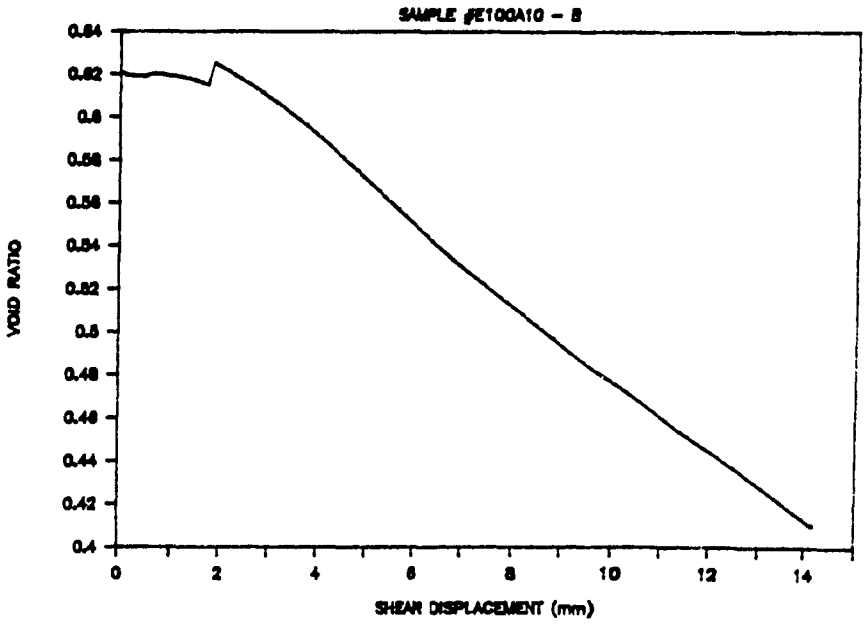
SAMPLE #E100A10 - B
VOID RATIO
SHEAR DISPLACEMENT (mm)

DENISON

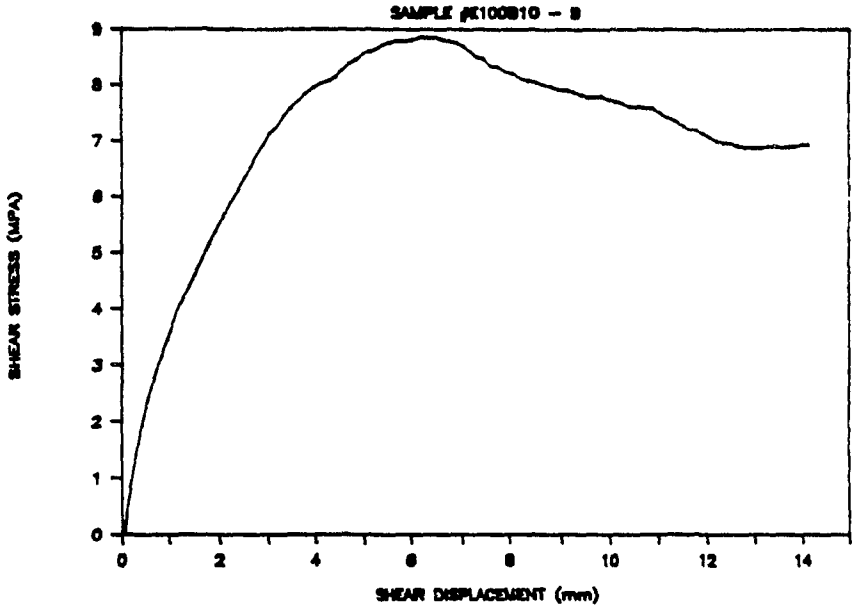
SAMPLE #E100810 - B
SHEAR STRESS (MPA)
0
1
2
3
4
5
6
7
8
9
0
2
4
6
8
10
12
14
SHEAR DISPLACEMENT (mm)

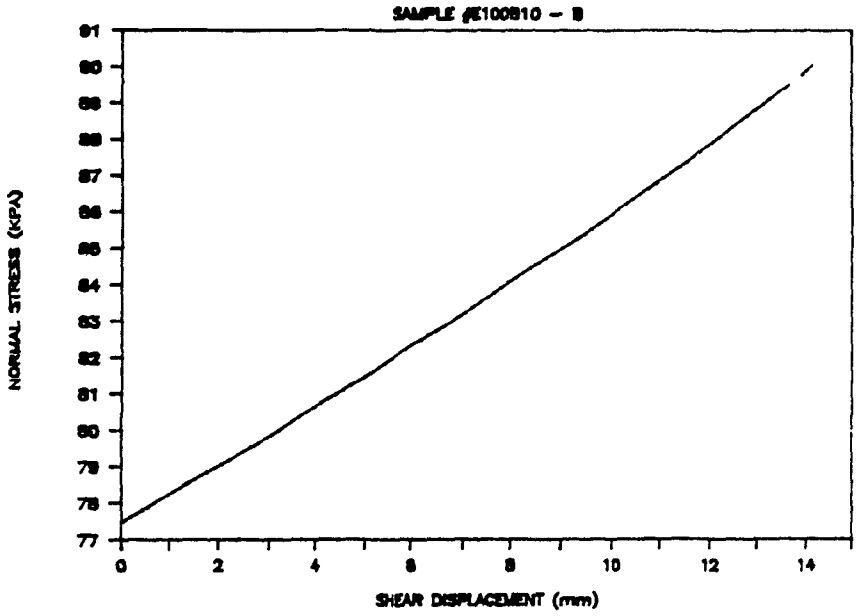
SAMPLE #E100810 - B
NORMAL STRESS (KPA)
77
78
79
80
81
82
83
84
85
86
87
88
89
90
91
0
2
4
6
8
10
12
14
SHEAR DISPLACEMENT (mm)

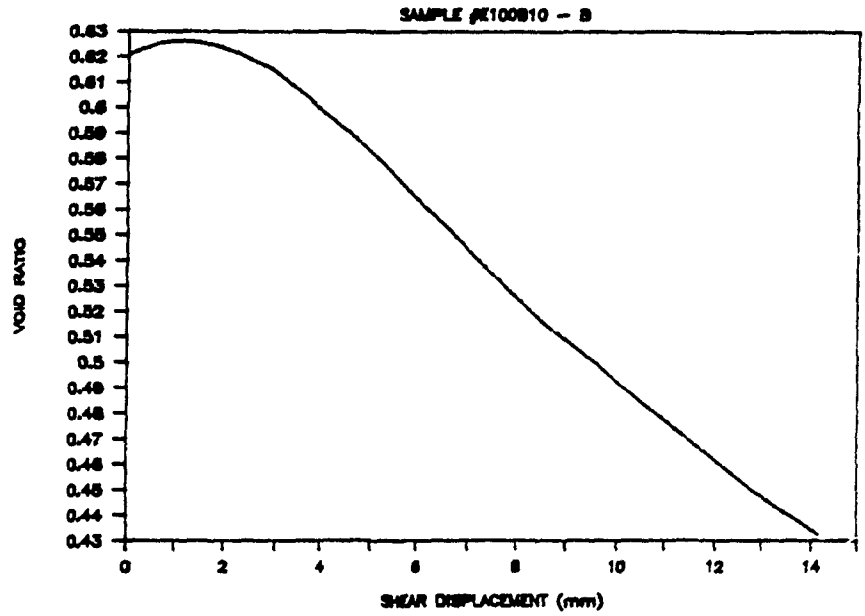
SAMPLE #E100810 - B
VOID RATIO
0.43
0.44
0.45
0.46
0.47
0.48
0.49
0.5
0.51
0.52
0.53
0.54
0.55
0.56
0.57
0.58
0.59
0.6
0.61
0.62
0.63
0
2
4
6
8
10
12
14
SHEAR DISPLACEMENT (mm)

DENISON

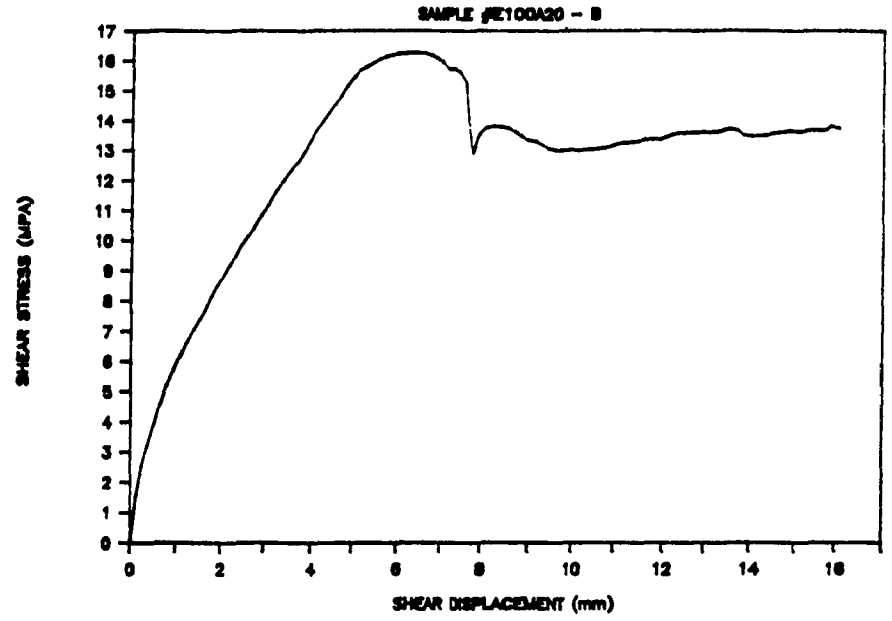
SAMPLE #E100A20 - B
SHEAR STRESS (MPA)
SHEAR DISPLACEMENT (mm)

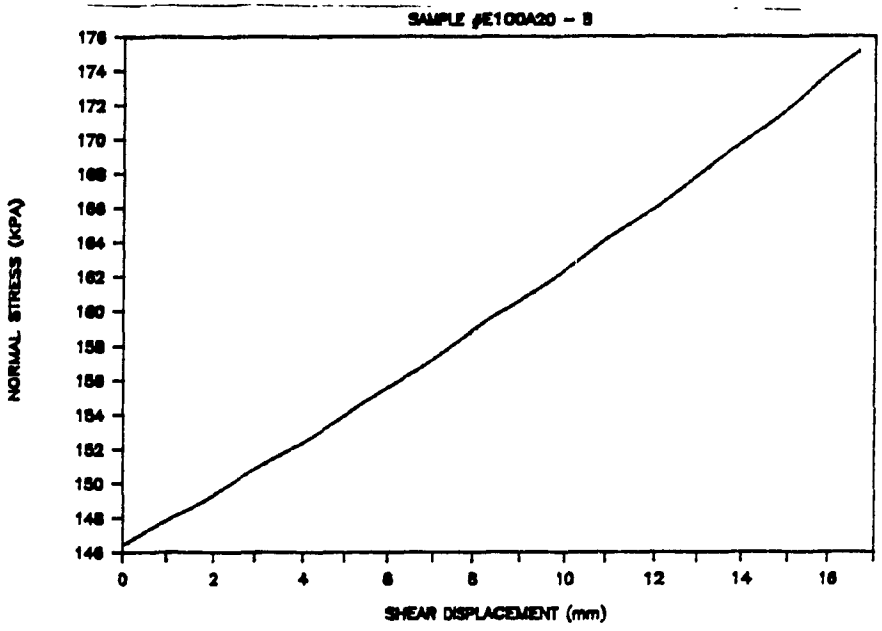
SAMPLE #E100A20 - B
NORMAL STRESS (KPA)
SHEAR DISPLACEMENT (mm)

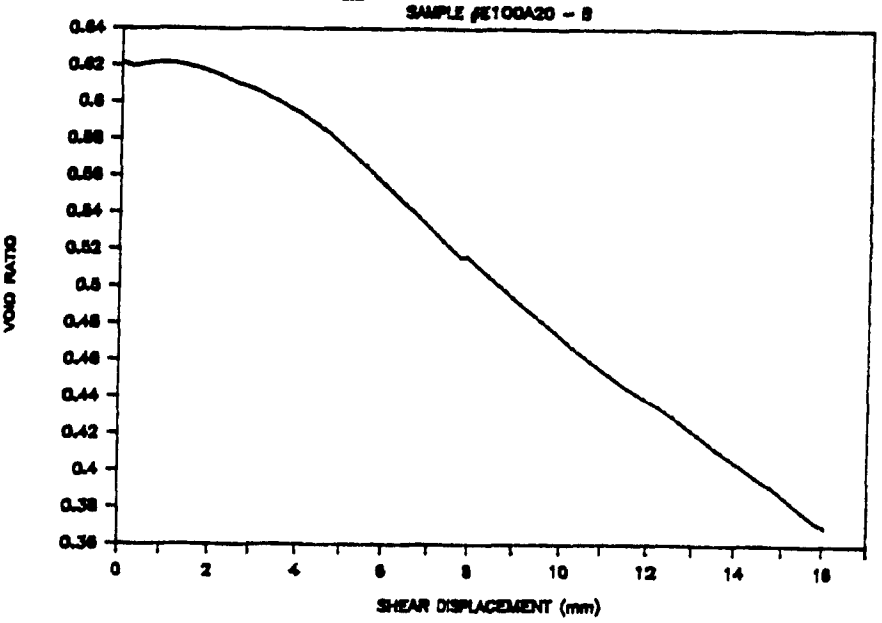
SAMPLE #E100A20 - B
VOID RATIO
SHEAR DISPLACEMENT (mm)

DENISON

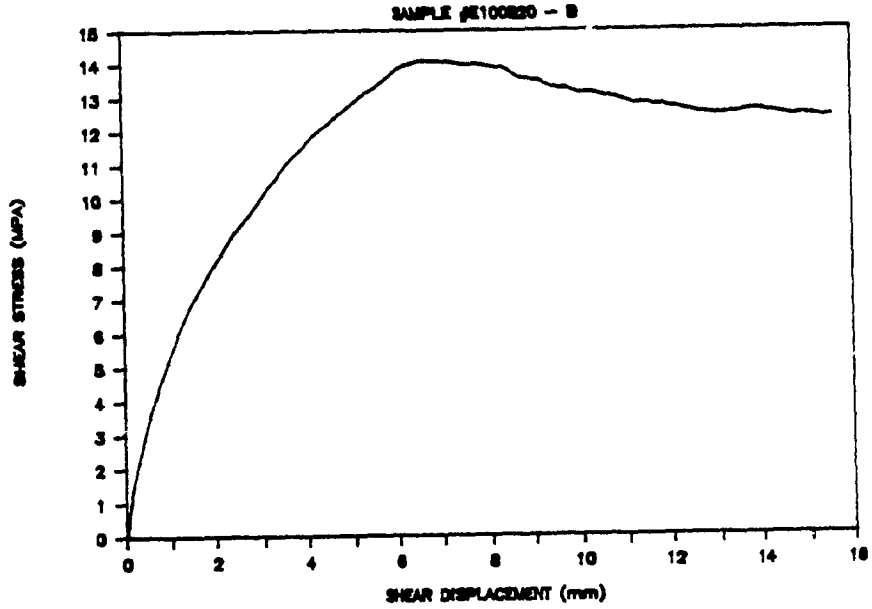
SAMPLE βE100820 – B
SHEAR STRESS (MPA)
SHEAR DISPLACEMENT (mm)

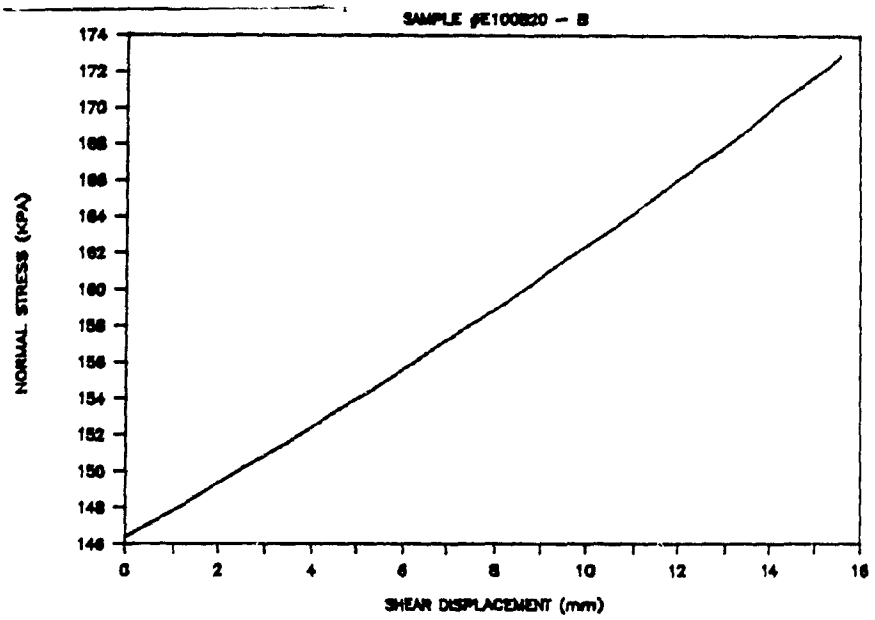
SAMPLE βE100820 – B
NORMAL STRESS (KPA)
SHEAR DISPLACEMENT (mm)

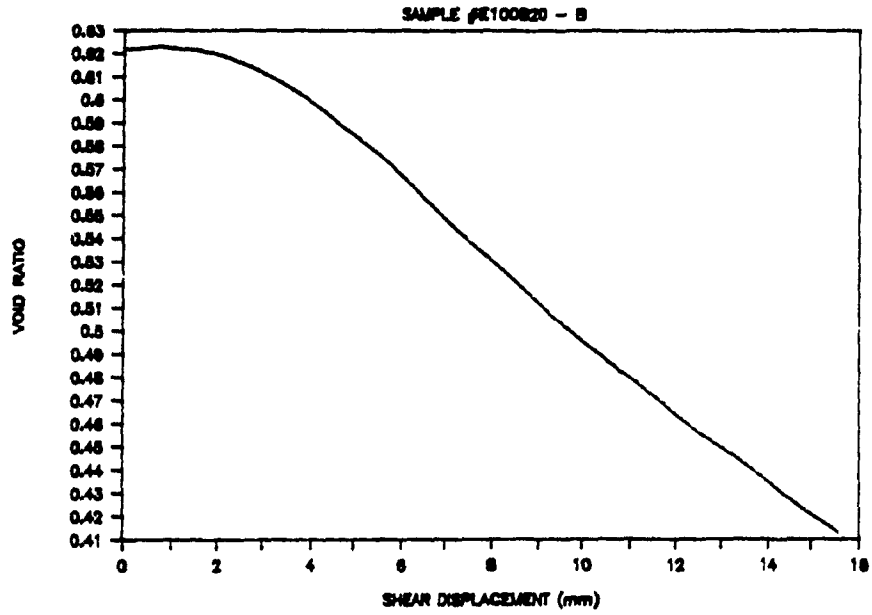
SAMPLE βE100820 – B
VOID RATIO
SHEAR DISPLACEMENT (mm)

DENISON

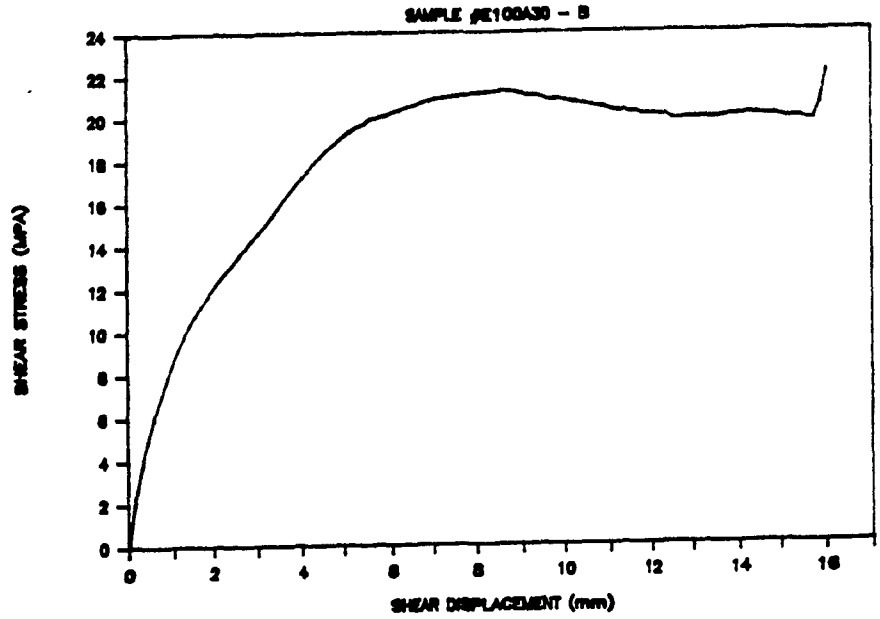
SAMPLE #E100A30 - B
SHEAR STRESS (MPA)
SHEAR DISPLACEMENT (mm)

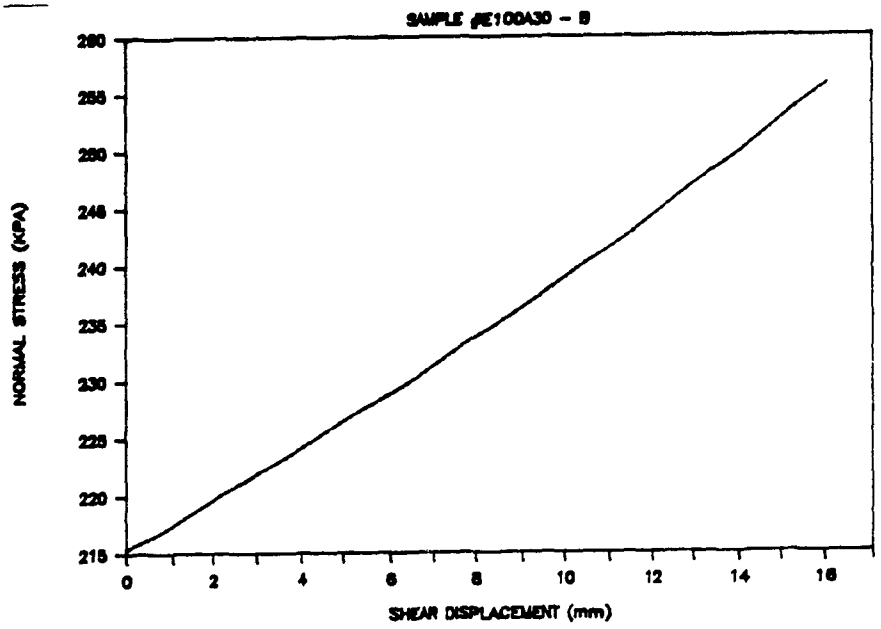
SAMPLE #E100A30 - B
NORMAL STRESS (KPA)
SHEAR DISPLACEMENT (mm)

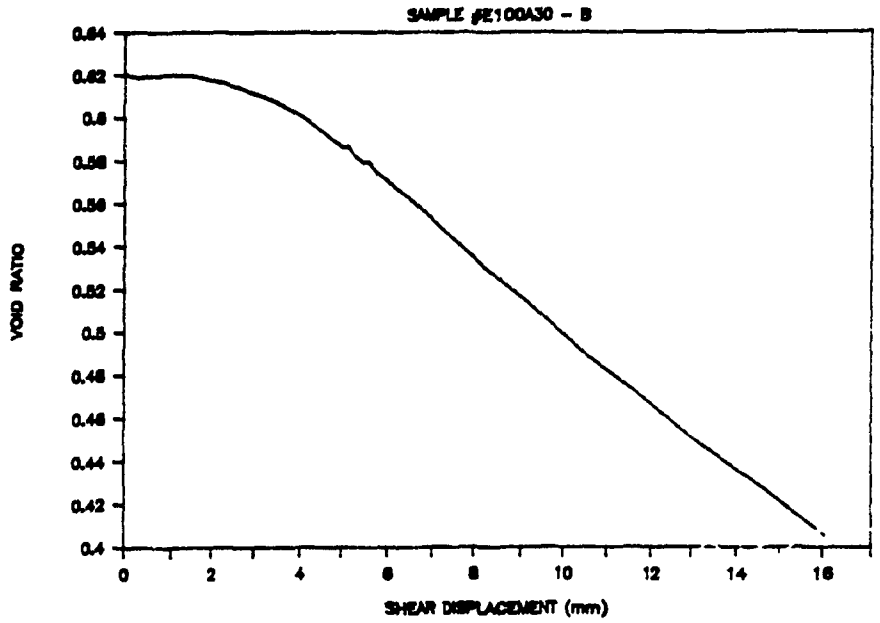
SAMPLE #E100A30 - B
VOID RATIO
SHEAR DISPLACEMENT (mm)

DENISON

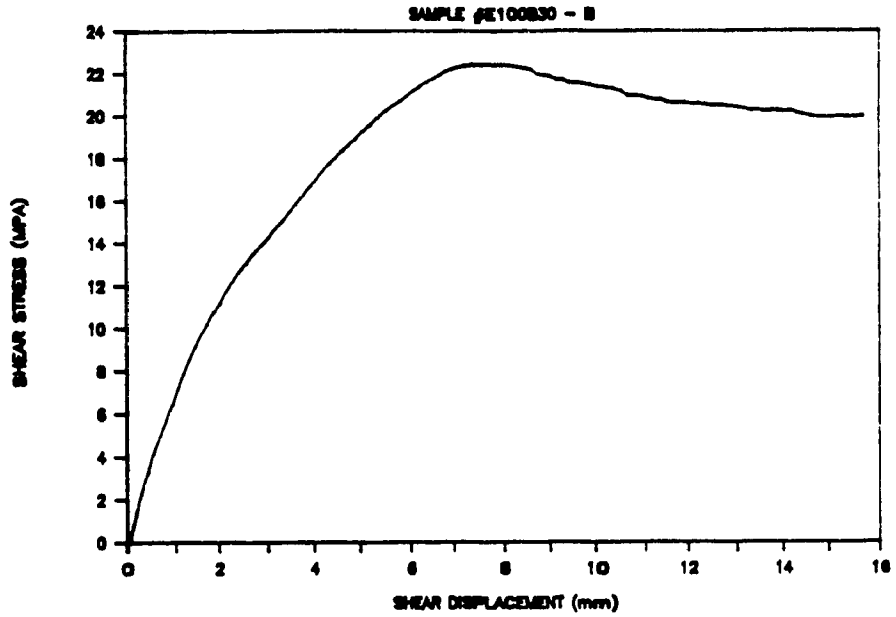
SAMPLE #E100830 - B
SHEAR STRESS (MPA)
SHEAR DISPLACEMENT (mm)

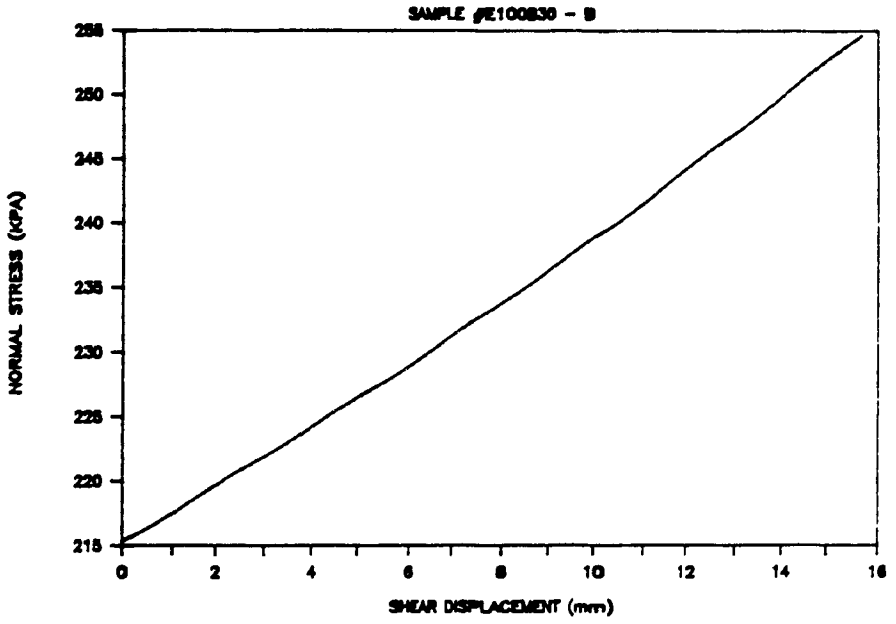
SAMPLE #E100830 - B
NORMAL STRESS (KPA)
SHEAR DISPLACEMENT (mm)

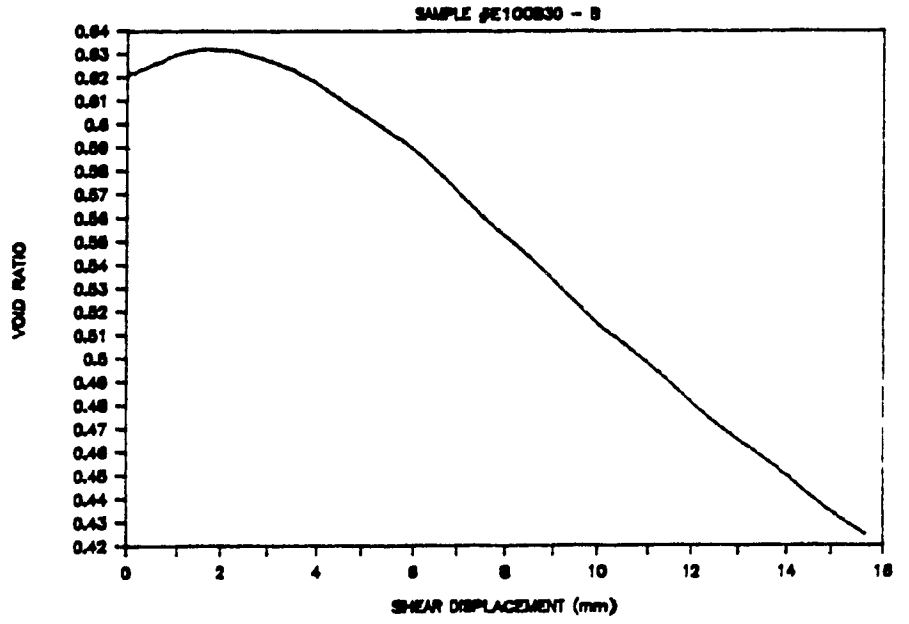
SAMPLE #E100830 - B
VOID RATIO
SHEAR DISPLACEMENT (mm)

DENISON

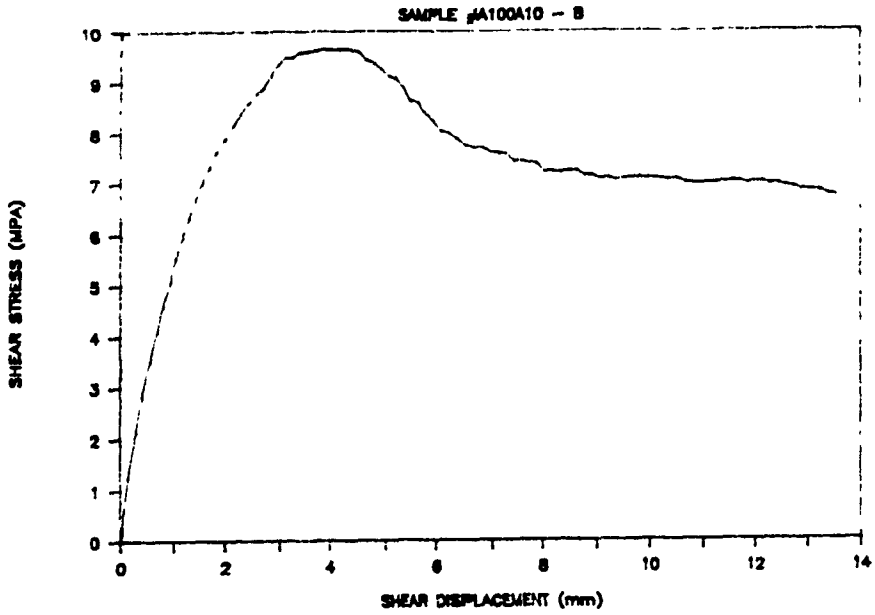
SAMPLE gA100A10 - S
SHEAR STRESS (MPA)
SHEAR DISPLACEMENT (mm)

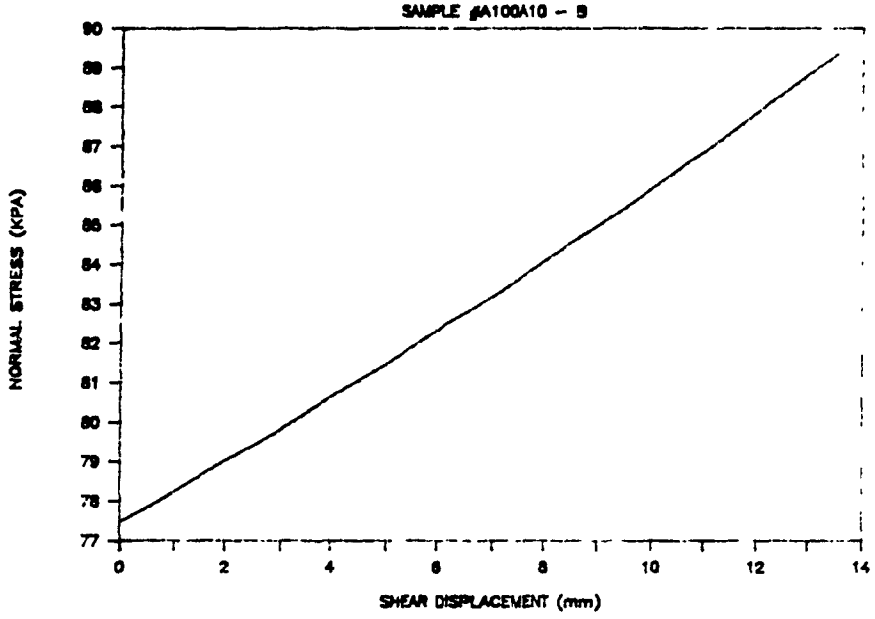
SAMPLE gA100A10 - S
NORMAL STRESS (KPA)
SHEAR DISPLACEMENT (mm)

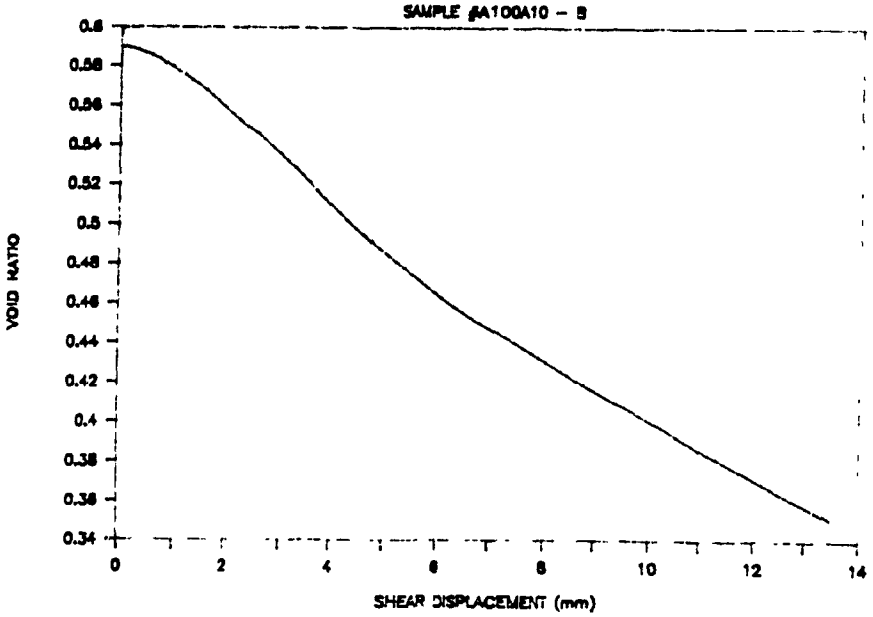
SAMPLE gA100A10 - S
VOID RATIO
SHEAR DISPLACEMENT (mm)

DENISON

SAMPLE #A100B10 - B

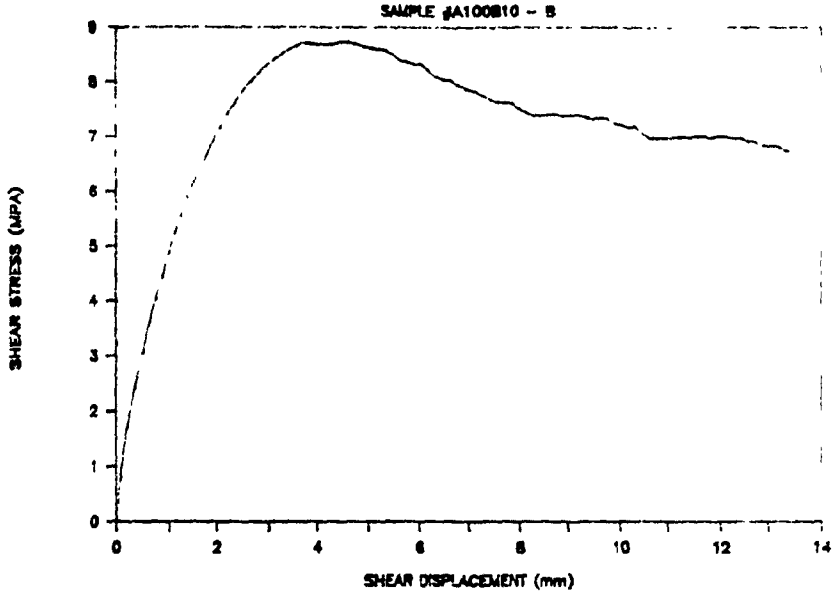

SAMPLE #A100B10 - B

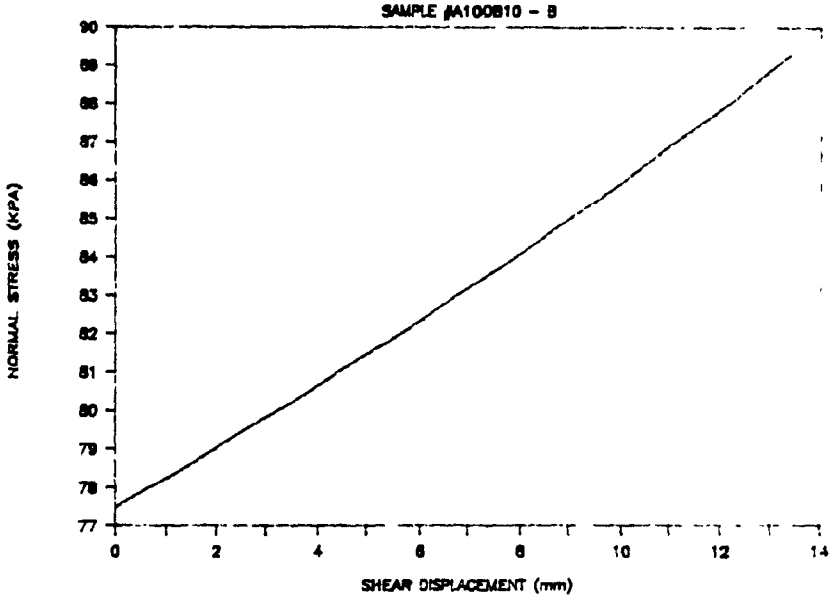

SAMPLE #A100B10 - B

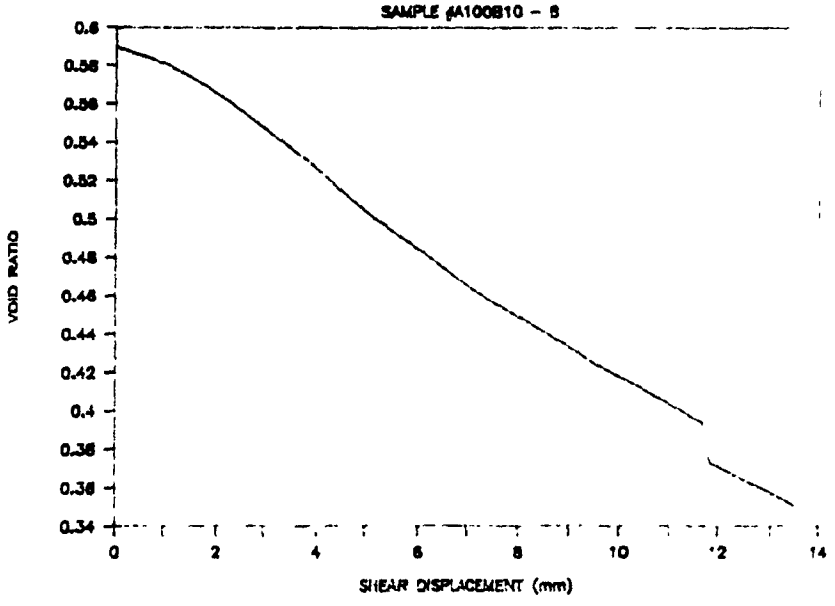

DENISON

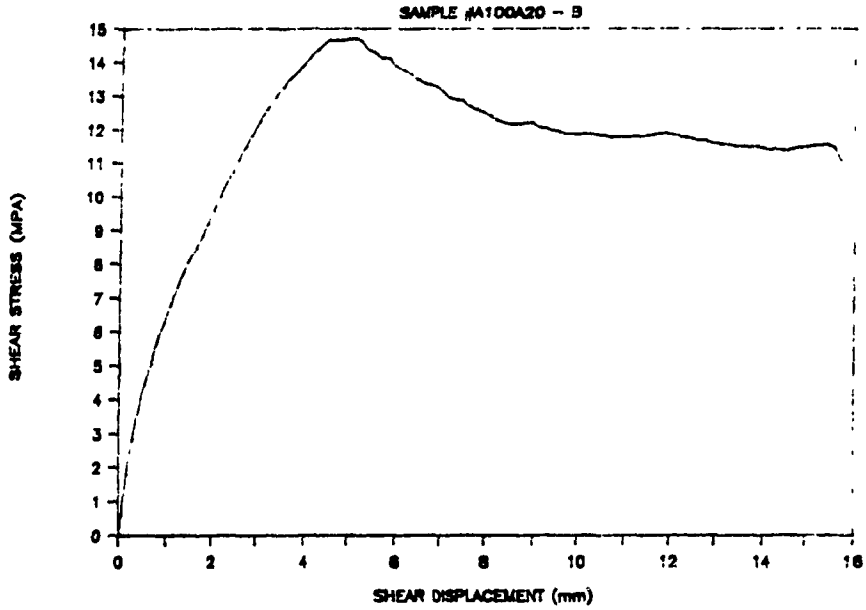
SAMPLE jA100A20 - B
SHEAR STRESS (MPA)
SHEAR DISPLACEMENT (mm)

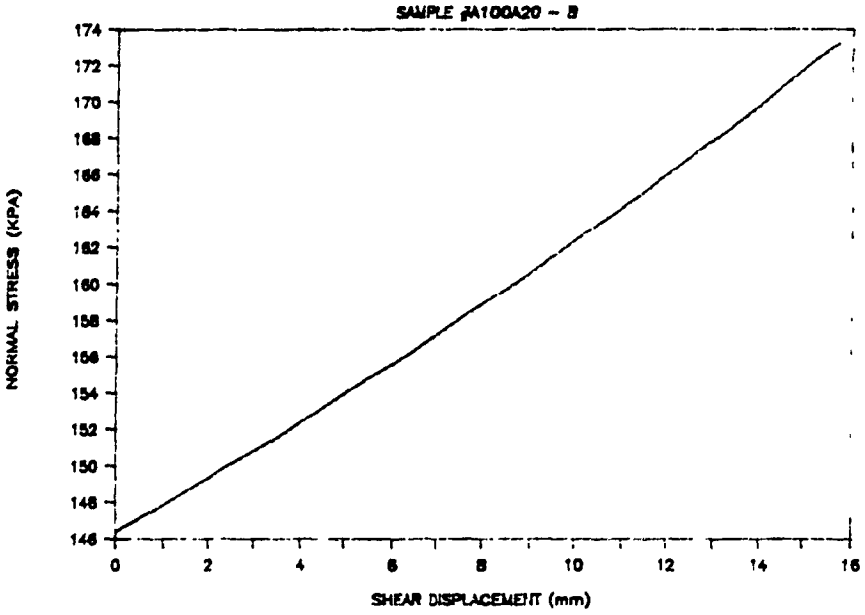
SAMPLE jA100A20 - B
NORMAL STRESS (KPA)
SHEAR DISPLACEMENT (mm)

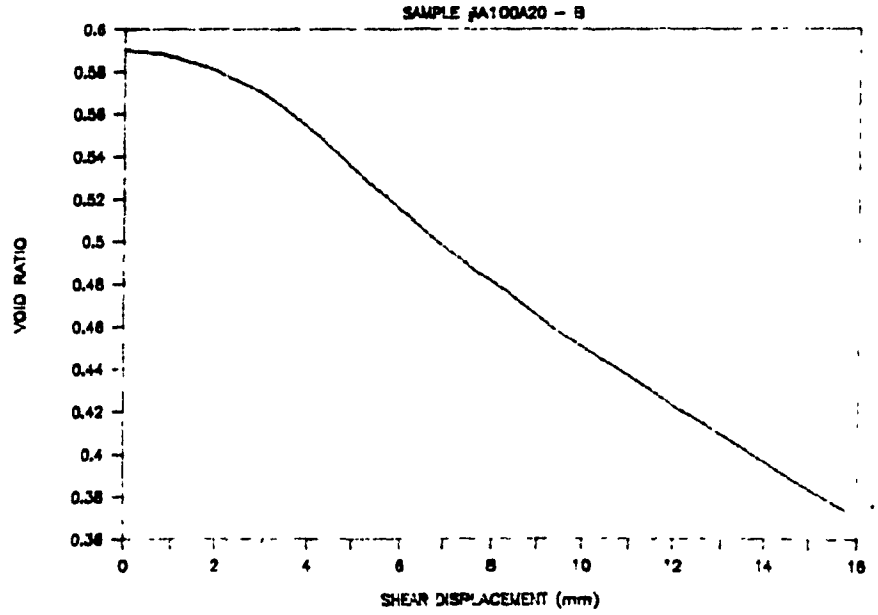
SAMPLE jA100A20 - B
VOID RATIO
SHEAR DISPLACEMENT (mm)

DENISON

SAMPLE #A100820 - B

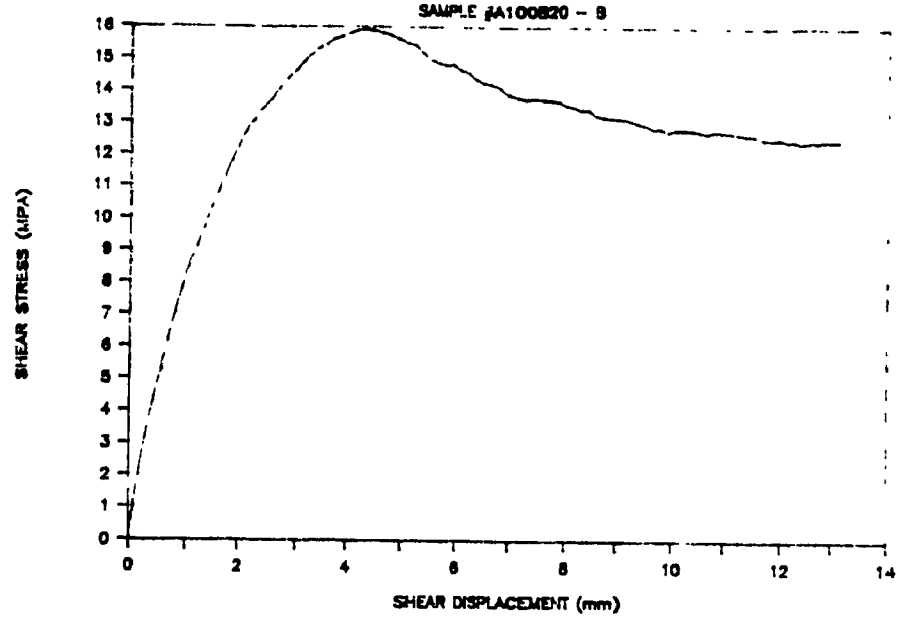

SAMPLE #A100820 - B

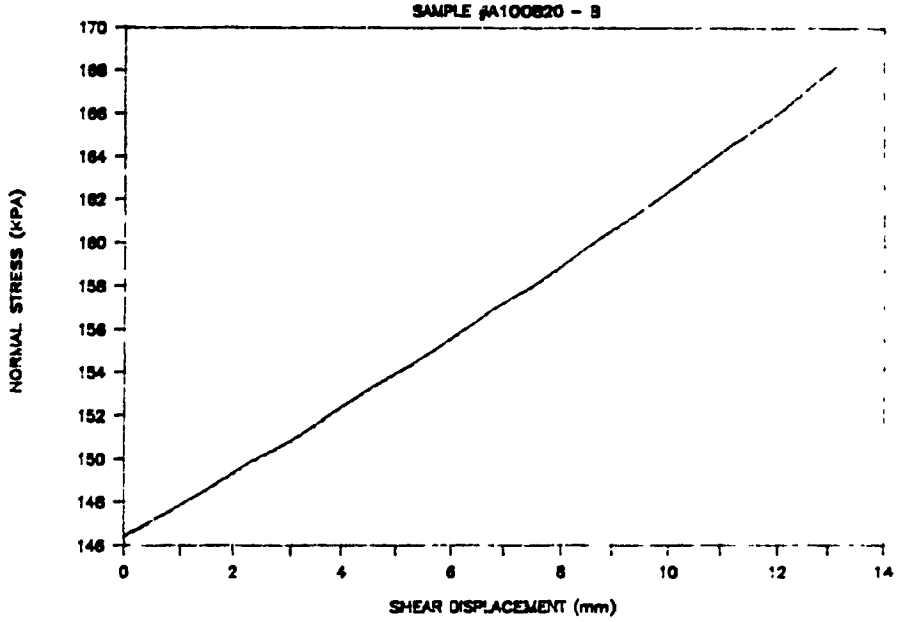

SAMPLE #A100820 - B

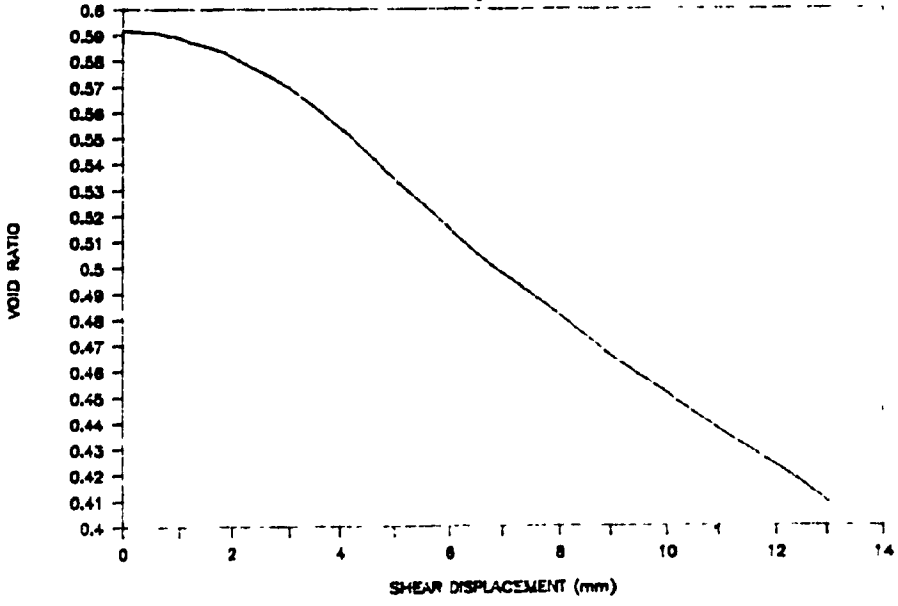

DENISON

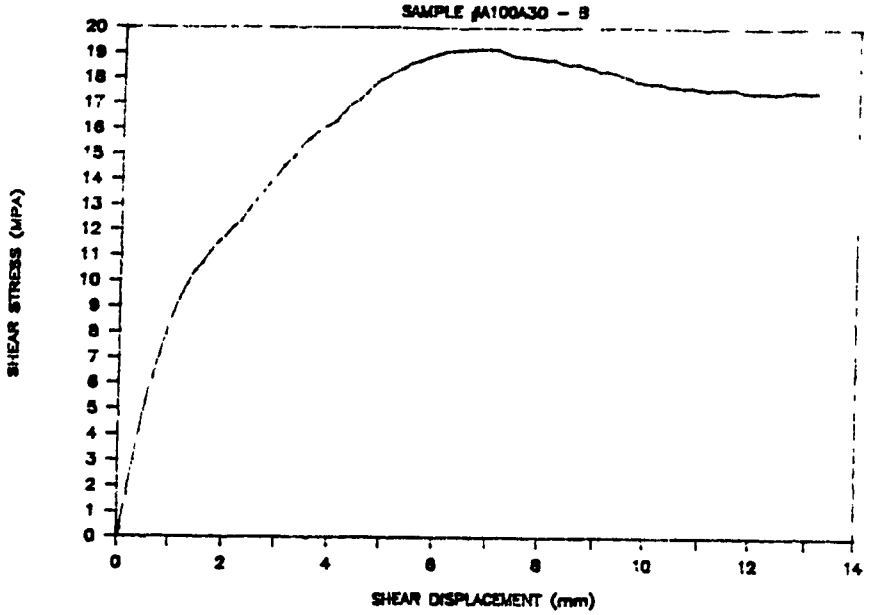
SAMPLE jA100A30 – B
SHEAR STRESS (MPA)
SHEAR DISPLACEMENT (mm)

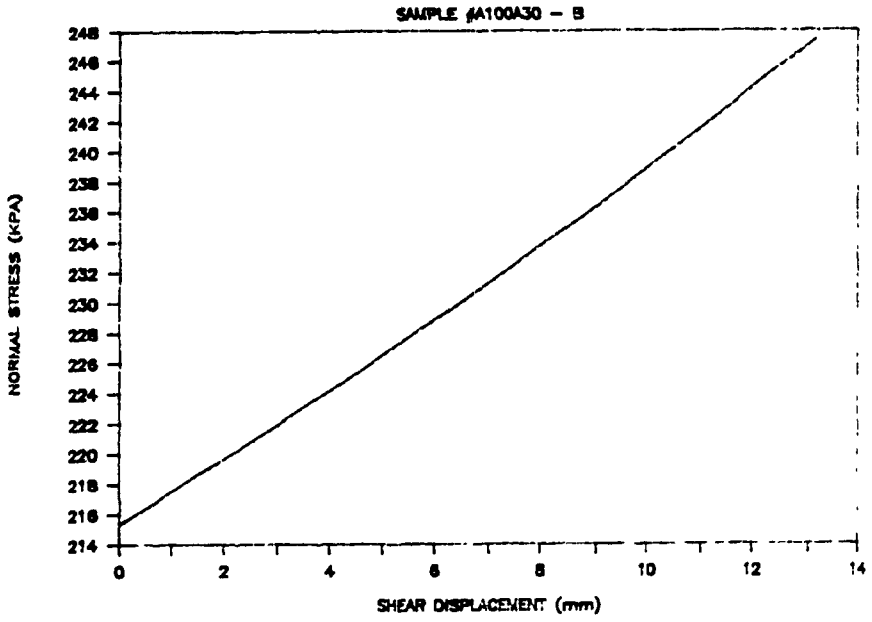
SAMPLE jA100A30 – B
NORMAL STRESS (KPA)
SHEAR DISPLACEMENT (mm)

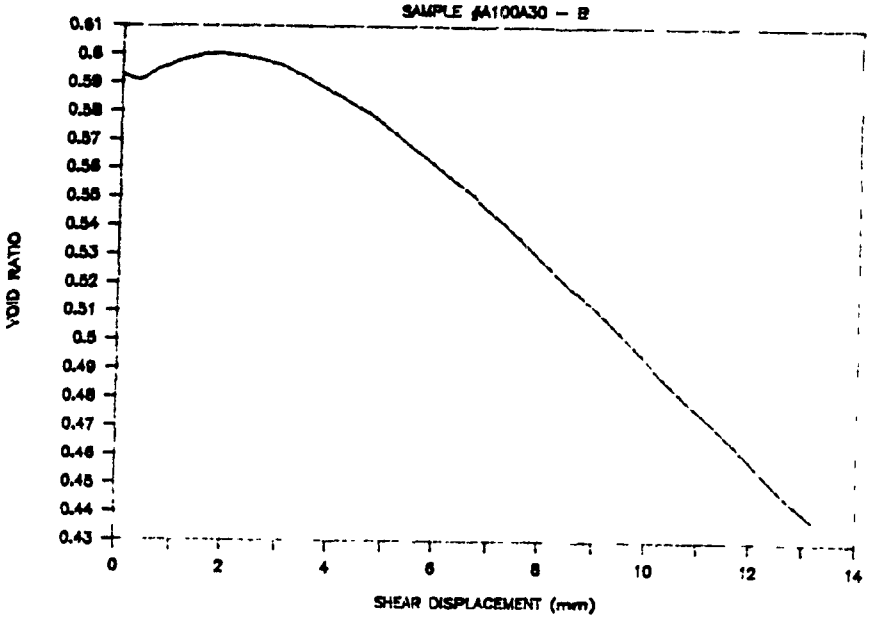
SAMPLE jA100A30 – B
VOID RATIO
SHEAR DISPLACEMENT (mm)

DENISON

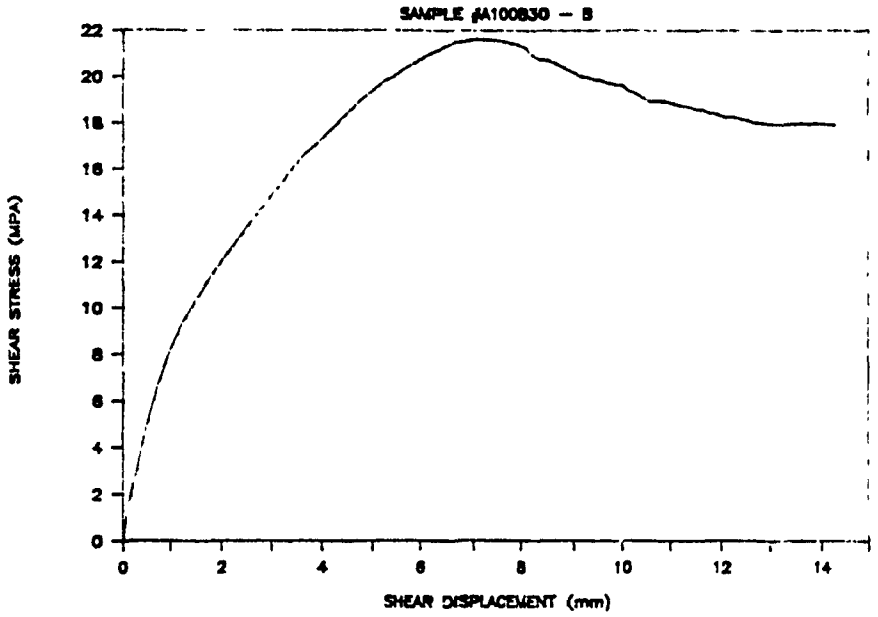
SAMPLE jA100830 – B
SHEAR STRESS (MPA)
SHEAR DISPLACEMENT (mm)

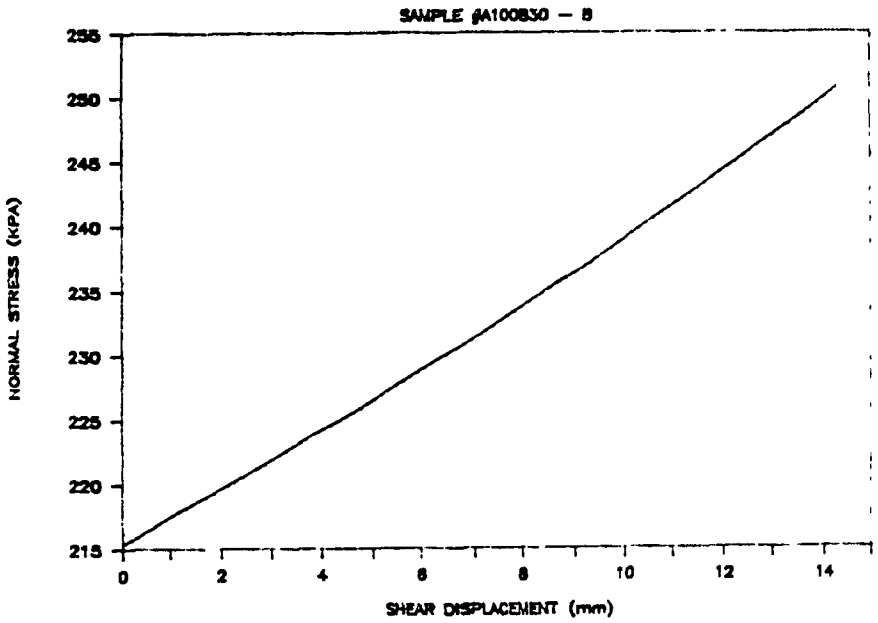
SAMPLE jA100830 – B
NORMAL STRESS (kPA)
SHEAR DISPLACEMENT (mm)

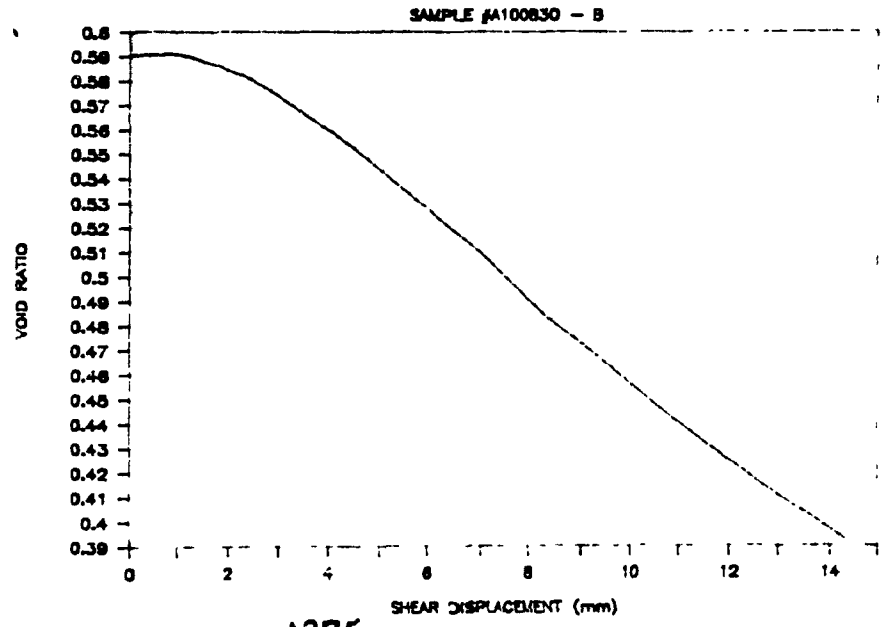
SAMPLE jA100830 – B
VOID RATIO
SHEAR DISPLACEMENT (mm)

DENISON

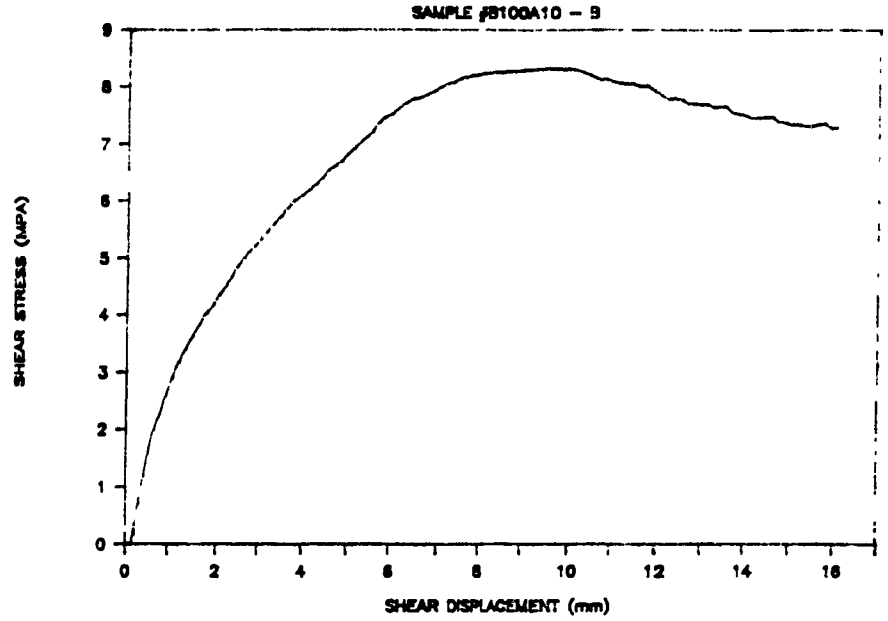
SAMPLE #B100A10 - B
SHEAR STRESS (MPA)
SHEAR DISPLACEMENT (mm)

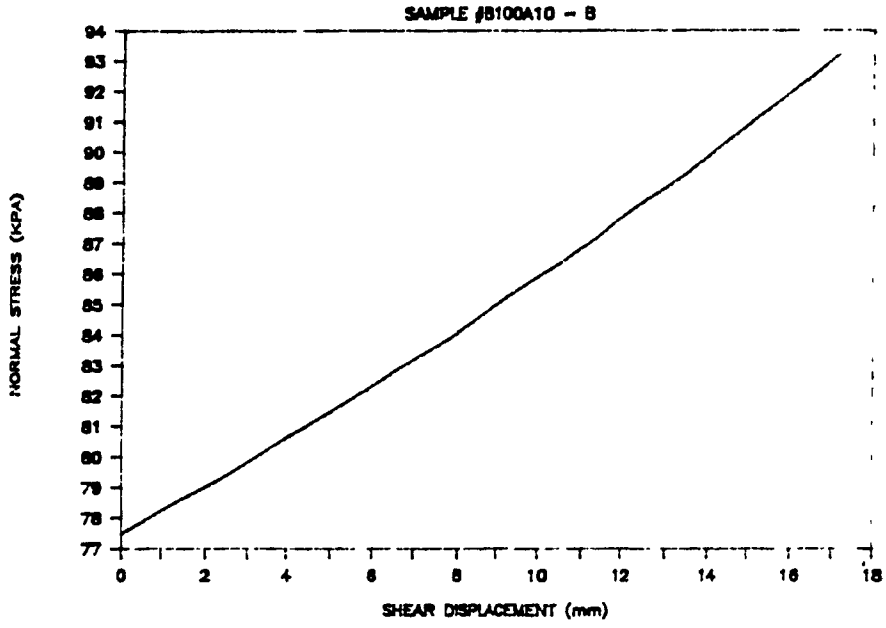
SAMPLE #B100A10 - B
NORMAL STRESS (KPA)
SHEAR DISPLACEMENT (mm)

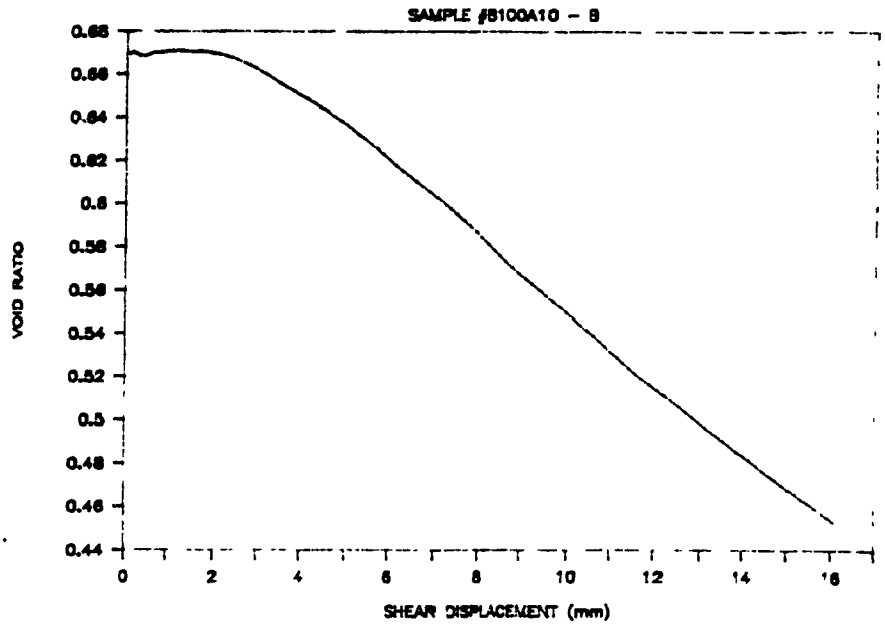
SAMPLE #B100A10 - B
VOID RATIO
SHEAR DISPLACEMENT (mm)

DENISON

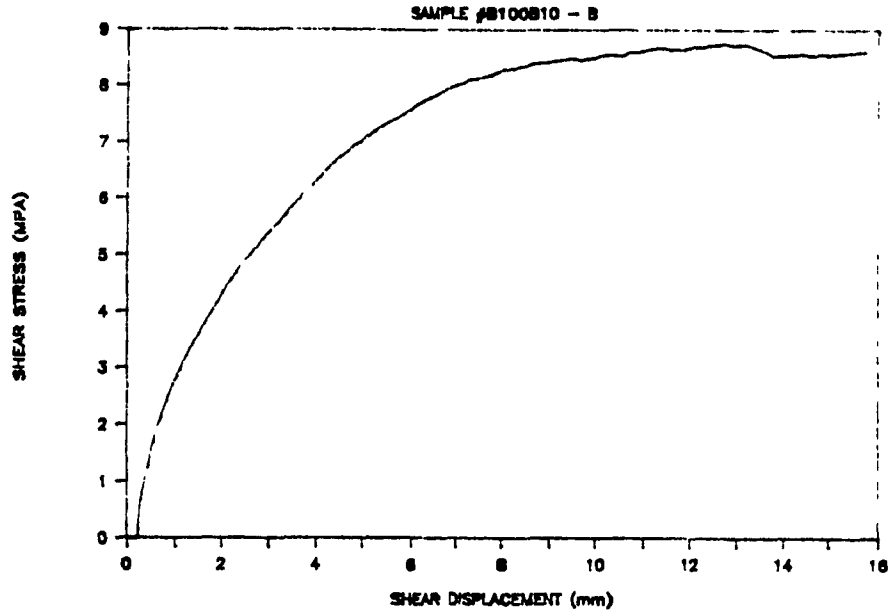
SAMPLE #B100810 - B
SHEAR STRESS (MPA)
0
1
2
3
4
5
6
7
8
9
0
2
4
6
8
10
12
14
16
SHEAR DISPLACEMENT (mm)

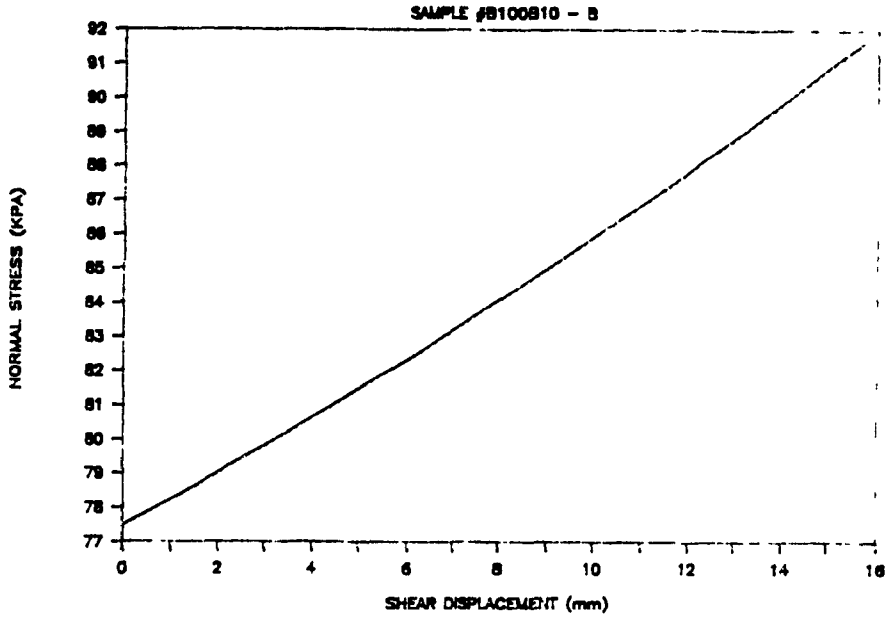
SAMPLE #B100810 - B
NORMAL STRESS (KPA)
77
78
79
80
81
82
83
84
85
86
87
88
89
90
91
92
0
2
4
6
8
10
12
14
16
SHEAR DISPLACEMENT (mm)

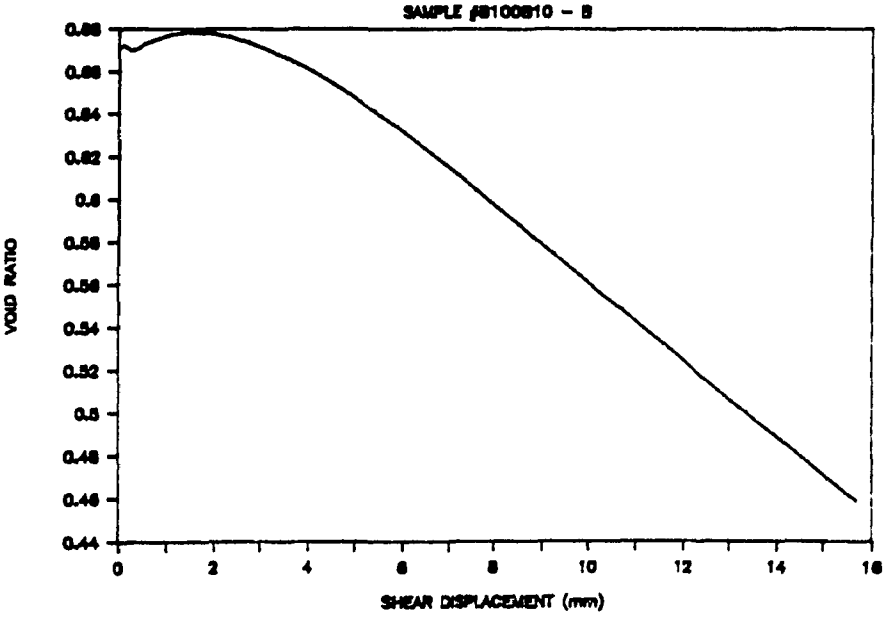
SAMPLE #B100810 - B
VOID RATIO
0.44
0.46
0.48
0.5
0.52
0.54
0.56
0.58
0.6
0.62
0.64
0.66
0.68
0
2
4
6
8
10
12
14
16
SHEAR DISPLACEMENT (mm)

DENISON

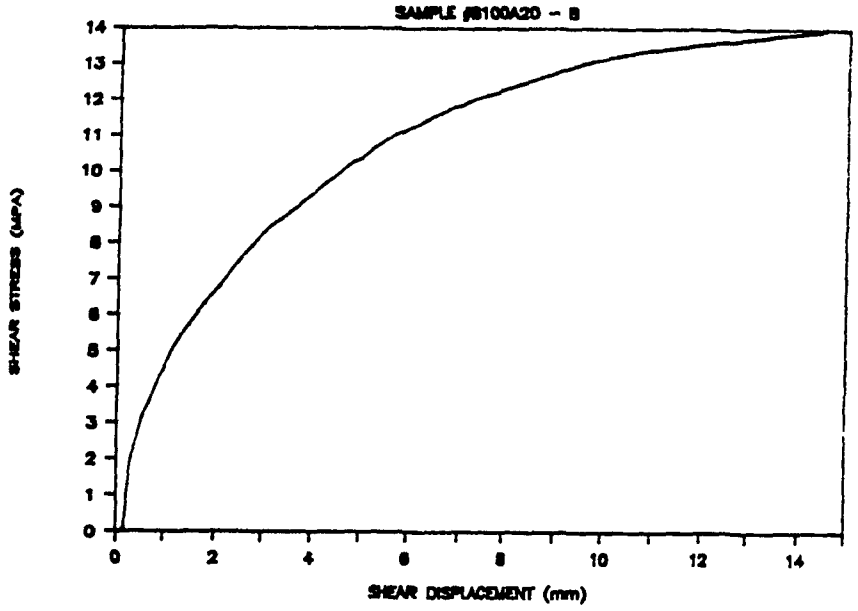
SAMPLE #B100A20 - B
SHEAR STRESS (MPA)
SHEAR DISPLACEMENT (mm)

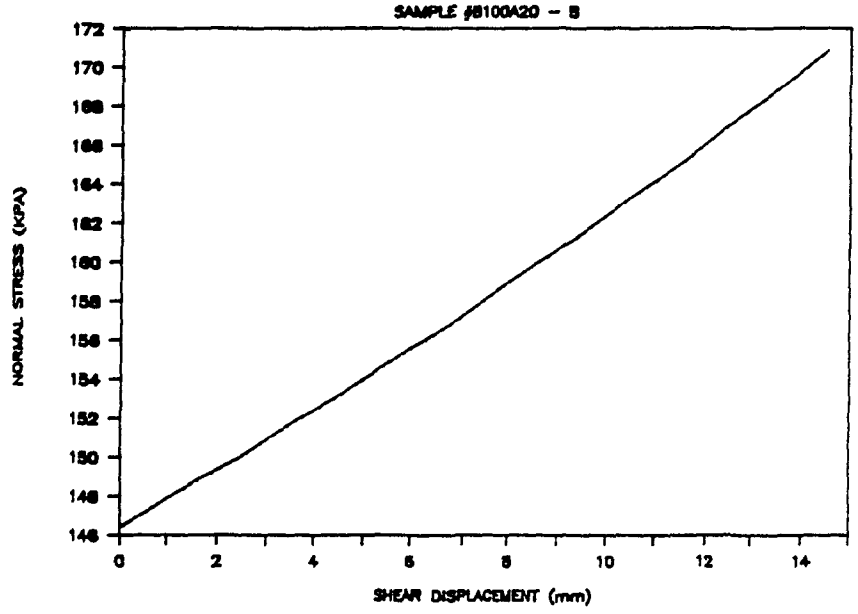
SAMPLE #B100A20 - B
NORMAL STRESS (KPA)
SHEAR DISPLACEMENT (mm)

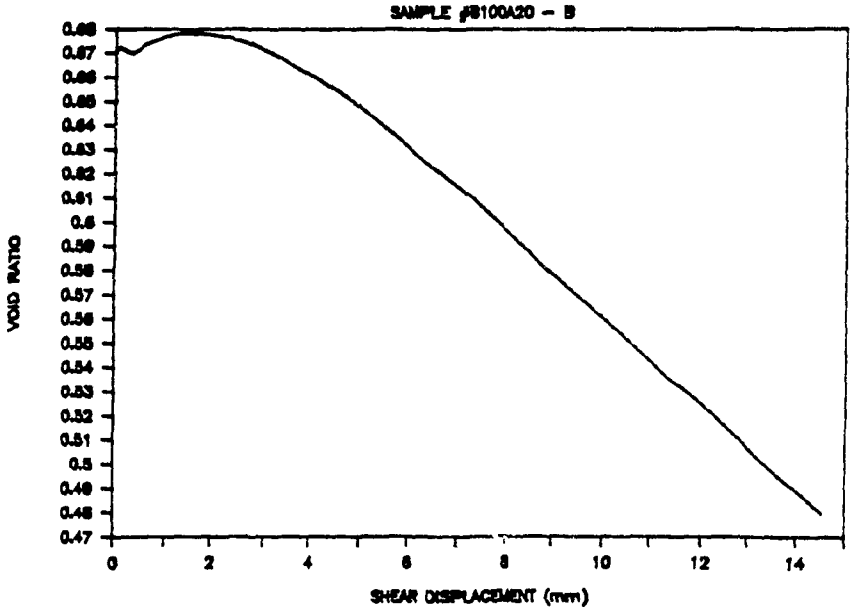
SAMPLE #B100A20 - B
VOID RATIO
SHEAR DISPLACEMENT (mm)

DENISON

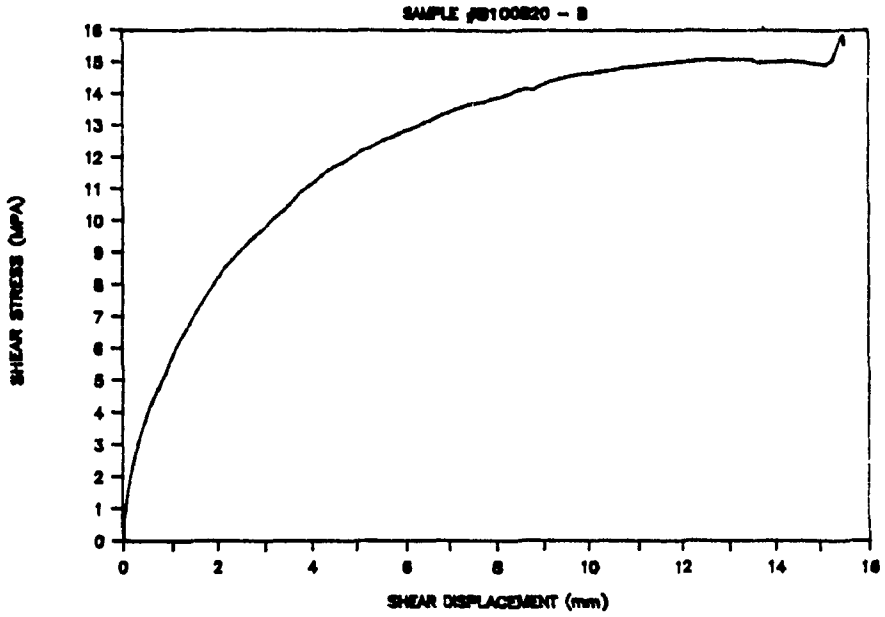
SAMPLE #B100820 -- B
SHEAR STRESS (MPA)
SHEAR DISPLACEMENT (mm)

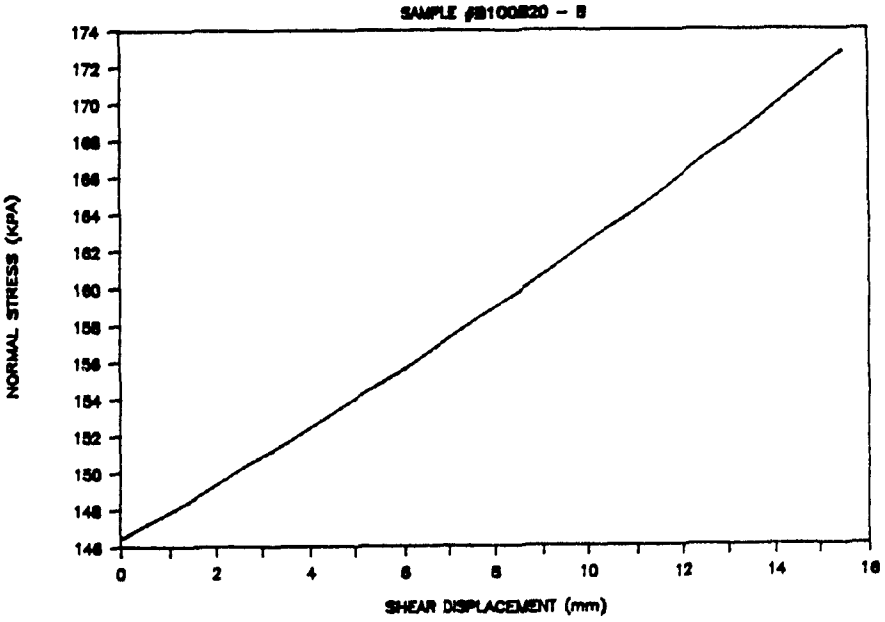
SAMPLE #B100820 -- B
NORMAL STRESS (KPA)
SHEAR DISPLACEMENT (mm)

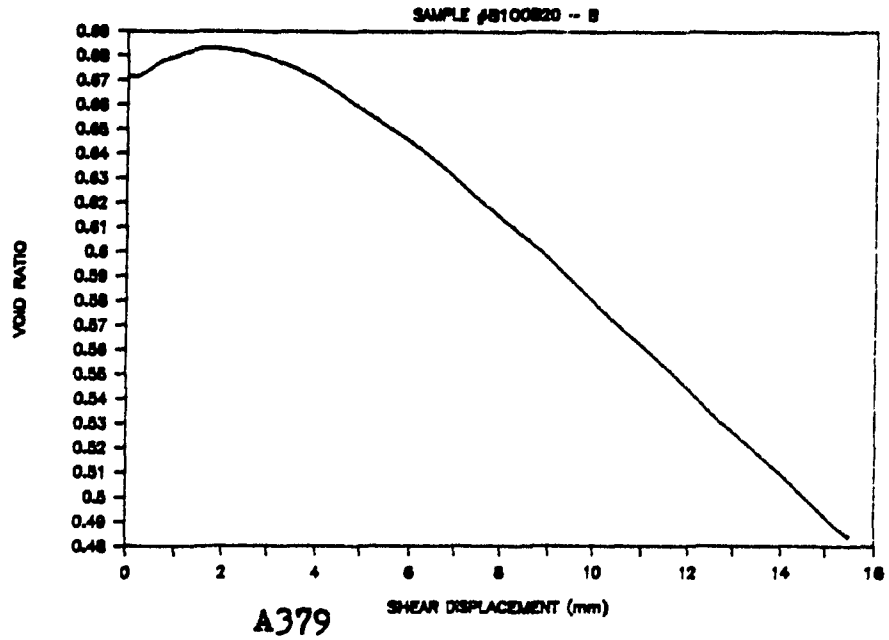
SAMPLE #B100820 -- B
VOID RATIO
SHEAR DISPLACEMENT (mm)

DENISON

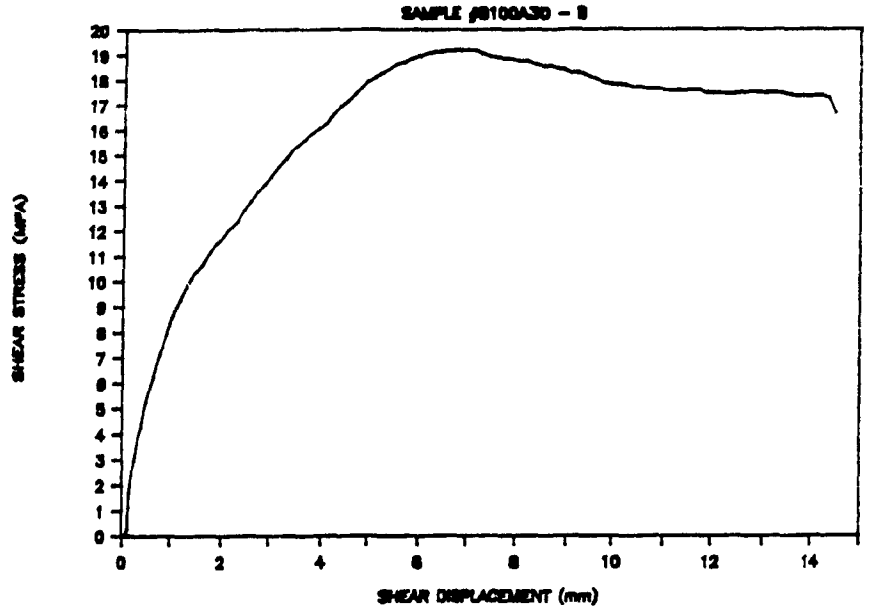
SAMPLE jB100A30 – B
SHEAR STRESS (MPA)
SHEAR DISPLACEMENT (mm)

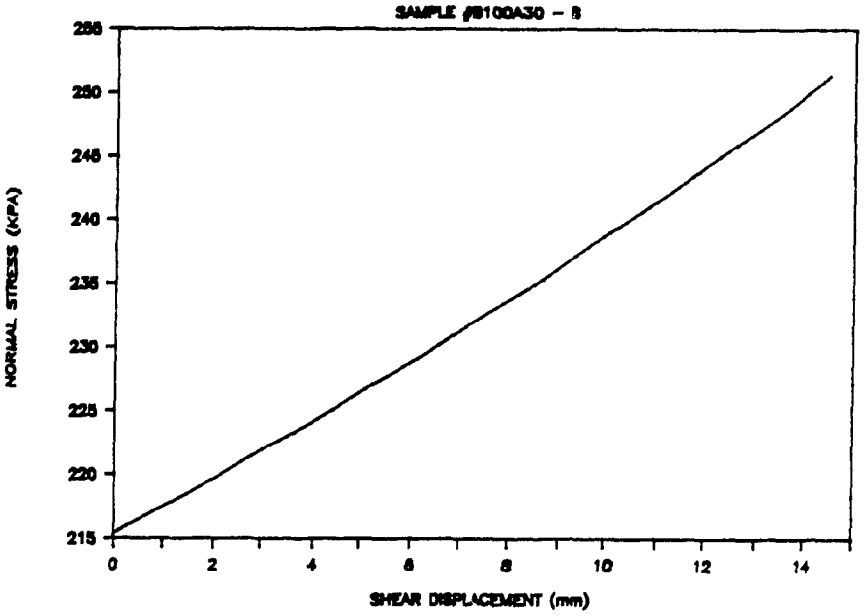
SAMPLE jB100A30 – B
NORMAL STRESS (KPA)
SHEAR DISPLACEMENT (mm)

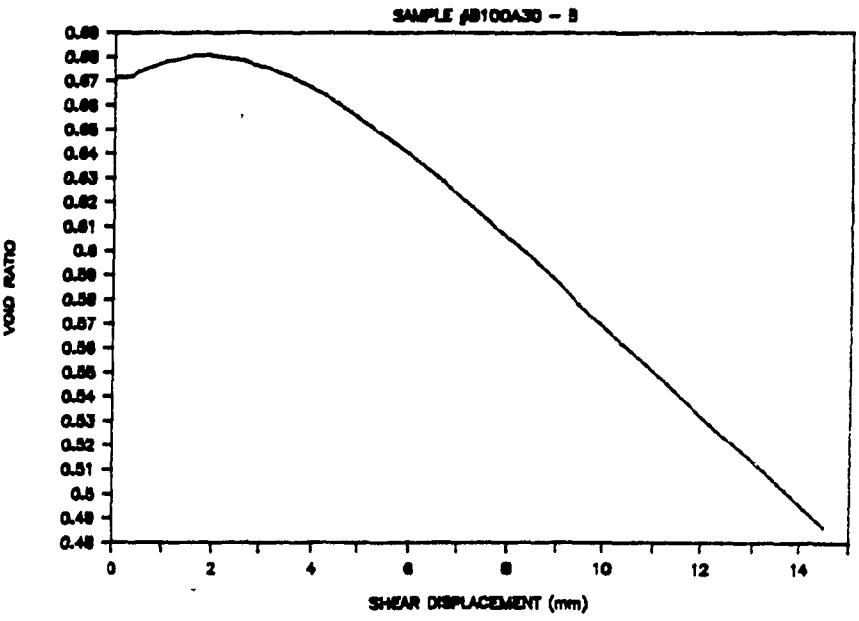
SAMPLE jB100A30 – B
VOID RATIO
SHEAR DISPLACEMENT (mm)

DENISON

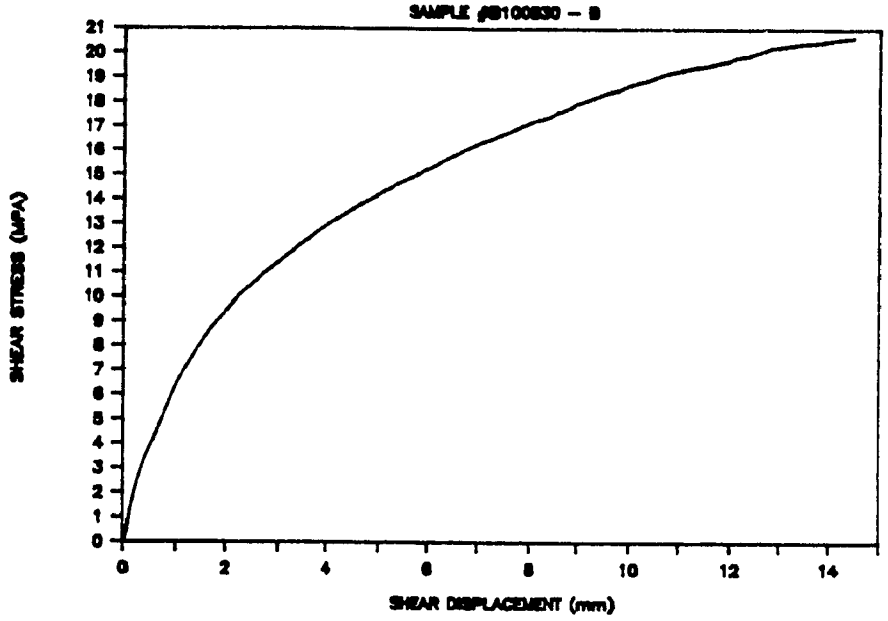
SAMPLE #B100830 - B
SHEAR STRESS (MPA)
SHEAR DISPLACEMENT (mm)

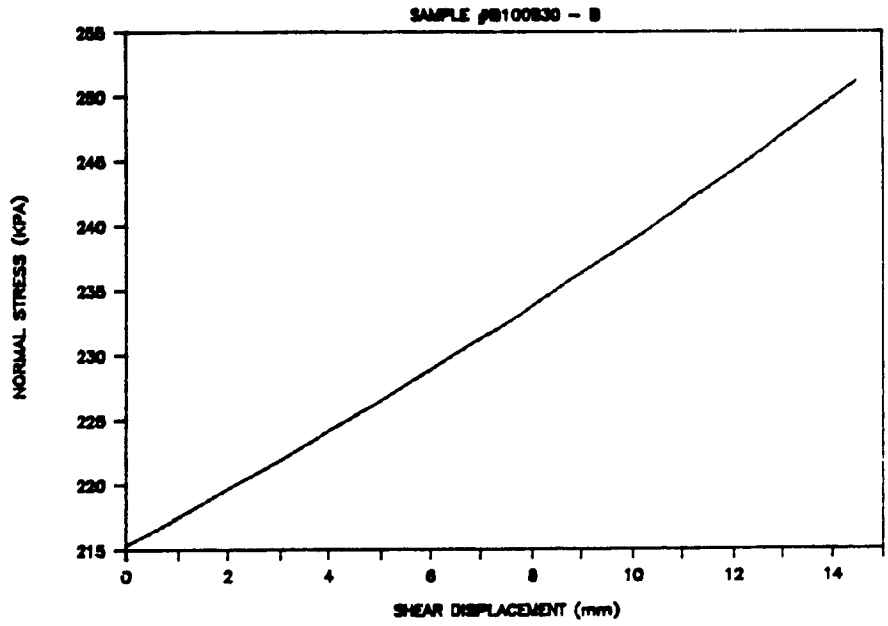
SAMPLE #B100830 - B
NORMAL STRESS (KPA)
SHEAR DISPLACEMENT (mm)

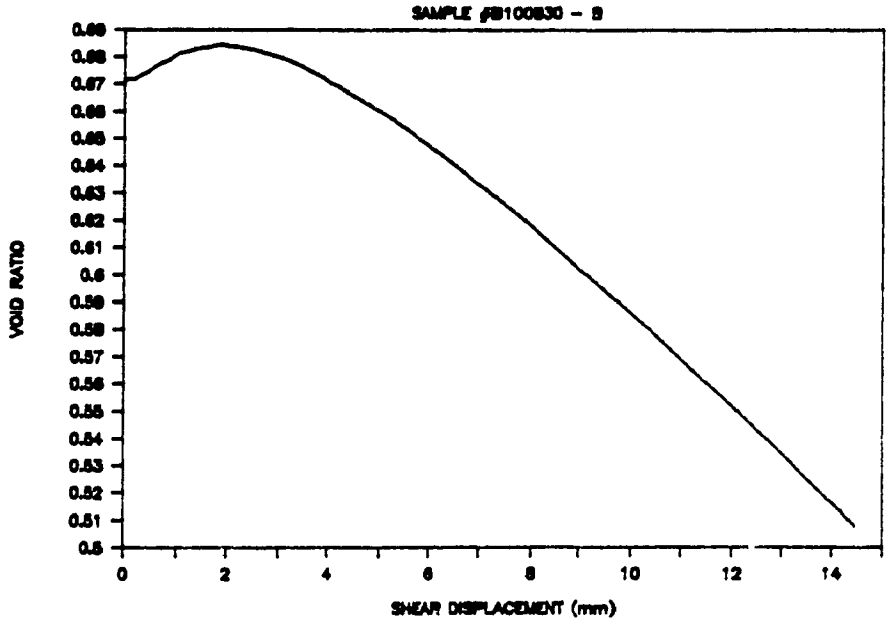
SAMPLE #B100830 - B
VOID RATIO
SHEAR DISPLACEMENT (mm)

DENISON

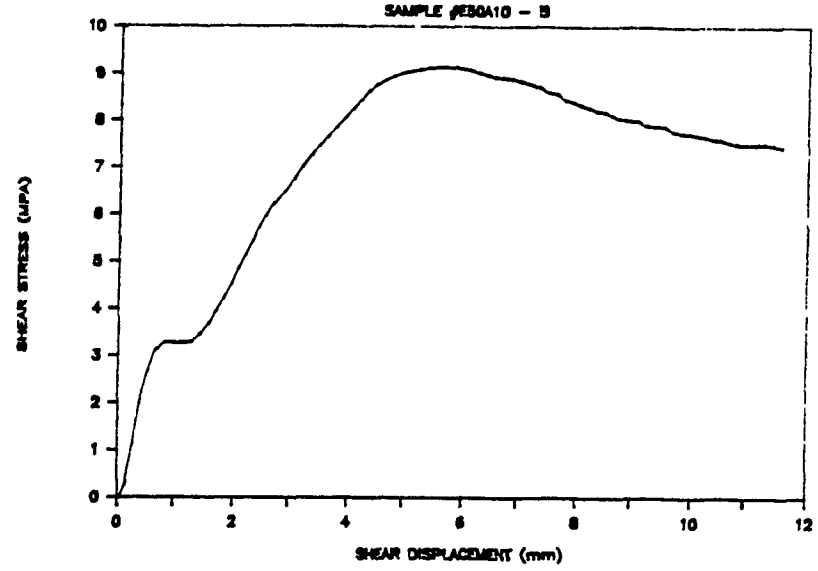
SAMPLE #E50A10 - B
SHEAR STRESS (MPA)
SHEAR DISPLACEMENT (mm)

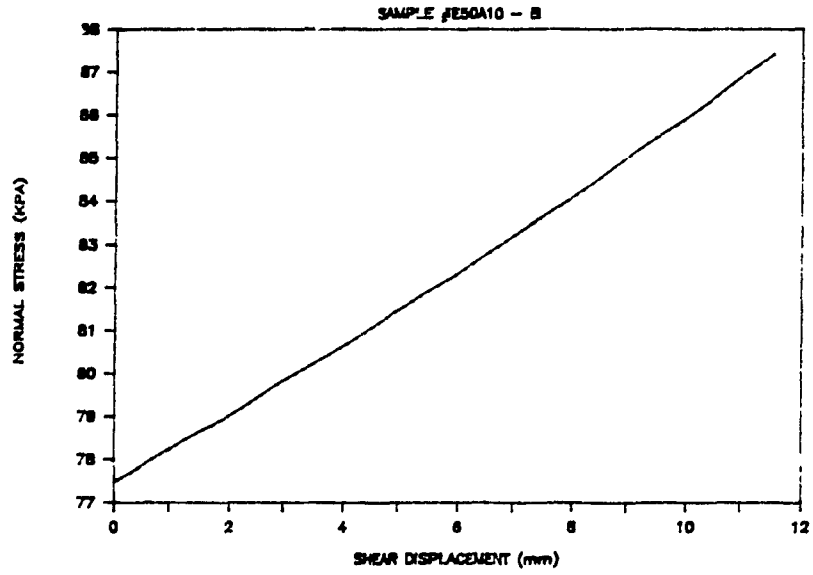
SAMPLE #E50A10 - B
NORMAL STRESS (KPA)
SHEAR DISPLACEMENT (mm)

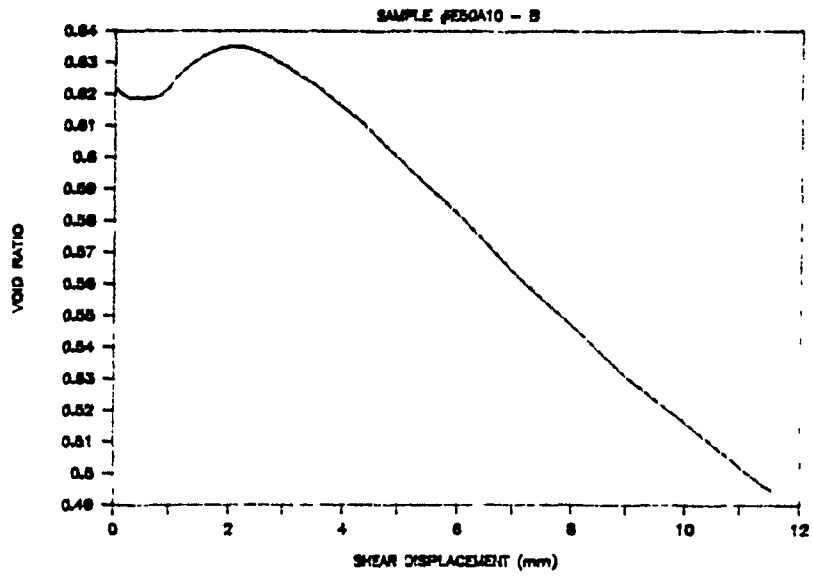
SAMPLE #E50A10 - B
VOID RATIO
SHEAR DISPLACEMENT (mm)

DENISON

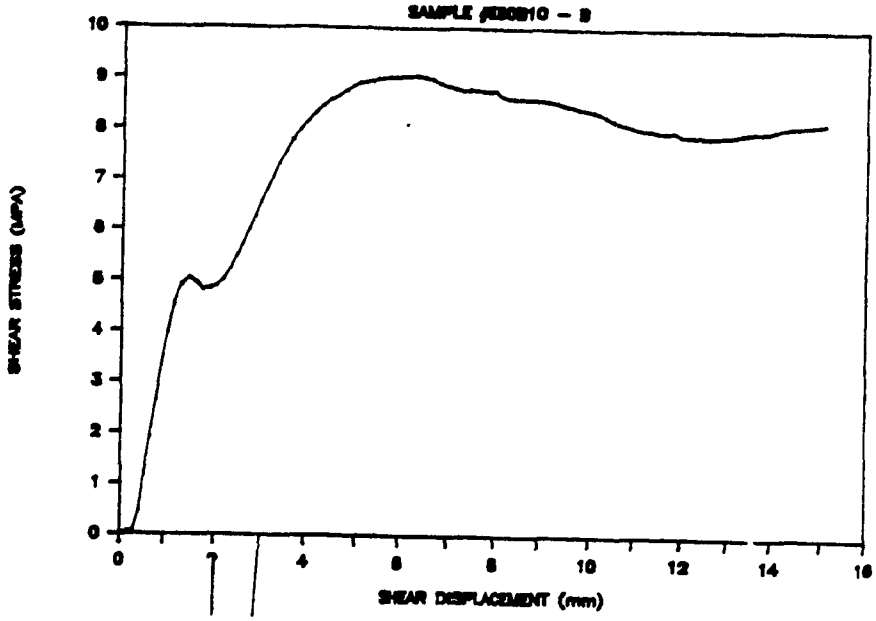
SAMPLE #E30810 – B
SHEAR STRESS (MPA)
SHEAR DISPLACEMENT (mm)

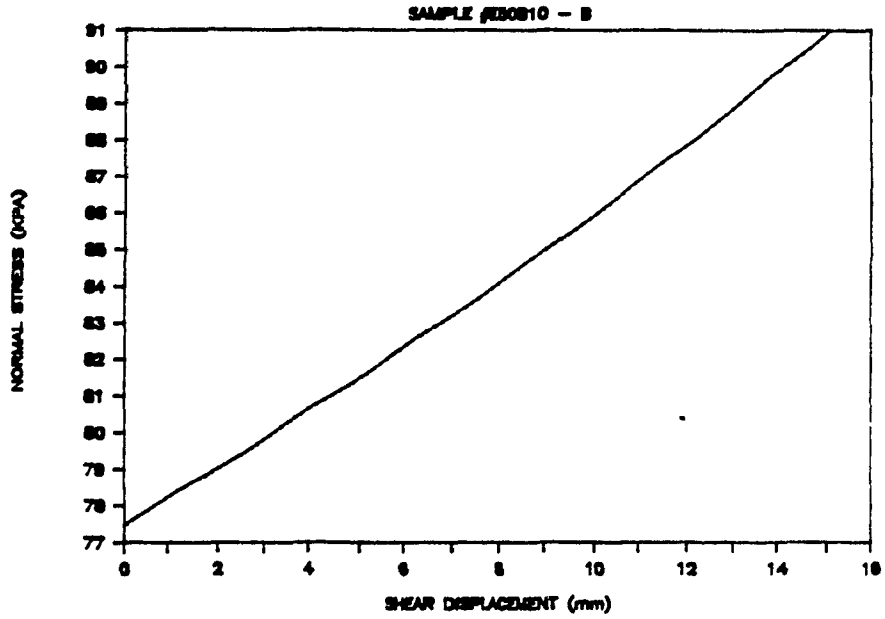
SAMPLE #E30810 – B
NORMAL STRESS (KPA)
SHEAR DISPLACEMENT (mm)

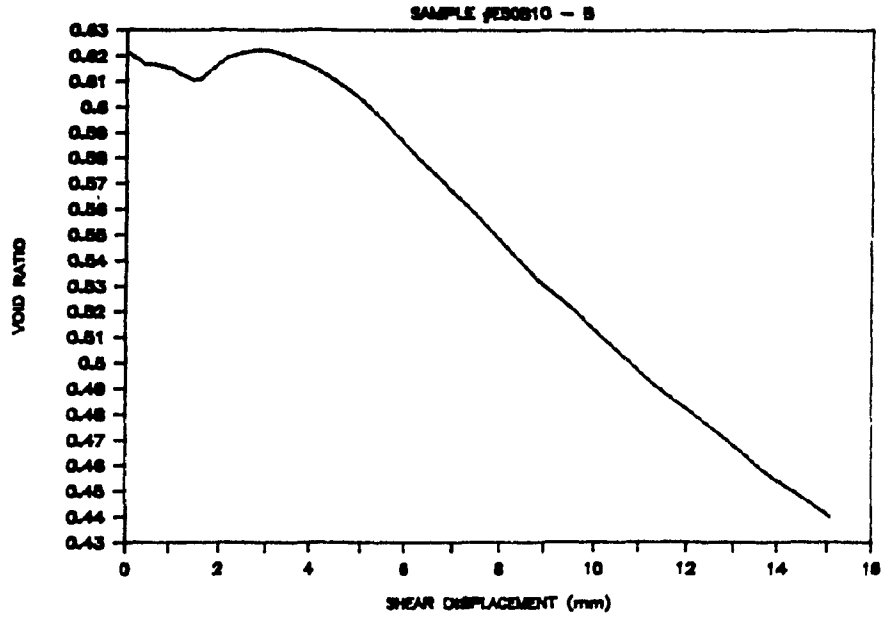
SAMPLE #E30810 – B
VOID RATIO
SHEAR DISPLACEMENT (mm)

DENISON

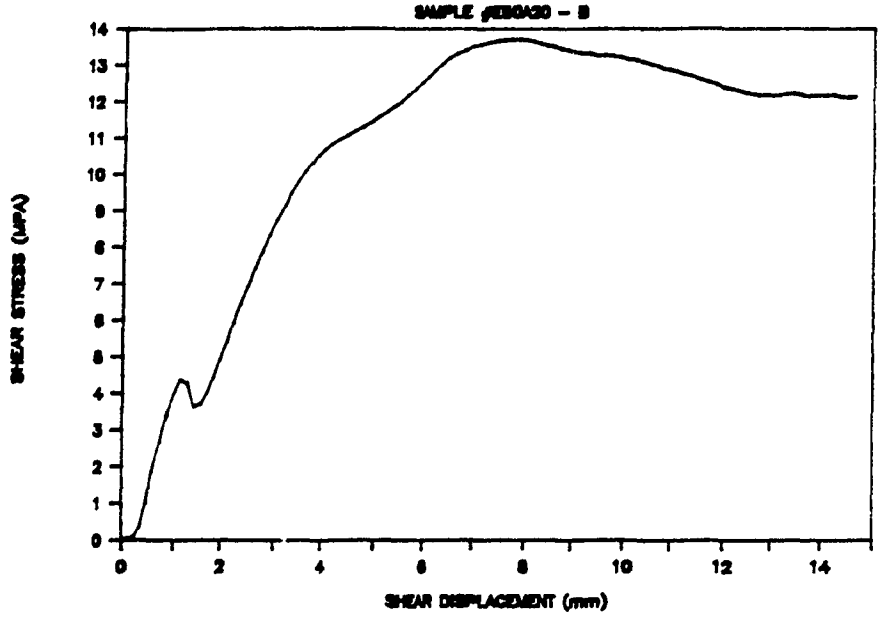
SAMPLE #EBGA20 - B
SHEAR STRESS (MPA)
SHEAR DISPLACEMENT (mm)

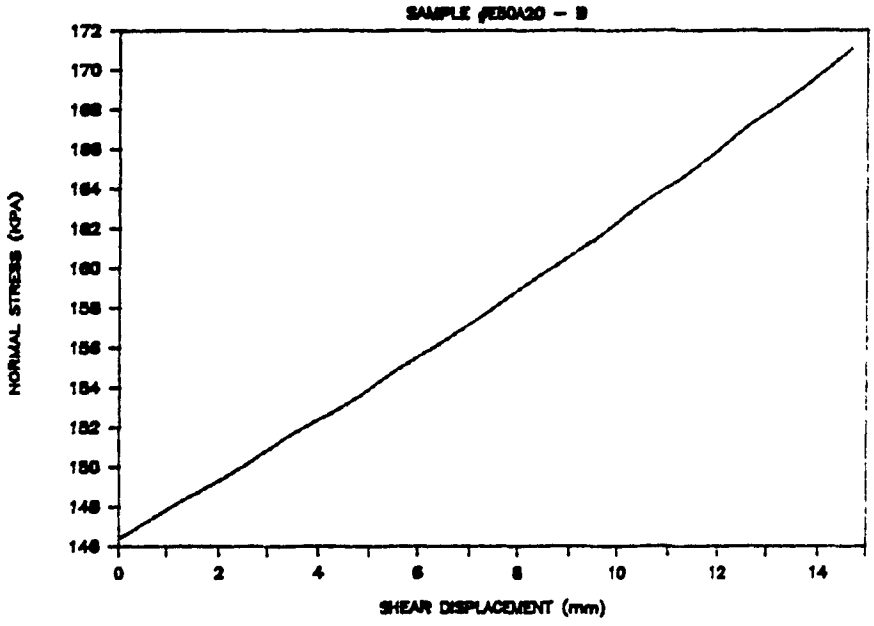
SAMPLE #EBGA20 - B
NORMAL STRESS (KPA)
SHEAR DISPLACEMENT (mm)

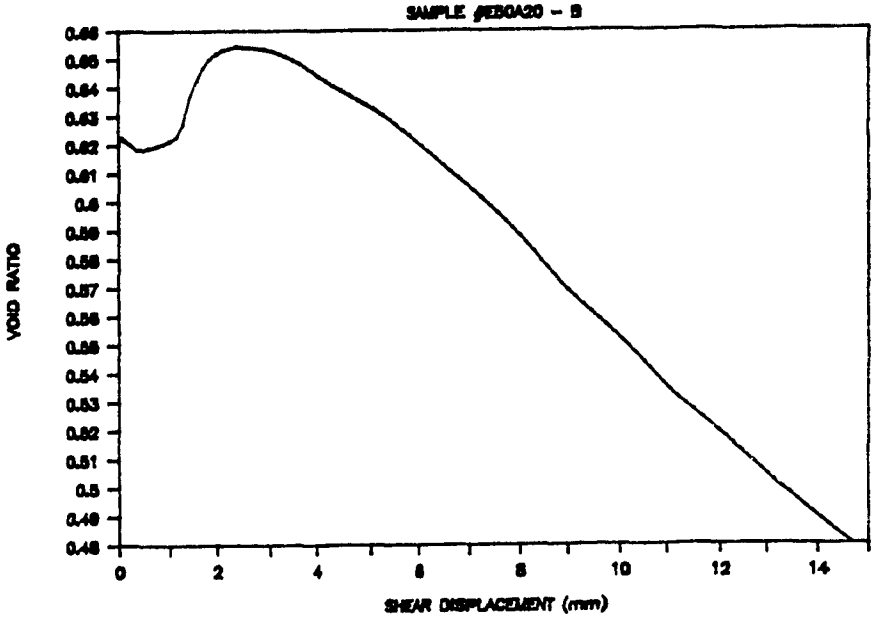
SAMPLE #EBGA20 - B
VOID RATIO
SHEAR DISPLACEMENT (mm)

DENISON

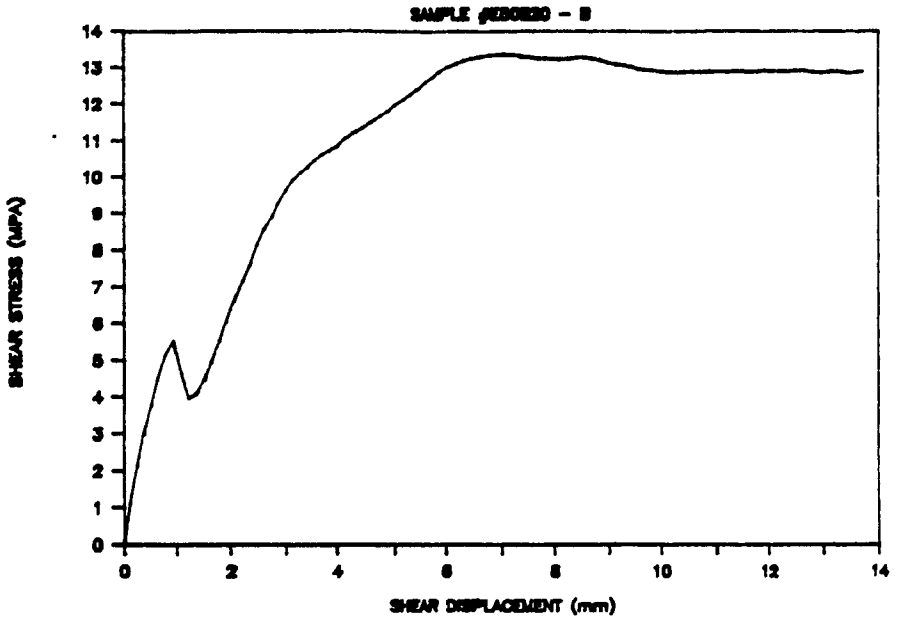
SHEAR STRESS (MPA)
SHEAR DISPLACEMENT (mm)

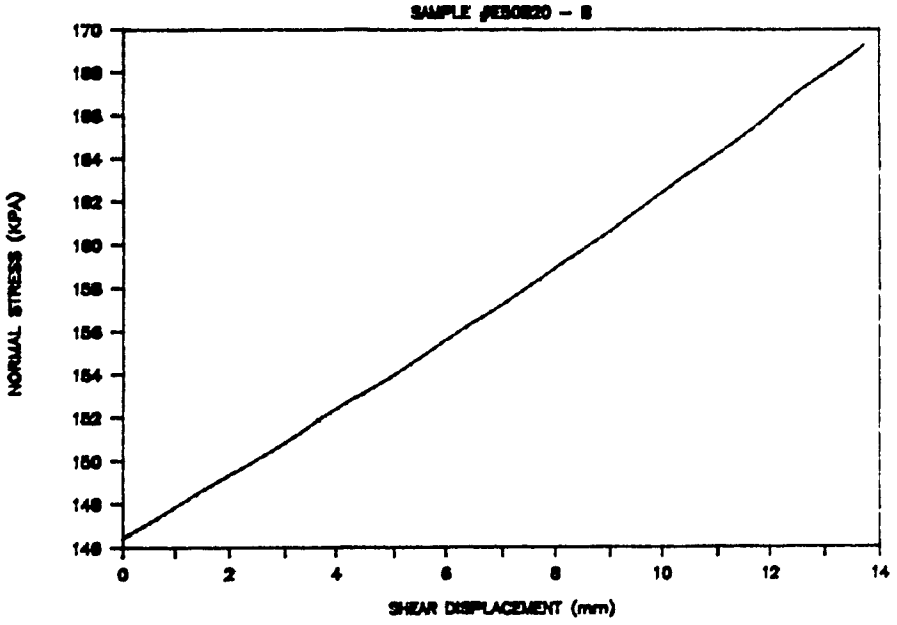
NORMAL STRESS (KPA)
SHEAR DISPLACEMENT (mm)

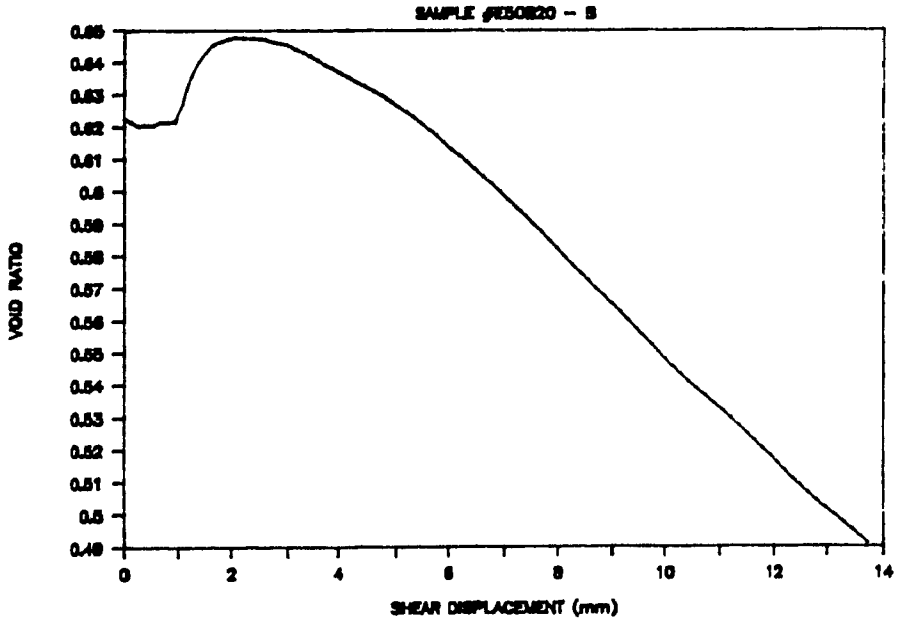
VOID RATIO
SHEAR DISPLACEMENT (mm)

DENISON

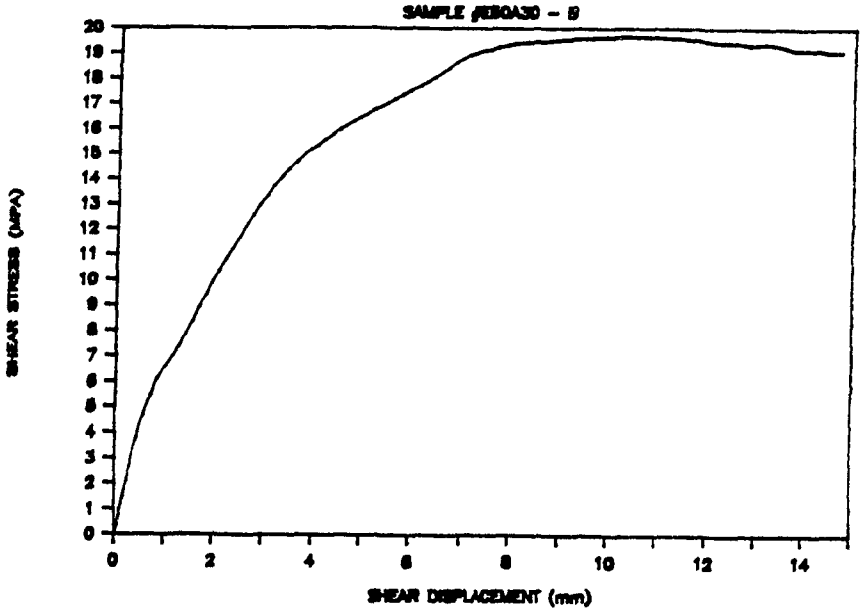
SAMPLE #E80A30 - B
SHEAR STRESS (MPA)
SHEAR DISPLACEMENT (mm)

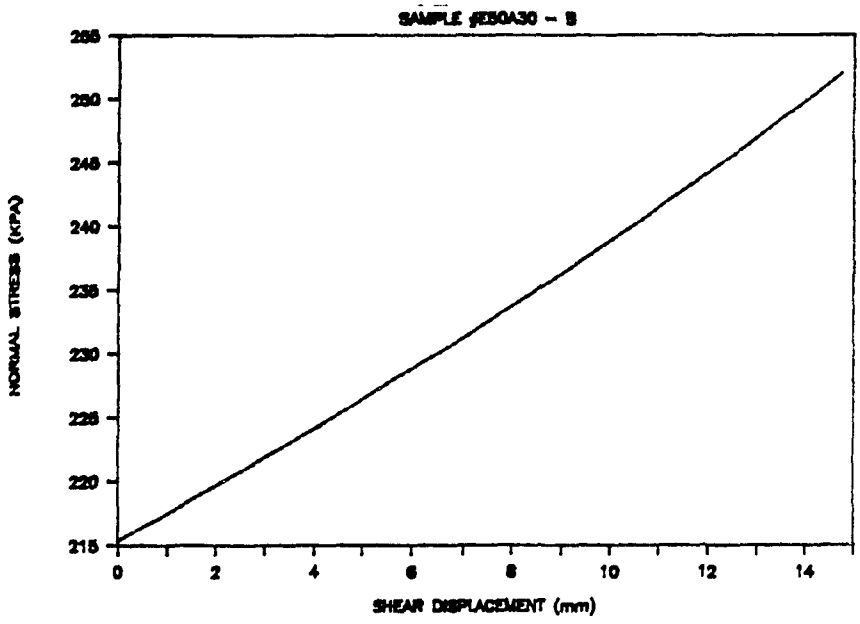
SAMPLE #E80A30 - B
NORMAL STRESS (KPA)
SHEAR DISPLACEMENT (mm)

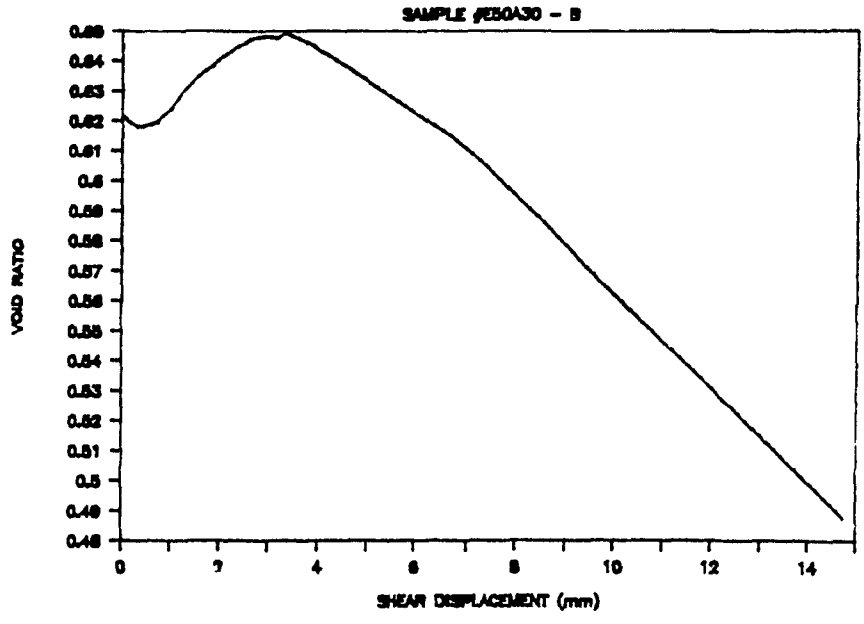
SAMPLE #E80A30 - B
VOID RATIO
SHEAR DISPLACEMENT (mm)

DENISON

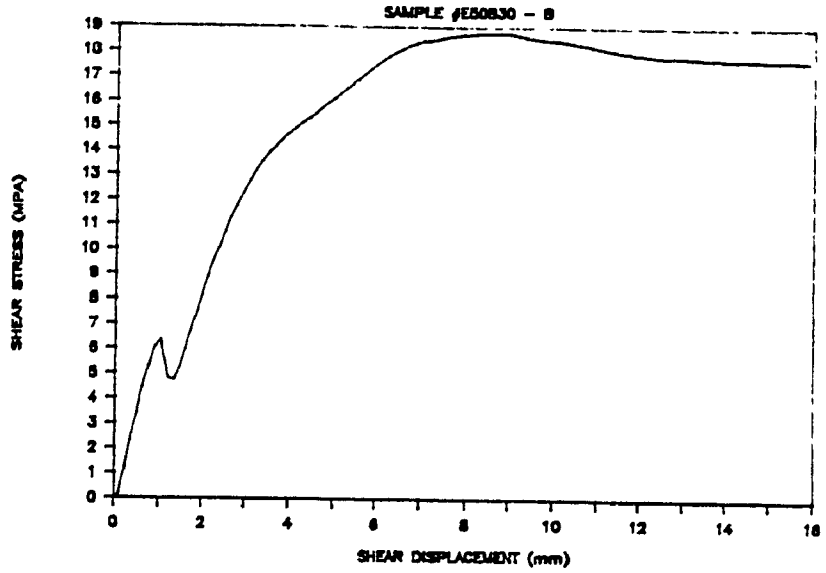
SAMPLE #E50830 - B
SHEAR STRESS (MPA)
SHEAR DISPLACEMENT (mm)

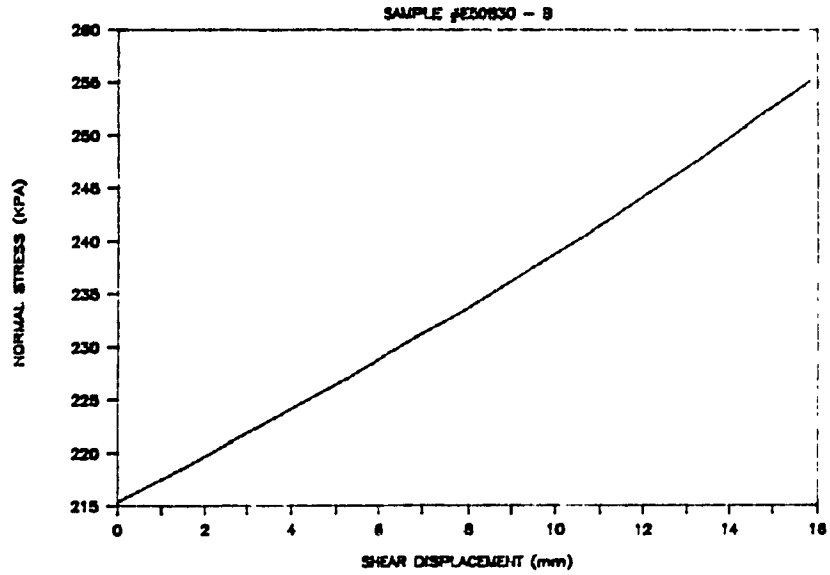
SAMPLE #E50830 - B
NORMAL STRESS (KPA)
SHEAR DISPLACEMENT (mm)

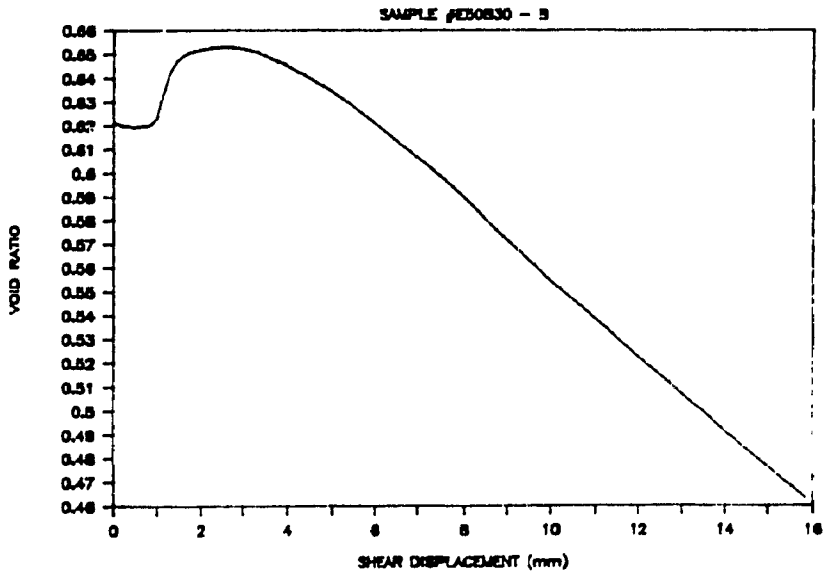
SAMPLE #E50830 - B
VOID RATIO
SHEAR DISPLACEMENT (mm)

DENISON

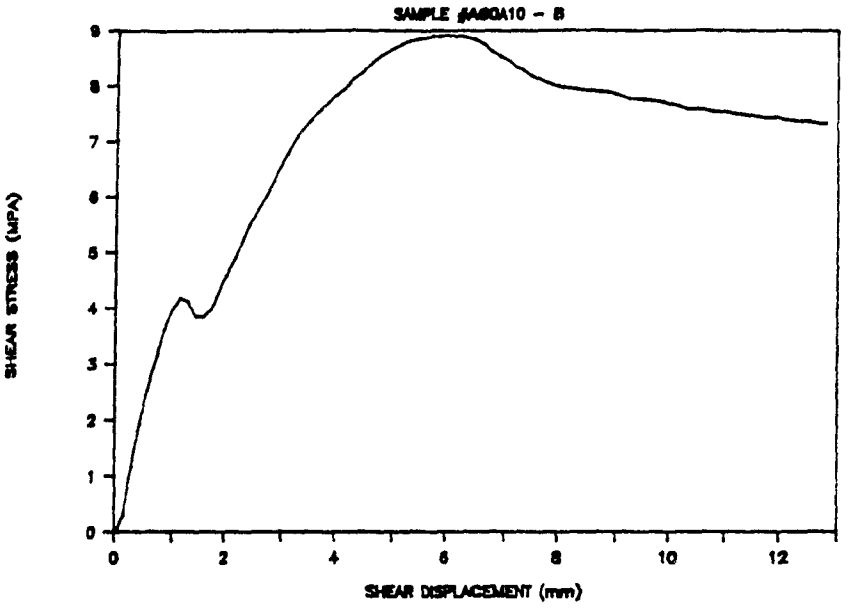
SAMPLE #A60A10 - B
SHEAR STRESS (MPA)
0
1
2
3
4
5
6
7
8
9
0
2
4
6
8
10
12
SHEAR DISPLACEMENT (mm)

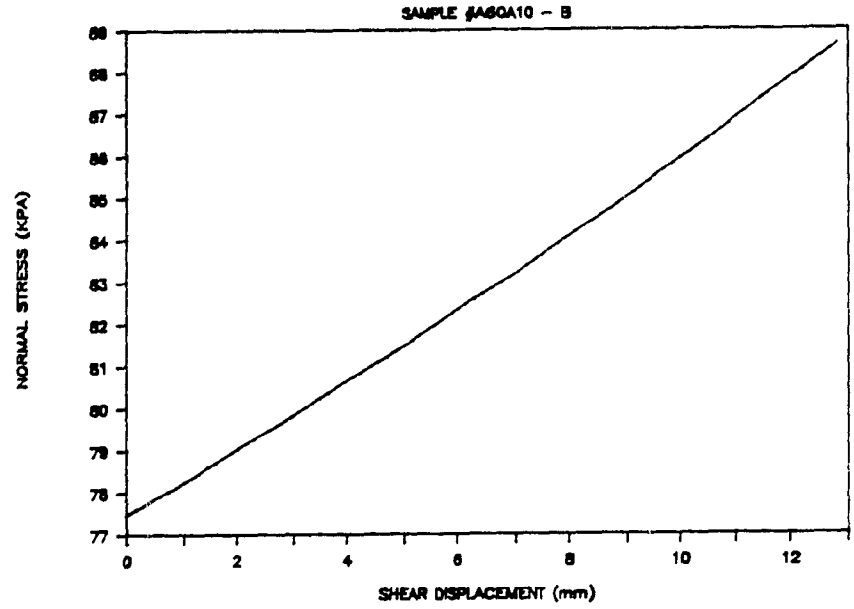
SAMPLE #A60A10 - B
NORMAL STRESS (KPA)
77
78
79
80
81
82
83
84
85
86
87
88
0
2
4
6
8
10
12
SHEAR DISPLACEMENT (mm)

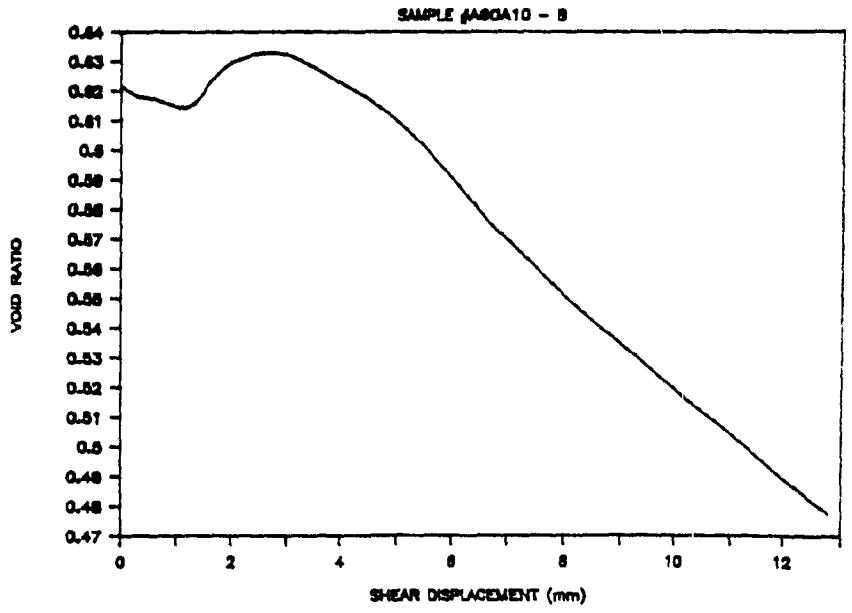
SAMPLE #A60A10 - B
VOID RATIO
0.47
0.48
0.49
0.5
0.51
0.52
0.53
0.54
0.55
0.56
0.57
0.58
0.59
0.6
0.61
0.62
0.63
0.64
0
2
4
6
8
10
12
SHEAR DISPLACEMENT (mm)

DENISON

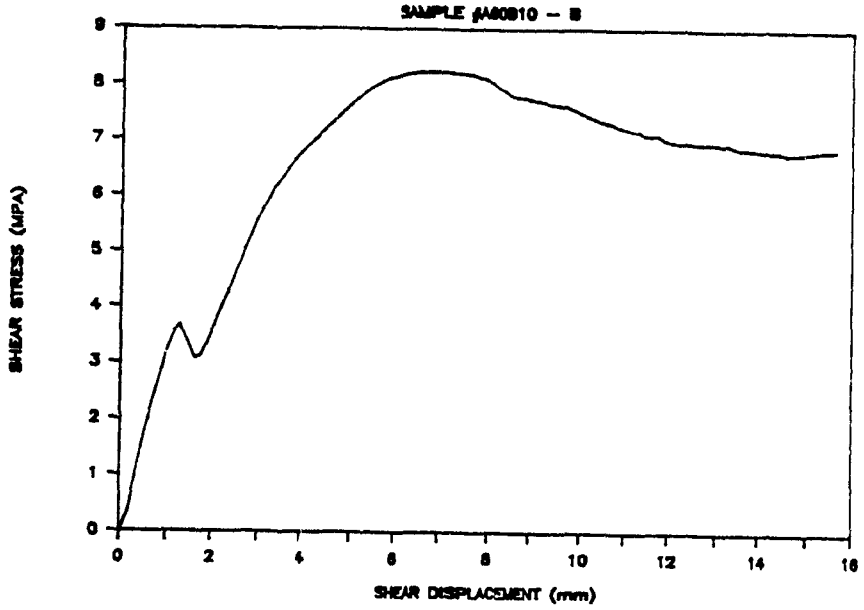
SAMPLE jA60810 – B
SHEAR STRESS (MPA)
SHEAR DISPLACEMENT (mm)

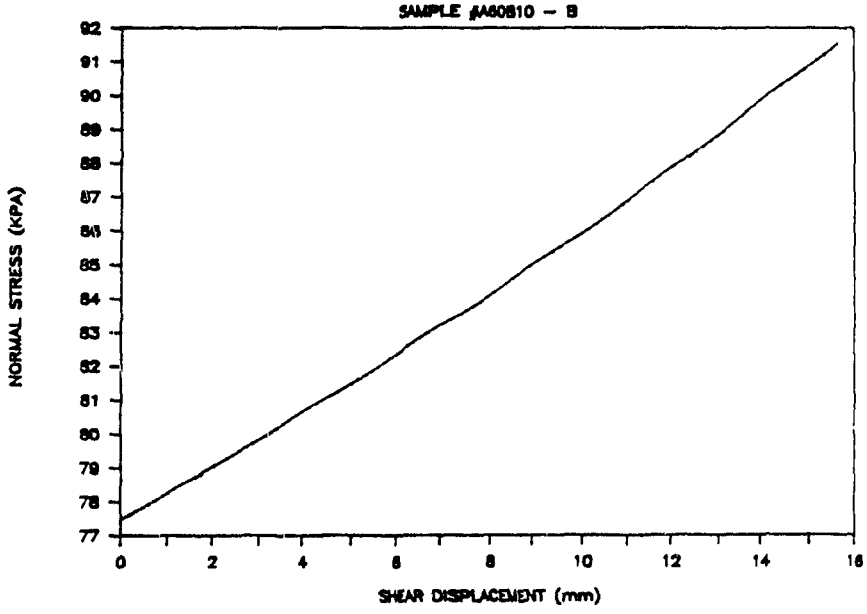
SAMPLE jA60810 – B
NORMAL STRESS (KPA)
SHEAR DISPLACEMENT (mm)

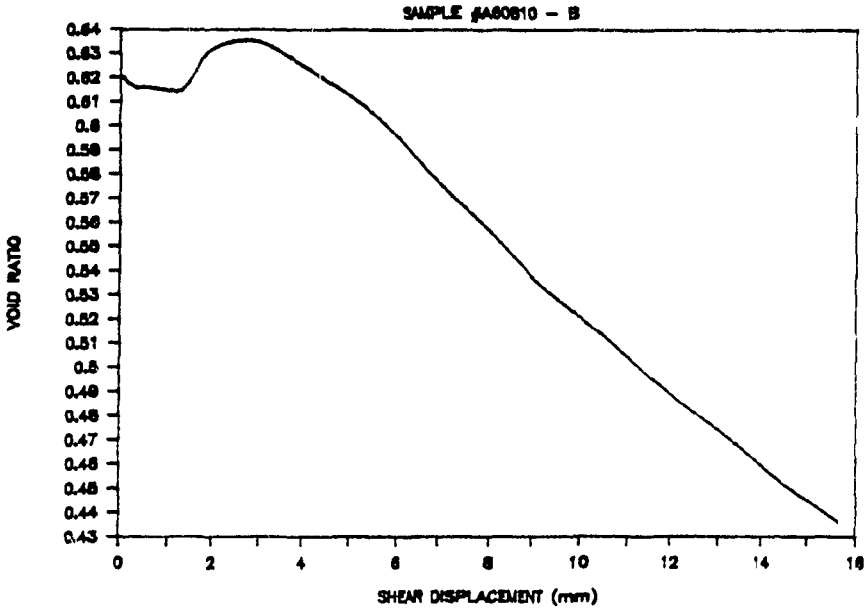
SAMPLE jA60810 – B
VOID RATIO
SHEAR DISPLACEMENT (mm)

DENISON

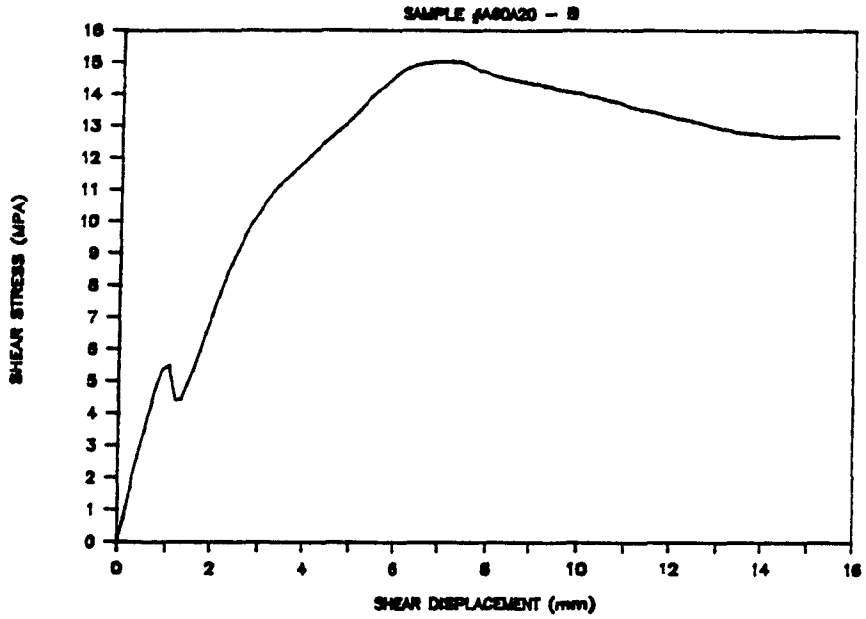
SAMPLE jA60A20 – B
SHEAR STRESS (MPA)
SHEAR DISPLACEMENT (mm)

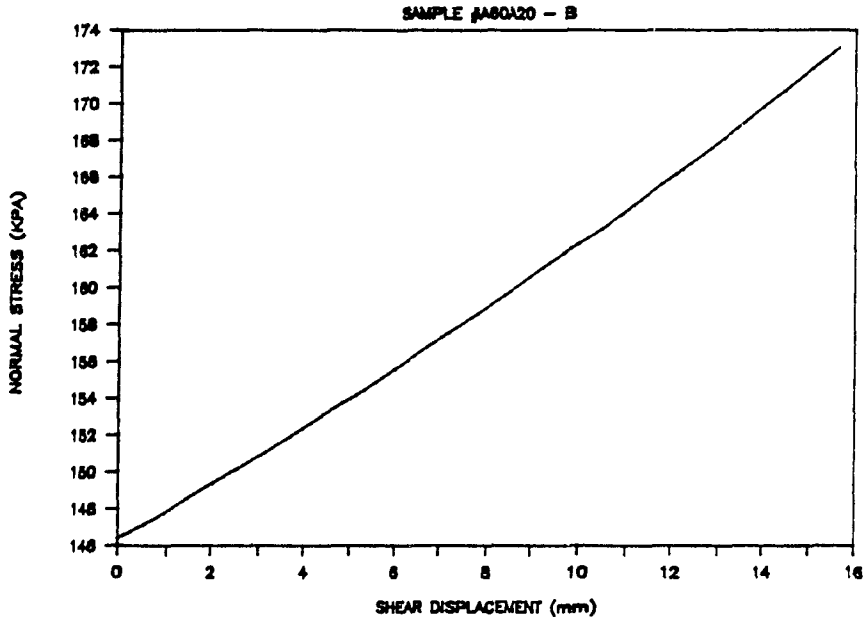
SAMPLE jA60A20 – B
NORMAL STRESS (KPA)
SHEAR DISPLACEMENT (mm)

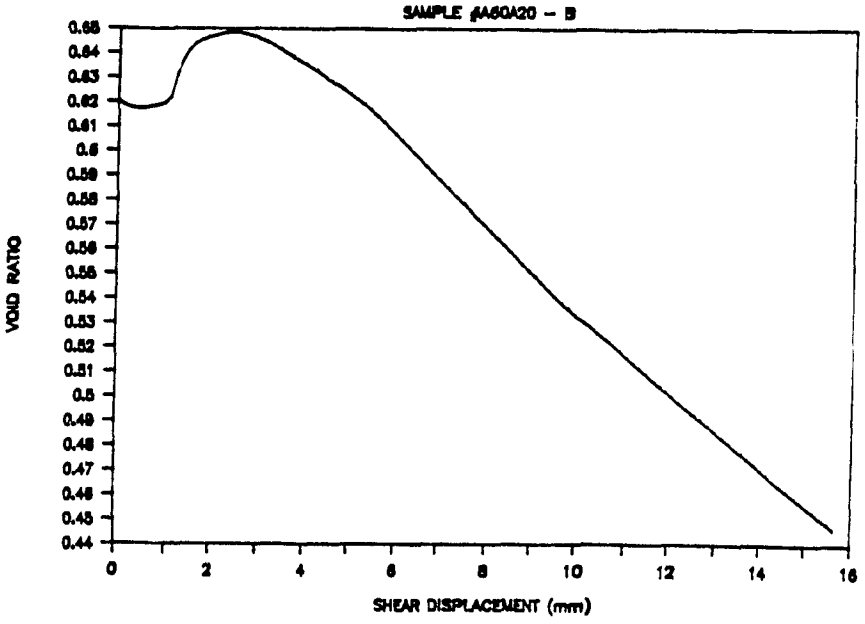
SAMPLE jA60A20 – B
VOID RATIO
SHEAR DISPLACEMENT (mm)

DENISON

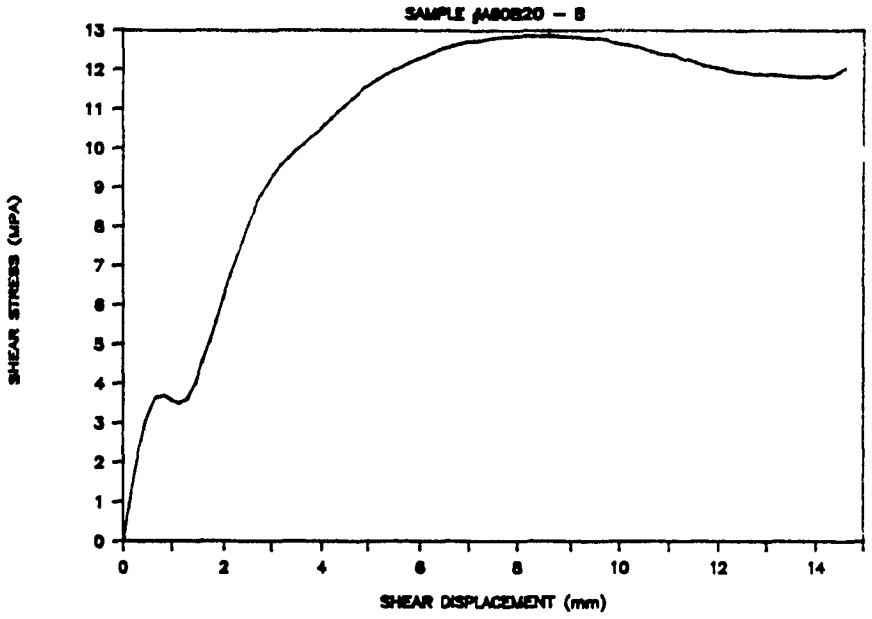
SAMPLE jA60820 – B
SHEAR STRESS (MPA)
SHEAR DISPLACEMENT (mm)

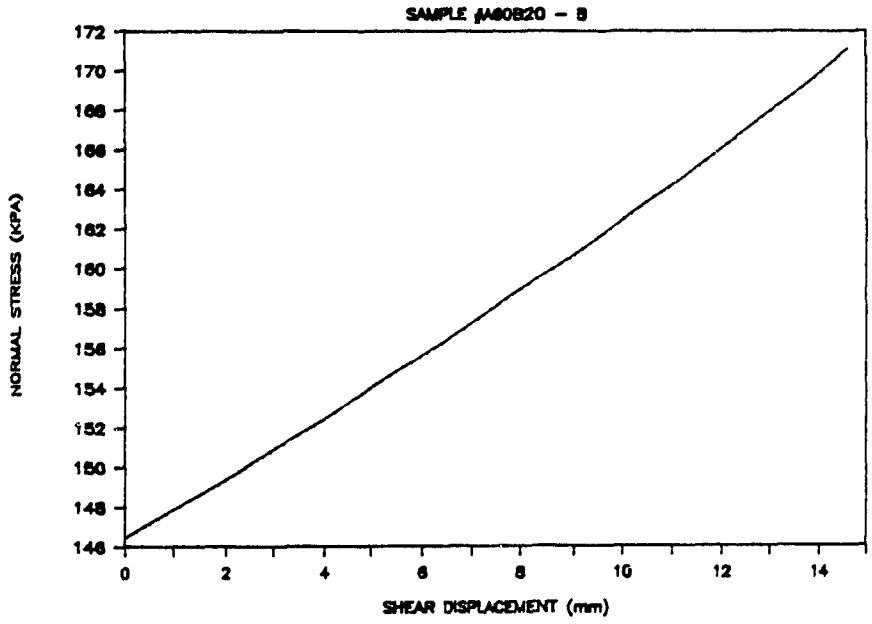
SAMPLE jA60820 – B
NORMAL STRESS (KPA)
SHEAR DISPLACEMENT (mm)

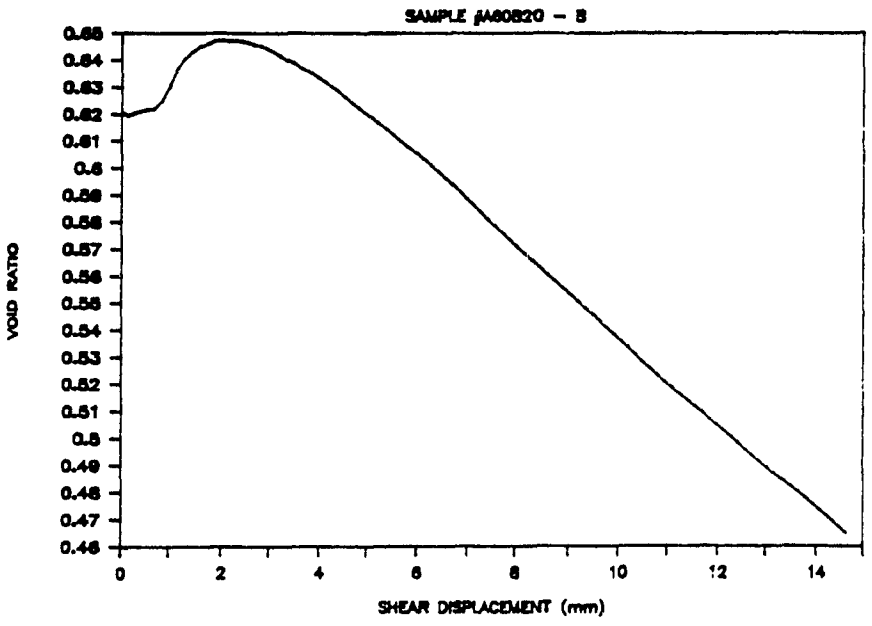
SAMPLE jA60820 – B
VOID RATIO
SHEAR DISPLACEMENT (mm)

DENISON

SAMPLE jA60A30 - B

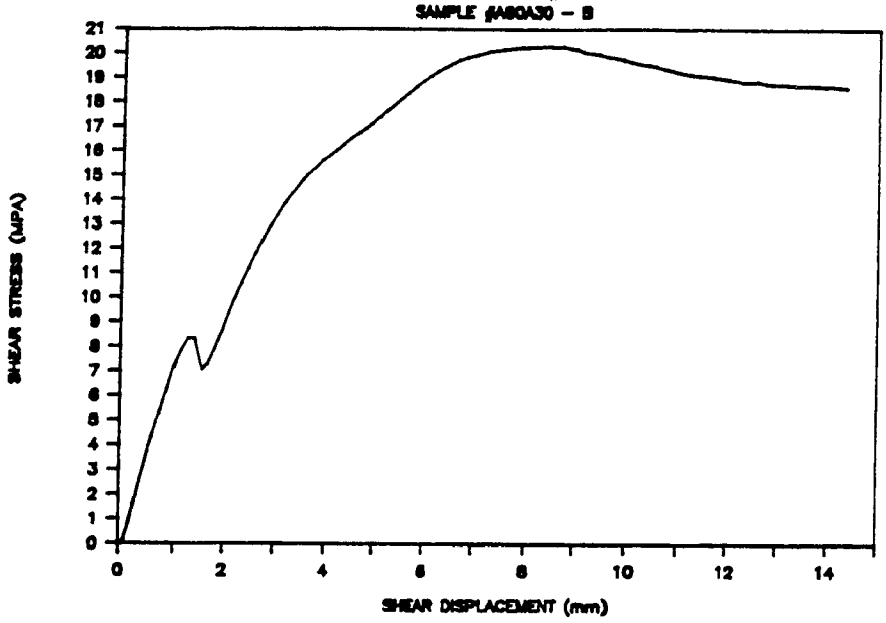

SAMPLE jA60A30 - B

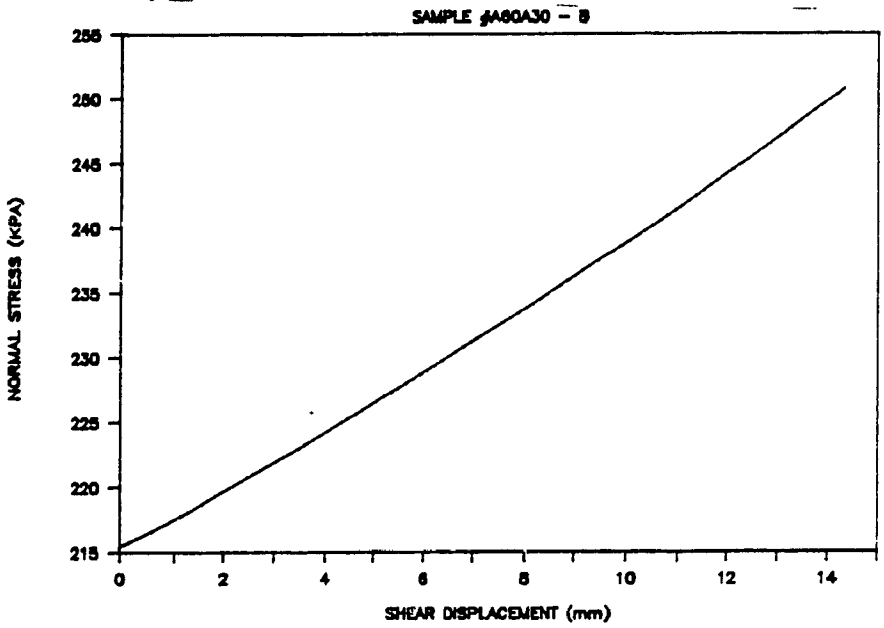

SAMPLE jA60A30 - B

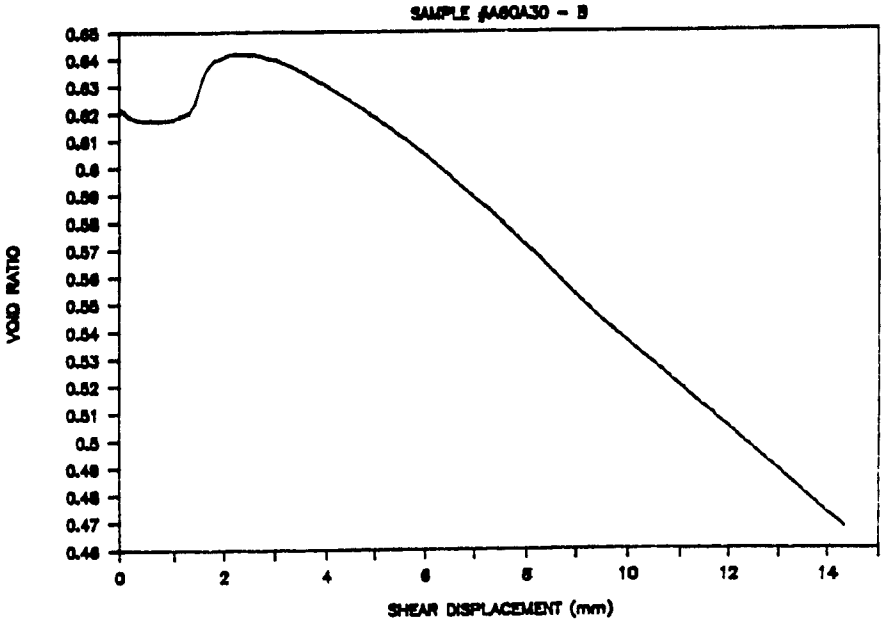

DENISON

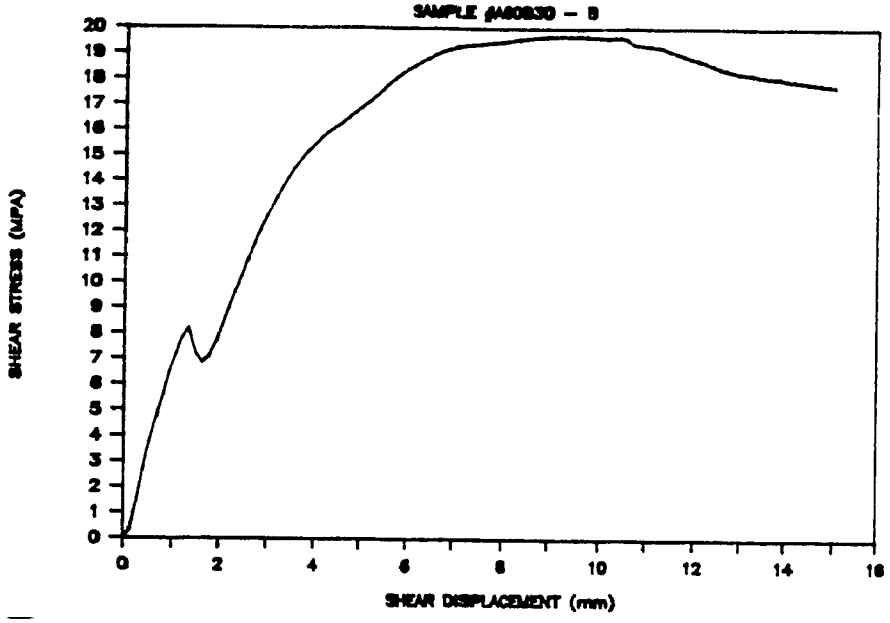
SAMPLE jA60B30 - B
SHEAR STRESS (MPA)
SHEAR DISPLACEMENT (mm)

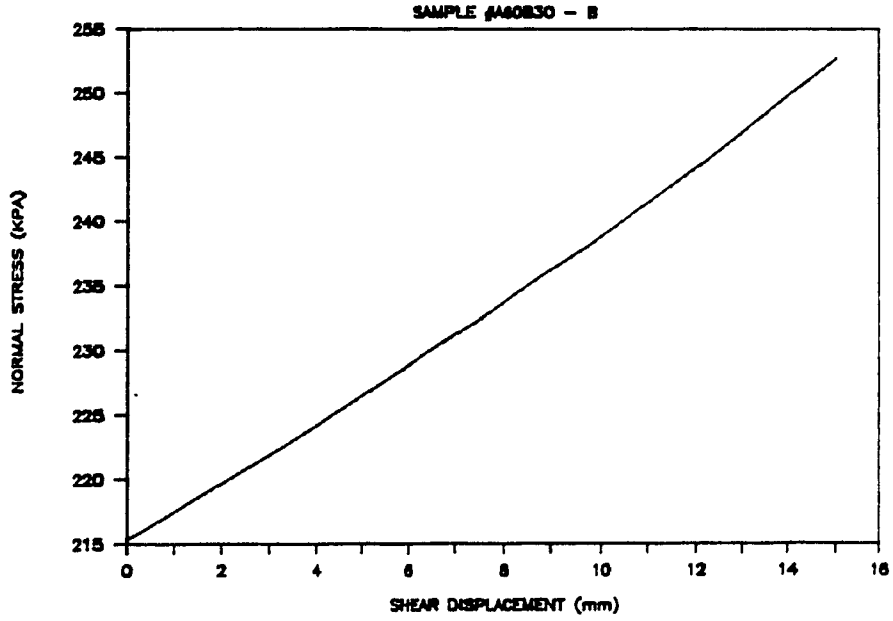
SAMPLE jA60B30 - B
NORMAL STRESS (KPA)
SHEAR DISPLACEMENT (mm)

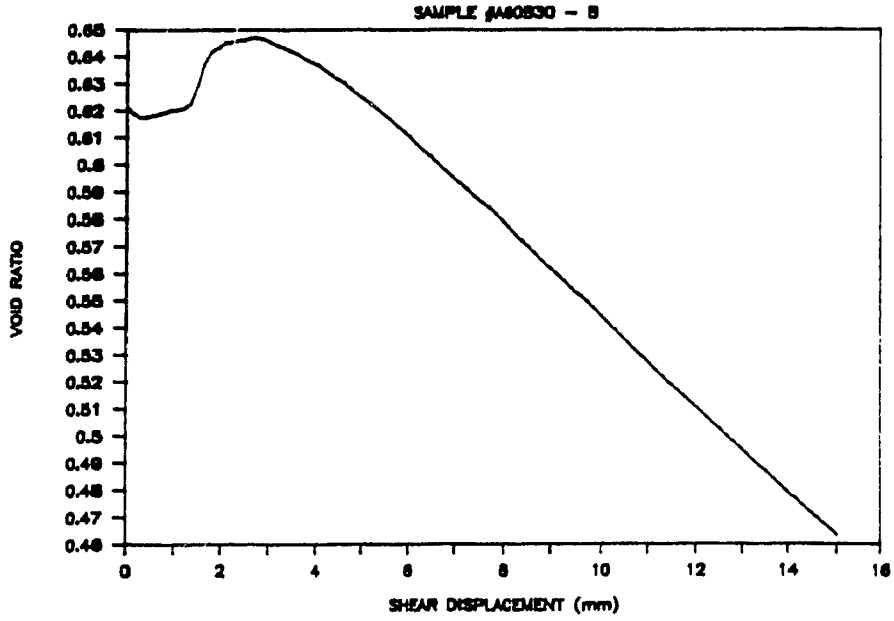
SAMPLE jA60B30 - B
VOID RATIO
SHEAR DISPLACEMENT (mm)

DENISON

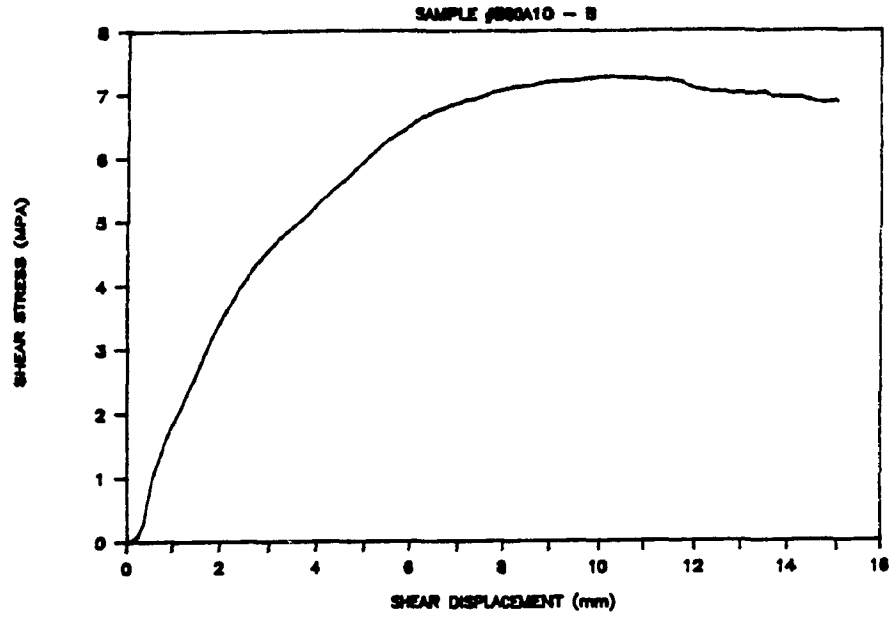
SAMPLE ßB60A10 – B
SHEAR STRESS (MPA)
SHEAR DISPLACEMENT (mm)

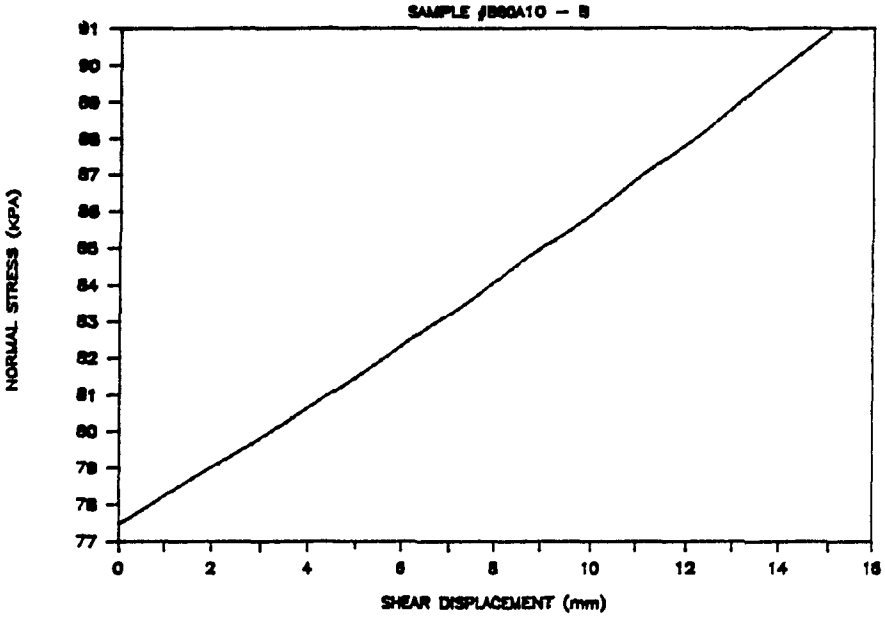
SAMPLE ßB60A10 – B
NORMAL STRESS (KPA)
SHEAR DISPLACEMENT (mm)

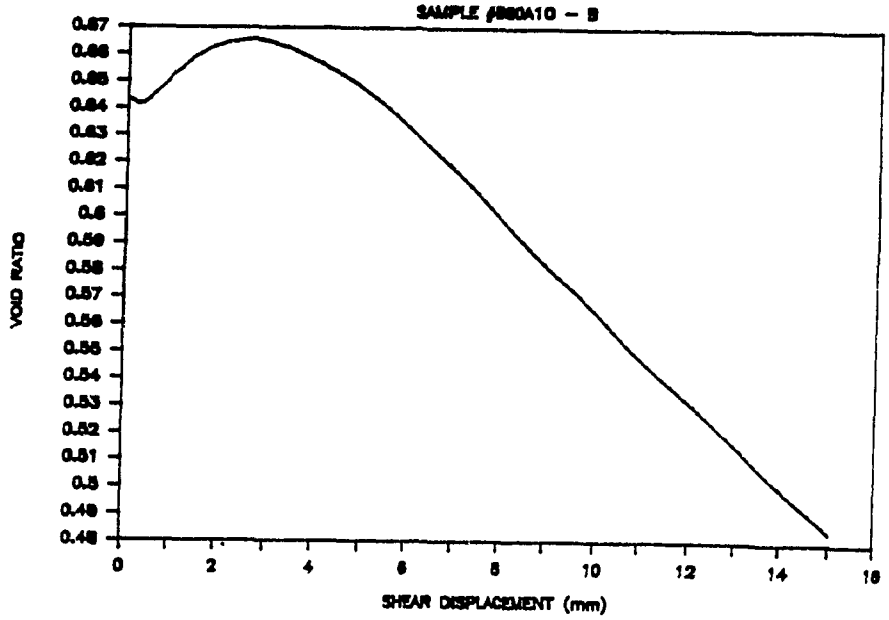
SAMPLE ßB60A10 – B
VOID RATIO
SHEAR DISPLACEMENT (mm)

DENISON

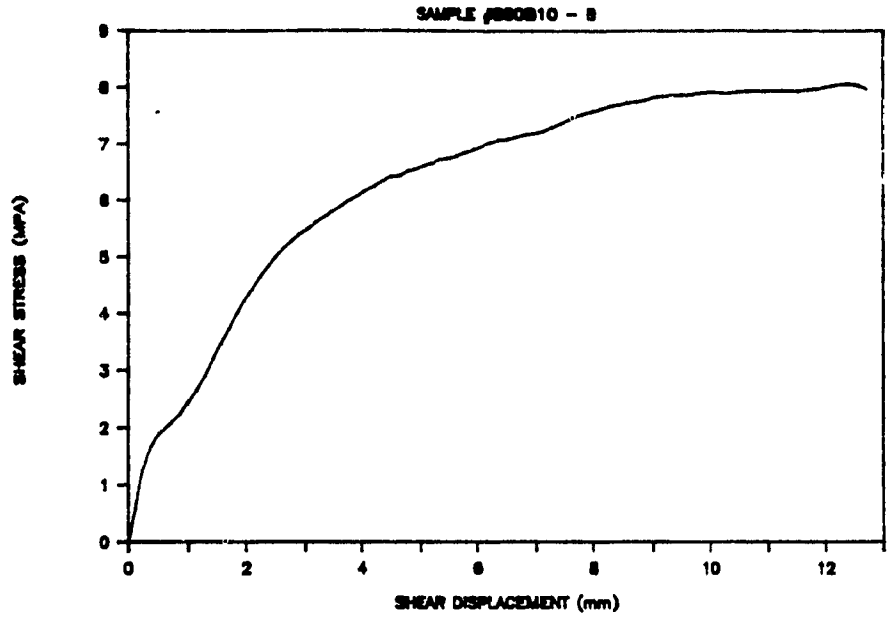
SAMPLE JB80B10 - B
SHEAR STRESS (MPA)
0
1
2
3
4
5
6
7
8
0
2
4
6
8
10
12
SHEAR DISPLACEMENT (mm)

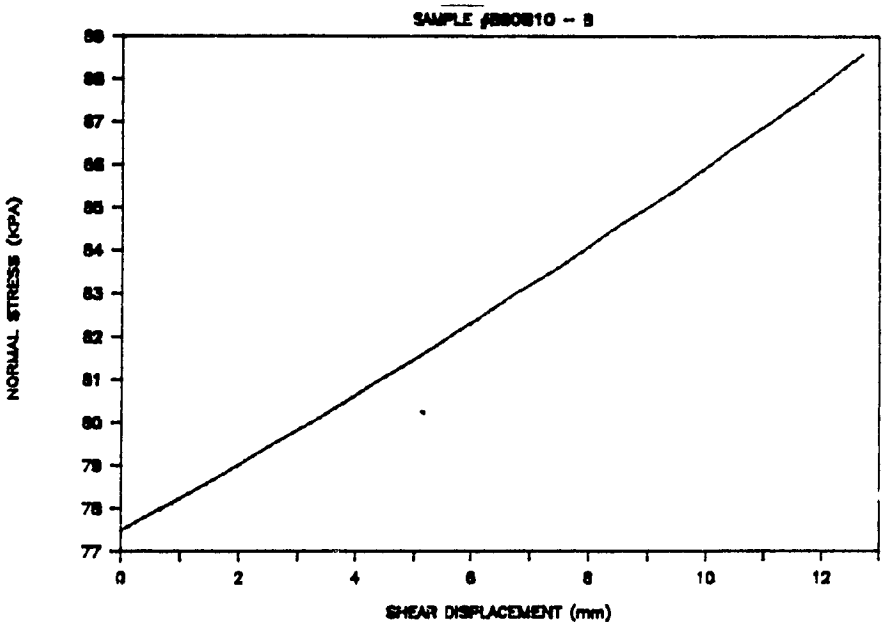
SAMPLE JB80B10 - B
NORMAL STRESS (KPA)
77
78
79
80
81
82
83
84
85
86
87
88
0
2
4
6
8
10
12
SHEAR DISPLACEMENT (mm)

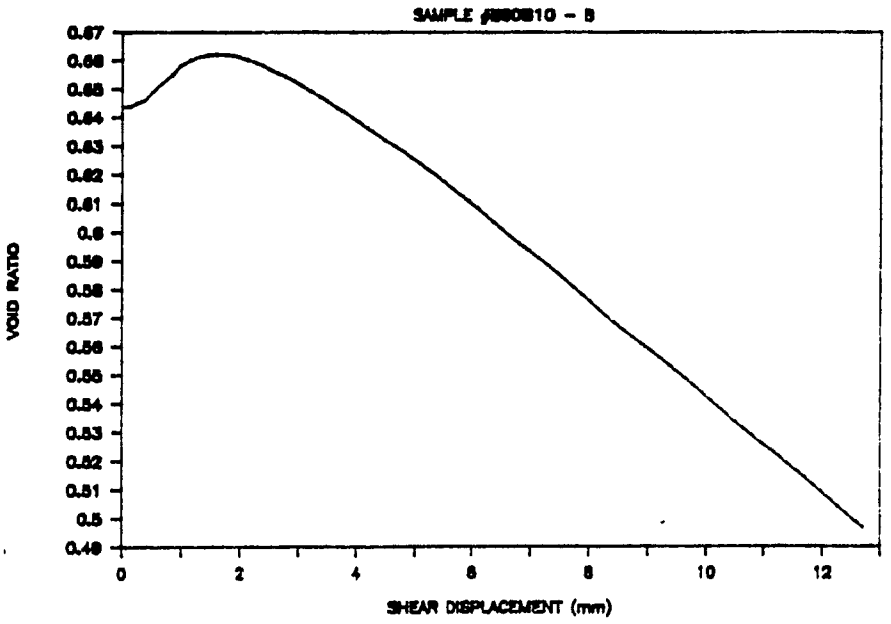
SAMPLE JB80B10 - B
VOID RATIO
0.49
0.5
0.51
0.52
0.53
0.54
0.55
0.56
0.57
0.58
0.59
0.6
0.61
0.62
0.63
0.64
0.65
0.66
0.67
0
2
4
6
8
10
12
SHEAR DISPLACEMENT (mm)

DENISON

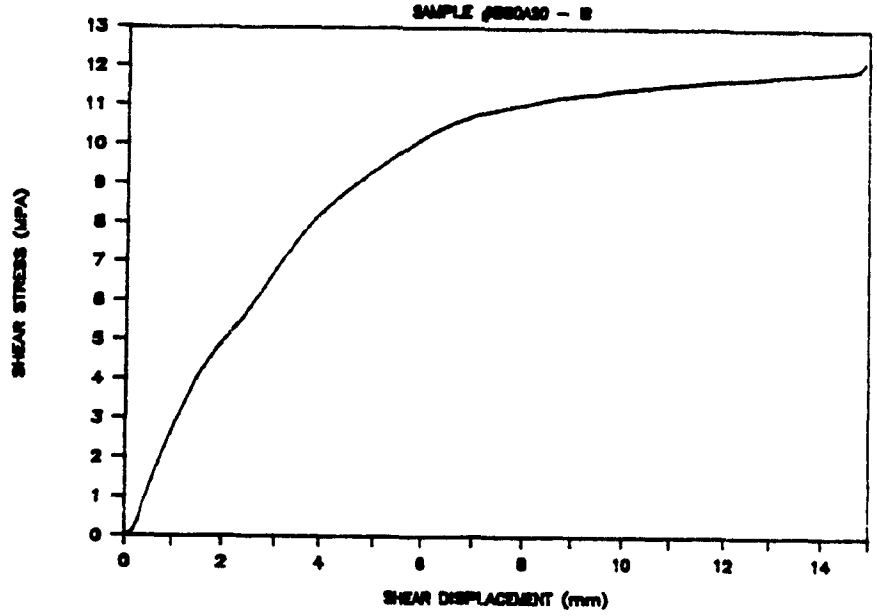
SAMPLE #B80A20 - B
SHEAR STRESS (MPA)
SHEAR DISPLACEMENT (mm)

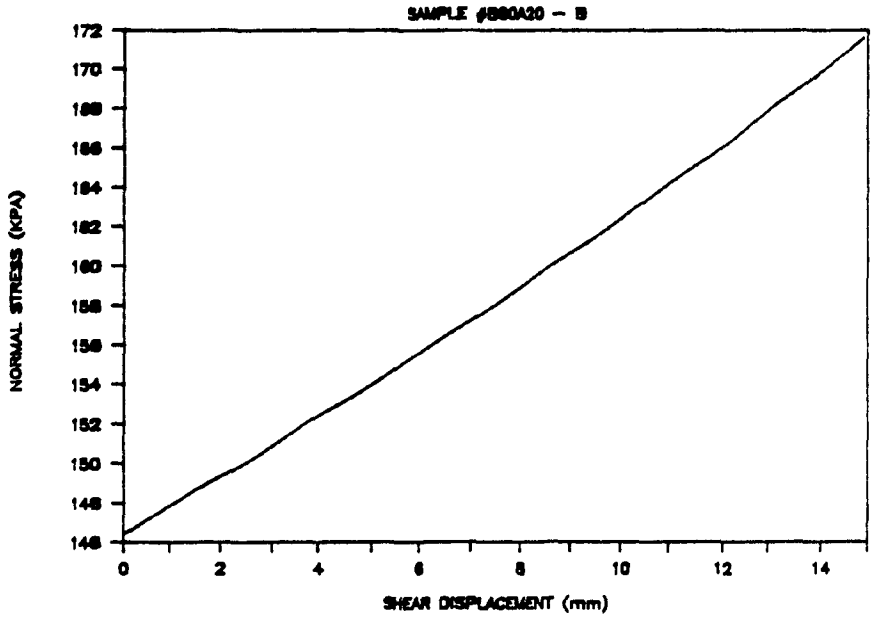
SAMPLE #B80A20 - B
NORMAL STRESS (KPA)
SHEAR DISPLACEMENT (mm)

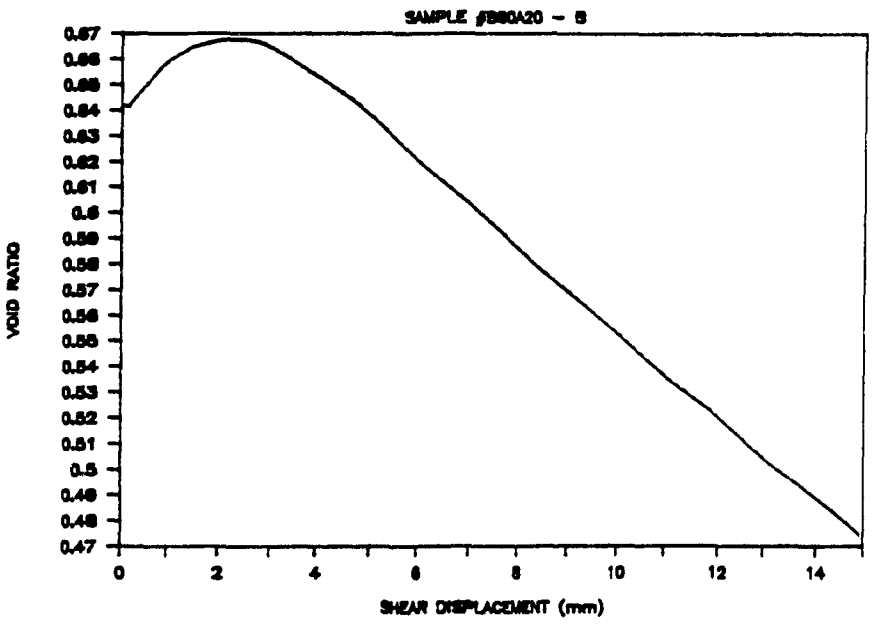
SAMPLE #B80A20 - B
VOID RATIO
SHEAR DISPLACEMENT (mm)

DENISON

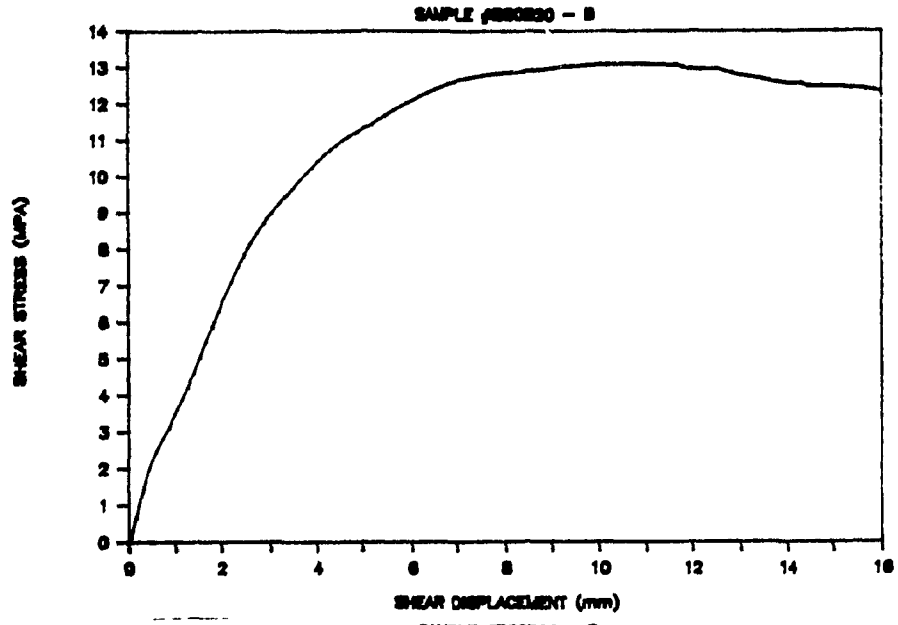
SAMPLE
SHEAR STRESS (MPA)
SHEAR DISPLACEMENT (mm)

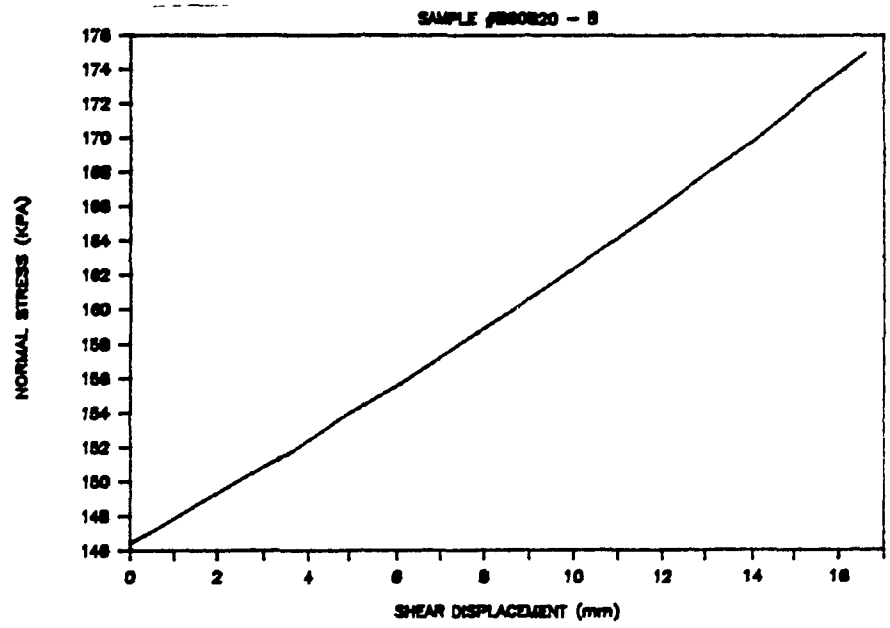
SAMPLE
NORMAL STRESS (KPA)
SHEAR DISPLACEMENT (mm)

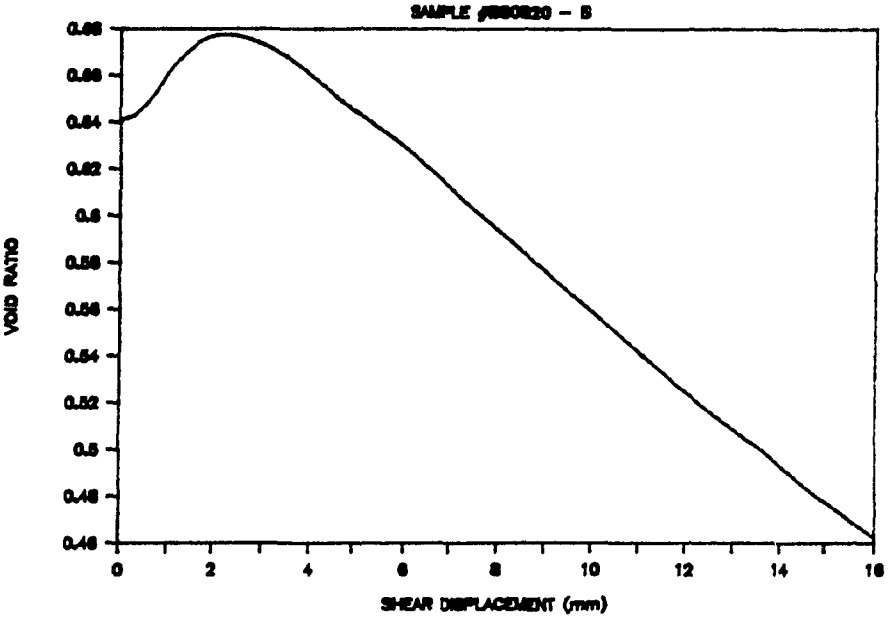
SAMPLE
VOID RATIO
SHEAR DISPLACEMENT (mm)

DENISON

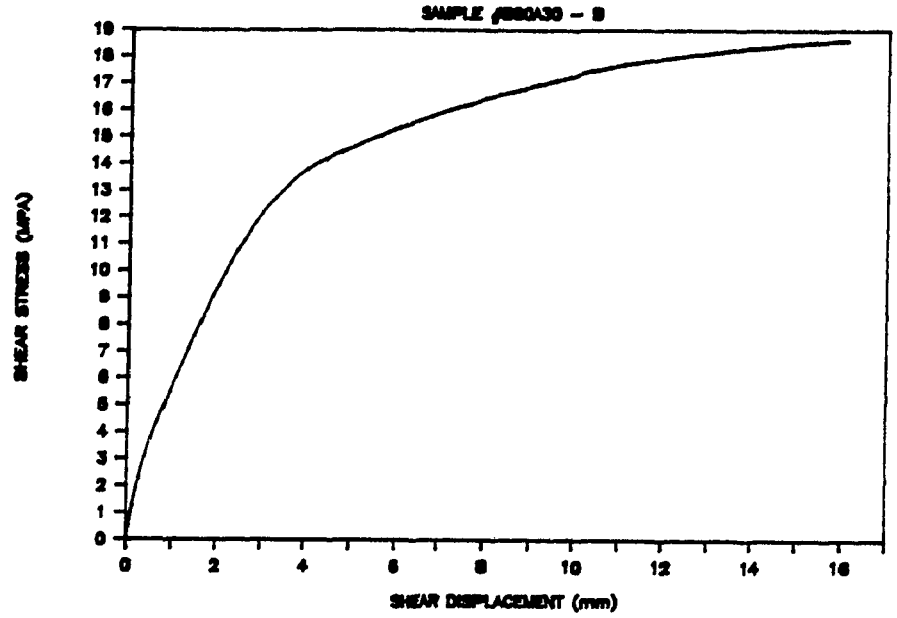
SAMPLE g880A30 - B
SHEAR STRESS (MPA)
SHEAR DISPLACEMENT (mm)

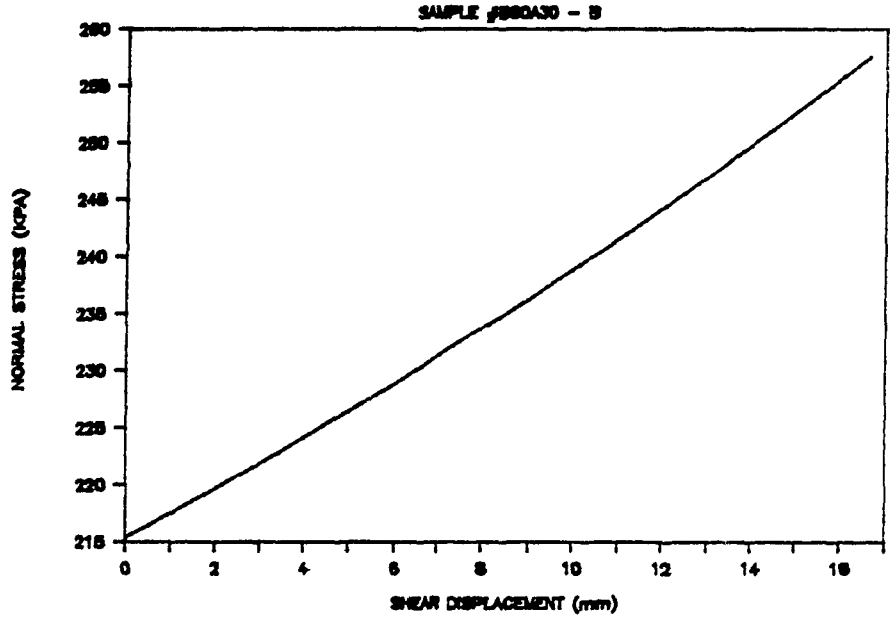
SAMPLE g880A30 - B
NORMAL STRESS (KPA)
SHEAR DISPLACEMENT (mm)

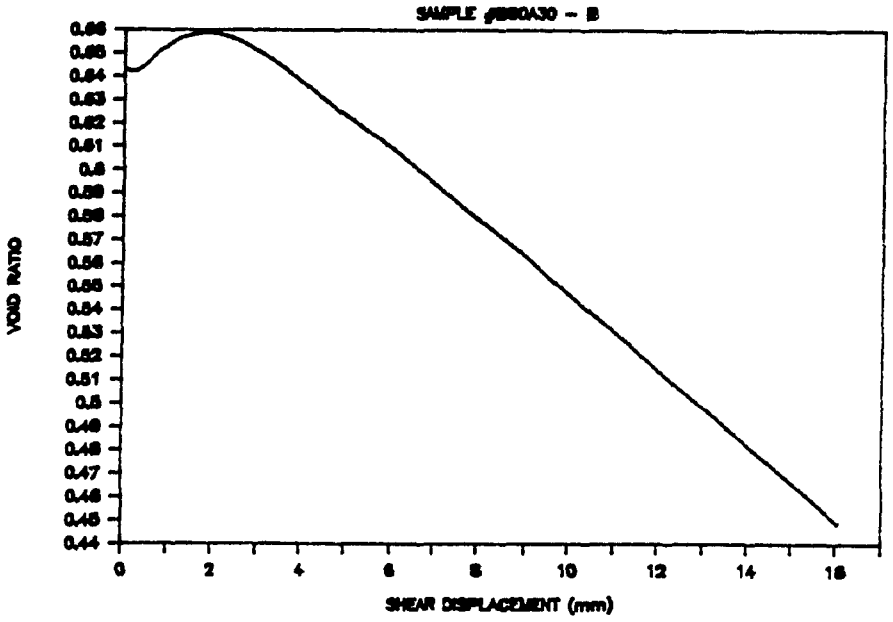
SAMPLE g880A30 - B
VOID RATIO
SHEAR DISPLACEMENT (mm)

DENISON

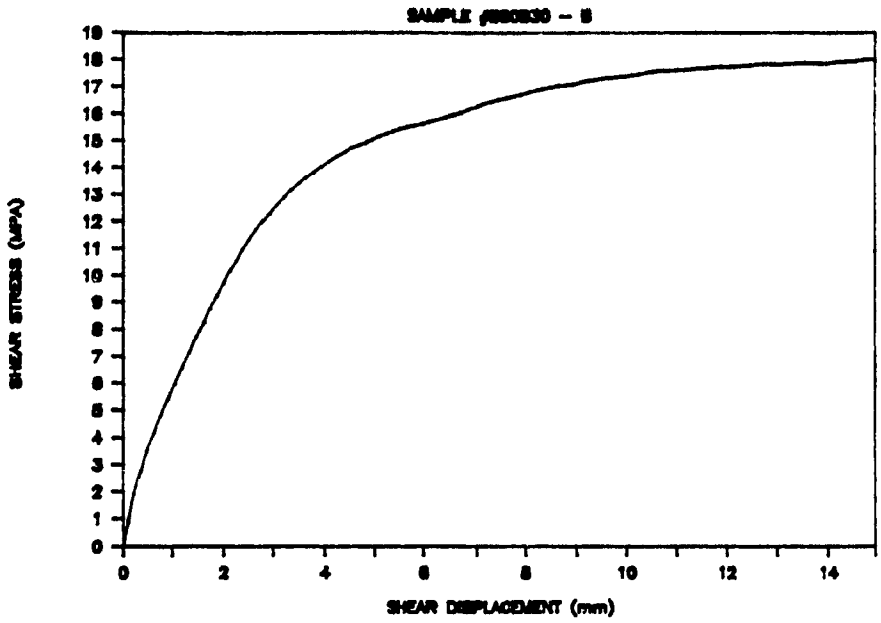
SHEAR STRESS (MPA)
SHEAR DISPLACEMENT (mm)

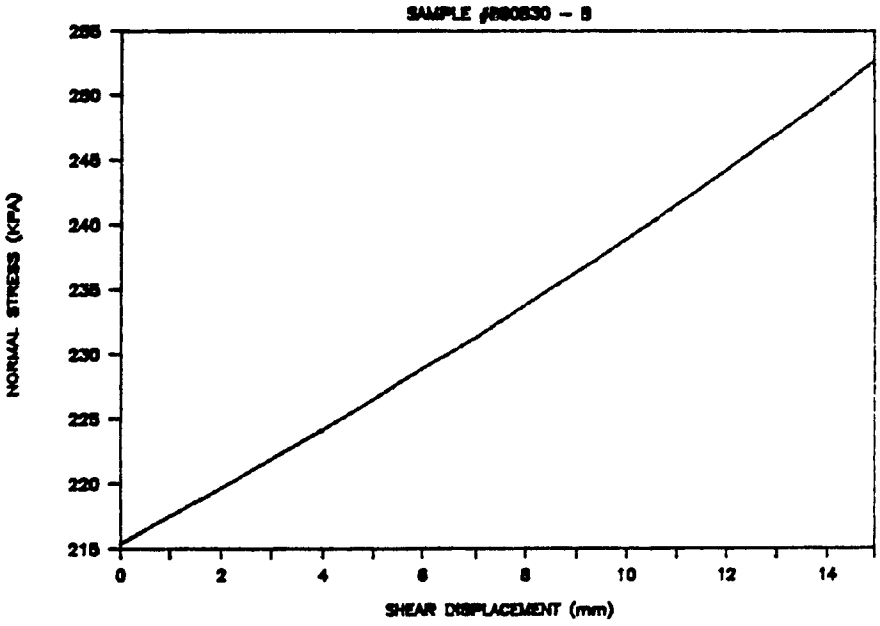
NORMAL STRESS (KPA)
SHEAR DISPLACEMENT (mm)

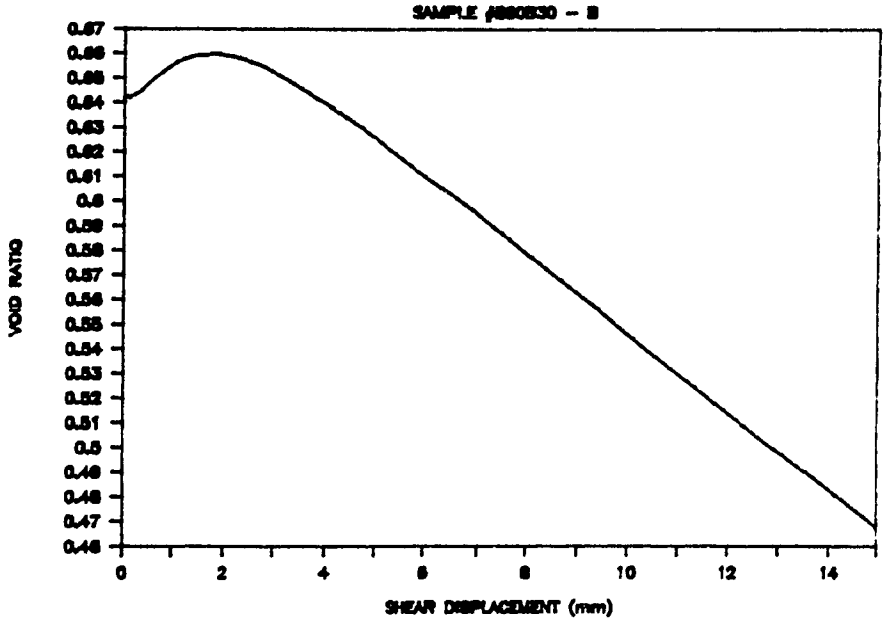
VOID RATIO
SHEAR DISPLACEMENT (mm)

DENISON

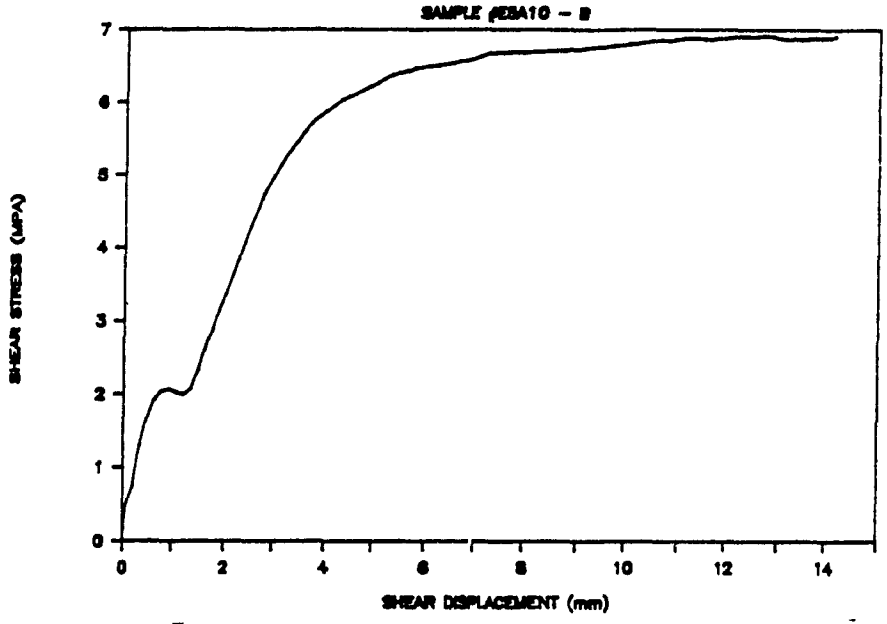
SAMPLE #EBA10 - B
SHEAR STRESS (MPA)
SHEAR DISPLACEMENT (mm)

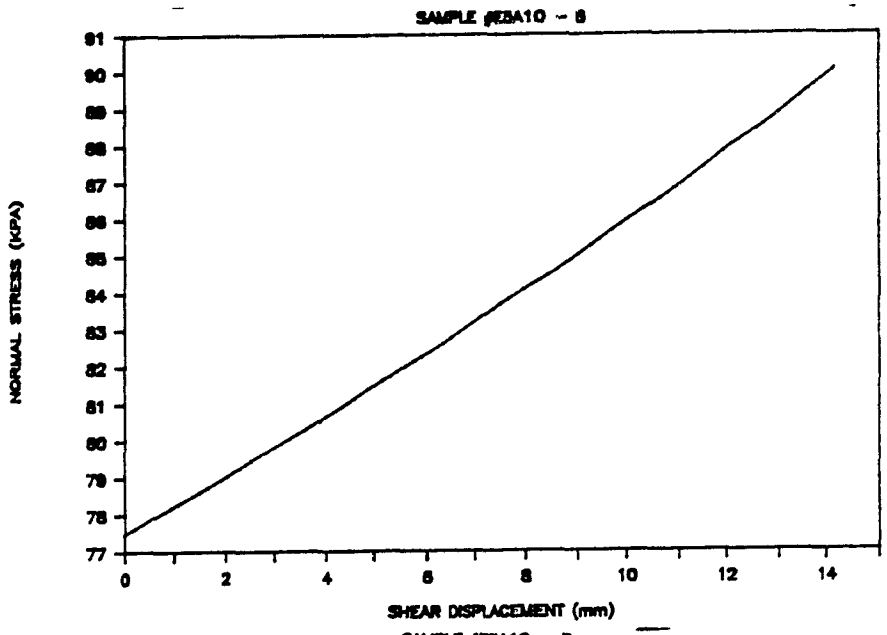
SAMPLE #EBA10 - B
NORMAL STRESS (KPA)
SHEAR DISPLACEMENT (mm)

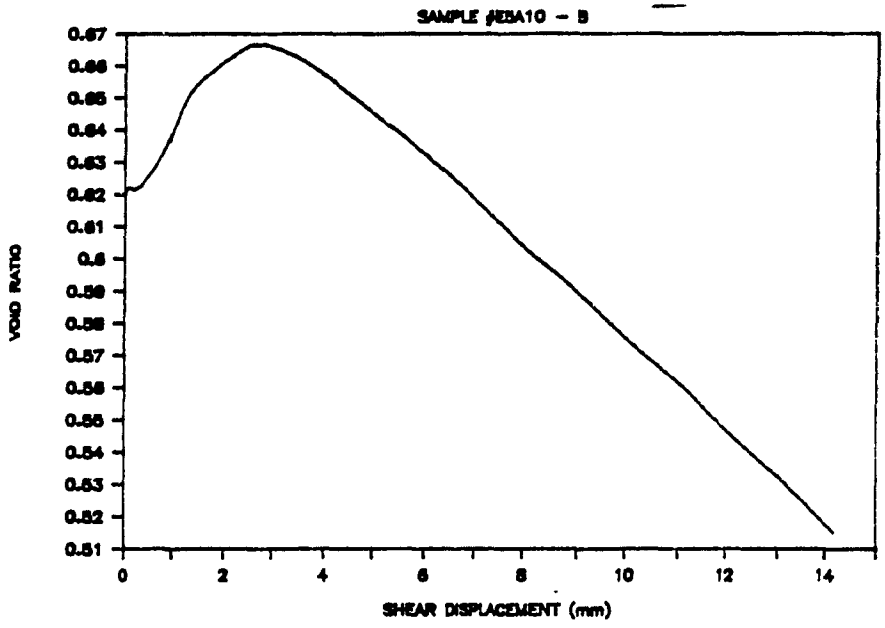
SAMPLE #EBA10 - B
VOID RATIO
SHEAR DISPLACEMENT (mm)

DENISON

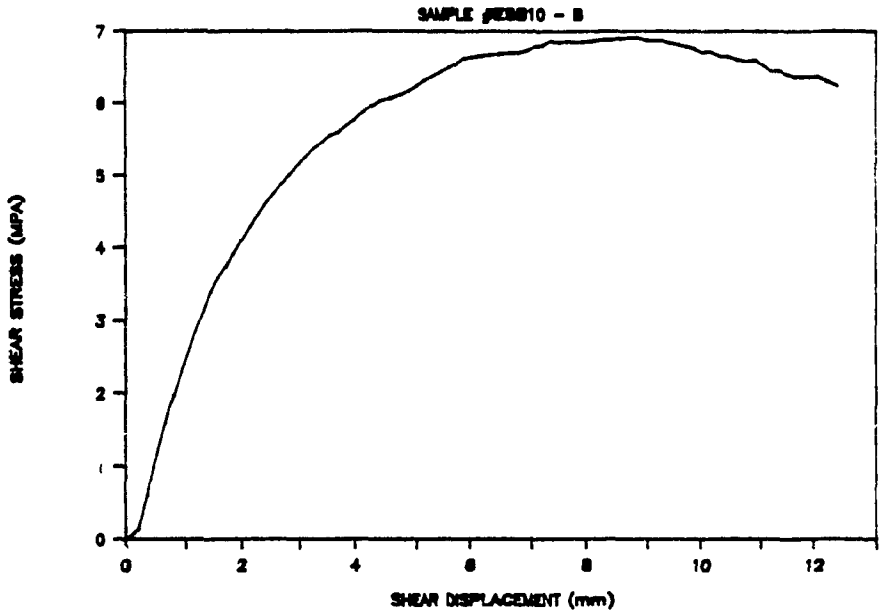
SAMPLE #E5810 - B
SHEAR STRESS (MPA)
0
1
2
3
4
5
6
7
0
2
4
6
8
10
12
SHEAR DISPLACEMENT (mm)

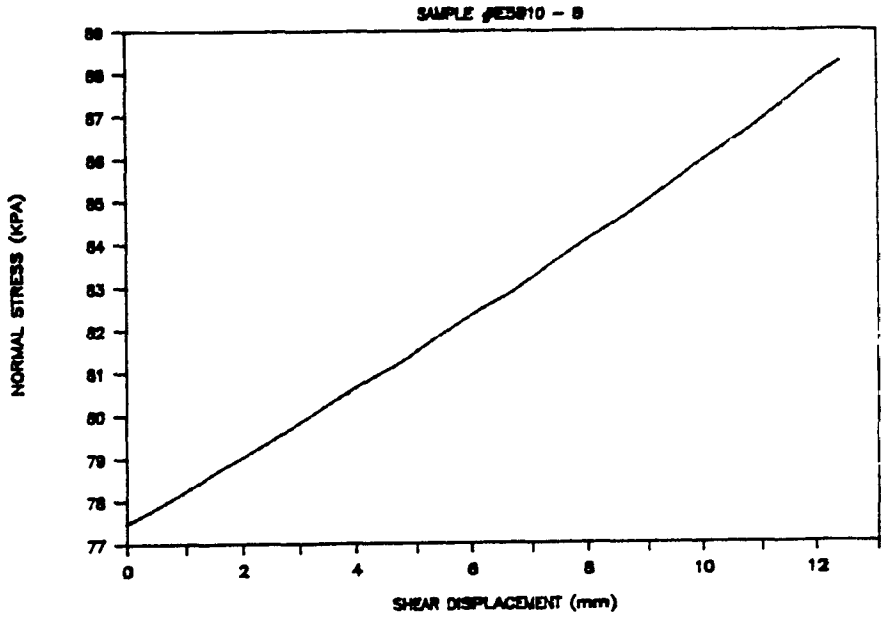
SAMPLE #E5810 - B
NORMAL STRESS (KPA)
77
78
79
80
81
82
83
84
85
86
87
88
0
2
4
6
8
10
12
SHEAR DISPLACEMENT (mm)

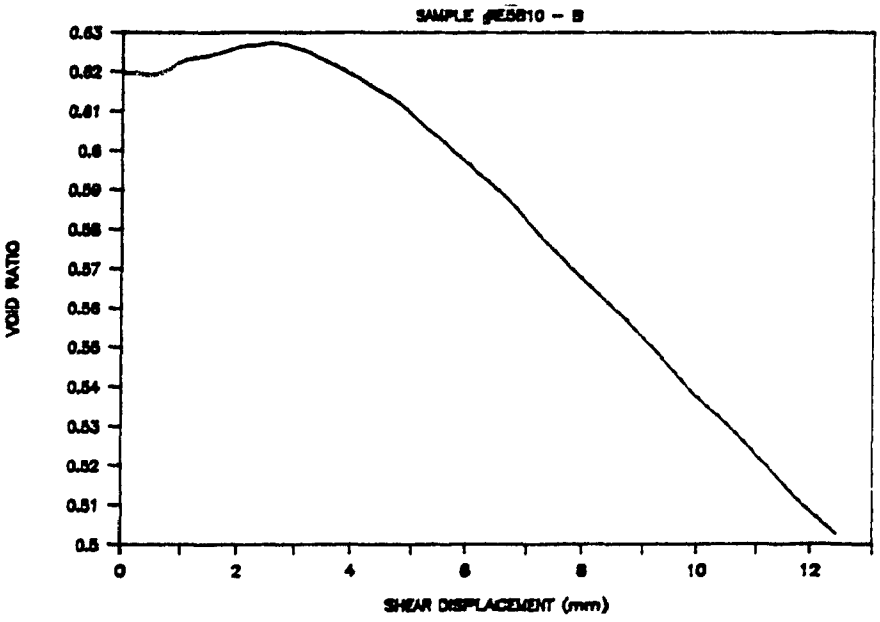
SAMPLE #E5810 - B
VOID RATIO
0.5
0.51
0.52
0.53
0.54
0.55
0.56
0.57
0.58
0.59
0.6
0.61
0.62
0.63
0
2
4
6
8
10
12
SHEAR DISPLACEMENT (mm)

DENISON

SAMPLE #E3A20 – 9

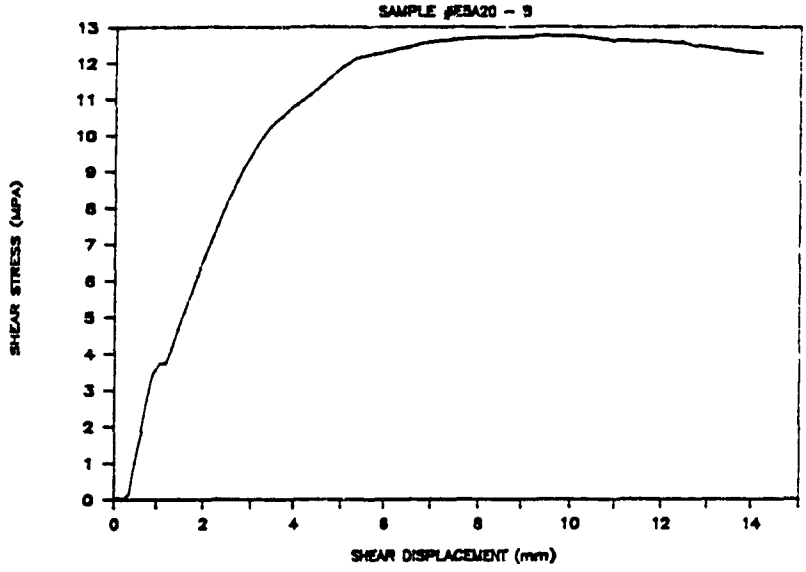

SAMPLE #E3A20 – 8

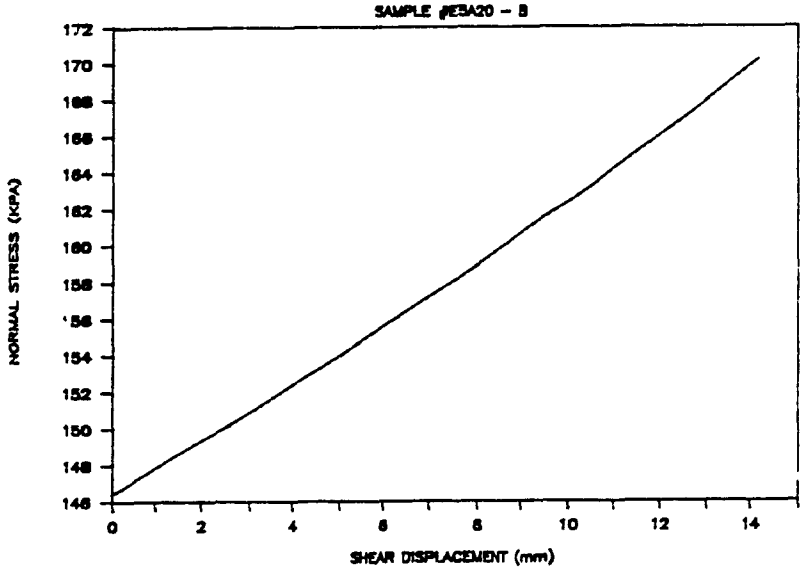

SAMPLE #E3A20 – 8

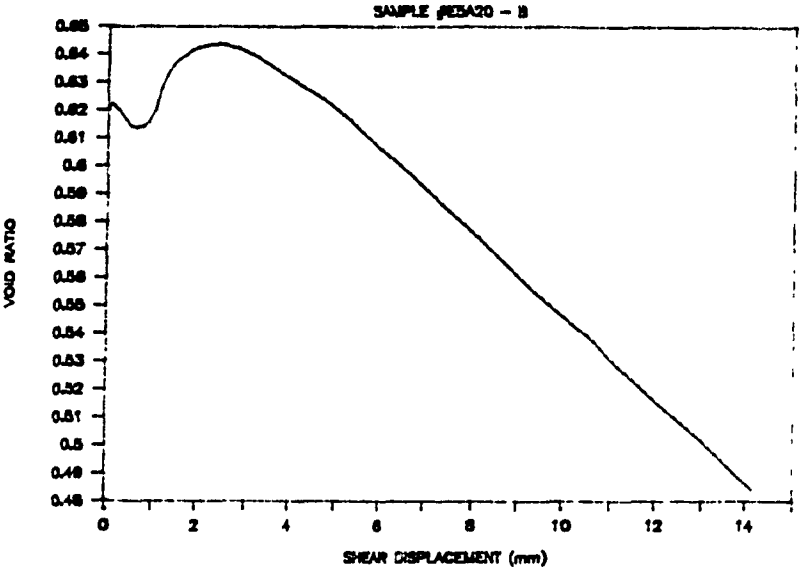

DENISON

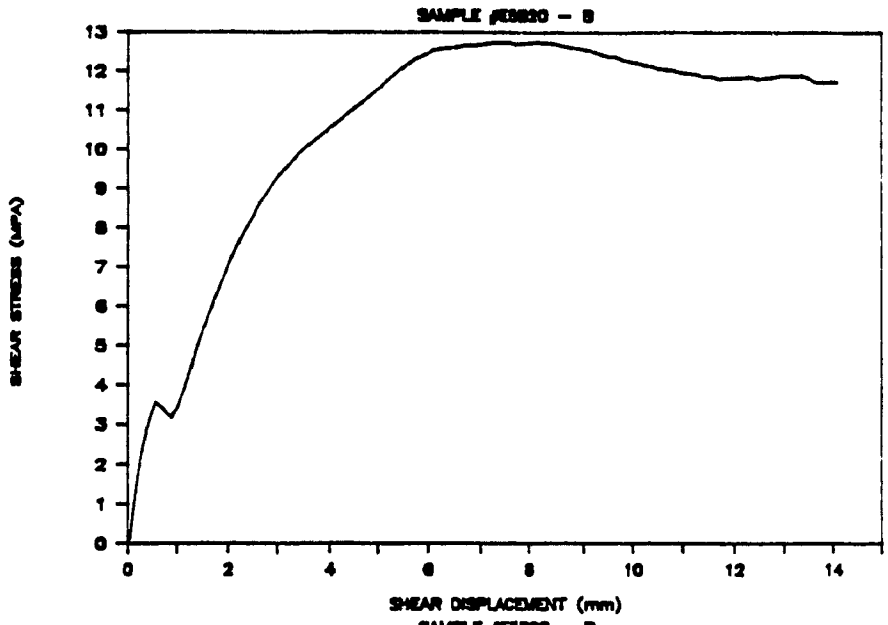
SAMPLE #E5820 – B
SHEAR STRESS (MPA)
SHEAR DISPLACEMENT (mm)

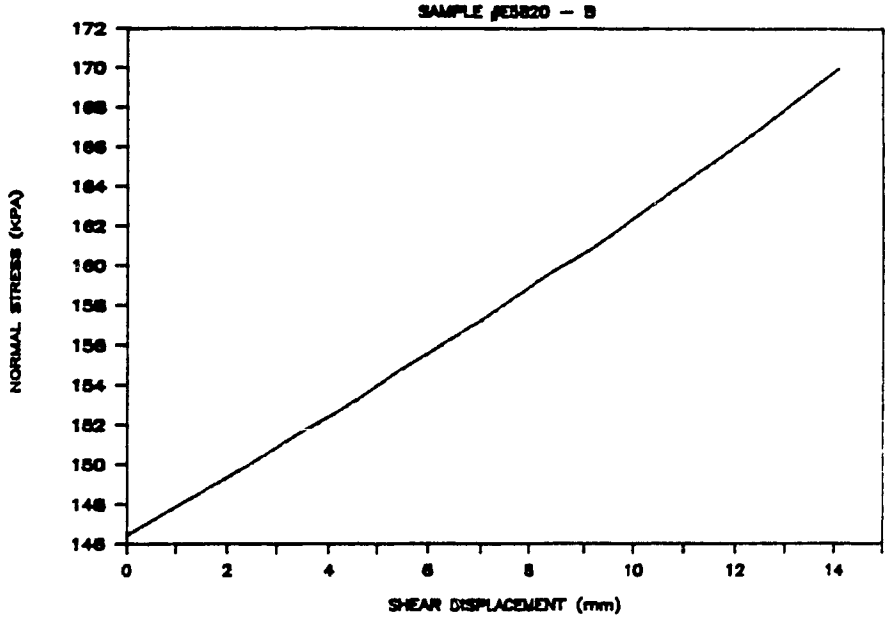
SAMPLE #E5820 – B
NORMAL STRESS (KPA)
SHEAR DISPLACEMENT (mm)

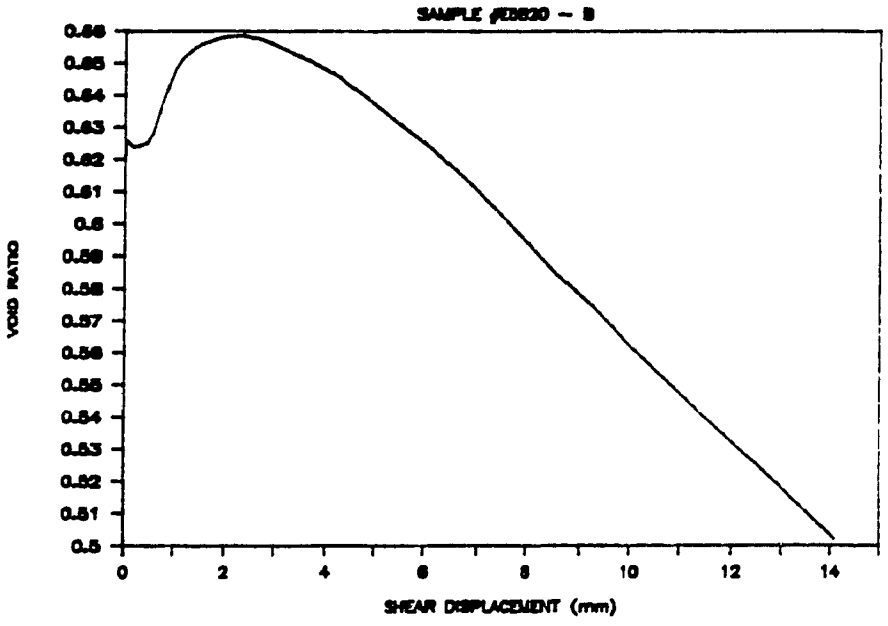
SAMPLE #E5820 – B
VOID RATIO
SHEAR DISPLACEMENT (mm)

DENISON

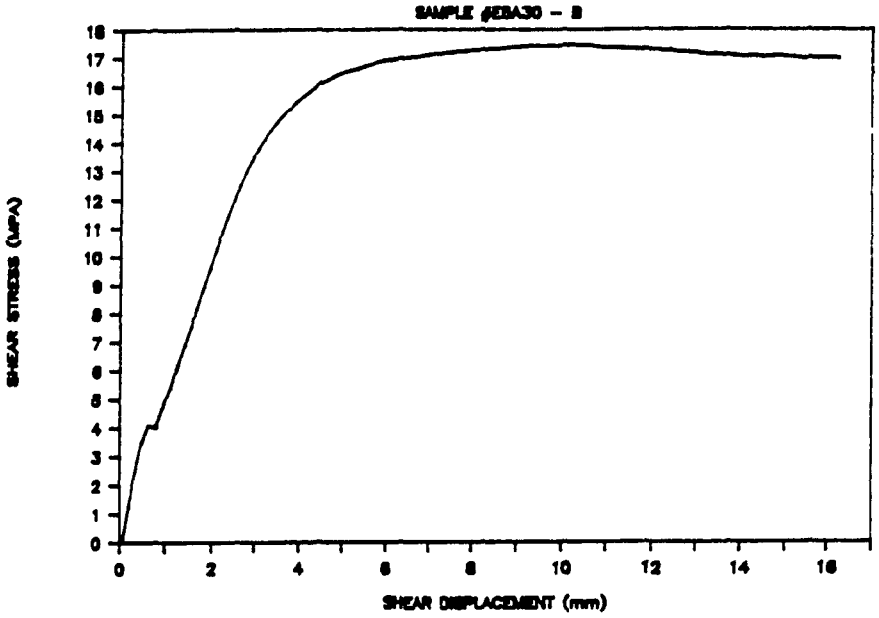
SAMPLE @EBA30 - B
SHEAR STRESS (MPA)
SHEAR DISPLACEMENT (mm)

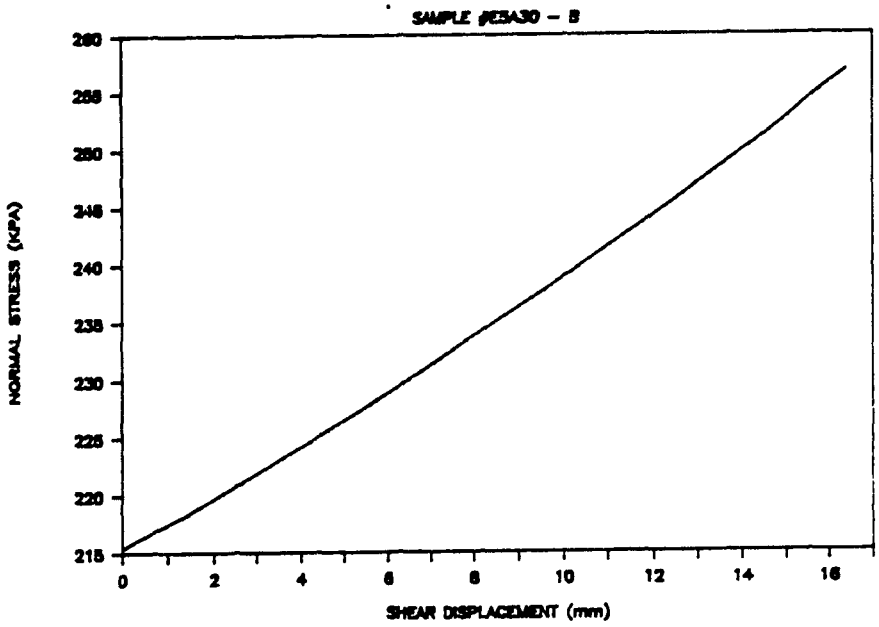
SAMPLE @EBA30 - B
NORMAL STRESS (KPA)
SHEAR DISPLACEMENT (mm)

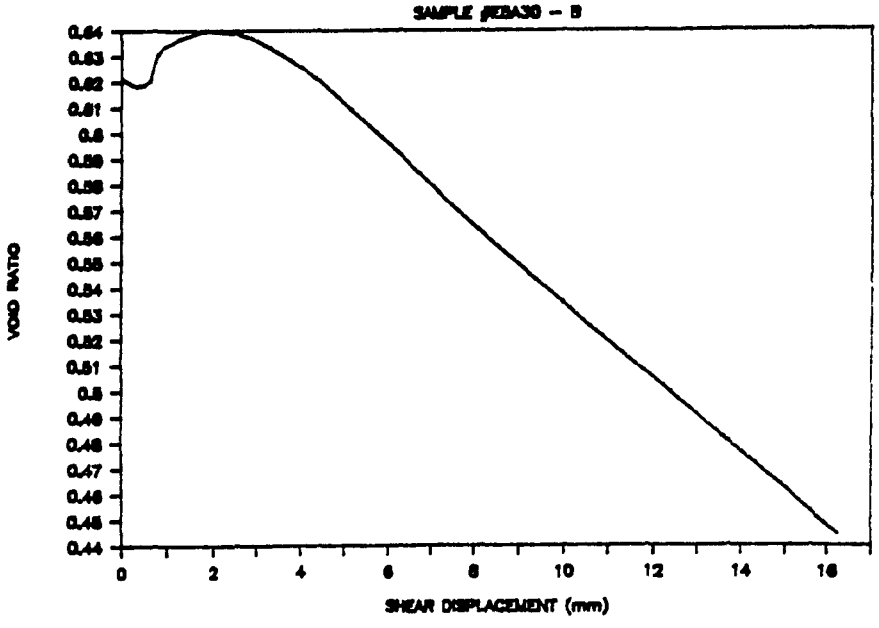
SAMPLE @EBA30 - B
VOID RATIO
SHEAR DISPLACEMENT (mm)

DENISON

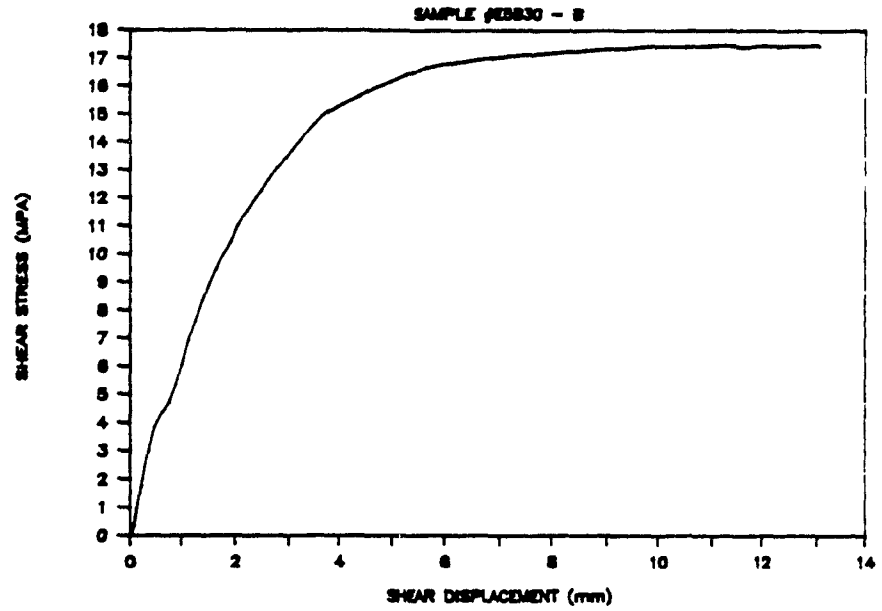
SAMPLE @ES830 - B
SHEAR STRESS (MPA)
SHEAR DISPLACEMENT (mm)

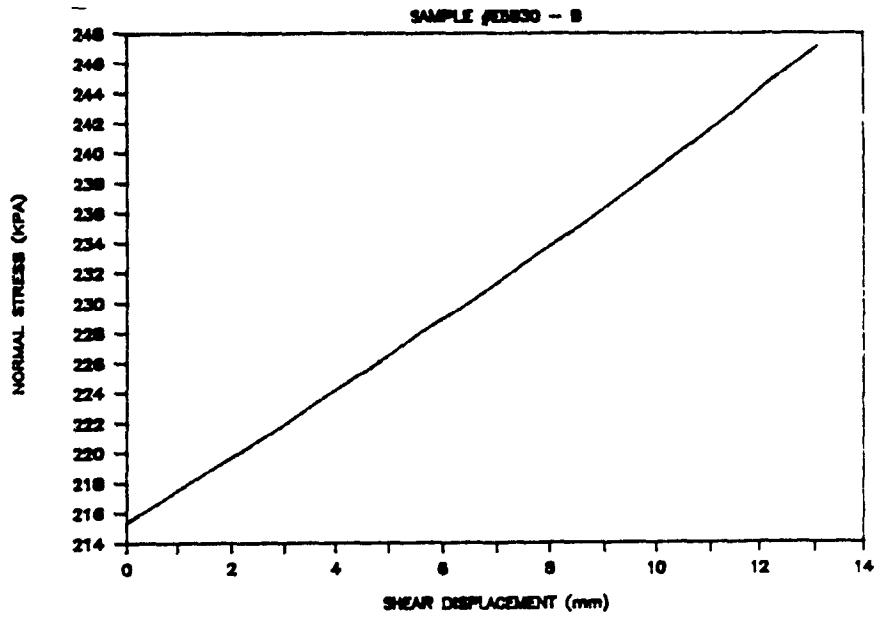
SAMPLE @ES830 - B
NORMAL STRESS (KPA)
SHEAR DISPLACEMENT (mm)

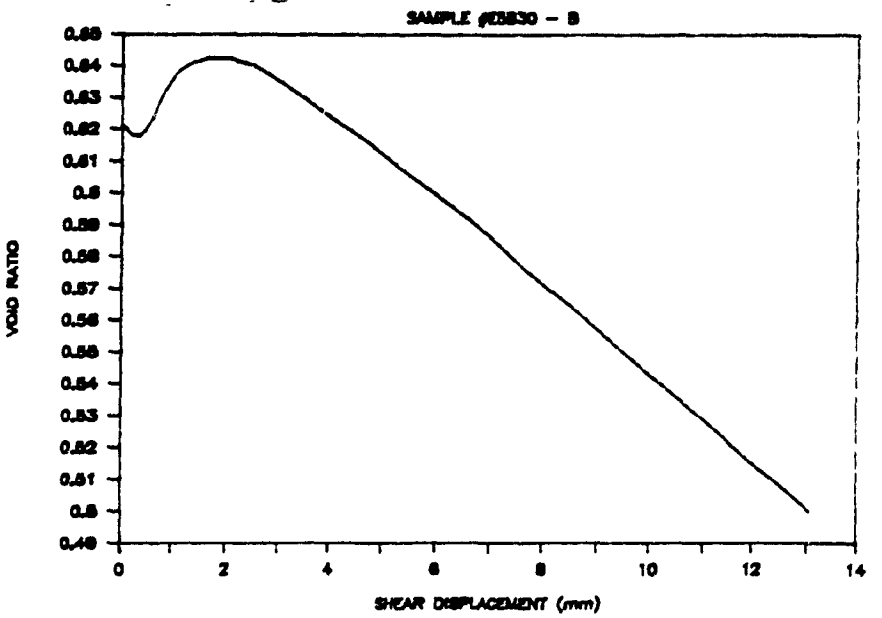
SAMPLE @ES830 - B
VOID RATIO
SHEAR DISPLACEMENT (mm)

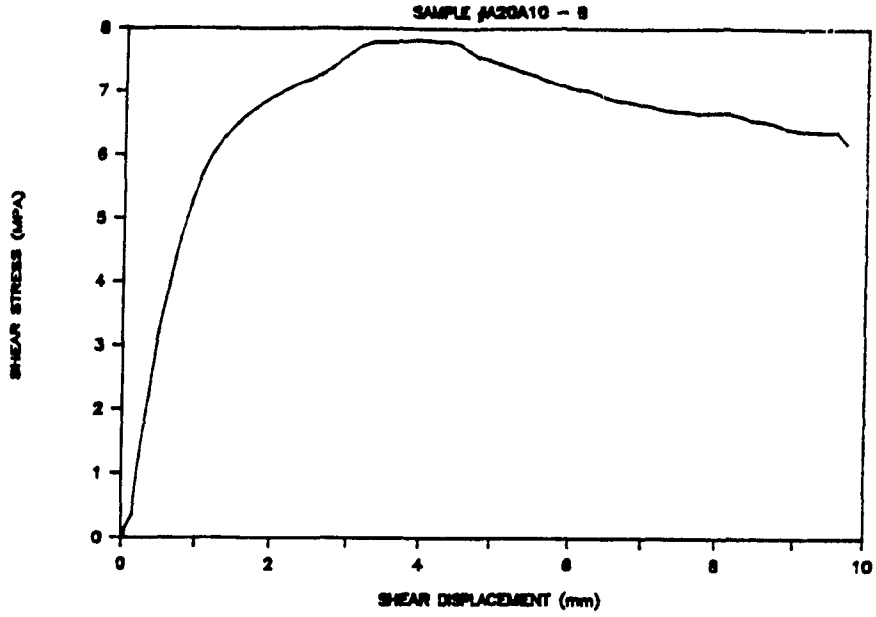
SAMPLE jA20A10 – B
SHEAR STRESS (MPA)
0
1
2
3
4
5
6
7
8
0
2
4
6
8
10
SHEAR DISPLACEMENT (mm)

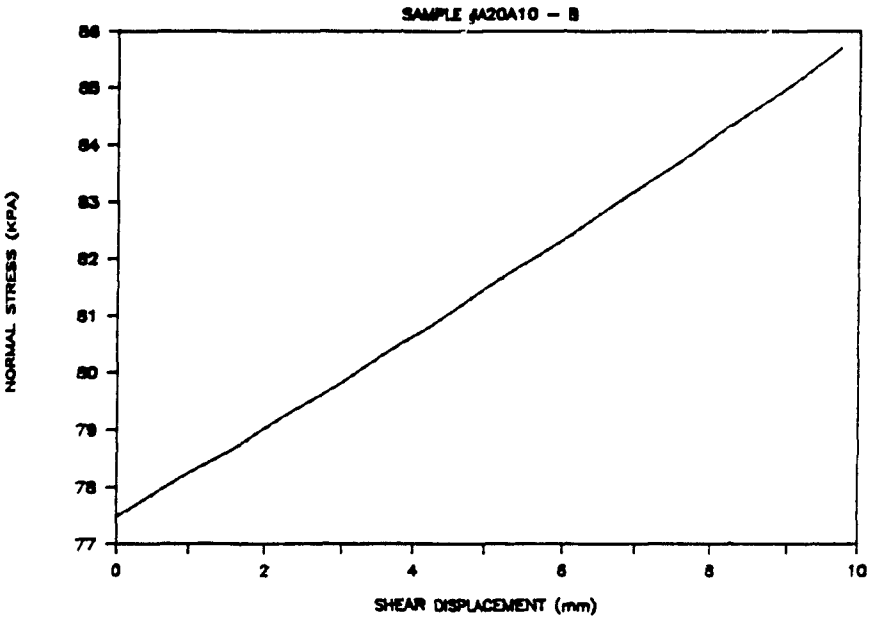
SAMPLE jA20A10 – B
NORMAL STRESS (KPA)
77
78
79
80
81
82
83
84
85
86
0
2
4
6
8
10
SHEAR DISPLACEMENT (mm)

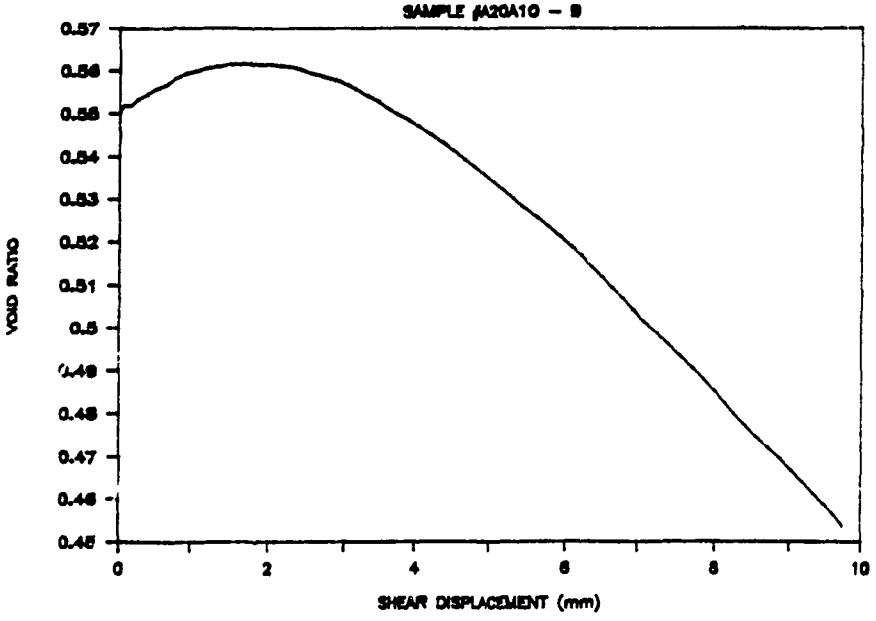
SAMPLE jA20A10 – B
VOID RATIO
0.45
0.46
0.47
0.48
0.49
0.5
0.51
0.52
0.53
0.54
0.55
0.56
0.57
0
2
4
6
8
10
SHEAR DISPLACEMENT (mm)

DENISON

SAMPLE #A20B10 – B

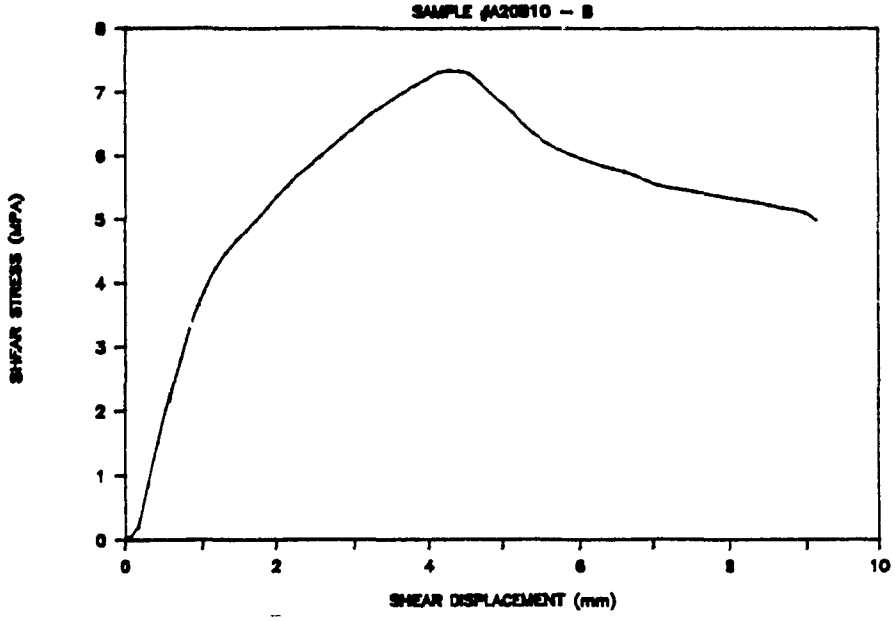

SAMPLE #A20B10 – B

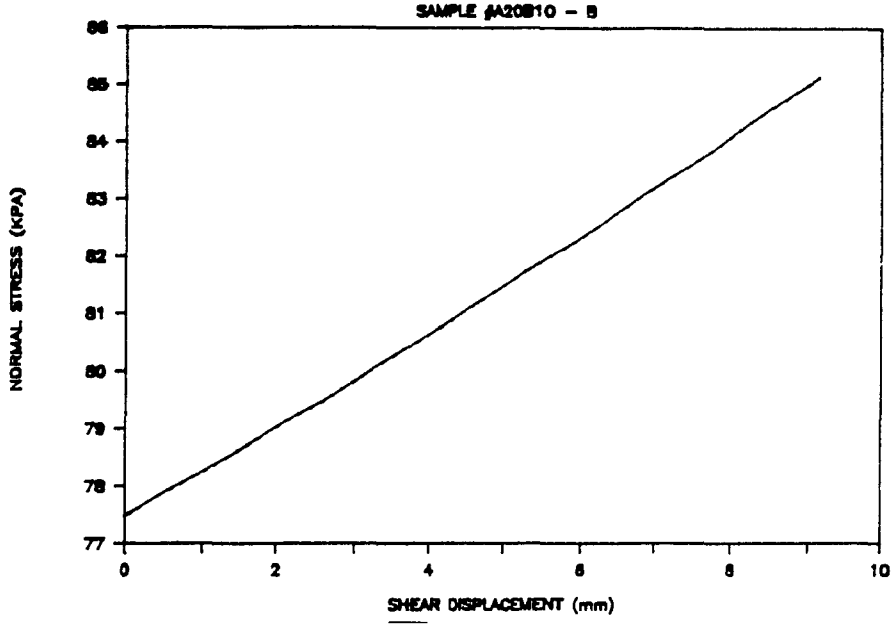

SAMPLE #A20B10 – B

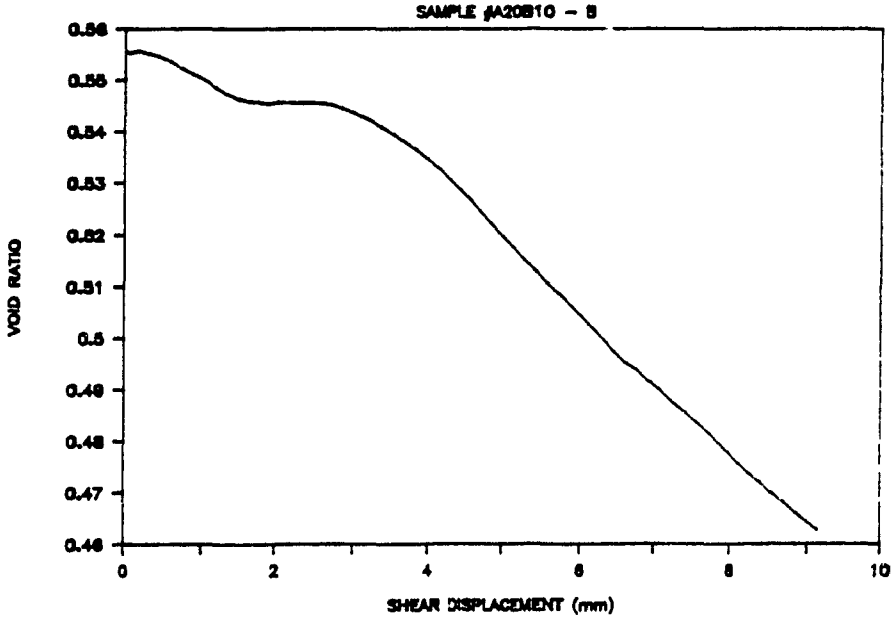

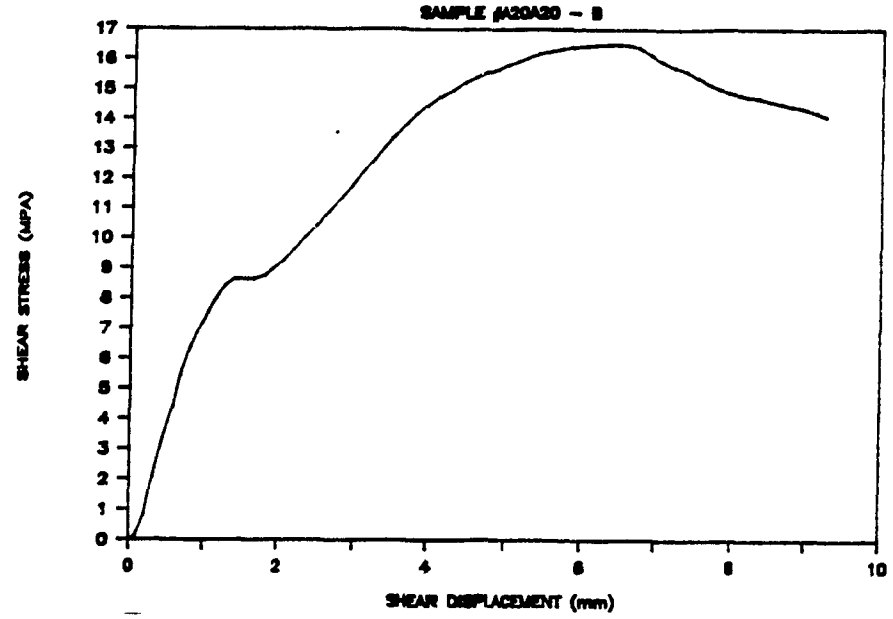
SAMPLE #A20A20 - B
SHEAR STRESS (MPA)
SHEAR DISPLACEMENT (mm)

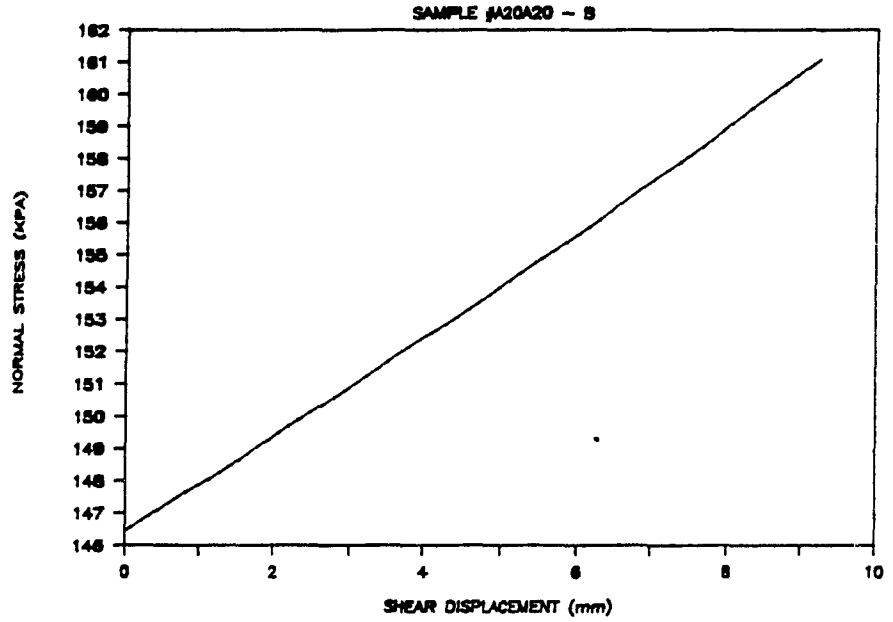
SAMPLE #A20A20 - B
NORMAL STRESS (KPA)
SHEAR DISPLACEMENT (mm)

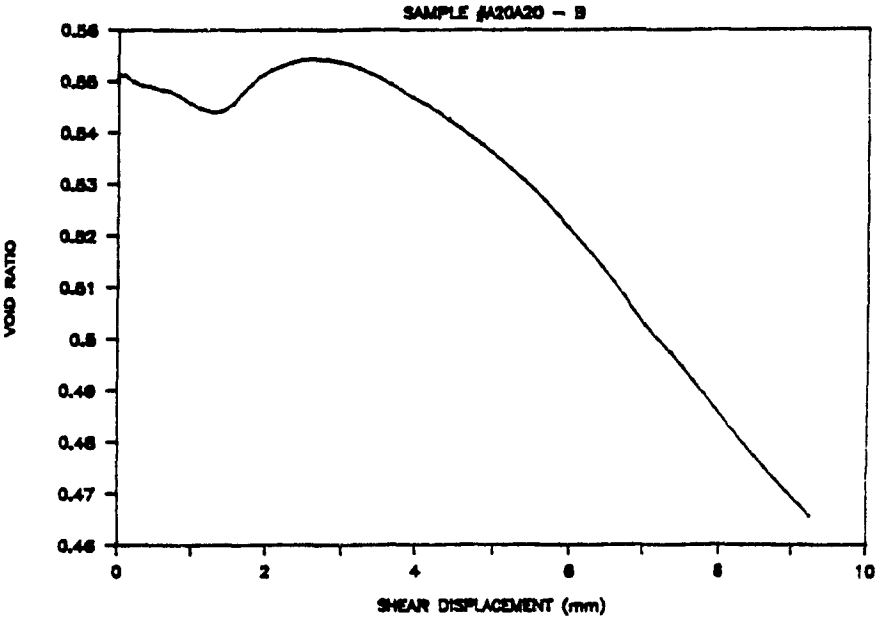
SAMPLE #A20A20 - B
VOID RATIO
SHEAR DISPLACEMENT (mm)

DENISON

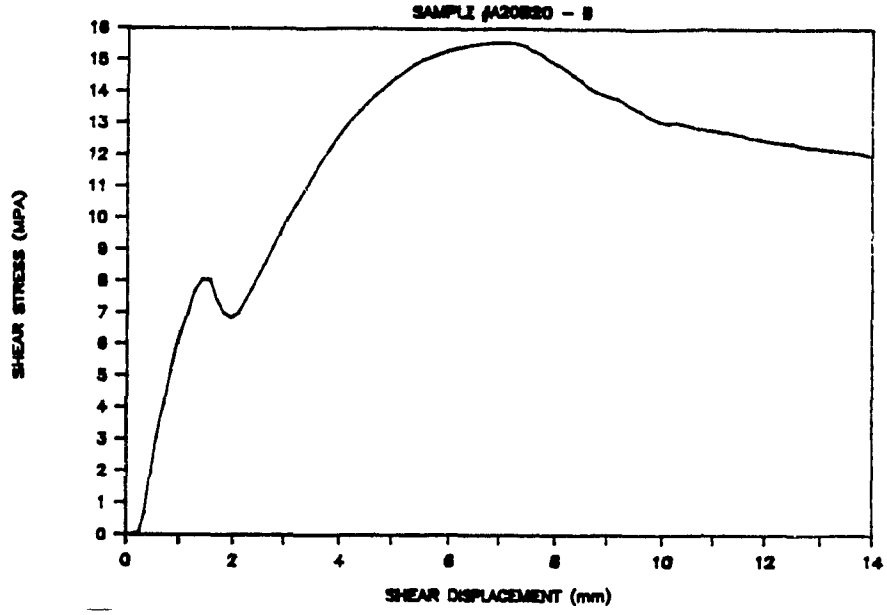
SAMPLE #A20B20 - B
SHEAR STRESS (MPA)
SHEAR DISPLACEMENT (mm)

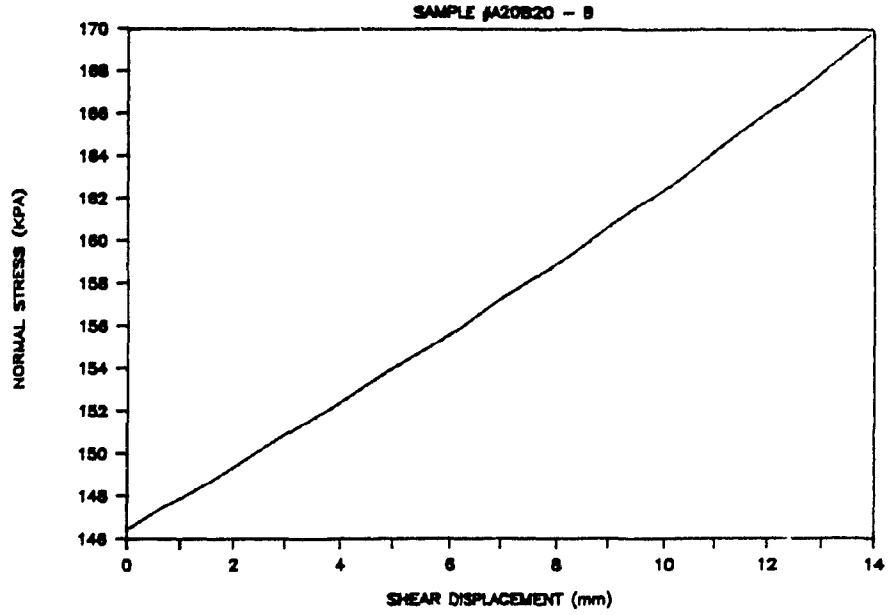
SAMPLE #A20B20 - B
NORMAL STRESS (KPA)
SHEAR DISPLACEMENT (mm)

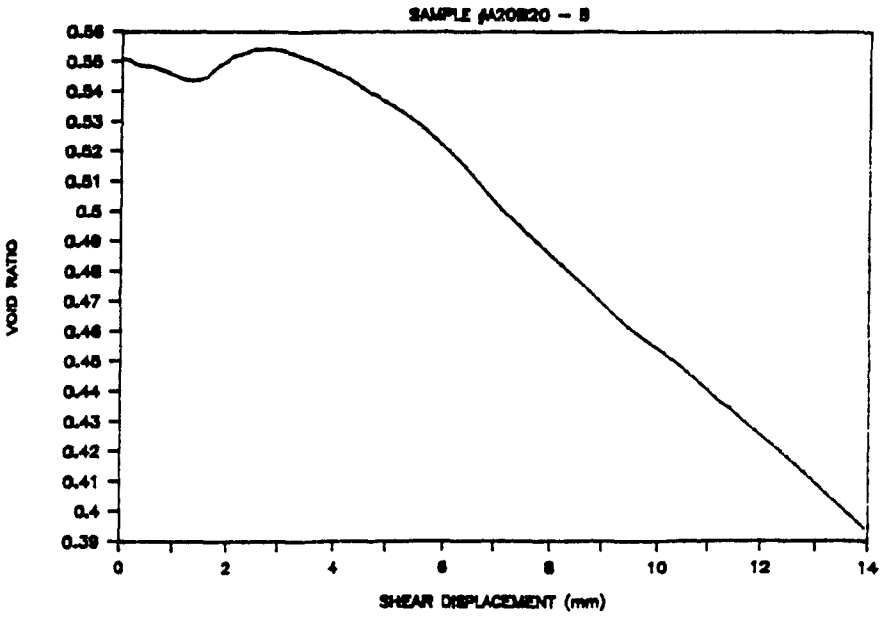
SAMPLE #A20B20 - B
VOID RATIO
SHEAR DISPLACEMENT (mm)

DENISON

SAMPLE #A20A30 - B

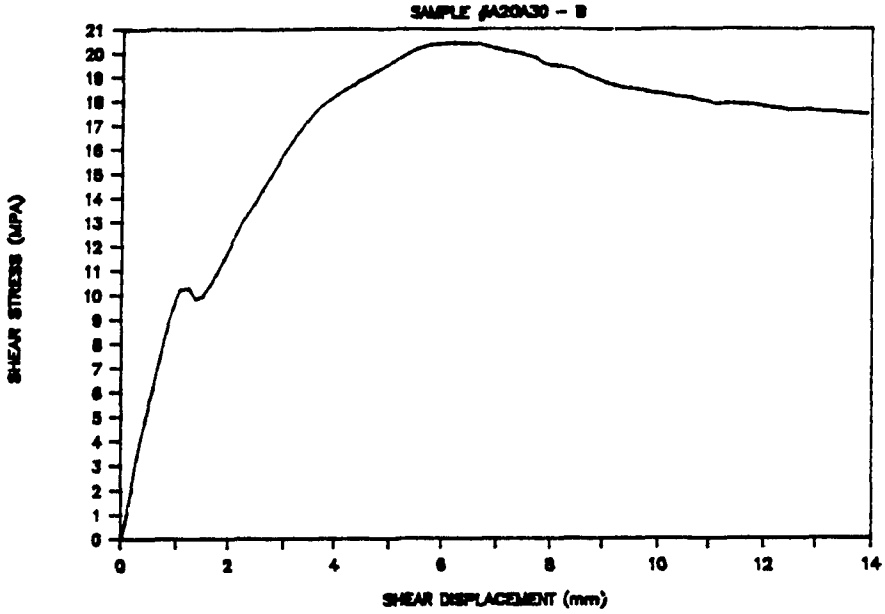

SAMPLE #A20A30 - B

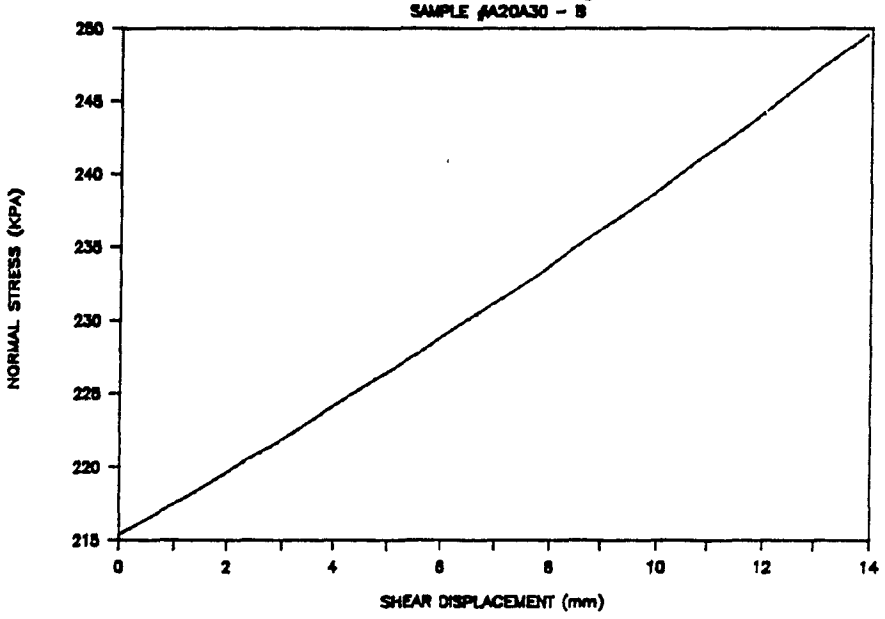

SAMPLE #A20A30 - B

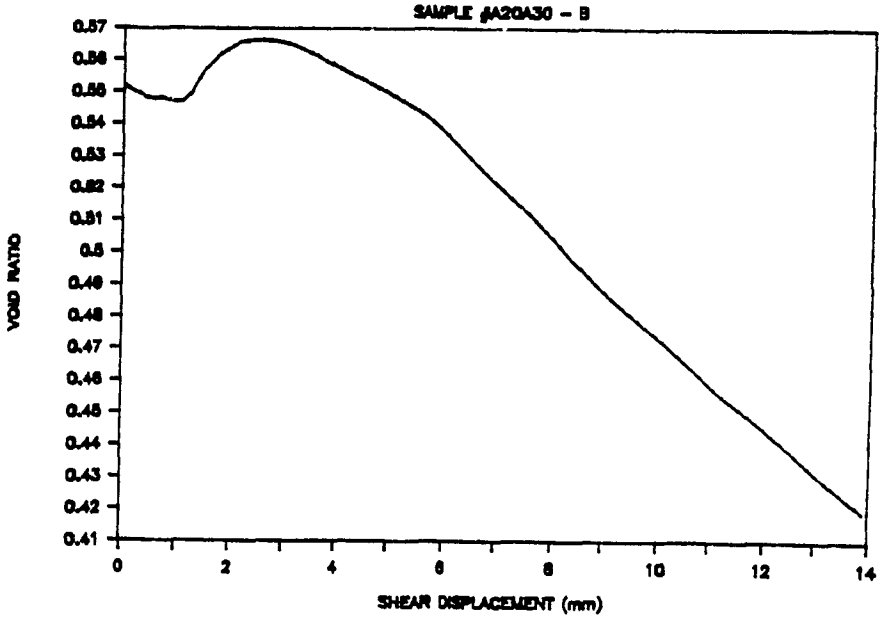

DENISON

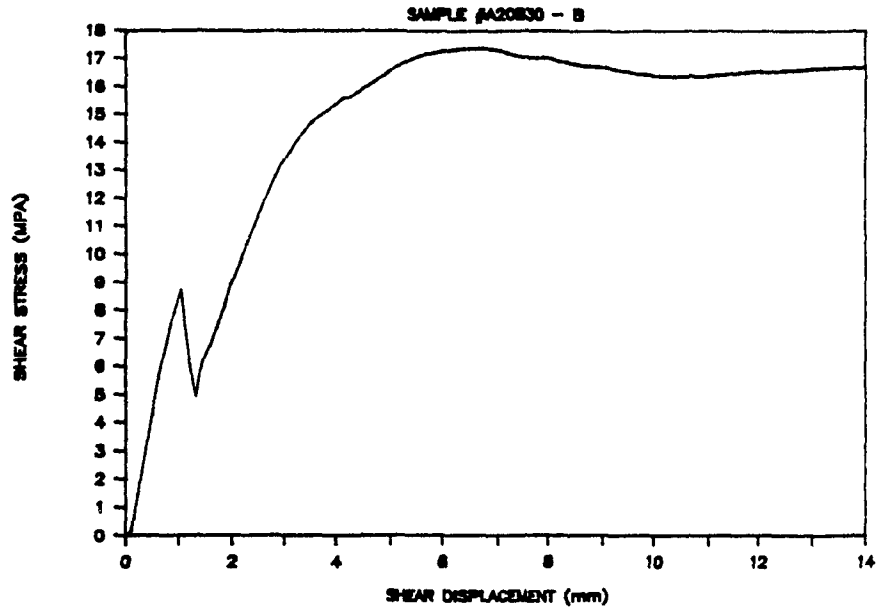
SAMPLE jA20B30 - B
SHEAR STRESS (MPA)
SHEAR DISPLACEMENT (mm)

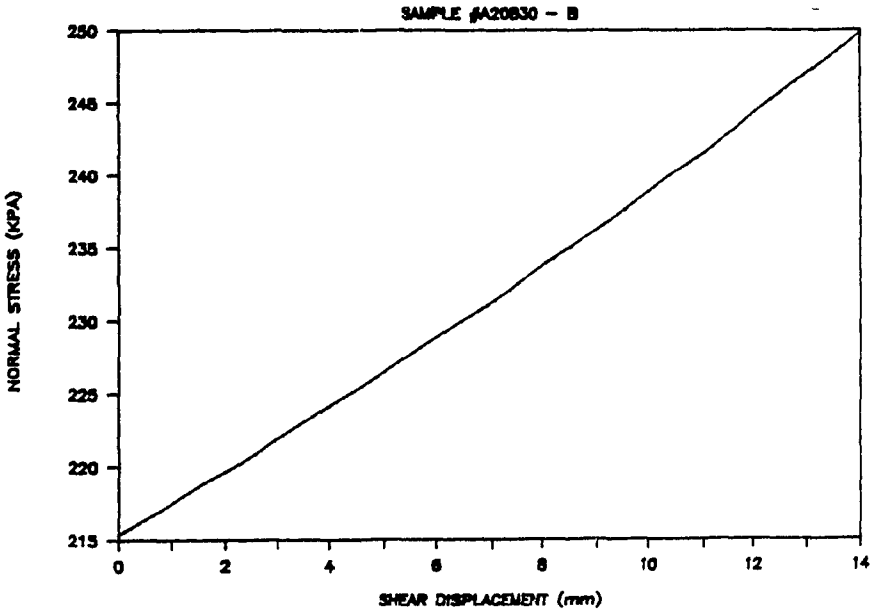
SAMPLE jA20B30 - B
NORMAL STRESS (KPA)
SHEAR DISPLACEMENT (mm)

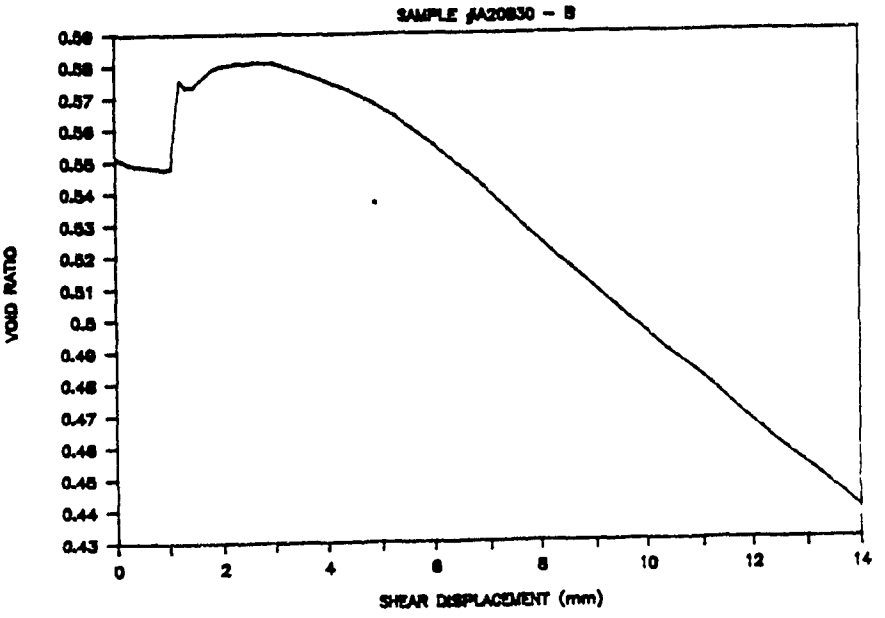
SAMPLE jA20B30 - B
VOID RATIO
SHEAR DISPLACEMENT (mm)

DENISON

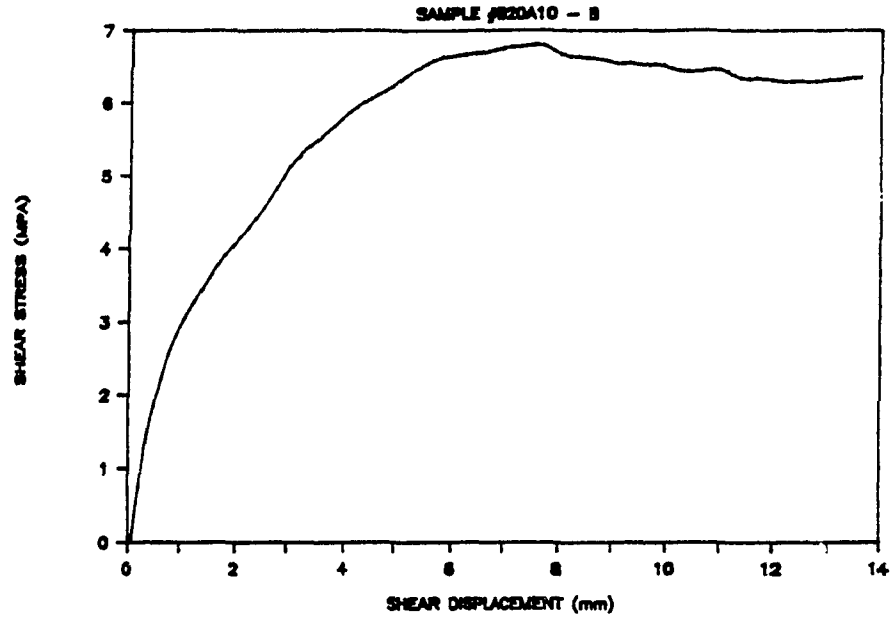
SAMPLE #B20A10 - B
SHEAR STRESS (MPA)
SHEAR DISPLACEMENT (mm)

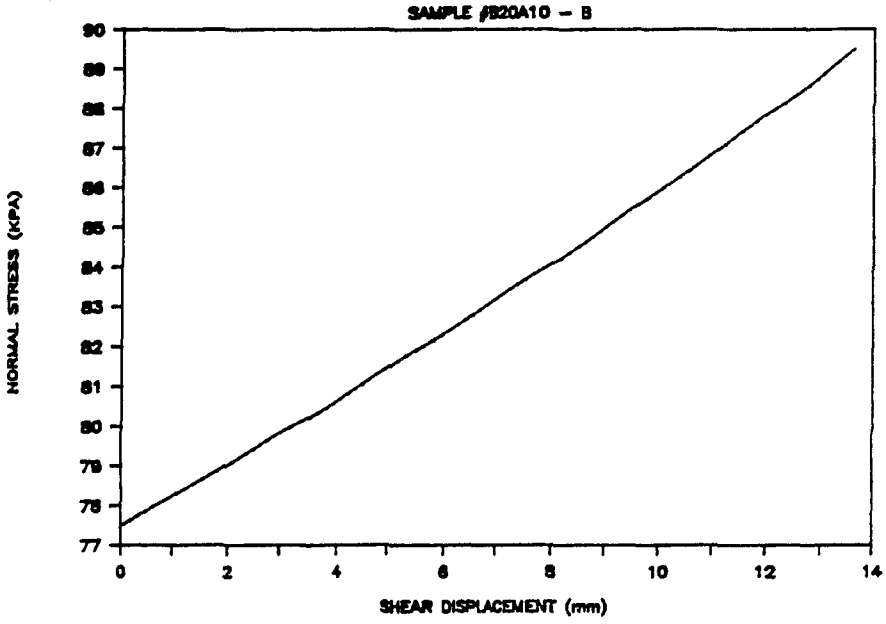
SAMPLE #B20A10 - B
NORMAL STRESS (KPA)
SHEAR DISPLACEMENT (mm)

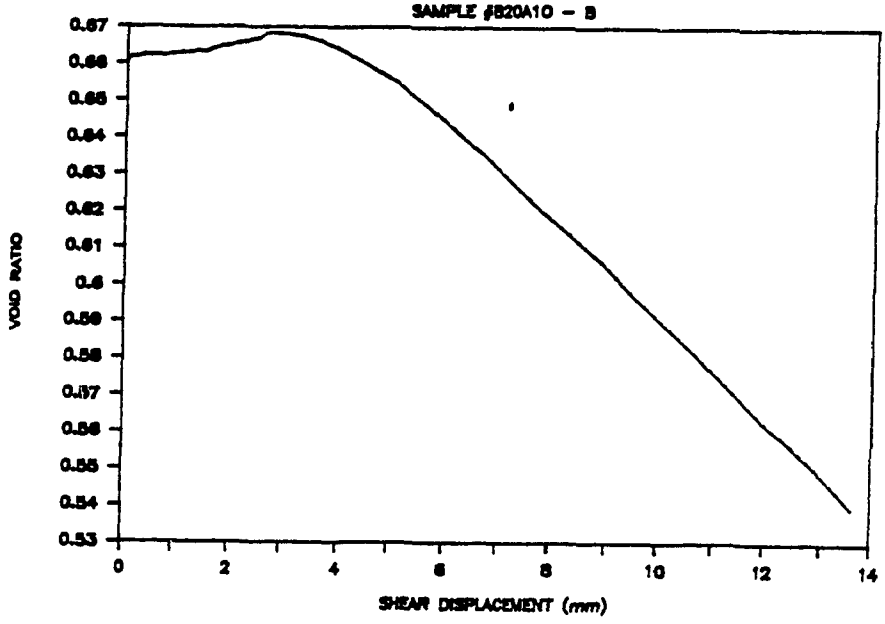
SAMPLE #B20A10 - B
VOID RATIO
SHEAR DISPLACEMENT (mm)

DENISON

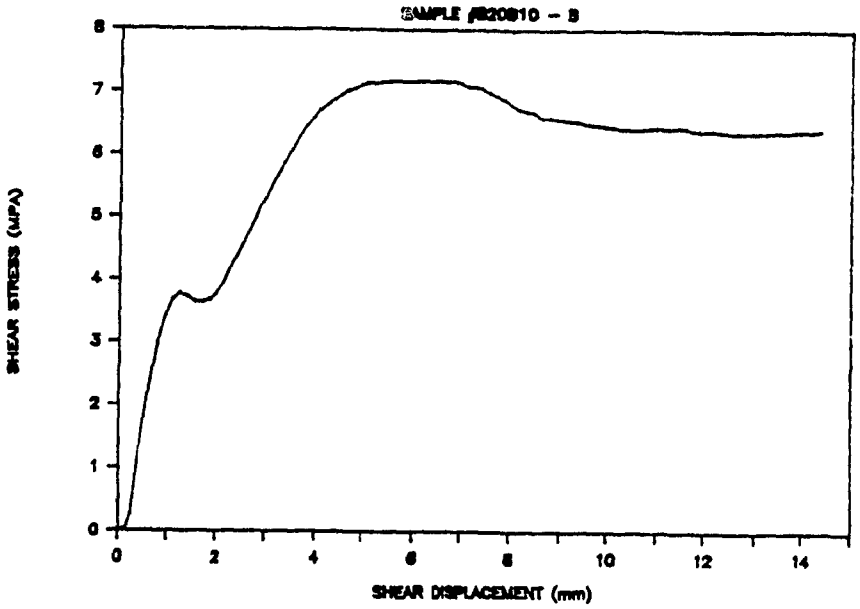
SAMPLE #820B10 - B
SHEAR STRESS (MPA)
SHEAR DISPLACEMENT (mm)

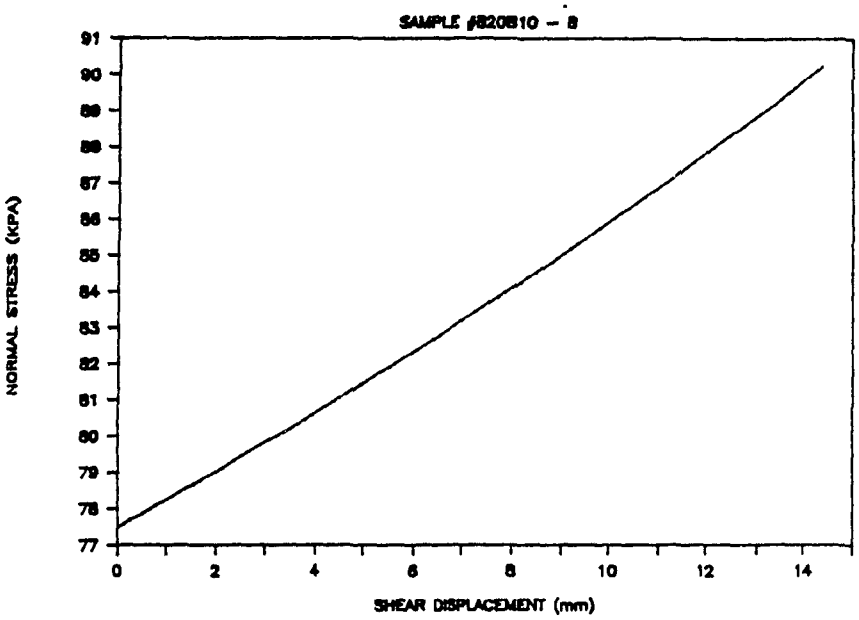
SAMPLE #820B10 - B
NORMAL STRESS (KPA)
SHEAR DISPLACEMENT (mm)

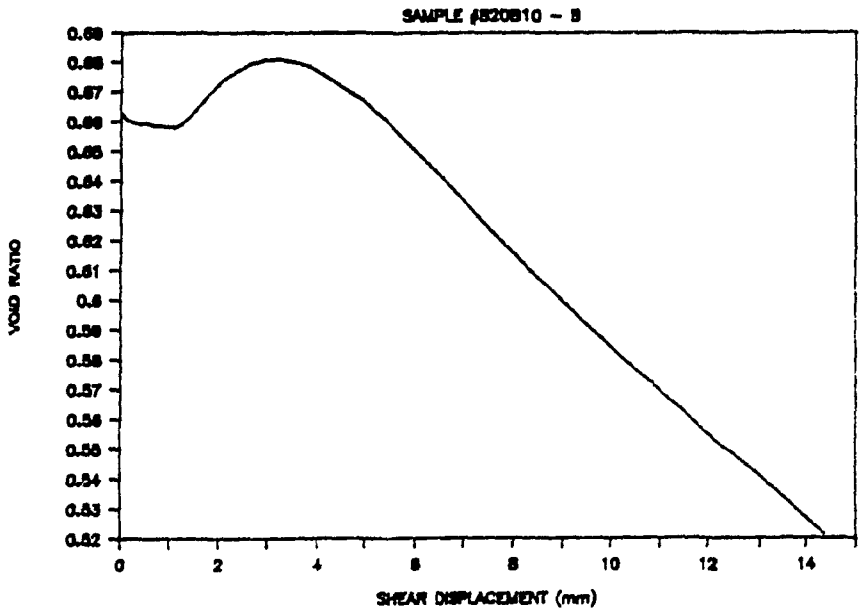
SAMPLE #820B10 - B
VOID RATIO
SHEAR DISPLACEMENT (mm)

DENISON

SAMPLE #B20A20 - B

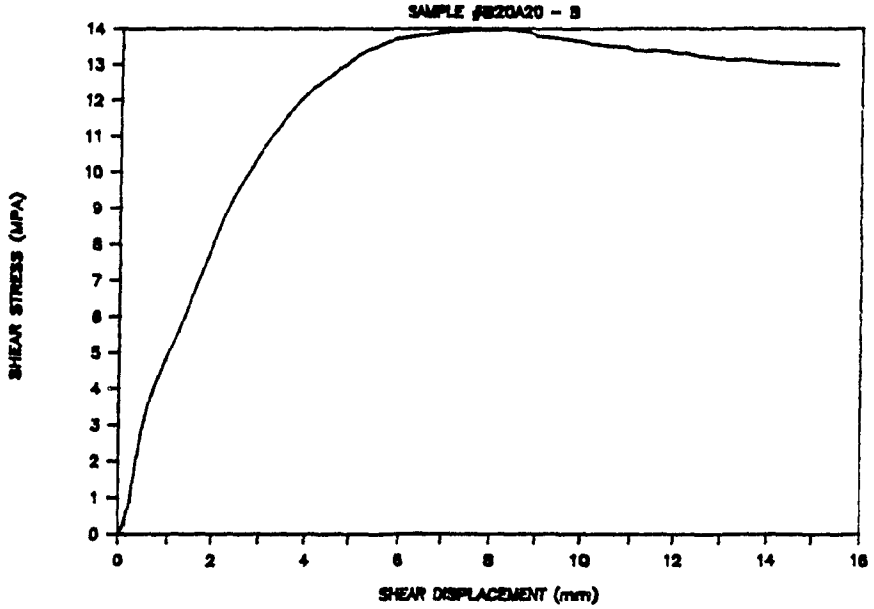

SAMPLE #B20A20 - B

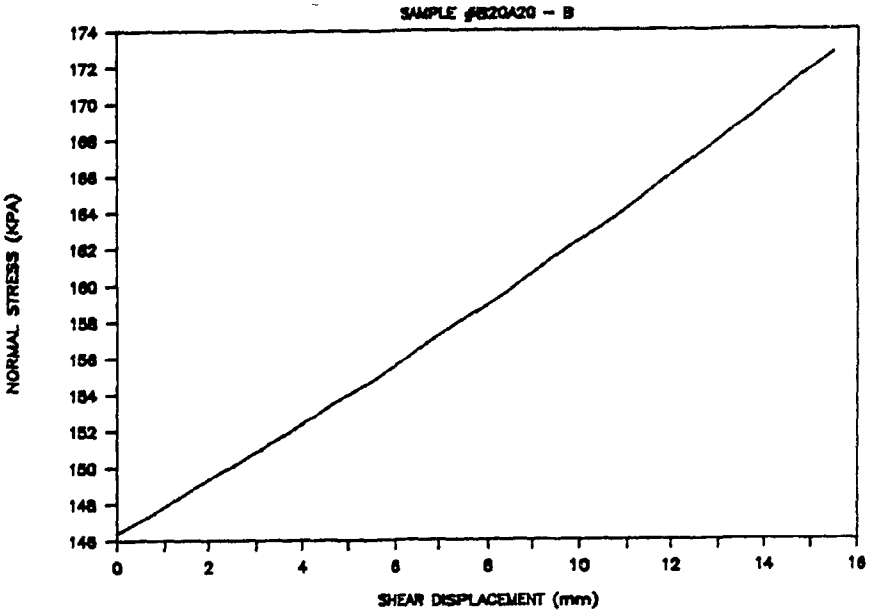

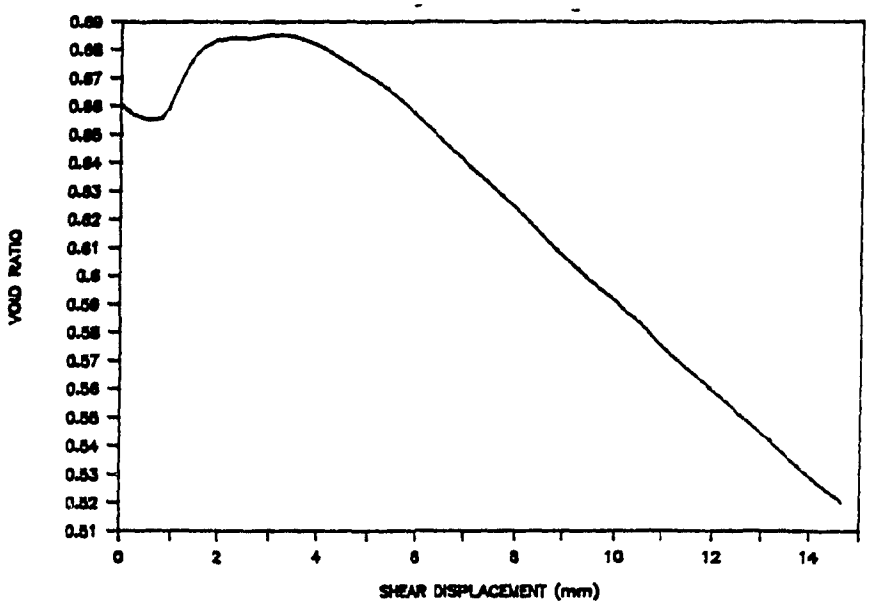

DENISON

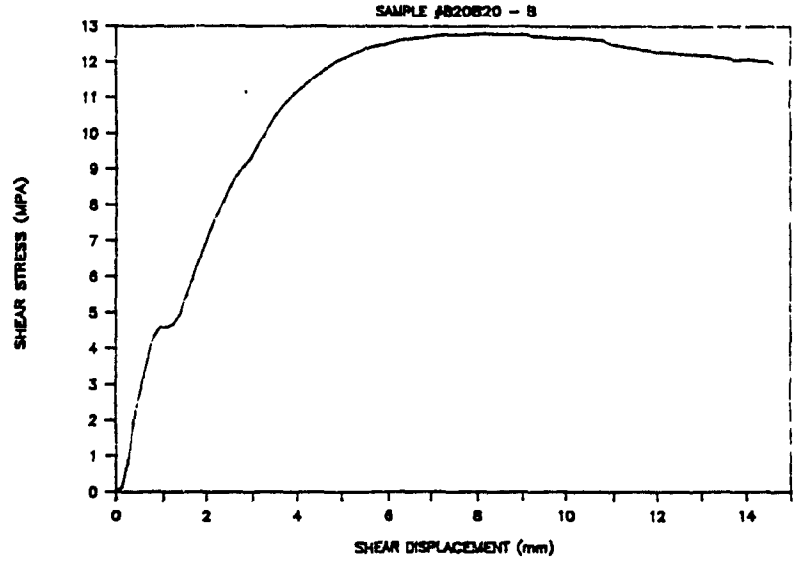
SAMPLE #B20B20 - B
SHEAR STRESS (MPA)
SHEAR DISPLACEMENT (mm)

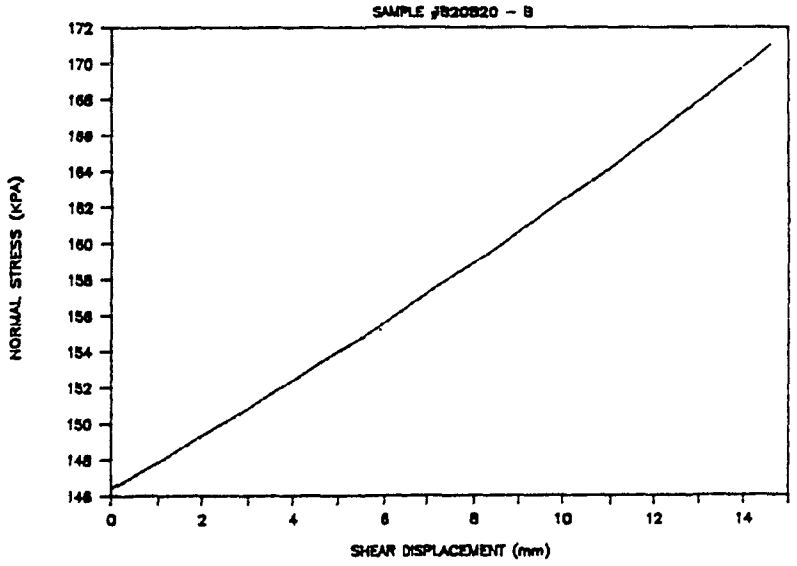
SAMPLE #B20B20 - B
NORMAL STRESS (KPA)
SHEAR DISPLACEMENT (mm)

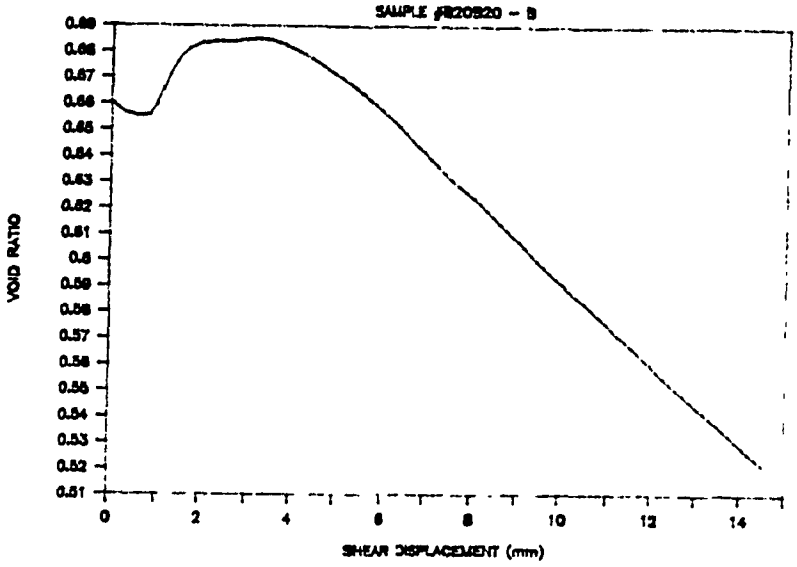
SAMPLE #B20B20 - B
VOID RATIO
SHEAR DISPLACEMENT (mm)

DENISON

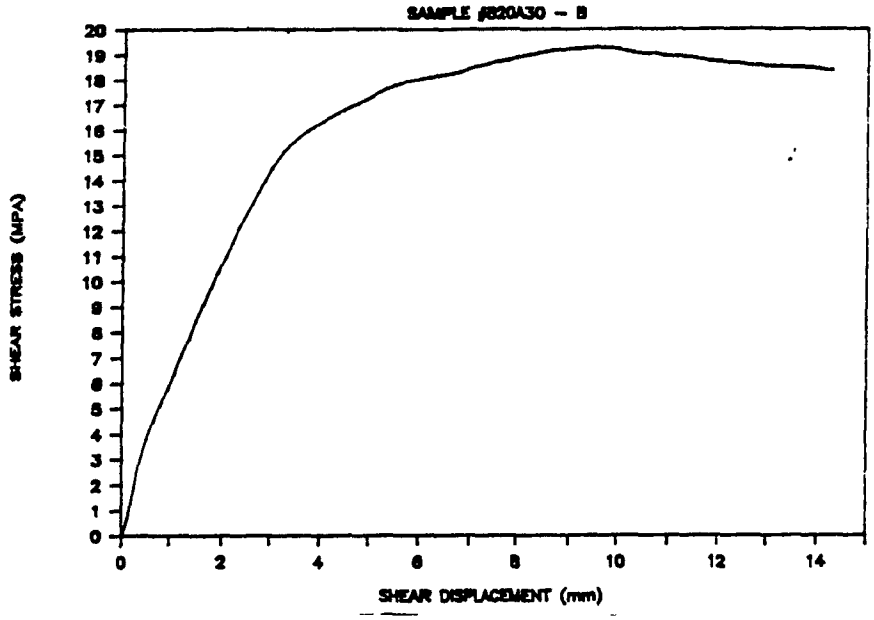
SAMPLE #B20A30 - B
SHEAR STRESS (MPA)
SHEAR DISPLACEMENT (mm)

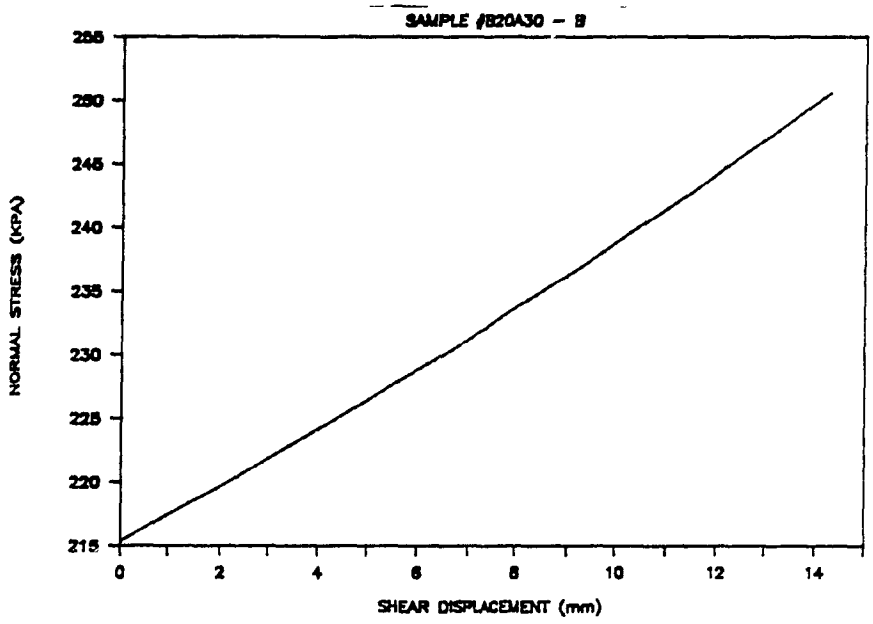
SAMPLE #B20A30 - B
NORMAL STRESS (KPA)
SHEAR DISPLACEMENT (mm)

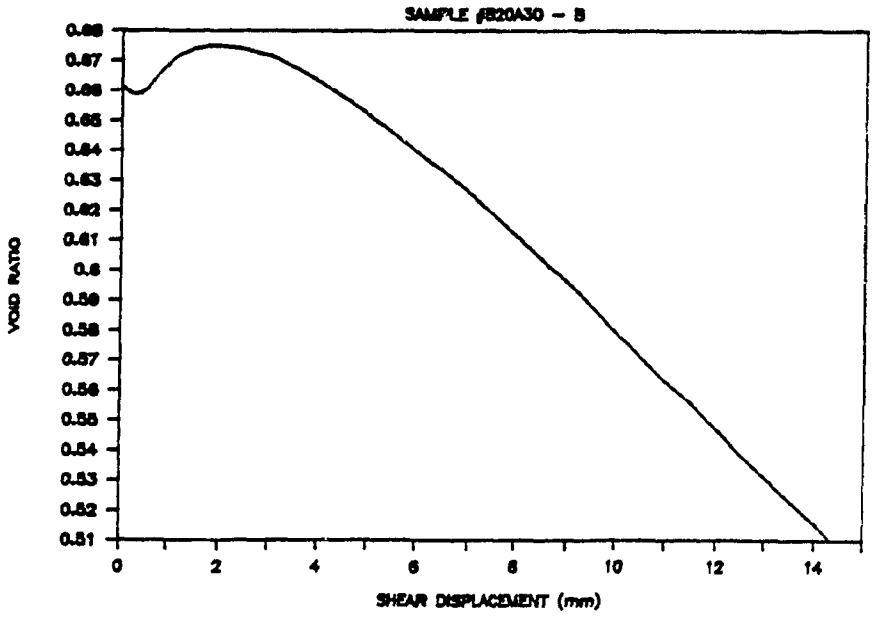
SAMPLE #B20A30 - B
VOID RATIO
SHEAR DISPLACEMENT (mm)

DENISON

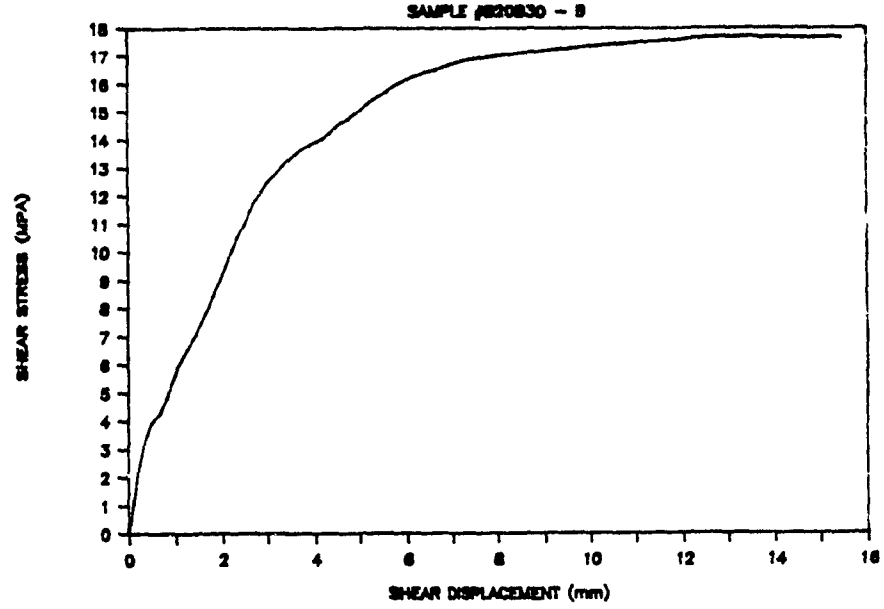
SAMPLE #820830 - 8
SHEAR STRESS (MPA)
SHEAR DISPLACEMENT (mm)

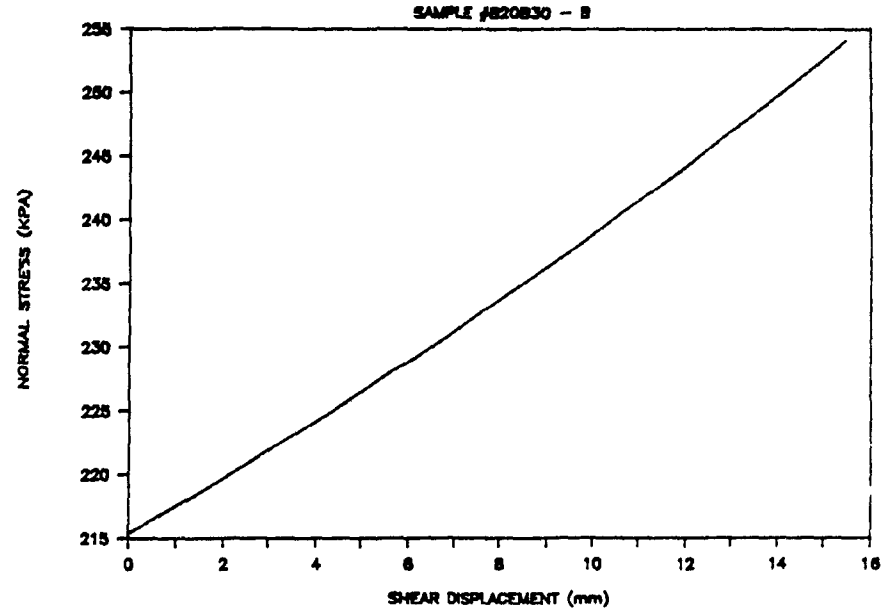
SAMPLE #820830 - 8
NORMAL STRESS (KPA)
SHEAR DISPLACEMENT (mm)

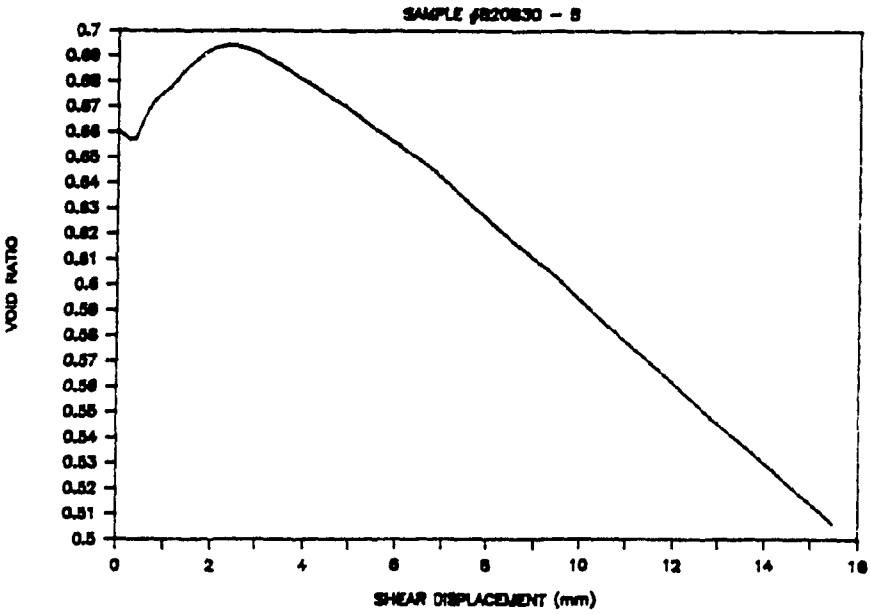
SAMPLE #820830 - 8
VOID RATIO
SHEAR DISPLACEMENT (mm)

APPENDIX D

ANALYZED SHEAR BOX DATA -
FAILURE ENVELOPES

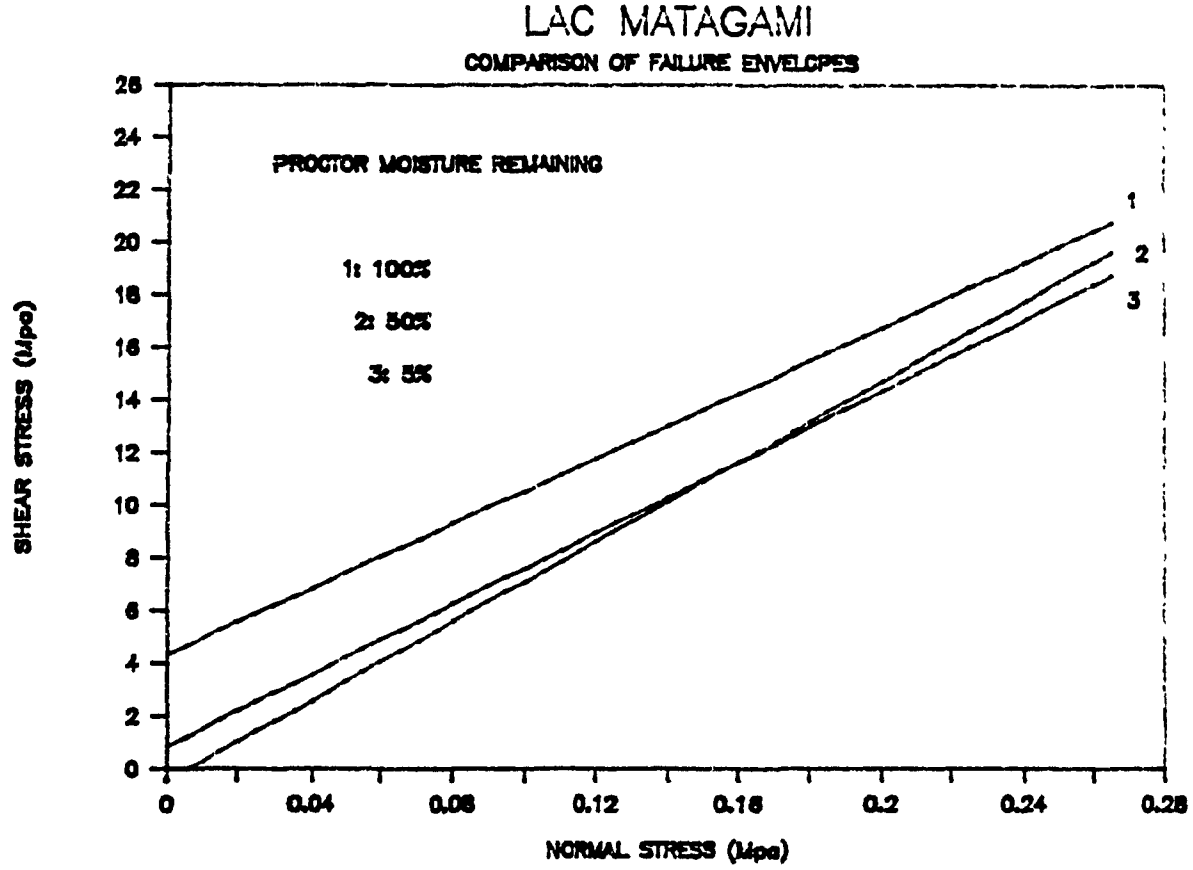
LAC MATAGAMI
COMPARISON OF FAILURE ENVELOPES
PROCTOR MOISTURE REMAINING
1: 100%
2: 50%
3: 5%
1
2
3
SHEAR STRESS (Mpa)
NORMAL STRESS (Mpa)
0
2
4
6
8
10
12
14
16
18
20
22
24
26
0.04
0.08
0.12
0.16
0.2
0.24
0.28

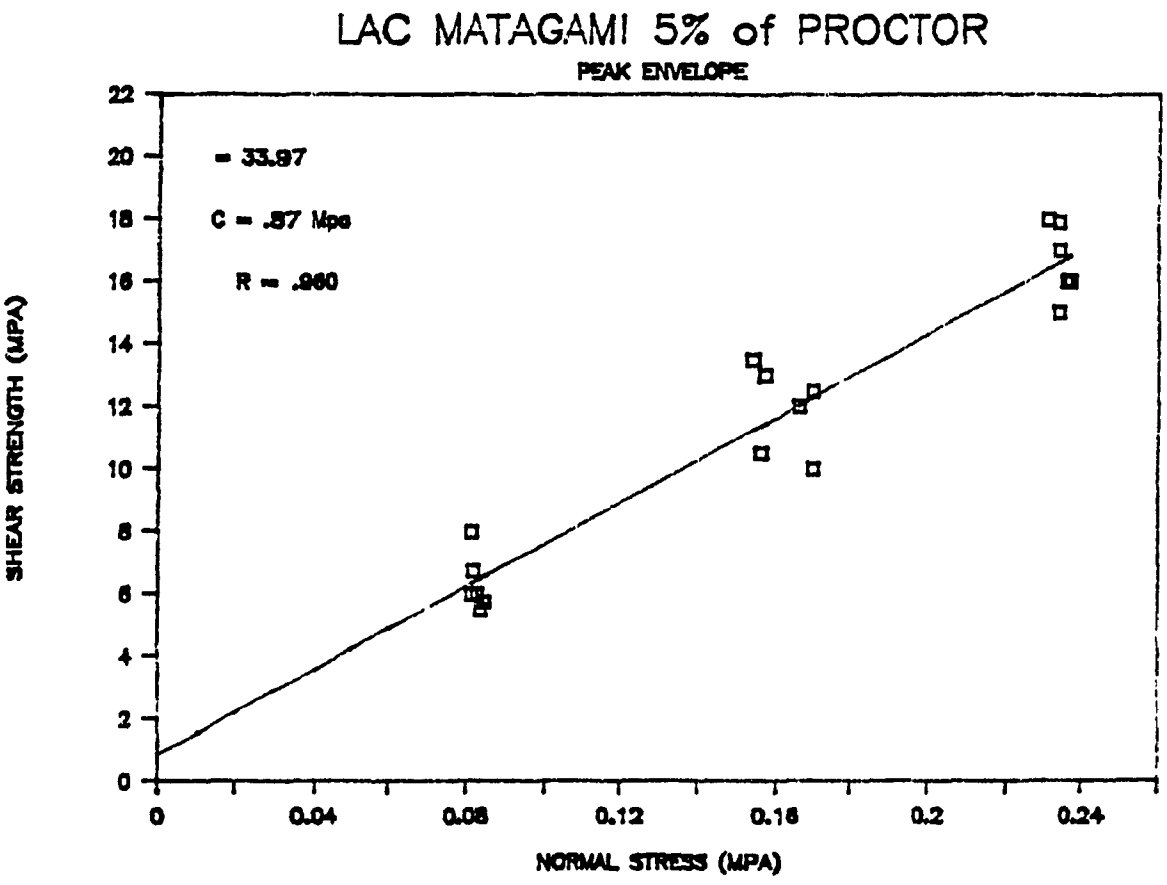
LAC MATAGAMI 5% of PROCTOR
PEAK ENVELOPE
= 33.97
C = .87 Mpa
R = .960
SHEAR STRENGTH (MPA)
NORMAL STRESS (MPA)
0
2
4
6
8
10
12
14
16
18
20
22
0.04
0.08
0.12
0.16
0.2
0.24

LAC MATAGAMI 50% of PROCTOR

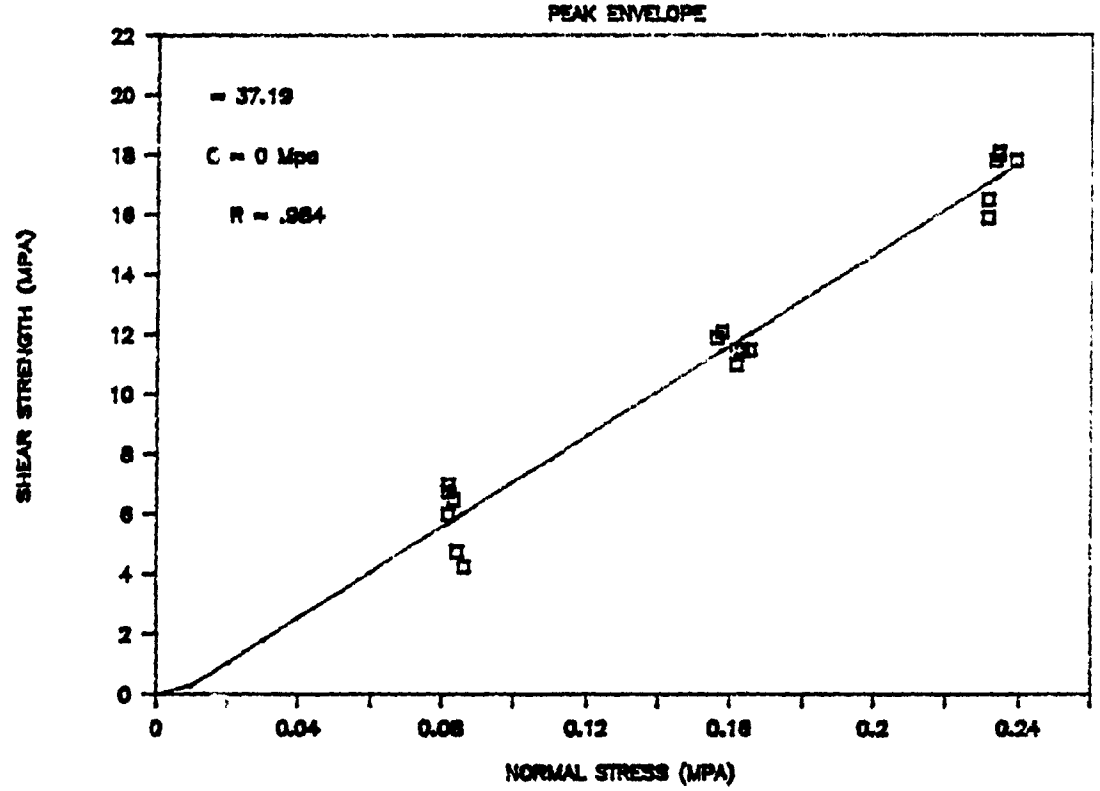

LAC MATAGAMI 100% of PROCTOR

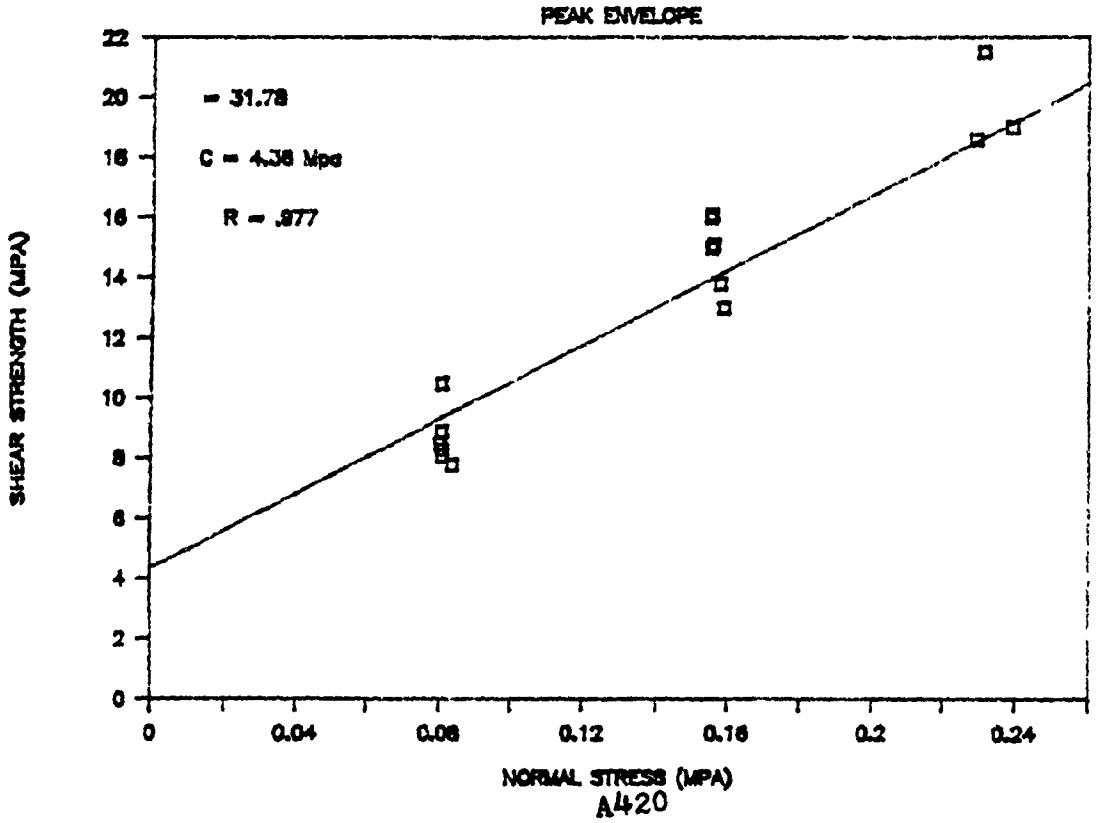

SIGMA MINES

COMPARISON OF FAILURE ENVELOPES

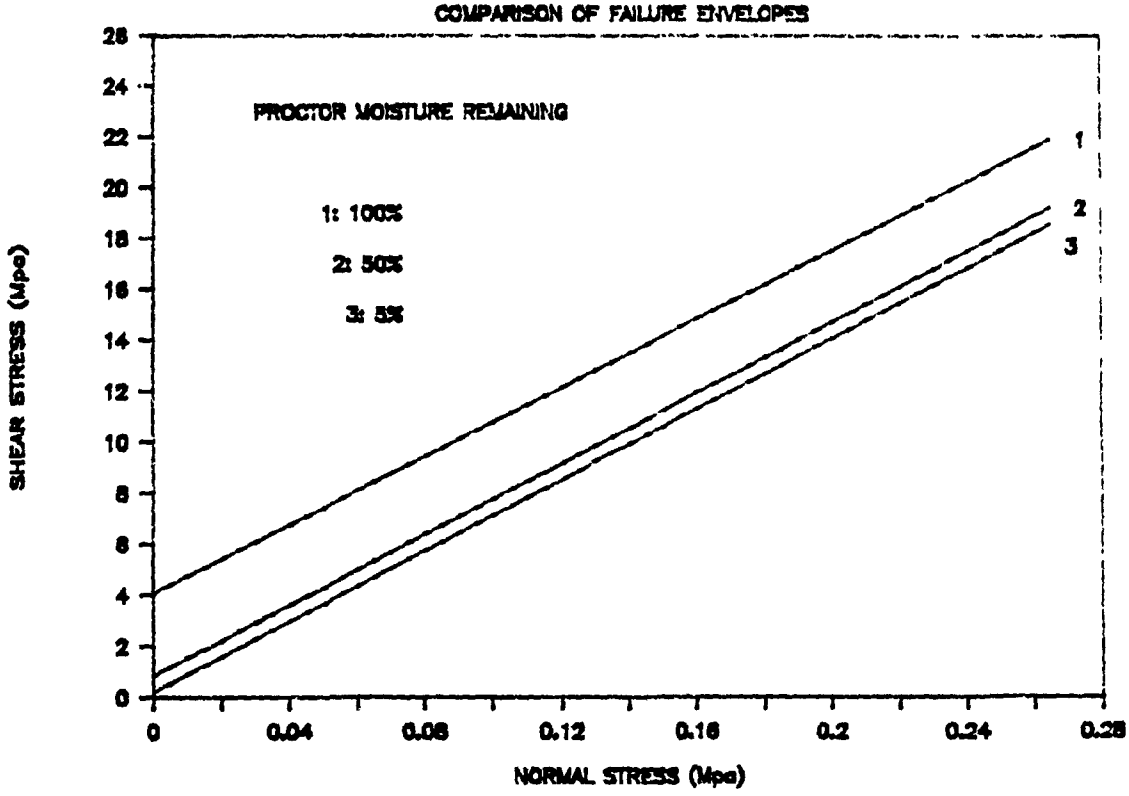

SIGMA 5% OF PROCTOR

PEAK ENVELOPE

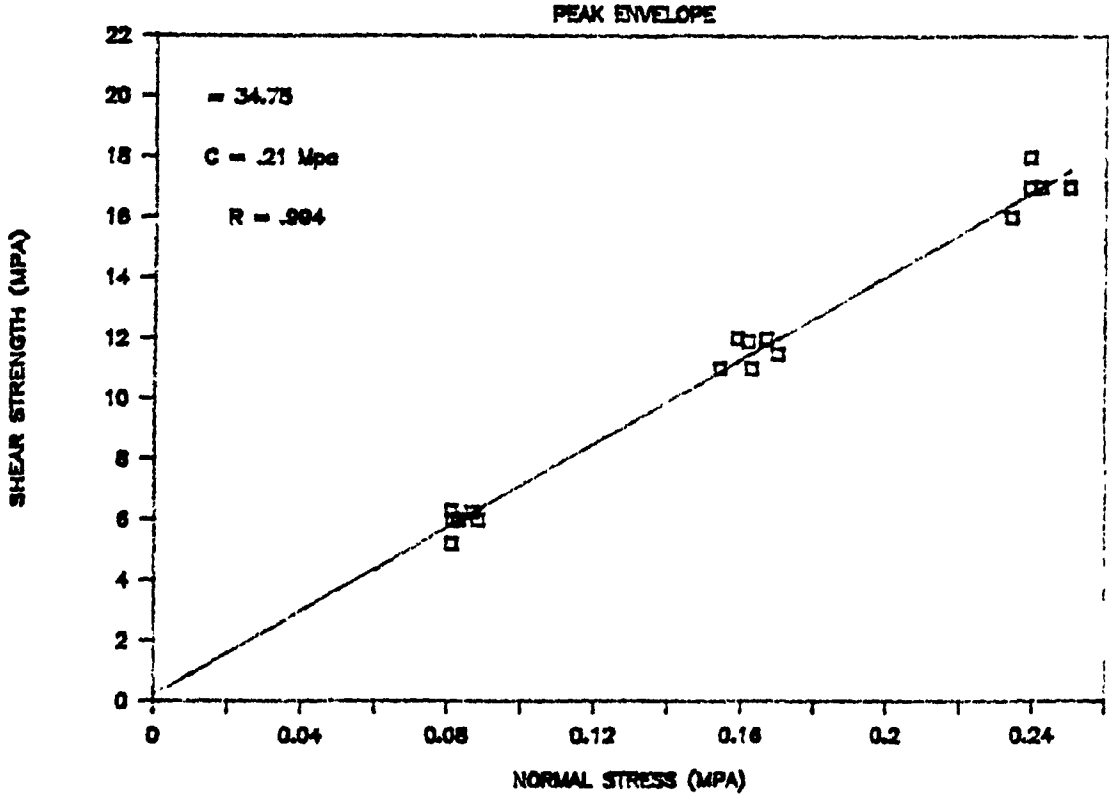

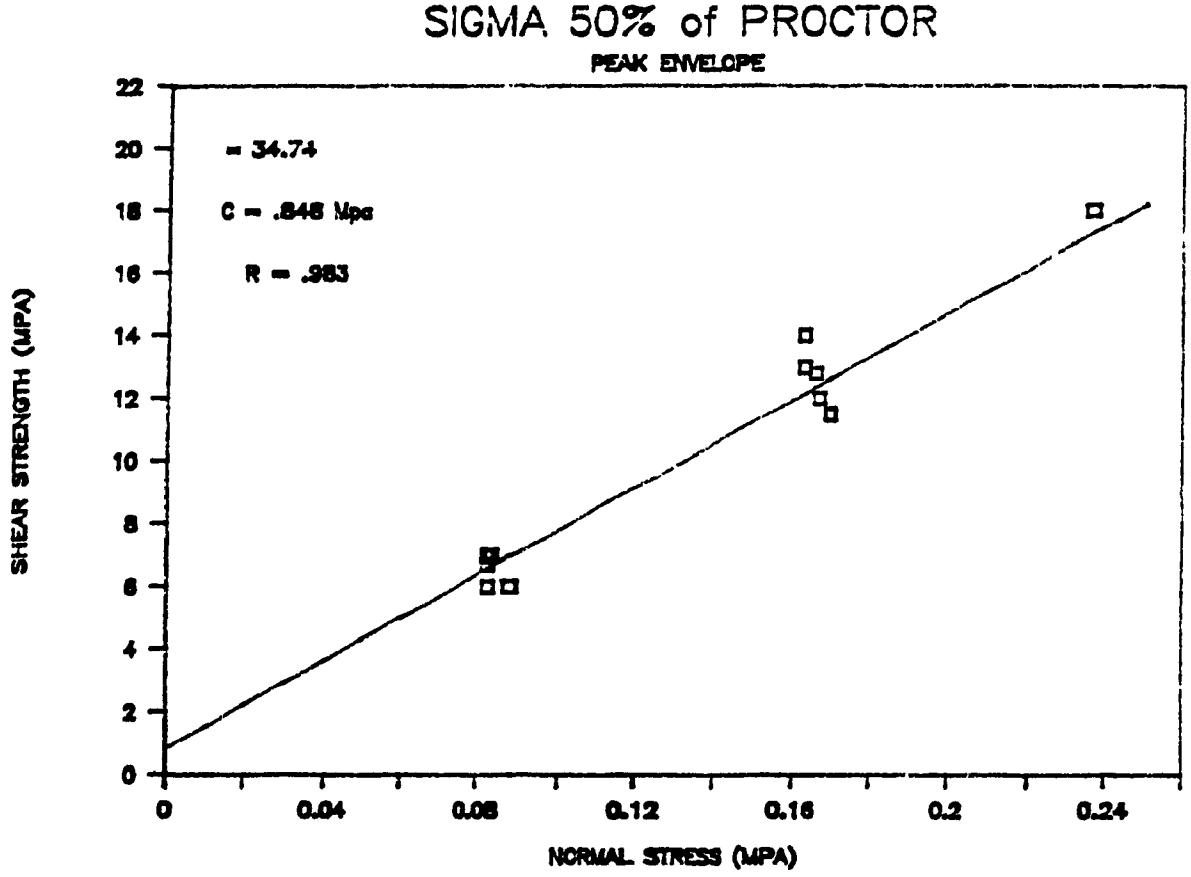
SIGMA 50% of PROCTOR
PEAK ENVELOPE
= 34.74
C = .848 Mpa
R = .983
SHEAR STRENGTH (MPA)
NORMAL STRESS (MPA)
0
2
4
6
8
10
12
14
16
18
20
22
0
0.04
0.08
0.12
0.16
0.2
0.24

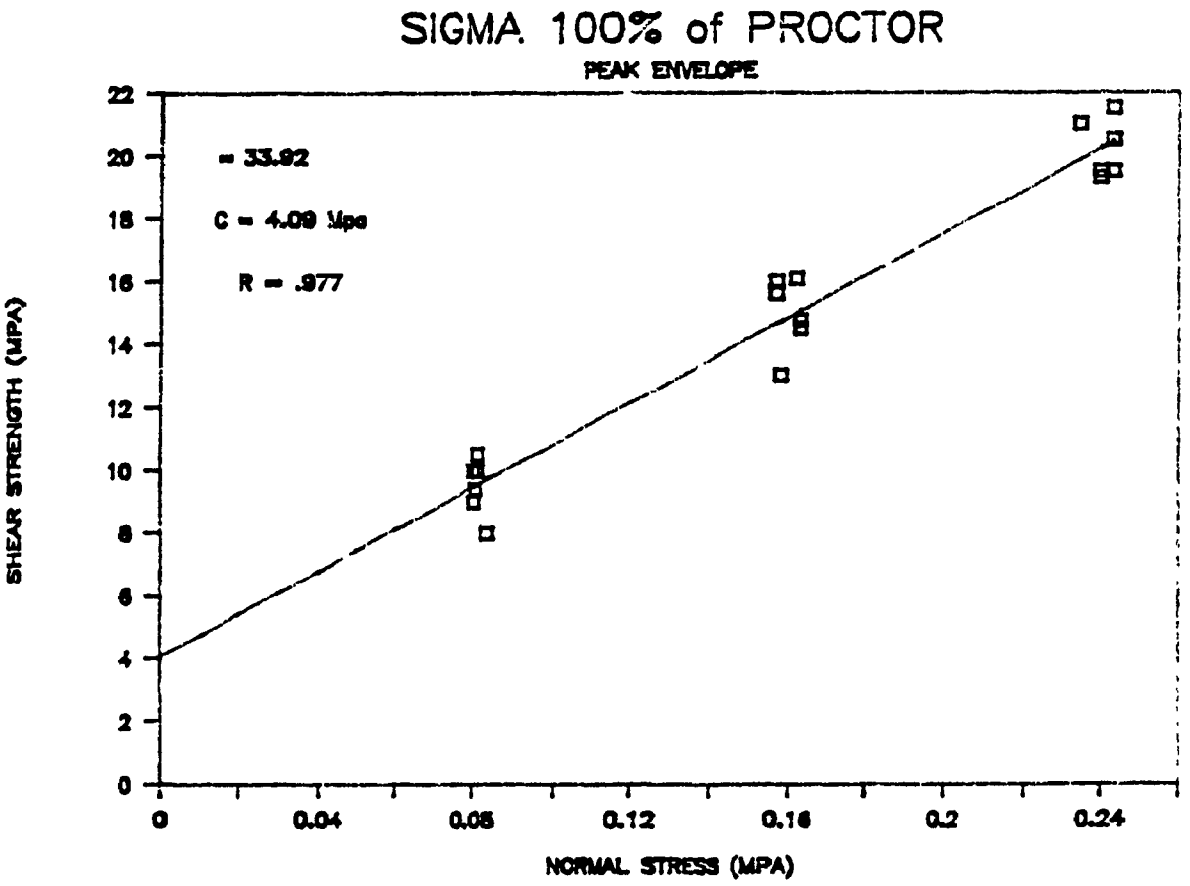
SIGMA 100% of PROCTOR
PEAK ENVELOPE
= 33.92
C = 4.09 Mpa
R = .977
SHEAR STRENGTH (MPA)
NORMAL STRESS (MPA)
0
2
4
6
8
10
12
14
16
18
20
22
0
0.04
0.08
0.12
0.16
0.2
0.24

DENISON SERIES A:

COMPARISON OF FAILURE ENVELOPES

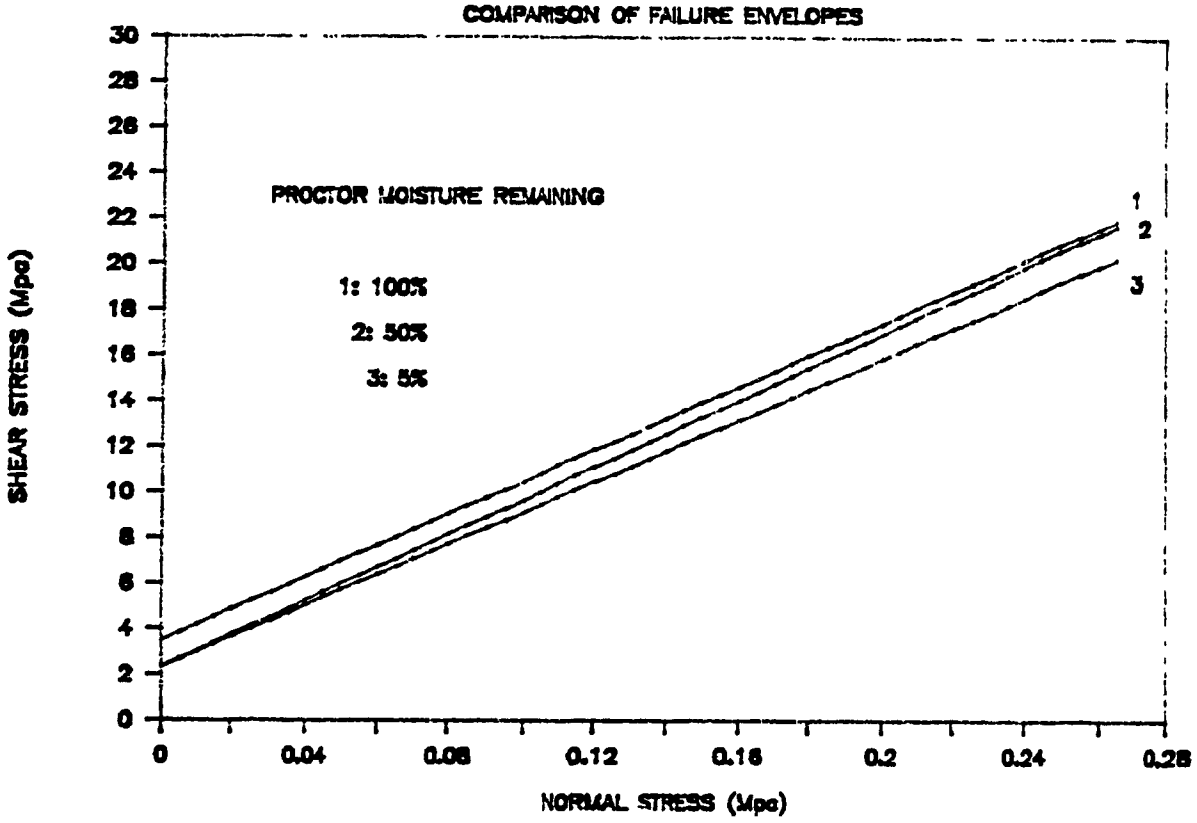

DENISON A – SERIES: 5% of PROCTOR

PEAK ENVELOPE

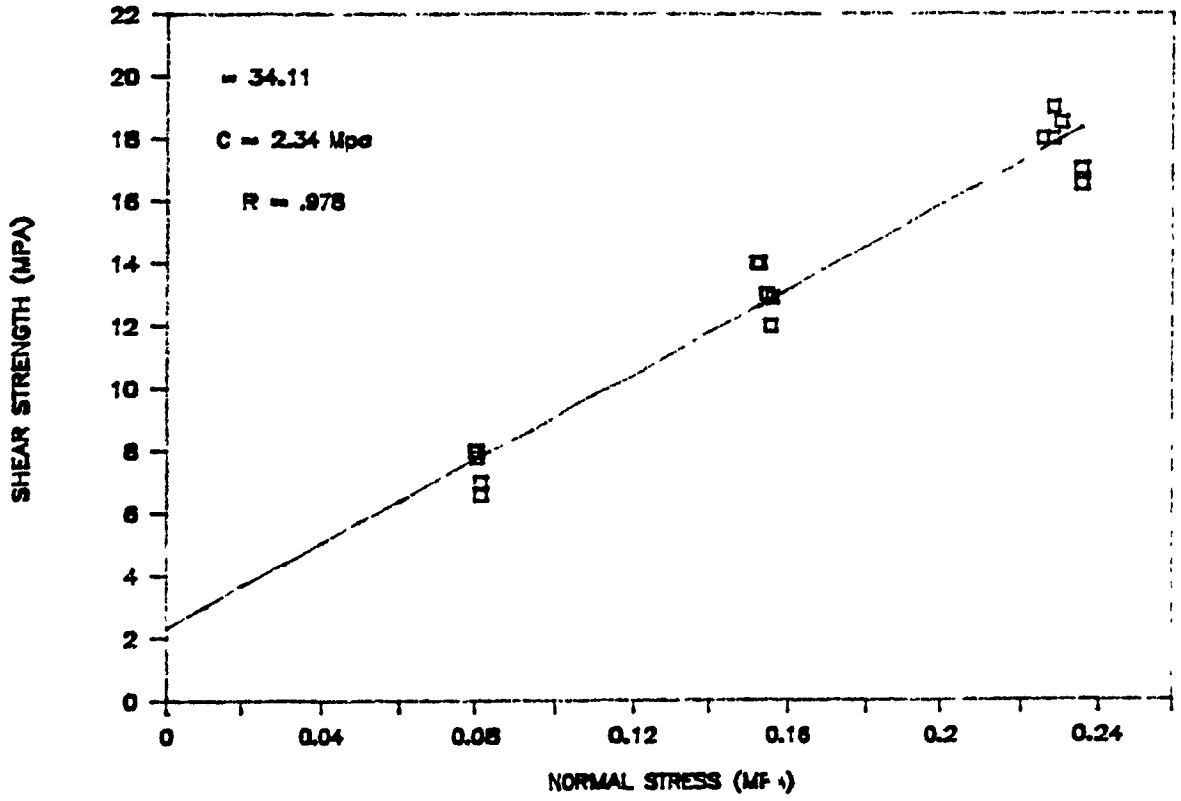

DENISON A — SERIES: 50% of PROCTOR

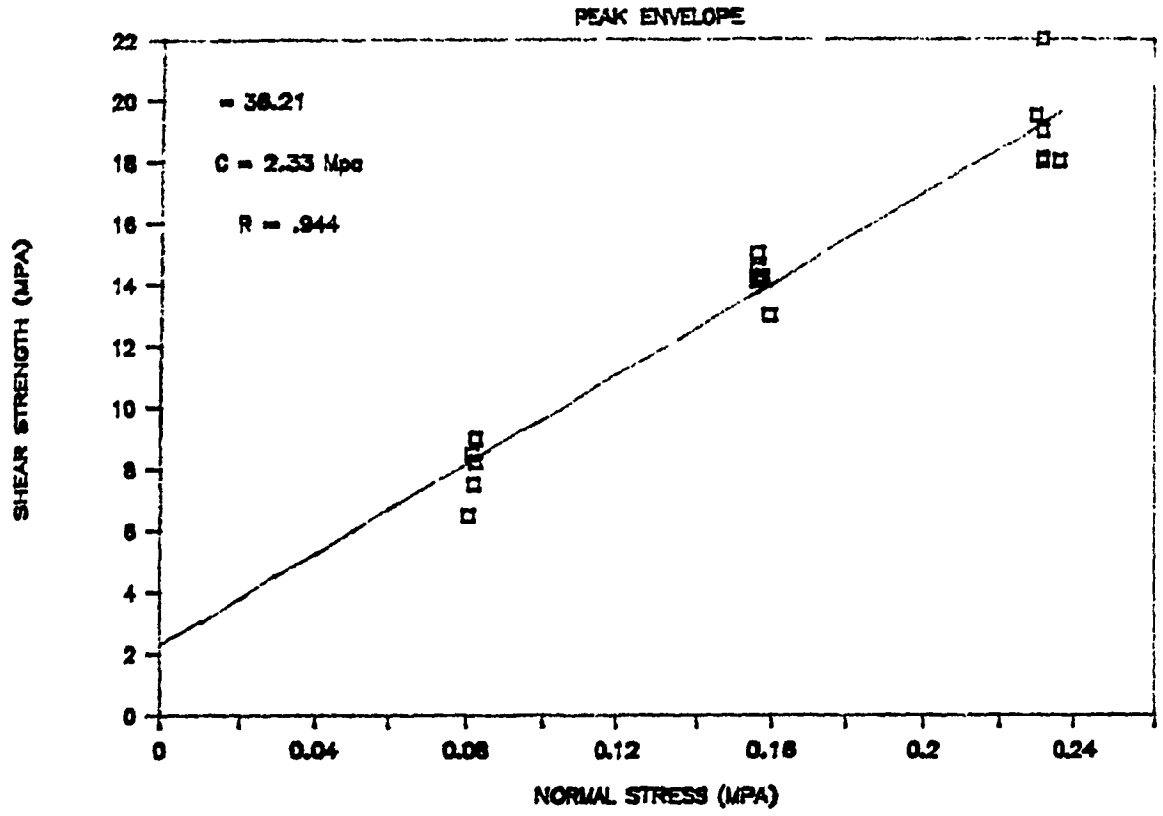

DENISON A — SERIES: 100% of PROCTOR

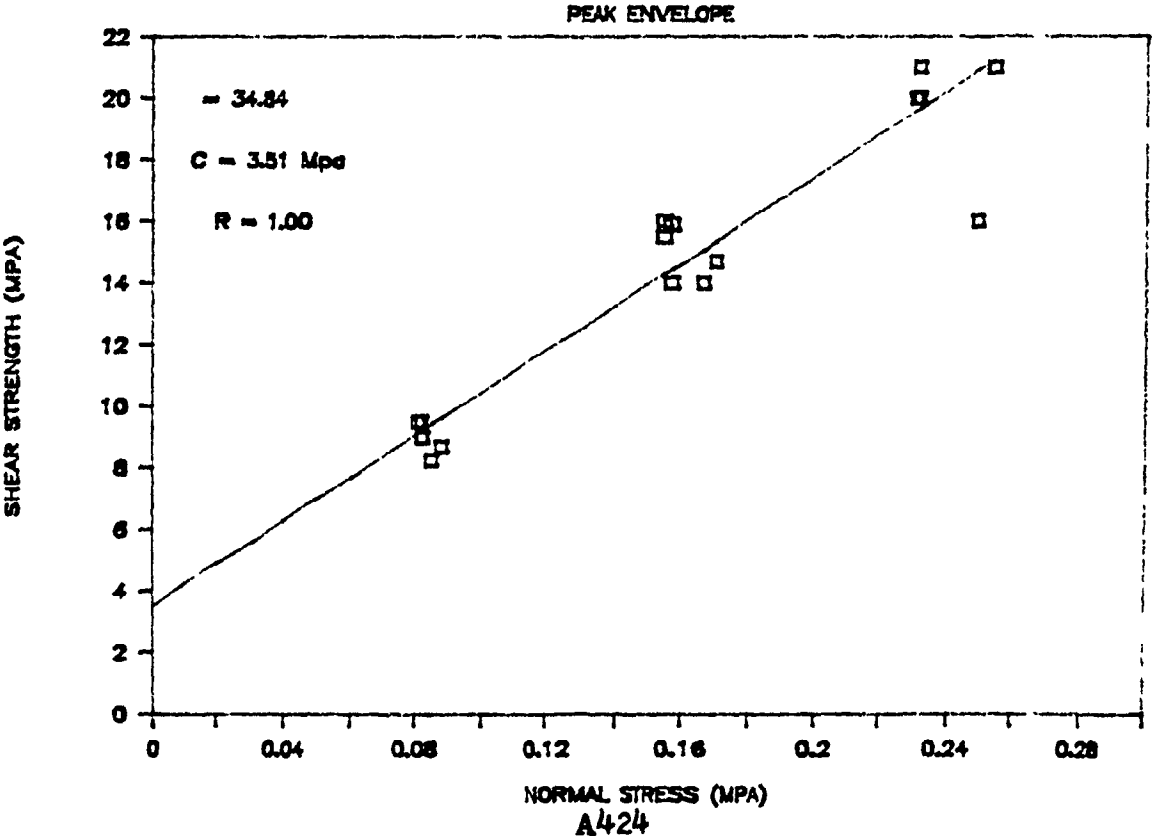

DENISON SERIES B:

COMPARISON OF FAILURE ENVELOPES

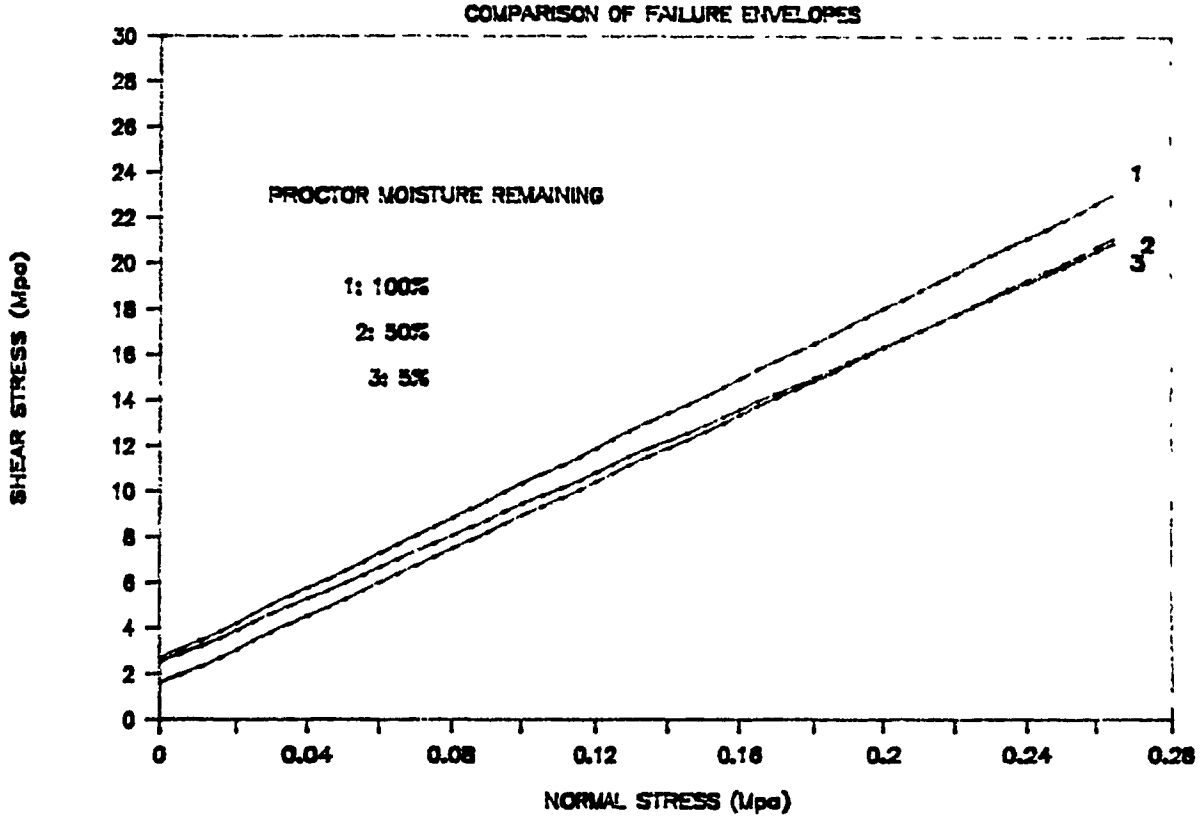

DENISON B – SERIES: 20% of PROCTOR

PEAK ENVELOPE

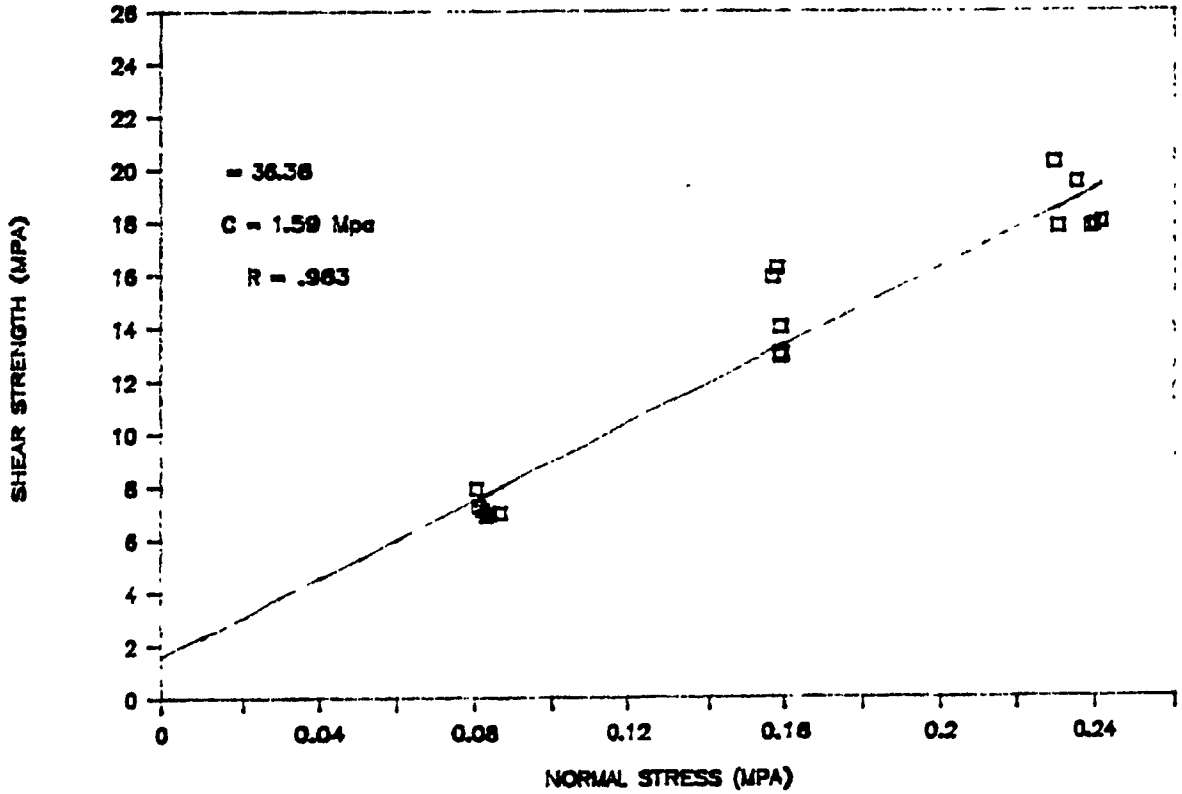

DENISON B -- SERIES: 50% of PROCTOR

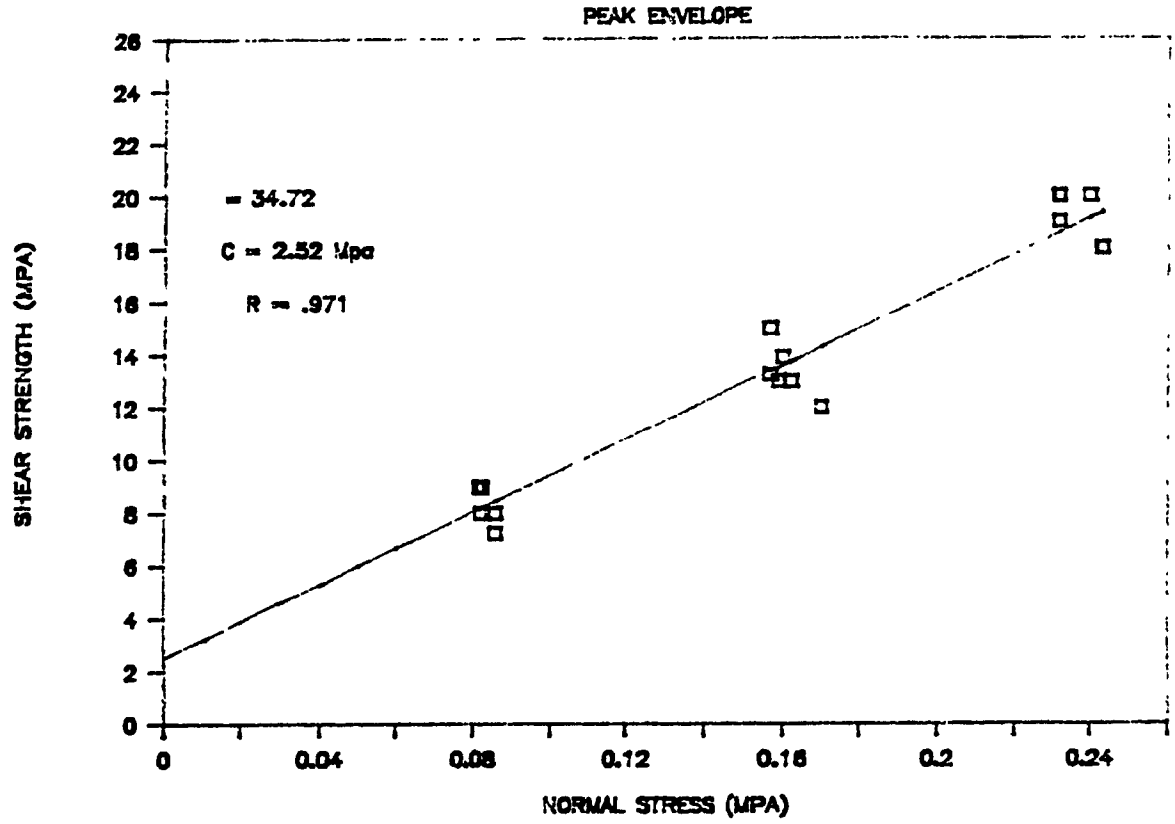

DENISON B -- SERIES: 100% of PROCTOR

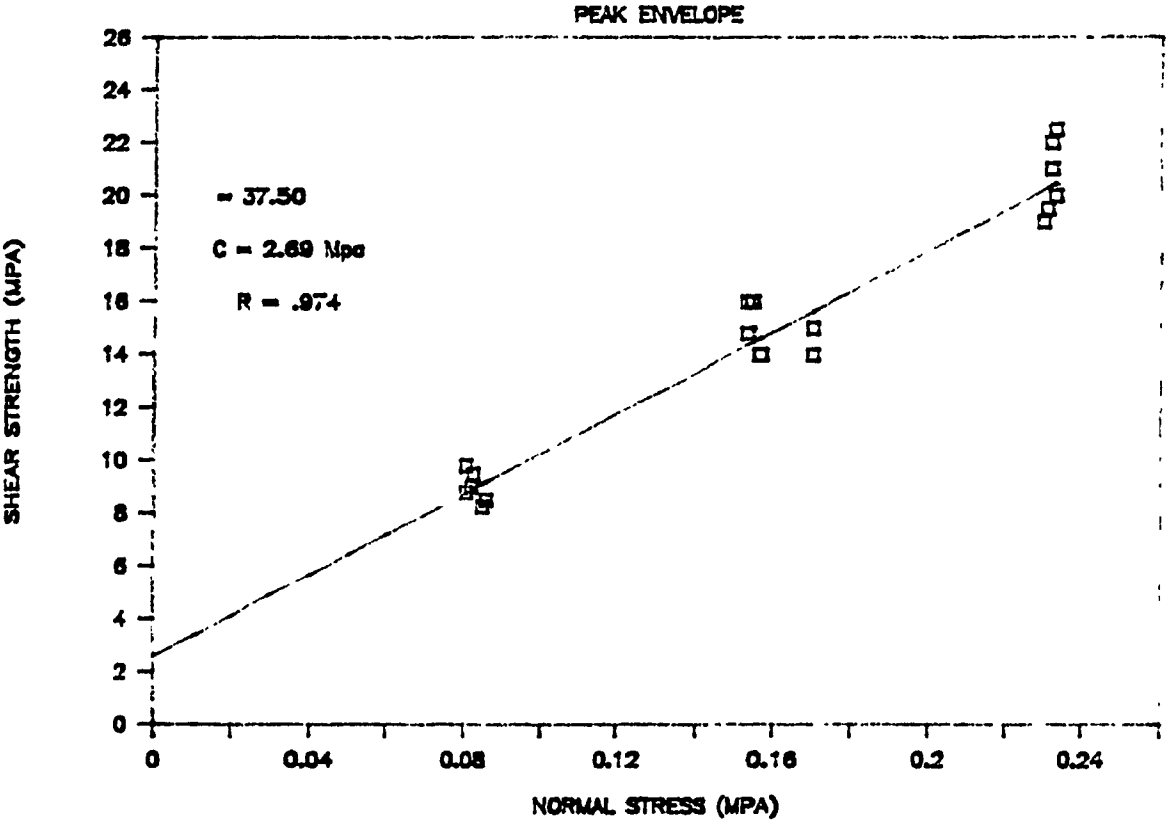

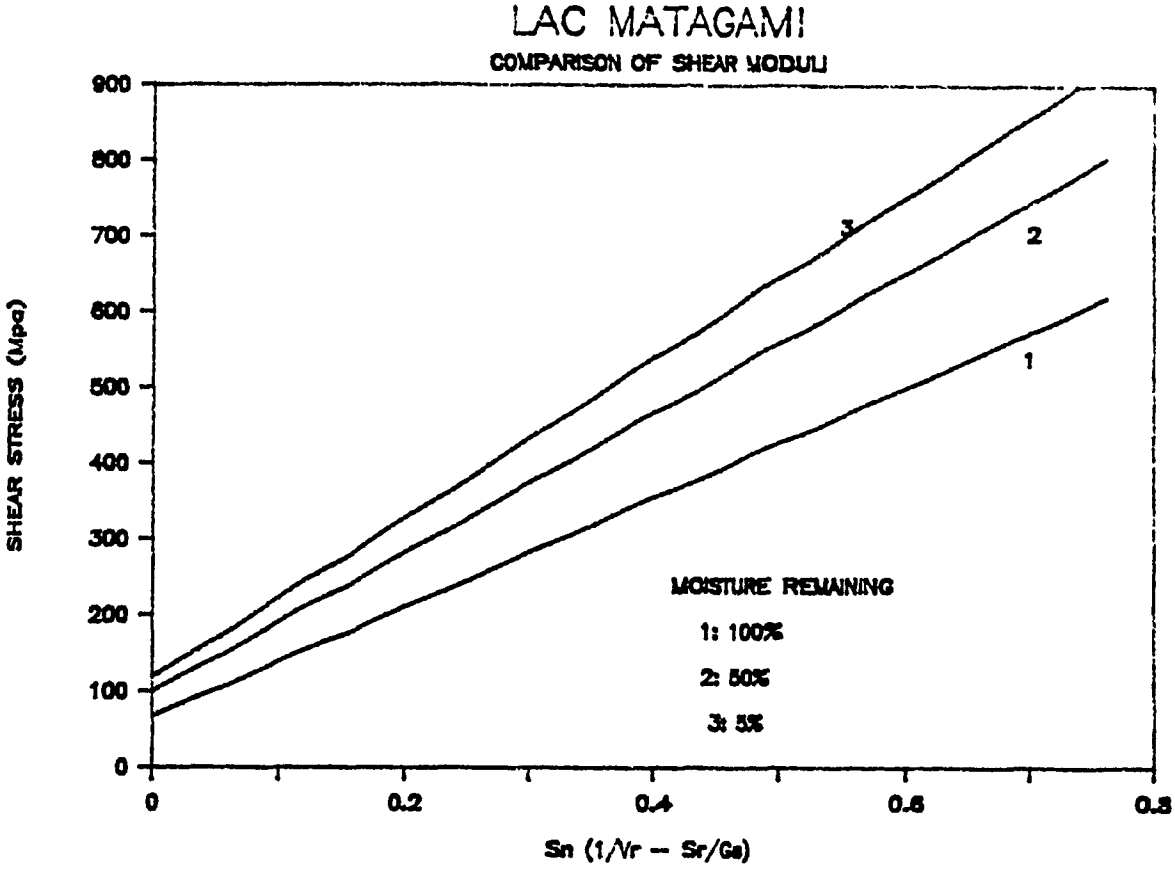
LAC MATAGAMI
COMPARISON OF SHEAR MODULI
SHEAR STRESS (Mpa)
900
800
700
600
500
400
300
200
100
0
0
0.2
0.4
0.6
0.8
Sn (1/Vr -- Sr/Ga)
3
2
1
MOISTURE REMAINING
1: 100%
2: 50%
3: 5%

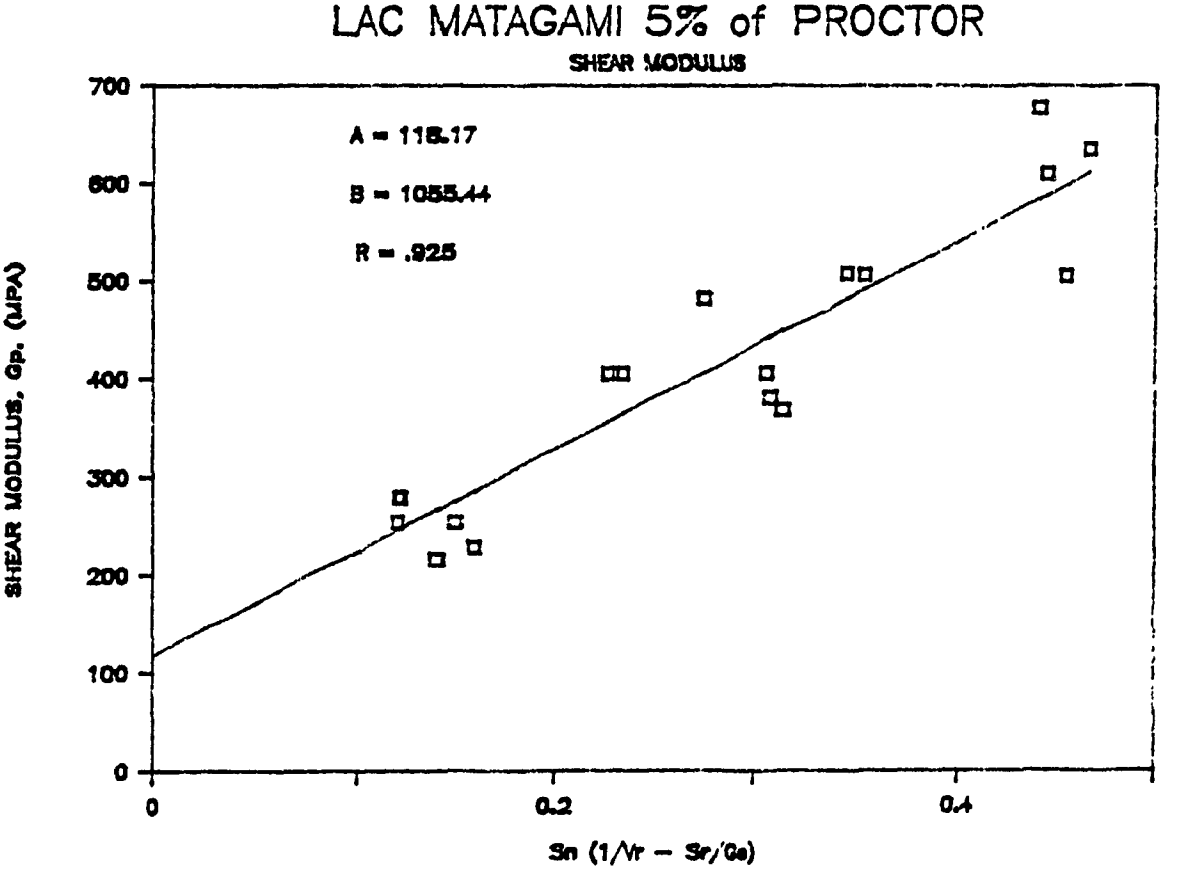
LAC MATAGAMI 5% of PROCTOR
SHEAR MODULUS
SHEAR MODULUS, Gp, (MPA)
700
600
500
400
300
200
100
0
0
0.2
0.4
Sn (1/Vr -- Sr/Ga)
A = 118.17
B = 1055.44
R = .925

LAC MATAGAMI 50% of PROCTOR

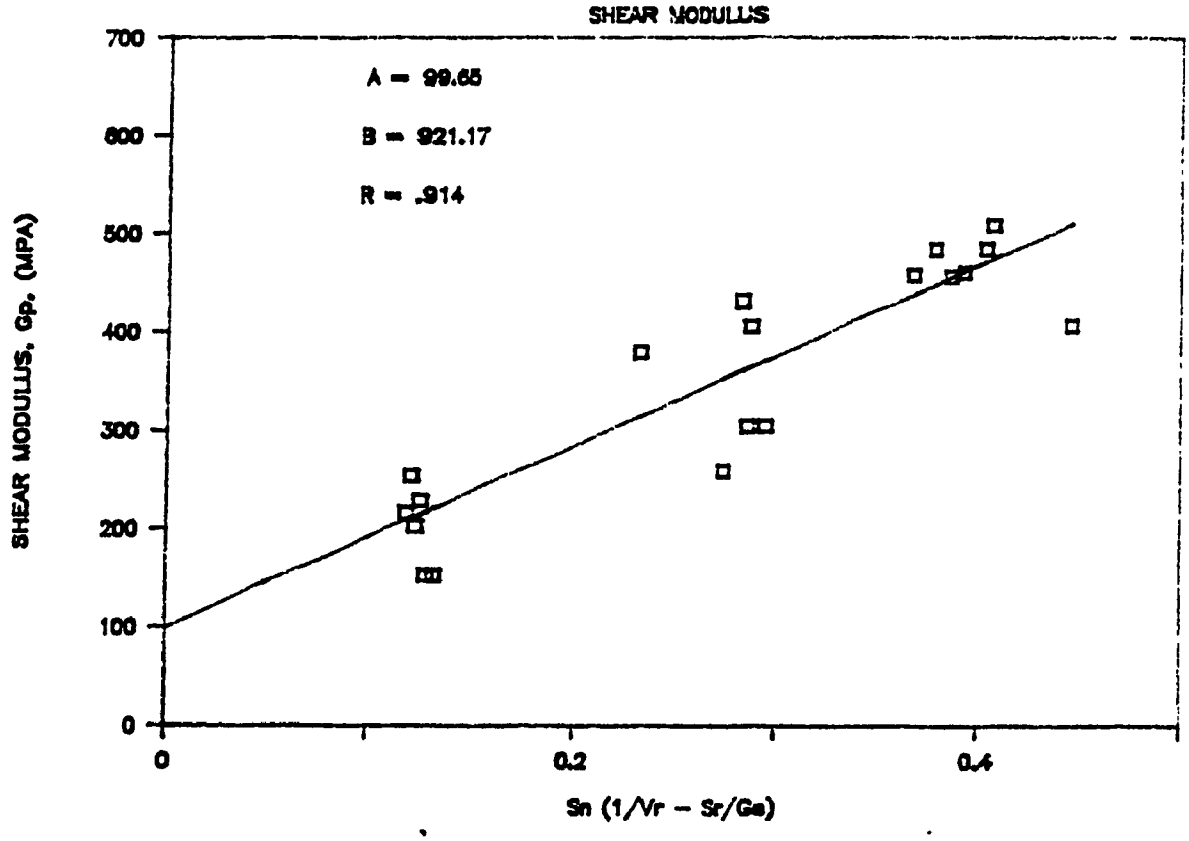

LAC MATAGAMI 100% of PROCTOR

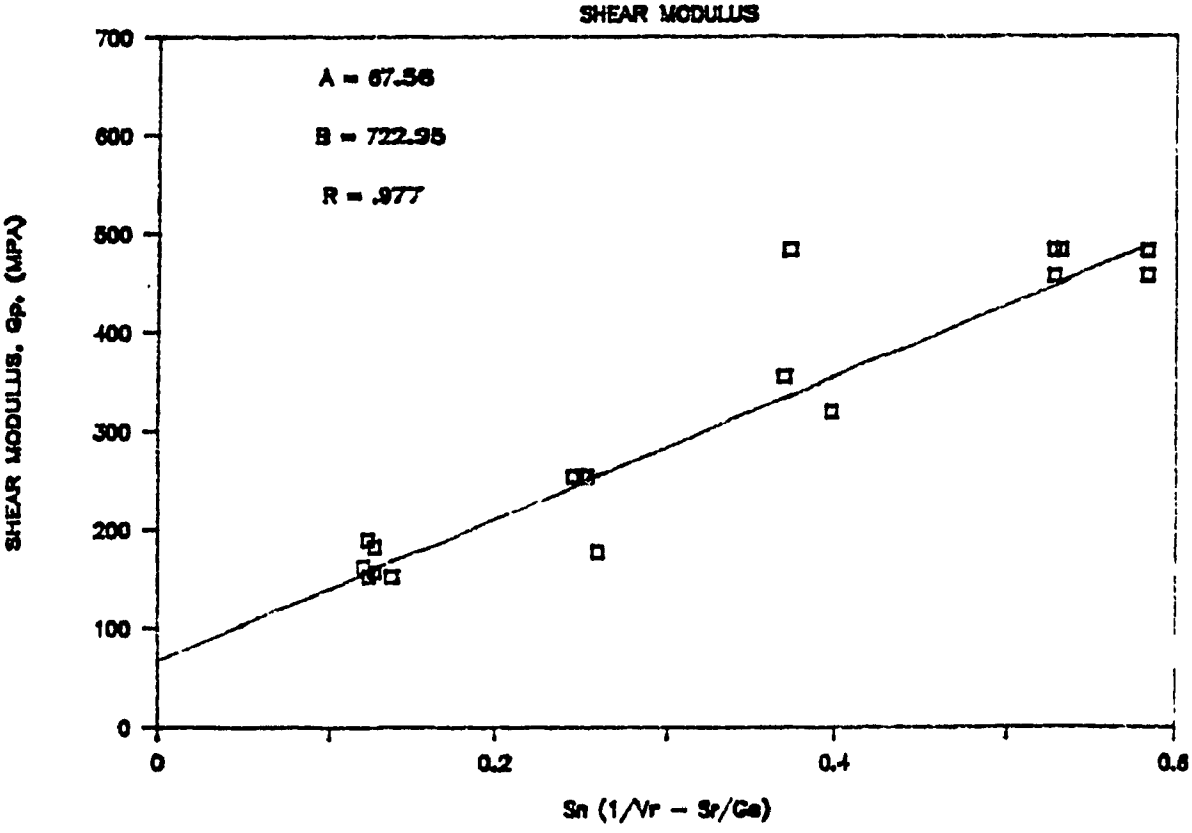

SIGMA MINE

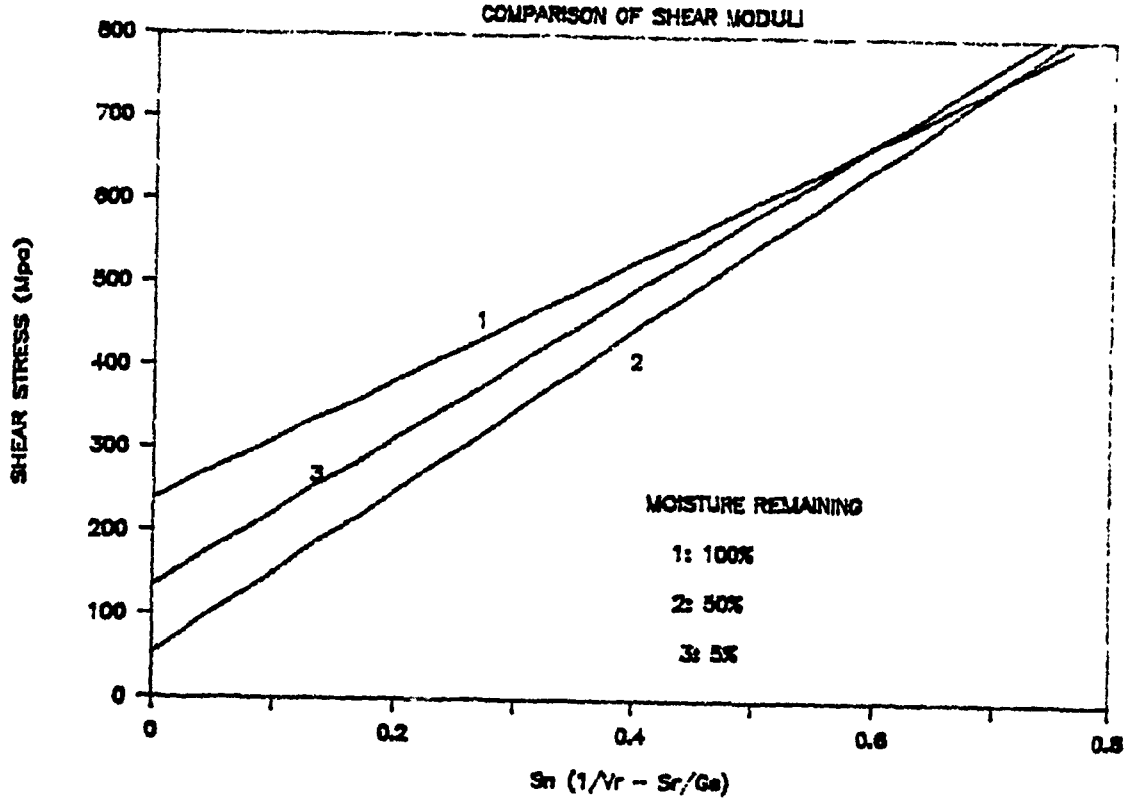

SIGMA 5% OF PROCTOR

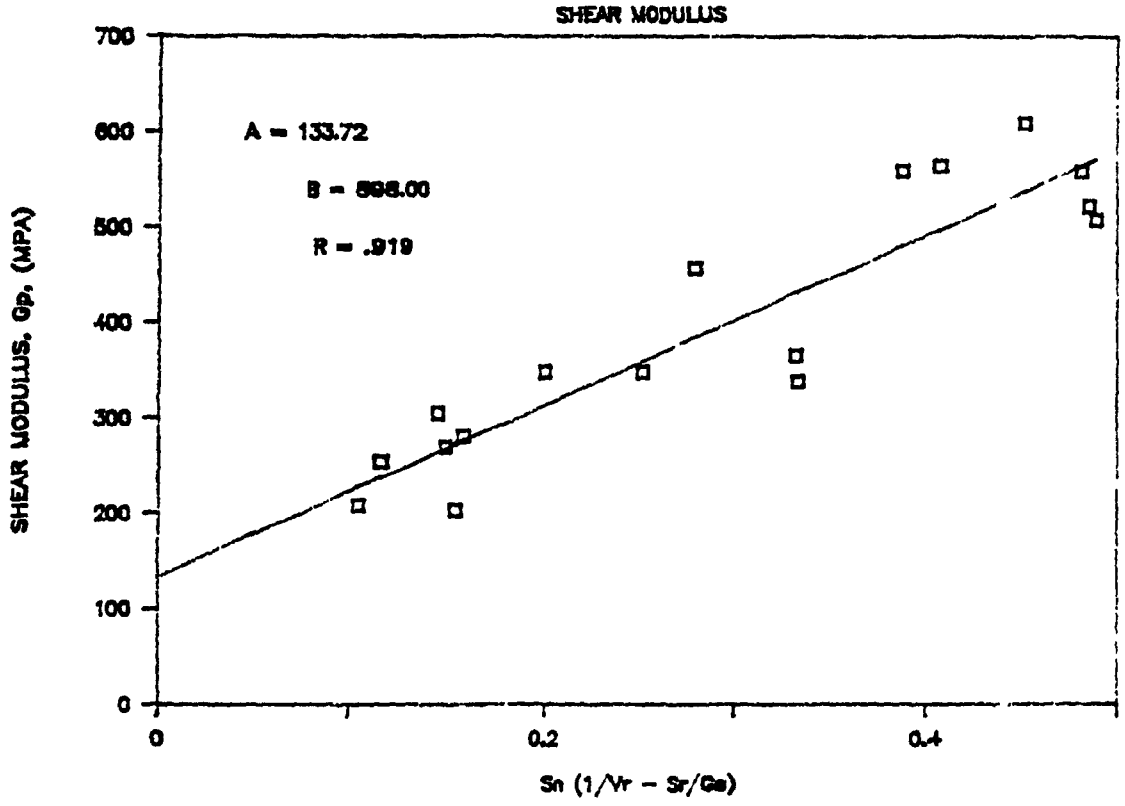

SIGMA 50% of PROCTOR

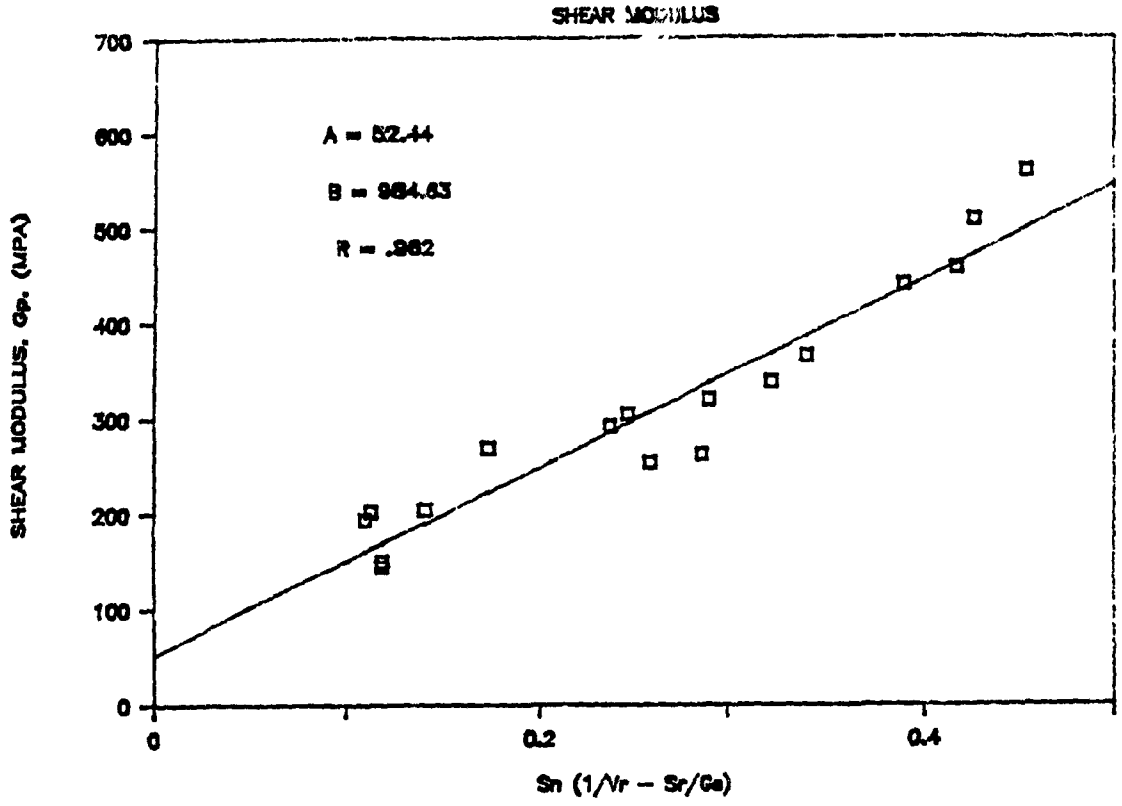

SIGMA 100% of PROCTOR

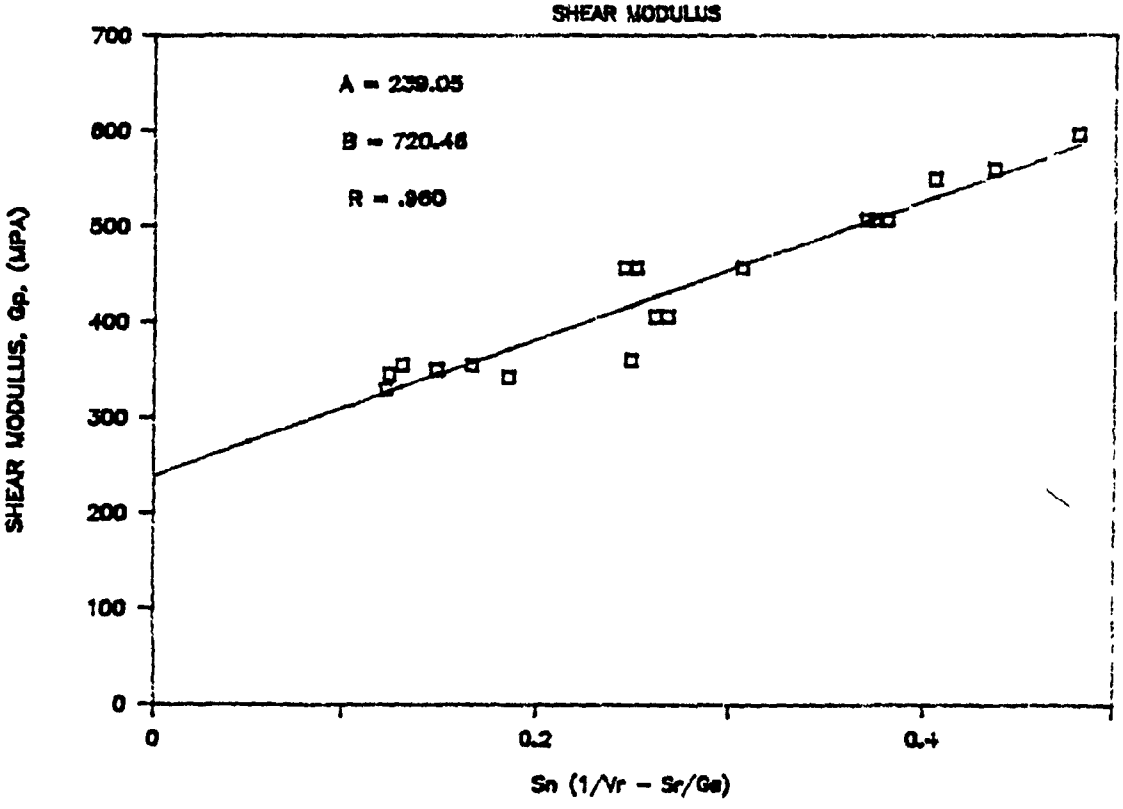

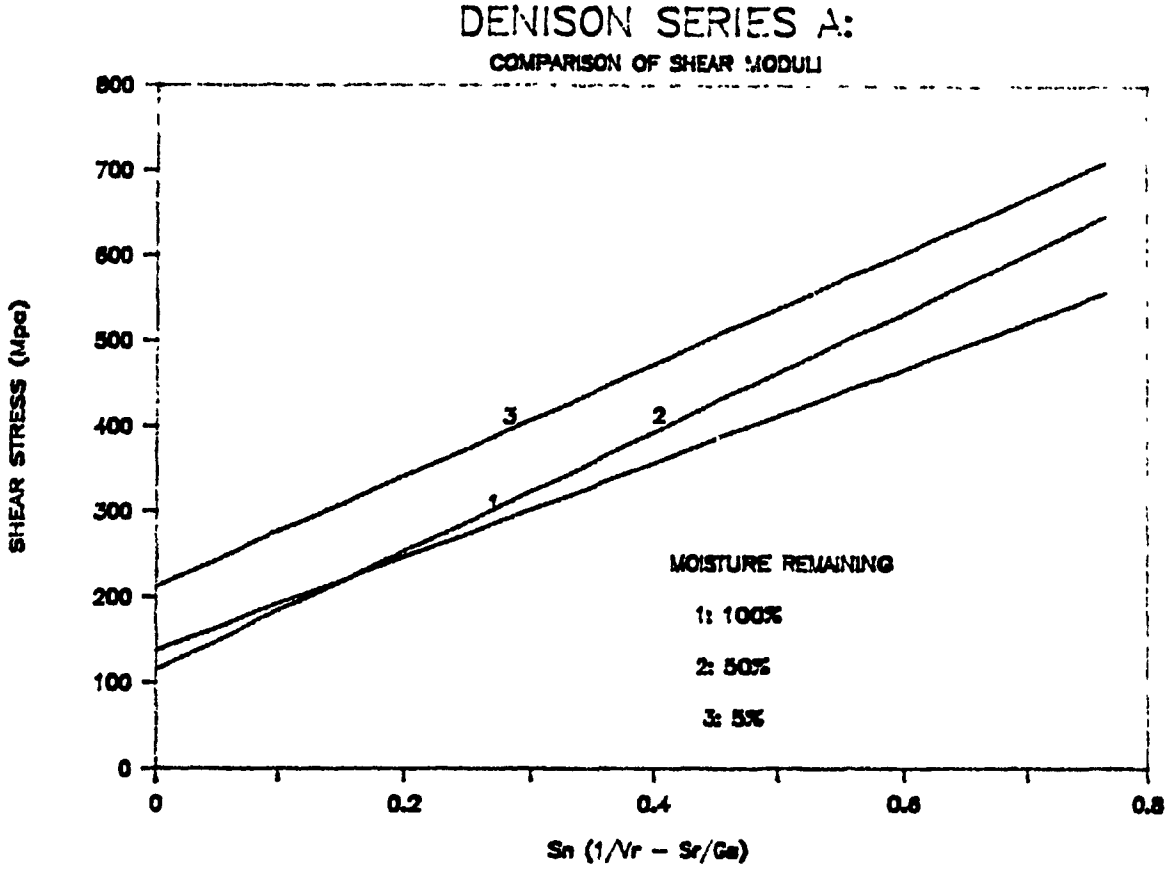
DENISON SERIES A:
COMPARISON OF SHEAR MODULI
SHEAR STRESS (Mpa)
800
700
600
500
400
300
200
100
0
0
0.2
0.4
0.6
0.8
Sn (1/Vr - Sr/Ga)
3
2
1
MOISTURE REMAINING
1: 100%
2: 50%
3: 5%

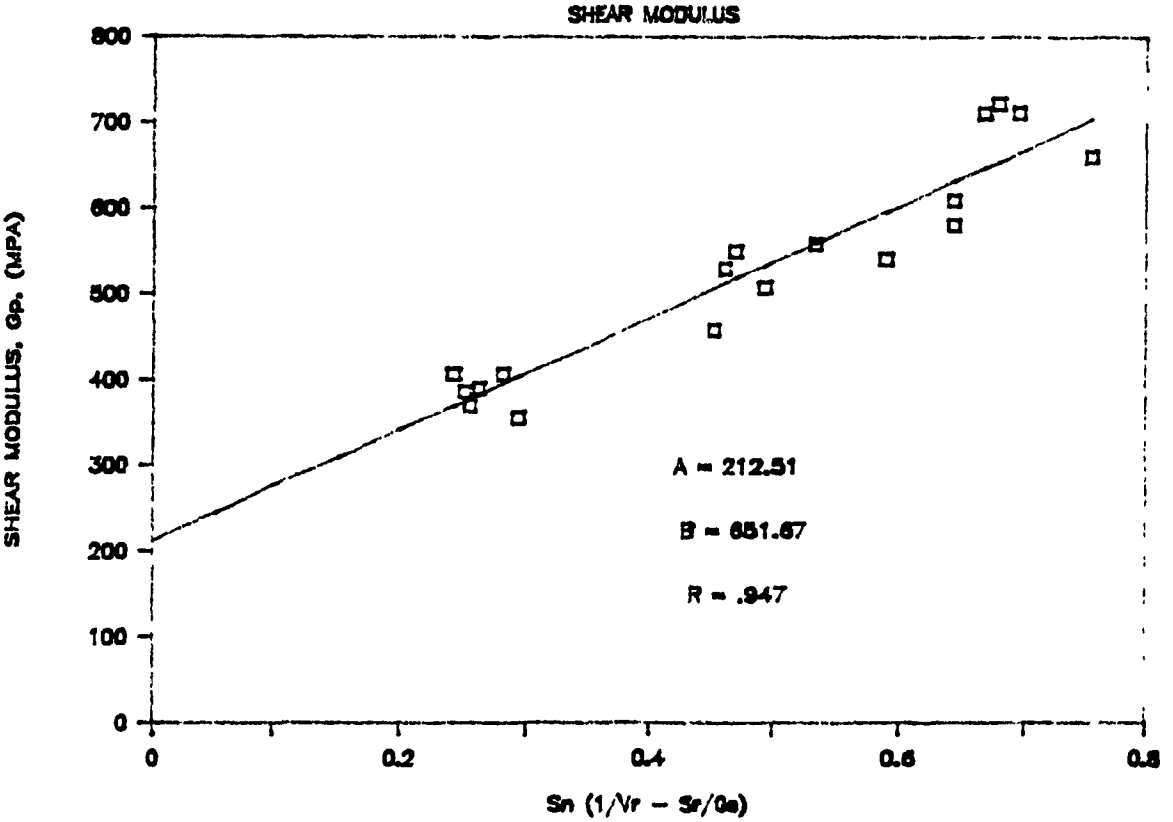
DENISON A - SERIES: 5% of PROCTOR
SHEAR MODULUS
SHEAR MODULUS, Gp, (MPA)
800
700
600
500
400
300
200
100
0
0
0.2
0.4
0.6
0.8
Sn (1/Vr - Sr/Ga)
A = 212.51
B = 651.67
R = .947

DENISON A – SERIES: 50% of PROCTOR

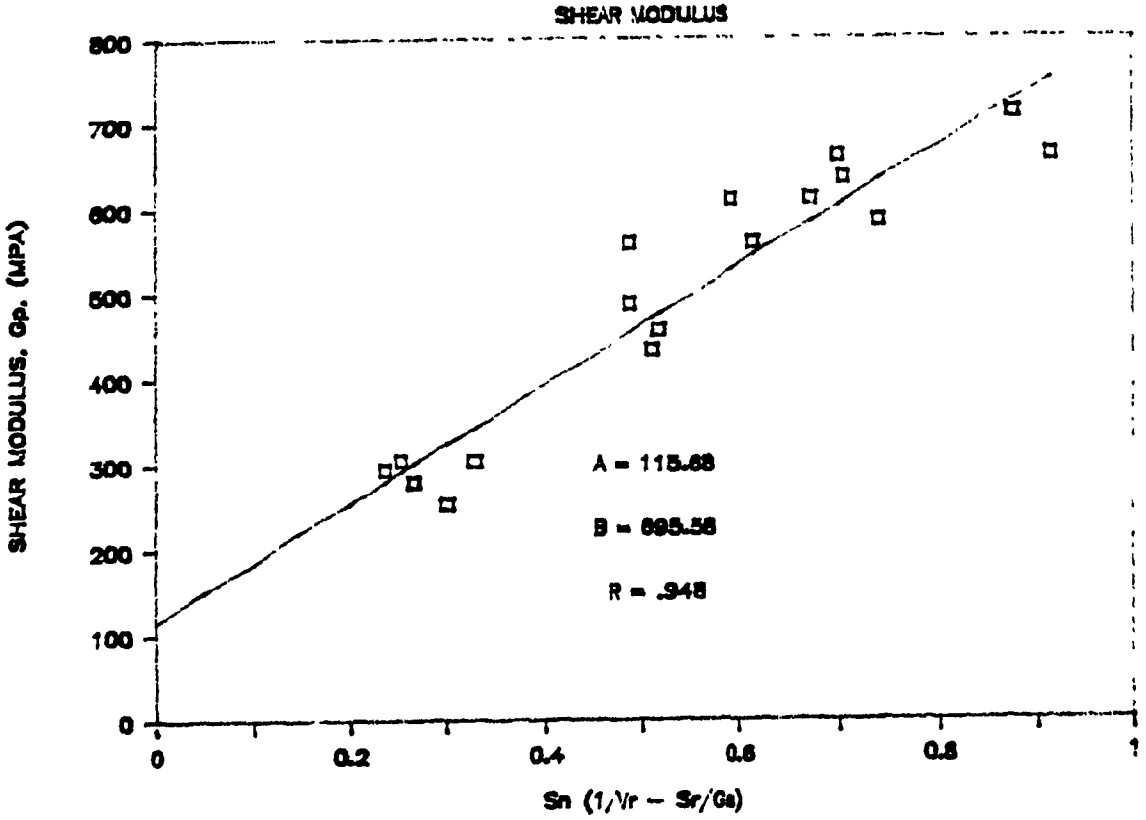

DENISON A – SERIES: 100% of PROCTOR

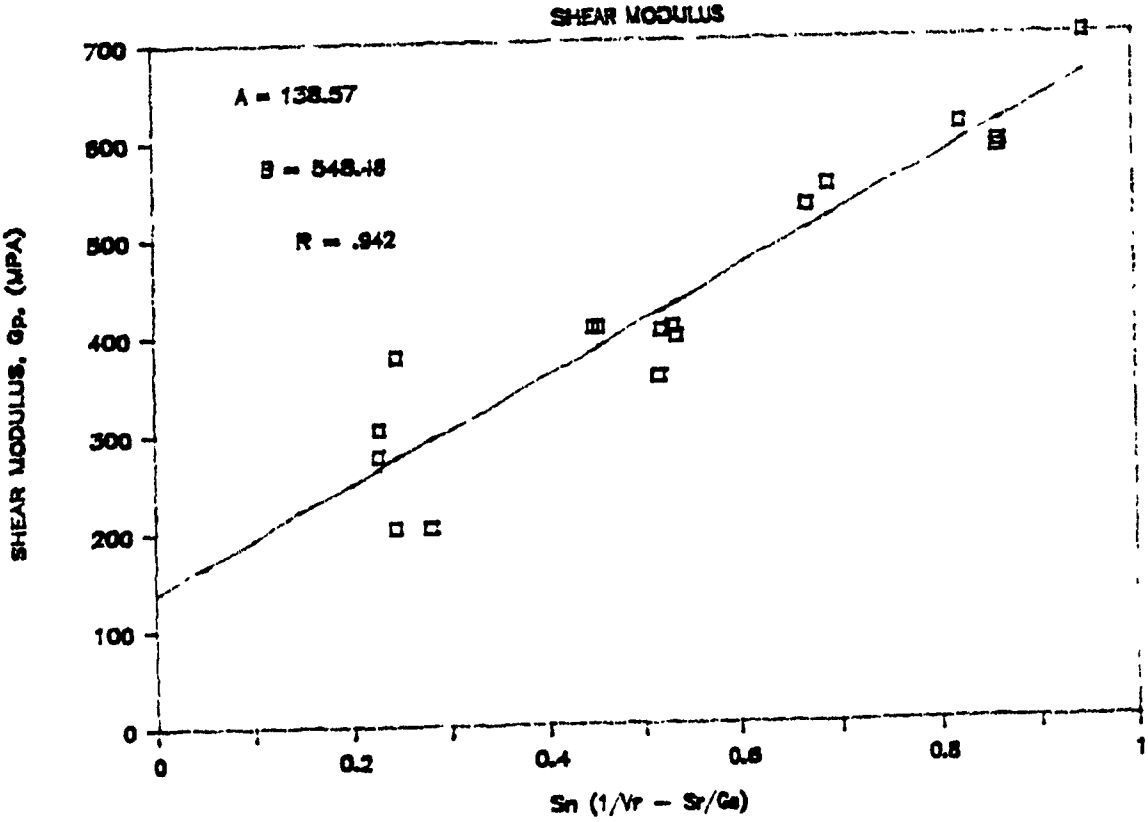

DENISON SERIES B:

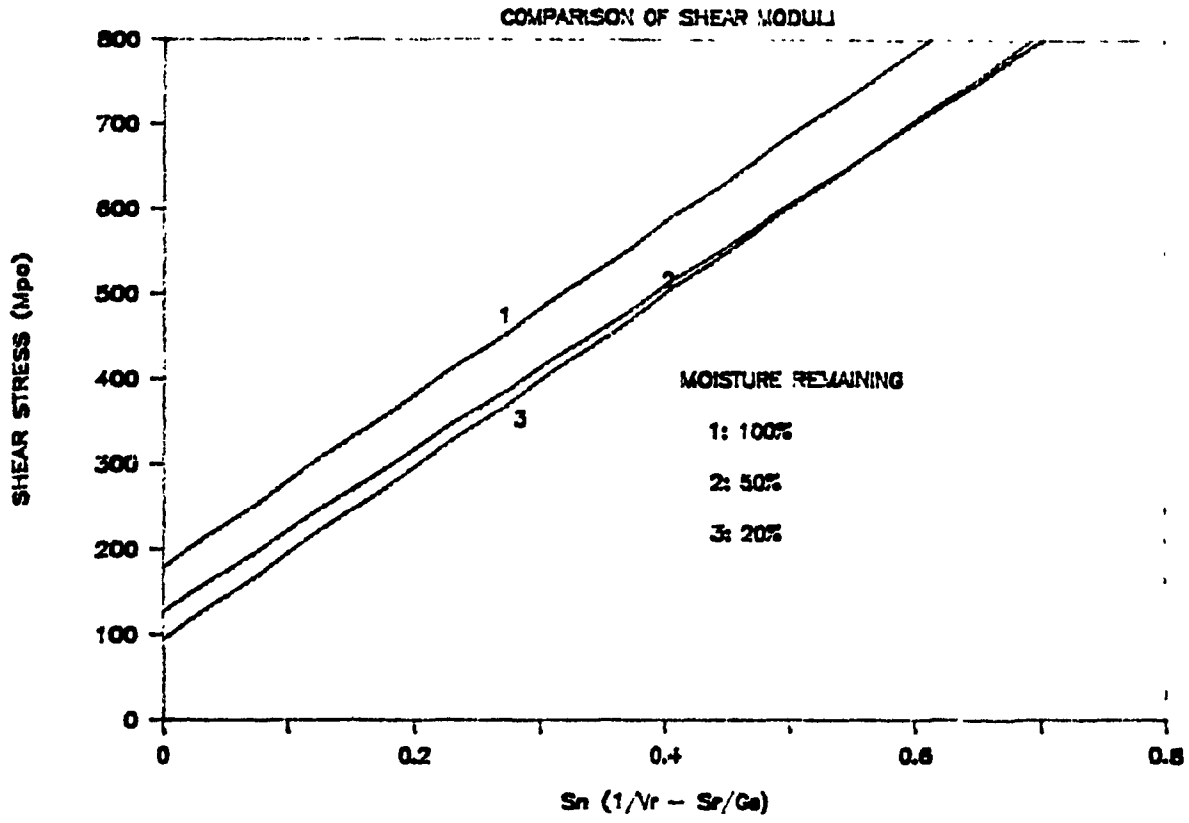

DENISON B – SERIES: 20% of PROCTOR

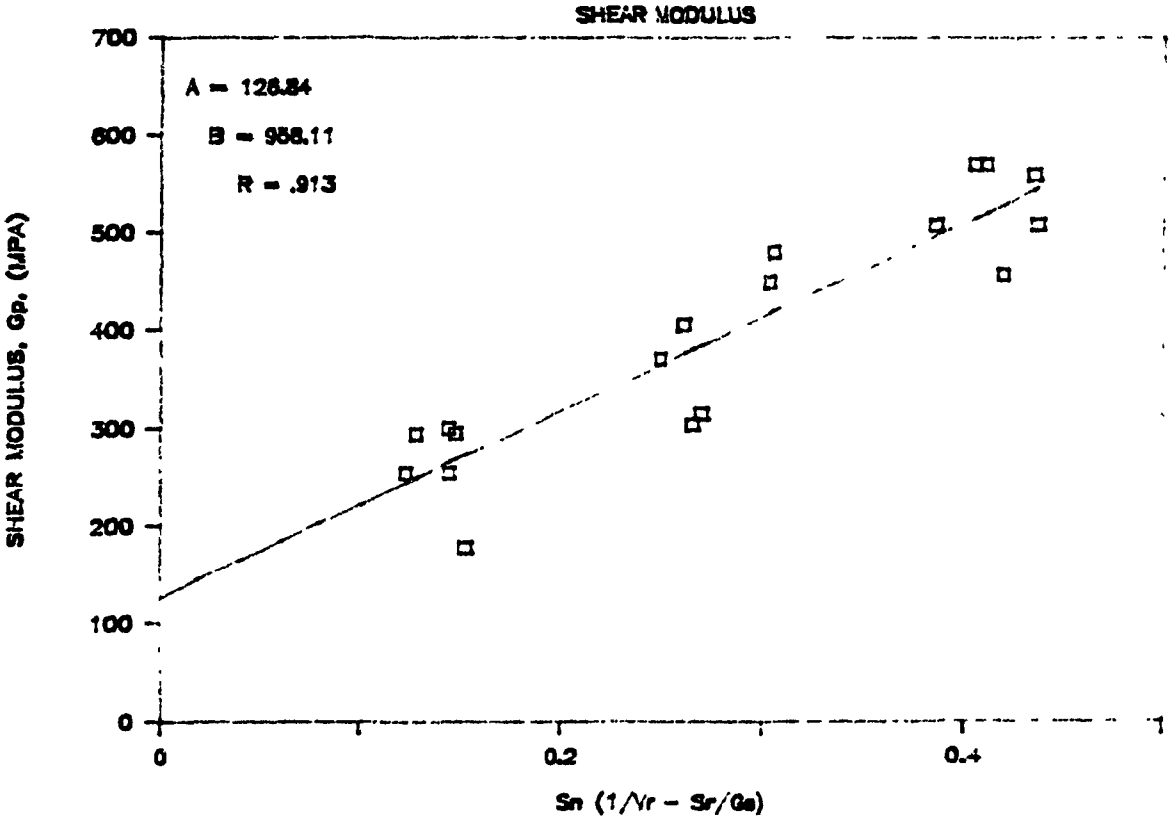

DENISON B — SERIES: 50% of PROCTOR

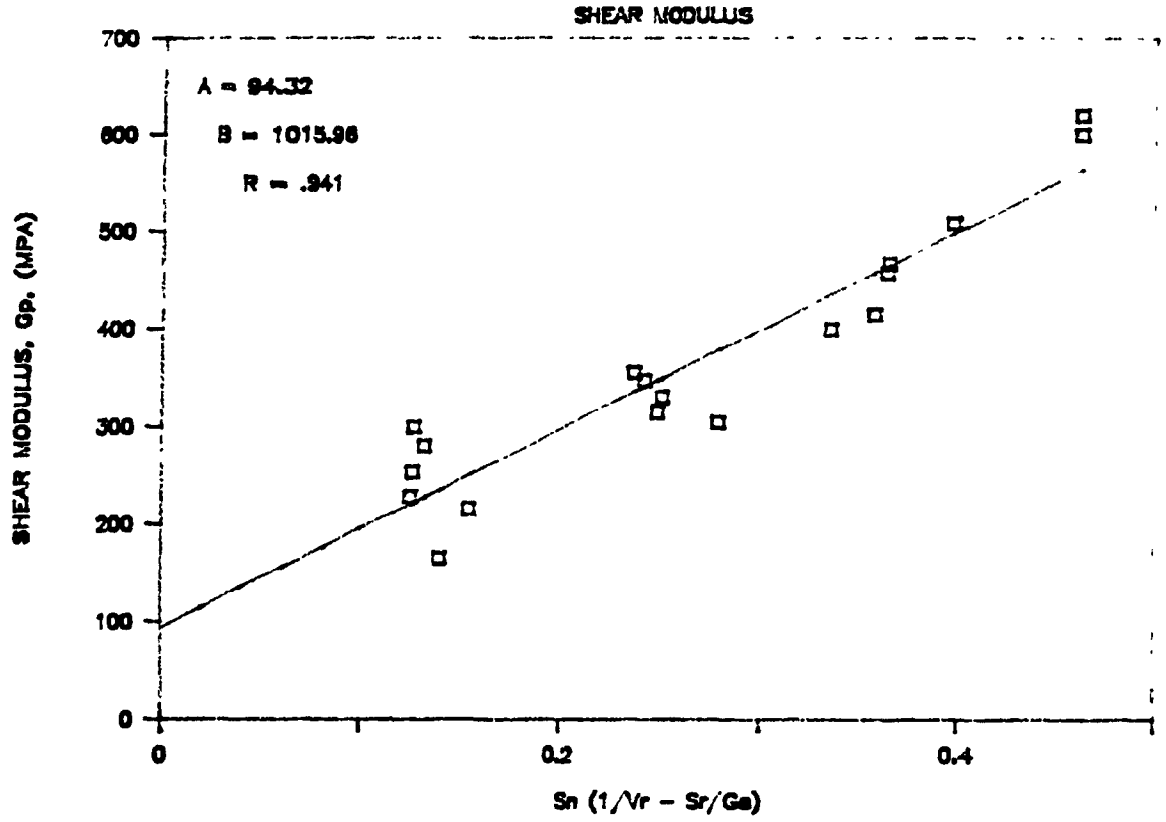

DENISON B — SERIES: 100% of PROCTOR

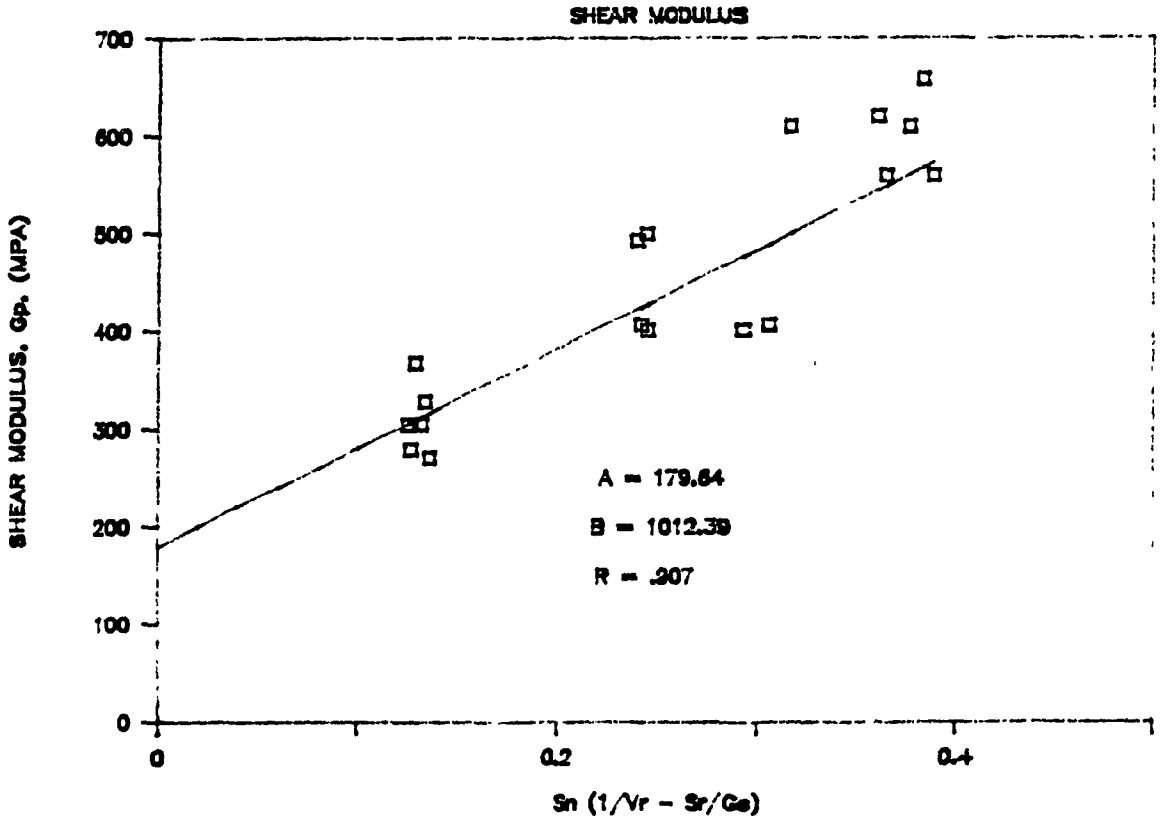

TABLE A -1 Master table for cemented mill tailings fill
Part 1
(See explanatory notes on p. A-16)

(1) ID	(2) Ref. No.	(3) T / C ratio (by wt)	(4) Cement content (% by wt)	(5) Uniaxial compressive strength 7 days (MPa)	(6) 14 days (MPa)	(7) 28 days (MPa)	(8) 90 days (MPa)
1	1	30:1	3.23	0.14	0.16	0.17	0.2
2	1	30:1	3.23	0.14	0.18	0.21	0.23
3	1	30:1	3.23		0.12	0.14	0.14
4	1	30:1	3.23	0.11	0.13	0.15	0.15
5	1	30:1	3.23		0.27	0.32	0.36
6	1	30:1	3.23	0.05	0.06	0.07	0.1
7	1	30:1	3.23		0.12	0.14	0.19
8	1	30:1	3.23	0.1	0.1	0.13	0.14
9	1	30:1	3.23	0.12	0.14	0.19	0.17
10	1	30:1	3.23	0.1	0.14	0.17	0.15
11	1	30:1	3.23	0.12	0.12	0.14	0.14
12	1	30:1	3.23		0.14	0.17	0.19
13	1	30:1	3.23	0.13	0.16	0.19	0.18
14	1	30:1	3.23		0.16	0.17	0.21
15	1	30:1	3.23	0.12	0.13	0.16	0.17
16	1	30:1	3.23		0.12	0.17	0.21
17	1	20:1	4.76	0.15	0.19	0.19	0.2
18	1	20:1	4.76		0.26	0.32	0.38
19	1	20:1	4.76		0.26	0.32	0.4
20	1	20:1	4.76			0.23	0.26
21	1	20:1	4.76	0.22	0.25	0.31	0.37
22	1	20:1	4.76			0.26	0.28
23	1	20:1	4.76		0.42	0.49	0.61
24	1	20:1	4.76		0.23	0.25	0.32
25	1	20:1	4.76	0.22	0.3	0.35	0.43
26	1	20:1	4.76		0.3	0.35	0.34
27	1	20:1	4.76	0.09	0.1	0.11	0.18
28	1	20:1	4.76		0.3	0.36	0.38
29	1	20:1	4.76			0.2	0.25
30	1	20:1	4.76			0.33	
31	1	20:1	4.76	0.25	0.27	0.3	0.35
32	1	20:1	4.76	0.21	0.23	0.26	0.28
33	1	20:1	4.76	0.22	0.27	0.29	0.32
34	1	20:1	4.76			0.17	0.23
35	1	20.1	4.76	0.2	0.24	0.29	0.32
36	1	20:1	4.76			0.12	0.28
37	1	20:1	4.76		0.26	0.31	0.38
38	1	20:1	4.76		0.28	0.3	0.34
39	1	20:1	4.76	0.18	0.21	0.23	0.3
40	1	15:1	6.25			0.59	0.72
41	1	15:1	6.25			0.39	0.69
42	1	10:1	9.09	0.61	0.73	0.88	0.91
43	1	10:1	9.09		0.79	0.87	

TABLE A -1 Master table for cemented mill tailings fill
Part 1 (continued)
(See explanatory notes on p. A-16)

(1) ID	(2) Ref. No.	(3) T / C ratio (by wt)	(4) Cement content (% by wt)	(5) Uniaxial compressive strength 7 days (MPa)	(6) 14 days (MPa)	(7) 28 days (MPa)	(8) 90 days (MPa)
44	1	10:1	9.09	0.72	0.88	1.02	
45	1	10:1	9.09		0.75	0.87	
46	1	10:1	9.09		0.64	0.74	
47	1	10:1	9.09	0.57	0.7	0.81	
48	1	10:1	9.09	0.19	0.27	0.34	0.52
49	1	8:1	11.11	0.54	0.65	0.76	0.83
50	1	8:1	11.11	0.72	0.83	0.91	
51	1	8:1	11.11	0.81	1.03	1.19	
52	1	8:1	11.11		1.12	1.43	
53	1	8:1	11.11	0.86	1.01	1.23	
54	1	8:1	11.11	0.65	0.8	0.93	
55	1	8:1	11.11	0.57	0.65	0.79	
56	1	8:1	11.11			1.41	
57	1	8:1	11.11	0.88	1.05	1.27	
58	4	30:1	3.23			0.08	
59	4	30:1	3.23			0.28	
60	4	30:1	3.23			0.09	
61	4	30:1	3.23			0.13	
62	4	30:1	3.23			0.19	
63	4		4.00			0.31	
64	4		8.00			1.03	
65	4		12.00			2.07	
66	4		16.00			3.52	
67	6		3.00	0.05	0.05	0.07	
68	6		3.00	0.05	0.05	0.07	
69	6		3.00	0.07	0.09	0.14	
70	6		6.00	0.12	0.16	0.19	
71	6		6.00	0.14	0.16	0.22	
72	6		6.00	0.16	0.22	0.32	
73	6		9.00	0.23	0.35	0.42	
74	6		9.00	0.22	0.32	0.39	
75	6		9.00	0.34	0.43	0.61	
76	6		12.00	0.65	0.84	0.99	
77	6		12.00	0.49	0.70	0.82	
78	6		12.00	0.47	0.63	0.75	
79	7	20:1	4.76			0.47	
80	7	10:1	9.09			0.78	
81	7	5:1	16.67			4.27	
82	10	40:1	2.44			0.01	
83	10	30:1	3.23			0.28	
84	10	20:1	4.76			0.48	
85	10	10:1	9.09			0.69	
86	10	8:1	11.11			1.38	

TABLE A -1 Master table for cemented mill tailings fill
Part 1 (continued)
(See explanatory notes on p. A-16)

(1) ID	(2) Ref. No.	(3) T / C ratio (by wt)	(4) Cement content (% by wt)	(5) Uniaxial compressive strength 7 days (MPa)	(6) 14 days (MPa)	(7) 28 days (MPa)	(8) 90 days (MPa)
87	10		12.50			2.07	
88	10	6:1	14.29			2.76	
89	10	5:1	16.67			3.45	
90	10	2:1	33.33			17.24	
91	10	40:1	2.44			0.28	
92	10	30:1	3.23			0.48	
93	10	20:1	4.76			0.69	
94	10	10:1	9.09			1.38	
95	10	8:1	11.11			2.07	
96	10		12.50			2.76	
97	10	6:1	14.29			3.45	
98	10	5:1	16.67			4.14	
99	11	10:1	9.09	0.71	0.98	1.2	
100	11	40:1	2.44	0.08	0.09	0.1	
101	11	40:1	2.44	0.11	0.21	0.37	
102	11	30:1	3.23	0.21	0.25	0.26	0.29
103	11	25:1	3.85	0.14	0.3	0.34	
104	11	25:1	3.85	0.15	0.19	0.2	
105	11	20:1	4.76	0.36	0.44	0.5	0.64
106	11	15:1	6.25	0.37	0.5	0.56	0.73
107	11		7.14	0.51	0.56	0.72	0.92
108	11	10:1	9.09	0.6	0.84	0.95	
109	11	6:1	14.29	1.32	1.38	1.7	2.05
110	13		4.00	0.06	0.09	0.1	0.14
111	13		6.00	0.14	0.24	0.41	0.76
112	13		8.00	0.32	0.47	0.66	0.87
113	13		10.00	0.28	0.46	0.74	1.11
114	13		15.00	0.71	1.14	1.86	3.57
115	14	40:1	2.44			0.1	
116	14	40:1	2.44			0.08	
117	14	40:1	2.44			0.06	
118	14	40:1	2.44			0.22	
119	14	20:1	4.76			0.15	
120	14	20:1	4.76			0.21	
121	14	20:1	4.76			0.66	
122	14	20:1	4.76			0.23	
123	14		7.00			0.4	
124	14		7.00			0.26	
125	14		7.00			0.45	
126	14	10:1	9.09			0.67	
127	14	10:1	9.09			0.4	
128	18	10:1	9.09			0.67	
129	18	8:1	11.11			2.9	

TABLE A -1 Master table for cemented mill tailings fill
Part 1 (continued)
(See explanatory notes on p. A-16)

(1) ID	(2) Ref. No.	(3) T / C ratio (by wt)	(4) Cement content (% by wt)	(5) Uniaxial compressive strength 7 days (MPa)	(6) 14 days (MPa)	(7) 28 days (MPa)	(8) 90 days (MPa)
130	18	6:1	14.29			4.3	
131	18	5:1	16.67			5	
132	18	4:1	20.00			8.3	
133	18	3:1	25.00			12.2	
134	18	2:1	33.33			13.7	
135	19	30:1	3.22			0.17	
136	19		4.40			0.28	
137	19		5.00			0.3	
138	19	16:1	5.90			1.07	
139	19	16:1	5.90			0.59	
140	19		6.00			0.56	
141	19		6.00			0.28	
142	19		8.00			1.08	
143	19		10.00			1.65	
144	21	30:1	3.23	0.14		0.21	
145	21	20:1	4.76	0.17		0.23	
146	21	12:1	7.69	0.27		0.41	
147	21	8:1	11.11	0.48		0.63	
148	22	25:1	3.85			0.22	
149	22	25:1	3.85			0.14	
150	22	25:1	3.85			0.1	
151	22	15:1	6.25			0.43	
152	22	15:1	6.25			0.35	
153	22	15:1	6.25			0.28	
154	22	10:1	9.09			0.63	
155	22	10:1	9.09			0.63	
156	22	10:1	9.09			0.72	
157	32	20:1	4.76	0.22		0.28	
158	32	10:1	9.09	0.7		0.93	
159	32	6:1	14.29	1.37		2.18	
160	32	20:1	4.76	0.40		0.38	0.41
161	32	30:1	3.23	0.22		0.28	0.3
162	32	40:1	2.44	0.19		0.22	0.21
163	32	12:1	7.69	0.46		0.64	
164	32	8:1	11.11	0.89		1.15	
165	32	16:1	5.90	0.32		0.4	
166	32		4.00	0.15		0.19	
167	32		3.03	0.11		0.16	
168	32	10:1	9.09	0.53		0.88	1.03
169	32	30:1	3.23	0.09		0.14	0.19
170	32	30:1	3.23	0.09		0.11	
171	32	20:1	4.76	0.15		0.17	
172	32	10:1	9.09	0.45		1.03	

TABLE A -1 Master table for cemented mill tailings fill
Part 1 (continued)
(See explanatory notes on p. A-16)

(1) ID	(2) Ref. No.	(3) T / C ratio (by wt)	(4) Cement content (% by wt)	(5) Uniaxial compressive strength 7 days (MPa)	(6) 14 days (MPa)	(7) 28 days (MPa)	(8) 90 days (MPa)
173	32	6:1	14.29	0.85		1.54	
174	32	30:1	3.23	0.07		0.1	0.14
175	32	20:1	4.76	0.15		0.3	0.37
176	32	10:1	9.09	0.33		0.54	0.8
177	32	30:1	3.23	0.14		0.19	
178	32	20:1	4.76	0.23		0.35	
179	32	8:1	11.11	0.81		1.13	
180	32	30:1	3.23	0.14		0.19	
181	32	30:1	3.23	0.08		0.11	
182	32	15:1	6.25	0.35		0.47	
183	32	10:1	9.09	0.35		0.43	
184	32	10:1	9.09	0.65		0.82	
185	32	10:1	9.09	0.54		0.68	
186	32	30:1	3.23	0.12		0.15	
187	32	10:1	9.09	0.42		0.54	0.72
188	32	20:1	4.76	0.14		0.19	0.21
189	32	30:1	3.23	0.08		0.12	0.14
190	32	6:1	14.29	1.05		1.28	
191	32	10:1	9.09	0.48		0.67	
192	32	20:1	4.76	0.26		0.4	0.55
193	32	30:1	3.23	0.14		0.26	0.34

TABLE A -1 Master table for cemented mill tailings fill
Part 2
(See explanatory notes on p. A-16)

(1) ID	(9) Tail. ID	(10) Cu	(11) Cc	(12) Spec. Grav.	(13) Unit weight (g/cc)	(14) Pulp dens. (%)	(15) Water cont. (%)	(16) W / C ratio
1	7	2.44	1.00		1.49	68	32	9.92
2	5	9.67	1.27		1.30	68	32	9.92
3						68	32	9.92
4	8	3.79	0.96			68	32	9.92
5						68	32	9.92
6						68	32	9.92
7						68	32	9.92
8						68	32	9.92
9	3	3.26	0.95		1.57	68	32	9.92
10	2	4.30	0.96		1.62	68	32	9.92
11	4	14	1.79		1.31	68	32	9.92
12						68	32	9.92
13	6	9.50	1.11		1.47	68	32	9.92
14						68	32	9.92
15	1	7.27	0.89		1.39	68	32	9.92
16						68	32	9.92
17	4	14	1.79		1.31	68	32	6.72
18						68	32	6.72
19						68	32	6.72
20						68	32	6.72
21	3	3.26	0.95		1.57	68	32	6.72
22						68	32	6.72
23						68	32	6.72
24						68	32	6.72
25	2	4.30	0.96		1.62	68	32	6.72
26						68	32	6.72
27						68	32	6.72
28						68	32	6.72
29						68	32	6.72
30	8	3.79	0.96			68	32	6.72
31	7	2.44	1.00		1.49	68	32	6.72
32						68	32	6.72
33	5	9.67	1.27		1.30	68	32	6.72
34						68	32	6.72
35	6	9.50	1.11		1.47	68	32	6.72
36						68	32	6.72
37						68	32	6.72
38						68	32	6.72
39	1	7.27	0.89		1.39	68	32	6.72
40	8	3.79	0.96			68	32	5.12
41	1	7.27	0.89			68	32	5.12
42						68	32	3.52
43						68	32	3.52

TABLE A -1 Master table for cemented mill tailings fill
Part 2 (Continued)
(See explanatory notes on p. A-16)

(1) ID	(9) Tail. ID	(10) Cu	(11) Cc	(12) Spec. Grav.	(13) Unit weight (g/cc)	(14) Pulp dens. (%)	(15) Water cont. (%)	(16) W / C ratio
44						68	32	3.52
45						68	32	3.52
46						68	32	3.52
47						68	32	3.52
48						68	32	3.52
49	1	7.27	0.89		1.39	68	32	2.88
50	5	9.67	1.27		1.30	68	32	2.88
51	3	3.26	0.95		1.57	68	32	2.88
52						68	32	2.88
53	7	2.44	1.00		1.49	68	32	2.88
54	6	9.50	1.11		1.47	68	32	2.88
55	4	14	1.79		1.31	68	32	2.88
56	8	3.79	0.96			68	32	2.88
57	2	4.30	0.96		1.62	68	32	2.88
58						55	45	13.95
59						75	25	7.75
60						60	40	12.4
61						65	35	10.85
62						70	30	9.3
63						68	32	8
64						68	32	4
65						68	32	2.67
66						68	32	2
67	36	3.05	1.13					
68	37	3.56	1.16					
69	38	5.08	0.88					
70	36	3.05	1.13					
71	37	3.56	1.16					
72	38	5.08	0.88					
73	37	3.56	1.16					
74	36	3.05	1.13					
75	38	5.08	0.88					
76	38	5.08	0.88					
77	37	3.56	1.16					
78	36	3.05	1.13					
79		4.7	0.81	3.01	1.96	26		5.24
80		4.7	0.81	3.01	1.96	27		2.72
81		4.7	0.81	3.01	1.96	29		1.47
82								
83								
84								
85								
86								

TABLE A -1 Master table for cemented mill tailings fill
Part 2 (Continued)
(See explanatory notes on p. A-16)

(1) ID	(9) Tail. ID	(10) Cu	(11) Cc	(12) Spec. Grav.	(13) Unit weight (g/cc)	(14) Pulp dens. (%)	(15) Water cont. (%)	(16) W / C ratio
87								
88								
89								
90								
91								
92								
93								
94								
95								
96								
97								
98								
99	42	9.64	1.11			72	28	3.08
100	43	5.15	1.43			72	28	11.48
101	42	9.64	1.11			72	28	11.48
102						72	28	8.68
103	42	9.64	1.11			72	28	7.28
104	43	5.15	1.43			72	28	7.28
105						72	28	5.88
106						72	28	4.48
107						72	28	3.92
108	43	5.15	1.43			72	28	3.08
109						72	28	1.96
110								
111								
112								
113								
114								
115						70	30	12.3
116						70	30	12.3
117						70	30	12.3
118								
119						70	30	6.3
120						70	30	6.3
121								
122						70	30	6.3
123						70	30	4.29
124						70	30	4.29
125						70	30	4.29
126						70	30	3.3
127						70	30	3.3
128								
129								

TABLE A -1 Master table for cemented mill tailings fil
Part 2 (Continued)
(See explanatory notes on p. A-16)

(1) ID	(9) Tail. ID	(10) Cu	(11) Cc	(12) Spec. Grav.	(13) Unit weight (g/cc)	(14) Pulp dens. (%)	(15) Water cont. (%)	(16) W / C ratio
130								
131								
132								
133								
134								
135								
136								
137								
138								
139								
140								
141								
142								
143								
144	45	4.19	1.34	3.72		65	35	10.85
115	45	4.19	1.34	3.72		65	35	7.35
146	45	4.19	1.34	3.72		65	35	4.55
147	45	4.19	1.34	3.72		65	35	3.15
148	48	5.73	1.24			68	32	8.32
149	47	2.75	1.38			68	32	8.32
150	46	8.96	0.64			68	32	8.32
151	48	5.73	1.24			68	32	5.12
152	47	2.75	1.38			68	32	5.12
153	46	8.96	0.64			68	32	5.12
154	47	2.75	1.38			68	32	3.52
155	46	8.96	0.64			68	32	3.52
156	48	5.73	1.24			68	32	3.52
157	56	2.76	0.98	2.84	1.55			
158	56	2.76	0.98	2.84	1.55			
159	56	2.76	0.98	2.84	1.55			
160				2.85		78	22	4.62
161				2.85		78	22	6.82
162				2.85		78	22	9.02
163	62	5.12	1.2	2.97		68	32	4.16
164	62	5.12	1.2	2.97		68	32	2.88
165	62	5.12	1.2	2.97		68	32	5.44
166	62	5.12	1.2	2.97		68	32	8
167	62	5.12	1.2	2.97		68	32	10.56
168				2.84				
169				2.84				
170				2.82		58	42	13.02
171				2.82		58	42	8.82
172				2.82		58	42	4.62

TABLE A -1 Master table for cemented mill tailings fill
Part 2 (Continued)
(See explanatory notes on p. A-16)

(1) ID	(9) Tail. ID	(10) Cu	(11) Cc	(12) Spec. Grav.	(13) Unit weight (g/cc)	(14) Pulp dens. (%)	(15) Water cont. (%)	(16) W / C ratio (%)
173				2.82		58	42	2.94
174				2.96		68	32	9.92
175				2.96		68	32	6.72
176				2.96		68	32	3.52
177								
178								
179								
180	63	4	0.98					
181	64	3.13	0.91					
182	63	4	0.98					
183	64	3.13	0.91					
184	63	4	0.98					
185				3.02		65	35	3.85
186				3.02		65	35	10.85
187						68	32	3.52
188						68	32	6.72
189						68	32	9.92
190				3.4		68	32	2.24
191				3.4		68	32	3.52
192				3.4		68	32	6.72
193				3.4		68	32	9.92

TABLE A -1 Master table for cemented mill tailings fill
Part 3
(See explanatory notes on p. A-16)

(1) ID	(17) Poros.	(18) Perc. rate (mm/h)	(19) DF (MPa)	(20) c (MPa)	(21) phi (deg.)
1					
2					
3					
4				0.07	33.8
5					
6					
7					
8					
9					
10					
11					
12					
13					
14					
15				0.1	12.4
16					
17					
18					
19					
20					
21					
22					
23					
24					
25					
26					
27					
28					
29					
30				0.14	25.6
31					
32					
33					
34					
35					
36					
37					
38					
39				0.12	24.7
40				0.17	35.8
41				0.14	26.1
42					
43					

TABLE A -1 Master table for cemented mill tailings fill
Part 3 (Continued)
(See explanatory notes on p. A-16)

(1) ID	(17) Poros.	(18) Perc. rate (mm/h)	(19) DF (MPa)	(20) c (MPa)	(21) phi (deg.)
44					
45					
46					
47					
48					
49					
50					
51					
52					
53					
54					
55					
56					
57					
58					
59					
60					
61					
62					
63					
64					
65					
66					
67					
68					
69					
70					
71					
72					
73					
74					
75					
76					
77					
78					
79	0.35			0.82	
80	0.35			0.17	
81	0.35				
82					
83					
84					
85					
86					

TABLE A -1 Master table for cemented mill tailings fill
Part 3 (Continued)
(See explanatory notes on p. A-16)

(1) ID	(17) Poros.	(18) Perc. rate (mm/h)	(19) DF (MPa)	(20) c (MPa)	(21) phi (deg.)
87					
88					
89					
90					
91					
92					
93					
94					
95					
96					
97					
98					
99					
100					
101					
102					
103					
104					
105					
106					
107					
108					
109					
110				0	24
111				0.16	23
112				0.24	28.5
113				0.32	30
114				0.45	34.5
115					
116					
117					
118					
119					
120					
121					
122					
123					
124					
125					
126					
127					
128					
129					

TABLE A -1 Master table for cemented mill tailings fill
Part 3 (Continued)
(See explanatory notes on p. A-16)

(1) ID	(17) Poros.	(18) Perc. rate (mm/h)	(19) DF (MPa)	(20) c (MPa)	(21) phi (deg.)
130					
131					
132					
133					
134					
135					
136					
137					
138					
139					
140					
141					
142					
143					
144					
145					
146					
147					
148					
149					
150					
151					
152					
153					
154					
155					
156					
157	0.4542				
158	0.4542				
159	0.4542				
160					
161					
162					
163					
164		361			
165		602			
166					
167		823			
168					
169					
170					
171					
172					

TABLE A -1 Master table for cemented mill tailings fill
Part 3 (Continued)
(See explanatory notes on p. A-16)

(1) ID	(17) Poros.	(18) Perc. rate (mm/h)	(19) DF (MPa)	(20) c (MPa)	(21) phi (deg.)
173					
174					
175					
176					
177					
178					
179					
180					
181					
182					
183					
184					
185					
186					
187					
188					
189					
190					
191					
192					
193					

NOTES re Table A-1

Column no.	Description
1	Sequential ID number
2	Reference number (see reference list)
3	Tailings/cement ratio by weight
4	Cement content (% of total dry weight) - as reported or calculated from col. 4
5	Uniaxial compressive strength after 7 days curing time (MPa)
6	Uniaxial compressive strength after 14 days curing time (MPa)
7	Uniaxial compressive strength after 28 days curing time (MPa)
8	Uniaxial compressive strength after 90 days curing time (MPa)
9	Tailings ID number as per Table A-2, when grain size distribution provided
10	Coefficient of uniformity
11	Coefficient of curvature
12	Specific gravity of dry tailings
13	Unit weight of dry tailings (g/cc)
14	Pulp density of fill = mass of solids / mass of slurry (%)
15	Water content = mass of water / mass of slurry (%)
16	Water / cement ratio by weight
17	Porosity
18	Percolation rate (mm/h)
19	Deformation modulus (MPa)
20	Cohesion (MPa)
21	Angle of internal friction (degrees)

TABLE A -2 Grain size distributions
(see note p. A-17)

(1) Tail. ID	(2) Ref. No.	(3) D10	(4) D30	(5) D50	(6) D60	(7) D70	(8) D80	(9) D90	(10) Type
1	1	11	28	57	80	110	150	220	Tailings
2	1	33	67	116	142	175	222	315	Tailings
3	1	50	88	135	163	197	245	340	Tailings
4	1	1	5	11	14	20	28	46	Tailings
5	1	6	21	43	58	80	105	140	Tailings
6	1	4	13	28	38	53	69	97	Tailings
7	1	32	50	68	78	87	96	115	Tailings
8	1	33	63	100	125	150	187	250	Tailings
9	2	2	8	22.5	34	50	76	115	Tailings
10	2	5.5	18	36	47.5	65	88	130	Tailings
11	2	7	7.5	11	12.5	15	18	28	Tailings
12	2	4	11	22	30	40	54	197	Tailings
13	2	3	35	71	92	116	147	197	Tailings
14	2	4	42	83	110	145	190	255	Tailings
15	2	30	65	96	117.5	143	175	223	Tailings
16	2	18	31.5	47.5	59	72	90	122	Tailings
17	2	27	43	61	73	88	107	130	Tailings
18	2	35	55.5	79	95.5	115	137	170	Tailings
19	2	7	53	220	380	585	820	1000	Tailings
20	2	62.5	126	177	212	255	306	392	Tailings
21	2	25	131	200	237	280	350	485	Nat. Sands
22	2	90	196	307	365	422	480	545	Nat. Sands
23	2	122	196	250	277	312	380	506	Nat. Sands
24	2	152.5	240	330	395	475	585		Nat. Sands
25	2	15	43	72	88	102	118	155	Exper. fill
26	2	18.5	47.5	73	82	102	117	143	Exper. fill
27	2	12.5	40	67.5	85	100	117	138	Exper. fill
28	2	25	54	78	92.5	108	123	145	Exper. fill
29	2	53	133	194	225	390			Sandfill
30	2	177	236	312	350	262			Sandfill
31	2	23	77	134	170	205			Tailings
32	6	15	46	73	87	102	117	140	Exper. fill
33	6	12	42.5	70	85	102	117	140	Exper. fill
34	6	26	54	82.5	92	108	127	157	Exper. fill
35	6	2.5	29	95.5	128	162	200	243	Tailings
36	6	58	107.5	154	177	202	228	262	Tailings
37	6	48	97.5	146	171	196	225	263	Tailings
38	6	26	55	104.5	132	165	203	257	Tailings
39	9	25	32	38	44				Tailings
40	9	17	25	33	38				Tailings
41	9	12	20	27.5	32				Tailings
42	11	5.5	18	38	53				Tailings
43	11	14	38	55	72				Tailings
44	17	34	49	72.5	87.5				Tailings

TABLE A -2 Grain size distributions (cont'd)

(1) Tail. ID	(2) Ref. No.	(3) D10	(4) D30	(5) D50	(6) D60	(7) D70	(8) D80	(9) D90	(10) Type
15	21	21.5	51	77	90	112	148	205	Sandfill
46	22	53	127	275	475	625	1050	2250	Sandfill
47	22	150	292.5	365	412	462	525	594	Tailings
48	22	30	80	137.5	172	215	265	340	Tailings
49	23	2.5	8	17.5	26				Tailings
50	24	42	58	80	95				Tailings
51	25	30	72.5	87	90				Tailings
52	27	19.5	50	92	117				Tailings
53	30	14	40	67	83				Tailings
54	30	108	263	485	630				Tailings
55	31	37	52.5	72	83				Tailings
56	32	39	64	91	107.5	125	147	182	Tailings
57	32	31	52	70	82	96	113	131	Tailings
58	32	42.5	68	89	97.5				Tailings
59	32	350	900	4500	13250				Rockfill
60	32	1610	7700	21700	32200				Rockfill
61	32	1935	2330	25700	42750				Rockfill
62	32	25	62	100	128	163	195	250	Tailings
63	32	43	85	140	172	210			Tailings
64	32	32	54	75	100	128	160	203	Tailings

Note. Cols. 3 - 9: grain sizes expressed in micrometres

TABLE A-3 Master table for cemented rockfill
(explanatory notes on p. A-16 apply)

(1) ID	(2) Ref. No.	(3) T / C ratio (by wt)	(4) Cement content (% by wt) (%)	(5) Uniaxial compressive strength 7 days (MPa) (MPa)	(6) 14 days (MPa) (MPa)	(7) 28 days (MPa) (MPa)	(8) 90 days (MPa) (MPa)
1001	7	20	16.6			12.93	
1002	7	10	9.09			5.69	
1003	7	5	4.76			2.33	
1004	8		2			0.63	
1005	8		3			1.38	
1006	8		6			2.19	
1007	8		8			3.13	
1008	8		10			4	
1009	8		9			1.27	
1010	8		9			3.23	
1011	8		9			3.63	
1012	8		9			3	
1013	8		9			1.77	
1014	45		2.5			2.5	
1015	45		3.5			4.9	
1016	45		5			6.2	
1017	45		6			7.4	
1018	45		7			8	
1019	45		10			18.3	
1020	46		3.3			2	
1021	46		6.8			4.7	
1022	46		11.3			12.1	
1023	32		3		1.44	1.3	
1024	32		4		1.61	1.74	
1025	32		5		2.08	2.61	

TABLE A-4 Master table for fly ash
Part 1
(see explanatory notes on p. A-23)

(1) ID	(2) Ref. No.	(3) T / C ratio (by wt)	(4) Cement content (% by wt)	(5) 28-d uniaxial comp. strength (MPa) 0% flyash	(6) 10% flyash	(7) 20% flyash	(8) 25% flyash
1	1	8:1	11.1	1.43	1.32	1.39	
2	1	8:1	11.1	1.43	1.39	1.28	
3	1	20:1	4.76	0.49	0.32	0.26	
4	1	20:1	4.76	0.49	0.29	0.3	
5	1	30:1	3.23	0.32	0.17	0.18	
6	1	30:1	3.23	0.32	0.15	0.13	
7	32	6:1	14.3	2.18			2.02
8	32	10:1	9.09	0.93			0.79
9	32	20:1	4.76	0.29			0.29
10	32	10:1	9.09	0.88			
11	32	10:1	9.09	0.88			
12	32	30:1	3.23	0.14			
13	32	30:1	3.23	0.14			
14	32	30:1	3.23	0.28			0.32
15	32	40:1	2.43	0.22			0.22
16	32	20:1	4.76	0.38			0.34
17	32	30:1	3.23	0.11			0.1
18	32	10:1	9.09	1.03			0.55
19	32	20:1	4.76	0.17			0.17
20	32	6:1	14.3	1.54			1.49
21	32	8:1	11.1	1.13			1.01
22	32	20:1	4.76	0.35			0.29
23	32	30:1	3.23	0.19			0.14
24	32	10:1	9.09	0.54			0.51
25	32	20:1	4.76	0.19			0.19
26	32	30:1	3.23	0.12			0.1
27	49	20:1	4.76	4.4			
28	49	20:1	4.76	4.4			
29	49	20:1	4.76	4.4			
30	49	20:1	4.76	4.4			

TABLE A-4 Master table for fly ash
Part 2
(see explanatory notes on p. A-16)

(1) ID	(9) 28-day uniaxial comp. strength (MPa) 30% flyash	(10) 50% flyash	(11) 60% flyash	(12) 75% flyash	(13) 100% flyash	(14) Spec. Grav.	(15) Unit weight (g/cc)
1							
2							
3							
4							
5							
6							
7		1.78				2.84	1.55
8		0.77				2.84	1.55
9		0.22				2.84	1.55
10		0.59				2.84	
11		0.9				2.84	
12		0.14				2.84	
13		0.14				2.84	
14		0.21		0.12	0.12	2.85	
15		0.17		0.06	0.11	2.85	
16		0.54		0.22	0.08	2.85	
17		0.1				2.82	
18		0.55				2.82	
19		0.16				2.82	
20		1.34				2.82	
21		0.81					
22		0.35					
23		0.14					
24		0.58					
25		0.15					
26		0.08					
27	2.6		1.6				
28	3.8		2.1				
29	1.6		2.6				
30	3.2		2.4				

TABLE A-4 Master table for fly ash
Part 3
(see explanatory notes on p. A-16)

(1) ID	(16) Pulp dens. (%)	(17) Void ratio	(18) W / C ratio (%)	(19) Origin of fly ash
1				
2				
3				
4				
5				
6				
7		0.83		Thunder Bay
8		0.83		Thunder Bay
9		0.83		Thunder Bay
10				Thunder Bay
11				Detroit
12				Detroit
13				Thunder Bay
14	78			Type 10, Thunder Bay
15	78			Type 10, Thunder Bay
16	78			Type 10, Thunder Bay
17	58			Type 10, Thunder Bay
18	58			Type 10, Thunder Bay
19	58			Type 10, Thunder Bay
20	58			Type 10, Thunder Bay
21				Type C
22				Type C
23				Type C
24	68			Detroit Type c
25	68			Detroit Type c
26	68			Detroit Type c
27			1.2	Type F - Source 1
28			1.2	Type C - Source 1
29			1.2	Type F - Source 2
30			1.2	Mixture C1 + F1 + F2

NOTES re Table A-4

Column no.	Description
1	Sequential ID number
2	Reference number (see reference list)
3	Tailings/cement ratio by weight
4	Cement content (% of total dry weight) - calculated from col. 4
5 - 13	Uniaxial compressive strength after 7 days curing time (MPa), with Portland cement replaced with the indicated percentage of fly ash by weight
14	Specific gravity of dry tailings
15	Unit weight of dry tailings (g/cc)
16	Pulp density of fill = mass of solids / mass of slurry (%)
17	Void ratio of tailings
18	Water / cement ratio by weight
17	Porosity = volume of voids / total volume
18	Percolation rate (mm/h)
19	Origin and type of fly ash (when available)

REFERENCES

1. Weaver, W.S., and Luka, R., "Laboratory studies of cement-stabilized mine tailings", CIMM Transactions, Vol. LXXIII, pp. 204-217.

2. Thomas, E.G., Nantel, J.H., and Notley, K.R., Fill technology in underground metalliferous mines, International Academic Services Ltd., 1979.

3. Thomas, E.G., "Cemented hydraulic fill mix design as it applies to mine scheduling", Jubilee Symposium on Mine Filling, 1973, pp. 137-145.

4. Singh, K.H., "Cemented hydraulic fill for ground support", CIM Bulletin, Jan. 1976, pp. 69-74.

5. Manca, P.P., Massaci, G., Massidda, L., and Rossi, G., "Stabilization of mill tailings for mining backfill with Portland cement and fly ash", The Institution of Mining and Metallurgy, 1984, pp. A48-A54.

6. Thomas, E.G., "Selection and specification criteria for fills for cut-and-fill mining", Application of rock mechanics to cut and fill mining, Institution of Mining and Metallurgy, 1980, pp. 128-132.

7. Arioglu, E., "Engineering properties of cemented aggregate fill for Uludag tungsten mine of Turkey", Mining with Backfill, A.A. Balkema, 1983, pp. 3-8.

8. Knissel, W., and Helms, W., "Strength of cemented rockfill from washery refuse - results from laboratory investigations", Mining with Backfill, A.A. Balkema, 1983, pp. 31-37.

9. Thomas, E.G., "Characteristics of cemented deslimed mill tailing fill prepared from finely ground tailing", Mining with Backfill, A.A. Balkema, 1983, pp. 59-66.

10. Dhar, B.B., Shanker, K.V., and Sastry, V.R., "Hydraulic filling - an effective way of ground control", Mining with Backfill, A.A. Balkema, 1983, pp. 113-120.

11. Ross-Watt, D.A.J., "Initial experience in the extraction of blasthole pillars between backfilled stopes", Mining with Backfill, A.A. Balkema, 1983, pp. 199-228.

12. Arioglu, E., Yuksel, A., and Agralı, Z., "Strength characteristics of lime-stabilized mine tailings", Mining Science and Technology, pp. 161-166.

13. Hassani, F.P., Scoble, M.J., and Pichacchia, L., "The significance of cement content to hydraulic backfill design", Proceedings, 87th Annual General Meeting of CIM, 1985.

14. Mitchell, R.,J., and Wong, B.C., "Behaviour of cemented tailings sands", Canadian Geotechnical Journal, 1982, pp. 289-295.

15. Nantel, J., and Lecuyer, N., "Assessment of slag backfill properties for the Noranda Chadbourne project", CIM Bulletin, Jan. 1983, pp. 57-60.

16. Thomas, E.G., "A review of cementing agents for hydraulic fill", Jubilee Symposium on Mine filling, 1973, pp. 65-75.

17. Swain, H.D., "An investigation into the use of pyrrhotite as a cementing agent for backfill", Jubilee Symposium on Mine Filling, 1973, pp. 77-85.

18. Liangduan, W., "The design and practice of cut and fill method at Fankou lead-zinc mine", Mining with Backfill, A.A. Balkema, 1983, pp. 293-300.

19. Rawling, J.R., Toguri, J.M., and Cerigo, D.G., "Strength and permeability of cement-stabilized backfill", Noranda Reasearch Centre, Dec. 1966, pp. 43-47.

20. Craig, R.F., Soil Mechanics, 3rd Ed., Van Nostrand Reinhold Publ., 1983.

21. Ontario backfill survey, 1986.

22. Ontario backfill survey, 1986.

23. Gignac, L., "Filling practices at Brunswick Mining No. 12 Mine", State-of-the-art Review, pp. 30-36.

24. Piciacchia, L., Scoble, M.J., Rowlands, N., "The integration of backfill non-linear behaviour into finite element modelling for underground mine design", Department of Mining and Metallurgical Engineering, McGill University.

25. Aitchison, G.D., Kurzeme, M., and Willoughby, D.R., "Geomechanics considerations in optimising the use of mine fill", Jubilee Symposium on Mine Filling, 1973, pp. 35-48.

26. Arioglu, E., "Design aspects of cemented aggregate fill mixes for tungsten stoping operations", Mining Science and technology, pp. 209-214.

27. Soderberg, R.L., and Busch, R.A., "Bulkheads and drains for high sandfill stopes", U.S.B.M. Spokane Research Center, 1985.

28. Ontario backfill survey, 1986.

29. Ontario backfill survey, 1986.